USAF TEST PILOT SCHOOL

FLYING

QUALITIES

TEXTBOOK

VOLUME II
PART 2

APRIL 1986

Vol.1- AD-A170957
Vol 2-pt 1- AD-A170959

EDWARDS AFB, CALIFORNIA

CHAPTER 9
ROLL COUPLING

9.1 INTRODUCTION

Divergence experienced during rolling maneuvers has frequently been referred to as "inertial coupling." This leads to a misconception of the problems involved. The divergence experienced during rolling maneuvers is complex because it involves not only inertial properties, but aerodynamic ones as well. The material in this chapter is intended to offer a physical explanation of the more important causes of roll coupling.

Coupling results when a disturbance about one aircraft axis causes a disturbance about another axis. An example of uncoupled motion is the disturbance created by an elevator deflection. The resulting motion is restricted to pitching motion, and no disturbance occurs in yaw or roll. An example of coupled motion is the disturbance created by a rudder deflection. The ensuing motion will be some combination of both yawing and rolling that results in coupling problems large enough to threaten the structural integrity of the aircraft.

There are numerous contributions to the roll coupling characteristics of an aircraft. Only three will be considered here:

Inertial Coupling

The I_{xz} Effect

Aerodynamic Coupling

These effects occur simultaneously in a complex fashion. Therefore, divergence cannot be predicted by analyzing these effects separately. The complicated interrelationship of these parameters can best be seen by analyzing the aircraft equations of motion.

$$\text{Roll } \dot{p} = \frac{\Sigma L}{I_x} - qr\left(\frac{(I_z - I_y)}{I_x}\right) + (\dot{r} + qp)\frac{I_{xz}}{I_x} \qquad (9.1)$$

$$\text{Pitch } \dot{q} = \frac{\Sigma M}{I_y} - pr\left(\frac{(I_x - I_z)}{I_y}\right) - (p^2 - r^2)\frac{I_{xz}}{I_y} \qquad (9.2)$$

$$\text{Yaw } \dot{r} = \frac{\Sigma N}{I_z} - pq\left(\frac{(I_x - I_z)}{I_z}\right) - (qr - \dot{p})\frac{I_{xz}}{I_z} \qquad (9.3)$$

$$\text{Drag } \dot{u} = \frac{\Sigma F_x}{m} - qw + rv \qquad (9.4)$$

$$\text{Lift } \dot{w} = \frac{\Sigma F_z}{m} - pv + qu \qquad (9.5)$$

$$\text{Side } \dot{v} = \frac{\Sigma F_y}{m} - ru + pw \qquad (9.6)$$

Consider Equations 9.1 - 9.3, derived from moment equations. In each case, the first term on the right-hand side of the equations represents the aerodynamic contribution, the second term the inertial contribution, and the third term the I_{xz} effects. It can be seen that these three contributions to roll coupling can combine to adversely or proversely affect pitch, roll, and yaw acceleration, and thus the tendency for the aircraft to diverge.

"Divergence" in roll coupling is characterized by a departure from the intended flight path that will result in either loss of control or structural failure. As defined, this "divergence" is what we are concerned with in roll coupling. Smaller roll coupling effects that do not result in divergence will not be considered. It should be noted that divergence about any one axis will be closely followed by divergence about the others.

9.2 INERTIAL COUPLING

Inertial coupling did not become a problem until the introduction of the century series aircraft. As the fighter plane evolved from the conventional design of the P-47 and P-51, through the first jet fighter, the F-80, and then to the F-100 and other century series aircraft, there was a steady change in the weight distribution. During this evolution, more and more weight was concentrated in the fuselage as the aircraft's wings grew thinner and shorter. This shift of weight caused relationships between the moments of inertia to

change. As more weight was concentrated along the longitudinal axis, the moment of inertia about the x axis decreased relative to the moments of inertia about the y and z axis. This phenomena increases the coupling between the lateral and longitudinal equations. This can be seen by examining Equation 9.2

$$\dot{q} = \frac{\Sigma M}{I_y} - pr\left(\frac{I_x - I_z}{I_y}\right) - (p^2 - r^2)\frac{I_{xz}}{I_y} \qquad (9.2)$$

As I_x becomes much smaller than I_z, the moment of inertia difference term $(I_x - I_z)/I_y$ can become large. If a roll rate is introduced, the term $pr\,(I_x - I_z)/I_y$ may become large enough to cause an uncontrollable pitch acceleration.

Modern fighter design is characterized by a long, slender, high density fuselage with short, thin wings. This results in a roll inertia which is quite small in comparison to the pitch and yaw inertia. The more conventional low speed aircraft may have a wingspan greater than the fuselage length and a great deal of weight concentrated in the wings. A comparison of these configurations is presented in Figure 9.1.
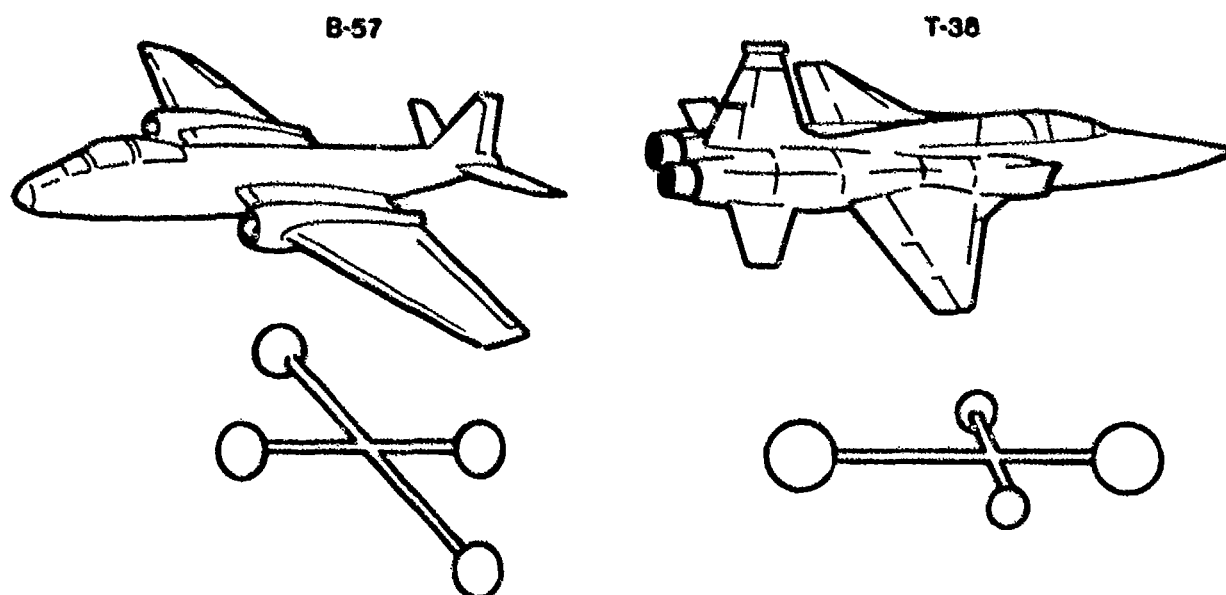

FIGURE 9.1.   CONVENTIONAL AND MODERN AIRCRAFT DESIGN

The mass distribution of these aircraft can be represented by a pair of dumbbells. The axis with the larger dumbbell will tend to align itself with the plane that is perpendicular to the roll axis. Therefore, inertial coupling for the B-57 is different than that of the T-38. A roll will have little effect on angle of attack for the B-57 and increase it for the T-38.

The conventional B-57 design presents considerable resistance to rotation about the x axis and does not generate high roll rates. On the other hand, the T-38 design presents a relatively small resistance to rotation about the x axis and attains high rates of roll. High roll rates enhance the tendency toward inertial coupling.

This analysis of inertial coupling will consider rolls about two different axes, the inertial axis and the aerodynamic axis. The inertial axis is formed by a line connecting the aircraft's two "centers of inertia" as shown in Figure 9.2. The aerodynamic axis is the stability x axis first introduced in the investigation of the left-hand side of the equations of motion. It is merely the line of the relative wind. Aircraft rotation in a roll is generally assumed to be about this axis. To visualize this, recall that to produce a rolling moment a differential in lift must be created on the wings. For the time being, let us assume that the aircraft will roll about the relative wind, or aerodynamic axis.
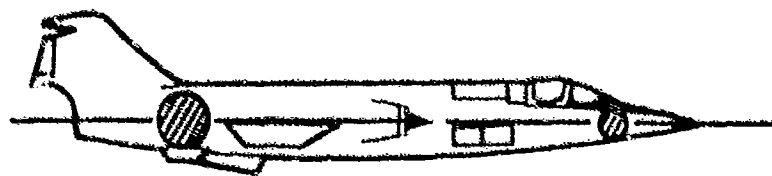

FIGURE 9.2. AIRCRAFT INERTIAL AXIS

First, consider a roll when the aerodynamic and inertial axes are coincident as illustrated in Figure 9.3. In this case, there is no force created by the centers of inertia that will cause the aircraft to be diverted

from its intended flight path, and no inertial coupling results. Now, observe what happens when the inertial axis is displaced from the aerodynamic axis.
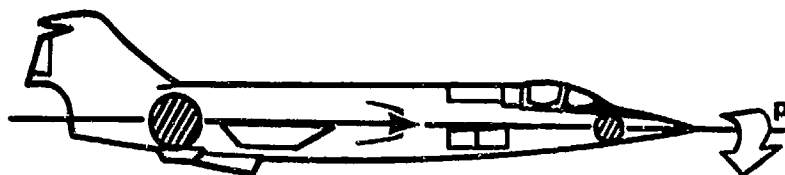

FIGURE 9.3. AERODYNAMIC AND INERTIAL AXES COINCIDENT

As the aircraft is rotating about the aerodynamic axis, centrifugal force will act on the centers of inertia. Remembering that centrifugal force acts perpendicular to the axis of rotation, it can be seen that a moment will be created by this centrifugal force. For the case depicted in Figure 9.4, where the aerodynamic axis is depressed below the inertial axis, a pitch up will result. Conversely, if the aerodynamic axis is above the inertial axis, a pitch down will result.
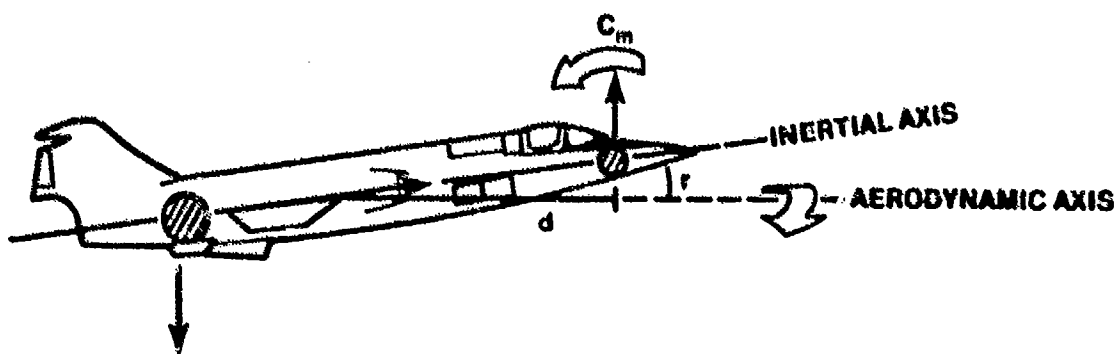

FIGURE 9.4. AERODYNAMIC AND INERTIAL AXES NONCOINCIDENT

To appreciate the magnitude of the moment thus developed, refer to Figure 9.4 and consider the following:

$$\text{Centrifugal Force (CF)} = \frac{mV^2_{\text{Tangential}}}{r} \qquad (9.7)$$

$$V_{\text{Tangential}} = r\omega = rp \qquad (9.8)$$

Therefore,

$$CF = mrp^2$$

The moment created by this centrifugal force is

$$M = (CF)(d) = mrp^2 d \qquad (9.9)$$

For modern designs, m is large. Also, r will be larger for a low aspect ratio wing. (The aircraft will operate at a higher angle of attack.) As previously discussed, p will be large. For long, dense fuselages, d will be large. Thus, the moment created by inertial coupling will be large.

9.3 THE I_{xz} EFFECT

Three products of inertia (I_{xy}, I_{yz}, and I_{xz}) appear in the equations of motion for a rigid aircraft. By virtue of symmetry, I_{xy} and I_{yz} are both equal to zero. However, the product of inertia I_{xz} can be of an appreciable magnitude and can have a significant effect on the roll characteristics of an aircraft.

The parameter, I_{xz}, can be thought of as a measure of the nonuniformity of a mass distribution along the x axis, and the mass of the aircraft can be considered to be concentrated on this axis. The axis about which $I_{xz} = 0$ is defined as the inertial axis.

The I_{xz} parameter is a measure of how the inertial axis is displaced from the aircraft x axis. A typical aircraft design can be represented by two centers of mass in the xz plane designated m_1 and m_2 in Figure 9.5. It can be seen that if the aircraft is rolled about the x axis, a pitch down will result. The inertial pitching moment (up or down) generated by a roll is a

function of (1) the axis about which the roll is performed and (2) the inclination of the inertial axis with respect to the roll axis. A roll about the aerodynamic axis in Figure 9.6a will produce a pitch down while the same roll in Figure 9.6b will produce a pitch up. Thus, when an aircraft is rolled about an axis which differs from its inertial axis, pitching moments develop which tend to cause the aircraft to depart from its intended flight path. Depending on its orientation, the I_{xz} parameter modifies the effect of inertial coupling.
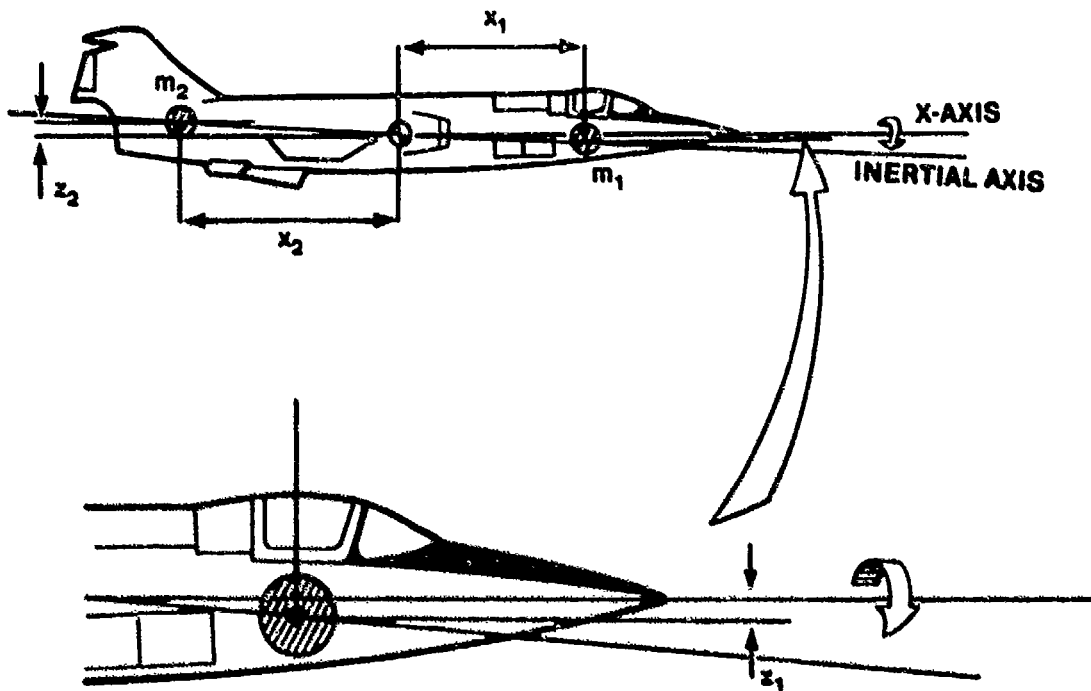
FIGURE 9.5. INERTIAL AXIS BELOW AERODYNAMIC AXIS

To appreciate the magnitude of this parameter, consider Figure 9.5. From Equation 9.9, the moment produced by the forward center of mass is,

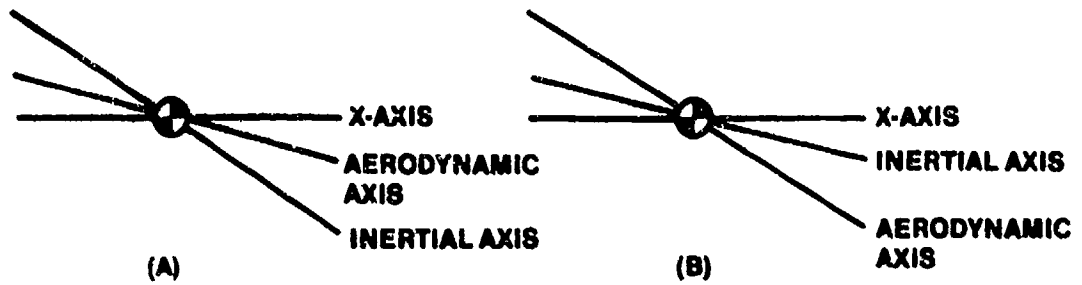$$M_1 = (C.F.) (x_1) = m_1 x_1 p^2 z_1 \qquad (9.10)$$

FIGURE 9.6. THE I_{xz} EFFECT

Similarly, the moment produced by the aft center of mass is

$$M_2 = m_2 x_2 p^2 z_2 \qquad (9.11)$$

The total pitch moment is therefore

$$M_T = M_1 + M_2 = m_1 x_1 p^2 z_1 + m_2 x_2 p^2 z_2 \qquad (9.12)$$

$$M_T = p^2 \, (m_1 x_1 z_1 + m_2 x_2 z_2) \qquad (9.13)$$

But for a simplified system

$$I_{xz} = m_1 x_1 z_1 + m_2 x_2 z_2 \qquad (9.14)$$

Therefore,

$$M_T = p^2 I_{xz} \qquad (9.15)$$

Thus, it can be seen that the magnitude of the pitching moment depends on the roll rate and the magnitude of the I_{xz} parameter relative to the roll axis.

9.4 AERODYNAMIC COUPLING

This analysis of roll coupling is not concerned with all aerodynamic coupling terms $\left(C_{n_p}, C_{n_{\delta_a}}, C_{\ell_r}, C_{\ell_{\delta_r}}, \text{ etc.} \right)$. Only the "kinematic coupling" aspects of aerodynamic coupling will be considered.

Kinematic coupling is the actual interchange of α and β during a rolling maneuver. This interchange is an important means by which the longitudinal and lateral motions are capable of influencing each other during a rapid roll.

To understand how this interchange of α and β occurs, consider Figure 9.7. In this figure the aircraft is assumed to have either infinitely large inertia or negligible stability. Thus it will roll about its inertial axis. In (I) the aircraft initiates a roll from a positive angle of attack. In (II) the initial angle of attack is converted to a positive sideslip angle of equal magnitude after 90° of roll. In (III) the aircraft has again exchanged β and α and after 180° of roll has an angle of attack equal in magnitude but opposite in sign to the original α. The interchange continues and in (IV) this $-\alpha$ is converted to $-\beta$.
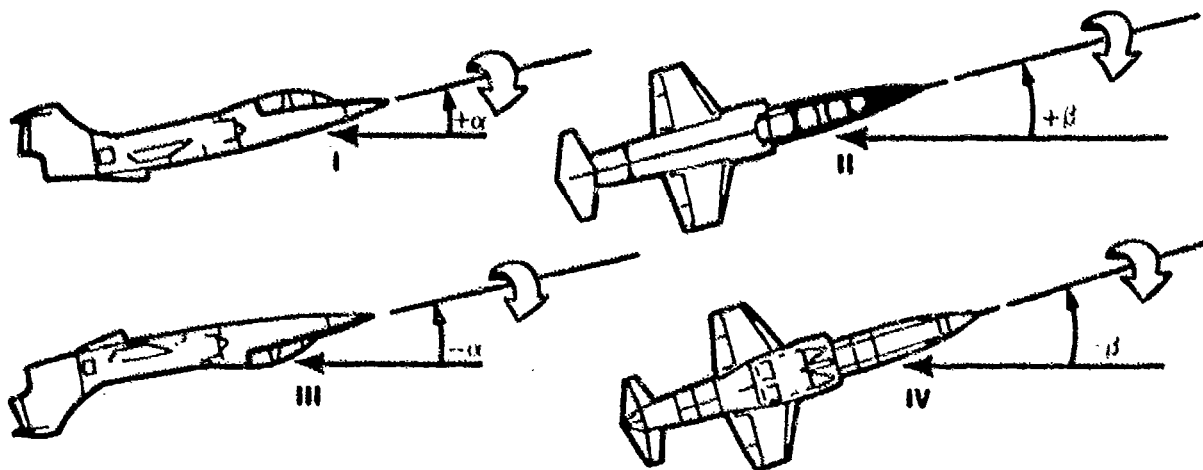
FIGURE 9.7. KINEMATIC COUPLING. ROLLING OF AN AIRCRAFT WITH INFINITELY LARGE INERTIA OR NEGLIGIBLE STABILITY IN PITCH AND YAW

Next, consider an aircraft with infinitely large stability in pitch and yaw or negligible inertia. Refer to Figure 9.8.
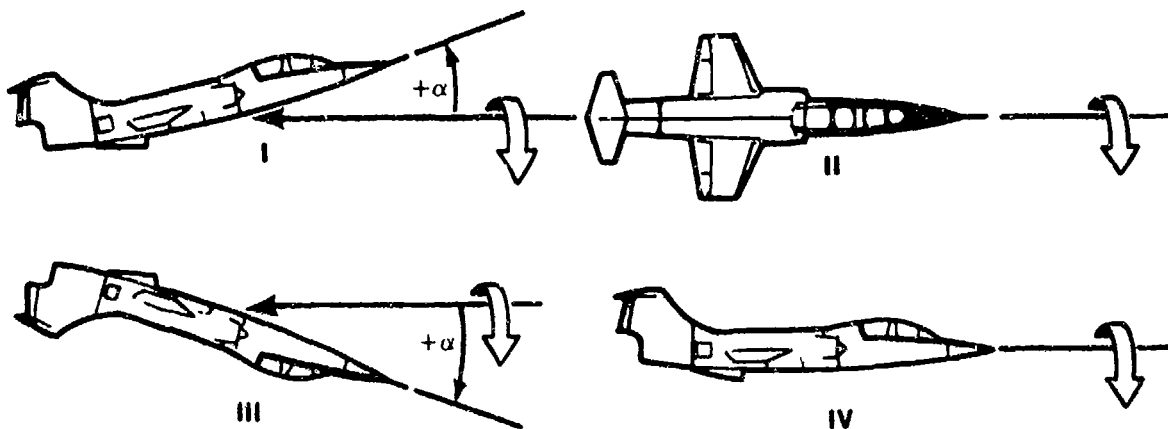
FIGURE 9.8.   NO KINEMATIC COUPLING.   ROLLING OF AN
AIRCRAFT WITH INFINITELY LARGE STABILITY
OR NEGLIGIBLE INERTIA IN PITCH AND YAW

In this case, the aircraft will roll about its aerodynamic axis, and no interchange of α or β will occur.

Since aircraft do not have infinitely large inertia or stability, neither of these extremes can occur. Some combination of these effects will always result during a roll. The amount of kinematic coupling will depend upon the relative values of C_{n_β} and C_{m_α} and roll rates. This can be shown with two empirical relationships:

$$\dot{\alpha} = -Kp\beta \qquad\qquad (9.16)$$

$$\dot{\beta} = Kp\alpha \qquad\qquad (9.17)$$

These relationships show that any roll rate will cause an interchange of α and β. The exact amount depends on the magnitude of K which is determined by the relative values of the moments of inertia and C_{m_α} and C_{n_β}. It can also be seen that for a given aircraft, the rate of interchange of α and β depends on the roll rate. The higher the roll rate, the greater the kinematic coupling. As roll rate increases, a point is reached where the stability of the aircraft

is insufficient to counter the α and β build up. This divergence could ultimately result in departure from controlled flight. This point is of special interest to designers and is often the subject of an in-depth mathematical analysis. Although little can be determined from Equations 9.16 and 9.17, they provide a basis for showing how an aircraft's dynamic response can be used to make some rough predictions about the kinematic coupling characteristics. It has been shown in dynamics that the natural frequency of the short period mode is a function of C_{m_α}. Likewise the natural frequency of the Dutch Roll mode is a function of C_{n_β}.

Assume that an aircraft is rolled at a rate that creates a disturbance in β at a rate equal to the maximum rate that the natural aircraft stability can damp out the disturbance. Thus,

$$\dot{\beta} = Kp\alpha = f(\omega_n)_{\text{Dutch Roll}} \qquad (9.18)$$

In this case, there would be no buildup of β, and a condition of neutral stability in yaw would result. However, if the roll rate were increased slightly above this value, then successively larger increases in β would occur and divergence would result. This analysis can also be followed through for an initial disturbance in α. It is not important which diverges first, α or β, since any divergence about one axis will quickly drive the other divergent. As a matter of interest however, supersonically C_{n_β} decreases more rapidly than C_{m_α} and therefore, most modern aircraft will diverge in yaw first, supersonically.

It can be shown on an analog computer that when $C_{m_\alpha} = C_{n_\beta}$ a stable condition will exist at all roll rates. This is often referred to as a "tuned condition", and is a possible dodge for an aircraft designer to use in a critical flight area. However, it is difficult to capitalize on this occurrence because of the wide variation of the stability derivatives with Mach.

It may be that an aircraft will possess stability parameters such that a roll coupling problem exists at a given roll rate. However, if a relatively long time is required before large values of α and β are generated, then the aircraft may be rolled at the maximum value by restricting the aircraft to one 360° roll. In this situation, the aircraft is diverging during the roll, but at such a slow rate that by the time the aircraft has rolled 360°, the maximum allowable α or β of the aircraft has not been exceeded.

9.5 AUTOROTATIONAL ROLLING

It has been shown that during rolling maneuvers, large angles of attack and sideslip may occur as a result of inertial and kinematic coupling. For some aircraft, certain conditions of α and β will produce a rolling moment that is in the same direction as the roll. If this moment is equal or greater than the moment created by roll damping, the airplane will continue an uncommanded roll. In some cases, it may not be possible to stop the aircraft from rolling, although full lateral control is held against the roll direction. This is known as autorotational rolling or "auto roll". There are various conditions that can cause auto roll. It can occur at a positive or negative angle of attack with any combination of sideslip angle. It is highly dependent on aerodynamic design. However, flight control and stability augmentation systems can also have a large effect. Auto roll is normally caused by the development of sideslip due to kinematic or inertial coupling and the effect of C_{ℓ_β} once this sideslip has developed. On some aircraft with highly augmented flight control systems, an auto roll may result from control inputs commanded by the system itself.

A good example of auto roll occurs in the F-104 at negative angles of attack. For analysis sake, let us assume the aircraft is rolled to the right. In this case the negative α is converted into negative β (refer to Figure 9.7, III and IV). The vertical stabilizer for the F-104 is highly effective, therefore the $-\beta$ develops a significant rolling moment to the right which reinforces the rolling motion. Since the F-104 is a fuselage loaded aircraft, the rolling motion causes the airplane to pitch down. This increases the $-\alpha$ and further complicates the problem. If allowed to continue, this motion

9.12

could diverge until the aircraft departs from controlled flight. If an auto roll of this type were to begin, the pilot should pull back on the stick to make α positive. With +α, kinematic coupling will tend to decrease the roll rate.

Although no analysis of the effects of augmented flight control systems (SAS, CAS, etc.) will be presented here, note that these types of systems are prone to cause auto roll tendencies. Rate feedbacks are hard to tailor to improve handling qualities throughout the flight regime without adversely affecting roll coupling tendencies somewhere in that regime. It is up to the flight test pilot and engineer to accurately predict where problems may exist and thoroughly investigate these areas.

9.6 CONCLUSIONS

As an aircraft's inertias are disproportionately increased in relation to its aerodynamic stabilities in pitch and yaw, the aircraft will be liable to pitching and yawing motions during rolling maneuvers. The more typical case is a divergence in yaw by virtue of an inadequate value of C_{n_β}.

The peak loads resulting from roll coupling generally increase in proportion to the initial incidence of the inertial axis and progressively with the duration of the roll and the rapidity of aileron application at the beginning and the end of the maneuver. The most severe cases naturally should be expected in a flight regime of low C_{n_β} and high dynamic pressures.

The rolling pull-out maneuver in a high performance aircraft is especially dangerous. It combines many unfavorable features: high speed, hence high roll rate capability; high acceleration which favors poor coordination and inadvertent excitation of transients by the pilot; and high dynamic pressures which at large values of α and β may break the aircraft.

Most high performance aircraft incorporate roll rate limiters in addition to angular damping augmentors. In these aircraft, a lateral control with enough power for low speed is almost certain to be too powerful for high speeds. Fortunately, limiters of various kinds are not too difficult to incorporate in a fully powered control system.

It is obvious that flight testing in suspected regions of roll coupling warrants a cautious methodical approach and must be accompanied by thorough computer studies that stay current with the flight test data. The only way that the pilot can discover the exact critical roll limit in flight is when he exceeds it, which is obviously not the approach to take. Because of this, flight tests are generally discontinued when computer studies indicate that the next data point may be "over the line".

The following example is cited. The Bell X-2 rocket ship was launched from its mother ship at Edwards in 1956. The pilot flew a perfect profile, but the rocket engine burned a few critical seconds longer than the engineers predicted, resulting in a greater speed (Mach 3.2) and greater altitude (119,800 feet) than planned. Unknown to the pilot, he was progressively running out of directional stability. When he was over the point at which he had preplanned to start his turn toward Roger's Dry Lake he actuated his controls. The X-2 went divergent with a resultant loss of control. The accident investigation revealed the cause to be a greater loss in directional stability than planned, resulting in divergent roll coupling.

A combination of reasonable piloting restrictions coupled with increased directional stability has provided the solution to roll coupling problems in the present generation of aircraft. The problem is one of understanding since a thinking pilot would no more exceed the roll limitations imposed on an aircraft than he would the structural "G" limitations.

Besides pilot education, some other methods to eliminate roll coupling divergence are:

1. Roll Rate Limiters

2. Angular Damping Augmentors

3. Placarded Roll Limits, such as:

    a. "G" limits

    b. Total allowable roll at maximum rate

    c. Altitude limits

    d. Mach limits

    e. Flap position limits

9.1. Given the following sketch and the fact that centrifugal force = mV^2_{TANG}/r, derive an expression for pitching moment as a function of α. Make a sketch.
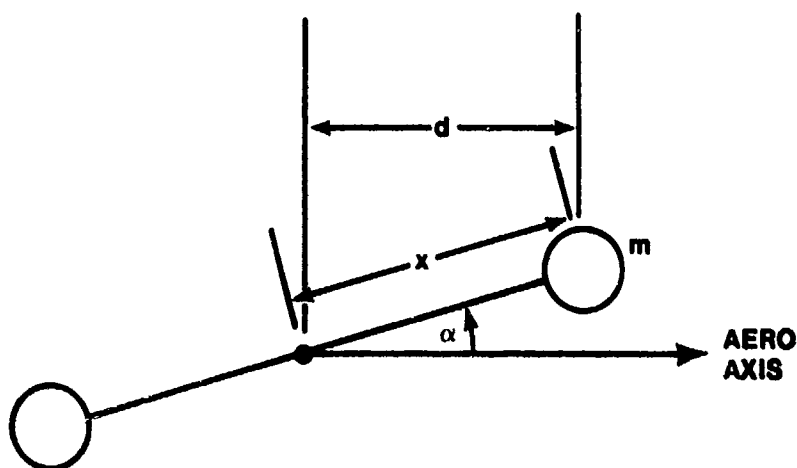
9.2. Given the following expressions taken from AFFTC-TR-79-18 (F-16 High Angle-of-Attack Report)

$$\dot{\alpha} = q - \tan\beta(p\cos\alpha + r\sin\alpha) + \frac{Z}{mV\cos\alpha\cos\beta} + \frac{r\tan\alpha\tan\beta}{mV\cos\beta}$$

$$\dot{\beta} = p\sin\alpha - r\cos\alpha + \frac{Y}{mV\cos\beta}$$

assume small angles (α, β) and negligible forces (Y, Z);

show that

$$\dot{\alpha} = q - p\beta$$

$$\dot{\beta} = p\alpha - r$$

9.3. Use the above expressions for $\dot{\alpha}$ and $\dot{\beta}$ and the expressions below:
(Assume a "principal axes" system)

$$G_y = \dot{q} I_y - rp (I_z - I_x) + (p^2 - r^2) I_{xz}$$

$$G_z = \dot{r} I_z - pq (I_x - I_y) + (qr - \dot{p}) I_{xz}$$

$$m = C_{m_\alpha} \alpha\, q S \bar{c} \qquad\qquad n = C_{n_\beta} \beta\, q S \bar{c}$$

Consider that for neutral divergence stability $p = r = \alpha = \beta = 0$.
Show that the critical roll rate for pitch and yaw divergence is

$$p_y{}^2 = \frac{C_{m_\alpha}\, q S \bar{c}}{I_x - I_z}$$

$$p_z{}^2 = \frac{C_{n_\beta}\, q S \bar{c}}{I_y - I_x}$$

9.16

9.1. $M = mx^2p^2 \sin 2\alpha$

CHAPTER 10

HIGH ANGLE OF ATTACK

10.1 GENERAL INTRODUCTION TO HIGH ANGLE-OF-ATTACK FLIGHT

From the designer to the pilot, everyone associated with the flying qualities of high performance military aircraft, particularly of the fighter or attack variety, is or should be aware of the importance of the high angle of attack flight regime. It is here that the aircraft will spend a significant amount of its time when performing the mission for which it was designed. It is here that the aircraft must display its most outstanding performance. It is also here that the aircraft, when pushed beyond its limits of controllability, can seemingly defy all laws of physics and principles of flight with which its surprised and often bewildered pilot is acquainted. The frequency of inadvertent loss of control at high angle of attack is such that many combat aircraft pilots are becoming firmly convinced that all pilots may be divided into two categories: those who have departed controlled flight, and those who will. Most thoroughly convinced are those pilots who fall into the former category.

The unfortunate fact concerning departure from controlled flight at high angle of attack is that many aircraft and pilots are lost each year due to failure to recover from the out-of-control flight condition. The circumstances surrounding the losses are varied. Departures from controlled flight may occur unintentionally during high-g maneuvers or intentionally during a nose-high deceleration to zero airspeed in an attempt to gain an advantage over an opponent in combat maneuvering; the aircraft may spin and the gyration be identified too late for recovery or a steep spiral may be mistakenly identified as a spin, causing recovery controls to be misapplied. Whatever the circumstances, departures from controlled flight result all too often in catastrophe (10.1:1). For this reason, test pilots in particular must be familiar with every facet of the high angle-of-attack flight regime.

10.2 INTRODUCTION TO STALLS

Stall speed is the minimum steady speed attainable, or usable, in flight. A sudden loss of lift occurring at a speed just below that for maximum lift is considered the "conventional" stall, although it has become increasingly common for the minimum speed to be defined by some other characteristic, such as a high sink rate, an undesirable attitude, loss of control about any axis, or a deterioration of handling qualities.

For rather obvious safety and operational reasons, determination of stall characteristics is a first-order-of-business item in flight testing a new aircraft. Stall speeds are also required early in the test program for the determination of various test speeds.

10.2.1 Separation

Separation, a condition wherein the streamlines fail to follow the body contours, produces a large disturbed wake behind the body and results in a pressure distribution greatly different from that of attached flow. On an aircraft, these changes in turn may produce:

a. A loss of lift (Figure 10.1)

b. An increase in drag

c. Control problems due to:

1. Control surfaces operating in the disturbed wake

2. Changes in the aerodynamic pitching moment due to a shift in the center of pressure and an altered downwash angle

d. A degradation of engine performance

Separation occurs at a point where the boundary layer kinetic energy has been reduced to zero, therefore the position and amount of separation is a function of the transport of energy into and out of the boundary layer and dissipation of energy within the boundary layer.
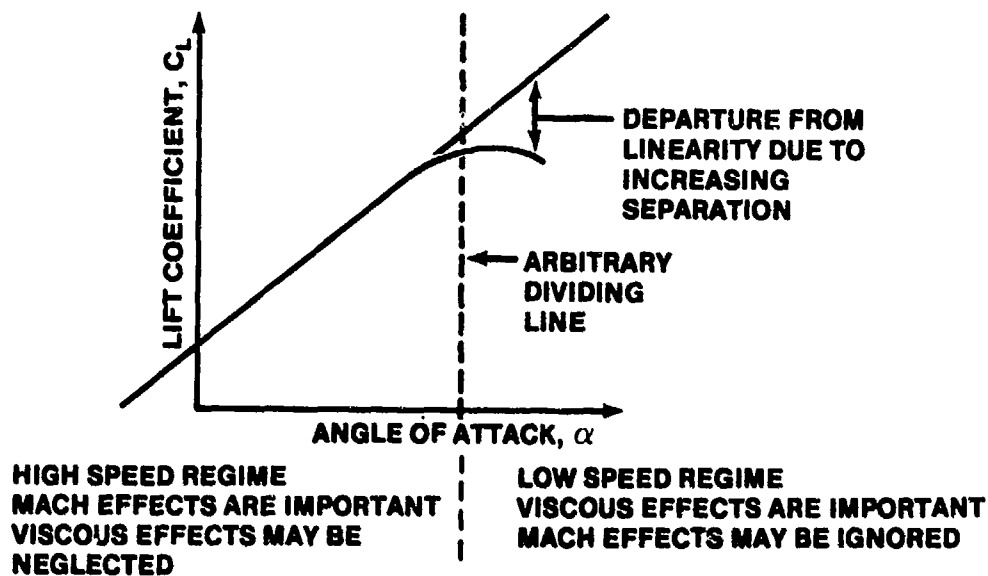
Figure labels (reading from the plot):

- LIFT COEFFICIENT, C_L (vertical axis)
- ANGLE OF ATTACK, α (horizontal axis)
- DEPARTURE FROM LINEARITY DUE TO INCREASING SEPARATION
- ARBITRARY DIVIDING LINE

HIGH SPEED REGIME
MACH EFFECTS ARE IMPORTANT
VISCOUS EFFECTS MAY BE
NEGLECTED

LOW SPEED REGIME
VISCOUS EFFECTS ARE IMPORTANT
MACH EFFECTS MAY BE IGNORED

FIGURE 10.1.   SEPARATION

Some factors which contribute to energy transport are:

a.   Turbulent (non-laminar) flow: Higher energy air from upper stream
     tubes is mixed into lower stream tubes.   This type flow,
     characterized by a full velocity profile, occurs at high values of
     Reynolds number (R_e) and involves microscopic turbulence.

b.   Vortex generators: These devices produce macroscopic turbulence to
     circulate high energy air down to lower levels.

c.   Slats and slots: These devices inject high energy air from the
     underside of the leading edge into the upper surface boundary layer.

d.   Boundary Layer Control: The blowing type of Boundary Layer Control
     (BLC) injects high energy air into the boundary layer while the
     suction type removes low energy air.

Two examples of energy dissipation functions are:

a.   Viscous friction: Energy loss varies with surface roughness and
     distance traveled.

b.   Adverse pressure gradient: Boundary layer energy is dissipated as
     the air moves against the adverse pressure gradient above a cambered
     airfoil section.   The rate of energy loss is a function of:

10.3

1. **Body contours** - Camber, thickness distribution, and sharp leading edges are examples.

2. **Angle of attack** - Increased angle of attack steepens the adverse pressure gradient.

Some typical coefficient of lift versus angle of attack (C_L versus α) curves illustrating these effects are shown in Figure 10.2.
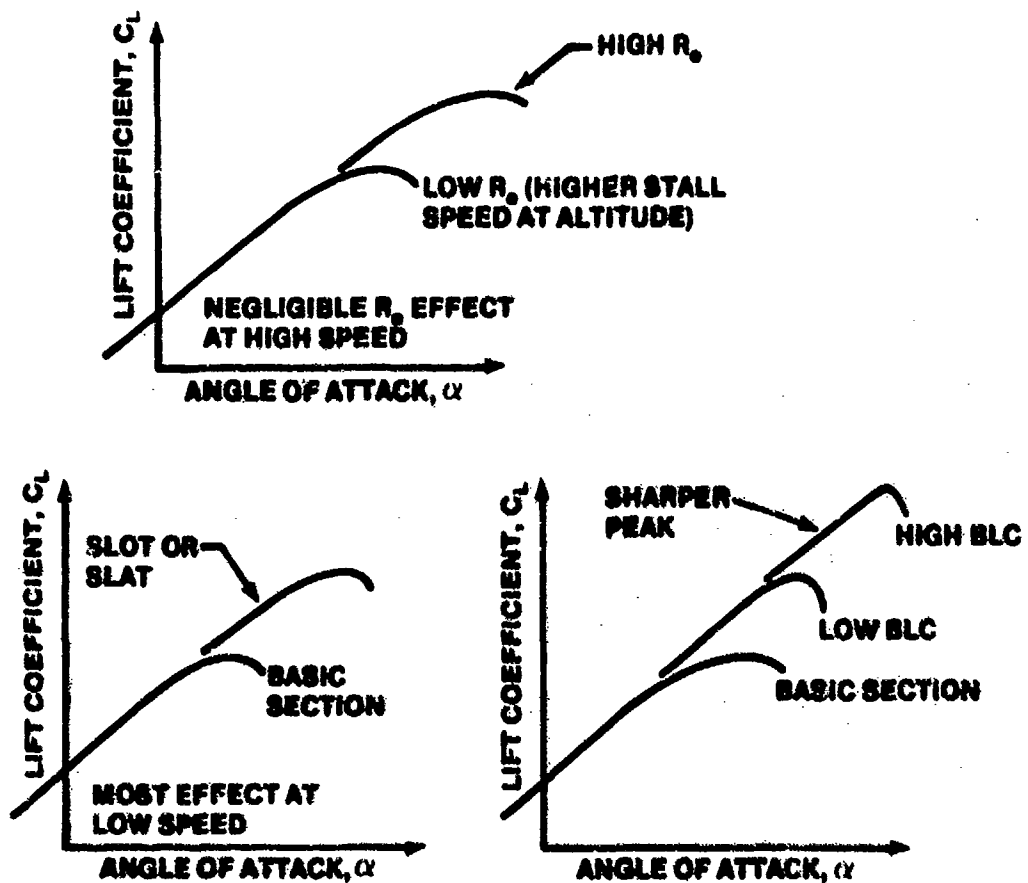

FIGURE 10.2. SEPARATION EFFECTORS

10.2.2 Three-Dimensional Effects

A three-dimensional wing exhibits aerodynamic properties considerably different from those of the two-dimensional airfoil sections of which it is formed. These differences are related to the planform and the aspect ratio of the wing.

10.2.3 Planforms

Downwash, a natural consequence of lift production by a real wing of less than infinite span, reduces the angle of attack at which the individual wing sections are operating (Figure 10.3).

THE EFFECTIVE ANGLE OF ATTACK
OF THE AIRFOIL SECTION IS REDUCED
BY DOWNWASH

α = ANGLE OF ATTACK
α_0 = SECTION ANGLE OF ATTACK
α_i = INDUCED ANGLE OF ATTACK
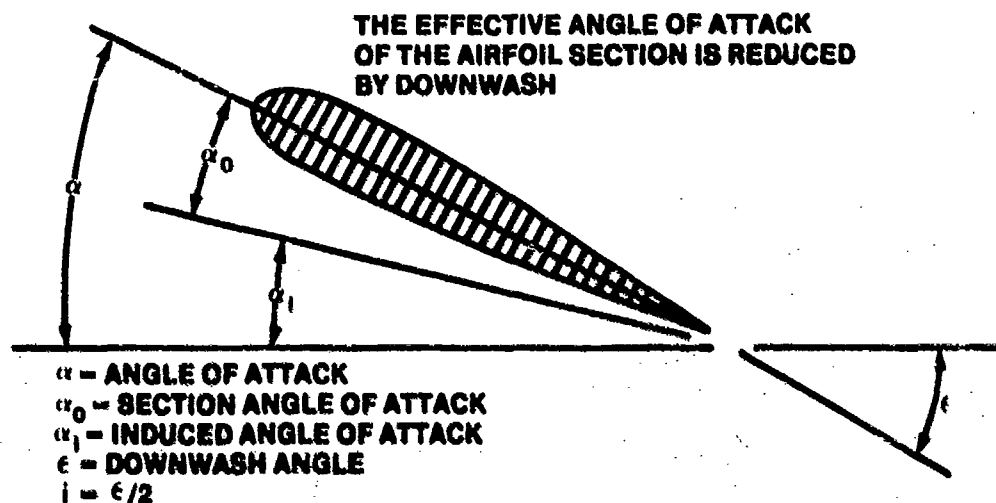ϵ = DOWNWASH ANGLE
$i = \epsilon/2$

FIGURE 10.3. DOWNWASH EFFECT ON ANGLE OF ATTACK

An elliptical wing has a constant value of downwash angle along its entire span. Other planforms, however, have downwash angles that vary with position along the span. As a result, the lift coefficient for a particular wing section may be more or less than that of nearby sections, or that of the overall wing. Airfoil sections in areas of light downwash will be operating at high angles of attack, and will reach stall first. Stall patterns therefore depend on the downwash distribution, and vary predictably with planform as shown in Figure 10.4.

Sweptback and delta planforms suffer from an inherent spanwise flow (Figure 10.5). This is caused by the outboard sections being located to the rear, placing low pressure areas adjacent to relatively high pressure areas.
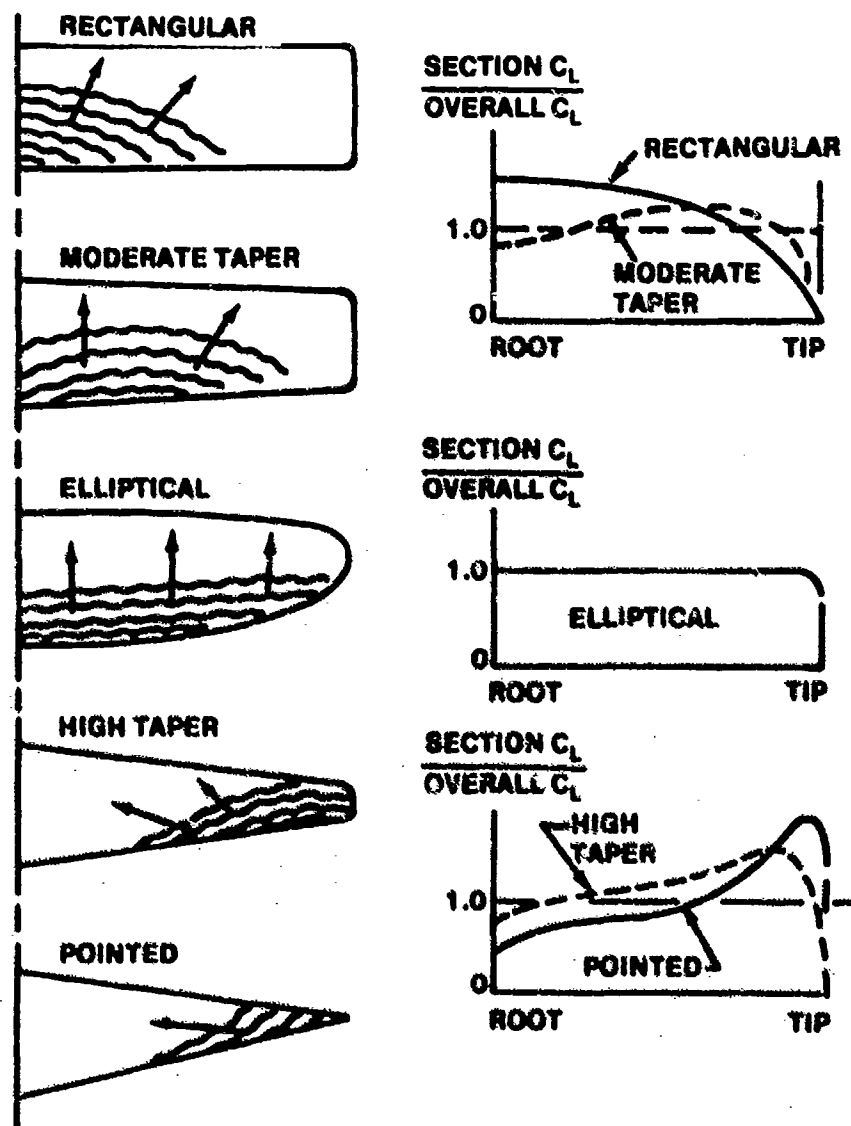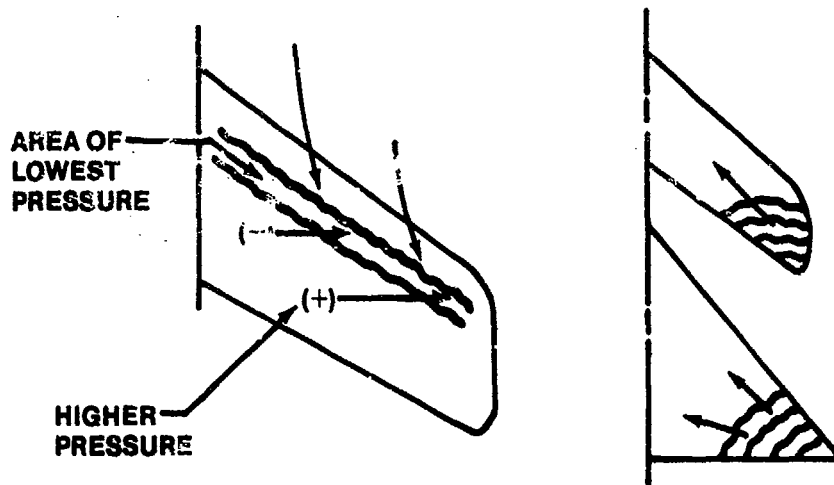

FIGURE 10.4.   STALL PATTERNS

FIGURE 10.5. SPANWISE FLOW

This spanwise flow transports low energy air from the wake of the forward sections outboard toward the tips, inviting early separation. Both the sweptback and delta planforms display tip-first stall patterns.

Pointed or low chord wing tips are unable to hold the tip vortex, which moves further inboard with increasing angle of attack, as shown in Figure 10.6.
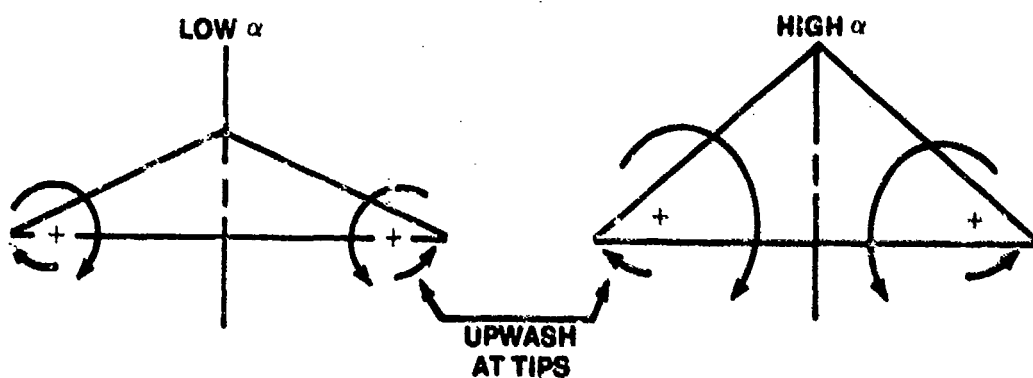

FIGURE 10.6. TIP VORTEX EFFECTS

The extreme tips operate in upwash and in the absence of aerodynamic fixes such as twist or droop, are completely stalled at most angles of attack.

10.2.4 Aspect Ratio

Aspect ratio may be considered an inverse measure of how much of the wing is operating near the tips. Wings of low aspect ratio (much of the wing near the tip) require higher angles of attack to produce a given lift.

The curves shown in Figure 10.7 illustrate several generalities important to stall characteristics. High aspect ratio wings have relatively steep lift curve slopes with well defined peaks at $C_{L_{max}}$. These wings have a relatively low angle of attack (and hence pitch angle) at the stall, and are usually characterized by a rather sudden stall break.

Low aspect ratio wings display the reverse characteristics: high angle of attack (high pitch angles) at slow speeds and poorly defined stalls. They can frequently be flown in a high sink rate condition to the right of $C_{L_{max}}$ where drag increases rapidly.
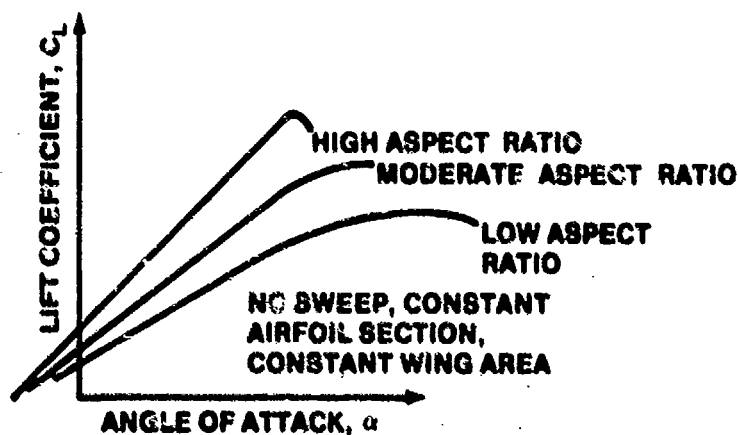

FIGURE 10.7. ASPECT RATIO EFFECTS

10.2.5 Aerodynamic Pitching Moment

On almost all planforms the center of pressure moves forward as the stall pattern develops, producing a noseup pitching moment about the aircraft center of gravity (cg).

This moment is not great on most straight wing planforms and the characteristic root stall of these wings adds a compensating nosedown moment such that a natural pitchdown tendency exists at high angles of attack. This occurs because the stalled center section produces much less downwash in the vicinity of the horizontal tail, decreasing its download. If the tail actually enters the turbulent wake, the nosedown moment may be further intensified due to a decrease in elevator effectiveness. This latter case usually provides a natural stall warning in the form of an airframe and control buffet.

On swept-wing and delta planforms the moment produced by the center of pressure (cp) shift is usually more pronounced and the moment contributed by the change in downwash at the tail is noseup. This occurs because the wing root section remains unstalled, producing greater lift and greater downwash as the angle of attack increases. The inboard movement of the tip vortex system also increases the downwash behind the center of the wing. Horizontal tails, even in the vicinity of this increased downwash, will produce more download. If the tail is mounted such that it actually enters the downwash area at high angles of attack, such as on the F-101, an uncontrollable pitchup may occur.

Many fixes and gimmicks have been used to alter lift distribution and stall patterns. Tip leading edge extensions, tip slots and slats, tip washout and droop, fences and root spoilers are but a few. Horizontal tail position is also subject to much adjustment such as has been necessary on the F-4C.

10.2.6 Load Factor Considerations

The relationship between load factor (n) and velocity may be seen on a V-n diagram, as shown in Figure 10.8. Every point along the lift boundary curve, the position of which is a function of gross weight, altitude, and aircraft configuration, represents a condition of $C_{L_{max}}$ (neglecting cases of insufficient elevator power). It is important to note that for each configuration, $C_{L_{max}}$ occurs at a particular α_{max}, independent of load factor, i.e., an aircraft stalls at the same angle of attack and C_L in accelerated flight, with n = 2.0, as it does in unaccelerated flight, with n = 1.0. The total lift (L) at stall for a given gross weight (W) varies with load factor since

10.9

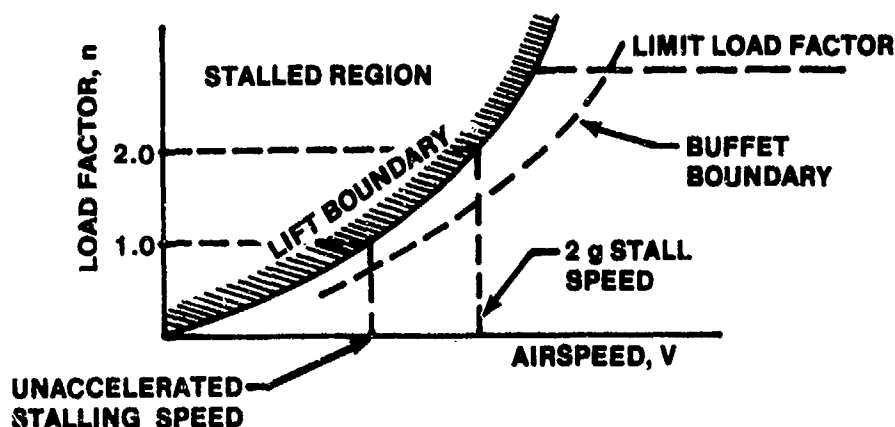$L = nW$. The increased lift at the accelerated stall must be obtained by a higher dynamic pressure (q).

FIGURE 10.8. LOAD FACTOR EFFECTS

$$q_{stall} = 1/2\rho \; V_{stall}^2 = \frac{nW}{C_{L_{max}} S} \qquad (10.1)$$

$$V_{stall} = \sqrt{\frac{2nW}{\rho C_{L_{max}} S}} \qquad (10.2)$$

or

$$V_{s_e} = \sqrt{\frac{2nW}{\rho_0 C_{L_{max}} S}}$$

Thus stall speed is proportional to n, making accurate control of normal acceleration of primary importance during stall tests.

10.10

10.3 INTRODUCTION TO SPINS (10.2: 1-1,1-2)

The early glider flights of the Wright brothers often ended by dropping off on one wing, out of control, with a wingtip eventually striking the Kitty Hawk, North Carolina, sand in a rotary motion. While the low altitude of these flights prevented motion from developing fully, it seems clear that these were departures into incipient spins.

In those early days of manned flight the spin was as dangerous as it is today. When the Wright brothers first tried warping the wings to roll into a turn, they found that the banking was accompanied by a dangerous tendency to diverge in yaw at high angle of attack. Adding a fixed vertical fin helped stabilize the 1902 glider, but the loss-of-control problem persisted. Orville Wright reasoned that a hinged vertical rudder could produce a counter yawing moment to keep the yaw from starting and thus enable the flyer to remain under control. This was tried first with rudder deflection connected to the wing-warp control, then with the pilot controlling the rudder separately. The fix was effective but required the pilot's constant attention. Proper spin recovery controls were not generally known until 1916, when flight test experiments on spin recovery procedures were conducted at the Royal Aircraft Factory, Farnborough, in an FE-8. Wing Commander Macmillan is responsible for a fascinating early history of the spin in Aeronautics, 1960-62 issues.

For early airplanes the spin recovery technique was at least rational if not instinctive: forward stick and rudder opposing the yawing motion should stop the rotation and unstall the wing. Once these recovery controls were known, World War I pilots used the spin as a maneuver to lose altitude without gaining airspeed. Then in the 1920's some of the more peculiar spin modes were recognized as problems. Accident summaries from that era show spins were involved in about three percent of all accidents reported and in twenty to thirty percent of the fatal accidents.

Analytical studies and dynamic wind tunnel testing to reduce the stall/spin problem were reported in England as early as 1917. Autorotation was observed in the wind tunnels, and the first analytical prediction methods were developed by Glauert and Lindemann. Gates and Bryant presented a comprehensive survey of spinning in 1927. About 1930, a method of determining the flight path and attitude of a spinning aircraft was put into use.

Rotation rates about and accelerations along the principal axes, as well as vertical velocity were measured and recorded photographically. This information was used to define the motion of the aircraft and could then be used in conjunction with the analytical prediction methods.

In the 1920's and 1930's, several forms of testing were being performed. One safety measure used in full-scale testing was to attach external ballast, that when released would cause the center of gravity of the airplane to move forward, thus returning the airplane to a controllable configuration. Because of the hazards involved in stall/spin flight testing, researchers hesitant to use full-scale aircraft tried free-flight models. One of the early spin models was dropped from the top of a 100-foot balloon hangar at Langley Field. This proved an inadequate means of obtaining data, and soon vertical wind tunnels were being built to investigate spinning (1930 in the United States, 1931 in England). In 1945, the U.S. Army Air Force dropped an instrumented model from a Navy blimp to study spin entry and recovery.

As jet aircraft were developed, the inertial characteristics of fighters in particular were changed to the point that spins and other post-stall motions became more troublesome and even required different recovery techniques. Most stall/spin problems were identified by the Wright Air Development Center Spin Symposium; some analysis methods had been developed, and the electronic digital computer provided a useful tool with which to examine the stall/spin problem.

Then suddenly the emphasis was shifted to space. With little management interest and rather poor expectations of improvement, resources for stall/spin research were quite limited. Our Air Force tended to concentrate on performance improvements, which have often aggravated stability and control problems at high angles of attack. Today, a large and costly Air Force accident record and a renewed emphasis on maneuver capability have led to a concerted effort to solve the problems associated with aircraft operating in the stall/spin flight regime.

Large aircraft have also experienced stall/spin problems. For example, several B-58s were lost in spins. Automatic trimming of the control-stick force was mechanized in such an insidious way that an inattentive pilot might not be aware of a slowdown to stall speed. Trouble with fuel management could result in an extreme aft center of gravity, at which B-58 stability and

control were deteriorated. The C-133, on long flights, would climb to an altitude approaching its absolute ceiling. Poor stall warning and a vicious stall while trying to fly there are thought to have caused the disappearance of several C-133 aircraft. It has become customary to require analysis and spin tunnel testing of all U.S. military airplanes even though flight demonstration of large, low-maneuverability types is limited to stalls with only moderate control abuse.

The military specification for flying qualities defines good high angle of attack characteristics in terms that are qualitative rather than quantitative. The airplane must exhibit adequate stall warning, and in addition the stall must be easily recoverable. We now emphasize resistance to violent departures from controlled flight, while retaining requirements for recovery from attainable post-stall motions. The definitions of good high angle of attack characteristics will differ for the various classes of aircraft; but with respect to fighter aircraft, a pilot should not have to worry about loss of control while flying within his useful maneuver envelope. We shall need quantitative requirements that will be of more use in the design stage for all classes of airplanes.

Generally post-stall design and testing have emphasized spins and spin recovery, taking the point of view that assurance of recoverability from the worst possible out-of-control situation guarantees safety. This philosophy falls short in several respects. Resistance to departure has not been emphasized adequately. The motions can be disorienting, and recovery control inputs such as ailerons with the spin are unnatural. And as airplanes grow larger and heavier, altitude loss becomes excessive. F-111 instructions, for example, are to eject if spin recovery has not commenced upon reaching 15,000 feet altitude. Spins and spin recovery should not be neglected, but emphasis needs to shift to departure resistance and early recovery.

10.3.1 Definitions

10.3.1.1 Stall Versus Out-Of-Control. Stalls and associated aerodynamic phenomena have been previously described, but it is worth repeating the formal definition of a stall from page 76 of MIL-F-8785C (Reference 10.3). In terms of angle of attack, the stall is defined as the lowest of the following:

a. Angle of attack for the highest steady load factor normal to the flightpath that can be attained at a given speed or Mach.

b. Angle of attack, for a given speed or Mach, at which abrupt uncontrollable pitching, rolling, or yawing occurs. Angular limits of 20° (Classes I, II, or III) or 30° (Class IV) are specified in Paragraph 3.4.2.1.2 of Reference 10.3.

c. Angle of attack for a given speed or Mach, at which intolerable buffeting is encountered.

d. An arbitrary angle of attack allowed by Paragraph 3.1.9.2.1 of Reference 10.3, which may be based on such considerations as ability to perform attitude corrections, excessive sinking speed, or ability to execute a go-around.

Reference defines the stall angle of attack more simply: the angle of attack for maximum usable lift at a given flight condition. This latter definition is the one most useful in this course, but the student must understand that "maximum usable lift" is determined from one of the four conditions given above.

10.3.1.2 Departure. Departure is defined as that event in the post-stall flight regime that precipitates entry into a PSG, spin, or deep stall condition (MIL-F-83691A, Reference 10.4, Paragraph 6.3.9). Notice two things about this definition. First, departure occurs in the post-stall flight regime; that is, the stall always precedes departure. It can be inferred then that the angle of attack for maximum usable lift is always less than the angle of attack at which departure occurs. The second point is that only one of three motions may result after departure - the aircraft enters either a PSG, spin, or deep stall (of course, a PSG can progress into a spin or deep stall). Implicit in this definition is the implication that an immediate recovery cannot be attained. For example, a light aircraft whose stall is defined by a g-break, may recover immediately if the longitudinal control pressure is relaxed. However, note that movement or position of controls is not mentioned in the definition. The same light aircraft that would not depart if control pressures were relaxed at the stall may depart and enter a spin if pro-spin controls are applied at the stall. Hence, in discussing susceptibility or resistance to departure one must specify control positions as well as loading and configuration.

The departure event is usually a large amplitude, uncommanded, and divergent motion. Such descriptive terms as nose slice or pitch-up are commonly used to describe the event. Large amplitude excursions imply changes in yaw, roll, or pitch greater than 20° (Class I, II, and III) or 30° (Class IV) (Reference 10.3, Paragraph 3.4.2.1.2). Uncommanded motions are motions not intended by the pilot, even though the control positions are legitimately causing the departure. The aircraft may not follow the pilot's commands for a number of reasons: the high angle of attack may render the control surface ineffective when moved to its desired position; or the pilot may be unable to position the stick to put the surface in the desired position due to lateral or transverse g loads. In either of these conditions the aircraft motion is "uncommanded." Finally, a divergent motion is one which either continuously or periodically increases in amplitude. The T-33 usually exhibits a "bucking" motion after the stall in which the nose periodically rises and falls. However, the motion is not divergent unless aggravated by full aft stick or some other pro-spin control. The T-38 will sometimes exhibit a non-divergent lateral oscillation near the stall angle of attack. Neither of these motions are normally counted as departures, though their occurrance does serve as warning of impending departure if further misapplications of controls are made. With this sort of background it is easy to see why a departure is so hard to define, yet is relatively easy for a pilot to recognize. Next, one must examine the terms "post-stall gyration," "spin" and "deep stalls," used to define a departure.

10.3.1.3 Post-Stall Gyration. A post-stall gyration is an uncontrolled motion about one or more axes following departure (Reference 10.4, Paragraph 6.3.10). PSG is a very difficult term to define concisely because it can occur in so many different ways. Frequently, the motions are completely random about all axes and no more descriptive term than PSG can be applied. On the other hand, a snap roll or a tumble are post-stall gyrations. The main difficulty lies in distinguishing between a PSG and either the incipient phase of a spin or an oscillatory spin. The chief distinguishing characteristic is that a PSG may involve angles of attack that are intermittently below the airplane's stall angle of attack, whereas a spin always occurs at angles of attack greater than stall.

10.3.1.4 Spin. A spin is a sustained yaw rotation at angles of attack above the aircraft's stall angle of attack (Reference 10.4, Paragraph 6.3.11). This definition bears a bit of explanation in that a spin is certainly not altogether a yaw rotation. Only the perfect flat spin ($\alpha = 90^\circ$) could satisfy that constraint. The inference is, however, that the yaw rotation is dominant in characterizing a spin. Indeed, to a pilot, the recognition of a sustained (though not necessarily steady) yaw rate is probably the most important visual cue that a spin is occurring. Even though roll rate and yaw rate are often of nearly the same magnitude, the pilot still ordinarily recognizes the spin because of the yaw rate. In steep spins (with α relatively close to α_s), it is quite easy to confuse the roll rate and yaw rate and pilots sometimes have difficulty in recognizing this type of motion and treating it as a spin. The steep inverted spin is particularly confusing since the roll and yaw rates are in opposite directions. Once again though, the yaw rate determines the direction of the spin and the required control manipulations to recover. All in all, it is well to remember that the spin is truly a complicated maneuver involving simultaneous roll, pitch, and yaw rates and high angles of attack. Even though the overall rotary motion in a spin will probably have oscillations in pitch, roll, and yaw superimposed upon it, it is still most easily recognized by its sustained yawing component.

10.3.1.5 Deep Stall. A deep stall is an out-of-control flight condition in which the airplane is sustained at an angle of attack well beyond that for α_s while experiencing negligible rotational velocities (Reference 10.4, Paragraph 6.3.12). It may be distinguished from a PSG by the lack of significant motions other than a high rate of descent. The deep stall may be a fairly stable maneuver such as a falling leaf, or it can be characterized by large amplitude angle of attack oscillations. For an aircraft to stay in a deep stalled condition, significant oscillations must be limited to the longitudinal axis. Lateral and directional control surfaces are either stalled or blanked out. Depending on the pitching moment coefficient, recovery may or may not be possible.

10.3.2 Susceptibility And Resistance To Departures And Spins

Susceptibility/resistance to departures and spins has become an extremely important design goal for high performance aircraft. Reference 10.5 offers

convincing proof that such design emphasis is overdue. But, for the designer to meet this requirement in an aircraft and for the test pilot to test against this requirement, it is essential that the words "susceptible" and "resistant" be understood alike by all concerned.

Susceptibility to departures and spins is normally determined with reference to the type of maneuver flown (test phase). If any aircraft departs or spins during a particular phase (as identified in Table 10.1), then it is given a departure/spin susceptibility assessment according to Table 10.2.

TABLE 10.1
TEST PHASES

Phase	Control Application
A – Stalls	Pitch Control applied to achieve the specified AOA rate, lateral-directional controls neutral or small lateral-directional control inputs as normally required for the maneuver task.
	Recovery initiated after the pilot has positive indications of: (a) a definite g-break or (b) a rapid angular divergence, or (c) the aft stick stop has been reached and AOA is not increasing.
B – Stalls with aggravated control inputs	Pitch control applied to achieve the specified AOA rate, lateral-directional controls as required for the maneuver task. When condition (a), (b), or (c) has been attained, controls briefly misapplied, intentionally or in response to unscheduled aircraft motions, before recovery attempt is initiated.
C – Stalls with aggravated and sustained control inputs	Pitch control applied to achieve the specified AOA rate, lateral-directional controls as required for the maneuver task. When condition (a), (b), or (c) has been attained, controls are misapplied, intentionally or in response to unscheduled aircraft motions, and held for three seconds before recovery attempt is initiated.
D – Post-stall gyration, spin, and deep stall attempts (this phase required only for training aircraft which may be intentionally spun and for Class I and IV aircraft in which sufficient departures or spins did not result in Test Phase A, B, or C to define characteristics.)	Pitch control applied abruptly, lateral-directional controls as required for the maneuver task, when condition (a), (b), or (c) has been attained, controls applied in the most critical positions to attain the expected spin modes of the aircraft and held up to 15 seconds before recovery attempt is initiated, unless the pilot definitely recognizes a spin mode.

TABLE 10.2
SUSCEPTIBILITY/RESISTANCE CLASSIFICATION

TEST PHASE	CLASSIFICATION	
	Departures	Spins
A - Stalls	extremely susceptible	extremely susceptible
B - Stalls with aggravated control inputs	susceptible	susceptible
C - Stalls with aggravated and sustained control inputs	resistant	resistant
D - Post-stall gyration, spin, and deep stall attempts	extremely resistant	extremely resistant

10.3.2.1 **Extremely Susceptible To Departure (Spins) (Phase A)**. An aircraft is said to be extremely susceptible to departure (spins) if the uncontrolled motion occurs with the normal application of pitch control alone or with small roll and yaw control inputs. The only allowable roll and yaw control inputs are those normally associated with a given maneuver task. In short, an airplane that departs or enters a spin during Phase A of the flight test demonstration falls within this category (Reference 10.4, Paragraph 3.4.1.8).

10.3.2.2 **Susceptible To Departure (Spins) (Phase B)**. An aircraft is said to be susceptible to departure (spins) when the application or brief misapplication of pitch and roll and yaw controls that may be anticipated in normal operational use cause departure (spin). The amount of misapplied controls to be used will be approved by the procuring activity for Phase B of the flight test demonstration. In other words, each aircraft will be stalled and aggravated control inputs will be briefly applied to determine departure (spin) susceptibility.

10.3.2.3 **Resistant To Departure (Spins) (Phase C)**. An aircraft is said to be departure (spin) resistant if only large and reasonably sustained misapplication of controls results in a departure (spin). "Reasonably sustained" means up to three seconds before recovery is initiated (Reference 10.4, Table 1). This time delay may be increased for aircraft without positive indication of impending loss of control. This aircraft departs (spins) during Phase C of the flight test demonstration.

10.19

10.3.2.4 **Extremely Resistant To Departure (Spins) (Phase D)**. An aircraft is said to be extremely resistant to departure (spins) if these motions occur only after abrupt, inordinately sustained application of gross, abnormal, pro-departure controls. Aircraft in this category will only depart (spin) in Phase D of the flight test demonstration when the controls are applied and held in the most critical manner to attain each possible mode of post-stall motion and held for various lengths of time up to 15 seconds or three spin turns, whichever is longer.

10.3.3 **The Mechanism Of Departure (10.6)**

As an aircraft approaches stall conditions the aerodynamic changes produced by flow breakdown over the wing and tail result in degraded stability and control effectiveness. It is the extent of this degradation that determines whether the aircraft is departure-prone or departure-resistant. Use of controls to prevent departure may not be effective because both aileron and rudder effectiveness are greatly reduced in the stall and, in addition, adverse yaw characteristics may prohibit the use of ailerons.

If the aircraft becomes directionally unstable but still retains a stable dihedral effect of sufficient magnitude, its departure will not be divergent. When both directional stability and dihedral effect become unstable, then any disturbance such as a gust or control input can result in a departure. The departure may be self-terminating or it may result in subsequent spin entry. Once a departure has occurred, an important question arises: is there any restoring tendency which will impede further uncontrolled excursions and if so, how is it manifested?

If the aircraft has a pitch down at the stall, or if the longitudinal control retains full effectiveness, the departure may be terminated through reduction in angle of attack. There may even be a restoring tendency at large sideslip angles where the vertical tail emerges from the wing-body interference field to restore both directional stability and dihedral effect enough to attenuate the departure tendency.

When increasing angles of attack and sideslip both result in further degradations in directional stability and dihedral effect and longitudinal control is not effective (or is not applied), departure and subsequent spin entry are highly probable.

The stability derivatives C_{n_β} and C_{ℓ_β} play an important role in high performance aircraft operating at high AOA's. As AOA is increased, C_{n_β} decreases to the point where it becomes negative; at this point, sideslip angles could start to diverge due to lack of directional stability. A stable dihedral effect (C_{ℓ_β}) will normally tend to decrease sideslip angle by rolling into the direction of yaw. This roll-off tendency prevents a pure yaw divergence thereby providing a natural aerodynamic recovery from a departure.

Since aircraft react to combinations of C_{n_β}, C_{ℓ_β} and kinematic as well as inertial coupling, a parameter which includes all of these effects is useful in predicting departure susceptibility. This parameter is called the Directional Departure Parameter (C_{n_β} Dynamic).

10.3.3.1 <u>Directional Departure Parameter</u>. The directional departure parameter represents an aircraft's directional stability with respect to its flight path rather than its body axes. Consider an aircraft body and stability axes as shown in Figure 10.9.
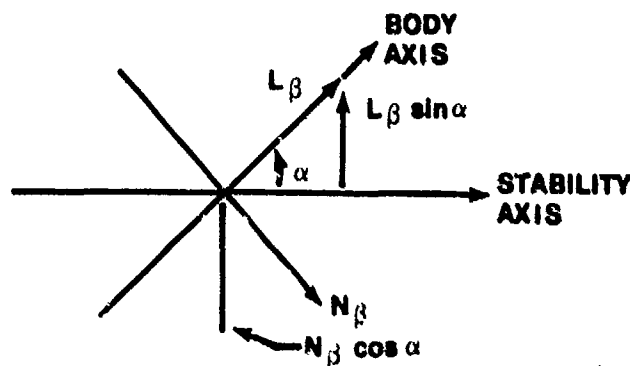

FIGURE 10.9.   STABILITY AXIS RESOLUTION

Resolving the body axes rolling and yawing moments (in terms of dimensional stability derivatives) into the stability axes, we get

$$N_{\beta_s} = N_\beta \cos \alpha - L_\beta \sin \alpha \qquad (10.3)$$

Recalling that the normalizing factors for each dimensional derivative are

$$N_\beta = \frac{1}{I_z} C_{n_\beta} \qquad\qquad L_\beta = \frac{1}{I_x} C_{\ell_\beta}$$

and substituting these relationships into Equation 10.3

$$\frac{1}{I_z} C_{n_{\beta_s}} = \frac{1}{I_z} C_{n_\beta} \cos \alpha - \frac{1}{I_x} C_{\ell_\beta} \sin \alpha$$

multiplying by I_z we get

$$\boxed{C_{n_{\beta DYN}} = C_{n_\beta} \cos \alpha - \frac{Iz}{Ix} C_{\ell_\beta} \sin \alpha}$$

(10.4)

where

$C_{n_{\beta DYN}}$ = Directional Departure Parameter - stability axes

C_{n_β} = Directional stability derivative - body axes

C_{ℓ_β} = Dihedral effect derivative - body axes

Normally a departure can be anticipated when $C_{n_{\beta DYN}}$ is negative. Notice that even if C_{n_β} goes negative, $C_{n_{\beta DYN}}$ may remain positive if the inertia ratio I_z/I_x is high and if C_{ℓ_β} is negative (stable). Most modern fighter aircraft have a high inertia ratio which is beneficial as long as C_{ℓ_β} remains negative. However, once C_{ℓ_β} becomes positive, the high inertia ratio will have an adverse effect on $C_{n_{\beta DYN}}$ and departure susceptibility. In general, a high negative (stable) C_{ℓ_β} is desired for fighter type aircraft. For a given value of $C_{n_{\beta DYN}}$, if C_{ℓ_β} is negative and small in magnitude, a yaw divergence can be expected; conversely if C_{ℓ_β} is negative and large in magnitude, a roll divergence can be expected. A comparison of C_{n_β} and $C_{n_{\beta DYN}}$ for the A-7 and F-18 aircraft is shown in Figures 10.10 and 10.11, respectively.

10.22

10.3.3.2 Lateral Control Departure Parameter (LCDP). The lateral control departure parameter has been used in various forms for different uses. It is developed from the simplified rolling and yawing moment equations assuming the aircraft to be laterally and directionally trimmed. The lateral control departure parameter predicts at what angle of attack roll reversal is expected to occur when using ailerons. Reversal in this sense does not mean aeroelastic aileron reversal, but that condition where the rolling moment due to sideslip, resulting from adverse yaw, overpowers the rolling moment commanded by the ailerons. To the pilot this condition is known as reverse aileron command or roll reversal.

This parameter has been correlated with spin entry tendency due to aileron adverse yaw for several fighter aircraft. The expression for LCDP also contains sideslip derivatives and is

$$LCDP = C_{n_\beta} - \frac{C_{n_{\delta_a}}}{C_{\ell_{\delta_a}}} C_{\ell_\beta}$$
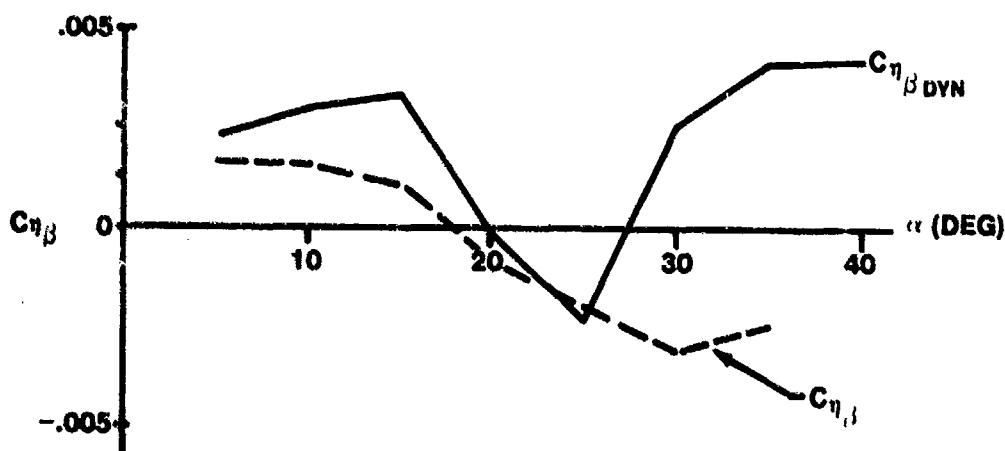
(10.5)
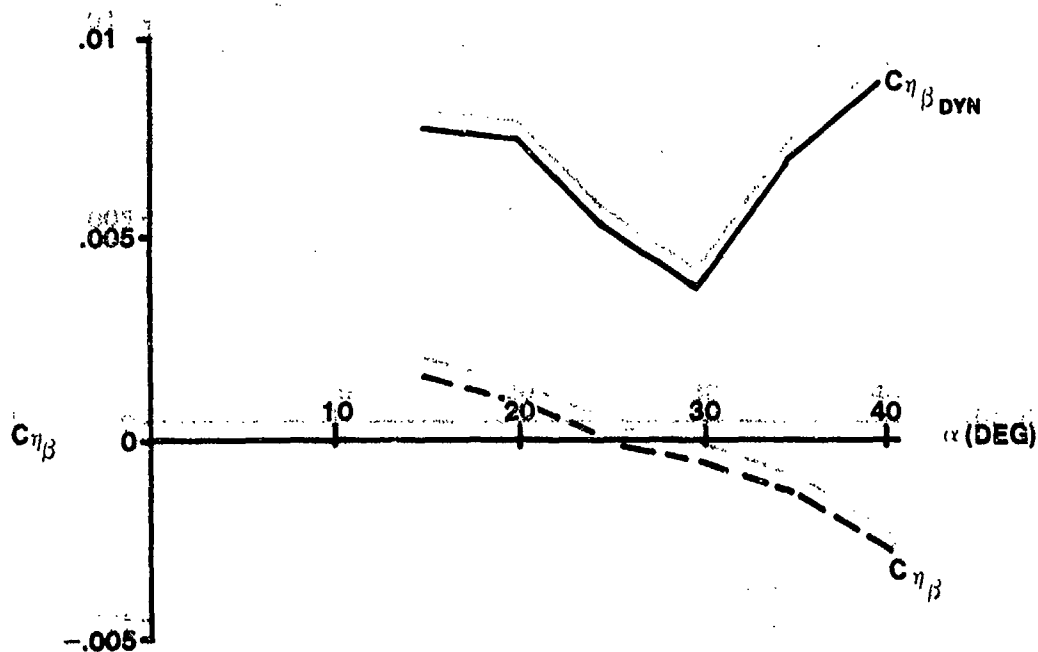

FIGURE 10.10. DIRECTIONAL STABILITY, A-7

FIGURE 10.11. DIRECTIONAL STABILITY, F-18

Aileron reversal occurs when LCDP becomes negative. Note the similarity of the role that dihedral effect plays in this expression relative to its role in $C_{n_{\beta DYN}}$. It again acts as a "multiplier" and the benefit or detriment in this case depends upon the sign of $C_{n_{\delta_a}}$. If the aircraft has adverse yaw due

to aileron $C_{n_{\delta_a}}$ is negative , then a stable dihedral effect $-C_{l_\beta}$ will have

an adverse effect. The opposite is true if the aircraft has proverse yaw. If the aircraft has an unstable dihedral effect, then the combined effects of LCDP and $C_{n_{\beta DYN}}$ will determine the type of departure following an aileron input.

10.3.4 Spin Modes

Adjective descriptors are used to describe general characteristics of a given spin and these adjectives specify the spin mode. Average values of angle of attack, for example, would allow categorization of the spin as either

10.24

upright (positive angle of attack) or inverted (negative angle of attack). An average value of angle of attack would also allow classification of a spin as either flat (high angle of attack) or steep (lower angle of attack). Finally, the average value of the rotational rate and the oscillations in angular rates about all three axes determines the rate and oscillatory character of the spin. One descriptive modifier from each of these groups may be used to specify the spin mode, see Table 10.3.

TABLE 10.3
SPIN MODE MODIFIERS

Sense	Attitude	Rate	Oscillations
Erect	Extremely steep	Slow	Smooth
Inverted	Steep	Fast	Mildly Oscillatory
	Flat	Extremely Rapid	Oscillatory
			Highly Oscillatory
			Violently Oscillatory

The most confusing thing about mode identificaction is the proper use of the attitude and oscillation modifiers. Perhaps the following tabulated data, Table 10.4, extracted from Reference 10.7, will provide insight into understanding how to use these terms.

Table 10.4 Note: One mode reported in Reference 10.7 has been omitted from this table because the terminology did not fully conform to that of Reference 10.4. It was called "highly oscillatory" with angle of attack excursions of 180°.

10.25

TABLE 10.4
F-4E SPIN MODES

Mode	Average AOA (deg)	AOA Oscillations (deg)	Yaw Rate (deg/sec)	Roll Rate (deg/sec)	Pitch Rate (deg/sec)
Steep-Smooth	42	± 5	40-50	50	15
Steep-Mildly Oscillatory	45-60	± 10	45-60	---	--
Steep-Oscillatory	50-60	± 20	50-60 (with large oscillations)	Same as yaw rate	--
Flat-Smooth	77-80	Negligible	80-90	25	7

10.3.5 Spin Phases

A typical spin may be divided into the phases shown in Figure 10.12.
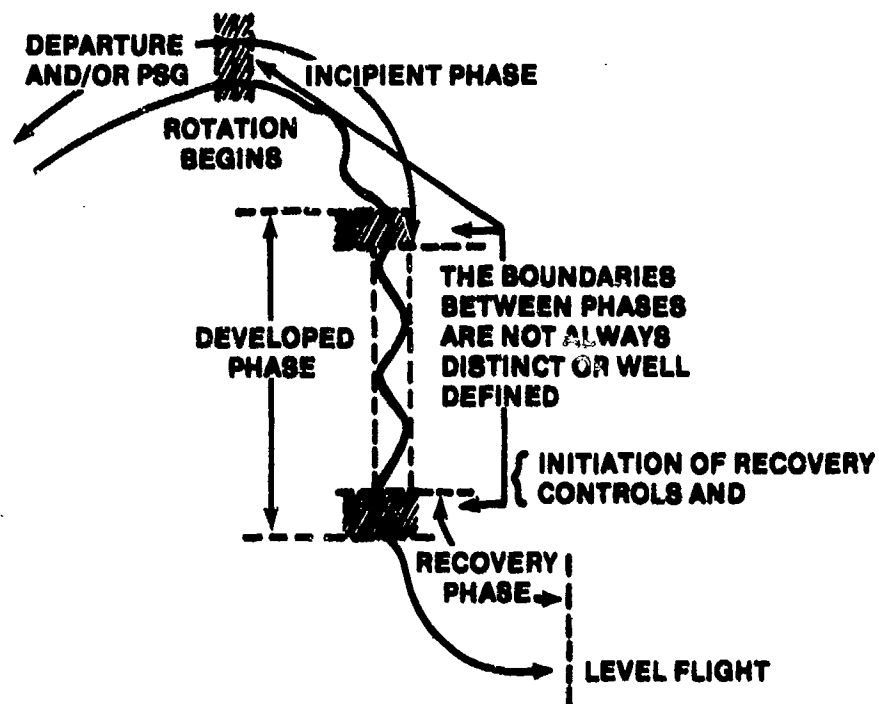
FIGURE 10.12. SPIN PHASES

10.26

10.3.5.1 <u>Incipient Phase</u>. The incipient phase of a spin is the initial, transitory part of the motion during which it is impossible to identify the spin mode. However, notice in Figure 10.12 that the yaw rotation begins as the incipient phase begins; that is, the visual cue to the pilot is of a sustained (though by no means steady) yaw rotation. A further distinction between the PSG (if one occurs) and the incipient phase of the spin is that the angle of attack is continuously above the stalled angle of attack (α_s) for the aircraft in the incipient phase of the spin. During a PSG the angle of attack may intermittently be less than α_s. This incipient phase continues until a recognizable spin mode develops, another boundary very difficult to establish precisely. In fact the test pilot may not recognize such a mode until he has seen it several times; but careful examination of data traces and film may reveal that a "recognizable" mode has occurred. In this case "recognizable" does not necessarily mean recognizable in flight, but distinguishable to the engineer from all available data. In short, the incipient phase of the spin is a transitory motion easily confused with a PSG, but distinctly different from either a PSG or the developed phase of the spin.

10.3.5.2 <u>Developed Phase</u>. The developed phase of a spin is that stage of the motion in which it is possible to identify the spin mode. During this phase it is common for oscillation to be present, but the mean motion is still abundantly clear. The aerodynamic forces and moments are not usually completely balanced by the corresponding linear and angular accelerations, but at least equilibrium conditions are being approached. Generally it is evident in the cockpit that the developed phase is in progress, though the exact point at which it began may be quite fuzzy. Since the aircraft motion is approaching an equilibrium state, it is frequently advisable to initiate recovery before equilibrium is achieved. For example, during the T-38 test program warning lights were installed to signal a buildup in yaw rate. Test pilots initiated recovery attempts when these lights came on. Still, in the flat spin mode with recovery initiated at 85° per second, a peak yaw rate of 165° per second was achieved. The longitudinal acceleration at the pilot's station was approximately 3.5 g and the spin was terminated by deployment of the spin chute (10.8: 10, 11). The developed spin, while it may be more comfortable due to less violent oscillations, can be deceptively dangerous, and the spin phase which follows can be disastrous.

10.3.5.3 Fully Developed Phase. A fully developed spin is one in which the trajectory has become vertical and no significant change in the spin characteristics is noted from turn to turn. Many aircraft never reach this phase during a spin, but when they do, they are often very difficult to recover. The smooth, flat spin of the F-4 is a classic example whereby this phase is attained and from which there is no known aerodynamic means of recovery. But a fully developed spin obviously requires time and altitude to be generated; how much time and how much altitude are strong functions of entry conditions. As a general rule, departures that occur at high airspeeds (high kinetic energy) require more time and altitude to reach the fully developed phase than departures which occur at low kinetic energy. Finally, the spin characteristics that remain essentially unchanged in the fully developed phase include such parameters as time per turn, body axis angular velocities, altitude loss per turn, and similar quantities. However, the definition does not prohibit a cyclic variation in any of these parameters. Hence a fully developed spin can be oscillatory.

With this rather lengthy set of definitions in mind, it is now appropriate to look more closely at spinning motions and at the aerodynamic and inertial factors which cause them and the PSG.

10.3.6 The Spinning Motion

Because the PSG is a random and usually a highly irregular motion, it is very difficult to study. On the other hand, the spin can approach an equilibrium condition and is therefore much more easily understood. Further, since the PSG is affected by the same aerodynamic and mass loading characteristics as the spin, an understanding of the spin and the factors affecting it are appropriate to the purposes of this course.

10.3.6.1 Flightpath Description. An aircraft spin is a coupled motion at extreme attitudes that requires all six equations of motion for a complete analysis. It is usually depicted with the aircraft center of gravity describing a helical path as the airplane rotates about an axis of rotation. Figure 10.13 shows such a motion. Notice that the spin axis of rotation may be curved and that the spin vector ω is constantly changing. Such a motion is highly complex, but by making some approximations a simplification results which can be very useful in understanding the spin and its causes.
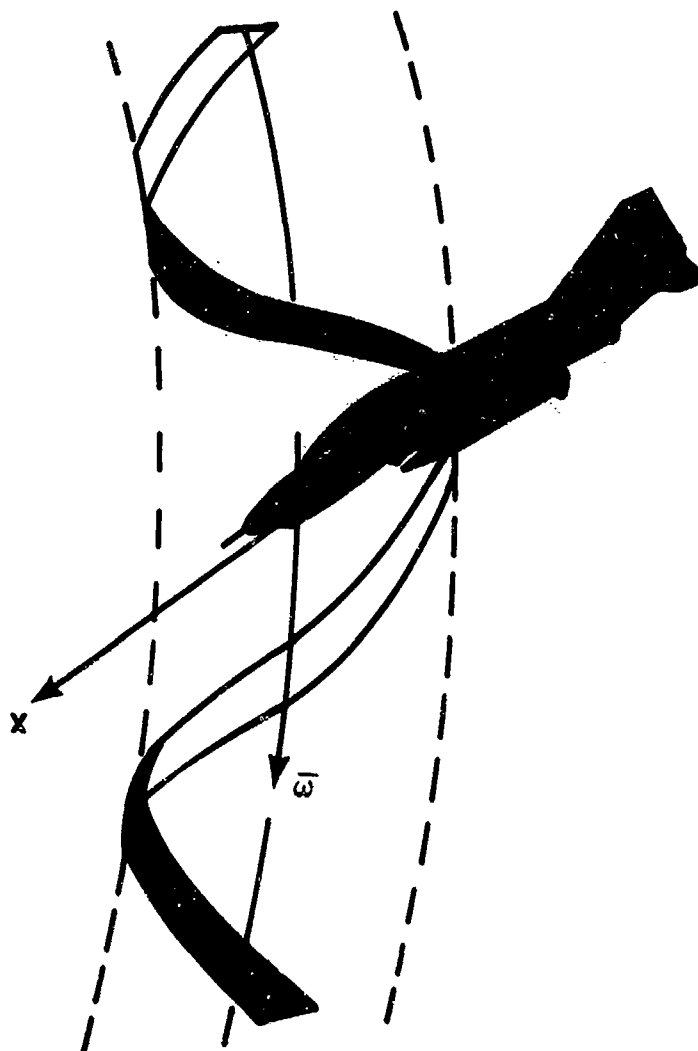
FIGURE 10.13.   HELICAL SPIN MOTION

In a fully developed spin with no sideslip the spin axis is vertical as indicated in Figure 10.14.
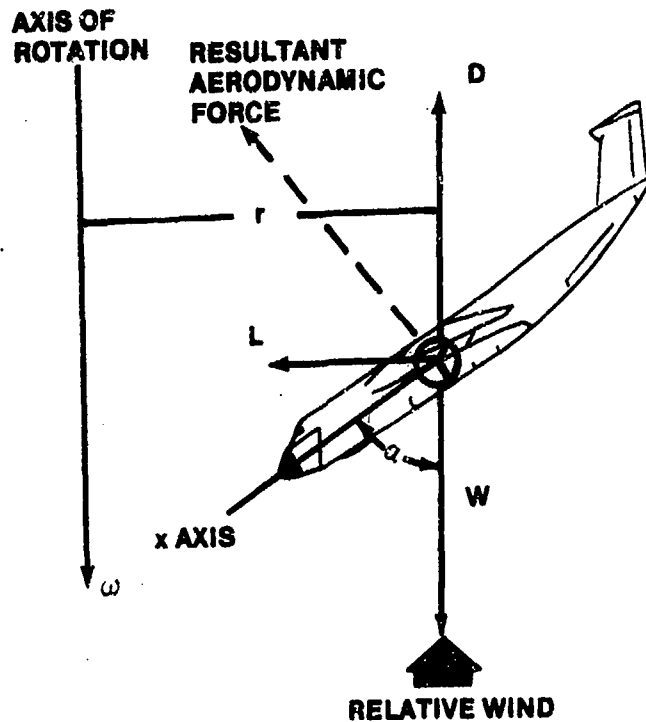
10.29

FIGURE 10.14. FORCES IN A STEADY SPIN WITHOUT SIDESLIP

If side force is ignored, the resultant aerodynamic force acts in the x-z plane and is approximately normal to the wing chord. Taking the relative wind to be nearly vertical, a summation of vertical forces gives

$$W = D = 1/2 \, \rho \, V^2 S \, C_D \qquad (10.6)$$

A similar summation of horizontal forces suggests that the lift component L balances the centrifugal force so that

$$mr\omega^2 = L = 1/2 \, \rho \, V^2 S \, C_L \qquad (10.7)$$

Equation 10.6 suggests that as AOA increases (and C_D increases), the rate of descent (V) must decrease. Furthermore, at a stalled AOA, C_L decreases as AOA increases. With these two facts in mind it is clear that the left hand side of Equation 10.7 must decrease as the AOA increases in a spin. The rotation rate, ω, tends to increase as AOA increases hence, the radius of turning, r, must decrease rapidly as AOA increases. These observations point up the fact

10.30

that in a fully developed spin, ω and the relative wind are parallel, and become more nearly coincident as the AOA increases. In fact the inclination (η) of the flightpath (relative wind) to the vertical is given by

$$\tan \eta = \frac{r\omega}{V}$$

A typical variation of η with AOA is from about 5.5° at $\alpha = 50^{\circ}$ to 1° at $\alpha = 80^{\circ}$ (10.8:533). So, it is not farfetched to assume that ω is approximately parallel to the relative wind in a fully developed spin.

All of these observations have been made under the assumption that the wings are horizontal and that sideslip is zero. The effects of bank and sideslip, while extremely important, are beyond the scope of this course, but References 10.8 and 10.9 offer some insight. It is noteworthy that this simplified analysis is valid only for a fully developed spin. However, the trends of the underlying physical phenomena will give a greater appreciation of the other phases of the spin and of the post-stall gyration.

10.3.6.2 Aerodynamic Factors. In the post-stall flight regime the aircraft is affected by very different aerodynamic forces than those acting upon it during unstalled flight. Many aerodynamic derivatives change sign; others which are insignificant at low angles of attack become extremely important. Probably the most important of these changes is a phenomenon called autorotation which stems largely from the post-stall behavior of the wing.

10.3.6.3 Autorotative Couple Of The Wing. If a wing is operating at α_1 (low angle of attack) and experiences a $\Delta\alpha$ due to wing drop, there is a restoring moment from the increased lift. If, on the other hand, a wing operating at α_2 ($\alpha_2 > \alpha_s$) experiences a sudden drop, there is a loss of lift and an increase in drag that tends to prolong the disturbance and sets up autorotation. These aerodynamic changes are illustrated in Figure 10.15.
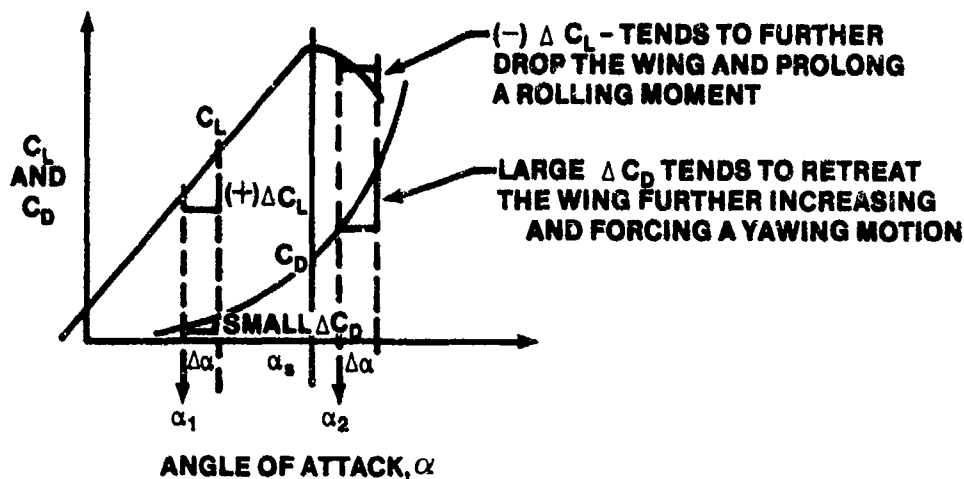
(−) ΔC_L - TENDS TO FURTHER DROP THE WING AND PROLONG A ROLLING MOMENT

LARGE ΔC_D TENDS TO RETREAT THE WING FURTHER INCREASING AND FORCING A YAWING MOTION

ANGLE OF ATTACK, α

FIGURE 10.15.   CHANGES IN C_L AND C_D WITH $\alpha < \alpha_s$ AND $\alpha > \alpha_s$

Consider now a wing flying in the post-stall region of Figure 10.15 and assume that some disturbance has given that wing an increase in α which tends to set up a yawing and rolling motion to the right as shown in Figure 10.16. The angle of attack of the advancing wing (Section A) corresponds to α_2 in Figure 10.15 while the angle of attack of the retreating wing (Section R) corresponds to $\alpha_2 + \Delta\alpha$ in Figure 10.15.   Figure 10.17 shows these two sections and illustrates why the advancing wing is operating at a lesser angle of attack than the retreating wing.   In each case the velocity vectors are drawn as they would be seen by an observer fixed to the respective wing section.   The difference in the resultant aerodynamic forces, R_A and R_R are resolved into components along the xyz body axis as in Figure 10.18.   Notice that ΔF_x is in a positive x-direction, while ΔF_z is in a negative z-direction. ΔF_x forms a couple as depicted in Figure 10.19 that tends to sustain the initial yawing moment to the right.   Of course, ΔF_z contributes a similar rolling couple about the x-axis which tends to sustain the initial rolling moment to the right.   Ordinarily, the autorotative couples generated by the wing are the most important aerodynamic factors causing and sustaining a spin. However, the other parts of the aircraft also have a part to play.
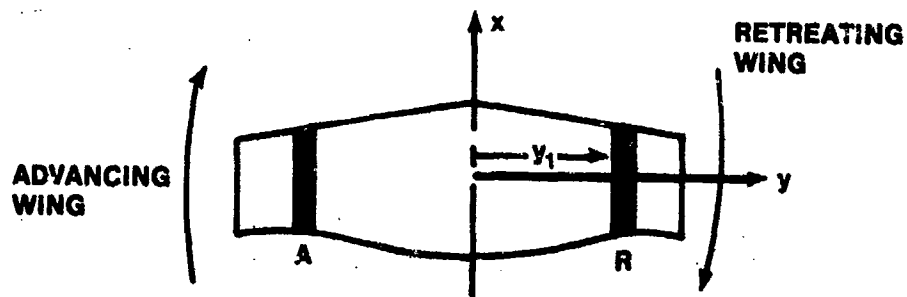
10.32

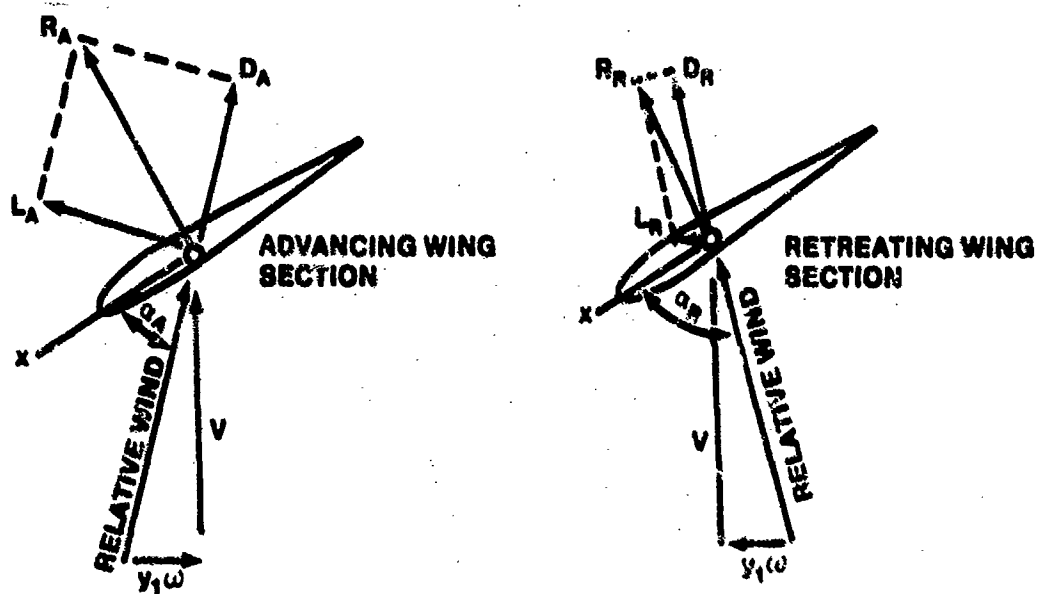FIGURE 10.16.   PLAN VIEW OF AUTOROTATING WING

FIGURE 10.17.   DIFFERENCE IN AOA FOR THE ADVANCING AND RETREATING
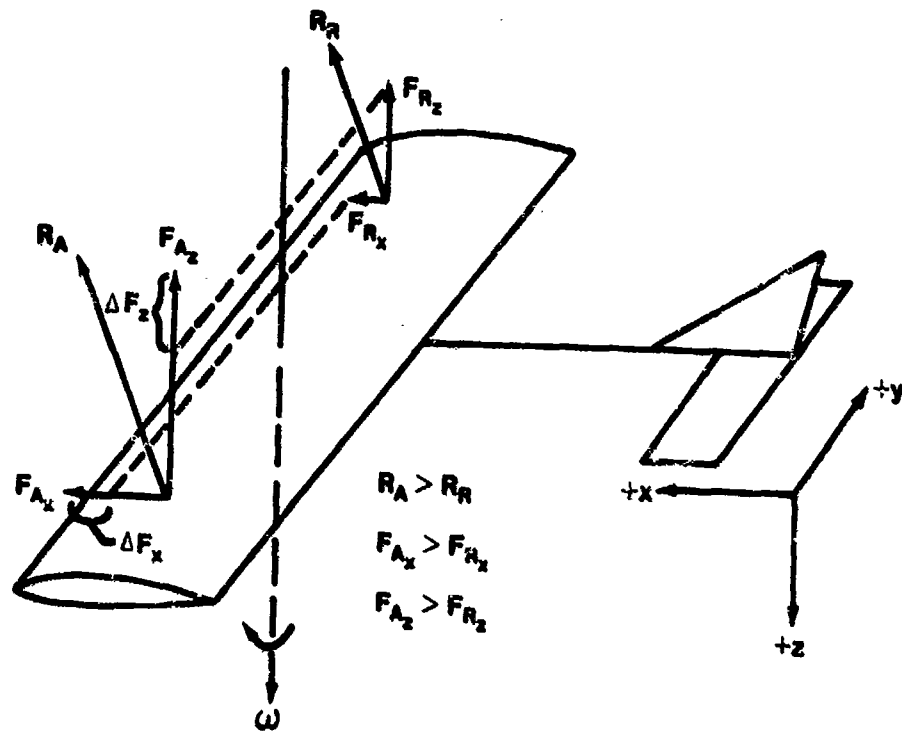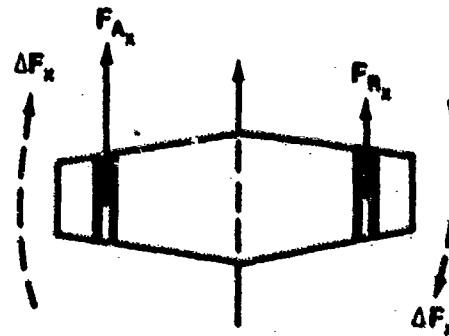WING IN AUTOROTATION

10.33

FIGURE 10.18.   DIFFERENCE IN RESULTANT AERODYNAMIC FORCES

$F_{A_x} - F_{R_x} = \Delta F_x$ YAW SUSTAINING

SIMILARLY

$F_{A_z} - F_{R_z} = \Delta F_z$ ROLL SUSTAINING

FIGURE 10.19.   AUTOROTATIVE YAWING COUPLE

10.34

10.3.6.4 <u>Fuselage Contributions</u>. The aerodynamic forces on the fuselage at stalled angles of attack are very complex, are highly dependent on fuselage shape, and may either oppose or increase the autorotative couples. Sidewash flow over the fuselage greatly affects the dihedral effect C_{ℓ_β} and may even increase it to values greater than those observed for unstalled flight (10.8:529). Weathercock stability C_{n_β} will also be affected significantly by sideshape, as illustrated in Figure 10.20. The fuselage in Figure 10.20A acts much like an airfoil section and may well generate a resultant aerodynamic force which would contribute to the yawing autorotative couple. Of course the fuselage shape will determine the relative size of "lift" and "drag" contributed by the rotating nose section. A box-like fuselage cross-section will probably give a resultant aerodynamic force opposing the yaw autorotation. An extreme example of this type of fuselage cross-section reshaping is the strakes added to the nose of the T-37, as in Figure 10.20B. Clearly the flow separation produced by the strakes in a flow field with considerable sidewash reorients the resultant aerodynamic force in such a way as to produce an anti-spin yawing moment. Such devices have also been used on the F-111, F-16, F-18, and F-20.

10.3.6.5 <u>Changes In Other Stability Derivatives</u>. All of the other stability derivatives, especially those depending on the lift curve slope of the wing, behave in a different manner in the post-stall flight regime. However, a fuller discussion of the post-stall behavior of such derivatives as C_{ℓ_p}, C_{n_p}, C_{n_r}, and combinations of these derivatives is given in (10.8:529). For the purposes of this course it suffices to say that C_{ℓ_p} becomes positive and C_{n_r} may become positive in the post-stall flight regime; C_{n_r} may also become greater in stalled flight. Each of these changes contributes to autorotation, the aerodynamic phenomenon which initiates and sustains a spin. However, aerodynamic considerations are by no means the only factors affecting the post-stall motions of an aircraft. The inertia characteristics are equally important.
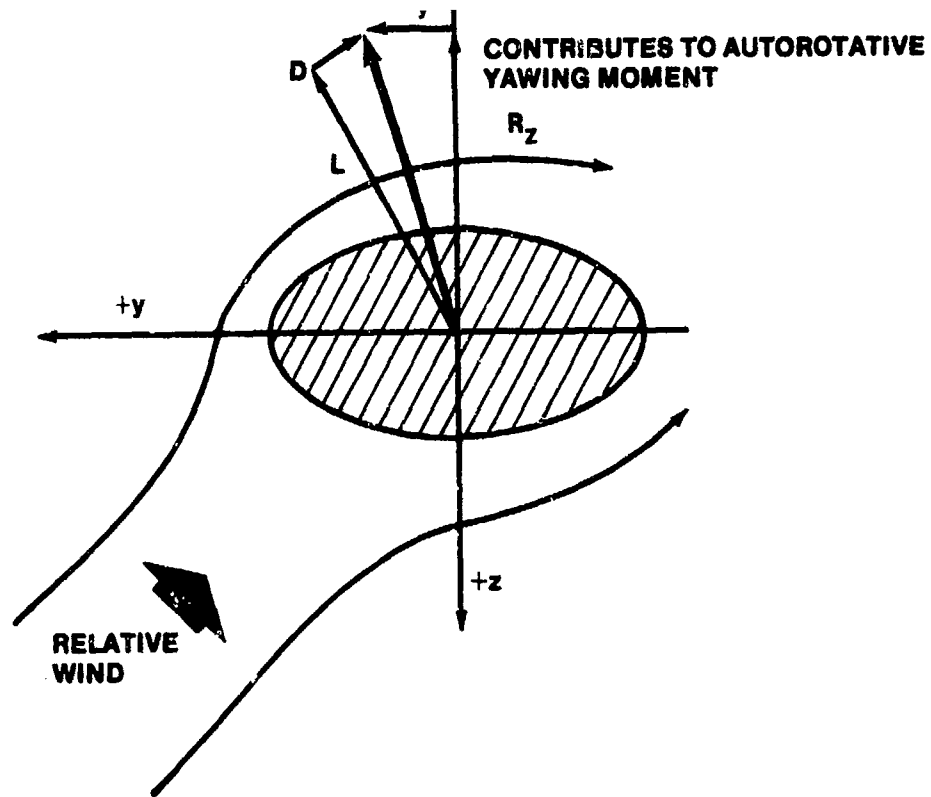
CONTRIBUTES TO AUTOROTATIVE
YAWING MOMENT

FIGURE 10.20A.   PLAIN FUSELAGE

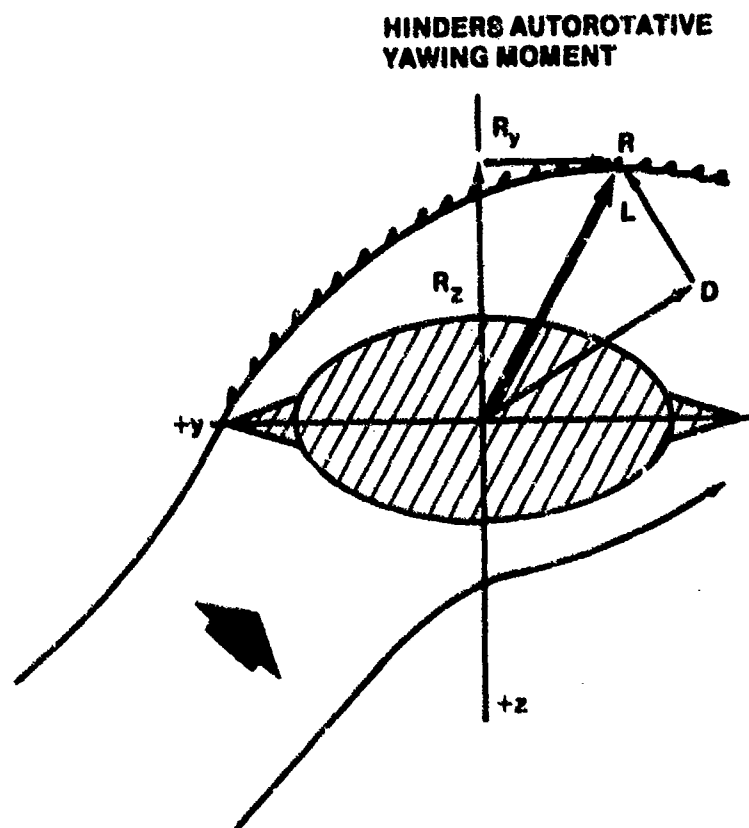HINDERS AUTOROTATIVE
YAWING MOMENT

FIGURE 10.20B.   FUSELAGE WITH STRAKES

10.36

10.3.6.6 Aircraft Mass Distribution

10.3.6.6.1 Inertial axes. For every rigid body there exists a set of inertial axes for which the products of inertia are zero and one of the moments of inertia is the maximum possible for the body. For a symmetrical aircraft, this inertial axis system is frequently quite close to the body axis system. For the purpose of this course, the small difference in displacement is neglected, and the inertial axes are assumed to lie along the body axes. Figure 10.21 illustrates what the actual difference might be.
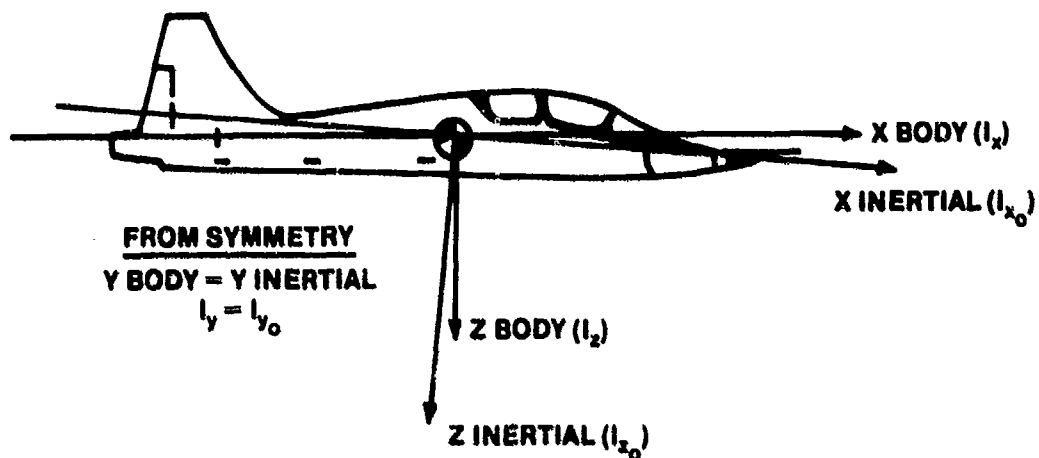

FIGURE 10.21. BODY AND INERTIAL AXES PROXIMITY

10.3.6.6.2 <u>Radius of gyration.</u> The center of gyration of a body with respect to an axis is a point at such a distance from the axis that, if the entire mass of the body were concentrated there, its moment of inertia would be the same as that of the body. The radius of gyration (K) of a body with respect to an axis is the distance from the center of gyration to the axis. In equation form

$$(y^2 + z^2) \ dm = I_x = K_x{}^2 m$$
$$(x^2 + z^2) \ dm = I_y = K_y{}^2 m$$
$$(x^2 + y^2) \ dm = I_z = K_z{}^2 m$$

or

$$K_i{}^2 = I_i/m, \tag{10.8}$$
$$i = x, \ y, \ or \ z$$

10.3.6.6.3 <u>Relative aircraft density.</u> A non dimensional parameter called relative aircraft density (μ) is frequently used to compare aircraft density to air density.

$$\mu = \frac{m/Sb}{\rho} = \frac{m}{\rho Sb} \tag{10.9}$$

10.3.6.6.4 Relative magnitude of the moments of inertia. The aircraft mass distribution is frequently used to classify the aircraft according to loading. Because aircraft are "flattened" into the xy plane, I_z is invariably the maximum moment of inertia. I_x is greater or less than I_y depending on the aircraft's mass distribution. The relative magnitudes of the moments of inertia are shown in Figure 10.22. As will be seen in the next paragraph the relative magnitudes of I_x, I_y, and I_z are of utmost importance in interpreting the equations of motion.

10.3.7 Equations Of Motion

Maneuvers within the post-stall flight regime can be analyzed by using all six equations of motion and integrating them numerically on a computer. From such studies, predictions of rate of rotation, angle of attack, magnitude of the oscillations, optimum recovery techniques, and other parameters can be made. However, such studies must use rather inaccurate theory to predict stability derivatives or else depend on wind tunnel data or free flight model tests to provide the aerodynamic data. Hence, many researchers prefer to rely almost completely on model tests for predictions prior to flight tests. Correlation between model tests and aircraft flight tests is generally good. But model tests also have limitations. Spin tunnel tests primarily examine developed or fully developed spins; there is no good way to investigate PSG's or the incipient phase of the spin in the spin tunnel. Reynolds number effects on both spin tunnel and free flight models make it very difficult to accurately extrapolate to the full scale aircraft. Engine gyroscopic effects are not often simulated in model tests. Finally, model tests are always done for a specific aircraft configuration, which is a distinct advantage for a flight test program even though it does not suit the purposes of this course. However, it would be foolish to ignore either computer analyses or model test in preparing for a series of post-stall flight tests. For obvious reasons, this course will be restricted to a much simplified look at the equations of motion as applied to a fully developed spin.

WING LOADED
$I_z > I_x > I_y$

NEUTRALLY LOADED
$I_z > I_x \cong I_y$

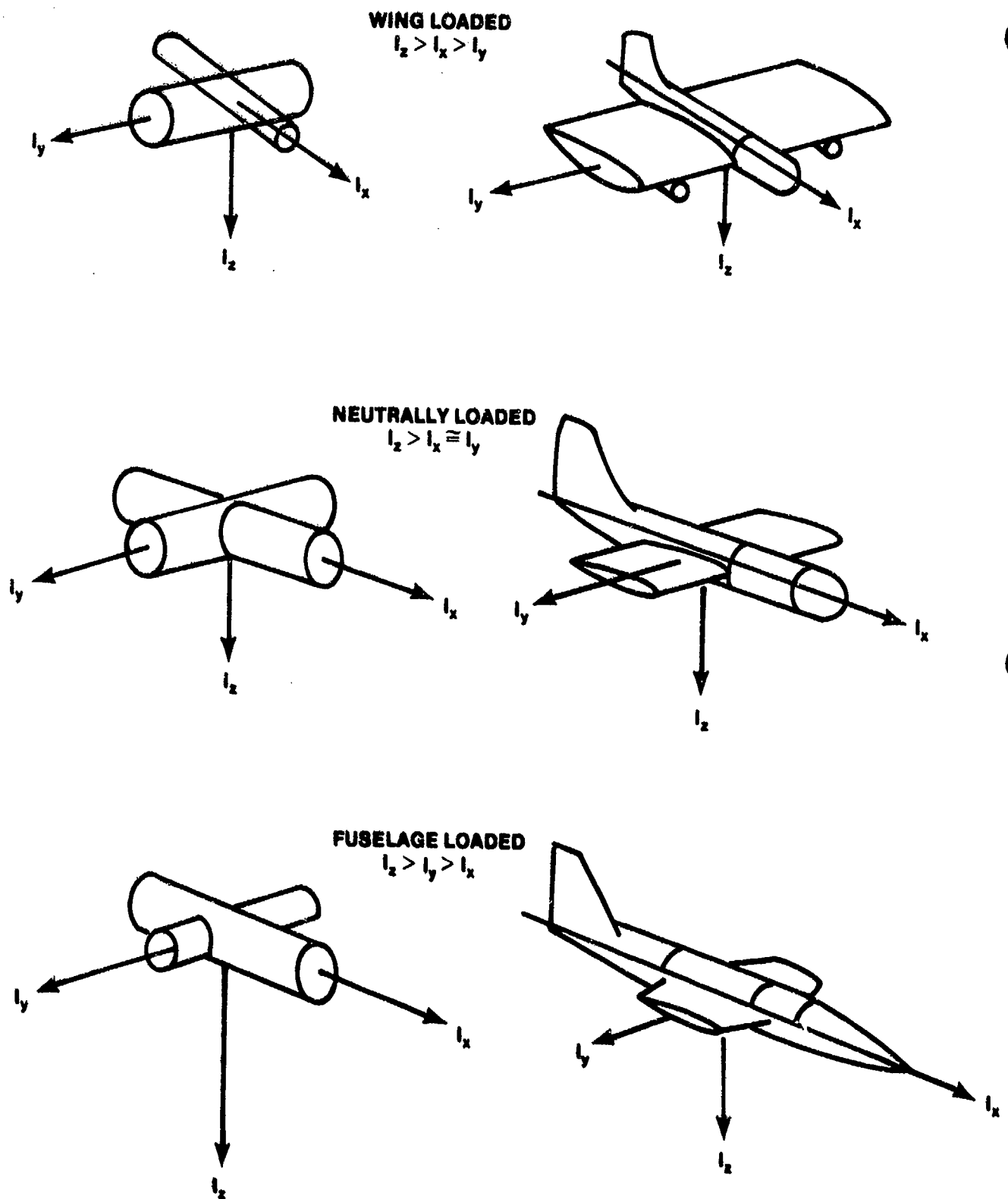FUSELAGE LOADED
$I_z > I_y > I_x$

FIGURE 10.22. AIRCRAFT MASS DISTRIBUTION

10.3.7.1 Assumptions. The analytical treatment used in this chapter is based on many simplifying assumptions, but even with these assumptions, good qualitative information can be obtained. The most important assumption is that only a fully developed spin with the wings horizontal will be considered. The wings horizontal, fully developed spin involves a balance between applied and inertial forces and moments. Some of the ramifications of this assumption are:

a. Initially, it will also be assumed that the applied moments consist entirely of aerodynamic ones, although other factors will be considered in later paragraphs.

b. With the wings horizontal, $\bar{\omega}$ lies entirely within the xz plane. Also, with the aerodynamic and inertia forces balanced, $q = 0$, ie $\bar{\omega} = p\bar{i} + r\bar{k}$.

c. The rate of descent (V) is virtually constant, as is altitude loss per turn.

d. $\bar{V}$ and $\bar{\omega}$ are parallel.

e. The time per turn is constant, or $\bar{\omega}$ is constant. Hence, $\dot{p} = \dot{q} = \dot{r} = 0$.

10.3.7.2 Governing Equations. The reference frame for expressing moments, forces, accelerations, etc., is the xyz body axis frame which rotates at the same rate as the spin rotation rate $\bar{\omega}$. The origin of the xyz axes is centered at the aircraft's cg and translates downward at a rate equal to the constant rate of descent $\bar{V}$. With this background the forces acting on the aircraft can be examined.

10.3.7.2.1 Forces. The external forces applied to the aircraft and expressed in an inertial reference frame follow Newton's second law.

$$\bar{F} = m\,\dot{\bar{V}}$$

Expressing $\bar{V}$ in the xyz reference frame,

$$\bar{F} = m\,(\dot{\bar{V}} + \omega \times \bar{V})$$

but since $\bar{V}$ is constant in the fully developed spin and since $\bar{\omega}$ and $\bar{V}$ are parallel,

$$\bar{F} = 0$$

The elimination of the force equations in this fashion merely reinforces the idea that the rotary motion is the important motion in a spin and one would expect the significant equations to be the moment equations.

10.3.7.2.2 <u>Moments</u>. The moment equations to be considered have already been developed in Chapter 4 and are repeated below.

$$G_x = \dot{p} I_x + qr (I_z - I_y) - (\dot{r} + pq) I_{xz} \tag{4.5}$$

$$G_y = \dot{q} I_y - pr (I_z - I_x) + (p^2 - r^2) I_{xz} \tag{4.3}$$

$$G_z = \dot{r} I_z + pq (I_y - I_x) + (qr - \dot{p}) I_{xz} \tag{4.6}$$

Using the assumption that the body axes, xyz, are also the inertial axes and considering G to consist of aerodynamic moments only, these equations become

$$\mathcal{L} = \dot{p} I_x + qr (I_z - I_y) \qquad \text{ROLLING MOMENT} \tag{10.10}$$

$$\mathcal{M} = \dot{q} I_y - pr (I_z - I_x) \qquad \text{PITCHING MOMENT} \tag{10.11}$$

$$\mathcal{N} = \dot{r} I_z + pq (I_y - I_x) \qquad \text{YAWING MOMENT} \tag{10.12}$$

Solving for the angular accelerations shows the contributions of each type of moment to that acceleration.

$$\dot{p} = \frac{\mathcal{L}}{I_x} + \frac{I_y - I_z}{I_x} q r \tag{10.13}$$

$$\dot{q} = \frac{\mathcal{M}}{I_y} + \frac{I_z - I_x}{I_y} p r \tag{10.14}$$

$$\dot{r} = \frac{\mathcal{N}}{I_z} + \frac{I_x - I_y}{I_z} p q \tag{10.15}$$

$$\underset{\text{aerodynamic}}{\text{term}} \qquad \underset{\text{inertial}}{\text{term}}$$

10.42

The body axis angular accelerations can also be exercised in terms of aerodynamic coefficients and the relative aircraft density.

$$\frac{\mathcal{L}}{I_x} = \frac{\frac{1}{2}\rho V^2 Sb}{K_x^2 m} C_\ell = \frac{V^2}{\frac{2m}{\rho Sb} K_x^2} C_\ell$$

$$\frac{\mathcal{L}}{I_x} = \frac{V}{2\mu K_x^2} C_\ell \qquad (10.16)$$

In a similar manner,

$$\frac{\mathcal{N}}{I_z} = \frac{V^2}{2\mu K_z^2} C_n \qquad (10.17)$$

It is common practice in post-stall/spin literature to define C_m on the basis of wingspan instead of on the basis of wing chord as is done in most other stability and control work. This change is made to allow a consistent definition of μ:

where $\qquad \mu = \dfrac{m}{\rho Sb}$ $\qquad\qquad\qquad (10.18)$

and is indicated by a second subscript; that is, C_m becomes $C_{m,b}$.
Then

$$\frac{\mathcal{M}}{I_y} = \frac{V^2}{2\mu K_y^2} C_{m,b} \qquad (10.19)$$

Equations 10.13 through 10.15 then become

$$\dot{p} = \frac{V^2 C_\ell}{2\mu K_x^2} + \frac{I_y - I_z}{I_x} qr \qquad (10.20)$$

$$\dot{q} = \frac{v^2 C_{m,b}}{2\mu K_y^2} + \frac{I_z - I_x}{I_y} pr \qquad (10.21)$$

$$\dot{r} = \frac{v^2 C_n}{2\mu K_z^2} + \frac{I_x - I_y}{I_z} pq \qquad (10.22)$$

With this brief mathematical background it is now appropriate to consider the aerodynamic prerequisites for a fully developed spin to occur.

10.3.7.3 <u>Aerodynamic Prerequisites</u>. For a fully developed upright spin with the wings horizontal, $p = q = r = q = 0$ and Equations 10.20, 10.21, and 10.22 yield

$$C_\ell = 0 \qquad (10.23)$$

$$-\frac{v^2 C_{m,b}}{2\mu K_y^2} = \frac{I_z - I_x}{I_y} pr \qquad (10.24)$$

$$C_n = 0 \qquad (10.25)$$

What do each of these results imply about a stable condition like the fully developed spin?

10.3.7.4 <u>Pitching Moment Balance</u>. By examining Equation 10.24 in association with $C_{m,b}$ versus α curve for an aircraft, it is at least possible to identify regions where a fully developed spin can occur.

First, the angle of attack must be above the stall angle of attack. This condition is obvious, since the definition of a spin demands $\alpha > \alpha_s$.

Second, $C_{m,b}$ must be opposite in sign to the inertial term on the right hand side of Equation 10.24. For an upright spin this requirement means that $C_{m,b}$ must be negative. This fact is clear if one observes that $I_z > I_x$ and that p and r are of the same sign in an upright spin (Figure 10.23). In fact, it is possible to express the rotation rate in a convenient form by slightly rearranging Equation 10.24. Recall that

$$\frac{\mathcal{M}}{I_y} = \frac{v^2 C_{m,b}}{2\mu K_y^2}$$

(10.19)

Figure 10.23 illustrates the fact that with wings level

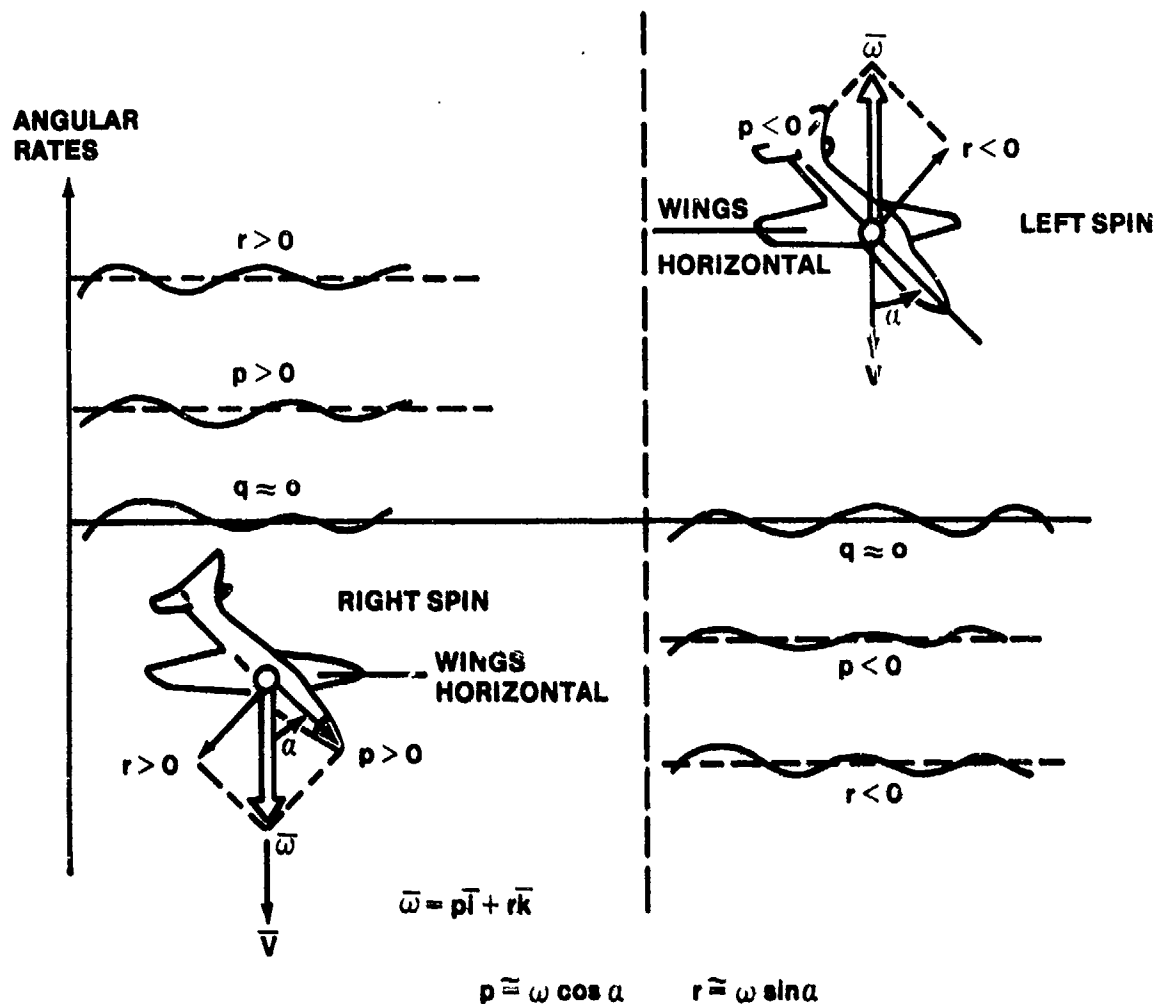$$p = \omega \cos \alpha \text{ and } r = \omega \sin \alpha$$

FIGURE 10.23.   SPIN VECTOR COMPONENTS

$$-\frac{\mathcal{M}}{I_y} = \frac{I_z - I_x}{I_y} \omega^2 \cos \alpha \sin \alpha$$

10.45

$$\omega^2 = \frac{-m}{1/2 \ (I_z - I_x) \ \sin 2 \alpha} \tag{10.26}$$

Equation 10.26 suggests that the minimum rotation rate occurs near an α of 45°, although strong variations in M_{aero} may preclude this minimum. In fact, there is one additional prerequisite which must be satisfied before a fully developed spin can occur.

The slope of $C_{m,b}$ versus α must be negative or stabilizing and must be relatively constant. This is required simply because a positive $dC_{m,b}/d\alpha$ represents a divergent situation and would therefore require a pitching acceleration, $\dot{q} = 0$. But this angular acceleration would violate the assumption of a constant ω in a fully developed spin. Said another way, any disturbance in angle of attack would produce a $\Delta C_{m,b}$ tending to restore $C_{m,b}$ to its initial value only so long as $dC_{m,b}/d\alpha < 0$. To summarize these constraints, consider Figure 10.24. Aircraft B can enter a fully developed, upright spin at any AOA above α_s insofar as the pitching moment equation is concerned because its $C_{m,b}$ versus α is always negative and $dC_{m,b}/d\alpha$ is always negative. However, Aircraft A can meet the three constraints imposed by the pitching equation only in the shaded areas. Of course, the pitching moment equation is not the sole criterion; the rolling and yawing moment equations must also be considered.
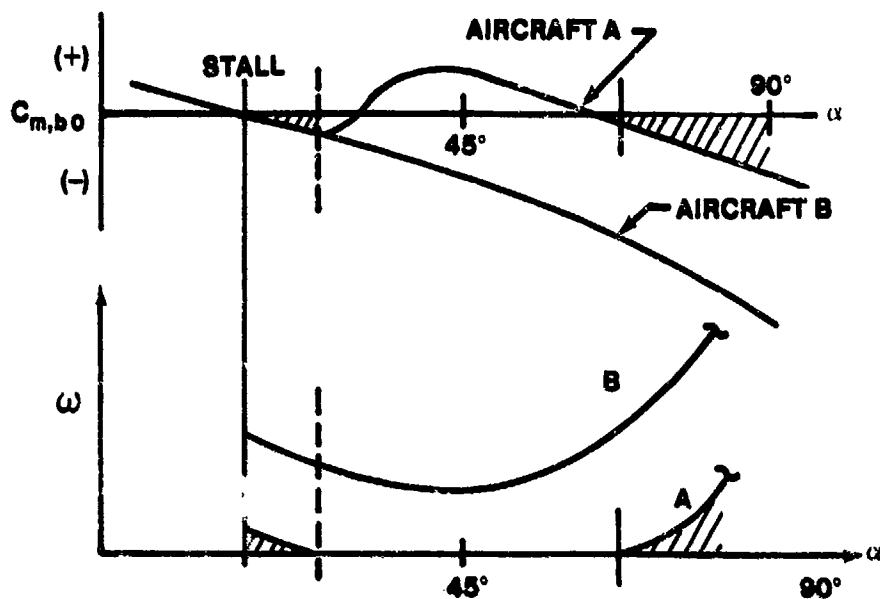
FIGURE 10.24. AERODYNAMIC PITCHING MOMENT PREREQUISITES

10.3.7.5 Rolling and Yawing Moment Balance. Equations 10.23 and 10.25 suggest at least four other conditions which must be satisified to have a fully developed spin occur. Although not specifically pointed out previously, all the aerodynamic derivatives, even $C_{m,b}$ are functions of both α, β, and the rotation rate ω. Having considered $C_{m,b}$ as a function of α alone, it is convenient to consider C_n and C_ℓ as functions of ω alone. There is little justification for this choice other that the fact the lateral-directional derivative is more directly linked to rotation rate while the longitudinal derivative is more directly linked to angle of attack. But it is well to keep in mind that all these variables do affect $C_{m,b}$, C_ℓ, and C_n.

The conditions imposed on both C_n and C_ℓ to allow a fully developed spin is that they must be equal to zero, and the derivatives with respect to ω must be negative. The first of these conditions is explicitly stated by Equations 10.23 and 10.25. But the second requirement ($dC_\ell/d\omega < 0$ adn $dC_n/d\omega < 0$) stems from the fact that a fully developed spin must be a stable condition. If an

10.47

If an increase in ω will produce an increased C_ℓ or C_n, then any change in rotation rate will cause the autorotative moments to diverge away from the supposedly stable initial condition. Figure 10.25 illustrates this point.
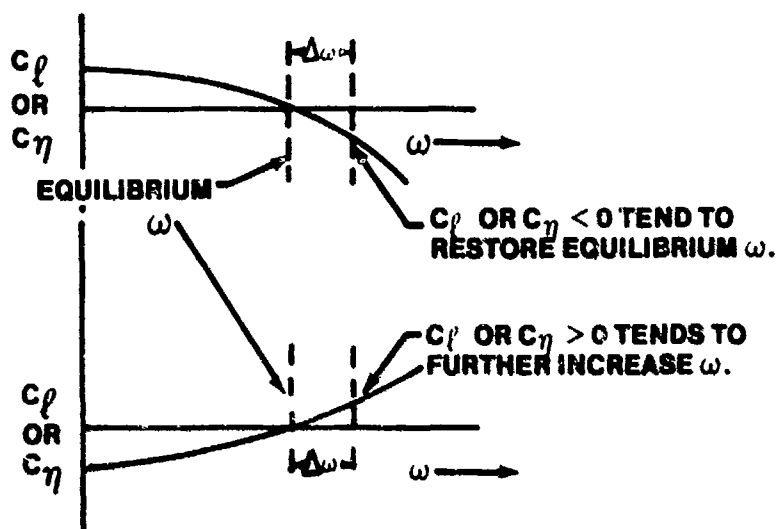

FIGURE 10.25. STABILIZING AND DESTABILIZING SLOPES FOR C_ℓ AND C_n VERSUS ω

Obviously, these aerodynamic prerequisites must all be met for a fully developed spin to exist in a true equilibrium form. Of course, oscillatory spins may occur with some relaxation of one or more of these conditions. It is extremely rare to observe an ideal case which would precisely meet all these conditions in an actual spin. So, while exactly satisfying all these conditions is essential for a fully developed spin to actually exist, it is common to estimate spin parameters with less than perfect fulfillment of these prerequisites. An example of how such estimations are made will be considered next.

10.3.7.6 Estimation Of Spin Characteristics. Reference 10.10, Appendix B, describes in detail a method of estimating spin characteristics which was designed to estimate initial conditions for a computer study investigating possible steady state spin modes of the McDonnell F-3H Demon. Although this

estimation method was only intended to help predict initial conditions for the numerical integration and thus save computer time, it serves as an excellent example of how model data and the aerodynamic prerequisites discussed earlier can be combined to get a "first cut" at spin characteristics.

The aerodynamic data on which this example is based were measured by steadily rotating a model about an axis parallel to the relative wind in a wind tunnel. Hence, no oscillations in angular rates are taken into account. This limitation on the aerodynamic data is indicated by the subscribt "rb" (rotation-balance tunnel measurements). In addition, the data are presented as a function of a non dimensional rotation rate, $\omega b/2V$. To help simplify the estimation process and partly because the rolling moment data were not as "well-behaved" as the yawing moment data, the rolling moment data were ignored. However, all the other prerequisites were observed. The estimation method is outlined below and the interested student is referred to Reference 10.10, Page 18, for a more complete description and a numerical example.

10.3.7.6.1 Determining $C_{m,rb}$ from aerodynamic data. Use the $\omega b/2V$ and α for which $C_{n,rb} = 0$ and $dC_{n,rb}/d\ (\omega b/2V) < 0$ to determine $C_{m,rb}$. This amounts to using the model data to determine aerodynamic pitching moments for which the aerodynamic yawing moment is zero.

10.3.7.6.2 Calculating inertial pitching moment. Using a modified form of Equation 10.26, and recognizing that the inertial pitching moment is the negative of the aerodynamic pitching moment on a fully developed spin, $-C_{m,rb}$ is calculated.

$$\omega^2 = \frac{-m}{1/2\ (I_z - I_x)\ \sin 2\ \alpha}$$

$$= \frac{-C_{m,rb}\ \frac{1}{2}\ \rho\ V^2\ S\ b}{1/2\ (I_z - I_x)\ \sin 2\ \alpha}$$

Solving for $-C_{m,rb}$

$$-C_{m,rb} = \frac{I_z - I_x}{\rho\ S\ b}\ \left(\frac{\omega}{V}\right)^2\ \sin 2\ \alpha \tag{10.27}$$

10.49

10.3.7.6.3 Comparing Aerodynamic Pitching Moments and Inertial Pitching Moments. Plot $C_{m,rb}$ versus α from the wind tunnel data and the results of Equation 10.27 on the same plot, like Figure 10.26.
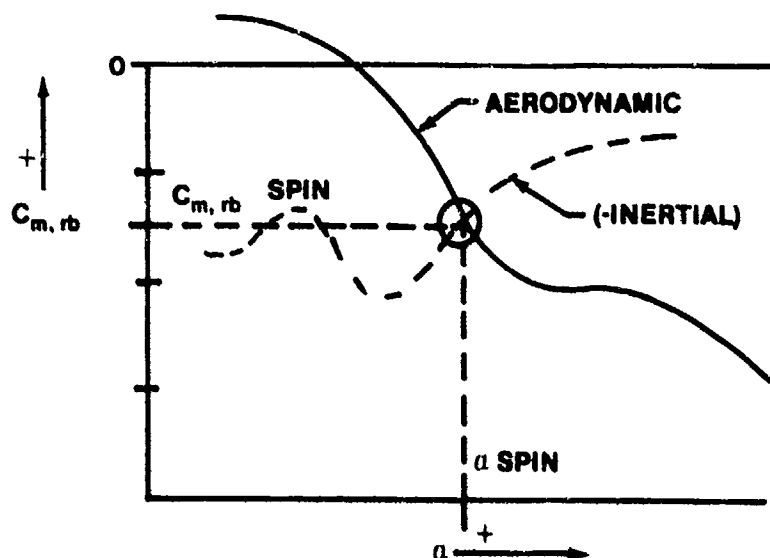

FIGURE 10.26.   AERODYNAMIC PITCHING MOMENTS COMPARED
TO INERTIAL PITCHING MOMENTS

The intersection of the two curves indicates a possible fully developed spin. From this plot the angle of attack of the potential spin is read directly and the value of $C_{m,rb}$ is used to calculate the potential rotation rate.

10.3.7.6.4 Calculation of ω. Rearranging Equation 10.27

$$\left(\frac{\omega}{V}\right)^2 = \frac{(-C_{m,rb})\ (\rho Sb)}{(I_z - I_x)\ \sin 2_\alpha}$$

(10.28)

the ratio ω/V can be calculated. But Equation 10.6 allows calculation of V if C_D is known. The model force measurements provide C_D and then

$$V^2 = \frac{W}{1/2\ \rho\ S\ C_D}$$

10.50

It follows that

$$\omega^2 = \frac{(-C_{m,rb})\ (\rho\ Sb)\ W}{(I_z - I_x)\ (\sin 2\alpha)\ 1/2\ \rho\ S\ C_D}$$

$$\omega^2 = \frac{-2C_{m,rb}\ b\ W}{C_D\ (I_z - I_x)\ \sin 2\ \alpha} \tag{10.29}$$

10.3.7.6.5 <u>Results</u>. A typical set of results from the numerical integration of the six equations compared with the estimated parameters is given in Table 10.5 (10.10:26,27).

TABLE 10.5
TYPICAL COMPUTER RESULTS VERSUS ESTIMATION

Computer Results			Estimation		
α (deg)	ω (rad/sec)	V (ft/sec)	α (deg)	ω (rad/sec)	V (ft/sec)
36.0	1.88	294	38.2	1.90	285
37.0	1.92	372	45.1	1.83	327
Oscillated out of spin			48.2	1.89	453
51.8	2.18	619	50.5	2.18	620
80.0	4.72	494	70.0	3.50	515
36.5	2.80	380	37.4	2.69	365

10.3.7.6.6 <u>Gyroscopic influences</u>. Only aerodynamic moments have been considered so far in expanding the applied <u>external</u> moments. Ordinarily the aerodynamic moments are the dominant ones, but gyroscopic influences of rotating masses can also be important. The NF-104, for example, had virtually no aerodynamic moments at the top of its rocket-powered zoom profile. There is convincing evidence that gyroscopic moments from the engine dominate the equations of motion at these extreme altitudes (10.11.13). The externally applied moments should be generalized to include gyroscopic influences and other miscellaneous terms (anti-spin rockets, anti-spin chutes, etc.). The applied external moments become

10.51

$$G_x = \mathcal{L} + L_{gyro} + L_{other} \qquad (10.30)$$

$$G_y = \mathcal{M} + M_{gyro} + M_{other} \qquad (10.31)$$

$$G_z = \mathcal{N} + N_{gyro} + N_{other} \qquad (10.32)$$

In the next paragraph a simplified expansion of the gyroscopic terms is considered.

10.3.7.6.6.1 <u>Gyroscopic Theory</u>. By virtue of its rotation, a gyroscope tends to maintain its spin axis aligned with respect to inertial space. That is, unless an external torque is applied, the gyro spin axis will remain stationary with respect to the fixed stars. If a torque is applied about an axis that is perpendicular to the spin axis, the rotor turns about a third axis that is orthogonal to the other two axes. On removing this torque the rotation (precession) ceases – unlike an ordinary wheel on an axle which keeps on rotating after the torque impulse is removed.

These phenomena, all somewhat surprising when first encountered, are consequences of Newton's laws of motion. The precessional behavior represents obedience of the gyro to Newton's second law expressed in rotational form, which states that torque is equal to the time rate of change of angular momentum.

$$\bar{T} = \frac{d\bar{H}}{dt} \qquad (10.33)$$

with $\bar{T}$ = external torque applied to the gyroscope

$\bar{H}$ = angular momentum of the rotating mass

$\bar{H} = I\,\bar{\Omega}$

with I = moment of inertia of the rotating mass

$\bar{\Omega}$ = angular velocity of the rotating mass.

Equation 10.33 applies, like all Newton's laws, only in an inertial frame of reference. If it assumed that $\bar{H}$ is to be expressed within a frame of reference rotating at the precession rate of the gyroscope, $\dot{\bar{H}}/_{inertial} = \dot{\bar{H}}/_{rotating} + \bar{\omega}_p \times \bar{H}$. If the gyro spin rate is unchanged then $\bar{H}$ measured in the rotating frame will be zero and Equation 10.34 becomes

$$\bar{T} = \bar{\omega}_p \times \bar{H} \tag{10.34}$$

The direction of precession for a gyro when a torque is applied is given by Equation 10.34 This direction is such that the gyro spin axis tends to align itself with the total angular momentum vector, which in this case is the vector sum of the angular moment due to the spinning rotor and the angular momentum change due the applied torque, $\Delta\bar{H}$ as shown in Figure 10.27. The law of precession is a reversible one. Just as a torque input results in an angular velocity output (precession), an angular velocity input results in a torque output along the corresponding axis.
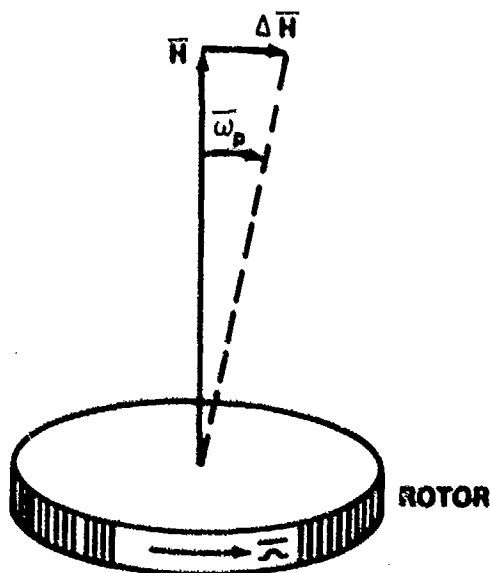
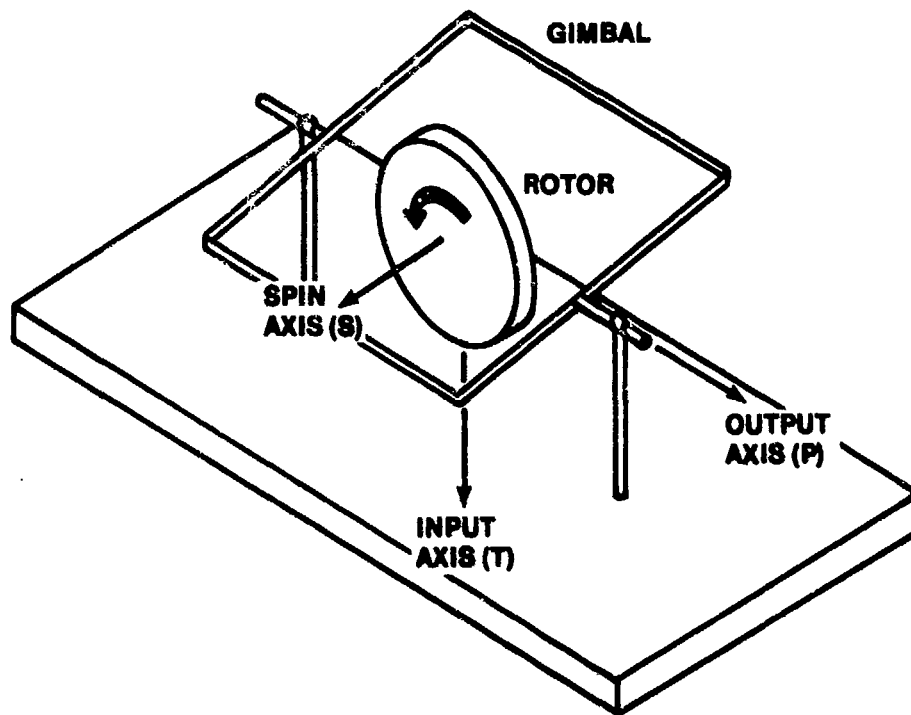FIGURE 10.27. DIRECTION OF PRECESSION

FIGURE 10.28.   GYROSCOPE AXES

Three axes are significant in describing gyroscope operation; the torque axis, the spin axis and the precession axis. These are commonly referred to as input (torque), spin, and output (precession). The directions of these axes are shown in Figure 10.28. They are such that the spin axis rotated into the input axis gives the output axis direction by the right hand rule. The direction of rotational vectors such as spin, torque, and precession can be shown by means of the right hand point in the direction of rotation, the thumb extended will point along the axis of rotation. For gyro work, it is convenient to let the thumb, forefinger, and middle finger represent the spin, torque, and precession axes respectively. Figure 10.29 illustrates this handy memory device.
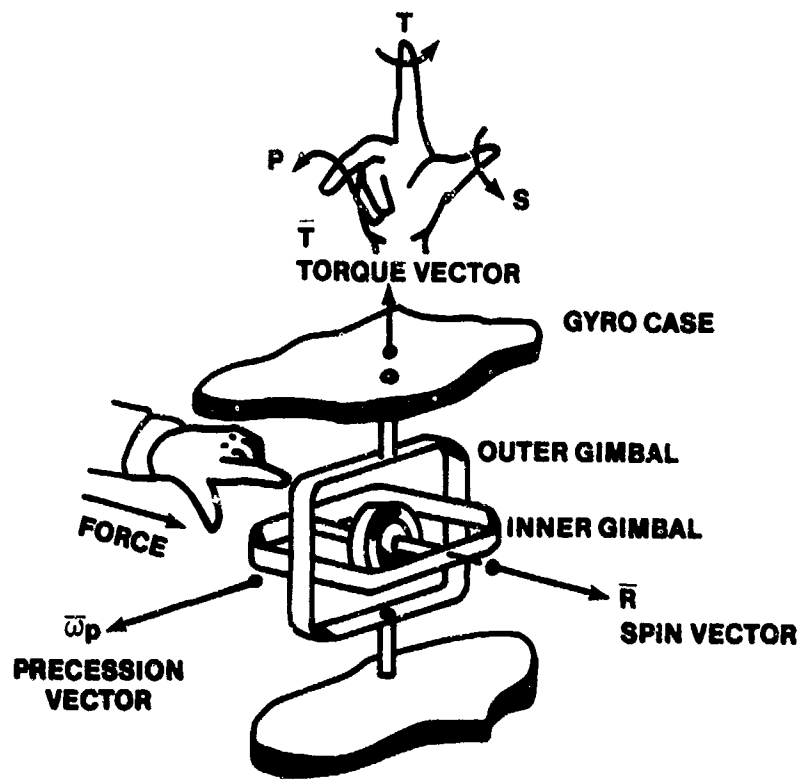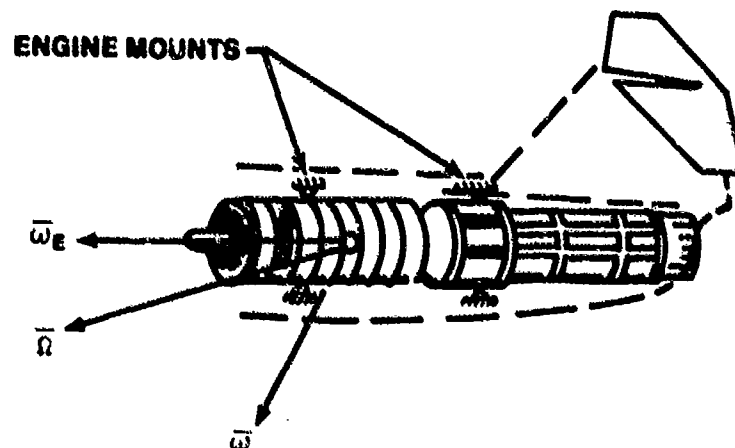
FIGURE 10.29.   SPIN, TORQUE AND PRECESSION VECTORS

FIGURE 10.30.   ANGULAR VELOCITIES OF THE ENGINE'S ROTATING MASS

10.3.7.6.6.2 **Engine Gyroscopic Moments.** In Figure 10.30, consider the rotating mass of the engine as a gyroscope and analyze the external torque applied to the engine mounts of an aircraft in a spin. Then the total angular velocity of the rotating mass is the vector sum of $\bar{\omega}_E + \bar{\omega}$, with $\bar{\omega}_E$ being the engine RPM (assumed constant) and ω being the aircraft's spin rotation rate.

$$\bar{\Omega} = \bar{\omega}_E + \bar{\omega}$$

But

$$\bar{\omega} \ll \bar{\omega}_E$$

$$\bar{\Omega} = \bar{\omega}_E$$

If one also assumes that the rotational axis of the engine is parallel to the x-axis,

$$\bar{\Omega} \cong \omega_E \bar{i}$$

Then the angular momentum of the engine is

$$\bar{H}_E = I_E \omega_E \bar{i} \tag{10.35}$$

with I_E = moment of inertia of the engine about the x-axis.

Considering Figure 10.30 again and applying Equation 10.34, the external torque applied to the engine must be the precession rate of the aircraft, $\bar{\omega}$, crossed into the engine's angular momentum.

$$\bar{T} = \omega \times \bar{H}_E \tag{10.36}$$

But the moment applied by the engine through the engine mounts to the spinning aircraft is equal but opposite in sign (Newton's Third Law).

$$\bar{G}_{gyro} = -\bar{\omega} \times \bar{H}_E$$

$$\bar{L}_{gyro} + \bar{M}_{gyro} + \bar{N}_{gyro} = - \begin{vmatrix} \bar{i} & \bar{j} & \bar{k} \\ p & q & r \\ I\omega_E & 0 & 0 \end{vmatrix}$$

$$\bar{L}_{gyro} = 0 \; \bar{i} \tag{10.37}$$

$$\bar{M}_{gyro} = (- I_E \omega_E \; r) \; \bar{j} \tag{10.38}$$

$$\bar{N}_{gyro} = (I_E \; \omega_E \; q) \; \bar{k} \tag{10.39}$$

Then Equations 10.13, 10.14, and 10.15 can be expanded to:

AERO	INERTIAL COUPLING (sometimes called gyrodynamic term)	GYROSCOPIC TERM (an engine effect)	MISCELLANEOUS (rockets, spin chutes,etc.)

$$\dot{p} = \frac{\mathcal{L}}{I_x} + \frac{I_y - I_z}{I_x} q r + \frac{L_{gyro}}{I_x} + \frac{L_{other}}{I_x} \tag{10.40}$$

$$\dot{q} = \frac{\mathcal{m}}{I_y} + \frac{I_z - I_x}{I_y} p r + \frac{M_{gyro}}{I_y} + \frac{M_{other}}{I_y} \tag{10.41}$$

$$\dot{r} = \frac{\mathcal{n}}{I_z} + \frac{I_x - I_y}{I_z} p q + \frac{N_{gyro}}{I_z} + \frac{N_{other}}{I_z} \tag{10.42}$$

Equation 10.26 becomes:

$$\omega^2 = - \frac{\mathcal{m} + I_E \omega_E r}{1/2 \; (I_z - I_x) \sin 2\alpha} \tag{10.43}$$

Equation 10.43 shows that the effect of the engine gyroscopic moment is to shift the ω vs α curves is shown in Figure 10.31. An engine that rotates in a counter clockwise direction (as viewed from the intake) will cause all aircraft to spin faster in a right, upright spin and slower in a left upright spin. Generally speaking, however, this engine gyroscopic moment is negligible in comparison to the other external moments.
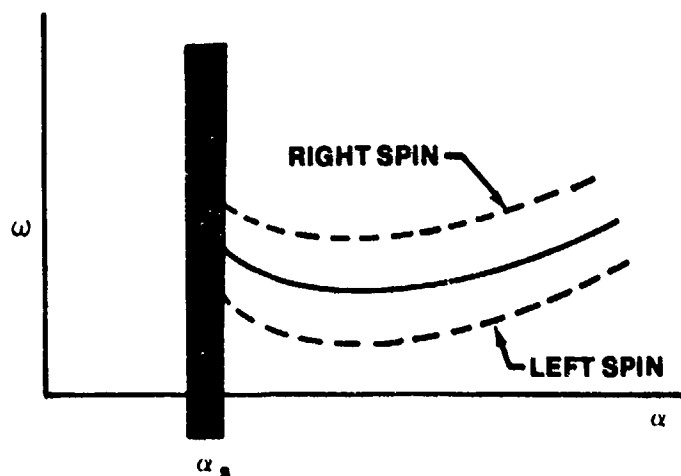

FIGURE 10.31. EFFECT OF M_{GYRO} ON SPIN ROTATION RATE

10.3.7.6.7 Spin Characteristics of Fuselage-Loaded Aircraft. It is appropriate to consider briefly some of the spin characteristics peculiar to modern high performance aircraft in which the mass is generally concentrated within the fuselage (I_y larger than I_x and almost as large as I_z). It can be shown that a system that has no external moments or forces tends to rotate about its largest principal axis, that, in the case of an aircraft, is the z axis. In an actual spinning aircraft, the external moments are not zero and thus the aircraft spins about some intermediate axis. For the idealized spin thus far considered, the pitching moment equation leads one to the observation that fuselage-loaded aircraft will probably spin flatter than their wing-loaded counterparts.

10.3.7.6.7.1 Fuselage-Loaded Aircraft Tend to Spin Flatter Than Wing-Loaded Aircraft. For a fully developed spin

$$G_y = - pr (I_z - I_x) \tag{10.44}$$

In an aircraft, $(I_z - I_x)$ can never be zero. Hence, if $G_y = 0$ the p must

10.58

be zero, in which case $\bar{\omega} = r\bar{k}$ and the spin is flat ($\bar{\omega} = p\bar{i}$ is excluded by the definition of a spin). If the spin is not flat, then both p and r exist and, in an upright spin, have the same algebraic sign. Because $(I_z - I_x)$ is always positive, examination of Equation 10.44 shows that G_y must always be negative (or zero) for an upright spin.

The smaller the pitch attitude (θ in Figure 10.32) the flatter the spin, and θ can be defined as $\sin^{-1} p/\omega$ for the spin depicted in Figure 10.32. θ varies with the relative magnitude of $(I_z - I_x)$, as can readily be seen by rearranging Equation 10.44.

$$p = \frac{|G_y|}{r(I_z - I_x)}$$

Since p becomes smaller as $(I_z - I_x)$ increases, it is clear that fuselage-loaded aircraft tend to spin flatter than wing-loaded aircraft. But what about the effect of increasing I_y upon the roll equation?

10.3.7.6.7.2 Fuselage-Loaded Aircraft Tend to Exhibit More Oscillations. On aircraft where I_y is approximately equal to I_z in magnitude, the fully developed spin is more likely to be oscillatory. In the limit, if $I_y = I_z$, the reference spin could be wing down, since any axis in the yz plane would be a maximum inertial axis. Although these facts suggest that the bank angle is easily disturbed and that a developed spin often occurs with the bank angle not zero, a restoring tendency does exist which leads to periodic oscillations in bank angle. Consider again the rolling moment equation.

$$G_x = \dot{p} I_x + q r (I_z - I_y) \tag{10.45}$$

If a "0" subscript is used to represent the reference or steady-state conditions,

$$G_{x_0} = \dot{p}_0 I_x + q_0 r_0 (I_z - I_y)$$

If instantaneous values are represented by Equation 10.45, the change in external moments due to the perturbations of the angular acceleration and angular velocities is

$$(G_x - G_{x_0}) = (\dot{p} - \dot{p}_0) I_x + (q r - q_0 r_0)(I_z - I_y)$$

Assuming perturbations in roll will not significantly change r_0, r r_0 and

$$\Delta G_x = \Delta p\, I_x + \Delta q\, (I_z - I_y) r_0$$

$$\Delta \dot{p} = \frac{\Delta G_x}{I_x} - \Delta q\, \frac{I_z - I_y}{I_x}\, r_0$$

The second term on the right side of Equation 10.46 serves to damp oscillations in that it reduces the ability of perturbations in rolling moment (ΔG_x) to produce perturbations in roll acceleration (Δp). For fuselage-loaded aircraft, in which ($I_z - I_y$) is small, the damping is much reduced. Thus, any perturbations in the motion tend to persist longer in fuselage-loaded aircraft than they do in wingloaded aircraft.

10.3.7.7 Sideslip. It is beyond the scope of this course to deal with the effects of sideslip in any detail. However, it is noteworthy that sideslip need not be zero in a developed spin; in fact it usually is not. Reference 10.8, Page 535, shows that sideslip in a spin arises from two sources: wing tilt with respect to the horizontal (ϕ) and the inclination of the flight path to the vertical (η).

$$\beta \cong \phi - \eta \tag{10.47}$$

If then, one considers a spin with a helical flight path as opposed to a vertical flight path, the inclination of the flight path to the vertical is positive and equal to the helix angle. Then, in order to maintain zero sideslip, the retreating wing must be inclined downwards by an amount equal to the helix angle in order to have zero sideslip. However, it is quite common to have fully developed spins (with the spin axis vertical, not the flight path) with varying amounts of sideslip. Sideslip on a stalled wing will generally increase the lift on the wing toward which the sideslip occurs and reduce the lift on the opposite wing. It is easy to understand that a small amount of sideslip can produce a large rolling moment and thereby significantly alter the balance of rolling moments. These qualitative comments are quite cursory and the inquisitive student may wish to pursue these effects further. Reference 10.8 offers an expanded discussion, but to adequately discuss sideslip effects in any detail one must consider all three

moment equations and their coupling effects. The consideration of sideslip leads to the general conclusion that the rolling couple can be balanced over a wide range of angles of attack and spin rotation rates.
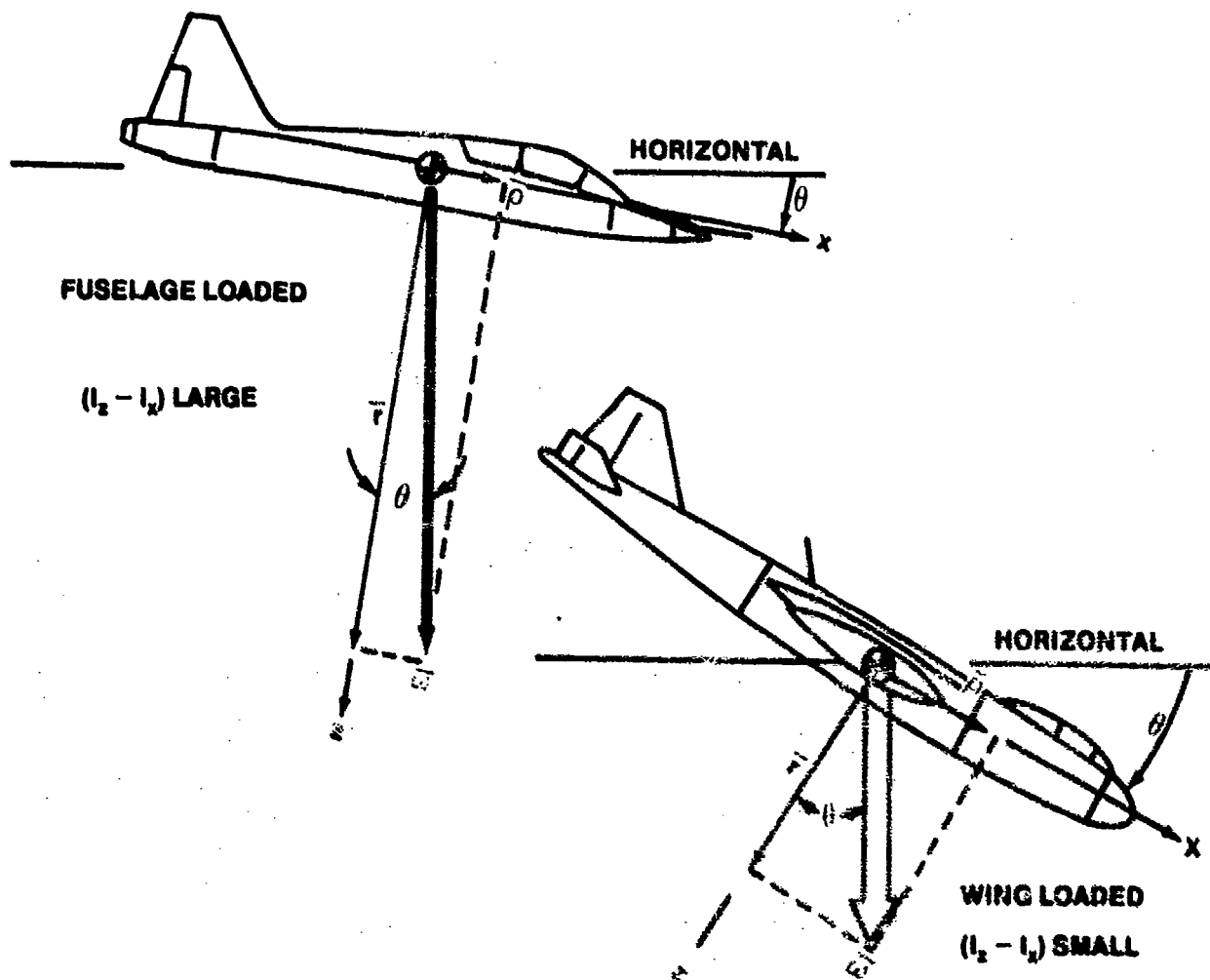

FIGURE 10.32. EFFECT OF MAGNITUDES OF I_z AND I_x ON SPIN ATTITUDE

10.3.7.8 Inverted Spins. Since PSG's are definitely uncontrolled aircraft motions, there is no guarantee that all spins will be upright. The test pilot particularly (and operational pilots as well) will continue to experience

inverted spins and PSG's which may be mainly inverted aircraft motions. As
Reference 10.12, Page 1, points out,

"...inverted spins cannot be prevented by handbook entries that 'the airplane resists inverted spins'."

It is, therefore, essential that the test pilot have some appreciation of the nature of the inverted PSG/spin. As usual, the analytical emphasis will necessarily be restricted to the fully developed spin, but the qualitative comments which follow also apply in a general way to other types of post-stall motion.

The most common pilot reaction to an inverted post-stall maneuver is, "I have no idea what happened! The cockpit was full of surprise, dirt, and confusion." Why? First, negative g flight is disconcerting in and of itself, particularly when it is entered inadvertently. But even experienced test pilots can be upset and their powers of observation reduced in an anticipated inverted spin. This disorientation usually takes one of two forms: (1) inability to distinguish whether the motion is inverted or upright or (2) inability to determine the direction of the spin. Each of these problems will be considered separately.

10.3.7.8.1 <u>Angle of Attack in an Inverted Spin</u>. The angle of attack in an inverted spin is always negative (Figure 10.33). It might appear that it would be easy to determine the difference in an upright or inverted spin; if the pilot is "hanging in the straps," it is an inverted spin. Such an "analysis" is accurate in some spin modes (the Hawker Hunter has an easily recognized smooth, flat mode such as this); however, if the motion is highly oscillatory, not fully developed, or a PSG, the pilot's tactile senses are just not good enough. If the aircraft has an angle of attack indicator, this is probably the most reliable means of determining whether the maneuver is erect or inverted. Lacking an angle of attack system, the pilot must rely on the accelerometer or his sensory cues, neither of which are easy to interpret. But what about determining spin direction?

UPRIGHT SPIN

+z

INVERTED SPIN

+z

α > 0 →

α < 0 →
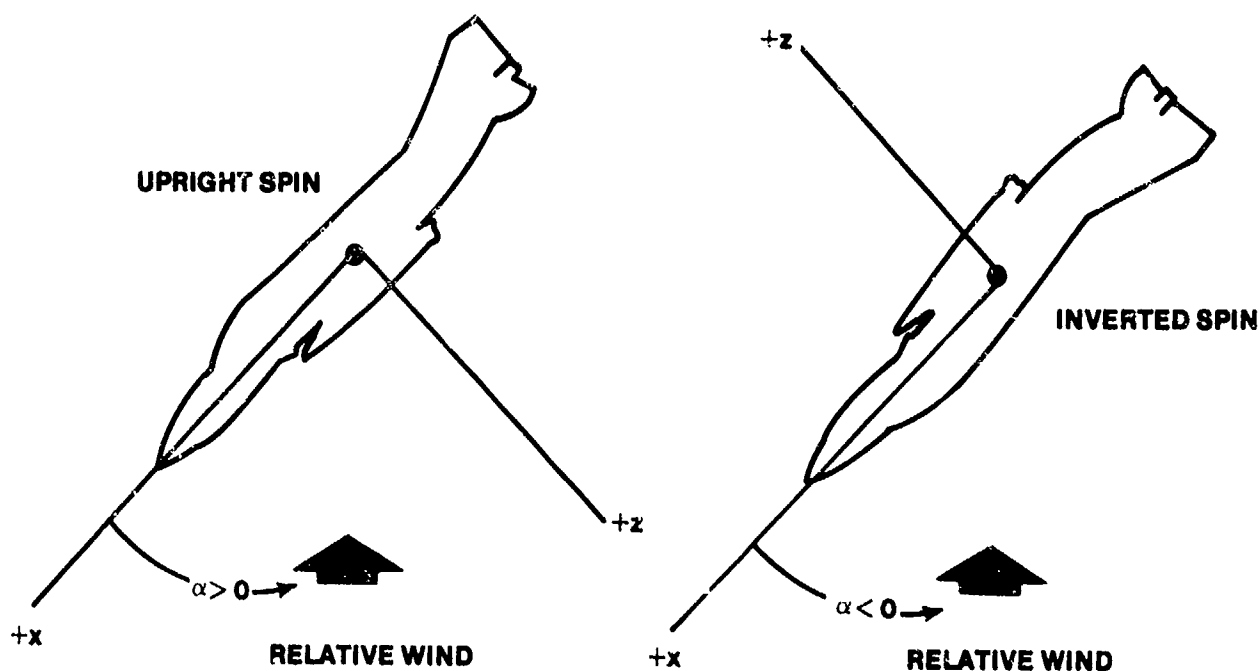
+x

RELATIVE WIND

+x

RELATIVE WIND

FIGURE 10.33. ANGLE OF ATTACK IN AN INVERTED SPIN

10.3.7.8.2 Roll and Yaw Directions in an Inverted Spin. Consider two identical aircraft, one in an upright spin and the other in an inverted spin as shown in Figure 10.34. Notice that the spin direction in either an upright or an inverted spin is determined by the sense of the yaw rate. Notice also that in an inverted spin the sense of the roll rate is always opposite that of the yaw rate. It is common for pilots to mistakenly take the direction of roll as the spin direction. The chances of making this error are considerably enhanced during a PSG or the incipient phase of the spin when oscillations are extreme. In steep inverted spins ($|\alpha|$ nearly equals $|\alpha_s|$) the rolling motion is the largest rotation rate and further adds to the confusion. However, there is a reliable cockpit instrument, the turn needle, which always indicates the direction of yaw. With such confusion possible, what about the previously obtained equations of motion? Is it necessary to modify them for the inverted spin?
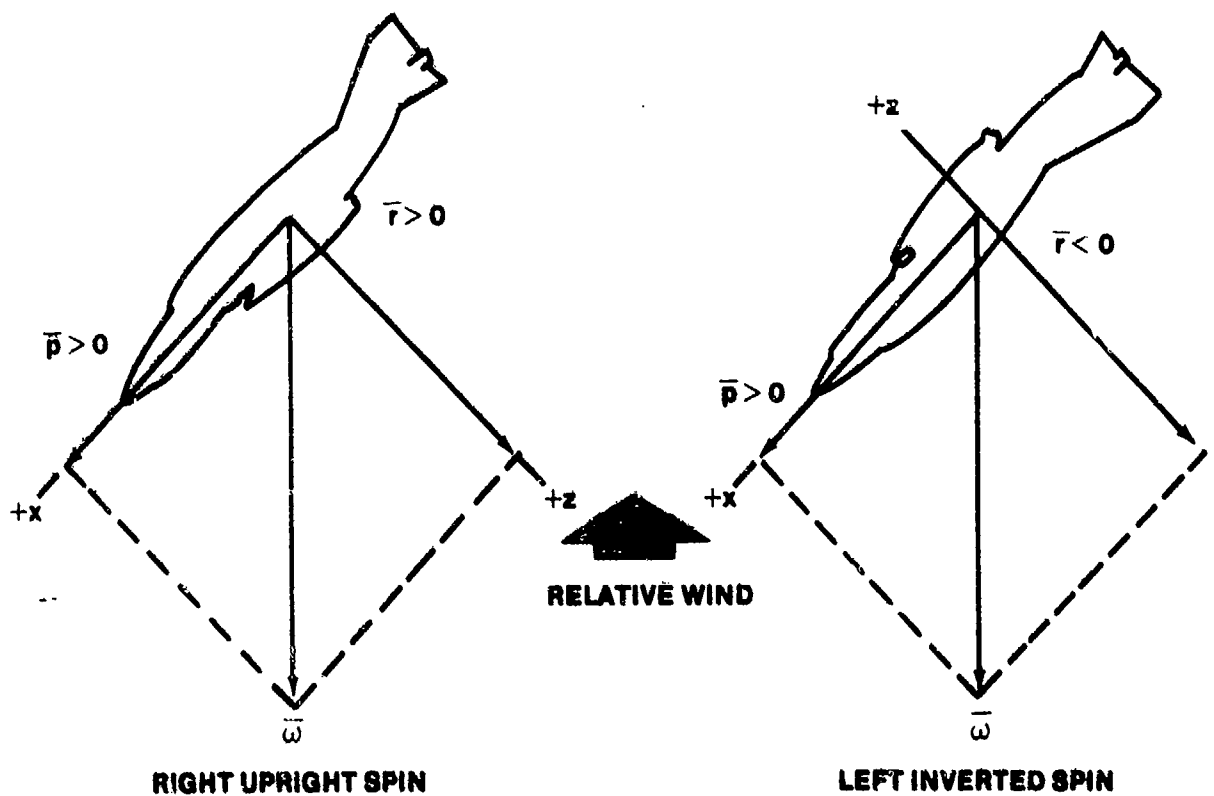
FIGURE 10.34. ROLL AND YAW RATES IN AN INVERTED SPIN

10.3.7.8.3 Applicability of Equations of Motions: All the equations previously described are directly applicable to the inverted spin. Of course, the differences in sign for angle of attack and the lack of aerodynamic data collected at negative angle of attack pose a significant practical problem in trying to do detailed analyses of the inverted spin. But for the qualitative purposes of this course, the equations of motion are usable. However, it is instructive to note the difference in the sense of the pitching moments between an upright and an inverted spin. Recall that in an upright spin the applied external pitching moment (dominated by the aerodynamic pitching moment) had to be negative to balance the inertial term, as Equation 10.44 for a fully developed spin shows.

$$G_y = -pr \, (I_z - I_x) \qquad (10.44)$$

10.64

But when p and r are of opposite signs, as in the inverted spin, the applied external moment must be positive. This fact is illustrated in Figure 10.35, where the mass of the aircraft is represented as a rotating dumb-bell.
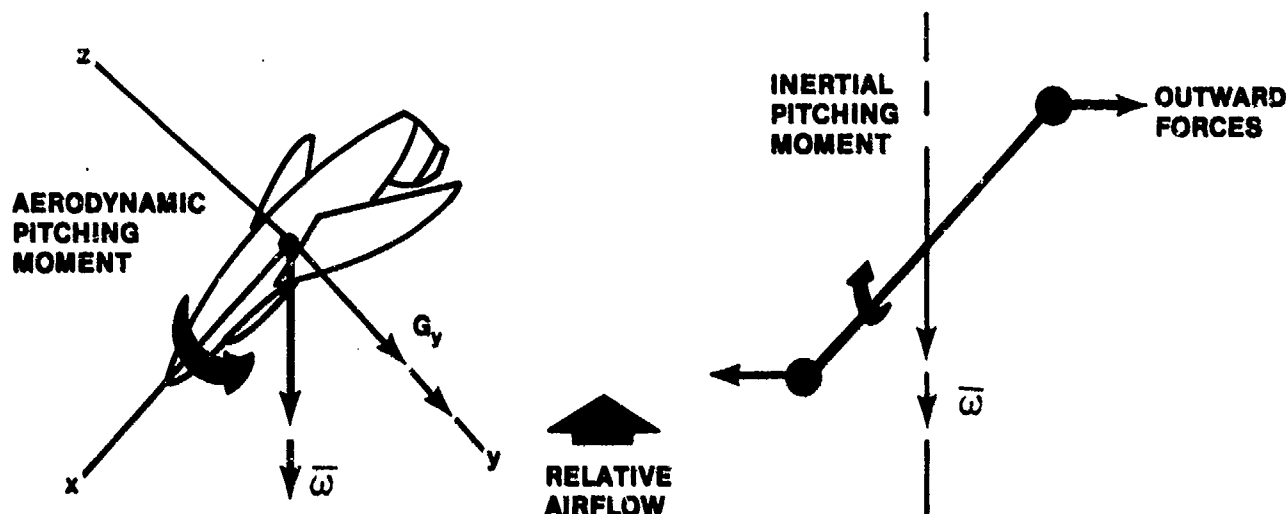

FIGURE 10.35. PITCHING MOMENTS IN AN INVERTED SPIN

It is apparent that in the inverted spin the external pitching moment is positive; that is, expressed as a vector, it lies along the positive y axis. As a final point, the recovery from PSG's/spins, both erect and inverted, must be examined in some detail.

10.3.8 Recovery

Obtaining developed spins today is generally difficult, but when obtained, the very factors that make this difficult may also make it difficult to recover from the spin. Current and future aircraft designs may be compromised too much for their intended uses to provide adequate aerodynamic control for termination of the developed spin; also, there is a problem of pilot disorientation associated with developed spins. As a result, the PSG and the incipient phase of the spin must be given more attention than they have received in the past, and preventing the developed spin through good design and/or proper control techniques has become a primary consideration.

Current aircraft have greater weight and appreciably larger moments of inertia about the y and z axes then those of World War II aircraft. With the resulting high angular momentum, it is difficult for a spin to be terminated as effectively as a spin in earlier airplanes by aerodynamic controls which are generally of similar size. Furthermore, controls which are effective in normal flight may be inadequate for recovery from the spin unless sufficient consideration has been given to this problem in the design phase.

10.3.8.1 Terminology. The recovery phase terminology was purposely omitted from previous discussion of spin phases for inclusion here. Referring to Figure 10.12, the recovery phase begins when the pilot initiates recovery controls and ends when the aircraft is in straight flight; however, there are several terms used to differentiate between the subparts of this phase.

10.3.8.1.1 Recovery. Recovery is defined as the transitional event from out-of-control conditions to controlled flight. In more useable terms, this period of time normally is counted from the time the pilot initiates recovery controls and that point at which the angle of attack is below α_s and no significant uncommanded angular motions remain. The key phrase in this expanded definition is "angle of attack below α_s;" once this objective is attained the aircraft can be brought back under control provided there are sufficient altitude and airspeed margins to maneuver out of whatever unusual attitude remains.

10.3.8.1.2 Dive Pullout and Total Recovery Altitude. The dive pullout is the transition from the termination of recovery to level flight. Total recovery altitude is the sum of the altitude losses during the recovery and dive pullout.

10.3.8.2 Alteration of Aerodynamic Moments. The balanced condition of the developed spin must be disturbed in order to effect a recovery, and prolonged angular accelerations in the proper direction are needed. Several methods for obtaining these accelerations are available but not all are predictable. Also, the accompanying effects of some methods are adverse or potentially hazardous. The general methods available for generating anti-spin moments follow with the applicable terms of the general equations also given.

Conventional means of spin recovery use flight controls to alter the aerodynamic moments (C_ℓ, $C_{m,b}$, and C_n); configuration changes are seldom used to accomplish spin recovery. The all-important question is "How should the flight controls be used to recover from a PSG or a spin?"

1. Modify Aerodynamic moments
   a. With flight controls
   b. Configuration changes (gear, flaps, strakes)

2. Reposition the aircraft attitude on the spin axis

$$\dot{p} = \frac{v^2}{2\mu K_x^2} \quad C_\ell \quad + \frac{I_y - I_z}{I_x} \quad q\,r \quad\quad\quad \frac{L_{other}}{I_x}$$

$$\dot{q} = \frac{v^2}{2\mu K_y^2} \quad C_{m,b} \quad + \frac{I_z - I_x}{I_y} \quad p\,r \quad - \frac{I_E\,\phi_E}{I_y}\,r \quad \frac{M_{other}}{I_y}$$

$$\dot{r} = \frac{v^2}{2\mu K_z^2} \quad C_n \quad + \frac{I_x - I_y}{I_z} \quad p\,q \quad + \frac{I_E\,\phi_E}{I_z}\,q \quad \frac{N_{other}}{I_z}$$

3. Variations in Engine Power

4. Spin chutes Spin Rockets

10.3.8.3 Use cf Longitudinal Control. The longitudinal control surface can only be effective if it can drive the angle of attack below α_s. Rarely is the elevator capable of producing this much change in pitching moment in a fully developed spin, but its use during a PSG or the incipient phase of a spin may well reduce angle of attack sufficiently. However, forward stick during a fully developed upright spin will merely cause many spin modes to progress to a higher rotation rate, which is also usually flatter. Model tests and computer studies should thoroughly investigate this control movement before it is recommended to the test pilot. Then a thorough flight test program must be conducted to confirm these predictions before such a recommendation is passed on to operational users.

10.3.8.4 Use of Rudder. Considering only the alteration of C_ℓ, $C_{m,b}$, or C_n by deflection of the appropriate control surfaces, the use of rudder to change C_n has proven to be the most effective in recovering from a developed spin.

Rudder deflection, if the rudder is not blanked out, produces a reduction in yaw rate which persists. The reduction in yaw rate reduces the inertia pitching couple and the angle of attack consequently decreases. Once the rotation rate has been reduced sufficiently, the longitudinal control can be used to reduce angle of attack below α_s.

Notice that the use of ailerons to produce an anti-spin rolling moment has not been discussed. Generally, in stalled flight the ailerons are not effective in producing moments of any significance, though they can still be the primary anti-spin control by causing a small change in bank angle and thereby reorienting the aircraft attitude on the spin axis so that the inertial terms operate to cause recovery.

10.3.8.5 Use of Inertial Moments. By using ailerons to reorient the aircraft attitude on the spin axis, a component of $\bar{\omega}$ can be generated on the y body axis, creating pitch rate, q. Pitch rate can then cause aircraft inertial moments to affect roll and yaw acceleration. Determining how the ailerons should be applied to reorient the aircraft attitude depends upon the relative magnitude of I_x and I_y. This can be seen from the roll and yaw acceleration equations listed below:

$$\dot{p} = \ldots + \frac{I_y - I_z}{I_x} q r \ldots$$

(10.48)

$$\dot{r} = \ldots + \frac{I_x - I_y}{I_z} p q$$

(10.49)

For instance, consider Equation 10.48 and a fuselage-loaded aircraft in a right, upright spin. $(I_y - I_z)/I_x$ is negative, while $\bar{r}$ is positive. In order to generate anti-spin roll acceleration (negative $\dot{p}$), then q must be positive. Similarly, q must be positive to generate anti-spin yaw acceleration (Equation 10.49). For a fuselage-loaded aircraft, the pitch rate must be positive in an upright spin (right or left) to develop anti-spin yawing and rolling acceleration. Aileron applied in the direction of the spin causes the aircraft body axes to tilt so as to produce a positive component of $\bar{\omega}$ along the y-axis (see Figure 10.36).

Another way to help achieve a positive pitch rate is to hold aft stick until the rotation rate begins to drop. This procedure is common in some fuselage-loaded aircraft, although it is unacceptable in others (F-104 for

example). However, the most important factor is the relative sizes of I_x and I_y. Considering that $(I_x - I_y)/I_z$ is approximately six times greater for the F-104 than for the T-28, it is little wonder that aileron is a more important spin recovery control in the F-104 than is the rudder.

A similar analysis of Equations 10.48 and 10.49 shows that aileron against the upright spin in a wing-loaded aircraft will produce an anti-spin yaw acceleration, but a pro-spin roll acceleration. Since wing-loaded aircraft generally spin more nose low than fuselage-loaded aircraft (with $p \cong r$), and since they generally are recoverable with rudder and elevator, aileron-against recovery procedures are rarely recommended.

10.3.8.6 **Other Recovery Means.** The other two terms which can produce anti-spin accelerations include engine gyroscopic terms and emergency recovery devices.

10.3.8.6.1 Variations in Engine Power. The gyroscopic terms are usually so small that they have little effect on recovery characteristics. Furthermore, jet engines often flame out during PSG or spin motions, particularly if the throttle is not at idle. So, although there are potential pitch and yaw accelerations available from the gyroscopic terms, NASA experience indicates that changes in engine power are generally detrimental to recovery.

10.3.8.6.2 Emergency Recovery Devices. Emergency recovery devices may take many forms - anti-spin parachutes attached to the aft fuselage, anti-spin parachutes attached to the wing tip, anti-spin rockets, strakes, etc. The design of such devices is a complex subject worthy of careful engineering in its own right. Certainly such design considerations are not the concern of test pilots, but the reliability of the device, its attachments, and its jettison mechanism are of vital concern. The pilot is also likely to be concerned with tests to validate this reliability.

10.3.8.6.3 Recovery from Inverted Spins. Recovery from inverted spins is generally easier than recovery from upright spins, particularly if the rudder is in undisturbed airflow. In fact many aircraft will recover from an inverted spin as soon as the controls are neutralized. In any case rudder opposite to the turn needle may be recommended, often in conjunction with aft stick. Some fuselage-loaded T-tailed aircraft may require anti-spin aileron. An analysis of Equations 10.48 and 10.49 shows that in an inverted spin aileron against the spin is the correct anti-spin control for a fuselage-loaded aircraft.
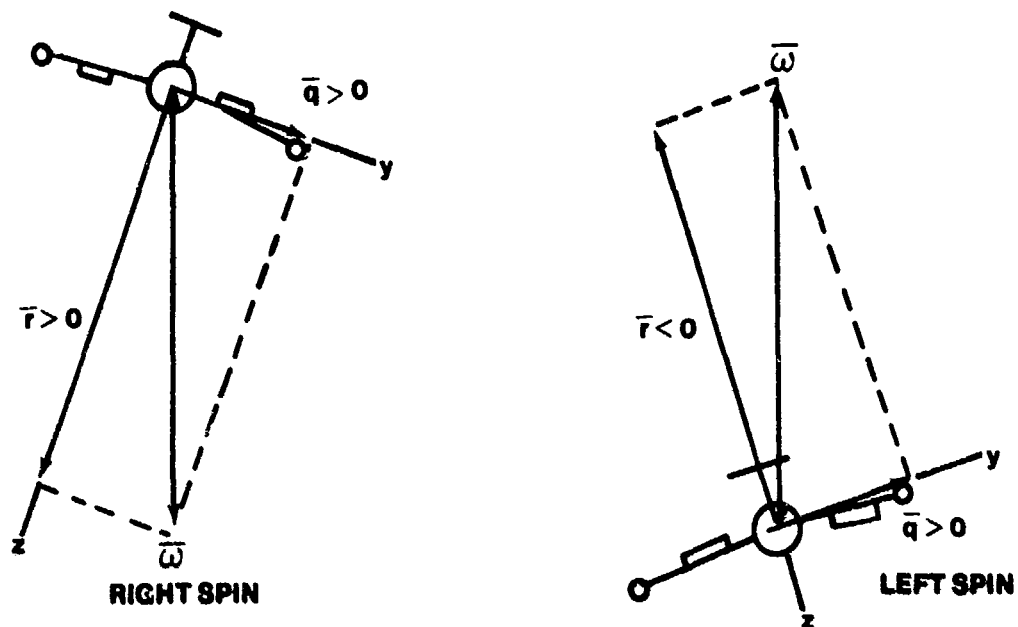
FIGURE 10.36. AILERON WITH RECOVERY PROCEDURE

10.3.9 Spin Theory Review

A brief review of some basic assumptions and prerequisites is in order. For a stabilized spin to exist, there must be a balance of moments (in particular, pitching moments). Therefore the sum of the inertial pitching moment $(\bar{M}_i)$ and the aerodynamic pitching moment $(\mathcal{M})$ must equal zero. For equilibrium, all accelerations must also be equal to zero, i.e., $\dot{p} = \dot{q} = \dot{r} = \dot{\omega}$ $= \dot{v} = 0$. For simplicity, assume a wings level spin with no sideslip (i.e., $\bar{q}$ $= 0 = \beta$; in reality, these are mutually exclusive assumptions). Since for an erect spin M_i is always positive (nose-up), it follows from the first assumption that $_a$ must therefore always be negative (nose-down). For this to occur, $C_m < 0$. As a corollary to this prerequisite, for stability in the spin along the pitch axis, C_{m_α} must also be negative, otherwise the aircraft would pitch itself up and out of the spin (as α increased, and $\bar{M}_i$ would

10.70

both increase). Two other important prerequisites discussed in the spin course are the requirements to have $\alpha > \alpha_{STALL}$ and a sustained yaw rate. Summarizing these assumptions and prerequisites for a stabilized, wings level spin:

a. $\bar{M}_i + \bar{\mathcal{M}} = 0$

b. $\dot{\bar{p}} = \dot{\bar{q}} = \dot{\bar{r}} = \dot{\bar{\omega}} = \dot{\bar{v}} = 0$

c. $\bar{q} = 0$

d. $\beta = 0$

e. $C_m < 0$

f. $C_{m_\alpha} < 0$

g. $\alpha > \alpha_{STALL}$

h. Sustained Yaw Rate

As shown in Figure 10.37, assume an aircraft in a stabilized, erect spin to the right. Resolving the spin vector, $\bar{\omega}$, into body axis rotations gives

$$\bar{p} = \bar{\omega} \cos \alpha \qquad (10.50)$$

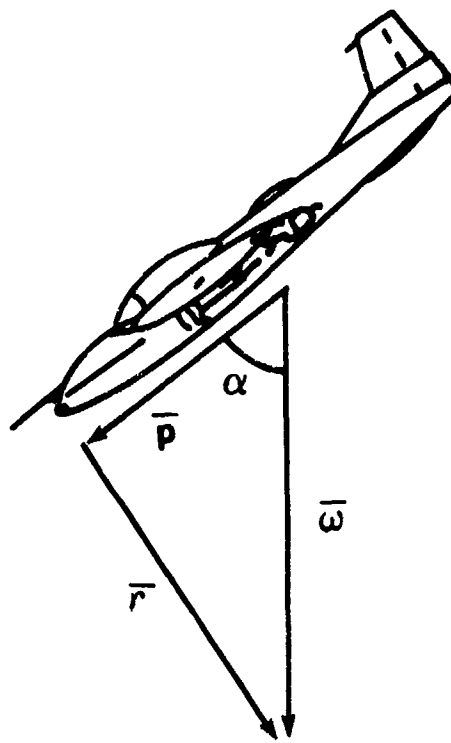$$\bar{r} = \bar{\omega} \sin \alpha \qquad (10.51)$$

FIGURE 10.37.   RESOLUTION OF SPIN VECTOR, $\bar{\omega}$

The three equations of motion used to describe an aircraft in a spin are:

$$G_x = \dot{p}I_x - qr\,(I_y - I_z) \tag{10.45}$$

$$G_y = \dot{q}I_y - rp\,(I_z - I_x) \tag{10.46}$$

$$G_z = \dot{r}I_z - pq\,(I_x - I_y) \tag{10.47}$$

where principal body axes have been assumed (i.e., $I_{xy} = I_{xz} = I_{yx} = 0$). G_x, G_y, and G_z are applied moments only and are therefore produced by aerodynamic moments $\mathscr{L}$, $\mathscr{m}$ and $\mathscr{n}$, respectively. Substituting and using the fact that $\dot{p} = \dot{q} = \dot{r} = 0$ for a stabilized spin yields:

$$\mathscr{L} = -qp\,(I_y - I_z) \tag{10.54}$$

$$\mathscr{m} = -rp\,(I_z - I_x) \tag{10.55}$$

$$\mathscr{n} = -pq\,(I_x - I_y) \tag{10.56}$$

10.72

An examination of the pitch equations, $\mathcal{M} = -rp(I_z - Ix)$, is in order. From the first assumption $(\mathcal{M} = -M_i)$ it is obvious that $M_i = rp\,(I_z - I_x)$. Substituting for r, p, the components of ω, $M_i = (\omega \sin \alpha)\,(\omega \cos \alpha)\,(I_z - I_x)$. Using the trigonometric identity, $\sin 2\theta = 2 \sin\theta \cos\theta$,

$$M_i = \frac{\omega}{2}\,(\sin 2\alpha)\,(I_z - I_x) = \omega^2\,\frac{(I_z - I_x)}{2}\,\sin 2\alpha \qquad (10.57)$$

Plotting M_i vs α, it is apparent that a curve, whose amplitude depends on the value $\omega^2\,(I_z - I_x)/2$ is obtained (Figure 10.38). (Intuitively, the strength of the inertial pitching moment is expected to increase as ω increases.):
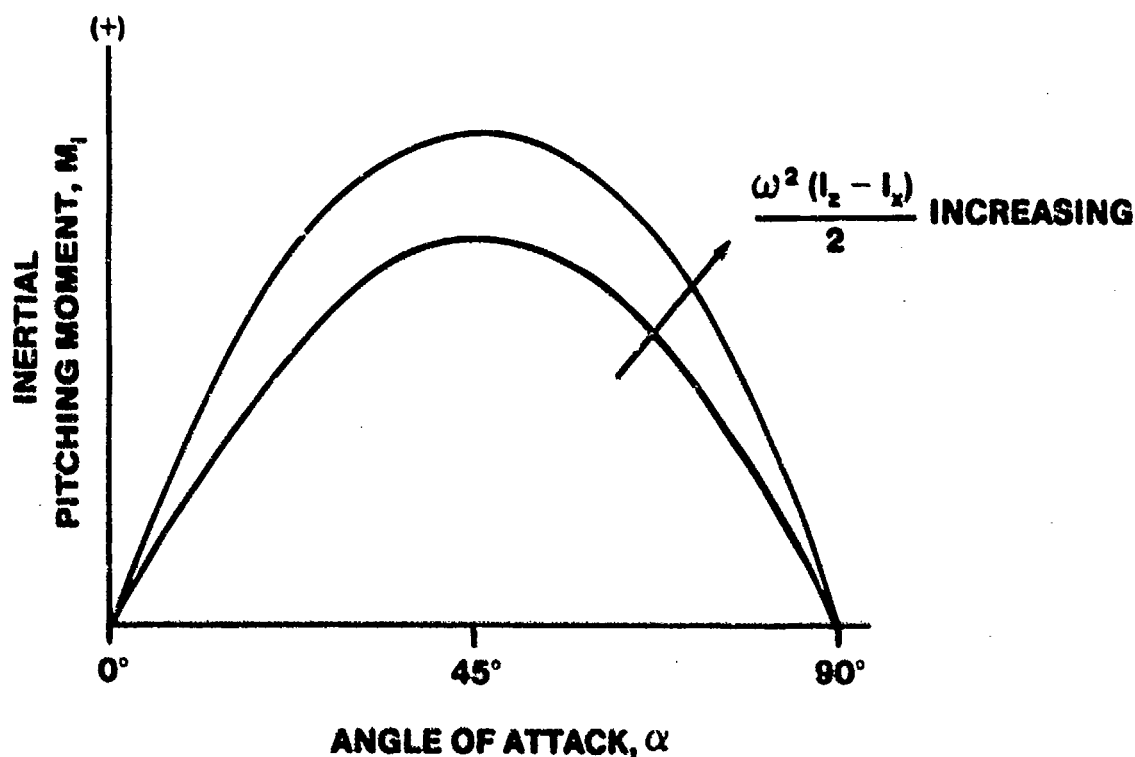

FIGURE 10.38. INERTIAL PITCHING MOMENT
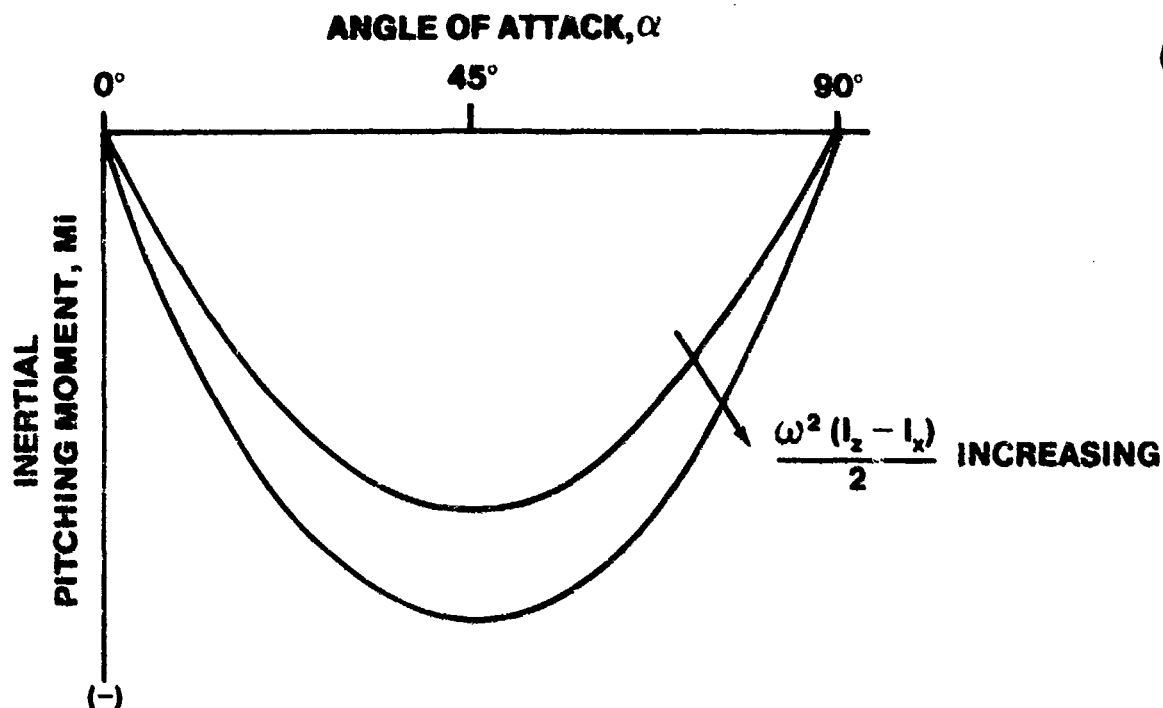
ANGLE OF ATTACK, α

FIGURE 10.39.   INERTIAL PITCHING MOMENT

For a stabilized erect spin of a "normal" aircraft, there are two prerequisites

$$C_m < 0 \text{ and } C_{m_\alpha} < 0.$$

Examining $\mathcal{M}$ gives $\mathcal{M} = C_m \, 1/2\rho \, V^2 Sc$. Therefore, a plot of $\mathcal{M}$ vs α yields Figure 10.40.
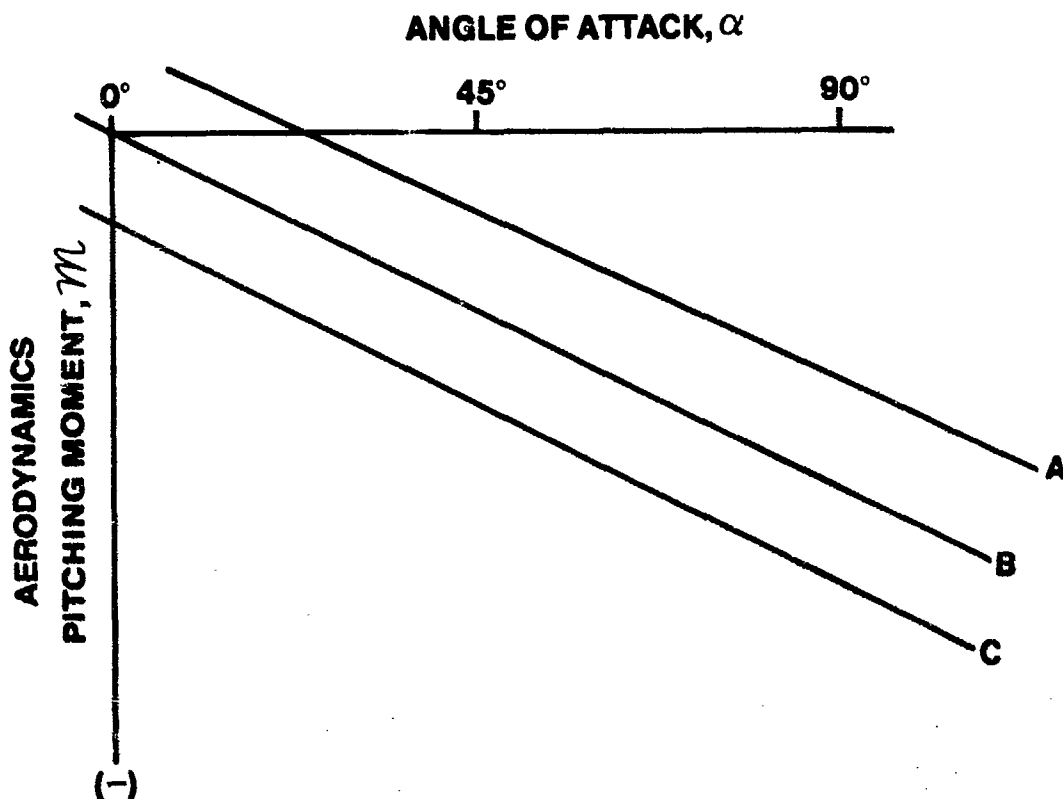
FIGURE 10.40.   AERODYNAMIC PITCHING MOMENTS

Curve A represents full aft stick.   Curve B represents neutral stick and Curve C represents full forward stick.   (Note: In the A-37, Curve B lies closer to Curve C than to Curve A.)   Superimposing the $\mathcal{M}$ and $-M_i$ curves vs α, the value of α where a stabilized erect spin can occur can be located, i.e., where $\mathcal{M} = -M_i$ (Figure 10.41).

At first glance, one might suspect an infinite number of values for α where a spin could occur, depending on how M_i is drawn which, in turn, depends on the choice of a value of ω, the spin rate.   However, the pitch axis is not the only axis involved and consideration must be given to the yaw and roll axis stabilities to determine the value of α and ω for a stabilized spin. That analysis is conducted using rotary balance wind tunnel data and is not considered here.   The purpose here is to examine the effects on the spinning aircraft once the stabilized conditions are known.
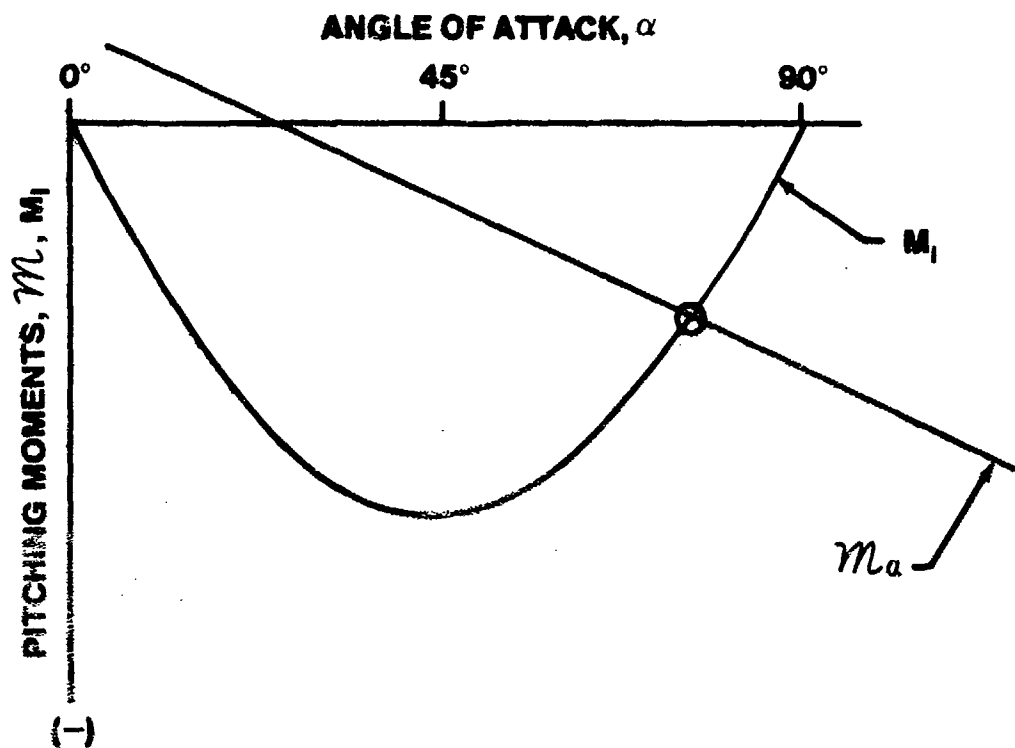
ANGLE OF ATTACK, α

FIGURE 10.41.   INERTIAL AND AERODYNAMIC PITCHING MOMENTS

The statement, "flatter pins spin faster", bears examination. Intuitively, this seems logical since the flatter the spin becomes, (i.e., α increases) a more nose-down moment is created due to $\mathcal{M}$. To remain stabilized the aircraft must spin faster to generate a large nose-up moment from M_i. This can also be seen by referring to Figure 10.42.

Assuming the $\mathcal{M}$ curve doesn't change, i.e., holding the stick fixed, the spin occurs at point A for one value of ω and α. If the spin rate can be stabilized at a higher rate (remember yaw and roll stabilities come into play) then without changing $\mathcal{M}$, the aircraft must flatten out to point B. Also, if the spin became flatter for whatever reason, a new and higher spin rate would develop to compensate. Hence, the flatter the spin, the faster the spin and vice versa.
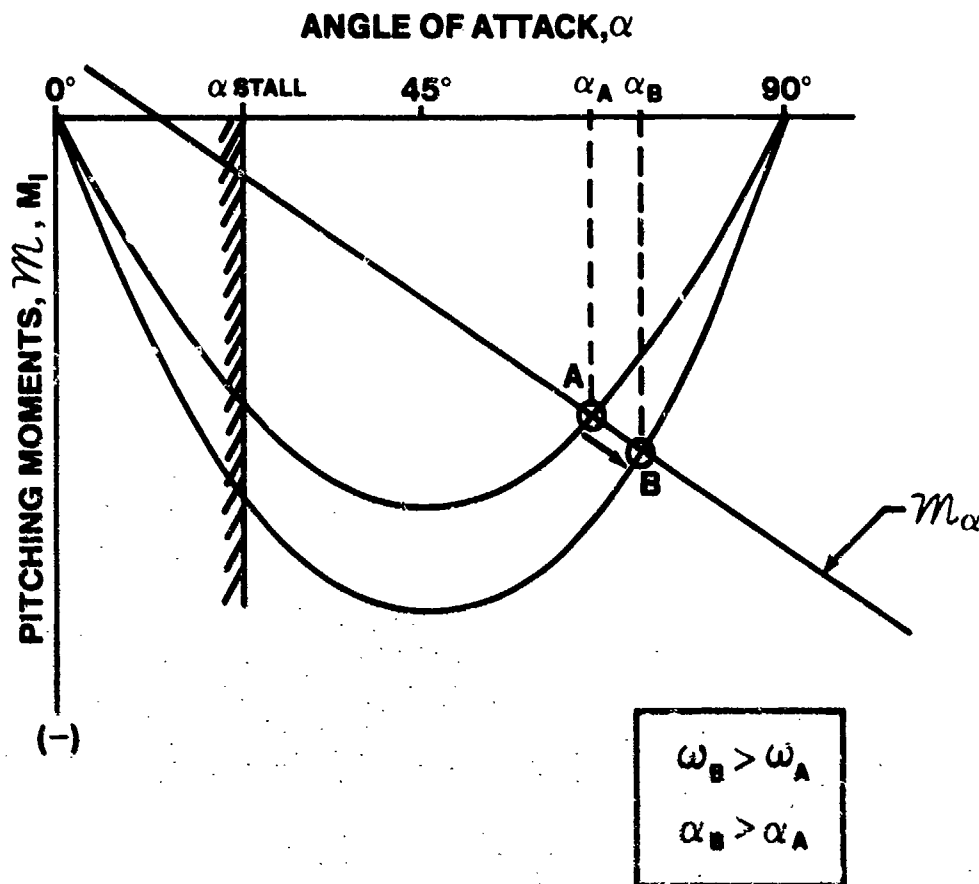
ANGLE OF ATTACK, α

FIGURE 10.42. EFFECT OF ANGLE OF ATTACK ON SPIN RATE

Next, the effect of forward stick on the spin mode must be examined. First of all, two points must be considered: (1) the elevator remains effective in the A-37 for generating some pitching moment and (2) the aircraft seeks to maintain the equilibrium angle of attack existing before the control input. An explanation of the effects is shown in Figure 10.43.

Two curves are shown depicting $\mathcal{M}$ vs α for full aft and full forward stick. During an erect spin in the A-37, the stick is held full aft and thus the spin occurs at Point A. If the stick is moved slowly to the full forward position, the aircraft will seek a new equilibrium spin mode. The aircraft tries to maintain the initial AOA (α_A), but because the elevator is still somewhat effective, α can be reduced only a slight amount. Because more nose-down aerodynamic pitching moment has been generated by moving the stick full forward, (even though α has decreased slightly) the inertial pitching

moment must also increase in magnitude in order to reach equilibrium. But M_i can only increase by allowing the spin rate, ω, to increase. The elevator is not effective enough to decrease α all the way to α_c, which is still on the original spin rate curve. Therefore, α decreases only slightly to α_B and the aircraft must spin faster to compensate, i.e., at Point B. Note that now there is a seeming contradiction, i.e., the aircraft is spinning steeper and faster, however, this is due to the fact that the $\mathcal{M}$ curve along which the aircraft must operate changed. In the previous discussion (flat and fast) the curve was held constant. Summarizing this effect, full forward stick will create the fastest spin mode at a lower α and full aft stick will create the slowest spin mode at a higher α. This explains why aft stick is important in a recovery; it slows the spin down (along with opposite rudder) thereby reducing M_i to a point where the elevator has enough authority to overcome it (i.e., $|m| > |M_i|$) and pitch the aircraft down out of the spin.
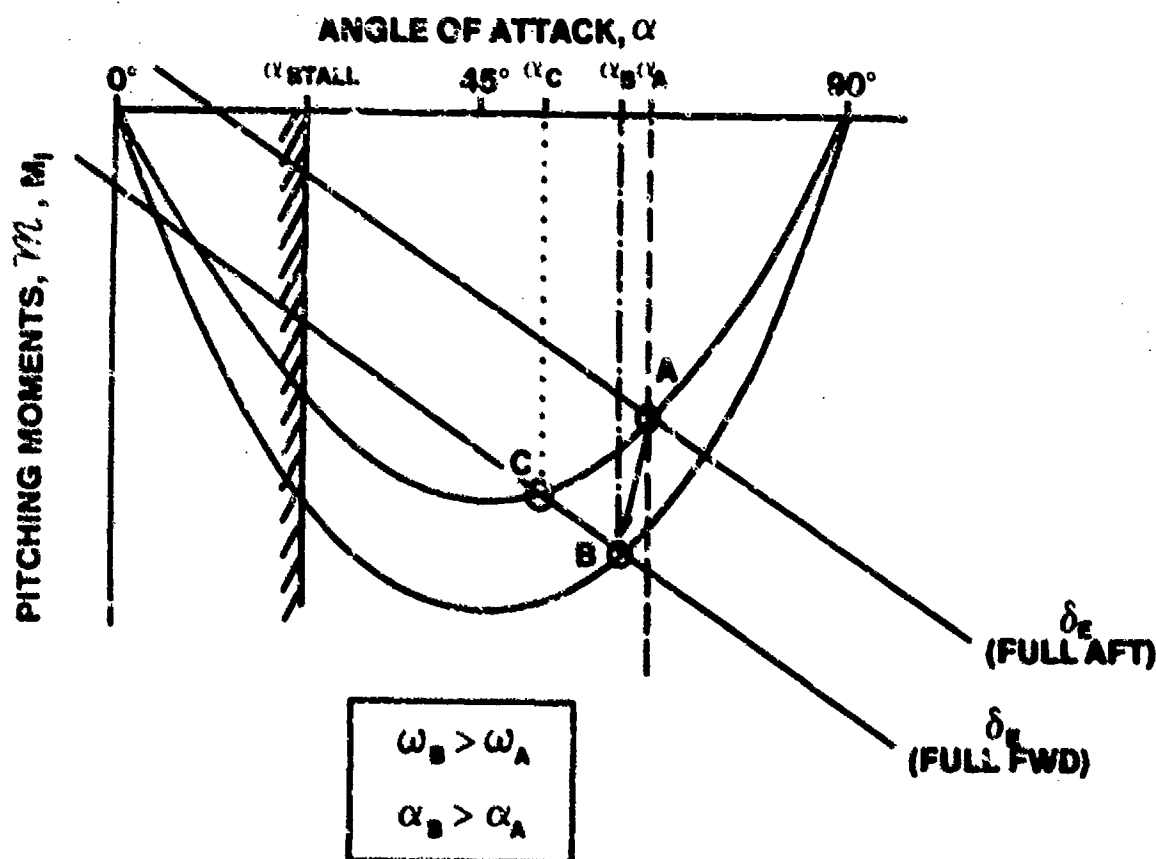

FIGURE 10.43.   EFFECT OF STICK POSITION ON SPIN RATE

Finally, the use of ailerons in a spin must be examined. To do this it must be understood that use of the ailerons uses roll to reorient the aircraft along the spin axis slightly, thereby creating a pitch rate, q. This pitch rate then couples in the equations of motion to create a yaw acceleration or deceleration, depending on the aircraft's inertial loading. Ailerons with the turn needle always create a positive pitch rate, regardless if the aircraft is erect or inverted. The equation of motion of importance is the yaw acceleration equation

$$\dot{r} = \frac{n}{I_z} + pq\left(\frac{I_x - I_y}{I_z}\right)$$

For a wing-loaded aircraft like the A-37, $I_x > I_y$. Considering an erect spin to the right, r and p are positive and aileron with the turn needle (i.e., right aileron) causes q to be positive. Pro-spin rudder is held until recovery, thus N_a is positive. Therefore, r is positive and is accelerating since $\dot{r}$ is also positive. From the previous discussion (faster/flatter), since putting in aileron increases ω but has no appreciable effect on the m curve, α must therefore increase as aileron is applied in the direction of the spin. Typically in the A-37, aileron with the spin will increase the yaw rate 10-15% and α will increase approximately 10°.

Admittedly, this is a simplified analysis. There are many more complex interrelationships occurring in the other two axes of motion in much the same way as in the pitch axis. However, this simplified view is still sound and should promote understanding of what occurs in a stabilized spin.

10.4 HIGH ANGLE OF ATTACK FLIGHT TESTS

10.4.1 Stall Flight Tests

Stalls, a familiar maneuver mastered by every pilot when first learning to fly, must not be taken for granted in a test program. There is a rather large collection of examples from flight test history to document the need for caution. Designs that combine an inherent pitchup tendency with measurable spin characteristics have contributed much to these examples. Stalls are usually first demonstrated by a contractor pilot, but it is possible for a military test pilot to find himself doing the first stalls in a particular

configuration, especially on test bed research programs where frequent modifications and changes are made after the vehicle has been delivered by the contractor.

The cautious approach starts with good preplanning. Discussion with the appropriate engineering talent of the predicted stall characteristics, and development of the most promising recovery technique for each stage of the stall, including possible post-stall gyrations is a necessity. In marginal cases, a suggestion for further wind tunnel testing or other alternative investigations might be warranted. The most favorable loading and configuration to be used in the initial stages must be determined. Stall and spin practice in trainer aircraft will enhance pilot performance during any out-of-control situations that might develop.

If pitchup or other control problems seem remotely possible, the first runs should terminate early in the approach to the stall and the data carefully examined (on the ground) for trends such as lightening or reversal of control, excessive attitudes, or sink rates. Advancing this data systematically on subsequent flights and avoiding the mistake of suddenly deciding in flight, because things are going well, to take a bigger step than planned is a necessity.

Stall characteristics must be evaluated in relation to their influence on mission accomplishment. Thus, both normal and accelerated stalls must be performed under entry conditions which could result from various mission tasks. However, prior to evaluating stalls entered from these conditions, a more controlled testing approach should be employed. This approach allows lower deceleration rates into the stall and lower pitch attitudes at the stall, thereby reducing chances for "deep-stall" penetration without adequate buildup. After the controlled stall investigation, if stall characteristics permit, simulated inadvertent stalls should be investigated under conditions representative of operational procedures.

10.4.2 The Controlled Stall Test Technique

The easiest and safest approach to controlled stall testing is to divide the investigation into three distinct parts:

1. Approach to the stall
2. Fully developed stall
3. Stall recovery

10.4.2.1 Approach to Stall. During this phase of the investigation, adequacy of stall warning and retention of reasonable airplane controllability are the primary items of interest. Assessment of stall warning requires subjective judgement by the pilot. Only the pilot can decide when he has been adequately warned. Warning must occur sufficiently in advance of the stall to allow prevention of the stall by normal control applications after a reasonable pilot reaction time. However, stall warning should not occur too far in advance of the stall. For example, it is essential that stall warning for approach configuration occur below normal approach speed. Reference 10.3 specifies definite upper and lower airspeed limits within which warning should occur. Stall warning which occurs too early is not only annoying to the pilot but is meaningless as an indication of proximity to the stall.

The type of stall warning is very important. Primary stall warning is generally in the form of airframe buffet, control shaking, or small amplitude airplane oscillations in roll, yaw, or pitch. Other secondary cues to the approach of the stall may be high pitch attitude, large longitudinal control pull forces (of course, this cue can be destroyed by "trimming into the stall"), large control deflections or sluggish control response. In any case, stall warning, whether natural or artificial, should be unmistakable, even under conditions of high pilot workload and stress and under conditions of atmospheric turbulence. If an artificial stall warning device is installed, approach to the stall should be evaluated with the device operative and inoperative to determine if the device is really required for normal operations.

During this phase of the evaluation, the test pilot must evaluate stall warning with the intended use and operational environment in mind. He must remember that he is specifically looking for the stall warning under controlled conditions. The operational pilot probably will not be. Will the operational pilot, preoccupied by other tasks and not concentrating on stalls, recognize the approach of a stall and be able to prevent it?

The general flying qualities of the airplane should be investigated during the approach to the stall as well as stall warning characteristics. Longitudinal, lateral, and directional control effectiveness for maintaining a desired attitude may deteriorate significantly during the approach to the

stall. Loss of control about any axis such as uncontrollable pitch-up or pitch-down, "wing drop," or directional "slicing" may define the actual stall. During the approach to the stall, the test pilot should be particularly aware of the amount of longitudinal nose-down control available because of the obvious influence of this characteristic on the ability to "break" the stalled condition and make a successful recovery.

This phase of stall investigation usually begins with onset of stall warning and ends at the stall, therefore the test pilot will certainly be concerned with the manner in which the airplane stalls and the ease of recovery. However, primary emphasis is placed on obtaining an accurate assessment of stall warning and general flying qualities during the approach to the stall. During initial investigations, it may be prudent to terminate the approach short of the actual stall, penetrating deeper and deeper with each succeeding approach until limiting conditions or the actual stall are reached. In addition, the rate of approach should be low initially, approximately one knot per second for normal stalls and two knots per second for accelerated stalls. As experience is gained, deeper penetrations at faster deceleration rates must be performed unless safety considerations dictate otherwise.

The test pilot should record at least the following data during the approach to the stall:

    a.   Airspeed, angle of attack, and altitude at stall warning

    b.   Type and adequacy of stall warning

    c.   Longitudinal control force at stall warning (either measured or estimated)

    d.   Qualitative comments regarding controllability and control effectiveness

    e.   Aircraft weight

10.4.2.2 Fully Developed Stall. Stall has been defined as the minimum steady speed attainable, or usable, in flight. This minimum may be set by a variety of factors, for example:

    a.   Reaching $C_{L_{max}}$ – the conventional stall

    b.   Insufficient longitudinal control to further decrease speed – lack of elevator power

c. Onset of control problems (Loss of control about any axis)

    (1) Pitchup
    (2) Insufficient lateral-directional control to maintain attitude
    (3) Poor dynamic characteristics

d. Back-side problems

    (1) High sink rate
    (2) Insufficient wave-off capability
    (3) Excessive pitch attitude

During this phase of the investigation, the primary objective is to accurately define the stall and the associated airplane behavior. The stall should be well-marked by some characteristic, such as pitch-up or pitch-down or lateral or directional divergence. In general, any pitch-up or directional divergence at the stall is undesirable because pitch-up may precipitate a deep stall penetration and directional divergence may lead to a spin. Pitch-down at the stall and lateral divergence may be acceptable. However, severe rolling, pitching, or yawing or any combination of the three are obviously poor characteristics.

Control effectiveness as evidenced by the pilot's ability to control or induce roll, pitch, or yaw should be evaluated in the stall, if airplane behavior permits this to be done safely. Obviously, control effectiveness should be evaluated with a suitable build-up program. Initially, control inputs only large enough to effect an immediate coordinated recovery should be used. As experience is gained, the airplane should be maintained in the stalled condition for longer and longer periods of time, and the effectiveness of all controls evaluated with larger and larger control deflections.

Actual flight test techniques to be used during stall testing must be agreed upon by the contractor, the System Program Office (SPO) and the flight test center performing the tests. Two flight test methods for defining the stall and the associated airplane behavior are presented below.

10.4.2.2.1 Level Flightpath Method. This method, involving a level flightpath, is an older method that is valid only for unaccelerated stalls. It has several disadvantages that limit its application, but in certain cases such as VSTOL testing or initial envelope extension it might prove useful. It has been largely replaced by the second method that involves a curved flightpath and is valid for both accelerated and unaccelerated stalls (Figure 10.44).
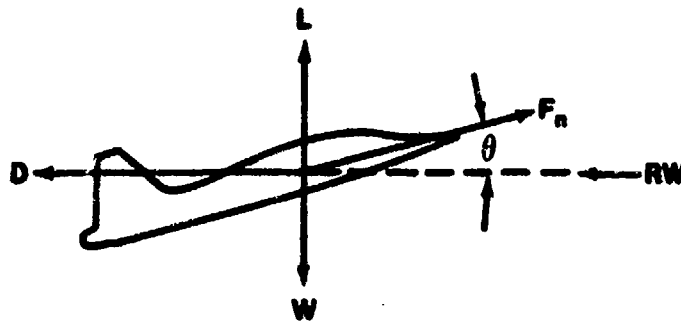
FIGURE 10.44. LEVEL FLIGHT PATH METHOD

$L + F_n \sin \theta = W$ and the flightpath is straight. In order to slow the aircraft to stall speed, however, an acceleration (a_D) in the drag direction must be obtained by adjustment of thrust or drag such that D is greater than $F_n \cos \theta$. This represents a disadvantage of the method, since a particular trim power or drag configuration cannot be maintained to the stall.

10.4.2.2.2 Curved Flightpath Method. Reference 10.3, Paragraph 6.2.2, requires that stall speed (V_s) be defined at 1-g normal to the flightpath, and that the aircraft be initially trimmed at approximately 1.2 V_s, after which trim and throttle settings remain constant. To achieve these requirements, once the trimmed conditions have been set the aircraft pitch attitude is increased to achieve a slight climb (less than 500 FPM), so as to initiate a bleed rate of one or two knots per second. Experience has shown that undesirable dynamic effects are encountered if bleed rates much in excess of one or two knots per second are used. Based on experience, arbitrary maximum bleed rates of one knot per second for unaccelerated stalls, and two knots per second for accelerated stalls have been set. Once the initial climb has been established, pitch attitude is controlled so as to maintain or increase the rate of climb (1500 FPM maximum). This technique conservatively assures a stall speed at 1-g normal to the flightpath. Stall speeds occurring at load factors other than 1-g normal to the flightpath shall be corrected as described in Reference 10.3, Paragraph 6.2.2. A tolerance of $\pm$ 500 feet from desired stall altitude is allowed.

The test pilot should record at least the following data regarding the stall:

1. Airspeed, angle of attack, and altitude at stall

2. Load factor

3. Characteristic which defines the stall

4. Longitudinal control force at the stall (either measured or estimated). The ratio of longitudinal control forces at stall and stall warning is a rough indication of longitudinal stability in the high angle of attack region and an indication of the ease of inadvertent stalling.

5. Qualitative descriptive comments

6. Aircraft weight

10.4.2.3 Stall Recovery. During this phase of the investigation, primary items of interest are the ease of recovery (the pilot's task), general flying qualities during the recovery, altitude required for recovery and the determination of an optimum recovery technique.

The recovery is started when the stall or minimum steady speed has been attained. For a conventional stall this is indicated by the inability to maintain the desired load factor -- usually a sudden break is apparent on the cockpit accelerometer.

The goal of the recovery must be specified. For example, the goal of recovery for configurations commensurate with combat maneuvering may be to regain sufficient control effectiveness about all three axes to perform offensive or defensive maneuvering tasks; the attainment of level flight may not be critical in these configurations. The goal of recovery for takeoff and approach configurations should be attainment of level flight with a minimum loss of altitude and the regaining of sufficient control effectiveness to safely maintain stall-free conditions. In each case, the test pilot must clearly define "stall recovery."

In a test program, all promising recovery procedures consistent with the objectives should be tried. It is important to have the recovery specified in detail before each drill -- not to wait until the stall breaks to decide what procedure is to be used. There are no iron-clad rules for recovery -- a "standard procedure" such as full military power could be disastrous in certain vehicles. Keep the instrumentation running throughout the recovery until the goal has been attained. In the case of minimum altitude loss, this

would be when rate of descent is zero and the aircraft is under control (the altimeter is the first indication of R/C = 0).

During initial investigation, the stall recovery procedures specified in pertinent publications should be utilized and the ease of effecting recovery evaluated. If no procedure has been developed, initial recovery must be accomplished with a "preliminary" technique formulated from all available technical information. As experience is gained, various modifications to the recovery procedure should be made until an optimum procedure is determined. In arriving at an optimum procedure for use by the operational pilot, the test pilot must not only consider the effectiveness of the technique (in terms of altitude lost or maneuverability regained), but must also consider the simplicity of the technique.

The test pilot should record at least the following data regarding stall recovery:

1.   Qualitative comments on ease of recovery

2.   Optimum recovery technique

3.   Altitude lost in recovery

4.   Qualitative comments on control effectiveness

10.4.3 Spin Flight Tests

10.4.3.1 <u>Spin Project Pilots Background Requirements</u>. Under current stall/post-stall/spin demonstration specification (Reference 10.4, Paragraph 3.3), military pilots will participate on high angle of attack investigations concurrently with the contractor's pilots. Therefore, it is imperative that the military test pilots assigned to a high angle of attack investigation be thoroughly familiar with all available background information concerning the investigation. This paragraph summarizes the preparation required for post-stall/spin investigations. The discussion is purposely general in nature; it will not specifically address the tests flown in the curriculum at the USAF Test Pilot School. These flights are described in detail in the current Flying Qualities Phase Planning Guide.

The methods available to the modern test pilot for pre-flight test spin research are:

1. Conventional wind tunnel

2. Dynamic models

   a) Wind tunnel free flight model
   b) Radio controlled model

3. Vertical spin tunnel

4. Rotary balance

5. Simulator

10.4.3.1.1 Conventional Wind Tunnel. Literature research should begin with the best and most current wind tunnel data available. Take careful note of any configuration or mass changes which were made since the available wind tunnel data were obtained. Look questioningly at the angle of attack and angle of sideslip ranges tested in the tunnel. Go over this data very carefully with the flight test engineers and try to ascertain the probable spin modes and optimum recovery techniques for each of them, as well as the optimum recovery procedure for post-stall gyrations if one is known. Start looking, even at this stage, for the simplest recovery technique possible. If possible, obtain analytical data to confirm or deny the possibility of using a common recovery procedure for both post-stall gyrations and spins (Reference 10.4, Paragraph 3.4.3). Spin test reports of similar aircraft should be reviewed thoroughly, but care must be exercised in extrapolating results. The spin characteristics of aircraft which are quite similar in appearance can vary drastically. Attempt to predict the effect that various loadings and configurations will have on post-stall/spin characteristics so that initial tests can be planned conservatively. As examples the A ` has loadings from which recovery is not acceptable (10.13:6) and highly asymmetric loadings in the A-7D may prolong recovery to an unacceptable degree. Flight tests of the A-7D were not performed with loadings of greater than 13,000 foot-pounds of asymmetry (10.14:11).

10.4.3.1.2 <u>Dynamic Mode Techniques</u> (10.15:13-2). As a result of the complexity of the stall/spin problem, and the lack of proven alternate predictive methods, the most reliable source of information on stall/spin characteristics prior to actual flight tests of the particular airplane has been tests of dynamically scaled airplane models. A properly scaled dynamic model may be thought of as a simulator with the proper values of the various aerodynamic and inertial parameters.

Several unique dynamic model test techniques for stall/spin studies have been developed including: (1) the wind-tunnel free-flight technique, (2) the outdoor radio-controlled model technique, and (3) the spin-tunnel test technique.

10.4.3.1.2.1 <u>Model Scaling Considerations</u> (10.15:13-2). Dynamic models must be scaled in each of the fundamental units of mass, length, and time in order to provide test results that are directly applicable to the corresponding full-scale airplane at a given altitude and loading condition. As a result of scaling, the motions of the model are geometrically similar to those of the full-scale airplane and motion parameters can also be scaled.

Some limitations of the dynamic model test techniques are apparent. For example, the model is tested at a value of Reynolds number considerably less than those of the full-scale airplane at comparable flight conditions. Although the linear velocities of the model are smaller than full-scale values, the angular velocities are greater than full-scale values.

The discrepancy in Reynolds number between model and full-scale airplane can be an important factor which requires special consideration for stall/spin tests. During spin-tunnel tests, large Reynolds number effects may be present which cause the model to exhibit markedly different characteristics than those associated with correct values of Reynolds number.

The fact that the angular velocities of the model are much faster than those of the airplane poses special problems with regard to controllability of the model for certain techniques. Because the human pilot has a certain minimum response time, it has been found that a single human pilot cannot satisfactorily control and evaluate dynamic flight models.

The stall and spin of an airplane involve complicated balances between the aerodynamic and inertial forces and moments acting on the vehicle. In order to conduct meaningful tests with dynamic models, it is important that

these parameters be properly scaled. Simply scaling dimensional characteristics without regard to other parameters will produce erroneous and completely misleading results.

As a result of the shortcomings of theoretical methods, the most reliable source of information on stall/spin characteristics prior to full-scale flight tests has been tests of dynamically scaled models.

10.4.3.1.2.2 The Wind-Tunnel Free-Flight Technique (10.15:13-2). The wind-tunnel free-flight technique, is used specifically to provide information on flight characteristics for angles of attack up to and including the stall. The test setup for this model test technique is illustrated by the sketch shown in Figure 10.45. Two pilots are used during the free-flight tests. One pilot controls the longitudinal motions of the model. The second pilot controls the lateral-directional motions of the model. The model is powered by compressed air, and the level of thrust is controlled by a power operator. The human pilots do not sense accelerations as the pilot of an airplane does, and must therefore, fly with sight cues as the primary source of information.

The cable attached to the model serves two purposes. The first purpose is to supply the model with compressed air, electric power for control actuators, and control signals. The second purpose of the cable is concerned with safety. A portion of the cable is a steel cable that passes through a pulley above the test section. This part of the flight cable is used to catch the model when a test is terminated or when an uncontrollable motion occurs. The entire flight cable is kept slack during the flight tests by a safety-cable operator who accomplishes this job with a high-speed pneumatic winch.

The model incorporates limited instrumentation for measurements of motion and control deflections.

The wind-tunnel free-flight technique can produce valuable information during studies of flight motions at high angles of attack and at the stall. Various phases of a typical investigation would include: (1) flights at several angles of attack up to and including the stall to evaluate dynamic stability characteristics, (2) an evaluation of pilot lateral control techniques at high angles of attack, and (3) an evaluation of the effects of stability augmentation systems.

The wind-tunnel free-flight technique has several inherent advantages: (1) because the tests are conducted indoors, the test schedule is rot subject to weather conditions; (2) the tests are conducted under controlled conditions and a large number of tests can be accomplished in a relatively short period of time; (3) airframe modifications are quickly evaluated and (4) models used in the technique are relatively large (11.10-scale for most fighter configurations) and can, therefore, be used in force tests to obtain static and dynamic aerodynamic characteristics for analysis of the model motions and as inputs for other forms of analysis, such as piloted simulators.
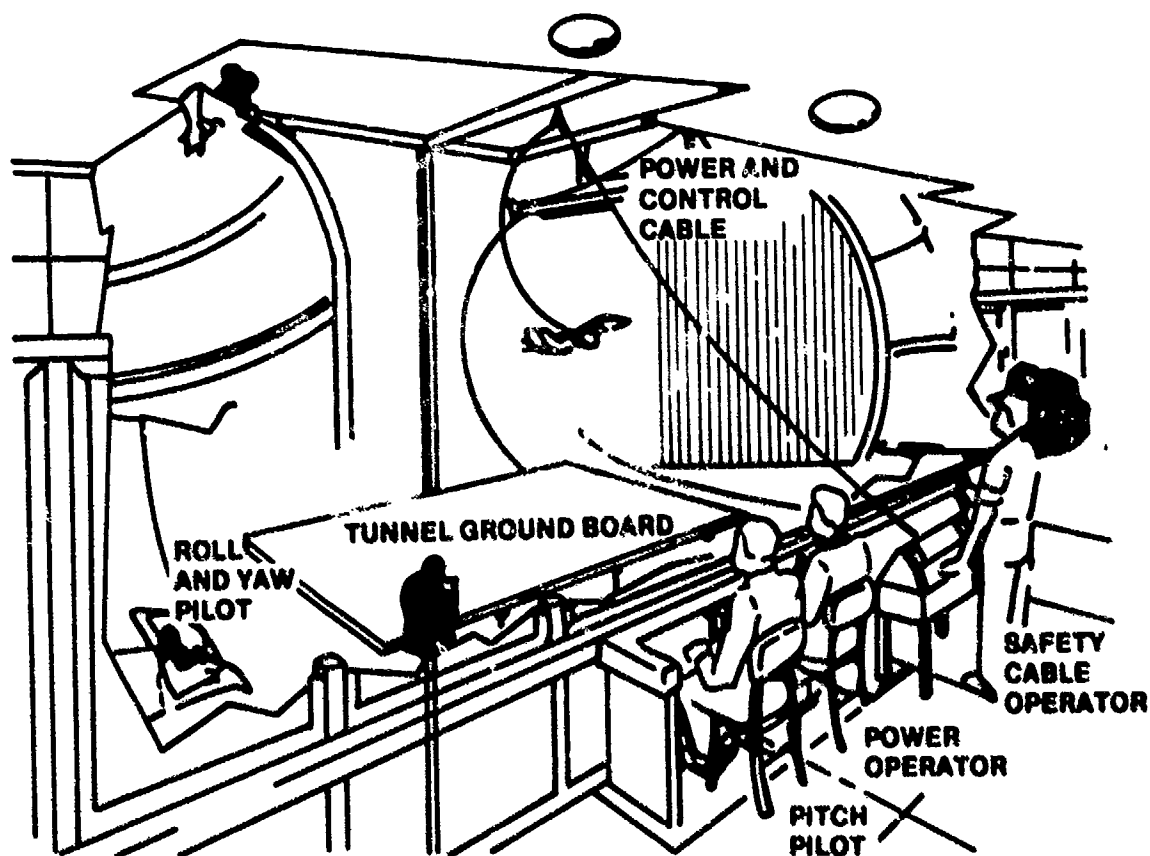

FIGURE 10.45. TEST SETUP FOR WIND-TUNNEL FREE-FLIGHT TESTS
(10.15:13-8)

10.4.3.1.2.3 The Outdoor Radio-Controlled Model Technique. (10.15:13-3, 4). A significant void of information exists between the results produced by the wind-tunnel free-flight test technique for angles of attack up to and including the stall, and the results produced by the spin-tunnel test technique, which defines developed spin and spin-recovery characteristics.

The outdoor radio-controlled model technique has, therefore, been designed to supply information on the post-stall and spin-entry motions of airplanes. The radio-controlled model technique consists of launching an unpowered, dynamically scaled, radio-controlled model into gliding flight from a helicopter, controlling the flight of the model from the ground, and recovering the model with a parachute. A photograph showing a typical model mounted on the launching rig of a helicopter is shown in Figure 10.46.
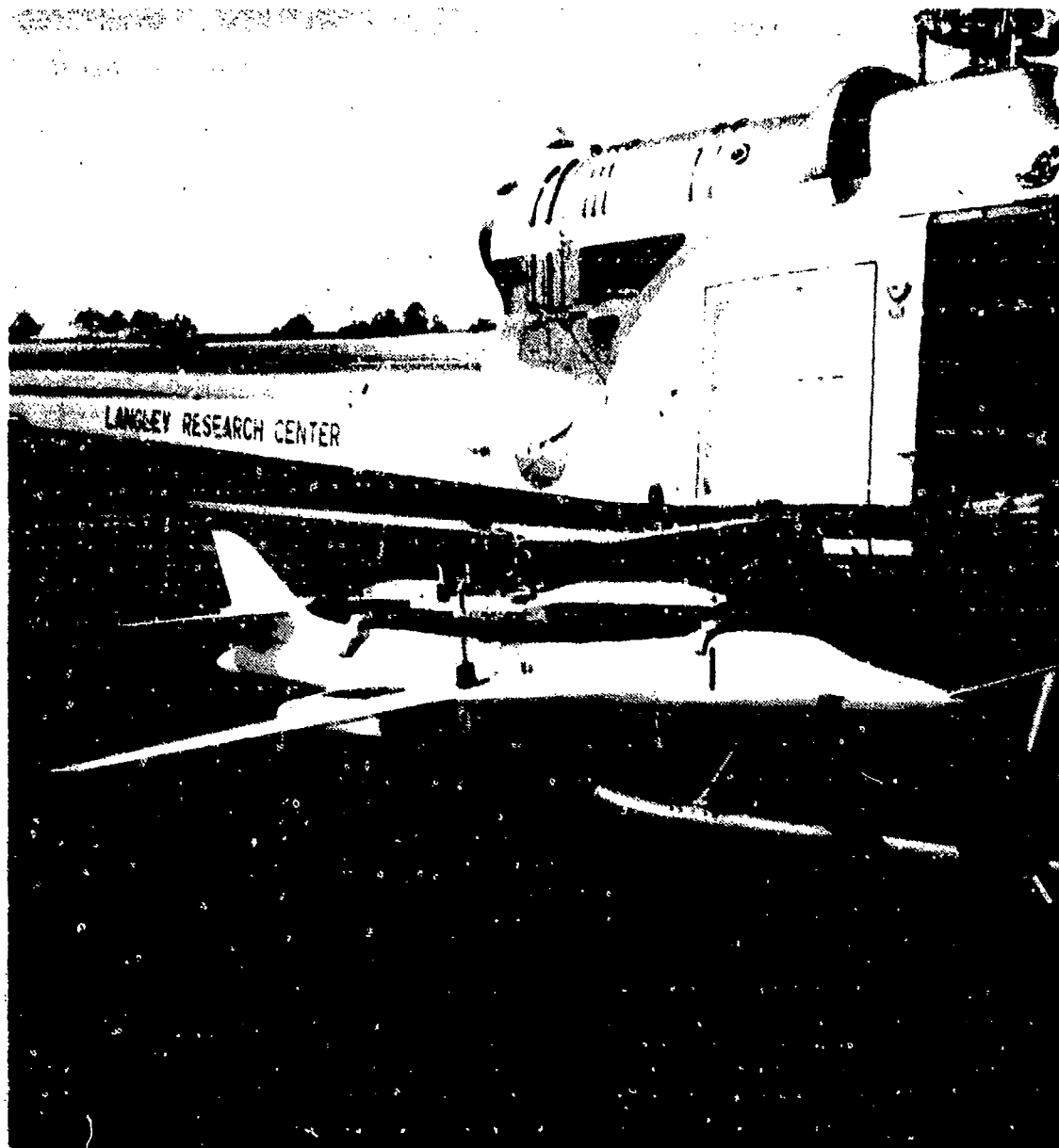

FIGURE 10.46.   B-1 RADIO CONTROLLED DROP MODEL MOUNTED ON A HELICOPTER

The models used in these tests are made relatively strong to withstand high landing impact loads of 100 to 150 g's. They are constructed primarily of fiberglass plastic, with the fuselage case being thick hollow shells and the wings and tails having solid balsa cores with fiberglass sheet coverings. Radio receivers and electric actuators are installed to provide individual operation of all control surfaces and a recovery parachute. Proportional-type control systems are used in this technique.

The models are trimmed for approximately zero lift, and launched from the helicopter at an airspeed of about 40 knots and an altitude of about 5000 ft. The models are allowed to dive vertically for about five seconds, after which the horizontal tails are moved to stall the model. After the stall, various control manipulations may be used; for example, lateral-directional controls may be moved in a direction to encourage any divergence to develop into a spin. When the model has descended to an altitude of about 500 ft., a recovery parachute is deployed to effect a safe landing.

The outdoor radio-controlled model technique provides information which cannot be obtained from the other test techniques. The indoor free-flight tests, for example, will identify the existence of a directional divergence at the stall, but the test is terminated before the model enters the incipient spin. In addition, only 1-g stalls are conducted. The radio-controlled technique can be used to evaluate the effect of control inputs during the incipient spin, and accelerated stalls can be investigated. At the other end of the stall/spin spectrum, spin-tunnel tests may indicate the existence of a flat or nonrecoverable spin mode, but it may be difficult for the airplane to attain this spin mode from conventional flight - the difference being that models in the spin tunnel are launched at about 90° angle of attack with a forced spin rotation. The radio-controlled test technique determines the spin susceptibility of a given airplane by using spin entry techniques similar to that of the full-scale airplane.

The radio-controlled technique determines (1) the spin susceptibility of a configuration, (2) control techniques that tend to produce developed spins, and (3) the effectiveness of various control techniques for recovery from out-of-control conditions.

There are several limitations of the radio-controlled technique that should be kept in mind. The first is that the tests are conducted out-of-doors. The test schedule is, therefore, subject to weather conditions,

10.92

and excessive winds and rain can severely curtail a program. This technique is relatively expensive. Expensive flight instrumentation is required to record the motions of the model; and the large size of these models requires the use of powerful and reliable electronic equipment. Costs are compounded by the fact that the model and its electronic equipment frequently suffer costly damage on landing impact. Because of this higher cost and the slow rate at which radio-controlled drop model tests can be accomplished, this technique is used only in special cases where the simpler and cheaper wind-tunnel and spin-tunnel techniques will not give adequate information; for example, when it is necessary to know whether an airplane can be flown into a particular dangerous spin mode, or when one wants to investigate recovery during the incipient spin. Conversely, most of the exploratory work, such as developing "fixes" for a departure at the stall or investigating a variety of spin-recovery techniques, is done in the wind tunnels.

10.4.3.1.3 The Spin-Tunnel Test Technique (10.15:13-4,5). The best known test technique used today to study the spin and spin-recovery characteristics of an airplane is the spin-tunnel test technique. A cross-sectional view of the NASA Langley Vertical Spin Tunnel is shown in Figure 10.47.

In this tunnel, air is drawn upward by a fan located above the test section. Models are hand-launched at about 90° angle of attack, with pre-rotation, into the vertically rising airstream. The model then seeks its own developed spin mode or modes. For recovery, the tunnel operator deflects the aerodynamic controls on the model to predetermined positions by remote control.

In a spin-tunnel investigation, the program consists of (1) determination of the various spin modes and spin-recovery characteristics, (2) study of the effect of center-of-gravity position and mass distribution, (3) determination of the effect of external stores, and (4) determination of the size and type parachute required for emergency spin recovery.

In a typical spin-tunnel test program, tests are made at the normal operating loading condition for the airplane. The spin and spin-recovery characteristics are determined for all combinations of rudder, elevator, and aileron positions for both right and left spins. In effect, a matrix of both
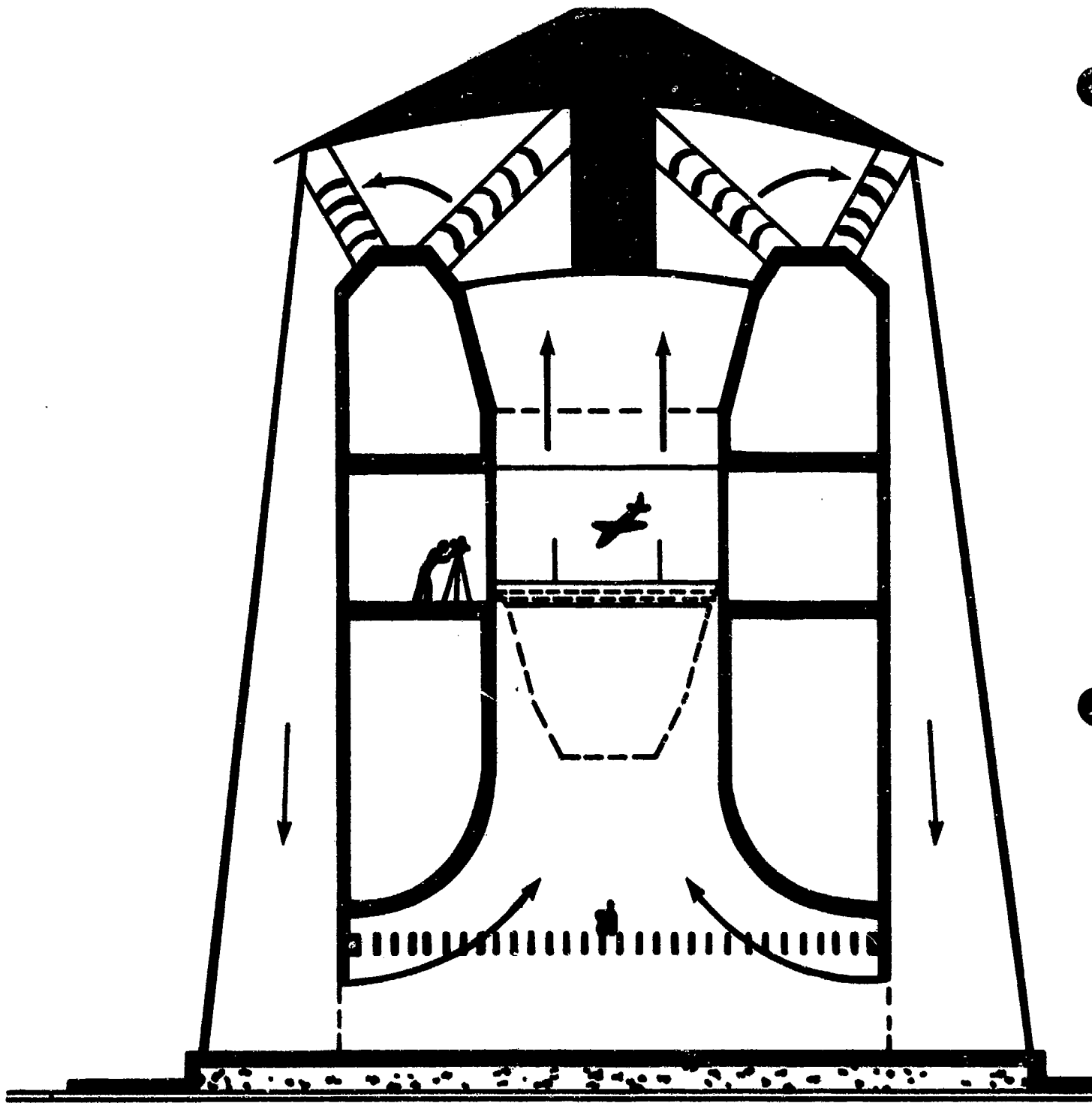
FIGURE 10.47.   CROSS-SECTIONAL VIEW OF NASA LANGLEY VERTICAL SPIN TUNNEL
(10.15:13-9)

the spin and spin-recovery characteristics are obtained for all control settings for the normal loading operating condition. Using these data as a baseline, selected spin conditions are treated again with incremental changes to the center of gravity and/or mass conditions. Then, based on the effects of these incremental changes, an analysis is made to determine the spin and spin-recovery characteristics that the corresponding airplane is expected to have. Also, the effectiveness of various control positions and deflections are analyzed to determine which control techniques are most effective for recovery. After the spin-recovery characteristics for the normal loading conditions have been determined, additional tests are made to determine the effects of other loading conditions, store configurations (including asymmetric stores), and other items of interest such as speed brakes and leading and trailing-edge flaps.

The parachute size required for emergency spin recovery is determined for the most critical spin conditions observed in the spin-tunnel tests, and is checked at other conditions throughout the test program. If the parachute size is found to be too small for other conditions, the size is adjusted so that the parachute finally recommended for use on the spin demonstration airplane will be sufficient to handle the most critical spins possible on the airplane for any loading.

As a result of the combination of the relatively small scale of the model and the low tunnel speeds, spin-tunnel tests are run at a value of Reynolds number which is much lower than that for the full-scale airplane. Experience has shown that the differences in Reynolds number can have significant effects on spin characteristics displayed by models and the interpretation of these results. In particular, past results have indicated that very significant effects can be produced by air flowing across the forward fuselage at angles of attack approaching 90°. These effects are influenced by the cross-sectional shape of the fuselage forebody and may be extremely sensitive to Reynolds number variations. Particular attention is, therefore, required for documentation of this phenomenon prior to spin-tunnel tests. This evaluation has been conducted in the past with the aid of static force tests over a wide Reynolds number range.

10.4.3.1.4 Rotary-Balance Tests (10.15:15-5,6). The rotary-balance test technique has produced significant information regarding the complex aerodynamic characteristics of airplane configurations during spinning motions. Six-component measurements are made of the aerodynamic forces and moments acting on the wind-tunnel model during continuous 360° spinning motions at a constant angle of attack. Past studies identified some of the major factors which influence spin characteristics such as the autorotative tendencies of unswept wings and certain fuselage cross-sectional shapes. The characteristics of the basic configuration, the effects of individual and combined control deflections, the effects of tail surfaces and nose strakes, and the effects of spin radius and sideslip are determined. Test results identify configuration features which can have large effects on the aerodynamic spin characteristics of modern aircraft. Some pro-spin flow mechanisms have been identified.

Test results have also indicated that the aerodynamic moments (particularly yawing and pitching moments) exhibited by current military configurations vary nonlinearly with spin rate. Nonlinear moments have a large effect on calculated spin motions, and agreement is obtained with dynamic model tests for smooth, steady spins when such data are used as inputs for the calculations. On the other hand, conventional calculation techniques using conventional linearized static and dynamic stability derivatives often produce completely erroneous results.

The results of rotary-balance tests conducted for several current fighter configurations indicate that the aerodynamic characteristics of these vehicles during spins are extremely complex phenomena which tend to be Reynolds number dependent and which vary nonlinearly with spin rate. Computer studies of spinning motions have indicated that data obtained from rotary-balance tests will be required for the development of valid theoretical spin prediction techniques.

10.4.3.1.5 Simulator Studies (10.13: 15-6,7). The model test techniques previously discussed have several critical shortcomings. For example, the inputs of the human pilot have been minimized or entirely eliminated. In addition, the use of unpowered models and space constraints within the wind tunnels do not permit an evaluation of the spin susceptibility of airplanes during typical air combat maneuvers. Finally, the effects of

sophisticated automatic control systems are not usually evaluated because of space limitations within the models. In order to provide this pertinent information, a piloted simulation test technique has been developed as a logical follow-on to the model tests.

Simulator application to the stall/spin area is dependent on the development of a valid mathematical model of the airplane under consideration. In view of the present lack of understanding of aerodynamic phenomena at spin attitudes, the simulation studies are currently limited to angles of attack near the stall, and fully developed spins are not simulated. Rather, the studies are directed toward an evaluation of the spin susceptibility or stall/departure characteristics of the airplane during typical air combat maneuvers and the effects of automatic control systems on these characteristics.

Simulation studies have indicated that it is an extremely valuable tool for stall/spin research. Correlation of results with those obtained from full-scale flight tests for several current fighters has indicated agreement, particularly with regard to the overall spin resistance of the configurations.

Extension of piloted simulation techniques to high angles of attack provides valuable insight as to the spin susceptibility of fighter configurations during representative air combat maneuvers. In addition, use of simulators is an effective method for the development and evaluation of automatic spin prevention concepts.

10.4.3.2 **Pilot Proficiency.** It is imperative that the test pilot engaged in a post-stall/spin test program have recent experience in stalls and in spinning aircraft as similar as possible to the test aircraft. Obviously, such aircraft should be those cleared for intentional spins. Coupled departures in a mildly spinning aircraft may be helpful in simulating the post-stall gyrations of an aircraft not cleared for intentional departures. Lack of spin practice for as little as three months will reduce the powers of observation of even the most skilled test pilot. Therefore, he should practice until he is at ease in the post-stall/spin environment immediately prior to commencing the data program. Centrifuge rides, with simulated instrumentation procedures and required data observations, can also be useful.

10.4.3.3 **Chase Pilot/Aircraft Requirements.** A highly qualified chase pilot in an aircraft compatible with the test aircraft increases the safety factor

and adds another observer. The chase pilot should participate fully in the preparation phase. In fact it is preferable that more than one pilot be assigned to a given project. Not only does such an arrangement permit more than one qualitative opinion, but by alternating between post-stall/spin and chase assignments, each pilot gets at least two viewpoints. He can evaluate the post-stall/spin characteristics both as an in-the-cockpit observer and from the somewhat more detached chase position. Of course, from a flying safety viewpoint the benefits of a competent chase pilot should be in an airplane with performance compatible with that of the test aircraft. His responsibilities include: staying close enough to observe and photograph departures, post-stall gyrations, and any spins; staying out of the way of an uncontrollable test aircraft; and being immediately in position to check any unusual circumstances such as lost panels, malfunctioning drag/spin chutes, or control surface positions. And, of course, if necessary, he can call out canopy jettison/ejection altitudes. All these responsibilities point up the importance of a well-prepared, observant chase pilot in a similar aircraft.

10.4.4 Data Requirements

The following two paragraphs are intended to provide only general guidance. The test plan for the specific project must be consulted for more detailed and specific requirements.

10.4.4.1 Data to be Collected. The flight test engineer will be primarily concerned with the required quantitative data. Rates of pitch, roll, and yaw, angular accelerations about each axis, control surface positions, angle of attack, indicated airspeed, and altitude are but a few of the typical time histories plotted meticulously by engineers. The pilot's most important data gathering is qualitative. Can all the necessary controls and switches be reached easily? What are the cockpit indications on production instruments of loss of control warning, departure, post-stall gyration, and spins? Can these indications be readily interpreted, or is the pilot so disoriented that he could not determine what action to take? What visual cues are available at critical stages of the recovery? Reference 10.14 gives an appropriate example of such a critical stage in the A-7D recovery sequence:

On several occasions during recovery from fully developed spins, yaw rotation slowed, AOA decreased below 22 units, and roll rotation increased prior to release of anti-spin controls. Pilots found it easy to confuse roll rate for yaw rate leading to the "Auger" maneuver defined as rolling at unstalled AOA with anti-spin controls.

This sort of qualitative finding can be and usually is the most important kind of result from a spin test program. Hence, it is poor practice to ask the pilot to neglect cockpit observations to gather quantitative data which should be recorded by telemetry or on-board recording devices. Project pilots must guard against this pilot overload by looking carefully at the available instrumentation, both airborne and ground-based.

10.4.4.2 Flight Test Instrumentation. The scope of the post-stall/spin test program will determine the extent of the instrumentation carried on board the aircraft. A qualitative program with a limited objective may require virtually no special instrumentation (10.16:1), while extensive instrumentation may be mandatory for a full-blown stall/post-stall/spin investigation. Table 10.6 shows typical on-board instrumentation for a complete evaluation. Of course, this instrumentation is not appropriate for every investigation; each program is a special case.

TABLE 10.6

TYPICAL FLIGHT TEST INSTRUMENTATION

Parameter	Time History[1]	Pilot's Panel
Angle of attack	X	X
Production angle of attack	X	X
Angle of sideslip	X	
Swivel boom airspeed	X	X
Swivel boom altitude	X	X (coarse altimeter)
Produce airspeed	X	
Production altitude	X	
Bank angle	X	
Pitch angle	X	
Pitch rate	X	
Roll rate	X	
Yaw rate	X	
Normal acceleration	X	X (sensitive indicator)
Accelerations at all crew stations	X	
All control surface positions	X	
Stick and rudder positions	X	
Stick and rudder forces	X	
All trim tab positions	X	
SAS input signals	X	
Engine(s) oil pressure	X	X
Hydraulic pressures	X	X

Fuel used (each tank)	X	X
Film, oscillograph, or tape-correlations and amount remaining	X	X
Event marker	X	X
Spin turn counter	X	X
Elapsed time	X	
Critical structural loads	X	X
Pilot warning signal(s)2		X
Emergency recover device indicators	X	X

[1]Magnetic tape, telemetry.

[2]Pilot warning sigals may include maximum raw rate indicators, spin direction indicators, minimum altitude indicators, and other such devices to help lower the pilot's workload. They may take the form of flashing lights, horns, oversized indicators, etc.

The prospective test pilot should particularly note the kinds of parameters to be displayed in the cockpit. In this area he must protect his own interests by assuring that the indicators and controls available to him are complete, but that they do not overload his capacity to observe and to safely recover the aircraft. Simulations, preferably under stress of some kind (in a centrifuge, for example), may help the pilot decide whether or not the cockpit displays and controls are adequate.

Finally, Reference 10.4, Paragraph 6.4.2.3, directs preparation of a technical briefing film and suggests that an aircrew training film may be produced at the option of the procuring activity. Usually, it is advisable to have one or more movie cameras mounted on or in the test aircraft to provide portions of this photographic coverage. Motion pictures taken over the pilot's shoulder may provide visualization of the departure motion, readability of production instruments, information about the adequacy of the restraint system, or other similar data. A movie camera taking pictures of the control surface positions can produce dramatic evidence of the effectiveness or lack of effectiveness of recovery controls. These cameras and recording devices should be made as "crash-proof" or at least as "crash-recoverable" as possible.

Further information on flight test instrumentation, cockpit displays, and cameras may be found in Paragraphs 3.2.2, 3.2.3, and 3.2.4 of Reference 10.4.

10.4.4.3 Safety Precautions. Stall/post-stall/spin test programs are usually regarded with suspicion by program managers and flying supervisors. Many such investigations have resulted in the loss of expensive, highly instrumented test aircraft and crew fatalities. Post-stall/spin test are hazardous. Careful attention to detail in several areas will minimize the dangers involved.

10.4.4.3.1 Conservative Approaches. Use a conservative build-up approach to incrementally expand the areas of investigation, choosing safe increments until the aircraft's uncontrolled motions are better understood (10.4:3.4). How can the test pilot plan to assure that such an approach is actually followed?

First, the entire program is usually broken down into phases. Even the terms now in use - stall/post-stall/spin - suggest the basic phases of such an investigation, although in practice the phases are generally broken down in more detail. Table 10.7 lists the recommended phases for such investigations.

Within these phases, there are several smaller steps to be taken with successive departures, post-stall gyrations, or spins. For example, aircraft loadings are normally changed gradually from clean to symmetric store loadings to asymmetric store loadings. The effects of these loading changes must be evaluated both for the aerodynamic effects and the changes in mass distribution. Unfortunately, it is not often obvious which effect is most damaging until after the tests are completed. One would also be ill-advised to use full pro-spin controls on the very first departure in phases B, C, or D. Delayed recoveries should be approached by sustaining the desired misapplication of controls in increments in each successive departure up to the maximum of 15 seconds as indicated in Phase D. Such conservatism in flying these tests is essential and must be adhered to scrupulously. However, it is also necessary to consider aircraft systems in order to plan a safe post-stall/spin program.

TABLE 10.7

TEST PHASES

Phase	Control Application
A - Stalls	Pitch control apr⸱ied to achieve the specified AOA rate, lateral-directional controls neutral or small lateral-directional control inputs as normally required for the maneuver task Recovery initiated after the pilot has positive indications of: (a) a definite g-break or (b) a rapid angular divergence, or (c) the aft stick stop has been reached and AOA is not increasing.
B - Stalls with aggravated control inputs	Pitch control applied to achieve the specified AOA rate, lateral-direction controls as required for the maneuver task. When condition (a), (b), or (c) from above has been attained, controls briefly misapplied, intentionally or in response to unscheduled aircraft motions before recovery attempt is initiated.
C - Stalls with aggravated and sustained control	Pitch control applied to achieve the specified AOA rate, lateral-directional controls as required for the maneuver task. When condition (a), (b), or (c) has been attained, controls are misapplied, intentionally or in response to unscheduled aircraft motions, held for three seconds before recovery attempt is initiated.
D - Post-stall Gyration, spin, and deep stall attempts (this phase required only for training aircraft which may be intentionally spun and for Class I and IV aircraft in which sufficient departures or spins did not result in Test Phase A, B, or C to define characteristics.	Pitch control applied abruptly, lateral-directional controls as required for the maneuver task, when condition (a), (b), or (c) has been attained, controls applied in the most critical positions to attain the expected spin modes of the aircraft and held up to 15 seconds before recovery attempt is initiated, unless the pilot definitely recognizes a spin mode.

10.4.4.3.2 <u>Degraded Aircraft Systems</u>. All systems are under an often unknown amount of strain during high angle of attack maneuvering. If the aircraft goes out of control in this flight regime, system design limits may well be exceeded. The propulsion/inlet system is often not designed to allow reliable operation of the engines during extreme angles of attack and sideslip. Engine flame out may result in loss of control in modern aircraft with hydraulic flight control systems. The test vehicle must have an alternate source of hydraulic power for the flight controls if there is a possibility that engine flameouts are likely to occur. However, do not overlook the behavior of the production hydraulic system: loss of production hydraulic pressure may be all that is necessary to prohibit intentional spins. In propeller-driven aircraft the hydraulic power used to govern the propeller pitch can also be a limiting factor, particularly during inverted spins. The electrical system may also be affected by engine flameout, and even a momentary failure can render instrumentation inoperative at a critical time. Hence, a reliable back-up electrical power source may be necessary. Other systems, such as the ejection system, pilot restraint system, or communications/ navigation system, may cause special problems during the post-stall/spin test program. The test pilot and test engineer must think through these special problems and, where necessary, add back-up systems to the test aircraft to assure safe completion of the program. Any backup systems that are required must not limit the range and scope of the tests; otherwise, they defeat their purpose.

10.4.4.3.3 <u>Emergency Recovery Device</u>. The ultimate back-up system, some sort of emergency recovery device, is so important that it deserves a paragraph all its own. Failure of this "last-ditch" system has in the past contributed to the discomfort of test pilot, engineer, and SPO director all too often. Reference 10.1, suggests that more attention must be given to the design of this system, perhaps to the extreme of making emergency recovery system components government-furnished equipment (GFE). While the feasibility of this rather drastic suggestion is questionable, it is imperative that more reliable systems be designed. Some of the things that must be scrutinized by the test pilot are:

1. Has the deployment/actuation mechanism demonstrated reliability through the expected envelope of dynamic pressures?

2. Are the moments generated large enough for all predicted spin rates?

3. Has the jettison mechanism demonstrated reliability throughout the expected envelope?

4. Are maintenance inspection procedures adequate for this system? (This system should be checked just prior to takeoff.)

5. Does the emergency recovery system grossly alter the aerodynamic and/or inertia characteristics of the test aircraft?

Obviously, no such list is complete, but the test pilot must carefully evaluate every component of the emergency recovery system: spin chute, spin rockets, or any other device.

10.4.4.3.3.1 <u>Spin-Recovery Parachute System Design</u> (10.18). There are three distinctly different branches of technology involved in the design of a spin-recovery parachute system - parachutes, spinning, and airplane systems. For a given airplane, the spin-recovery parachute must be designed to recover the airplane from its worst spin condition. Definition of this "worst condition" and the parachute size and riser length is generally obtained for military airplanes from tests of dynamic models in the NASA Langley spin tunnel.

10.4.4.3.3.1.1 <u>Parachute Requirements</u>. Positive and reasonably quick opening (approximately three to four seconds) of the spin-recovery parachute is necessary for all operating conditions so that the spin may be terminated as rapidly as possible to minimize altitude loss.

A stable parachute is required so that it will tend to trail with the relative wind at the tail of the airplane in a spin and thus apply a yawing moment that is always anti-spin; whereas an unstable parachute because of its large oscillations may apply a yawing moment that varies from anti-spin to pro-spin, and thus hinders or prevents recovery.

Determination of the correct parachute size and riser length is very important in the overall design of a recovery system. The riser length controls the position of the parachute in the wake of the spinning airplane and therefore affects the force that the parachute can apply to the airplane. Figure 10.48 is an illustration of a typical spin-recovery parachute system.
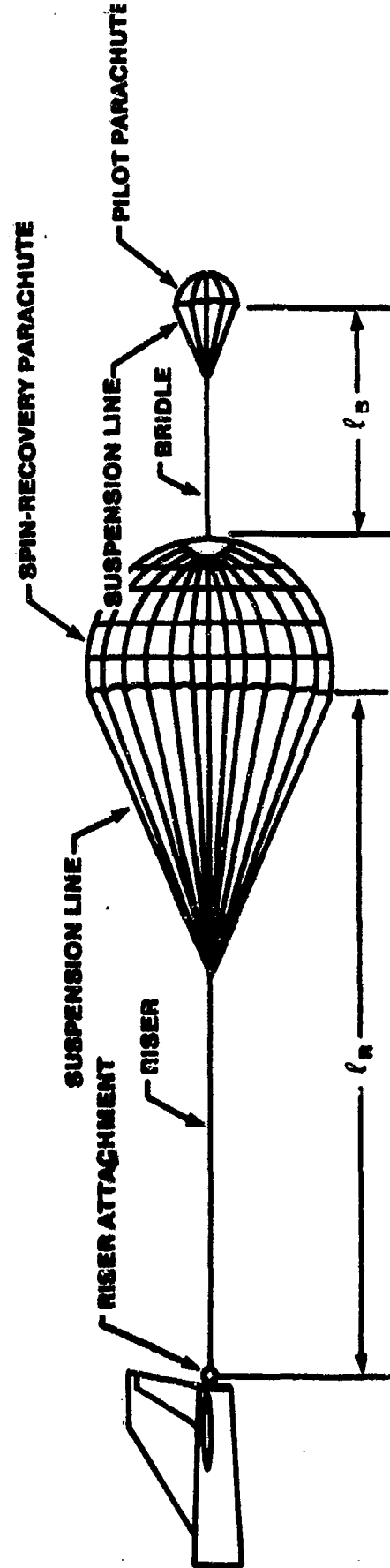
FIGURE 10.48. SKETCH OF SPIN-RECOVERY PARACHUTE SYSTEM AND ITS NOMENCLATURE

(10.18)

10.106

10.4.4.3.3.1.2   Parachute Compartment   (10.18).   A   fundamental
requirement in any parachute installation is to locate the compartment and the
riser attachment point as far aft on the airplane as possible. This approach
will reduce the possibility of the riser or parachute striking the airplane
and will also give the maximum moment arm for the parachute force to act on.
It should be assumed that the angle the riser makes with the fuselage
longitudinal axis can be as high as 90° if a flat or a highly oscillatory spin
mode exists. If the riser is likely to contact the jet exhaust because of the
attachment point location, then it must be protected against heat. Additional
protection of the riser might be necessary if there is a possibility of its
rubbing against the airplane structure after deployment. Since the riser
generally is made of fabric (for example, nylon), abrasions on or nicks in the
riser while it is in tension can cause it to fail very rapidly.

The parachute compartment should also be designed so that it does not
change the spin and recovery characteristics of the airplane by changing the
aerodynamic and/or inertia characteristics of the airplane with the
installation and thereby invalidate the tests. Two types of parachute
compartments are (1) one in which the compartment is permanently attached to
the airplane and deployment is initiated by pulling the deployment bag from
the compartment with a pilot parachute, and (2) one in which the compartment
is pulled away and completely separated from the airplane by a pilot parachute
which then pulls the compartment off the deployment bag when the riser is
fully extended.

Two major requirements for a satisfactory parachute compartment are that
it be designed so that (1) the extraction of the deployment bag by pilot
parachute or tractor rocket or by forceful ejection can be accomplished
regardless of the airplane attitude, and (2) the bag be undamaged during the
deployment process.

10.4.4.3.3.1.3   Parachute Deployment Methods   (10.18).   The two basic
methods for deploying the spin-recovery parachute from an airplane are the
line-first and the canopy-first methods shown in Figure 10.49. The line-first
method is preferred for several reasons, as indicated in the discussion of the
method.

10.4.4.3.3.1.3.1 Line-first method. In line-first method (Figure 10.49), a pilot parachute extracts the deployment bag from the parachute compartment, deploying first the riser, then the parachute suspension lines, and finally, the recovery parachute by pulling the deployment bag off the parachute. The primary advantage of this method is that it provides a clean separation of the deployment bag from the airplane and also ensures that the inflation of the spin-recovery parachute canopy will occur away from the airplane. Consequently, the possibility of the parachute fouling on the airplane and the effect of the airplane wake on the parachute are minimized. Furthermore, the snatch loads will be reduced because parachute inflation will occur after the riser is fully extended.

10.4.4.3.3.1.3.2 Canopy-first method. In the canopy-first method (Figure 10.49), a pilot parachute extracts the deployment bag from the parachute compartment. A pilot parachute extracts the spin-recovery parachute canopy from the bag, then the suspension lines, and finally the riser. The primary disadvantages of this method are (1) the increased possibility of the spin-recovery parachute canopy fouling on the airplane; (2) the high snatch loads that occur because the spin-recovery parachute canopy will become inflated before the riser has become fully extended; (3) the high opening shock loads; and (4) the possibility of the canopy being damaged, or only partly inflated, because the canopy and suspension lines become entangled. The only advantages of this method are (1) it requires a lower pilot parachute extraction force than the line-first concept because the spin-recovery parachute canopy is extracted easily regardless of the altitude of the spinning airplane; and (2) once the deployment starts, the parachute itself provides an additional force that helps complete the deployment of the canopy, suspension lines, and riser.

10.4.4.3.3.1.4 Basic Attachment Methods (10.18). The spin-recovery parachute riser is attached to the airplane by an attachment and release mechanism and this device has proven to be a critical item in the system design. For this reason, regardless of the type of mechanism used, no part of it should require such precise adjustment that lack of such adjustment could cause the mechanism to malfunction. The mechanism must perform the following critical functions: (1) attachment of the parachute riser to the airplane, (2) release of the parachute after spin recovery, and (3) automatic release of

the parachute in the event of inadvertent deployment during critical phases of flight. There are two basic methods normally used:

(1) Closed-jaw method (Figure 10.50) - The attachment of the riser to the airplane is made prior to take-off and provision is made for automatic release in the event of premature deployment.

(2) Open-jaw method (Figure 10.50) - The attachment is not made until immediately before a spin test.

Several factors must be considered in designing the attachment and release mechanism. For example, if the shackle, or D-ring, is locked in the attachment mechanism prior to take-off, as illustrated by the closed-jaw concept of Figure 10.50, it is essential from the standpoint of flight safety that provision be made so that the parachute will automatically jettison should it inflate inadvertently. This automatic jettisoning of the parachute can be accomplished by putting a weak link, such as a shear pin, in the system. Prior to the start of the spin tests, the weak link is bypassed by a locking mechanism capable of withstanding the opening shock load of the parachute. If the mechanism is left open until the start of the spin tests, however, as illustrated by the open-jaw concept of Figure 10.50b, the parachute would be automatically jettisoned since it would be unrestrained.

This approach does require, however, that steps be taken to ensure that the shackle is in position in the mechanism when the time comes to arm the system. A low-strength bolt or safety wire can be used to achieve the proper positioning. For either of the foregoing types of systems, a light is generally used to indicate that the system has been armed by bypassing the weak link or by closing the jaws.

In both the closed-jaw and open-jaw methods, the normal procedure for releasing the parachute after it has been deployed is by mechanical means. Provisions, however, should be made for emergency jettisoning of the parachute if the primary jettison system fails to operate. This jettisoning can be accomplished through the use of explosive bolts or pyrotechnic line cutters. If the explosive bolts are used, they should be of the nonfragmenting variety to ensure the safety of the airplane. The pyrotechnic line cutters have a disadvantage in that the cutters and the electric wires to them are subject to damage by the slipstream and therefore might fail to function.
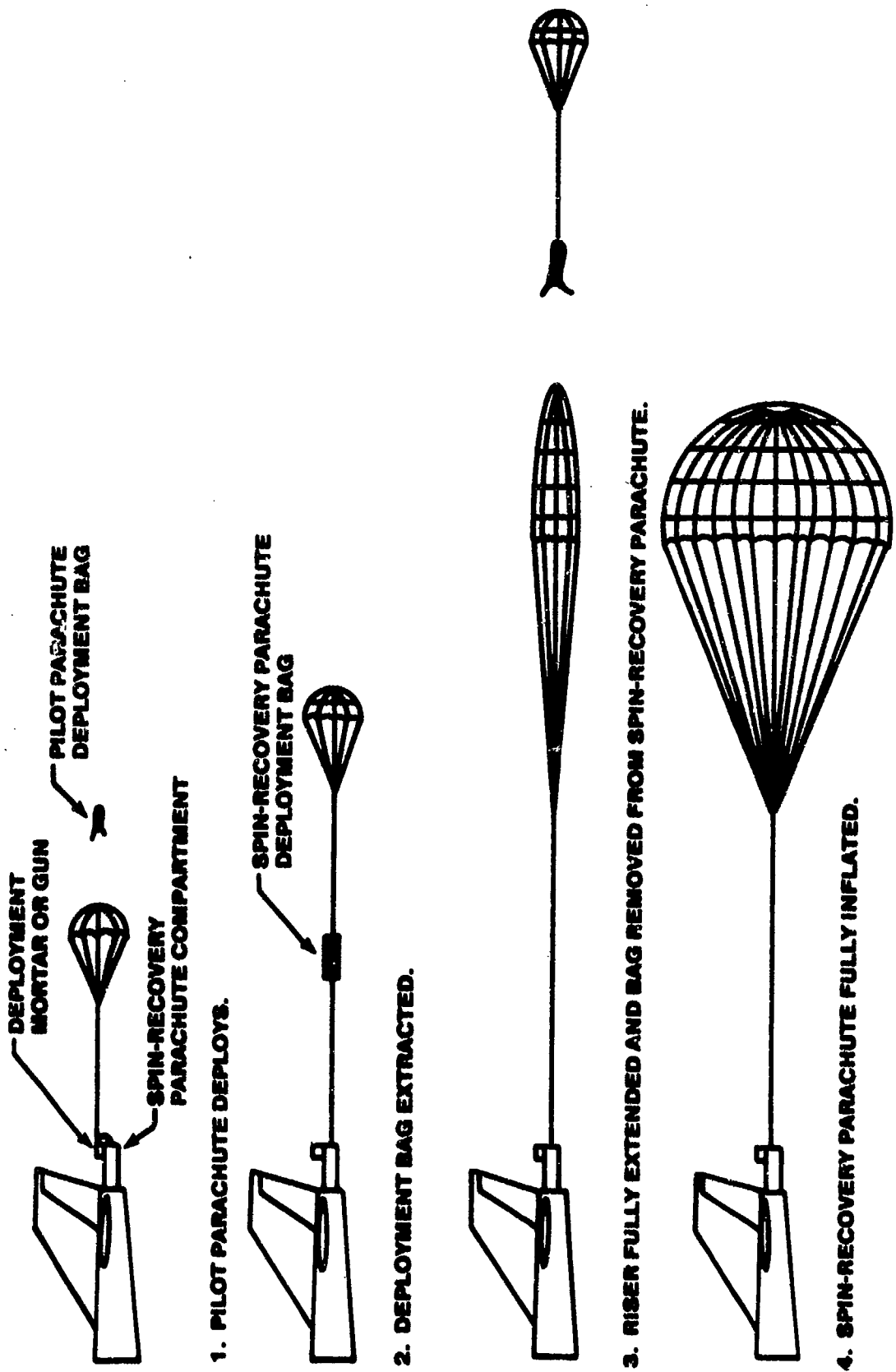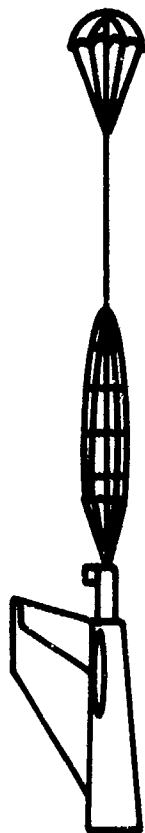
FIGURE 10.49. BASIC SPIN-RECOVERY PARACHUTE DEPLOYMENT TECHNIQUE
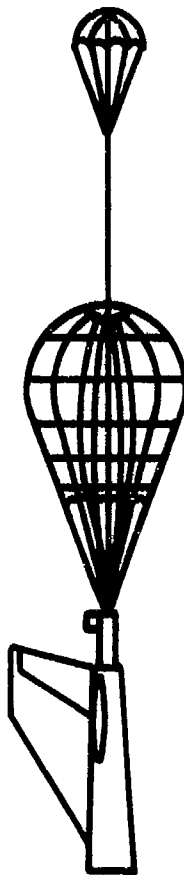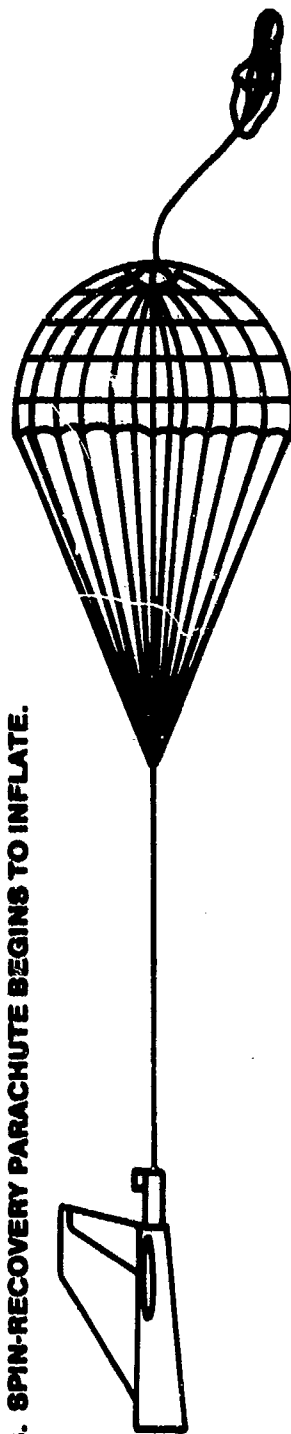(10.18)

10.110

PILOT PARACHUTE
DEPLOYMENT BAG

1. PILOT PARACHUTE DEPLOYS.

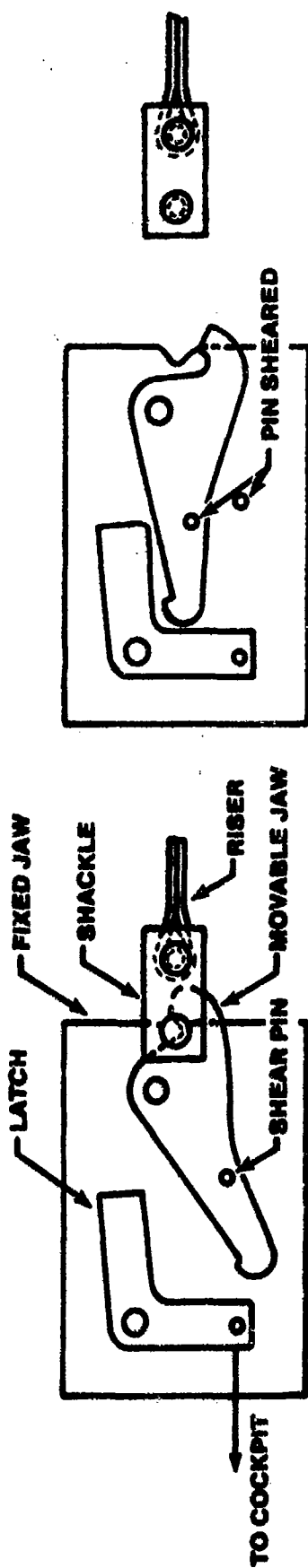2. SPIN-RECOVERY PARACHUTE CANOPY EXTRACTED.

3. SPIN-RECOVERY PARACHUTE BEGINS TO INFLATE.

4. RISER FULLY EXTENDED AND SPIN-RECOVERY PARACHUTE FULLY INFLATED.

(b) CANOPY-FIRST METHOD.

FIGURE 10.49. CONCLUDED

10.111

FIGURE 10.50. PARACHUTE ATTACHMENT AND RELEASE MECHANISMS

(10.18)

RISER

SHACKLE

PIN SHEARED

(2) IF PREMATURE PARACHUTE DEPLOYMENT OCCURS, PARACHUTE LOAD WILL SHEAR PIN

SPRING COMPRESSED

PIN TO LIMIT UPWARD MOVEMENT OF MOVABLE JAW

MOVABLE JAW

FIXED JAW

SHEAR PIN

LATCH

TO COCKPIT

(1) LATCH IS OPEN AND JAWS ARE OPEN FOR TAKEOFF, LANDING, AND NORMAL FLIGHT OPERATION TO ALLOW FOR PREMATURE JETTISONING OF PARACHUTE.

SPRING EXTENDED
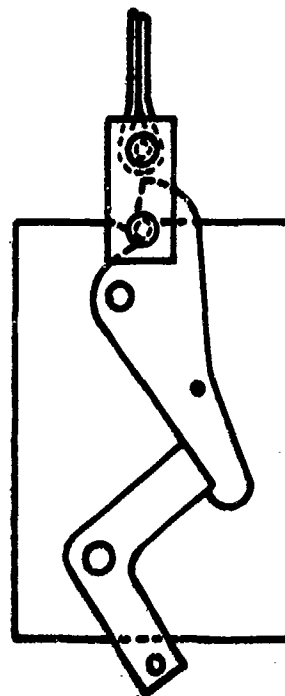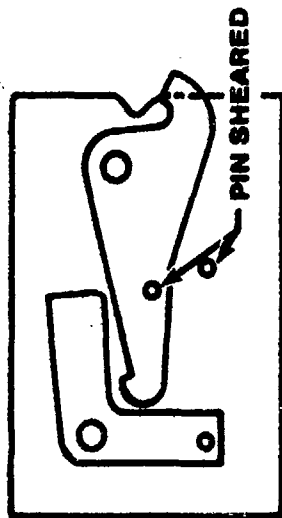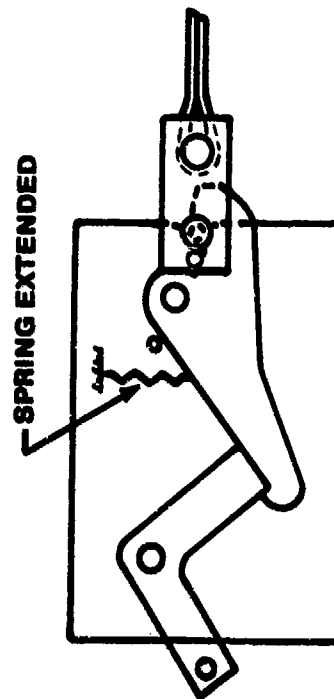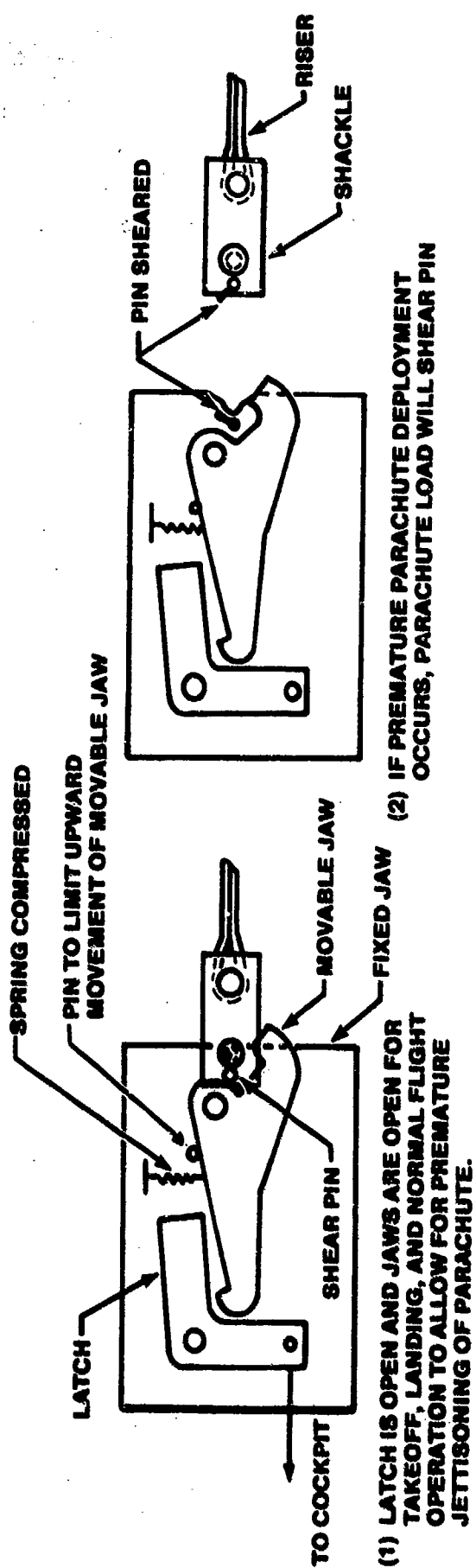
(3) FOR NORMAL DEPLOYMENT OF PARACHUTE, LATCH IS CLOSED AND JAWS ARE CLOSED PRIOR TO SPIN ENTRY TO RETAIN PARACHUTE RISER IN JAWS.

(b) OPEN-JAW CONCEPT.

FIGURE 10.50.   CONCLUDED

10.113

10.4.4.3.3.2 Alternate Spin-Recovery Devices. Although tail-mounted spin-recovery parachutes are used almost exclusively in full-scale spin demonstrations, rockets and wing-tip-mounted parachutes have been considered. Anti-spin rockets have been used occasionally, but wing-tip mounted parachutes have been used apparently only once.

10.4.4.3.3.2.1 Rockets (10.18). Rockets are generally used for spin recovery in special cases where the use of a parachute involves unusual problems. Tail-boom airplane configurations or tailless configurations with a very short tail moment arm might provide such unusual problems. Rockets, however, have many disadvantages when compared with tail-mounted parachutes as will be discussed later.

Rockets generally have been installed on or near each wing tip but there have been cases where the rocket was installed at the nose or the tail of the airplane. When the rockets are installed on the wing tips, their thrust is applied in a forward direction. Depending on the direction of the spin which should be determined by a sensor, the left or right rocket is fired to apply an anti-spin yawing moment (for example, in a right spin the right rocket would be fired).

When the spin-recovery rockets are added to the airplane, care should be taken that the rocket installation does not alter the spin and recovery characteristics of the airplane by altering the aerodynamic and/or inertia characteristics of the airplane and thereby invalidate the tests.

10.4.4.3.3.2.1.1 Thrust orientation. The effectiveness of the applied yawing moment produced by rockets mounted on the wing tips depends on the orientation of the rocket thrust line with respect to the principal axis of the airplane. In order to avoid a rolling moment that might be adverse, depending on the mass distribution of the airplane the rocket thrust should be aligned as closely as possible with the principal axis of the airplane.

10.4.4.3.3.2.1.2 Rocket impulse. On the basis of past experience with model spin-recovery rocket investigations, certain conclusions can be drawn regarding the nature of the rocket impulse required, rocket impulse being the product of the average value of the thrust and the time during which it acts. The rocket must not only provide a sufficient yawing moment for recovery, but the rocket must provide this moment for as long as the spin rotation is

present. Rockets that have the same impulse but different amounts of thrust and thrust durations may or may not produce satisfactory spin recoveries depending on the magnitude of the thrust and the thrust duration.

The primary advantages of a rocket-recovery system are:

(1) Definite known yawing moment is applied.

(2) Applied yawing moment is not affected by wake of airplane.

(3) Rockets do not have to be jettisoned after use.

(4) Fuselage or wing has to be strengthened only to withstand the yawing moment produced by the rockets.

The disadvantages of rockets are:

(1) Some type of sensor must be used to determine the direction of spin so that the proper rocket is fired.

(2) Duration of rocket thrust is limited.

(3) If duration of rocket thrust is too long and pilot does not terminate it when recovery is complete, the airplane may enter a spin in the opposite direction; conversely, if the rocket thrust is terminated prematurely the airplane may not recover from the spin.

(4) If the pilot does not regain control of the airplane following recovery by use of a rocket and the airplane enters a second spin there is no further emergency recovery system; whereas, with a tail-mounted recovery parachute, he can retain the stabilizing effect of the parachute until he is sure he has recovered control.

(5) Two installations are necessary if rockets are mounted on wing tips.

10.4.4.3.3.3 Wing-Tip-Mounted Parachutes (10.18). Tests were conducted until 1952 in the NASA Langley spin tunnel on dynamically scaled models using wing-tip-mounted parachutes. Full-scale airplane tests with wing-tip parachutes have apparently been made on only one airplane in the past 20 years. Wing-tip parachutes apply an anti-spin yawing moment to the airplane to effect a spin recovery; they also apply a rolling moment and, if the airplane has a swept wing, a pitching moment will be applied.

Even though wing-tip parachutes generally need be only about 50 to 60 percent as large as a tail parachute in order to effect a spin recovery, they have all the disadvantages of rockets. In addition if the mass of the airplane is distributed along the wing, the rolling moment produced by the parachute will retard spin recoveries.

10.4.4.3.4 **Special Post-Stall/Spin Test Flying Techniques.** In general, the test pilot must have indelibly fixed in mind what control actions he will take when the first departure occurs. An inadvertent departure can give just as meaningful (perhaps more meaningful) data as an intentional one - if the test pilot overcomes his surprise quickly enough to make preplanned and precise control inputs. The keys to avoiding confusion in the cockpit have already been mentioned, but they bear repeating. The test pilot must be recently proficient in post-stall gyrations and in spinning, and he must be so familiar with the desired recovery controls that they are second nature. Apart from overcoming the surprise factor through adequate preparation, the test pilot may need some other tricks in this highly specialized trade.

10.4.4.3.4.1 **Entry Techniques**

10.4.4.3.4.1.1 **Upright Entries.** For aircraft susceptible or extremely susceptible to spins, an upright spin may be easy to attain. In this case the test pilot's main concern may be how to produce repeatable characteristics; that is, he may seek to achieve the same entry g-loading, attitude, airspeed, and altitude in successive spins so that correlation between spins is easier. Of course, if the aircraft is resistant to spins, it may still be susceptible to departure and entry into a post-stall gyration. In this case, correlation of the data may be even more difficult since the random motions of a PSG are seldom repeatable. Again, the attempt usually is to achieve repeatable entry conditions so that over a large statistical sample the characteristics of the PSG become clear. Achieving several departures with repeatable entry conditions is one of the more demanding piloting tasks. Considerable proficiency is required to achieve the AOA bleed rates or airspeed bleed rates specified in Reference 10.4, Page 5. Once the baseline characteristics for a given configuration are relatively well known, the test pilot is called on to simulate entries appropriate to the operational use of the aircraft.

10.4.4.3.4.1.2 **Tactical Entries.** These entry maneuvers must be carefully thought out in light of the expected role of the aircraft. It is

often wise to consult directly with the using command, particularly if the aircraft has already entered operational service. Reference 10.4 suggests the types of tactical entries listed in Table 10.8 but past experience is no substitute for foresight in planning such tests. By carefully examining the tactics envisioned by operational planners, the test pilot should be able to recognize other possible tactical entries which may cause difficulty in the high angle of attack flight regime.

TABLE 10.8

TACTICAL ENTRIES

1. Normal inverted stalls
2. Aborted maneuvers in the vertical plane (vertical reversals, loops, or Immelmans)
3. High pitch attitudes (above 45°)
4. Hard turns and breaks as used in air combat maneuvering
5. Overshot roll-ins as for ground attack maneuvering
6. High-g supersonic turns and/or transonic accelerations/decelerations
7. Sudden idle power and/or speed brake decelerations
8. Sudden asymmetric thrust transients prior to stall

10.4.4.3.4.1.3 **Inverted Entries.** Obtaining entries into inverted post-stall gyrations or spins can be very difficult simply because aircraft often lack the longitudinal control authority to achieve a stall at negative angles of attack. The most straightforward way to depart the aircraft in an inverted attitude is to roll inverted and push forward on the stick until stall occurs at the desired g-loading. Many aircraft, however, have marginal elevator authority and it is necessary to misapply the controls to obtain an inverted departure. Pulsing the rudder or applying other pro-spin controls as the nose drops can help precipitate departure. In the OV-10, for example, the direction of applied aileron determines the direction of the inverted spin - provided full aileron deflection is used. However, if aerodynamic controls lack authority, the test pilot can also use inertial moments to precipitate inverted departures.

How the inertial terms can aid entry into a spin can best be seen by examining the pitch rate acceleration equation:

$$q = \frac{M_{aero}}{-I_y} + pr \frac{(I_z - I_x)}{I_y}$$

If the negative pitching acceleration generated by M_{aero}/I_y was too small to produce a stalled negative angle of attack, an additional negative pitching acceleration can be produced from (pr $(I_z - I_x)/I_y$). All that is necessary is for p and r to have opposite signs. Typically, the roll momentum is built up by rolling for at least 180° opposite to the desired direction of the inverted spin and then applying full prospin controls at the inverted position. Obviously, these control manipulations must be made at an angle of attack near the stall. Sometimes it is even advisable to apply a slight amount of rudder opposite to the roll during the roll momentum buildup period. A typical procedure designed to produce a left inverted spin is given below:

1. Establish a nose high pitch attitude.

2. Apply full right aileron and a slight amount of left rudder.

3. After a minimum of 180° of roll (360° or more may be advantageous in some aircraft), apply full left rudder, maintain full right aileron, and full forward stick (on some aircraft full aft stick may be used).

4. Recover using predicted or recommended recovery procedures.

This procedure must be modified to fit the characteristics of a particular aircraft, but it does illustrate the kind of control manipulation sometimes required in post-stall/spin investigations. Some aircraft will not enter an inverted spin using this sort of exaggerated technique, but using the inertial moments to augment aerodynamic controls has uncovered spin modes not obtained by other means. Reference 10.12 provides further information on the subject of inverted spinning.

10.4.4.3.4.2 Recovery Techniques

Out-of-Control Recoveries

The underlying principle of all recovery techniques is simplicity (refer to Paragraph 3.4.2 of Reference 10.4). The procedure to be used must not require the pilot to determine the nature or direction or the post-stall

gyration. In fact, Paragraph 3.4.2.2.2 of Reference 10.3 requires recovery from both post-stall gyrations and incipient spins using only the elevator control. Engine deceleration effects must be tested. Any part of the flight control system (the SAS, for example) which hinders desired control surface placement must be identified and carefully evaluated. Care must be taken to ensure that the recovery controls recommended to recover from a post-stall gyration will not precipitate a spin. The test pilot is primarily responsible for identifying reliable visual and cockpit cues to distinguish between post-recovery angular motions (steep spirals, rolling dives) and the post-st 11 gyration. Taken together, these requirements demand that the test pilot be a careful observer of the motion. In fact, he is likely to become so adept at making these observations that he must guard against complacency. His familiarity with the motions may cause him to over-estimate the operational pilot's ability to cope with the out-of-control motions. Paragraph 3.4.2.2.2 of Reference 10.3 specifies that the start of the recovery shall be apparent to the pilot within three seconds after initiation of recovery. This requirement is very stringent and will require very fine judgement on the part of the test pilot.

10.4.4.3.4.2.1 <u>Spin Recoveries</u>. The criteria for recovery from a spin are outlined in Table 10.9. (Paragraph 3.4.2.2.2 of Reference 10.3). These criteria are applicable to any spin modes resulting from any control misapplication specified in Reference 10.4. Timing of control movements should not be critical to avoid spin reversals or an adverse mode change.

Table 10.10 outlines the NASA Standard, NASA Modified, and NASA Neutral recovery procedures. These recoveries are by no means optimum for all aircraft and they must not be construed to be. In contrast, the F-4E recovery technique includes forward stick, which reflects the philosophy of simplifying out-of-control recovery procedures. Generally, forward stick is desirable for recovery immediately following a departure. The reason for retaining the forward stick is to keep the out-of-control recovery procedure like the spin recovery procedure. However, individual aircraft characteristics may dictate that out-of-control recovery procedures differ from spin recovery procedures. Such characteristics violate the specifications of References 10.3 and 10.4, but the test pilot must evaluate the need for two recovery procedures. He cannot assume that any "canned" recovery procedure will work nor that the

design meets the specifications. In summary, the test pilot's job is to assure that the operational pilot has a simple, reliable recovery procedure which will consistently regain controlled flight.

TABLE 10.9
RECOVERY CRITERIA

Class	Flight Phase	Turns for Recovery
I	Category A,B	1-1/2
I	PA	1
IV	Category A,B	2-1/2

TABLE 10.10
RECOVERY TECHNIQUES

NASA Standard	NASA Modified	NASA Neutral
(If ailerons were held during spin, neutralize)	Same	Neutralize all Controls
A. Full opposite rudder	A. Full opposite rudder and at the same time ease stick forward to neutral.	
B. Stick full aft	B. Neutralize rudder when rotation stops.	
C. When rotation stops - neutralize rudder (immediately)		
D. EASE stick forward to approximately neutral position.		

The following questions are taken from the AFFTC F-5F Spin report. They are intended to expose you to real high AOA terminology and to give you a feel for what factors come into play in high performance aircraft high AOA flight.

10.1 The F-5F had roll rate hesitations or even roll reversals when trying to roll at high AOA with ailerons. The main reason for this was
_____.

    a) adverse yaw
    b) kinematic coupling plus a moderate dihedral effect
    c) strong $C_{\ell_{\delta_a}}$

    d) negative $C_{m_{\delta_a}}$

10.2 Rudder rolls at or near stall AOA produced a roll about the stability axis with oscillations in roll rate superimposed. This was caused by
_____.

    a) moderate dihedral effect
    b) kinematic coupling
    c) strong directional stability
    d) a and b

10.3 A flat spin could be entered from an abrupt full aft stick input. During one g flight, a forward cg required _____ AOA's.

    a) lower
    b) higher

10.4 At the aft cg condition, the F-5F is _____ to departures when an abrupt full aft stick input is made.

    a) extremely susceptible
    b) susceptible
    c) resistant
    d) extremely resistant

10.5 The most critical full rudder/full aft stick maneuver to generate a PSG or spin, was a level, decelerating turn, applying full top rudder accompanied by a smooth full aft stick input below stall AOA. Large AOA values were obtained initially due to _____.

    a) aerodynamic longitudinal moments
    b) kinematic coupling
    c) inertial coupling

10.6 Following the same entry as question No. 10.5, inertial yaw acceleration was less with _____.

    a) abrupt aft stick
    b) smooth aft stick

10.7   An oscillatory spin sometimes occurred from a PSG even at nominal cg's.
       During recovery different control inputs gave the following results

       _____.

       a)   rudder against, was effective
       b)   adverse yaw due to ailerons helped the recovery
       c)   ailerons-with helped the airplane "roll out of the spin"
       d)   ailerons-with produced a pitching moment which resulted in an
            anti-spin yaw acceleration through the relationship

$$r = \dots \frac{I_x - I_y}{I_z} \, pq$$

Engine Operating Characteristics

Four double-engine and five single-engine flameouts were experienced during 195 maneuvers conducted during this program. The susceptibility of the engines to flameouts was dependent upon power setting and severity of the post-stall motions. Most of the flameouts occurred at power steerings at or above 95% RPM and above 40° AOA with large sideslip angles present. The flameouts typically occurred during the first significant AOA/sideslip excursion during the post-stall motions. The probability of engine flameout was significantly reduced when power during the maneuver entry was reduced to below 95% RPM. Left and right engines were equally susceptible to flameout during a given maneuver. All of the flameouts occurred in the vicinity of 35,000 feet pressure altitude. Flameout susceptibility should be less at lower altitudes. No engine flameouts were encountered during inverted out-of-control flight. These characteristics are the same as those obtained on the F-5E.

Aerodynamic Analysis

This section contains an explanation of the aerodynamics involved in the airplane characteristics which were described in previous sections. Trends in airplane stability and control were derived from analysis of flight test data. Similar trends are generally substantiated in wind tunnel and analytical data. Wind tunnel data presented in Appendix B was obtained as low Mach but exhibits trends evidenced throughout the subsonic Mach range.

Basic Airplane Erect Characteristics

Longitudinal

The slight nose drop tendency at stall (21 to 25 degrees AOA, depending on Mach) resulted from a decrease in lift and a significant increase in static longitudinal stability above stall AOA. The decrease in lift, as indicated by a local change in sign of the slope of normal force coefficient (C_N) versus AOA, is presented in Figures B1 and B2. The increase in longitudinal stability, as indicated by an increase in slope of pitching moment (C_m) versus AOA, is presented in Figures B3 and B4. Normal force coefficient again increased when AOA exceeded approximately 25°, as indicated by a restoration in the slope of C_N versus AOA, but was not always apparent to the pilot. Although C_N again increased above 25° AOA, a decrease in speed (due to increased drag) usually meant a decrease in normal load factor as AOA increased.

10.123

Flight test data indicated static longitudinal stability (C_m at zero

sideslip) as being stable up to 40° AOA, essentially neutral between 40 and 50° AOA, and again stable above 50° AOA. For post-stall AOA's less than 40°, longitudinal stability was only slightly reduced over that of the F-5E for respective nominal and aft cg's (nominal cg of the F-5E is 14% MAC and aft cg is 20% MAC). Above 40° AOA, the F-5E exhibited significantly less longitudinal stability than the F-5E. Above 50° AOA with an aft cg (16% MAC), the F-5F had approximately 40% less nosedown restoring pitching moment than the F-5F and F-5E which resulted in the decreased PSG and spin resistance of the F-5F (the other difference being large yawing moments at small sideslip angles, discussed later).

Trim AOA's with full aft stick were 28 and 31° with nominal and aft cg's, respectively, but higher AOA's were obtained when full aft stick was sustained. Directional instabilities and strong dihedral effect resulted in wing rock with considerable oscillations in roll rate, yaw rate, and sideslip when full aft stick was sustained. Inertial pitch coupling ($I_z - I_x/I_y$ pr) tended to increase AOA above maximum trim AOA. Also, a noseup pitching moment due to sideslip (positive C_{m_β}) existed above approximately 28° AOA. When full aft stick was sustained, sideslip oscillations reduced or eliminated the nosedown aerodynamic pitching moment, or even resulted in a net noseup moment, depending on the magnitude of the sideslip oscillations. AOA's in excess of 50° were achieved with aft cg when full aft stick was sustained while AOA's were usually obtained below 30° with nominal cg. The pitching moment due to sideslip was similar to that of the F-5E. Trim AOA with full aft stick was increased by four degrees over that of the F-5E due to the increased stabilator deflection (20° compared to 17°) and a slight reduction in longitudinal stability. The higher AOA's (as compared to the F-5E) obtained with sustained full aft stick with an aft cg resulted partially from the increased stabilator deflection but primarily from the decreased longitudinal stability above 40° AOA.

Abrupt full aft stick applications were capable of achieving in excess of 40 to 50° AOA with the nominal and aft cg's, respectively, without sustaining full aft stick (discussed later).

Lateral-Directional

The onset of wing rock at stall AOA was a result of static directional stability C_{n_β} becoming negative while maintaining sufficient dihedral effect

C_{ℓ_β} to prevent a pure nose slice from occurring. Excursions in sideslip

were self-terminating as the airplane rolled due to C_{ℓ_β} and thus reduced

sideslip through the interchange of AOA and sideslip. Dihedral effect was, however, reduced somewhat near stall AOA, especially with flaps UP. Above approximately 28° AOA, strong dihedral effect was restored while static directional stability generally remained negative. Flap deflection increased dihedral effect for AOA's up to approximately 35°. The static directional instability was of greater magnitude than that of the F-5E, but an increase in dihedral effect due to the installation of wing fences (Figure C1) resulted in improved lateral-directional characteristics over that of the F-5E for AOA's below approximately 32°.

Although airplane response to aileron was sluggish near or above stall AOA, no strong adverse effects were noted when full aileron was applied at high AOA. Aileron effectiveness $C_{\ell_{\sigma_a}}$ existed near or above stall AOA while

$C_{\lambda_{\ell_a}}$ decreased significantly as AOA was increased to stall and thereafter

retained near constant effectiveness at AOA's above stall. Negligible yawing moment due to aileron $C_{n_{\sigma_a}}$ existed near or above stall AOA while C_n was small or negative. The result of aileron input was that the airplane initially rolled (essentially about the body X-axis) in the direction of input and built up adverse sideslip due to an interchange of AOA and sideslip. As stall AOA was approached, attainable roll rates with the ailerons were greatly reduced due to the dihedral effect associated with this adverse sideslip and decreased aileron effectiveness. At or above stall AOA, the adverse sideslip tended to cause the roll to hesitate or even reverse direction.

Rudder became the primary roll control near stall AOA. Rudder effectiveness $C_{n_{\sigma_r}}$ did not noticeably decrease until stall AOA was exceeded. Little, if any, effectiveness remained above 50° AOA. Rudder rolls near but below stall AOA were rapid and smooth. During these rolls, typical peak yaw and roll rates of 30 and 100° per second, respectively, caused AOA to peak to approximately 30 degrees even with fixed longitudinal stick position during the roll. As stall AOA was exceeded, the roll hesitated and became more oscillatory. At or above stall AOA, rudder inputs resulted in yaw excursions to quite large proverse sideslip (due to negative C_{n_β}). A rapid roll due to dihedral effect followed. As the airplane rolled, sideslip changed sign due to an interchange of AOA and sideslip. Thus, adverse sideslip was created, causing a rolling moment (due to C_{ℓ_β}) opposite to the direction of control input. Depending on the magnitude of the adverse sideslip, the roll rate momentarily decreased, stopped, or even changed sign before sideslip again became proverse. Yaw rate normally remained the direction of rudder input. Above stall AOA the roll could be described as a continual rotation about the stability axis with roll oscillations (wing rock) superimposed. Examples of rudder rolls are presented in Figures A13 through A15. No problems existed in performing full rudder pedal rolls when longitudinal stick was maintained forward of or at that position required to trim the airplane at stall AOA. When full aft stick was applied (with aft cg) in conjunction with full rudder, however, peak AOA's in excess of 45° were obtained due to the stabilator deflection, inertial coupling, and pitching moment due to sideslip. With the attainment of these extreme AOA's, PSG or spin entry was possible (discussed later).

Significant yawing moments, observed in flight test data, were present at zero or small sideslip angles (less than $\pm 10^O$) above approximately 354° AOA. These moments were presumably the result of the asymmetric shedding of vortices from the nose of the airplane (determined during ongoing wind tunnel and water tunnel flow visualization tests by the contractor). Above 42° AOA was significantly smaller. Flight test data indicated these yawing moments to be positive from approximately 45 to 60° AOA and negative between approximately 60 and 70° AOA. The sign of those below 45° AOA was not consistent. The yawing moments above 42° AOA were approximately twice the

the magnitude of those of the F-5E. Whereas these moments were not significant for the F-5E, they were very influential in the behavior of the F-5F. The existence of the large yawing moments above 42° AOA was one of the two primary differences between the F-5F and F-5E which resulted in decreased PSG and spin resistance (the other being decreased longitudinal stability above 40° AOA, discussed later).

A propelling yaw damping derivative (positive C_{nr}) were evident above 50° AOA, with the strongest effect between 50 and 60° AOA. Significant effects due to positive C_n were evident when approximately 35° per second yaw rate was achieved in the 50 to 60° AOA region. The propelling yaw damping was similar to that of the F-5E.

PSG and Spin

The attainment of approximately 45° AOA by abrupt aft stick application alone was sufficient for PSG or spin entry. High AOA obtained in such a manner was initially accompanied by very small sideslip angles. Large yawing moments were present (discussed earlier) to establish a yaw excursion which was capable of causing PSG or spin entry. Figure A29 presents an example of an abrupt pullup at 150 KIAS with an aft cg which resulted in an unrecoverable flat spin. Although not pursued further, trends in data indicate certain conclusions about abrupt full aft stick inputs applied below stall AOA. With an aft cg in a one-g, wings level condition, abrupt full aft stick applied at 20° AOA or lower (greater than 130 KIAS) and sustained for as little as two seconds can result in an unrecoverable flat spin. With the nominal cg, such an input would be required at approximately 10° AOA or lower (greater than 160 KIAS) for spin entry to occur. Entry into a PSG or recoverable oscillatory spin, rather than a flat spin, may be possible with the nominal cg due to the increased nosedown aerodynamic pitching moment which could prevent the rapid transition to a flat spin by limiting AOA excursions. To achieve sufficient AOA for PSG or spin entry from an accelerated flight condition, the abrupt aft stick input must occur at significantly lower AOA. Above 250 KIAS, for instance, the input must occur at an AOA at least 5° lower than for the one-g, wings-level condition. Pitch damping C_{m_q} was the reason for the lower AOA

requirement for full aft stick input during accelerated flight. More horizontal tail was required to obtain a given AOA, less incremental horizontal tail input was available to increase AOA during an abrupt full aft stick input. In addition, the higher attainable pitch rates at the higher airspeeds produced more nosedown moment due to C_{mq} than at low airspeeds.

Full aft stick/full rudder or sustained full aft stick (smooth input) maneuvers achieved 45° AOA or higher with large sideslip oscillations (approximately $\pm 20^O$). The airplane was susceptible as with the abrupt full aft stick input alone. The large yawing moments at small sideslip angles did not completely dominate the motion in these maneuvers since less time was spent at $\pm 10^O$ sideslip than during the abrupt pullup maneuver. With the large sideslip oscillations, the natural "stability" (due to strong C_{ℓ}) often contained the yaw excursions. However, the effect of the large moments at small sideslip was evident and resulted in either decreasing or increasing the existing yaw rates or starting a yaw rate if non existed. Thus, any maneuver which achieved near 45° AOA had the potential for PSG or spin entry.

PSG or spin entry was possible without significant influence from the large yawing moments at small sideslip. If full aft stick/full rudder maneuvers were performed so as to achieve near 50° AOA with significant yaw rate (at least 25° per second), PSG entry was possible. Spin entry was possible if at least 35° per second yaw rate was established near 50° AOA. However, many full aft stick, full rudder deflection maneuvers (with or without cross controlled aileron) resulted in high yaw rate with lower AOA (less than 40°) or high AOA (greater than 50°) with low yaw rate but did not sustain both high AOA and high yaw rate. Two effects which often prevented a sustained high AOA were the nominal cg and high airspeed. The increased longitudinal stability at the nominal cg made it very difficult to sustain AOA's much above 40°. Maneuvers which maintained a nose low attitude, such as windup turns, maintained high enough speeds so that a substantial aerodynamic nosedown moment was present to counter the noseup inertial moment and thus prevent sustained at the extreme AOA's because of inertial yaw coupling ($I_x - I_y/I_z$ pq). Yaw rates in excess of 30° per second with MANEUVER flaps and in excess of 40° per second with flaps UP were obtained below 40° AOA. The higher

attainable yaw rates with flaps UP was due to less dihedral effect below approximately 35° AOA than with MANEUVER flaps. Therefore, the airplane was more susceptible to PSG/spin entry with flaps UP. The large positive pitch rates, involved in achieving even higher AOA, coupled with roll rate to produce an inertial yaw acceleration to oppose the established yaw rate. This opposition to yaw rate, along with decreased redder effectiveness at high AOA's, resulted in reduced yaw rates of less than 20° per second at the high AOA's. As a result, the following was the most critical full rudder/full aft stick maneuver from the standpoint of susceptibility to PSG or spin: a level, decelerating turn applying full rudder out of the turn and smooth full aft stick below stall AOA. Susceptibility was significantly increased when this maneuver was flown with the aft cg configured airplane or with flaps UP. Full rudder input below stall AOA produced sufficient yaw/roll rates to inertially couple AOA to large values. As the airplane pitched to high AOA/high pitch attitude (since rudder was applied away from the turn direction), the airspeed decreased rapidly. Thus, the aerodynamic nosedown moment was reduced and high AOA was more easily sustained. Smooth aft stick application (as opposed to abrupt) allowed the high AOA to be obtained with minimum pitch rate and thus minimum anti-spin inertial yaw acceleration. This maneuver established the high AOA while maintaining sufficient yaw rate to generate a substantial prospin yawing moment due to positive C_{n_β}. Therefore, a tendency towards continued rotation was established.

Forward stick was the key to recovery from the PSG. Considerable nose-down moment due to the stabilator was required to overcome both the noseup inertial moment due to the yaw and roll rates and noseup moment due to sideslip. Depending on the established yaw and roll rates, full forward stick could be required for recovery from the PSG. It was possible to accelerate the yaw rate somewhat with the application of abrupt forward stick. A negative pitch rate (or reduction in positive pitch rate), produced by the forward stick, coupled with roll rate to create a prospin inertial yaw acceleration (or reduced the typical anti-spin inertial yaw acceleration by reducing positive pitch rate). If sufficient forward stick was not applied to simultaneously reduce AOA, progression into a developed spin was probable. In some cases, especially with the aft cg, full forward stick applied immediately

upon recognition of loss of control did not effect recovery without entry into a spin.

When recovery was not effected from a PSG with the nominal cg, the propelling C_{n_r} increased yaw rate and an oscillatory spin was established. Full forward stick usually did not produce sufficient nosedown moment to reduce AOA due to the increased inertial noseup moment as yaw rate increased. Reduction in yaw rate to reduce the noseup inertial moment, while maintaining forward stick, was the key to recovery from the spin. Forward stick was maintained to allow maximum nosedown aerodynamic moment. However, effectiveness of the lateral-directional controls to reduce yaw rate was marginal at best. Rudder applied against the spin produced little, if any, yawing moment to slow the rotation due to loss of effectiveness at high AOA. Ailerons applied in the direction of spin produced little, if any, adverse yawing moment to oppose the rotation since yawing moment due to aileron was minimal at high AOA. Probably the most benefit of the lateral-directional spin recovery controls was the rolling moment of the aileron. A very small roll capability into the spin direction caused a slight wing-down orientation about the spin axis (inside wing down). This produced a small positive pitch rate which coupled with the roll rate to produce an anti-spin inertial yaw acceleration. Recovery or nonrecovery from the spin (above 50° AOA) was a result of the balance between this inertial anti-spin yaw acceleration and the prospin aerodynamic yaw acceleration primarily due to the positive C_{n_r}. AOA oscillations to lower than 50° resulted in an anti-spin aerodynamic yaw acceleration due to negative C_{n_r} and some rudder effectiveness, and resulted in a decrease in yaw rate. When yaw rate was reduced enough to allow a sustained AOA below 50°, recovery was accomplished by sustaining anti-spin controls. However, if AOA was sustained between 50 and 60° (region of strongest positive C_{n_r}) long enough, yaw rate could accelerate significantly, and progression into the higher rate, higher AOA unrecoverable flat spin could probably occur. With the aft cg, if recovery was not effected from a PSG, rapid transition into an unrecoverable flat spin occurred. This was due to the significantly reduced nosedown restoring pitching moment with the aft cg.

Centerline Tank Loading

Addition of a centerline tank (loading 5) to the basic airplane resulted in a significant degradation in static lateral-directional stability (Figures B11 and B12). Static directional stability was significantly degraded over that with the basic airplane for AOA's up to 30° and only slightly for higher AOA's. Dihedral effect was significantly reduced as compared to the basic airplane for all AOA's above approximately 10°. With flaps fully extended, $C_{\ell_{\beta}}$ was reduced to near zero in a small AOA region, near 22 to 24°. This AOA region was slightly larger, approximately 20 to 25° AOA, with minimal flap extension (as with MANEUVER flaps selected above 250 KIAS) or with flaps UP.

With MANEUVER flaps, stalls resulted in a nose slice tendency when stall AOA was attained. The motion following the nose slice consisted of wing rock with more yaw rate and larger sideslip angles than were evident with the basic airplane. Above 200 KIAS and especially above 250 KIAS (only $12/8^{\circ}$ LE/TE flaps), stalls resulted in a severe, abrupt nose slice at approximately 20° AOA. The nose translated purely in yaw until dihedral effect was restored at approximately 10° of sideslip. Restoration of dihedral effect was abrupt, resulting in large initial roll rate excursions. Large yaw rates were then combined with the large roll rates in the sane direction and AOA was inertially coupled abruptly to over 60°. The roll following the nose slice resulted in a large sideslip buildup to the opposite direction due to an interchange of AOA and sideslip. The directional instability was such that this sideslip caused either a reduction in established yaw rate or a yaw and roll opposite in direction to the nose slice. This abrupt yaw and roll resulted in a very large peak in inertial pitch acceleration, causing a peak AOA in excess of 75° during the PSG. Figures A9 and A26 present the maneuvers performed during this program with the centerline tank loading.

10.1   Money, A.F. and House, D.E. U.S. Navy Flight Test Evaluation and
         Operational Experience at High Angle-of-Attack. AGARD-CP-199,
         November, 1975.

10.2   Woodcock, R.J. & Weissman, R. The Stall-Spin Problem. AGARD-CP-199,
         November, 1975.

10.3   MIL-F-8785C. Flying Qualities of Piloted Airplanes. 5
         November 1980.

10.4   MIL-S-83691A (USAF) Stall/Post-Stall/Spin Flight Test Demonstration
         Requirements for Airplanes. 15 April 1972.

10.5   Ad Hoc Team Report on F-111 Stall/Post-Stall/Spin Prevention
         Program. Aeronautical Systems Division. 28 August 1970.

10.6   Titiriga, A. Jr., Ackerman, J.S., and Skow, A.M. Design Technology
         for Departure Resistance of Fighter Aircraft. AGARD-CP-199,
         November, 1975.

10.7   Nial, J.A. Spin Testing USN High Performance Airplanes. AGARD
         Report, November 1961.

10.8   Babister, A.W. Aircraft Stability and Control. New York, The
         MacMillian Company, 1961.

10.9   Kerr, T.H. "General Principles of Spinning," AGARD Flight Test
         Manual. Volume II, Chapter 8, New York, Pergamon Press, Inc., 1962.

10.10   Anglin, E.L., et al. Analytical Study of Aircraft Developed Spins
         and Determination of Moments Required for Satisfactory Recovery.
         NASA TN D-2181, 1964.

10.11   Hendrickson, C.L., et al. NF-104A Aerospace Trainer Evaluation.
         FTC-TR-65-37, Air Force Flight Test Center, Edwards AFB, California,
         December 1965.

10.12   Skalla, D.Z. Commander USN, A New Look at the Inverted Spin. Naval
         Air Test Center, Patuxent River, Maryland, 6 May 1968.

10.13   Wheatly, Gary F. Lieutenant Commander USN, Pilot Techniques for
         Spin Flight Testing. Naval Test Pilot School Staff Paper, Naval Air
         Test Center, Patuxent River, Maryland, 5 February 1968.

10.14   Milner, James R. Major, USAF, Limited A-7D Spin Tests.
         FTC-TR-70-14, Air Force Flight Test Center, Edwards AFB, California,
         May 1970.

10.15   Chambers, J.R. and Bowman, J.S. Jr. Stall/Spin Test Techniques used by NASA. AGARD-CP-199, November, 1975.

10.16   Fortner, Larry P., Major, USAF. T-37B Qualitative Spin Tests. FTC-TR-70-9, Air Force Flight Test Center, Edwards AFB, California, April 1970.

10.17   Nial, J.A. Spin Testing USN High Performance Airplanes. AGARD Report, November 1961.

10.18   Burk, S.M. Jr. Summary of Design Considerations for Airplane Spin-Recovery Parachute Systems. NASA TN D-6866, August, 1972.

CHAPTER 11

ENGINE-OUT THEORY AND FLIGHT TESTING

11.1 INTRODUCTION

This chapter examines the problems associated with an engine failure and how engine out flight testing is accomplished. The discussion will be divided into the control problem, the performance problem, pilot reaction times, and how the equations of motion are affected by an engine loss. In all cases, the failed engine will be considered the most critical. For a jet aircraft, this is an outboard engine; for a U.S. conventional propeller aircraft (clockwise rotation propeller) this would be the left outboard engine. If the loss of an important system (rudder, hydraulics, etc.) supported by a particular engine complicates the engine out performance or control problem to a greater degree than the asymmetric moment alone, then that particular engine would be considered critical.

The data gathered through engine-out testing is used to build the initial portions of the takeoff, climb, and landing performance data charts of an aircraft flight manual. Also, many important decisions regarding engine-out procedures must be sought. One very controversial area that needs major attention is that of pilot reaction time. Testing must always take into consideration that the aircraft will be flown by operational pilots not in a controlled test environment.

Engine-out testing is divided into two areas: the performance problem and the control problem.

11.2 THE PERFORMANCE PROBLEM

Reduced climb performance, service ceiling, and range capability accompany an engine failure as a natural consequence of decreased thrust and increased drag. But the effect of an engine failure on takeoff performance is a more complex subject. Basically, the requirement is for the aircraft to attain a takeoff velocity at a given lift coefficient. At any point during the takeoff roll the pilot needs a variety of speeds on which to base a decision to abort or continue. These definitions vary considerably between the military and the FAA. Part 25 of the FAA regulations details requirements on takeoff performance. The military usually receives its performance specifications from the System Program Office (SPO) or from a Statement of Need (SON) from a Major Air Command.

11.2.1 Takeoff Performance

At every instant throughout the takeoff roll, the pilot must have an acceptable course of action available in the event of engine failure. During the first part of the takeoff roll, this action will be to abort the takeoff. Beyond a certain point the action will be to continue the takeoff with the engine failed. The dividing point between these courses of action is a function of aircraft performance and control.

Consider an aircraft in a particular configuration and gross weight. For any given runway length there is a maximum speed to which it can accelerate on all engines, experience a critical engine failure, and then complete a maximum effort stop at the far end of the runway. This speed, the refusal speed, (V_R), is relatively high for long runways and relatively low for short ones (see Figure 11.1). Stopping technique and devices to be used must be specified. This speed could also be maximum braking speed (V_{MB}) depending on how the speeds are designed. However, V_R must never exceed V_{MB} in order to avoid hazardous conditions.
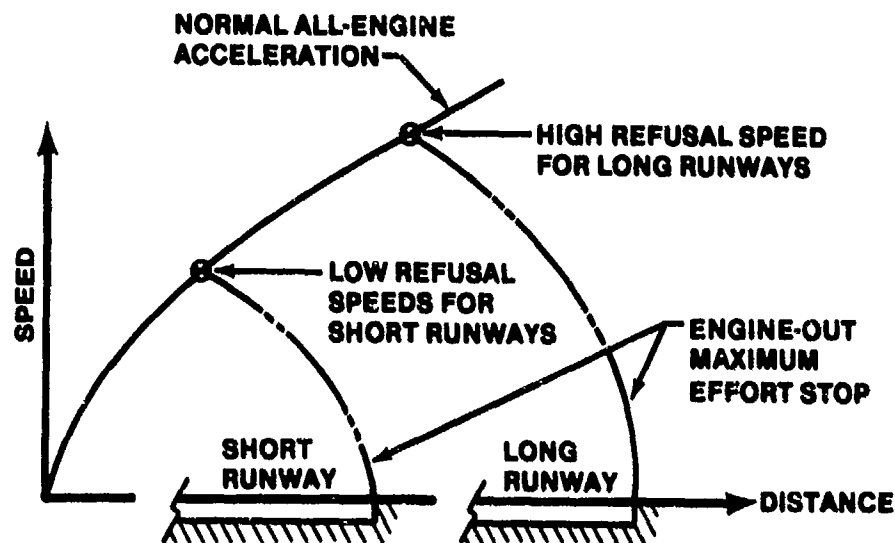
FIGURE 11.1. REFUSAL SPEED

Now consider the same aircraft attempting the takeoff under identical conditions. There is also a minimum speed to which it can accelerate on all

engines, lose the critical engine, and then continue the takeoff with the engine failed, becoming airborne at the far end of the runway. This speed, the minimum-continue speed, varies with runway length in a manner opposite that of refusal speed, i.e., it is relatively low for long runways (Figure 11.2).
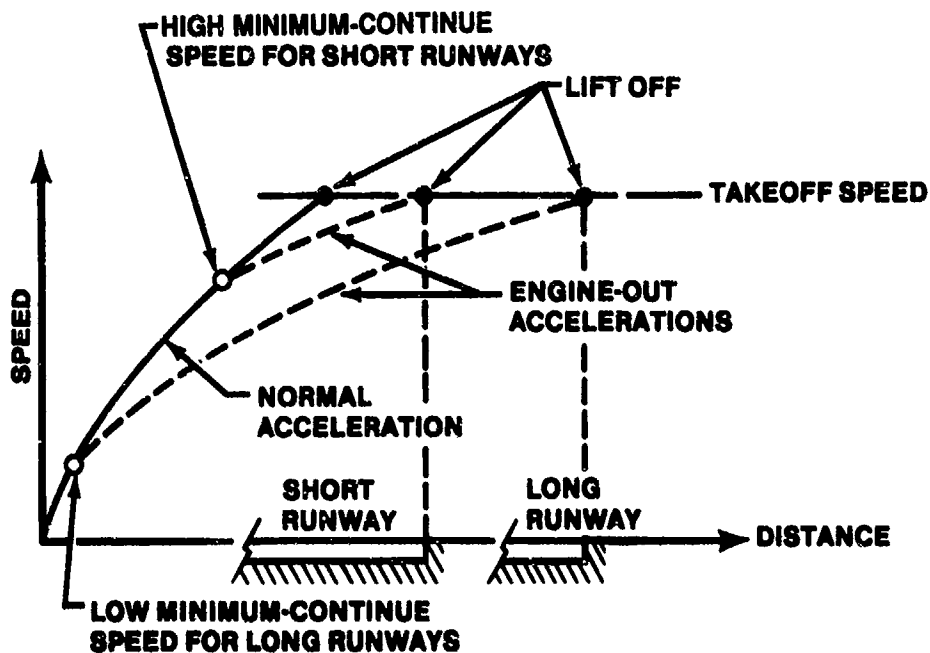
FIGURE 11.2.   MINIMUM-CONTINUE SPEED

11.3

The gap between the minimum-continue speed and the refusal speed reflects the size of the safety margins provided by a given runway for the particular conditions (Figure 11.3).
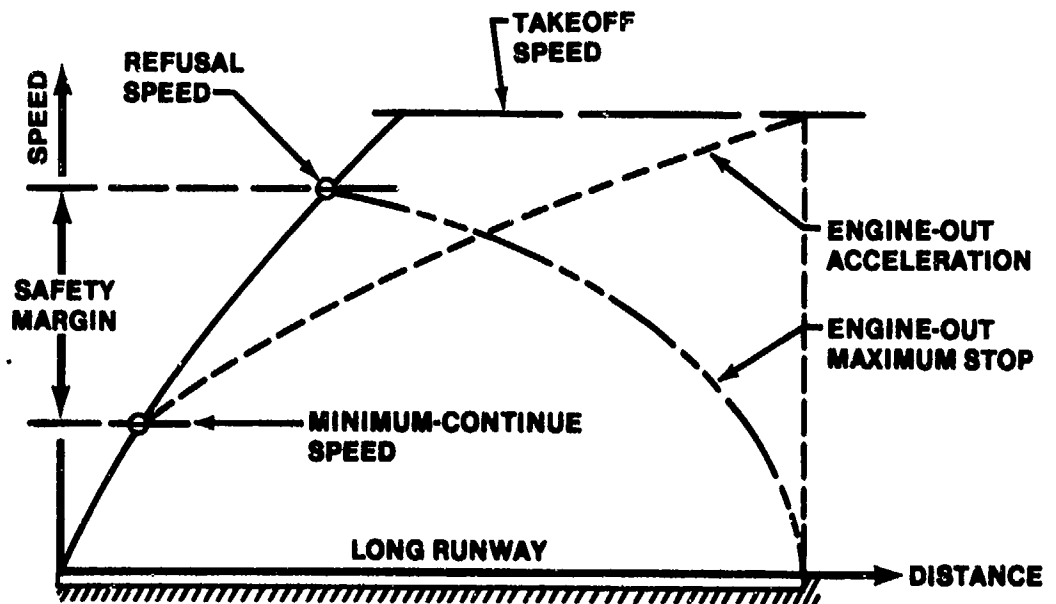
FIGURE 11.3. TAKEOFF SAFETY MARGIN

Obviously, if the runway is very short and the refusal speed is less than the minimum-continue speed, a situation exists where neither a safe takeoff nor an abort can be made if an engine failure occurs between the two speeds. (Figure 11.4).
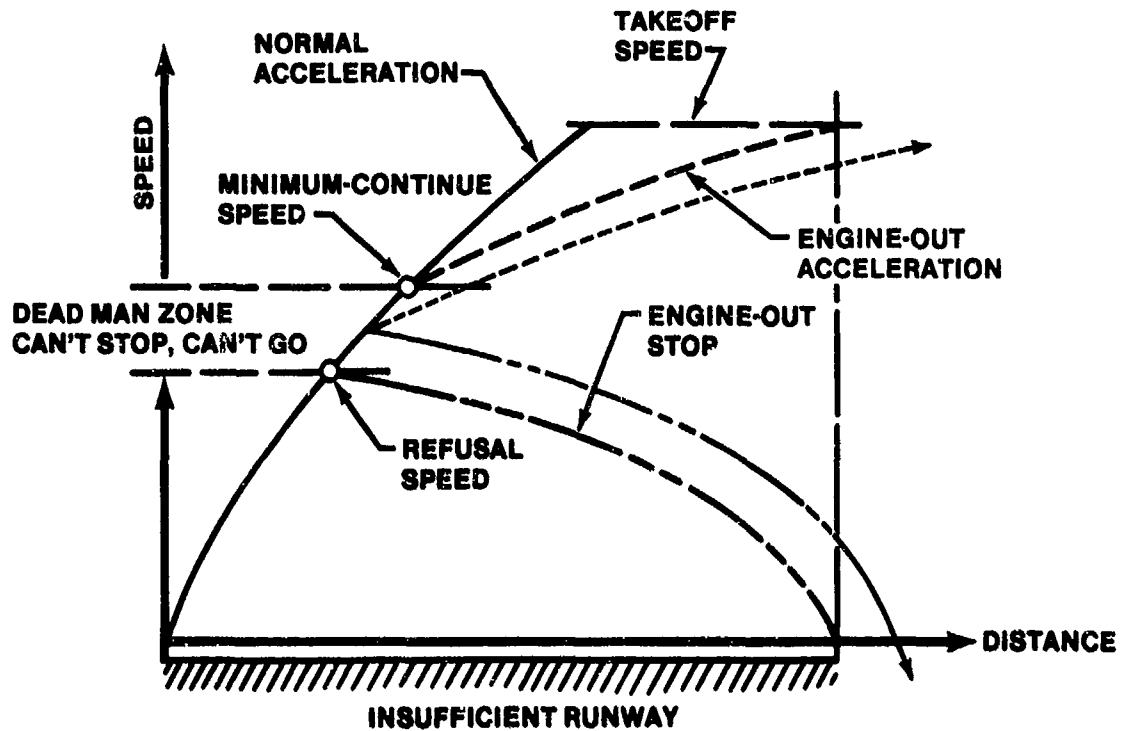
FIGURE 11.4. TAKEOFF DEAD MAN ZONE

The military normally uses a distance called Critical Field Length (CFL) to enable the pilot to immediately determine if the runway length is sufficient to provide a safety margin. The CFL is the total runway required to accelerate to a given speed, lose an engine, then continue the takeoff or abort in the same distance. The speed used in the CFL definition is the critical engine failure speed (V_{CEF}) (Figure 11.5).
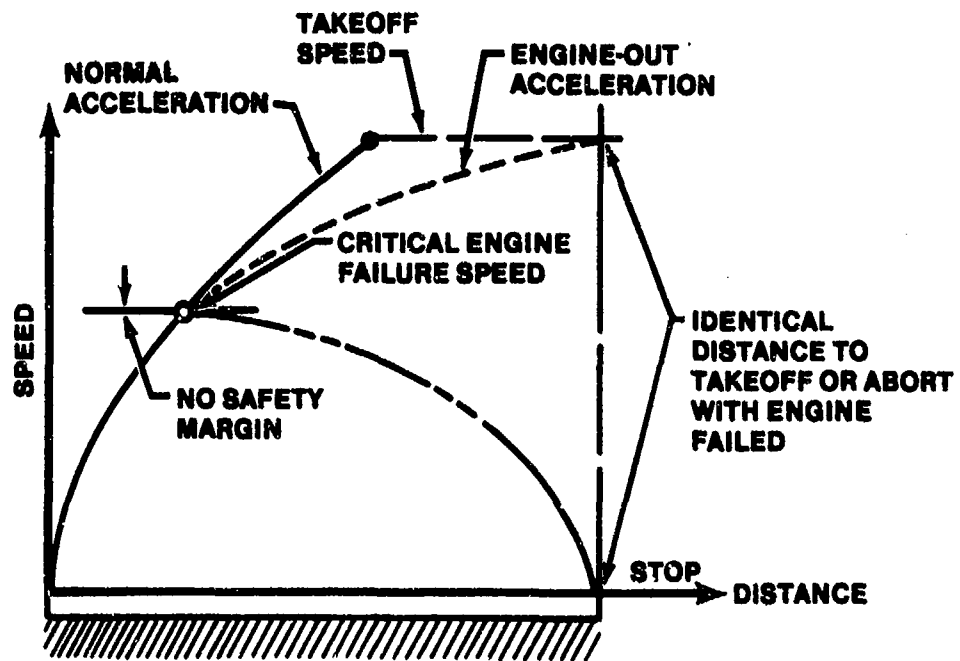
FIGURE 11.5. CRITICAL FIELD LENGTH/CRITICAL ENGINE
FAILURE SPEED

The next term to define is decision speed. Decision speed (V_1 or S_1) is the speed at which the pilot must decide whether to continue the takeoff or abort. Decision speed is usually the higher of V_{CEF} or ground minimum control speed. If S_1 is below V_R, as shown in Figure 11.6, then a safety zone exists such that the pilot can either takeoff or abort.
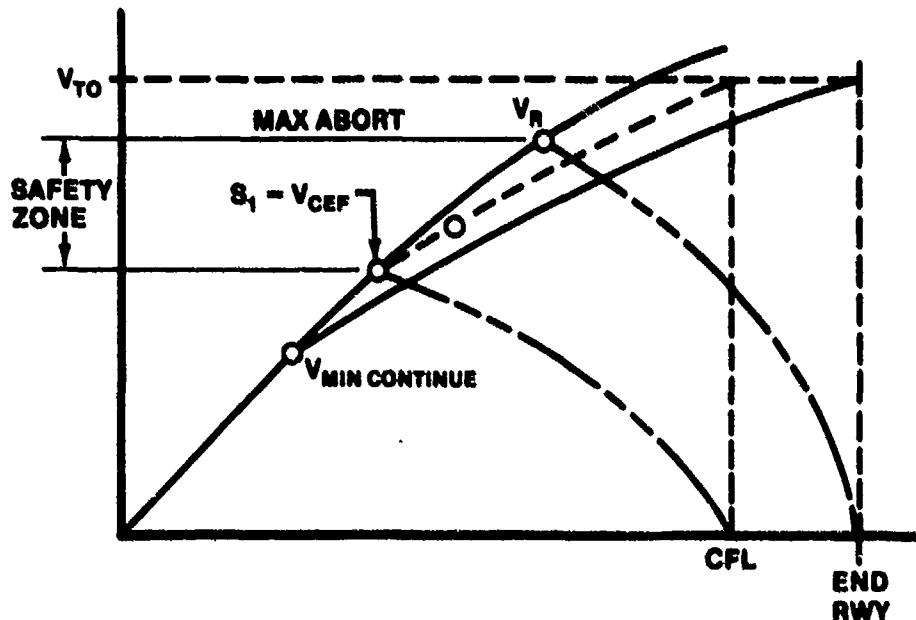
FIGURE 11.6. DECISION SPEED

11.6

All the previous performance discussions are concerned with what the aircraft will actually do. It still remains for the pilot or operational authority to decide at what particular speed or distance the course of action will change from abort to continue the takeoff in the event of engine failure. If the initial climb performance is going to be critical on the takeoff, the decision poi. may be near the higher speed end of the safety margin (Figure 11.7).
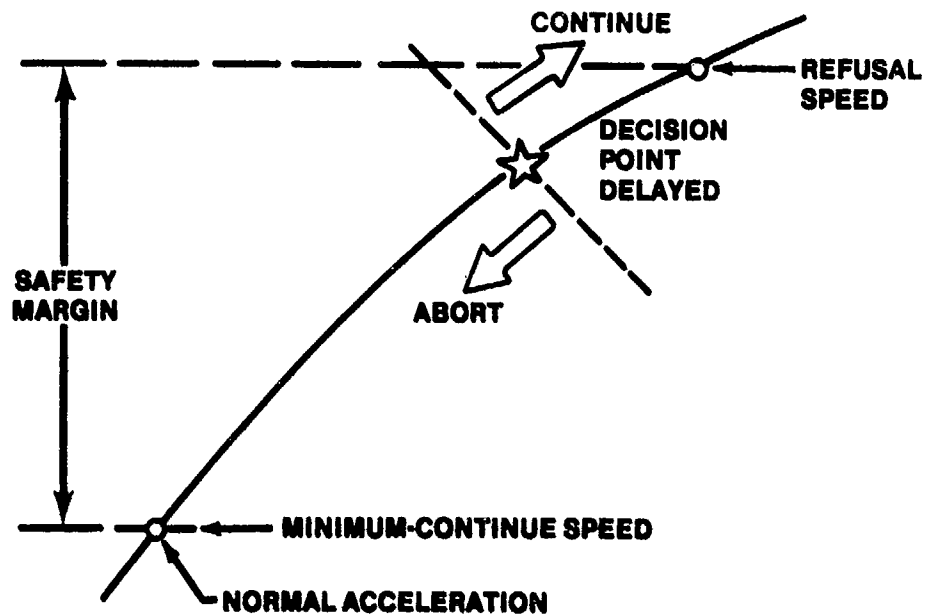
FIGURE 11.7. HIGH DECISION SPEED

The B-47 illustrates the opposite case. This aircraft had a very poor record for successful aborts and was operated with the decision speed relatively near the low speed end of the safety margin (Figure 11.8).
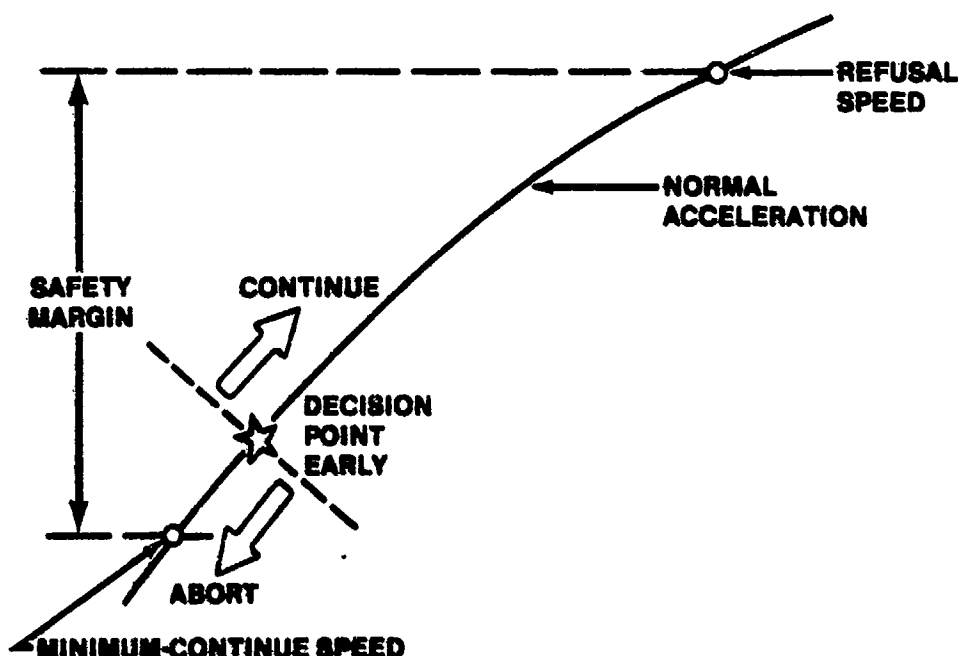
FIGURE 11.8. LOW DECISION SPEED

Other cases may be decided by the nature of the overrun or the terrain beyond the runway i.e., is it better to go off the far end of the runway almost stopped or almost flying?

What about the climbout after becoming airborne? The period between lift-off and attaining best engine-out climb speed can be very critical. Major air commands normally specify a minimum authorized rate of climb between 200 and 500 feet per minute for engine-out operations. This level of performance allows little margin for mismanagement of attitude or configuration. Flap retraction may have to be accomplished incrementally on a very tight speed schedule to keep sufficient lift for a positive climb gradient without excessive drag. Unexpected characteristics may be encountered in this phase. For example, the additional drag due to opening doors might make it desirable to delay gear retraction until late in the clean-up phase. In another instance, the time available to obtain the clean

11.8

configuration might be limited by the supply of water injection fluid if dry thrust is insufficient to maintain the climb. Careful flight test exploration of this phase is an obvious requirement.

11.3 THE CONTROL PROBLEM

The control problem is divided into the steady state case and the dynamic case. The dynamic case is an extension of the steady state case due to the rates and accelerations incurred during pilot reaction time and generally will dictate the maximum control inputs required. Figure 11.9 shows an aircraft in steady state equilibrium with a failed engine.
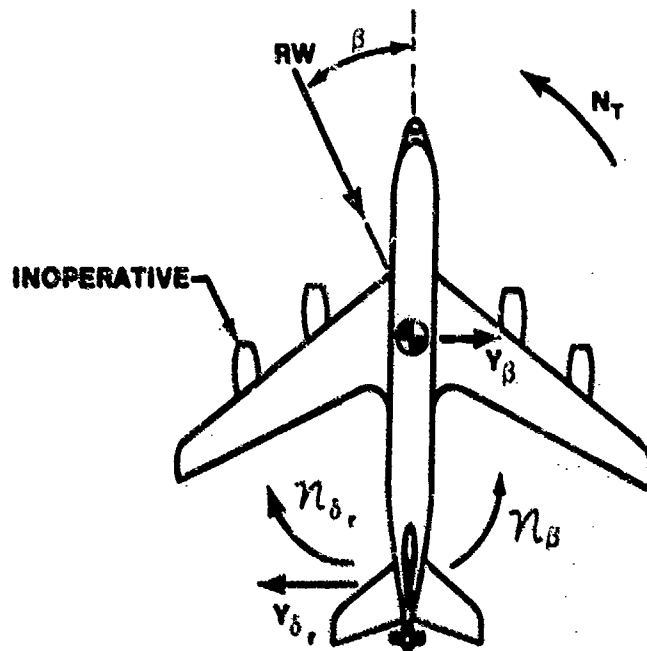
FIGURE 11.9. ENGINE-OUT STEADY STATE FLIGHT

Notice that the moment created by asymmetric thrust is opposed by rudder moment and that the rudder force is opposed by the side force generated by the sideslip angle at equilibrium. The yawing moment generated by the failed engine will be a function of basic engine parameters, temperature and pressure altitude. The other forces and moments are functions of airspeed, bank angle, and crosswind when on the ground.

11.9

11.3.1 Steady State Conditions

The Equations of Motion (EOM) are the starting point for examination of the asymmetric thrust condition. The longitudinal equations are not critical when examining engine-out control problems. These equations are balanced by the usual techniques for stabilized flight. The lateral-directional EOM are of most interest in achieving equilibrium during engine-out conditions.

If the torque and gyroscopic effects due to rotating engines or propellers are neglected, and if the restriction of steady unaccelerated flight is imposed, three lateral-directional force/moment equations can be written:

$$\mathcal{L}_{\delta_a} \delta_a + \mathcal{L}_{\delta_r} \delta_r + \mathcal{L}_{\beta} \beta = 0 \tag{11.1}$$

$$N_T + \mathcal{N}_{\delta_a} \delta_a + \mathcal{N}_{\delta_r} \delta_r + \mathcal{N}_{\beta} \beta = 0 \tag{11.2}$$

$$Y_{\delta_r} \delta_r + Y_{\beta} \beta + W \sin \phi = 0 \tag{11.3}$$

The roll equation, balanced by aileron deflection (δ_a), is usually not critical, although lack of roll authority could be a limiting case. The yawing moment equation and the sideforce equation (11.2 and 11.3) are the primary balancing equations for engine-out conditions. These examples are balanced using combinations of rudder deflection (δ_r), sideslip (β), and bank angle (ϕ).

The lateral-directional equations with asymmetrical thrust suggest there are four variables and three equations. The common way out of this dilemma is to select:

ϕ and solve for β, δ_a, δ_r

or to select

β and solve for ϕ, δ_a, δ_r

or to select

δ_r and solve for ϕ, β, δ_a

11.10

11.3.1.1 <u>Bank Angle Effects</u>. Three cases of equilibrium are of particular interest:

$$\text{Case 1:} \quad \phi = 0$$

$$\text{Case 2:} \quad \beta = 0$$

$$\text{Case 3:} \quad F_r = 0$$

<u>Case 1:</u> $\phi = 0$

Figure 11.10 shows the forces and moments for Case 1, the zero bank angle case, with the left engine inoperative. The aircraft is in equilibrium with no accelerations. The pilot would note this with constant heading, ball centered, turn needle centered, rudder opposing the failed engine and aileron opposite rudder to keep wings level.
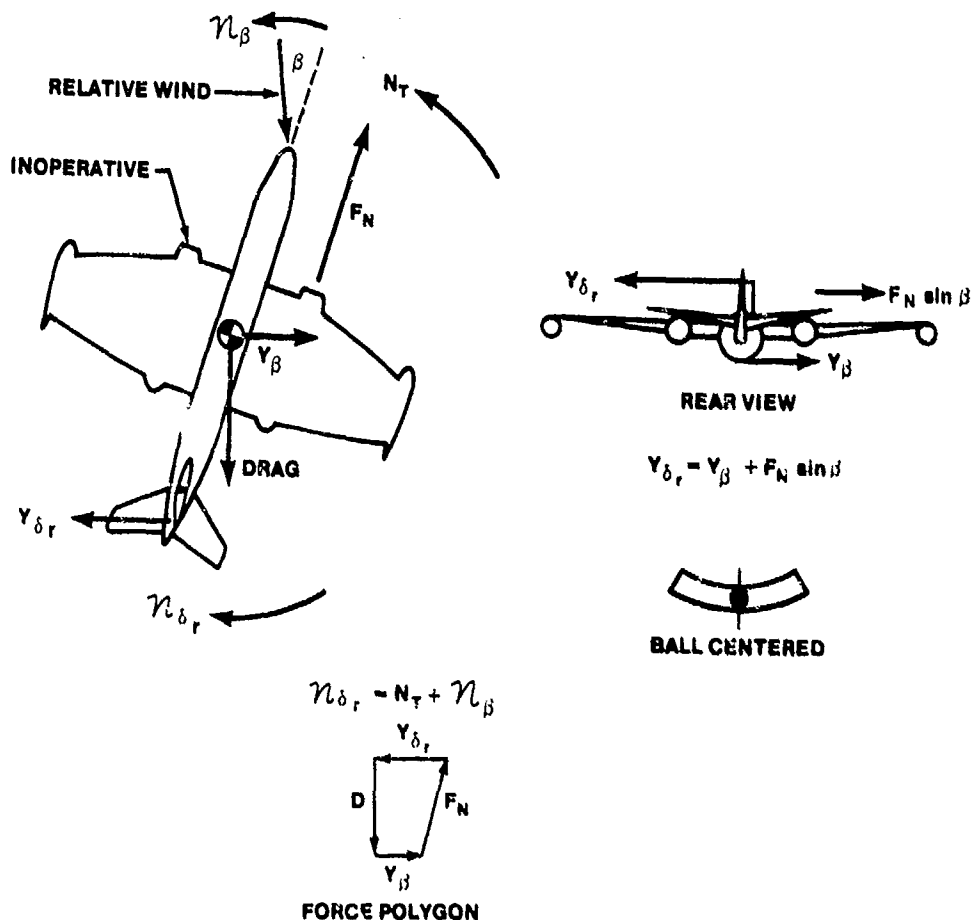
FIGURE 11.10. EQUILIBRIUM FLIGHT WITH WINGS LEVEL

11.11

The negative yawing moment created by the failed engine is balanced by a positive rudder deflection. The rudder deflection produces a negative sideforce that is balanced by the sideforce due to sideslip. For the zero bank case, the yawing and sideforce equations become

$$N_T + \mathcal{N}_{\delta_a} \delta_a + \mathcal{N}_{\delta_r} \delta_r + \mathcal{N}_\beta \beta = 0 \qquad (11.4)$$

$$W \sin \phi + Y_{\delta_r} \delta_r + Y_\beta \beta = 0 \qquad (11.5)$$

These equations can be solved simultaneously to determine the control deflections and sideslip required for balanced equilibrium flight. Assuming δ_a produces very little yawing moment

$$\delta_r = \frac{-N_T - \mathcal{N}_\beta \beta}{\mathcal{N}_{\delta_r}} \qquad (11.6)$$

and

$$\beta = \frac{N_T \, Y_{\delta_r}}{\mathcal{N}_{\delta_r} \, Y_\beta - \mathcal{N}_\beta \, Y_{\delta_r}} \qquad (11.7)$$

When the appropriate numbers are substituted for the derivatives, for a failed left engine (a negative N_T), β will be negative.

Case 2: $\beta = 0$

Another way to balance the sideforce resulting from the rudder deflection is by using the $W \sin \phi$ term in the sideforce equation (11.3). Figure 11.11 shows the forces and moments for the zero sideslip case.
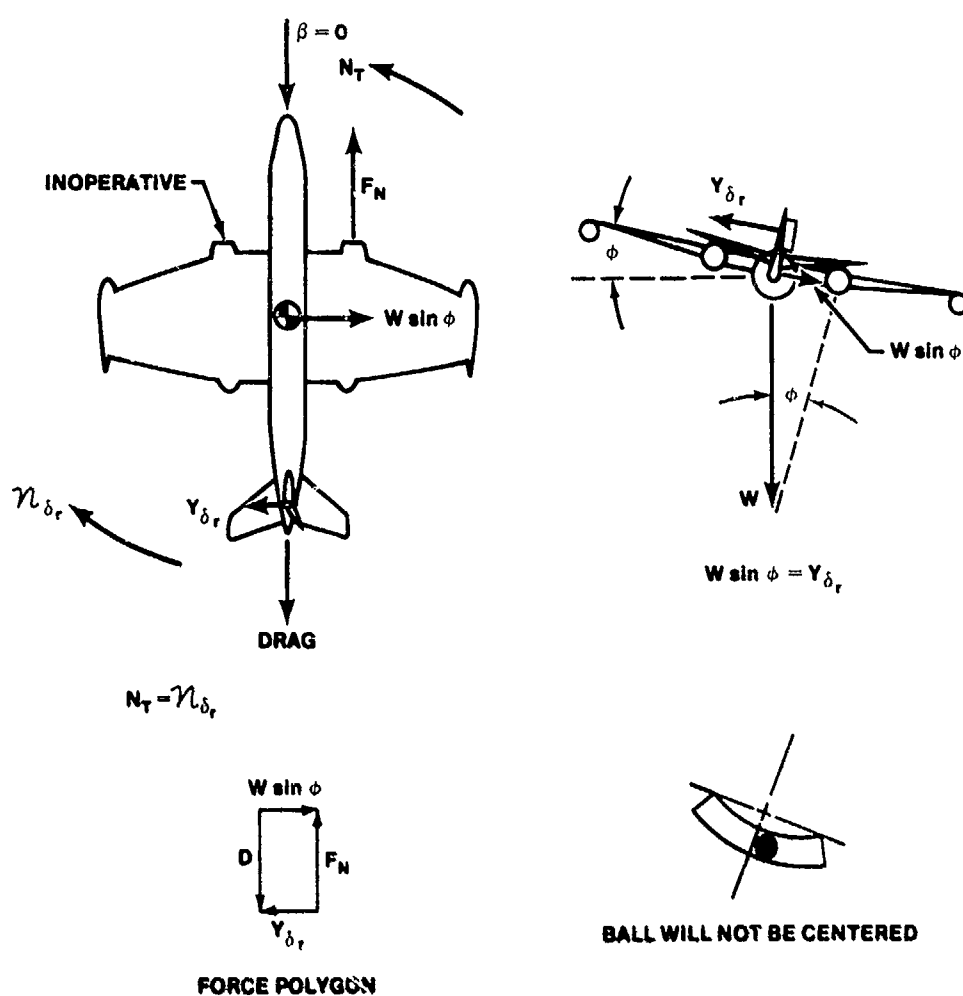
FIGURE 11.11. EQUILIBRIUM FLIGHT WITH ZERO SIDESLIP

The aircraft is in equilibrium with some bank toward the operating engine, a constant heading, and turn needle centered. The rudder deflection is in the same direction as the $\phi = 0$ case, however, less δ_r is required. The ball in the turn-and-slip indicator will be deflected in the direction of the bank angle.

With the sideslip equal to zero, the yaw and sideforce equations become

$$N_T + \mathcal{N}_{\delta_r} \delta_r = 0 \tag{11.8}$$

$$Y_{\delta_r} \delta_r + W \sin \phi = 0 \tag{11.9}$$

These equations can be solved to determine the amount of bank required to reduce the sideslip to zero.

$$\delta_r = \frac{-N_T}{\mathcal{N}_{\delta_r}} \tag{11.10}$$

and

$$W \sin \phi = Y_{\delta_r} \frac{N_T}{\mathcal{N}_{\delta_r}} \tag{11.11}$$

therefore

$$\sin \phi = \frac{1}{W} \frac{Y_{\delta_r} N_T}{\mathcal{N}_{\delta_r}} \tag{11.12}$$

Three important conclusions can be made from the previous discussion. First, bank angle can reduce the amount of rudder required to achieve equilibrium. Second, an increase in weight reduces the amount of bank required to reduce the sideslip to zero. Third, this configuration will have the least amount of drag. With $\beta = 0$, no sideforce is generated, and therefore, no drag due to sideforce is created.

Case 3: $F_r = 0$

The last steady state case to be examined is with zero rudder force. With an irreversible flight control system, δ_r will also be zero. With a reversible system, some rudder deflection will result from the sideslip being produced, however, for the purposes of this discussion δ_r will be considered equal to zero.

Figure 11.12 shows the forces and moments for Case 3. The aircraft is in equilibrium with rudder force equal to zero, constant heading, and turn needle centered. The bank angle required to achieve this steady state condition is considerably more than that required in Case 2. Also note, the ball in the turn-and-slip indicator will be deflected more in the direction of the bank.
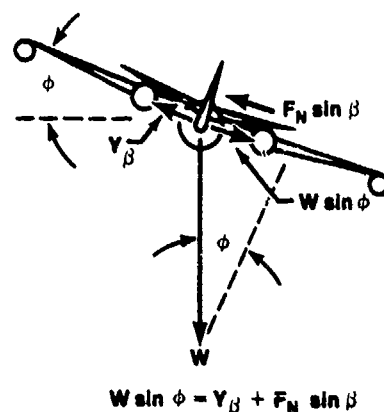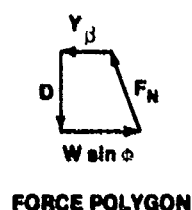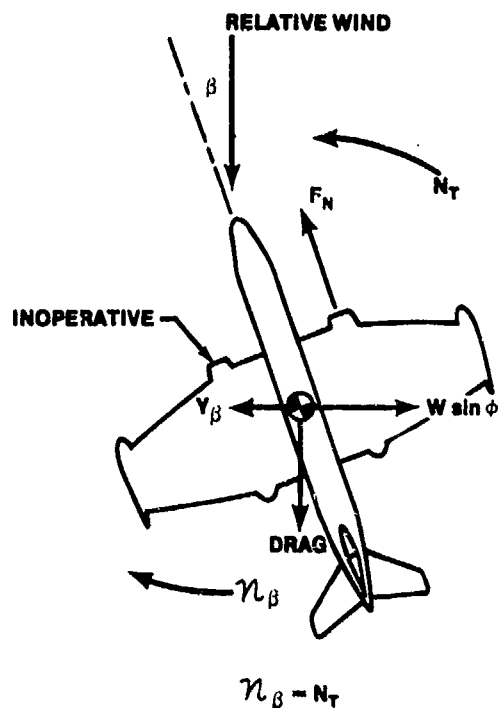
FIGURE 11.12. EQUILIBRIUM FLIGHT WITH ZERO RUDDER DEFLECTION

With the rudder force and δ_r equal to zero, the yaw and sideforce equations become

$$N_T + \mathcal{N}_\beta \beta = 0 \qquad (11.13)$$

$$Y_\beta \beta + W \sin \phi = 0 \qquad (11.14)$$

These equations can be solved to determine the amount of bank required to achieve equilibrium with $F_r = 0$.

$$\beta = \frac{-N_T}{\mathcal{N}_\beta} \qquad (11.15)$$

$$\sin \phi = \frac{1}{W} \frac{Y_\beta \, N_T}{\mathcal{N}_\beta} \tag{11.16}$$

From the above equations it can be seen that for a failed left engine (negative N_T), β must be positive to balance the equation. The amount of sideslip developed in this case is considerably more than that developed in Case 1 ($\phi = 0$). Also, to balance the sideforce equation the bank angle must be positive. The amount of bank required to achieve equilibrium with $F_r = 0$ is also more than that required to achieve $\beta = 0$. Given these two points, it should be recognized that this is the highest drag condition of the three cases discussed. Another thing to consider is the possibility of fin stall and loss of directional control due to the high sideslip and bank angles produced during this case.

It is important to note that for any asymmetric thrust condition there are numerous combinations of rudder deflection and bank angle that will balance the equations of motion. However, for a given bank angle there is only one rudder deflection that will result in equilibrium (steady state) flight.

11.3.1.2 **Air Minimum Control Speed** (V_{mca}). For a given set of asymmetric thrust conditions, there is a speed below which aerodynamic control alone is insufficient to maintain equilibrium. Figure 11.13 is a typical plot that shows the yawing moments due to asymmetric thrust and maximum rudder deflection, as a function of speed. Below the speed where the two curves cross, the yawing moment due to δ_r is no longer sufficient to overcome the moment due to asymmetric thrust and therefore steady state flight cannot be achieved. This speed is the air minimum control speed (V_{mca}).
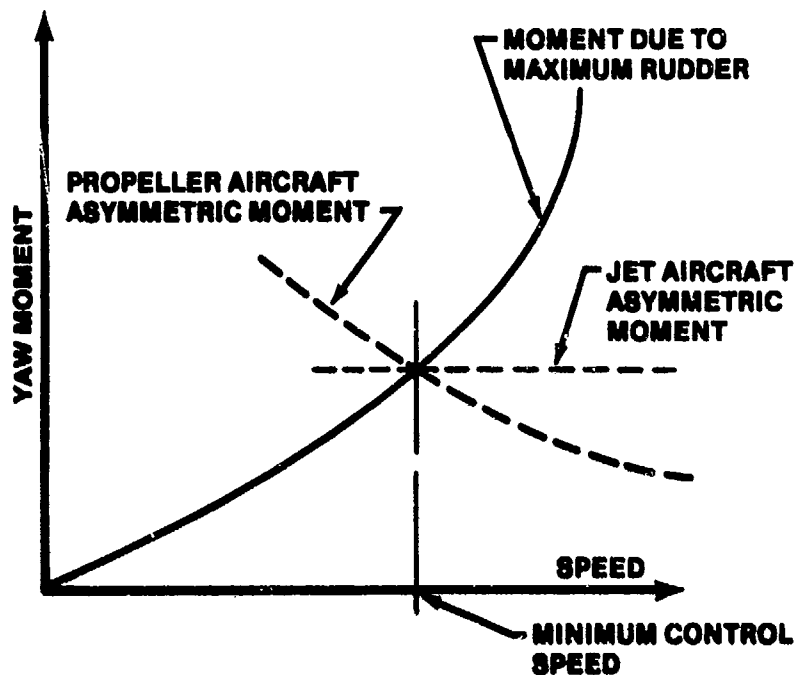
FIGURE 11.13. YAWING MOMENTS

Not shown in this figure is the effect of bank angle on the yawing moments as previously discussed.

11.3.1.3 Ground Minimum Control Speed (V_{mcg}). Ground minimum control speed is more complicated. The rudder moment and asymmetric moments are related the same as the in-flight case, but nosewheel steering can help oppose the asymmetric thrust moment, landing gear opposes side force, and crosswind can greatly affect the rudder moment available.

If the crosswind is from the direction of the failed engine, less rudder deflection is available to counteract the moment from the engine loss because some rudder is being used to correct the weathercock tendency caused by the

crosswind component. Figure 11.14 graphically depicts the major yawing moments encountered on the ground.
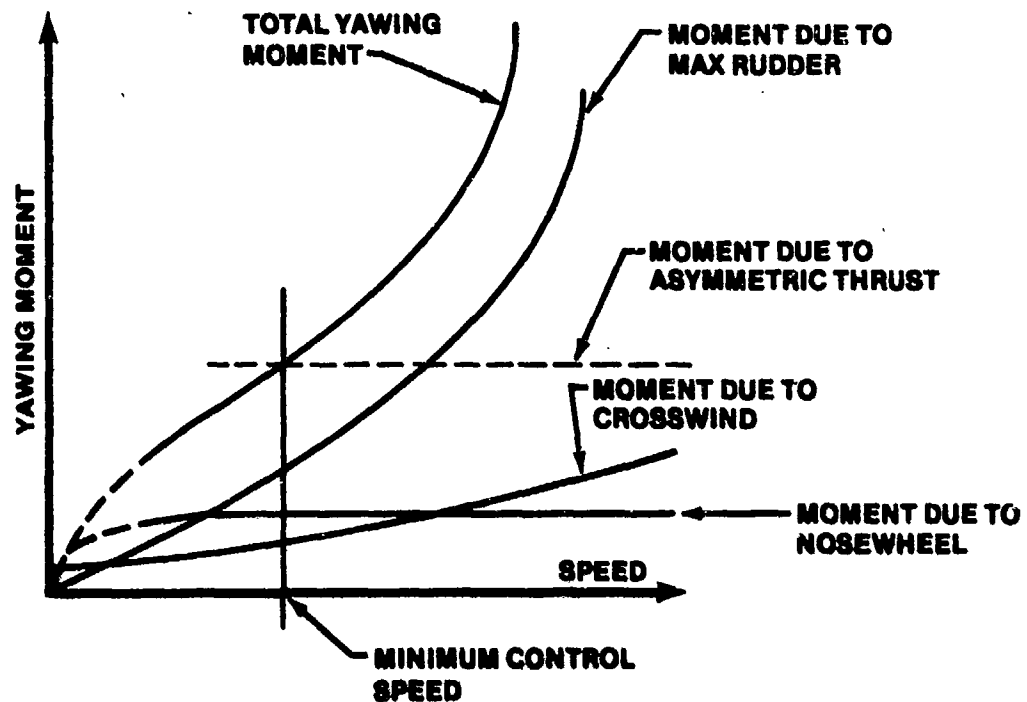
FIGURE 11.14. GROUND YAWING MOMENTS

11.3.1.4 <u>Minimum Lateral Control Speed Theory</u>. Lateral controllability has not generally been a problem in minimum control speed determination except on certain experimental powered-lift aircraft and a few propeller-driven airplanes such as the OV-10A where large portions of the wing are immersed in the propeller slipstream. On the first prototype versions of the OV-10A with the 30-foot wing span, nearly 55% of the wing was immersed in the propeller slipstream. Large asymmetric rolling moments caused by the loss of an engine led to severe lateral control problems which resulted in minimum control speeds between 80 to 120 KIAS depending upon the configuration, gross weight, and the criteria used to define them. For an aircraft capable of twin-engine approach speeds between 55 to 75 knots, this large gap between V_{mca} and approach airspeed was simply intolerable, at least to some Department of Defense managers, and the decision was made to lengthen the wings in an attempt to cure this problem. The result was a 40-foot wing OV-10A with marginal STOL capabilities.

With the development of Advanced Medium STOL Transport aircraft, the Air Force might procure in quantity, aircraft where minimum control speed may be

11.18

defined by the lack of lateral rather than directional controllability. Therefore, a review of the factors influencing the lateral control problem is in order.

The classical situation for wings-level air minimum lateral control speed is illustrated in Figure 11.15. This situation is the same as that illustrated in Figure 11.10 for the directional control speed case except that now, minimum control speed is defined as the minimum speed at which full lateral control deflection is reached. The propulsive rolling moment, L_T shown in figure 11.15 is that generated by propulsive lift and must be balanced by rolling moment due to lateral control deflection and also rolling moment due to sideslip. (The assumption is made that full rudder deflection has not been achieved.)
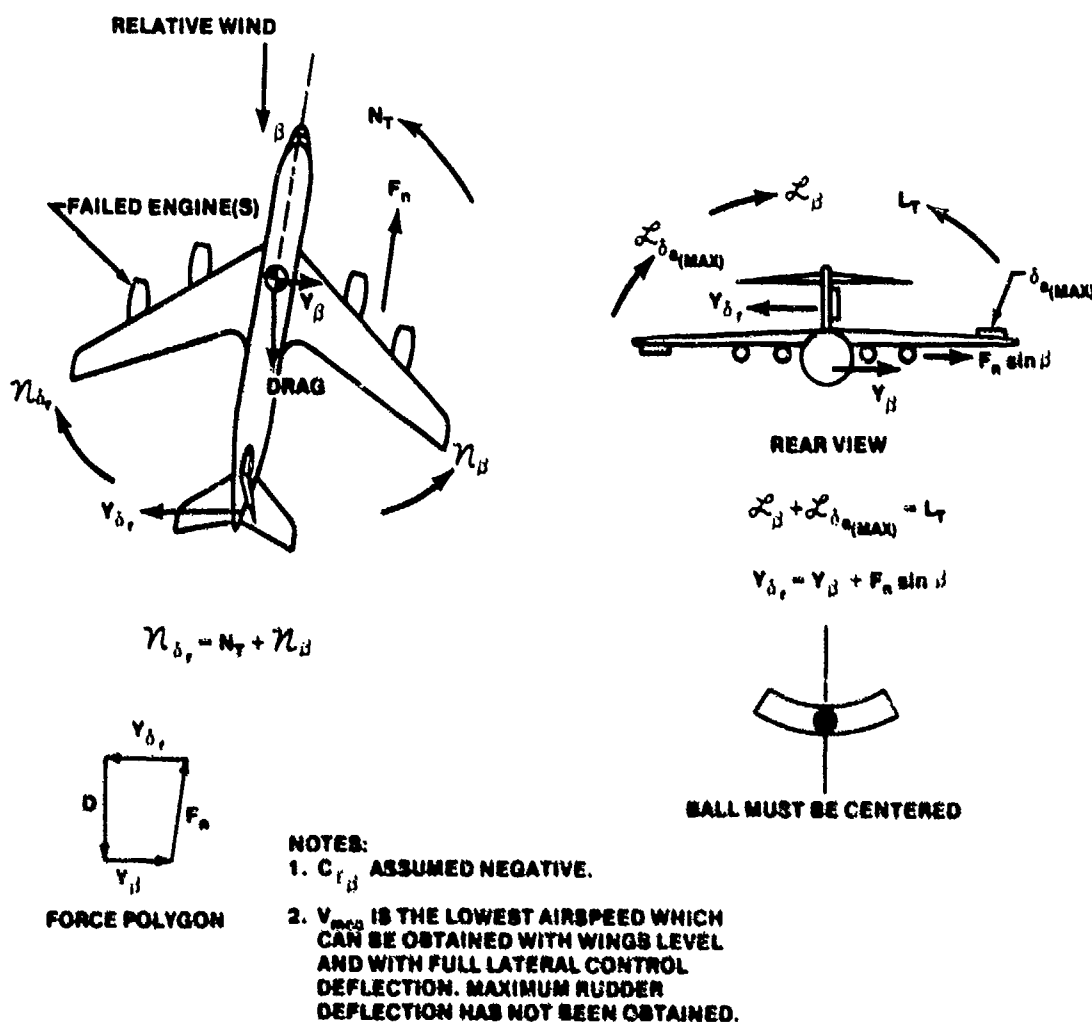
FIGURE 11.15.   AIR MINIMUM LATERAL CONTROL SPEED EQUILIBRIUM
CONDITION FOR WINGS LEVEL

Assume that airspeed is allowed to decrease below the V_{mca} established for the wings-level configuration shown in Figure 11.15. With the left engine(s) failed as shown, the aircraft will now begin to roll to the left since no additional lateral control remains to balance the rolling moment generated by the operating engine(s). The only way to bring the aircraft forces and moments back into equilibrium is to increase sideslip into the failed engine (Figure 11.16) and allow rolling moment due to sideslip, $\mathcal{L}_\beta$, to increase and therefore reestablish equilibrium. When the bank angle has reached 5°, the minimum lateral control speed has been obtained.

Sideslip must be from the failed engine side and bank angle must be into the failed engine.

$$n_{\delta_r} = N_T + n_\beta$$

FORCE POLYGON

$$Y_{\delta_r} + W \sin\phi = Y_\beta + F_n$$

$$\mathcal{L}_\beta + \mathcal{L}_{\delta_{a(MAX)}} = L_T$$

REAR VIEW

BALL WILL NOT BE CENTERED
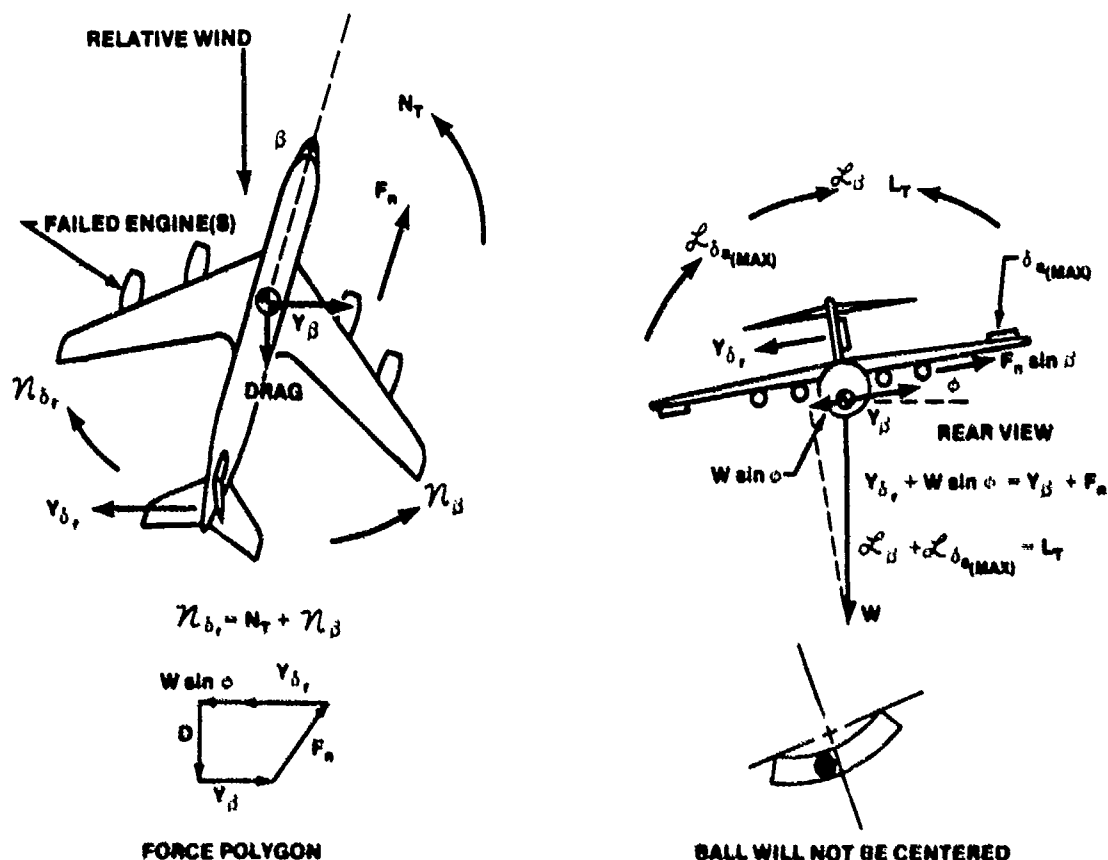
NOTE: IF AIRSPEED DECREASES BELOW WINGS-LEVEL V_{mca} (BASED ON FULL LATERAL CONTROL DEFLECTION), AIRCRAFT WILL BANK INTO THE FAILED ENGINE(S). EQUILIBRIUM CAN BE REESTABLISHED BY INCREASING SIDESLIP INTO THE FAILED ENGINE, THUS ALLOWING POSITIVE DIHEDRAL EFFECT TO PROVIDE ADDITIONAL ROLLING MOMENT INTO THE OPERATING ENGINE(S).

FIGURE 11.16. AIR MINIMUM LATERAL CONTROL SPEED EQUILIBRIUM CONDITION FOR WINGS BANKED 5 DEGREES

11.20

11.3.2 Dynamic Engine Failure

As stated earlier, the dynamic case is an extension of the steady state case due to rates and accelerations incurred during pilot reaction time. Before an aircraft can achieve equilibrium, the pilot must first overcome these rates and accelerations. The dynamic case usually requires more control authority and, therefore, is usually more restrictive than the steady state case.

One of the most important variables when considering the dynamic engine failure is the pilot's reaction time. Pilot reaction time is probably the most controversial and the most critical parameter in the dynamic case. Granted, an engine failure during cruise is not severe and pilot reaction time is not as critical a parameter. However, during critical phases of flight,such as takeoff or go-around, it becomes a very important variable. To fully understand what a "realistic time delay" is, the following discussion addresses the psychological factors involved with reaction time.

11.3.2.1 Reaction Time. Pilot reaction time is defined as "the time between the stimulus and the completion of the response". This includes time to recognize a problem, to deliberate (decision time), and react. To realistically calculate the reaction time, all those parts must be taken into account. Accepted figures for human reaction time for the simplest tasks in which no decision is required is .2 seconds. But reaction time is also a function of the stimulus, the complexity of the response and the body member being used, and can be up to one full second. For instance, it takes about 20% longer to respond with the feet than with the hands.

Recognition of the problem depends on the nature of the stimulus; its signal characteristics, complexity, and rate. If the stimulus (a warning light or bell) is received when the pilot's attention is diverted to doing other tasks, a longer time may result. We know that verbal signals are poor in a high ambient noise environment. On your particular aircraft and its cockpit environment, the time required can vary greatly from the simple recognizable task.

The decision process is increased greatly from a simple to a complex task. The pilot must decide in a very critical (even crisis) period whether he should abort a takeoff or continue it. If an extra stimulus is being

received, such as an "S-1" call, the new stimulus will not be processed until the original one has been completed. The added time delay from this multiple stimuli is called the "psychological reaction time." Figure 11.17 shows that even among a large sample of pilots, reaction time for a complex decision varies widely and takes considerably longer than that of a simple task.
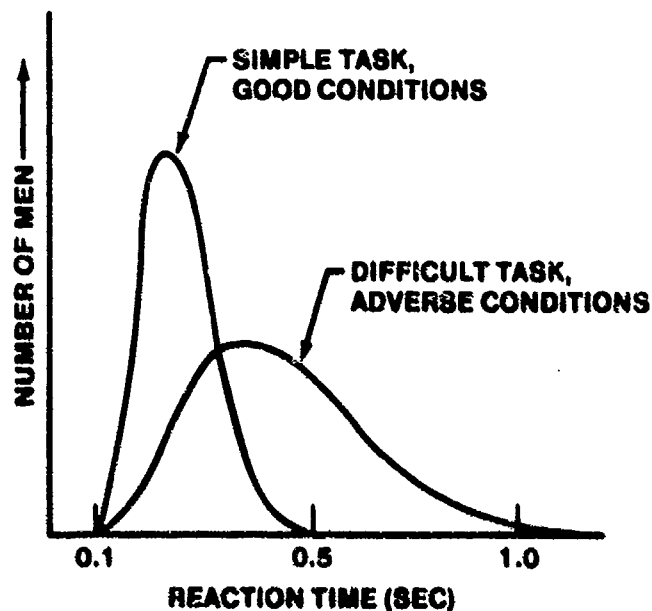

FIGURE 11.17. VARIATION IN REACTION TIME

A summary of reaction time from the recognition to the reaction for a simple task under laboratory conditions is shown in Table 11.1

11.22

TABLE 11.1
COMPOSITION OF REACTION TIME OR LAG TIME

1. RECEPTOR DELAYS.	.001 TO .038 SEC	⎫ RECOGNITION
2. NEUTRAL TRANSMISSION TO CORTEX	.002 TO .100 SEC	⎬
3. CENTRAL-PROCESS DELAYS	.070 TO .300 SEC	DECISION
4. NEUTRAL TRANSMISSION TO MUSCLE	.010 TO .020 SEC	⎫ REACTION
5. MUSCLE LATENCY AND ACTIVATION TIME	.030 TO .070 SEC	⎬
TOTAL REACTION TIME	.113 TO .578	

NOTES: 1. Simple Task, no choice of actions.

2. Subject is expecting stimulus in laboratory conditions.

Table 11.1 data could be used to predict a test pilot's reaction time to a simple task. This is possible because he knows what task is required (an abort or continued takeoff), the environment is controlled, and he has practiced the task many times. These typical numbers (.2 to .5 seconds) cannot be used to represent the operational pilot's true reaction time. Some of the critical questions to be taken into consideration in predicting accurate reaction time are:

a. What are the cues to be observed?

b. What is the total time from beginning of abort to max braking?

c. What are the takeoff speed overshoots during abort?

d. Can full braking be considered before other actions?

e. Has the runway length covered during the decision period been included?

It can become very easy during a test program to accept a smaller reaction time, if the times are driving your critical field lengths beyond the specification limits. Be careful, honest, and remember the operational pilot!

11.4 ENGINE-OUT FLIGHT TESTING

Military aircraft are usually designed with relatively low safety margins in order to attain the optimum performance. In fact, during war emergency operation the gross weight may be so high that engine-out operation is not possible at all. Flight tests of these critical phases, on or near the ground, require a high level of crew skill and proficiency; each point must be carefully planned and flown. Such tests are a normal part of the developmental testing of a new aircraft. They also play a vital part in side-by-side evaluations of assault or VSTOL transports where the ability to carry a useful load in and out of a given landing area is frequently limited by engine-out performance. Individual evaluations to determine if an aircraft meets the contractor's guarantees may also hinge on this area of operation.

11.4.1 In-Flight Performance

Normal performance flight test methods may be used to determine the climb, range, and endurance at altitude with engines inoperative.

11.4.2 Landing Performance

Restricted reversing capability and possible higher approach speeds required to maintain minimum safe speeds will affect landing performance. Normal flight test methods are valid, but caution must be exercised in go-around situations, especially at light gross weights.

11.4.3 Air Minimum Control Speed

It has been shown that an aircraft with an engine inoperative can be stabilized in straight unaccelerated flight using various combinations of bank angle and rudder deflections. It has also been shown that, for a given bank angle, there is a speed below which aerodynamic control with maximum rudder deflection is insufficient to maintain this equilibrium.

It is possible that there will be no minimum control speed for a multi-engine aircraft because it can be controlled down to aerodynamic stall. This is the desired situation, however it is important that in this particular situation the aerodynamic stall speed not be reported as the minimum control

speed, but rather "the aircraft is controllable down to aerodynamic stall" for the particular configuration tested.

MIL-F-8785C specifies that straight flight must be possible during takeoff with an engine failure and further specifies the control forces and deflections that may be used to accomplish this. It might, therefore, seem that a minimum control speed is only of academic interest. However, there may be instances where a multi-engine aircraft could meet the specifications at takeoff speed, but be operated at a speed in some operational or approach flight phase which would be lower than minimum takeoff speed. Hence, the asymmetric thrust minimum control speed must still be determined by flight test. MIL-F-8785C also states that a maximum of 5° bank angle and 180 pounds rudder force will be used during engine-out flight test for determination of V_{mca}.

The method used for gathering engine-out flight test data is known as the steady straight slow down method.

Prior to flight test, consideration must be given to the hazards associated with shutting down one engine during flight. On a twin-engine aircraft, these associated hazards may be such that the engine cannot be shutdown. If so, a method of simulating an engine shutdown must be devised so that the data may be analyzed accurately.

At a speed well above the predicted V_{mca}, maximum asymmetric thrust is established by shutting down, or simulating shutdown of, the most critical engine and setting the other symmetric engine at maximum thrust for the test conditions. With the aircraft in the specified configuration, a series of stabilized points are flown at decreasing speeds down to the speed where maximum rudder deflection occurs. This speed is the minimum control speed for the test conditions. The data recorded at each of the stable points should include but is not limited to, engine parameters (to determine thrust), temperature, pressure altitude, rudder force and deflection, aileron force and deflection, and bank angle.

The flight test profile should be flown with the wings level and with the wings banked at various bank angles, and is usually performed at two or more altitudes. If the aircraft has a rudder power assist system the profile should be repeated with the assist off.

The analysis of minimum control speed data can be easily extrapolated to off-standard day conditions if it is expressed in non-dimensional form. Thrust moment (N_T) may be non-dimensionalized by the following equation:

$$C_{n_T} = \frac{N_T}{qSb} \qquad (11.17)$$

where

q = dynamic pressure, lb/ft^2

S = wing area, ft^2

b = wing span, ft

The steady state equations of motion for the asymmetric power condition are:

$$C_{\ell_\beta} \beta + C_{\ell_{\delta_a}} \delta_a + C_{\ell_{\delta_r}} \delta_r = 0 \qquad \text{Roll} \qquad (11.18)$$

$$C_{n_T} + C_{n_\beta} \beta + C_{n_{\delta_r}} \delta_r + C_{n_{\delta_a}} \delta_a = 0 \qquad \text{Yaw} \qquad (11.19)$$

$$C_{Y_\beta} \beta + C_{Y_{\delta_r}} \delta_r + C_L \sin \phi = 0 \qquad \text{Sideforce} \qquad (11.20)$$

At high angles of attack and low airspeeds

$$C_{\ell_{\delta_r}} = 0$$

Solving Equation 11.18 for δ_a and Equation 11.20 for β, and substituting these relations into Equation 11.19 yields

$$C_{n_T} = K_1 \delta_r + K_2 C_L \sin \phi \qquad (11.21)$$

Where K_1 and K_2 are constants containing the stability derivatives in the original three equations.

For aircraft with reversible directional control systems, the equation for rudder pedal force, F_r, is

$$F_r = G \bar{q} S_r \bar{c} \, (b_1 \alpha_F + b_2 \delta_r) \qquad (11.22)$$

By an analysis similar to that above for thrust moment coefficient, it can be shown that a rudder pedal force coefficient (C_{F_r}) can be defined as

$$C_{F_r} = \frac{F_r}{qS_r} = K_3\delta_r + K_4C_L\sin\phi \qquad (11.23)$$

Equations 11.21 and 11.23 show that both C_{n_T} and C_{F_r} are both unique functions of rudder deflection, lift coefficient, and bank angle.

CALIBRATED AIRSPEED - (KT)
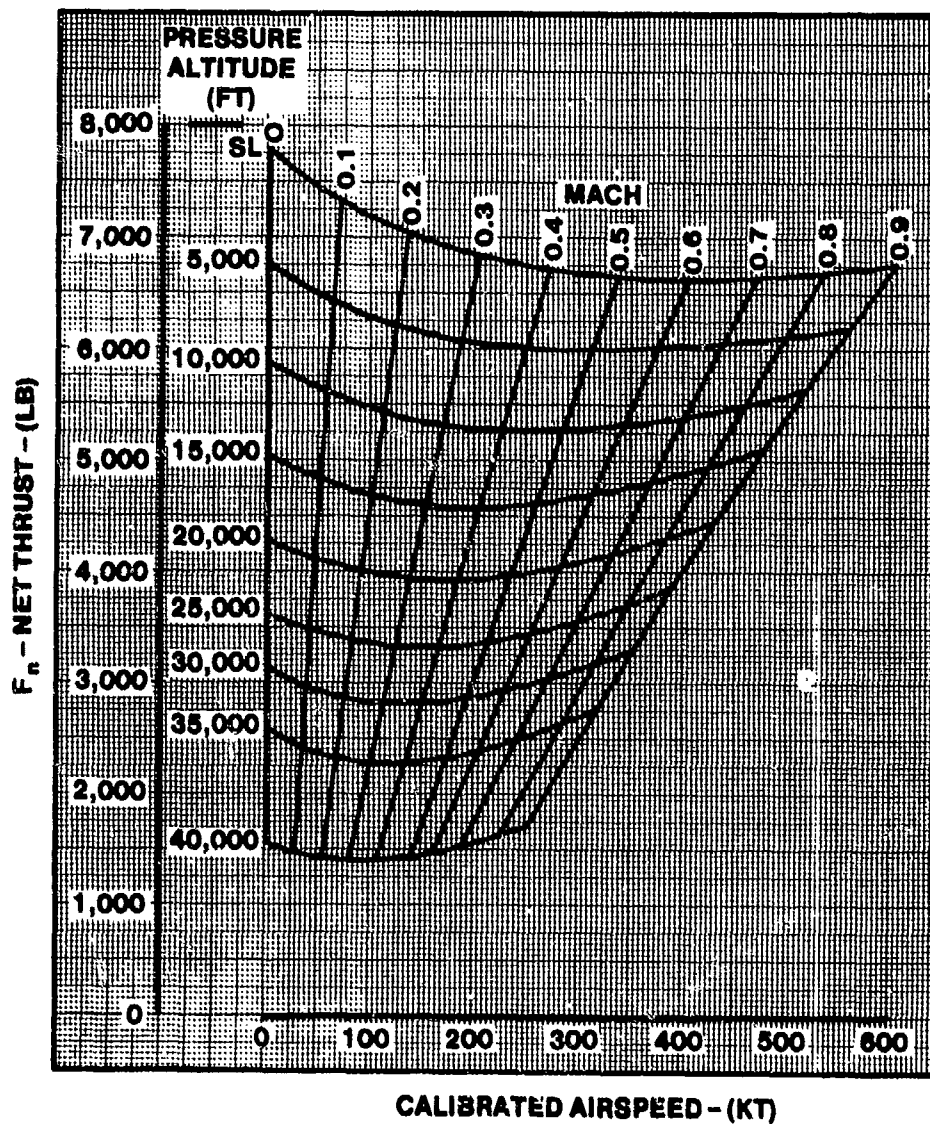
FIGURE 11.18A. ENGINE CHARACTERISTICS
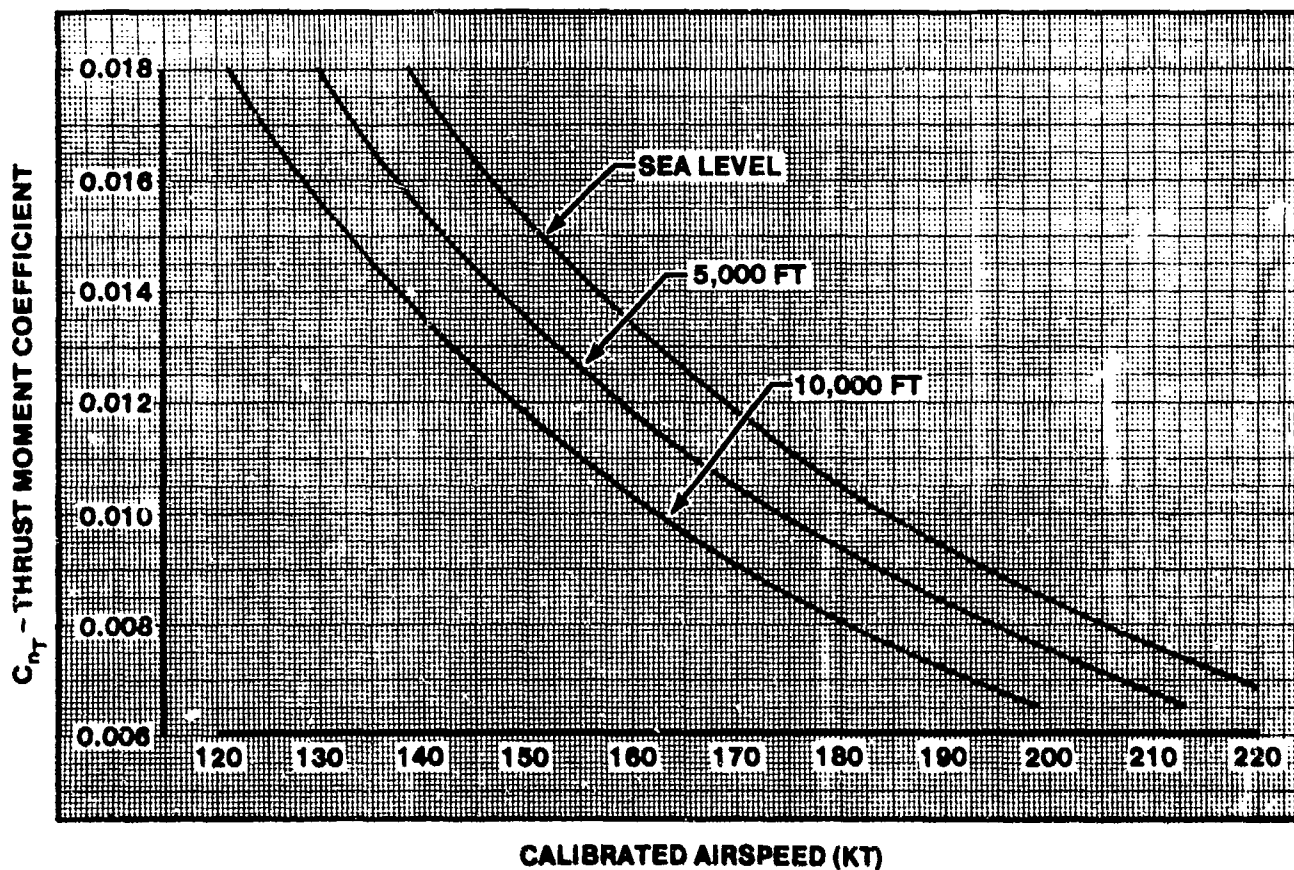
FIGURE 11.18B. NONDIMENSIONAL THRUST MOMENT COEFFICIENT
VERSUS AIRSPEED

Prior to commencing the flight test phase, an engine thrust deck is required (Figure 11.18A). Thrust moment coefficient is then easily calculated by Equation 11.17, and may be presented like that in Figure 11.18B. This same information can be gathered by instrumenting the engine for measurement.

During flight test, the rudder deflection required for a wings-level equilibrium point with asymmetric thrust is defined. The locus of all stabilized points represents a curve (Figure 11.19A) on which the thrust moment coefficient must be exactly balanced by the associated rudder deflection. Note for a given airplane and thrust level, a coefficient can be identified as the maximum allowable using full rudder.

11.28
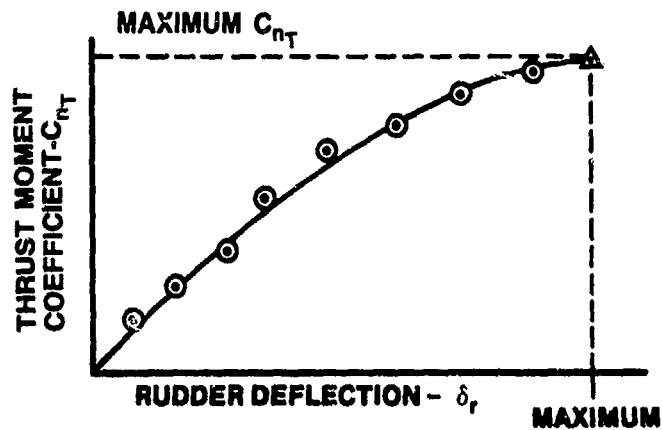
FIGURE 11.19A.   NONDIMENSIONAL THRUST MOMENT COEFFICIENT (C_{n_T})

At each altitude in Figure 11.18B, the speed associated with the maximum C_{n_T} is the   static air minimum control speed.   Finally, a generalized plot of V_{mca} for   standard day conditions may appear like that in Figure 11.19B.   The safety advantages of this method are obvious: being able to accurately predict sea level data for a hazardous flight condition without ever having to test there!
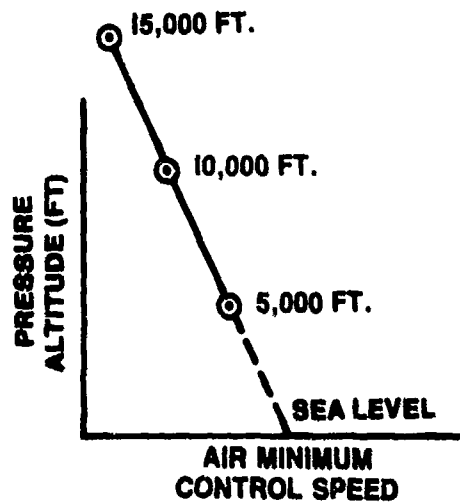
FIGURE 11.19B.   STATIC AIR MINIMUM DIRECTION CONTROL SPEEDS

The speed at which the rudder force limit (180 pounds) imposed by MIL-F-8785C is reached can also be determined using the flight test data. Flight test thrust moment coefficient is plotted vs. rudder pedal force coefficient $\left(C_{F_r}\right)$ as shown in Figure 11.20.
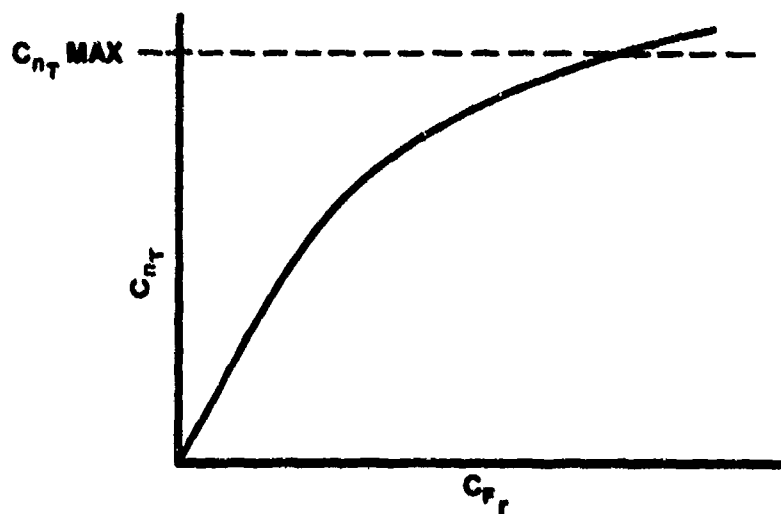
FIGURE 11.20.   RUDDER FORCE COEFFICIENT

For any C_{n_T} and $F_r = 180$ lbs., C_{F_r} can be <u>calculated</u> for different altitudes. These points can be plotted and straight lines drawn to the origin as shown in Figure 11.21.

FIGURE 11.21. V_{mca} LIMITING FACTORS

These lines represent lines of constant rudder force equal to 180 pounds. If the altitude line intersects the C_{F_r} curve prior to intersecting the maximum C_{n_T} line, as in the sea level case, then 180 pounds rudder force will be reached before maximum rudder deflection and this will be the limiting factor. If the constant rudder force line intersects the maximum C_{n_T} line first, then maximum rudder deflection will occur before 180 pounds rudder force and δ_r becomes the limiting factor.

11.4.3.1 <u>Weight Effects</u>. The previous discussion addressed only wings level flight and therefore, no weight effects were present. To determine the effects of aircraft weight the $C_L \sin \phi$ term of Equation 11.20 must be considered.

The thrust moment coefficient from the wings banked flight test data is calculated the same way as for the wings level data and plotted vs. $C_L \sin \phi$ as shown in Figure 11.22.

δ_{r_3} = MAX δ_r

δ_{r_2}

δ_{r_1}

C_{n_T}

$C_L \sin \phi$
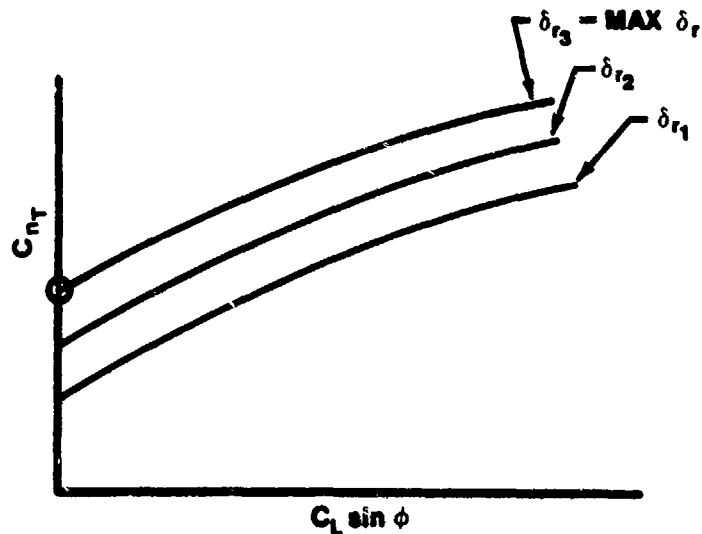
FIGURE 11.22. THRUST MOMENT COEFFICIENT

In actual flight testing to determine values for the flight manual, only the minimum control speed at maximum rudder deflection is necessary (in this case δ_{r_3}). One important anchor point of this plot is the maximum C_{n_T} determined from the wings level data analysis previously accomplished. This point is plotted at $C_L \sin \phi$ equal to zero. Also note from the plot that as bank angle increases ($C_L \sin \phi$ increasing), thrust moment coefficient for maximum δ_r increases, which corresponds to a decrease in minimum control speed.

For any altitude, airspeed, and weight, there is a unique value of C_{n_T} associated with full asymmetric thrust, and a corresponding unique value of lift coefficient. If an altitude, airspeed, gross weight and bank angle are assumed, it is possible to compute and plot corresponding values of C_{n_T} and $C_L \sin \phi$ as shown in Figure 11.23.
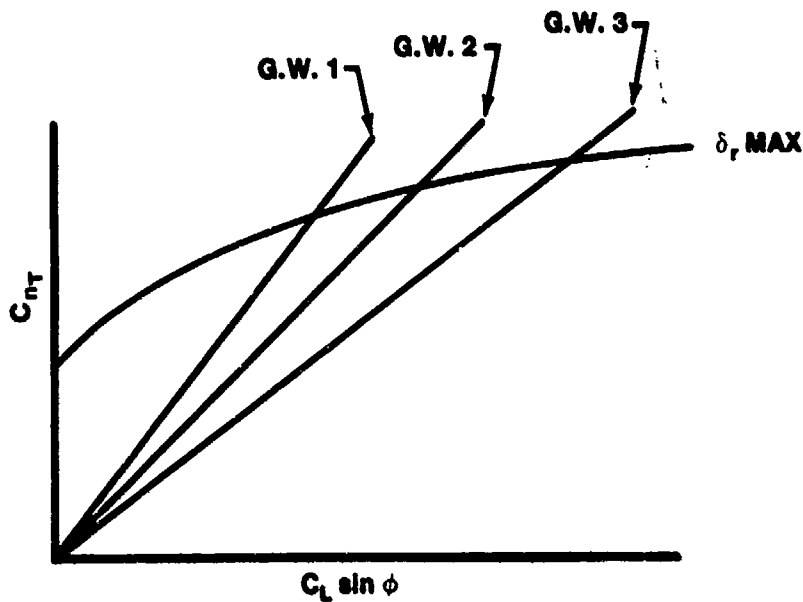
FIGURE 11.23.   WEIGHT EFFECTS ON C_{n_T}

These lines represent lines of constant gross weight with GW3 greater than GW1. Note from this plot that as gross weight increases the maximum C_{n_T} that can be balanced also increases, which corresponds to a decrease in minimum control speed as in the increasing bank case.

11.4.3.2 Altitude Effects. Another way to analyze the data is to plot variations of C_{n_T} and $C_L \sin \phi$ at constant weight and bank angle as a function of altitude as shown in Figure 11.24.
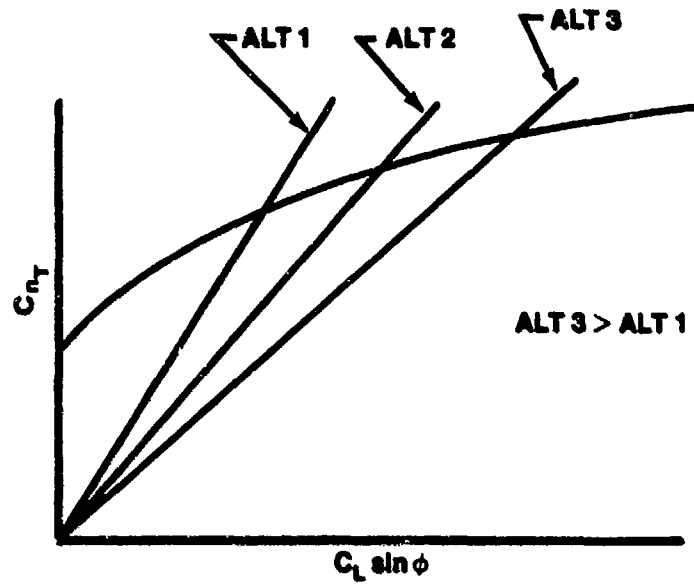
FIGURE 11.24. ALTITUDE EFFECTS ON C_{n_T}

Note from this plot that as altitude increases so does C_{n_T}.

The analysis of rudder force coefficient is performed the same as with the wings level flight test data and can be superimposed on either Figure 11.23 or Figure 11.24. Figure 11:25 is an example of this plot.
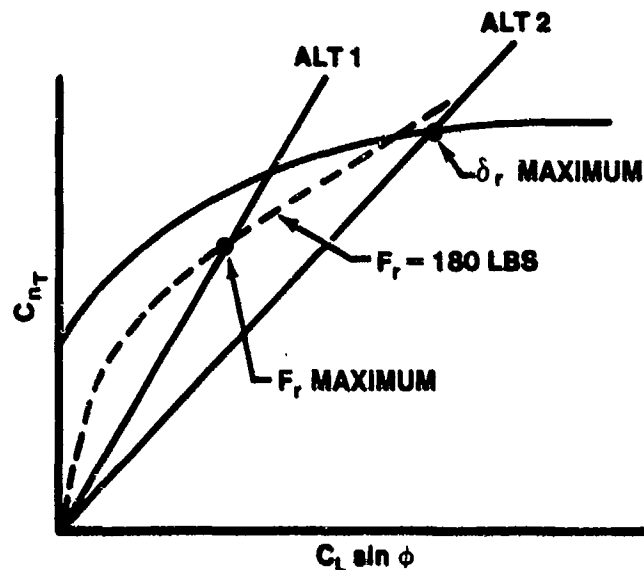
FIGURE 11.25.   RUDDER FORCE COEFFICIENT

As in the wings level data, if the rudder force coefficient (dashed) line intersects the altitude line first, the minimum control speed is rudder force limited.

11.4.4   Secondary Method Of Data Analysis

The previous discussion of engine-out data analysis is limited in that an accurate thrust deck is needed to calculate values of C_{n_T}. If a thrust deck is not available, another method of analyzing the data must be used.

With the aircraft in the specified configuration, and with the critical engine failed, a series of stabilized points are recorded at decreasing speeds. A plot of the critical control parameter (this will most frequently be rudder deflection) versus airspeed is made to determine the minimum control speed. (Figure 11.26.)
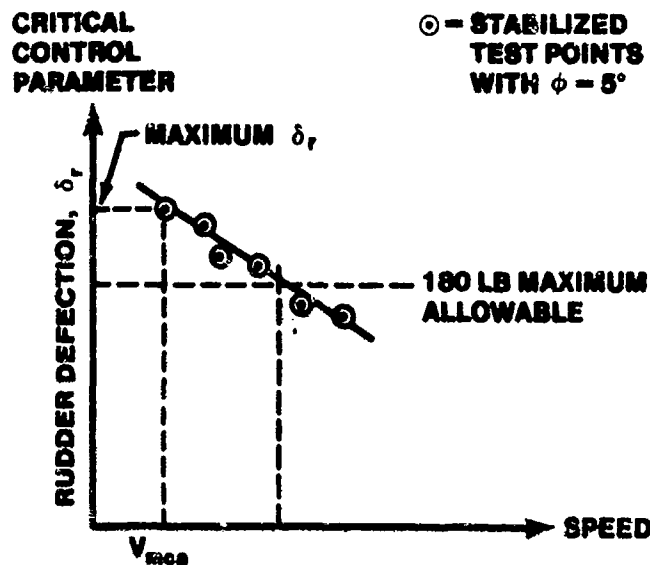
FIGURE 11.26.   AIR MINIMUM CONTROL SPEED

The test must be accomplished at more than one altitude, including one as low as is safely possible, to provide accurate extrapolation to sea level as shown in Figure 11.27.
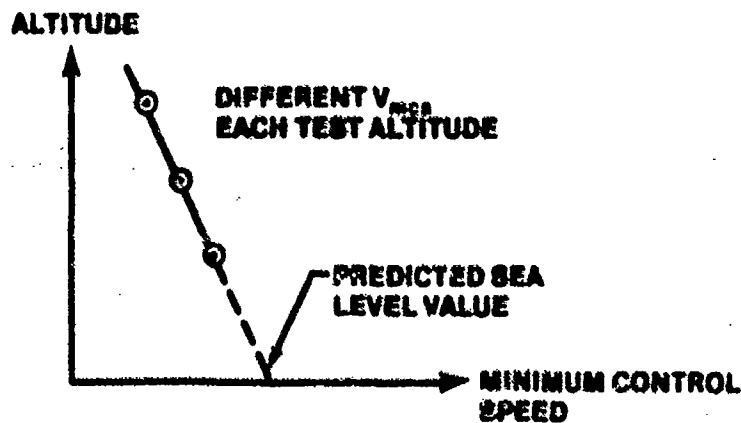
FIGURE 11.27.   PREDICTED SEA LEVEL V_{mca}

Note from this plot that the minimum control speed usually increases at lower altitude due to increased engine thrust.

11.36

11.4.5 Lateral Control Data Analysis

There is no proven non-dimensional technique to generalize minimum control speed data where lateral controllability is the determining factor. An attempt has been made however, to describe an analysis procedure which may be applicable to these aircraft.

On powered-lift or immersed-wing aircraft, very large lift vectors are generated on each wing because of the blowing effect. Under asymmetric power conditions, these large lift vectors result in large rolling moments which can be illustrated by Figure 11.28.
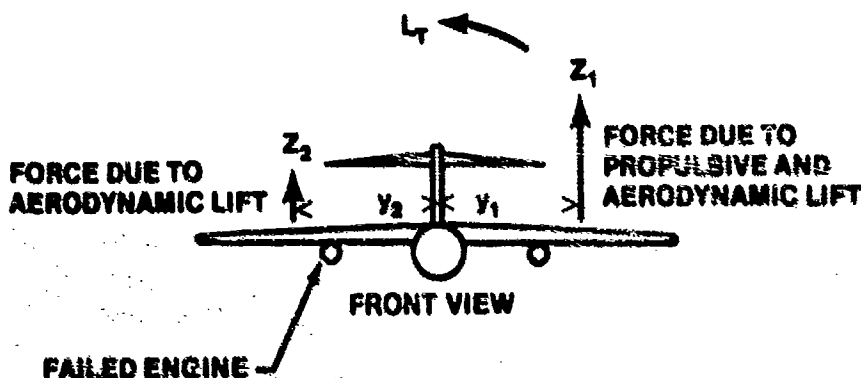
FIGURE 11.28. ROLLING MOMENTS WITH ASYMMETRIC THRUST

The total rolling moment, L_T on the aircraft is

$$L_T = -y_2 z_2 + y_1 z_1$$

where z_1 and z_2 = lift due to both propulsive and aerodynamic lift or aerodynamic lift alone whichever the case may be, [lb]

y_1 and y_2 = distance from aircraft centerline to lift vectors z_1 and z_2 respectively (y_1 and y_2 not necessarily equal), [ft]

The nondimensional rolling moment coefficient is

$$C_{\ell_T} = \frac{L_T}{qSb}$$

(11.24)

Equation 11.18 now becomes

$$C_{\ell_r} + C_{\ell_\beta}\beta + C_{\ell_{\delta_a}}\delta_a + C_{\ell_{\delta_r}}\delta_r = 0$$

(11.25)

Equations 11.19 and 11.20 remain the same. If an analysis is made similar to that previously shown for the directional control problem, it can be shown that

$$C_{n_T} + K_5 C_{\ell_T} = K_6 \delta_a + C_L \phi$$

(11.26)

where K_5 and K_6 are constants assuming that the control and stability derivatives shown in Equations 11.19, 11.20, and 11.25 are zeros or constants near the angles of attack and airspeeds at which the lateral minimum control speed will occur.

Unfortunately, the magnitudes and directions of the propulsive lift component of the thrust vector and the yawing moment component of the thrust vector are nearly impossible to determine on a powered-lift aircraft. For a conventional aircraft, engine thrust can be assumed to act along the engine centerline which is usually aligned near the aircraft centerline. On a powered-lift airplane, the thrust vector varies according to angle ϵ as shown in Figure 11.29.
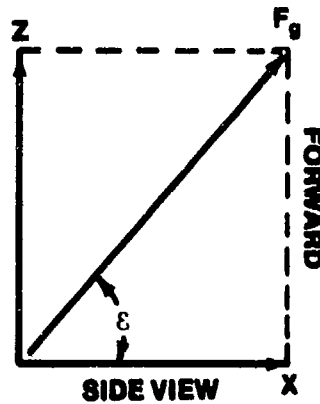
FIGURE 11.29. GROSS THRUST VECTOR

where

F_g = gross thrust vector, lb

ϵ = angle of downstream jet momentum vector, deg.

Angle ϵ is influenced by the flap angle setting but is not equal to this angle. Therefore, the component forces Z and X are nearly impossible to determine. These two vectors are functions of the gross thrust vector, therefore the following substitution may yield acceptable non-dimensional results

$$C_j = f(\delta_{cw}, C_L, \phi) \qquad (11.27)$$

where

C_j = gross thrust coefficient = F_g/qS

δ_{cw} = lateral control wheel, position, deg.

The substitution of δ_{cw} for δ_a is made because roll control may be a function

of spoiler deflection as well as aileron deflection.

The relationship shown in Equation 11.27 may not be correct for some powered-lift airplanes because of variations in the stability and control derivatives near the minimum control speed. However, in lieu of more complicated techniques it may yield satisfactory nondimensional results.

11.4.5.1 Ground Minimum Control Speed. The ground minimum control speed (V_{mcg}) will differ from the flight value because of:

1. The inability to use sideslip and the restriction on the use of bank angle.

2. Crosswind components.

3. The additional yaw moments produced by the landing gear, which in turn vary within the landing gear configuration; the amount of steering used; the vertical loads on each gear and runway condition.

There are three basic test methods for V_{mcg} testing: One involving acceleration, the second involving deceleration, and the third involving throttle chops during takeoffs.

Some high performance aircraft accelerate in the test condition and the acceleration method is required. The asymmetric yawing moment is gradually increased (by throttle manipulation) as increasing speed provides more control. The speed where sufficient control is available to hold the full asymmetric power condition is the minimum control speed. This method requires considerable skill and coordination to obtain good results – the aircraft is essentially at minimum control speed throughout the acceleration.

If the aircraft will decelerate with the asymmetric power condition set up (symmetrical pairs of non-critical engines may also be retarded) the "back-in" method may be used. The test is started at a ground speed in excess of the expected minimum and the power condition is set. As the speed decreases, more aerodynamic control deflection is required; the speed where directional control cannot be maintained is the minimum control speed.

These first two methods are considered static tests because no yaw rates or accelerations are allowed to develop.

The third, and primary method used at AFFTC relies heavily on good prediction of ground minimum control speeds. An incremental test speed above

11.40

the predicted speed is chosen. The test aircraft is accelerated on all engines to this speed and an engine chopped. Since the test speed is above the predicted speed, the aircraft should be easily controllable. If so, then the test speed will be reduced in increments down to the predicted speed. If at any speed down to the predicted speed, the aircraft deviates more than 30 feet with full controls used, the test is aborted. In this case, a new speed will be needed above the predicted speed. Since test pilots are performing the tests, knowing that an engine will be failed, some additional pilot reaction time must be added. The minimum acceptable reaction time for operational use would be one second.

11.4.5.2 Dynamic Engine Failure. To define the dynamic situation of an engine loss, pilot reaction time and the rates and accelerations that develop during that time have to be added to the steady state case.

The objectives of flight tests are to anticipate operational problems, duplicate realistic time delays, and arrive at a speed and recovery technique to give the average pilot a safe margin. The only realistic way to prove an aircraft can be recovered from a dynamic engine failure is to flight test it.

The military specification (MIL-F-8785C, Paragraph 3.3.9.3) requires that a pilot be able to avoid dangerous conditions that might result from the sudden loss of an engine during flight. The method to test compliance with this specification is to stabilize with symmetrical power and suddenly fail the most critical engine. After observing a realistic time delay for pilot realization and diagnosis, the pilot arrests the aircraft motion and achieves the equilibrium engine-out condition. Since it obviously requires more control to arrest the motion than to maintain equilibrium, this dynamic situation must be considered in determining the minimum control speeds.

Minimum control speed should not be set by any factor other than insufficient control. If the aircraft stalls before reaching the minimum control speed, a statement that "at this gross weight, the aircraft is controllable down to the stall" is preferable to calling the stall speed the "minimum control speed".

CHAPTER 12

AEROELASTICITY

12.1 INTRODUCTION

Aeroelasticity is the science which deals with the mutual interaction of aerodynamic, elastic, and inertial forces and the aircraft's structural responses to these forces. If aircraft could be designed as perfectly rigid structures, then the interaction of these forces would not be important. The weight penalties and the resultant loss of aircraft performance make this design option impractical. This chapter is intended to introduce the flight test crew to the subject of aeroelastic phenomena in aircraft. Paragraph 12.3 deals with material used in aircraft structures, including structural design considerations and use of composite materials in aircraft structures. Paragraph 12.4 introduces aircraft structural response to loads and Paragraph 12.5 presents static and dynamic aeroelastic phenomena due to the interaction of the forces mentioned above.

This subject area has taken on increased importance to the flight test crew in recent years. New high strength-to-weight and high stiffness-to-weight materials are being used in aircraft. New aircraft design and fabrication techniques allow the structural weight to be minimized, thus increasing the flexibility of today's aircraft. Active feedback control surface actuation to alleviate dynamic loads and flutter on aircraft is being used to further decrease aircraft structural weight and thus gain increased performance. New composite aircraft structures require the test crew to better understand materials and structural response to loads. This chapter is intended to introduce the test team to this important subject area.

12.2 ABBREVIATIONS AND SYMBOLS

A, a	amplitude or area
ac	aerodynamic center
b	semi-chord or torsional damping
c	wing chord or distance from neutral axis to outermost fiber
cg	center of gravity
$C_{L_{max}}$	variation of lift coefficient with angle of attack
C_{L_α}	variation of the lift coefficient with angle of attack
$C_{L_{\delta_a}}$	variation of the lift coefficient with aileron deflection
d	linear damping or diameter
E	modulus of elasticity (Young's Modulus)
e	strain or the distance between the aerodynamic center and the elastic axis
EA	elastic axis
F, f	force or frequency
f_b	bending stress
f_c	compressive stress
f_n	normal stress or natural frequency
f_p	proportional limit stress
f_s	shear stress
f_t	tensile stress
G	Modules of Rigidity
g	gravity or flutter damping
h	vertical displacement
I	moment of inertia
J	polar moment of inertia

K	spring stiffness
K_α	torsional stiffness
K_x	bending stiffness
L	lift or length
L_{δ_a}	lift due to aileron deflection
$L_{\Delta\theta}$	variation in lift due to wing twist
ΔL_{δ_a}	variation in lift due to aileron deflection
M	Mach or moment
m	mass
M_{aero}	aerodynamic moment
M_{ac}	moment about the aerodynamic center
$M_{ac_{\delta a}}$	moment about the aerodynamic center due to aileron deflection
P	load
q	dynamic pressure
q_D	dynamic pressure at divergence speed
q_R	dynamic pressure at aileron reversal speed
r	radius
S	wing area or shear force
T	axial force
t	material thickness or time
U_D	divergence speed
U_F	flutter speed
U_R	aileron reversal speed
α	angle of attack or coefficient of thermal expansion
ω	frequency

ω_d	damping frequency
ω_F	flutter frequency
ω_n	undamped natural frequency
ω_α	undamped natural torsional frequency
σ	stress
σ_{ENG}	engineering stress
σ_{TR}	true stress
σ_u	ultimate stress
σ_y	yield stress
ϵ	strain
ϵ_{ENG}	engineering strain
ϵ_{TR}	true strain
γ	shear strain
μ	Poisson's ratio
δ	change in length
a	aileron deflection
ζ	damping ratio
ϕ	phase angle

12.3 AIRCRAFT STRUCTURAL MATERIALS

12.3.1 Introduction to Design

The primary responsibility of the engineer is the design, construction, and maintenance of structures and machinery, etc. In his function as a designer, he makes use of the principles of thermodynamics, electricity, and the statics and dynamics of solids and fluids, but he is ultimately limited by the materials at his disposal. In the past, design of a mechanism or system

has often been a function separate from the consideration of the material of which the mechanism was to be constructed. This process was adequate when there were a very limited number of materials available. Now, it is estimated that a designer must choose from as many as 75,000 alternative materials. In addition, the capability of designing specific materials for an application exists. This has a far reaching effect on the process of design; now the designer must consider from the outset the materials and fabrication techniques to be used.

Perhaps even more significant is the growing tendency toward development and use of metamorphic materials: those that change properties as the service environment changes. Some examples are metals that form metal oxide coatings in a corrosive environment and inhibit further corrosion, steels that are "self-healing" in order to prevent crack propagation, and polymers that are formed into final shape "in place." These materials demand a unified design approach that considers the material as a dynamic part of the system rather than passive and static.

Because of the intimate interaction between the part and the material, it is necessary that designers understand basic material properties and materials engineers understand the design process. At least, they must be able to communicate in a mutually comprehensible manner since they must work together throughout the design process. The purpose of this section is to briefly introduce the design process and some material properties of concern to the "designer." The design process is discussed first, then material properties, fabrication, and finally an example of their interaction.

12.3.2 The Design Process

The formulation of aircraft performance, size, and carriage requirements by using commands starts the design process. These requirements are carried through the acquisition process, modified through cost and current (and projected) state-of-the-art and off-the-shelf technology compromises. The end product of the acquisition cycle is the contractual specification that defines as specifically as possible the performance requirements the system must meet. It is this specification that dictates the design and the design process.

For a new development of an aircraft or weapon system, the definition of its mission dictates the design. While the iterations of the design cycle may

be similar among cargo, fighter, and heavy bomber aircraft, the tolerances, structural requirements, and size limitations differ widely. The typical flight profiles dictate the loads and mission load cycles to be considered by the structural designers. Wing and control surface sizes and locations are, in part, determined by the performance requirements, and these in turn influence the structural load paths to ensure proper margins of safety. Static and dynamic loads are analyzed according to the required flight characteristics and internal and external carriage requirements. Sizing, structural design, material selection, propulsion interface and support, avionics locations and functions, control system development, aerodynamic considerations, radar and IR signatures, and human factors engineering are analyzed, developed, coordinated, compromised, modified, and integrated through innumerable iterations. Each nut, bolt, washer, and rivet is analyzed and examined to ensure that critical load paths at worst case conditions exhibit satisfactory margins of safety under static and dynamic loadings. Figure 12.1 depicts a simplification of this process before any aluminum is formed, composite is wound, or fastener installed. The airframe design process, from an aerodynamic viewpoint, must also contain sufficient structure to permit landing and taxi loads.

Once the basic analyses have been completed and preliminary design has given way to initial fabrication, mock-ups are used as a tool to determine actual form and fit of hardware, avionics, control systems, oxygen and pressurization systems, ducting, hydraulics, and electrical routings. As this sizing progresses, structural components undergo load testing to determine the accuracy and fidelity of analyses and to update simulations. Fabrication leads to installation and integration, yielding structures that finally begin to look and feel like aircraft. Selection of materials is covered elsewhere in the chapter, but is a continuing process in design in an attempt to provide required shape, strength, size, and airflows at minimum weight. The design process continues through flight testing the entire system, improving on previous attempts to upgrade performance with minimum cost and weight.
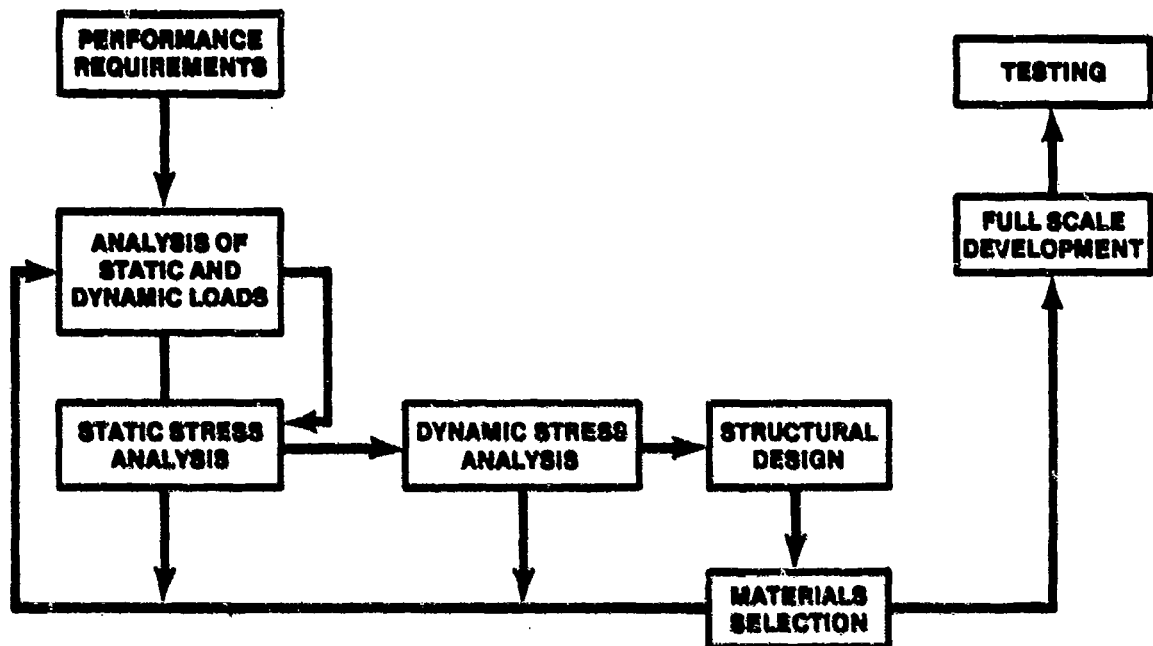
FIGURE 12.1. DESIGN PROCESS

12.3.3 Material Properties

The value of an engineering material is highly relative depending on the specific circumstances under which it is to be used. There are as many different materials suitable for a given design as there are different designs to accomplish a certain design goal. However, there is a "best" material for a certain design when a sufficient number of conditions are set for the material to meet.

There are a number of material properties that are basic in almost all engineering designs. For some applications, more than one property may be needed, such as high strength associated with good electrical conductivity and corrosion resistance. As more conditions are introduced, the selection narrows down. Obviously, an infinite number of conditions such as the three above can be set to finally limit the choice of available materials. Unfortunately, the ideal material for a particular application having a combination of optimum values for various properties does not always exist and a compromise is necessary at this stage to reach a definite decision. This is

only possible by understanding the properties which describe the character of
the material.

Some of these properties will be discussed in more detail on the
following pages. These properties are: mechanical, physical, chemical,
thermal, electrical, and optical. In addition, availability, cost,
fabrication techniques, reliability, and maintainability must be considered.
Though not often thought of as material properties, they are usually based on
a combination of properties, design, and economics.

12.3.3.1 **Mechanical Properties.** The mechanical properties of most concern at
present are stiffness, strength, toughness, ductility, hardness, and fracture
toughness. This discussion will treat only tensile loads, but the same
analysis could be made for compressive and shear loads.

Stiffness. When stiffness is considered, there are two definitions that
must be understood. The first is stiffness as it refers to the ratio of
stress (σ) to strain (ϵ) in the elastic region of the stress-strain diagram
shown in Figure 12.2. Stiffness in this sense is Young's Modulus (E); in
torsion the analogous parameter is G, modulus of rigidity.
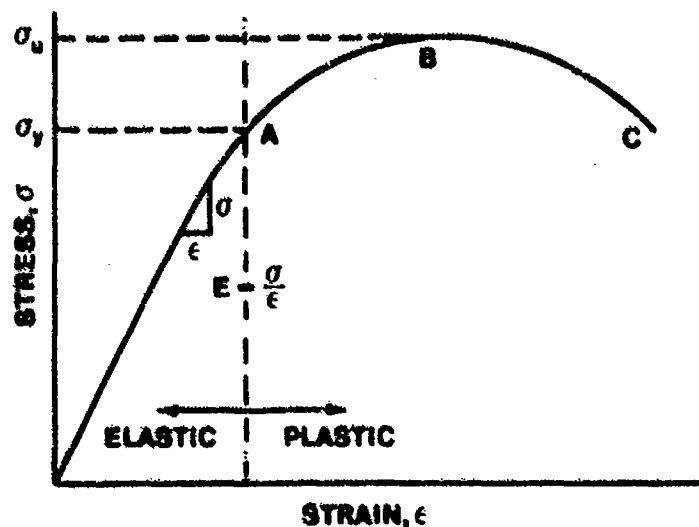
FIGURE 12.2. TYPICAL STRESS-STRAIN DIAGRAM

Stiffness (E) is closely related to the bonding between atoms in metals and ceramics and the bonding (number or type) between chains in polymers. For a given metal or ceramic, there is little that can be done to significantly change the value of E for the material. In the case of polymers, the value of E can be changed because interchain bonding can be varied.

Stiffness (E) is not necessarily related to the strength of a material which will be seen when strength is considered. Figure 12.3 shows what is meant by this statement. Material A has the highest E but the yield strength is less than for Material B which has a lower E. The meaning of yield strength will be discussed in the next section.
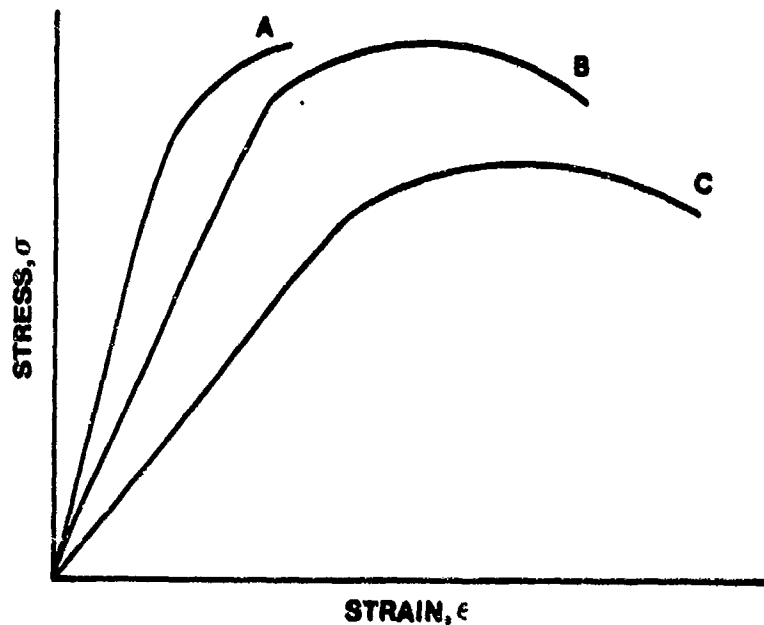
FIGURE 12.3. STRESS-STRAIN DIAGRAM, DIFFERENT MATERIALS

Strength. The strength of a material is a mechanical property of the material. It also depends on what the failure criteria are defined to be. There are several "strengths" depending on what constitutes failure: (1) yield strength (σ_y); (2) ultimate strength (σ_u); and (3) rupture or breaking strength. The common failure criteria are:

1. Excessive elastic deformation - related to σ_y since when stress is equal to σ_y, plastic deformation begins.

2. Excessive plastic deformation - an example of this is creep in jet engine turbine blades.

3. Fracture - separation of the material due to ductile or brittle fracture, fatigue, or creep. There are other failure criteria such as loss of appearance, which often must be considered. The three listed above are of major concern and will be developed further.

Strength data for a given material are usually obtained from simple tensile tests of standard specimens and are displayed on a stress-strain diagram as shown in Figure 12.2. Normally, materials display a region of elastic response and one of plastic response. The response is taken to be elastic (completely recoverable under ideal conditions) up to the yield strength (σ_y). Thereafter, the response is plastic, and the deformation is not completely recoverable when the load is removed - some permanent set being retained. The ultimate strength (σ_u) at Point B represents the ratio of the maximum load applied to the specimen to the original specimen's cross-sectional area (A_0). From Point B to C, the specimen continues to be loaded. However, the load is decreasing in magnitude and the cross-sectional area is decreasing. Consequently, the σ/ϵ curve decreases. Point C represents the complete separation of the material (fracture).

Figure 12.2 showed an engineering σ/ϵ curve in which all loads were divided by A_0. Engineering stress (σ_{ENG}) is

$$\sigma_{ENG} = \frac{P}{A_0} \qquad (12.1)$$

and engineering strain (ϵ_{ENG}) is given by

$$\epsilon_{ENG} = \frac{\delta}{\ell_0} = \frac{\ell_f - \ell_0}{\ell_0} \qquad (12.2)$$

However, during the test, the cross-sectional area clearly decreases and the length increases. If instantaneous values of cross-sectional area (A_i) and length are used rather than the original values, true stress and strain (σ_{TR}, ϵ_{TR}) are obtained. These equations are

$$\sigma_{TR} = \frac{P}{A_i} \tag{12.3}$$

and

$$\varepsilon_{TR} = \int_{\ell_0}^{\ell_f} \frac{d\ell}{\ell} = \ln\left(\frac{\ell_f}{\ell_0}\right) \tag{12.4}$$

but

$$\ell_f = \ell_0 + \delta,$$

so ε_{ENG} and ε_{TR} can be related by

$$\varepsilon_{TR} = \ln(1 + \varepsilon_{ENG})$$

Figure 12.4 shows a comparison of true and engineering stress-strain diagrams. The true σ/ε curve continues to increase even after the load decreases because the instantaneous cross-sectional area (A_i) is decreasing at a faster rate due to necking of the specimen. This discussion will consider engineering stress and strain since the engineer is concerned with the original areas, lengths, etc., in the design phase.

Materials are often characterized as ductile or brittle depending on the extent of their plastic behavior. Figure 12.5 shows hypothetical materials of varying ductility. Material A is entirely brittle and fractures while still responding elastically. Ceramics display this type of behavior. Material B undergoes some plastic deformation before fracture and is characterized as being ductile. The strain in the plastic region of the σ/ε curve is a measure of the ductility of the material. If the material is greatly strained before fracture, the material is considered to be ductile. Ductile and brittle are relative terms; thus, Material B is ductile relative to Material A and brittle relative to Material C. There are three additional mechanical properties of great concern that are related to ductility: hardness, toughness, and fracture toughness.
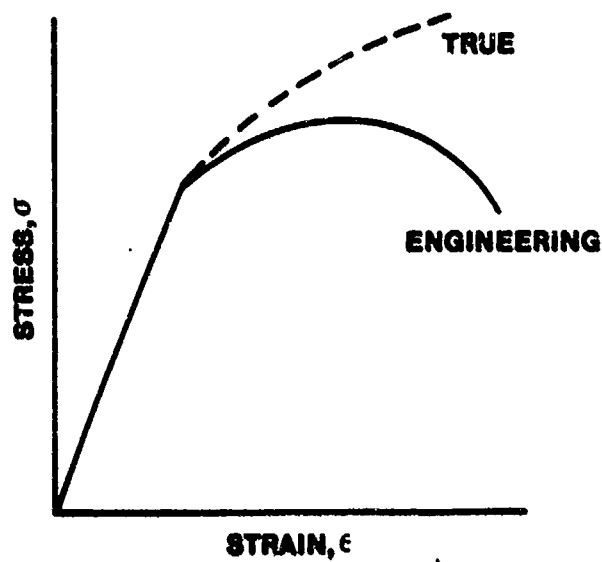
FIGURE 12.4.   COMPARISON OF TRUE AND ENGINEERING STRESS-STRAIN DIAGRAMS
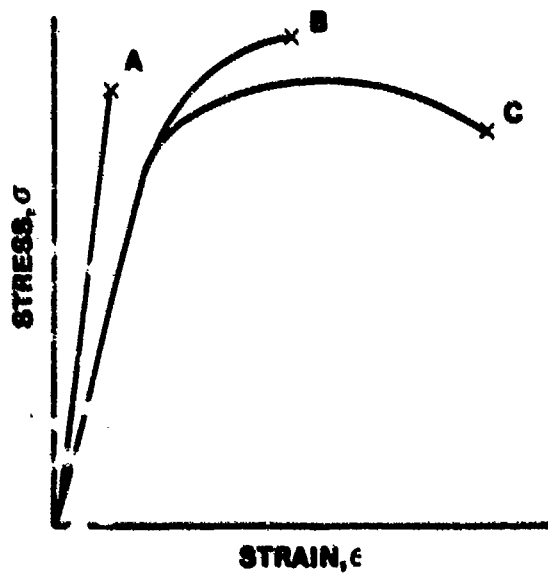
FIGURE 12.5.   EFFECT OF DUCTILITY ON STRESS-STRAIN CHARACTERISTICS

Hardness. There are a number of ways to measure the hardness of a material: abrasion, rebound, cutting, indentation, etc. The most common method for metals is by indentation. Penetrators of specified geometry and material are forced into the metal by known loads and the depth of penetration measured. The depth of penetration is then a measure of the metal's hardness. Since the penetrator is forced into the metal, the metal is plastically deformed indicating that hardness and ductility are directly related. If the material is ductile, it can be easily deformed plastically and consequently is soft. If the material is brittle, it cannot be easily deformed plastically and is therefore a hard material. Hardness, then, is a measure of the resistance of a material to indentation.

For many metals (particularly steels), there is a direct relationship between the hardness and the ultimate or tensile strength of the material. The approximate relationship for carbon and low alloy steels is

$$\sigma_u = 480 \ (BHN) \tag{12.6}$$

where BHN is the Brinell Hardness Number - the result of a Brinell Hardness Test. Other hardness numbers could be obtained from Rockwell or Vickers Hardness Tests and then related to the BHN.

Toughness. Toughness is a measure of the ability of a material to absorb energy in the plastic range. One way to measure toughness would be by using the area under the σ/ϵ diagram. Thus, in Figure 12.5, Material C would have to be the toughest and Material A the least tough.

In the elastic range, there is a property related to toughness which is called resilience. Resilience is a measure of the capacity to absorb energy in the elastic range and is the area under the elastic portion of the σ/ϵ curve. Resilience is important when considering such things as leaf springs for automobiles. The material must always operate within the elastic range and absorb energy in that range.

There are other properties of importance such as electrical, thermal, magnetic, optical, chemical, and physical. Only electrical, thermal, and chemical properties will be briefly mentioned here.

12.3.3.2 Electrical. Some materials are conductors and others insulators; semiconductors fall in between. The electrical conductivity of a material

depends on the type of bonding. If the valence electrons are bound as they are in ionic and covalent bonding, then the material is an insulator. If the valence electrons are free to move as in the metallic bond, the material is a conductor. At very high temperatures the ions in ceramics may become electrical conductors.

12.3.3.3 Thermal. Thermal conductivity and the coefficient of thermal expansion are also related to bonding. Thermal conductivity requires that electrons be free to move so the same materials that conduct electricity are normally thermal conductors. Those that are electrical insulators are thermal insulators. The coefficient of thermal expansion (α) is inversely related to the strength of the atomic bonds. Therefore, as bond strength increases, α decreases. Many designs are subjected to a thermal environment, and thermal stresses are set up that result in failure of the part. Another thermal effect is creep or accelerated plastic deformation that only becomes a problem at about one-half the material's melting point on an absolute scale.

12.3.3.4 Chemical. Chemical properties, as used here, refer to the corrosion and oxidation properties of the material.

12.3.4 Conclusion

The design process is a rather long and exhaustive process because of the great number of factors to be considered and the interplay of mechanics and materials. Good design is possible only if the designer is familiar with materials and every materials engineer is familiar with the design process.

12.3.5 Composite Materials

12.3.5.1 Introduction to Composite Materials. Early man had a variety of natural materials such as wood, clay, stone, copper, and iron available. Although he did not understand the basis for a material's behavior, he selected materials that met his needs. The early Egyptians are an example of men who, not having a natural material available to meet their needs, combined two materials to form a composite that overcame their limitations. They combined mud with straw to produce reinforced bricks which they used to build their cities.

This cycle continues and even more so in today's highly technological world. Design ideas limited by materials lead to the development of new, more advanced materials. The need for higher performance materials to overcome present design limitations has created a new class of materials called composites. A composite material is a combination of two or more constituents from the three general classifications of materials: metals, ceramics and/or polymers. Composite materials were created to provide materials with improved mechanical properties such as stiffness, strength, and high temperature stability. The development of composite materials is a revolutionary advancement in materials technology. Until recently, materials selection was a substitution affair where the question was, "What material can I use in place of alloy X?" The material selection was often a secondary decision that did not influence the design. A composite material allows the materials engineer to incorporate the required properties which greatly affect the design and should be considered early in the preliminary design phase.

The importance of composites becomes clear if one examines material properties on a density-corrected basis. Table 12.1 illustrates this fact by comparing mechanical properties (density corrected) to show the specific properties. It is apparent that very little flexibility in material selection actually exists for conventional materials. Composite materials combine a reinforcing material with high specific strength and specific stiffness with a low density matrix material that results in a system that is synergistic (properties of the whole are greater than the sum of the individual constituents).

These materials are especially useful in aerospace applications where weight is an extremely important and driving design parameter. Development of composites has been primarily financed by research and development in the aerospace industry conducted by both private industry and government. A large variety of laminated composite structures have been designed and flight tested. A large number of materials can be classified as composite materials; however, this chapter will be confined to the more advanced fiber reinforced composites that utilize continuous and discontinuous fibers as the reinforcement material.

TABLE 12.1

MECHANICAL PROPERTIES

Materials	ρ (lb/in^3)	E(psix10^6)	E/ρ (inx10^3)	TS(psix10^3)	Ductility %
Steel (Hot Rolled) (Metal)	.283	30	105	65	30
Steel (Cold Rolled) (Metal)	.283	30	105	85	20
Aluminum (Metal)	.100	10	100	63	7
Titanium (Metal)	.165	17	103	165	15
Beryllium (Metal)	.067	42	625	83	16
Pine Wood (Polymar)	.0145	1.3	90	7	—
Silica Glass (Ceramic)	.079	10	126	—	—
Graphite Whiskers	.060	102	1700	2845	—
Boron/w Wire	.095	55	580	400	—
Boron Epoxy (Composite)	.075	20	270	133	—

12.3.5.2 <u>Continuous Fiber Reinforcement Materials.</u> A composite material is composed of two basic components - a reinforcing fiber which is surrounded by a soft light-weight matrix. The majority of advanced composite materials utilize continuous fiber reinforced materials fabricated from ceramics and metals. The fiber must have a high specific strength to carry the load in the composite structure and a high specific stiffness to supply the required structural rigidity. Designs require the fibers to be uniformly aligned to maximize the contribution of fiber strength properties to the composite structure. Ideally, the fiber axis should be aligned parallel to the maximum

loading axis of the structure. Since a single row of fibers is called a lamina (Figure 12.6) and one must stack up lamina in a sequence to form a laminated structure (Figure 12.7) where the fiber orientation can be varied, the materials engineer can design in a wide variety of material properties. Another benefit the fiber offers is that it will prevent crack propagation through the matrix.

The strength and stiffness requirements for fibers limits the material selection primarily to ceramics and metals. Table 12.2 shows the primary materials being investigated; for metals, boron, tungsten and steel are the most promising. For ceramics, graphite, glass and silicon carbide hold great promise. Boron fibers are the most versatile metal fibers. Research and development have concentrated on these fibers. Tungsten and steel are of interest for high temperature applications. Graphite is the most attractive ceramic fiber and it can be made into a variety of fiber shapes and lengths. Its primary disadvantage is cost. Glass is cheaper by comparison and does have some very attractive properties; however, it requires special surface coating protections called sizes to protect the fiber from degradation by the environment and from handling during manufacture. Ceramic fibers exhibit the greatest strengths and are very stable, but they can be difficult to bond and usually require a coating to promote better interfacial bonding. The metals tend to exhibit lower strengths but are easier to bond. However, interfacial reactions can degrade the fiber properties.

FIBER

MATRIX

LAMINA CONSTRUCTION

FIGURE 12.6.

LAMINA
THICKNESS

LAMINA (ONE LAYER)

0, 45, 90, 0 LAMINATE GEOMETRY
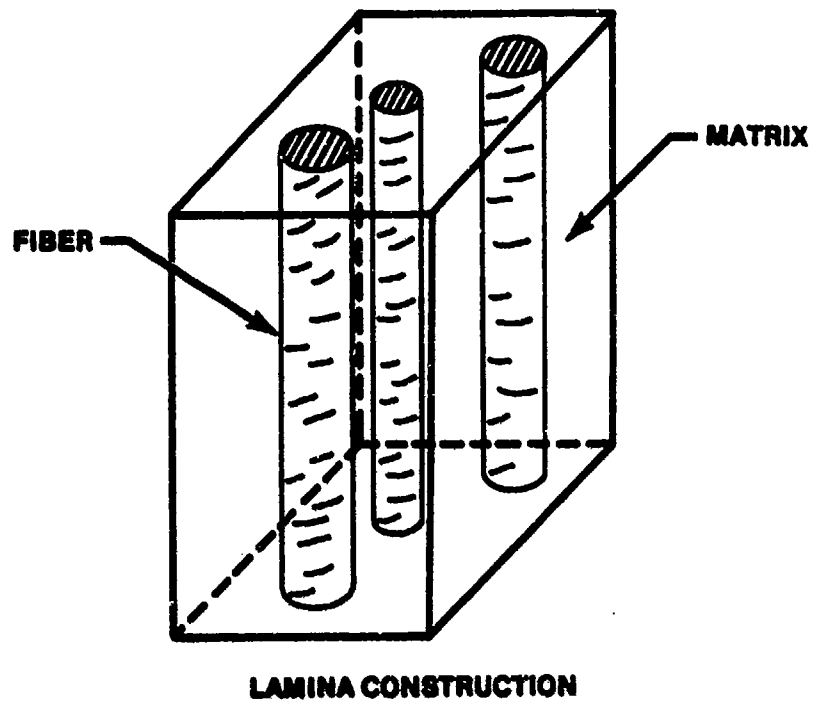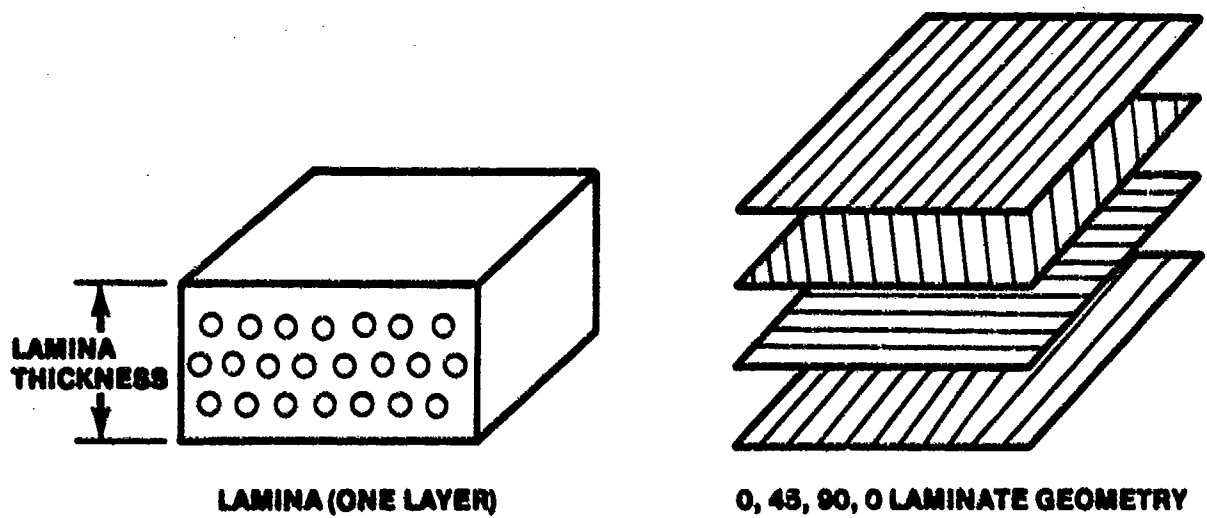
FIGURE 12.7.   LAMINATED STRUCTURE

TABLE 12.2

PROPERTIES OF FIBER AND MATRIX MATERIALS

	Melt Point ($^\circ$F)	Density (lb/in^3)	Tensile St. (Ksi)	Strength Density ($\times 10^6$)	E ($\times 10^6$ Psi)	Modulus Density ($\times 10^7$ in)
AMORPHOUS FIBERS						
S-Glass	1540	.090	650	7.2	12.6	14.0
SiO$_2$	3020	.079	850	10.8	10.5	13.3
DISCONTINUOUS FIBERS (SINGLE CRYSTAL)						
Al$_2$O$_3$	3700	.143	3000	21.4	62	43.4
SiC	4870	.116	3000	26.1	70	60.8
Graphite	6600	.060	2845	47.4	102	170
POLYCRYSTALLINE FIBERS						
Al$_2$O$_3$	3700	.144	300	2.6	25	21.9
Graphite	6600	.054	200	3.7	30	56.5
Tungsten	6150	.697	580	.8	59	8.5
Steel	2550	.280	600	2.1	29	10.3
MULTIPHASE FIBERS						
Boron/W	4170	.095	400	4.2	55	57.8
SiC/W	4870	.148	300	2.0	70	43.3

	Cont. Use Tem. (^{0}C)	Elongation (%)	Tensile Strength (Ksi)	Modulus ($\times 10^6$ Psi)
MATRIX MATERIALS				
Polycarbonate	120	80	9	.34
Polysulfone	150	50	10	.36
Epoxy-BPA	145	4.8	13	.36
Epoxy-CA	150	3.5	19	.78
Phenolic	160	2	9	.45

The fibers can exhibit a variety of crystalline structures which affect their properties. Single crystal discontinuous fibers are of an order of magnitude stronger than all the other fibers; however, they are microscopically small and difficult to fabricate. Polycrystalline fibers have lower strengths due to the imperfections present in the larger fibers. Amorphous fibers are strong but highly susceptible to damage and degradation.

There are a variety of manufacturing processes used to fabricate reinforcement fibers. Glass fibers are typically prepared by making the material molten and then extruding it through small orifices ($\approx$ .005 inch) which removes water. The fibers are fired at a temperature to densify. Metal fibers are made using the wire drawing process; however, to reduce the fiber down to .005 inch requires diamond dies which are very expensive. There are other processes such as electromechanical, liquid metal, vapor deposition, and numerous proprietary processes.

The fabrication of boron fibers is very interesting and unique. A tungsten wire .005 inch in diameter is passed through a long glass tube that contains boron gas such as boron trichloride (BCL_3). Pressure is maintained in the tubes to force the boron to deposit on the tungsten filament which is heated electrically. The entire process takes less than two minutes and produces a filament between .003" - .005" in diameter. The time can be adjusted to yield other diameters but .008 inch is presently the upper limit. The fibers are usually produced in continuous lengths of 10,000 feet. The only supplier of boron fibers in quantity is the AVCO Corporation in Lowell, Massachusetts. One advantage of composite fibers is that they can be processed by winding around mandrels. They are then woven into two-dimensional cloths and three-dimensional mats that are then impregnated with the matrix. This process can be a definite advantage in producing complex shapes.

12.3.5.3 Matrix Materials. The second basic component material is the binding or matrix material. The fibers carry load and give structural rigidity. The matrix material bonds the fibers and holds them in a specific alignment. It transfers loads through shear mechanisms to the fibers. The matrix material must be light weight so that the benefits of the specific

strength and specific stiffness are not depleted. Similarly, a soft ductile material will assure full fiber strength is utilized and provide good plastic behavior for transferring load by shear mechanisms. The matrix also serves to protect the fibers from the environment which may tend to attack the fibers and degrade properties. This is especially true of glass fibers. The matrix will arrest crack propagation occurring in fibers since it acts as a foreign material interface and will deflect the cracks. Other properties the matrix can contribute include toughness, fatigue strength, oxidation resistance, corrosion resistance, etc. The matrix material requirements have limited selection to polymers and metals. Polymers such as epoxies, phenolics, and polysulfones, and metals such as titanium and aluminum possess the lower strength/high ductility behavior that is necessary in a matrix. Epoxies and aluminum have been extensively researched and most components that are flying on aircraft or are in the development stages are made from these matrices. The phenolics and titanium are still in their early stages but hold great promise for higher temperature applications. Unlike fibers, these materials can usually be fabricated using conventional techniques already established which reduce costs. The polymers are temperature limited, can be sensitive to humidity, and possess a wide variation in properties such as chemical and corrosion resistance. Important considerations in design are the stresses and life expectancies required of these matrix materials. These polymers also exhibit shrinkage which must be accounted for in the processing since it can be as great as 15%. Typical matrix properties are shown in Table 12.2.

12.3.5.4 Manufacturing of Composite Materials. Careful consideration must be given to the decision concerning which fiber to combine with which matrix to yield the optimum design. All design parameters must be considered in order for the materials engineer to design in the required properties. This further requires that material selection and assessment be made early in the preliminary design phase.

Regardless of the selection of fiber and matrix, they both must be properly bonded together. The bonding surface between fiber and matrix is called the interfacial bond, and it has an enormous effect upon composite material properties and fabrication. The metallurgical reactions that occur

are complicated and difficult to control. Poor bonding at the interface results in premature failures. The fiber shape is also important. The greater the surface area available for bonding, the better the bonding will be. Thus, non-circular cross sections promote superior bonding.

There are a number of techniques employed to control interfacial reaction zones to limit property degradation while promoting good bonding. The ceramic tend to be thermodynamically stable and show smaller reaction zones. They do not, however, bond as well to the matrix and therefore require a coating such as polymeric or metallic coating. These coatings are especially required in metal matrix composites. When boron was initially used, it often had to be coated with silicon carbide to bond it with aluminum and titanium. Advances in composite technology and fiber treatment have eliminated these requirements.

Interface reactions result in the destruction of the fiber. The three most prevalent reactions that occur include diffusion between fiber and matrix which can leave a penetration zone with recrystallization that causes premature failure of the fibers. In addition, precipitation reactions and/or solid solution reactions can produce fracture initiation sites leading to failure.

A variety of manufacturing processes are utilized that allow the designer latitudes which conventional materials do not possess. The fibers can be wound around a mandrel and then impregnated with the resin matrix material or a "prepreg" (partially cured) composite can be wound on a mandrel. The "prepreg" composite is often used to allow forming of lamina into desired shapes and then using a mold under heat and pressure to produce final curing. The metal matrix composites can be handled in this same manner. Often, large sheets of composite material are precut into ply patterns which are hand-assembled and then finish processed. Composites can be woven into two-dimensional and three-dimensional shapes which are then impregnated with the matrix and cured. This type of fabrication gives the designer tremendous capabilities that otherwise would not be available.

12.3.5.5 Design Applications. As composites become more common, it is necessary for engineers accustomed to dealing with metals to become more versatile in their thinking. The various properties of metals are generally

considered to be isotropic - the same in all directions. The design trade-offs mentioned earlier are thus fairly straightforward. It is common when dealing with metals to consider such properties as modulus, E, as constants. This, in fact, is not the case with composite materials. Composites are anisotropic; that is, having different strength, stiffness and thermal properties in the various directions. This produces an added complexity for the designer but also provides him with more flexibility and a chance to truly optimize a structure. If the designer fully understands the anisotropic nature of a material, he is able to design the material to meet the specific design requirements (strength, stiffness, etc.) of his structure in its specific directions. This, of course, forces the designer to analyze the strengths and stiffnesses required in his structure based upon such factors as the expected loads and allowable deflections. Since structures are often loaded in only one or two directions, a composite can be made strong in those directions. This can be compared with fabricating steel or aluminum where, in order to meet a maximum strength requirement in one direction, the material, because of its basic nature, is equally strong in other directions. It can thus be seen that a composite can be used more efficiently and produce a second weight savings in addition to the one inherent in its high strength-to-weight or stiffness-to-weight ratios.

12.3.5.6 Economic Factors. Composite materials have gained a reputation for being expensive. To some extent, this reputation is deserved. As graphite and boron filaments were first being developed in the 1960's, costs of $600 per pound and $400 per pound, respectively, were common. With increased production, these costs are now on the order of $100 per pound for boron and $50 per pound for graphite, which still does not favorably compare with a few dollars per pound for steel. However, the cost to be considered is not the material cost but the cost of the finished product or the dollars per payload of the final system.

The cost of compositing includes the tape fabrication, laying the tape into layers and the final assembly of the part including its joining to other parts of the structure. Metal parts, of course, have forming and machine costs associated with them. The Navy built a composite wing for a Target Drone using graphite epoxy. While the material costs were higher than the

aluminum it replaced, the manufacturing steps in fabricating the wing were reduced from approximately 50 for the aluminum to 3 for the graphite. The savings resulting from this are quite obvious.

C.E. Cataldo, in an article on the use of composites for the space shuttle, estimates that composites can save 5-9% of the structural weight of approximately 200,000 pounds. This savings of 10,000-18,000 pounds, when compared to the original payload of 25,000-65,000 pounds, produces a payload increase of up to 40%. The cost savings resulting from this are so huge that they overshadow any material costs.

12.3.5.7 <u>Analysis of Composite Materials</u>. A technique used to determine the properties of a composite is based upon the volume fraction of its constituents. This rule of mixtures is illustrated in the following paragraphs.

If we stipulate that the fibers are uniformly aligned, as shown in Figure 12.7, and that a perfect bond exists between the fiber and matrix, then the strain is the same for the composite, the matrix, and the fiber

$$\epsilon_c = \epsilon_f = \epsilon_m$$

The total load in the composite will be the sum of the loads carried by the fiber and the matrix.

$$P_c = P_f + P_m$$

Utilizing the axial stress relationship and solving for P, the equation can be rearranged as follows

$$\sigma = \frac{P}{A} \quad \therefore P = \sigma A$$

$$\sigma_c A_c = \sigma_f A_f + \sigma_m A_m$$

Dividing by the area of the composite and noting it is equivalent to the sum of the areas of the fiber and matrix yields

$$\boxed{\sigma_c = V_f \sigma_f + V_m \sigma_m} \qquad\qquad (12.7)$$

where V_f and V_m are volume fractions. Note $V_f + V_m = 1$. Dividing by the strain yields

$$\boxed{E_c = V_f E_f + V_m E_m} \qquad\qquad (12.8)$$

EXAMPLE: Design a composite material with a modulus of elasticity of 11 GPa and a yield strength of 160 MPa. The properties of the fiber and matrix are shown below and have been measured for the limiting strain.

$E_f = 14.$ GPa $\qquad\qquad\qquad E_m = 7.$ GPA

$\sigma_f = 210.$ GPa $\qquad\qquad\qquad \sigma_m = 105.$ MPa

@ $\varepsilon_f = .015$ m/m $\qquad\qquad$ @ $\varepsilon_m = .015$ m/m

Consider both equations

a. $\sigma_c = V_f \sigma_f + V_m \sigma_m$ $\qquad\qquad$ b. $E_c = V_f E_f + V_m E_m$

$160 = 210 (V_f) + 150 (V_m)$ $\qquad\qquad$ $11 = 14 (V_f) + 7 (V_m)$

Note: $V_m = 1 - V_f$

$160 = 210 (V_f) + 150 (1 - V_f)$ $\qquad\qquad$ $11 = 14 (V_f) + 7 (1 - V_f)$

$V_{f_\sigma} = 0.524$ $\qquad\qquad\qquad\qquad$ $V_{f_\sigma} = 0.571$

Notice there are two answers and in order to meet both design requirements you must choose the largest value where the volume fraction of fibers would be 57.1%.

This type of analysis is often applied to composites and is adequate for properties such as density and certain mechanical properties such as the longitudinal stiffness. Note, however, that this relation says that the properties of a composite are bounded by those of its constituents.

As mentioned earlier, a simple analysis such as the rule of mixtures or ideas that one might be comfortable with in dealing with metals is not adequate in the analysis and design of composite structures. Since the mathematics of anisotropic elasticity and of composite laminate analysis are beyond the level of this course, this chapter will simply present an overview of some of the techniques used.

There are more steps with more complexity in the design of a structural composite than exist in the design of metal structures. The design cycle starting with the fiber and matrix constituents are illustrated in Figure 12.8. Note that this cycle is continuous. This implies that the material's design must be simultaneous with the structure's design. The final objective of the design process is, of course, to achieve an optimum structure. This can often be translated into minimum weight.

The design cycle shown in Figure 12.8 combines two basic approaches which have been labeled microscopic and macroscopic. The microscopic approach considers the mechanical and physical characteristics of possible fiber and matrix materials. These properties are normally considered to be isotropic; however, the structure as a whole is heterogeneous (non-homogeneous). Using various assumptions concerning the state of stress and strain between the fiber and matrix, the designer must select the proper constituent materials and decide upon the packing arrangement of the fibers and their proper volume fraction. As seen in Figure 12.9, the properties of the unidirectional laminate depend upon this microscopic analysis of the constituents. The reason the laminate or single layer of composite is made of fibers all oriented in one direction is that this allows ease of manufacture and analysis.

The next step is to determine the mechanical and physical characteristics of the building block laminate. This involves what is called a macroscopic

analysis. Here, the matrix and fiber are considered smeared together to form a homogenous but anisotropic material for analysis purposes. Such a procedure is advantageous since existing plate and shell theories can be applied to the analysis of these thin homogeneous anisotropic laminatae.
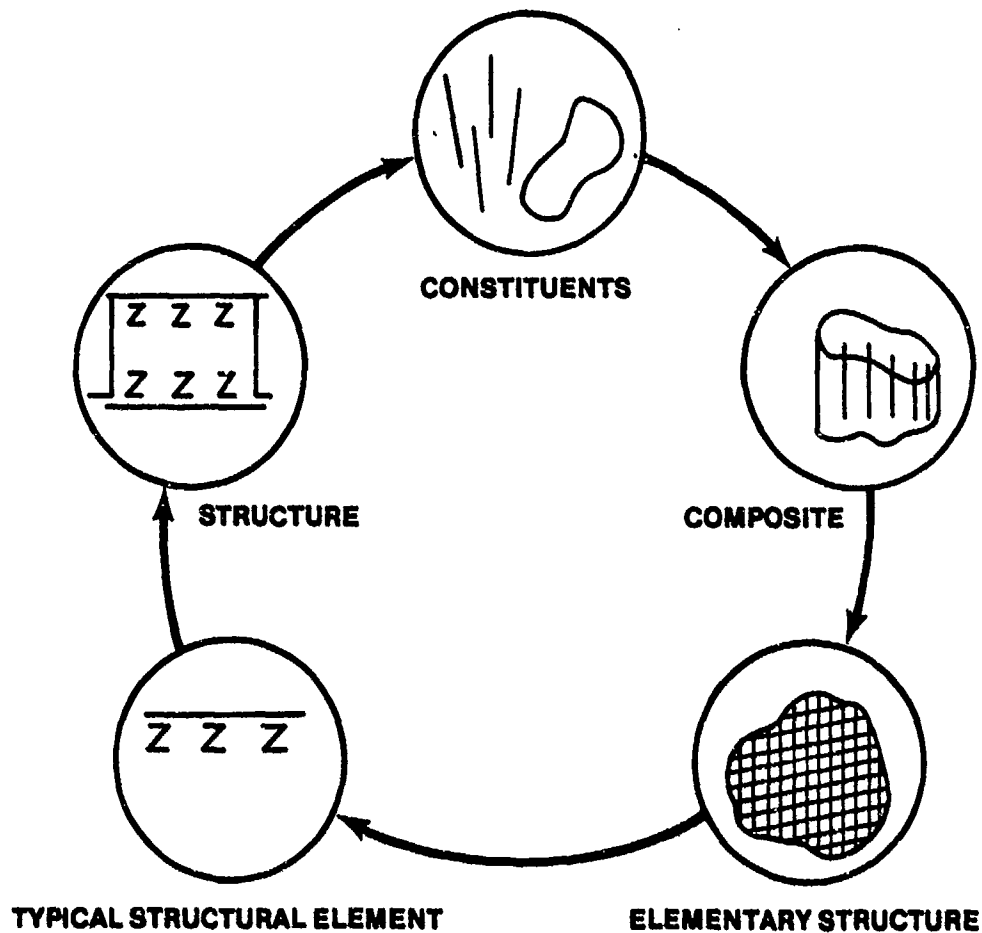
FIGURE 12.8.   COMPOSITE STRUCTURAL DESIGN AND ANALYSIS CYCLE

Laminate analysis involves determining the optimum number and orientation of the lamina necessary to provide the desired properties. Presently there is not a unique mathematical solution to this problem and the combination of computer iteration and experience guides the designer to a final laminate arrangement. An arrangement of 0, 45, 90, 0 for a four-ply structure is illustrated in Figure 12.7. Usually the optimization procedure produces

angles which might be difficult to manufacture; thus, it is common to change a calculated 0, 39, 87, +5 arrangement to the 0, 45, 90, 0 mentioned earlier for ease and economy of manufacture.

The final result of this analysis is a structure of lower cost, improved maintainability and increased performance. Table 12.3 shows some of the current applications of composites. During development, the aerospace industry tested composites in non-critical structures such as doors in the F-111 and in the wing of a Navy Target Drone. The use of materials and fabrication techniques previously untried was often done to the reluctance of both designers and users. Today, however, such materials are seeing use in primary aircraft structures such as the longitudinal spine of the B-1 and horizontal and vertical stabilizer sections of the F-15.
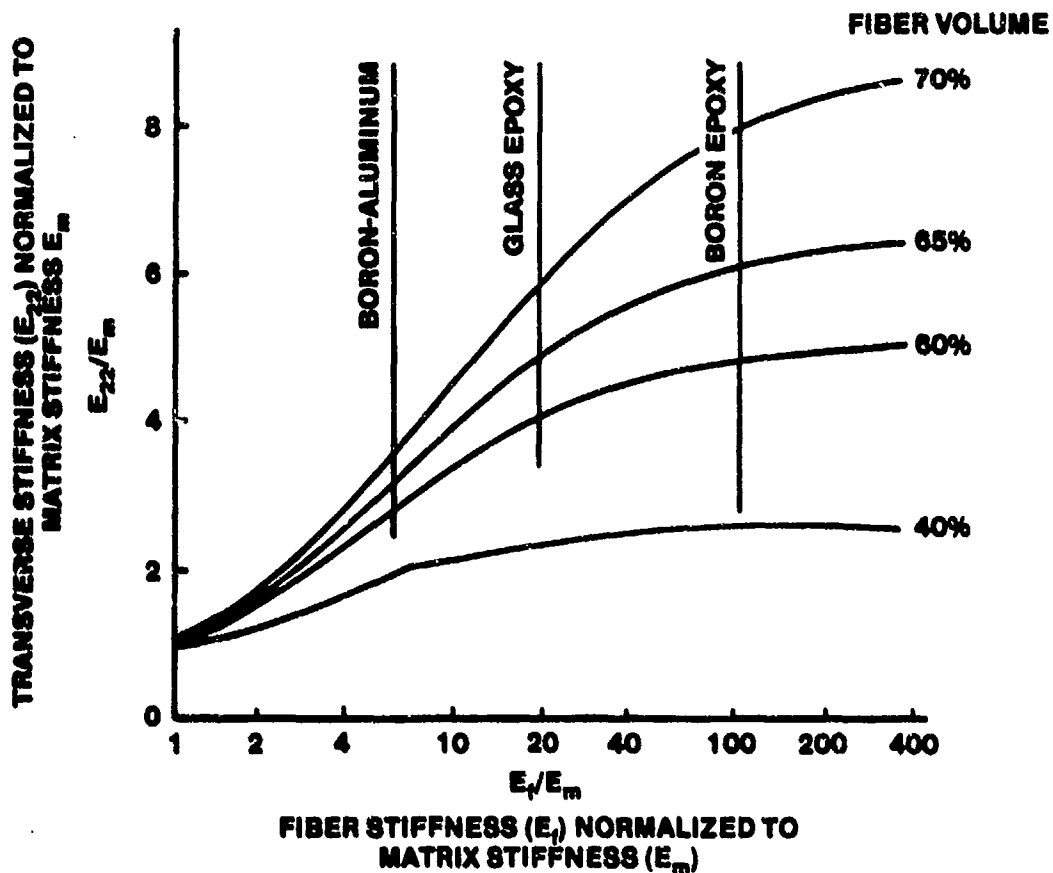
FIGURE 12.9. TRANSVERSE STIFFNESS IN UNIDIRECTIONAL LAMINATE

12.3.5.8 Discontinuous Fiber Reinforcement Materials. There are various types of discontinuous fiber reinforcement materials. In this paragraph, glass, whisker formation, and binary eutectic fiber reinforced composites will

be discussed. The discontinuous glass fiber reinforced composites are the most widely used composites in industry today. The primary advantages of these composite systems are in their manufacture. They utilize the technology applied to the polymeric and textile industries. This eliminates the need to make large capital investments in exotic manufacturing equipment. In addition, the fabrication of the glass fibers and polymeric matrices are well established and inexpensive. The glass can be chopped into fibers and randomly distributed throughout the matrix giving three-dimensional stiffening and strengthening. The procedure consists of mixing a polymeric with glass fibers and using conventional injection molding techniques to produce fiberglass types of structures. The fibers can be chopped up and blown into a meshed structure with a matrix added to form a "prepreg" that can be final cured into a finished product. The glass fibers can be woven into mats and impregnated with resin to form a continuous fiber reinforced composite. There are many epoxy and phenolic resins that can be used with the chopped fibers but these composites do not exhibit high strength levels. They are used for corrosion resistance, light weight, low cost manufacturing, optical properties, etc.

It is obvious from Table 12.2 that the single crystal whiskers possess an order of magnitude greater properties over the polycrystalline, amorphous and multiphase fibers. These whiskers are free from defects and dislocations, and their properties approach theoretical values. The obvious question is, "Why aren't these composite fibers being used throughout the industry?" The answer is technically complicated but economically simple. The whiskers are only 100-200 microns long which is the reason they can be fabricated defect-free. But they are also difficult to bond to the matrix and infinitely more difficult to align. The handling and fabrication of these whiskers requires expensive and sophisticated equipment. Economically they are impractical. A typical example is silicon carbide whiskers. They are grown using a sublimation technique that involves the prolysis of organosilanes, silicon compounds, and hydrocarbons in a hydrogen atmosphere at 1500-2000°C. Graphite can be formed into scroll-type fibers by combining sublimation techniques with DC arcing under high pressure in an inert atmosphere. Other techniques use evaporation and vapor-liquid-solid deposition processes, but all are prohibitively expensive.

TABLE 12.3

COMPOSITE APPLICATIONS AND DEVELOPMENT

SPACE SHUTTLE APPLICATIONS

Thrust Structure	Fuselage	Bulkheads	Tanks	Hot Structure	Shrouds
SKINS					
Boron-Epoxy	Ring Frames	Glass-Epoxy	Glass-Filament Wound with Liners	Carbon-Carbon	Boron-Epoxy
Boron-Alum.	Longerons	Graphite Epoxy		Graphite Coated	Boron-Alum.
Graphite-Epoxy	Stringers				Graphite Epoxy
	Skins				Glass-Honeycomb
	Beams				
BEAMS	Fittings		Graphite-Epoxy for small tanks	Boron-Polyimide 650°	
Same					
	Boron-Epoxy			Graphite-Polyimide 650°	
	Boron-Alum			Boron-Alum. 600°	
STRUTS	Graphite-Epoxy			Metal-Metal 2000-2500°	
Same	Glass-Epoxy				
				Borsic-Ti 800°	

12.30

TABLE 12.3 (continued)

COMPOSITE APPLICATIONS AND DEVELOPMENT

DEVELOPMENT STATUS

Current Developments (Near Term Payoff)	Advanced Development (Long-Term Payoff)	Future Development (New Concepts-New Materials)
Boron-Epoxy	Boron-Polyimide Graphite-Polyimide	In-Situ Reinforcements
Graphite-Epoxy	Wire Reinforced Metals	
Boron-Aluminum	Graphite-Aluminum	High Temperature Polmers
Carbon-Carbon	Beryllium Composites	Low Cost High Speed Production
	Hybrids	Advanced Hybrids

COMPOSITE TEMPERATURE CAPABILITIES

Maximum Temperature Capabilities

Polymer Matrices	Temperature (^{0}F)	Metal Matrices
S-Glass/Epoxy		
Boron/Epoxy	350*	
Graphite/Epoxy		
Graphite/Polyimide	600	Boron/Aluminum
	650	Graphite/Aluminum
	700	
	800	Borsic/Titanium
Carbon/Carbon	1000	Beryllium/Titanium
Carbon/Carbon (Uncoated)	1800	Borsic/Nickel
		Wire/Superalloys
Carbon/Carbon (Anti-Oxidant)	2400	Molybdenum/Columbium Tantalum

* Assuming Stable Care

The binary eutectic system offers the only real viable alternative to this problem which is available with today's technology. A binary eutectic occurs when a liquid transforms into a two-phase solid at constant temperature. The reaction is invariant and occurs only at a specific composition and a specific temperature. It is a specific point on the phase diagram. It should be noted that not all binary systems will exhibit this phenomenon and of those that do, not all can be controlled to produce an aligned microstructure.

The directional solidification (DS) of the eutectic is the key processing parameter. It is the directional cooling which permits the alignment of the whisker fibers within the matrix material. Controlling the cooling gradient by slowly withdrawing molten material from the furnace orients the fiber growth direction parallel to the uniaxial heat flow. The fiber and matrix materials freeze into a solid solution forming a discontinuous fiber reinforced composite material in one step. The growth rates, however, are only about a quarter of an inch per hour which means the manufacturing costs are quite high. The primary application of interest is in the turbine of an aircraft engine. The enormous property increases gained and the potential engine performance improvements justify the high manufacturing costs. The eutectic system receiving the most attention is the tantalum carbide fiber in a nickel base super alloy or cobalt based alloy. There are many shapes the fiber can take; however, it has been shown that rods or platelets give the best properties. These alloys are very stable. They compete with conventional alloys at room temperature but are vastly superior at high temperatures. Their properties do not degrade even at levels close to their melting point. Since the whiskers grow naturally within the matrix, there are no bonding problems. Experiments conducted on the interfacial bond strength show it is stronger than the fiber itself. This is probably due to the unique matching of preferred crystallographic planes that occur during processing. Figure 12.10 center shows a DS turbine blade. The DS blade's composite structure is compared to other forming techniques -- a conventional casting left and a single crystal turbine blade right.

A low volume fraction of fiber will give a rod-like reinforcement structure, whereas near equal fractions of matrix and fibers produce a

platelet structure. The rod fibers are superior and more predictable; however, they only supply uniaxial strengthening. The platelets have a two-dimensional strengthening effect. In addition, studies on solute atoms, dislocation mobility, temperature, strength and plastic properties show that intermetallic compounds make better fibers than do ceramics or metals. These materials offer great advancements to aircraft and engine performance.
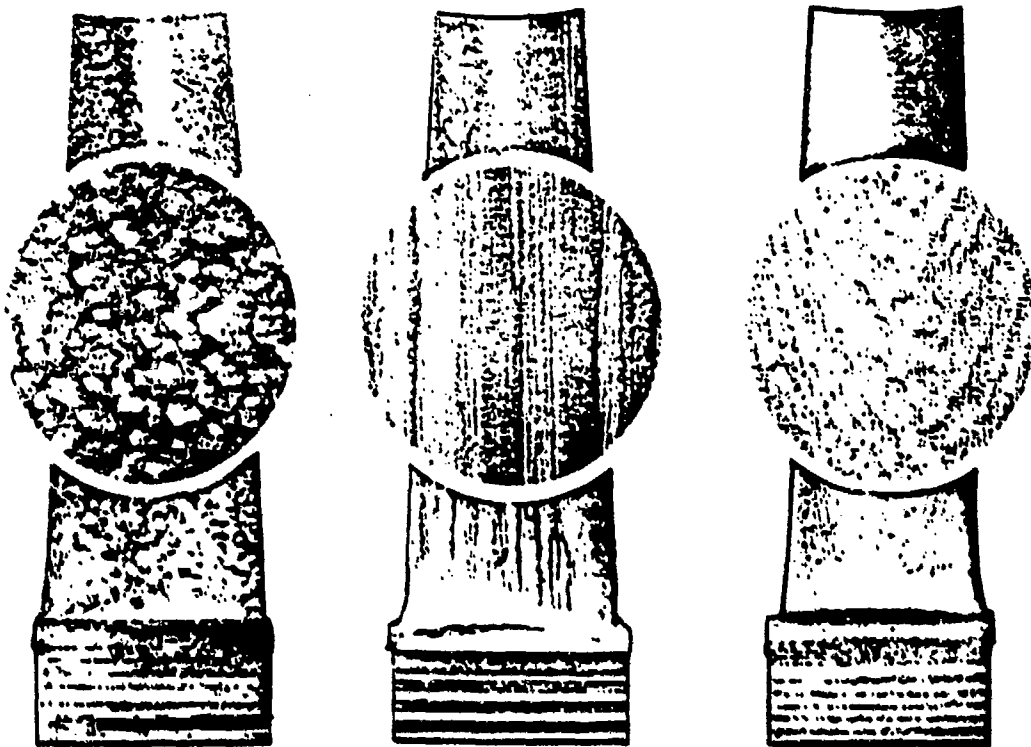
FIGURE 12.10. MICROSTRUCTURE OF CONVENTIONALLY CAST (LEFT),
DIRECTIONALLY SOLIDIFIED (CENTER) AND SINGLE
CRYSTAL (RIGHT) TURBINE BLADES

12.3.5.9 GLOSSARY

__Fiber__ - Reinforcing component of the composite that supplies the strength and stiffness properties.

__Matrix__ - Soft light-weight bonding component of the composite that holds the fibers.

__Lamina__ - A single layer of fibers surrounded by matrix material.

__Laminate__ -A structure build up using lamina at various orientations to yield a structural element.

__Prepreg__ - A partially cured composite laminate that is pliable and can be shaped and then finish cured.

__Interfacial Bond__ - Surface bond between the fiber and the matrix.

__Eutectic Composite__ - A two-phase solid where one phase acts as fiber reinforcement and the second phase is the matrix.

__Whisker__ - A small single crystal fiber that is defect free (length is 100-200 microns).

12.4 FUNDAMENTALS OF STRUCTURES

This section on the fundamentals of structures has been prepared to provide a practical combination of theory and application to the operational problems of aircraft, missiles, and space craft. For this reason only the minimum mathematical relationships are provided.

There are three fundamental objectives that will be addressed:

(1) Acquaint the reader with the basic properties of structural materials and the particular qualities of these materials that make them suitable in particular structures.

(2) Furnish the reader the fundamental reasons for operating strength limitations and good maintenance practices.

(3) Equip the reader with the ability to recognize and diagnose the causes of structural and mechanical failures.

These objectives are first served by describing the principal requirements of any aircraft, missile, or space craft structure. The most important basic requirement is that the primary structure should be of the lowest possible weight. All of the basic items of performance and efficiency of a configuration are seriously affected by the structural weight. This is especially true when the extremes of performance are demanded of a configuration. For example, during preliminary design of a long range jet aircraft, a configuration weight growth factor of twenty may be typical. In other words, if the weight of any single item, e.g., landing gear structure, were to increase one pound, the gross weight of the aircraft must increase twenty pounds to maintain the same performance. Any additional weight would require more fuel, more thrust, larger engines, greater wing area, larger landing gear, heavier structure, more fuel, etc., until the aircraft gross weight had increased twenty times the original weight change.

Long range missiles and space craft usually encounter a design growth factor which is considerably in excess of any typical aircraft. Some typical long range ballistic missiles have demonstrated preliminary design growth factors on the order of 80 to 200. Of course, such configurations

represent an extreme of performance but serve notice of the great significance of structural weight. A limiting situation can exist when the demands for performance exceed the "state-of-the-art". If performance demands are extreme and basic powerplant capabilities are relatively low, the growth factors approach infinite values and impractical gross weights result for the configuration.

While the structure must be of the lowest possible weight, it must also be easily accessible for repair, inspection, and maintenance. There must be adequate protection from the environment to prevent corrosion, ionizing radiation, etc. In many instances, the accommodation for easy access for simple maintenance must be forsaken simply to obtain reduced structural weight.

The primary structure must be the minimum weight structure which can safely sustain the loads typical of operation. The actual nature of the most critical loads will depend to a great extent upon the design mission of the vehicle. During design and development, the mission must be thoroughly analyzed to define the most critical loads that will determine the minimum necessary (size and weight) of the structural elements. From an apparent infinite number of possible situations, the most critical conditions must be defined. Generally, there are three important areas of structural design, any one of which (or combination) could provide the most critical requirements of the structure.

12.4.1 Static Strength Considerations

Static loads refer to those loads which are gradually applied to the structure. The effects of the onset of loading or the repetition of loading deserve separate consideration. Throughout the operation of its mission, a vehicle structure encounters loads of all sorts and magnitudes. Various loads may originate during manufacture, transport, erection, launch, flight gusts and maneuvers, landing, etc. These various conditions may be encountered at various gross weights, e.g., positions, altitudes, pressurization, etc. If particular elements of the structure are separated for study, it is appreciated that these elements are subject to a great spectrum of varying loads.

For the considerations of static strength, it is important that this spectrum be analyzed to select the maximum of all loads encountered during

normal (or intended) operation. This maximum of all normal service loads is given special significance by assigning the nomenclature of "limit" load. The specific requirement of the structure is that it must be able to withstand "limit" load without ill effect. Most certainly the structure must withstand limit load without objectionable permanent deformation.

Specific requirements are different for various structural applications, and, in some cases, a "yield" factor of safety of 1.15 must be incorporated. This requirement would demand that the primary structure be capable of withstanding a load 15% greater than limit without "yielding" or deforming some objectionable amount. If such requirements were specified for a fighter aircraft, the aircraft could be safety maneuvered to limit "G" without causing the aircraft to be permanently deformed. If such requirements were specified for a typical missile, the missile could be fueled and static tested without causing the structure to be permanently deformed. Of course, the number of times this action could be repeated without ill effect would not be part of the static strength consideration.

A separate provision must be made to account for the possibility of a one-time application of some severe load greater than limit. For example, the previously mentioned fighter aircraft may require some flight maneuver load greater than limit in order to avert a disaster of collision. The same idea applies to the missile where malfunction of equipment may cause higher than normal tank pressurization. In either of these examples, some load greater than limit is always a (remote) possibility and, within reasonable limits, should not cause a catastrophic failure of the primary structure. There must be some provision for the possibility of a single critical load greater than limit.

Experience with piloted aircraft has shown that an "ultimate" factor of safety of 1.5 is satisfactory. Thus, a primary structural element should be capable of withstanding one load 50% greater than limit without failure. Of course, loads which generate stresses greater than the "yield" point will cause objectionable permanent deformation of the structure and render it unsuitable for continued operation. The principal concern is that the primary structure withstand the "ultimate" load without failure. To be sure, the ultimate load can be resisted only by a sound structure, i.e., no cracks, corrosion, eccentricity, etc.

12.37

In the previous discussion the yield factor of safety of 1.15 and ultimate factor of safety of 1.5 have been selected for example since these values are representative of piloted aircraft. On the other hand, certain missile configurations may have factors of safety well below that of piloted aircraft, e.g., yield factor of safety of 1.0, ultimate factor of safety of 1.2. In order to complete the picture, some ground support equipment may have an ultimate factor of safety of five or six, and a typical bridge structure may have an ultimate factor of safety of twenty. The factors of safety for airborne vehicles must be as low as is consistent with the safety and integrity of the structure.

When specific limit loads, yield and ultimate factors of safety are defined, there will be no deliberate addition of strength above these specified minimums. The reason is simple: undesirable structural weight would be added. However, the normal variation of material strength properties must be accounted for by designing to minimum guaranteed strength or specific levels of probability. In either case, it is possible that a considerable percentage of the structures will exceed the strength requirements by slight margins. This is an expected result when the structure is required to meet or exceed the minimum specified values.

As a result of these static strength considerations, the primary structure must withstand limit load without objectionable permanent deformation and ultimate load without failure. Because of the yield factor of safety and certain material characteristics, objectionable permanent deformation does not necessarily take place immediately above limit load. This could lead to difficulty in appreciating over-stress conditions since objectionable permanent deformation does not necessarily occur just beyond limit load. However, at ultimate load, failure is imminent.

12.4.2 Rigidity and Stiffness Considerations.

"Strength" could be defined as the resistance to applied loads. On the other hand, "stiffness" could be defined as the resistance to applied deflections. This particular distinction between strength and stiffness is a necessary consideration since the development of adequate strength does not ensure the attainment of adequate stiffness and rigidity. In fact, the

particular requirements of stiffness must be given consideration which is separate (but not completely independent) from the basic strength considerations.

The stiffness characteristics of a structure are very important in defining the response of the structure to dynamic loads. In order to distinguish a dynamic load from the ordinary static load, inspect Figure 12.11 where a weight, W, is suspended by a spring which has a stiffness, K.

GRADUALLY APPLIED LOADING   **SUDDEN LOADING**

$$\delta = \frac{W}{K}$$

POSITION FOR STATIC EQUILIBRIUM
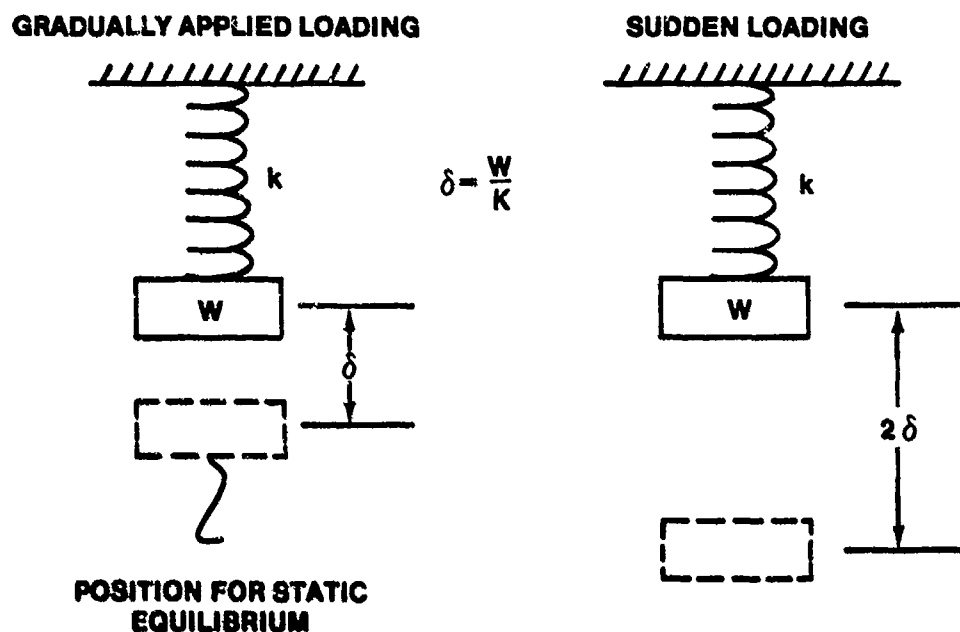
FIGURE 12.11. TIME DEPENDENCE OF LOAD APPLICATION

If the weight were lowered slowly and the force gradually applied to the spring, the spring would deflect slowly until the spring supports the entire weight with an equilibrium deflection of $\delta = W/K$. Alternatively, if the weight is suddenly dropped onto the spring, the input energy of the sudden loading will cause the spring to deflect twice as greatly, 2δ. Then the weight will oscillate back and forth, finally coming to rest at the same equilibrium deflection as for the gradually applied load. During the first plunge when the spring is deflected 2δ, the spring is subject to an instantaneous load which is twice the weight. Under the dynamic loading illustrated, the dynamic load is twice as great at the static load. Of

12.39

course, if the weight had been projected downward onto the spring with an initial velocity, the input energy would be greater and the dynamic amplification of load would be increased considerably.

The previous example serves only to point out the serious nature of dynamic loads. In a more typical (and complex) aircraft or missile structure, many degrees of freedom exist and the response may show the coupling between various possible modes of oscillation. In any case, the energy of load input, the rate of onset, and the characteristic response of the structure must be examined to determine the critical amplification of loads. The stiffness characteristics and the existence of damping, either natural or synthetic, must be tailored - if possible - to minimize critical amplification of loads.

Vibration of structures may provide critical situations and create a source of damaging loads. The fundamental nature of a vibrating system is best illustrated by the simple spring-mass system of Figure 12.12. If a weight, W, is suspended on a spring of stiffness, K, a small disturbance of the system will cause the weight to oscillate at some frequency which is dependent on spring stiffness and weight.

PLATFORM EXCITATION IS
$$a \sin 2\pi f(t)$$

SPRING-MASS NATURAL FREQUENCY IS
$$f_n = \frac{1}{2\pi}\sqrt{\frac{kg}{W}}$$

CYCLIC AMPLITUDE OF OSCILLATING WEIGHT IS $\underline{A}$
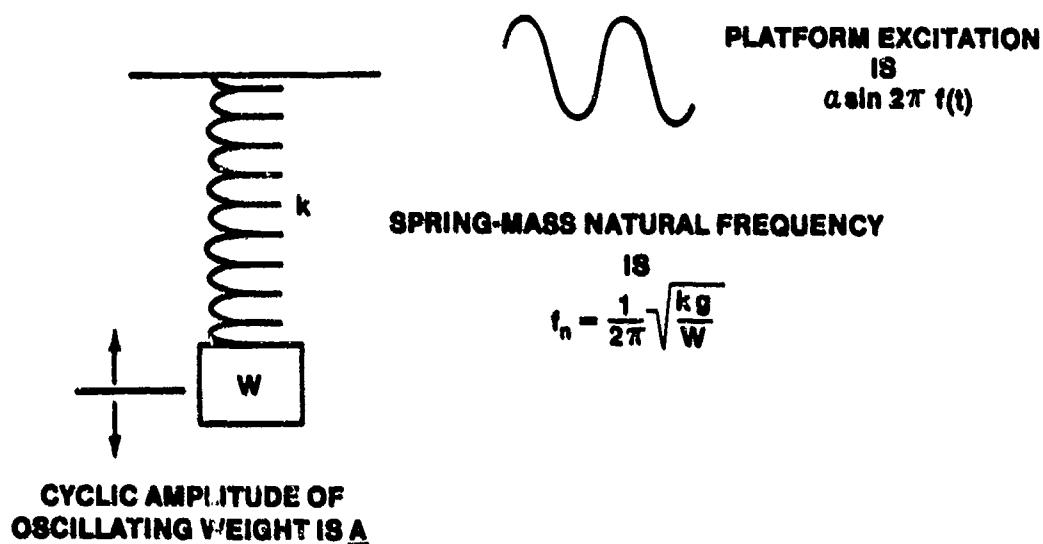
FIGURE 12.12.   FUNDAMENTAL NATURE OF A VIBRATING SYSTEM

This "natural" frequency is related by Equation 12.9.

$$f_n = \frac{1}{2\pi} \sqrt{\frac{Kg}{W}}$$

(12.9)

where f_n = natural frequency, cps

K   = spring stiffness, lbs/w.

g   = acceleration due to gravity, 386

W   = weight, lbs.

In order to consider the possibility of a forced vibration of this system, suppose the platform is moved back and forth with a sinusoidal motion, $a \sin 2\pi f(t)$, where f is the frequency of excitation and a is the amplitude of excitation. The cyclic motion of the platform will induce a cyclic motion of suspended weight. The amplitude of motion of the weight, A, is related to the platform excitation and the natural frequency of the spring-mass system. Equation 12.10 defines this relationship:

$$A = \frac{a}{1 - (f/f_n)^2}$$

(12.10)

where   A = amplitude of weight motion

a = amplitude of platform motion

f = excitation frequency of platform

f_n = natural frequency of spring-mass system

A careful inspection of Equation 12.10 points out one of the undesirable possibilities of a forced vibration of a structure. As the excitation frequency of the platform equals the natural frequency of the system (f/f_n=1), a resonant condition develops and the amplitude of weight motion approaches an infinite value. Of course, this resonant condition could cause sudden failure of the spring.

If the platform is subjected to an excitation frequency which is well below the natural frequency, the weight amplitude is very nearly the same as

the platform amplitude. The weight would move along with the platform with only slightly greater than static deflection of the spring. When the excitation frequency is considerably greater than the natural frequency, the weight is essentially isolated while the platform oscillates. The cyclic deflection of the spring would approach the cyclic displacement of the oscillating platform. If damping, or resistance to motion, is introduced into the system, the resonant condition will simply produce less than infinite motion of the oscillating weight. Above and below the resonant condition, damping will alter the motion depending on the amount of damping present in the system.

While the simple system illustrated does not portray the behavior of complex structures, the fundamental relationships are the same. During design of a structure the stiffness and mass distribution must be tailored to ensure that the ordinary environment of vibration does not allow any approach to resonant conditions and produce damaging loads.

Aeroelastic problems are encountered due to the interaction of aerodynamic forces and elastic deflection of the structures. Since elastic deflections are involved, the inherent stiffness and rigidity of the structure is a principal quality determining the extent of aeroelastic problems.

Static aeroelastic problems involve only the relationship of the aerodynamic forces and elastic deflections without the generation of inertia forces. A typical static aeroelastic problem encountered in aircraft is the phenomenon of "aileron reversal". Deflection of an aileron produces a section pitching moment tending to twist the wing in torsion. Thus, if an aileron is deflected down at high speed, the wing may develop such significant twisting deflection that the aircraft may roll opposite to the direction desired. Of course, sufficient stiffness must be provided in the structure to prevent aileron reversal or any significant loss of control effectiveness within the intended range of flight speeds.

A more disastrous sort of aeroelastic problem is referred to as "divergence." Suppose that a surface is subjected to a slight up gust when at very high speed. If the change in lift occurs forward of the elastic center, the surface will tend to twist leading edge up as well as bend up. The twist represents additional angle of attack, more lift, more bend, more twist, etc., until a sudden failure results. Such a failure is sudden and catastrophic

without warning. It is obvious that divergence could not be tolerated and sufficient stiffness must be present to prevent divergence within the anticipated flight range. In addition, below the divergence speed there must be sufficient stiffness to ensure no serious change in load distribution due to this sort of interaction between aerodynamic forces and elastic deflections.

All of the static aeroelastic problems are specific to the stiffness qualities of the structure and the dynamic pressure of flight. Thus, any specific operating limitation imposed will be relative to a certain dynamic pressure hence, indicated, calibrated, or equivalent airspeed.

The dynamic or oscillatory aeroelastic problems introduce an additional variable: inertia forces. Thus, dynamic aeroelastic problems involve some combination of aerodynamic forces, elastic deflections, and inertia forces. "Flutter" is one such problem. If a surface with particular mass and stiffness distribution were exposed to an airstream, the oscillatory aerodynamic forces may combine with the various natural oscillatory modes of the surface to produce an unstable motion. Flutter is essentially an aerodynamically excited oscillation in which airstream energy is extracted to amplify the energy of the structural oscillation.

Flutter is not necessarily limited to control surfaces or wing surfaces. Structural panels may encounter flutter conditions which are just as critical and damaging.

During design, the review and analysis of possible flutter behavior constitutes one of the most highly complex studies. The mass and stiffness distribution must be arranged to prevent flutter from occurring during normal operation. There is the implication that any alteration of stiffness or mass distribution due to service operation could cause a possible dangerous reduction of the speed at which flutter would occur.

This fact is important with respect to all of the conditions requiring adequate stiffness of the primary structure. Any alteration of stiffness may produce a dangerous change in dynamic response, vibration, or aeroelastic behavior.

12.4.3 Service Life Considerations

When considering the service life of a structure, the entire gamut of loads must be taken into account. To achieve satisfactory performance during

service operation, a structure must withstand the cumulative effect of all varieties of load that are typical of normal use. Normal periods of overhaul, inspection, and maintenance must be anticipated.

Creep is the continued plastic straining of a part subjected to stress. Of course, creep is of a particularly serious nature when the part is subject to stress at high temperature since elevated temperatures reduce the resistance to plastic flow. Gas turbine components, reentry configurations, rocket combustion chambers and nozzles represent some of the typical structures in which creep is important.

If a part is exposed to stress at high temperature, the part will continue to strain at a constant stress. If the exposure time is increased to some critical point, the creep rate will suddenly increase and failure will occur. Such failures due to creep can take place at well below the static ultimate strength of the material. Of course, the creep stress must be supplied for sufficient time to generate the condition of failure. It is typical of all metals that any increase in applied stress or temperature will increase the creep rate and reduce the time required to cause failure.

The creep damage is accumulated throughout the life of a structure, with the times at high stress and temperature causing the most rapid rate of accumulation. In order for a structure to perform satisfactorily in service, the spectrum of varying loads and temperatures must not cause a critical accumulation of creep damage. In other words, service use should not cause either creep deformation sufficient to prevent operation or creep failure by fracture or buckling. In some applications of turbines, machinery and mechanism, the limit of creep deformation may be the appropriate design consideration. The primary airframe structure may not be adversely affected by such creep deformations and the final failure by fracture or buckling may be the critical consideration.

In special high temperature structures the anticipated service life has distinct limitations. For example, gas turbine powerplants may have turbine structural elements which must be replaced at regular intervals while the shaft, case, and compressor withstand only ordinary inspection. If certain turbine elements were required to demonstrate the same time life as less highly stressed or heated parts, such life may not be at all possible. As a result the design service life of such high temperature, high stress parts may be set by design limitations rather than arbitrary desirable values.

Fatigue is the result of repeated or cyclic loads. If a metal part is subjected to cyclic stress of sufficient magnitude, a crack will eventually form and propagate into the cross-section. When the remaining cross-section cannot withstand the existing loads, a final rupture occurs as if by static load. The most important aspect of fatigue is that the failure is progressive by the accumulation of fatigue damage. When a critical level of damage is accumulated, a crack forms and propagates until final failure takes place. When a part is exposed to the variety of repeated loads during service operation, the cumulative fatigue must be limited so that failure does not occur within the anticipated service life.

In order to prevent fatigue failures, the structural design must bring into consideration many important factors. First, a reasonable estimate of the service life must be made and the typical spectrum of service loads must be defined. Then the fatigue characteristics of the materials must be determined by laboratory test of specimens. The effect of stress concentrations, corrosion environment, residual stresses, and manufacturing quality control must be analyzed. With these factors known, the concept of cumulative damage can be applied to determine the dimensions of the part necessary to prevent fatigue failure during the anticipated service life.

The normal scatter and variation in material properties encountered in fatigue tests will not allow prediction of the specific life of individual parts. A more appropriate consideration would be to account for the variability of material characteristics and load spectrum by the definition of failure probability. In other words, as parts in service approach the design service life, the probability of fatigue failure increases. If parts are exposed to service well beyond the design service life, failure probability will be quite high and the incidence of failures and malfunction of equipment will increase.

The use of periodic inspection and maintenance is very unnecessary to ensure failure free operation. Regular inspection must guarantee that parts do not incur excessive deformation or cracks during exposure to fatigue and creep conditions. There is always the possibility of short periods of high stress or temperature which could cause acceleration of creep or fatigue damage and precipitate a premature failure. This is a very important obligation of the maintenance facility.

The various considerations of static strength, stiffness, and service life will all contribute specific demands on a structure. Just which of these considerations predominate will depend upon the exact nature of the structure. An aircraft may show that any one of the static strength, service life, or stiffness requirements may predominate. In the design of most powerplant systems, the service life considerations of creep and fatigue usually predominate. Very short life missile structures may show that the static strength considerations prevail during design. However, if the missile must withstand considerable transportation, handling, and continuous functional checks, service life considerations may be important.

12.4.4 Load and Stress Distribution

Fundamentally, there are two types of loads which can be applied to an element of structure. There are "axial loads" which are applied along the axis of the part (Figure 12.13) and there are "transverse" loads - often referred to as "shear loads" - which are applied normal or perpendicular to the axis of the part (Figure 12.14). Any complicated load condition to which a structure is subjected can be resolved to the various axial or transverse loads acting on a particular part. Since the inherent strength properties of a structural material are based upon the element strengths of its crystals and grains, a more appropriate definition of load condition on a part is the amount of load per unit of cross section area. Thus load per unit area is referred to as "stress" and all basic properties of structural materials are based upon stress or load per unit of cross section area. Of course, as there are two basic types of loads -- axial and transverse -- there are two basic types of stress which result from these loads -- axial or "normal" stresses of tension and compression and the transverse or "shear" stresses.

TENSION   COMPRESSION
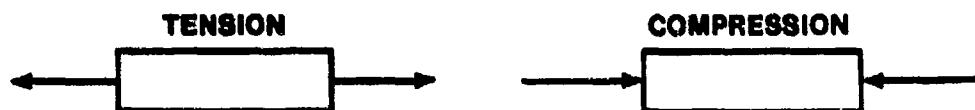
FIGURE 12.13. AXIAL LOADS

Axial tension applied to a material will produce certain types of effects and certain types of failures, while axial compression in the same type of material will produce completely different effects in different types of failures.

**PURE
SHEAR**
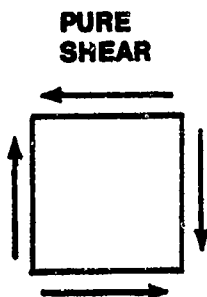
FIGURE 12.14. TRANSVERSE LOADING

A shear stress applied to a particular material results in a somewhat unusual pattern. If a shear is applied to an element of material in a vertical direction, that element will experience balancing shears in a horizontal direction of an equal magnitude. This must be so in order that the element be in equilibrium in rotation.

In any case in which the basic loads — either axial or transverse — are resolved on a cross-section of a part, the stresses are then computed for each element of the part as the amount of load per unit of area.

For normal stress,

$\sigma = P/A$

σ = normal stress, psi

P = loads in lbs

A = area, in^2

For shear stress,

$\sigma_s = P/A$

σ_s = shear stress   (12.11)

P = loads in lbs

A = area, in^2

As an example of the typical stress distribution in a loaded structure, the following example problem is provided. This example will best furnish an

interpretation of the idea of stress and the function of certain structural components.

Figure 12.15 illustrates a typical beam structure. In this case there is a simplified spar or beam subjected to a concentrated load at the right end. The left end is mounted or fixed to a rigid wall surface. For simplicity, it is assumed that the spar (or beam) is the entire effective structure and that all loads will be resisted by this part. The problem will be to investigate the stresses at Points A and B in this spar structure which result from the application of the shear load at Point C. The beam has a constant cross-section throughout the span as shown in Figure 12.15. The spar flanges of this type structure furnish the primary bending resistance, while the spar web connecting the spar flanges provides the primary resistance to shear loads. The rivets attach the spar web to the spar flange, and there are vertical stiffeners attached to the web to maintain the form, shape, and stability of the structure. The distribution of stress at Point A in the beam is best visualized by taking a section through the beam at Point A and supplying the internal loads at the Section A which are necessary to resist the applied external shear load at C, thus maintaining equilibrium of the structure. This is shown in Figure 12.16.

WEB TO FLANGE RIVETS ARE SPACED ¾ IN.

APPLIED
FORCE
OF 10,000 LB

UPPER SPAR FLANGE
X-SECTION AREA = 4.0 IN.²

10 IN. BETWEEN CENTROIDS
OF FLANGE AREAS

SPAR WEB
IS 0.1 IN. THICK

WEB TO FLANGE RIVETS
ARE ¾ IN. DIAMETER

LOWER SPAR FLANGE
X-SECTION AREA = 2.0 IN.²
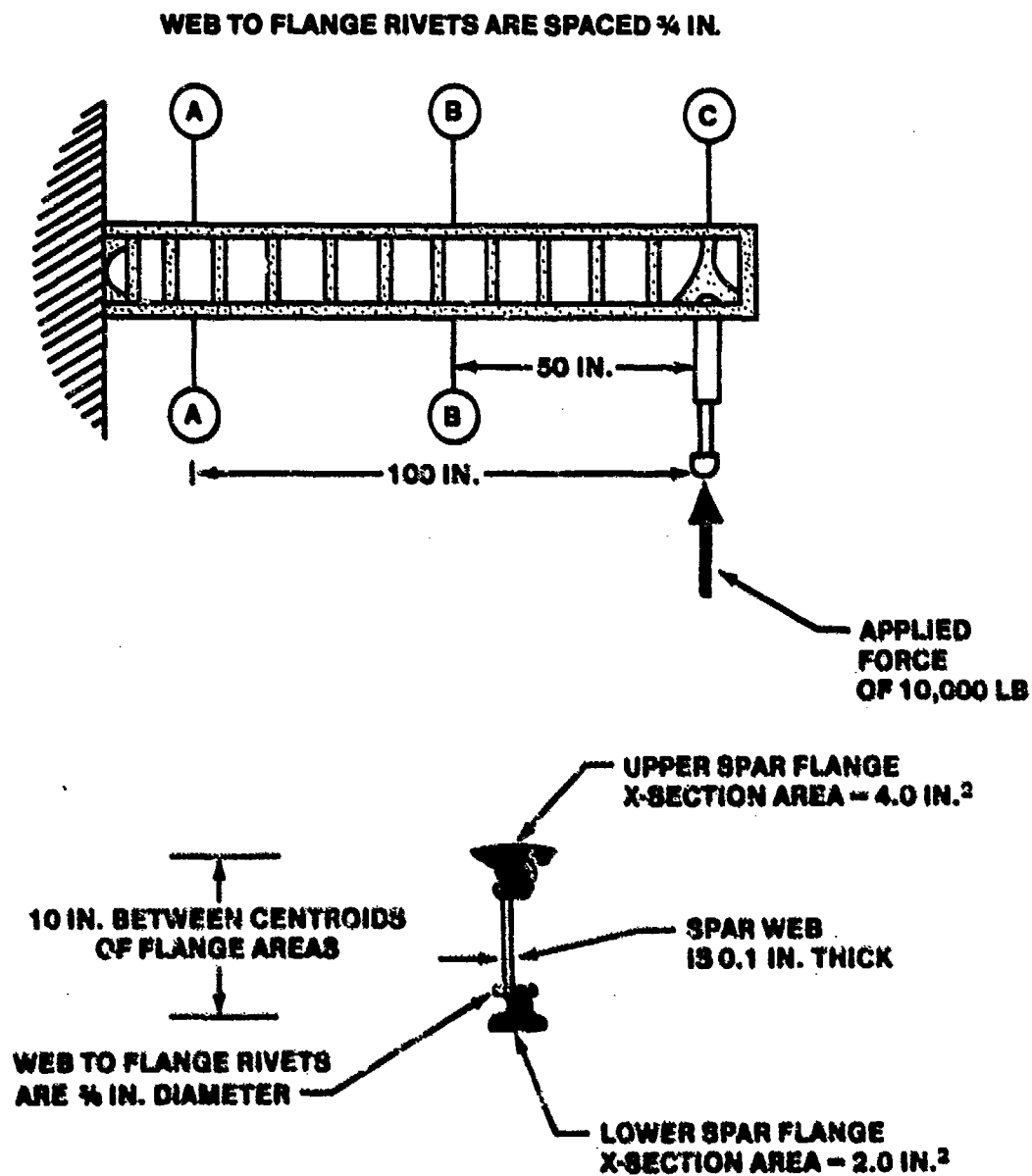
FIGURE 12.15.   TYPICAL BEAM STRUCTURE

12.49

First, to maintain an equilibrium in a vertical direction, there must be a resisting shear load on Section A of 10,000 lbs in a vertical direction down, which resists the applied shear load up at Point C. Due to the lever arm of force at Point C, there is a bending moment produced in the structure at Point A. The magnitude of this bending moment is the product of the force and the lever arm, i.e., 10,000 lbs times 100 in = 1,000,000 in lbs of moment at Section A. As the spar flanges provide the primary resistance to bending, there will be a compression axial load developed in the upper spar flange and a tension axial load produced in a lower spar flange. These axial loads in the spar flanges for this untapered beam must be equal to maintain equilibrium of a structure in a horizontal direction. These axial forces in the spar flanges will be referred to as "P" pounds of load. These two forces of P, acting as a couple at a distance of 10 in apart (the distance between the centers of gravity of areas of the upper and lower spar flanges) must provide internal balance in the structure to the applied external bending moment of 1,000,000 in-lbs In other words, P x 10 in must equal 1,000,000 in-lbs The P pounds of load in a flange is then computed to be 100,000 lbs.

$$P_{lb} \times 10^{"} = 1,000,000 \text{ in-lbs}$$
$$P = 100,000 \text{ lbs}$$

To determine the stress in the upper flange, the compression load is distributed over the compression area

$$\sigma_c = P/A = 100,000 \text{ lbs}/4 \text{ sq in} = 25,000 \text{ lbs/in}^2$$

The tension stress in a lower flange is the load divided by the area

$$\sigma_t = P/A = 100,000 \text{ lb}/2 \text{ sq in} = 50,000 \text{ lbs/in}^2$$

Since the spar web furnished primary resistance to shear loads, there is a shear load of 10,000 lbs acting on the effective area of the web. The effective area of this web is the depth times the thickness. In this case, depth is taken as 10 inches and the thickness is 1/10 of an inch which produce
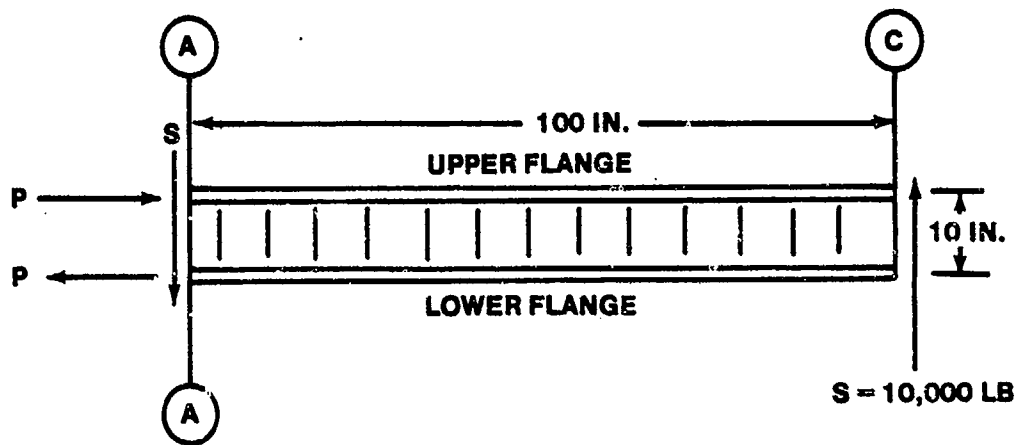
FIGURE 12.16. STATIC STRUCTURAL EQUILIBRIUM

one square inch of cross sectional area. This shear stress in the web is then load divided by area

$$\sigma_s = P/A = 10,000 \text{ lb/1 sq. in.} = 10,000 \text{ lbs/in}^2$$

To investigate the stress distribution at Section B, the same fundamental procedure is employed (Figure 12.17). That is, the section at Point B is furnished with the loads on the cross-section necessary to place the structure in equilibrium. The bending moment to be resisted by the spar flanges is the 10,000 lbs of force acting at the 50 inch lever arm. This produces a bending moment of 500,000 in lbs and results in axial loads in the spar flanges of 50,000 lbs each.
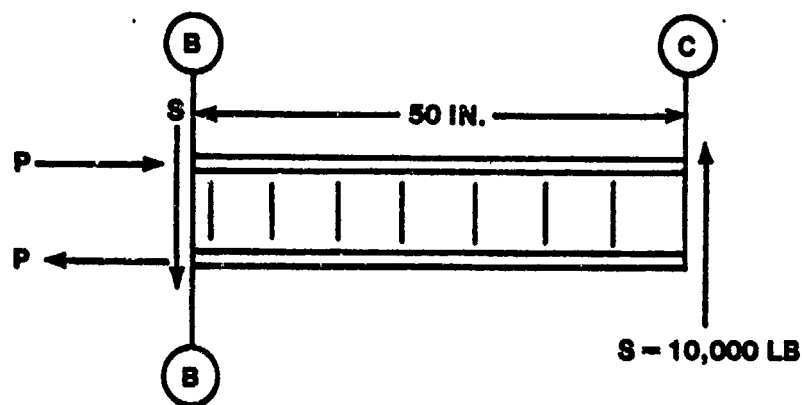
FIGURE 12.17. SHEAR STRESS DISTRIBUTION

The compression stress in the upper flange is then

$$\sigma_c = P/A = 50,000 \text{ lb/ sq in } = 12,500 \text{ lbs/in}^2$$

The tension stress in the lower flange is

$$\sigma_t = P/A = 50,000 \text{ lb/2 sq in } = 25,000 \text{ lbs/in}^2$$

Since the same amount of shear load must be supplied on Section B to provide equilibrium in a vertical direction and resistance to the applied 10,000 lbs shear load, the shear stress in the spar web remains the same 10,000 psi throughout the span of the beam and it does so as long as there is no change in the shear load across the beam.

To determine the stress in the rivets attaching the spar web to the flanges, the function of the rivets must be made clear. The point of load application at Section C on the beam has a vertical load of 10,000 lbs applied. This concentrated load of 10,000 lbs must be appropriately distributed to the web by a fitting. The desired result, as in Figure 12.18, is to distribute the concentrated shear load of 10,000 lbs to the edge of the spar web such that for the 10 inch effective depth of the web there is 1,000 lbs of load for each 1 inch along the edge.

PURPOSE OF THE FITTING IS TO
DISTRIBUTE THE CONCENTRATED LOAD
OF 10,000 LB TO A UNIFORM SHEAR
IN THE WEB OR 1000 LBS/IN.
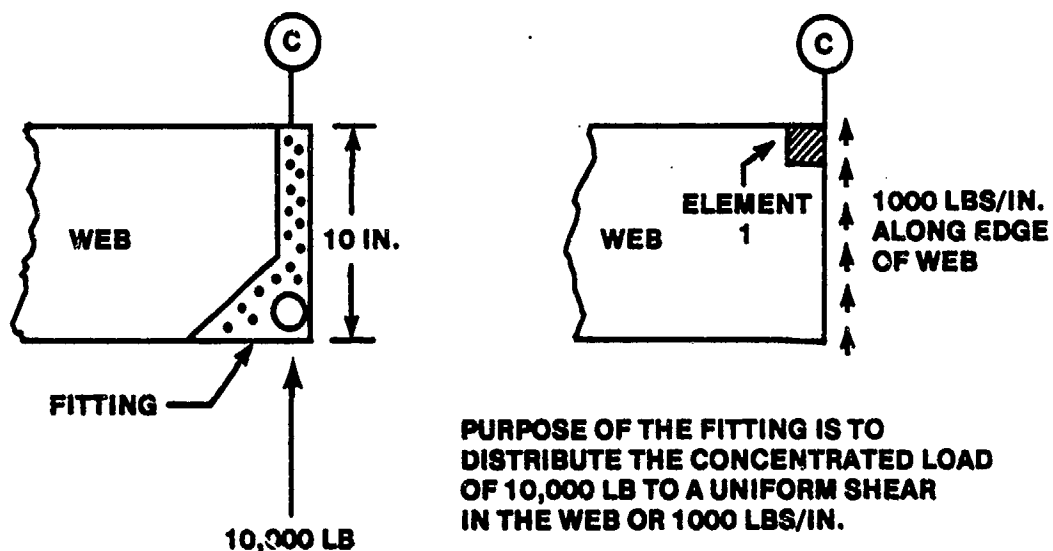
FIGURE 12.18.   DISTRIBUTION OF CONCENTRATED SHEAR LOAD

The Element 1 in the upper right hand edge of the web at Section C has applied on its edge 1,000 lbs shear load. Figure 12.19 illustrates the manner in which this 1,000 lbs of load applied to this 1 inch Element 1 is resisted.

At the left hand side, there is a shear load down of 1,000 lbs balancing the applied 1,000 lbs. This shear load on the left hand edge is furnished by the adjacent element of the web to the left of Element 1. Since an element of structure with an applied shear load must also have balancing shears at 90°, there will exist (or must exist) on Element 1 shear loads on the upper and lower edges as shown. The shear load on the upper edge of Element A is supplied by the next piece of structure in contact with the edge of the web. This load must come from the spar flange and is transmitted by the "web-to-flange" rivets. The primary function of the "web-to-flange" rivets is then to provide a continuity of shear and to balance the applied vertical shear load in a horizontal direction. The shear load of the lower side of Element 1 is supplied by the next element immediately underneath Element 1 in the web. If the spacing of rivets attaching the web to the flange is three-quarters of an inch, the load for each rivet in shear will be 3/4 of 1,000 lbs (rivets spaced 3/4 inch) or 750 lbs per rivet. With the diameter of the rivet given as 3/8 of an inch, the rivet stress in shear could then be computed as the

12.53

load divided by area:

$$\text{Rivet stress} = \frac{\text{load}}{\text{area}}$$

$$\sigma_s = \frac{750 \text{ lbs}}{(\pi/4)(3/8)^2 \text{in.}^2}$$

$$\sigma_s = \frac{750 \text{ lbs}}{.1104 \text{ in}^2}$$

$$\sigma_s = 6800 \text{ psi}$$
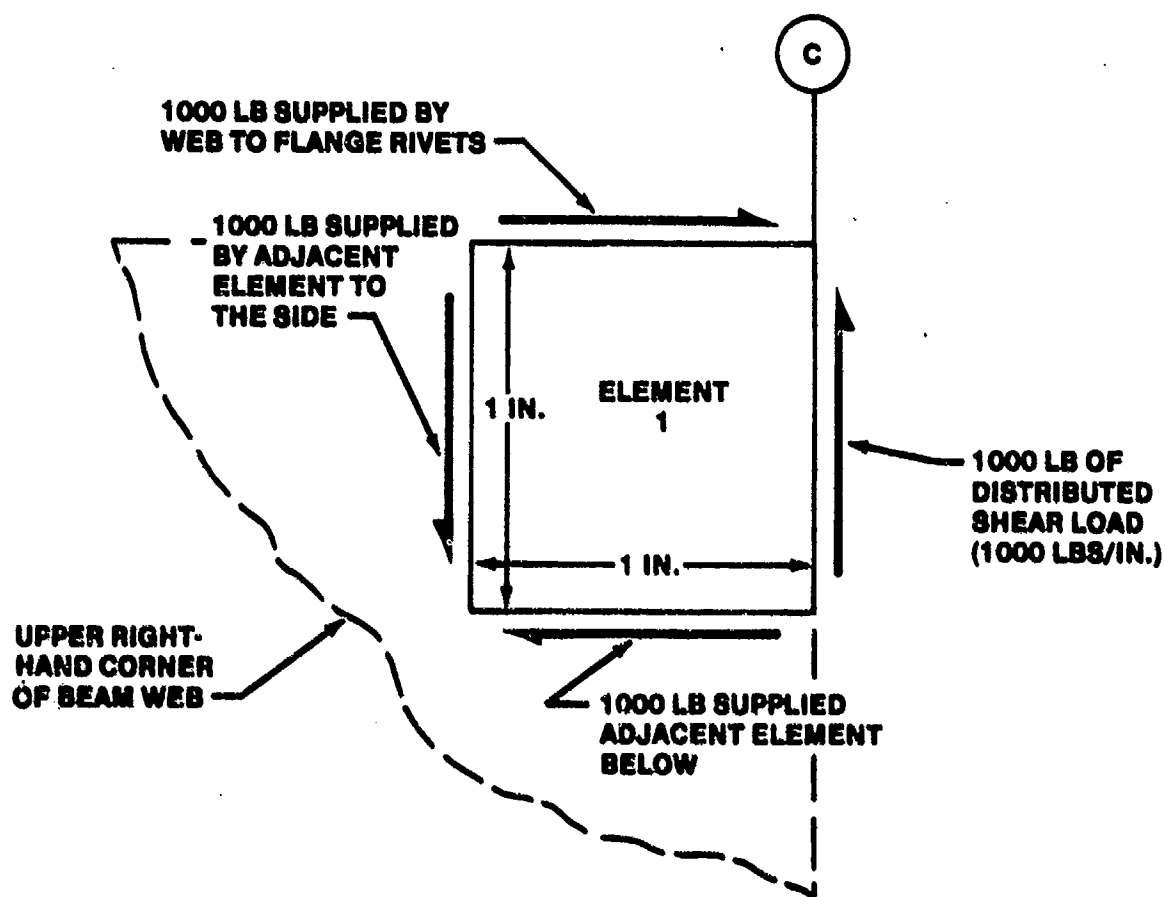
FIGURE 12.19.   SHEAR ELEMENT
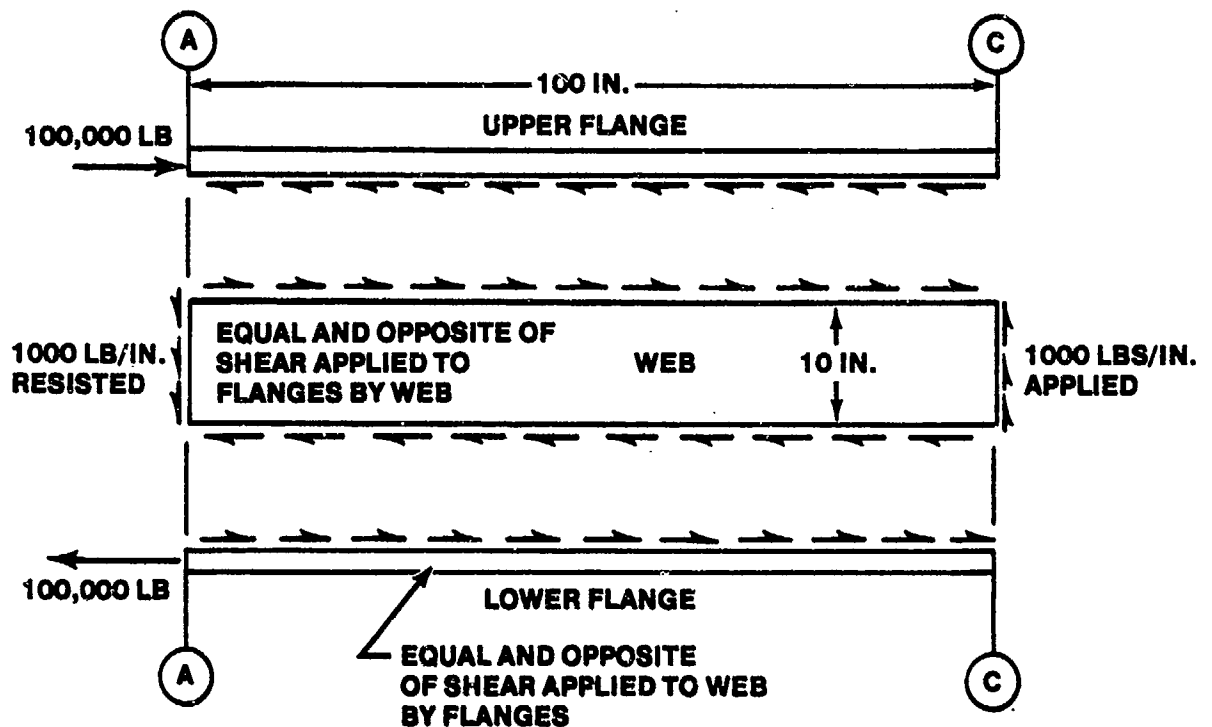
FIGURE 12.20. SPAR FLANGE AND WEB LOADS

Figure 12.20 gives an illustration of the upper and lower spar flange removed from the structure and the loads applied to spar flanges and the web.

The flange loads of 100,000 lbs at Section A are the result of the accumulated axial force from the distributed shear loads of 1,000 lbs per inch for the entire length of 100 inches. This distributed load at Section A (100 inch length) and 50,000 lbs at Section B (50 inch length).

The vertical stiffeners attached to the web have no particular stress — either compression tension or shear - until the web of the spar begins to buckle. (Figure 12.21)

The primary function of these vertical stiffeners is to maintain the form and stability and to provide support for the web panel, thereby preventing or delaying the shear buckling of the web. When buckling occurs in the web, the
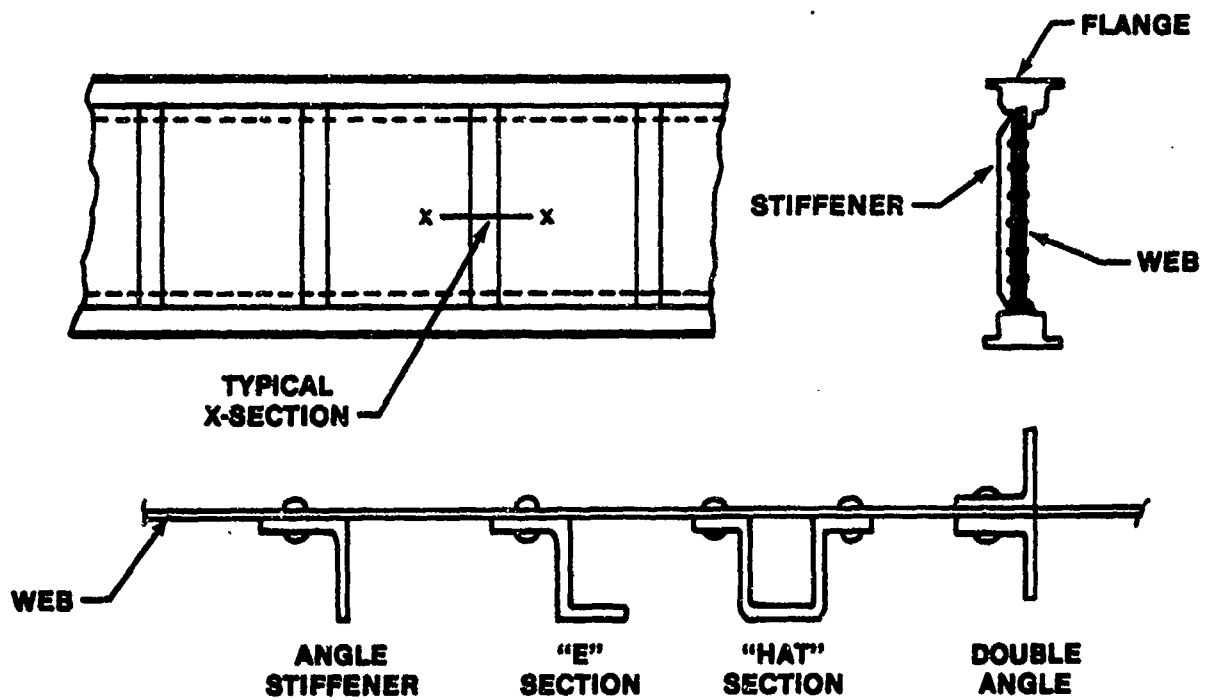
FIGURE 12.21.   VERTICAL STIFFENERS

vertical stiffeners must withstand compression loads to prevent collapse of the structure.

The function and importance of the spar web can be best emphasized by two examples shown in Figure 12.22. If there were no web between the pinned flanges and a shear load applied, no resisting loads would be developed in the flanges. The structure would collapse to the shape shown with no resistance to the applied load.

**STRUCTURE OFFERS
NO RESISTANCE TO AN
APPLIED LOAD**

**NO
WEB**

**FLANGES
PINNED
TO WALL**
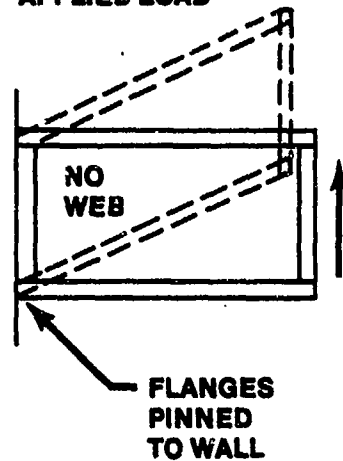
**BENDING OF FLANGES
PRODUCES LITTLE
RESISTANCE TO AN
APPLIED LOAD**

**NO
WEB**

**FLANGES
FIXED
IN WALL**

**WITH
WEB**
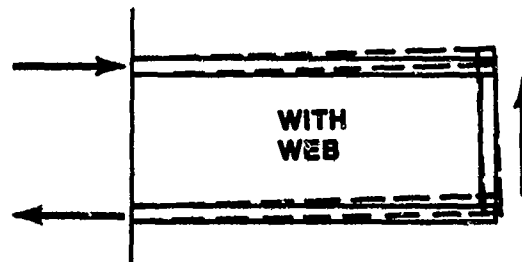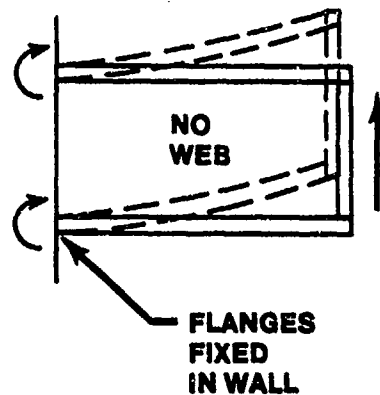
**THE WEB RESISTS SHEAR
AND ALLOWS BENDING TO BE
RESISTED BY AXIAL LOADS
IN THE FLANGES**

FIGURE 12.22.   SPAR WEB FUNCTION

If there were no web between the fixed flanges, a shear load applied would produce "secondary" bending of the flanges. Since the bending resistance of the flanges is quite small, prohibitive stresses and deflections would result. Obviously, the more efficient structure is the web-flange combination which resists shear in the web and bending by axial loads in the flanges.

Actually, there is very rarely such a thing as a "lightening hole" in a shear web. More usually these holes are for access in maintenance and production and are a structural penalty for anything but minimum gage thickness structures (light planes, gliders, airships, etc.).

The previous example problem of the stress distribution in a simplified structure has considered that there were no particular complications to

produce anything other than pure axial and shear stresses. In a more detailed analysis, consideration would be made of the contribution of the web to bending resistance, the complication and magnification of stress due to rivet holes, etc.

There are, of course, examples in which the distribution of stress in a structural element is complicated by the particular manner of loading. There follow certain examples of the particular stress as distributed in typical structures if there is bending, torsion, etc., and the resulting stresses remain in the elastic range of the material characteristics. By "elastic range", it is implied that stresses may be applied, then released, and no permanent deformation of the structure would be incurred.

12.4.5 Pure Bending

Figure 12.23 illustrates the use of a solid, rectangular bar with pure bending moments applied. The stresses at Section A will be distributed as shown with the upper portion of Section A subjected to a compression stress which will be a maximum at the outer surface and the lower surface of Section A subjected to a tensile stress which will be a maximum at the outer surface.

The point at which the stress is zero - neither tension nor compression - is referred to as the "neutral axis". For a symmetrical, rectangular section this point would be midway between the upper and lower surfaces. The neutral axis for a homogenous material subjected to elastic bending is always located at the center of gravity (or "centroid") of cross sectional area.

COMPRESSION

(A)

SECTION A

NEUTRAL
AXIS

TENSION

(A)

UPPER
SURFACE

COMPRESSION

NEUTRAL
AXIS

STRESS DISTRIBUTION
ON SECTION A

LOWER
SURFACE

TENSION
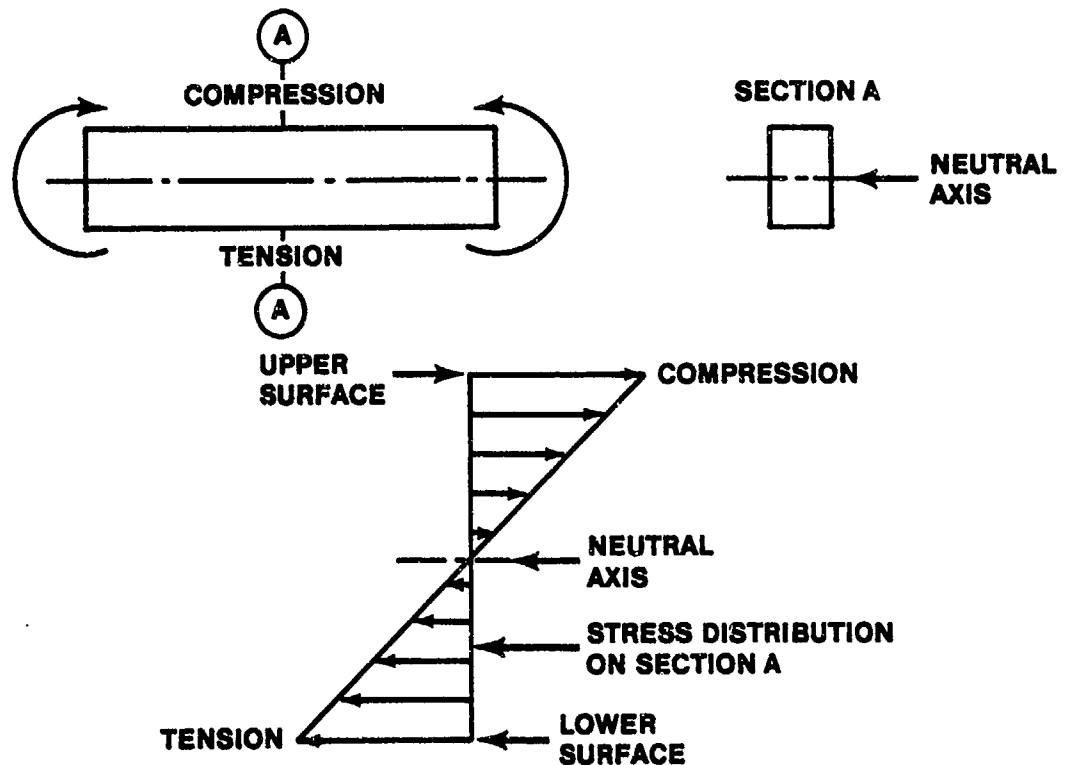
FIGURE 12.23.   PURE BENDING OF A SOLID, RECTANGULAR BAR

In Figure 12.24 there is an unsymmetrical cross-section subjected to pure bending. For the cross-section shown, the neutral axis will be closer to the upper surface of the part than the lower surface. The stress distribution illustrated in Figure 12.24 will continue to be a linear variation of stress between the two maximum stresses at the upper and lower surfaces. However, as the neutral axis is closer to the upper surface, the magnitude of compression stress will be smaller than the tensile stress on the lower surface. This must be so, since the compression load produced by the smaller compression stress distributed over the larger area above the neutral axis will be equal to the tension load produced by the higher tensile stress acting over the smaller tensile area below the neutral axis. Thus, equal and opposite compression and tensile loads exist which furnish equilibrium to the cross-section in the horizontal direction.

12.59
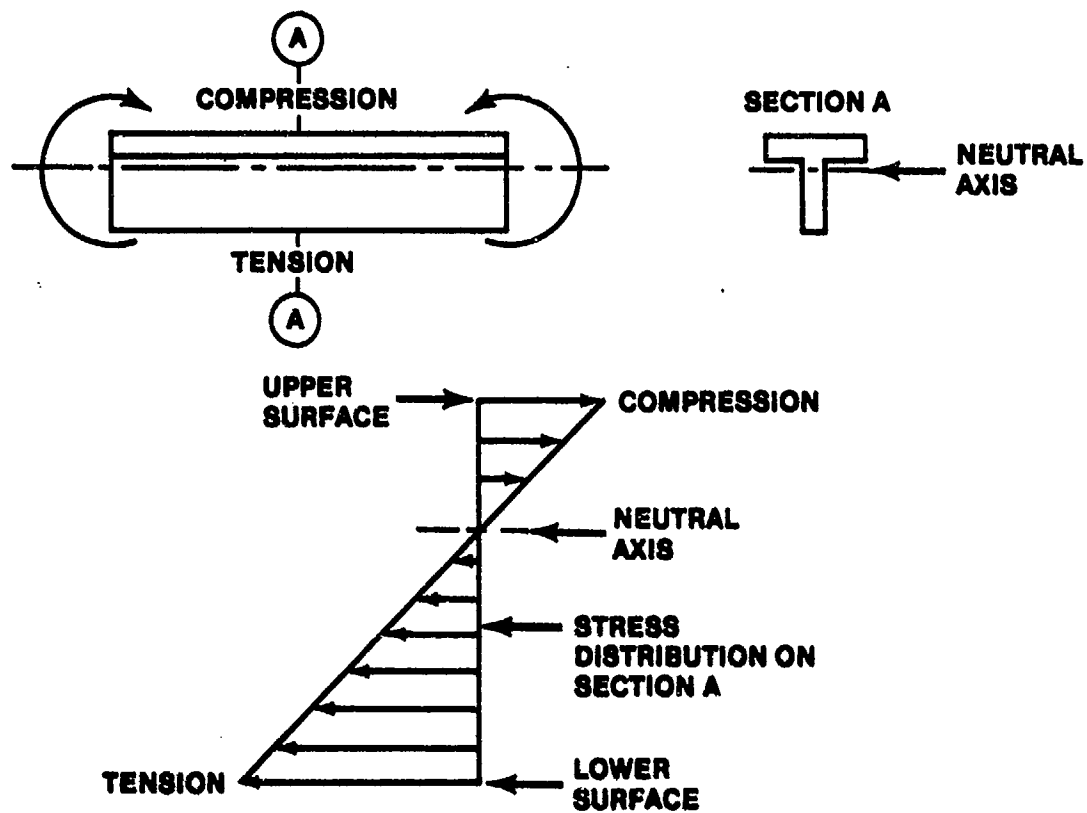
FIGURE 12.24. PURE BENDING OF AN UNSYMMETRICAL CROSS-SECTION

For beams or other structures subjected to bending moments,

$$\sigma_{b_{max}} = \frac{Mc}{I} \qquad (12.12)$$

12.60

Where $\sigma_{b_{max}}$ = maximum bending stress, psi

M = bending moment on cross-section, lb in

c = distance from neutral axis to outermost fiber, in

I = moment of inertia of cross-section, in^4

If the stress on some other fiber is desired, the equation is simply σ_b = My/I, where y is the distance from the neutral axis to the fiber under consideration.

The term "moment of inertia" appears in the previous equations. As has been explained, the bending stress in a fiber depends on its distance from the neutral axis. If the material can tolerate a given amount of stress, the largest moment can be resisted when the area resisting it is as far as possible from the neutral axis. The moment of inertia is a quantity which takes the shape of the cross-section into account in determining the amount of bending moment which can be resisted by a given cross-section without exceeding a specified stress. For several cross-section shapes the following apply:

$$I = \frac{1}{12} b h^3 \qquad \text{(rectangular)}$$

$$I = \frac{1}{36} b h^3 \qquad \text{(triangular)}$$

$$I = \frac{\pi}{64} D_0^4 \qquad \text{(circular)}$$

$$I = \frac{\pi}{64} D_0^4 - D_i^4 \qquad \text{(doughnut)}$$

Where I = moment of inertia about the neutral axis, in^4

b = rectangle or triangle width, in

h = rectangle or triangle height, in

D_0 = outside diameter, in

D_i = inside diameter, in

12.4.6 Pure Torsion

Figure 12.25 illustrates the condition of pure torsion applied to a solid, circular shaft. With torsion applied to the part, the stress produced on Section A is primarily that of shear - a shear stress which is a maximum at the outer surface and varies linearly to zero at the axis of the part.

For circular shafts subjected to torsion moments,

$$\sigma_{s_{max}} = \frac{Tc}{J} \tag{12.13}$$

Where $\sigma_{s_{max}}$ = maximum shearing stress, psi

  T   = torsional moment or twisting moment, lb in

  c   = radius from axis to outermost surface, in

  J   = "polar moment of inertia" of cross-section, in^4

Use $f = Mr/J$ if the stress at a distance r from the axis is desired.

The polar moment of inertia, J, is used for determining strength of sections subjected to torsion.

Only the circular sections have simple equations for this sort of stress distribution. These are as follows:

$$J = \frac{\pi}{32} D_0^{\,4} \qquad \text{(circular)}$$

$$J = \frac{\pi}{32} \; D_0^{\,4} - D_i^{\,4} \qquad \text{(doughnut)}$$

Where J = polar moment of inertia, in^4

  D_0, D_i = outside and inside diameters, in

For sections other than circular, reference may be made to any of the more standard texts on strength of materials.
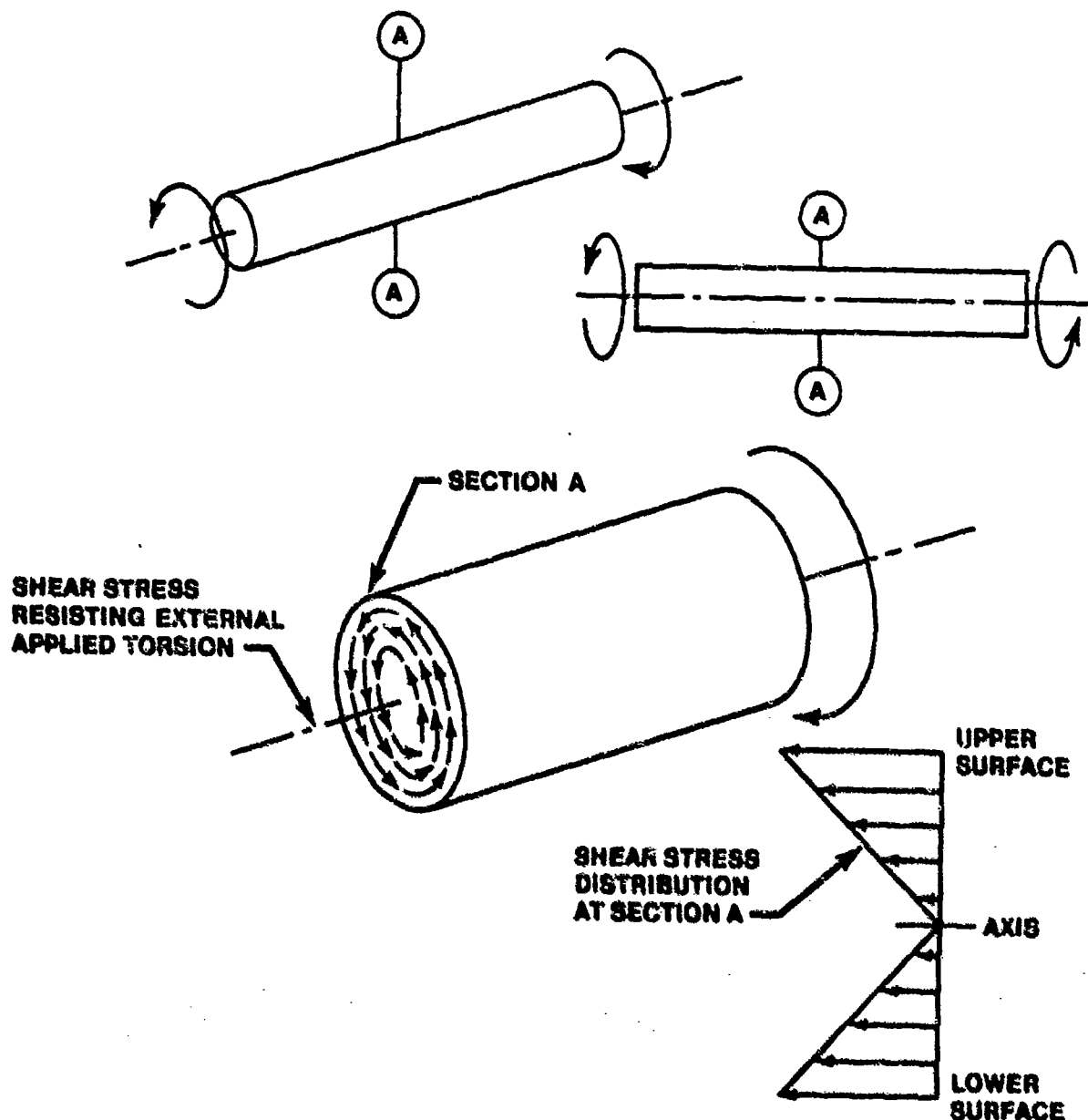
FIGURE 12.25. PURE TORSION OF A SOLID, CIRCULAR SHAFT

Figure 12.26 illustrates the conditions in which a continuous, hollow cross section is subjected to torsion. In this instance, the shear stress is a constant value around the periphery of the cross section. Since the shear load distributed around the periphery must provide an internal resisting moment equal to the external applied moment, the shear stress for this continuous shell structure may be computed by use of the following relationship:

$$\sigma_s = \frac{T}{2At} \qquad\qquad (12.14)$$

where σ_s = shear stress, psi

T = applied torque, in-lbs

A = enclosed area of cross-section, sq in

t = shell thickness, in

THICKNESS, t

CONTINUOUS HOLLOW TUBE

ENCLOSED AREA, A

APPLIED TORQUE, T

SLOTTED HOLLOW TUBE

THICKNESS, t

UNROLLED WIDTH, b

APPLIED TORQUE, T
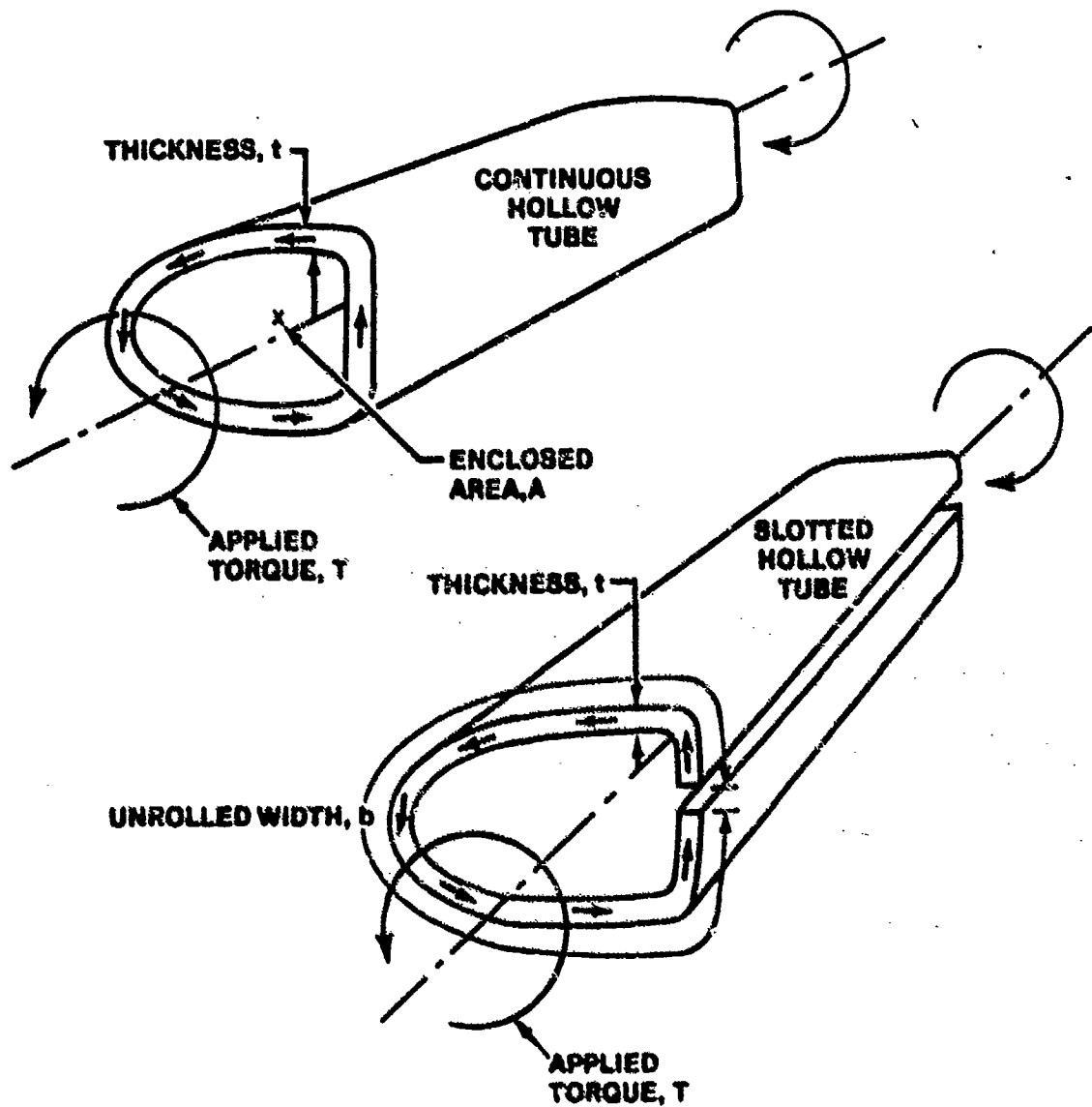
FIGURE 12.26.   PURE TORSION OF A HOLLOW TUBE

If this section were slotted in a longitudinal direction, a very large amount of the torsional rigidity would be lost. There would be no continuous shear stress distributed around the periphery of the shell and high local shear stresses with great deflections would be encountered. The maximum shear stress in this case could be calculated by application of the following equation:

$$\sigma_{s_{max}} = \frac{3T}{bt^2} \tag{12.15}$$

where $\sigma_{s_{max}}$ = maximum shear stress, psi

T = applied torque, in-lbs

b = unrolled width, in

c = shell thickness, in

Any shell structure subjected to torsional loading which has a cutout or slot will have a tendency to develop much higher stresses and may be excessively flexible.

12.4.7 Bolted or Riveted Joints

Figure 12.27 illustrates a typical type of bolted or riveted joint which is encountered in more conventional structures. In such a joint, the load applied to element A is transferred by the bolt and distributed to elements B and C. This transfer of load by the bolt produces a shear stress on the bolt cross-section. The bolt shear stress is

$$\sigma_s = \frac{load}{area}$$

$$\sigma_s = \frac{P/2}{\pi/4\ d^2} = \frac{2P}{\pi d^2} \tag{12.16}$$

The tensile load developed in the plate creates a critical tensile stress along section x. The average tension stress at section x is

$$\sigma = \frac{load}{area} \tag{12.17}$$

$$\sigma = \frac{P}{(w-d)t}$$

12.65
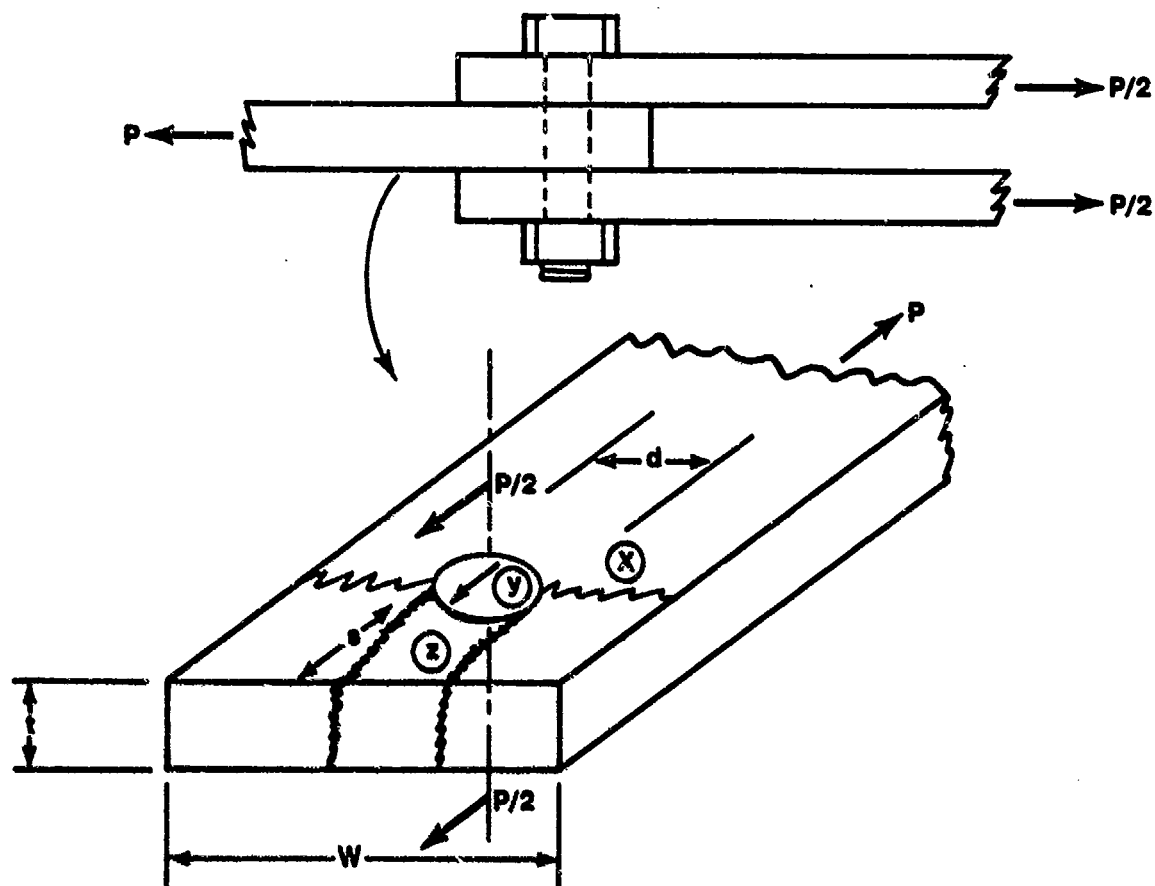
FIGURE 12.27. DOUBLE LAP JOINT, BOLT IN DOUBLE SHEAR

In addition, the bolt bearing on the surface of the hole (surface Y) may create a critical compressive stress. The average bearing stress in the plate at the bolt hole is:

$$\sigma_{br} = \frac{load}{area} \tag{12.18}$$

$$\sigma_{br} = \frac{P}{dt}$$

The application of the bearing load creates a shear stress along Sections z which tends to tear out the edge of the plate.

12.66

The "edge tear-out" stress is

$$\sigma_s = \frac{\text{load}}{\text{area}}$$

$$\sigma_s = \frac{P}{2\,ts} \tag{12.19}$$

These simple equations represent only the simple average stresses in order to appreciate some of the fundamental requirements of a joint. There is the obvious possibility that friction between the plates may accomplish part of the shear transfer and the hole may create considerable stress concentration to cause peak stresses well above the computed average.

12.4.8 Pressure Vessels

The use of highly pressurized containers in various aircraft and missiles creates significant structural problems. Some of the more simplified situations are represented by the stresses created in pressurized spherical and cylindrical shells. These vessels are illustrated in Figure 12.28.
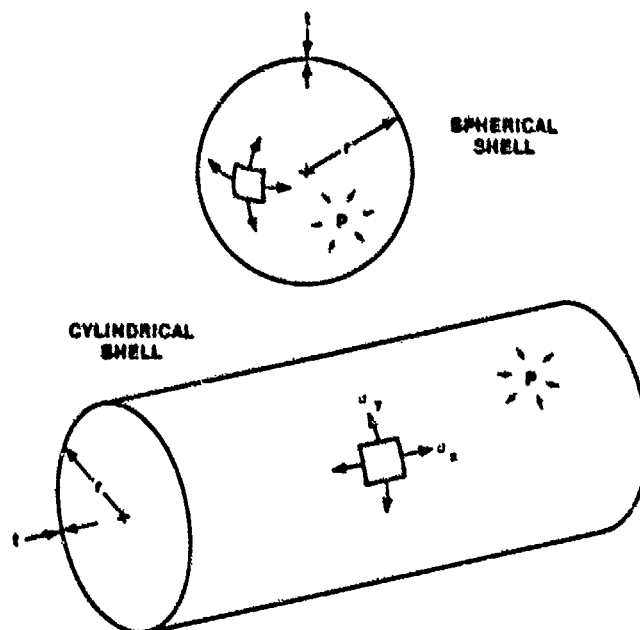
FIGURE 12.28. STRESS IN PRESSURIZED VESSELS

The stress in a pressurized spherical shell is uniform and constant in all directions along the surface. The resulting tensile stress is due to the pressure load being distributed over the effective shell area

$$\sigma = \frac{load}{area} \qquad (12.20)$$

$$load = (pressure)\ (area)$$

$$= (p)\ (\pi r^2)$$

$$area = 2\pi rt$$

$$\sigma = \frac{p\pi r^2}{2\pi rt}$$

$$\sigma = \frac{pr}{2t}$$

In order to consider the stresses in a pressurized cylindrical shell, the existence of two separate stresses must be noted. The longitudinal stress, σ_x is related as follows:

$$\sigma_x = \frac{load}{area}$$

$$\sigma_x = \frac{p\pi r^2}{2\pi rt}$$

$$\sigma_x = \frac{pr}{2t} \qquad (12.21)$$

This is identical to the relationship developed for the pressurized spherical shell. However, an additional stress, σ_y, is developed which is referred to as the "hoop" stress.

$$\sigma_y = \frac{load}{area}$$

$$load\ per\ unit\ length = 2pr$$

$$area\ per\ unit\ length = 2t$$

$$\sigma_y = \frac{2pr}{2t}$$

$$\sigma_y = \frac{pr}{t} \qquad (12.22)$$

(NOTE: $\sigma_y = 2f_x$)

For this situation the hoop stress incurred is twice the longitudinal stress developed. An important fact is concluded from this relationship: If a failure due to pressure occurs in a uniform cylindrical shell, the hoop stresses will predominate in the mode of failure.

12.4.9 Component and Principal Stresses

Two factors determine the strength and manner of failure of any structural member. One, of course, is the property and character of the structural material. The other is the maximum normal stresses ("principal stresses") and maximum shear stresses which exist in various areas of a part. Whenever there is a normal stress applied to a part there will exist various magnitudes of normal and shear stresses at planes different to the direction of loading. Also, any time a shear stress is applied to a part, there will exist at certain planes various magnitudes of normal and shear stresses. The various components of the applied primary stress must be investigated to determine the influence upon strength and failure type.

A typical example of component stress is illustrated in Figure 12.29. Figure 12.29A shows a specimen of material with a pure axial tension load applied. If a section or cut is made in this specimen at Section X, it is seen that a constant tension stress exists on this plane perpendicular to the direction of loading. Figure 12.29B shows the same specimen subjected to the same pure axial tension load but with a cut made along Section Y. An investigation of the stresses acting on Section Y shows that there still exists a uniform tensile stress across the section. However, the tensile stress which exists on plane Y will have components which are perpendicular and parallel to the surface of the cut. One of these components which is perpendicular to the face of the section will be a normal tensile stress of a smaller magnitude than the tensile stress applied to the cross-section. Along the surface of Section Y will be a component of stress parallel to the surface. This is a shear stress -- it is a component of the primary applied tensile stress.

Since the tensile stress component perpendicular to the face of the cut will be of a smaller magnitude than the applied tensile stress, it will have no particular or immediate influence on strength or mode of failure. However, the shear stress component parallel to the face of the section is a stress of an altogether different nature. It may have a decided effect on strength and failure type as some materials are much more critical in shear than in normal stress (particularly ductile metals).
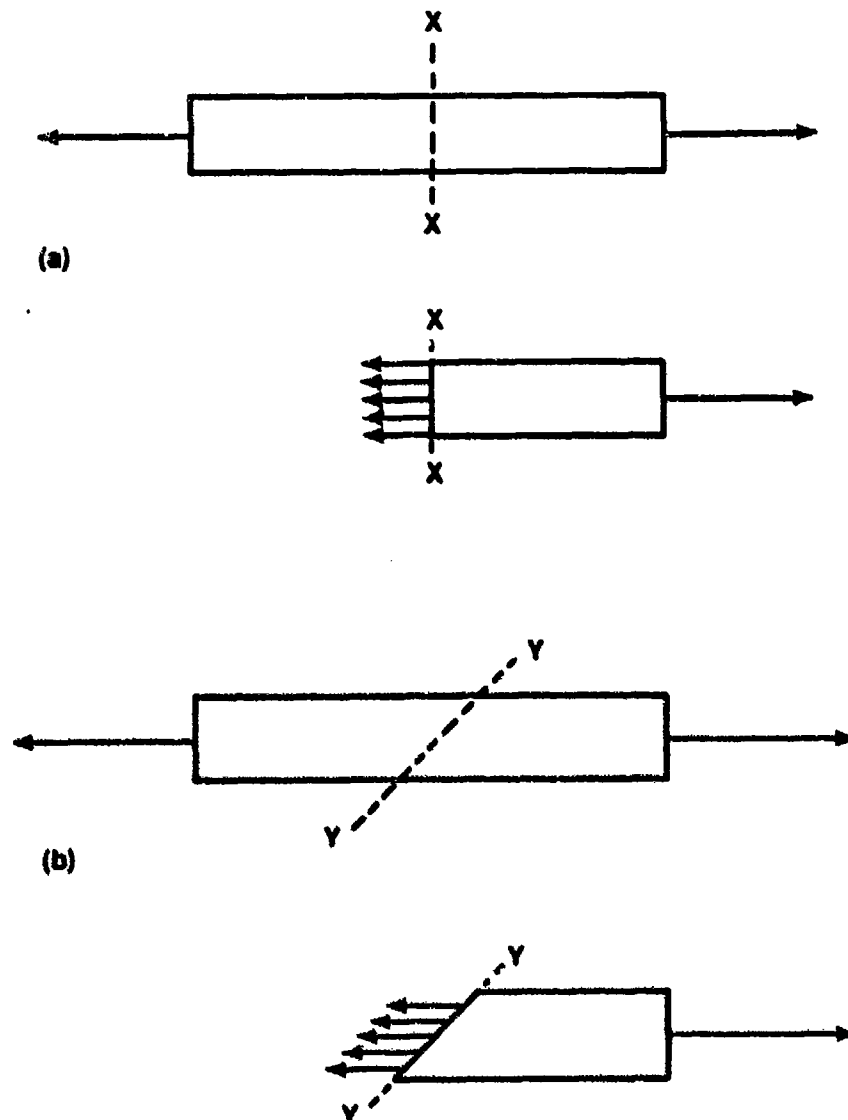
FIGURE 12.29.   COMPONENT STRESSES

Figure 12.30A shows a part loaded in tension with a section cut along the direction of applied stress. It is obvious there would be no shear stress

(due to force components) along this Section Z. Since shear stresses do not exist either at a section perpendicular to the direction of applied stress, or at a section parallel to the direction of applied stress, it is reasonable to assume that between these limits the existing shear stress will be a maximum on a section at 45° to the direction of primary load application.
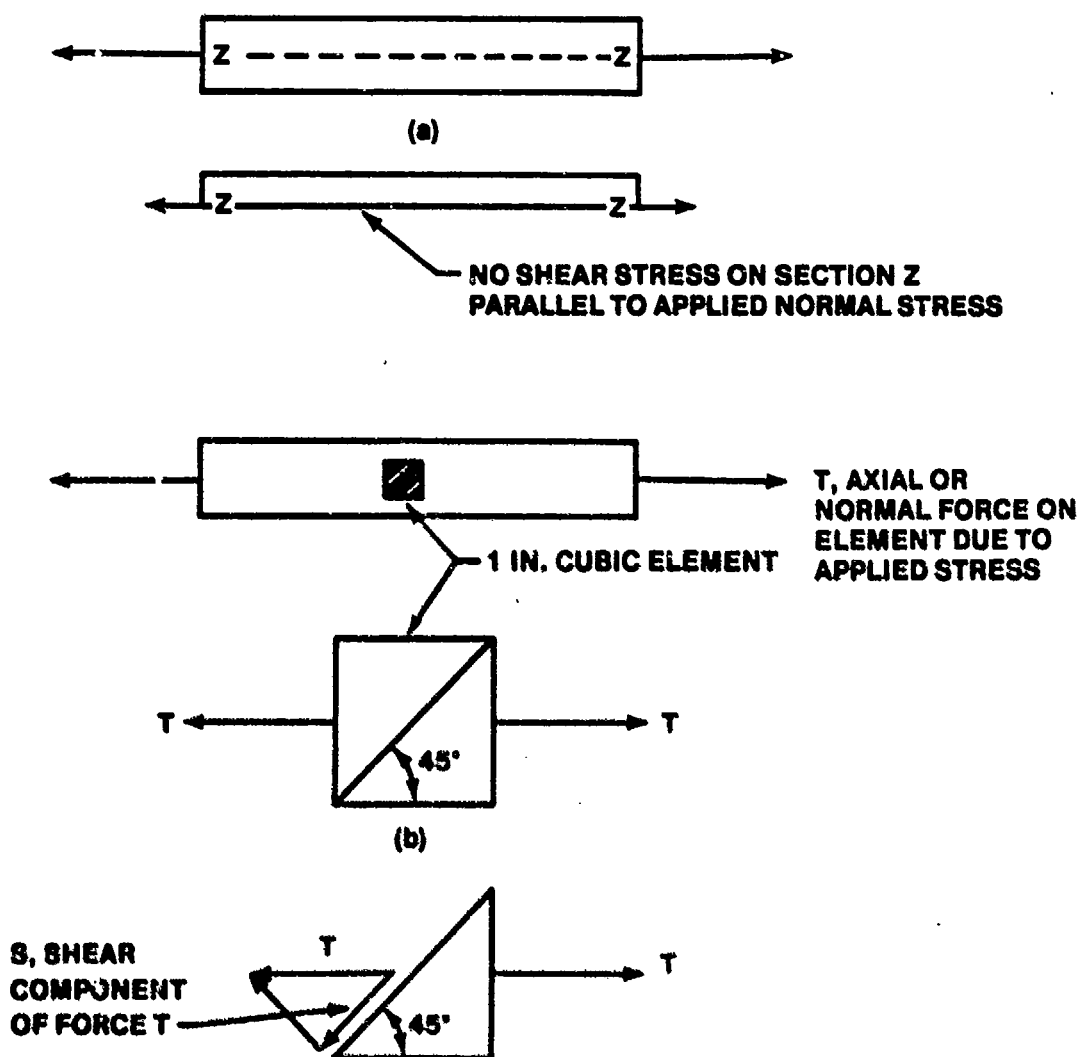
FIGURE 12.30. COMPONENT SHEAR STRESSES

To determine the magnitude of the maximum shear stress, it is best to take a one inch cube of material from the basic specimen and examine the forces existing in this element. There is applied to the sides of this one-

inch element (as in Figure 12.29B) a load which is the tensile stress on the specimen cross-section. Since the section or cut is to be located at 45° to the applied stress, the component of force distributed along the diagonal will be as follows:

$$S = T \sin 45°$$
$$S = .707 \ T$$

This shear force will be distributed over the diagonal surface which, for the one inch element, will be 1.414 inches. The shear stress is then

$$= \frac{.707 \ T}{1.414}$$

$$= .50 \ T$$

Thus, an applied axial stress will produce a maximum component shear stress which is one-half the magnitude of the applied stress. Knowledge of the presence of the component shear stress and its existence as a maximum at 45° is basic to a discrimination between ductile and brittle failure types.

An example of the existence and orientation of the maximum component shear stress is provided in Figure 12.31 where two specimens of metal - one very ductile and one very brittle - are subjected to failing tensile loads. The brittle type material will fracture with a clean break at 90° to the direction of loading. The ductile specimen will exhibit fracture planes at 45° to the direction of the applied tensile stress thus verifying the existence of component shear stresses. This 45° type of fracture from pure tensile loads is referred to as the "ductile" or "shear" type of failure.
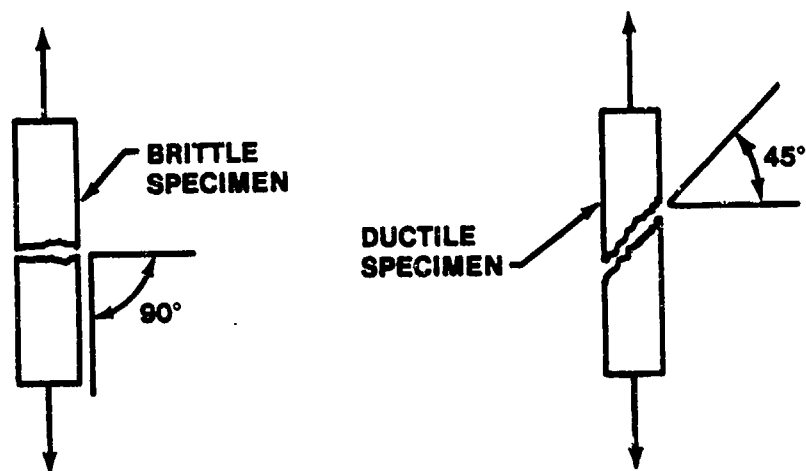
FIGURE 12.31.   EFFECT OF DUCTILITY ON FRACTURE

The condition of an applied pure shear presents a different and slightly more complex problem concerning component and principal stresses. Consider a one inch cubic element subjected to pure shear (Figure 12.32).

If a Section A is taken at a diagonal of 45° in one direction, it is apparent that there must be a compression force on the diagonal to statically balance the action of the two shear forces applied along the edges of the element. The two shear forces have components at 45° which are additive and must be balanced.

$$C = S \sin 45^\circ + S \cos 45^\circ$$
$$C = (2) (.707)S$$
$$C = 1.414 S$$

Since the compression force is distributed along the diagonal the compression stress may be found as

$$\text{compression stress} = \frac{1.414 \ S}{1.414}$$

$$= 1.000 \ S$$

12.73
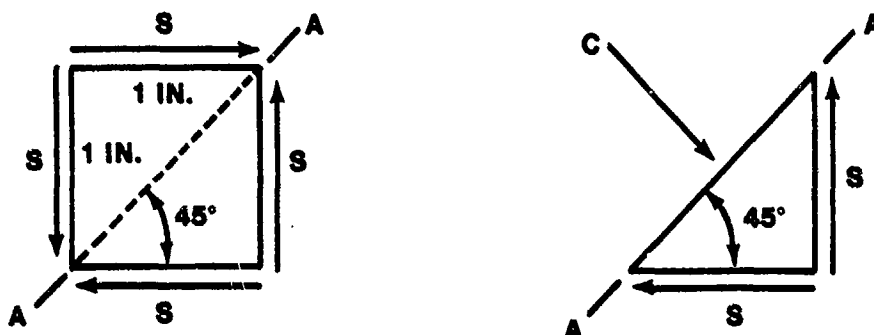
FIGURE 12.32. APPLIED PURE SHEAR - SECTION AA ANALYSIS

Thus, for the case of pure shear applied to an element, there exists at one 45° section a compression stress equal in magnitude to the applied shear stress. The existence of this component compression stress is evident in the failure mode of a thin walled tube subjected to a failing torsion load (torsion, of course, produces a uniform pure shear). If the walls of the tube are sufficiently thin, the tube will fail primarily in buckling due to the principal compression stress existing in the 45° direction.
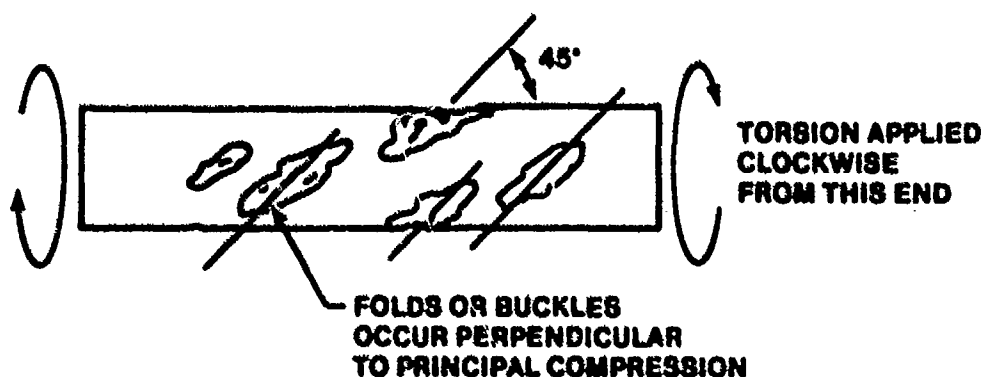
FIGURE 12.33. BUCKLING FAILURE DUE TO TORSION

12.74

If the same one-inch element of Figure 12.32 (shown in Figure 12.34) is subjected to the same pure shear condition - but sectioned along Plane B, a different stress situation results. If the element is cut along Section B, it is apparent that a tension force, T, must be sufficient to balance the components of the two shear forces along the edge. This situation will produce a tension stress distributed along the diagonal which is equal in magnitude to the applied shear stress. The presence of this tension stress is verified by the mode of failure of a brittle shaft in torsion (twisting a piece of chalk produces the same result) (Figure 12.35). In this case, a fracture will begin as a 45° spiral surface which is perpendicular to the principal tension stress.

It must be remembered that component stresses may have a definite bearing on the strength and mode of failure of any structure. Any normal or shear stress applied to a part will produce component and principal stress that cannot be neglected.
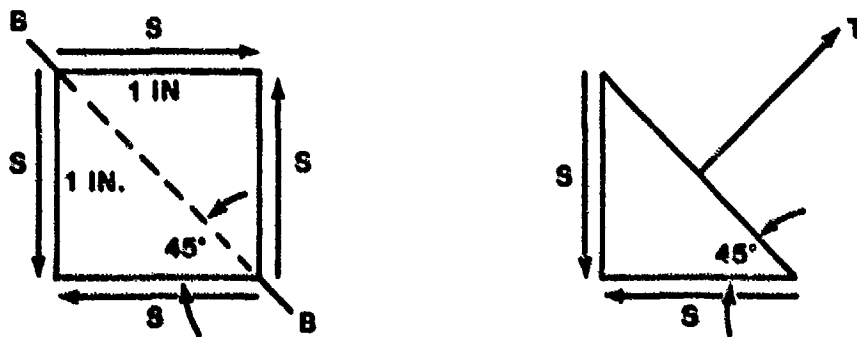
FIGURE 12.34. APPLIED PURE SHEAR - SECTION B-B ANALYSIS
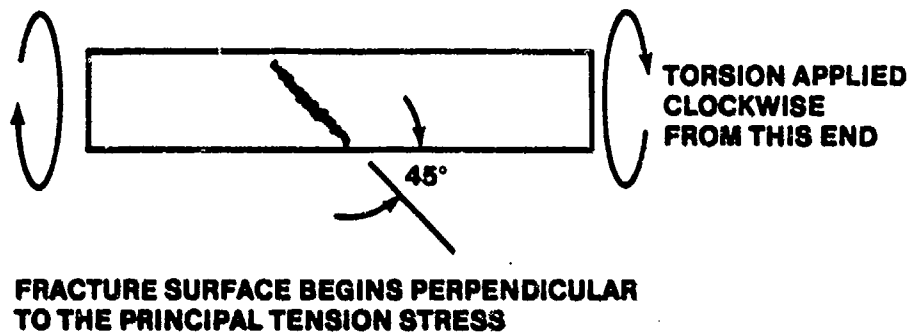
FIGURE 12.35. BRITTLE FAILURE DUE TO TORSION

12.4.10 Strain Resulting from Stress

Any structure which is subjected to stress must deform under load, even though the deformation may not be visible to the naked eye. Recall from the previous sections that stress is the true measure of state for a part subjected to load. Strain is a similar means of measure. In order to fully evaluate the state of being of a stressed material, all deformations must be considered on a unit basis. Strain is thus defined as deformation per unit of length and in most engineering terminology is referred to by "e" or "ε" (epsilon).

Suppose a steel bar 100 inches in length is subjected to a tensile stress of 30,000 psi - as in Figure 12.36. The total change in length throughout the 100-inch length would be about 0.1 inches. If subjected to uniform stressing, the part would be subjected to a uniform strain which is as follows:

$$\text{strain} = \frac{\text{total deformation}}{\text{original length}}$$

$$\varepsilon = \frac{\Delta L}{L} \qquad\qquad (12.23)$$

$$\varepsilon = \frac{0.1 \text{ in}}{100 \text{ in}}$$

$$\varepsilon = .001 \text{ inches per in}$$

To produce a total deformation of 0.1 inches in 100 inches of length, the strain must be .001 in/in or 0.1%.
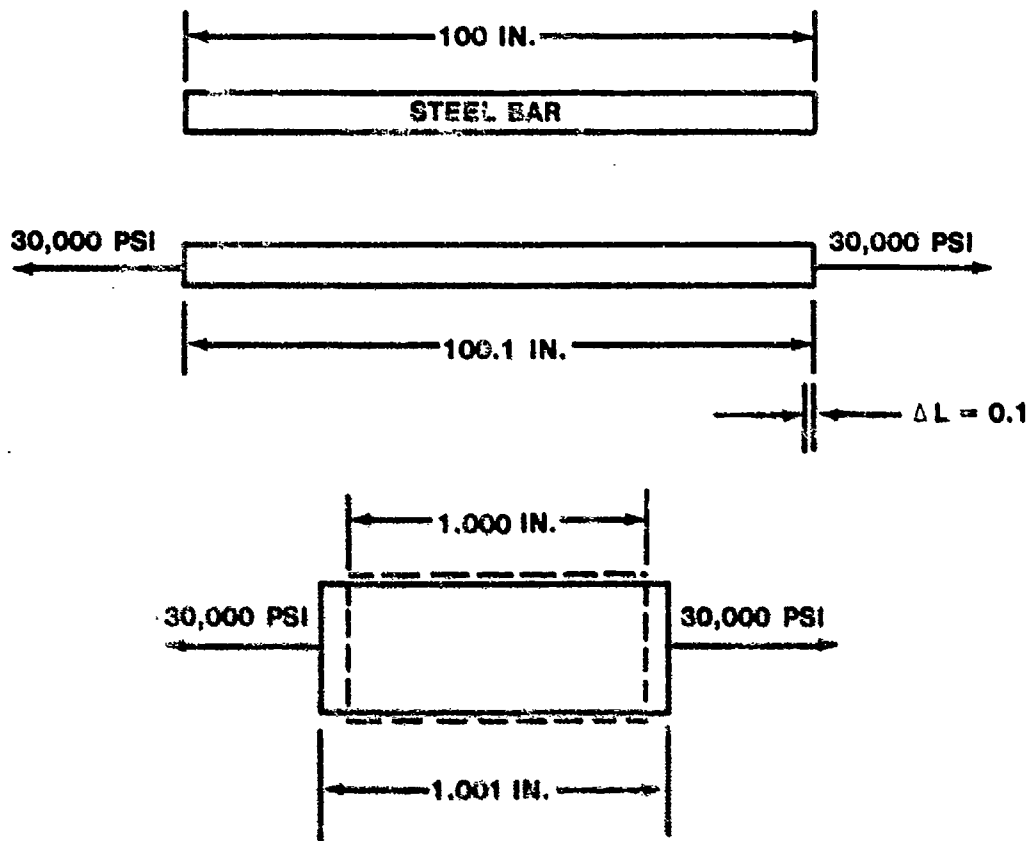
FIGURE 12.36.   AXIAL STRAIN

In addition to the longitudinal strain of the part shown in Figure 12.36, there will be a lateral contraction of the metal. For most metals there is a definite relationship between this transverse strain and the longitudinal strain and it is important when considering combined stresses that are dependent upon deflections. The proportion between the lateral strain and the longitudinal strain has been given the name "Poisson's ratio, μ (mu)" and for most homogenous metals this ratio has the approximate magnitude of 0.3 (μ = 0.3). In the case of the previous example the longitudinal extension strain of .001 would be accompanied by a lateral contraction strain of .0003.

Thus, it is important to remember that any metal subjected to stress must strain. The amount of strain, while not necessarily visible, must be present

12.77

and is very important. Just as large stresses may produce numerically small strain, any small strain forced on a structure may produce large stresses.

Shear stress also produces shear strains. Shear strain, while not necessarily denoting a change in length, does describe a change in relative position of the part. Figure 12.37 should illustrate this fact.
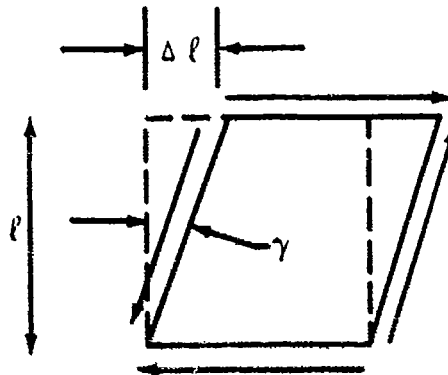
FIGURE 12.37. SHEAR STRAIN

Shear strain is most properly described by the angle of strain, γ (gamma) in radians. When a shear stress is applied to an element, the shear strain, γ, can be computed as the proportion of the change in position of one side, Δℓ, to the original length, ℓ.

$$\gamma = \frac{\Delta \ell}{\ell} \qquad (12.24)$$

One of the most important properties of an aircraft material is its stiffness. If a part were subjected to a particular level of stress, small strains would indicate a stiff or rigid material; large strains would indicate a flexible material. The accepted method of measuring the stiffness or rigidity of a material is to compute a proportion between the applied axial stress and the resulting axial strain. This proportion is known as the "Modulus of Elasticity" or "Young's Modulus" and is denoted by the letter, E.

$$E = \frac{\sigma}{\epsilon} \qquad (12.25)$$

where E = modulus of elasticity, psi

σ = stress, psi

ε = strain, in/in

Typical values for this Modulus of Elasticity are

Steel   E = 30,000,000 psi

Aluminum Alloy E = 10,000,000 psi

Magnesium Alloy E = 7,000,000 psi

By a comparison of these values it is seen that an aluminum alloy part subjected to a given stress would strain three times as greatly as a steel part subjected to the same stress level.

There is no true modulus of elasticity in shear. However, for computing shear deflections there exists an equivalent quantity known as the "modulus of rigidity" or "shear modulus" and is denoted by the letter G.

$$G = \frac{\sigma_s}{\gamma} \qquad (12.26)$$

where G = modulus of rigidity, psi

σ_s = shear stress, psi

γ = shear strain, in/in

For most metals the shear modulus is approximately 40% of the elastic modulus - e.g.

Steel   G = 12,000,000 psi

Aluminum Alloy G = 4,000,000 psi

For homogenous materials the Modulus of Rigidity may be determined by the following equation:

$$G = \frac{E}{2(1+\mu)} \qquad (12.27)$$

where G = Modulus of Rigidity

E = Modulus of Elasticity

μ = Poisson's ratio

Bending stresses will cause bending deflections. In this case, no general strain relationship can be defined that is similar to simple axial strain. Since bending stresses do vary throughout the cross-section there will be a variation of axial strains proportional to the axial stress.

For the initially straight beam that is shown in Figure 12.38, an applied pure bending moment will produce a deflection of pure curvature.
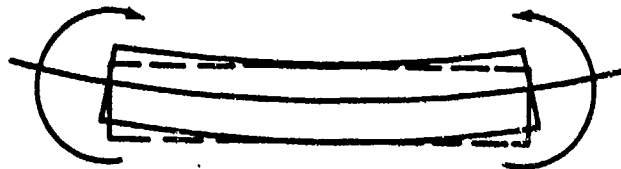
FIGURE 12.38. PURE CURVATURE

Pure bending imposed will cause compression strains on the lower surface, and zero strain at the neutral axis. The result of these strains is a bending of the beam to the arc of a circle with no change in length of the neutral axis. Of course, if one end of the beam is held stationary the other end deflects upward - but only because of the curvature of bending (Figure 12.39).
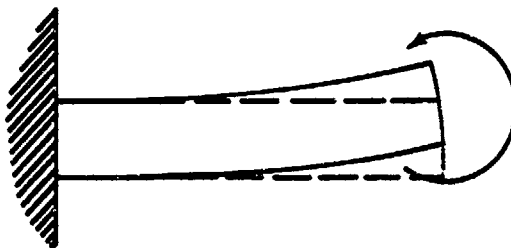
FIGURE 12.39. BENDING DEFLECTION OF CANTILEVER BEAM

A somewhat similar condition exists for a length of shaft subjected to a pure torsion loading. The shear stress distributed on the cross-section will produce shear strains, which are angular displacements. The net effect is to produce a uniform twist throughout the length of the shaft. If a straight line were to be drawn on the shaft, as in Figure 12.40, this line would be displaced upon load application and would finally occupy the position indicated by the dotted line. The helix angle of displacement would depend upon the shear strains developed at the surface of the shaft.
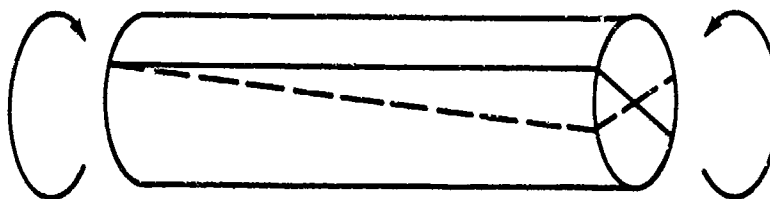
FIGURE 12.40. ANGULAR DISPLACEMENT DUE TO TORSION

Actually, only two factors determine the strain for a particular material subjected to stress. One, of course, is the magnitude of stress; the second is the type of material and characteristic stiffness. The actual amount of

deflection of a loaded structure will depend on the physical arrangement of the structure and the cumulative effect of the local strains existing in various components of the structure.

12.4.11 Stress-Strain Diagrams and Material Properties

In order to evaluate the properties of a material and the possible structural application, it is necessary to determine strains corresponding to various levels of applied stress. Laboratory tests are then conducted which subject a specimen of material to various magnitudes of stress while strains are recorded at each stress. If the stresses and corresponding strains are then plotted on a graph, many useful and important properties of the material may be observed.
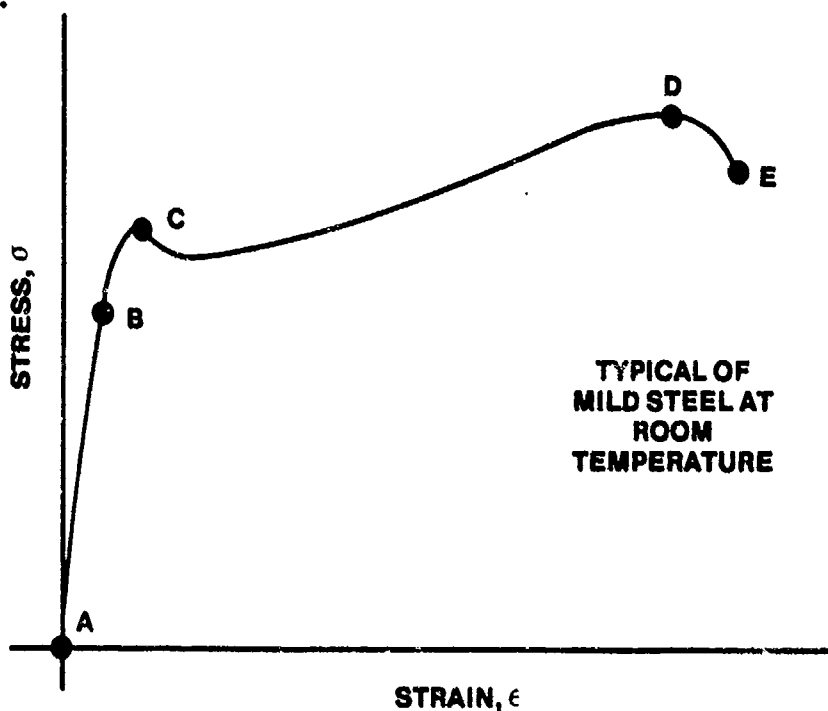
FIGURE 12.41. STRESS-STRAIN DIAGRAM OF TYPICAL MILD STEEL

Figure 12.41 shows a typical "stress-strain" diagram for a mild steel at room temperature. As the stress is first applied and increased, the strain begins and increases in direct proportion to the stress - i.e., the stress-strain diagram is a straight line from A to B; therefore, this material would snap back to zero strain upon the release of stress. Because of the elastic nature of the material in this range of stress, the stress range from A to B is referred to as the "elastic or proportional range" of the

material. This definition then implies that stresses up to Point B will not cause permanent deformation of the material.

If the applied stress is gradually increased above the value at Point B, the plot of stress vs. strain will deviate slightly from a straight line. There will then be some small - but measurable - permanent strains thus incurred. Hence, Point B is the end of the elastic or proportional range of the material and the value of stress at Point B is termed the "elastic or proportional limit; σ_p."

Should the stress be gradually increased up to Point C, a noticeable yielding of the material will be apparent; at Point C the strain suddenly increases without further increase in stress. In fact, with most ductile steels, there may be a decrease in stress resisted by the material as large plastic strain takes place. It is obvious that any stress above the value at Point C will produce very large and objectionable permanent strains. To verify this condition, assume that a stress is applied up to Point X on the diagram in Figure 12.42. The strain at this point is quite large. If the stress were to be released, the material would "relax" along the dotted line shown which is parallel to the original straight line from B to A. At Point Y the stress is again zero but a large permanent deformation has taken place. The value of stress at Point C is logically termed the "yield point" or "Yield stress, σ_y", of the material and is the stress beyond which large and objectionable permanent strains take place.

The stress-strain diagram of Figure 12.42 does show that the material is capable of withstanding stresses greater than the yield stress - but not without large permanent strains. If the stresses above Point C are gradually applied, the material will continue to withstand higher and higher stresses until the very ultimate strength capability is reached at Point D. If any attempt is made to subject the specimen to a stress greater than the value at Point D, failure will begin and will be complete at Point E. Since the value of stress at Point D is the very highest stress the material can withstand without failure, it is termed the "ultimate strength" or "ultimate stress, σ_U", of the material.

The two most important strength properties which are derived from the stress-strain diagram are the "yield strength" and the "ultimate strength." There is a direct analogy between these two properties and the operating

strength limitations of an airframe structure. If the material shown on the stress-strain diagram is never subjected to a stress above the yield point, no significant or objectionable permanent strains will take place; if an airframe structure is never subjected to a load condition greater than the "limit" load, no significant or objectionable permanent deformations will be incurred. If the material shown in the stress-strain diagram were subjected to a stress above the yield point, large and undesirable permanent strains will take place; if an airframe is subjected to a load condition greater than the "limit" load, undesirable permanent deformation of the structure may be anticipated, e.g., permanently distorted fuselage, bent wings, deformed tanks, etc. If an attempt is made to subject a material to a stress greater than the ultimate, failure will then occur; if any flight condition is attempted which produces loads greater than "ultimate" load, actual failure of the airframe is imminent.
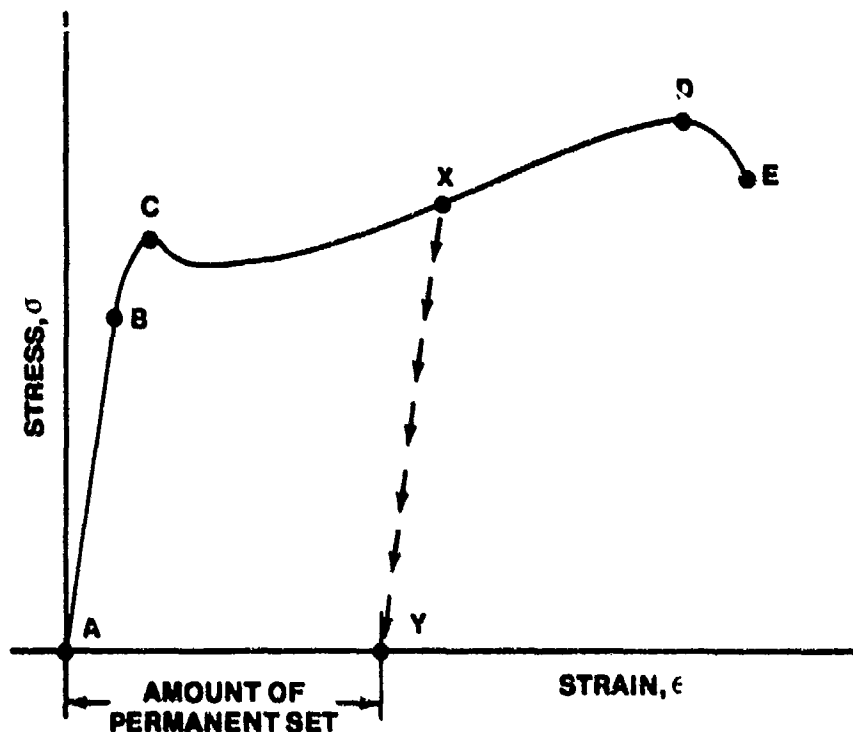
FIGURE 12.42.   PERMANENT SET

The basic stress-strain diagram of Figure 12.43 readily defines five of the most important static strength properties of a material:

1.   The elastic or proportional limit is the end of the elastic region of the material.   A part subjected to stresses at or below the proportional limit will experience no permanent deformation.   Upon the release of stress the part will snap back to the original unstressed shape.

2. The yield strength is the highest practical value of stress to which a material should be subjected. Stresses between the proportional limit and the yield point will cause only slight and hardly measurable permanent deformation. Any stress above the yield point will result in large and objectionable permanent deformation.

3. The ultimate strength is the very maximum of stress which a material can withstand without failure. Extremely large and undesirable permanent deformations will ordinarily result when this point is approached.

4. The fracture point, or the effective stress at time of failure, is determined primarily to evaluate the manner of fracture and the ductile quality of the material.

5. The total strain or total elongation of the material at the point of fracture is an indication of the ductility of the material. Any metal which would have less than five per cent elongation in a two inch test length is considered to be brittle - ordinarily too brittle to be applicable to an ordinary aircraft or missile structure.
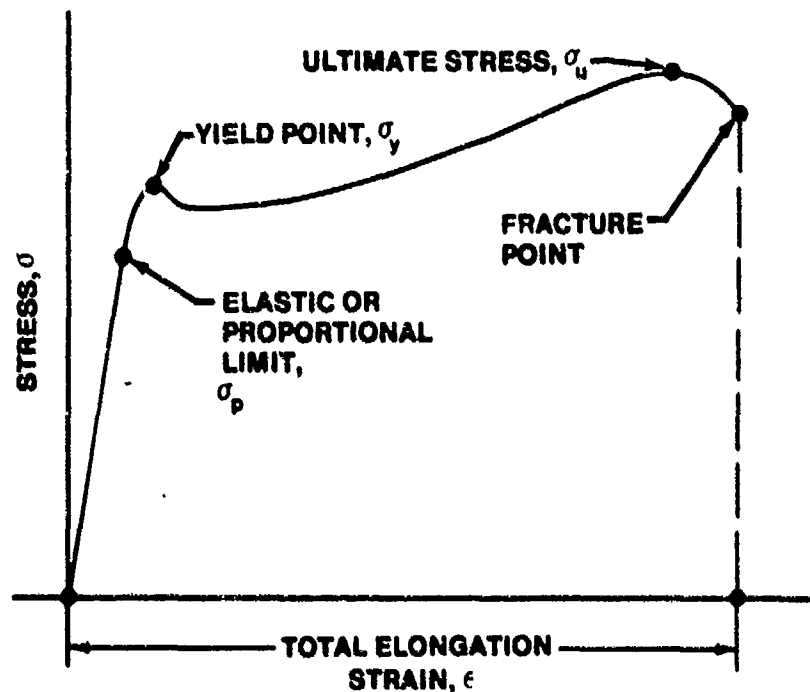
FIGURE 12.43. DEFINITION OF STATIC MATERIAL PROPERTIES

At this point, it is appropriate to present some of the variations in the stress-strain diagrams due to manner of loading or material type. One point to consider is that stress-strain diagrams are not usually used in connection with shear properties of a material. The proportional limit, ultimate strength, etc., in shear are not true properties because of "section or form" considerations. Cross-section dimensions and area distribution will cause significant variations in the shear strength capabilities.

Many materials used in aircraft construction (aluminum alloys, magnesium alloys, and some steels) do not exhibit a definite yield point or a distinct proportional limit. Figure 12.44 illustrates this fact. In such an instance it is necessary to define the yield point and proportional limit as a given departure from the original straight line of 0.0001 in/in. The yield stress is determined as the stress which produces a departure from the original straight line of 0.002in/in (Figure 12.45). In this case an applied stress equal to the yield stress would result in a permanent set of 0.2%. This amount is considered admissible for ordinary purposes.
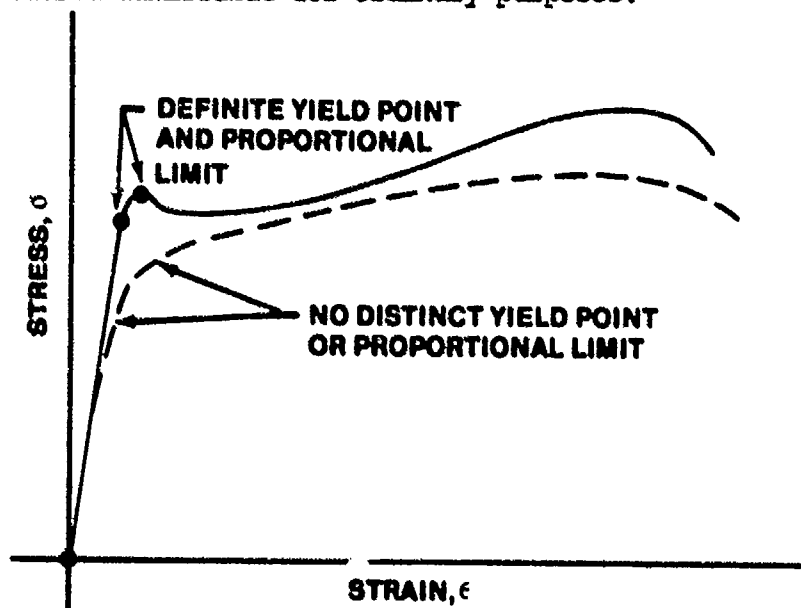
FIGURE 12.44. VARIATIONS IN STRESS-STRAIN RELATIONSHIPS

Compression stress-strain diagrams are similar to tension stress-strain diagrams except that the departure from proportionality generally occurs sooner and more gradually. Compression stress-strain diagrams are more difficult to obtain correctly because of buckling of the specimen. As
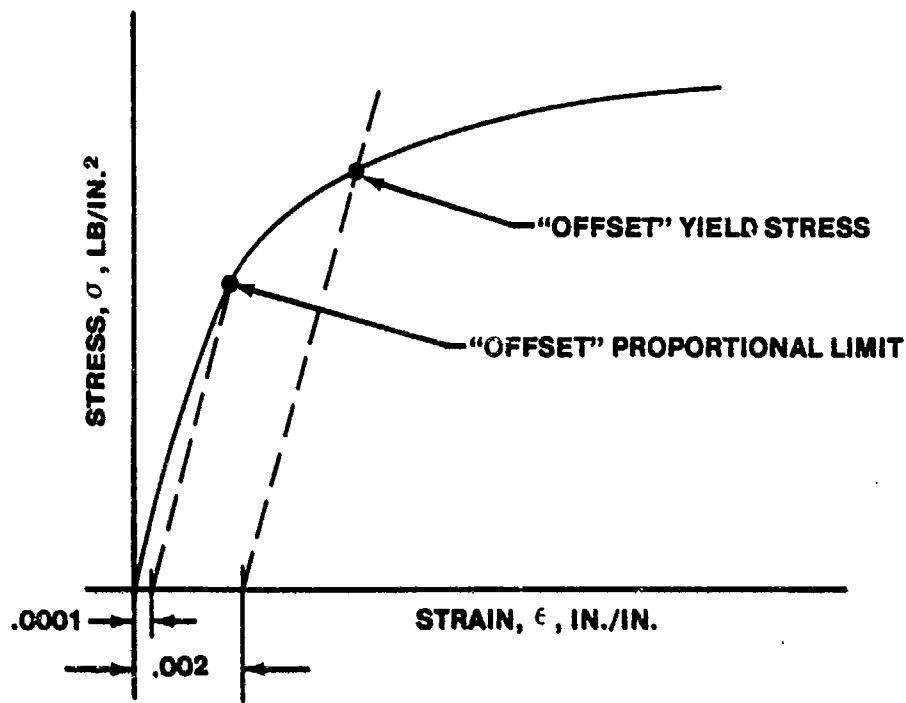
FIGURE 12.45.   DEFINITION FOR VARIANT STRESS-STRAIN RELATIONSHIP

compression buckling of a specimen constitutes a failure, it is obvious that compression ultimate strength is not true property and could not be determined as a specific quality of a metal.   The stiffness of a metal and the physical arrangement of the structure combine to decide the stability of the structure when subjected to compression loads (Figure 12.46).
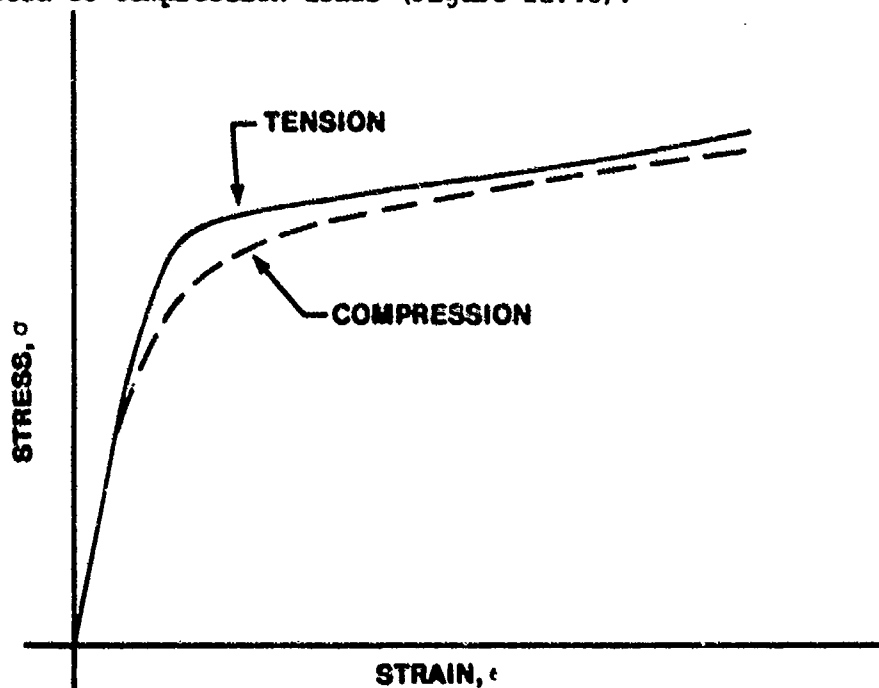

FIGURE 12.46.   COMPRESSION STRESS-STRAIN COMPARISON

In order to determine other material properties expressed by the stress-strain diagrams a closer examination must be made of certain areas of the stress-strain diagram.

By an inspection of the straight line portion of the stress-strain diagram, an evaluation may be made of the inherent stiffness of the material. In the elastic range of a material the proportion between stress and strain is the Modulus of Elasticity (sometimes called "Young's Modulus") and the magnitude of this proportion is a direct measure of the inherent stiffness. A high value for the Modulus of Elasticity will indicate a very stiff or rigid material while a low value indicates low stiffness or greater flexibility (Figure 12.47).
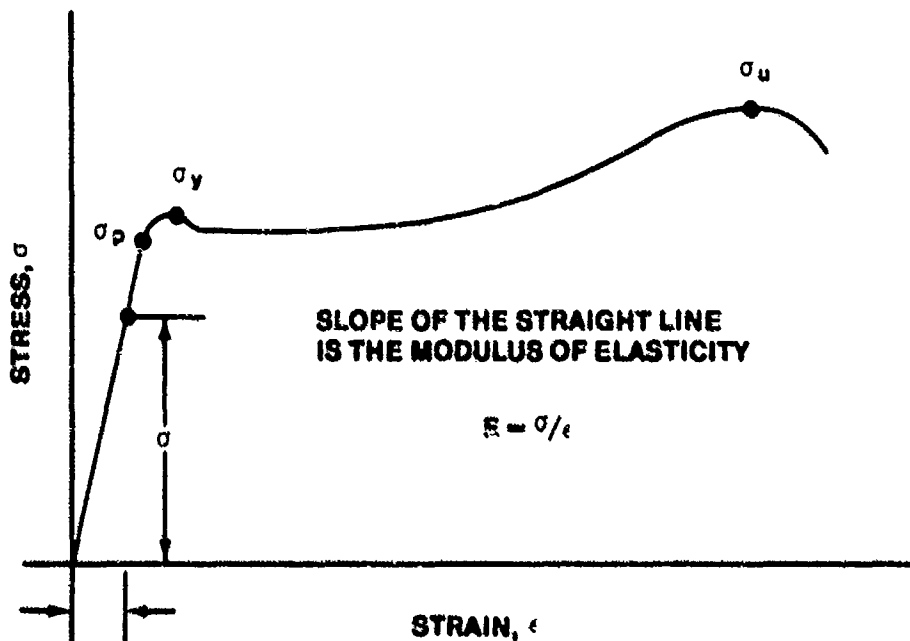
FIGURE 12.47. DEFINITION OF MODULUS OF ELASTICITY

When the stress-strain diagrams for three different materials are compared, the difference in the slopes and the proportions of inherent stiffness are readily apparent as shown in Figure 12.48.

Only two solutions exist: (1) lower the value of the operating stress or (2) change to a material type which has a higher elastic stiffness (higher E).

STRAIN, ε , IN./IN.

MATERIAL	E
STEEL	~ 30,000,000 PSI
ALUMINUM ALLOY	~ 10,000,000 PSI
MAGNESIUM ALLOY	~ 7,000,000 PSI
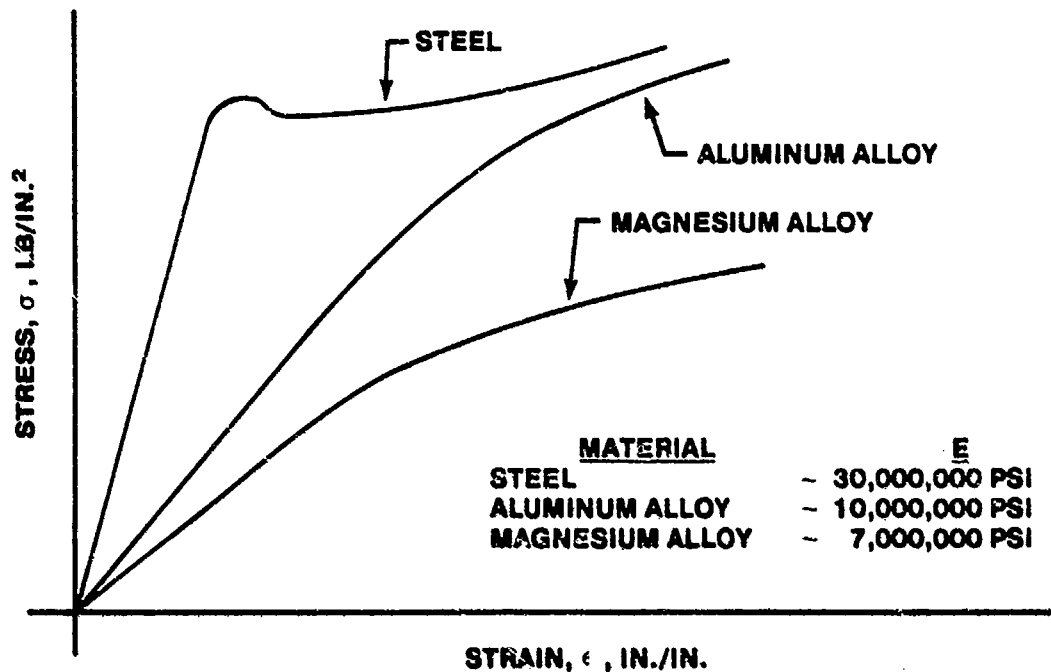
FIGURE 12.48. MODULES OF ELASTICITY COMPARISON

One important point to consider is that the Modulus of Elasticity, E, cannot be altered by heat treatment or changed any significant amount by use of a different alloy. Thus, the Modulus of Elasticity is an intrinsic property of the type of metal. Figure 12.49 shows the typical stress strain diagrams for steel in various conditions of heat treatment. Notice that the origin of each has the same slope. While the strength and ductility are changed by heat treatment, the stiffness of the elastic material remains unaltered. Increasing hardness by heat treatment will simply increase the stress at which plastic flow begins. Thus, if elastic deflections of a part which are excessive already exist, the problem will not be solved by heat treatment of changing alloy.
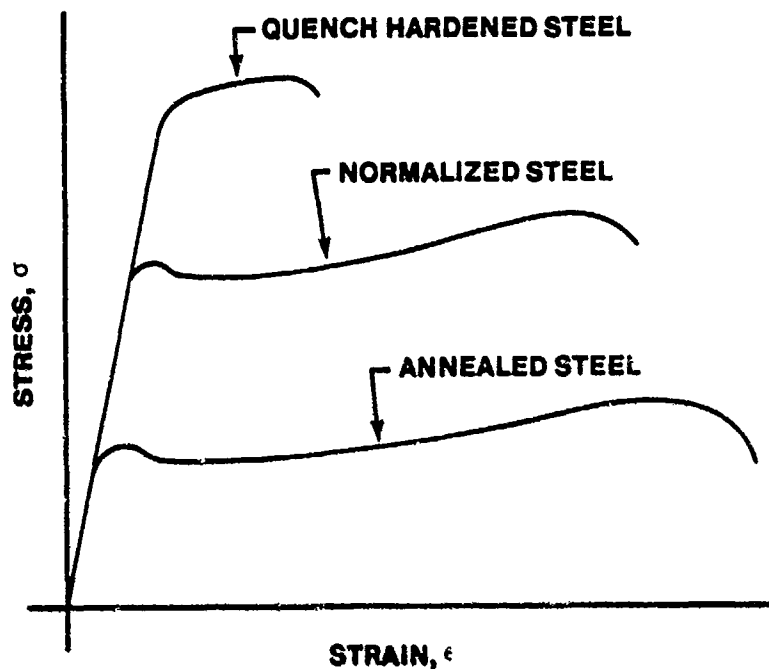
FIGURE 12.49. EFFECTS OF HEAT TREATMENT

Actually, the elastic modulus of a given metal will vary only with temperature, elevated temperature producing a lower Modulus of Elasticity. For example, a high strength aluminum alloy at 600° F will exhibit a Modulus of Elasticity which is only one-half the value shown at room temperature.

The elastic range of a material is the area of most general interest for ordinary structural investigation. However, when investigating the phenomenon of buckling of short columns and the behavior of structures at loads near ultimate, the stiffness of a metal in the plastic range is of particular interest. As was previously noted, the proportion between stress and strain is defined as the Modulus of Elasticity. At any stress below the proportional limit, this proportion is one fixed and constant value. Above the proportional limit, this proportion is one fixed and constant value. Above the proportional limit, this definition results in a proportion which is known as the "secant Modulus". Once beyond the proportional limit, the proportion between stress and strain will noticeably decrease. Hence, the Secant Modulus will have a value lower than the Modulus of Elasticity. Another method of measuring the stiffness in the plastic range is the slope of a line drawn tangent to the stress-strain diagram at some stress above the proportional limit. The slope of this tangent line defines a value known as the "Tangent

Modulus". The Tangent Modulus then measures an "instantaneous" stiffness while the Secant Modulus measures a "gross" or "cumulative" stiffness. Figure 12.50 gives the procedure of calculation of these properties and Figure 12.51 illustrates the typical variations of the Secant and Tangent Modulus for an aluminum alloy.

The loss of stiffness in the plastic range is appreciated when it is realized that small changes in stress will produce larger changes in strain than in the elastic region.

The energy storing and energy absorbing characteristics are of particular importance in defining the properties of a material. Any stress produced in a material requires the application of a force through a distance and, as a consequence, a certain amount of work is done. Consider a cubic inch element of steel with a gradually applied stress of 30,000 psi (as in Figure 12.52). As the stress is gradually increased from zero to 30,000 psi, the strain gradually increases from zero to

$$G = \frac{\sigma}{E} = \frac{30,000}{30,000,000} = .001 \text{ in/in}$$
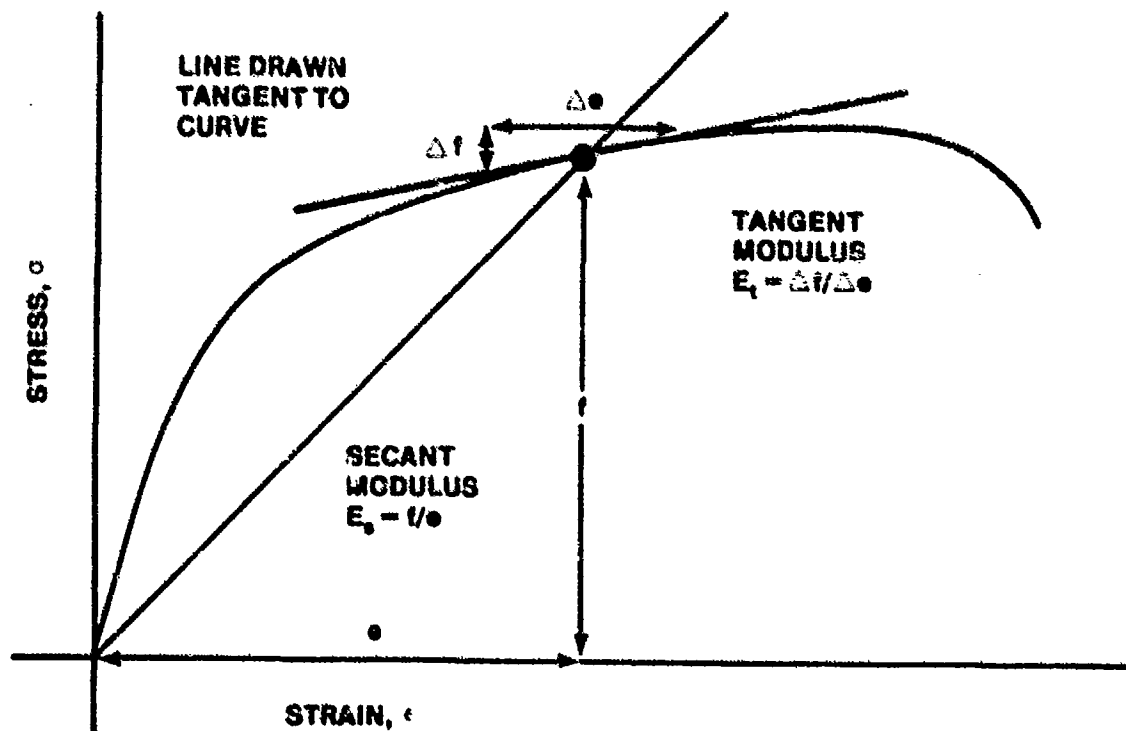
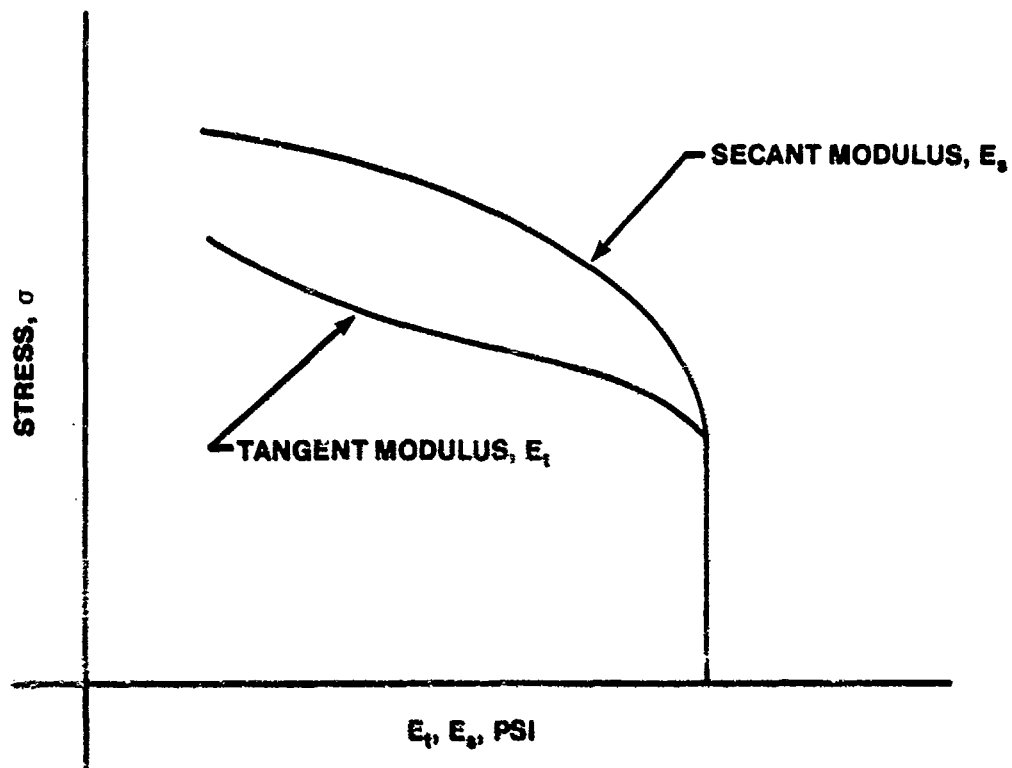FIGURE 12.50. DEFINITION OF SECANT AND TANGENT MODULI

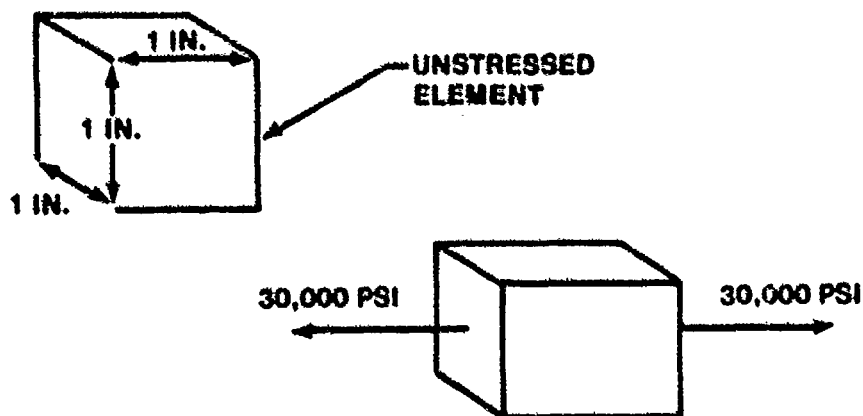FIGURE 12.51.   VARIATION OF SECANT AND TANGENT MODULI

FIGURE 12.52.   APPLICATION OF STRESS

The work done during this gradual stressing is the product of the average force and the distance.

$$\text{Work done} = \left[\frac{30,000}{2} \ \frac{\text{lb}}{\text{in}^2} \right] \times \left[.001 \ \frac{\text{in}}{\text{in}} \right]$$

$$= 15 \ \frac{\text{in-lb}}{\text{in}^3}$$

Thus, 15 inch-pounds of work would be required to produce the final stress of 30,000 psi in the cubic inch element. This amount of work is actually represented by the area enclosed on the stress-strain diagram at this particular stress level (Figure 12.53). This area principle is then used with the stress-strain diagram to describe the energy properties of a material.

If a material is stressed to the proportional limit, all work done in producing this stress is stored elastically in the material. Therefore, the area under the straight line portion of the stress-strain diagram is a direct measure of the energy storing capability and is referred to as the "Modulus of Resilience". Of course, the manner of loading-tension. compression, shear, etc., must be specified since the work done will be different depending on the manner of loading.
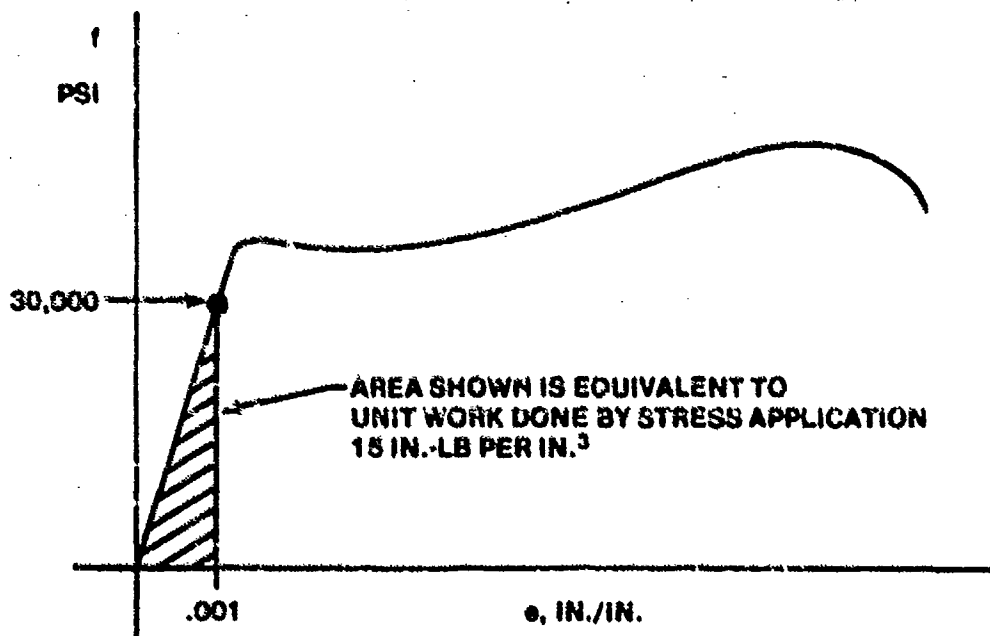

FIGURE 12.53. WORK DONE BY STRESS APPLICATION

If a material were stressed all the way to failure, the entire area under the stress-strain diagram is a measure of the work required to fail the material. The toughness or energy absorbing quality of the material is evaluated in this manner.
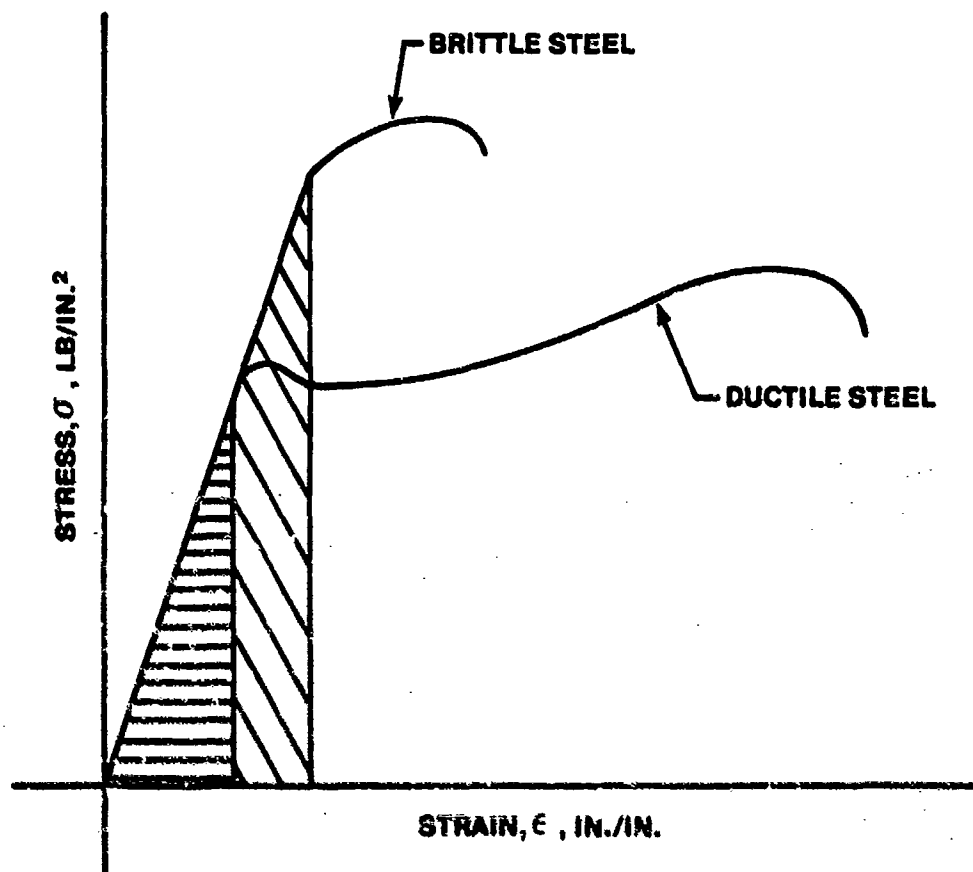

FIGURE 12.54. ENERGY STORING CAPABILITIES (RESILIENCE) OF DUCTILE AND BRITTLE STEELS

A comparison of the stress-strain diagrams for a ductile and brittle steel should define the properties of "resilience" and "toughness". The shaded areas shown in Figure 12.54 denote the energy storing capabilities for the ductile and brittle steels. The brittle material has the higher elastic limit and consequently a higher "Modulus of Resilience". The shaded areas of Figure 12.55 denote the energy absorbing capabilities of the same materials. The ductile material, while having lower strengths, devlops much greater strains. As a result, the ductile material will require a greater amount of work to produce failure and is then the tougher material. The additional work

required to break the softer, more ductile, material goes into forcing the metal particles to slip relative to each other. When a specimen of ductile material is fractured during a laboratory test, this effect may be appreciated by handling the broken specimen of ductile material immediately after failure. A ductile specimen will be warm to the touch as the work absorbed by the material is converted into heat.
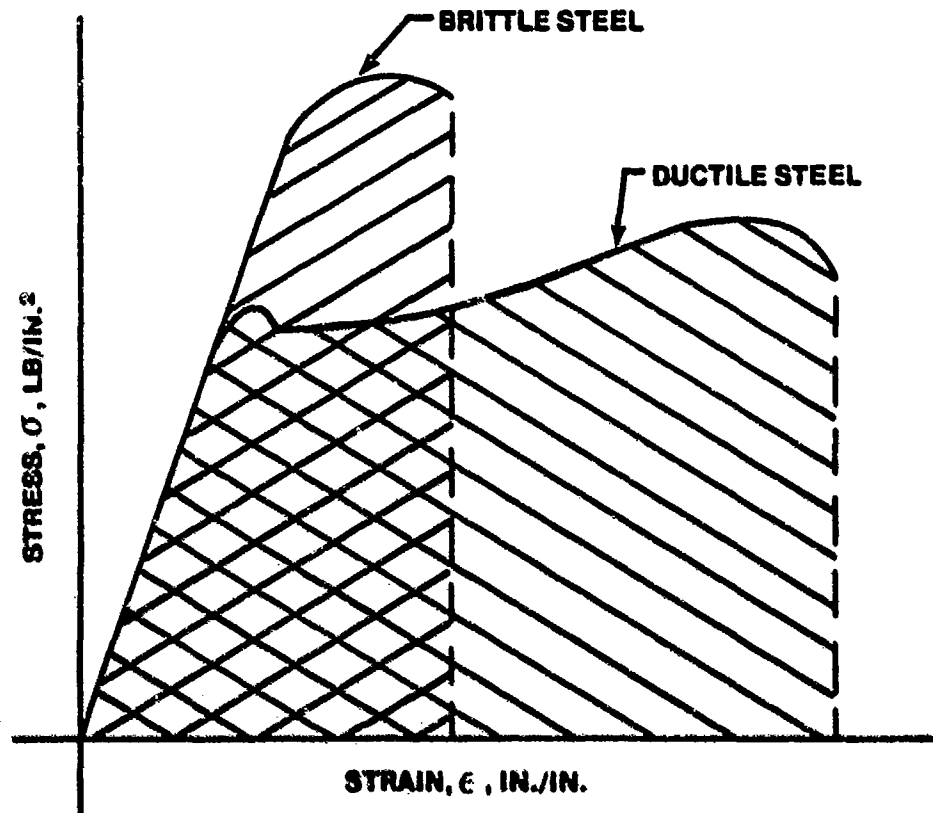

FIGURE 12.55.   ENERGY ABSORBING CAPABILITIES (TOUGHNESS)
OF DUCTILE AND BRITTLE STEELS

It may seem strange that it is possible to fail the more ductile metal at a lower stress but still require that more work be done. If so, remember that work is the product of average force and distance.

It would be desirable for a structural material to have a high yield point, high resilience, high ultimate strength, and also high toughness. However, materials which have very high strength usually have low ductility and low toughness. The balance between the strength requirements and

toughness (or energy absorbing) requirements will depend on the particular application in a structure. As examples of the two extremes consider: (1) a reciprocating engine valve spring and (2) protective crash helmet or protective headgear. In the fabrication of a valve spring, a material must be selected which has very high strength and great resilience. Such a material would necessarily have low toughness but in such an application toughness is unimportant and resilience is given primary consideration. In the construction of a true protective crash helmet or hard hat, sharp impact blows first must be distributed then the energy of impact absorbed as far as is possible. This requires a thickness of a crushable material for the inner lining which has high toughness per unit weight. Actual strength is not necessarily a factor since energy absorption requirements predominate.

The stress-strain diagram of a material will then furnish all necessary information to determine the static strength properties. Actually there are 10 important points of information that may be gained from an inspection of the stress-strain diagram. As shown in Figure 12.56 these points are as follows:
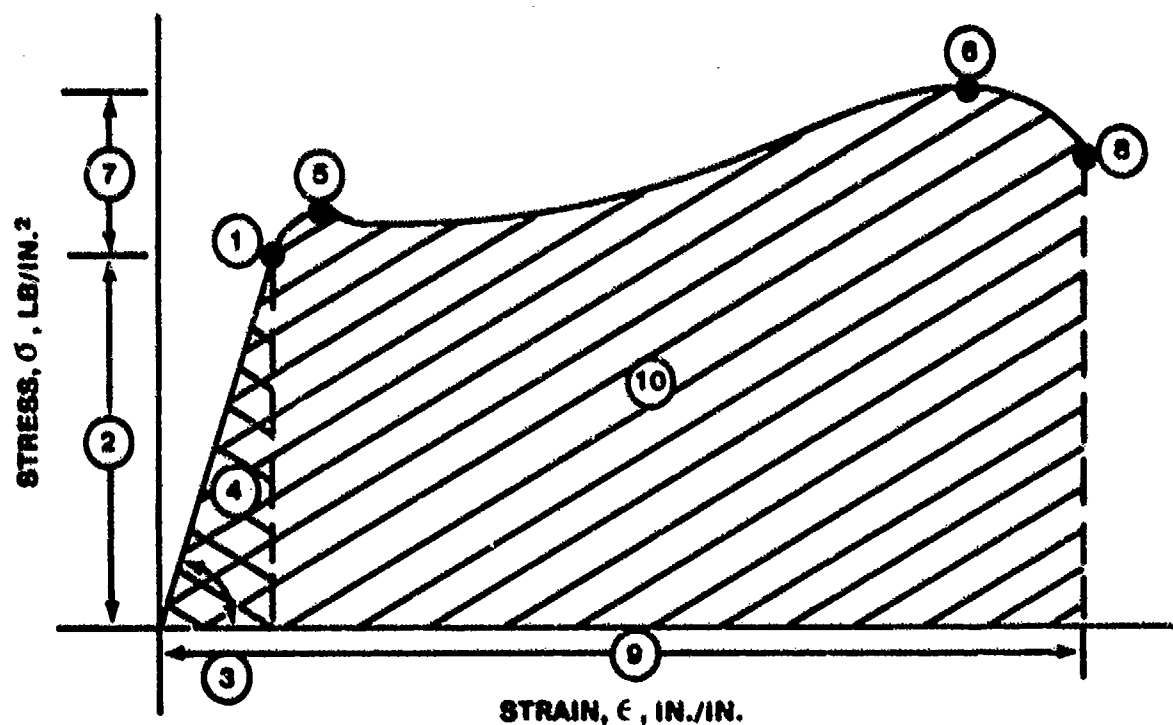

FIGURE 12.56. STATIC STRENGTH PROPERTIES

(1) The proportional limit is the stress which denotes the end of proportionality between stress and strain. If not clearly defined, 0.0001 in/in offset is used.

(2) The elastic range of stress is the range of stress and strain up to the proportional limit.

(3) The Modulus of Elasticity is the slope of the straight line portion of the stress-strain diagram. This slope measures inherent stiffness. Beyond the proportional limit, the Secant or Tangent Modulus will be appropriate.

(4) The resilience is measured by the area under the straight line portion of the stress-strain diagram. This indicates ability to store energy elastically.

(5) The yield stress is the value of stress above which objectionable amounts of permanent strain are incurred. If not clearly defined, 0.002 in/in offset is used.

(6) The ultimate strength is the very highest stress that the material can withstand without failure. This represents the maximum load-carrying capability for static loads.

(7) The plastic range of stress is between the proportional limit and the ultimate stress. Permanent strains occur in this area. Below the yield stress these permanent strains are relatively small and insignificant; above the yield stress these permanent strains are large and objectionable.

(8) The fracture point is the effective stress at time of failure. It is noted primarily to evaluate the manner of failure and the ductile quality of the material.

(9) The total elongation is a measure of ductility. If less than five percent in a two inch specimen length, the material is considered brittle.

(10) The toughness of a material is represented by the total area under the stress-strain diagram. This indicates the amount of work required to fail the material and denotes energy absorption capability.

An interesting phenomenon in connection with the stress-strain diagram is "work hardening" or "strain hardening". Suppose that a material is subjected to a stress beyond the yield point and then released. If stress is subsequently reapplied, the new stress-strain diagram will be a straight line up to the point where stress was released and then it continues along the original curve. Figure 12.57 illustrates this process. The material which
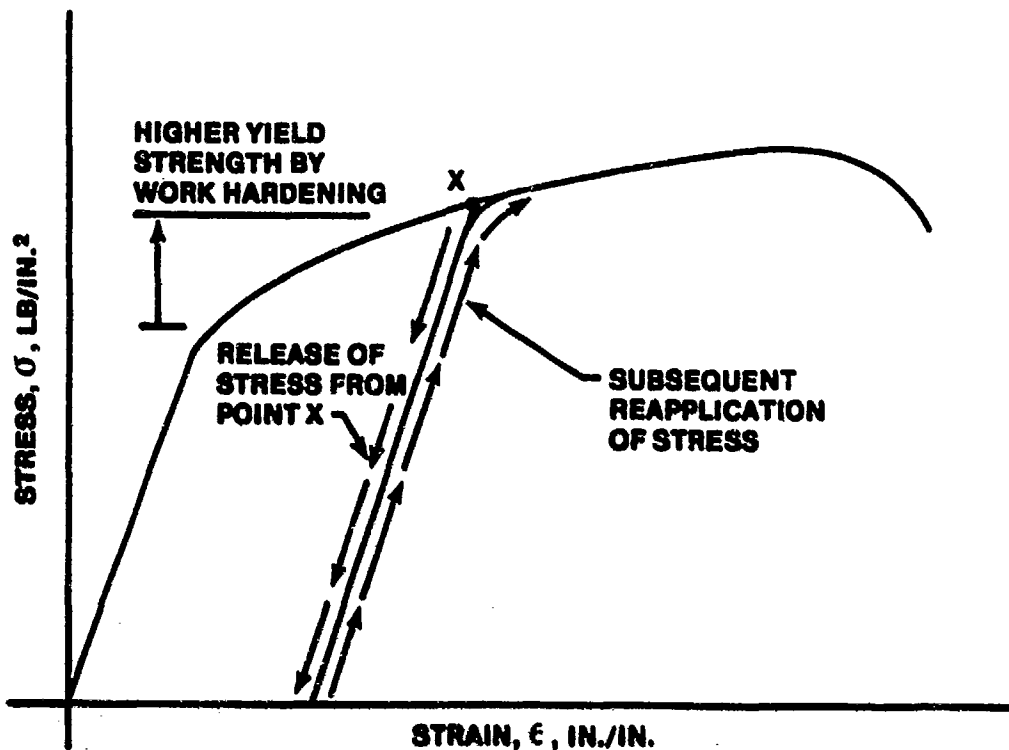
FIGURE 12.57. WORK HARDENING

has been permanently stretched will then have higher proportional and yield strengths. Many of the typical aircraft materials - aluminum alloys, stainless steels, etc. - are work hardened to produce these beneficial gains in strength properties. Of course, the work hardening must be limited to prevent loss of ductility and the formation of flaws and fissures.

The effects of ductility and the plastic range of stress are quite significant in predicting the failing load of a structure. The ultimate stress has been defined previously at the maximum stress a material will withstand without failing. This stress is designated as the "tension ultimate" (σ_{t_u}) or "shear ultimate" (σ_{s_u}) depending on the manner of loading and is determined by tests of small specimens. If these values of strength are used to predict the ultimate strength capability of large sections in bending and torsion, noticeable errors may result. An elastic stress distribution in bending may be predicted by the following relationships:

$$\sigma_b = \frac{My}{I}$$

where σ_b = bending stress, lb/in^2

M = applied bending moment, in-lb

y = element distance from neutral axis, in

I = moment of inertia of the cross-section, in^4

Such stress distribution is linear - varying directly with the element distance from the neutral axis, y. A typical elastic stress distribution is shown in Figure 12.58. Whenever stresses are produced which are beyond the proportional limit of the material, the bending stress distribution tends to remain linear but due to the loss of proportionality between stress and strain in the plastic range, the stress distribution is non-linear. Figure 12.59 shows a typical stress distribution resulting from bending loads which create stresses in excess of the proportional limit.

Notice that for a given maximum stress at the outer fiber, the inelastic bending stress distribution requires a greater applied bending moment than the elastic stress distribution. The reason for this is that the outer fibers begin to yield allowing the underlying fibers to develop a stress higher than predicted by elastic theory. Thus, the use of the equation
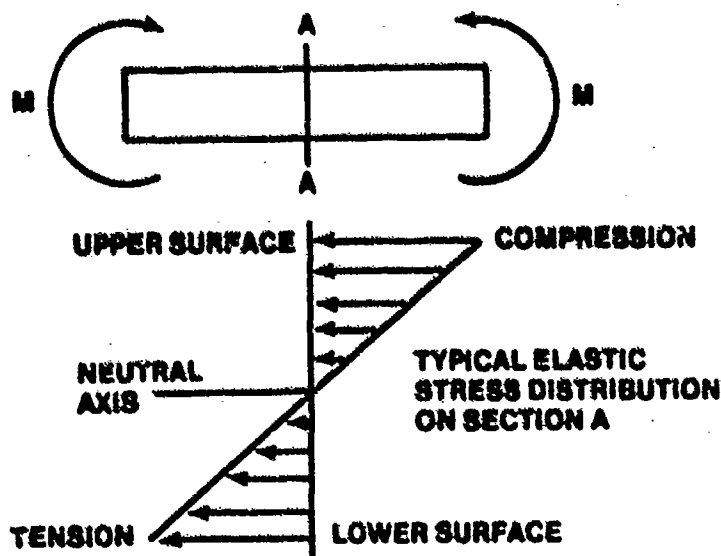
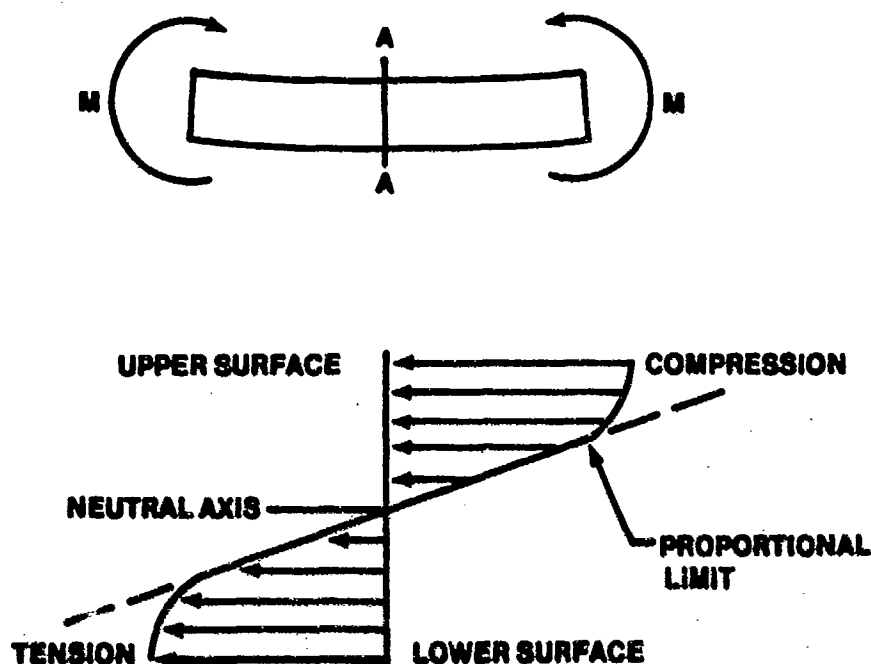FIGURE 12.58. ELASTIC STRESS DISTRIBUTION

FIGURE 12.59. PLASTIC (NON-LINEAR) STRESS DISTRIBUTION

$$\sigma_b = \frac{Mc}{I}$$

to compute the maximum bending stress is valid only for maximum stresses which do not exceed the proportional limit. In order to predict the failing load of a structure in bending, the same form of equation may be used with a fictitious ultimate stress referred to as the "bending modulus of rupture", σ_b. This bending modulus of rupture is defined by the following equation:

$$\sigma_b = \frac{M_b c}{I}$$

where σ_b = bending modulus of rupture, lb/in^2

M_b = bending moment to cause failure, in-lb

$$c \;=\; \text{distance to critical outermost element, in.}$$

$$I \;=\; \text{section moment of inertia, in}^4$$

If the material is ductile and no buckling of the section occurs, the bending modulus of rupture will be some value greater than the tensile ultimate strength. In a perfectly ductile, stable cross-section the bending modulus of rupture could be 1.5 times the tensile ultimate; in a very brittle, stable cross-section the bending modulus of rupture would be equal to the tensile ultimate. If the cross-section is composed of thin walled unstable elements which are apt to buckle, the bending modulus of rupture may be much less than the tensile ultimate strength. The bending modulus of rupture is obviously dependent upon the type of material (especially ductility) and the shape or form of the cross-section.

An analogous situation exists for sections subjected to torsion loading and is due to the form of the cross-section and the character of the material. In order to predict the failing torsion load of a structure, another fictitious stress is used which is referred to as the "torsion modulus of rupture", σ_{s_t}. This torsion modulus of rupture is defined by the following equation:

$$\sigma_{s_t} \;=\; \frac{M_{t_b}\, C}{J}$$

where σ_{s_t} = torsion modulus of rupture, psi

M_{t_b} = torque or moment to cause failure, in-lb

c = distance to critical outermost element, in

J = polar moment of inertia of cross-section in^4

If a metal is subjected to a stress in the plastic range, the strain will continue to change in the direction of stress although the stress is held constant. This is a condition which is most common to metals at high stresses and high temperatures and the phenomenon is known as "creep". Figure 12.60 is a typical creep curve for a metal at a constant stress and temperature.
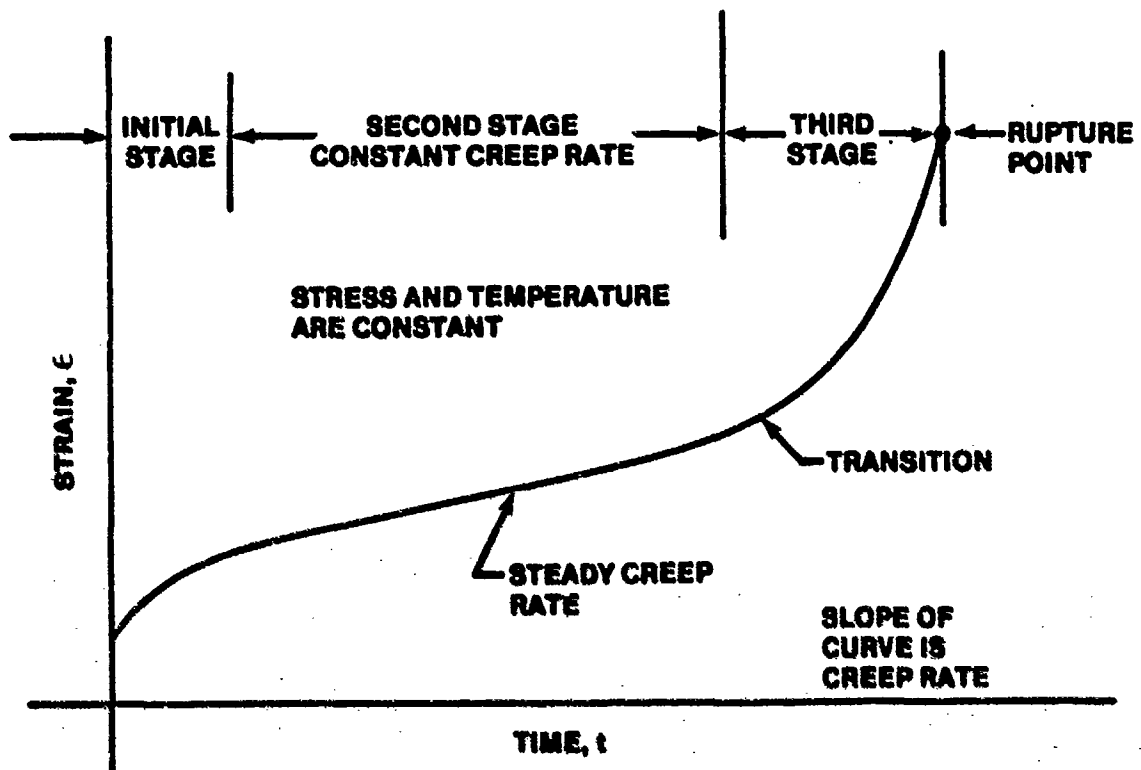
FIGURE 12.60.   CREEP CURVE FOR A METAL AT CONSTANT STRESS AND TEMPERATURE

Upon the application of stress, a high initial creep rate will develop, then decrease to the minimum value of steady creep. During the second stage the creep rate is essentially constant. After a period of time the third and final stage of creep will take place with an increase in creep rate and final rupture. Since the stress to cause rupture varies inversely with time and temperature, creep problems are of the greatest importance in light weight, high temperature structures.

In the design of high temperature structures the amount of deformation allowable may be a more severe criteria than actual rupture strength. This would be the case for components which - if excessively strained - would not function properly or would fail at loads lower than normally anticipated.

Stress-strain diagrams for a material may be greatly altered when the rate of stressing is very high. When stress is applied very suddenly (almost instantaneously) the result is "impact" stresses. The amount of energy absorbed under impact conditions may be significantly different from the

energy absorbed when the load is applied steadily and gradually. The actual speed or rate at which a material is stressed will determine what changes in energy absorption take place. In the case of an ordinary structural material, an increase in the rate of stressing (above that of very gradual load application) will initially produce a slight increase in the energy absorbed. With continued increase in rate of stressing, a "critical speed" will be reached and the energy absorbed will be at maximum. Above this speed the toughness will be greatly reduced. If the stress-strain diagrams for impact stressing were recorded and compared with the stress-strain diagram obtained from gradual load application, the result would be similar to Figure 12.61.
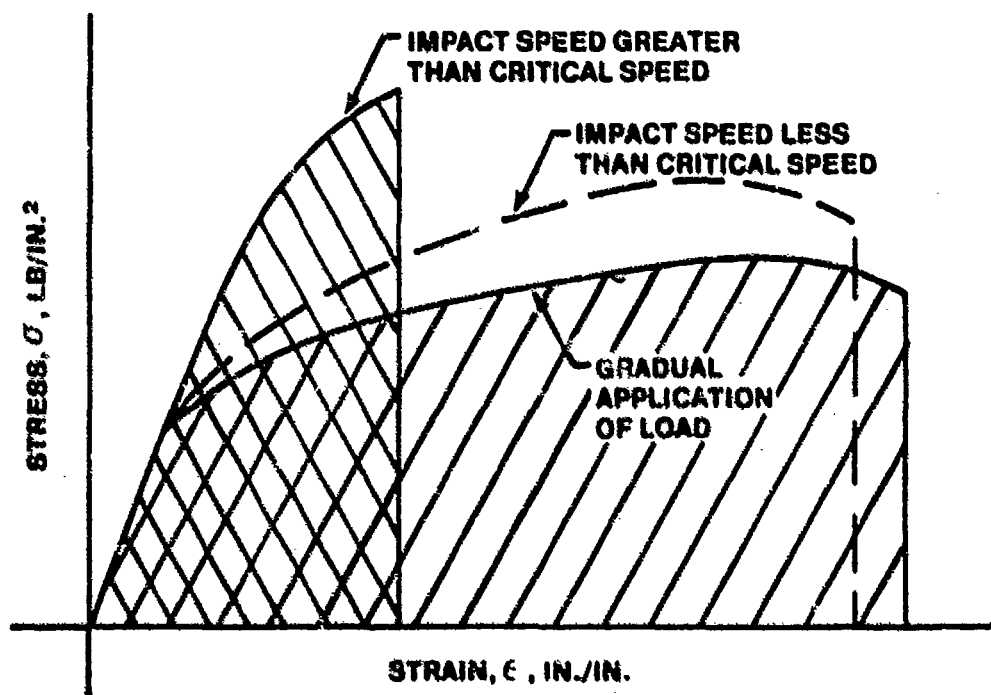

FIGURE 12.61.   EFFECTS OF APPLICATION RATE ON STRESS

When stress is applied above the critical speed, the failing stress would be higher but the elongation would be greatly reduced. In fact, the effect of impact stresses beyond the critical speed is to produce brittle type failures in tough or ductile materials. On the other hand, a brittle material will not show any great effect of high stress rates since there is very little ductility or energy absorbing capability for gradually applied loads.

While impact stresses near the critical speed are not ordinarily encountered in airframe structures, due consideration must be given to the case of dynamic machinery and mechanisms. The effect of impact stresses is most important when there are severe discontinuities in the shape of a part or when a part is operated at low temperatures.

Figures 12.62-12.69 are illustrations of failure of different types of materials under tension, torsion or shear.
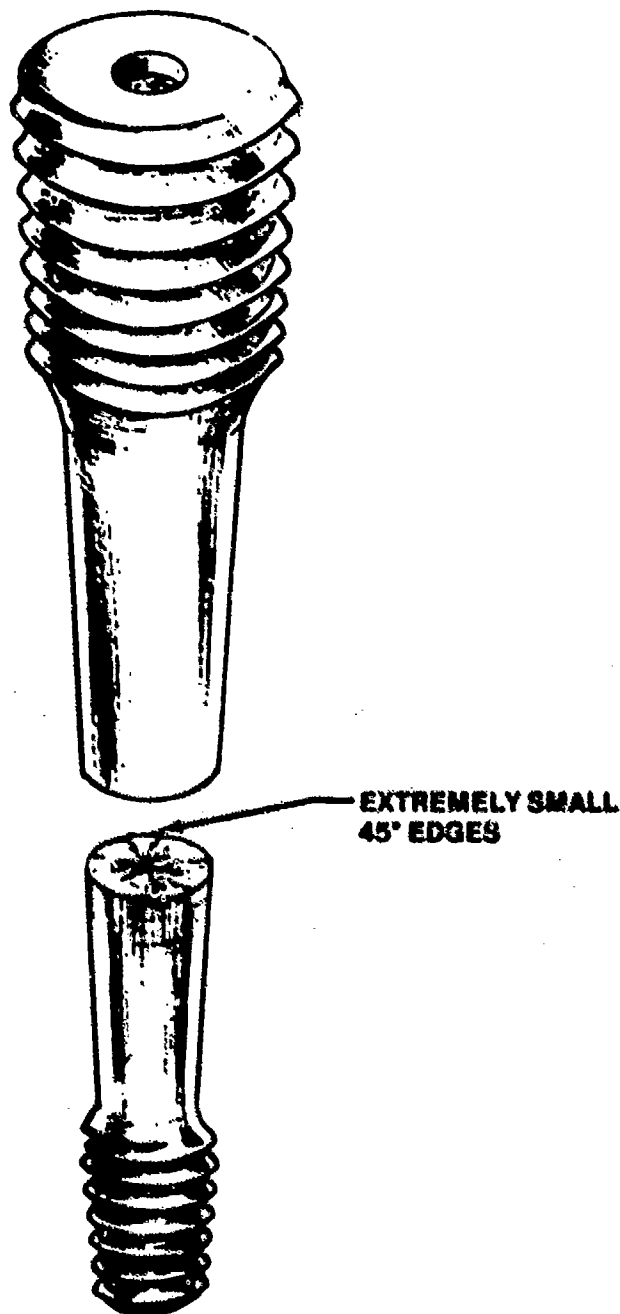

EXTREMELY SMALL 45° EDGES

FIGURE 12.62. BRITTLE TENSION FAILURE

ROUGH GRANULATED
TENSION TYPE ZONE

P CONE
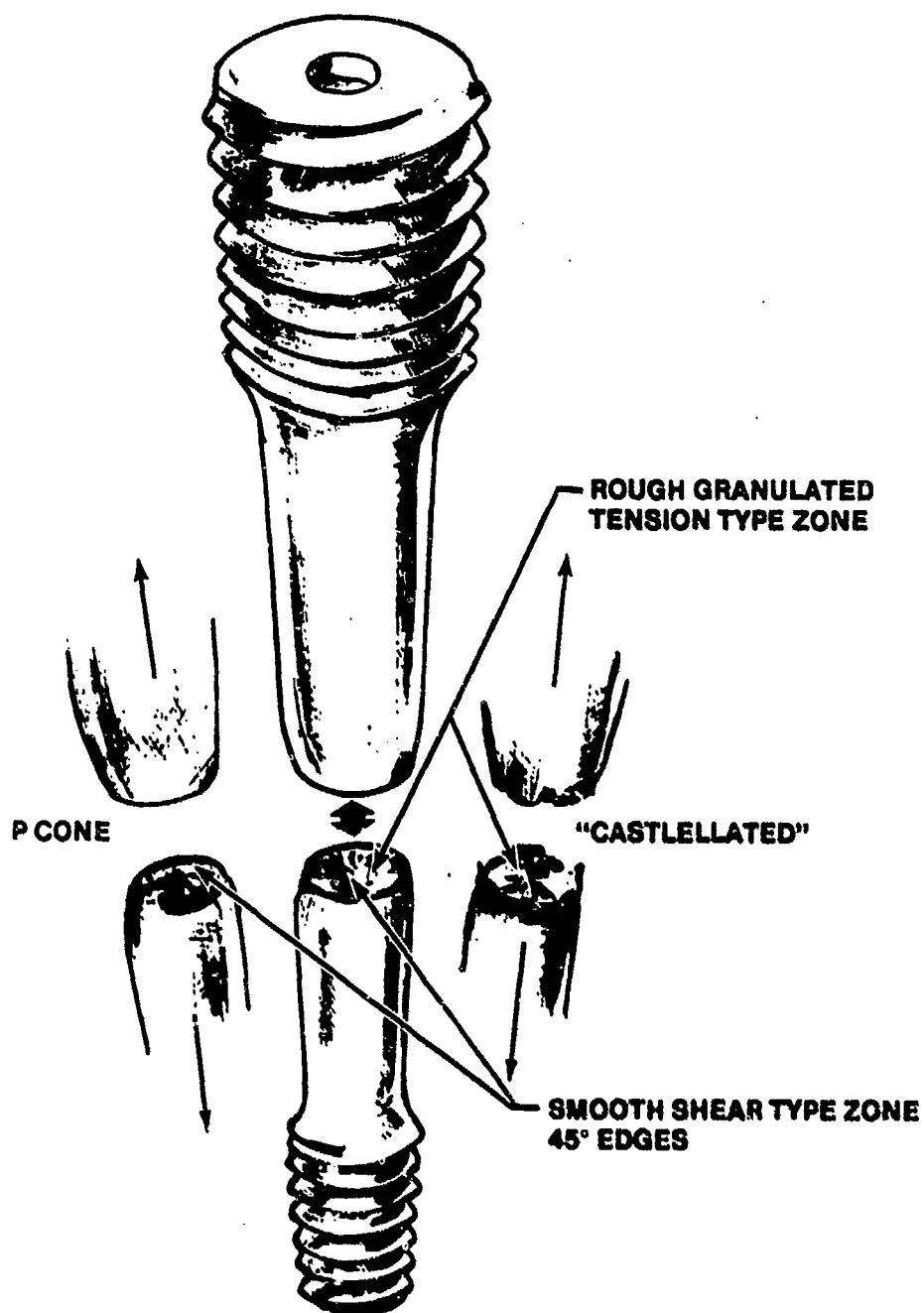
"CASTLELLATED"

SMOOTH SHEAR TYPE ZONE
45° EDGES

FIGURE 12.63. MEDIUM DUCTILITY TENSION FAILURE
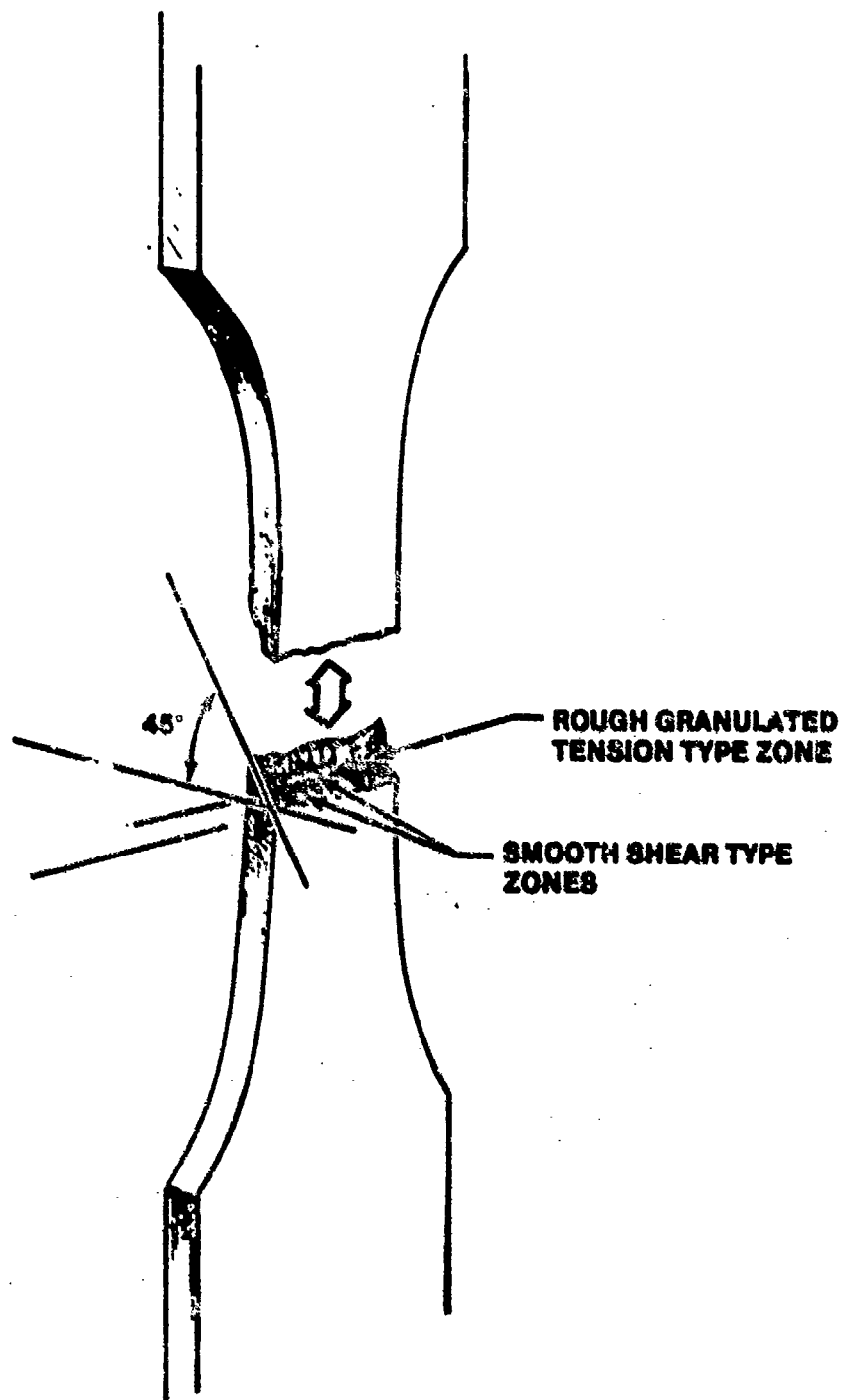
FIGURE 12.64.   HIGHLY DUCTILE TENSION FAILURE SHEET OR THIN BAR STOCK
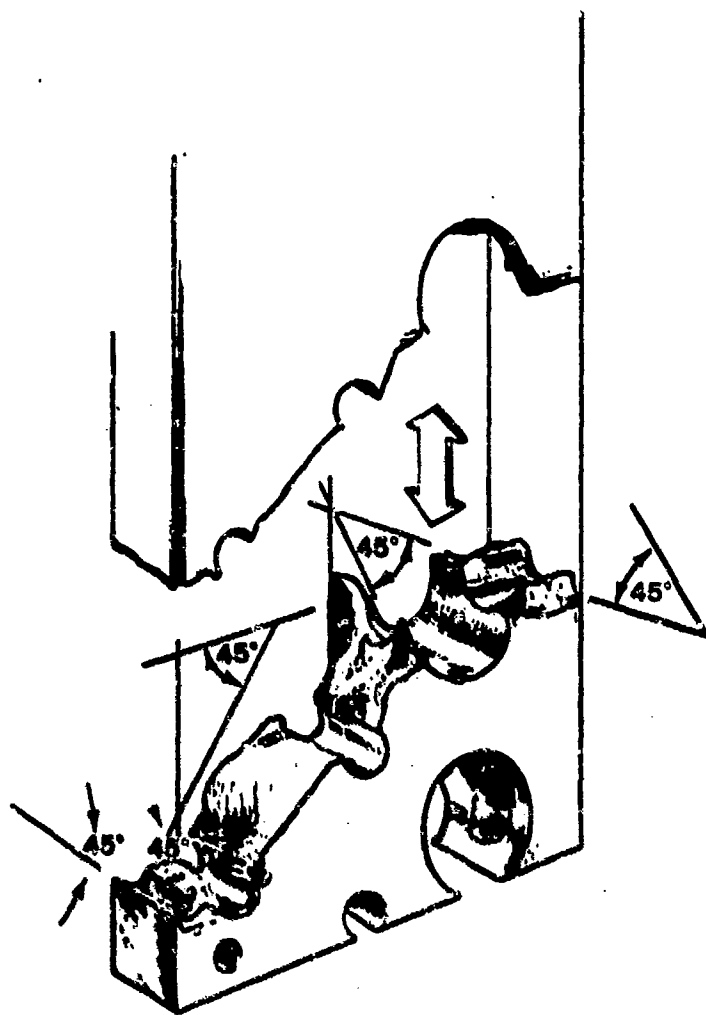
FIGURE 12.65. TYPICAL TENSION FAILURE DUCTILE AIRCRAFT MATERIAL

DUCTILE

SMOOTH SURFACE
SHEAR TYPE

FAINT CONCENTRIC
CIRCLES

ROUGH GRANULATED
TENSION TYPE ZONE

BRITTLE
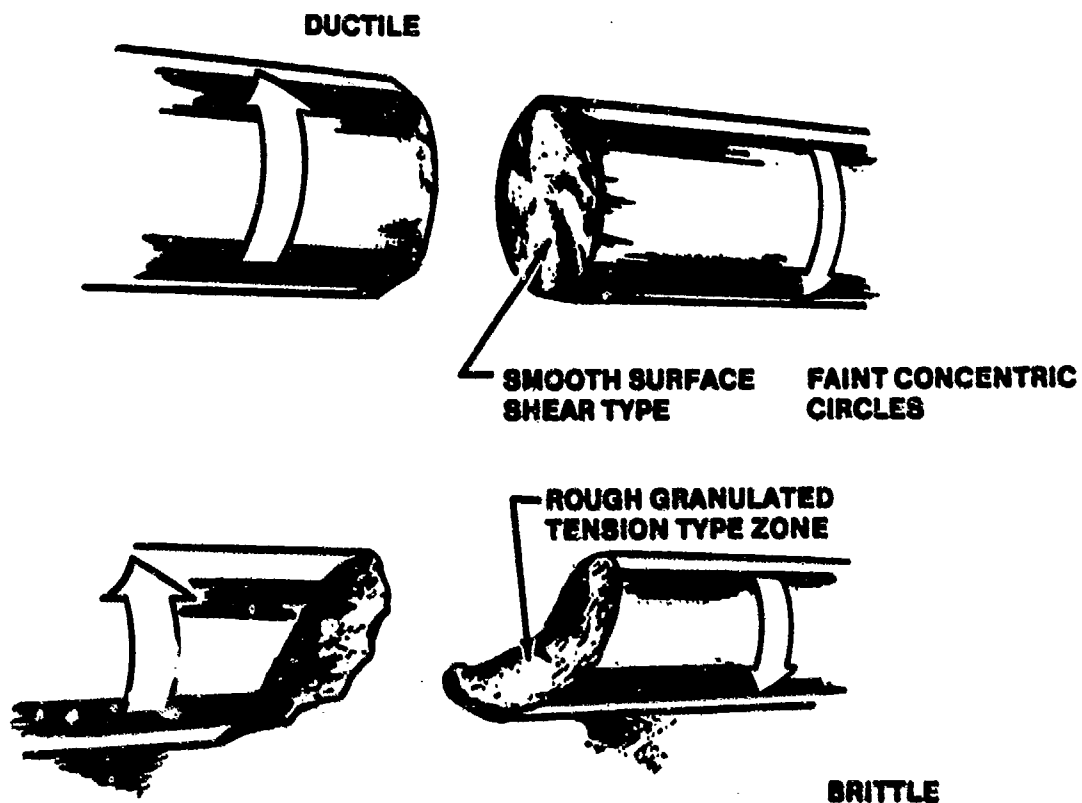
FIGURE 12.06.   TORSION FAILURE
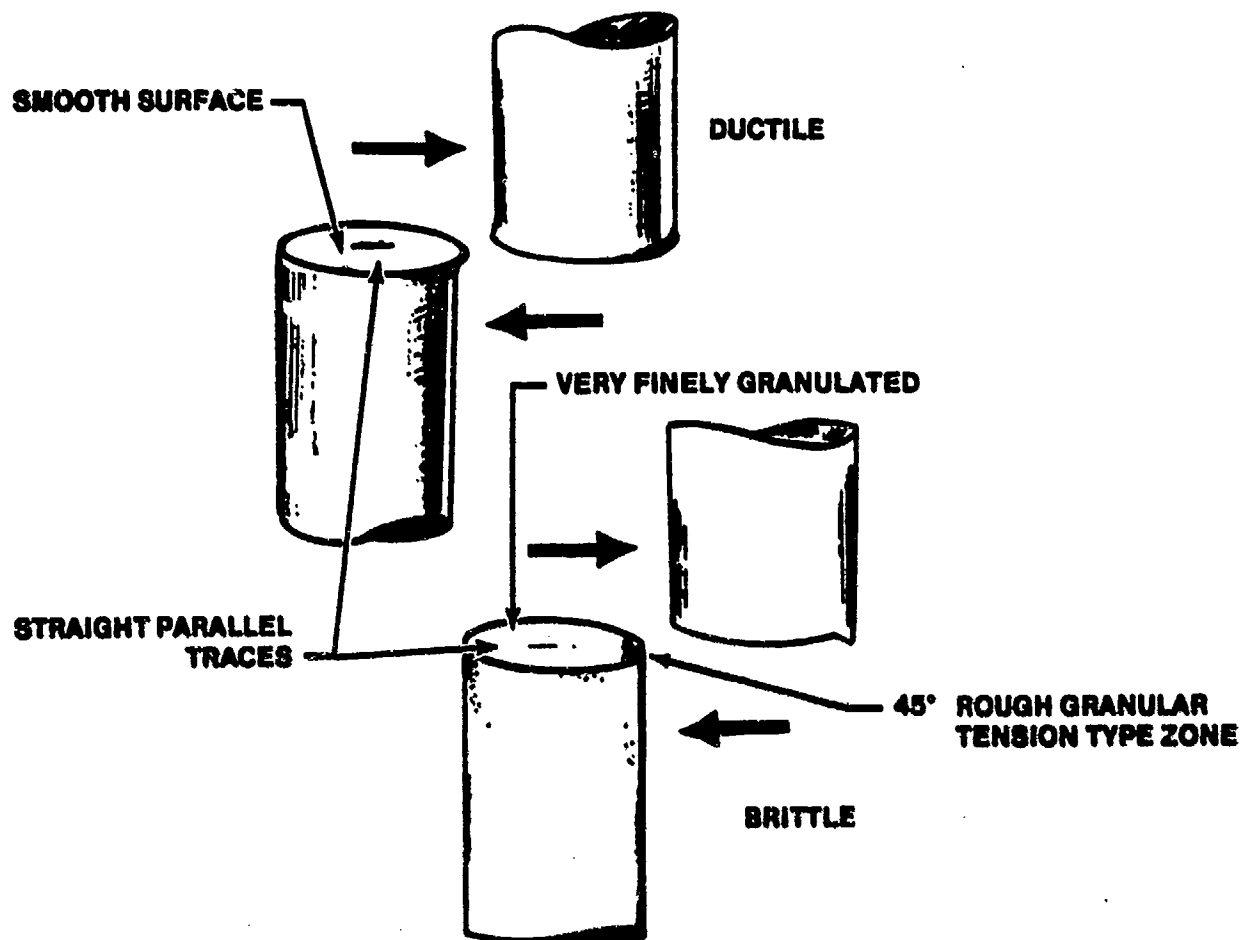
FIGURE 12.67.   SHEAR FAILURE

45° BUCKLES DUE TO RESOLVED COMPRESSION
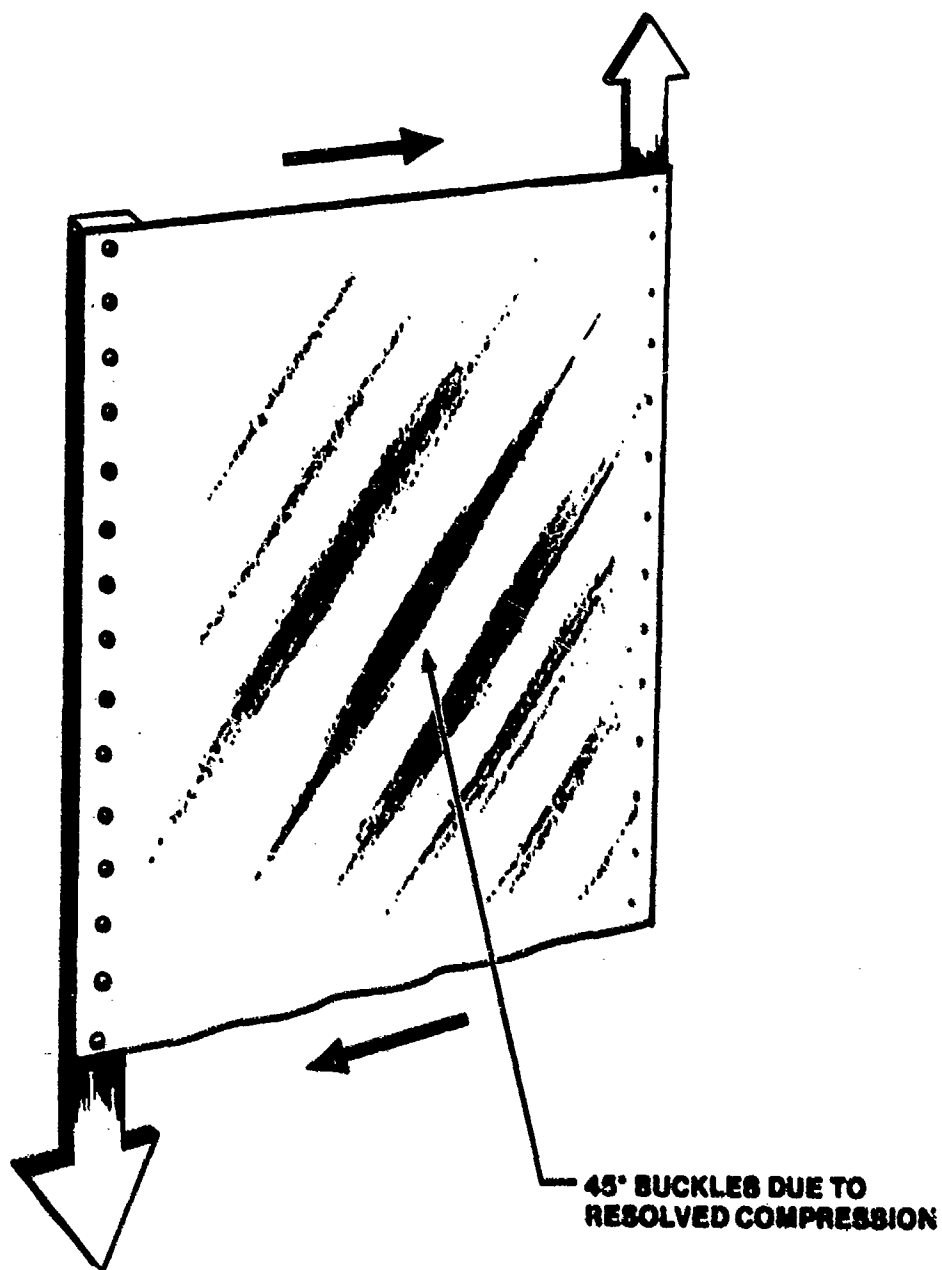
FIGURE 12.68.   SHEAR IN PANELS COMPRESSION TYPE FAILURE
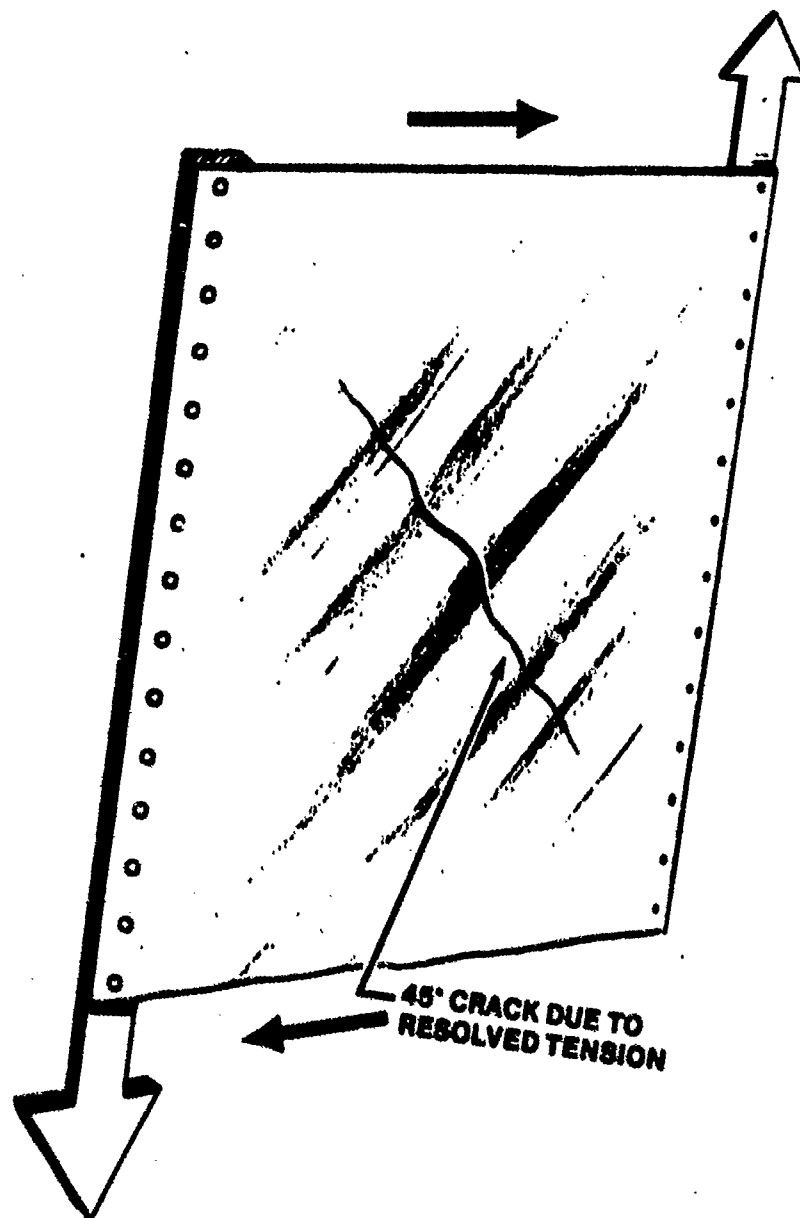
FIGURE 12.69. SHEAR IN PANELS TENSION TYPE FAILURE

45° CRACK DUE TO
RESOLVED TENSION

12.5 AEROELASTICITY

12.5.1 INTRODUCTION AND DEFINITIONS

Except for a few isolated examples in the TPS curriculum, the aircraft has been treated as a rigid body. That is, no bending, twisting, or deformations were assumed to occur on the structure in the definition and derivation of the performance and stability characteristics. For example, lateral bending of the fuselage was ignored in determining the steady straight sideslip equations. Or the effects of wing bending and subsequent load redistribution were not taken into account in the lift, drag, and moment equations.

In reality, though, airplanes deform under aerodynamic loads. These effects can be significant, especially in high speed lightweight aircraft at high maneuvering accelerations, or in the large category aircraft such as the C-5A, Boeing 747 or Lockheed L-1011 during normal flight conditions. The degree to which the analytical computations are affected is dependent upon flight conditions. However, aeroelastic effects must be included in any precision analysis. We therefore must treat the stability derivatives as functions of dynamic pressure (q), as well as Mach (M) and angle of attack (α). Designing and building a totally rigid airplane is not practical because of the weight penalty (the development of lightweight composites has lessened the problem somewhat but high cost becomes a major factor in that area). The designer is thus faced with the dilemma of conflicting requirements for lightweight (for improved aircraft performance) versus structural rigidity (to preclude aeroelastic effects).

The study of aeroelasticity is important, therefore, simply because the aeroelastic problem is a reality. A decision has to be made as to how much rigidity can be sacrificed before the bending, twisting and inertial effects of the structure restrict the performance and handling qualities. Is there assurance that catastrophic structural failure will not occur somewhere in the aircraft's flight regime?

Aeroelasticity is often defined as the science which studies the mutual interaction between aerodynamic, elastic and inertial forces of an airplane in flight. Again, the phenomenon would be nonexistent if aircraft structures were perfectly rigid but the weight/cost penalties for that privilege would be too severe. By itself, structural bending or flexibility is not

objectionable. The problems arise when the deformations in turn cause changes in the aerodynamic forces. If the deformations and aerodynamic forces vary rapidly, inertial forces become important.

In 1946, A.R. Collar presented a paper to the Royal Aeronautical Society that ingeniously classified problems in aeroelasticity by means of a triangle of forces. Referring to Figure 12.70, the three types of forces (aerodynamic, elastic, and inertial) are placed at the vertices of a triangle. Each aeroelastic phenomena can be located on the diagram according to its relation to the three vertices. For example, dynamic aeroelastic phenomena such as flutter, F, lie within the triangle, since they involve all three types of forces and must be bonded to all three vertices. Static aeroelastic phenomena such as wing divergence, D, lie outside the triangle on the upper left side, since they involve only aerodynamic and elastic forces. Although it is difficult to define precise limits in aeroelasticity, the classes of problems connected by solid lines to the vertices are usually accepted as principal ones. Of course, other borderline fields can also be placed on the diagram. For example, mechanical vibrations, V, and rigid body aerodynamic stability, DS, are connected by dotted lines. It is very likely that in certain cases the dynamic stability problem is influenced by aircraft flexibility and it would therefore be moved within the triangle to correspond with DAS, where it would be regarded as a dynamic aeroelastic problem.

Collar's Aeroelastic Triangle (or more completely "Aeroinertia-Elastic" Triangle) was revised to a tetrahedron some 15 years later by I.E. Garrik to include Aerothermoelasticity, Figure 12.71. Aerodynamic thermal effects associated with high-speed flight vehicles introduce deformations, streses, and changes in material properties that can greatly extend the field of aeroelasticity. This chapter will not formally address Aerothermoelasticity, except to introduce it as an influencing factor of aeroelasticity in high-speed flight.

Static Aeroelastic Phenomena:

These phenomena are the ones which are concerned with steady state (i.e. non-oscillatory) aerodynamic loads, and the associated steady state distortion. Static implies the absence of inertial forces, thus it requires only coupling between the aerodynamic and elastic forces of the aircraft. It includes the following classical cases:

A: AERODYNAMIC FORCE   AEROELASTIC PHENOMENA
E: ELASTIC FORCE
I: INERTIAL FORCE

                         F: FLUTTER
                         B: BUFFETING
RELATED FIELDS   Z: DYNAMIC RESPONSE
                         L: LOAD DISTRIBUTION
V: MECHANICAL VIBRATIONS   D: DIVERGENCE
DS: DYNAMIC STABILITY   C: CONTROL EFFECTIVENESS
                         R: CONTROL SYSTEM REVERSAL
                         DSA: AEROELASTIC EFFECTS ON DYNAMIC STABILITY
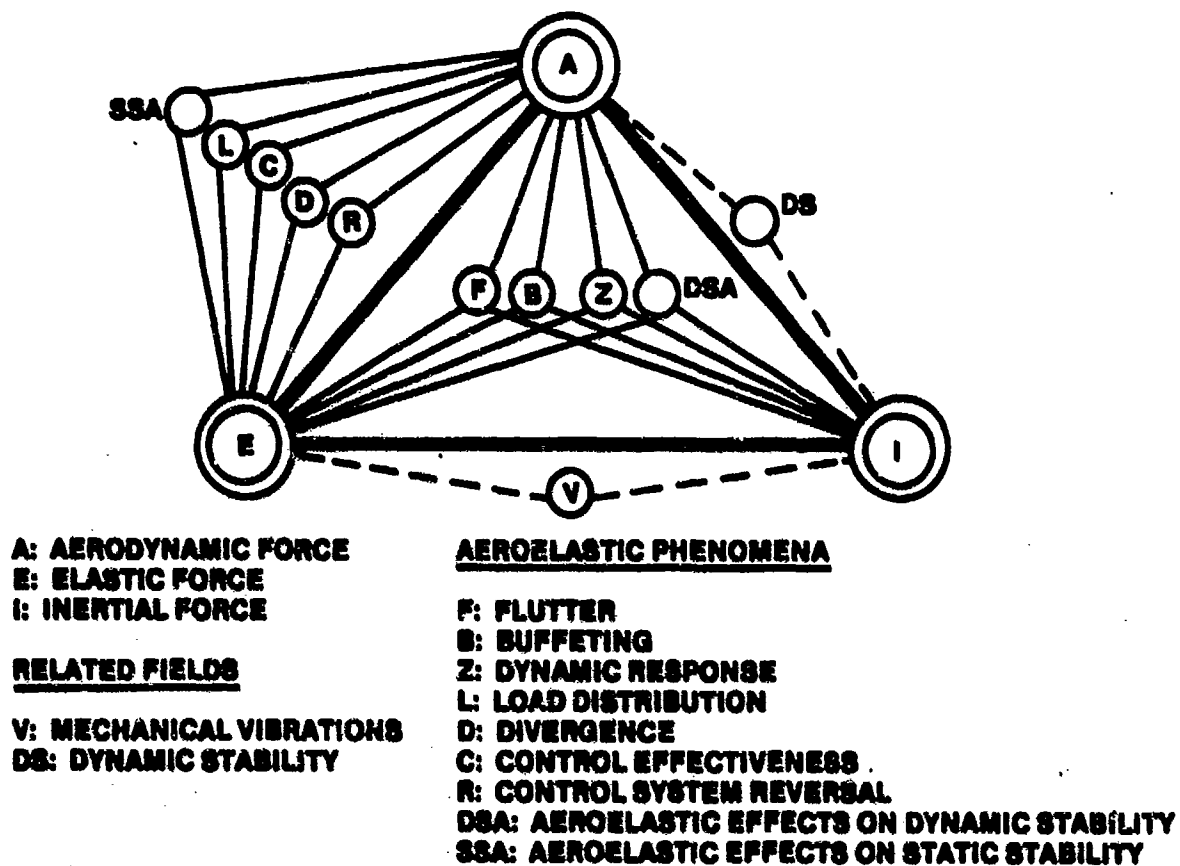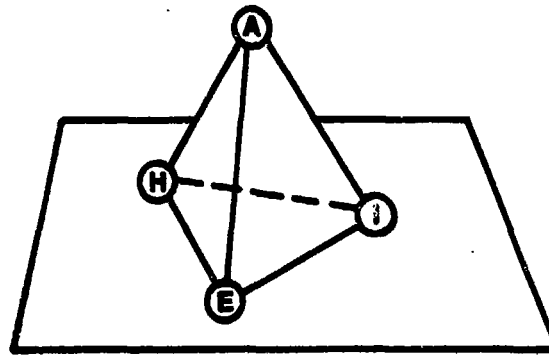   SSA: AEROELASTIC EFFECTS ON STATIC STABILITY

FIGURE 12.70. COLLAR'S AEROELASTIC TRIANGLE OF FORCES

A: AERODYNAMIC FORCE
E: ELASTICITY FORCE
I: INERTIA FORCE
H: HEATING

FIGURE 12.71.   TETRAHEDRON OF AEROTHERMOELASTICITY

Aeroelastic Effects on Static Stability, SSA.   As the aerodynamic and
elastic forces combine, the deformations of the structure can be of
sufficient magnitude to influence the static stability derivatives.

Load Distribution, L.   Influence of elastic deformation of the structure
on the distribution of aerodynamic pressures over the structure.

Control Effectiveness, C.   This phenomena attempts to evaluate the
influence of the elastic deformations on the controlability of the
aircraft.

Torsional Divergence, D.   A static instability of a lifting surface at a
speed U_D called the divergence speed where the elasticity of the lifting
surface plays an essential role in the instability.   At a speed slightly
above the wing divergence speed, the elastic restoring moment about a
spanwise with elastic axis can no longer balance the aerodynamic moment
created by the airloads.

Control Reversal, R.   A condition occurring in flight at a speed called
the control reversal speed, where the intended effects of displacing a
control surface are nullified by the elastic deformations of the
structure.   For example, a right roll aileron deflection may result in a
roll to the left because of a wing twist caused by the deflected
ailerons.   The B-47 for example exhibited an aileron control reversal
phenomena at .80 Mach.

Dynamic Aeroelastic Phenomena:

In dynamic aeroelastic problems, we are concerned with the oscillatory
motion of various parts of aircraft, and particularly interested in the
conditions under which these oscillatory modes tend to diverge (increase in
amplitude), because this may result eventually in the structural failure.   As
mentioned previously, dynamic aeroelastic phenomena are the interaction

between aerodynamic, inertial, and elastic forces. Some examples of this problem are:

Flutter, F. A self-excited dynamic instability of the structural components of an aircraft, usually involving the coupling of separate vibration modes, where the forcing function for oscillation is drawn from the airstream. The coupling of the bending and twisting modes of a wing results in a bending-torsional wing flutter. Other examples of flutter modes are: wing-aileron, tail-fuselage, and bending-torsion-aileron. Simply stated, flutter is the dynamic instability of an elastic body in an airstream. Flutter speed U_F and corresponding frequency are defined as the lowest airspeed and frequency where a flying structure will exhibit sustained, simple harmonic oscillations.

Buffeting, B. Transient vibrations of aircraft structural components due to aerodynamic impulses produced by the wake behind wings, nacelles, fuselage pods, or other components of the airplane. The problem can be serious in fighter aircraft during maneuvering to $C_{L_{max}}$ at high speed, often resulting in rugged transient vibrations on the tail due to aerodynamic impulses from the wing wake. Since these impulses are quite random there is no analytic theory to adequately describe the phenomenon. Cures are usually made as necessary by proper positioning of the tail assembly.

Aeroelastic Effects on Dynamic Stability, DSA. Changes in an aircraft dynamic stability can result due to elastic bonding, twisting, or deformation of its structure (e.g., the changes in the short period frequency and damping due to fuselage bending).

Mechanical Vibration, V. A mechanical vibration of the airplane structure mainly due to the coincidence of a powerful engine harmonic with an airframe frequency. Aerodynamic interaction may not be necessary.

It should be noted from the above discussion that flutter and divergence corresponded to conditions of aeroelastic instability, and that speeds beyond the critical flutter and divergence speeds will result in an eventual structural failure. However, control reversal is not a condition of instability, and speeds beyond control reversal speed will result only in a reversal of the action of the control system and not necessarily in a failure of the structure. Control effectiveness influences maneuverability, and it is important that the control system designer has a thorough understanding of this phenomena.

Thus, the three critical airspeeds involving aeroelasticity are flutter (U_f), divergence (U_D), and aileron reversal (U_R) speeds. In the early design

stages of an aircraft, the comparative values of these speeds must be completely analyzed. Figure 12.72 shows the relation between the critical speeds for a typical wing with varying amounts of forward and backward sweep.
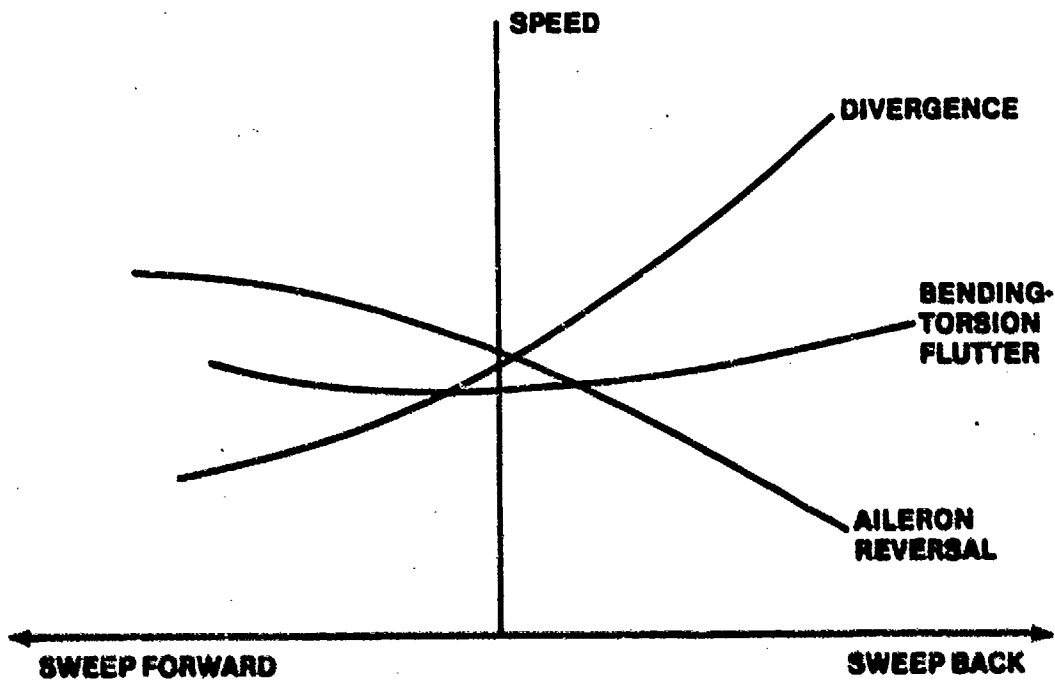

FIGURE 12.72. EFFECT OF WING SWEEP ON CRITICAL SPEEDS

12.5.2 Historical Background

Aeroelastic problems were relatively unknown until World War II. Prior to that time, aircraft speeds were relatively low and the load requirements and lack of design refinements produced an aircraft structure rigid enough to preclude most aeroelastic phenomena. Except for the time spans of the two World Wars, aircraft top speeds had increased approximately 19 knots per year from 1910 to 1955. As the speed of aircraft began to increase with no increase in load or stiffness requirements, the designers and pilots began to encounter problems associated with aeroelasticity.

When airplanes were first built there were no logical stiffness criteria for design. Hence, increasing speeds led to the wide variety of aeroelastic problems. Control surface flutter first occurred at about 110 knots; wing

flutter started at around twice that speed. The strength questions posed by the speed increase were solved partly by material developments and partly by constructional techniques, but not before many in-flight failures had occurred.

Samuel P. Langley was probably the first airplane designer affected. His misfortune occurred just prior to the Wrights' first flight. During the launch of Langley's monoplane off the Potomac River houseboat, catastrophic wing divergence occurred. His failure with the monowing and the Wrights' success with the biplane, combined with the lack of a torsional stiffness criterion for the monowing, resulted in the favoring of the dual wing design during the early period. The partiality was understandable since no designer wanted to over-stiffen the wing at the expense of added weight.

Although a few externally braced monoplanes were built prior to World War I, military monoplane design virtually stopped between 1917 and the mid-thirties. During the biplane era, the most common aeroelastic problem was tail flutter. One of the first documented cases occurred on the tail of the British twin-engined Handley Page 0/400 bomber at the start of the first war. The noted aerodynamicists Lanchester and Bairstow investigated the reasons for the flutter incidents and the following is a quote from Lanchester's report:

> "The difficulty experienced is that at certain critical speeds of flight a tail wobble is set up, involving heavy torsional stresses on the fuselage, the type of vibration being an angular oscillation approximately about the axis of the fuselage; I am informed that the angular magnitude of this oscillation amounts at times to something approaching 15°, and is undoubtedly extremely dangerous to the structure of the machine. I gather that the experience of the pilots when this vibration is at its worst is terrifying."

The problem was being caused by the coupling between the fuselage torsion mode and the anti-symmetrical elevator excitation mode. In the latter, the left and right elevators oscillated about their hinge lines in opposite phase. There was no interconnecting torque tube to prevent the occurrence. The other mode was merely the low frequency torsional oscillation of the aircraft fuselage. Since the vibrating frequencies of these two separate oscillatory modes were almost the same, a resonant coupling occurred, with the resulting tail wobble phenomenon. A same type of tail flutter problem was experienced by the DH-9 in 1917, resulting in several fatalities. The fix used then was

the same one used for the Handley Page bomber. It has been a design feature ever since for reversible flight control systems - the left and right elevators were connected with a stiff torque tube.

Wing problems appeared with the return of the monowing. Insufficient torsional rigidity led to divergence, loss of aileron effectiveness, and flutter. An early problem occurred on the Fokker D-8. The aircraft was built for WWI and due to superior performance was immediately placed in combat. Within a few days several wing failures occurred during high speed dives. The wing torsional stiffness criterion used in the initial design was the same as that previously used for biplanes.

The Army ran static strength tests and discovered that the wings were more than capable of withstanding the 6g design limit. Why then, the failures? Confronted with the dilemma, Fokker decided to conduct his own static tests. He found that although the wing did indeed have the design strength, under increasing loads the angle of incidence at the wing tips increased, relative to the roots: the necessary condition for divergence. In the high speed dives the air loads increased faster at the tips and the resulting torsion caused the wings to fail.

After the war, the U.S. Army encountered a violent but nondestructive case of wing-bending/aileron-rotation flutter on the same Fokker D-8. The cure for the problem, as with virtually any control surface type flutter, was mass balancing of the control surface.

The period of monoplane development, because of the accompanying resurgence of aeroelastic problems, initiated the first serious research in the field of aeroelasticity. Early day techniques were mainly cut-and-try. Many analytic theories were presented on wing load distribution, wing divergence, loss of lateral control and aileron reversal. Potential flow flutter analysis was sufficiently understood by 1935 to be incorporated into aircraft design but the majority of airplane designers were reluctant to trust the mathematicians to formulate criteria for the strength and rigidity of aircraft structural components.

From 1934 to 1937, the perennial arms race resulted in the development of many new types of aircraft. Numerous cases of flutter appeared, mainly of the wing or tail type. The accidents served to underscore the critical nature of mass distribution and control surface mass balancing. In 1938, a panel of

scientists boarded a four-engined Junker aircraft for an in-flight observation of a planned flutter test. All perished when a catastrophic condition occurred. The accident served due warning to the community of the difficulties and hazards of flight flutter testing.

With the development of improved excitation and measuring equipment, and a better theoretical understanding of the nature of the flutter problem, flutter testing came of age during the late forties. Analytic predictions are still imprecise, but with improved model and wind tunnel technology, and with the tremendous surge in the development of the high speed computers, investigation of aeroelastic phenomena is becoming more and more a controlled science.

12.5.3 Mathematical Analysis

The mathematical treatment of aeroelastic phenomena is somewhat complex and tedious. It requires a knowledge of the structural properties of the vehicle and of the nature of the aerodynamic forces acting on the surface of the airplane. Many textbooks and other publications exist which treat the subject in thorough detail (References 12.1, 12.2, 12.10, and 12.11). This chapter will attempt to only touch upon the essential and basic ideas behind the mathematical formulation.

Specifically, we will look at wing torsional divergence, aileron reversal, and flutter. The first two are static phenomena and are not significant present-day problems. We treat them because they are easy to analyze and visualize. Flutter is always a primary design consideration and will therefore be treated in detail.

12.5.4 Wing Torsional Divergence

If a wing in steady flight is slightly perturbed, an aerodynamic moment will be induced which tends to twist the wing further. Since the structure's stiffness is independent of speed of flight, and the aerodynamic moment is proportional to the flight velocity squared, there may exist a critical speed at which the elastic stiffness of the wing is barely able to sustain the wing in its deformed state. This speed is called the divergence speed and the wing is said to be torsionally divergent.

More simply stated, wing divergence is the condition where the aerodynamic moment exceeds the elastic restoring moment in torsion. Figure 12.73 illustrates a typical cambered wing section moving with a flight speed U.

$$\alpha = \alpha_r + \theta$$
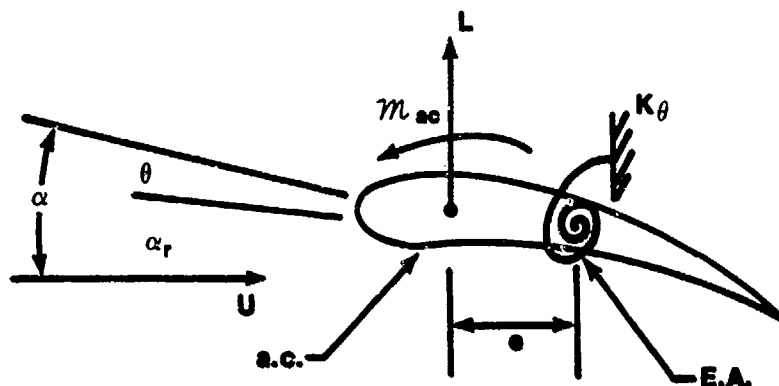
α_r = INITIAL ANGLE OF ATTACK (RIGID)

θ = ANGLE OF TWIST

FIGURE 12.73. CAMBERED WING SECTION

Acting at the aerodynamic center is the lift (L) and the moment about the a.c. (m_{ac}). The elastic restoring moment on the wing opposing the total aerodynamic moment is depicted by a linear coiled spring with spring constant K_θ attached at the elastic axis (E.A.) located a distance e behind the a.c. The elastic axis is defined as the axis about which the wing section would twist, subjected to pure moment. A vertical force applied at the E.A. would effect only a vertical deflection (bending). No twisting would result. For the sake of definition, the bending and twisting of a wing are illustrated separately in Figure 12.74.
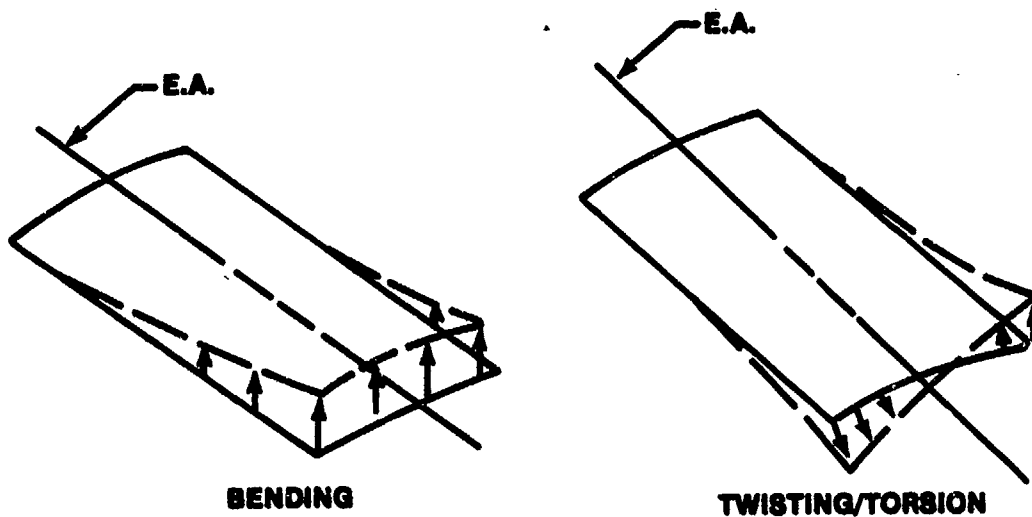
FIGURE 12.74. WING BENDING AND TWISTING

For the wing section in Figure 12.73, the angle of attack on the airfoil is composed of two parts: α_r, the angle of attack that a rigid wing would see, and θ, the angle resulting from elastic twist. At equilibrium, the aerodynamic moment about the elastic axis must equal the elastic restoring moment $K_\theta \theta$.

Aerodynamic moment about the elastic axis

$$\mathcal{M}_{AERO} = Le - \mathcal{M}_{ac} = K_\theta \theta$$

From subsonic aerodynamics, we know that

$$L = q \, S \, C_{L_\alpha} = q \, S \, C_{L_\alpha} (\alpha_r + \theta) \text{ and}$$

$$\mathcal{M}_{ac} = q \, S \, c \, C_{Mac}$$

Equating the moments,

$$K_\theta \theta = \mathcal{M}_{AERO} = Le - \mathcal{M}_{ac}$$

$$= qS \left[e\, C_L\, (\alpha_r + \theta) - c\, [C_{Mac}] \right]$$

Solving for the twist angle θ,

$$\theta = \frac{qS \left(e\, C_{L_\alpha}\, \alpha_r - c\, C_{Mac} \right)}{K_\theta - q\, Se\, C_{L_\alpha}} \qquad (12.30)$$

At the divergence condition the twist angle grows without bound (i.e., $\theta \to \infty$). This condition occurs mathematically when the denominator of Equation 12.30 equals zero.

$$K_\theta - q\, Se\, C_{L_\alpha} = 0$$

where $\quad q = q_D$ (Dynamic Pressure at Divergence)

$$q_{D_2} = \frac{\rho}{2}\, U_D^2 = \frac{K_\theta}{Se\, C_{L_\alpha}}$$

or, solving for the divergence speed U_D,

$$\boxed{U_D = \sqrt{\frac{K_\theta}{\frac{\rho}{2}\, Se\, C_{L_\alpha}}}} \qquad (12.31)$$

The design parameters affecting the divergence of straight wings are primarily the wing torsional stiffness (K_θ) and the offset distance e. Increasing K_θ is a costly process at the expense of considerable weight. An approach more frequently employed is to proportion the wing structurally so as to move the elastic axis forward. Aft wing sweep lessens the divergence problem since swept wing tip angles of attack are effectively reduced by wing bending.

If a real, three dimensional, wing were considered, the actual divergence speed must be obtained by integration across the span of the wing since local spanwise properties will vary.

12.5.5 Aileron Reversal

The aeroelastic problem of aileron reversal is closely related to wing torsional divergence in that both depend strongly upon the torsional stiffness of the wing. The history of this subject closely parallels that of wing torsional divergence; however, it was during World War II that the problem came into importance. The increasing speeds and the requirements for rolling performance precipitated the problem greatly. Following WW II, and with the advent of thin-wings, moderately high aspect ratio, and sweepback, the aileron reversal speed became of prime importance.

Aircraft with conventional planforms may suffer serious loss of aileron, elevator, and rudder control effectiveness due to elastic deformations of the structure. The aileron controls the rolling motion of an aircraft, and when placed downward, the lift over the wing is increased and a rolling moment is produced. The down aileron also produces a twisting moment on the wing which tends to twist the wing nose down and reduce the angle of attack and hence this reduces the rolling moment. A similar situation exists for the up aileron wing. The up aileron produces a torque which increases the angle of attack and decreases the effective rolling moment. Since the wing stiffness is independent of the flight velocity and the aerodynamic force ineffective in producing a rolling moment and the resulting wing segment twist and aileron deflection produce no effective change in lift. Beyond this critical speed, the effect of ailerons is actually reversed. This analysis also applies to the other control surface and is sometimes known as "Control Surface Effectiveness." Figure 12.75 shows how aileron effectiveness as measured by the ratio of rolling velocity to aileron angle is affected by forward speed for a WW II fighter-type aircraft at sea level.

Avoidance of aileron reversal in a straight wing with conventional ailerons is a matter of providing sufficient wing torsional stiffness. If the wing is swept back aileron reversal is a serious problem and wing bending stiffness must also be increased. This sometimes becomes prohibitively large in a weight analysis, hence, the other means are employed. Spoilers, fully moving wing tips, and even moving the aileron inboard all produce suitable means to combat this occurrence. Figure 12.76 shows that the aileron reversal speed can be increased by changing the configuration of the aileron controls. Additionally, this figure shows that control effectiveness can be increased

with decreasing sweepback. Inboard ailerons are used in the F-4, while the T-38 has ailerons at the semi-span position. Often aircraft are fitted with two sets of aileron surfaces, the outboard being locked out at high speeds and only the inboard ailerons being used for roll control. The cases of elevator and rudder control effectiveness and reversal are usually less critical than those of aileron, they are, however, more complicated due to the large deformations of the fuselage and attachments.
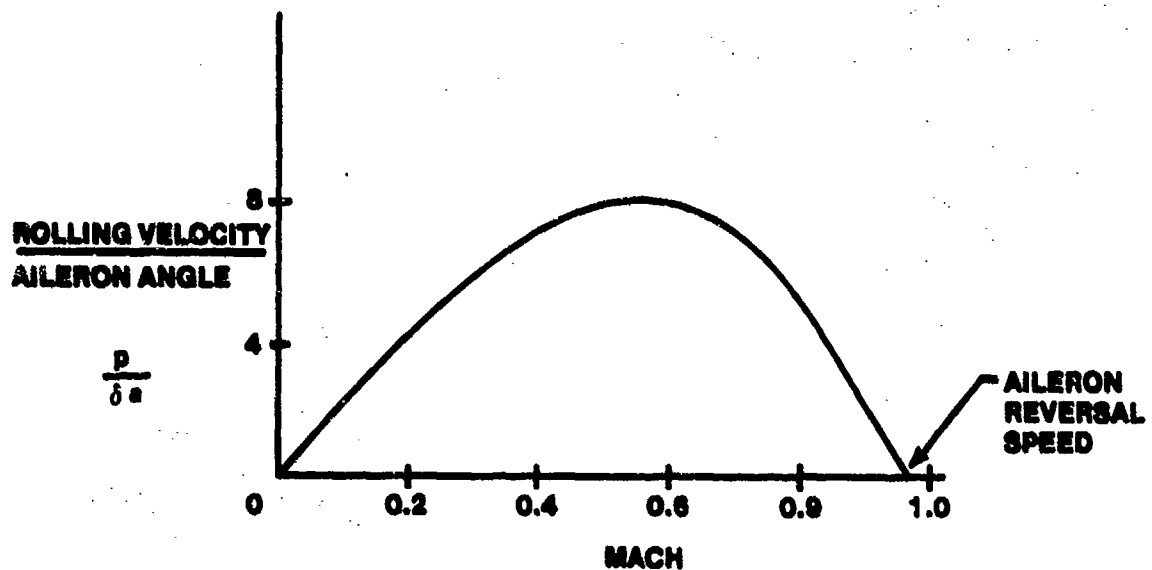

FIGURE 12.75. AILERON EFFECTIVENESS

It should be noted that flutter and divergence correspond to conditions of aeroelastic instability, and that speeds beyond critical flutter and divergence speeds will result in an eventual structural failure. Control reversal is not a condition of instability, and speeds beyond the control reversal speed will result only in a reversal of the action of the control system and not necessarily a failure of the structure. The prime concern here is the loss of maneuverability. With the advent of fully boosted systems, additional complications result because of the deformations resulting in the controlling mechanism and the enormous mechanical advantage available.
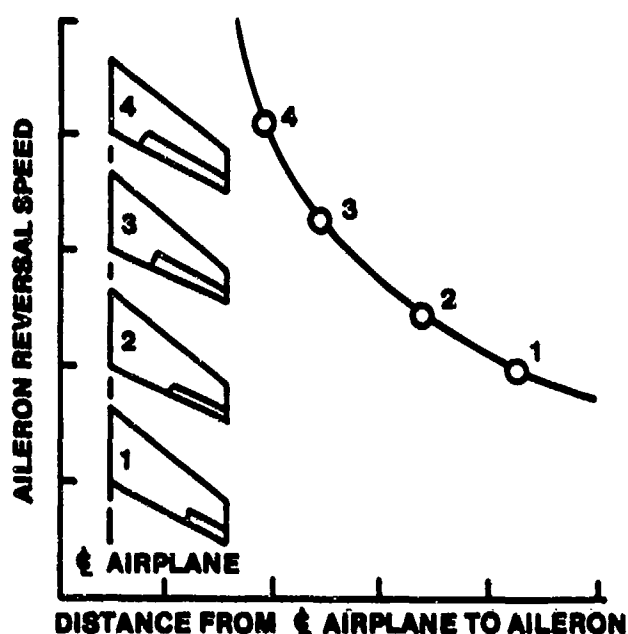

FIGURE 12.76. AILERON REVERSAL SPEED VS AILERON POSITION

Figure 12.77 illustrates a typical cambered wing section with ailerons. σ_a represents a downward deflection of the aileron. If the wing were rigid, the aileron displacement would be accompanied by an increase in lift. However, for an elastic wing the deflected aileron would also cause a nose-down twist of the wing, reducing the effective angle of attack. The nose down twisting moments increase with the square of airspeed whereas the elastic restoring moment stays constant. At some critical airspeed U_R, called the aileron reversal speed, the increase in lift caused by the deflected aileron is completely negated by the loss in lift due to the reduction of the effective angle of attack caused by the twist. The mathematics follow. Again, the elastic restoring moment is $K_\theta \theta$.

Aero dynamic moment about the elastic axis

$$\mathcal{M}_{AERO} = Le - \mathcal{M}_{ac} - \mathcal{M}_{ac_{\delta_a}}$$

where $\mathcal{M}_{ac_{\delta_a}}$ is the contribution to the moment about the a.c. due to aileron deflection.

$$L = q S C_{L_\alpha} (\alpha_r - \theta) + q S C_{L_{\delta_a}} \delta_a$$

or

$$L = q S \left[C_{L_\alpha} (\alpha_r - \theta) + C_{L_{\delta_a}} \delta_a \right]$$

Substitution into the moment equation yields

$$\mathcal{M}_{AERO} = q Se \left[C_{L_\alpha} (\alpha_r - \theta) + C_{L_{\delta_a}} \delta_a \right]$$
$$- q Sc \left[C_{Mac} + C_{M_{\delta_a}} \delta_a \right]$$

Again, equating elastic and aerodynamic moments,

$$K_\theta \theta = \mathcal{M}_{AERO} = Le - \mathcal{M}_{ac} - \mathcal{M}_{ac_{\delta_a}}$$

$$= q Se C_{L_\alpha} (\alpha_r - \theta) - q Sc C_{Mac}$$

$$+ q Se C_{L_{\delta_a}} \delta_a - q Sc C_{M_{\delta_a}} \delta_a$$

Solving for the twist angle θ,

$$\theta = \frac{q S \left(e\, C_{L_{\delta_a}} - c\, C_{M_{\delta_a}} \right) \delta_a}{K_\theta + q\, Se\, C_{L_\alpha}} + \frac{q S \left(e\, C_{L_\alpha}\, \alpha_r - c\, C_{Mac} \right)}{K_\theta + q\, Se\, C_{L_\alpha}} \quad (12.32)$$

Ultimately, we will be interested in only the change in twist angle due to a change in aileron deflection i.e., $\partial\theta/\partial\delta_a$. Consequently, the second term in the θ equation drops out since it remains invariant with a change in aileron deflection. As a result,
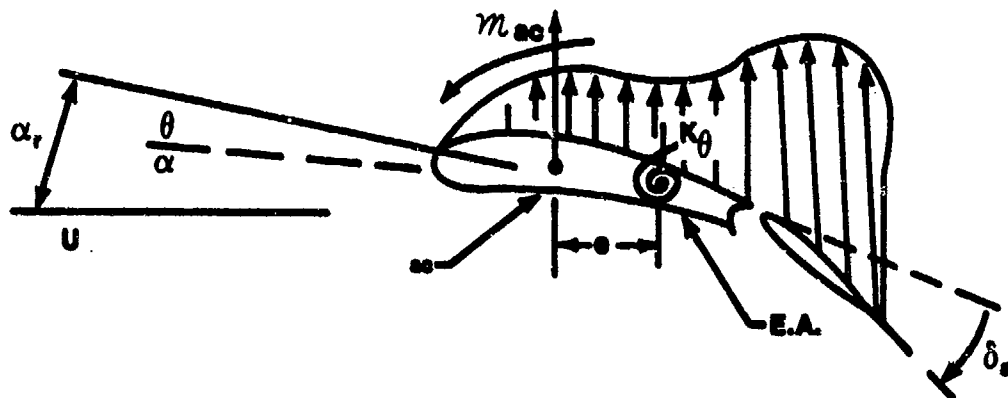

FIGURE 12.77. CAMBERED WING SECTION WITH AILERON

$$\frac{\partial\theta}{\partial\delta_a} = \frac{q S \left(e\, C_{L_{\delta_a}} - c\, C_{M_{\delta_a}} \right)}{K_\theta + q\, Se\, C_{L_\alpha}} \quad (12.33)$$

At U_R, the change in lift due to a change in aileron deflection, ΔL_{δ_a}, becomes zero.

$$\Delta L_{\delta_a} = 0$$

The change in lift ΔL_{δ_a} is represented by

$$\Delta L_{\delta_a} = L_{\delta_a} + L_{\Delta\theta}, \text{ where}$$

$L_{\delta a}$ = lift increase due to the increase in camber = $q S C_{L_{\delta_a}} \delta_a$

$L_{\Delta\theta}$ = lift decrease due to the leading edge twist = $- q S C_{L_\alpha} \dfrac{\partial\theta}{\partial\delta_a}$

Therefore,

$$\Delta L_{\delta_a} = q S C_{L_{\delta_a}} \delta_a - q S C_{L_\alpha} \frac{\partial\theta}{\partial\delta_a}$$

Substituting Equation 12.33 for $\partial\theta/\partial\delta_a$ yields

$$\Delta L_{\delta_a} = q S \left[C_{L\delta_a} \delta_a - C_{L_\alpha} \frac{q S \left(e C_{L_{\delta_a}} - c C_{M_{\delta_a}} \delta_a \right)}{K_\theta + q S e C_{L_\alpha}} \right]$$

Rearranging and cancelling, we obtain

$$\Delta L_{\delta_a} = \frac{q S \left(K_\theta C_{L_{\delta_a}} + q S c C_{L_\alpha} C_{M_{\delta_a}} \right) \sigma_a}{K_\theta + q S e C_{L_\alpha}} \tag{12.34}$$

At the reversal speed $\Delta L_{\delta_a} = 0$. Since q, S, and δ_a in the numerator of Equation 12.34 are all non-zero, the terms within the parentheses must vanish to satisfy the equation

$$K_\theta C_{L_{\delta_a}} + q_R S c C_{L_\alpha} C_{M_{\delta_a}} = 0$$

where $q = q_R$ (Dynamic Pressure at Control Reversal)

$$q_R = - \frac{K_\theta C_{L_{\delta_\alpha}}}{S c C_{L_a} C_{M_{\delta_a}}}, \qquad \text{or}$$

12.129

$$U^R = \sqrt{-\frac{K_\theta \, C_{L_{\delta_a}}}{\frac{\rho}{2} S c \, C_{L_\alpha} \, C_{M_{\delta_a}}}}$$

(12.35)

All the terms are positive except for $C_{M_{\delta_a}}$ so U_R is, of course, real. A noteworthy observation is the fact that the reversal speed is independent of twist axis location (e). The aerodynamic moment at the reversal condition is a pure couple and therefore independent of axis position. Also notice the U_R decreases with a decrease in altitude.

Preventing aileron reversal in a straight wing is a matter of increasing torsional stiffness (K_θ), increasing the aileron effectiveness $\left(C_{L_\delta} \right)$, or of decreasing the magnitude of C_{M_δ}. In the case of swept wings, where aileron reversal has been a serious problem, bending stiffness must also be increased. Since weight increases accompany stiffness increases other methods should be employed. Alternative methods such as spoilers and all moving wing tips have proved beneficial. Also, the effective K_θ is increased as the aileron locations are moved inboard.

12.5.6 Flutter

First we assume a cantilever straight wing without ailerons mounted in a wind tunnel and with no airflow. When the model is disturbed, oscillations are induced which gradually damp out since the elastic structure provides a damping ratio of its own, known as structural damping, usually from 2% to 8%. As the speed of the wind flow is increased, the rate of damping of the oscillations increases due to aerodynamic damping. With further increases of speed, a point is reached where the damping starts to decrease rapidly. At the next point, the Critical Flutter Speed, the oscillation can just maintain itself with steady amplitude. Speeds above the critical flutter speed trigger a violent oscillation and subsequent destruction of the section when subjected to a small disturbance. This airfoil is said to have oscillatory instability and is said to flutter. Moreover, once the oscillation starts, it is self sustained and no further external forces or forcing functions are required.

Additional types of flutter can involve aileron motion where there may be one or more ranges of speeds for which flutter occurs. The aileron flutter induces the wing to flutter. Usually these regimes are bounded at both ends by critical speeds where one has an oscillation of constant amplitude.

The oscillatory motion of a fluttering cantilever wing has both bending and torsional components. If the airfoil is rigid in torsion and is constrained to have only a flexural degree of freedom, it will not flutter. With only torsional degrees of freedom it can flutter only if the angle of attack is near the stall angle. Thus, coupling of several degrees of freedom is a necessary portion of flutter. Furthermore, bending movements at all points across the span are approximately in phase with one another. The torsional movements are all approximately in phase; however, the bending mode is usually considerably out of phase with the torsional movement. This phase difference is responsible for flutter.

An airplane wing is an elastic body and has infinitely many degrees of freedom in vibration. The basic construction allows any elastic deformation in the chordwise section to be described by (1) deflection of a reference point, (2) and angle of rotation about that point. With control surfaces, the freedom to turn about the hinge line is so much more important than elastic deformation that this deflection is best described by an angle of rotation about its hinge line.

One must consider three variables in wing flutter (this does not include a time variable):

(1) Bending
(2) Torsion
(3) Control surface rotation

A flutter mode which contains all three is termed ternary flutter. A flutter mode which contains only two (usually the first two) is called binary flutter. Occasionally, a single degree of freedom oscillation may exist. This usually occurs with control surfaces and is referred to as "buzz."

In general the design criteria requires that an aircraft must be able to fly near U_f without the appearance of undesirable marginal stability in its structural vibrations. Yet, bending and torsional flutter can emerge suddenly

and violently, and at about five knots above U_f the wing will possibly destroy itself after two or three cycles of oscillations.

The classical type of flutter nearly always involves the coupling of two or more degrees of freedom. The analysis can be very complex, depending upon the desired detail. We shall attempt only an elementary treatment here, with emphasis on formulation and physical interpretation. The basic second order system will be studied in depth because it conveniently demonstrates the stability problem, the basis of all flutter phenomena. We will be mainly concerned with the changes in system response resulting from changes in damping and/or excitation frequency.

Figure 12.78 shows a typical wing section with two degrees of freedom: x, a vertical displacement downward (bending), and α, the angular deflection about the elastic axis. For simplification, the E.A. and the c.g. are coincident.

Unlike the static divergence and control reversal problems, the flutter analysis will require knowledge of the mass and inertial properties of the wing since an oscillatory motion will be involved, resulting in a "generation" of inertial forces. By use of Newton's second law, the equations of motion for the wing in the two degrees of freedom can be derived.
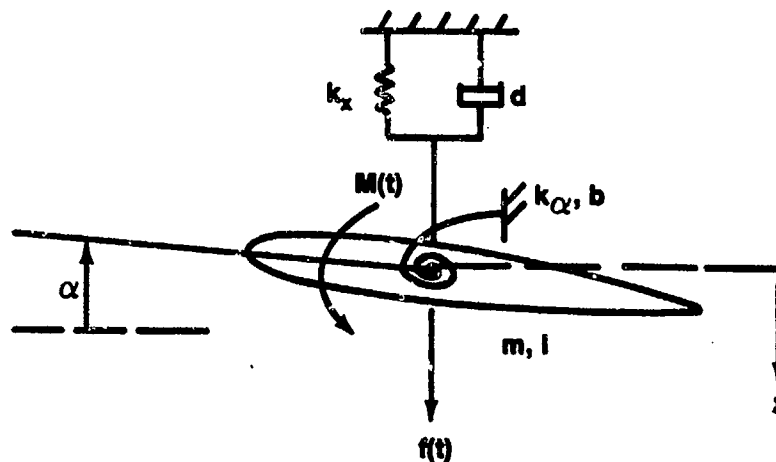
FIGURE 12.78.   TWO DEGREE OF FREEDOM WING SECTION

NOTE: f(t) = time varying force acting at c.g.

               M(t) = time varying moment acting on wing section

               m = mass of section

               I = moment of inertia about c.g.

               k_x, k_α = spring constants of displacement (bending)
                                   and torsion, respectively

               d, b = bending and torsion damping coefficients

$$m \ddot{x} + d \dot{x} + k_x x = f(t)$$

$$I \ddot{a} + b \dot{a} + k_a a = M(t)$$

As the equations stand, for small displacements there is neither inertial nor elastic coupling between the two degrees of freedom. That is, in the absence of the external driving forces f(t) and M(t), the free body motion is independent in both x and a. The motions do not interfere. This is obvious from inspection (no a in the x equation, and vice versa) and is the result of our collocating the c.g., the axis of twist, and the displacement axis. The only way coupling can be introduced is through the driving forces f(t) and M(t).

Before showing how the equations can be coupled aerodynamically, let's first look at the solutions to the equations. As they are presented, the equations are linear and can be solved separately. The solution for x, for example, is the sum of a transient (homogeneous) and a steady-state solution.

$$x(t) = x_t(t) + x_s(t)$$

Placing the x equation in standard form

$$\ddot{x} + 2\zeta\omega_n\dot{x} + \omega_n^2 x = f'(t)$$

where

$$\omega_n^2 = \frac{K_x}{m}$$

$$\zeta = \frac{d}{2\sqrt{mk_x}}$$

$$f'(t) = \frac{f(t)}{m}$$

The undamped natural frequency ω_n*, is the frequency the system would oscillate in the absence of damping. The damping ratio ζ is simply a convenient way of representing the degree of damping (due to the dash-pot coefficient, d) relative to the size of the mass and spring constants. The method for finding the transient solution can be found in numerous texts on differential equations.

$$x_t = e^{-\zeta\omega_n t} (C_1 \cos \omega_d t + C_2 \sin \omega_d t) \qquad (12.38)$$

$$\omega_d = \omega_n \sqrt{1 - \zeta^2}, \quad 0 \le \zeta < 1$$

where the constant ω_d is the damped frequency, and for obvious reasons is less than the undamped frequency ω_n. We see that the transient response has the form of a sinusoidal oscillation whose envelope decreases exponentially with time.

To solve for the steady-state solution x_s, knowledge of the driving force $f(t)$ is required. Flutter has been observed to be sinusoidal, therefore we can assume that the nature of the driving force is also sinusoidal.

NOTE: *In this example, ω_n is the undamped translational structural frequency.

$$f(t) = F \cos \omega t$$

We can then assume a steady-state solution of the form

$$x_s = A \cos (\omega_t + \phi)$$

Substitution into the differential equation yields values for the constants. Chapter 3 of Reference 11 gives the details to the solution.

$$A = \frac{F/k_x}{\sqrt{\left(1 - \frac{\omega^2}{\omega_n^2}\right)^2 + \left(2 \zeta \frac{\omega}{\omega_n}\right)^2}}$$

and

$$\phi = \tan^{-1}\left(\frac{-2 \zeta \frac{\omega}{\omega_n}}{1 - \frac{\omega^2}{\omega_n^2}}\right)$$

The steady-state response with amplitude A and phase angle ϕ is of the same form as the driving force. The amplification factor $A/(F/k_x)$ is the ratio of the amplitude A of the steady-state solution to the static deflection F/k_x due to a constant force of magnitude F. Figure 12.79 shows a plot of the amplification factor versus frequency for different values of ζ.
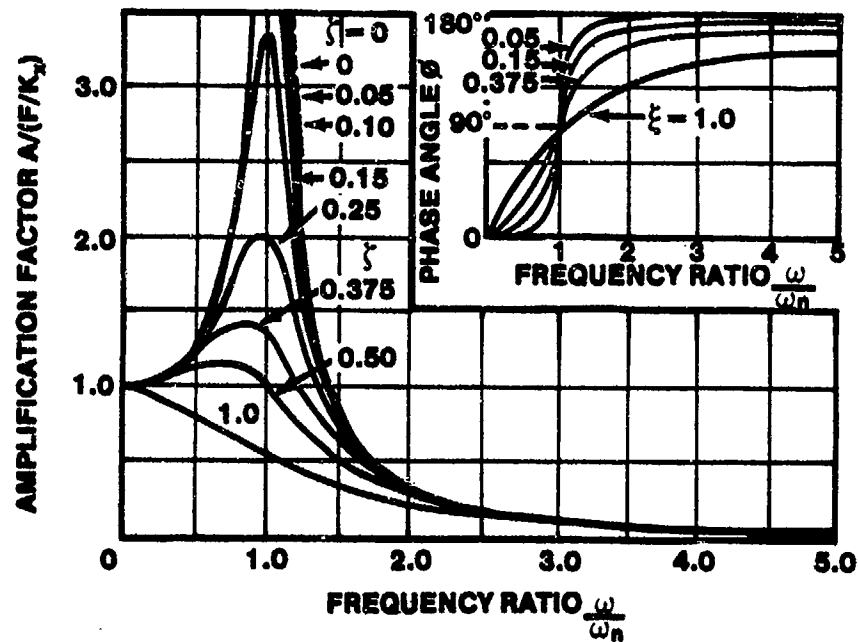
FIGURE 12.79. AMPLIFICATION FACTOR AND PHASE ANGLE VERSUS FREQUENCY RATIO

The amplification factor is unity when the input frequency is zero, regardless of the damping ratio ζ. It is important to note that when the forcing frequency (ω) equals the undamped natural frequency (ω_n), the amplification factor is $1/(2\zeta)$. Consequently, any amount of damping is very critical in holding down the response. Lack of damping results in an unbounded output.

Note also that at the critical frequency ($\omega = \bar{\omega}_n$) the phase angle ϕ is 90°, regardless of ζ. It can be shown that during this condition, the response (bending) velocity $\dot{x}_s$ is exactly in phase with the driving force $f(t)$, which is the condition for maximum power input into the oscillating wing system from the external force.

How do we relate the above analysis to a meaningful wing flutter problem? Looking back at Figure 12.78 we can take the x degree of freedom as the basic wing bending mode with natural frequency of oscillation $\omega_n = \sqrt{k_x/m}$, a value obviously dependent upon the mass and elastic properties of the wing. The external force $f(t)$ can be inferred to be the aerodynamic lift acting on the given wing section.

$$f(t) = -L(t) = -q \, S \, C_{L_\alpha} \, \alpha(t)$$

If $\alpha(t)$ were to vary sinusoidally at frequency ω, we'd have

$$f(t) = -q \, S \, C_{L_\alpha} \, \alpha_0 \cos \omega t \quad (\alpha_0 \text{ is the magnitude of the angle of attack variations with time})$$

or,

$$f(t) = F \cos \omega t$$

This is exactly the same type of external driving force described in the example above. Such a variation in α can also result from the rotational equation of motion.

$$I\ddot{\alpha} + b\dot{\alpha} + k_\alpha \alpha = M(t)$$

Solving for the free body response [$M(t) = 0$], the solution is similar to the displacement transient solution (Equation 12.38)

$$\alpha(t) = e^{-\zeta_T \omega_\alpha t} \left[C_1 \cos \left(\omega_\alpha \sqrt{1-\zeta_T^2} \right) t + C_2 \sin \left(\omega_\alpha \sqrt{1-\zeta_T^2} \right) t \right]$$

In most wing structures, bending damping is much greater than torsional damping. Therefore, without loss of generality we can assume torsional structural damping (ζ_T) to be small. The solution then has the approximate form

$$\alpha(t) = C_1 \cos \omega_\alpha t + C_2 \sin \omega_\alpha t,$$

where $\omega_\alpha = \sqrt{k_\alpha / I}$ represents the natural undamped torsional frequency of the wing. If the initial conditions are picked appropriately, $\alpha(t)$ can be represented by

$$\alpha(t) = \alpha_0 \cos \omega_\alpha t \qquad (12.39)$$

The critical condition now occurs when $\omega = \omega_\alpha = \omega_n$ i.e., when the natural frequencies of wing bending and wing torsion are the same. Substituting $\omega = \omega_\alpha$ in Equation 12.39 yields

$$\alpha(t) = \alpha_0 \cos \omega t$$

or,

$$\cos \omega t = \frac{\alpha(t)}{\alpha_0}$$

Substituting this into the forcing function for displacement $f(t)$ gives

$$f(t) = \frac{F}{\alpha_0} \alpha(t)$$

If F/α_0 is set equal to some constant A, then

$$f(t) = A\alpha(t)$$

Equation 12.36 then becomes

$$m \ddot{x} + d \dot{x} + k_x x = A \alpha(t)$$

In this example the result is aerodynamic coupling between the two degrees of freedom, bending and torsion. Under certain conditions of damping, the end product from the coupling will be classical bending-torsional flutter.

A side view of the flight path of the wing in bending-torsional flutter is shown in Figure 12.80.
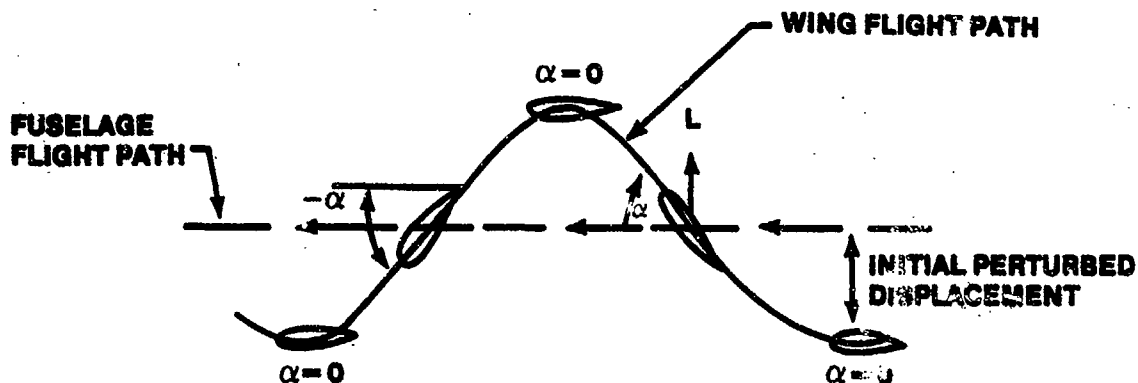
FIGURE 12.80. BENDING-TORSIONAL FLUTTER $(\omega = \omega_\alpha = \omega_n)$

This is a very simplified explanation of wing bending-torsion flutter. The bending mode is coupled aerodynamically with the torsion mode to effect the dynamic instability. The physical interpretation is rather straightforward but precise predictions on actual wing flutter speeds and frequencies are extremely difficult to obtain analytically. In our example, several specific assumptions and simplifications were made: (1) the elastic axis was placed at the c.g., (2) the wing section was treated as a rigid one, and (3) the aerodynamic damping and air mass accelerations were ignored. However, these assumptions did not detract from the general ideas basic to the dynamic instability.

Other types of flutter which may occur usually involve the rotation of some control surface about its hinge line. Wing bending/aileron rotation flutter, or fuselage torsion/rudder rotation flutter are examples. It is also possible, in fact more common for more than two modes to be present, such as in wing bending/wing torsion/aileron rotation flutter. Theodore Theodorsen presented a NACA paper in 1935 which treats the three-degree-of-freedom wing-aileron airfoil in somewhat complete and tedious detail.

12.5.7 Structural Modeling

To expand the analysis to treat the total aircraft structure and to cover all interactions between structural components is considerably more difficult.

The problem is basically twofold in the derivation of the equations of motion. First, the free body mass and structural relationships have to be determined. Second, the aerodynamic forces acting on the entire surface have to be derived. These forces will in turn depend upon the deflections, velocities, and accelerations of the structure.

General equations can be formulated by treating the aircraft as composed of a large number of discrete masses. Rewriting Equation 12.36 in matrix form yields the general equation

$$[m] \ \{\ddot{x}\} \ + \ [d] \ \{\dot{x}\} \ + \ [k] \ x \ = \ f(t)$$

The brackets [] signify a square matrix and the braces indicate a column matrix. Represented are n simultaneous equations in degrees of freedom x_i^* (i = 1, 2, ..., n). The equations are difficult to formulate and difficult to solve. The main problem lies in determining the stiffness coefficients K_{ij}.

To obtain the harmonic solution to the above equations a continuous forcing function, F_i, is applied equal to the structural damping d_{ij}. As a result, the forcing function and structural damping cancel and the equations are simplified to

$$[m] \ \{\ddot{x}\} \ + \ [k] \ \{x\} \ = \ 0$$

Next, a matrix of flexibility influence coefficients C_{ij} is defined as the inverse of the stiffness matrix

$$[c] \ = \ [k]^{-1}$$

The equations now become

$$[c] \ [m] \ \{\ddot{x}\} \ + \ \{x\} \ = \ 0$$

The influence coefficients are preferred to the stiffness coefficient because they are more conveniently determined by actual measurements on the structure or a scaled model. Using the simple spring relationship shown in Figure 12.81, the force F required to deflect a spring (or wing section equivalent) a distance x in static equilibrium is governed by

$$F = kx$$

Or, taking a different view, the displacement x resulting from the application of a force F is given by

$$x = 1/k \ F = C \ F.$$

*The coordinate x_i can represent either a displacement or an angular deflection.
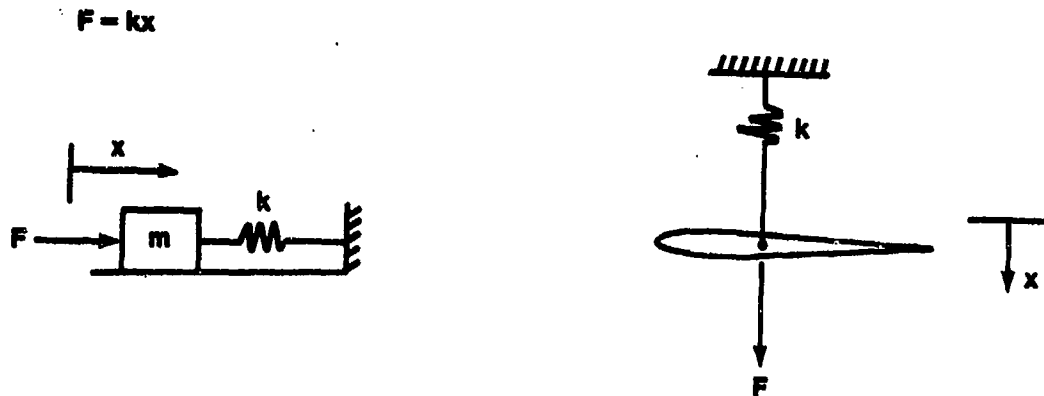

FIGURE 12.81.   SIMPLE SPRING RELATIONSHIP

If we assume, for example, that a wing in Figure 12.82 is approximated by five separate sections, the displacement at section 3 due to forces F_2 and F_4 applied at stations two and four, respectively, is given by

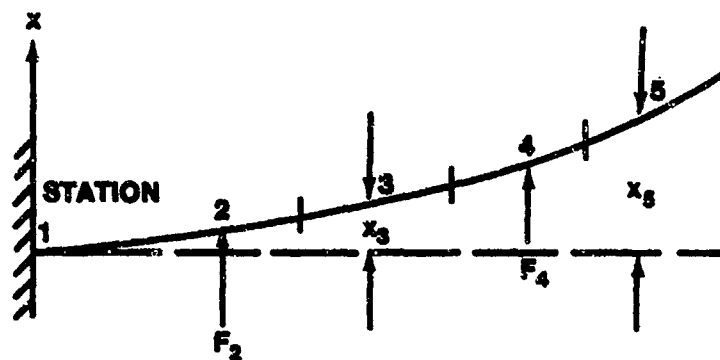$$X_3 = C_{32} \ F_2 + C_{34} \ F_4$$

FIGURE 12.82. CANTILEVER WING

In general, a displacement at Station (or mass point) i due to the existence of forces at Station j is given by the following relationship:

$$x_i = C_{i1} F_1 + C_{i2} F_2 + \ldots + C_{in} F_n$$

$$x_i = \sum_{j=1}^{n} C_{ij} F_j$$

Conversely, a force at Station i will cause deflections at Stations j, governed by

$$F_i = k_{i1} x_1 + k_{i2} x_2 + \ldots + k_{in} x_n$$

$$F_i = \sum_{j=1}^{n} k_{ij} x_j$$

The C_{ij} can be determined by

$$C_{ij} = \left. \frac{x_i}{F_j} \right]_{F_k = 0, \ k \neq j}$$

Therefore C_{ij} will not become undefined.

For example, if a unit force were applied at station 27, (i.e., $F_{27} = 1$) and all other forces were zero, all the $C_{i,27}$ can be determined from

$$C_{i,27} = x_i$$

On the other hand, the $k_{27,j}$ are not as conveniently determined since it is difficult to isolate a force when a unit displacement is applied at any station. Consequently, it is much easier and more accurate to measure a displacement than to measure a force and the influence coefficient is more often used.

For the equations

$$[c] \ [m] \ \{\ddot{x}\} + \{x\} = 0$$

we can assume sinusoidal solutions of the form

$$x_i = A_i \sin \omega t, \ or$$

$$\{x\} = \{A\} \sin \omega t$$

Substitution into Equation 12.40 leads to

$$-\omega^2 \ [c] \ [m] \ \{A\} \sin \omega t + \{A\} \sin \omega t = 0$$

or, since $\sin \omega t \neq 0$

$$\boxed{\frac{1}{\omega^2} \ \{A\} = [c] \ [m] \ \{A\}}$$

This is a standard eigenvalue problem which can be solved using iterative techniques. Values of the model vectors or mode shapes A can be found, corresponding to a specific frequency ω. There are as many eigenvalue solutions ω and corresponding eigenvectors A as there are degrees of freedom in the system. That is, an n degree of freedom system has n mode shapes and frequencies. The concept of mode shapes is so basic to flutter analysis that further discussion is justified at this time.

12.5.8 Structural Vibrations - Mode Shape Determination

The basic discussion of mode shapes and frequencies will use the uniform cantilever beam of length L shown in Figure 12.83 as an example.
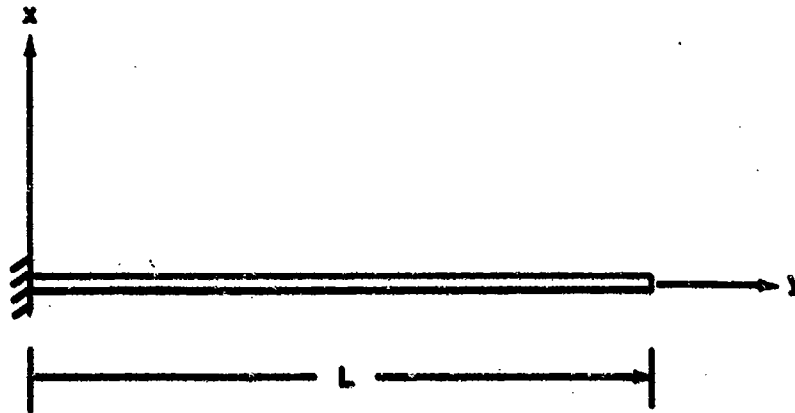

FIGURE 12.83.   UNIFORM CANTILEVER BEAM

What do the natural mode shapes represent and how do we compute them? The real question to address is: If the beam were to vibrate freely at some resonant condition* what vibrating shape would it assume and what would the frequency of vibration be?

Since the beam is continuous it has an infinite number of mass points and, consequently, an infinite number of degrees of freedom. We state, without proof, that there are also an infinite number of distinct vibration shapes, each of which has a unique vibration frequency.

The Equation of Motion for this system leads one to a complex or double eigenvalue problem, where the eigenvector determines the modal shape of the beam, $X(y)$, and corresponding eigenvalue, ω_z, represents the square of the vibration frequency. These eigenvalues are derived given the mass and stiffness distributions, and the specific boundary conditions. For the beam

*Definition: Resonant Condition - Vibrating at a maximum amplitude in phase with an oscillating input at the systems undamped natural frequency, ω_n.

12.144

in Figure 12.83 the boundary conditions are: zero displacement and slope at the fixed end $(y = 0)$, and zero shear and moment at the free end $(y = L)$. The eigenvectors are solutions to homogeneous equations so that if $X_k(y)$ is a mode shape, $C\,X_k(y)$ is one also. As a result, each mode shape function represents relative displacements along the beam. The absolute values are determined from the initial conditions.

The differential equation for the cantilever beam as given in Reference 1 is

$$EI\,\frac{d^4x}{dy^4} + m\,\frac{d^2x}{dt^2} = 0$$

(12.41)

where

E = modulus of elasticity
I = area moment of inertia
m = mass distribution.

Equation 12.41 is a separate partial differential equation with a solution $x(y, t)$ a product of a function of y only, $X(y)$, times a function of time only, $T(t)$.

$$x(y,t) = X(y)\,T(t)$$

Substituting $x(y,t)$ into Equation 12.41 yields

$$EI\,\frac{d^4X}{dy^4}\,T + m\,\frac{d^2T}{dt^2}\,X = 0$$

or

$$-\frac{1}{T}\,\frac{d^2T}{dt^2} = \frac{EI}{m}\,\frac{d^4X}{dy^4}\,\frac{1}{X}$$

Since y and t are independent, they can be equated to a separation constant. In this example the separation constant will be the square of the mode shape frequency, ω^2. The result will be two linear differential equations.

$$\frac{d^2T}{dt^2} + \omega^2 T = 0$$

$$\frac{EI}{m}\frac{d^4x}{dy_4} - \omega^2 X = 0$$

or,

$$\frac{d\,X}{dy_4} - \frac{\omega^2}{a^2} X = 0$$

where

$$a = \sqrt{\frac{EI}{m}}$$

The solutions to Equations 12.42 and 12.43 are

$$T = A \sin \omega t + B \cos \omega t$$

$$X = C \sinh \sqrt{\frac{\omega}{a}}\, y + D \cosh \sqrt{\frac{\omega}{a}}\, y$$

$$+ E \sin \sqrt{\frac{\omega}{a}}\, y + F \cos \sqrt{\frac{\omega}{a}}\, y,$$

where, A, B, C, D, E, and F are constants. Applying the boundary conditions for a uniform cantilever beam: $X(o) = 0$, $X'(o) = 0$, $X''(L) - 0$, and $X'''(L) = 0$, yields the following transcendental equation. The solution of which gives the mode shape frequency ω_1.

$$\cos \sqrt{\frac{\omega}{a}}\, L + \frac{1}{\cosh \sqrt{\frac{\omega}{a}}\, L} = 0, \qquad (12.44)$$

where

$$a = \sqrt{\frac{EI}{m}}$$

The solution to Equation 12.44 can be found by iterative techniques or through graphic depiction. What follows is the graphical solution that satisfies Equation 12.44.

The abcissas of the points of intersection of the curves yield values for $\sqrt{\frac{\omega}{a}}\, L$,

$$\sqrt{\frac{\omega}{a}}\, L = 0.597\ \pi,\ 1.49\ \pi,\ \frac{5}{2}\ \pi,\ \frac{7}{2}\ \pi,\ \frac{9}{2}\ \pi,\ \ldots$$

or

$$\omega_1 = (0.597)^2 \left(\frac{\pi^2}{L}\right) a$$

$$\omega_2 = (1.49)^2 \left(\frac{\pi^2}{L}\right) a$$

.
.
.

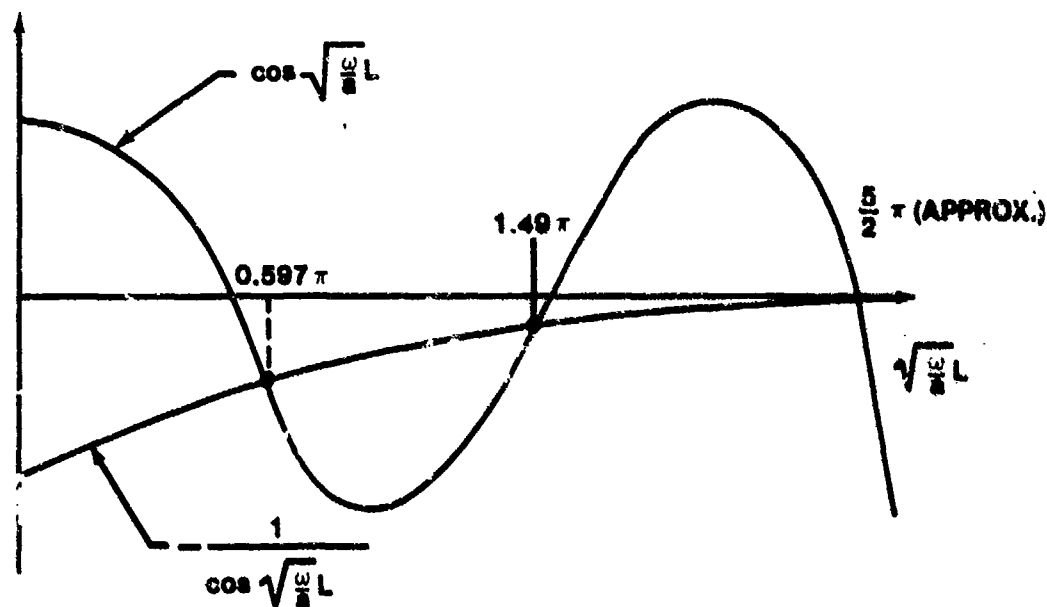$$\omega_1 = \left(i - \frac{L^2}{2}\right)\left(\frac{\pi^2}{L}\right) a,\ \text{(i sufficiently large)}.$$

FIGURE 12.84. GRAPHICAL SOLUTION TO THE TRANSCENDENTAL EQUATION OF A UNIFORM CANTILEVER BEAM

12.147

Having determined the model frequencies, ω_1, the specific mode shapes, $X_i(y)$, can be derived by substituting the frequency values ω_1 into the general mode shape equation for the cantilever.

$$X_i(y) = \left[\left(\frac{\sin\sqrt{\frac{\omega_i}{a}}L - \sinh\sqrt{\frac{\omega_i}{a}}L}{\cosh\sqrt{\frac{\omega_i}{a}}L + \cos\sqrt{\frac{\omega_i}{a}}y} \right) \left(\sinh\sqrt{\frac{\omega_i}{a}}y - \sin\sqrt{\frac{\omega_i}{a}}y \right) + \left(\cosh\sqrt{\frac{\omega_i}{a}}y - \cos\sqrt{\frac{\omega_i}{a}}y \right) \right]$$

Where D is a constant determined by the boundary conditions. Do not be concerned at how these equations were derived. They are simply the solutions of the fourth order differential equation for the vibrating cantilever beam. The important thing to note is that there are an infinite number of solutions ω_i, and that for each ω_i there corresponds an $X_i(y)$. Figure 12.85 shows four of the lowest frequency mode shapes.

The significance of the application of mode shapes and frequencies is that any vibration of any elastic body will be a summation of individual mode shape vibrations. The characteristics of mode shapes are such that (1) for each natural vibration frequency there exists one and only one natural mode shape, (2) in the vibration of any single mode, the displacements of the structure reach their zeros and their extreme simultaneously [as is evident from the solution $x(y,t) = X(y) T(t)$], (3) the natural mode shapes are linearly independent (i.e., no shape can be formed by any linear combination of the others), and (4) in any free vibration of a beam, wing, aircraft structure, bridge, and so forth, any combination of natural modes can exist simultaneously without mutual interference. In the case of aircraft flutter, the mode shapes become coupled due to the action of the external aerodynamic driving forces, which are in turn functions of the critical mode shapes. Using the general discrete mass free body problem discussed earlier, we can relate to a specific aircraft example.

$$\text{(c)} \quad [m]\,\ddot{x} + x = 0$$

with solution

$$\frac{1}{\omega^2} \{A\} = [c] [m] \{A\}$$

The "wing" in Figure 12.82 has five separate stations, each with mass m_i and each having two degrees of freedom, x_i, a vertical displacement, and α_i an angular rotation about the elastic axis as shown in Figure 12.86.

x

y

L

$a = \sqrt{\dfrac{EI}{m}}$

FUNDAMENTAL MODE
$i = 1$

$\omega_1 = (0.597)^2 \left(\dfrac{\pi}{L}\right)^2 a$

FIRST HARMONIC
$i = 2$

$\omega_2 = (1.49)^2 \left(\dfrac{\pi}{L}\right)^2 a$

SECOND HARMONIC
$i = 3$

$\omega_3 = \left(\dfrac{5}{2}\right)^2 \left(\dfrac{\pi}{L}\right)^2 a$

THIRD HARMONIC
$i = 4$

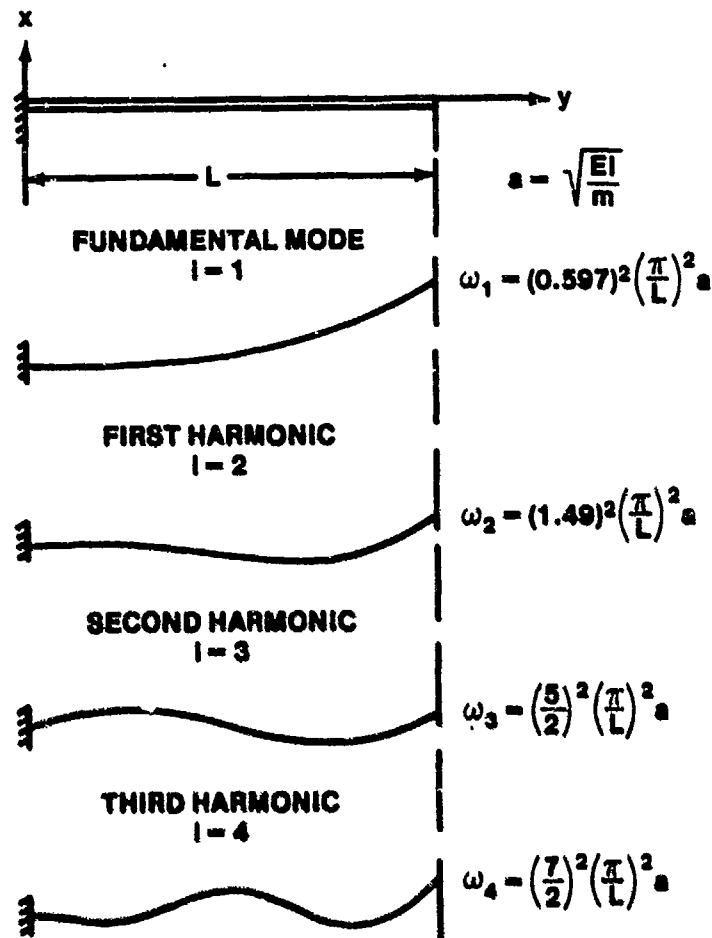$\omega_4 = \left(\dfrac{7}{2}\right)^2 \left(\dfrac{\pi}{L}\right)^2 a$

FIGURE 12.85.   FREQUENCY MODE SHAPE FOR A VIBRATING BEAM

The model vector $\{A\}$ is comprised of ten-degrees of freedom; five vertical displacements and five angular deflections.

$$\{A\} = \begin{bmatrix} x_1 \\ \cdot \\ \cdot \\ x_5 \\ \alpha_1 \\ \cdot \\ \cdot \\ \alpha_5 \end{bmatrix}$$
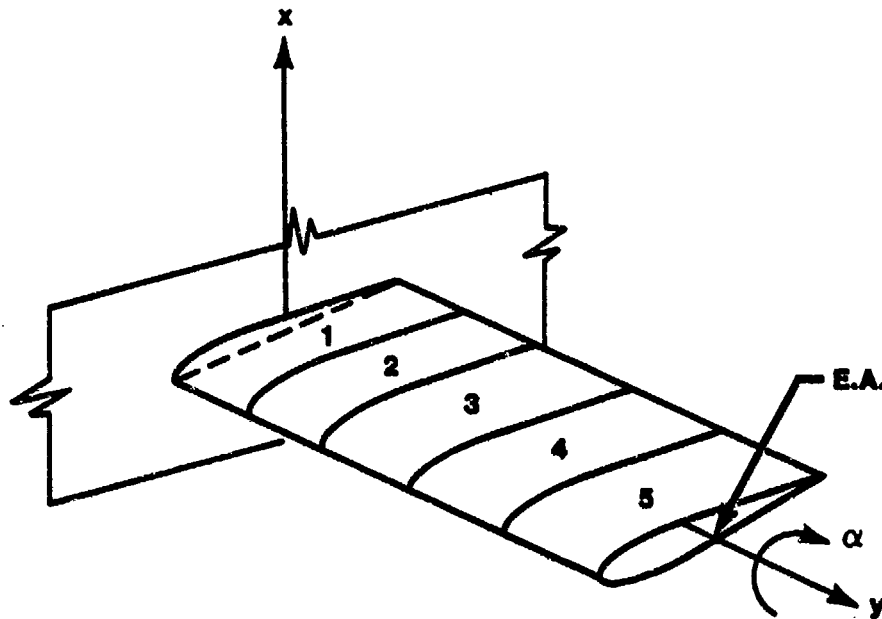

FIGURE 12.86.   CANTILEVER WING

From experimental measurements we can determine the mass and moment of inertia of each section, along with the influence coefficients (D_{ij}) for the total wing with respect to the ten degrees of freedom. Recall that C_{28} represents the vertical deflection x_2 at wing Station 2 due to a unit moment applied at wing Station 3 (α_3 being the eighth degree of freedom by definition).

The matrix equation

$$\frac{1}{\omega^2} \{A\} = [c] [m] \{A\}$$

thus, represents 10 simultaneous equations in the 11 unknowns ω, X_1, ... , α_5. Again, the mode shapes are relative displacements in the A matrix. A typical solution might be

12.150

$$\omega = 3.5, \quad A \begin{bmatrix} 1.00 \\ 1.21 \\ 1.63 \\ 2.23 \\ 3.05 \\ 0.74 \\ 1.13 \\ 1.74 \\ 2.57 \\ 3.49 \end{bmatrix}$$

At any given time, therefore, the wing station deflections for the given 3.5 rad/sec mode might be represented by

$$\{x\} \;=\; K \; \{A\} \; \sin (3.5t \;+\; \phi_1)$$

where the values K and ϕ_1 would depend on the initial conditions. Other modes at different frequencies will, of course, exist simultaneously. Flutter is the result of the aerodynamic coupling of these modes.

Even for simple structures the mode shapes and frequencies may be difficult to determine analytically. As a result, many simplifying assumptions are normally made. For the wing just described, the assumption that is can be represented by five rigid sections seems a bit gross, but for the low frequency mode shapes the simulation is quite reasonable. In actual aircraft problems the critical modes are usually the lower frequency ones for very fundamental reasons. The large bending and structural deformations are the ones which more efficiently extract energy from the airstream. These are usually the lower frequency modes.

A useful technique for the flutter analyst is to assume that a structure will take on certain predetermined mode shapes based on previous observations of similar type structures. The assumed mode shape can then be used in the energy equations to arrive at the particular mode shape frequency. This technique aids in the solution of complex structures but there is obviously an accompanying reduction in accuracy. The subject of mode shapes will be brought up again in the discussion of ground vibration tests.

12.5.9 Wind Tunnel Modeling

The use of aircraft models has produced solutions to practical problems in the areas where existing theory is not yet dependable. Particularly in dealing with flutter, the testing of wind tunnel models with properly scaled mass and stiffness properties has often yielded better results than equivalent analytical efforts.

12.5.10 Buckingham π Theorem

Model theory must be based on a clear understanding of the principles of dimensional analysis. The writing of equations in dimensionless form with a reduction in the number of variables was generalized by Buckingham in his "π Theorem" which states that if a physical situation can be represented by the equation

$$\psi \ (S_1, \ S_2, \ S_3, \ \ldots, \ S_n) = 0$$

where the n arguments S_i include all the primary quantities (mass, length, time, etc.), the secondary quantities, and dimensional constants which must be considered in the problem, the equation can be rewritten in the form

$$\phi \ (\pi_1, \ \pi_2, \ \pi_3, \ \ldots, \ \pi_{n-m}) - 0$$

in which π_1, π_2, $\ldots$, π_{n-m} are the (n-m) independent products of the arguments $S_1, \ldots, S_n$, which are dimensionless in primary quantities. The form of these dimensionless π's can be found by a formal procedure but they can usually be constructed by inspection. Typical π's in general use are aspect ratio AR, reduced frequency $k = \omega b/V$, Mach M, and Reynolds number Re. There are two main advantages in using dimensionless variables. First, since the dimensionless equation of motion is completely unaffected by scale effects the values of the dimensionless variables should be the same for both the original problem and its model.

As a sample problem we can use the wing twist relationship derived earlier to determine the wing divergence speed.

$$\theta \ = \ \frac{q \ S \ (e \ C_{L\alpha} \ \alpha_r + c \ C_{Mac})}{K_\theta - q \ Se \ C_{L\alpha}}$$

12.152

θ, α_r, C_{L_α} and C_{Mac} are already dimensionless. The other quantities have the dimensions as indicated (n + 5).

$$q - \frac{F}{L^2} \qquad\qquad S - L^2$$

$$K_\theta - FL \qquad\qquad e - L$$

$$c - L$$

Force (F) and length (L) were chosen as the primary quantities (m = 2).

By inspection we can form independent dimensionless ratios e/c and qSc/K_θ so that the equation may be rearranged to read

$$\theta = \frac{\left(\frac{qSc}{K\theta}\right)\left[\left(\frac{e}{c}\right)C_{L_\alpha}\alpha_r + C_{Mac}\right]}{1 - \left(\frac{qSc}{K_\theta}\right)\left(\frac{e}{c}\right)C_{L\alpha}}$$

The number of arguments has been reduced by two, as predicted by the Theorem (since there are the two primary quantities F and L in the equation). The equation really implies that any model of the semi rigid wing having the same shape (C_{Mac} and C_{L_α}) must have the same dimensionless location of the elastic axis (e/c), the same rigid angle of attack (α_r), and the same ratio of aerodynamic to elastic forces ($qSc/K\theta$). It is also desirable to have similar Mach and Reynolds numbers if the effects are significant.

12.5.11 Aeroelastic Model

All aeroelastic models are designed along three fundamental airplane properties: (1) structural stiffness distribution, (2) mass distribution, and (3) the external shape. The model designer has to decide beforehand which of the properties will require a more exact simulation, depending on the nature of the planned tests. Property (1) is important for accurate loading measurements and property (3) is important for aerodynamic force evaluations. A flutter model obviously requires an accurate reproduction of all three properties and is therefore difficult to design.

The usual first approach is to attempt a scaled replica. However, for low speed models the required skin thickness (using the same material) may be prohibitively small. For a more workable thickness a softer material must be used but this in turn tends to reduce the accuracy of the stiffness reproduction. It also limits the amount of structural detail which can be obtained. The designer most often finds that the best plan is to lay out a simplified structure, making sure that it does not use up too much of the available mass. A shell is then formed to enclose the structure with the proper external shape. Finally, the remaining mass is distributed over the sections. The type of construction used for both the structure and the external shell depends upon the size, speed range, and ratio of the air density between aircraft flight altitude and test chamber conditions.

The types of aeroelastic testing fall into three general areas, whether with models or with full scale airplanes. The first area requires no airstream, such as in fatigue, static loading, and ground vibration tests. The second and third test areas involve airflow, in either the tunnel or full scale flight. The second area encompasses the static phenomena divergence, (control effectiveness) and the third area includes the unsteady phenomena such as flutter, gust loading and dynamic stability.

The test programs for nearly all prototypes include "shake testing", to determine the normal modes of vibration. These derived mode shapes and frequencies can be compared with the analytical calculations to verify the mass and stiffness properties of the math model. Sometimes the experimental data serve as the basis for a new set of calculations.

Once an adequate model is built the testing takes place. There are basically two different approaches to the problem. In the first, the testing is designed to evaluate the coefficients in the differential equation governing the problem. In the second approach the model is designed and tested as an analog. The model can simulate parts of airplanes, such as wings or tails, or the whole airplane. Each scheme has peculiar advantages and drawbacks as well as the usual problems of excitation, mounting and measurement. The particular details of tunnel testing and measurement is a total subject in itself.

12.5.12 Wind Tunnel Model Flutter Prediction Methods

Four methods used to measure the subcritical (below the actual flutter speed) response characteristics are co/quad, randomdec, power spectral density (PSD), and peak-hold spectrum methods. These methods are used to measure the frequency and damping (or an inverse response amplitude proportional to the damping in the peak-hold spectrum case) in the predominant or critical vibration modes. By suitably plotting and extrapolating the subcritical damping in the vibration mode or modes of interest, the flutter point can usually be established. With each method, the response can be approximated by that of a single-degree-of-freedom system. All of these methods can be used real-time, that is, used to translate the response time history samples into quantitative information for the test engineer while the test is in progress.

Briefly, the co/quad method measures the in-phase and out-of-phase components of the forces response generated by the sinusoidal frequency sweep technique. The randomdec method, a relatively new method used in the F-16 flight flutter testing, makes use of ensemble averaging of transient response to random excitation. The PSD method is a well-known procedure for the analysis of random response data. It is obtained directly from an ensemble average of the square of the magnitude of the Fourier transform of a number of segments of the time history. In the peak-hold spectrum method, Fourier components of a number of time history segments are determined and the envelope of the peak values of these components is obtained as a function of frequency.

Co/Quad Method. The co/quad method involved measuring the forced response of a model to an input force such as that generated by a trailing-edge control surface as illustrated schematically in Figure 12.87. If a transfer function relating the response to the input force is determined as a function of frequency, then the damping on each mode can be obtained. Cross spectrum between the control surface command signal and the model dynamic response can be determined with a co/quad analyzer. This type analyzer presents two outputs in terms of in-phase (called co for coincident) and out-of-phase (called quad for quadrature) components between signals. Several means of calculating the damping are available directly from a co and quad type of presentation. As indicated in Figure 12.87, the damping of a

mode can be estimated from the out-of-phase component by the frequencies labeled f_A and f_B. These are the frequencies at the half-power points and the structural damping g can be expressed in terms of these frequencies (Figure 12.87).
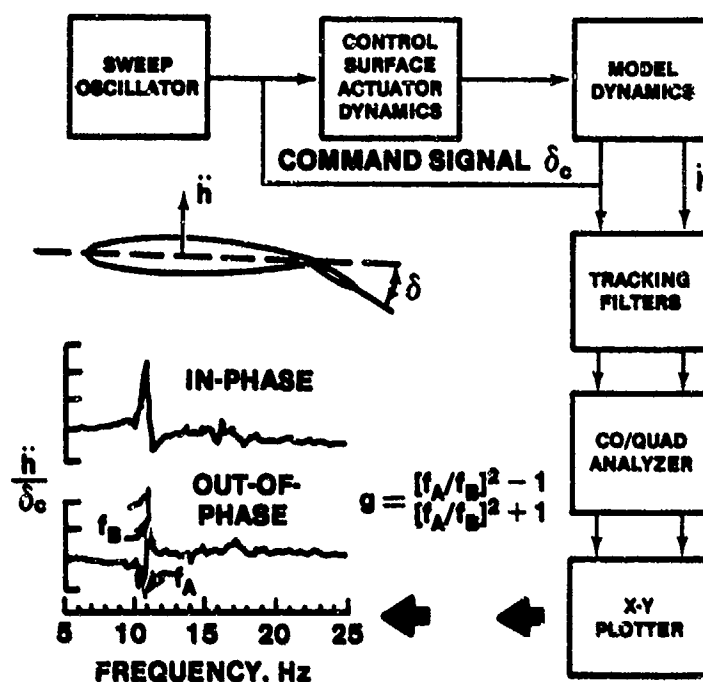

FIGURE 12.87. IMPLEMENTATION OF CO/QUAD METHOD

Randomdec Method. The Random Decrement method is basically an ensemble averaging of the turbulence-induced random vibrations of the test article. As is illustrated in Figure 12.88, triggering each data sample at a constant level, Y_t. Assuming linear superposition, the time history of each sample can be regarded as the combined solution from (1) an initial step displacement, (2) an initial velocity and (3) a random forcing function. Note that the Figure 12.88C sample represents the response to the same initial displacement as Figure 12.88B, a different initial velocity with the opposite sign, and a different random forcing function. It can be reasoned intuitively that when a large number of samples are averaged, only the response to the constant initial displacement will remain because the average of responses due to the

alternating initial velocities and the random forcing functions will tend to zero. Thus, it is seen that the ensemble average converges toward the transient response to an initial step. For a constant trigger level, the ensemble average (Randomdec Signature) will be constant even if the amplitude of the forcing function varies. If the ensemble average is made up of samples with initial positive slopes only, then the resulting trace represents the transient response to a combined step and initial velocity. Under these conditions the Randomdec Signature would vary with the intensity of the forcing function, thus minimizing the use of the signature trace as a failure detector. However, the damping as determined from the decay rate of the signature trace would be valid.
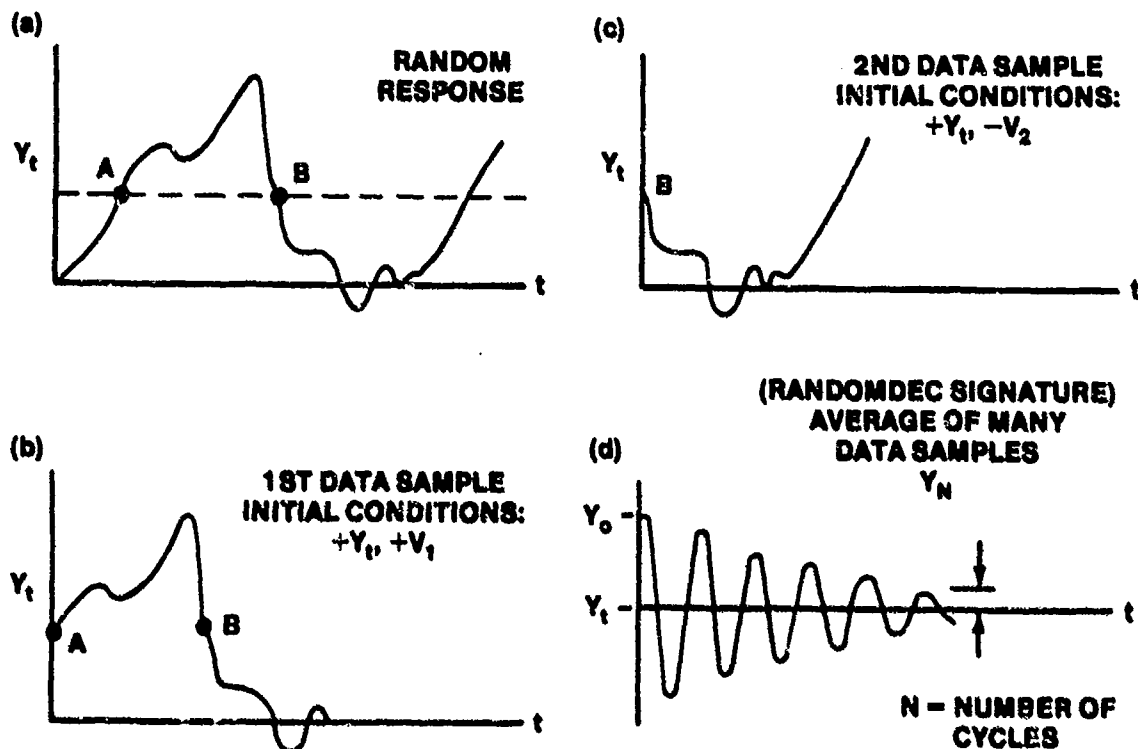
FIGURE 12.88. RANDOM DECREMENT CONCEPT

Structural damping, g, may be determined directly by

$$g = \frac{1}{N\pi} \log_e \left(\frac{Y_0}{Y_N} \right)$$

PSD and Peak-Hold Spectrum Methods. The PSD and the peak-hold spectrum methods are implemented as shown in Figure 12.89. Both methods are implemented using a spectroscope. This analyzer employs time compression techniques to achieve minimum analysis time for the frequency-tuned band-pass filter to convert the input signal from the time domain to the frequency domain. Following compression, the input signal is frequency analyzed. Shown on the left of Figure 12.89 is a typical PSD obtained from the model dynamic response h. The resulting signature has a peak for each structural mode and, for well-separated peaks, the damping ratio may be obtained. As indicated in Figure 12.89, the structural damping is equal to the frequency bandwidth, taken at the half-power point, and divided by the mode frequency.

An additional mode of operation of a spectroscope allows for detection and storage of the peak values of frequency windows. In this mode of operation, an ensemble spectrum composed of frequency windows is obtained.

Upon receipt of each subsequent spectrum, peak filter response at each location is updated in a positive direction. That is, only an increase in value causes an update to the new higher value. On the right of Figure 12.89, a typical peak-hold spectrum is shown. With this method the damping parameter
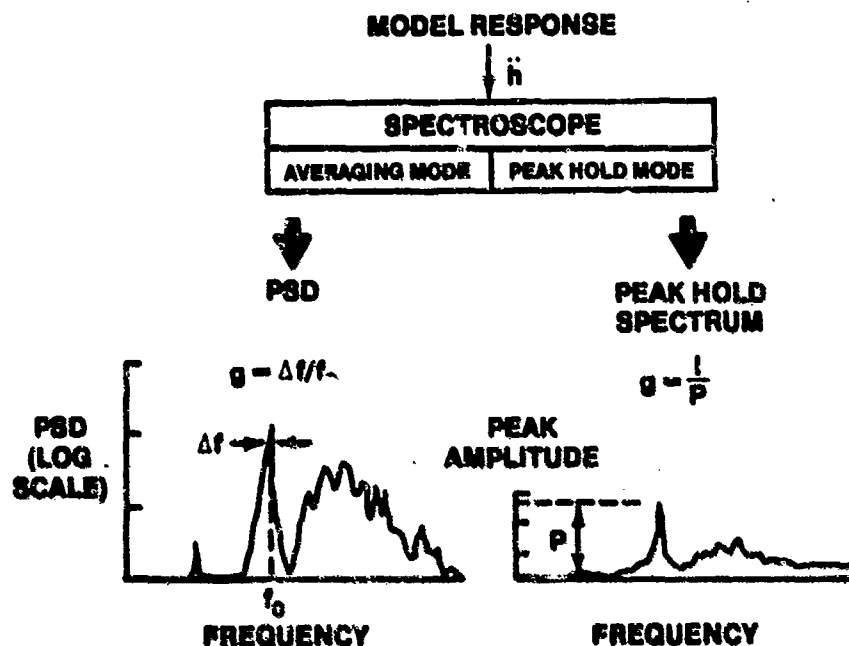
MODEL RESPONSE $\ddot{h}$

SPECTROSCOPE	
AVERAGING MODE	PEAK HOLD MODE

PSD

PEAK HOLD
SPECTRUM

$g = \Delta f/f$

$g = \frac{1}{P}$

PSD
(LOG
SCALE)

Δf

PEAK
AMPLITUDE

P

f_0

FREQUENCY

FREQUENCY

FIGURE 12.89. IMPLEMENTATION OF SPECTRUM METHODS

is not obtained. However, the reciprocal of the peak spectrum amplitude 1/P is proportional to the damping ratio and is used as a measure of system stability. The peak-hold method can be applied using two forms of excitation, model response to tunnel turbulence and model response to sinusoidal force.

Typical results obtained from the four subcritical response methods are presented and compared in Figures 12.90 and 12.91. Figure 12.90 presents the variation of structural damping coefficient of a delta wing flutter model with dynamic pressure. The damping results obtained with co/quad, randomdec, and PSD are indicated with open symbols. The model fluttered at a dynamic pressure of 5.89 kPa (123 lbf/ft^2) as indicated with the closed symbol. A plot of the inverse amplitude of the peak spectrum (used as the stability criteria) is presented in Figure 12.90B as a function of dynamic pressure. Shown are results from forced excitation and random excitation (turbulence).

12.159
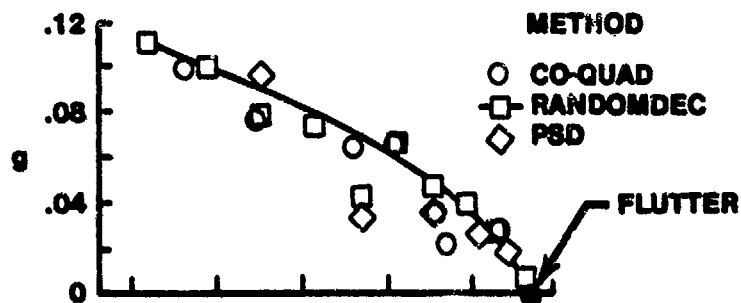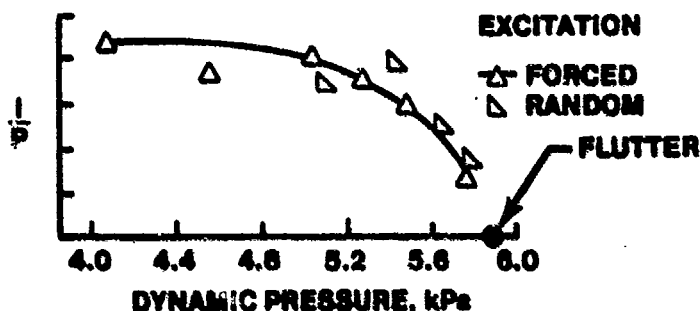
FIGURE 12.90. COMPARISON OF SUBCRITICAL METHODS, DELTA-WING MODEL (M = 0.90)

Further illustration of the type of data generated with the use of the four subcritical methods is presented in Figure 12.91. Shown are the data plots from which the damping levels presented in Figure 12.90 were obtained. The wind-tunnel conditions were the same for each method (Mach M = 0.90; dynamic pressure q = 5.42 kPa (113 lbf/ft^2).

12.5.13 Ground Vibration Testing (GVT)

As mentioned earlier, the primary purpose of ground vibration testing (shake testing) is to measure the structural mode shapes and frequencies. Sometimes the data serve to generate a new set of calculation. At other times, the measured mode shapes serve as the model for flutter predictions, especially when the effects of configuration changes on flutter speeds are being investigated.
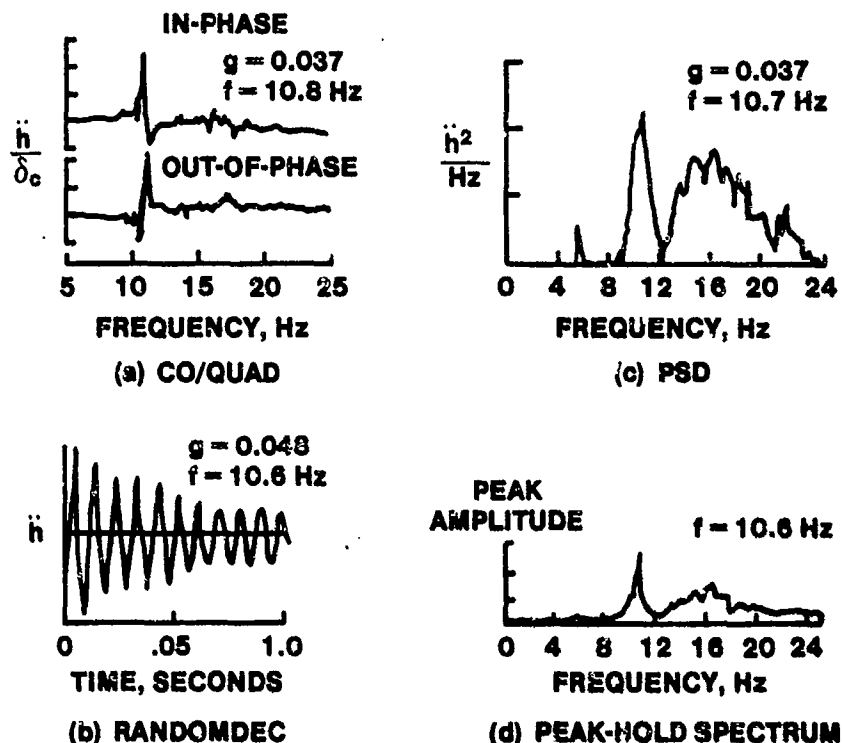
FIGURE 12.91. ILLUSTRATION OF SUBCRITICAL METHODS

$$M = 0.90; \quad q = 5.42 \text{ kPa } (113 \text{ lbf/ft}^2)$$

The X-24B "lifting body" is an excellent example of a reconfigured aircraft (from the X-24A). The structural modifications include the addition of right and left strake/aileron combinations and the modification of the two outboard vertical fins. The fin, strake and aileron form a single sub-assembly mated to the airframe. From analyses and previous test experience with the X-24A, the only possible flutter problems would occur with the strake/aileron and fin/rudder components. For further definition of the model characteristics of these components a ground vibration test program was conducted.

The objective in the program (as in all GVT's) was to measure the frequency, mode shape and structural damping for each significant mode of the

new tail section configuration. Especially important was the degree of interaction between the strake/aileron and the fin/rudder in the vibration modes.

For GVT, there is always the requirement to isolate the rigid body modes so that the highest frequency of rigid body motion is well below the lowest frequency of any structural vibration or mode shape. For example, if the natural frequency of rotation of the elevators were 10 Hz, the aircraft as it is supported should not have a pitch frequency close to the 10 Hz value. Otherwise there may be a problem in properly isolating and in determining the existence of that particular elevator rotation mode.

Ideally, the way to isolate the rigid body modes is to suspend the aircraft through the c.g. by a long cable but the methods cannot conveniently be employed. Two practical techniques are (1) to support the vehicle on air cushion stands, or (2) to suspend the aircraft with soft-spring ceiling mounted suspension systems. The approach used on the X-24B was to deflate the tires to half pressure.

The way to excite the structural modes on ground vibration tests is through some variable frequency vibrating device attached to the structure. Typically used are constant force electromagnetic or hydraulic shakers on which there is precise frequency tuning and an automatic frequency sweep feature.

For the X-24B, electromagnetic shakers with current feedback and individual gain and phase controls were used to input the sinusoidal forcing function to the structure. Seven excitation conditions involving six different shaker locations were required to completely investigate the model characteristics. Seven accelerometers were used to obtain data during the test. Acceleration measurements were recorded at predetermined grid points marked on the structure.

The test procedure was to first conduct a frequency sweep from 10 to 200 Hz at each of six different shaker locations. Possible modes were identified by observing Lissajous patterns on an oscilloscope of input force versus reference acceleration, and of other acceleration ratios. Essentially, at resonant condition the force would be in phase with the velocity and this situation would be indicated by the scope patterns. Once a mode was spotted the shaker could be retuned more precisely to the resonant frequency.

Acceleration and phase measurements were than taken along the predetermined grid locations labeled on the structure. Structural damping values were obtained by dimping the armature current to the shakers and measuring the vibration decay traces.

The mode shape and frequency data would be used in a flutter analysis whereby the aerodynamic forces (through a Theodorsen type analysis) would be evaluated in their interaction with the structure. Any conditions of instability could be predicted and the results used to refine the V-g diagrams or equivalent.

12.5.14 Flight Test

Most of the preflight functions have been accounted for. We can now approach the subject at the user's level and discuss the subject of flight test. Is the aircraft free of aeroelastic problems and if so, to what extent?

The criteria for strength and dynamic instabilities are listed in Reference 12.18. V_L, the limit speed for the basic and high drag configurations, is the maximum attainable speed commensurate with the operational use of the airplane, considering shallow and steep dive angles, thrust, operation, and nonoperation of speed brakes, and inadvertent upsets from gusts, or as specified in the contract documents. The airplane or its components should not exhibit flutter, buzz, divergence or other aeroelastic, aerothermoelastic or aeroservoelastic instabilities. The fifteen percent safety margin shall be shown by analytical or experimental data (including flight test up to V_L). In addition, the damping coefficient g for any critical flutter mode or any significant dynamic response mode shall be at least three percent (0.03) for all altitudes and flight speeds up to V_L.

Reference 12.18 also furnishes guidelines on how the math analyses are to be performed, specifying the use of (1) compressible aerodynamics in high subsonic flight, (2) finite span assumptions, and (3) three-dimensional flow effects, if significant. Model and ground vibration tests are also specified when necessary.

For the project manager or project pilot, then, what should the important considerations be in the formulation of the test program. The driving force should be the probability of the flutter condition and its anticipated seriousness. For example, if the airplane were apt to destroy itself well

12.163

inside its performance envelope the program would be handled differently from that of a flutter clearance demonstration where the predicted safety margin was 50%.

If the program were solely for flutter, the problem would probably be very specific. In a larger prototype eval program, flutter investigations are usually clearance demonstrations, although there might be occasions when specific problems are anticipated.

At a critical flutter condition the damping ratio of one of the modes becomes zero. The object of flight flutter testing is, then, to obtain a measure of the damping values associated with the flight modes and their trends as the airspeed is progressively increased so that, from the damping trends as sub-critical conditions, the approach of a critical condition may be indicated and its speed determined by extrapolation.

Prototype airplanes represent tremendous investments in time and money. Extensive analytical, model and shake tests are performed in the design and development phase so that for most of the newer aircraft the flutter margins will have been assured. If not, the predictions on speed and damping for the problem areas will be reasonably accurate. On the initial flights the tests will be carried out to increasingly higher speeds and an actual occurrence of flutter can be spectacularly destructive. Even though many preventive measures may have been taken by the designers the possibility of such an occurrence cannot be overlooked.

For most fighter type aircraft the problem areas will not be with the basic airplane but instead with the various wing stores configurations. On large bomber or transport aircraft an aeroelastic instability may exist on the basic airplane. Regardless of whether the aircraft is new or old, large or small, the primary consideration in the program formulation should be the seriousness and probability of the flutter condition.

Other considerations in the program development are time and monetary constraints. Is the problem serious enough that the airplane may face either a grounding or a severe restriction on the envelope until a solution is found? A grounding of the entire T-37 fleet due to a potential rudder flutter problem would place an unacceptable restriction on the USAF UPT program. An airspeed restriction on a front line attack aircraft due to a possible wing flutter
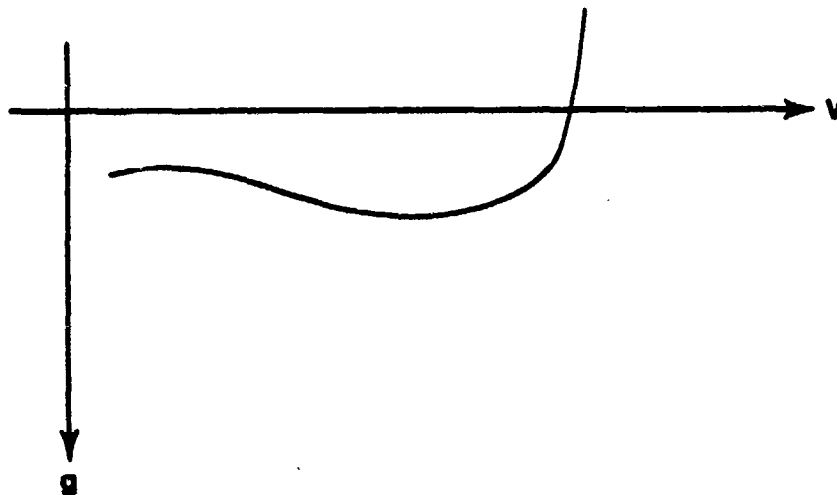
FIGURE 12.92. HYPOTHETICAL V-g DIAGRAM

problem would be intolerable during a crisis situation. In either case there
is an immediate need to find a solution - as was the case for the wing
divergence problem of the Fokker D-8 during WW I.

Along with the time constraint is the problem of money. Are there enough
funds to conduct a thorough, ground vibration test (time permitting)? What
about money to contract for an in-depth mathematical analysis? These factors
are discussed separately simply for clarity.

In preparing the test plan, of prime importance is attitude and
understanding of the details of the testing to be performed. Are all test
specifications and the pertinent aircraft characteristics totally familiar?
Can critical speeds be achieved in level flight? Will there be time at the
test points for adequate frequency sweeps by an on-board excitation system?
Do the handling qualities change significantly in the transonic range? Will
the on-board method of excitation will be adequate?

During the late 30's the Germans encountered destructive flutter on
several flight tests due to their inability to detect its onset. The
recording equipment was not satisfactory in obtaining the required data at the

time needed. The excitation equipment was inadequate in properly exciting and controlling the critical modes at subcritical speeds. It is extremely important that the approach to a critical flutter condition be recognized by observing the subcritical airplane response. Damping trends become very important as the airspeeds are increased toward the potential flutter condition, especially if the V-g diagram is of the type shown in Figure 12.92 where the slope steepens quickly at the critical condition.

12.5.15. In-flight Excitation

To assure that the critical mode is adequately excited at subcritical speeds, a special excitation system may have to be manufactured. The following methods for in-flight excitation presently exist:

(1) Manual Pulses (stick raps) - can excite frequencies up to six or seven HZ or with powered control systems, up to 10 to 12 Hz depending on aircraft size and servo capabilities. The main advantages of this technique are convenience and cost. A quick, solid rap with the open palm to the side of the stick is the method usually employed. It was used on the F-8 supercritical wing flutter investigation. The same technique was used with the TACT-F-111 except that a wooden mallet was used instead of the open hand. The main disadvantages are lack of frequency selection and the inability to excite the higher frequency modes. It is difficult to manually simulate an impulse input. The energy content in the high frequency modes is usually deficient.

(2) Ballistic Charges "Bonkers" - pulse charges have been used to excite flutter modes. These mini-explosions more closely simulate the ideal impulse with its large frequency content. The disadvantage is that these charges are usually one shot devices, if pyrotechnic.

(3) Sinusoidal Shakers (inertial Exciters) - these devices consist of either a rotating out-of-balance wheel or a mass wand oscillating at a desired frequency. The obvious advantage is frequency selectivity. The disadvantage of inertia exciters becomes apparent at low frequencies (i.e., below 3 c.p.s.) when an extremely large out-of-balance, or equivalent, is required to produce the desired force and the weight of the exciter may become prohibitive. Also, in the case of the wheel there may be an excess of shaking force at the high frequencies. The F-5, YF-17 and B-1 prototypes used mass shakers for flutter excitation.

(4) Oscillating Vanes - In this method an auxiliary aerofoil, of symmetrical section, is attached externally to the aircraft structure and is made to oscillate with a sinusoidal change of incidence by a variable-frequency driving mechanism. The method is

best suited to the excitation of low-frequency modes. In order to control the force exerted by the aerofoil it is necessary to provide some type of force-measuring like between the aerofoil and the aircraft structure and also to have independent control of incidence as well as of frequency. Nevertheless, it may be difficult to control the force with accuracy in the transonic region when large changes of lift may occur with small changes in Mach. Care must be taken to ensure that the installation of the aerofoil does not significantly affect the flutter characteristics of the aircraft. Oscillating Vanes were used in the C-141, C-5A, B-52, and A-10 test programs.

(5) Autopilot/Autostabilizer Excitation - As the state-of-the-art is advanced and more sophisticated control augmentation systems are developed, increasing dependence will be place on Autopilot/Autostabilizer systems for flutter excitation. This method may be adopted for tests on aircraft having powered flying controls. A sinusoidal voltage signal of variable frequency is fed, as an error signal, into the autopilot and this produces appropriate oscillations of the main control surfaces. Alternatively, the signal may be fed to the autostabilizer unit to produce the same result. Both methods will be effective down to zero frequency but it may be difficult to excite the higher-frequency modes of the aircraft because of attenuation which may be inherent in the transmissibility characteristics of the power control system. The advantages are obvious but the control system response plus freeplay and stiffness must be very accurately known. The F-15 flight test program involved use of the CAS for flutter excitation. The Advanced Aerial Refueling Boom (AARB) flight test program used its fly-by-wire control system to program frequency sweeps and control inputs to excite various structural modes.

(6) Turbulence - with the growth of statistical analysis applications, much more use will also be made of turbulence and other atmospheric phenomena as sources of excitation for flutter testing. A spectral density analysis of a random input can be analyzed against the output to find the correlation function. The main disadvantages are that there is no control over the amplitude and frequency characteristics of the input, and that turbulence is hard to find. Another disadvantage is that an on-line computer is required to make the responses meaningful, real time. The YF-16 test program incorporated the use of turbulence as a flutter excitation method.

The selection of the excitation method is very important. The critical mode must have sufficient excitation at subcritical speeds so that the damping behavior can be observed. This point cannot be overemphasized.

Experience has shown that it is preferable to apply the excitation as close as possible to the surfaces whose flutter characteristics are under

particular investigation, as it is not always possible to obtain adequate forced amplitudes of the surfaces under observation, by excitation at a remote point in the structure. This will mean that in a general flutter investigation is may be necessary to provide separate excitation equipment for the wings and tail end of the aircraft. For example, if inertial exciters were being used, it might be necessary to install an exciter outboard in each wing with the ability to operate in and out of phase and, in addition, independent vertical and lateral excitation in the rear fuselage. The detail positions of the exciters would be dictated by local space and strength consideration, always bearing in mind that the exciters must be placed as far as possible away from nodal lines for the modes of vibration of interest in the flutter problem.

Other areas which might need some attention in the test plan formulation are pilot-static calibrations, use of a back-up pilot in the safety/photo chase role, and so forth. The test plan must be thorough and explicit with regard to all responsibilities and functions. Yet it must be realistic enough that no one has any problems sticking to the rules.

During the early 50's at Wright-Patterson AFB flutter tests were conducted on the P-80 to obtain data on the effects of tip tank fuel c.g. travel. Lead weights were used to control the variables. The wing modes were excited by elevator raps for the symmetrical case and aileron raps for the anti-symmetrical case.

The test program was planned to cover a predetermined speed range for each flight. At each data point the pilot would excite the wings and take oscillograph records. After each flight the data would be analyzed and the speed range established for the next sortie.

After two uneventful flights the pilot felt that too much time was being wasted in flying and collecting the data so he decided to take the initiative to speed up the program. A few more airspeed increments were flown that the test card had called for and a wing bending-torsion flutter condition developed. Fortunately, he was able to jettison the tip tanks before a catastrophic failure occurred. However, the wings were so badly ripped that they could not be repaired. Analysis of the subcritical response on the oscillograph showed that there was sufficient flutter onset warning even

though the pilot could feel no change in the aircraft prior to the flutter occurrence. The moral is - develop a sound test plan and stick to it.

12.5.16 Flight Test Execution

There are also do's and don'ts in the flying and test plan execution.

(1) Precision flying is a must - do not exceed the maximum intended aerodynamic pressure. Practice build-up runs should be flown so that the procedures become rote and the pilot knows exactly how the critical speeds will be approached.

(2) There must be a minimum crew. For multi-place aircraft each crewmember must be thoroughly familiar with the egress procedures following an emergency. In past cases of flutter testing of cargo type aircraft where the risks were high, knotted ropes were secured along the floor in converging lines toward the exits. If the aircraft became uncontrollable in flight the crewmembers would be able to pull themselves toward the exits for bailout.

(3) The pilot must be completely familiar with the recovery techniques if a flutter condition were to be encountered. There would be an immediate need to reduce the q and the pilot must fully understand the effects on the airplane of throttle chops, immediate g loadings, use of S/B, stores release, and so forth. In other words, what is the exact response for the pilot if a flutter condition were encountered.

(4) An investigation should start at the higher altitudes, working first toward the Mach limits. In subsequent flights, the lower altitude, high q limits could be approached.

(5) If at any time the damping becomes less than predicted, or if they reach minimum planned for levels, recover the aircraft and regroup.

(6) The weather on test day should be near perfect. Turbulence (unless used as the excitation source) might prematurely excite the critical condition. Obstructions to vision such as cloud layers or heavy haze are not desirable during high speed dives. Strong wind shears can lead to dangerous dive attitude changes.

(7) A decision must be made on whether to test over land or over water. There is usually less turbulence and more altitude for dive recoveries over the latter. The disadvantages are distance to the recovery base and the difficulty of wreckage retrieval should an accident occur.

(8) Real time TM with computer hook up is highly recommended. This set-up would allow the engineers to monitor energy distribution of the excited modes and determine the adequacy of excitation at a subcritical speed. Also, the damping trends will be better defined so that engineering decisions based simply on successive oscillograph traces can be avoided.

(9) The aircrew should monitor the data analysis to ensure that they clearly understand how the tests are proceeding. Their inputs relative to mission progression and foreseeable problems are often times invaluable. Many of the "rules" just presented are common sense in nature.

Nevertheless, they are emphasized simply because of the many occasions in previous flight tests where catastrophes happen simply because of a failure in understanding or of communication by the aircrew. Back in 1941, flutter tests were being conducted on the twin engined AT-8. Ground vibration tests in conjunction with a wing analysis predicted a bending-torsion flutter at 217K. During the preliminary flight tests, however, no large wing oscillations were encountered even at speeds up to 221 K (only small persistent oscillations were recorded).

Consequently, a 3/8 in-lb rotational unbalance shaker was placed at the 42% semi-span on the left wing rear spar. The procedure for the pilot and flutter engineer crew was to climb to 15 thousand feet, start a gentle powered dive and tune the shaker to resonance at each incremental speed build-up. Approaching 200 K, the wing oscillations became so large that the pilot became somewhat concerned. However, since he felt that the engineer in back was watching the same oscillations without getting excited the situation was under control. It turned out that the flutter engineer was on his knees controlling the knobs on the excitation and recording equipment and was not in fact observing the large oscillations.

This example illustrates the importance of each person involved knowing what his and everyone else's responsibility is in a hazardous test program. Another misconception was noted then and at other times prior and subsequent: If the flutter engineer is aboard things must be okay.

A successful test program requires that the crew thoroughly understand the problem, the aircraft capabilities and characteristics, the whys and wherefores in the data accumulation and analyses, and the individual responsibilities in the flight test execution. Like in all group efforts (and so well exemplified in the game of football), a sound game plan, followed by total concentration in individual execution is a must. Happy landing.

12.5.17 Brief Example

We will very briefly discuss the Northrop T-38 as an example of how flutter characteristics of a prototype aircraft are determined through design, analysis, tunnel and ground vibration tests. The emphasis is not on detail but on overall approach. Some of the measures taken to identify and eliminate possible problem areas will be discussed.

Non-steady aerodynamic theories are usually conservative in that the calculated speeds at which instability will occur are usually lower than actual. Because of this, and due to the limitations of beam theory analyses the basic flutter inputs into the T-38 design philosophy were to be derived from wind tunnel model tests. Analytic calculations were made mainly to define speed increments resulting from structural changes and variations in the surface boundary conditions.

Ground vibrations tests on the airplane were run primarily to verify the calculated modes and to illuminate deficiencies in the structural boundaries and the safety margins on the final wing design. Flutter flight test confirmed the safety margins on the production aircraft.

The vibration and flutter analyses of each of the T-38 aerodynamic surfaces were based on the following assumptions: (1) Spanwise distributions of bending and torsional stiffness were represented along a straight swept elastic axis; (2) Surface mass distributions were represented by inertially equivalent strips perpendicular to the elastic axis as shown in Figure 12.93; (3) Oscillating surface aerodynamic forces were approximated by two-dimensional aerodynamic forces calculated for streamwise strips as shown in Figure 12.94, and (4) A flutter mode was represented by a superposition of a finite number of natural vibration modes.
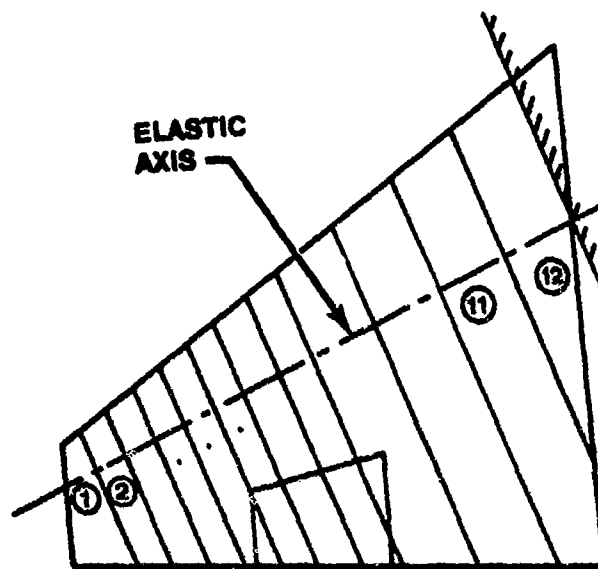
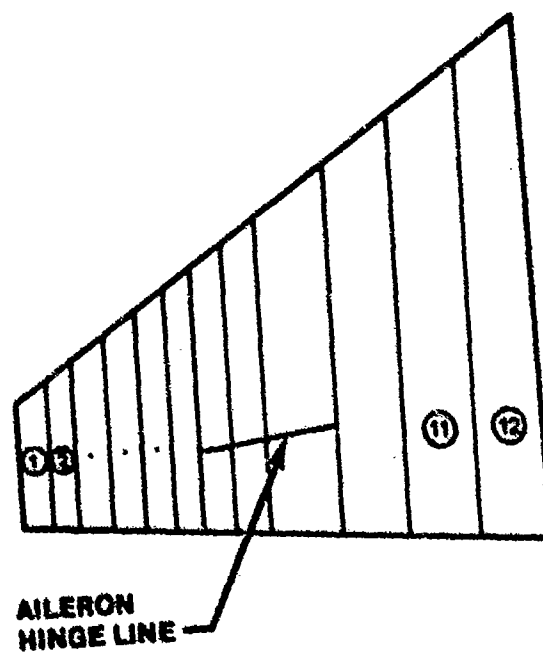FIGURE 12.93.   STRUCTURAL MODEL OF T-38 WING

FIGURE 12.94.   AERODYNAMIC MODEL OF T-38 WING

12.172

The first two assumptions lead to a static beam problem with inertia loadings induced by the mass section oscillations. The strip theory aerodynamic terms used in the flutter analysis were initially based on the incompressible flow oscillating wing section theory of Theodorsen. In follow-up analyses the lift curve slopes were adjusted from the infinite AR 2π value to wind tunnel derived ones.

The three low speed tunnel models used the spanwise mass distribution shown in Figure 12.93. The high speed models simulated the actual aircraft structure with scaled down skins and spars. All models were vibrated prior to the tunnel tests to verify the dynamic simulation.

The general results of the wing tests are as follows. Flutter boundary determination was difficult because of the high stability of the wing. No flutter occurred during the transonic tests at Cornell where 115% limit velocities were achieved at Mach between 0.78 and 0.94. A mild flutter may have occurred with the addition of aft ballast at M = 0.86. Based on an analytical extrapolation comparing the bare wing with the ballasted one a safety margin of 32% was predicted.

Tunnel tests at AEDC revealed a possible low damping region at M = 0.85 and q = 2340 (V_e = 850 K). The wing was lost at q = 3480. Even a conservative estimate yielded a safety margin of 38%.

The high speed wing tests at Cornell covered a range of aileron rotation to second wing bending (ω_β/ω_2) from 0.92 to 1.48. No aileron flutter or buzz instability was observed. Very briefly, the overall conclusions of the T-38 flutter characteristics were as follows:

Wing and Aileron - no special problems were found in this area.

Vertical Fin and Rudder - except for the destabilizing effect of a three pound extended fuel vent, the vertical fin did not present any major stability problems.

Horizontal Stabilizer - this was initially the most critical of the T-38 aerodynamic surfaces. Flutter problem areas were associated with actuator stiffness, torque tube bending stiffness, freeplay in the actuator system, and the possibility of fuselage vertical bending/horizontal stabilizer bending flutter. The presence of freeplay in the actuator system resulted in a significant decrease in model flutter speeds. As a result, rigging procedures were adopted to eliminate freeplay on the airplane.

The level of pitch stiffness on the stabilizer was found to be deficient during the ground vibration tests. Increases in horn size and hydraulic cylinder stiffness were required to alleviate the coupled stabilizer pitch - torsion problem. In fact, one of the more significant recommendations made in the report was that more rigid controls were required in the future on the specific problem of actuator stiffness and freeplay.

It is appropriate at this time to present a quote from the "DISCUSSION AND CONCLUSIONS" section of the report.

"Identification and elimination of the T-38 flutter problem areas has required a coordinated effort in the fields of theoretical analysis, ground vibration testing, and wind tunnel flutter model testing. No one of these investigations would have been completely effective without the additional information received from the other studies. The final confirmation of aircraft flutter freedom has come from the best possible source - flight flutter tests of the production aircraft."

BIBLIOGRAPHY

12.1.   Cataldo, C.E. "Overview of Composites for Space Shuttle Structures," George C. Marshall Space Flight Center, Alabama.

12.2.   Rosen, B. W. "Structural Composites - Design and Analysis," Materials Sciences Corporation, Blue Bell, PA (Drexel University Seminar).

12.3.   Lovelace, A.M. and Tsai, S.W. "Composites Enter the Mainstream of Aerospace Vehicle Design," Astronautics and Aeronautics, pp. 56-61, July 1970.

12.4.   Tsai, S.W. "Mechanics of Composite Materials, Part I, Introduction," AFML-TR-66-149, June 1966.

12.5.   McQuillen, E.J. and Shih, H.L. "Graphite-Epoxy Wing for BWM-34E Supersonic Aerial Target," Journal of Aircraft, Vol. 8, No. 6, pp 480-486, June 1971.

12.6.   Chow, P.C., Carleone, J. and Hsu, C.M. "Effective Elastic Constants of Layered Media," Report No. 71-18, Mechanics and Structures Advanced Study Group, Drexel University, Philadelphia, PA., October 1971.

12.7.   Materials (A Scientific American Book), W.H. Freeman and Co., San Francisco, 1967.

12.8.   Nicholls, R. "Composite Construction Materials Handbook," Prentice-Hall, Inc., Englewood Cliffs, NJ., 1976.

12.9.   Broutman, L.J. and Krock, R.H. "Modern Composite Materials," Addison-Wesley Publishing Co., Menlo Park, CA., 1967.

12.10. BISPLINGHOFF, R.L., ASHLEY, H., and HALFMAN, R.L. Aeroelasticity, Adison-Wesley Publishing Co., Inc., MA, 1955.

12.11. ABRAMSON, H.N. The Dynamics of Airplanes, The Ronald Press Co., New York, 1958.

12.12   GARRICK, I.E. Editor, Aerodynamic Flutter, AIAA Selected Reprint Series, March, 1969.

12.13   LONG, J.A., Jr., and BERRY, R.L. X-24-B Ground Vibration Test (Speedbrake/Aileron/Fin/Rudder), AFFTC FTC-TR-73-23, June, 1973.

12.14   LONG, J.A., Jr. Flutter Test Techniques as Demonstrated in the NASA F-8 Supercritical Wing Program, Flight Test Technology Branch Office Memo, Air Force Flight Test Center, January, 1973.

12.15   SCHWARTZ, S., and ROONEY, T.R. T-38 Flutter Characteristics
        Summary, NAI-58-11, Northrop Corp., Hawthorne, CA, June, 1960.

12.16   McCRACKEN, D.W. Flutter Boundary Testing, from the Pilots Handbook
        for Critical and Exploratory Flight Testing, SETP, CA. 1972.

12.17   TOLVE, L.A. History of Flight Flutter Testing, Lockheed Aircraft
        Corp., Marietta, GA.

12.18   MILITARY SPECIFICATION, MIL-A-008870A (USAF), Airplane Strength and
        Rigidity, Flutter, Divergence, and Other Aeroelastic Instabilities,
        31 Mar 1971.

12.19   KARAMCHETI, K. Principles of Ideal-Fluid Aerodynamics, John Wiley
        and Sons, Inc., New York, 1966.

12.20   THOMSON, W.T. Vibration Theory and Applications, Prentice-Hall,
        Inc., New Jersey, 1965.

12.21   KORDES, E.E. Chairman, NASA Symposium on Flutter Testing
        Techniques, NASA SP-415, October 9-10, 1975.

12.22   THEODORSON, T. General Theory of Aerodynamic Instability and the
        Mechanism of Flutter, NACA Report No. 496, 1935.

CHAPTER 13

FEEDBACK CONTROL THEORY

13.1 FUNDAMENTALS OF FEEDBACK CONTROL THEORY

Pilots might be inclined to associate the phrase "control system" with only aircraft flight control systems. Although the control system theory of this course has a large application to flight control systems, this material applies to any process or system in which control is exercised over some output variable. Examples of these controlled variables are: the speed of an automobile, the temperature of a room, the attitude of a spacecraft, ad infinitum.

Feedback control system theory is often called several different things. It might be found under any of the following headings or titles: Control Systems, Automatic Control Systems, Servo-Mechanisms, or our term, Feedback Control Systems.

First, the difference between "open-loop" and "closed-loop" control will be discussed. Consider the roll channel of an aircraft flight control system in which the pilot input is assumed to be a rate command. That is, the pilot commands a roll rate ($\dot{\phi}$) proportional to the stick displacement. Figure 13.1 shows a diagram of this system. The input is a low power input representing a selected value of roll rate.
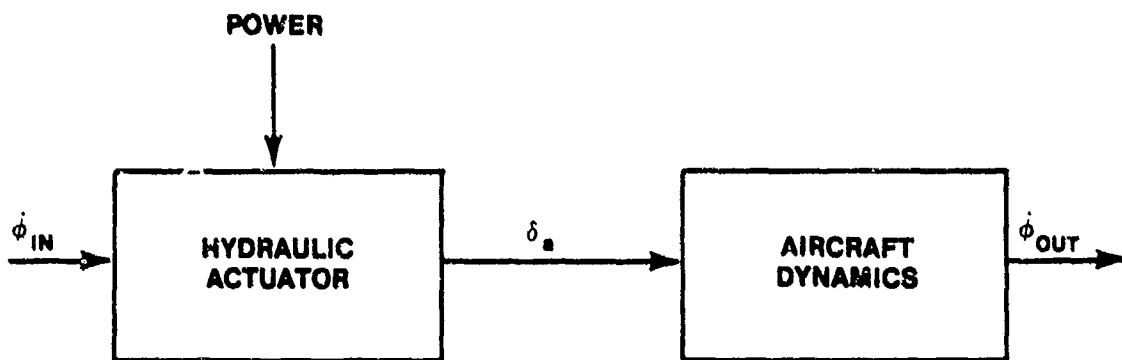

FIGURE 13.1   OPEN-LOOP CONTROL SYSTEM

This mechanical signal is then amplified in a hydraulic control valve/actuator combination to position the ailerons accordingly (δ_a). The deflected ailerons then react with the airstream to produce a roll moment in the required direction. The magnitude of the resultant roll rate ($\dot{\phi}_{out}$) is a function primarily of the dynamic pressure (q) and the moment of inertia about the longitudinal axis (I_x). Both are part of aircraft dynamics.

There are innumerable examples of the "non-feedback" or "open-loop" type of control systems. For instance, a gasoline engine in an automobile has a low power input, the throttle position, which controls the speed of the vehicle expending a large amount of power. In a simple electronic amplifier a very small input signal controls a much larger output signal. In all open-loop control systems the output has no influence on the input whatsoever. The input quantity controls the output only directly through the intermediate components. Referring back to the aircraft roll control system, a lateral stick displacement of a specified amount will not command a constant roll rate under all conditions. As the conditions in the intermediate components change, such as the dynamic pressure, moment of inertia, hydraulic pressure, temperature of hydraulic fluid, condition of hydraulic components, temperature effects on modulus of elasticity of metal components, etc., the resultant roll rate for a specified input will vary.

The performance of any control system with respect to maintaining the output quantity as close as possible to the input quantity can be substantially improved by feeding back the output for comparison with the input. The use of the difference resulting from this comparison as an actuating signal constitutes a feedback or closed-loop control system.
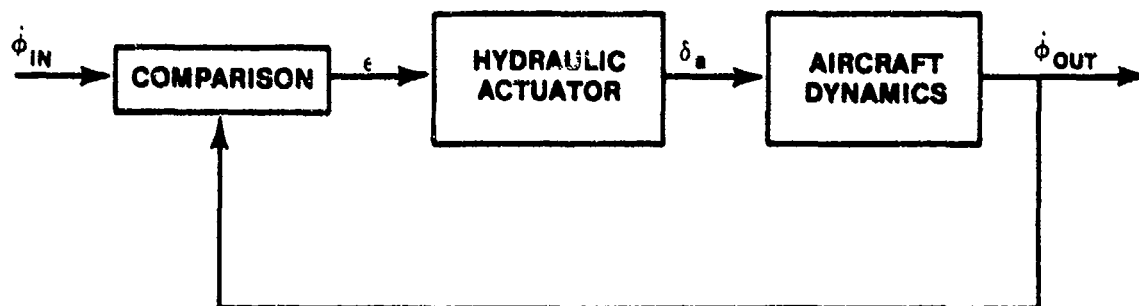

FIGURE 13.2. CLOSED-LOOP CONTROL SYSTEM

Figure 13.2 shows how the open-loop system of Figure 13.1 can be changed to a closed-loop system by the addition of an outer feedback loop to compare the input with the output. Thus, the effect of variations in the intermediate components can be eliminated in that a corrective signal (ϵ) will continue to exist until the output properly matches the input.

A serious disadvantage of closed-loop control systems, however, is that they can make an otherwise stable system unstable. The possibility of instability is the prime reason for the existence of the science of feedback control system analysis. The first and major effort in control system analysis is the determination of whether or not the closed-loop system is stable. After this fact is established, other response characteristics may be found.

Stability, with respect to control systems is defined as follows: A stable system is a system in which the transients die out with increasing time.

13.2 NOMENCLATURE

The following nomenclature is used in this chapter:

$$R = \text{input variable}$$

$$C = \text{output variable}$$

Each of these might represent any quantity depending on the system such as angular or linear position, current, voltage, degrees of temperature, etc, or the time rate of change of those above.

The following symbol represents a summer or differential. It indicates the algebraic summation of the input quantities according to the arrows and
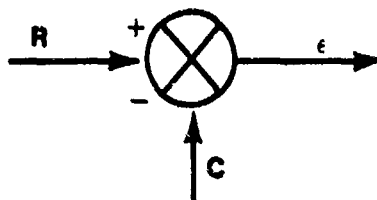

FIGURE 13.3. SUMMER OR DIFFERENTIAL

the signs. The example in Figure 13.3 shows

$$\epsilon = R - C \qquad (13.1)$$

The symbol for gain or amplification factor is K.

Control systems are generally described through the use of block diagrams as in Figures 13.1 and 13.2. However, instead of words to indicate the process or operation occurring within each block, there appears what is called a transfer function (Figure 13.4). The term "transfer function" might be thought of as what is done to the input to produce the output. Although the transfer functions within the blocks are generally written in terms of some operator notation, they are often described graphically, especially for nonlinear systems. A definition of transfer function is: the ratio of the output to the input expressed in Laplace operator notation, assuming zero initial conditions. The transfer function is essentially a mathematical model of the system and embodies all the physical characteristics of the system i.e., mass, damping, etc.

$$R \longrightarrow \boxed{\begin{array}{c} \text{TRANSFER} \\ \text{FUNCTION} \end{array}} \xrightarrow{\quad C \quad}$$
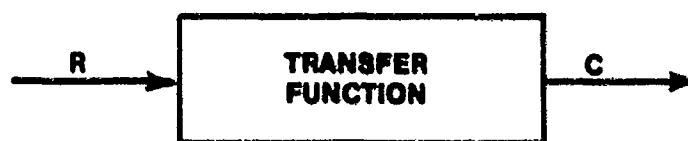
$$C = \left[\begin{array}{c} \text{TRANSFER FUNCTION} \\ \text{(IN OPERATOR} \\ \text{NOTATION)} \end{array} \right] \times R$$

$$\frac{C}{R} = \left[\begin{array}{c} \text{TRANSFER FUNCTION} \\ \text{(IN OPERATOR} \\ \text{NOTATION)} \end{array} \right]$$

FIGURE 13.4. TRANSFER FUNCTION

13.3 DIFFERENTIAL EQUATIONS - CLASSICAL SOLUTIONS

Differential equations for a control system will illustrate the types of responses to be expected from first and second order systems. These two examples are used throughout this course because higher-order systems produce a transient response consisting of the sum of first and second-order responses.

The reason the transient response is significant rather than the steady state or complete response, concerns the stability of the system. Since positive stability requires that the transients die away with increasing time, the transient solution of the differential equation describing the system is most important to the analysis. The transient solution also provides other important response characteristics.

Figure 13.5 shows a simplified block diagram of VTOL Auto Pitch Control with inertia, I_y, and limited aero-damping proportional to pitch rate. Pitch attitude is maintained by reaction control jets. These jets produce a torque proportional to a valve position. Torque = $\mu\epsilon$, where μ is the gain of the valve and ϵ the input to the valve. The loop is closed by comparing the output pitch attitude to the commanded pitch attitude.
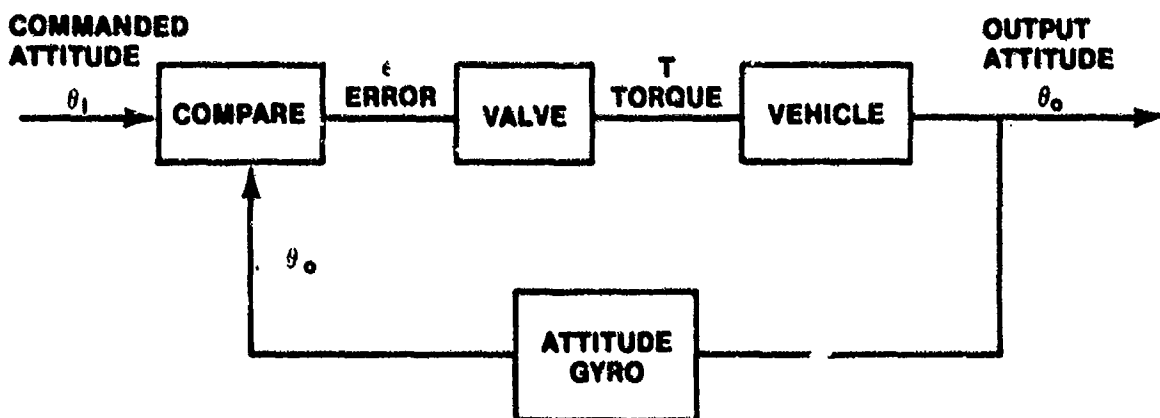

FIGURE 13.5. VTOL AUTOMATIC PITCH CONTROL BLOCK DIAGRAM

This comparison produces the error signal, ε, which is the input to the linear valve. The resulting torque, $\mu\varepsilon$, is applied to the vehicle to change the pitch attitude.

Two situations will be considered in order to simplify the problem. In the first case, only the effect of viscous damping will be considered. This will result in a first-order differential equation. The second case will include both inertia and viscous friction and will result in a second-order system. The first and second-order differential equations will be solved for the transient response.

13.3.1 First-Order System

Using Figure 13.5, including only the effect of damping on the vehicle, the differential equation of the system can be written by equating the applied torque to the absorbed torque. The torque applied by the reaction jets is absorbed by the viscous friction (aero-damping) of the vehicle.

$$\mu\varepsilon = b\dot{\theta}_0$$

The output of the comparator, $\varepsilon = \theta_i - \theta_0$ that produces the system differential equation or the equation of motion

$$\mu(\theta_i - \theta_0) = b\dot{\theta}_0$$

Applied Torque = Absorbed Torque

Using the operator "p" notation (where $p = d/dt$) to determine the system transient response, the homogeneous equation becomes

$$\frac{b}{\mu}p\,\theta_0 + \theta_0 = 0$$

13.6

$$\left(\frac{b}{\mu} p + 1\right) \theta_0 = 0$$

the root of the characteristic equation is

$$p = -\frac{\mu}{b}$$

Since the transient response is assumed to be

$$\theta_0(t)_{transient} = \sum_{i=1}^{n} C_i e^{p_i t} \tag{13.2}$$

where p_i's are the roots of the characteristic equation, the transient response for our first order system is

$$\theta_0(t)_{transient} = Ce^{-(\mu/b)t} \tag{13.3}$$

For positive gain μ, and damping factor b, is always stable. Thus, a first-order system has only real roots of the characteristic equation and the transient response is either an exponential increase or decrease depending on the sign on the time constant. The time constant is the reciprocal of the coefficient of t in the exponent of e (b/μ in our case).

The time constant, generally given the symbol τ, can be defined as the value of time that makes the exponent of e equal to -1. In one time constant the exponential $e^{-t/\tau}$ has decreased from the value 1 to the value 0.368. Figure 13.6 shows a plot of the transient response of a first-order stable system. Time constants are discussed in more detail in Paragraph 13.5.4.
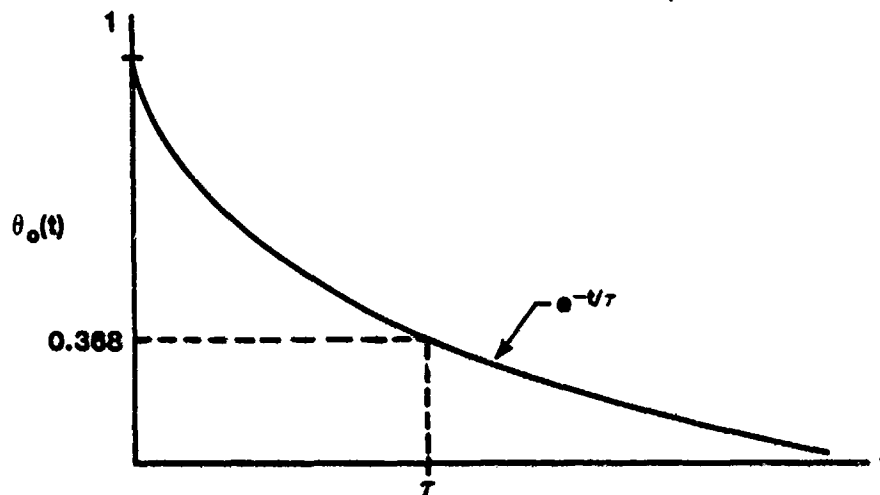
13.7

FIGURE 13.6. PLOT OF FIRST ORDER TRANSIENT RESPONSE

A stable transient response requires the root of the characteristic equation be negative.

13.3.2 Second-Order System

Equating applied torque to absorbed torque of Figure 13.5 again, but including the inertia and damping effects yields

$$\mu\varepsilon = b\dot{\theta}_0 + I\ddot{\theta}_0$$

again

$$\varepsilon = \theta_i - \theta_0$$

and

$$\upsilon(\theta_i - \theta_0) = b\dot{\theta}_0 + I\ddot{\theta}_0$$

$$I\ddot{\theta}_0 + b\dot{\theta}_0 + \mu\theta_0 = \mu\theta_i$$

is the equation of motion of the system. The homogeneous equation in operator notation is

13.8

$$\theta_0 (Ip^2 + bp + \mu) = 0$$

The characteristic equation is

$$Ip^2 + bp + \mu = 0 \tag{13.4}$$

whose roots are

$$P_{1,2} = \frac{-b \pm \sqrt{b^2 - 4\mu I}}{2I} \tag{13.5}$$

Depending on the relative magnitudes of the gain, damping factor, and inertia, the roots of the characteristic equation might be real or complex thereby indicating different types of response. If the roots turn out to be real, the transient response is merely the sum of the two resulting first-order exponential terms. If the roots are complex, however, they always appear in complex conjugate pairs in the following form:

$$P_{1,2} = \sigma \pm j\omega_d$$

where σ is the real part and ω_d the imaginary part of the roots. These complex roots yield a solution of the form

$$\theta_0(t)_{transient} = C_1 e^{(\sigma+j\omega_d)t} + C_2 e^{(\sigma - j\omega_d)t} \tag{13.6}$$

After complex variable manipulations, this expression can be shown to be equivalent to

$$\theta_0(t) = Ae^{\sigma t} \cos(\omega_d t + \phi) \tag{13.7}$$

where A and ϕ are derived from the coefficients C_1 and C_2.

This is the form of the solution whenever the characteristic equation has complex conjugate roots.
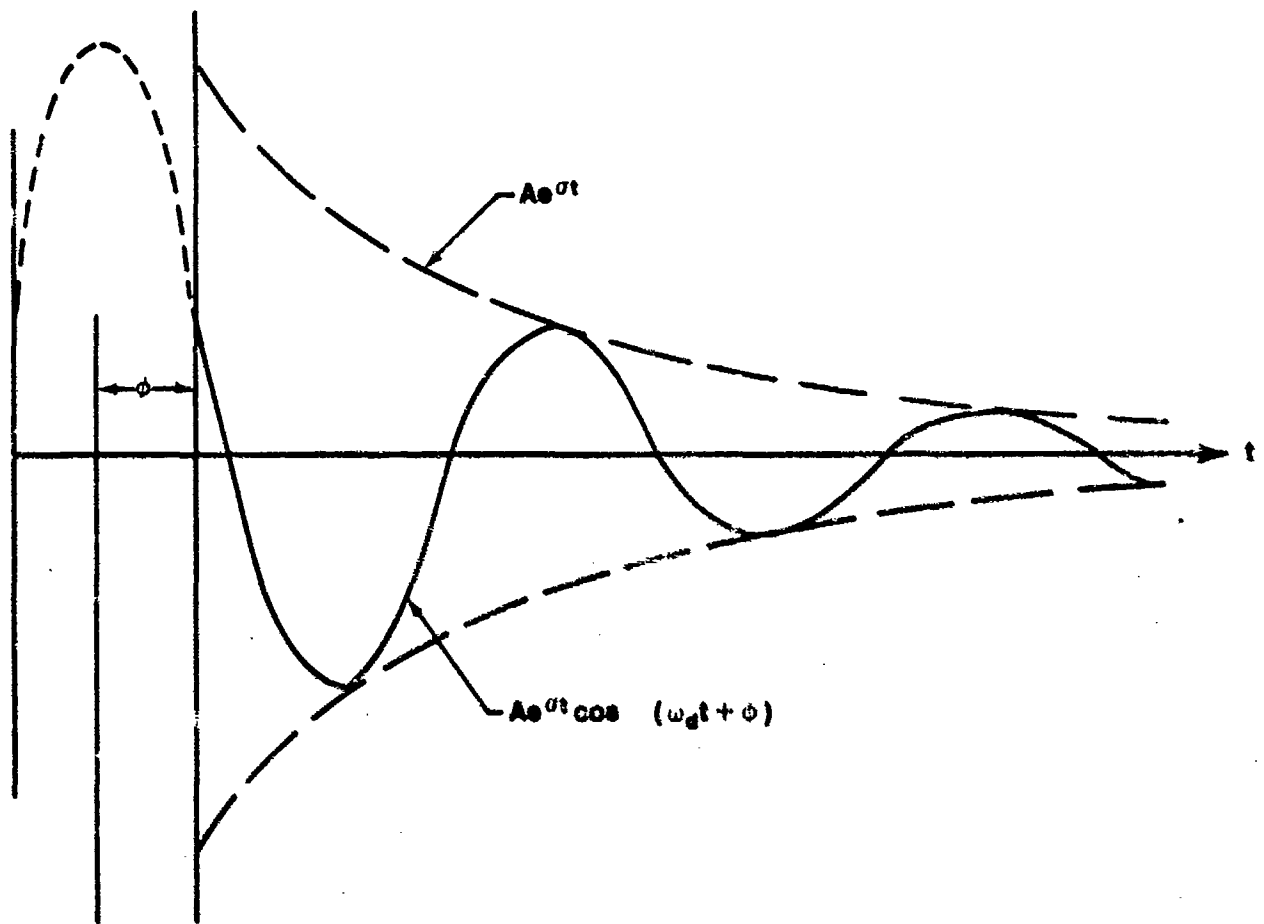

FIGURE 13.7. EXPONENTIALLY DAMPED SINUSOID - TYPICAL SECOND-ORDER SYSTEM RESPONSE

It is called an exponentially damped sinusoid and consists of a sine wave of frequency ω_d whose magnitude is $Ae^{\sigma t}$; that is, it is decreasing exponentially with time if σ is a negative quantity. A typical second-order response is plotted in Figure 13.7.

Referring back to the solution of the characteristic equation, Equation 13.5, the real part can be recognized as the exponent of e

$$\sigma = -\frac{b}{2I} \qquad (13.8)$$

and the imaginary part as the frequency of the oscillation of the transient response

$$\omega_d = \sqrt{\frac{b^2 - 4\mu I}{4I^2}} \qquad (13.9)$$

The quantity b represents the effective damping of the system. If b equals $2\sqrt{\mu I}$ the two roots $p_{1,2}$ are equal. This is the critical level of damping and is written $b' = 2\sqrt{\mu I}$.

The damping ratio is defined as the ratio of actual damping to the critical value of damping

$$\zeta = \frac{\text{actual damping}}{\text{critical damping}} = \frac{b}{b'} = \frac{b}{2\sqrt{\mu I}} \qquad (13.10)$$

When ζ is greater than zero but less than one the roots are complex and the solution is a damped sinusoid of the form of Figure 13.8 and is called underdamped. When ζ is greater than one the roots are real and the response is overdamped. When ζ is negative, the system is unstable.

The undamped natural frequency, ω_n is defined as the frequency of oscillation of the transient if the damping is zero. From Equation 13.9

$$\omega_n = \sqrt{\frac{\mu}{I}} \qquad (13.11)$$

The response in the case of no damping is a sine wave of constant amplitude.

Second-order equations (or factors in more complex systems) are frequently written in terms of the damping ratio and undamped natural frequency. Factoring μ from Equation 13.4 leaves

$$\frac{I}{\mu} p^2 + \frac{b}{\mu} p + 1 = 0 \qquad (13.12)$$

13.11

where I/μ can be recognized as $1/\omega_n^2$ and b/μ equals $2\zeta/\omega_n$. The characteristic equation becomes

$$\frac{1}{\omega_n^2} p^2 + \frac{2\zeta}{\omega_n} p + 1 = 0$$

Multiplying by ω_n^2 produces the standard form of the second-order system.

$$p^2 + 2\zeta\omega_n p + \omega_n^2 = 0 \tag{13.13}$$

The roots of this equation are

$$p = \sigma \pm j\omega_d = -\zeta\omega_n \pm j\omega_n\sqrt{1 - \zeta^2} \tag{13.14}$$

And the transient response in terms of ζ and ω_n is

$$c(t)_{\text{transient}} = Ae^{-\zeta\omega_n t} \cos\left(\omega_n t \sqrt{1 - \zeta^2}\, t + \phi\right) \tag{13.15}$$

Figure 13.8 shows a family of curves representing the response to a step input of a second-order system as a function of ζ. These curves illustrate the fact that the amount of overshoot and the time to arrive at the input value are a function of ζ.
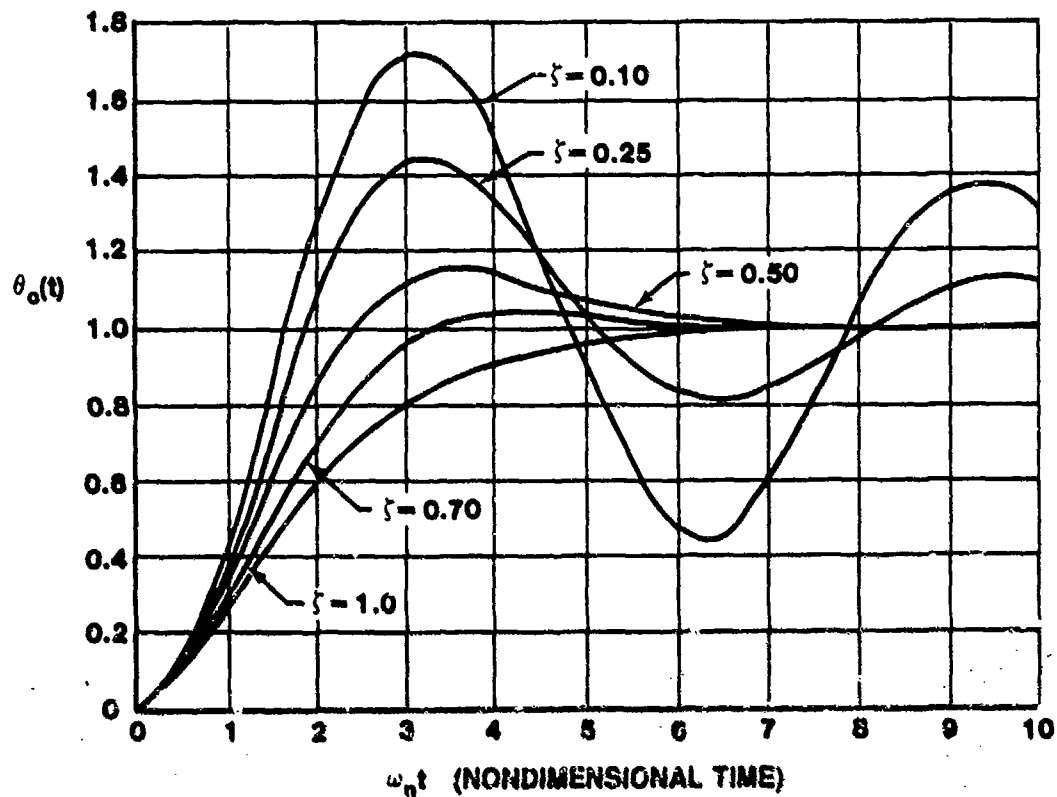
FIGURE 13.8.   SECOND-ORDER TRANSIENT RESPONSE VERSUS ζ

13.4   TRANSFER FUNCTIONS

The first and second-order equations derived in the previous paragraph were solved using the classical method to show the types of response to be expected from each type system.   In practice, this approach is extremely laborious, if not impossible, for more complicated systems.   Therefore, more advanced techniques are used which do not produce the total solution but do indicate whether or not the system is stable; and if not, provide information about how to make the system stable.   These sophisticated techniques generally use Laplace transforms.   The use of operational calculus offers a definite advantage in that transfer functions can be manipulated using the normal rules of algebra.   It also imposes a severe restriction.   The systems to be

analyzed must be representable by linear differential equations with constant coefficients. The method of determining these transfer functions will now be described.

First, we will consider the system of Figure 13.5 in which only damping was included. Its equation of motion is

$$\frac{b}{\mu} \dot{\theta}_0 + \theta_0 = \theta_i$$

Letting $\tau = b/\mu$ we have

$$\tau\dot{\theta}_0 + \theta_0 = \theta_i$$

Taking the Laplace transform using the notation $\mathcal{L}[\theta_0(t)] = \theta_0(s)$

$$\tau s\theta_0(s) - \tau\theta_0(0^+) + \theta_0(s) = \theta_i(s)$$

where

$\theta_0(0^+)$ is the value of $\theta_0(t)$ at $t = 0^+$

$$\theta_0(s)[\tau s + 1] = \theta_i(s) + \tau\theta_0(0^+)$$

$$\theta_0(s) = \frac{\theta_i(s)}{\tau s + 1} + \frac{\tau\theta_0(0^+)}{\tau s + 1}$$

Thus we see that the input to the system is acted upon by the transfer function

$$\frac{1}{\tau s + 1} \tag{13.16}$$

and also the initial condition is acted upon by this transfer function.

From this brief discussion we can see that if we assume all the initial conditions to be zero we obtain the relationship

$$\frac{\theta_0(s)}{\theta_i(s)} = \frac{1}{\tau s + 1} \tag{13.17}$$

Our first-order system can then be described in the manner of Figure 13.4 where $G(s) = 1/(\tau s + 1)$, the transfer function.

The transfer function of our second-order system in which the inertia and damping were considered will now be determined using the same procedure. From its equation of motion,

$$I \ddot{\theta}_0 + b \dot{\theta}_0 + \mu \theta_0 = \mu \theta_i$$

taking the Laplace transform and assuming all initial conditions to be zero we have

$$\frac{I}{\mu} s^2 \theta_0(s) + \frac{b}{\mu} s \theta_0(s) + \theta_0(s) = \theta_i(s)$$

$$\theta_0(s) \left[\frac{I}{\mu} s^2 + \frac{b}{\mu} s + 1 \right] = \theta_i(s)$$

The transfer function is then

$$\frac{\theta_0(s)}{\theta_i(s)} = \frac{1}{\dfrac{I}{\mu} s^2 + \dfrac{b}{\mu} s + 1} \tag{13.18}$$

The transfer functions that have been developed for first and second-order systems (Equations 13.17 and 13.18) are obtained from the equation of motion of the whole system with the feedback loops closed (Figure 13.5). Therefore, they are called closed-loop transfer functions.

The denominator of Equation 13.18 is equivalent to Equation 13.12 and is the characteristic equation of the system.

13.5 TIME DOMAIN ANALYSIS

Much of the work of the control system engineer is done in the s-domain to take advantage of simplicity of solution, but the response of a system is in the time domain. The time response of a system is divided into two parts: (1) the transient response, and (2) the steady-state response.

$$c(t) = c_{trans}(t) + c_{s.s.}(t) \qquad (13.19)$$

In order to analyze a control system, we discuss the performance of the system in terms of time response to a specific input. For a given system, a specific input will result in a predictable transient response and a steady-state error. Control system performance specification can be stated in terms of the transient behavior of the system and the allowable steady-state error. In general, the steady-state error can be a function of time; however, we usually want $\lim_{t \to \infty} e(t)_{ss} = 0$.

In reality, control system specification and obtainable real world solutions are a compromise. The first order of business in analyzing a control system is to determine if the system is stable. If it is stable, then it will be tested to determine if it meets the performance specifications. The response of the system to specific test inputs will provide several measurements of performance.

13.5.1 Typical Time Domain Test Input Signals

13.5.1.1 The step input is the most commonly used test signal. This input is simply an instantaneous change in the reference input variable (Figure 13.9).
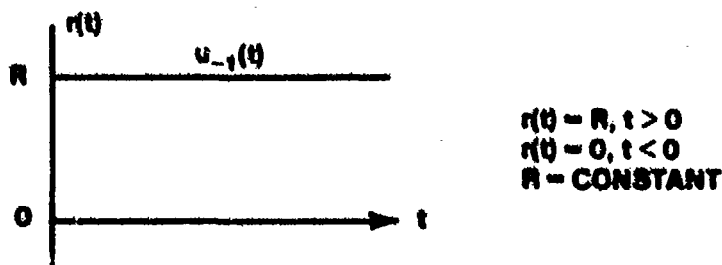

FIGURE 13.9. STEP INPUT

$$r(t) = u_{-1}(t)$$

where $u_{-1}(t)$ is the unit step function. The quantity $r(t)$ is not defined at $t = 0$. The Laplace transform of the unit step is

$$\mathcal{L}\{u_{-1}(t)\} = \frac{1}{s} \qquad (13.20)$$

Therefore the Laplace of $r(t) = Ru_{-1}(t)$ is R/s.

13.5.1.2 <u>Ramp Function</u>. The ramp signal is the integral of the unit step and is often called the velocity input (Figure 13.10).
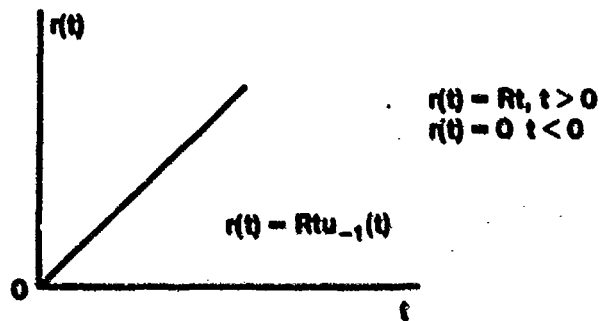
r(t) = Rt, t > 0
r(t) = 0 t < 0

r(t) = Rtu_{-1}(t)

FIGURE 13.10. RAMP INPUT

$$r(t) = Rt\, u_{-1}(t)$$

and

$$\mathcal{L}\{Rt\, u_{-1}(t)\} = \frac{R}{s^2} \qquad (13.21)$$

13.5.1.3 <u>Parabolic Input</u>. The parabolic input signal (Figure 13.11) is the integral of the ramp signal and is often referred to as the acceleration input.
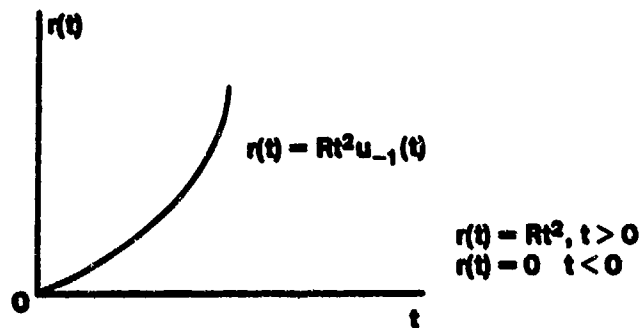
FIGURE 13.11. PARABOLIC INPUT

$$r(t) = Rt^2 u_{-1}(t)$$

and

$$\mathcal{L}\{Rt^2 u_{-1}(t)\} = \frac{2R}{s^3} \tag{13.22}$$

13.5.1.4 Power Series Input. An input made up of the sums of a step, ramp and a parabola would be a power series of power 2.

$$r(t) = R\left[1 + t + \frac{t^2}{2}\right] u_{-1}(t) \tag{13.23}$$

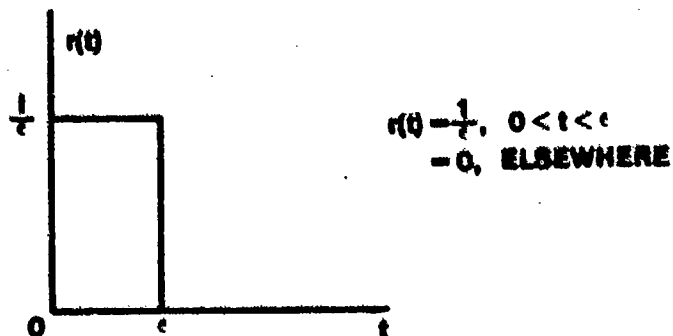13.5.1.5 Unit Impulse. Another useful input is the unit impulse (Figure 13.12).

FIGURE 13.12. UNIT IMPULSE

13.18

As $\varepsilon \to 0$, the function $r(t)$ approaches the impulse function $\delta(t)$.

$$\mathcal{L}\{\delta(t)\} = 1 \qquad (13.24)$$

13.5.2 Time Response of a Second-Order System

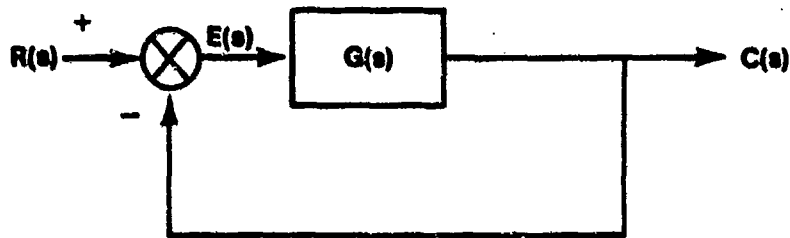Consider the closed loop block diagram in Figure 13.13

FIGURE 13.13. CLOSED-LOOP CONTROL SYSTEM

where

$$C(s) = \frac{G(s)\ R(s)}{1 + G(s)} \qquad (13.25)$$

Let

$$G(s) = \frac{K}{s(s + a)}$$

$$C(s) = \frac{\dfrac{K}{s(s + a)}\ R(s)}{1 + \dfrac{K}{s(s + a)}}$$

$$= \frac{K}{s^2 + as + K}\ R(s)$$

This equation can be generalized in terms of ζ and ω_n.

Let $a = 2\zeta\omega_n$, $K = \omega_n^2$.

Then the control ratio $C(s)/R(s)$ is

$$\frac{C(s)}{R(s)} = \frac{\omega_n^2}{s^2 + 2\zeta\omega_n s + \omega_n^2} \qquad (13.26)$$

For a unit step input, $R(s) = 1/s$, and

$$C(s) = \frac{C(s)}{R(s)}\ R(s)$$

$$C(s) = \frac{\omega_n^2}{s\left(s^2 + 2\zeta\omega_n s + \omega_n^2\right)} \qquad (13.27)$$

Taking the inverse Laplace gives the transient response

$$c(t) = 1 - \frac{1}{\beta} e^{-\zeta\omega_n t} \sin(\omega_n \beta t + \phi) \qquad (13.28)$$

where $\beta = \sqrt{1 - \zeta^2}$ and $\phi = \tan^{-1} \beta/\zeta$. The transient response of this system varies according to the selected value of ζ. Figure 13.14 depicts this variation.

Several standard performance specification terms common throughout industry are illustrated in Figure 13.15.
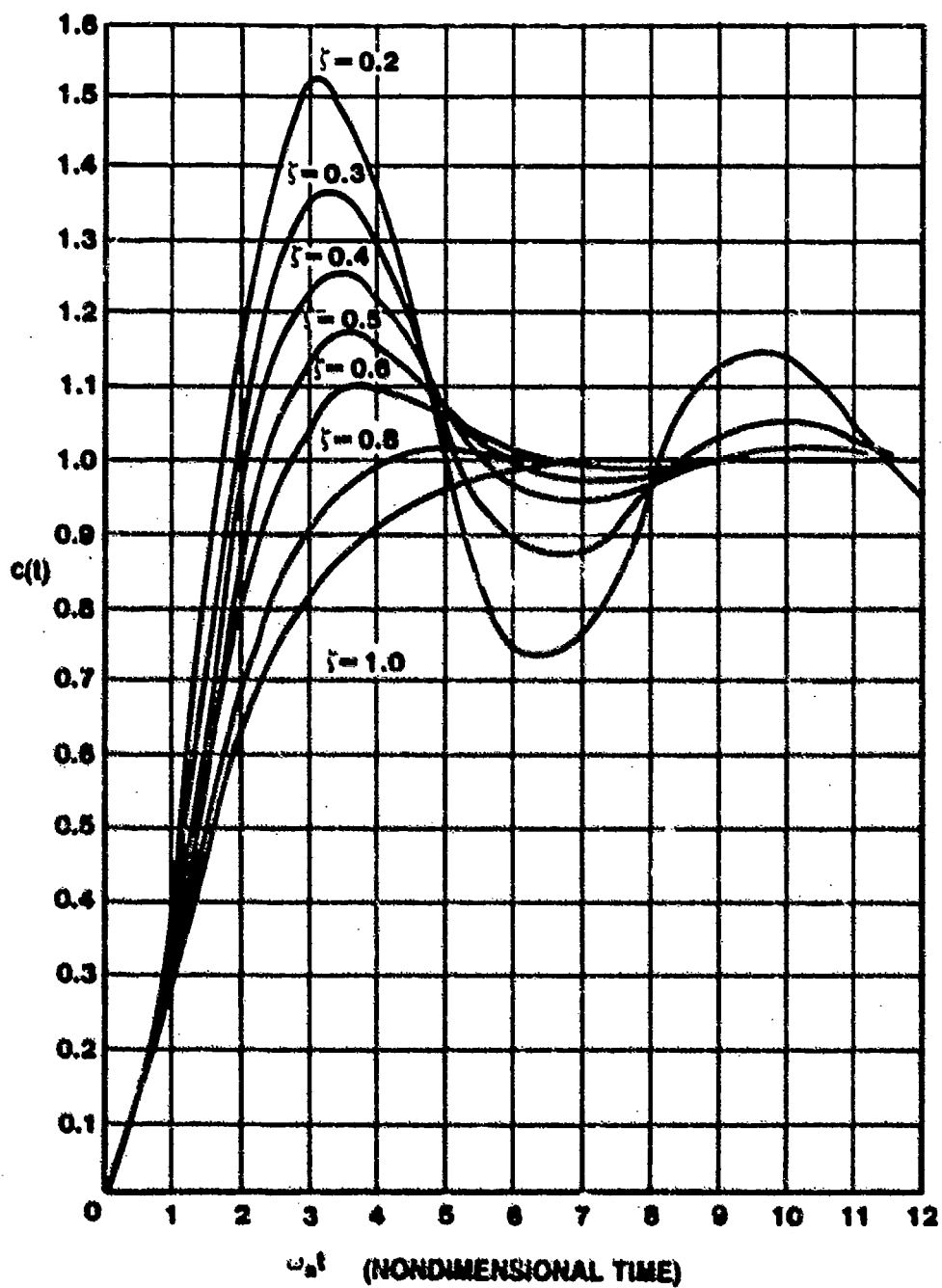
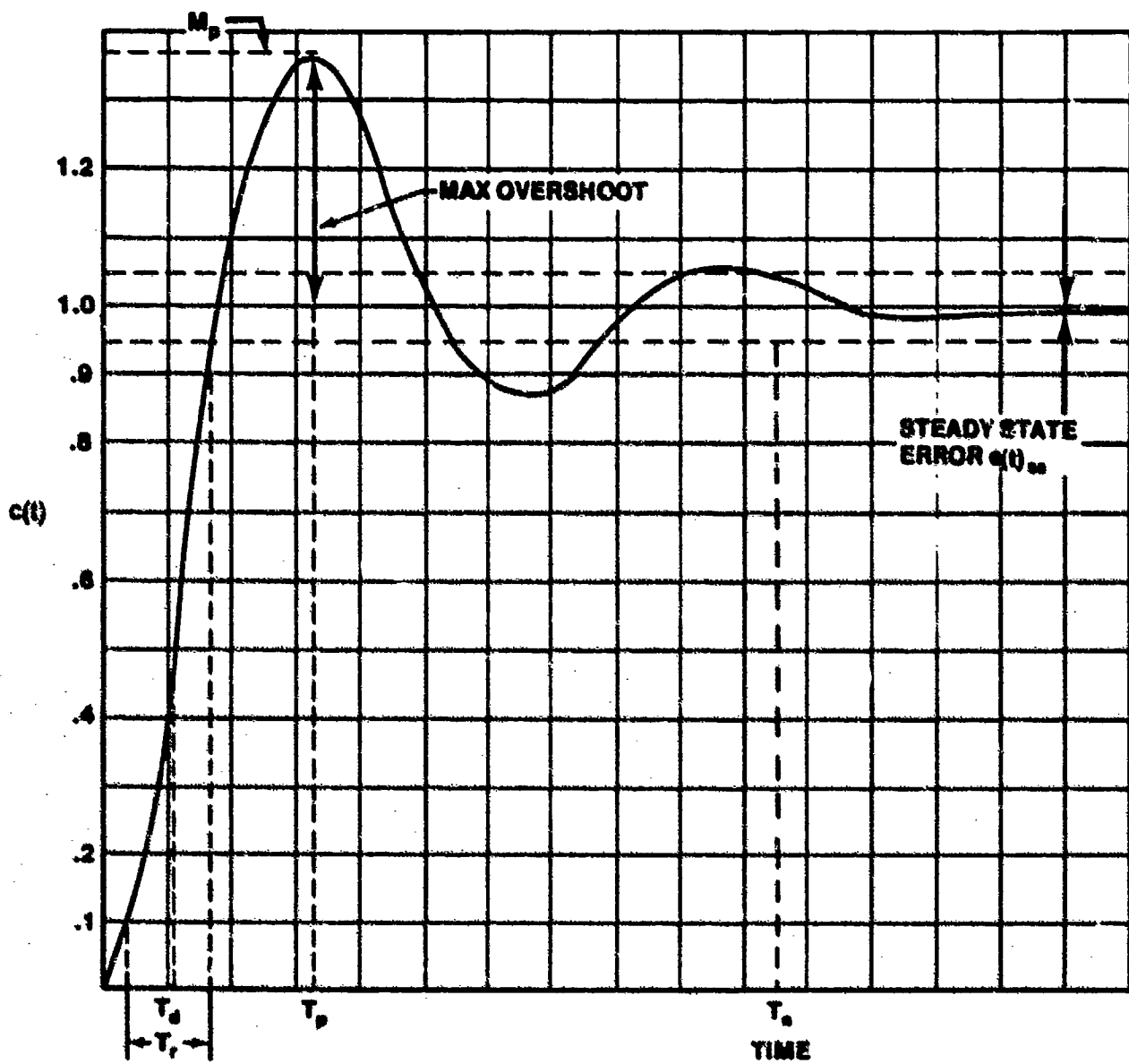FIGURE 13.14. TRANSIENT RESPONSE OF A SECOND-ORDER SYSTEM TO A STEP INPUT

FIGURE 13.15.   TIME DOMAIN SPECIFICATIONS

These transient performance specifications are usually defined for a unit step input.

1. Overshoot - indicated by largest error between input and output during the transient state. We can determine the magnitude by using the previously developed equation for a step input to a second order system.

$$c(t) = 1 - \frac{1}{\sqrt{1 - \zeta^2}} e^{-\omega nt} \sin\left(\omega_n \sqrt{1 - \zeta^2} + \tan^{-1} \frac{\sqrt{1 - \zeta^2}}{\zeta}\right) \quad (13.29)$$

Taking the derivative of this equation and equating to zero yields

$$\frac{dc(t)}{dt} = 0 = \frac{1}{\sqrt{1 - \zeta^2}} \zeta\omega_n e^{-\zeta\omega nt} \sin\left(\omega_n \sqrt{1 - \zeta^2} + \tan^{-1} \frac{\sqrt{1 - \zeta^2}}{\zeta}\right)$$

$$- \frac{1}{\sqrt{1 - \zeta^2}} e^{-\zeta\omega nt} \omega_n \sqrt{1 - \zeta^2} \cos\left(\omega_n \beta t + \tan^{-1} \frac{\sqrt{1 - \zeta^2}}{\zeta}\right) \quad (13.30)$$

This derivative is zero when $\omega_n \sqrt{1 - \zeta^2} = 0, \pi, 2\pi$, etc.
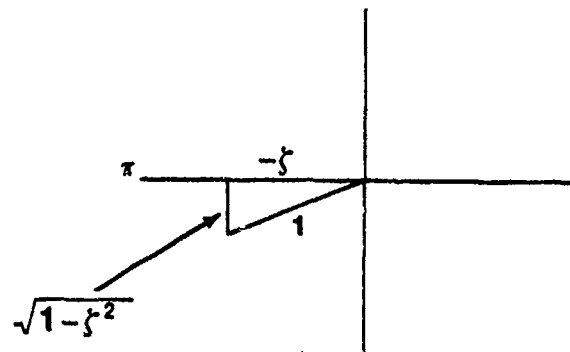The peak overshoot occurs at the first value after zero (with initial conditions equal to zero).

Therefore, the time to maximum or peak overshoot is

$$\boxed{T_p = \frac{\pi}{\omega_n \sqrt{1 - \zeta^2}}} \quad (13.31)$$

Substituting this value into $c(t)$ yields the peak response, M_p.

$$M_p = 1 - \frac{1}{\sqrt{1 - \zeta^2}} \exp\left(\frac{-\zeta\omega_n \pi}{\omega_n \sqrt{1 - \zeta^2}}\right) \sin\left(\pi + \tan^{-1} \frac{\sqrt{1 - \zeta^2}}{\zeta}\right)$$

Note: $\sin\left(\pi + \tan^{-1}\dfrac{\sqrt{1-\zeta^2}}{\zeta}\right) = \sin\left(-\tan^{-1}\dfrac{\sqrt{1-\zeta^2}}{\zeta}\right)$

$$= -\sqrt{1-\zeta^2}$$

And

$$\boxed{M_p = 1 + \exp\left(-\frac{\zeta\pi}{\sqrt{1-\zeta^2}}\right)} \qquad (13.32)$$

The overshoot for the unit step input is

$$\text{Overshoot} = M_p - 1 = \exp\left(-\frac{\zeta\pi}{\sqrt{1-\zeta^2}}\right) \qquad (13.33)$$

and the percent of overshoot

$$\text{P.O.} = \frac{M_p - 1}{1} \times 100\%$$

$$= 100\exp\left(-\frac{\zeta\pi}{\sqrt{1-\zeta^2}}\right) \qquad (13.34)$$

2. Time Delay, T_d, is the time required for the response to a unit step to reach 50% of its final value.

3. Rise Time, T_r, is the time required for the response to a unit step to rise from 10% to 90% of its final value.

4. Settling Time, τ_s, is the time required for the response to a unit step to decrease to and to stay within a specific percentage of its final value. Commonly used values are 2% or 5% of the final value.

13.5.3 Higher-Order Systems

The relationships developed in the preceding paragraph using ω_n and ζ apply equally well for each complex-conjugate pair of poles of an nth-order system. The distinction is that the dominant ζ and ω_n apply for that pair of complex-conjugate poles which lie closest to the imaginary axis. The values of ζ and ω_n are dominant because the corresponding transient term has the longest settling time and the largest magnitude. Therefore, the dominant poles primarily determine the shape of the time response, $c(t)$. A nondominant pole(s) has a real axis component that is at least six times further to the left than the corresponding component of the dominant pole(s). Components of $c(t)$ due to nondominant pole(s) die out relatively quickly, and can be neglected. (13.1:245)

13.5.4 Time Constant, τ

The time constant is used as a measure of the exponential decay of a response. For first-order systems, the transient response is an exponential function described by Ae^{-mt}, Figure 13.16.
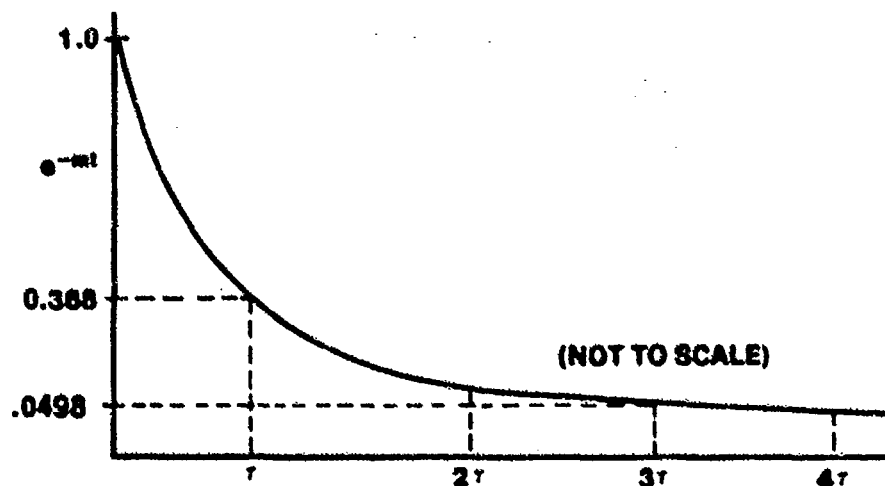

FIGURE 13.16. PLOT OF EXPONENTIAL e^{-mt}

The value of time which makes the exponent of e equal to -1 is defined as the time constant, τ

$$-m\tau = -1$$

$$\tau = \frac{1}{m}$$

In one time constant the exponential e^{-mt} will decrease from a value of 1.0 to a value .368. Table 13.1 shows values for other time constants.

TABLE 13.1

TIME CONSTANT TABLE

t	e^{-mt}
1τ	.368
2τ	.135
3τ	.0498
4τ	.0183

The time constant is another way of specifying settling time. The exponential will decay to 37% of its initial value in τ seconds (one time constant). In 3τ the exponential is within approximately 5% and in 4τ approximately 2% of its final value. For a second-order underdamped system of the form

$$c(t) = 1 - \frac{1}{\beta} e^{-\zeta\omega_n t} \sin(\omega_n \beta t + \phi)$$

the response is bounded by the exponent of the form $(1/\beta)e^{-mt}$. The specifications of ζ and ω_n determine the bounding exponential curve. The time constant, τ, for these systems is

$$\tau = \frac{1}{\zeta\omega_n} \tag{13.35}$$

13.6 STABILITY DETERMINATION

The most important area of the analysis of a closed-loop control system is the determination of stability. A system is said to be stable if the output of the system corresponds to the input after transients die out. A system is said to be unstable if the transients do not die out or if they grow larger following a disturbance.

Stability is an inherent characteristic of the system and depends only upon the system itself, not upon the input or forcing function. Hence, if a system is unstable, any input will cause the system to diverge. If the system is stable, any bounded input will cause a bounded response.

The problem in determining stability is ascertaining whether or not the transients of a system will die out BEFORE the system is built.

We must determine the conditions under which a system will become unstable and be able to tell when this happens in the analysis of the system. Several methods are available for determining stability: root locus, Bode plot, Routh's stability criterion, and Nyquist Criterion. Only the root locus and the Bode plot methods will be presented in this chapter.

13.6.1 Stability in the s-Plane

Since this course is concerned with linear systems, i.e., those whose differential equations are linear with constant coefficients, the transient response is of the form

$$c(t)_{transient} = \sum_{i=1}^{n} k_i e^{s_i t}$$

where n is the order of the differential equation and the values of s are the roots of the characteristic equation which are, in general, complex.

$$s = \sigma + j\omega_d \qquad (13.36)$$

σ is the real part of the complex variable s and ω_d is the imaginary part of the complex variable s. The notation used to indicate this is

$$\sigma = \text{Re}\{s\}$$

$$\omega_d = \text{Im}\{s\}$$

Previously, we discussed only a first and second-order system and saw the type of transient response to be expected from each. The characteristic equation of higher-order systems, however, can in theory be factored into the product of several first and second-order factors depending on the order of the equation. This is demonstrated in Equations 13.37 and 13.38

$$A_n s^n + A_{n-1} s^{n-1} + \ldots A_0 = 0 \tag{13.37}$$

Can be expressed

$$(\tau_1 s + 1)(\tau_2 s + 1) \ldots \left(\frac{s^2}{\omega_{n_1}^2} + \frac{2\zeta_1}{\omega_{n_1}} s + 1 \right) \left(\frac{s^2}{\omega_{n_2}^2} + \frac{2\zeta_2}{\omega_{n_2}} s + 1 \right) \ldots = 0 \tag{13.38}$$

The transient response of a complex system is the sum of those associated with each of the first and second-order factors. Each root of the characteristic equation must be of one of the forms shown in Figure 13.17. Opposite the possible values of the roots on the left are shown the corresponding transient response components as a function of time. Note that complex or imaginary roots always occur in complex-conjugate pairs. That is, they have imaginary parts of equal magnitude but are opposite in sign.

All the possible values of s can also be described through use of a complex plane -- in this case the s-plane. A complex plane is one in which the value of the real part of the complex variable is the distance along the abscissa and the magnitude of the imaginary part is described along the ordinate. These are called the real and imaginary axes, respectively. The complex variable, s, is then a position vector in the complex s-plane where $\sigma = \text{Re}\{s\}$ is the magnitude of the real component and $\omega_d = \text{Im}\{s\}$ is the imaginary component.

Figure 13.18 shows the s-plane. If the values of s, which are the roots of the characteristic equation, are plotted in the s-plane, they produce a transient solution component as indicated. Areas in the s-plane in which roots produce stable and unstable responses are also shown. Roots yielding marginally or neutrally stable output are all on the imaginary axis. Roots associated with non-oscillatory response are all on the real axis. A root of the characteristic equation at the origin (s = 0) has a transient solution equal to a constant.

The mathematical definition of a stable system is one in which the roots of the equation have only negative real parts. In other words, where $s = \sigma + j\omega_d$ are the roots of the characteristic equation, $\sigma < 0$ produces a stable system.
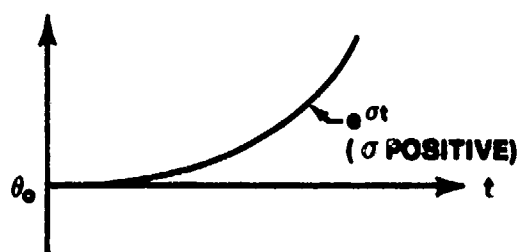
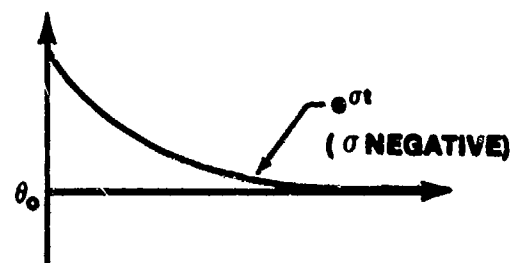| VALUE OF s	TIME RESPONSE	PICTORIAL SOLUTION

σ (POSITIVE) $Ce^{\sigma t}$
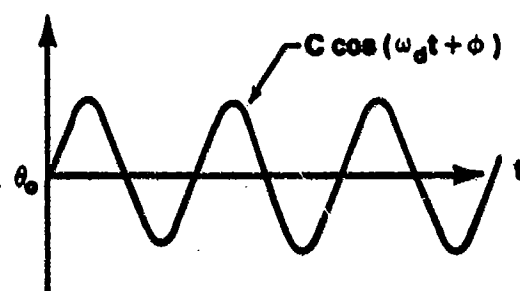

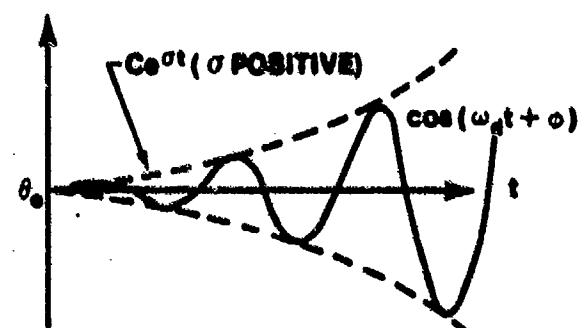σ (NEGATIVE) $Ce^{\sigma t}$

$\pm j\omega_d$ $C\cos(\omega_d t + \phi)$

$\sigma \pm j\omega_d$
(σ POSITIVE) $Ce^{\sigma t}\cos(\omega_d t + \phi)$

$\sigma \pm j\omega_d$
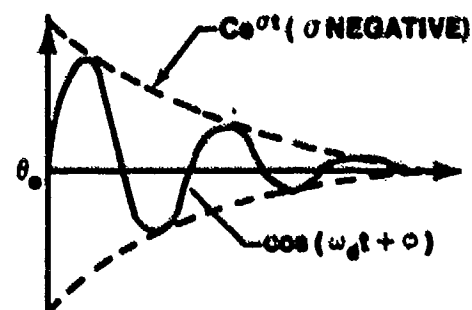(σ NEGATIVE) $Ce^{\sigma t}\cos(\omega_d t + \phi)$

FIGURE 13.17. TRANSIENT SOLUTION OF LINEAR
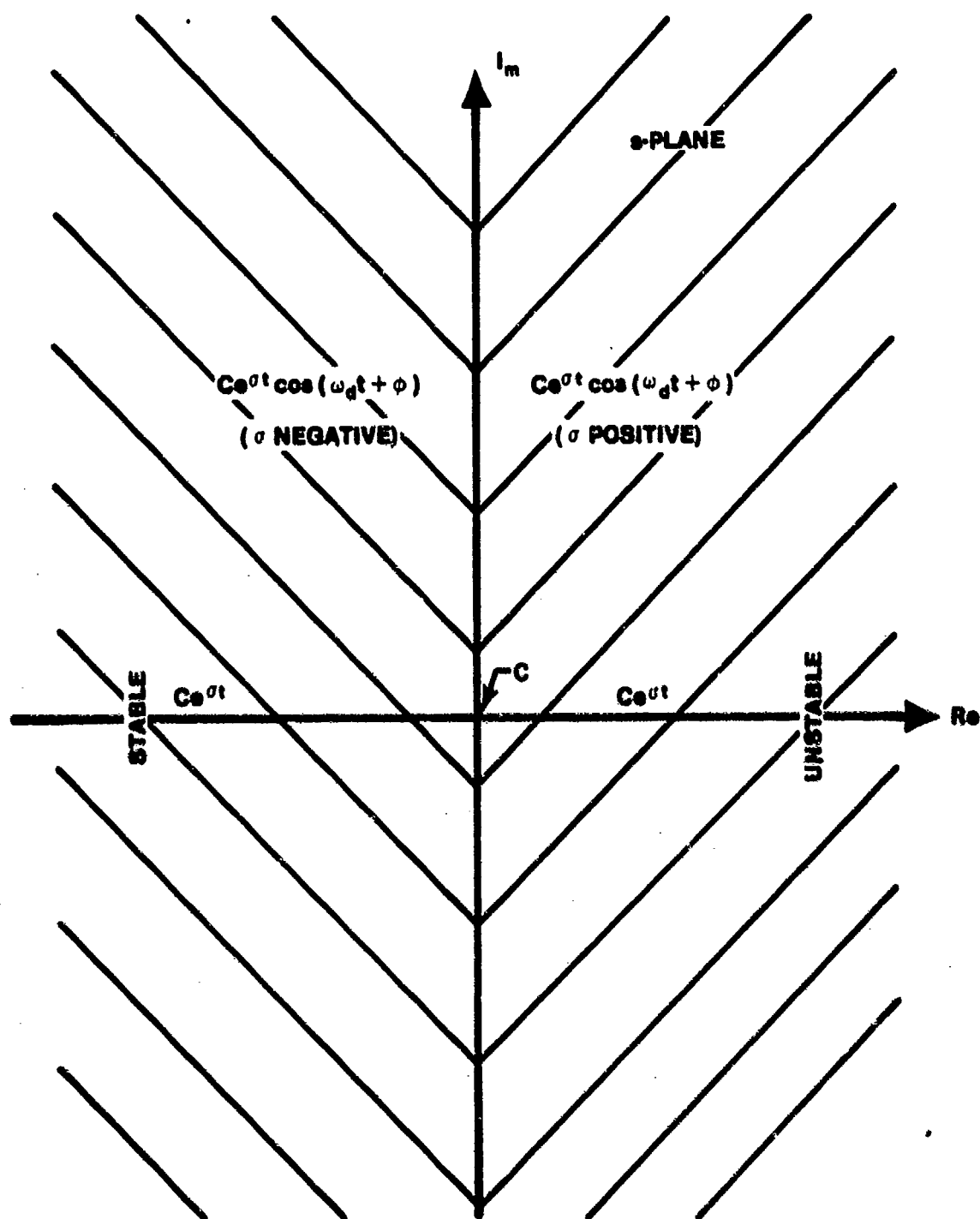CONSTANT COEFFICIENT EQUATIONS

FIGURE 13.18.   COMPLEX s-PLANE

13.6.2 Additional Poles and Zeros

The results of adding a real pole or a real zero to the basic second-order control ratio as given by Equation 13.26 will be investigated. When a pair of complex-conjugate poles are dominant, the approximations developed in Paragraph 13.5.2 yield accurate results. The addition of a third real pole to a second-order transfer function can significantly alter the system time response $c(t)$, and the approximations given in Paragraph 13.5.2 no longer give accurate results.

The effects of a third real pole can be seen by considering the control ratio

$$\frac{C(s)}{R(s)} = \frac{K}{\left(s^2 + 2\zeta\omega_n s + \omega_n^2\right)\left(s - p_3\right)} \; ; \left(K = \omega_n^2 p_3\right) \qquad (13.39)$$

The time response resulting from a unit step input is

$$c(t) = 1 + 2\left|A\right| e^{-\zeta\omega_n t} \sin(\omega_d t + \phi) + B e^{p_3 t} \qquad (13.40)$$

The transient term due to the real pole, p_3, has the form $B e^{p_3 t}$, where B is always negative. Therefore, the peak overshoot is reduced, and the settling time, t_s, may be increased or decreased. This is the typical effect of adding a third real pole. The further to the left p_3 is, the smaller the magnitude of B, and therefore the effect on $c(t)$. Typical time responses as a function of the real pole location are shown in Figure 13.19 (13.1:350).
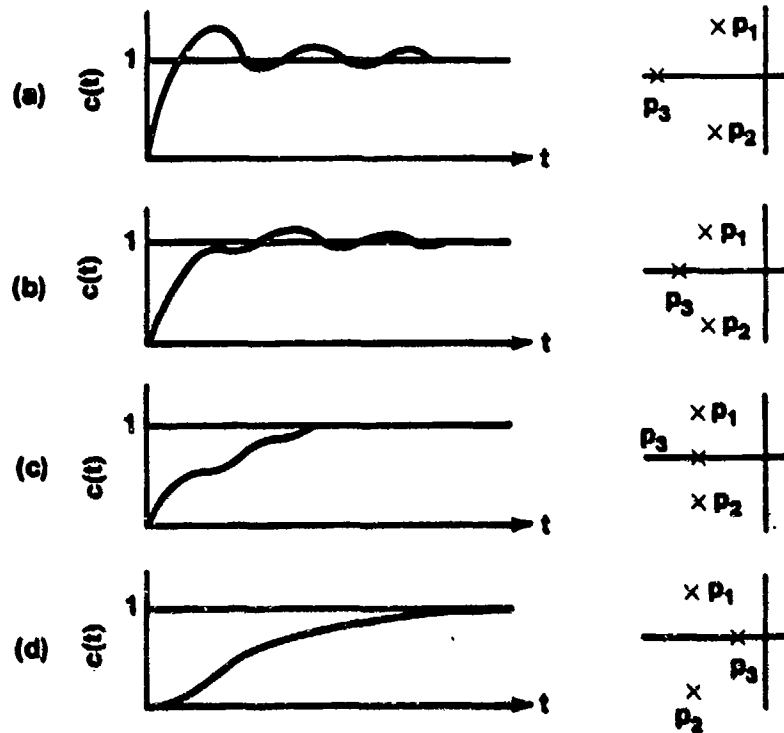
FIGURE 13.19.   TIME RESPONSE AS A FUNCTION
OF REAL POLE LOCATION

The time response is also altered by the addition of a real zero to the basic second-order transfer function of Equation 13.26.   The control ratio now becomes

$$\frac{C(s)}{R(s)} = \frac{K(s - z)}{\left(s^2 + 2\zeta\omega_n s + \omega_n^2\right)}, \quad \left(K = \omega_n^2 / z\right) \qquad (13.41)$$

The time response resulting from a unit step input is

$$c(t) = 1 + \frac{1}{\omega_d} \left[(z - \zeta\omega_n)^2 + \omega_d^2\right]^{1/2} e^{-\zeta\omega_n t} \sin(\omega_d t + \phi) \qquad (13.42)$$

where

$$\phi = \tan^{-1} \frac{d}{z - \zeta\omega_n} \qquad (13.43)$$

13.33

From Equations 13.42 and 13.43, it is seen that the addition of a real zero affects both the magnitude and phase of the transient part of $c(t)$. The real zero tends to increase the overshoot and decrease the phase angle of $c(t)$. This effect becomes more dramatic as the zero approaches the imaginary axis. This is illustrated in Figure 13.20 for a stable second-order system with $\zeta\omega_n$ held constant.
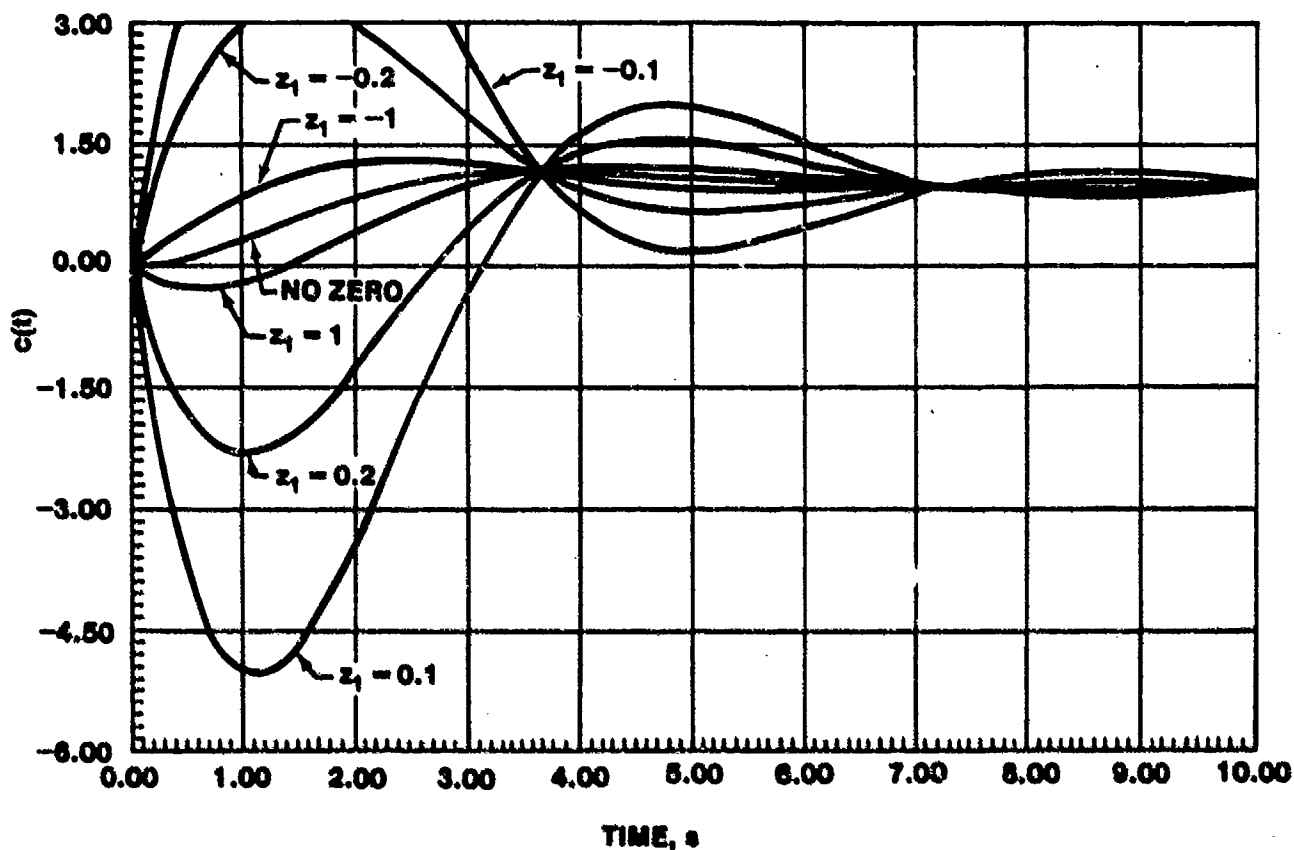
FIGURE 13.20. TIME RESPONSE OF A SECOND-ORDER SYSTEM
AS A FUNCTION OF REAL ZERO LOCATION

Several things can be seen by examining the responses in Figure 13.20. First, it should be noted that rise time is decreased and the overshoot is increased with the addition of a real zero. This effect is more noticeable as the zero moves closer to the imaginary axis. This is to be expected, because when the zero is at the origin, it acts as a pure differentiator of the input. Differentiation of the unit step input yields the unit impulse. When the zero is in the right half plane, the response is stable but the direction of the

initial response is opposite to the final steady-state value. Additionally, it should be noted that the initial slope of the response is not zero as is true for a second-order system without a zero (13.2:91). The block diagram of a system zero is shown in Figure 13.21.
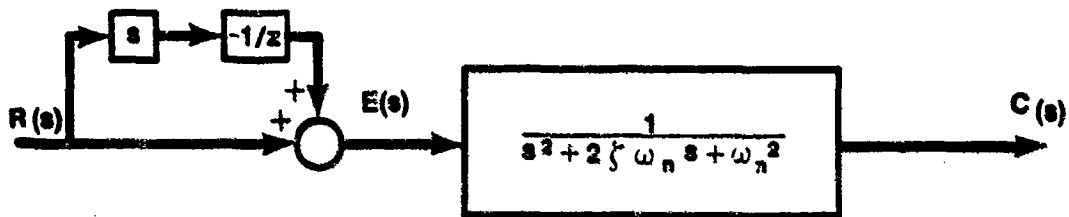
FIGURE 13.21.   BLOCK DIAGRAM OF A SECOND-ORDER
SYSTEM WITH A REAL ZERO

From Figure 13.21 it can be seen that the zero operates on the input signal to produce a signal proportional to both the magnitude and the derivative (rate of change) of the input signal. Therefore, the system will react not only to the magnitude of input, but also to its rate of change. If R(s) is changing rapidly, then E(s) is large and the system responds faster. (13.1:360).

13.7   STEADY-STATE FREQUENCY RESPONSE

We have looked at the time domain analysis and specifications of control systems. In the time domain analysis, the typical test inputs were the step, ramp, and parabola. The frequency response technique, introduced in this paragraph, is a valuable tool to the control systems engineer and provides a standardized method representing the total performance of a system. The input for steady-state frequency response is the sinusoid

$$r(t) = A_1 \sin \omega t$$

The basis for the frequency response method is that a system's response to a sinusoid will be a sinusoid at the same frequency, but the response will

differ in magnitude and phase angle. All that is needed to completely specify the steady-state frequency response is to be able to find the magnitude of the output and the phase angle.

The fact that the output is a sinusoid of the same frequency can be shown by analyzing a sinusoid input to a first-order system described by

$$G(s) = \frac{B}{s + \frac{1}{\tau}} \qquad (13.44)$$

The input, $r(t) = A_1 \sin \omega t$ in Laplace transform is

$$R(s) = \frac{A_1 \omega}{s^2 + \omega^2}$$

$$C(s) = G(s) R(s)$$

and

$$C(s) = \frac{B}{s + \frac{1}{\tau}} \frac{A_1 \omega}{s^2 + \omega^2}$$

Using partial fraction expansion yields

$$C(s) = \frac{C_1}{s + \frac{1}{\tau}} + \frac{C_2 s}{s^2 + \omega^2} + \frac{C_3}{s^2 + \omega^2}$$

Finding the coefficients C_1, C_2, and C_3 can be a tedious process. By inspection we can write the form of the solution as

$$c(t) = C_1 e^{-t/\tau} + C_2 \cos \omega t + \frac{C_3}{\omega} \sin \omega t$$

Another form of this equation is

$$c(t) = C_1 e^{-t/\tau} + A_0 \sin (\omega t + \phi) \qquad (13.45)$$

The steady-state response can be written as

$$c(t)_{ss} = A_0 \sin (\omega t + \phi) \qquad (13.46)$$

$\swarrow$ Magnitude $\uparrow$ Phase Angle

which tells us that the steady-state response will always have the same frequency as the input but will differ in phase angle and magnitude. The transient response due to the exponential term, $C_1 e^{-t/\tau}$, decays to zero as $t \to \infty$.

The Laplacian operator, s, contains both real and imaginary components and to evaluate coefficient C_3 the complex variable "s" would be selected to be $\pm j\omega$ (i.e. purely imaginary). Thus

$$s = \sigma + j\omega_d$$

and for a constant amplitude-input sinusoid, σ is zero, (Figure 13.22), therefore

$$s = j\omega$$
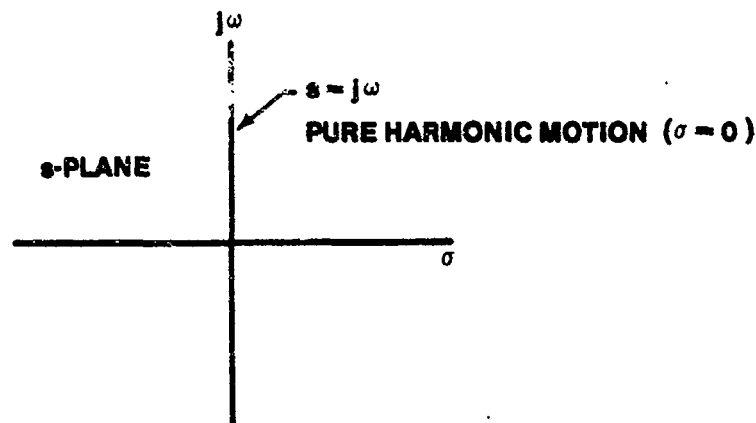
FIGURE 13.22. S-PLANE - PURE HARMONIC MOTION

The frequency response function, jω, is defined by replacing s with jω in the system transfer function (Equation 13.44).

$$G(s) = \frac{B}{s + \frac{1}{\tau}}$$

becomes

$$G(j\omega) = \frac{B}{j\omega + \frac{1}{\tau}}$$

It is important to remember that we are talking about the steady-state frequency response only when we replace s with the frequency response function, jω.

13.7.1 Complex Numbers

In the study of feedback control systems, the relative magnitude and time relationship between such quantities as position, speed, voltage, current, force, and torque are the items of interest. These are all real physical quantities which behave according to the laws of nature. It is frequently convenient, however, to represent these physical quantities by complex mathematical symbols that indicate more than the information describing the

real quantities themselves. The use of complex variables to represent real physical quantities has the advantage of simplifying the mathematical process necessary to solve the problem. On the other hand, it has the disadvantage of obscuring the true value of the real physical quantities.

It is the purpose of this chapter to introduce the complex variable notation which will be used later. Complex quantities are usually expressed in one of four forms:

(a) rectangular

(b) polar

(c) trigonometric

(d) exponential

The equivalence of these four forms will now be demonstrated.

13.7.1.1 Rectangular Form. The complex quantity z is drawn on the complex plane in Figure 13.23. It can be thought of as a position vector in the complex plane.
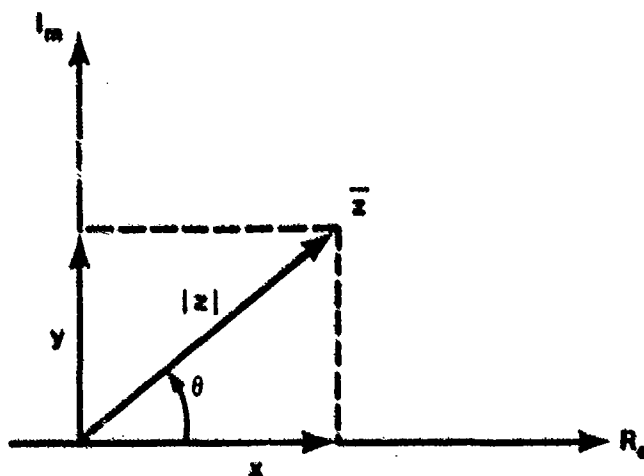
FIGURE 13.23. THE COMPLEX PLANE

The real part is measured along the horizontal or real axis and the imaginary part is measured along the vertical or imaginary axis.

In rectangular form the complex variable, z, is

$$\bar{z} = x + jy$$

where j is the imaginary quantity $\sqrt{-1}$.

13.7.1.2 Polar Form. Any position in the complex plane can also be defined
by the angle, θ, of the position vector z, and its magnitude, z (Figure
13.23). In polar form the complex quantity, z, is

$$\bar{z} = |z| \angle \theta$$

In terms of the rectangular form parameters,

$$|\bar{z}| = \sqrt{x^2 + y^2}$$

$$\theta = \tan^{-1} y/x$$

13.7.1.3 Trigonometric Form. The trigonometric form of the position vector
in the complex plane can be written again using Figure 13.23. We see that

$$\cos \theta = \frac{x}{\sqrt{x^2 + y^2}}$$

and

$$\sin \theta = \frac{y}{\sqrt{x^2 + y^2}}$$

Therefore,

$$\cos \theta + j \sin \theta = \frac{x}{\sqrt{x^2 + y^2}} + j \frac{y}{\sqrt{x^2 + y^2}}$$

Multiplying both sides by

$$|\bar{z}| = \sqrt{x^2 + y^2}$$

We have

$$|\bar{z}| \, [\cos \theta + j \sin \theta] = \sqrt{x^2 + y^2} \left[\frac{x}{\sqrt{x^2 + y^2}} + j \frac{y}{\sqrt{x^2 + y^2}} \right]$$

The trigonometric form is then

$$\bar{z} = |\bar{z}| \, [\cos \theta + j \sin \theta]$$

13.7.1.4 <u>Exponential Form</u>. The exponential form of a complex quantity · is most convenient for mathematical manipulation. It will be shown equivalent to the trigonometric form.

The MacLaurin series expansion e^x is

$$e^x = 1 + x + \frac{x^2}{2!} + \frac{x^3}{3!} + \dots$$

Letting $x = j\theta$

$$e^{j\theta} = 1 + j\theta - \frac{\theta^2}{2!} - j\frac{\theta^3}{3!} + \dots \qquad (13.47)$$

Now, $\sin \theta$ and $\cos \theta$ can be defined by series expansions as follows:

$$\sin \theta = \theta - \frac{\theta^3}{3!} + \frac{\theta^5}{5!} - \frac{\theta^7}{7!} + \dots \qquad (13.48)$$

$$\cos \theta = 1 - \frac{\theta^2}{2!} + \frac{\theta^4}{4!} - \frac{\theta^6}{6!} + \dots \qquad (13.49)$$

Recalling that $j^2 = -1$, Equation 13.48 and 13.49 may be written

$$\cos \theta = 1 + \frac{(j\theta)^2}{2!} + \frac{(j\theta)^4}{4!} + \frac{(j\theta)^6}{6!} + \dots \qquad (13.50)$$

$$j \sin \theta = \frac{j\theta}{1!} + \frac{(j\theta)^3}{3!} + \frac{(j\theta)^5}{5!} + \frac{(j\theta)^7}{7!} + \ldots \qquad (13.51)$$

Adding Equation 13.50 to 13.51 yields

$$\cos \theta + j \sin \theta = 1 + \frac{j\theta}{1!} + \frac{(j\theta)^2}{2!} + \frac{(j\theta)^3}{3!} + \ldots \qquad (13.52)$$

The right side of Equation 13.52 is equal to Equation 13.47, therefore

$$e^{j\theta} = \cos \theta + j \sin \theta$$

and finally

$$|\bar{z}| = |\bar{z}| \, e^{(j\theta)} \qquad (13.53)$$

We have proven the four forms of the complex variable z to be consistent. They are summarized below

Rectangular $\qquad \bar{z} = x + jy$

Polar $\qquad \bar{z} = |\bar{z}| \; \underline{/\theta}$

Trigonometric $\qquad \bar{z} = |\bar{z}| \, [\cos \theta + j \sin \theta]$

Exponential $\qquad \bar{z} = |\bar{z}| \, e^{j\theta}$

13.7.2 Bode Plotting Technique

With this background in complex notation we will develop the Bode technique of frequency response. Beginning with a generalized transfer function (Equation 13.54), we will manipulate it into the frequency response standard form, sometimes called the Bode form (Equation 13.55).

$$G(s) = \frac{K\, s^m\, (s + a_1)(s + a_2)\; s^2 + 2\zeta\omega_{n_1} s + \omega_{n_1}^2}{s^n\, (s + a_3)(s + a_4)\; s^2 + 2\zeta\omega_{n_2} s + \omega_{n_2}^2} \qquad (13.54)$$

Equation 13.54 must be normalized as follows:

$$G(s) = \frac{K\, a_1\, a_2\, \omega_{n_1}^2\, s^m\, (\tau_1 s + 1)(\tau_2 s + 1)\left(\dfrac{s^2}{\omega_{n_1}^2} + \dfrac{2\zeta s}{\omega_{n_1}} + 1\right)}{a_3\, a_4\, \omega_{n_2}^2\, s^n\, (\tau_3 s + 1)\,(\tau_4 s + 1)\left(\dfrac{s^2}{\omega_{n_2}^2} + \dfrac{2\zeta s}{\omega_{n_2}} + 1\right)} \qquad (13.55)$$

where

$$\tau_1 = \frac{1}{a_1}, \quad \tau_2 = \frac{1}{a_2} \text{ etc.,}$$

Let

$$K_n = \frac{K\, a_1\, a_2\, \omega_{n_1}^2}{a_3\, a_4\, \omega_{n_2}^2} \quad \text{and} \quad K = \text{static loop sensitivity}$$

Substitute $j\omega$ for s in Equation 13.55 and rewriting in the Frequency Response Standard Form

$$G(j\omega) = \frac{K_n (j\omega)^m\, (1 + j\tau_1\omega)(1 + j\tau_2\omega)\left(1 - \dfrac{\omega^2}{\omega_{n_1}^2} + j2\zeta \dfrac{\omega}{\omega_{n_1}}\right)}{(j\omega)^n\, (1 + j\tau_3\omega)\,(1 + j\tau_4\omega)\left(1 - \dfrac{\omega^2}{\omega_{n_2}^2} + j2\zeta \dfrac{\omega}{\omega_{n_2}}\right)} \qquad (13.56)$$

13.43

Equation 13.56 can be written in polar form

$$G(j\omega) = |G(j\omega)| \underline{/\phi(\omega)}$$

where $G(j\omega)$ is of the form $\sqrt{\overline{Re}^2 + \overline{Im}^2}$

and $\phi(\omega)$ of the form $\tan^{-1} \dfrac{\overline{Im}}{\overline{Re}}$

Furthermore, $G(j\omega)$ can be written in exponential form where

$$G(j\omega) = |G(j\omega)| \; e^{j\phi(\omega)} \tag{13.57}$$

To express $G(j\omega)$ in either of these formats will entail finding the magnitude $G(j\omega)$ and the phase angle $\phi(\omega)$. The Bode technique requires taking the log of $G(j\omega)$ to take advantage of addition and subtraction in lieu of multiplication, and division.

Taking the log of Equation 13.57 yields

$$\log |G(j\omega)| \; e^{j\phi(\omega)} = \log |G(j\omega)| + \log e^{j\phi(\omega)}$$

$$= \log |G(j\omega)| + j \; 0.4343 \; \phi(\omega)$$

The quantity, $j \; 0.434 \; \phi(\omega)$, is the imaginary part and in future discussion only the angle $\phi(\omega)$ will be used.

The unit of magnitude commonly used in control systems is the "decibel" and will be defined as

$$20 \log |G(j\omega)| = (\;\;) \; db \tag{13.58}$$

This quantity is often referred to as the log magnitude and is abbreviated Lm where

$$Lm \; G(j\omega) = 20 \log |G(j\omega)| \; db \tag{13.59}$$

13.44

Now, how does multiplication and division become addition and subtraction for Bode development? We will take the log of Equation 13.56 and multiply this by 20 which will give the amplitude ratio in decibels. The use of logarithms will allow us to add for multiplication and subtract for division.

The Im of Equation 13.56 becomes

$$20 \log \left|G(j\omega)\right| = 20 \log K + 20\, m \log \left|j\omega\right| + 20 \log \left|1 + j\, \tau_1 \omega\right|$$

$$+ 20 \log \left|1 + j\tau_2\omega\right| + 20 \log \left|1 - \frac{\omega}{\omega_{n_1}^2} + j\, \frac{2\zeta\omega}{\omega_{n_1}}\right|$$

$$- 20\, n \log \left|j\omega\right| - 20 \log \left|1 + j\tau_3\omega\right| - 20 \log \left|1 + j\tau_4\omega\right|$$

$$- 20 \log \left|1 - \frac{\omega}{\omega_{n_2}^2} + j\, \frac{2\zeta\omega}{\omega_{n_2}}\right| \qquad (13.60)$$

The associated phase angle of Equation 13.56 becomes,

$$\underline{/G(j\omega)} = \underline{/K} + m\, 90^\circ + \tan^{-1} \omega\tau_1 + \tan^{-1} \omega\tau, \omega\tau_2$$

$$+ \tan^{-1} \frac{2\zeta\omega/\omega_{n_1}}{1 - \frac{\omega^2}{\omega_{n_1}^2}} - n\, 90^\circ - \tan^{-1} \omega\tau_3$$

$$- \tan^{-1} \omega\tau_4 - \tan^{-1} \frac{2\zeta\omega/\omega_{n_2}}{1 - \frac{\omega^2}{\omega_{n_2}^2}}$$

13.45

It is immediately obvious that a point by point solution of these equations for varying input frequency, ω, would be very tedious. A technique known as the Bode plot simplifies this process. Notice in Equation 13.60 that there are four types of factors in the open-loop transfer function $G(j\omega)$.

1. Constant term, K_n

2. Pole or zero at origin, $(j\omega)^{\pm n}$
   ($+n$ = zero, $-n$ = pole)

3. Simple pole or zero, $(1 + j\omega\tau)^{\pm n}$

4. Quadratic pole or zero, $\left(1 - \dfrac{\omega^2}{\omega_n^2} + j2\zeta\dfrac{\omega}{\omega_n}\right)^{\pm n}$

The Bode plot uses semilog paper. Magnitude and phase angle are represented on the ordinate (linear scale) and frequency along the logarithmic scale as in Figures 13.24 and 13.25. Bode plot technique uses asymptotes and corrections to the asymptotes for each of the four types of factors listed above. All of the factors are individually plotted on the Bode diagram, and then are added and subtracted (taking advantage of logarithms) to achieve the composite curve. We will develop the technique for each of the four types of factors.

Constant term, K_n The magnitude of K_n in db is

$$20 \log |K_n| = \text{constant}$$

and the associated phase angle is

$$\text{Arg } (K_n) = 0^{\circ} \quad \text{or}$$

$$\text{Arg } (- K_n) = \pm 180^{\circ}$$

as shown in Figure 13.26.

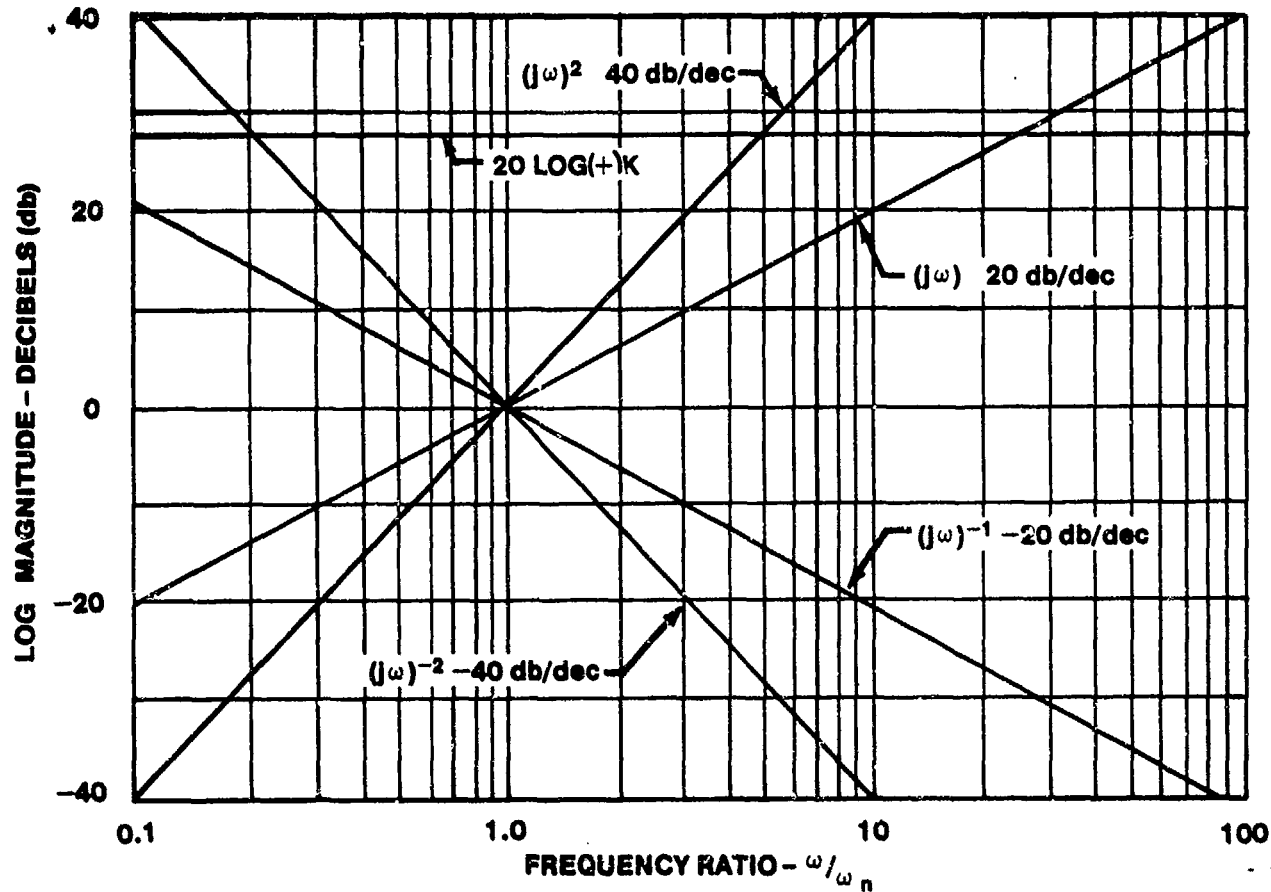The magnitude and phase angle are depicted respectively on Figures 13.24 and 13.25.

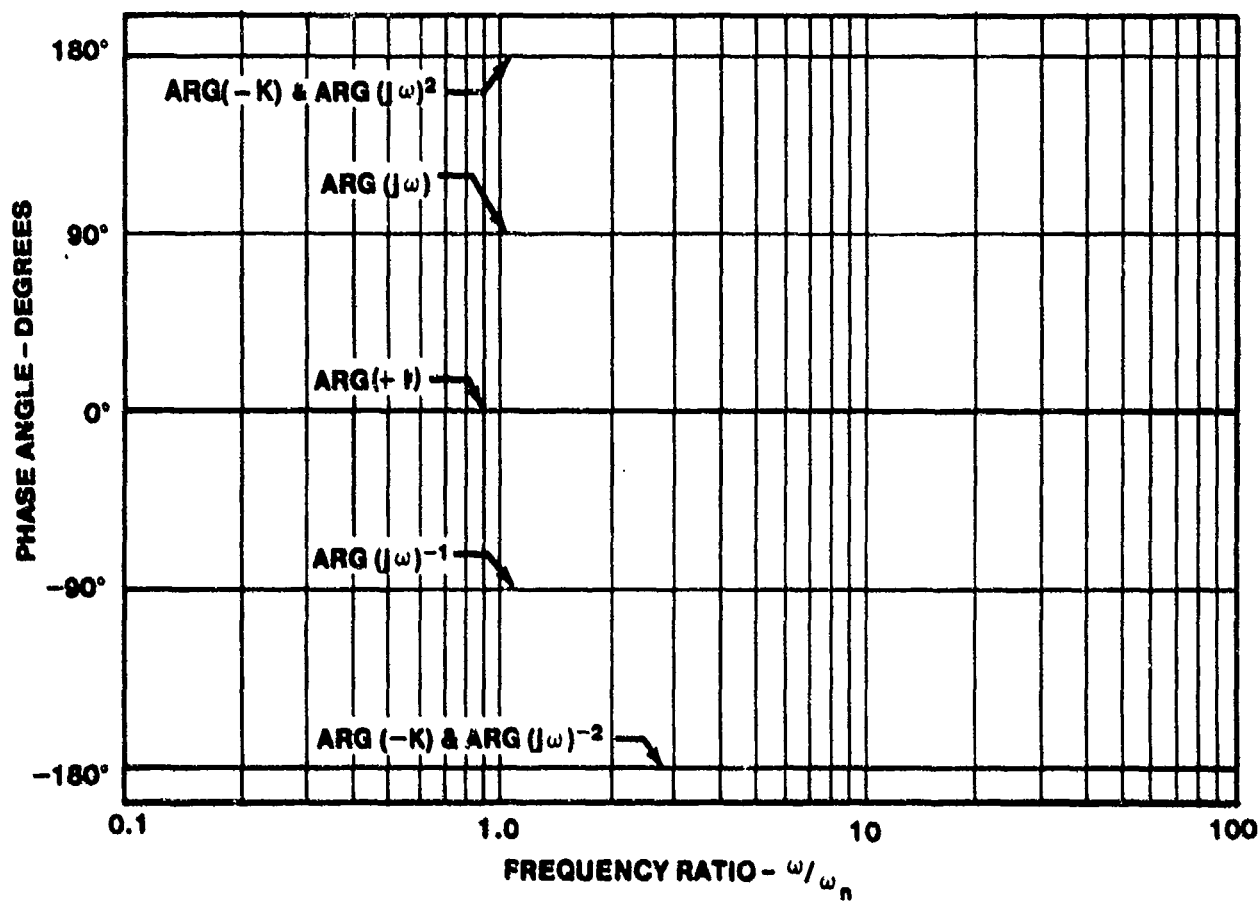FIGURE 13.24. BODE MAGNITUDE PLOT OF $(j\omega)^{\pm n}$ AND K

FIGURE 13.25. BODE PHASE ANGLE PLOT OF $(j\omega)^{\pm n}$ AND K

13.47
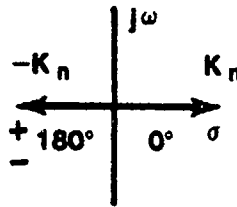
FIGURE 13.26.   PLOT OF A CONSTANT ON
THE COMPLEX PLANE

Pole or zero at origin, $(j\omega)^{\pm n}$. The magnitude of $(j\omega)^{\pm n}$ is

$$20 \log |(j\omega)^{\pm n}| = \pm 20 \, n \log \omega_{db}$$

which is the equation of a straight line with slope of ± 20 n db per decade.

A decade is a frequency band from f_1 to f_2 where $f_2/f_1 = 10$ and the number of decades from f_1 to f_2 is $\log (f_2/f_1)$. The octave is also used as a frequency ratio and is a frequency band from f_1 to f_2 where $f_2/f_1 = 2$. The number of octaves from f_1 to f_2 is given by $\log (f_2/f_1)/\log 2 = 3.32 \log f_2/f_1$. Also, ± 20 n db/decade $= \pm 6$ n db/octave. When $\omega = 1$, the equation $20 \log (j\omega)^{\pm n} = 0$. The straight line passes through the 0 db point at frequency $\omega = 1$, Figure 13.24. The phase angle

$$\text{Arg } (j\omega)^{\pm n} = \pm n \, 90^\circ$$

as shown in Figure 13.25.

Simple Pole or Zero, $(1 + j\omega\tau)^{\pm n}$ the magnitude of this term in db is expressed as

$$20 \log |(1 + j\omega\tau)|^{\pm n} = \pm 20 \, n \log (1 + j\omega\tau)$$

13.48

at very low frequency (i.e., $\omega\tau \ll 1$) the magnitude of this curve is 0 db. At frequencies where $\omega\tau \gg 1$ the magnitude asymptote has a slope of $\pm 20n$ db/decade. The 0 db asymptote and the $\pm 20n$ db/dec asymptote intersect at the corner frequency, $\omega_c = 1/\tau$, Figure 13.27.

The phase angle is expressed as

$$\text{Arg } (1 + j\omega\tau)^{\pm n} = \pm n \tan^{-1} \omega\tau$$

At $\omega = 0$, $\phi = 0^\circ$ and at
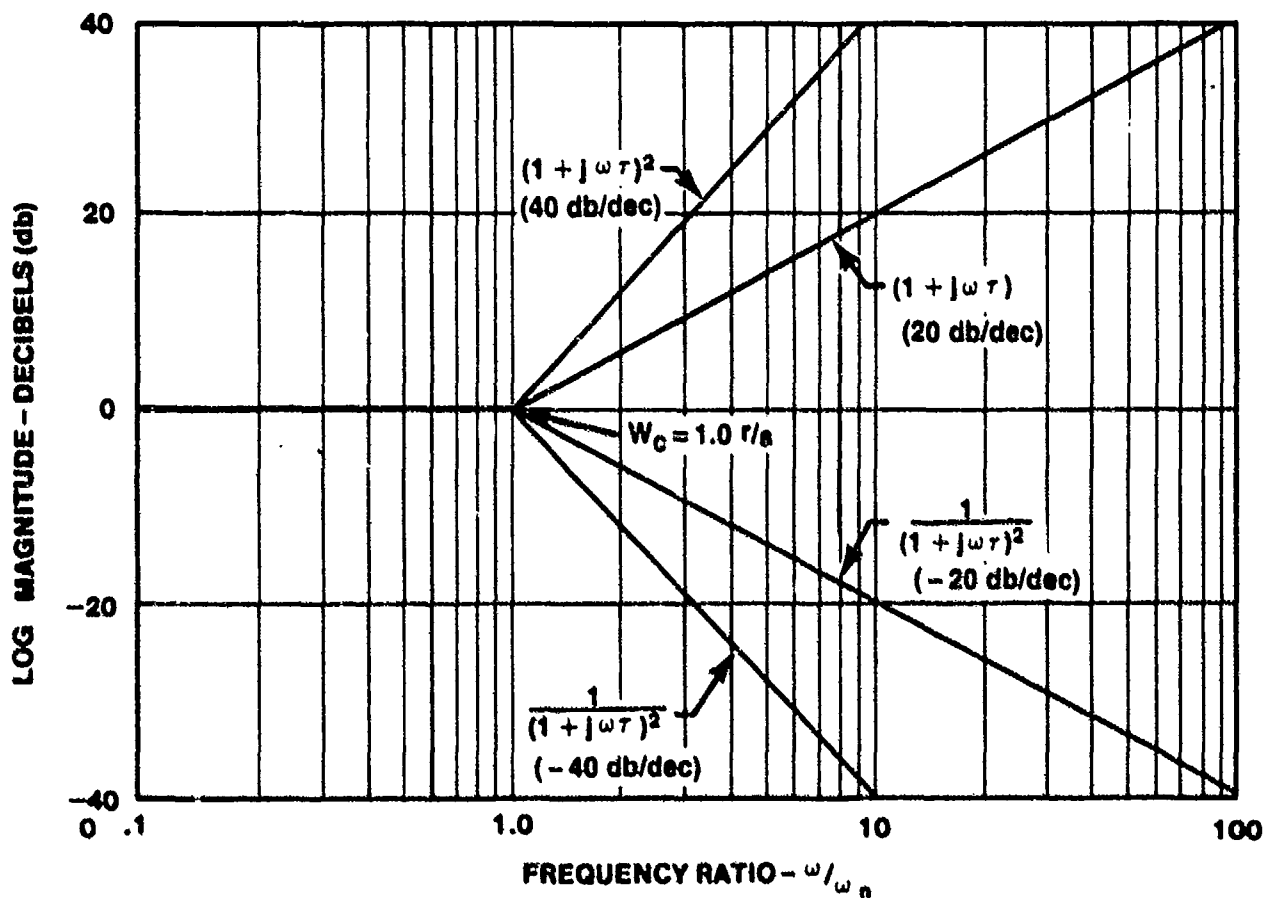
$\omega = \infty$, $\phi = \pm n \pi/2$ radians

FIGURE 13.27. BODE MAGNITUDE PLOT OF TERM $(1 + j\omega\tau)^{\pm n}$

Table 13.2 shows the variation of the phase angle with normalized frequency ω/ω_c, for n = -1.

TABLE 13.2

PHASE ANGLE VARIATION WITH NORMALIZED FREQUENCY $\left[(1 + j\omega\tau)^{-1}\right]$

$\dfrac{\omega}{\omega_c}$	$\tan^{-1}\omega\tau$
0	0
.1	$-5.7°$
.5	$-26.5°$
1.0	$-45.0°$
2.0	$-63.4°$
10.0	$-84.3°$
∞	$-90.0°$

The following techniques are used to plot the $(1 + j\omega\tau)^{\pm n}$ factor.

1. Locate corner frequency, $\omega_c = 1/\tau$.

2. Draw +20n db/decade asymptotes through the corner frequency (+20n db/dec for zero terms and -20n db/dec for pole terms).

3. A straight line can be used to approximate the phase shift. The line is drawn from $0°$ at one decade below the corner frequency to n $(\pm 90°)$ (+ for zero term, - for pole term) at one decade above the corner frequency. The maximum deviation using this approximation is about $6°$. The specific phase angle values are shown in Table 13.2 and the appropriate corrections can be applied if desired. These corrections are shown in Figure 13.28.

4. The error to the magnitude curve (created by using the asymptote technique) can be determined analytically. First determine the error at the corner frequency $\omega_c = 1/\tau$.

$$\pm 20n \log \sqrt{1 + \omega_c^2 \tau^2} \quad \text{becomes} \quad \pm 20n \log \sqrt{1 + \frac{\tau^2}{\tau^2}}$$

and

$$\pm 20n \log \sqrt{2} = \pm 10n \log 2 = \pm 3.01n \text{ db}$$

This shows that the asymptote can be corrected by adding approximately $\pm 3n$ db at the corner frequency. Likewise for a frequency one decade above the corner frequency,

$$\omega = 10 \, \omega_c = \frac{10}{\tau}$$

and

$$\pm 20n \log \sqrt{1 + 100 \, \tau^2/\tau^2} = \pm 20n \log \sqrt{101}$$

and

$$-10 \log 101 = -20.043 \text{ db (actual, for } n = -1)$$

Our straight line asymptote used -20 db so the total error at one decade is -.043 db. Similarly the error at $\omega_c/10$ can be found. At $\omega = 2\omega_c$ (one octave) $= 2/\tau$, the actual Lm for $n = -1$ is

$$-20 \log \sqrt{1 + 4 \, \tau^2/\tau^2} = -10 \log 5 = -6.9897 \text{ db}$$

The asymptote method produced a value of -6 db at this point, thus an error -.9897, or approximately -1.0 db.

Therefore, the straight line asymptotes can be made closer to the actual Lm curve by applying a $\pm 3n$ db correction at ω_c and a $\pm 1n$ db correction 1 octave above and 1 octave below ω_c.
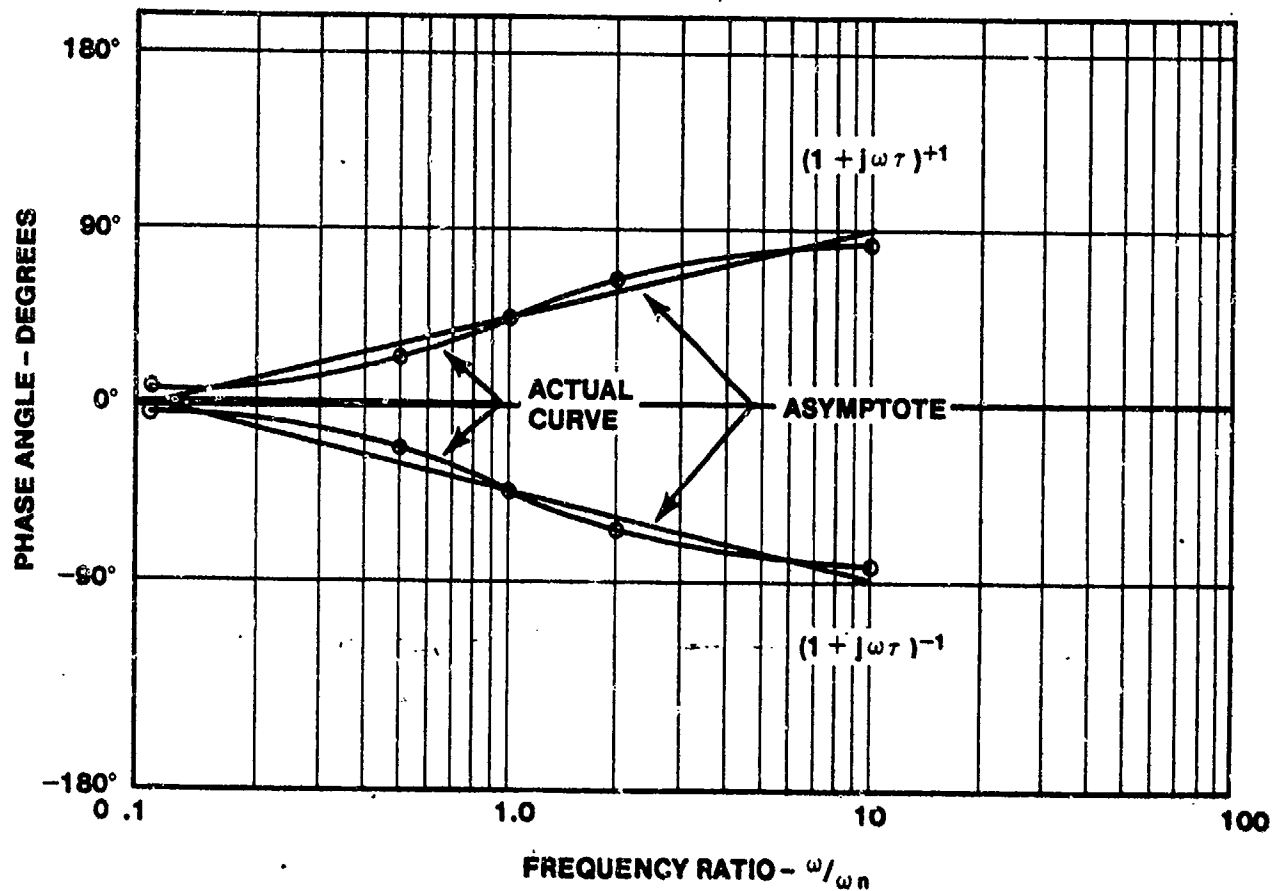
FIGURE 13.28. BODE PHASE ANGLE PLOT OF $(1 + j\omega\tau)^{\pm n}$

<u>Quadratic Term.</u> $[1 + 2\zeta/\omega_n \ j\omega + (j\omega/\omega_n)^2]^{\pm n}$

Consider the quadratic term

$$G(s) = \frac{1}{\left(1 + \frac{2\zeta s}{\omega_n} + \frac{s^2}{\omega_n^2}\right)^n}$$

(13.61)

The log magnitude of $G(j\omega)$, Equation 13.61, in db is

$$20 \log G(j\omega) = -20 n \log \sqrt{\left[1 - \left(\frac{\omega}{\omega_n}\right)^2\right]^2 + 2\zeta\left(\frac{\omega}{\omega_n}\right)^2}$$

(13.62)

and the phase angle is

13.52

$$\text{Arg } G(j\omega) = -n \tan^{-1} \left[\frac{2\zeta \frac{\omega}{\omega_n}}{1 - \left(\frac{\omega}{\omega_n}\right)^2} \right] \qquad (13.63)$$

If $\zeta > 1$, the quadratic term can be factored into two first-order factors plotted following the technique of the previous section. If $\zeta < 1$ the quadratic factors into a complex-conjugate pair and we plot the entire quadratic without factoring. The influence of the damping ratio, ζ, on the magnitude plot and phase angle plot is illustrated in Figure 13.29. From Figure 13.29 we see that the maximum value of the resonant peak is a function of ζ. The maximum value of the resonant peak is given by

$$M_r = \frac{1}{2\zeta \sqrt{1 - \zeta^2}} \qquad (13.64)$$

and the frequency at which this peak occurs is

$$\omega_r = \omega_n \sqrt{1 - 2\zeta^2} \qquad (13.65)$$

The asymptote technique will provide accurate curves provided corrections are applied.

LOG MAGNITUDE – DECIBELS (db)

PHASE ANGLE, DEG

15

10

5

0

-5

-10

-15

-20

-25

-30

0°

-20°

-40°

-60°

-80°

-100°

-120°

-140°

-160°

-180°

$\zeta = 0.10$

$\zeta = 0.15$

$\zeta = 0.20$

$\zeta = 0.25$

$\zeta = 0.30$

$\zeta = 0.50$

$\zeta = 0.71$

$\zeta = 1.00$

12 db/ OCTAVE

0.1

1

5

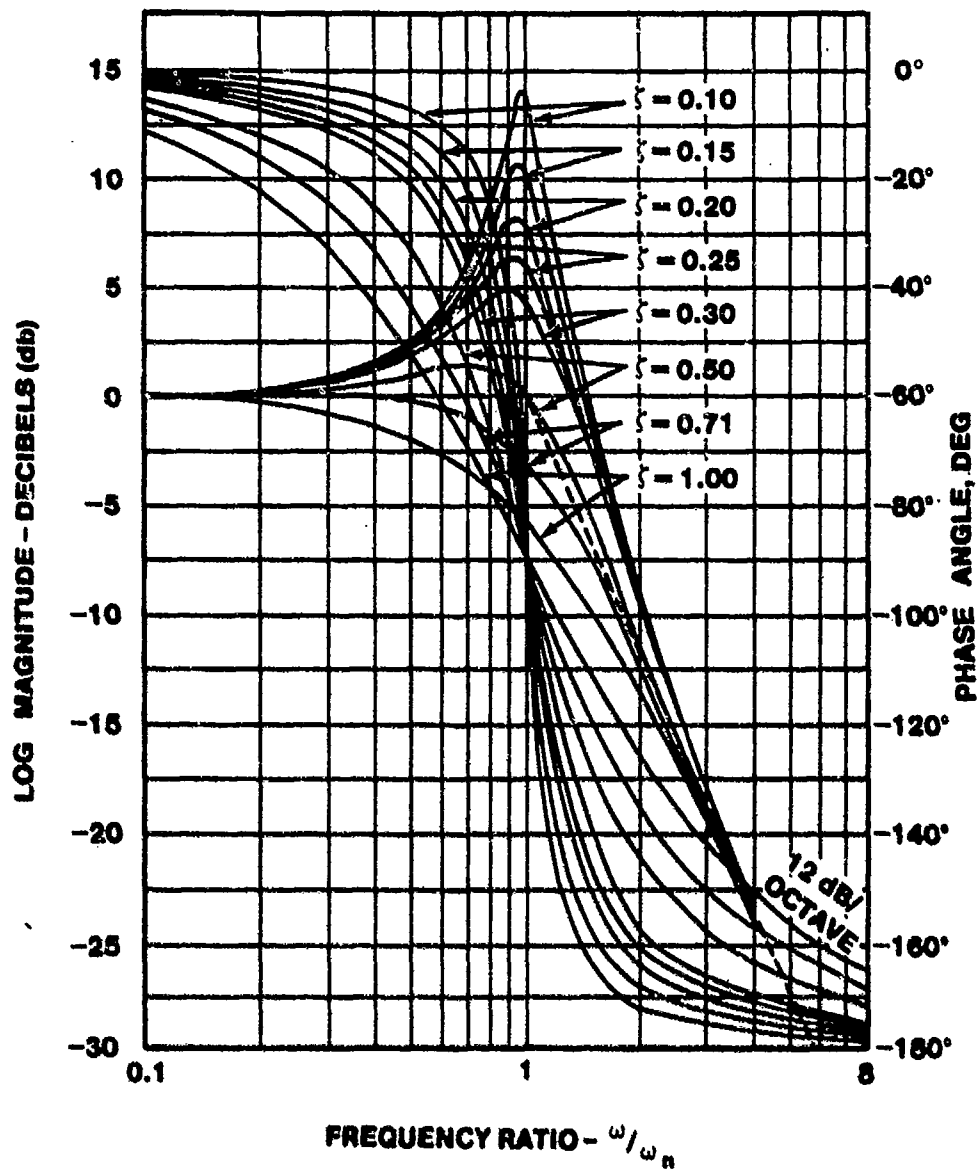FREQUENCY RATIO – ω/ω_n

FIGURE 13.29. BODE DIAGRAM FOR $G(j\omega) = \left[1 + (2\zeta/\omega_n)\, j\omega + (j\omega/\omega_n)^2\right]^{-1}$

13.54

At very low frequency $\frac{\omega}{\omega_n} \ll 1$

$$20 \log \ G(j\omega) \ \approx \ - 20 \ n \log 1 \ = \ 0 \ db$$

Therefore, at low frequencies the asymptote for the quadratic term is a straight line with a slope of zero. At high frequency $\omega/\omega_n \gg 1$, Equation 13.62 can be approximated as

$$20 \ \log \ G(j\omega) \ \approx \ -20 \ n \ \log \sqrt{\left(\frac{\omega}{\omega_n}\right)^4}$$

$$\approx \ -40 \ n \ \log \left(\frac{\omega}{\omega_n}\right) \ db$$

The last equation represents the equation of a straight line with slope of -40 ndb/dec. If the quadratic is in the numerator (i.e., +n) the slope is positive. The two asymptotes intersect at ω_n, hence, ω_n is considered the corner frequency of the quadratic factor. The actual magnitude plot for the quadratic factor differs strikingly from its asymptote plot in that the amplitude curve depends not only on ω_n, but also on ζ. From Figure 13.29, several values of Lm around ω_n can be plotted for a specific ζ to obtain an accurate magnitude plot.

The phase angle plot for a quadratic factor can be obtained by locating the $\pm 90°n$ point at ω_n and obtaining a few points either side of ω_n for a specific value of ζ from Figure 13.29.

To summarize, the procedures for plotting the quadratic term are:

a. Determine the value of ζ and ω_n.

b. Plot the zero db asymptote from low frequencies to ω_n and a $\pm 40n$ db/dec asymptote beginning at ω_n.

c. Use the curves presented in Figure 13.29 to correct the asymptotes in the vicinity of the corner frequency.

d. At the corner frequency, ω_n, locate the $\pm 90°n$ phase point. Using the curves of Figure 13.29 for the specific ζ, plot enough data points to permit sketching the phase angle curve.

When each of the four types of factors are plotted on the Bode plot, all the magnitude curves and phase angle curves are summed at different frequencies to complete the composite curves. The following problem will illustrate the simplicity of this technique.

Example Problem:

Given:
$$G(s) = \frac{640s\ (s + 1000)}{(s + 10)\ (s^2 + 80s + 6400)}$$

where

$$2\zeta\omega_n = 80, \quad \omega_n = 80, \quad \zeta = 0.5$$

1. First put G(s) into the frequency response standard form.

$$G(j\omega) = \frac{(640)\ (1000)\ (j\omega)\ (1 + j\ .001\omega)}{(6400)\ (10)\ (1 + j\ .1\omega)\ \left(1 - \frac{\omega^2}{6400} + j\ \frac{80\omega}{6400}\right)}$$

where

$$K_n = \frac{(640)\quad (1000)}{(6400)\quad (10)} = 10$$

13.56

2. Find the corner frequencies where $\omega_c = 1/\tau$. For a quadratic term the natural frequency ω_n is the corner frequency ω_c.

   Zeros: $\omega_c = 1000$, +20 db/dec

   Poles: $\omega_c = 10$, -20 db/dec; $\omega_c = 80$, -40 db/dec

3. Plot the individual magnitude and phase angle terms on the Bode. Also $20 \log K_n = 20 \log 10 = 20$ db.

4. Apply the appropriate corrections at the corner frequencies.

5. Add the curves.

6. Figures 13.30 and 13.31 show the contribution of the separate factors and the composite curve for the example.

We must emphasize that the development on the Bode plot presented here is based on the steady-state frequency response of an open-loop system to a sinusoidal input. Techniques exist to arrive at the closed-loop frequency response, but these are beyond the scope of our study. The closed-loop frequency response graph is a plot of magnitude ratio, $M(j\omega) = C(j\omega)/R(j\omega)$, and phase angle, ϕ, versus frequency. One method of determining the closed-loop frequency response is by using the Nichol's chart (Reference 13.3).
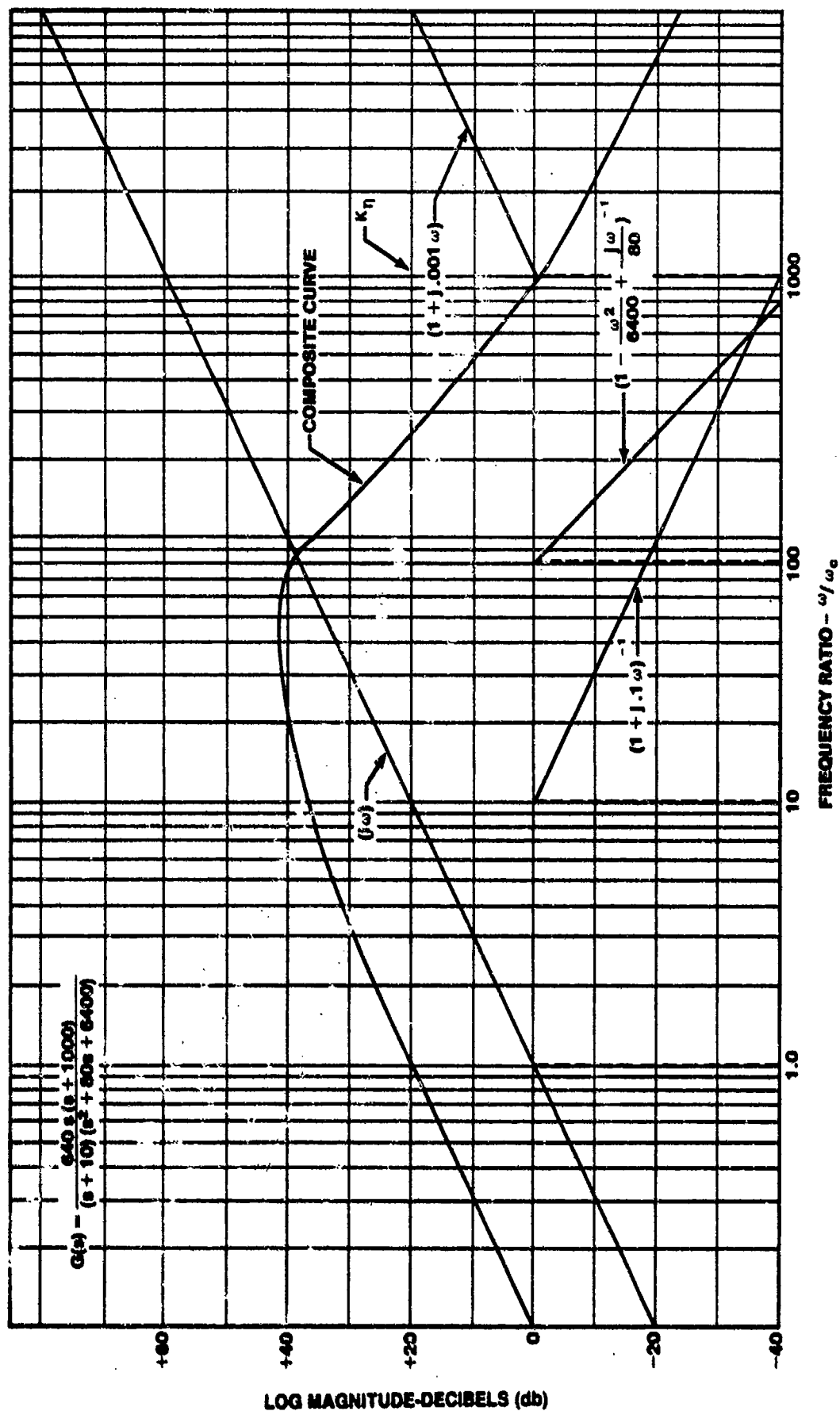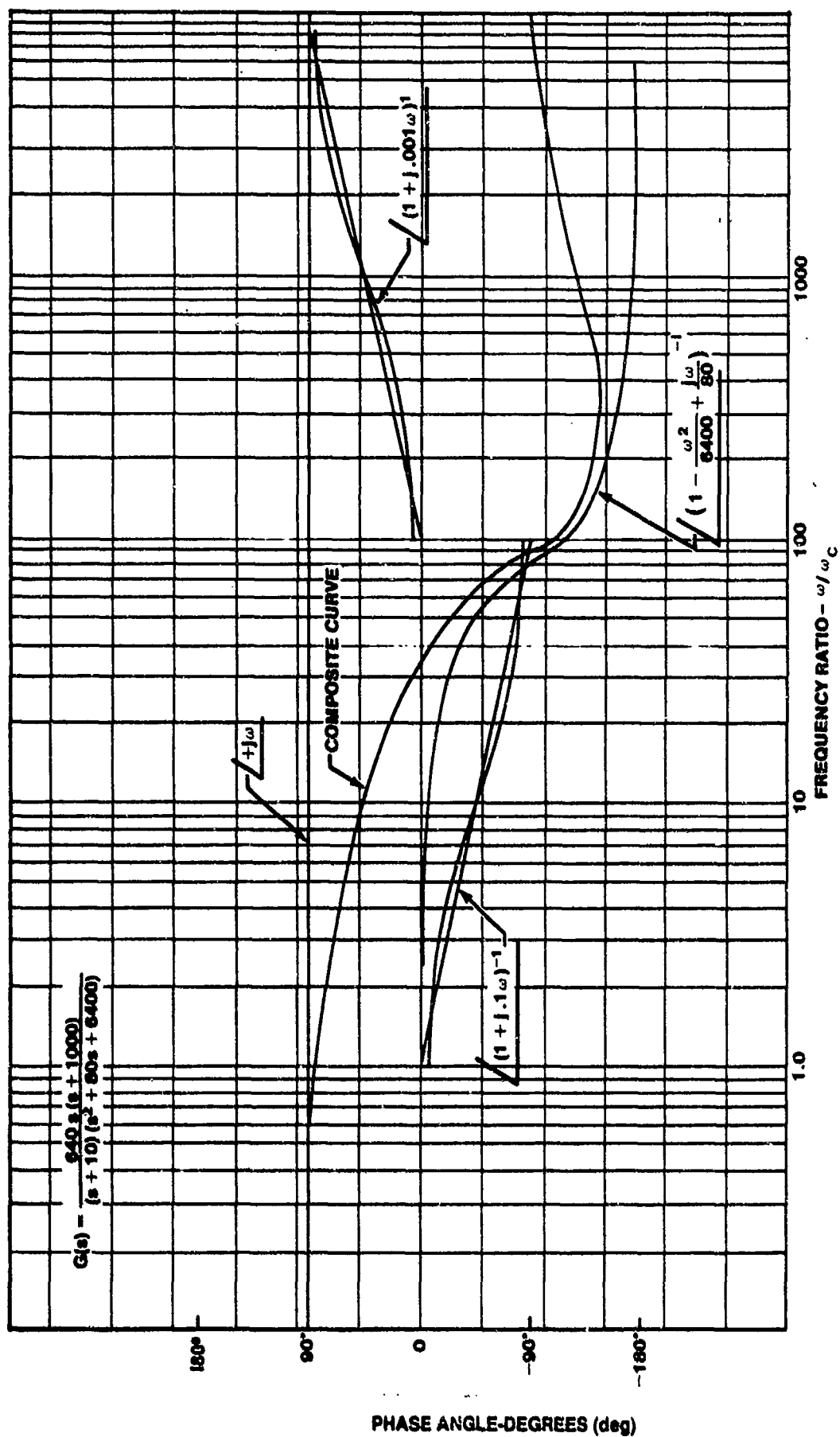
FIGURE 13.30. BODE LOG MAGNITUDE PLOT

13.58

FIGURE 13.31. BODE PHASE ANGLE PLOT

13.59

13.7.3 Relative Stability

The relative stability of a closed-loop system can be determined by looking at the Bode plot of the open-loop transfer function, KGH(jω). Several terms are used to relate stability by the Bode Plot. The mathematical basis for these relationships comes from the Nyquist Stability Criteria. The terms are:

13.7.3.1 Gain Margin. Gain margin is the additional amount of gain, measured in decibels, that the magnitude ratio can be increased before the system goes unstable. The gain margin is defined as the reciprocal of the open-loop transfer function, GH(jω), evaluated at the frequency where the phase angle is $-180°$.

$$\text{Gain Margin} = 20 \log_{10} \frac{1}{GH(j\omega)}$$

This quantity is illustrated in Figure 13.32.

13.7.3.2 Phase Margin. Phase margin is the amount of phase shift, measured in degrees, that the phase angle curve can be displaced to produce instability in the system. Phase margin is measured at the frequency where the Lm plot crosses the 0 db line.

$$\text{Phase Margin} = +180° + \phi$$

$$(\phi = \text{phase angle measured at 0 db})$$

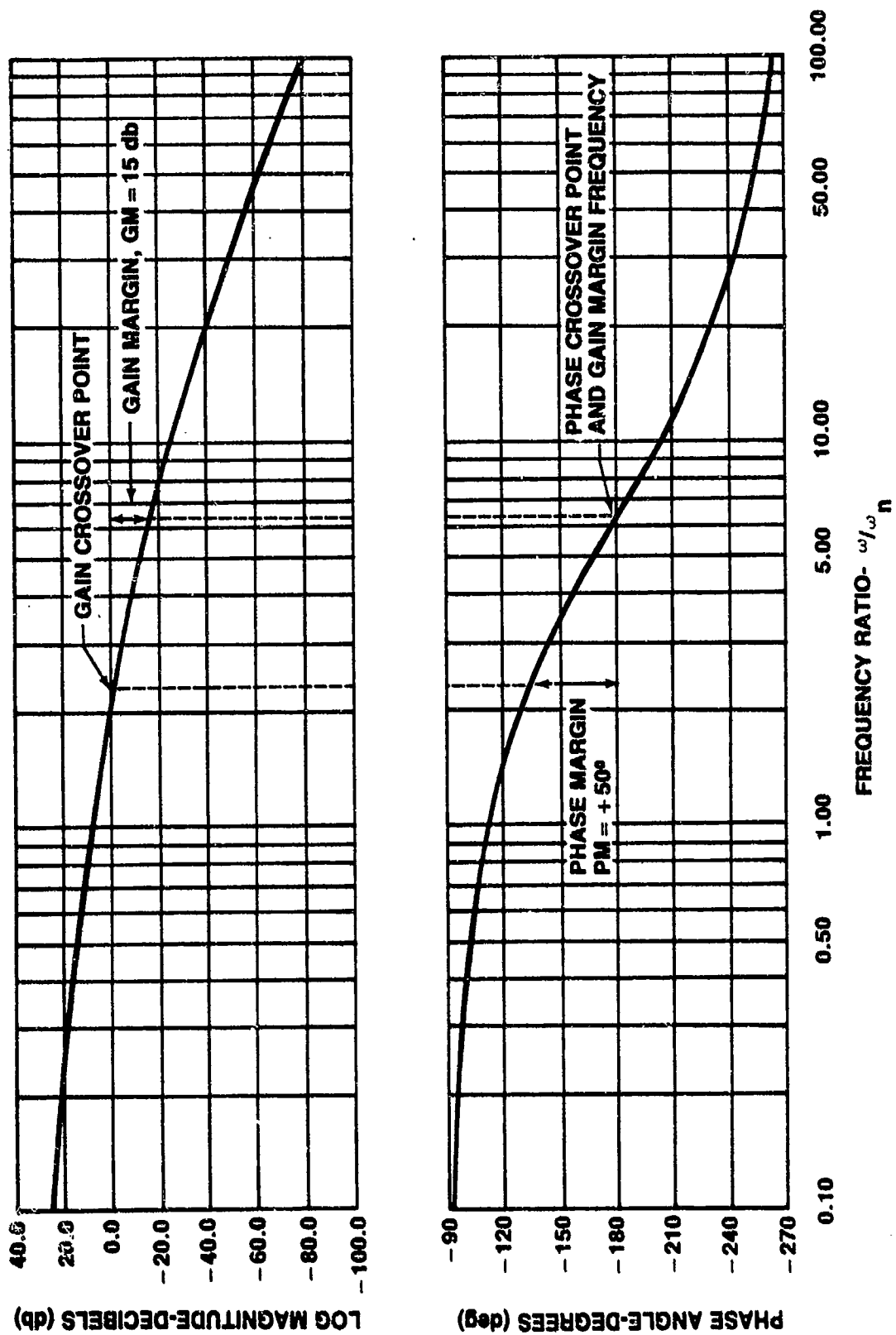This quantity is illustrated in Figure 13.32.

FIGURE 13.32. BODE PLOT RELATIVE STABILITY RELATIONSHIPS

Stability requires that the phase margin be positive, i.e., the phase angle at the 0 db crossover point must be greater than -180°.

13.7.3.3 The Gain Crossover Point is defined as the point or points where the magnitude curve crosses the zero db axis.

13.7.3.4 The Phase Crossover Point is the point on the Bode phase angle plot at which the phase angle is -180°. The frequency at which the phase crossover occurs is called the gain margin frequency.

13.7.4 Frequency Domain Specifications

There are several terms used to express the specifications of systems in the frequency domain. Although these terms are usually used to define the closed-loop response, they can also be used to express characteristics of the open-loop Bode plot.

13.7.4.1 Bandwidth (BW). The definition of bandwidth of a system depends on an accurate description of the problem. Normally the bandwidth is defined as the frequency at which the magnitude ratio $M(j\omega) = C(j\omega)/R(j\omega)$ has dropped to 70.7% of the zero frequency level or 3 db down from the zero frequency level as shown in Figure 13.33. This does not cover all cases in that the magnitude ratio at zero frequency may be low as in Figure 13.34. In this case the bandwidth is defined as the frequency range over which the magnitude ratio does not vary more than -3 db from its value at a specified frequency. For the purposes of this course the bandwidth can also be determined as the -3 db point on the Im plot of the open-loop system. This value should correspond closely to the bandwidth of the closed-loop system.
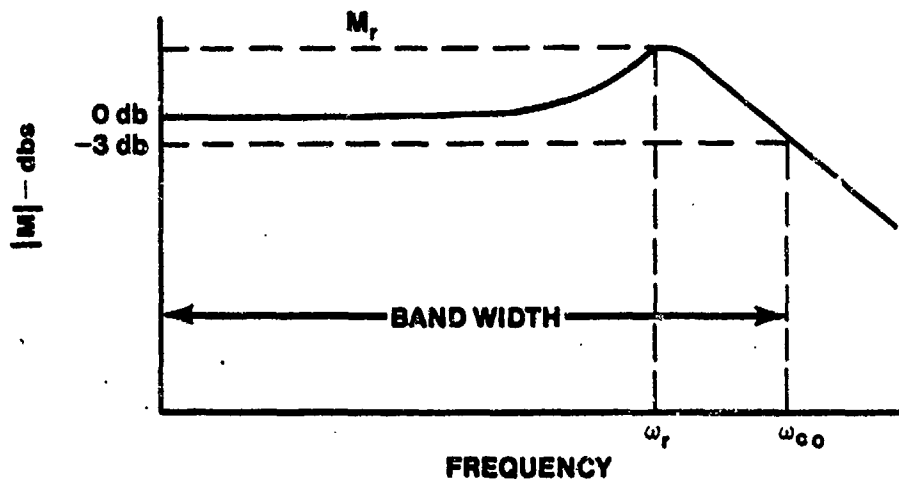
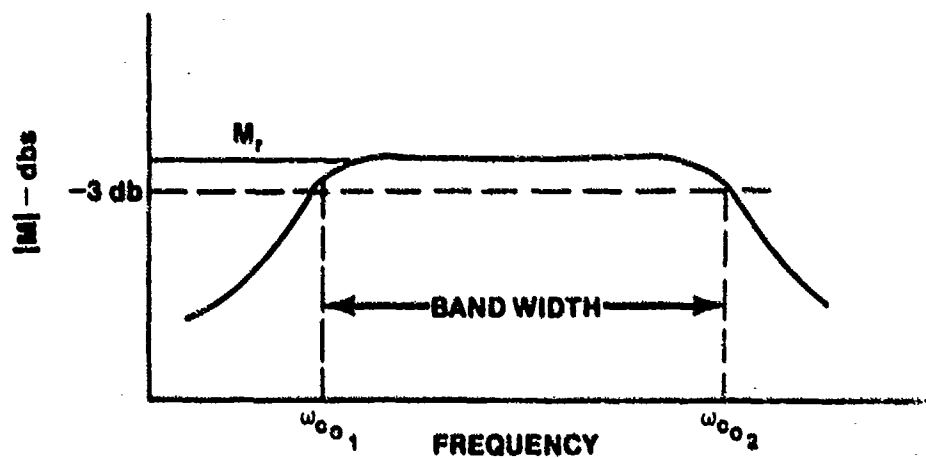FIGURE 13.33.   FREQUENCY DOMAIN CHARACTERISTICS

FIGURE 13.34.   FREQUENCY DOMAIN CHARACTERISTICS

13.63

The frequency at which the -3 db point is reached is called the cutoff frequency, ω_{co}. Bandwidth is important for two reasons. First, it is indicative of the noise filtering characteristics of the system. System noise is always present and the bandwidth and the corresponding cutoff frequency dictate at what frequency the response and thus the noise will be filtered. Secondly, the bandwidth is a measure of the transient response properties of a system. A large bandwidth will allow higher frequencies to pass to the output and the system may be characterized by fast rise time and large overshoots. However, if the bandwidth is narrow, only low frequency signals are passed and the time response will generally be slow and sluggish.

13.7.4.2 Resonant Peak, M_r. If the system is of second-order or higher, it may have a resonant peak, M_r. For a second-order system there exists exact mathematical relationships between ζ, the damping ratio, and ω_r, the frequency at which M_r occurs. A higher-order system can often be approximated by a second-order system to simplify the solution. The resonant peak, M_r, Figure 13.33, is an indication of the relative stability of the system as a high value of M_r corresponds to a large overshoot in the time domain. Typical values of M_r for usable stable systems may vary from 1.1 to 1.5.

13.7.5 Experimental Method of Frequency Response

A Bode plot may be determined experimentally and ultimately will provide the system transfer function. The method depicted in Figure 13.35 will allow for measurement of the magnitude ratio and phase angle versus frequency.
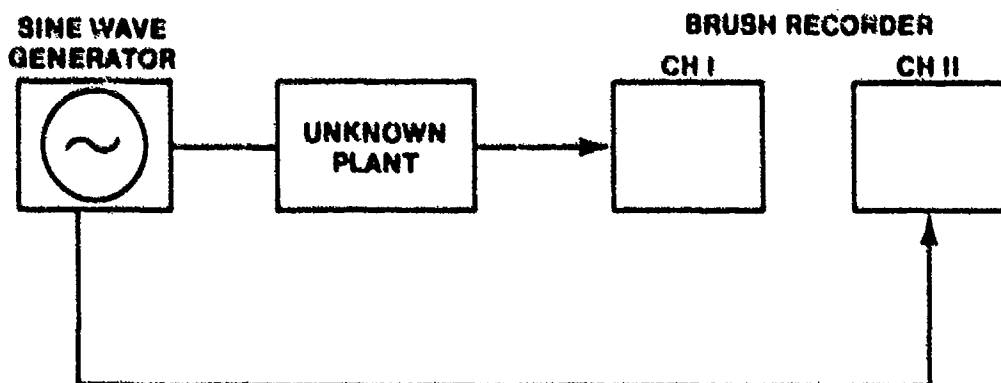

FIGURE 13.35. EXPERIMENTAL BODE TECHNIQUE

Once the Lm and phase angle versus frequency curves are plotted, asymptotes care fitted on the curve and determine the corner frequencies. If a resonant peak occurs, use the techniques discussed previously to determine ζ and ω_n.

In our discussion, we have been talking about open-loop systems that do not have poles and/or zeros in the right-half of the s-plane (RHP). These systems are known as minimum phase systems. A nonminimum phase system is one which has an open-loop pole and/or zero in the RHP. A nonminimum phase factor is of the form

$$(1-j\zeta\omega)^{\pm n} \quad \text{or} \quad \left[1 + \left(\frac{\omega}{\omega_n}\right)^2 \pm j2\zeta\frac{\omega}{\omega_n}\right]^{\pm n}$$

If a system is known to be minimum phase, only the Lm plot is required to fully determine the system transfer function; while both the Lm and phase angle plots are required to determine the system transfer function if the system is nonminimum phase. For example, consider the following transfer functions:

$$G_1(s) = \frac{(s+1)}{(s+10)}, \quad G_2(s) = \frac{(s+1)}{(s-10)}, \quad G_3(s) = \frac{(s-1)}{(s+10)}, \quad \text{and } G_4(s) = \frac{(s-1)}{(s-10)}$$

All four transfer functions have similar Lm plots, but their phase angle plots are all different ($G_1(s)$ is minimum phase; $G_2(s)$, $G_3(s)$, and $G_4(s)$ are all nonminimum phase).

13.8 CLOSED-LOOP TRANSFER FUNCTION

For reasons to be seen shortly, complex control systems are most often represented by a block diagram in the form of Figure 13.36 where the forward transfer function, G, and the feedback transfer function, H, are expressed as functions of s, the Laplace transform variable. The closed-loop transfer function of Figure 13.36 will now be developed in terms of the forward and feedback transfer functions for our first and second-order systems. No transfer function present in the feedback loop is called unity feedback (in Figure 13.5, $H(s) = 1$).

13.65
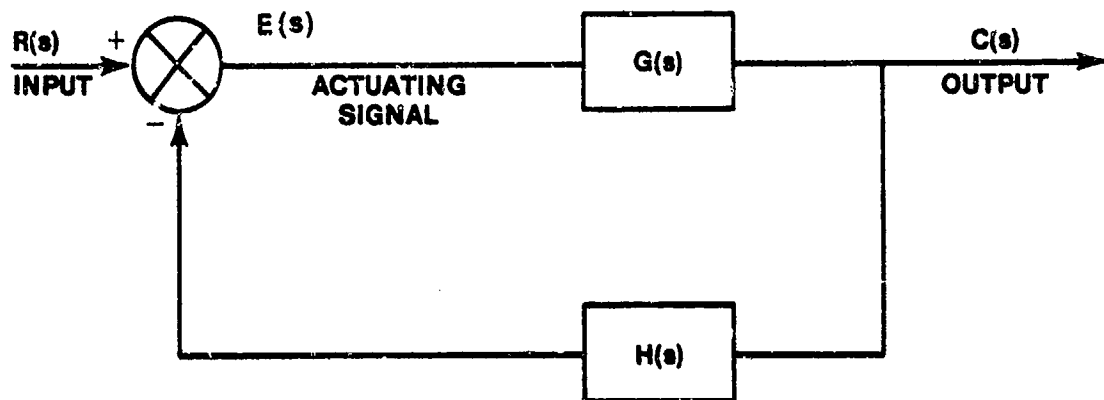
FORWARD TRANSFER FUNCTION — G(s)
FEEDBACK TRANSFER FUNCTION — H(s)
OPEN-LOOP TRANSFER FUNCTION (OLTF) — G(s)/H(s)
CLOSED-LOOP TRANSFER FUNCTION (CLTF) — C(s)/R(s)
ACTUATING SIGNAL — E(s)

FIGURE 13.36.   STANDARD FORM OF FEEDBACK CONTROL SYSTEM

In order to find G(s) of the first-order system (Figure 13.5), equate torques and assume only damping present

$$\mu\varepsilon = b\dot{\theta}$$

taking the Laplace transform and noting that $G(s) = \theta(s)/E(s)$ we find

$$\mu E(s) = bs\theta(s)$$

$$G(s) = \frac{\theta}{E}(s) = \frac{1}{\frac{b}{\mu}s}$$

again letting

$$\tau = \frac{b}{\mu}$$

$$G(s) = \frac{1}{\tau s} \qquad (13.66)$$

The same procedure for the case including inertia yields the following torque summation:

$$\mu\epsilon = I\,\dot\theta + b\,\dot\theta$$

$$E(s) = \frac{I}{\mu} s^2\,\theta(s) + \frac{bs}{\mu}\,\theta(s)$$

$$G(s) = \frac{\theta}{E}(s) = \frac{\mu}{Is^2 + bs} \qquad (13.67)$$

Thus, we have the forward transfer function for our two systems. Referring to Figure 13.36, we will now derive an expression for the closed-loop transfer function in terms of G and H.

$$G(s) = \frac{C(s)}{E(s)}$$

and also

$$E(s) = R(s) - H(s)\,C(s)$$

substituting

$$G(s) \ [R - H(s) \ C(s)] \ = \ C(s)$$

$$R(s) \ G(s) \ = \ C(s) \ [1 + GH(s)] \qquad (13.68)$$

the system closed-loop transfer function becomes

$$\frac{C}{R} \ (s) \ = \ \frac{G(s)}{1 + GH(s)} \qquad (13.69)$$

This is a very important relationship which should immediately be committed to memory.

    As noted previously, the block diagram of Figure 13.36 is the standard form of the feedback control system. When in this form the closed-loop transfer function can be quickly found by Equation 13.69. But most important, the characteristic equation of the system from which the transient response is determined is immediately evident. Referring to Equations 13.68 and 13.69 we will show that the characteristic equation is found from the denominator of the right hand term in Equation 13.69.

$$1 + GH(s) \ = \ 0$$

The characteristic equation is merely 1 plus the system open-loop transfer function, GH(s), which is directly available.

But first, applying our closed-loop transfer function expression to the first-order system we use the forward transfer function of Equation 13.66. Since the system has unit feedback, H(s) = 1 and

$$GH(s) = \frac{1}{\tau s}$$

Therefore, using Equation 13.69 yields

$$\frac{C}{R}(s) = \frac{G(s)}{1 + GH(s)} = \frac{\frac{1}{\tau s}}{1 + \frac{1}{\tau s}}$$

$$\frac{C}{R}(s) = \frac{1}{\tau s + 1}$$

which is consistent with Equation 13.16, the transfer function derived from the equation of motion of the entire system.

In the case of the second-order system, since H(s) is unity

$$GH(s) = \frac{\mu}{Is^2 + bs}$$

For this system, using Equation 13.69

$$\frac{C}{R}(s) = \frac{G(s)}{1 + GH(s)} = \frac{\frac{\mu}{Is^2 + bs}}{1 + \frac{\mu}{Is^2 + bs}}$$

$$\frac{C}{R}(s) = \frac{1}{\frac{Is^2}{\mu} + \frac{bs}{\mu} + 1} \tag{13.70}$$

13.69

is again consistent with the more direct method leading to Equation 13.18. The denominator of Equation 13.70 is the characteristic equation introduced by Equation 13.12.

Transfer functions are written to describe either whole systems or parts of systems using the appropriate differential equation. When control systems described by block diagrams, are reduced to some standard form, they quickly yield both the transfer function of the entire closed-loop system and its characteristic equation.

We will now discuss the technique of manipulating control systems in block diagram notation to obtain the desired form.

13.9 BLOCK DIAGRAM ALGEBRA

It was seen that the simplification resulting from the use of operational calculus is further increased when transfer functions and block diagrams are introduced. The special methods of predicting the transient response of a system without solving its equation of motion are most conveniently employed when the block diagram is of the form of Figure 13.36.

In practice, individual transfer functions are written for each integral unit of a more complex system. For example, the system of Figure 13.37 represents the pitch axis of an aircraft autopilot where the input is the commanded pitch attitude and the output the actual aircraft attitude. The autopilot, the elevator servo, and the aircraft itself are described separately in G_1, G_2, and G_3 respectively. As long as it is realized that transformed quantities are used the G(s) can be discarded and only G used.

The system of Figure 13.37 can be simplified by combining the inner loop into a single transfer function. If we let G_4 be the closed-loop transfer function of the inner loop we have

$$G_4 = \frac{G_2}{1 + G_2}$$

Figure 13.37 can then be redrawn as shown in Figure 13.38. This diagram is then further reduced by noting that

$$G_1 = \frac{\delta_i}{E}, \quad G_4 = \frac{\delta_e}{\delta_i}, \quad G_3 = \frac{C}{\delta_e}$$

and

$$G_1 G_4 G_3 = \frac{\delta_i}{E} \frac{\delta_e}{\delta_i} \frac{C}{\delta_e} = \frac{C}{E}$$

Denoting

$$G_5 = G_1 G_4 G_3 = \frac{G_1 G_2 G_3}{1 + G_2}$$
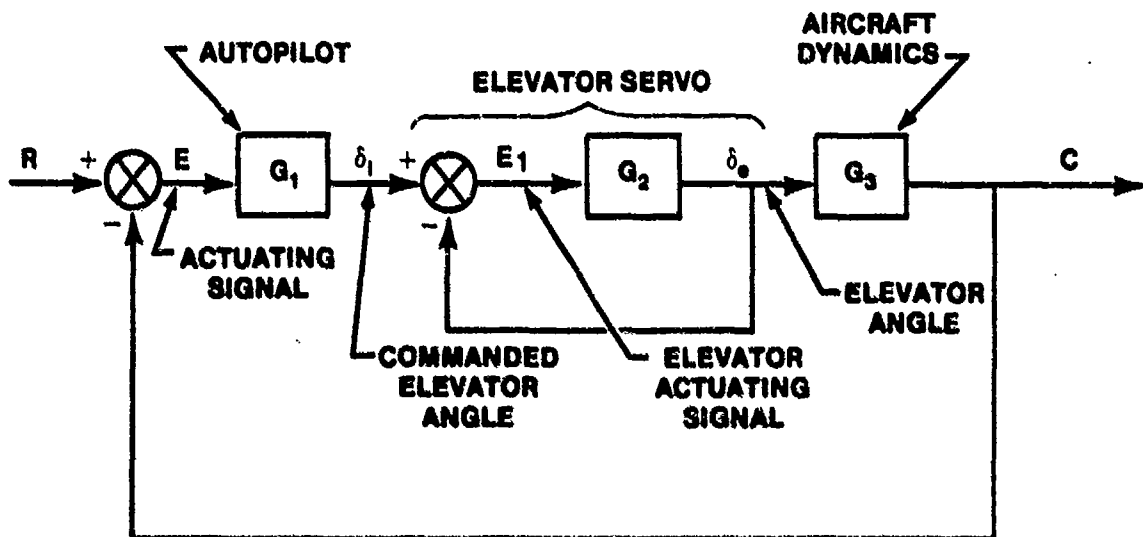
FIGURE 13.37.   AIRCRAFT PITCH AXIS CONTROL SYSTEM
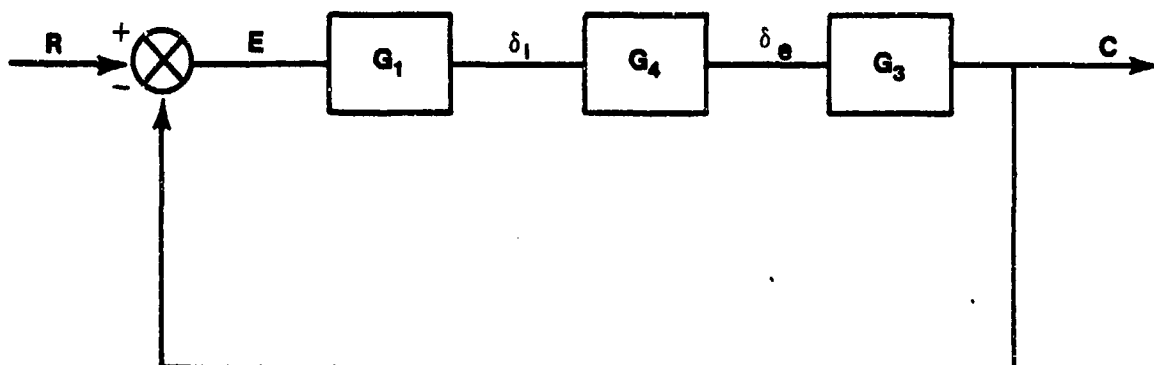
FIGURE 13.38.   (FIGURE 13.37 REDUCED)
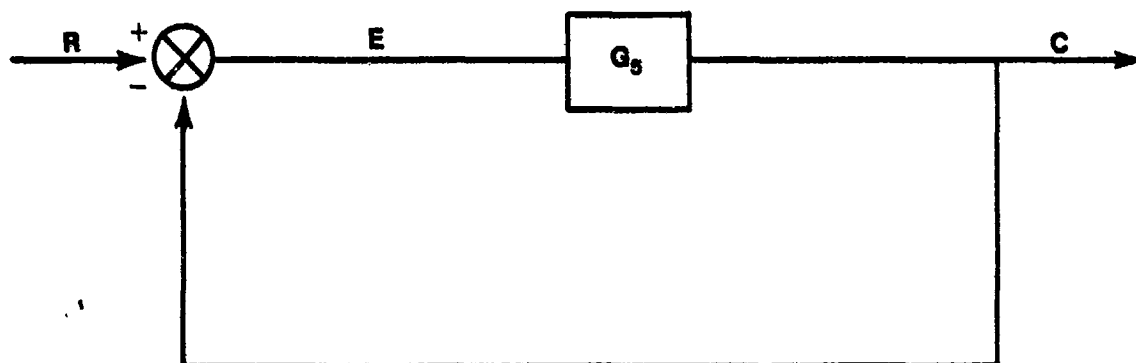
FIGURE 13.39.   (FIGURE 13.37 FURTHER REDUCED)

We have, finally, the control system described in the proper form in Figure 13.39.

The following block diagram identities, Figure 13.40, will assist in manipulating complex control systems into the standard form for analysis.
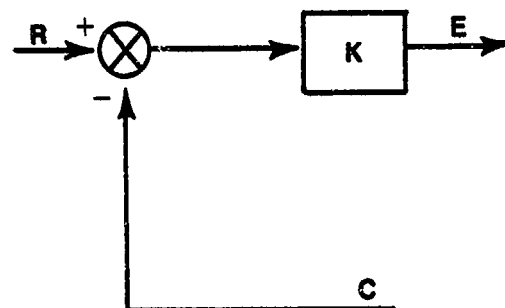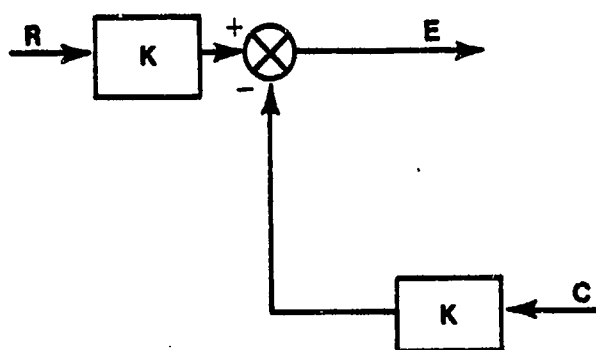
(a)
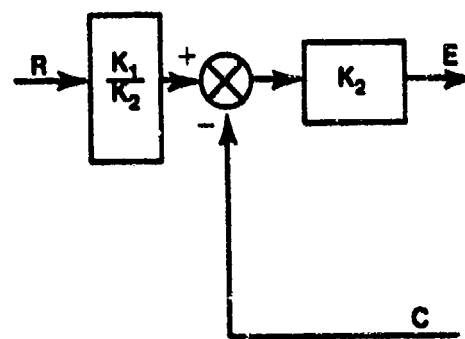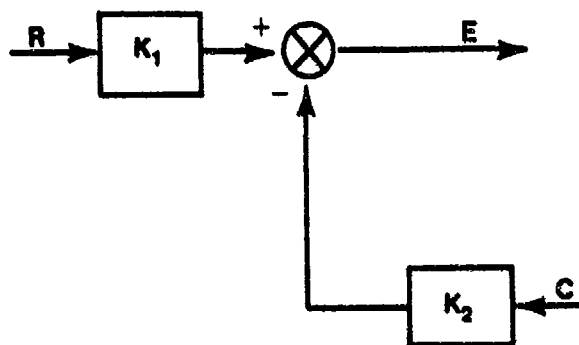
(b)

FIGURE 13.40. BLOCK DIAGRAM IDENTITIES

13.73
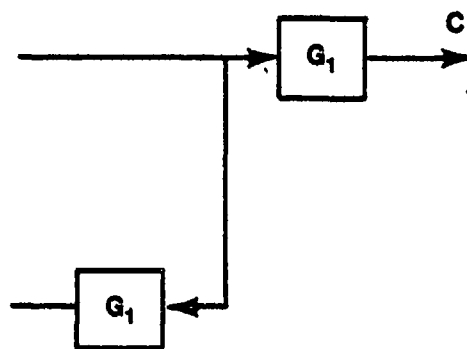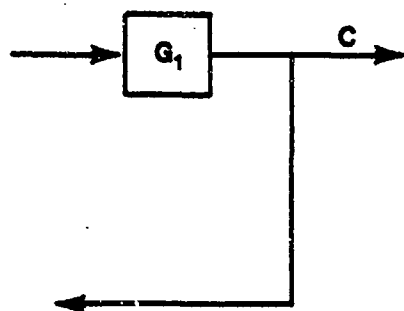
(c)
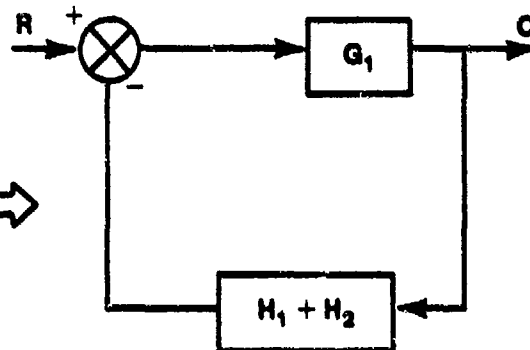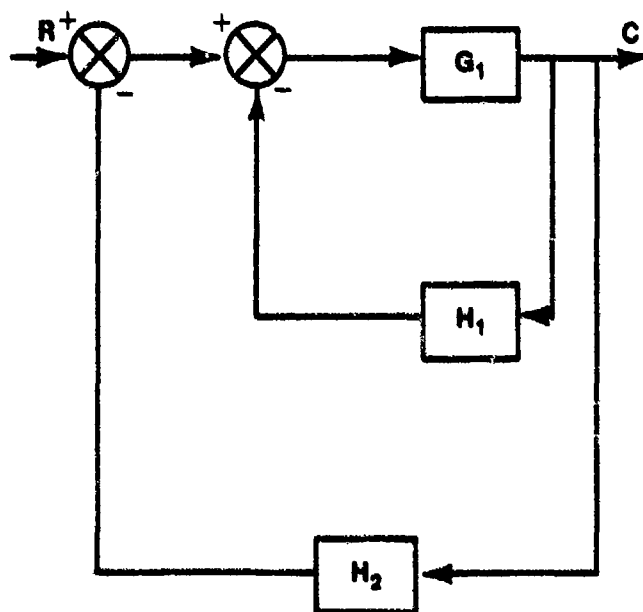
(d)

FIGURE 13.40. CONT. BLOCK DIAGRAM IDENTITIES
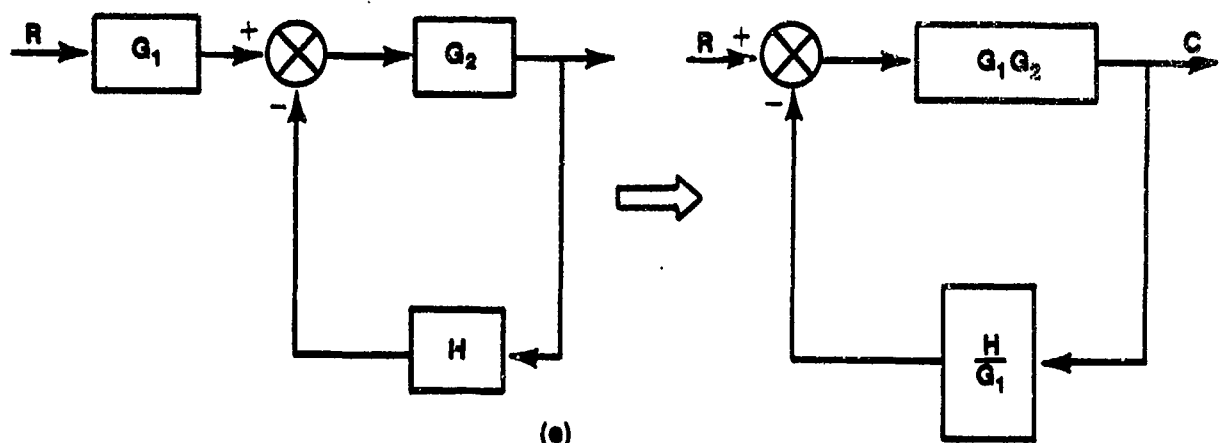
FIGURE 13.40. CONT. BLOCK DIAGRAM IDENTITIES

13.10 STEADY-STATE PERFORMANCE

The steady-state accuracy of a system is of considerable importance and is often related in terms of the steady-state error. Figures of merit for steady-state performance are the error constants, K_p, K_v, and K_a often referred to as the position, velocity and acceleration error·constants.

A technique used to indicate the steady-state performance of a system is to classify the system by "Type". The number of free or pure integrators in the forward loop is the Type system (system must be stable and represented by unity feedback). For a specified input function, an n-type system will produce a mathematically predictable steady-state error. Consider the unity feedback system in Figure 13.41. A unity feedback system is used in this development since we will be relating the performance as a function of the steady-state error, $e(t)_{ss}$, where

$$e(t)_{ss} = r(t)_{ss} - c(t)_{ss}$$

For this relationship to be valid in this development, the reference input r(t) and the control variable c(t) must be dimensionally the same and must be to the same scale.
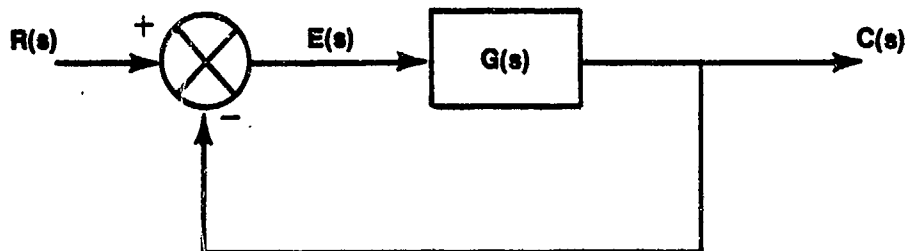
FIGURE 13.41.   UNITY FEEDBACK SYSTEM

$$E(s) = R(s) - C(s)$$

and

$$C(s) = E(s) \, \dot{G}(s)$$

therefore

$$E(s) = R(s) - E(s) \, G(s)$$

$$E(s) \, [1 + G(s)] = R(s)$$

$$\frac{E(s)}{R(s)} = \frac{1}{1 + G(s)}$$

The error signal $E(s)$ is a function of the plant, $G(s)$, and the reference input $R(s)$.

$G(s)$ can be represented by

$$G(s) = \frac{K_n(\tau_1 s + 1)(\tau_2 s + 1) \, \text{——}}{s^n (\tau_a s + 1)(\tau_b s + 1)\left(\dfrac{s^2}{\omega_n^2} + \dfrac{2\zeta s}{\omega n} + 1\right) \, \text{——}}$$

Defines "Type"

13.76

where n = 0, 1, 2, ... For a Type 0 system n = 0; i.e., no free integrators in the forward loop. G(s) must be expressed in the above form to properly evaluate the overall gain, K_n, of the transfer function. This gain is often referred to as the "DC" gain or "type" gain.

We will seek to show the relationships between the inputs, the n-type system and the steady-state error. First consider the general error and apply a step, ramp, and a parabolic input.

$$E(s) = \frac{R(s)}{1 + G(s)}$$

13.10.1 Step Input

Let $r(t) = Ru_{-1}(t)$ and $R(s) = R/s$ and apply the final value theorem. Recall for any function $F(s)$.

$$\lim_{s \to 0} s\, F(s) = \lim_{t \to \infty} f(t) \qquad E(s) = \frac{1}{1 + G(s)} R(s)$$

$$e(t)_{ss} = \lim_{s \to 0} \frac{s\, R/s}{1 + G(s)}$$

$$= \frac{R}{1 + \lim_{s \to 0} G(s)}$$

K_p Position Error Constant. The position error constant, Kp, is defined as

$$K_p = \lim_{s \to 0} G(s)$$

Therefore,

$$e(t)_{ss} = \frac{R}{1 + K_p}$$

For a Type 0 system

$$G(s) = K_0 \frac{(\text{---})(\text{---})}{(\text{---})(\text{---})}$$

$$K_p = \lim_{s \to 0} G(s) = \lim_{s \to 0} K_0 \frac{(\text{---})(\text{---})}{(\text{---})(\text{---})}$$

$K_p = K_0$, the overall gain of the transfer function.

For a Type 0 system a step input yields

$$e(t)_{ss} = \frac{R}{1 + K_0}$$

and the steady-state error is represented graphically in Figure 13.42
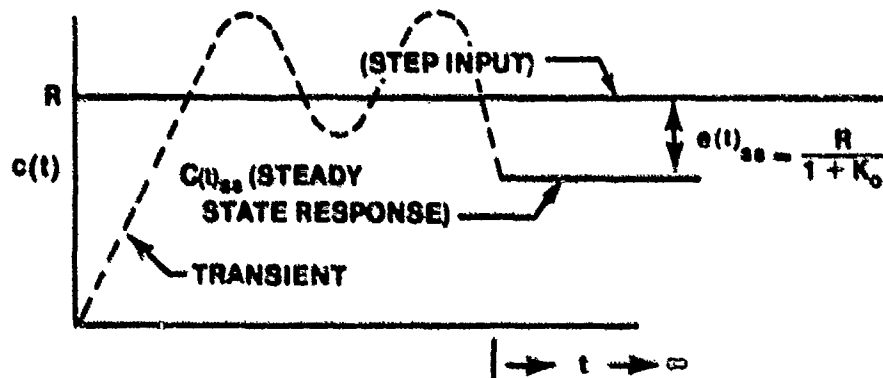
FIGURE 13.42.   STEADY-STATE ERROR,
TYPE 0 SYSTEM - STEP INPUT

For a Type 1 system

$$G(s) = \frac{K_1 (\text{---})(\text{---})}{s (\text{---})(\text{---})}$$

$$K_p = \lim_{s \to 0} G(s) = \lim_{s \to 0} \frac{K_1 (\text{---}) (\text{---})}{s (\text{---}) (\text{---})}$$

$$K_p = \infty$$

Therefore,

$$e(t)_{ss} = \frac{R}{1 + \infty} = 0$$

The resulting error from a step input into a Type 1 system is zero. Similarly for a Type 2 and 3 system with a step input, the resulting error is zero.

13.10.2 Ramp Input

Consider a ramp input $r(t) = Ru_{-1}(t)$, $R(s) = R/s^2$

Therefore,

$$E(s) = \frac{R/s^2}{1 + G(s)}$$

$$e(t)_{ss} = \lim_{s \to 0} \frac{s \, R/s^2}{1 + G(s)}$$

$$= \lim_{s \to 0} \frac{R}{s + s \, G(s)}$$

$$= \frac{R}{\lim_{s \to 0} s \, G(s)}$$

K_v, Velocity Error Constant. The velocity error constant, K_v is defined as

$$K_v = \lim_{s \to 0} s \, G(s)$$

Therefore,

$$e(t)_{ss} = \frac{R}{K_v}$$

13.79

which is the error in displacement (of the output) due to a ramp input.

For a Type 0 system

$$K_v = \lim_{s \to 0} s\, K_0 = 0,$$

and the resulting steady-state error is infinite (Figure 13.43)
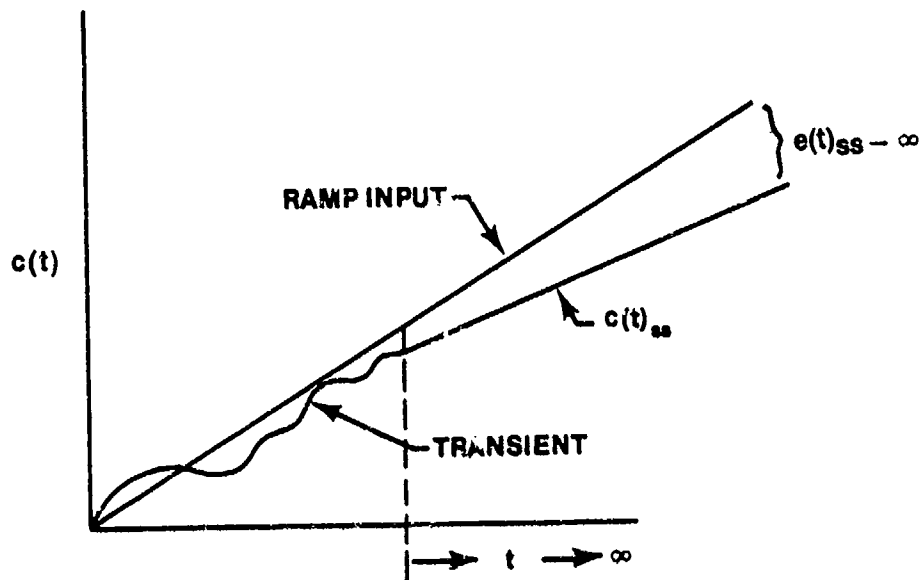
FIGURE 13.43.   STEADY-STATE ERROR - TYPE "0" SYSTEM, RAMP INPUT

For a Type 1 system

$$K_v = \lim_{s \to 0} \frac{s\, K_1}{s} = K_1,$$

the overall gain of the transfer function. The resulting $e(t)_{ss} = R/K_1$.
Therefore,

$$e(t)_{ss} = R/K_1$$

Figure 13.44 illustrates a Type 1 system with a ramp input.
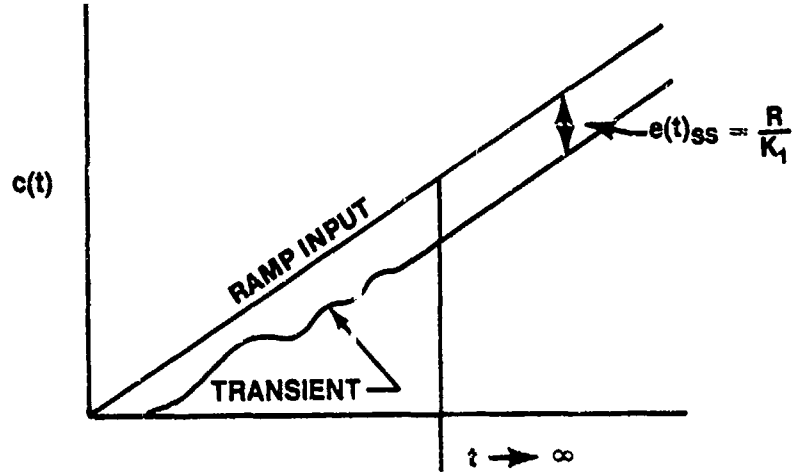
FIGURE 13.44.   STEADY-STATE RESPONSE OF A TYPE 1
SYSTEM WITH A RAMP INPUT

For Type 2 and Type 3 systems $K_v = \infty$ and the resulting steady-state error is zero.

13.10.3 Parabolic Input

Consider the input $r(t) = Rt^2 u_{-1}(t)/2$, $R(s) = R/s^3$

$$e(t)_{ss} = \lim_{s \to 0} \frac{s \dfrac{R}{s^3}}{1 + G(s)}$$

$$= \lim_{s \to 0} \frac{R}{s^2 + s^2 G(s)}$$

$$= \frac{R}{\lim_{s \to 0} s^2 G(s)}$$

K_a, Acceleration Error Constant. The acceleration error constant, K_a, is defined as

$$k_a = \lim_{s \to 0} s^2 G(s)$$

13.81

The steady-state error,

$$e(t)_{ss} = \frac{R}{K_a}$$

is the error in displacement (of the output) due to an acceleration type input.

For a Type 0 system

$$K_a = \lim_{s \to 0} s^2 K_0 = 0$$

and for a Type 1 system

$$K_a = \lim_{s \to 0} \frac{s^2 K_1}{s} = 0$$

For Type 0 and Type 1 systems a parabolic input will result in a parabolic output with the steady-state error, $e(t)_{ss}$, increasing to infinity (Figure 13.45).
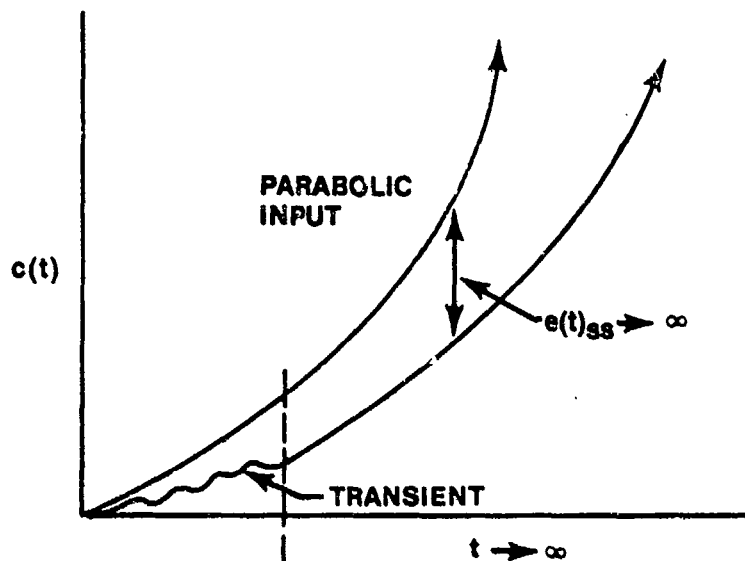
FIGURE 13.45.   STEADY-STATE RESPONSE OF TYPE 0 AND TYPE 1
SYSTEMS TO A PARABOLIC INPUT

For a Type 2 system

$$K_a = \lim_{s \to 0} \frac{s^2 K_2}{s^2} = K_2$$

the overall gain of the transfer function.

The steady-state error, $e(t)_{ss}$, is equal to R/K_2 (a constant) (Figure 13.46).
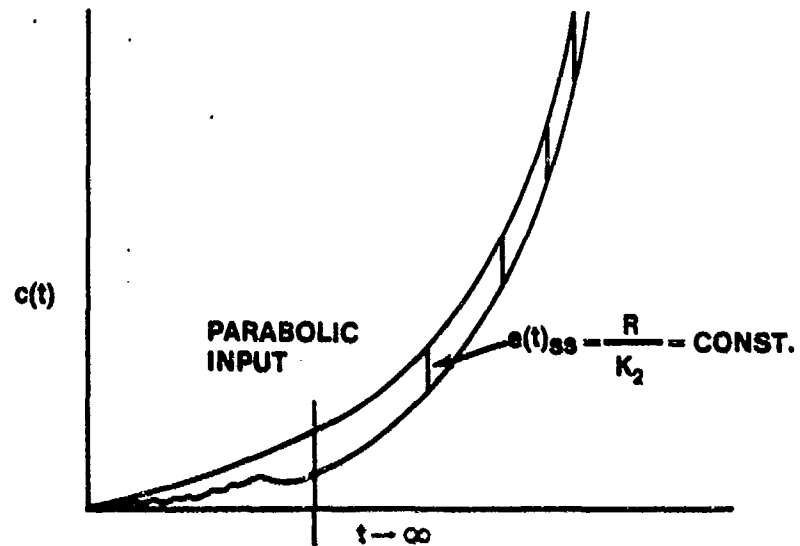
FIGURE 13.46. STEADY-STATE RESPONSE OF A TYPE 2
SYSTEM TO A PARABOLIC INPUT

For a Type 3 system

$$K_a = \lim_{s \to 0} \frac{s^2 K_3}{s^3} = \infty$$

Therefore the steady-state error is zero.

The information that has been developed is presented in tabular form in Table 13.3.

TABLE 13.3

STEADY-STATE ERROR

Type System	Error Constants			Steady-State Error		
	Step	Ramp	Parabolic	Step Input	Ramp Input	Parabolic Input
	$K_p =$	$K_v =$	$K_a =$	$e(t)_{ss} = \dfrac{R}{1 + K_p}$	$e(t)_{ss} = \dfrac{R}{K_v}$	$e(t)_{ss} = \dfrac{R}{K_a}$
0	K_0	0	0	$e(t)_{ss} = \dfrac{R}{1 + K_0}$	∞	∞
1	∞	K_1	0	$= 0$	$e(t)_{ss} = \dfrac{R}{K_1}$	∞
2	∞	∞	K_2	$= 0$	$= 0$	$e(t)_{ss} = \dfrac{R}{K_2}$
3	∞	∞	∞	$= 0$	$= 0$	$= 0$

13.10.4 Steady-State Response of the Control Variables

The foregoing discussion has been looking at the steady-state error, based on a specific input to a known plant, G(s). It is also interesting to look at the steady-state value of the control variable, $c(t)_{ss}$, for a known steady-state error signal, $e(t)_{ss}$.

Consider again the following equation:

$$G(s) = \frac{C(s)}{E(s)} = \frac{K_n \, (\tau_1 s + 1)(\tau_2 s + 1) \, \cdots}{s^n \, (\tau_a s + 1)(\tau_b s + 1) \, \cdots}$$

Rewriting yields

$$E(s) = \frac{(\tau_a s + 1)(\tau_b s + 1) \, \cdots}{K_n \, (\tau_1 s + 1)(\tau_2 s + 1) \, \cdots} \, s^n \, C(s)$$

Applying the final value theorem

$$e(t)_{ss} = \lim_{s \to 0} s\, E(s) = \lim_{s \to 0} \left[\frac{s\,(\tau_a s + 1)(\tau_b s + 1) \cdots}{K_n (\tau_1 s + 1)(\tau_2 s + 1) \cdots} s^n\, C(s) \right]$$

$$= \lim_{s \to 0} s\, \frac{[s^n\, C(s)]}{K_n}$$

Recall the differential theorem

$$[D^n c(t)] = s^n\, C(s)$$

with initial conditions equal to zero.

Applying the final value theorem to the differential theorem yields

$$\lim_{s \to 0} s\, [s^n\, C(s)] = D^n c(t)_{ss}$$

We may now write

$$e(t)_{ss} = \frac{D^n c(t)_{ss}}{K_n}$$

or

$$K_n\, e(t)_{ss} = D^n c(t)_{ss}$$

From this equation and the characteristics of the systems as shown in Table 13.3, the following conclusions are drawn regarding the steady-state response:

a. A type 0 system is one in which a constant actuating signal maintains a constant value of the output, i.e.,

$$K_0\, e(t)_{ss} = c(t)_{ss}$$

b.   A Type 1 system is one in which a constant actuating signal maintains a constant rate of change of the output, i.e.,

$$K_1 \, e(t)_{ss} = D \, c(t)_{ss}$$

c.   A Type 2 system is one in which the second derivative of the output is maintained constant by a constant actuating (error signal) i.e.,

$$K_2 \, e(t)_{ss} = D^2 \, c(t)_{ss}$$

13.10.5   Determining System Type and Gain From the Bode Plot

System type and gain can be obtained from a Bode Plot with the system in unity feedback form. The slope of the low frequency portion of the Lm curve determines the system type: a 0 db/dec slope represents a Type 0 system, -20 db/dec a Type 1 system, and a -40 db/dec slope a Type 2 system. The system gain (K_n) is determined from the Lm plot by projecting a vertical line from $\omega = 1.0$ rad/sec to the low frequency asymptote (or its projection) and reading across horizontally the Lm value. This Lm value represents

$$Lm \, G(j\omega) = 20 \log K_n$$

Depending on system type, $K_n = K_0$, K_1, or K_2. Figure 13.47 illustrates how the Bode Plot is used in the manner described.
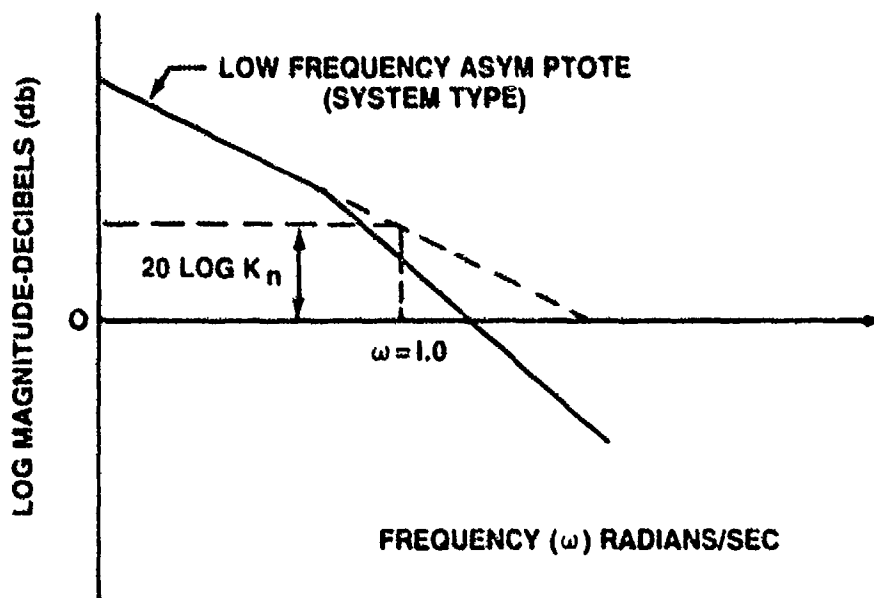
FIGURE 13.47.   SYSTEM TYPE AND GAIN FROM A BODE PLOT

13.10.6 Summary

The static error constant can be used to quickly determine the ability of control system to follow a specific input. The application of error constants is not limited to systems with inputs classified as one of the three basic types of test signals. For linear systems, the concept can easily be extended to systems with inputs that can be represented by a polynomial, i.e.,

$$r(t) = R\left(1 + t + \frac{t^2}{2}\right) u_{-1}(t)$$

The steady-state error is

$$e(t)_{ss} = \frac{R}{1 + K_p} + \frac{R}{K_v} + \frac{R}{K_a}$$

a superposition of the errors due to each input signal component acting alone.

The chief advantage to the foregoing approach to steady-state response is the ease and timeliness of arriving at the answer. The chief disadvantage of the error constant approach is that only one of the constants has a finite value which is not zero or infinity for a particular n-type system. In cases where the steady-state error is a function of time, the error constant approach only gives an answer of infinity for $e(t)_{ss}$ and does not provide an indication of how the error varies with time. Even though the steady-state error may turn out to be infinite, for an actual problem, the input may be applied for a finite time, thus the error will be finite. This finite error may be well within the specifications.

It would appear desirable to select a large value of K_n, the overall gain of the transfer function, to minimize the steady-state error; but not without a penalty. Too large a value of K_n may force the system unstable. As we will see when we get to root locus analysis, an adjustment of the system gain effects both the natural frequency and the damping ratio for a closed-loop system with complex poles. In many cases the exact value of K_n which results in unstable system operation may be found by analysis. Routh's criterion, for example, will provide the value and the application of the criterion may be found in the literature (Reference 1).

13.11 ROOT LOCUS

An accurate prediction of the system's performance can be obtained by deriving the differential equation of a control system and then determining its solution. This approach is not feasible, however, for any but the simplest system. Not only is the direct solution method extremely tedious, but if the response does not meet the required specifications, no indication is given of how to improve its performance.

The aim of the design engineer is to predict the performance of the system without solving its equations of motion. Also, he would like the analysis to indicate how to modify the system in order to produce the desired response characteristics. Several methods are available which both predict stability and indicate the type of compensation required. Of those, root locus will be discussed in this course. Another technique is Nyquist criterion. The theory and application of root locus will be described.

Definition: The root locus is a plot of the roots of the characteristic equation of the closed-loop system as the gain is varied from zero to infinity. The definition itself presents the underlying theory of the root locus method. The primary objective is to determine system stability. This leads to another question. What determines stability? The answer, is the transient solution, which is determined from the roots of the characteristic equation, which cannot have positive real parts and be stable.

The general approach used in the development of the root locus technique will be to plot a root locus for a simple system the hard way, i.e., successive analytic solutions for the roots of the characteristic equation for selected values of static loop gain, K. Then the significance of the root locus will be discussed for the simple system, and then for any system. Lastly, some rules will be developed which permit quick plots to be drawn using relatively little labor.

13.11.1 Poles and Zeros

This section will define what is meant by poles and zeros and also discuss their relationship in functions of interest here. Consider the system represented by the block diagram in Figure 13.48.
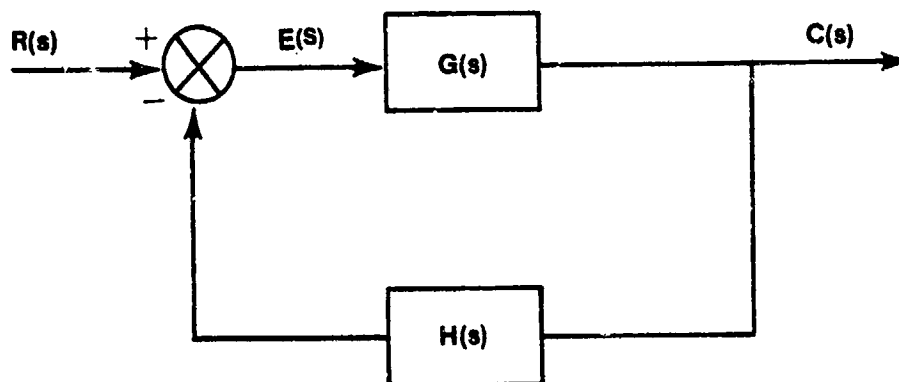
FIGURE 13.48. CLOSED-LOOP SYSTEM

where

$$\frac{C(s)}{R(s)} = \frac{G(s)}{1 + GH(s)}$$

and where in general

$$G(s) = \frac{K_n (\tau_1 s + 1)(\tau_2 s + 1)(\ldots)}{s^n (\tau_a s + 1)(\tau_b s + 1)(\ldots)} = K_n G'(s) = K_n \frac{N_G(s)}{D_G(s)} \qquad (13.71)$$

and

$$H(s) = K_h \frac{(\tau_\alpha s + 1)(\tau_\beta s + 1)(\ldots)}{(\tau_I s + 1)(\tau_{II} s + 1)(\ldots)} = K_h H'(s) = K_h \frac{N_H(s)}{D_H(s)} \qquad (13.72)$$

where the numbers τ_1, τ_2, $\ldots$; τ_a, τ_b, $\ldots$; τ_α, τ_β, $\ldots$; τ_I, τ_{II}, $\ldots$ may be real, complex or zero.

We now define two new terms:

ZERO — A zero of a function (like G(s)) is a value of s that makes that function zero.

POLE — A pole of a function (like G(s)) is a value of s that makes that function go to infinity.

13.90

For Example:

$$s = -\frac{1}{\tau_1} \text{ is a zero of } G(s)$$

$$s = -\frac{1}{\tau_\alpha} \text{ is a zero of } H(s)$$

$$s = -\frac{1}{\tau_a} \text{ is a pole of } G(s)$$

$$s = -\frac{1}{\tau_{II}} \text{ is a pole of } H(s)$$

In terms of the s-plane, (Figure 13.49), this means that there are values that cause $G(s)$ and $H(s)$ and incidentally their product $G(s)$ $H(s)$ to be zero and to be infinite. Figure 13.50 is a plot of the function $G(s)$ $H(s)$.
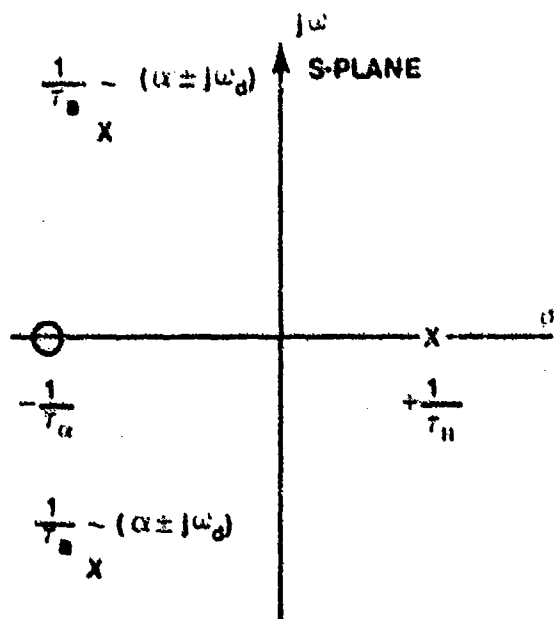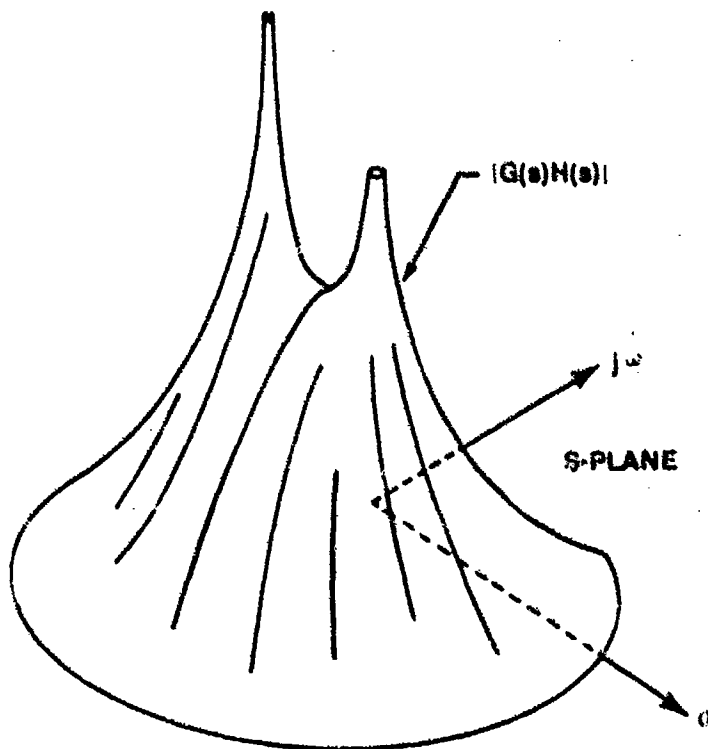
FIGURE 13.49. s-PLANE   FIGURE 13.50. SURFACE OF G(s) H(s)

13.91

The value of s which results in an infinite value of G(s)H(s) is the pole of G(s)H(s).

The pole gets its name from the appearance that a graph of the magnitude of G(s)H(s) makes as "s" assumes values near the point $+ 1/\tau_{I\!I}$ (Figure 13.51).
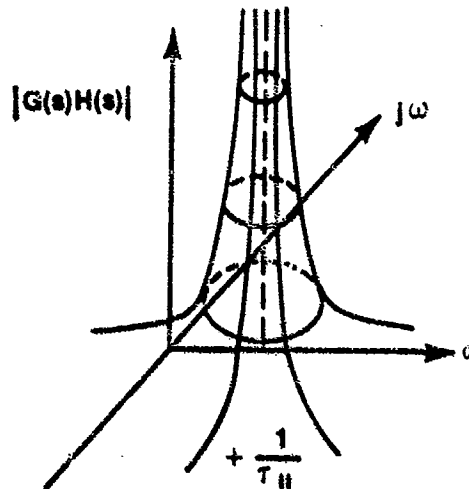
FIGURE 13.51. A POLE OF G(s)H(s)

Note that the poles and zeros of the function G(s)H(s) completely describe the function. When we take the composite function like G(s)/[1 + G(s)H(s)], where presumably we know the poles and zeros of G(s) and H(s), one must exercise caution regarding the transference of this information to the composite function.

For Example:

A zero of G(s) is also a zero of G(s)/[1 + G(s)H(s)]

A pole of G(s) does not result in a pole or zero of G(s)/[1 + G(s)H(s)]

A zero of H(s) does not result in a pole or zero of G(s)/[1 + G(s)H(s)]

A pole of H(s) is a zero of G(s)/[1 + G(s)H(s)]

A zero of 1 + G(s)H(s) is a pole of G(s)/[1 + G(s)H(s)]

13.92

Now, since we want to see if the transients die out let us take the expression C(s)/R(s) (Equation 13.69), solve it for C(s) and assume some form of excitation R(s). Actually any form of excitation (sine, unit step, unit ramp, etc.) may be used.

Substituting Equations 13.71 and 13.72 into Equation 13.69 yields

$$\frac{C(s)}{R(s)} = \frac{G(s)}{1 + G(s)H(s)}$$

$$= \frac{K_n \dfrac{N_G(s)}{D_G(s)}}{1 + K_n \dfrac{N_G(s)}{D_G(s)} K_H \dfrac{N_H(s)}{D_H(s)}}$$

$$= \frac{K_n N_G(s) D_H(s)}{D_G(s) D_H(s) + K_n K_h N_G(s) N_H(s)} \tag{13.73}$$

The zeros of $D_G(s) D_H(s) + K_n K_h N_G(s) N_H(s)$ are the same as the zeros of $1 + G(s)H(s)$ and Equation 13.73 can be factored into the form

$$C(s) = \frac{K_n N_G(s) D_H(s)}{(s - r_1)(s - r_2)(s - r_2) \dots}, \quad \frac{K_n N_G(s) D_H(s)}{(\text{roots from Root Locus})} \tag{13.74}$$

where, for convenience we let $\theta_i(s) = 1$, the unit impulse function. By partial fractions Equation 13.74 can be expanded into the form

$$C(s) = \frac{A_1}{s - r_1} + \frac{A_2}{s - r_2} + \frac{A_3}{s - r_3} + \dots$$

where r_i are the zeros of $1 + G(s)H(s)$ and the poles of $G(s)/[1 + G(s)H(s)]$. The factors, r_i, may be real or complex and positive or negative. Note that the inverse transform of each element leads to an exponential term. Assuming r_i is real and positive, then $(r_i = + \sigma_i)$ and

$$\frac{A_i}{s - r_i} = \frac{A_i}{s - \sigma_i} \rightarrow A_i \, e^{+\sigma_i t} \qquad (13.75)$$
<u>UNSTABLE</u>

and if r_i is negative then $(r_i = -\sigma_i)$

$$\frac{A_i}{s - r_i} = \frac{A_i}{s - (-\sigma_i)} = \frac{A_i}{s + \sigma_i} \rightarrow A_i \, e^{-\sigma_i t} \qquad (13.76)$$
<u>STABLE</u>

In the first case (Equation 13.75), the amplitude of the transient term gets large as time gets large because of the $e^{+\sigma_i t}$ term.

In the second case (Equation 13.76), the transient term disappears because as time gets large $e^{-\sigma_i t}$ goes to zero.

Thus, if a system under investigation has any positive real poles of $G(s)/[1 + G(s)H(s)]$ or a positive real zero of $1 + G(s)H(s)$ then the system is unstable.

Conversely, if the system being investigated has all negative real poles of $G(s)/[1 + G(s)H(s)]$ or all negative real zeros of $1 + G(s)H(s)$, then the system is stable.

If we assume that r_c is complex then we know there exists another zero of $1 + G(s)H(s)$ which is the complex conjugate of r_c, namely $\bar{r}_c$.

This pair of zeros of $1 + G(s)H(s)$ leads to a term in the partial fraction expansion where $r_c = \alpha_c + j\omega_c$ and $\bar{r}_c = \alpha_c - j\omega_c$ of the form

$$\frac{A_c s + A_d}{(s - \alpha_c)^2 + (\omega_c)^2}$$

which has the inverse transform of the form

$$K \, e^{a_c t} \cos(\omega_c t + \phi_c)$$

where if α_c is positive, $\alpha_c = +\sigma_c$, then we get an exponentially increasing cosine term (Figure 13.52).

$$\theta_o = K\, e^{\sigma_c t}\cos(\omega_c t + \phi_o)$$

$e^{\sigma_c t}$ FORMS THE ENVELOPE
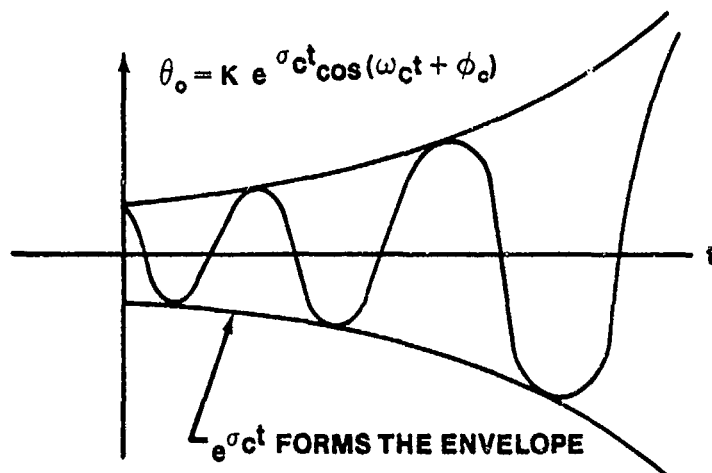
FIGURE 13.52. EXPONENTIALLY INCREASING COSINE TERM

However, if α_c is negative, $\alpha_c = -\sigma_c$. Then the response is of the form $Ke^{-\sigma_c t}\cos(\omega_c t + \phi_c)$ which is a cosine term with an envelope that decreases with time (Figure 13.53).

$$K\, e^{-\sigma_c t}\cos(\omega_c t + \phi_o)$$

$e^{-\sigma_c t}$ FORMS THE ENVELOPE
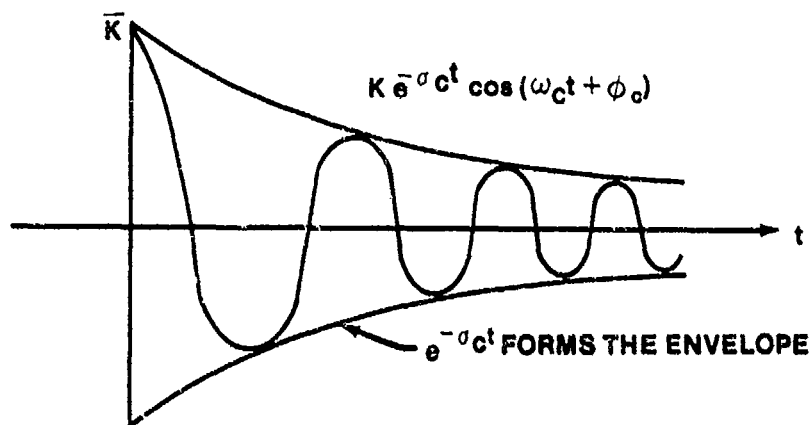
FIGURE 13.53. EXPONENTIALLY DECREASING COSINE TERM

Thus, we conclude that if a complex zero of $1 + G(s)H(s)$ has a positive real part, $\alpha = +\sigma_c$, then the system is unstable and if a complex zero of $1 + G(s)H(s)$ has a negative real part, $\alpha = -\sigma_c$, then the system is stable. Actually the conditions for real zeros and complex zeros are the same:

13.95

REAL PART POSITIVE -- SYSTEM UNSTABLE

REAL PART NEGATIVE -- SYSTEM STABLE.

Now what is the significance of the location of the zeros of $1 + G(s)H(s)$ upon the s-plane? Looking at the s-plane we find that if ANY zeros of $1 + G(s)H(s)$ are in the RHP the system is unstable. If ALL zeros of $1 + G(s)H(s)$ are in the LHP the system is stable.

Now knowing that instability is caused by a zero or zeros of $1 + G(s)H(s)$ with a positive real part, the problem of determining stability degenerates to the problem of determining whether or not there are any zeros of $1 + G(s)H(s)$ in the RHP or, equivalently, whether $1 + H(s)G(s)$ does indeed have a zero or zeros with positive real parts.

13.11.2 Direct Locus Plotting

The example to be used for direct root locus plotting will be the second-order system whose differential equation and transfer functions were derived earlier. The system is shown in Figure 13.54 and Equation 13.67 gives the forward transfer function: $H(s) = 1$.
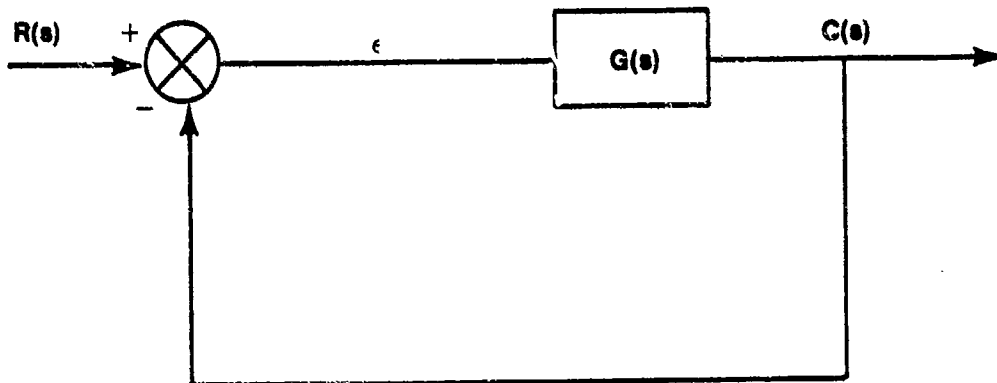
FIGURE 13.54. UNIT FEEDBACK SYSTEM

$$G(s) = \frac{\mu}{Is^2 + bs}$$

The following values will be assumed for the constants

$$I = 1$$

$$b = 2$$

$$\mu = K$$

Equation 13.67 becomes

$$G(s) = \frac{K}{s(s + 2)} \tag{13.77}$$

The problem is to determine the roots of the characteristic equation for all values of K and to plot these roots in the s-plane.

From Equation 13.69 the system closed-loop transfer function is

$$\frac{C}{R}(s) = \frac{G(s)}{1 + GH(s)}$$

$$\frac{C}{R}(s) = \frac{\dfrac{K}{s(s + 2)}}{1 + \dfrac{K}{s(s + 2)}} = \frac{K}{s^2 + 2s + K}$$

The system characteristic equation is

$$s^2 + 2s + K = 0 \tag{13.78}$$

The roots of Equation 13.78 are

$$s_{1,2} = -1 \pm \sqrt{1 - K}$$

The location of roots for various values of K is shown in Table 13.4.

TABLE 13.4

CLOSED-LOOP ROOT LOCATIONS AS A FUNCTION OF K

K	s_1	s_2
0	$0 + j0$	$-2 - j0$ (open-loop poles)
1/2	$-.3 + j0$	$-1.7 - j0$
1	$-1 + j0$	$-1 - j0$
2	$-1 + j1$	$-1 - j1$
3	$-1 + j\sqrt{2}$	$-1 - j\sqrt{2}$
∞	$-1 + j\infty$	$-1 - j\infty$

The points from Table 13.4 are plotted in the s-plane of Figure 13.55
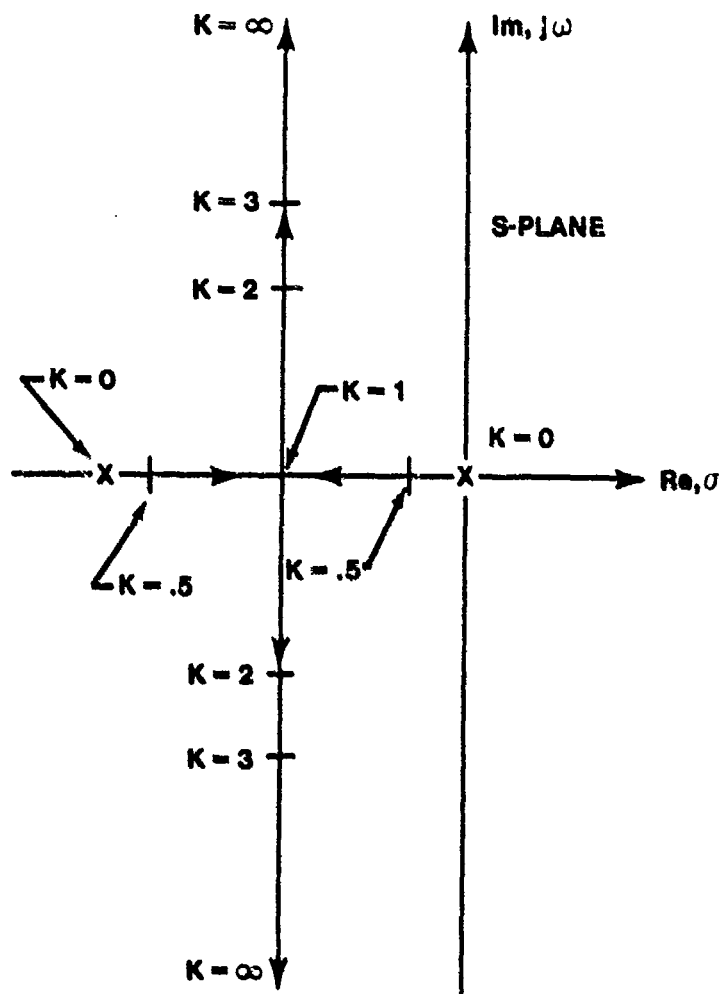
FIGURE 13.55.

Root Locus for GH(s) $= \dfrac{K}{s(s + 2)}$

The root locus of Figure 13.55, which is the locus of roots of the characteristic equation as a function of gain, quickly indicates whether or not the system is stable, and, also, the form of the transient response for any selected value of K. From the plot, it can be seen that for $0 < K < 1$ the roots are real and negative resulting in exponential decay from each root. For $1 < K < \infty$, however, the roots are complex with the real part negative. The corresponding transient response is oscillatory within an exponentially decaying envelope. For example, for $K = 1.5$ the approximate values of s from the locus are

$$s_1 = -1 + j\ 0.5$$

$$s_2 = -1 - j\ 0.5$$

The system transient response for $K = 1.5$ is then

$$c(t) = Ce^{-t} \cos(0.5t + \phi)$$

The time involved in constructing a root locus for a complex system in this manner is obviously prohibitive. This difficulty will be overcome later.

To further discuss the significance of the s-plane and the root locus we will consider a second-order characteristic equation in its standard form

$$s^2 + 2\zeta\omega_n + \omega_n^2 = 0$$

The roots of this equation are

$$s_{1,2} = \underbrace{- \zeta\omega_n}_{\sigma} \pm \underbrace{j\omega_n \sqrt{1 - \zeta^2}}_{\omega_d} \tag{13.79}$$

In order to realize what this means in the s-plane, refer to Figure 13.56a. Any arbitrary value of s will have, from Equation 13.79, a real part $\sigma = \zeta\omega_n$ and an imaginary part $\omega_d = \omega_n \sqrt{1 - \zeta^2}$. From these values shown in Figure 13.56, and the Pythagorean theorem, the magnitude of the position vector, s is found to be equal ω_n. The angle ϕ is also significant since

$$\cos \phi = \frac{\zeta \omega_n}{\omega_n} = \zeta$$

Figure 13.56a summarizes this information and shows how parameters important to the transient response can be easily obtained from the position of roots in the s-plane. From the root locus, then, the transient response characteristics for all values of gain, K, can be seen at a glance.

13.11.3 Angle and Magnitude Conditions

Now that the value of the root locus has been established, the rules will be developed which permit simplified plotting of complex systems. These rules are based on two conditions, the angle condition and the magnitude condition which evolve from the characteristic equation.

As stated many times, the closed-loop control system may be represented by

$$\frac{C}{R}(s) = \frac{G(s)}{1 + GH(s)}$$

from which the characteristic equation is

$$1 + GH(s) = 0$$
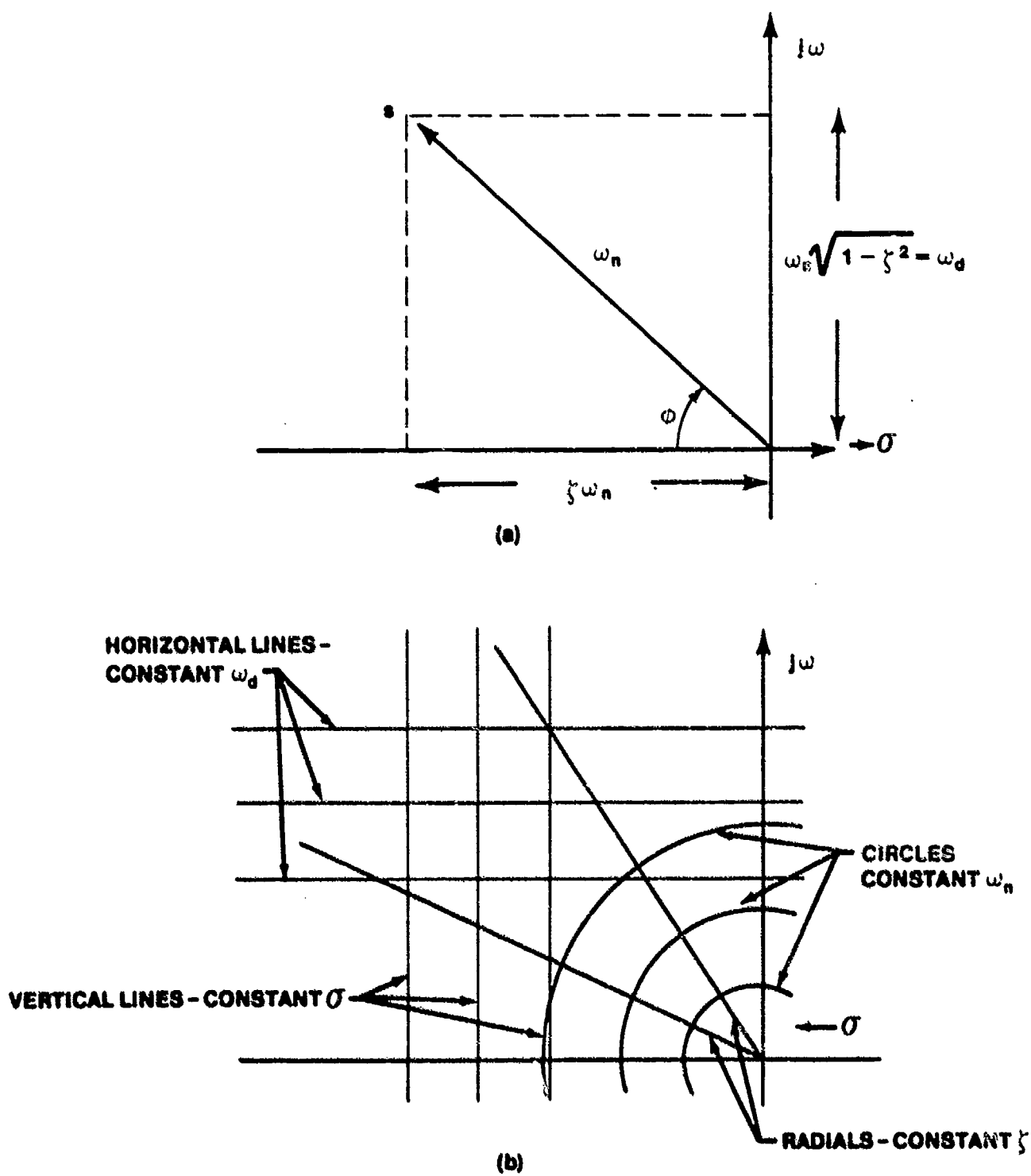
FIGURE 13.56.   SIGNIFICANCE OF s-PLANE PARAMETERS

13.102

The system open-loop transfer function can be written in the following form

$$GH(s) = \frac{K(s - z_1)(s - z_2) \cdots}{(s - p_1)(s - p_2) \cdots} \qquad (13.80)$$

where the static gain, K, is factored out and the z's and p's are the open-loop zeros and poles respectively.

Since the values of s to be determined must satisfy the relationship

$$1 + GH(s) = 0$$

we can say

$$GH(s) = -1 \qquad (13.81)$$

but, since s is, in general, complex, GH(s) is then a function of a complex variable and Equation 13.81 can be written

$$GH(s) = 1e^{j(1 + 2n)\pi} = 1 \, \underline{/(1 + 2n)\pi} \qquad (13.82)$$

where

$$n = 0, \pm 1, \pm 2, \pm 3, \ldots$$

Equation 13.82 says that in order for the value of s to be a zero of $1 + GH(s)$ the magnitude of the complex quantity GH(s) must be equal to 1 and the argument be some odd multiple of π. Hence the

Magnitude condition

$$\left| GH(s) \right| = 1 \qquad (13.83)$$

Angle condition

$$\underline{/GH(s)} = (1 + 2n)\pi \qquad (13.84)$$

$$n = 0, \pm 1, \pm 2, \pm 3 \ldots$$

Substituting Equation 13.8C into Equation 13.84, the angle condition becomes

$$\left/\dfrac{K(s - z_1)(s - z_2)\ \cdots}{(s - p_1)(s - p_2)\ \cdots}\right. = (1 + 2n)\pi \qquad (13.85)$$

Since each factor of GH(s) can be represented by a vector in the s-plane from the pole or zero to the s-point in question, Equation 13.85 can be written

$$\left/\dfrac{\underline{/s - z_1} + \underline{/s - z_2} + \cdots}{\underline{/s - p_1} + \underline{/s - p_2} + \cdots}\right. = (1 + 2n)\pi$$

or

$$\underline{/s - z_1} + \underline{/s - z_2} + \cdots - \underline{/s - p_1} - \underline{/s - p_2} - \cdots = (1 + 2n)\pi \qquad (13.86)$$

Thus, using the angle condition, any point in the s-plane can be investigated to determine whether or not it is a point on the root locus by measuring the angles of the vectors from the poles and zeros to the point in question, and adding them according to the left side of Equation 13.86. If this sum equals an odd multiple of π, the value of s satisfies the characteristic equation, and is on the root locus.

Figure 13.57 demonstrates the application of the angle condition. The vectors representing GH(s) for $s = s_0$ are shown in Figure 13.57. The angle condition test to determine if s_0 is on the root locus is

$$\phi - \theta_1 - \theta_2 = (1 + 2n)\pi \qquad (13.87)$$

From the figure,

$$\phi = 170^{\circ}$$

$$\theta_1 = 195^{\circ}$$

$$\theta_2 = 140^{\circ}$$

Equation 13.87 becomes

$$170 - 195 - 140 \neq \pm \pi$$

$$- 165 \neq \pm \pi$$

S-PLANE

$$GH(s) = \frac{(s + 2)}{(s + 3 + j2)(s + 3 - j2)}$$
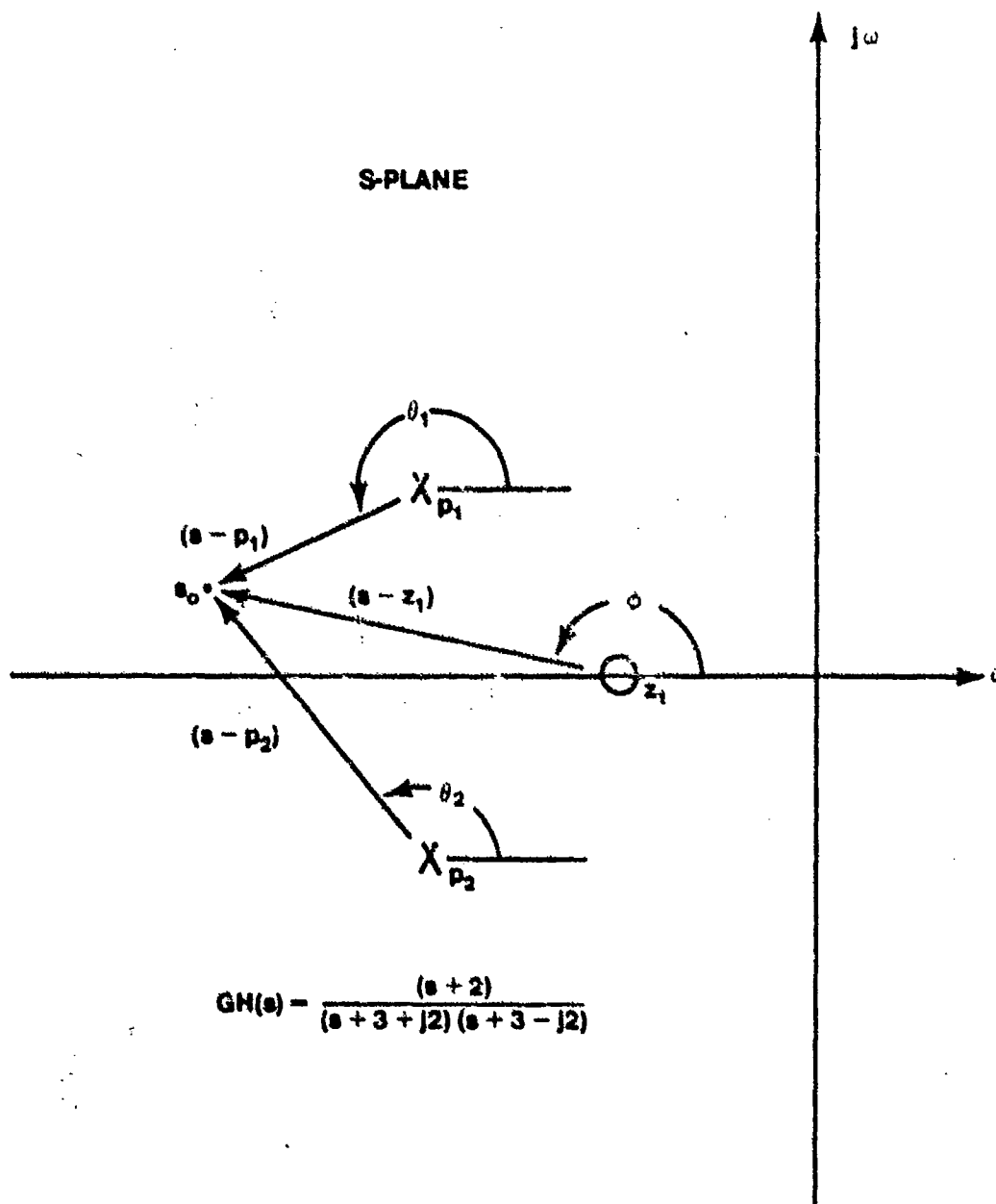
FIGURE 13.57. APPLICATION OF ANGLE CONDITION

Therefore, s_0 is not on the locus but is fairly close. Successive tries will allow converging on the point that satisfies the characteristic equation.

Combining Equation 13.80 and 13.83 the magnitude condition becomes

$$\frac{K \cdot |s - z_1| \cdot |s - z_2| \cdots}{|s - p_1| \cdot |s - p_2| \cdots} = 1$$

$$K = \frac{|s - p_1| \cdot |s - p_2| \cdots}{|s - z_1| \cdot |s - z_2| \cdots} \tag{13.88}$$

Equation 13.88 says that the magnitude of all the vectors from the poles to the s point in question, divided by the magnitudes of the vectors from the zeroes is equal to the gain, K. This condition allows us to determine the value of gain from any point on a locus in the s-plane.

The reader is encouraged to check the example system's root locus (Figure 13.55), to ensure it is consistent with both the angle and magnitude condition.

13.11.4 Rules for Root Locus Construction

The following rules for K > 0 will allow a sketch of the root locus to be drawn quickly. These rules are based upon the angle condition and an analysis of the characteristic equation.

a. The number of branches of the locus is equal to the number of open-loop poles (i.e., the order of the characteristic equation).

$$1 + GH(s) = 1 + \frac{K(s - z_1) \cdots (s - z_z)}{(s - p_1) \cdots (s - p_p)} = 0 \tag{13.89}$$

$$(s - p_1) \cdots (s - p_p) + K(s - z_1) \cdots (s - z_z) = 0$$

Since we have assumed a rational polynomial, $P \geq Z$, and the highest order of s is P.

P is the number of open loop poles, Z is the number of open loop zeros.

b. The Loci branches begin at the open-loop poles where $K = 0$. If we write the characteristic equation with the static gain factored out

$$1 + GH(s) = 1 + KGH'(s) = 0$$

then

$$KGH'(s) = -1$$

$$GH'(s) = -1/K \tag{13.90}$$

for $K = 0$, $GH'(s) = \infty$, which means s is at a pole of GH(s).

c. The branches end at the open-loop zeros where $K = \infty$. From Equation 13.90, when $K = \infty$, $GH'(s) = 0$, which is a zero of GH(s). When $P > Z$ (the usual case) the additional branches end at $s = \infty$ which may also be considered an open-loop zero.

d. The loci branches that do approach $s = \infty$ do so asymptotically to radial lines centered at

$$\gamma = \frac{\Sigma \text{ Re } (p's) - \Sigma \text{ Re } (z's)}{P - Z}$$

e. The angles of these asymptotes are given by

$$\gamma = \frac{(1 + 2n)\pi}{P - Z}$$

where

$$n = 0, \pm 1, \pm 2 \ldots$$

f. A point on the real axis is on a locus branch if it is to the left of an odd number of open-loop poles and zeros. This can be seen from Figure 13.58 in which it is obvious that the net angular contribution from a pair of complex conjugate poles or zeros to a search point on the real axis is $0°$. The real axis poles and zeros contribute zero or π when the search point is to the right or left of the pole or zero respectively. Therefore, the angle condition is satisfied only to the left of an odd number of open-loop poles and zeros.
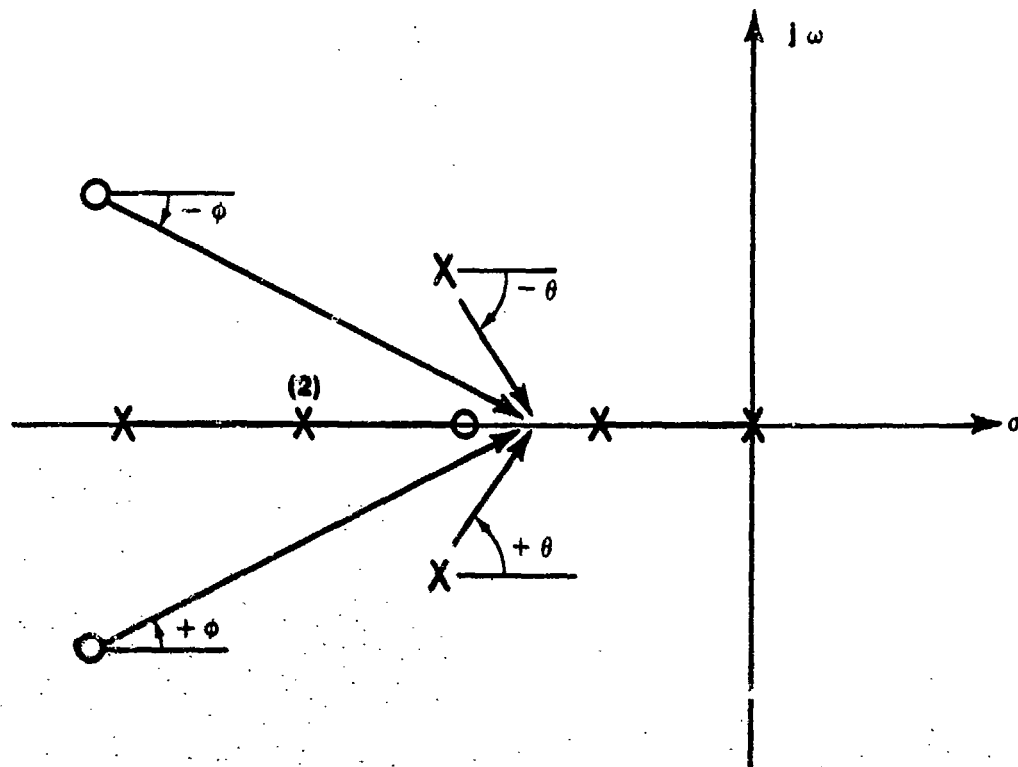
FIGURE 13.58.   REAL AXIS LOCI

g.   The angle of departure approach of a loci branch from (to) a complex
pole (zero) can be found using the angle condition as follows. If a
search point is chosen ϵ distance from a complex pole (zero), the
angle of this vector is the departure approach angle at that pole
(zero).

Consider the situation of Figure 13.59 where it is desired to find the
departure angle from p_1. If the magnitude of the vector from p_1 is ϵ then the
angle of the vectors from the other poles and zeros can be measured directly
to p_1. Solving the angle condition, Equation 13.86 for $\underline{/s - P_1}$ (an unknown
quantity) will yield the departure angle.
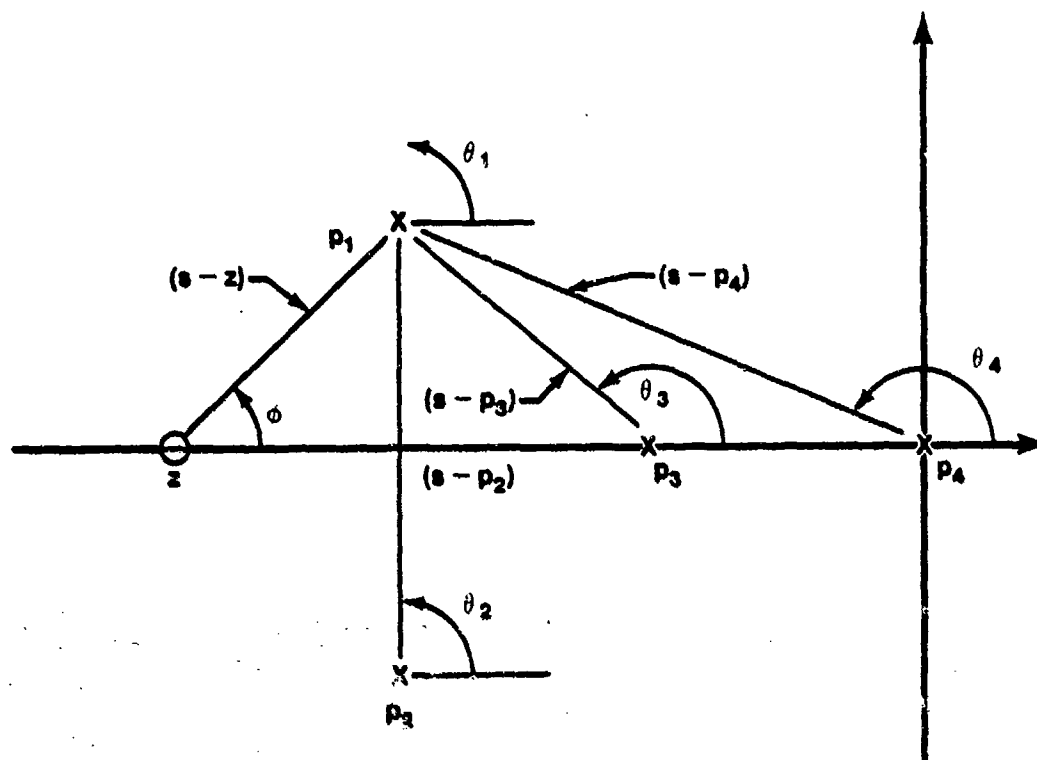
FIGURE 13.59. DEPARTURE ANGLE DETERMINATION

Equation 13.86 says

$$\underline{/s - z} - \underline{/s - p_1} - \underline{/s - p_2} - \underline{/s - p_3} - \underline{/s - p_4} = (1 + 2n)\pi$$

From Figure 13.59

$$\phi - \theta_1 - \theta_2 - \theta_3 - \theta_4 = (1 + 2n)\pi$$

$$\phi = 45^{\circ}$$

$$\theta_2 = 90^{\circ}$$

$$\theta_3 = 135^{\circ}$$

$$\theta_4 = 155^\circ$$

$$\theta_1 = 45^\circ - 90^\circ - 135^\circ - - 155^\circ - \pi$$

Departure angle is

$$\theta_1 = -155^\circ$$

h. The point at which the loci branches leave or enter the real axis are sometimes called "breakaway" or "breakin" point, respectively.

Figure 13.60 illustrates the computation of a breakaway point for the system whose oper-loop transfer function is

$$GH(s) = \frac{K}{s(s+1)(s+2)}$$

From the characteristic equation,

$$\frac{K}{s(s+1)(s+2)} = -1$$

$$K = -s(s+1)(s+2)$$

$$K = -s^3 - 3s^2 - 2s$$

To find the point where K is maximum, we can differentiate the expression for K and set it equal to zero. The solution of this equation should produce the desired result.

$$\frac{dK}{ds} = -3s^2 - 6s - 2 = 0$$

$$s_{1,2} = -1 \pm 0.574$$

$$s = -1.574 \text{ or } -0.426$$

S-PLANE

BREAKAWAY POINT

$$GH(s) = \frac{K}{s(s+1)(s+2)}$$
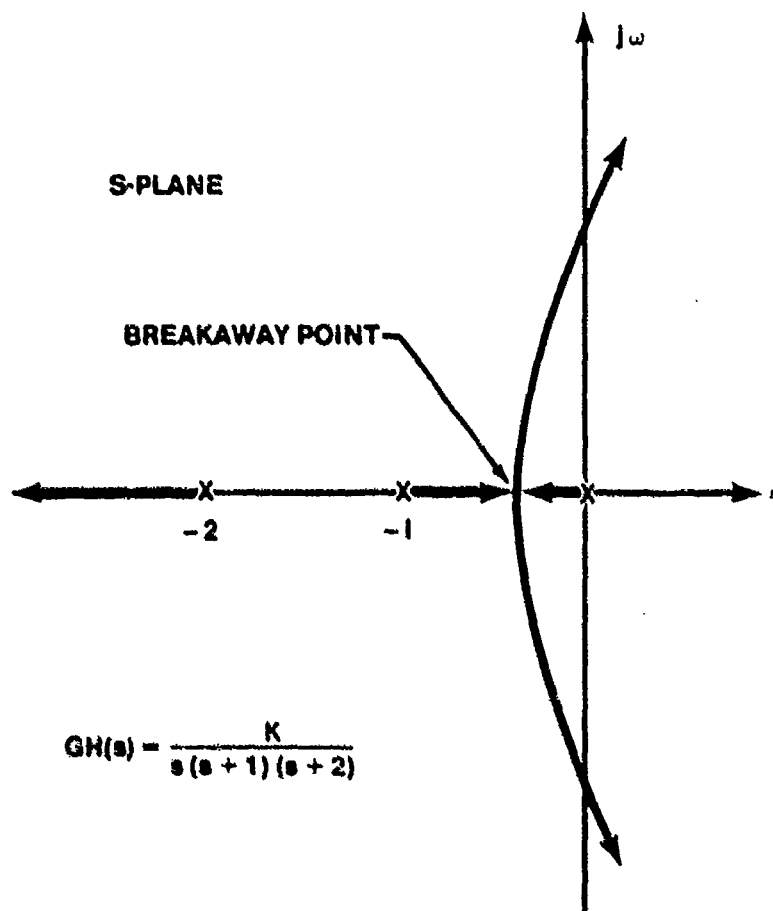
FIGURE 13.60. BREAKAWAY POINT COMPUTATION

It is obvious from Figure 13.60 that the latter solution, s = -0.4257, is the meaningful answer because it appears on a real axis locus. This, then is the breakaway point.

This method of computing breakaway points is restrictive in that more complex systems with higher-order transfer functions are difficult to solve since dK/ds is higher than second-order.

The fact that the root locus is always symmetrical about the real axis is advantageous in that only the upper half of the s-plane need be plotted. The lower half is just a mirror image. The reason for this should be obvious when one considers that complex roots always appear in conjugate pairs.

The rules above will permit a sketch of the root locus very quickly. If more accurate data is required, the branches can be checked using the angle condition and a protractor. After the locus is complete, the values of K that are deemed important can be computed using the magnitude condition.

Root Locus Examples:

Example 1:

$$G(s) = \frac{K'}{s(0.5s + 1)(0.2s + 1)}$$

$$H(s) = 1$$

Rewriting in the most useful form

$$GH(s) = \frac{10K'}{s(s + 2)(s + 5)}$$

Letting $10K' = K$, we can plot the locus and calibrate it in gain. In the actual system, however, the gain selected, K', will be a factor of 10 less than that found from the locus plot.

From the previous equation

$$P_1 = 0, P_2 = -2, P_3 = -5$$

$$P = 3, \quad Z = 0$$

Applying the rules developed in the previous section, the root locus of Figure 13.61 is plotted.

a. The number of branches is 3.

b. The locus branches begin at the poles s = 0, -2, -5, where K = 0.

c. Since there are no open-loop zeros, the 3 branches will end along asymptotes whose real axis intercepts are

$$\sigma = \frac{\Sigma \; Re \; (p's) - \Sigma \; Re \; (z's)}{P - Z}$$

$$\sigma = \frac{[0 - 2 - 5] - [0]}{3 - 0}$$

$$\sigma = -7/3$$

The asymptotes angles are

$$\gamma = \frac{(1 + 2n)\pi}{P - Z}$$

$$\gamma = \frac{(1 + 2n)\pi}{3} = 60^{\circ}, \; 180^{\circ}, \; 300^{\circ}$$

d. Real axis loci exist between s = 0 and s = -2, and from s = -5 to s = -∞.

e. There are no complex poles or zeros so rule (g) does not apply.

f. The breakaway point is found as follows:
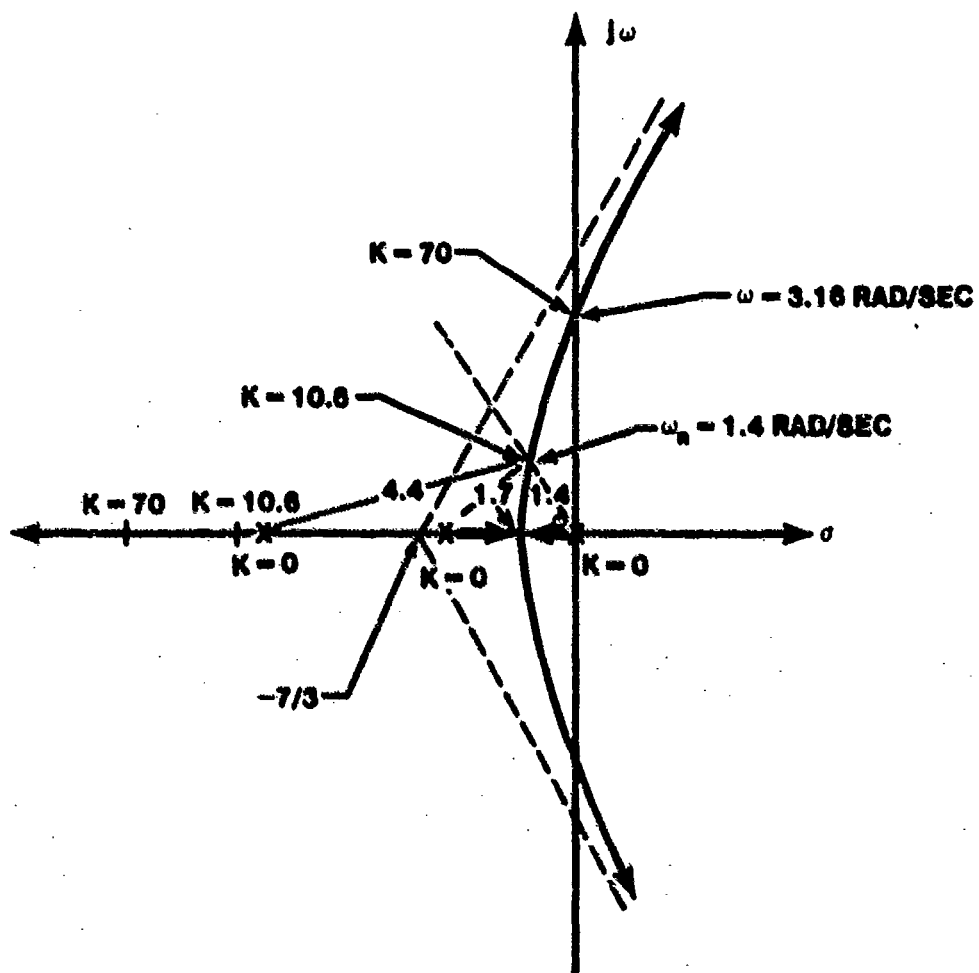
FIGURE 13.61. EXAMPLE OF A ROOT LOCUS

$$GH(s) = \frac{K}{s(s + 2)(s + 5)} = -1$$

$$K = -s(s + 2)(s + 5)$$

$$K = -s^3 - 7s^2 - 10s$$

$$\frac{dK}{ds} = -3s^2 - 14s - 10 = 0$$

$$s = -3.79, -0.88$$

Since - 3.79 is not on a locus branch, s = -0.88 is the breakaway point.

Now that the root locus is plotted, the desired values of K can be found. It is generally useful to know the value of K for which the system becomes unstable. By measuring the length of the vectors from each of the poles to the point where the locus crosses the imaginary axis into the LHP, we find

$$K = (3.16)(3.7)(6.0) = 70$$

The system is neutrally stable at K = 70 and the frequency of the oscillation will be 3.16 rad/sec. For K > 70, the roots of the characteristic equation are in the RHP where they have positive real parts and the system is unstable.

If some specific transient response parameter is required, such as $\zeta = 0.5$, the corresponding value of K can be determined.

Since

$$\cos^{-1} \zeta = \phi$$

$$\cos^{-1} 0.5 = 60^\circ$$

When the radial from the origin 60° from the negative real axis crosses, the root locus is the required operating condition and the gain for that point is

$$K = (4.4)(1.7)(1.4) = 10.6$$

To find the total transient response, however, it is necessary to find the point on all branches where K = 10.6. Each branch contributes one term to the transient response and they all must have the same value of K. Because the lower half plane is a mirror image, the lower root is the complex conjugate of the upper value. The point on the third branch along the real axis where K = 10.6 is found through trial and error. The transient solution, then, for K = 10.6, $\zeta = 0.5$, has a quickly damped pure exponential term and a dominant more slowly damped exponentially decaying oscillation at $\omega_n = 1.4$.

$$\theta_0(t)_{transient} = C_1 e^{-5.5t} + C_2 e^{-0.7t} \cos(1.2t + \phi)$$

Example 2:

$$GH(s) = \frac{K(s + 2)}{s(s + 3)(s^2 + 2s + 2)}$$

$$GH(s) = \frac{K(s + 2)}{s(s + 3)(s + 1 + j)(s + 1 - j)}$$

Applying the rules:

a. The number of branches is 4.

b. The locus branches begin on the open-loop poles at s = 0, -3, $-1 \pm j$.

c. One branch will end on the open loop zero at s = -2. The remaining 3 branches will end at s = ∞ along asymptotes centered at

$$\sigma = \frac{[0 - 3 - 1 - 1] - [-2]}{4 - 1}$$

$$\sigma = -1$$

with asymptote angles

$$\gamma = \frac{(1 + 2n)\pi}{4 - 1}$$

$$\gamma = 60°, \; 180°, \; 300°$$

d. Real axis loci exist between s = 0 and -2, and form s = -3 to - ∞.

e. The departure angle from the complex poles is found by

$$\theta = 45° - 135° - 90° - 26.5° + 180°$$

$$\theta = - 26.5°$$

Once the value of s for the imaginary axis crossing is found, a graphical solution for K using the magnitude condition can be used, i.e.,

$$K = \frac{(3.41)(2.81)(1.60)(1.19)}{2.59} \approx 7.04$$

We will continue this development to determine the closed-loop response for $\zeta = .5$. As the open-loop transfer function was specified

$$GH = \frac{K(s + 2)}{s(s + 3)(s^2 + 2s + 2)}$$

we shall further specify that

$$G(s) = \frac{K}{s(s^2 + 2s + 2)} \quad \text{and}$$

$$H(s) = \frac{(s + 2)}{(s + 3)}$$

It can be seen from the root locus plot that the transient response will have two pure exponentially decaying terms from the real axis branches and one oscillatory damped term from the complex loci. It should also be noted that the maximum ζ possible for the oscillatory terms is $\zeta = .7$ established by the

open-loop complex poles where K = 0. Although the ζ = .5 radial crosses the complex locus in the vicinity of $s_{1,2}$ = 0.5 $\pm$ .9j, the exact crossing can be found using the angle condition. A point on the ζ = .5 radial near the sketched locus is tried as a search point and if the point satisfies the angle condition, the point is on the locus and pins down the exact roots in question. A couple of search point narrows our locus to s = -.56 $\pm$ .96j. At this point the angle condition is satisfied, i.e., $\underline{/s - z_1}$ - $\underline{/s - p_3}$ - $\underline{/s - p_2}$ - $\underline{/s - p_4}$ - $\underline{/s - p_1}$ = π, or 33.6° - 120° - 77° - 21.2° - (-5°) = 179.6° $\cong$ π.

Next, the magnitude condition used at this point is = -.56 + j.96, to determine the value of gain, K.

$$K = \frac{|s| \quad |s + 3| \quad |s + 1 + j| \quad |s + 1 - j|}{|s + 2|}$$

$$= \frac{(2.36)\,(2.025)\,(1.12)\,(.45)}{1.74}$$

$$= 1.532.$$

So far we have determined two roots (a complex pair) and the value of gain for system operation. Two other roots lie on the real axis loci (one on each branch) and are found by trial and error by using the magnitude condition and finding a search point that will yield a value of K = 1.532.

A search point at s = -.8 is determined to be a root corresponding to a value of K = 1.532, i.e.,

$$\frac{(.8)\,(2.2)\,(1.025)^2}{(1.2)} = 1.54 = K$$

(close enough for a graphical solution)

Another search point at s = -3.81 also satisfies the magnitude condition, i.e.,

$$\frac{(.81)\,(3.81)\,(2.99)^2}{1.81} = 1.525 = K$$

(close enough for a graphical solution)

Thus we have located the four roots that correspond to the specified requirements. These roots are $s = -.8$, $s = -3.81$, $s = -.56 + 96j$, $s = -.56 - .96j$, with a corresponding operating gain of 1.53 (Figure 13.62).

Recalling Equations 13.71, 13.72, and 13.73 the closed-loop response can be written using the roots determined from the root locus, i.e.,

$$G(s) = K_n \frac{N_G(s)}{D_G(s)}$$

$$H(s) = K_H \frac{N_H(s)}{D_H(s)}$$

$$\frac{C(s)}{R(s)} = \frac{K_n N_G(s) D_H(s)}{D_G(s) D_H(s) + K_n K_h N_G(s) N_H(s)}$$

$$= \frac{K_n N_G(s) D_G(s)}{(\text{Roots from Root Locus})}$$

Substituting in the appropriate quantities yields

$$\frac{C(s)}{R(s)} = \frac{1.53(s + 3)}{(s + 3.81)(s + .8)(s^2 + 1.12s + 1.23)}$$

$$GH = \frac{K(s + 2)}{s(s + 3)(s^2 + 2s + 2)}.$$
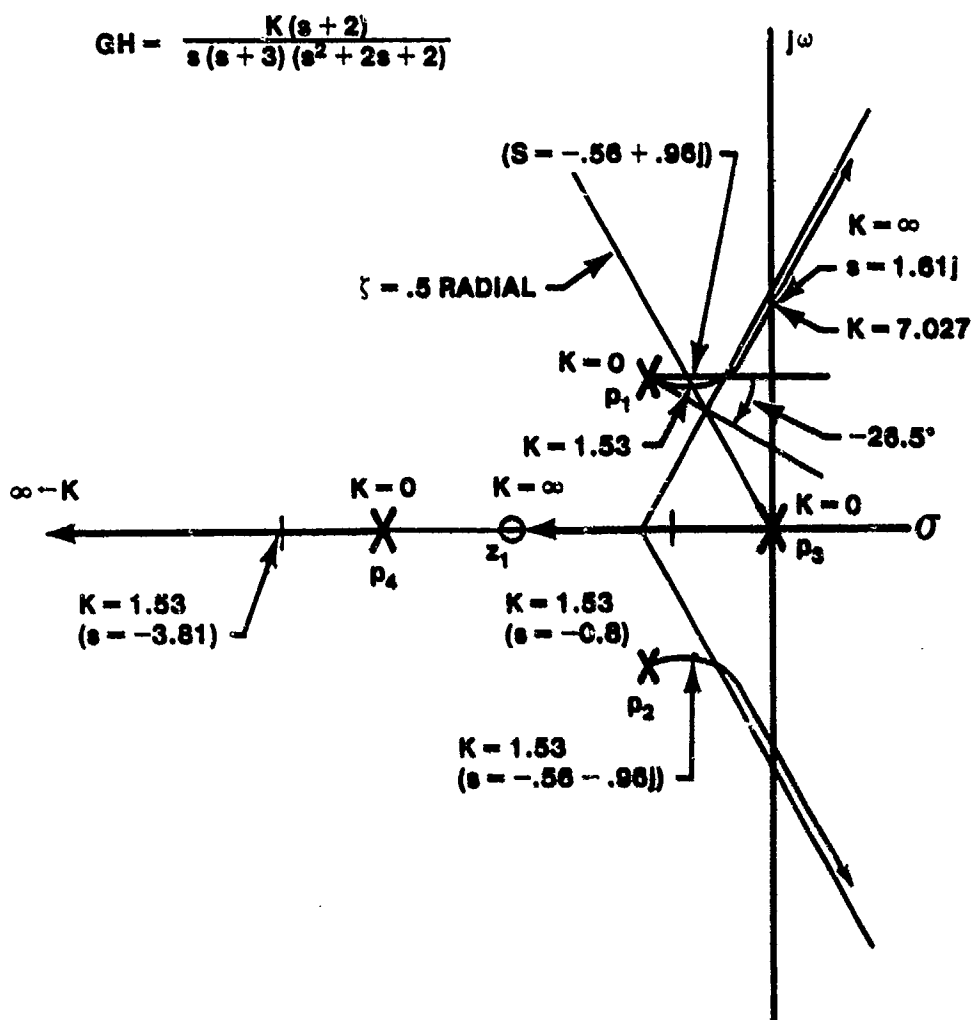
FIGURE 13.62. ROOT LOCUS PLOT

13.120

13.12 COMPENSATION TECHNIQUES

You have been introduced to theory and technique used to set up a control system problem and to analyze the results. Unfortunately the system often needs to be "fixed" to meet the desired performance specifications. This "fixing" is called compensation and is used to reshape the root locus to achieve the desired performance specifications. Generally, three performance specifications are changed by compensation: degree of stability, transient response, and steady-state error.

Actual compensation is achieved by addition of electrical network, and/or mechanical devices which may contain levers, springs, dashpots, gyros, etc. There are two positions in the control system where compensation is usually performed. In the feedback loop where it is referred to as feedback compensation and in the forward loop where it is called cascade compensation. In the forward loop the compensator is normally placed in the low energy point so the power dissipation will be small.

Common networks used to achieve compensation are lag, lead, and lead-lag, all of which are passive. Modern control systems often use active networks which modify the syst s o ensure the desired specifications are met by cancelling the undesirable characteristics and replacing them with the desired characteristics.

Our approach to compensation will be to look at our basic system then to see the effect of each type of compensation of shape of the root locus and the steady-state performance.

13.12.1 Feedback Compensation

13.12.1.1 Proportional Control (Unity Feedback). Consider the basic system in Figure 13.63.
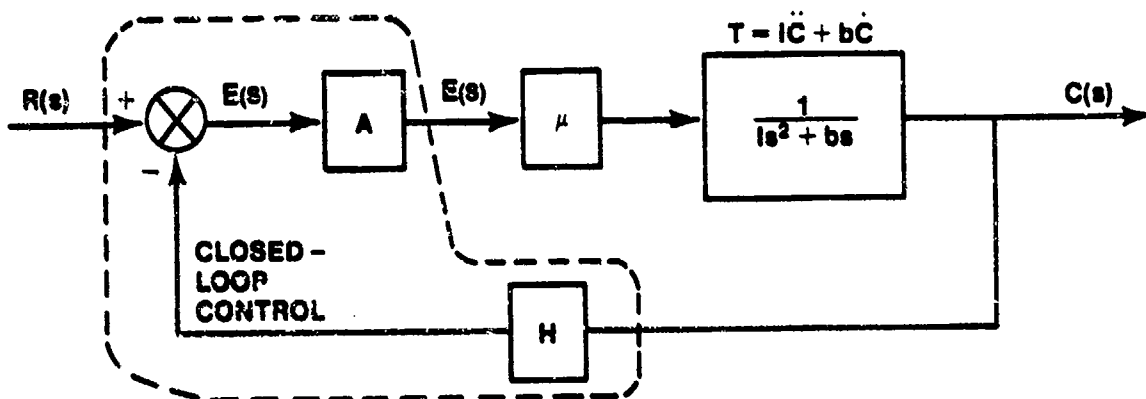
FIGURE 13.63.   BASIC SYSTEM

where for the first case

$$A = 1$$

$$G(s) = \frac{\mu}{Is^2 + bs} = \frac{\mu/I}{s(s + b/I)}$$

$$H(s) = 1$$

$$GH(s) = \frac{\mu/I}{s(s + b/I)}$$

The closed-loop transfer function is

$$\frac{C}{R}(s) = \frac{\mu/I}{s^2 + \frac{b}{I}s + \frac{\mu}{I}} \tag{13.90}$$

and

$$\omega_n = \sqrt{\mu/I}$$

and

$$\zeta = \frac{b}{2\sqrt{\mu I}}$$

Figure 13.64 is the root locus of this basic system.

$$GH = \frac{\mu/I}{s(s+b/I)} = \frac{K}{s(s+b/I)}$$

$$\text{WHERE } K = \frac{\mu}{I}$$

$$K_p = \infty$$
$$K_v = \frac{\mu}{b}$$
$$K_a = 0$$
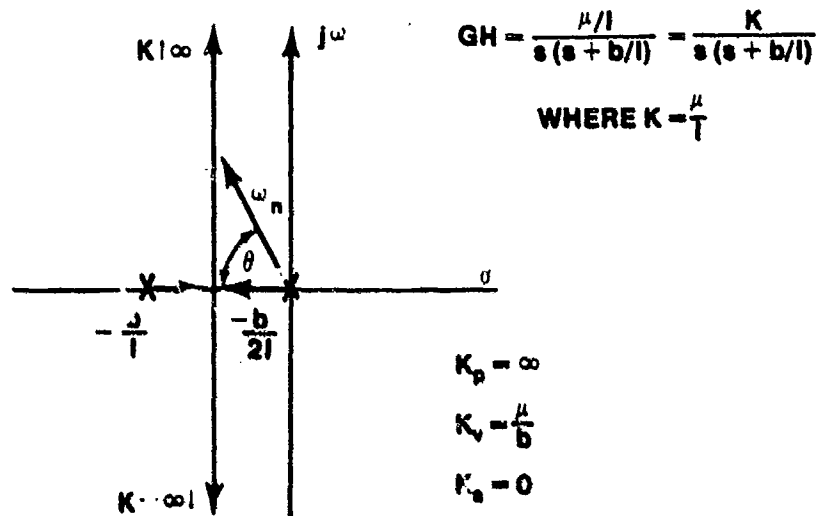
FIGURE 13.64. ROOT LOCUS OF BASIC SYSTEM WITH UNITY FEEDBACK

Application of a step, $R(s) = 10/s$, results in

$$C(s) = \frac{10}{s}\left(\frac{\mu/I}{s^2 + \frac{b}{I}s + \frac{\mu}{I}}\right) \qquad (13.91)$$

The inverse transform of Equation 13.91 is

$$c(t) = 10 - \frac{10}{\sqrt{1-\zeta^2}} e^{-\zeta\omega_n t} \sin(\omega_d t + \phi)$$

After a finite time the transients die out and the response settles down to the commanded value of 10 units with no steady-state error. If the damping term, b, was zero, the locus would move right to the imaginary axis and pure harmonic motion would result. By looking at the error coefficients K_p, K_v and K_a, we see that this system has zero error for a step, Rb/μ error for a ramp and has infinite error for a parabolic input.

The amount of viscous damping in a practical system is often limited by physical constraints. To cope with a lightly damped system, artificial damping is added. An investigation of Equation 13.90 reveals that the damping of the system can be increased by increasing the coefficient of the s term (θ term) in the denominator.

13.12.1.2 <u>Derivative Control (Rate Feedback)</u>. The problem of adding a $K\dot{C}$ term (Ks term) into the forward loop is solved by derivative control or rate feedback. Figure 13.65 shows the introduction of the $K\dot{C}$ term into the block diagram.
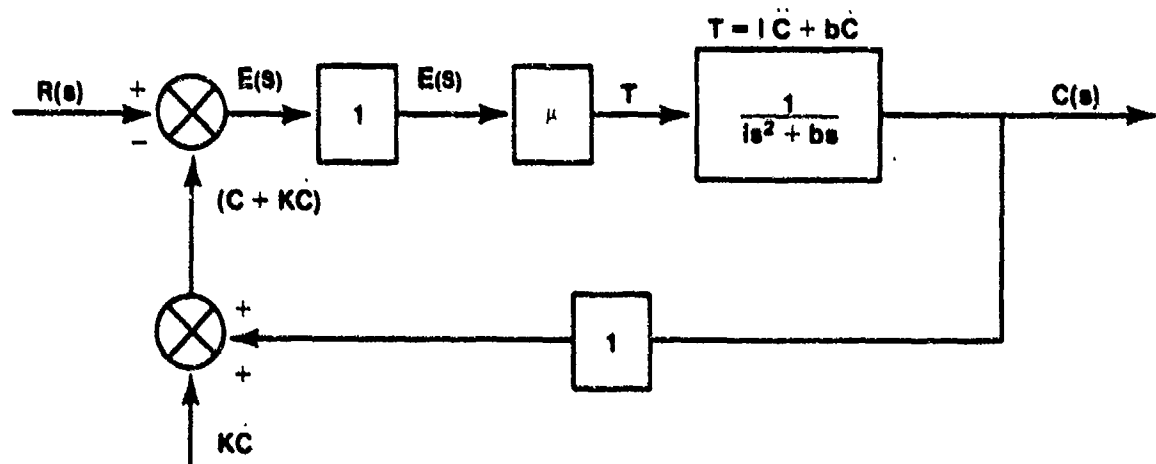
FIGURE 13.65. BASIC SYSTEM WITH INTRODUCTION OF $K\dot{C}$ TERM

The $K\dot{C}$ term can be achieved by taking the derivative of C and is often achieved by means of a rate gyro as shown in Figure 13.66.

13.124
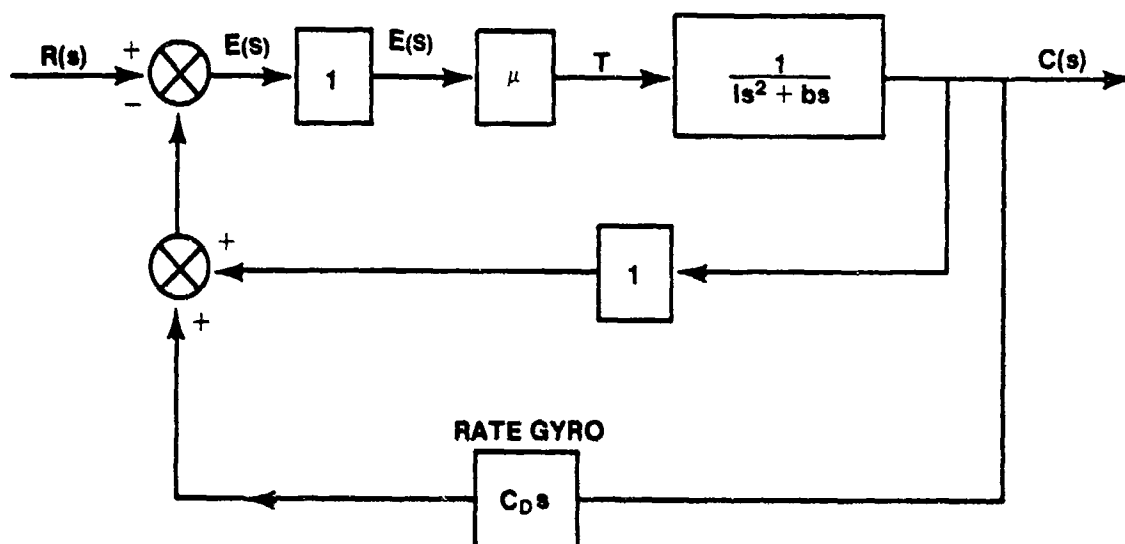
FIGURE 13.66.   BASIC SYSTEM WITH RATE GYRO
ADDED TO FEEDBACK LOOP
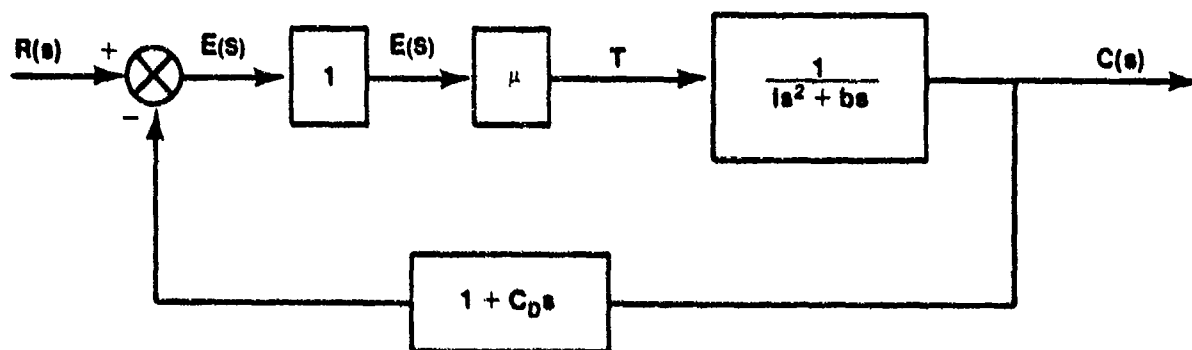
FIGURE 13.67.   REDUCTION OF FIGURE 13.66

The control ratio is written for Figure 13.67

$$\frac{C(s)}{R(s)} = \frac{\mu}{Is^2 + bs + \mu\,(1 + C_D s)}$$

$$= \frac{\mu/I}{s^2 + \left(\dfrac{b + \mu C_D}{I}\right)s + \dfrac{\mu}{I}}$$

The natural frequency of the system is unchanged; however the damping has been increased by $\mu C_D/I$.

The effect of derivative control on the root locus is illustrated in Figure 13.68. The forward transfer function becomes

$$G(s) = \frac{\mu/I}{s(s + b/I)}$$

and the feedback transfer function is

$$H(s) = (1 + C_D s)$$

This in effect adds an open-loop zero to our open-loop transfer function.

$$GH(s) = \frac{\frac{\mu}{I}(1 + C_D s)}{s\left(s + \dfrac{b}{I}\right)} = \frac{\frac{\mu}{I} C_D\left(s + \dfrac{1}{C_D}\right)}{s\left(s + \dfrac{b}{I}\right)}$$

$$GH(s) = \frac{\frac{\mu}{I} C_D (s + 1/C_D)}{s(s + \frac{b}{I})} = \frac{K'(s + 1/C_D)}{s(s + b/I)}$$

WHERE $K' = \frac{\mu}{I} C_D$

CASE (a)

$$\frac{1}{C_D} < \frac{b}{I}$$

CASE (b)
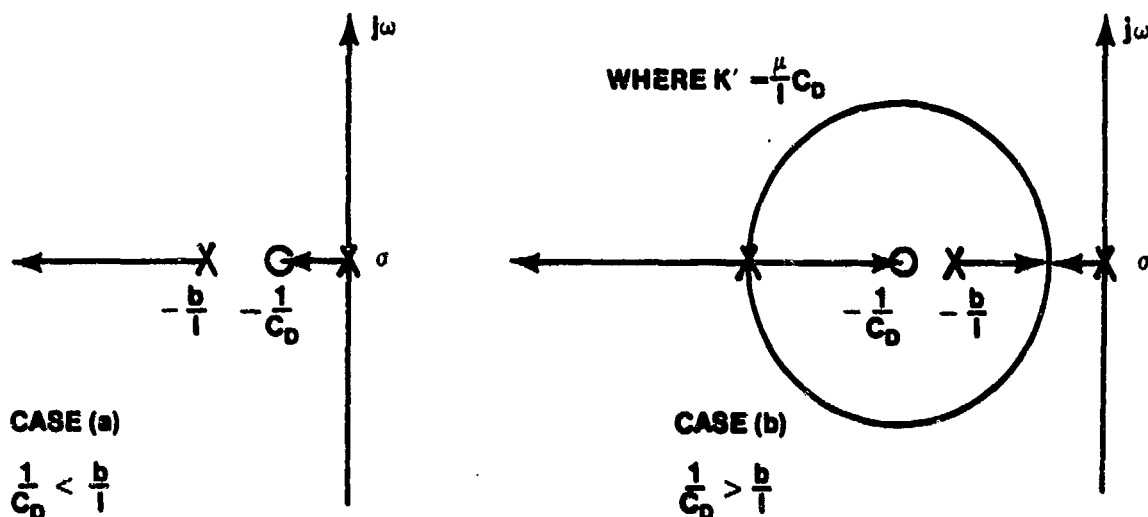
$$\frac{1}{C_D} > \frac{b}{I}$$

FIGURE 13.68.   ROOT LOCUS OF BASIC SYSTEM
WITH DERIVATIVE CONTROL

The value of C_D will determine if the response will have an oscillatory term.   In case (a) of Figure 13.68, $1/C_D < b/I$ will result in two first order roots and oscillation is not possible.   However in case (b) where $1/C_D > b/I$, the locus path allows for an oscillatory response over a wide range of static loop sensitivity ($\mu/I \ C_D$).   It is obvious from Figure 13.68 that high damping can be achieved with reasonably high values of static loop sensitivity (gain).   Before we can check the steady-state error, we must rearrange the block diagram (Figure 13.69 a, b, c) to unity feedback.
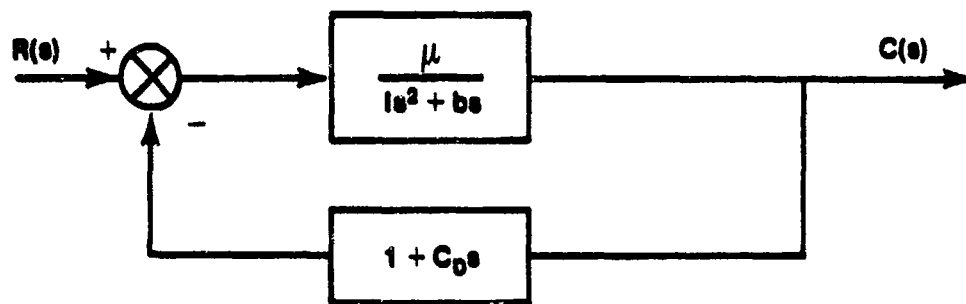
(a)
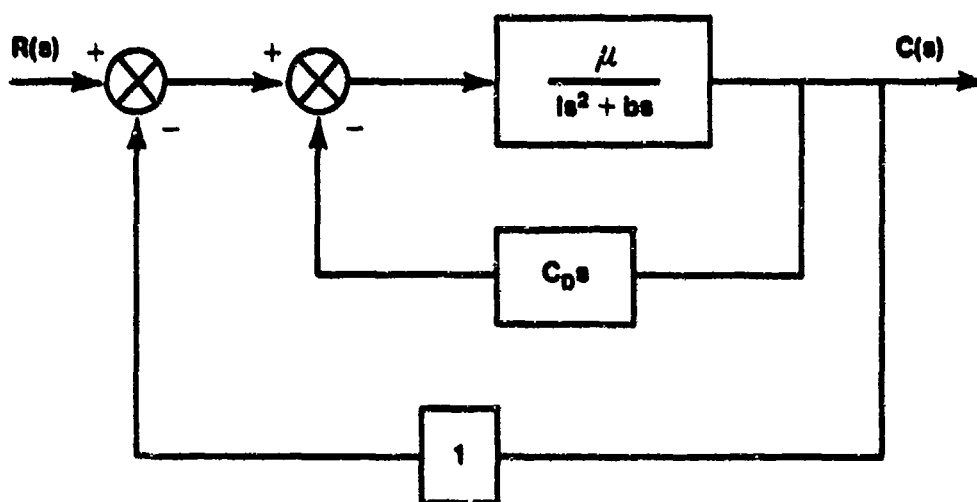
(b)
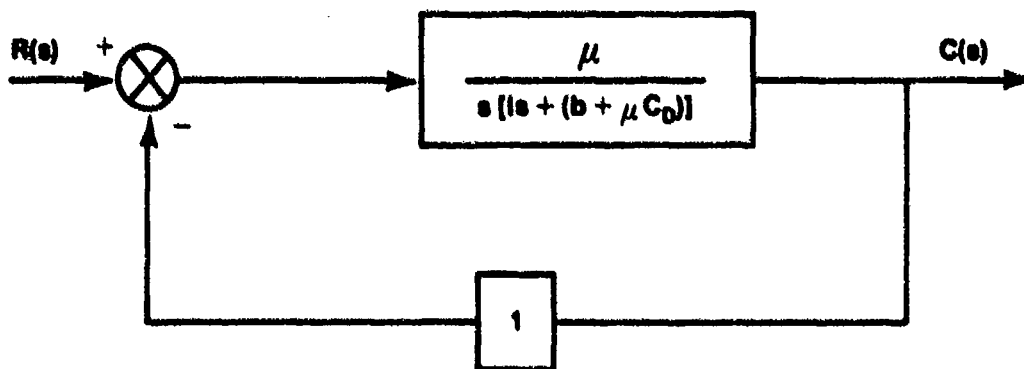
(c)

FIGURE 13.69.   REDUCTION OF DERIVATIVE CONTROL
BLOCK DIAGRAM TO UNITY FEEDBACK

The corresponding error coefficients are

$$K_p = \infty$$

$$K_v = \frac{\mu}{(b + \mu C_D)}$$

$$K_a = 0$$

Therefore we see the steady-state error will increase with the introduction of derivative control (system type remains the same).

We have discussed two types of feedback compensation and have found that the transient response can be improved by addition of derivative control, but only at the expense of the steady-state error. The other compensation techniques to be considered are used in the forward loop.

13.12.2 Cascade Compensation

The first forward compensation technique to be discussed is error rate compensation.

13.12.2.1 Error Rate Compensation. Error rate or ideal derivative compensation is used when the transient response of the system must be improved. This is achieved by reshaping the root locus by moving it to the left. This in effect decreases the system time constant, $\tau = 1/\zeta\omega_n$, thereby speeding up the response. Error rate compensation is achieved by adding the rate of change of the error signal to the error signal (Figure 13.70).
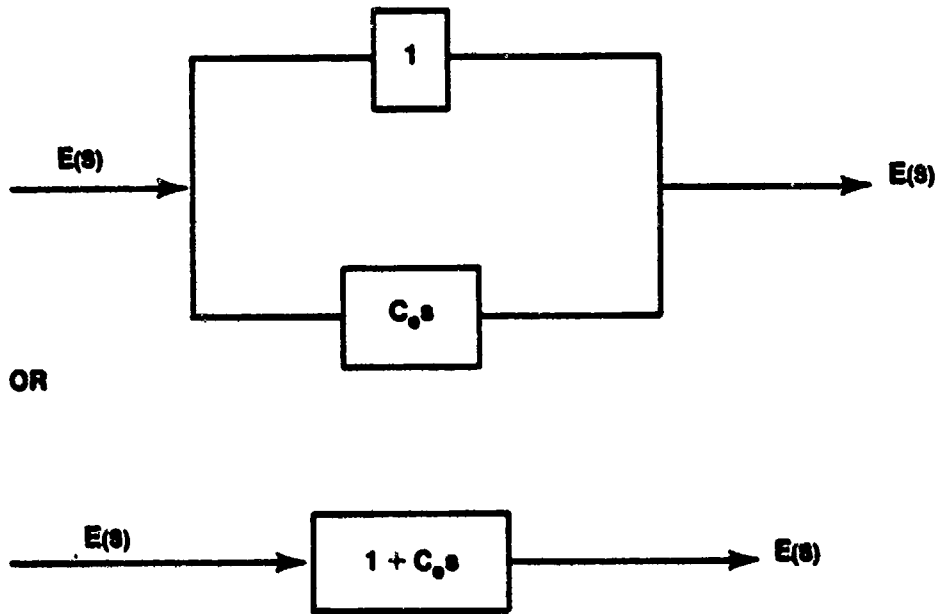
FIGURE 13.70.   IDEAL ERROR RATE COMPENSATOR

The physical effect of error rate can be described as introducing anticipation into the system.   The system reacts not only to magnitude of the error, but, also to its probable value in the future.   If the error is changing rapidly, then $E_1(s)$ is large and the system responds faster.   The net result is to speed up the system.   Figure 13.71 shows error rate added to the basic system.
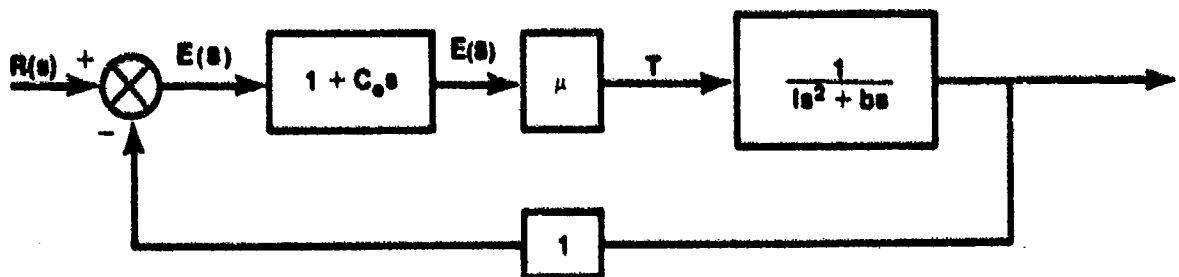
FIGURE 13.71.   BASIC SYSTEM WITH
                ERROR RATE CONTROL

Now the forward transfer function becomes

$$G(s) = \frac{\mu(1 + C_e s)}{Is^2 + bs}$$

$$= \frac{\frac{\mu}{I} C_e \left(s + \frac{1}{C_e}\right)}{s \left(s + \frac{b}{I}\right)}$$

and

$$H(s) = 1$$

Therefore the open-loop transfer function is

$$GH(s) = \frac{\frac{\mu}{I} C_e \left(s + \frac{1}{C_e}\right)}{s \left(s + \frac{b}{I}\right)}, \quad \text{and}$$

$$\frac{C(s)}{R(s)} = \frac{\frac{\mu}{I} C_e \left(s + \frac{1}{C_e}\right)}{s^2 + \left(\frac{b + C_e \mu}{I}\right)s + \frac{\mu}{I}}$$

We see that error rate has added a zero to the function as well as achieving artificial damping similar to derivative control. Although the open-loop transfer function, GH(s), of the derivative control and error rate control are similar, the closed-loop transfer functions are different due to the cascade zero of the error rate compensator. The root locus for error rate is illustrated in Figure 13.72. The zero, in effect, draws the locus to the left; thereby speeding up the response and making the system more stable.

$$GH(s) = \frac{\frac{\mu}{T}C_e(s + \frac{1}{C_e})}{s(s + \frac{b}{T})}$$

$$= \frac{K''(s + \frac{1}{C_e})}{s(s + \frac{b}{T})}$$

$$\text{WHERE } K'' = \frac{\mu}{T}C_e$$
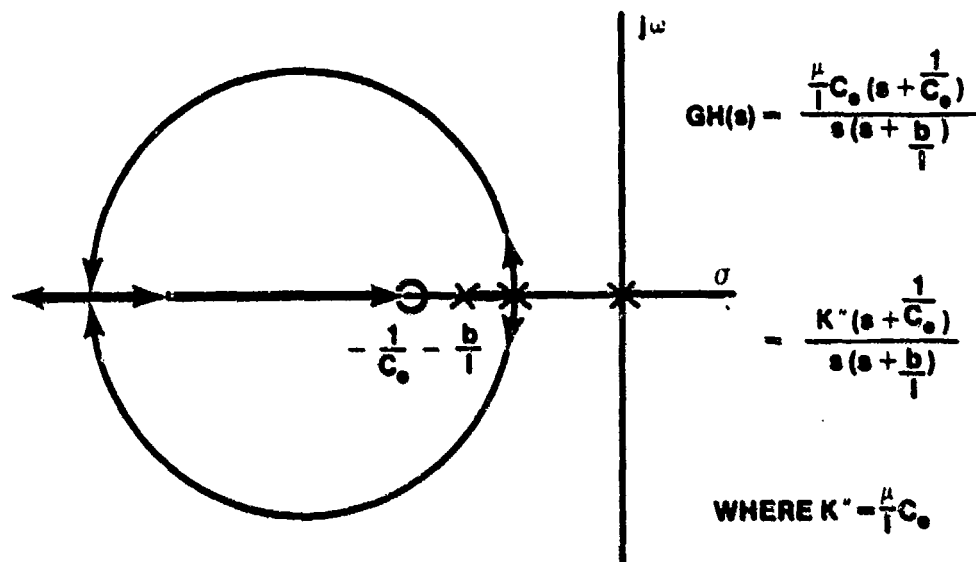
FIGURE 13.72.   ROOT LOCUS OF BASIC SYSTEM WITH
ERROR RATE COMPENSATION

Looking at the error coefficients we find

$$K_p = \infty$$

$$K_v = \frac{\mu}{b}$$

and

$$K_a = 0$$

Therefore the steady-state performance of the system is unchanged from the basic system.

In the real world an ideal differentiator is difficult to construct and other problems with differentiation of system noise arise. A passive element known as a lead compensator is used to approximate ideal error rate control. The transfer function of this device is

$$G_c(s) = \frac{A\left(s + \frac{1}{\tau}\right)}{\left(s + \frac{1}{\alpha\tau}\right)} = \frac{A(s + z_c)}{(s + p_c)}, \quad \alpha < 1$$

The pole p_c, is located far to the left so that the angle of the compensator is nearly all lead due to the zero, z_c, which is placed by trial and error to a point near the original locus. This normally results in a small increase in gain and a large increase in the undamped natural frequency, thereby reducing settling time. Introduction of this lead compensation into the basic system could result in a locus as shown in Figure 13.73.

$$GH(s) = \frac{A\,\mu/I\,(s+z_c)}{s(s+p_c)(s+\frac{b}{I})} = \frac{K^{''}\,(s+z_c)}{s(s+p_c)(s+\frac{b}{I})}$$

WHERE $K^{''} = A\,\mu/I$
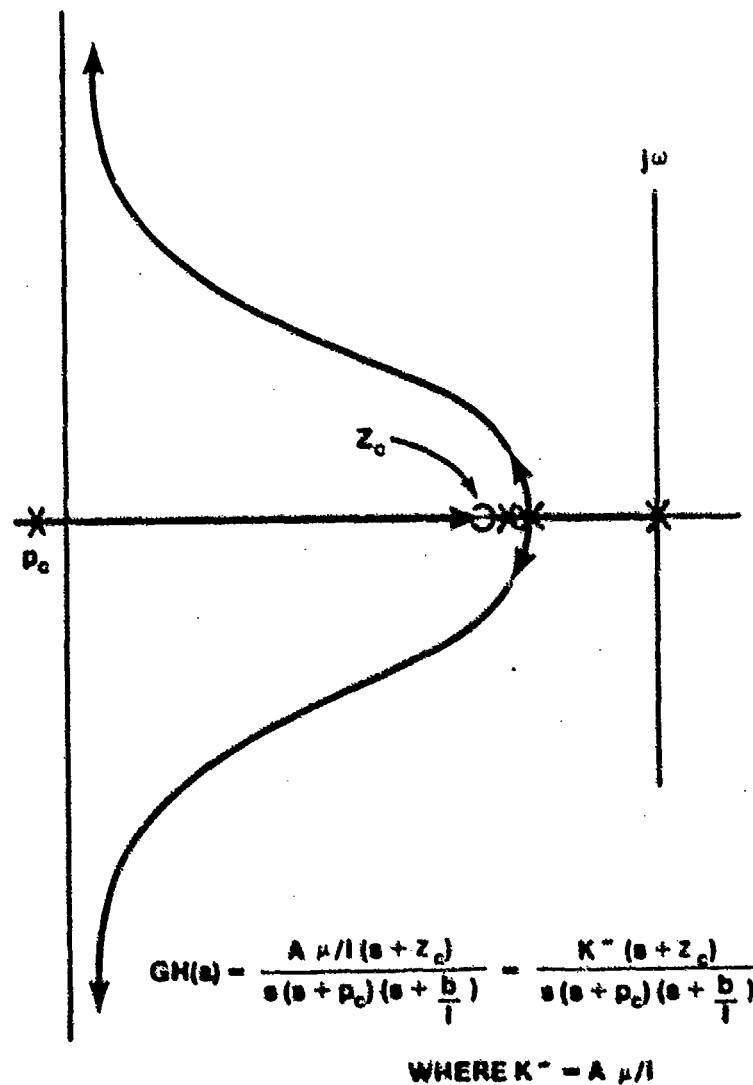
FIGURE 13.73.   LEAD COMPENSATION APPLIED
TO BASIC SYSTEM

13.12.2.2 Integral Control. The second cascade compensation technique is integral control. Often the transient response of a system is satisfactory but the steady-state error is excessive. Integral control produces an actuating signal that is proportional to both the magnitude and the integral of the error signal $E(s)$, Figure 13.74.
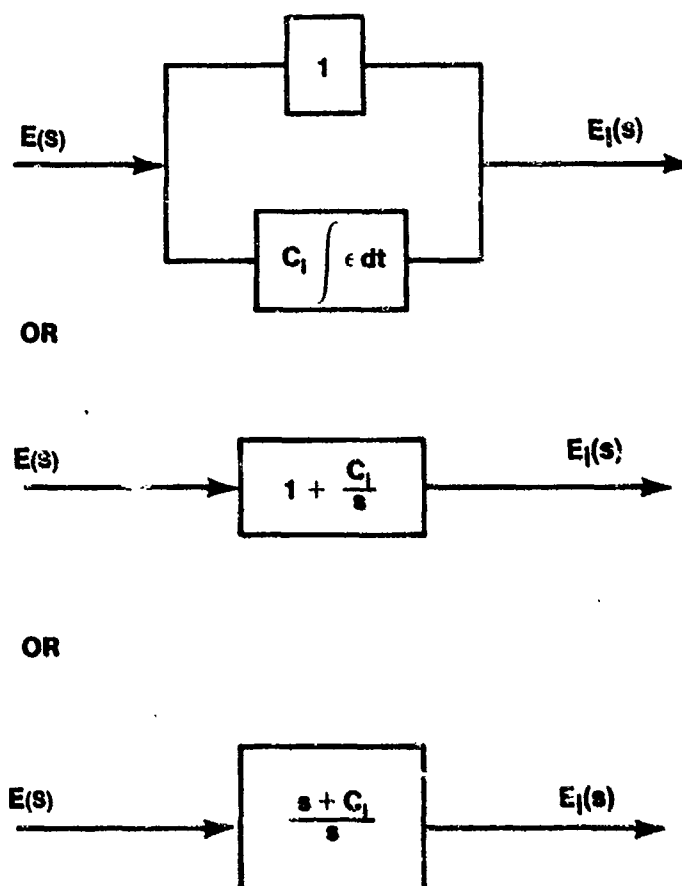
FIGURE 13.74. IDEAL INTEGRAL CONTROL

The net result is the increase in system type. The error $E_1(s)$ continues to increase as long as an error, $E(s)$, is present and eventually becomes large enough to produce an output signal equal to the input. The error, $E(s)$, is then zero. Since we are not interested in changing the time response of the system, the positioning of the zero becomes very important. The pole at the origin has the effect of moving the locus to the right and slowing down the

response. The zero must be placed very close to the origin to reduce the effect of the pole on the locus.

Figure 13.75 shows integral control added to out basic system.
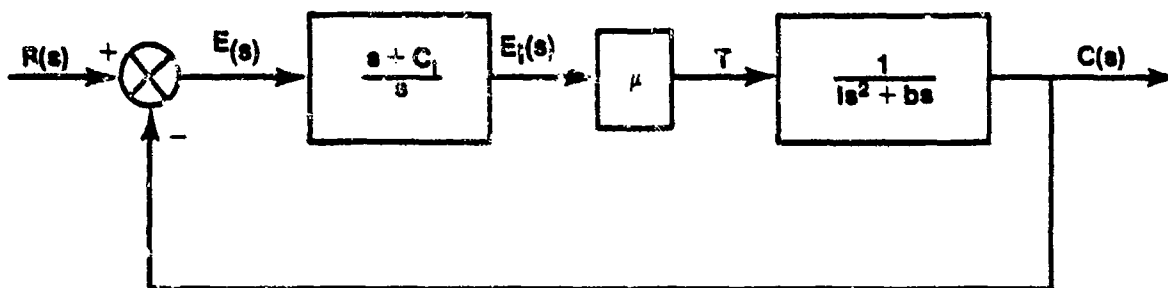
FIGURE 13.75.   BASIC SYSTEM WITH INTEGRAL CONTROL

Now the forward transfer function becomes

$$G(s) = \frac{\mu(s + C_i)}{s(Is^2 + bs)} = \frac{\frac{\mu}{I}(s + C_i)}{s^2\left(s + \frac{b}{I}\right)}$$

and

$$H(s) = 1$$

The open-loop transfer function is

$$GH(s) = \frac{\frac{\mu}{I}(s + C_i)}{s^2\left(s + \frac{b}{I}\right)} \tag{13.92}$$

Figure 13.76 is the root locus of Equation 13.92.

Where:

$$GH(s) = \frac{\frac{\mu}{T}(s + C_i)}{s^2 \left(s + \frac{b}{T}\right)}$$

$$= \frac{K(s + C_i)}{s^2 \left(s + \frac{b}{T}\right)}$$

WHERE $K = \frac{\mu}{T}$

$$\left[S_c = \frac{\left(-\frac{b}{T} + C_i\right)}{2}\right]$$

$C_i < \frac{b}{T}$

(IF $C_i > \frac{b}{T}$, COMPLEX LOCUS LIES IN RHP AND SYSTEM IS UNSTABLE FOR ALL K)
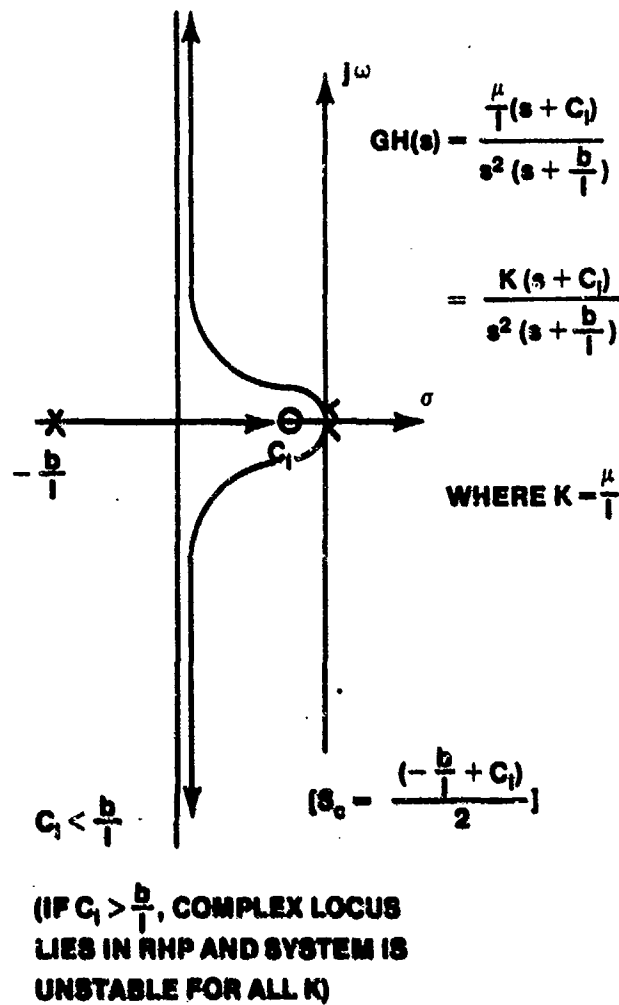
FIGURE 13.76.   ROOT LOCUS OF BASIC SYSTEM WITH INTEGRAL CONTROL

The additional pole at the origin increases the system type as well as the scaling of K along the loci. The change in the transient response for the ideal integral control is minimized by placing the zero very close to origin. In a real world system there is a limit to achieving this proximity.

The integral control compensator is achieved electrically by a lag network or mechanically by use of an integrating gyroscope.

The lag network transfer function is of the form

$$G_c(s) = \frac{A}{\alpha} \frac{(s + 1/\tau)}{\left(s + \frac{1}{\alpha\tau}\right)} , \qquad (13.93)$$

where $\alpha > 1$ and is usually about 10; therefore, Equation 13.93 is approximately

$$G_c(s) \approx \frac{A}{\alpha} \frac{(s + 1/\tau)}{s}$$

In design, if the pole and zero are placed very close (at the origin), the net angle contribution at the dominate poles can be kept to less than 5° and the locus is displaced only slightly. The resulting increased gain of the system and increased system type all result in decreased steady-state error.

The error coefficient for the compensated system became

$$K_p = \infty$$

$$K_v = \infty$$

$$K_a = \frac{\mu C_i}{b}$$

and the system will now handle a parabolic input with a $e(t)_{ss} = R\, b/\mu C_i$.

A summary of passive compensations contained in Table 13.5.

BLOCK DIAGRAM OF BASIC SYSTEM UNDER CONSIDERATION
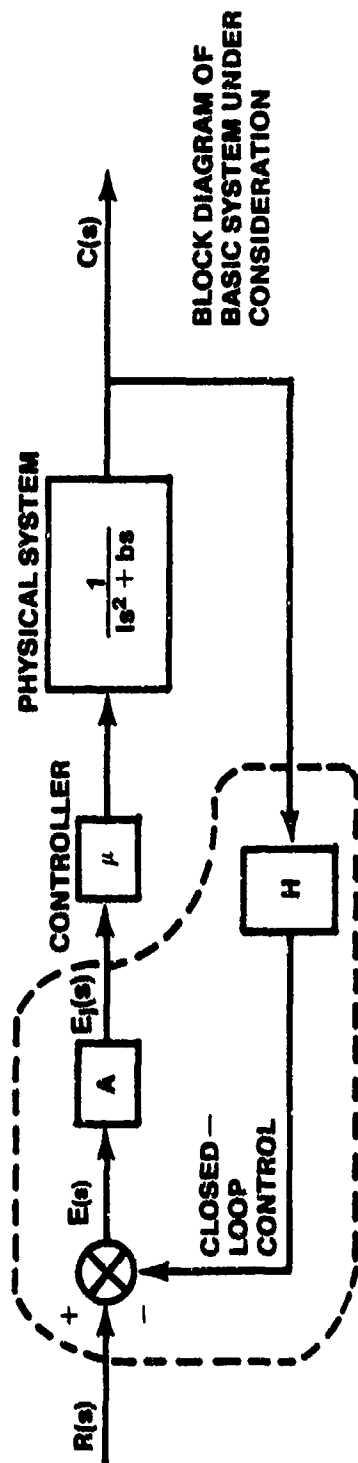
Table 13.5

PASSSIVE COMPENSATION

NAME	A	H	ω_n	ζ	$E_i(s)$	STEADY-STATE ERROR $[e(t)_{ss}]$		
						STEP	RAMP	PARABOLIC
PROPORTIONAL	1	1	$\sqrt{\dfrac{\mu}{I}}$	$\dfrac{b}{2\sqrt{\mu I}}$	$R-C$	$e(t)_{ss}=0$	$e(t)_{ss}=\dfrac{b}{\mu}R$	INFINITE ERROR
DERIVATIVE	1	$(1+C_D s)$	$\sqrt{\dfrac{\mu}{I}}$	$\left(\dfrac{b}{\mu}+C_D\right)\dfrac{1}{2}\sqrt{\dfrac{\mu}{I}}$	$R-C-C_D sC$	$e(t)_{ss}=0$	$e(t)_{ss}=\left(\dfrac{b}{\mu}+C_D\right)R$	INFINITE ERROR
ERROR RATE	$(1+C_e s)$	1	$\sqrt{\dfrac{\mu}{I}}$	$\left(\dfrac{b}{\mu}+C_e\right)\dfrac{1}{2}\sqrt{\dfrac{\mu}{I}}$	$E+C_e sE$	$e(t)_{ss}=0$	$e(t)_{ss}=\dfrac{b}{\mu}R$	INFINITE ERROR
INTEGRAL	$\left(1+\dfrac{C_i}{s}\right)$	1	3RD ORDER	3RD ORDER	$E+C_i \quad E/s$	$e(t)_{ss}=0$	$e(t)_{ss}=0$	$e(t)_{ss}$ $=\dfrac{Rb}{\mu C_i}$

13.13 SUMMARY

In this chapter an attempt has been made to present the fundamentals of control system analysis. Applications of the theory were held to a minimum so that full attention could be devoted to learning the tools and techniques used in this type of analysis.

Once the analysis techniques have been mastered the more interesting and appropriate area of flight control and handling qualities may be addressed. A knowledge of root locus theory and frequency response is essential in understanding the applications of feedback analysis to flight vehicle systems. Despite the introduction of modern control theory (state variables) and digital flight control, an understanding of these systems is still based in large measure on knowledge of classical feedback control systems.

BIBLIOGRAPHY

13.1. D'Azzo, J. J. and Houpis, C. H. <u>Linear Control System Analysis and Design, Conventional & Modern.</u> McGraw Hill Book Co., New York, N. Y., 2nd Edition, 1981.

13.2. Reid, J. G. <u>Linear System Fundamentals.</u> McGraw Hill Book Co., New York, N. Y., 1983.

13.3. James, H. M., Nichols, M. B. and Phillips, R. S. <u>Theory of Servomechanisms.</u> McGraw Hill Book Co., New York, N. Y., 1947.

CHAPTER 14

FLIGHT CONTROL SYSTEMS

14.1 INTRODUCTION

Modern aircraft design employs ever more sophisticated flight control designs, incorporating concepts such as fly-by-wire, fault tolerance, digital computation, integrated flight-fire-propulsion, and data multiplexing. Each of these features offers performance and survivability advantages. For instance, fault tolerant systems capable of reconfiguring aircraft flight control systems to compensate for lost aerodynamic control surfaces have obvious advantages for battle damaged aircraft. The flight test community must evaluate new aircraft to ensure that they can safely, efficiently and reliably accomplish their design missions. Aircraft systems must be evaluated during a test program to ensure that they enhance the aircraft to perform its design role effectively without decreasing reliability through unnecessary complexity.

In modern aircraft, the pilot no longer is directly linked to the aircraft aerodynamic control surfaces. The pilot provides inputs to an electronic flight control system which compares the pilot's command to the actual aircraft response. If the two are not in agreement, the flight control system compensates by actuating the aerodynamic control surfaces to provide the commanded response. In aircraft such as the F-16, the dynamics of the aircraft, and hence the handling qualities provided to the pilot, are no longer merely a function of the stability and control characteristics of the aircraft, but are strongly influenced, and even dictated by the flight control system. Modern flight control systems provide the pilot with an aircraft which is seemingly stable despite severe aerodynamic instabilities which exist in the unaugmented airframe (no flight control system attached).

The study of aircraft flight control systems is important because of the central role of the flight control system in today's aircraft. Modern aircraft are plagued by a host of handling qualities problems which degrade their ability to accomplish their missions. New technology offers capabilities that promise to enhance tomorrow's combat aircraft beyond the wildest dreams of today's pilots.

The course provides a fundamental understanding of basic aircraft control strategies, stressing the advantages and disadvantages of each type of feedback control commonly used in modern aircraft. The effects of various

control system elements, such as actuators, feel systems, electronic compensators, mechanical elements, and structural filters on the aircraft dynamic modes of motion are studied. Modern flight control systems are analyzed to gain an appreciation for their operation and potential handling qualities deficiencies. Simple multiloop techniques for the longitudinal axis and the more challenging coupled lateral-directional axes are analyzed. The analysis techniques require only root locus and time response programs available at the Test Pilot School. More advanced computer programs to ease the analysis problem are currently being created to augment the techniques discussed in this text. Two problems are provided for practicing the concepts discussed in the classroom.

Once the aircraft aerodynamic configuration is determined to meet the mission performance specifications, the requirement for a stability and control augmentation system usually arises to correct handling qualities deficiencies. Figure 14.1 provides a flow chart of a typical flight control system development effort. Fly-by-wire flight control systems not only compensate for poor stability and control characteristics, but provide the medium through which the pilot flies the aircraft. Flight control concepts must determine which feedback strategies solve the problems confronted.

REQUIREMENT

CONCEPT

INITIAL
DESIGN

ADVANCED
DESIGN

GROUND
SIMULATION

INFLIGHT
SIMULATION

FLIGHT TEST
OF AIRCRAFT

ACCEPTABLE SYSTEM

MAJOR
DEFICIENCIES
AND
PROBLEMS

DESIGN
CHANGES
REQUIRED

MINOR
DEFICIENCIES

SYSTEM
TWEAKING
REQUIRED
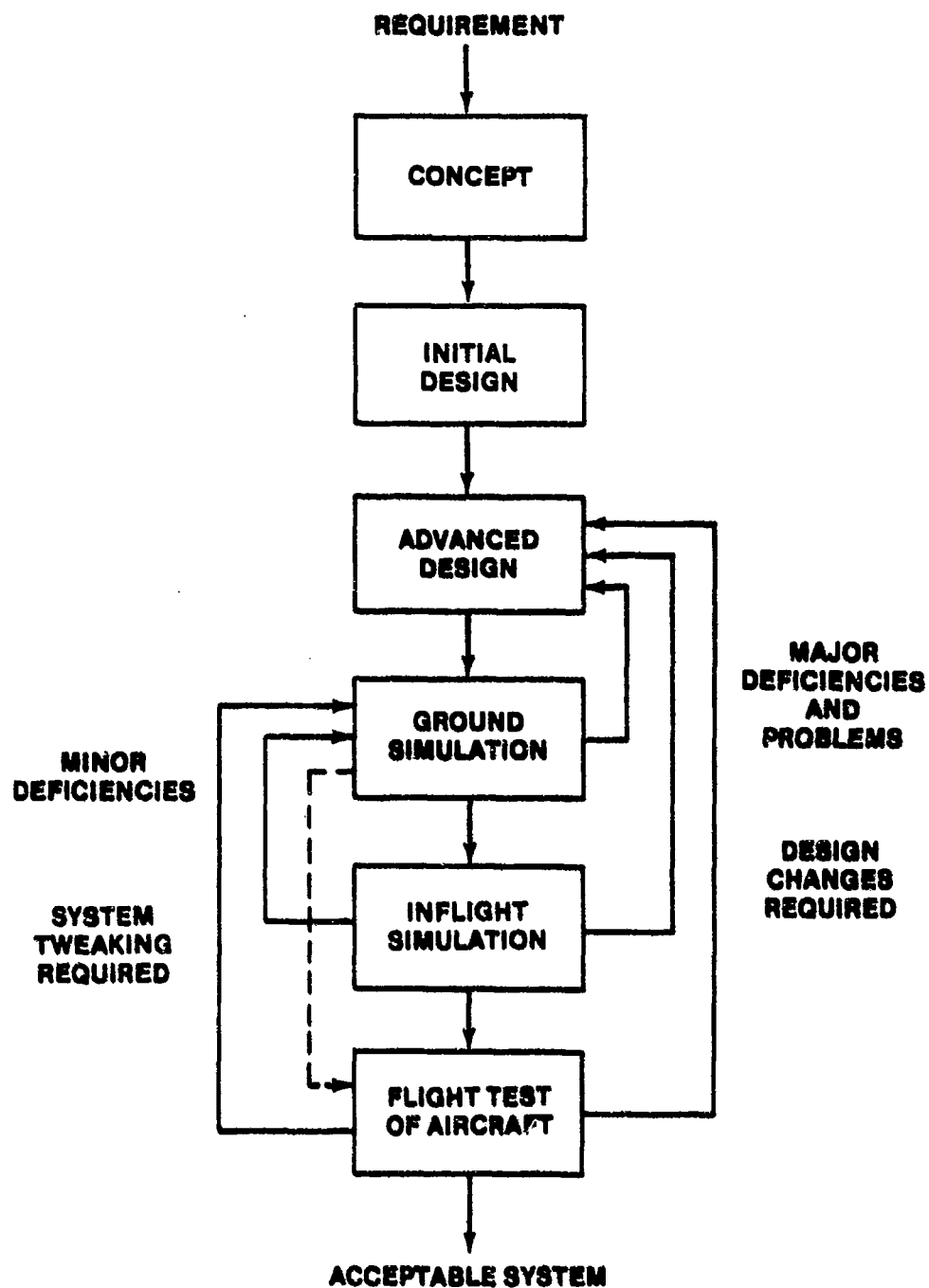
FIGURE 14.1.   FLIGHT CONTROL SYSTEM DEVELOPMENT FLOW CHART

Advanced design simulations of the flight control system, including piloted simulations, are accomplished. Sophisticated ground simulations with high quality visual systems (not necessarily the most visually aesthetic, but having minimal time delays which can overshadow major handling qualities problems) are used for a concerted piloted simulation phase. Both operational and test pilots should fly the simulation in as realistic a manner as possible. Major handling qualities deficiencies uncovered during the ground simulation phase should be corrected prior to flight. In-flight simulations should determine deficiencies before hardware or software for the flight test vehicle are finalized. Only flight tests can reveal all the problems associated with the system design. Once the flight control design has matriculated through all the iterations of design, simulation and flight test, the configuration is judged to be successful. It is unlikely that aircraft flight control system testing on aircraft like the F-16 will end so long as the aircraft is in the inventory. New mission requirements will arise and result in flight control system refinements because of new flying qualities difficulties.

Figure 14.2 presents a schematic of a flying qualities flight test program for a modern, highly augmented aircraft. A thorough understanding of the aircraft mission and the mission tasks is essential. Simplified linear analysis may reveal areas where handling qualities deficiencies are likely and will help the flight test organization become familiar with the system operation and design rationale. A detailed block diagram analysis aids in defining test points and specific areas that require attention.
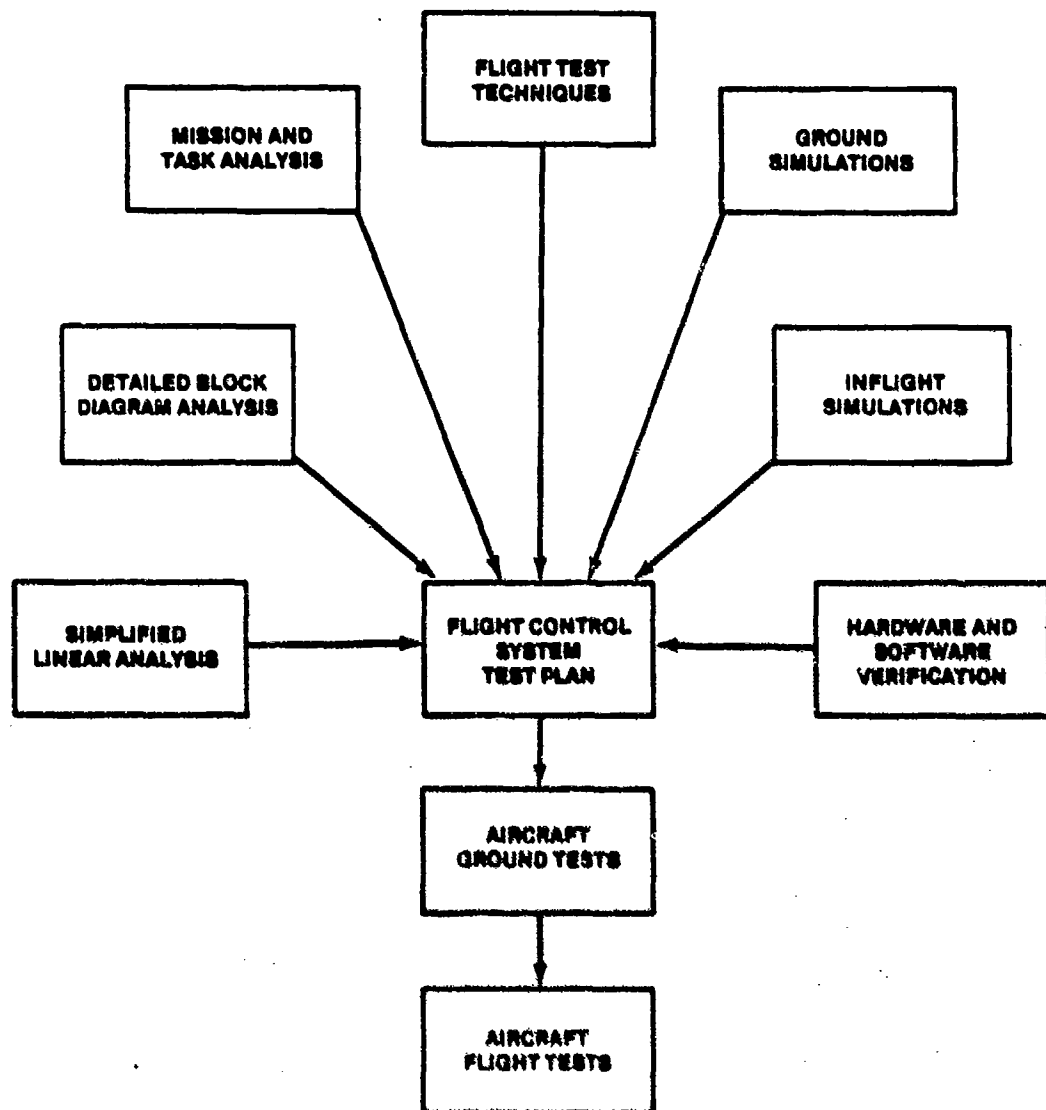
FIGURE 14.2. FLIGHT CONTROL SYSTEM TEST PLANNING CONSIDERATIONS AND TEST
CONDUCT

14.2 ELEMENTARY FEEDBACK CONTROL FOR AIRCRAFT

In a simplified augmentation system, as shown in Figure 14.3, aircraft motion parameters are fed back directly to the aircraft control surface. The system is an idealization since control surfaces cannot be moved without actuators, which introduce lag into the system. Additionally, aircraft motions cannot be sensed instantaneously or reproduced in a pure form.
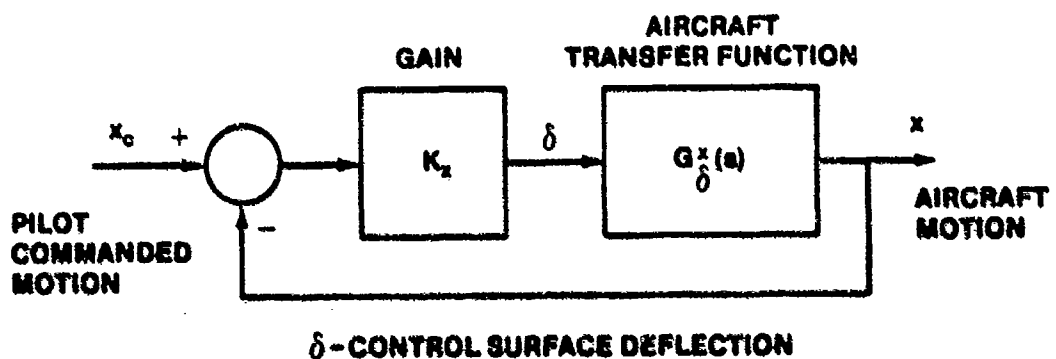
FIGURE 14.3. ELEMENTARY AIRCRAFT FEEDBACK CONTROL SYSTEM

Despite these simplifications, this analysis indicates the general effects of the feedback system on the aircraft dynamic modes of motion. Table 14.1 presents a list of commonly used feedback quantities. In most of the analysis to follow, the controller considered will be a simple gain.

TABLE 14.1
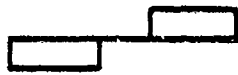
COMMON AIRCRAFT FEEDBACK PARAMETERS
AND ACTUATING AERODYNAMIC SURFACES

Feedback Parameter	Actuating Surface
1. Longitudinal Axis	
θ, pitch angle	δ_e, elevator deflection
q, pitch rate	δ_f, flap deflection
u, forward velocity	δ_t, engine throttle deflection
a_x, longitudinal acceleration	δ_{hc}, horizontal canard deflection
a_z, normal acceleration	
h, altitude	
$\dot{h}$, rate of climb	
α, angle of attack (w/U_0)	
2. Lateral-Directional Axes	
ϕ, bank angle	δ_a, aileron deflection
p, roll rate	δ_r, rudder deflection
r, yaw rate	δ_{vc}, vertical canard deflection
β, sideslip angle (v/U_0)	
a_y, lateral acceleration	

14.2.1 Aircraft Models and Sign Conventions

There are other sign conventions than the one used at the USAF Test Pilot School. Table 14.2 compares the NASA sign convention with the normal TPS sign convention.

TABLE 14.2
SIGN CONVENTION

CONTROL DISPLACEMENT	TPS	NASA
$+\delta_r$	(TER)	(TEL)
$+\delta_e$	(TEU)	(TED)
$+\delta_a$		

Understanding the sign convention is important prior to starting any analysis, as the phasing (summing junction signs) necessary to obtain proper operation in the feedback control system is dependent on the sign convention used. Just as positive pitch implies the aircraft nose going up and the tail going down (according to the right hand rule with the aircraft Y body axis pointing out the right wing), a positive elevator deflection implies the leading edge moving down and the trailing edge moving up. This means that a positive elevator input will produce a positive pitching motion. Using a similar definition, positive rudder produces positive yaw rate.

The sign convention can be quickly determined by observing the sign of the gain term in the aircraft transfer functions. The sign of the $G^{\theta}_{\delta_e}$, $G^{p}_{\delta_a}$ and $G^{r}_{\delta_r}$ gain term indicates the direction that the aircraft will (but may not indicate intermediate or final motion directions). A positive sign on $G^{\theta}_{\delta_e}$ indicates positive elevator trailing edge up in the Test Pilot School sign convention.

Aircraft transfer functions are obtained from the equations of motion developed from small perturbation theory, analytically computed, wind tunnel

or flight test derived stability derivatives. Appendix A provides the commonly used aircraft equations of motion and a brief description of how to obtain the transfer function relating an output dynamic motion parameter to a particular control surface input.

The longitudinal model of the aircraft is shown in Figure 14.4 for an elevator input. The single aerodynamic surface, when deflected, affects several aircraft motion parameters simultaneously. Normally, the aircraft block is simplified, as in Figure 14.4a, showing the elevator input and only the outputs of interest, pitch attitude for instance. The model in Figure 14.4b is always implied.
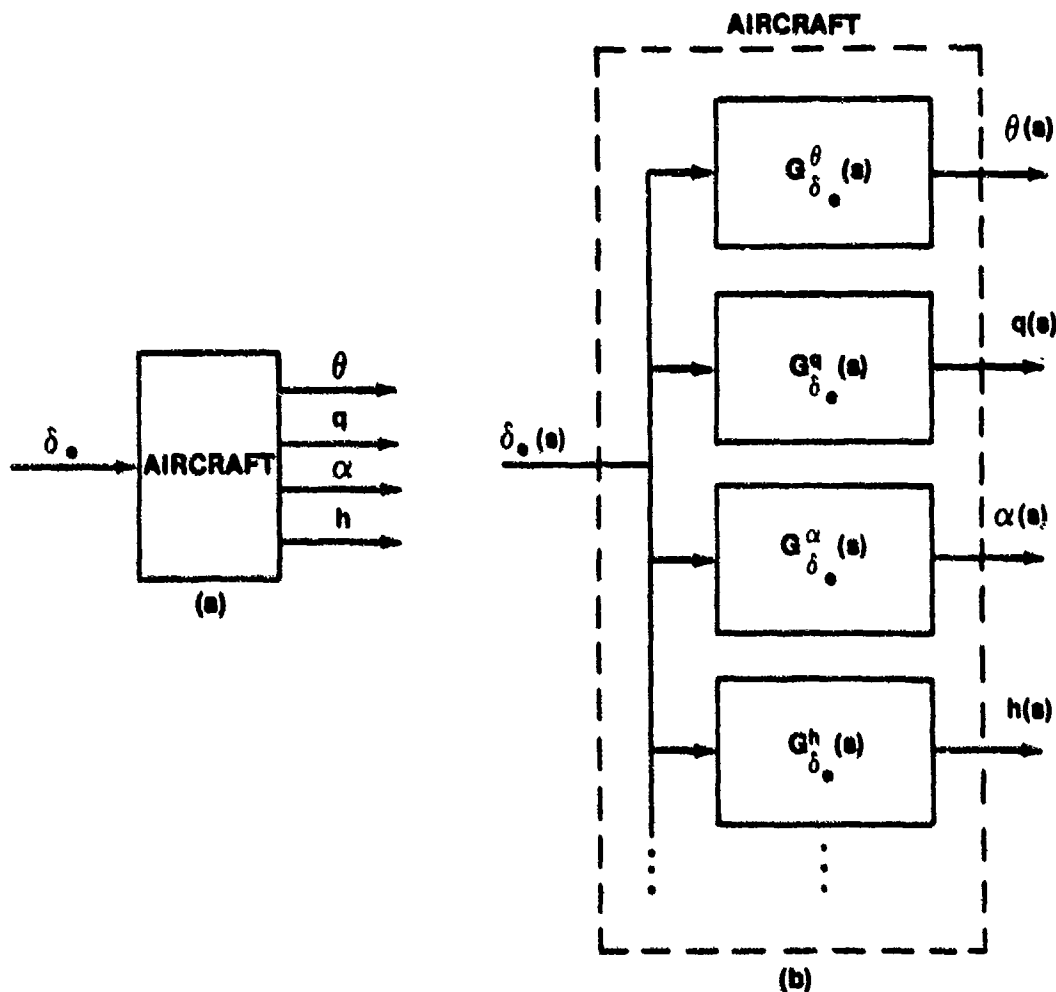
FIGURE 14.4. AIRCRAFT LONGITUDINAL AXIS MODEL

The lateral-directional axes model is shown in Figure 14.5. It is complicated by the fact that two controls can simultaneously affect all the aircraft motion parameters. Once again, the aircraft block is usually simplified, as in Figure 14.5a, but the more complete diagram of Figure 14.5b is always implied. If two controls are considered in the longitudinal axis, such as flap deflection in addition to the elevator input, then a more complex model, similar to the lateral-directional model, is necessary.

AIRCRAFT

$G^{\beta}_{\delta_a}(s)$

$G^{p}_{\delta_a}(s)$

$G^{r}_{\delta_a}(s)$

$G^{\beta}_{\delta_r}(s)$

$G^{p}_{\delta_r}(s)$

$G^{r}_{\delta_r}(s)$

$\delta_a(s)$

$\delta_r(s)$

$\beta(s)$

$p(s)$

$r(s)$

δ_a

δ_r

AIR-CRAFT

β

p

r

(a)

(b)
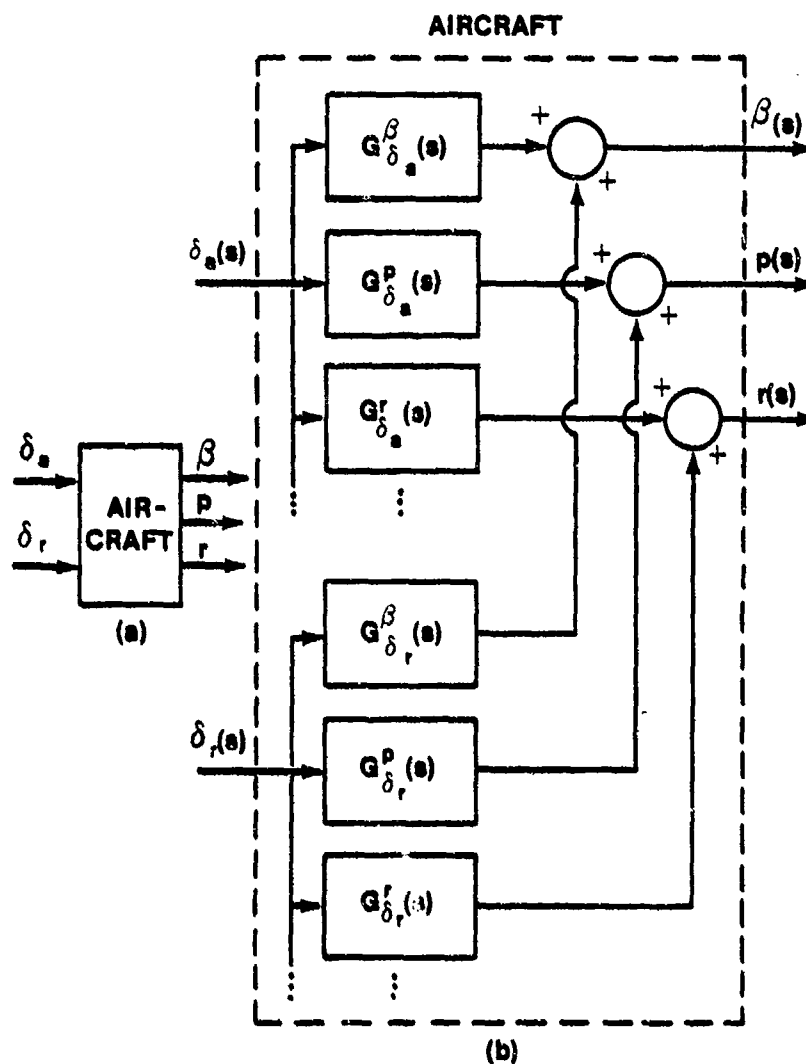
FIGURE 14.5. AIRCRAFT LATERAL-DIRECTIONAL AXES MODEL

14.2.2 Elementary Longitudinal Feedback Control

The purpose of the longitudinal flight control system is to provide acceptable short period dynamics to accomplish high gain tasks, such as gunnery, in-flight refueling, formation, and landing, and to provide adequate speed and maneuvering stability cues to the pilot. Slight phugoid instability can be tolerated for piloted flight, although not for autopilot operation. The effects of a single feedback loop stability augmentation system on the aircraft short period and phugoid dynamic modes will be analized.

14.2.2.1 Pitch Attitude Feedback to the Elevator. Figure 14.6 shows the block diagram of a pitch attitude feedback control system with a pure gain controller.
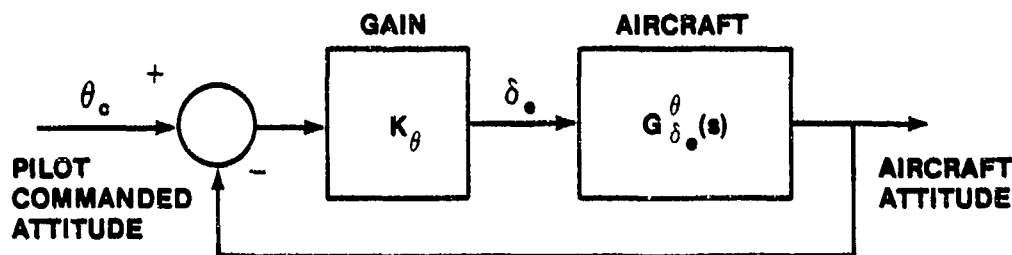
FIGURE 14.6. PITCH ATTITUDE COMMAND SYSTEM

The negative feedback compares the pilot input to the actual response and commands the appropriate elevator deflection. If the aircraft pitch attitude response is less than that commanded, an increased deflection of the elevator is required.

The unaugmented aircraft characteristics in Figure 14.7 are typical of a reasonably well behaved aircraft in cruising flight at moderate altitudes. The Bode plot of Figure 14.7a illustrates these characteristics, which include a wide separation between the short period and phugoid breakpoints, in both amplitude ratio and frequency, and the relatively heavy damping of the short period. Figure 14.7b presents the root locus of the open loop transfer

function to show how the closed loop characteristic roots of the augmented aircraft change as a function of the system gain. At moderate gain, the phugoid roots are driven close to the zeros, while the short period roots move to a higher natural frequency and a slightly lower damping ratio. This degradation of the short period damping is not necessarily undesirable unless the unaugmented aircraft short period damping is marginal. The important point to remember is that pitch attitude feedback increases the phugoid damping, effectively suppressing the phugoid dynamics--in this case, at the expense of the short period. The total system damping is unchanged by the pitch attitude feedback loop since none of the aerodynamic stability derivatives that contribute to dynamic damping, such as X_u, Z_α, M_α, or M_q are augmented by the feedback, a requirement if overall system damping is to be increased (see Appendix B).

Interceptor aircraft, during high altitude supersonic flight, often have similar characteristics to the situation described above except that the damping of the unaugmented aircraft short period is very low. The feedback of the pitch attitude degrades the damping ratio of the short period rapidly as
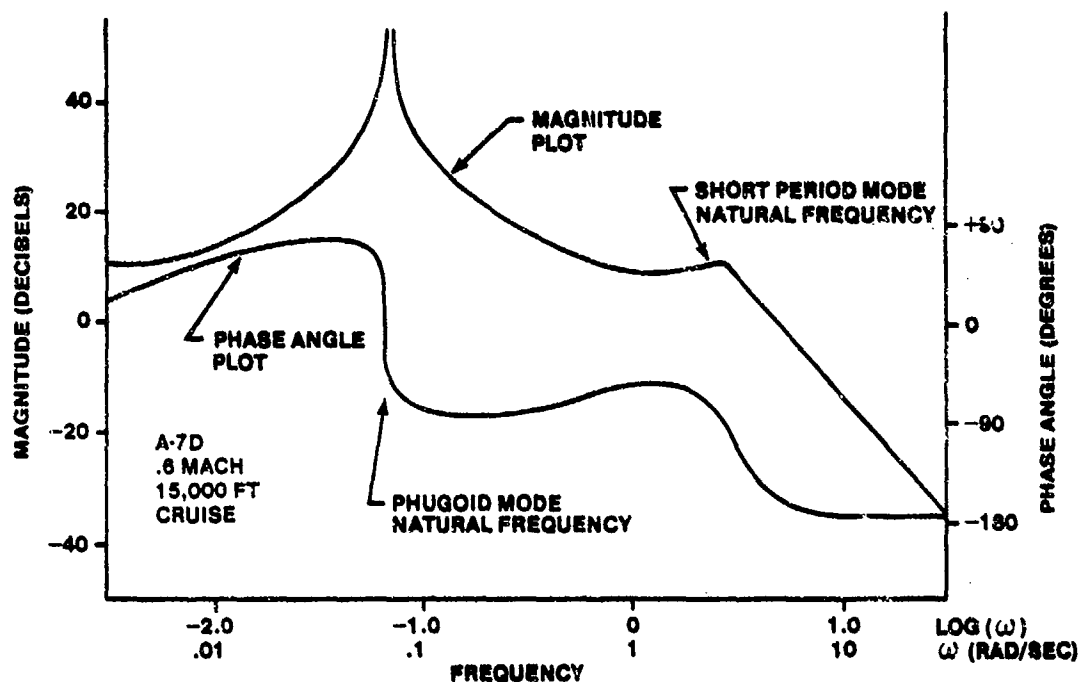
FIGURE 14.7A.   BODE OF PITCH ATTITUDE LOOP FOR AN AIRCRAFT WITH GOOD DYNAMICS
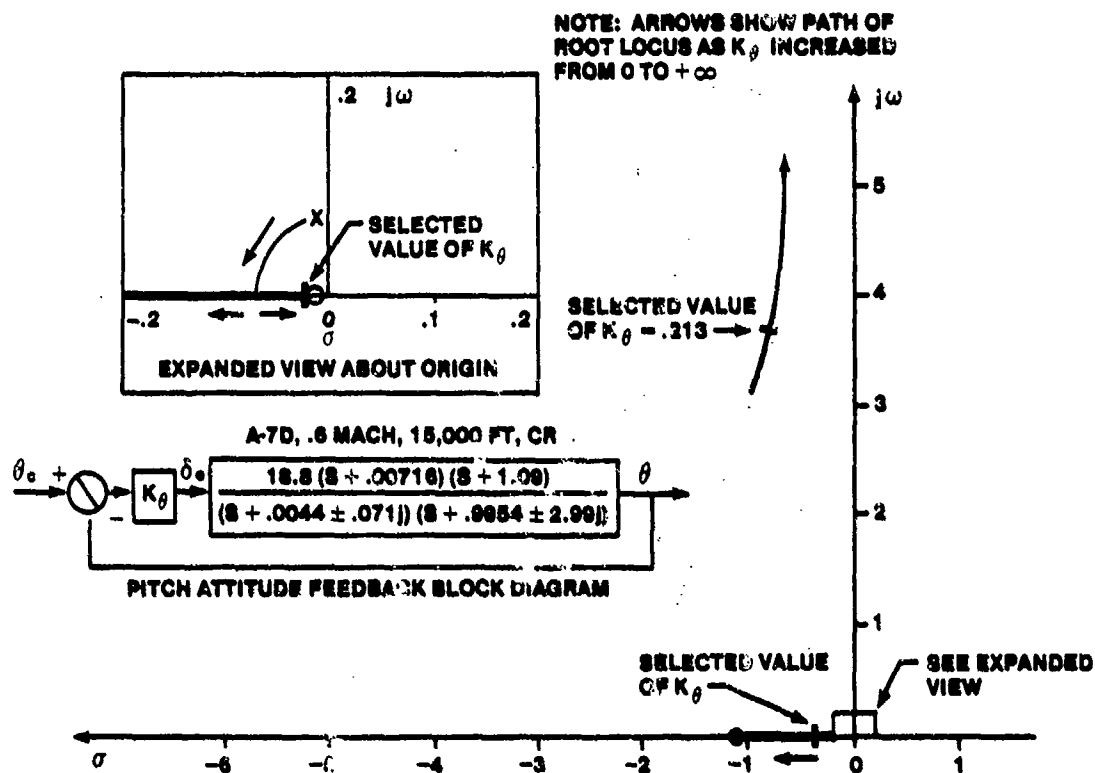
FIGURE 14.7B.   ROOT LOCUS PLOT OF PITCH ATTITUDE LOOP FOR AN AIRCRAFT WITH GOOD DYNAMICS

the gain increases. The suppression of the phugoid in this case exacts too
high a price by excessively destabilizing the short period mode.

Figure 14.8 presents an aircraft at high subsonic speed that exhibits a
longitudinal divergence (instability) commonly known as "tuck". Instead of
the normal phugoid oscillation, the mode is characterized by two real roots,
one stable and one unstable. This mode usually exhibits a slow increase in
speed and a nose down pitch attitude. This is the result of a sufficiently
negative stability derivative, which is caused when

$$\frac{\partial C_m}{\partial M} \quad \text{(proportional to } M_u\text{)}$$

the aerodynamic center shifts from the one-quarter mean aerodynamic chord
characteristic of subsonic flight towards the one-half mean aerodynamic chord
characteristic of supersonic flight. The root locus of the pitch attitude
feedback loop shows that at a moderate gain, the tuck mode moves from the
right half s-plane to the left half s-plane so that the closed loop aircraft
system becomes stable.

Another longitudinal instability is associated with the short period.
The short period roots degenerate to a set of real roots, one stable and the
other unstable. This is due to a sufficiently positive value of M_α and is
caused by an aft center of gravity condition in the aircraft (longitudinal
static instability or relaxed static stability). Figure 14.9 shows the effect
of pitch angle feedback on the F-16, an aircraft which uses an aft center of
gravity position to decrease trim drag during cruise and improve
maneuverability.

FIGURE 14.8. ROOT LOCUS PLOT OF PITCH ATTITUDE LOOP FOR AN AIRCRAFT WITH A
TUCK MODE
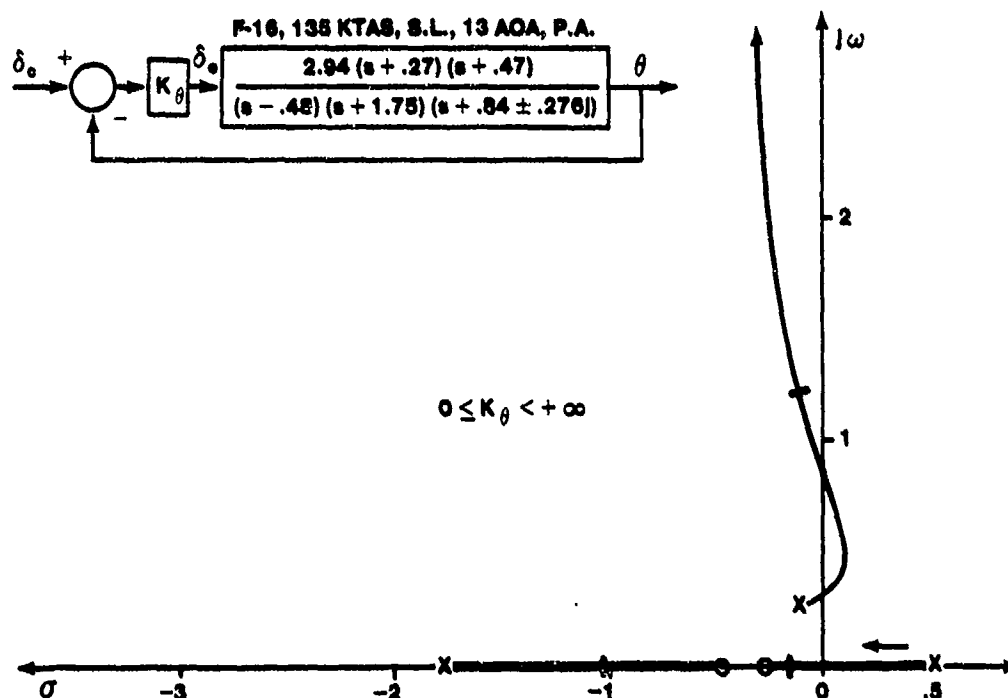
FIGURE 14.9. ROOT LOCUS PLOT OF PITCH ATTITUDE LOOP FOR A
LONGITUDINALLY STATICALLY UNSTABLE AIRCRAFT

14.15

Figure 14.10 shows the effect of pitch attitude feedback on the AV-8A
Harrier vertical takeoff and landing (VTOL) fighter during transition from
wingborne (conventional) flight to jetborne (VTOL) flight. The unstable
oscillatory pair are stabilized at a low value of gain and the damping of the
short period is initially increased. The behavior of the short period mode of
the augmented aircraft then behaves in a manner similar to conventional
aircraft in that the damping is reduced and the natural frequency increased as
the gain becomes larger. The two roots on the real axis remain stable for all
values of gain.

$$0 \leq K_\theta < +\infty$$

AV-8A, 160 KTAS, S.L., PA

$$\frac{6.59 \, (s + .065) \, (s + .521)}{(s + .203) \, (s + 1.69) \, (s - .123 \pm .364j)}$$

PITCH ATTITUDE FEEDBACK BLOCK DIAGRAM
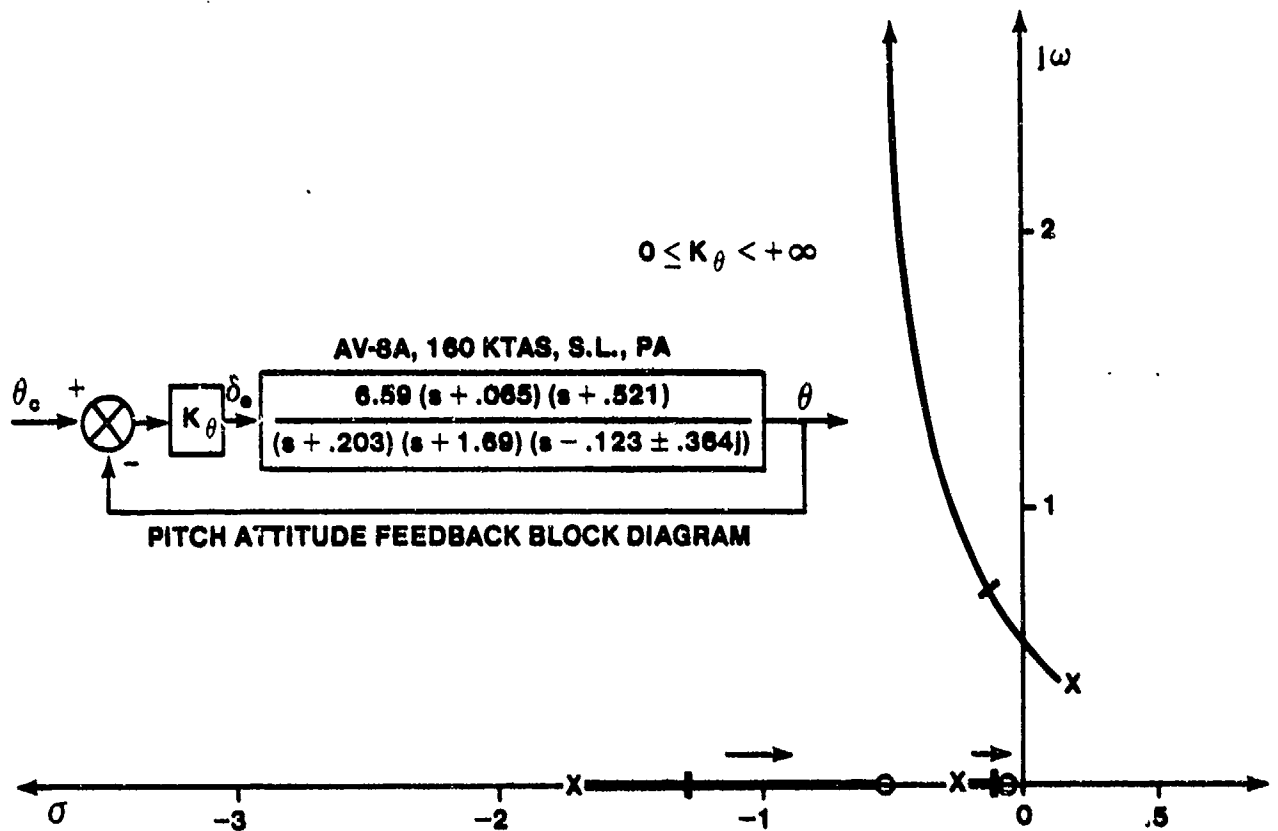
FIGURE 14.10.   ROOT LOCUS PLOT OF PITCH ATTITUDE LOOP FOR AN AIRCRAFT
WITH UNSTABLE OSCILLATORY MODE

In all the pitch attitude feedback augmentation schemes discussed above, the open loop gain does not become infinite at low frequency since a pole at the origin does not exist (type 0 system). The closed loop frequency response, therefore, has an amplitude ratio slightly less than one at low frequencies, as illustrated in Figure 14.11 for an aircraft with well behaved unaugmented characteristics and a selected value of system gain. The higher the gain, the lower the steady state error. But an infinite (or very large) gain cannot be used since the short period damping would approach zero. Several ways to eliminate the steady state error in the pitch attitude command system will be discussed in Paragraph 14.3.
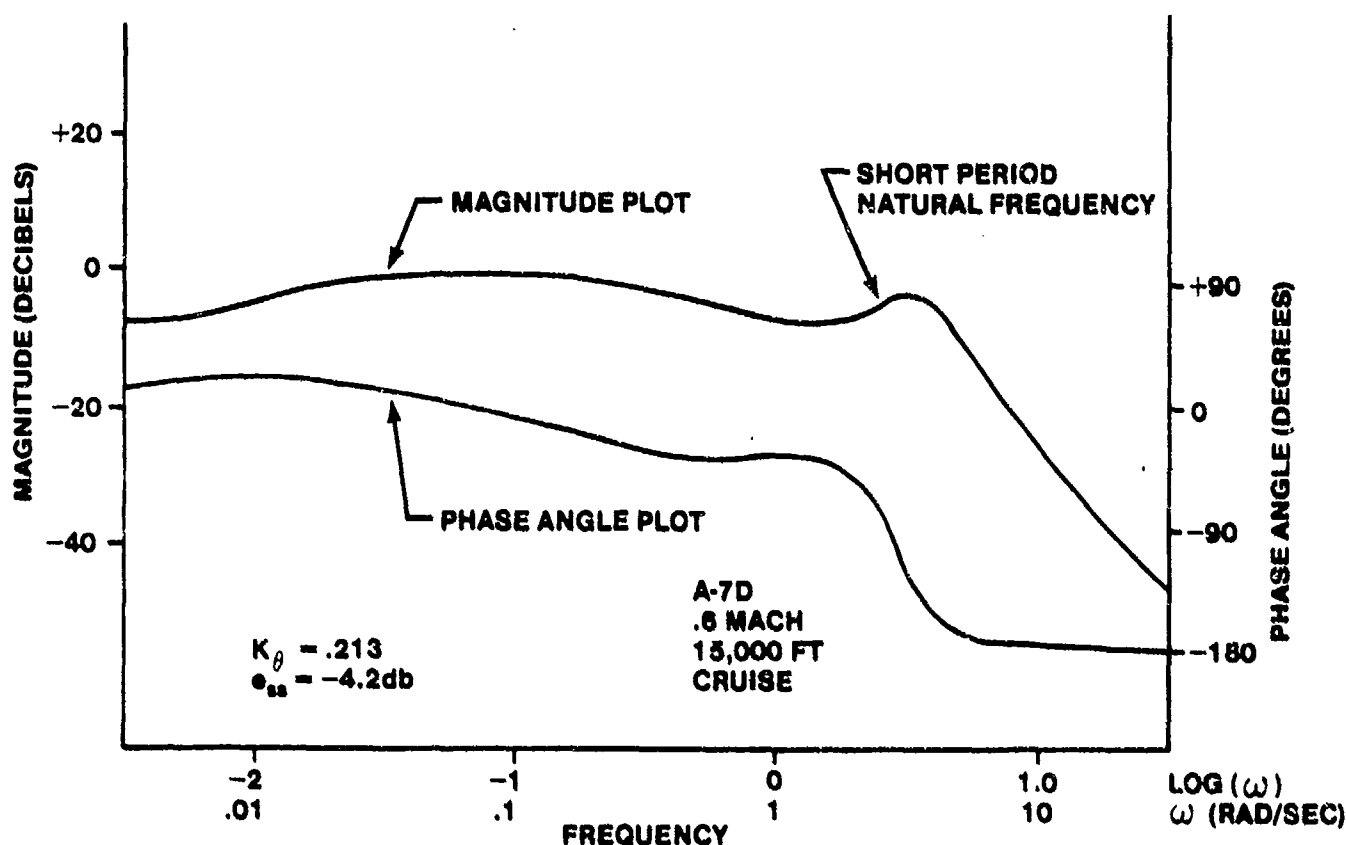
FIGURE 14.11.   BODE PLOT OF CLOSED LOOP PITCH ATTITUDE CONTROL SYSTEM
FOR AN AIRCRAFT WITH GOOD DYNAMICS

14.17

14.2.2.2 <u>Pitch Rate Feedback to the Elevator</u>. Figure 14.12 shows a block diagram of a pitch rate feedback control system, commonly called a pitch rate command system since the pilot stick input is compared directly to the aircraft pitch rate. This feedback effectively augments the pitch damping stability derivative, so that increasing the magnitude of the pitch damping directly increases the short period damping. The system uses a pure gain controller.
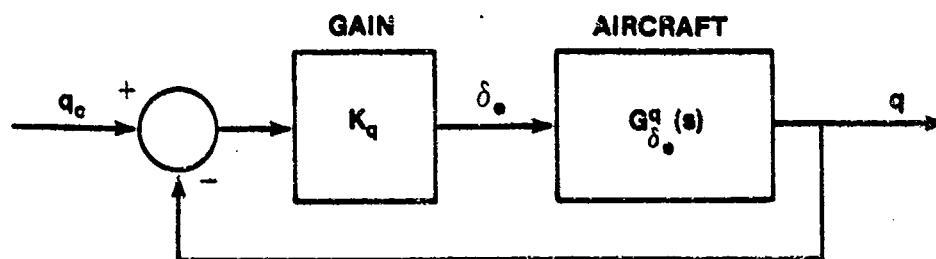
FIGURE 14.12.   PITCH RATE COMMAND SYSTEM

Figure 14.13 presents a root locus plot of the pitch rate command system implemented on a well behaved aircraft. At low gain, the aircraft short period roots move rapidly towards the real axis, dramatically increasing the short period damping while changing the short period natural frequency only slightly. At a relatively low gain, the two short period roots become real (overdamped). The phugoid roots move toward two zeros near the origin, but for the same values of gain that dramatically affected the short period, the phugoid mode damping is hardly changed and the natural frequency decreases only slightly. It is apparent from this analysis that the feedback of pitch rate to the elevator has little effect on the phugoid mode unless high gain is used. High gain, however, increase the short period response time causing a sluggish (slow) response to pilot inputs. This sluggishness is caused by the real axis root which approaches the zero near s = -1.
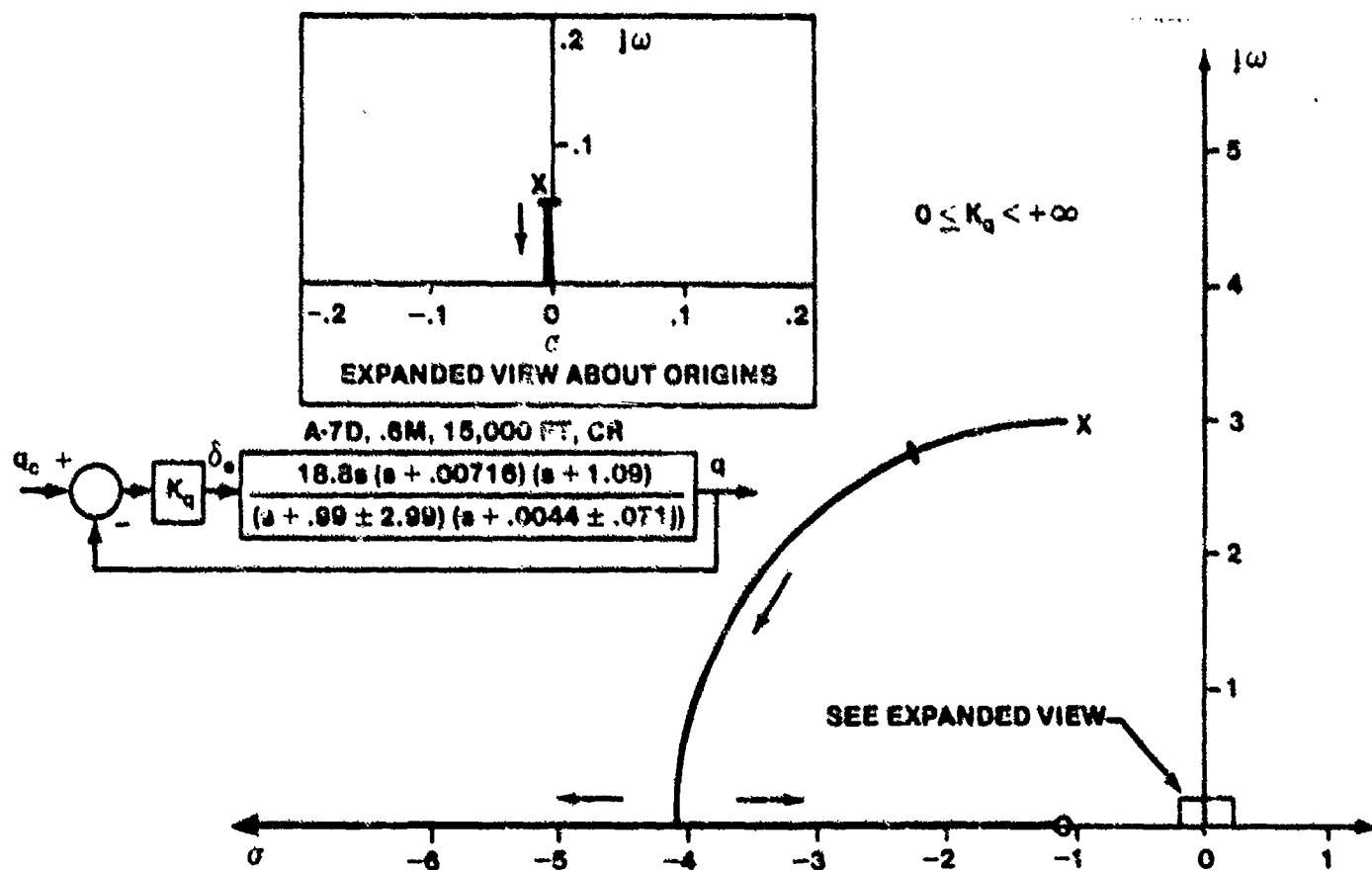
FIGURE 14.13. ROOT LOCUS PLOT OF PITCH RATE LOOP FOR AN AIRCRAFT WITH GOOD DYNAMICS

If the aircraft speed increases to the transonic region so that the tuck mode appears, the pitch rate feedback remains effective in damping the short period mode at low gain, as shown in Figure 14.14. The tuck mode root, however, remains unstable despite the augmentation system, showing that pitch rate feedback is ineffective in completely stabilizing the aircraft. The unstable tuck mode is usually not objectionable to the pilot as long as the time to double amplitude is large, where

$$T_2 = - \frac{\ln 2}{\sigma} \qquad (14.3)$$

Figure 14.15 presents the effects of a pitch rate command system on an aircraft with an unstable oscillatory mode. For some minimum gain the unstable roots move into the left half s-plane. The damping ratio increases and the natural frequency decreases rapidly with increasing gain. The oscillatory mode is effectively suppressed at a reasonably low gain.
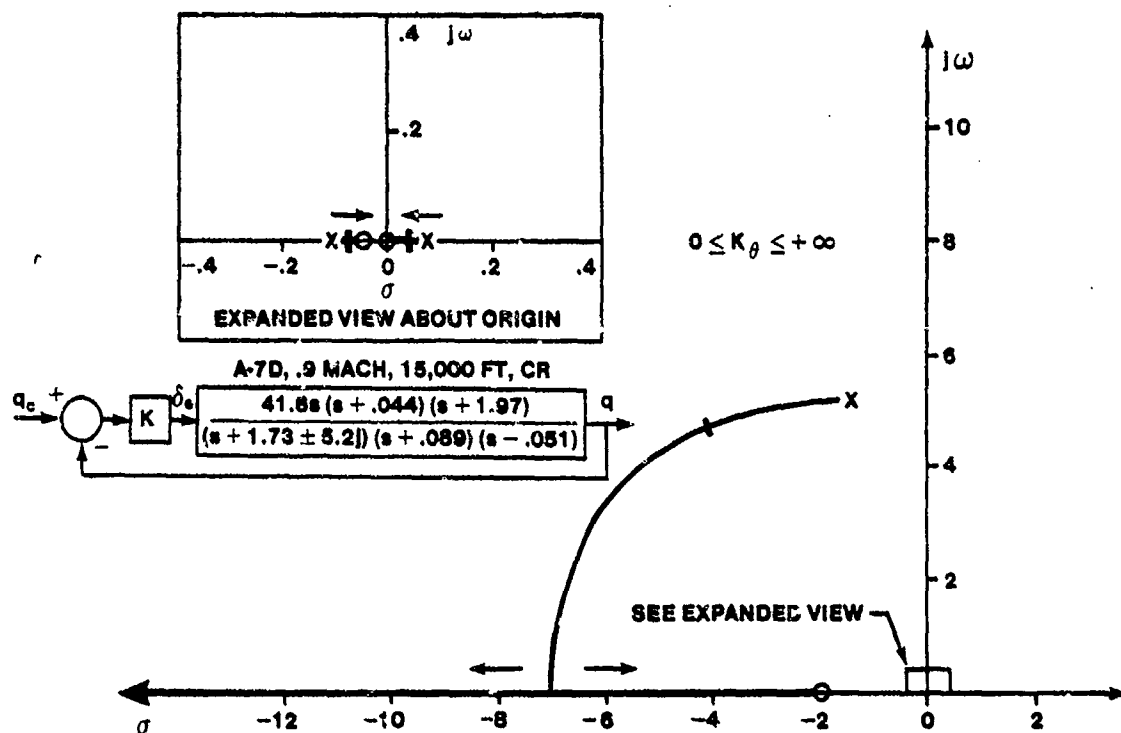
FIGURE 14.14. ROOT LOCUS PLOT OF PITCH RATE LOOP FOR
AN AIRCRAFT WITH A TUCK MODE
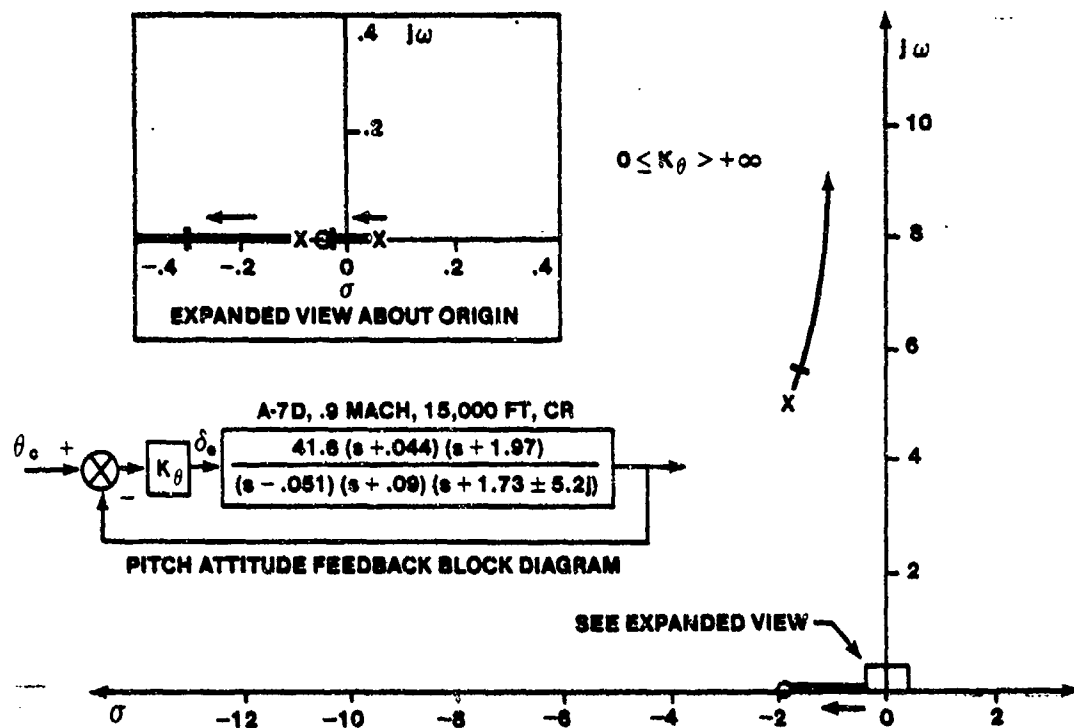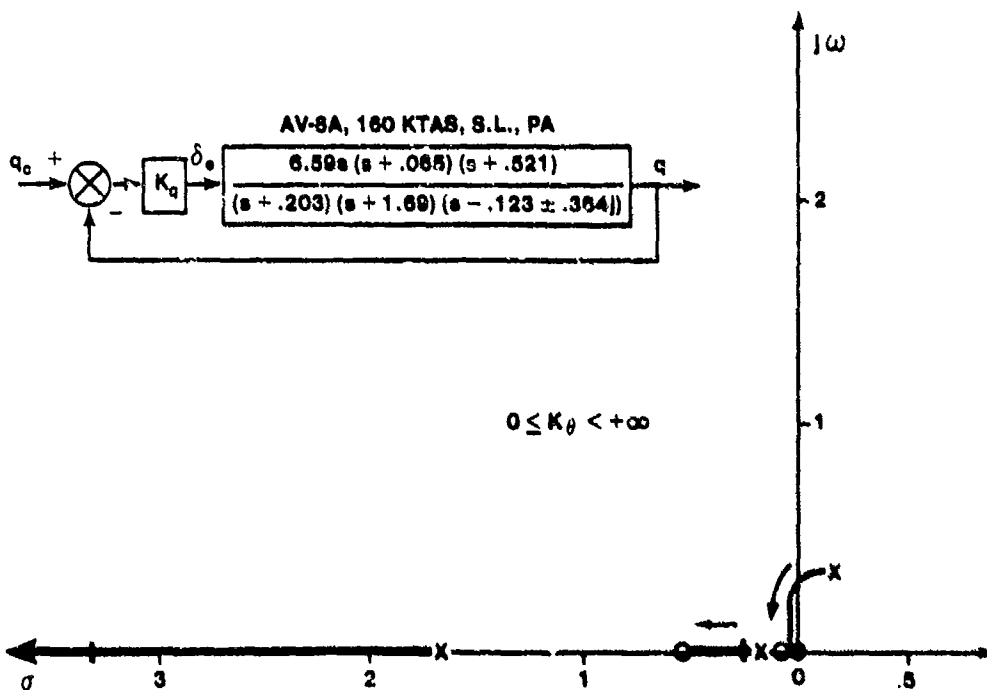

FIGURE 14.15. ROOT LOCUS PLOT OF PITCH RATE LOOP FOR AN
AIRCRAFT WITH UNSTABLE OSCILLATORY MODE

14.2.2.3 <u>Angle of Attack Feedback to the Elevator</u>. The effect of angle of attack feedback on the dynamics of the aircraft with generally acceptable characteristics is presented in Figure 14.16. The proximity of the complex zeros to the phugoid roots implies very little angle of attack change in the phugoid mode. The phugoid of the angle of attack feedback augmented aircraft is suppressed to a greater extent than for the unaugmented aircraft, but the phugoid characteristics are otherwise not appreciably altered. The short period roots are greatly affected. The magnitude of the M_α stability derivative is effectively increased (becomes more negative for improved static stability). From the short period approximate transfer function, the effect of increasing the magnitude of M_α is to increase the natural frequency of the short period, since

$$\omega_{n_{sp}} = Z_w M_q - M_\alpha \qquad (14.4)$$

The short period roots move rapidly with a gain increase. At extremely high gain, the short period roots become real, one going to the high frequency zero on the real axis and the other tending to negative infinity. Very high gain can ideally provide heavy short period damping. This is difficult to achieve in practice due to servo (actuator) and sensor lag effects that drive the short period roots into the right half s-plane. Also, high gains tend to drive the power servo to its limits for all but the smallest inputs or disturbances. Besides, high short period natural frequencies are undesirable to the pilot since the aircraft tends to respond too abruptly.

Figure 14.17 shows the root locus of an angle of attack command system for an aircraft which is statically unstable, longitudinally, where the center of gravity is aft of the center of lift, so that $M_\alpha > 0$.

A relatively low gain causes the unstable root to move into the left half s-plane. The two oscillatory roots move rapidly to the real axis, one moving towards the origin and the other towards the stable real axis root. At a low gain, two of the roots become a phugoid mode pair while the other two form the short period roots. As the gain increases, the phugoid frequency increases and the damping decreases. At very high gain, the phugoid is suppressed by the pair of zeros near the origin. The short period frequency increases and

the damping decreases with increasing gain. The effects of angle of attack feedback for the statically unstable aircraft are identical to that for the aircraft with reasonably good dynamics as the gain becomes very large. The aircraft possesses static stability once the characteristic roots move into the left half s-plane.

The feedback of the rate of change of angle of attack augments the M_α stability derivative, which increases the short period damping, as seen from the short period approximate transfer function, since

$$2\zeta_{sp}\omega_{n_{sp}} = -(Z_w + M_q + M_{\dot\alpha})$$ (14.2)

The use of angle of attack rate feedback is similar in its effects on the aircraft characteristic roots as the pitch rate feedback system. The difficulty in using this feedback strategy involves problems in accurately sensing the angle of attack rate.

14.2.2.4 <u>Normal Acceleration Feedback to the Elevator</u>. The acceleration at the aircraft center of gravity is

$$a_{z_{cg}} = U_0 (\dot\alpha - q) + g(\sin\theta_0) \theta$$ (14.5)

where the last term is normally negligible due to the small angle assumption for a 1 g trim condition. The transfer function is formed by combining the angle of attack rate and pitch rate transfer functions, such that

$$G_{\delta_e}^{a_{z_{cg}}}(s) = \frac{a_{z_{cg}}(s)}{\delta_e(s)} = U_0 \left(\frac{s\alpha(s)}{\delta_e(s)} - \frac{q(s)}{\delta_e(s)} \right)$$ (14.6)

It is seldom possible, or even desirable, to measure the normal acceleration at the center of gravity. If the accelerometer is located some distance away from the center of gravity (acceleration measured in the plane of symmetry) the normal acceleration measured is

$$a_z = a_{z_{cg}} - \ell_x \dot q$$ (14.7)
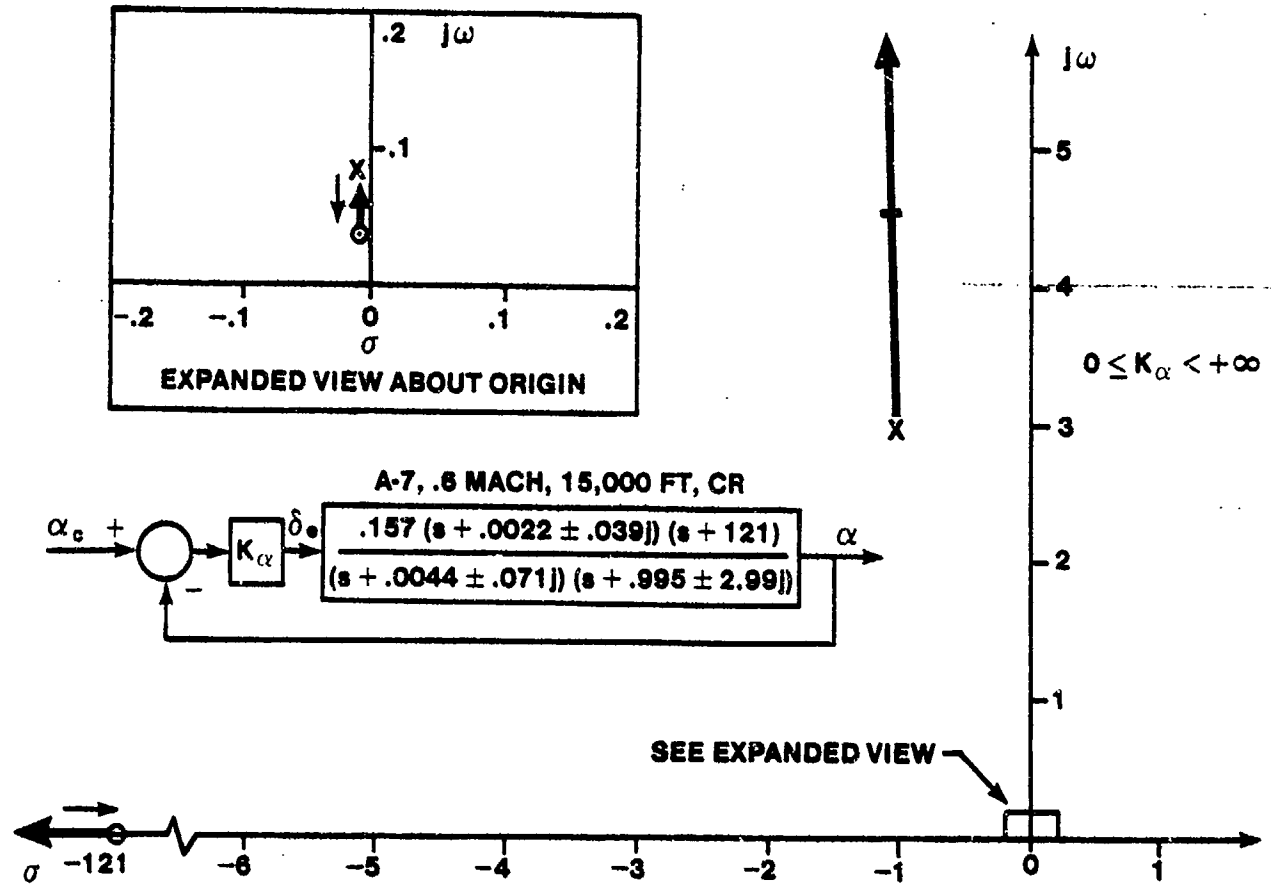
FIGURE 14.16.   ROOT LOCUS PLOT OF ANGLE OF ATTACK LOOP FOR
AN AIRCRAFT WITH GOOD DYNAMICS
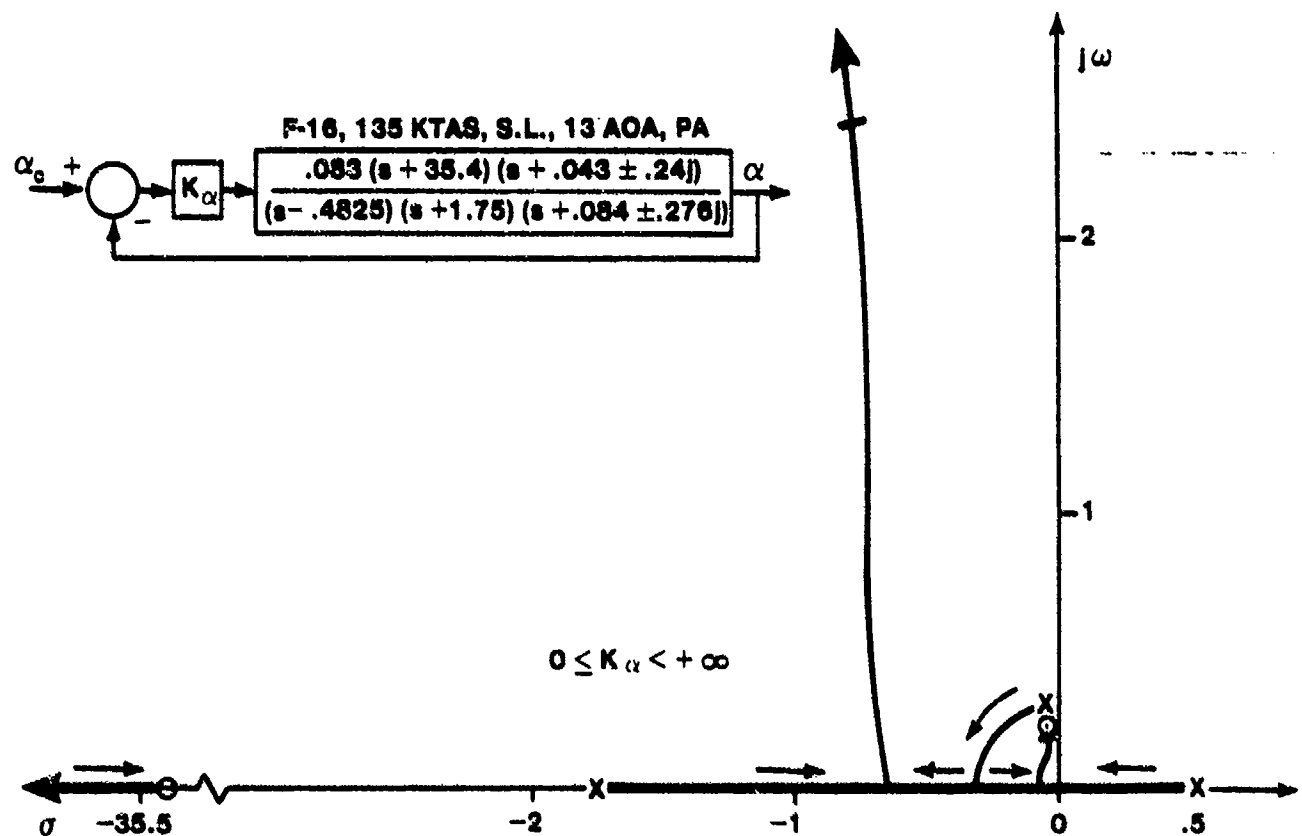
FIGURE 14.17.   ROOT LOCUS PLOT OF ANGLE OF ATTACK LOOP FOR A
LONGITUDINALLY STATICALLY UNSTABLE AIRCRAFT

and the aircraft transfer function for elevator inputs becomes

$$G_{\delta_e}^{a_z}(s) = \frac{a_z(s)}{\delta_e(s)} = U_0 \left[\frac{s\alpha(s)}{\delta_e(s)} - \frac{q(s)}{\delta_e(s)} - \frac{\ell_x}{U_0} \frac{sq(s)}{\delta_e(s)} \right] \qquad (14.8)$$

Figure 14.18 presents the block diagram and root locus plot of a load factor (g) command system with the accelerometer located at the aircraft center of gravity. Feedback is employed to compare the output to the input due to the nonminimum phase zero (right half s-plane zero) at s = 11.0 in the load factor transfer function,

$$\frac{n_z}{\delta_e(s)} = \frac{-3.09(s + 11.8)(s - 11)}{(s + 0.995 \pm 2.99j)}$$

Similar zeros occur quite frequently in aircraft transfer functions. The root locus analysis must be based on a 0° angle criterion rather than the -180° criterion normally used.

The short period roots move rapidly with only a small increase in gain. Initially, the short period damping decreases somewhat as the natural frequency increases. At a relatively high gain, the two oscillatory short period roots meet and become real. At very high gains, one of the real roots is driven to the right half s-plane, causing the system to become unstable. The effect is essentially the same as that of the angle of attack feedback situation for low system gains, since

$$n_z = \frac{L}{W} = \frac{\rho V_A^2 \, SC_{L_\alpha} \alpha}{2W} \qquad (14.9)$$
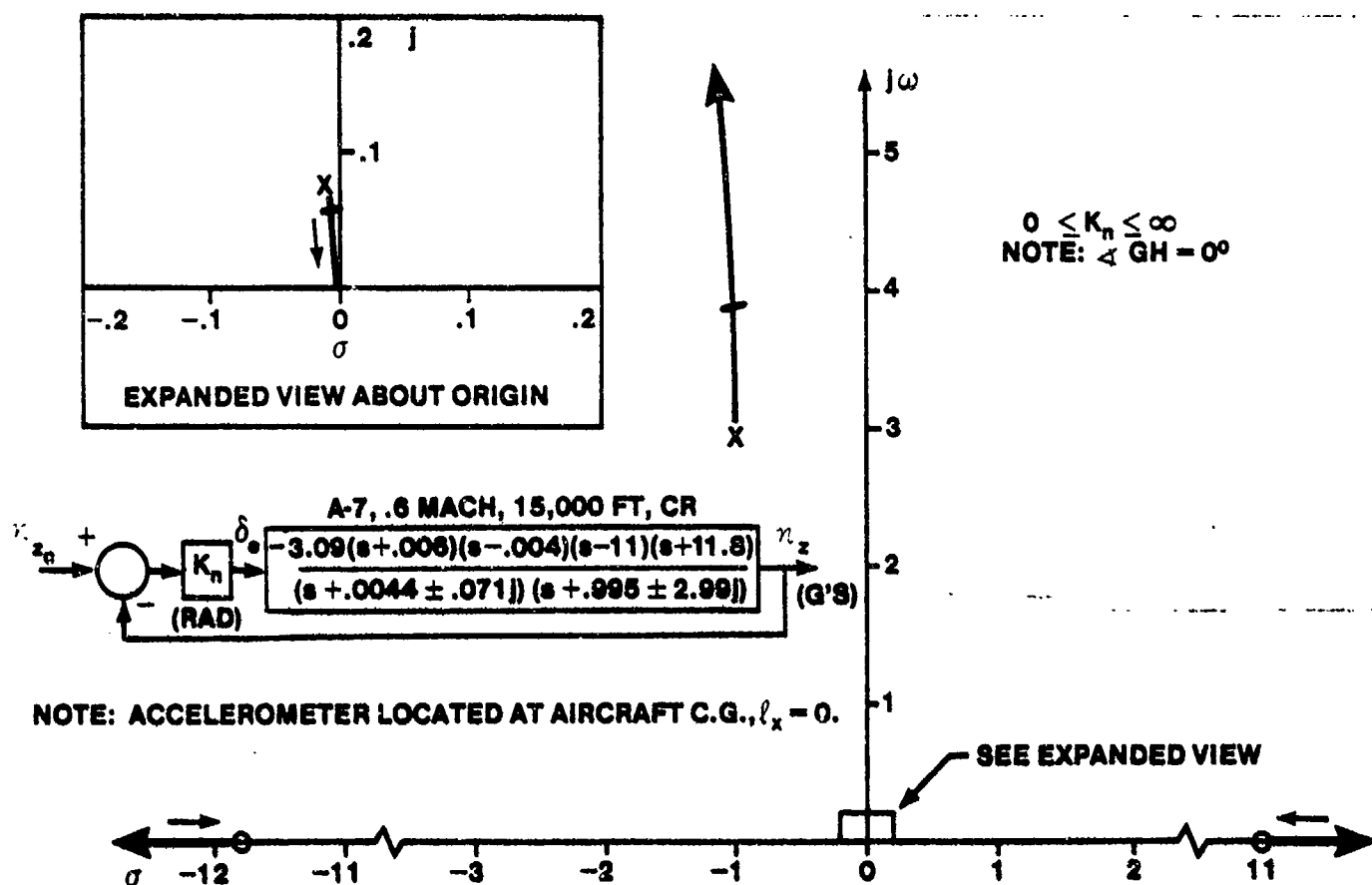
FIGURE 14.18. ROOT LOCUS PLOT OF LOAD FACTOR (G) COMMAND SYSTEM
FOR AN AIRCRAFT WITH GOOD DYNAMICS

where the density altitude, aircraft speed, wing area, weight, and lift curve slope are all essentially constant in the short term, making the load factor proportional to the angle of attack.

The phugoid natural frequency is reduced somewhat as the gain increases and the damping of the phugoid is not affected significantly until the gain becomes high. At very high gain, one of the phugoid roots will become an unstable real root.

An elevator actuator, a necessary part of any practical system, causes additional lag, which forces the short period roots to migrate into the right half s-plane as a complex pair at low gain.

14.26

If the accelerometer is located ahead of the center of gravity, the effect is to alter the zeros of the sensed load factor transfer function. This effect will be discussed in detail in Paragraph 14.3. Figure 14.19 shows a root locus plot of a g-command system with the accelerometer located ahead of the center of gravity. Advantages of the system over the case where the accelerometer is located at the center of gravity are twofold: an accelerometer at the center of gravity is impractical in that the center of gravity position shifts as fuel is burned or the payload is changed (weapons are released) and, when an actuator is added to the system, the short period roots are not driven into the right half s-plane as in the case of the accelerometer located at the center of gravity.

$$0 \le K_n < +\infty$$
$$\ell_x = 7.95 \text{ FT}$$

NOTE: MAGNITUDE OF K_n SAME AS FIGURE 14.18

EXPANDED VIEW ABOUT ORIGIN

A-7D, .6 MACH, 15,000 FT, CR

$$\frac{1.55 (s + .006) (s - .004) (s + .8427 \pm 16.091j)}{(s + .0044 \pm .071j) (s + .995 \pm 2.99j)}$$

SEE EXPANDED VIEW
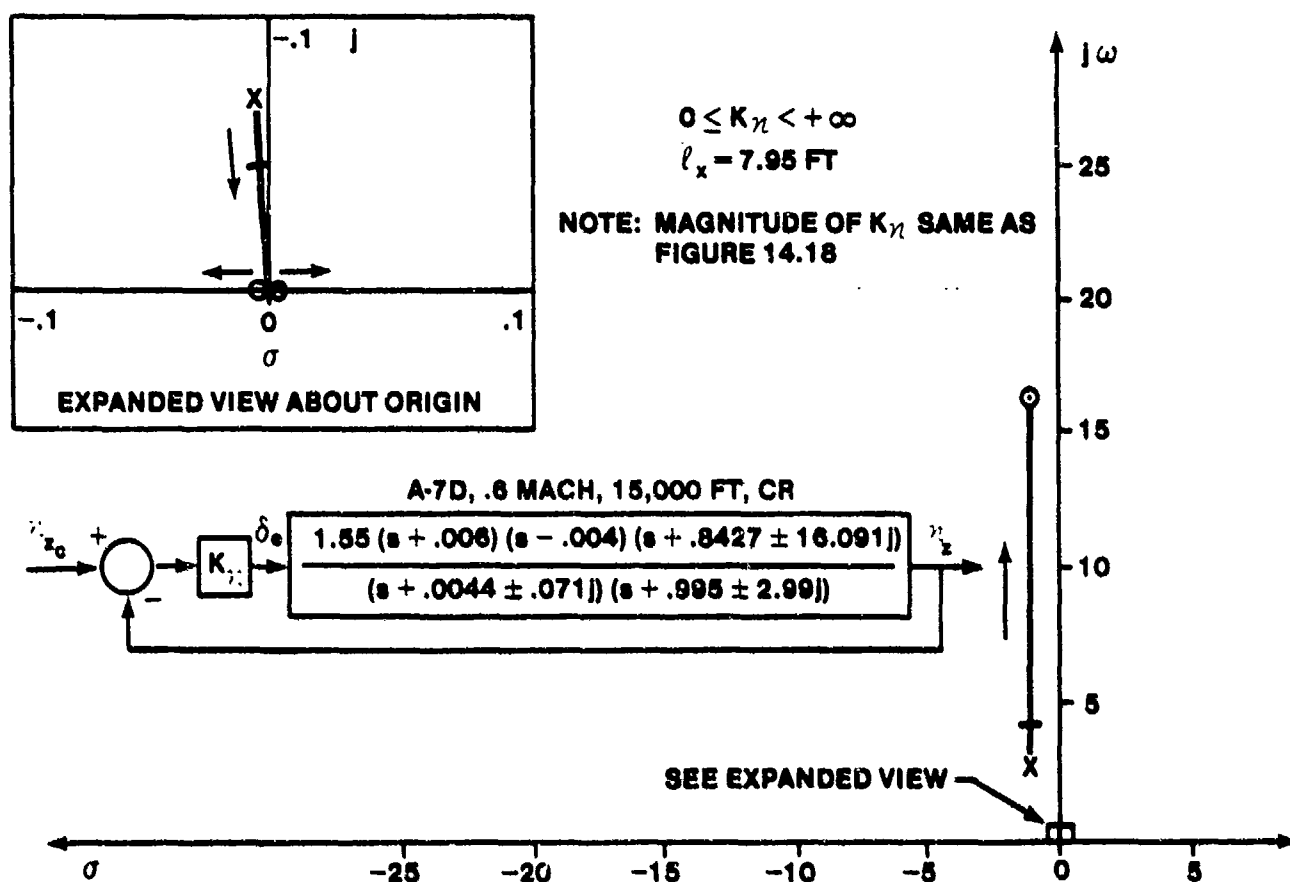
FIGURE 14.19.   ROOT LOCUS OF G COMMAND SYSTEM WITH ACCELEROMETER AHEAD OF CENTER OF GRAVITY

14.27

14.2.2.5 **Forward Velocity Error Feedback to the Elevator.** The use of the elevator to control airspeed has a powerful effect on the phugoid mode, as shown in Figure 14.20. The augmented phugoid roots move rapidly to a higher natural frequency and the phugoid damping is greatly increased. Comparatively large phugoid damping ratios can be achieved before the short period is altered significantly. The effect of velocity feedback is to augment the M_u stability derivative, which affects both the phugoid natural frequency and the damping, since, from the phugoid approximate transfer function,

$$\omega_{n_p}^2 = \frac{g \ (M_w Z_u - Z_w M_u)}{\omega_{n_{sp}}^2} \tag{14.10}$$

EXPANDED VIEW ABOUT ORIGIN

A-7, .6 MACH, 15,000 FT, CR

$$\frac{6.96 \ (s + .56 \pm .693 j) \ (s + 120)}{(s + .0044 \pm .071 j) \ (s + .995 \pm 2.99 j)}$$

$0 \leq K_u < \infty$

SEE EXPANDED VIEW
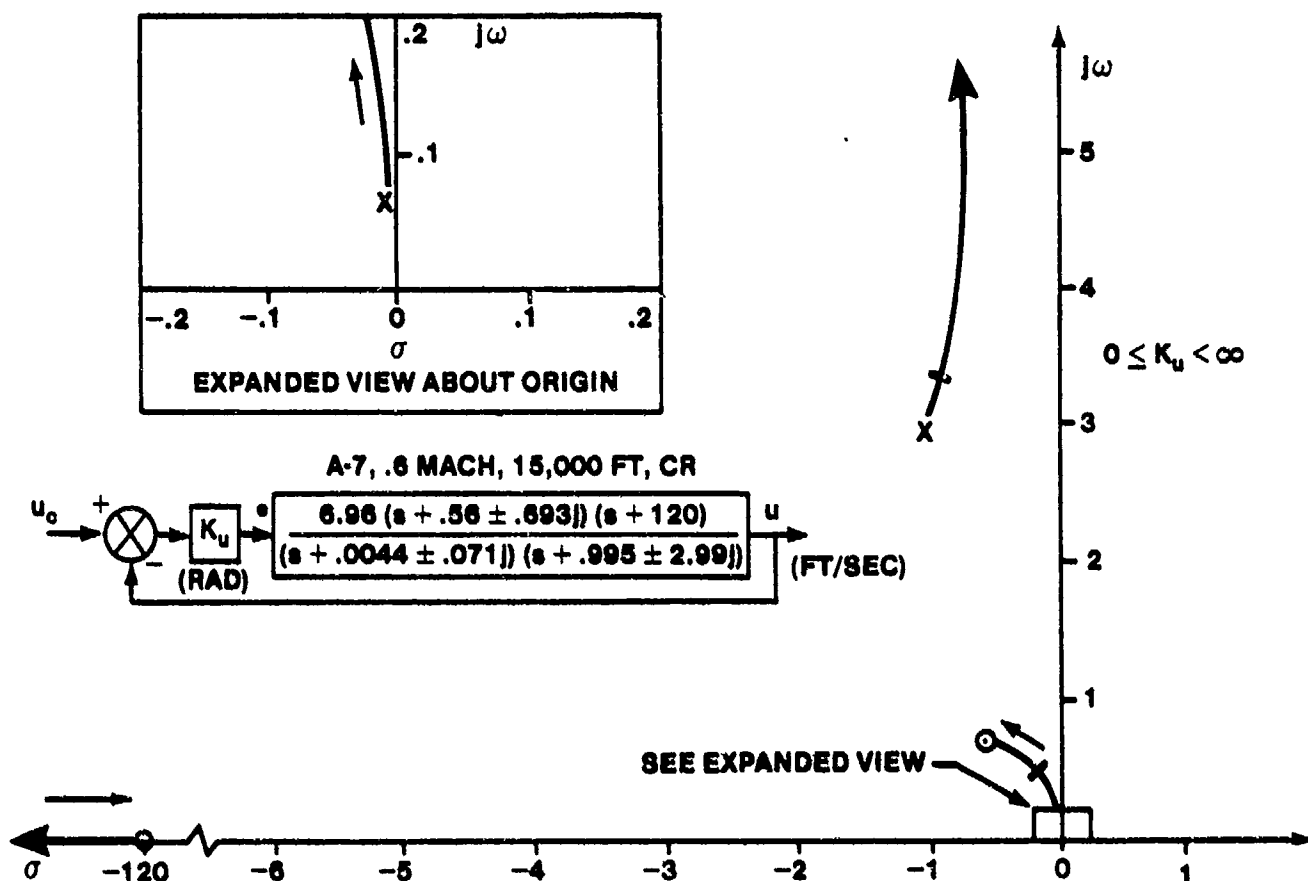
FIGURE 14.20. ROOT LOCUS PLOT OF FORWARD VELOCITY LOOP FOR
AN AIRCRAFT WITH GOOD DYNAMICS

14.28

and

$$2\zeta_p \omega_{n_p} = -X_u - \frac{(X_\alpha - g)}{\omega_{n_{sp}}^2} \cdot M_u \qquad (14.11)$$

where $Z_w < 0$ normally and $M_u > 0$.

From the above expressions, increasing M_u increases both

$$\omega_{n_p} \quad \text{and} \quad \zeta_p .$$

In many situations, the complex zero pair in the

$$G_{\delta_e}^u (s)$$

transfer function are by a pair of zeros on the real axis. In this situation, the phugoid damping due to velocity feedback is more pronounced than that of the example used above.

The same beneficial effect on the phugoid also occurs if a tuck mode is present. A relatively low forward loop gain will stabilize the tuck mode root while not significantly affecting the short period.

Although the augmented phugoid damping ratio is improved by the feedback of forward velocity error alone, the damping is improved further if forward acceleration is also fed back. This creates a new stability derivative, $M_{\dot{u}}$ which augments the $2\zeta_p \omega_{n_p}$ term in the approximate transfer function.

The effect of using pitch attitude control to regulate airspeed by applying a positive pitching moment whenever the speed is greater than that desired can be disconcerting to the pilot if the pitching moment is too great, especially in turbulence. The use of the elevator to control airspeed is not common in military aircraft.

14.2.2.6 <u>Altitude Error Feedback to the Elevator</u>. For small perturbations from straight and level flight, the vertical velocity of the aircraft (Figure 14.21) may be approximated as

$$\dot{h} = V_A \sin\gamma$$

where $\gamma = \theta - \alpha$ so that

$$\dot{h} = V_A(\theta - \alpha) \cong U_0(\theta - \alpha) \qquad (14.12)$$
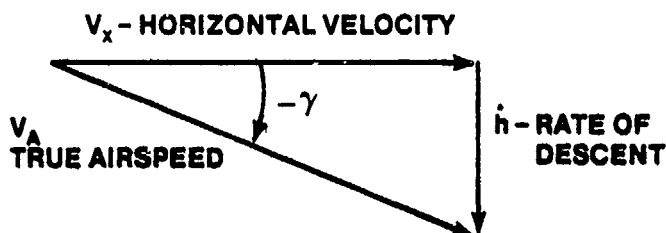
FIGURE 14.21. GEOMETRY FOR ALTITUDE RATE DETERMINATION

The transfer function relating the aircraft altitude to an elevator command becomes

$$\frac{h(s)}{\delta_e(s)} = \frac{U_0}{s}\left(\frac{\theta(s)}{\delta_e(s)} - \frac{\alpha(s)}{\delta_e(s)}\right) \qquad (14.13)$$

Because of the free s, the feedback of altitude to the elevator by itself drives the modified phugoid roots into the right half s-plane at very low gains, as can be seen in Figure 14.22. Several multiloop system configurations provide possibilities to overcome this instability. A common approach is to feed back altitude as an outer loop parameter with an inner attitude hold loop engaged. Another approach is to feed back a combination of altitude and altitude rate signals, but this is not common due to difficulties in sensing the rate of climb or descent without excessive lag in the sensor. One method to determine the rate of climb or descent is to compute the signal, using true airspeed from the air data system, pitch angle from the attitude reference system, and angle of attack from the AOA sensor.

A major problem occurs when the aircraft is on the back side of the thrust required versus airspeed curve. Flight in this regime is accomplished during some approaches to landing (carrier approaches, minimum run landings, and normal landings for some aircraft) or during steep climbs. When on the back side of the power curve, the zero near the origin in Figure 14.22 is in the right half s-plane, causing the pole at the origin to be driven unstable for all closed loop system gains. In principle, the peak of the thrust required curve could be determined and the sign of the gain changed to avoid divergence, but this would cause the phugoid roots to become unstable at very low gain. Altitude control using the elevator alone cannot be achieved for flight conditions near the performance reversal airspeed.
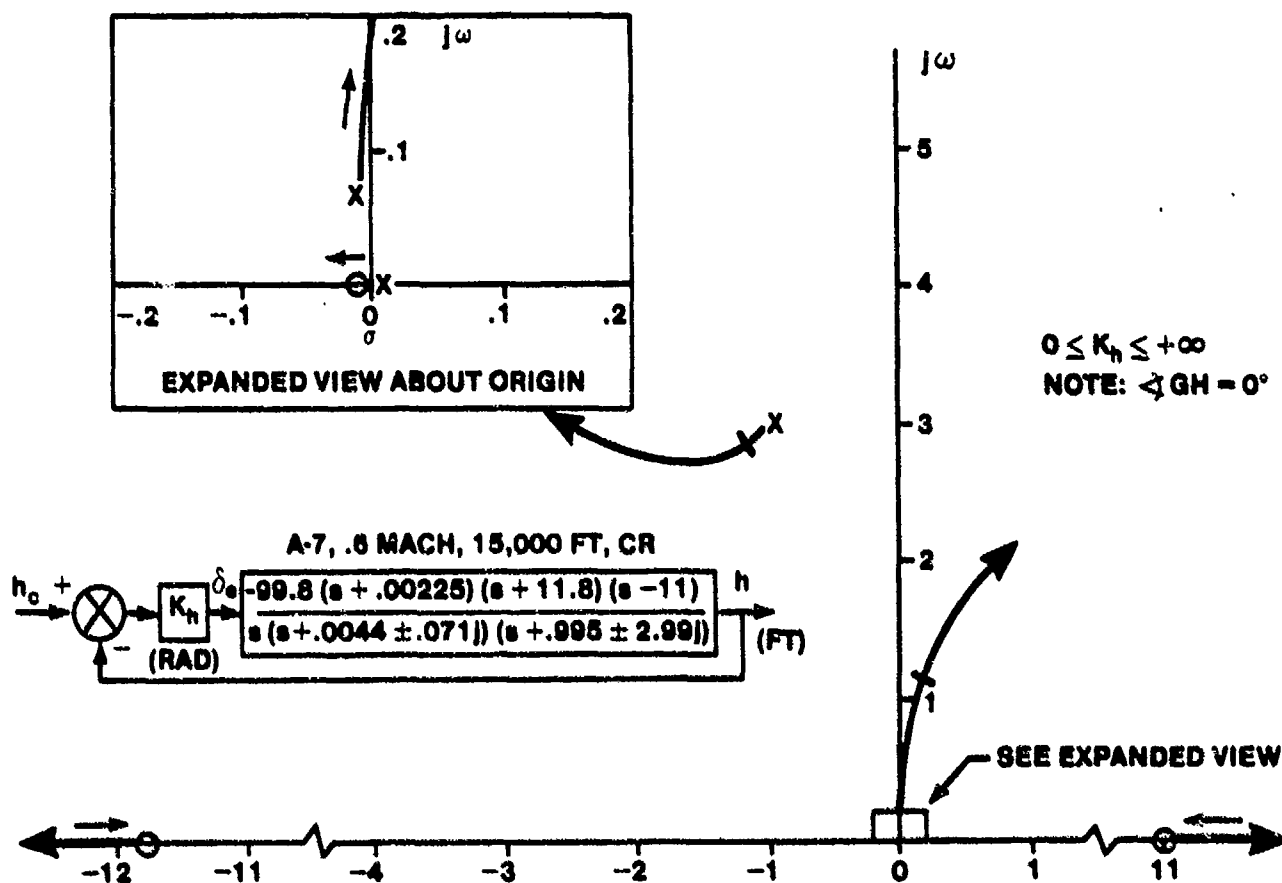
FIGURE 14.22. ROOT LOCUS PLOT OF ALTITUDE HOLD LOOP FOR AN AIRCRAFT WITH GOOD DYNAMICS

14.31

14.2.3 Elementary Lateral-Directional Feedback Control

The primary purpose of the lateral-directional stability augmentation system is to provide acceptable Dutch roll characteristics while retaining a sufficiently fast roll response for the aircraft. The spiral mode stability is often sacrificed in augmentation systems, since the pilot can easily control a slight tendency for the aircraft to increase its bank angle during a turn. Poor Dutch roll characteristics are usually quite annoying, especially if the aircraft is disturbed by turbulence or if the pilot is trying to perform tight tracking tasks such as formation flying, air-to-air or air-to-ground tracking, or approach and landing. Autopilots must provide stable roots for all the dynamic modes of the aircraft.

14.2.3.1 <u>Bank Angle Feedback to the Ailerons.</u> Bank angle and roll rate are the primary feedbacks used in single loop roll control systems. In cruising flight, the spiral mode time constant is typically very large and the aircraft can be either neutrally stable, slowly convergent, or slightly divergent. The neutrally stable or divergent spiral modes are unacceptable for unattended operation, and the slowly convergent spiral mode is only slightly better. One purpose of the lateral autopilot is to provide a higher degree of spiral stability. This is achieved through the use of roll angle feedback, which effectively creates roll static stability. Bank angle stability is also provided with this system, and a tendency to maintain the roll attitude orientation of the aircraft in the presence of turbulence is gained. Automatic pilot bank angle guidance commands can be imposed on the system for flight path control, a necessary capability for automatic landing systems.

Figure 14.23 shows the root locus of a bank angle feedback for the A-7D which has good rolling characteristics. The proximity of the numerator zeros to the Dutch roll roots indicates that very little aileron excitation of the Dutch roll dynamics occurs. The performance of the roll attitude hold system shows promise for relatively low gain. The spiral mode of the unaugmented aircraft is slightly stable but unacceptably slow to converge. The augmentation system decreases the convergence time by moving the root further to the left. This is accomplished at the expense of the roll mode time constant, which increases with increasing gain. For somewhat higher gain, the

spiral mode and roll mode roots combine and separate from the real axis. For moderate gain, a well damped oscillatory pair are provided, with damping decreasing and natural frequency increasing as the gain increases.

Figure 14.24 presents the root locus for the C-5 in which the Dutch roll dynamics are not well suppressed by the numerator zeros. The roll mode and spiral mode roots behave in a similar manner to the previous case for low to moderate gains. The Dutch roll roots, however, move slightly towards a higher natural frequency. The Dutch roll damping increases slightly for low gains, but then decreases steadily as the natural frequency increases with increasing gain. The roll angle feedback is not successful in suppressing Dutch roll dynamics and poor lateral ride quality could be expected.
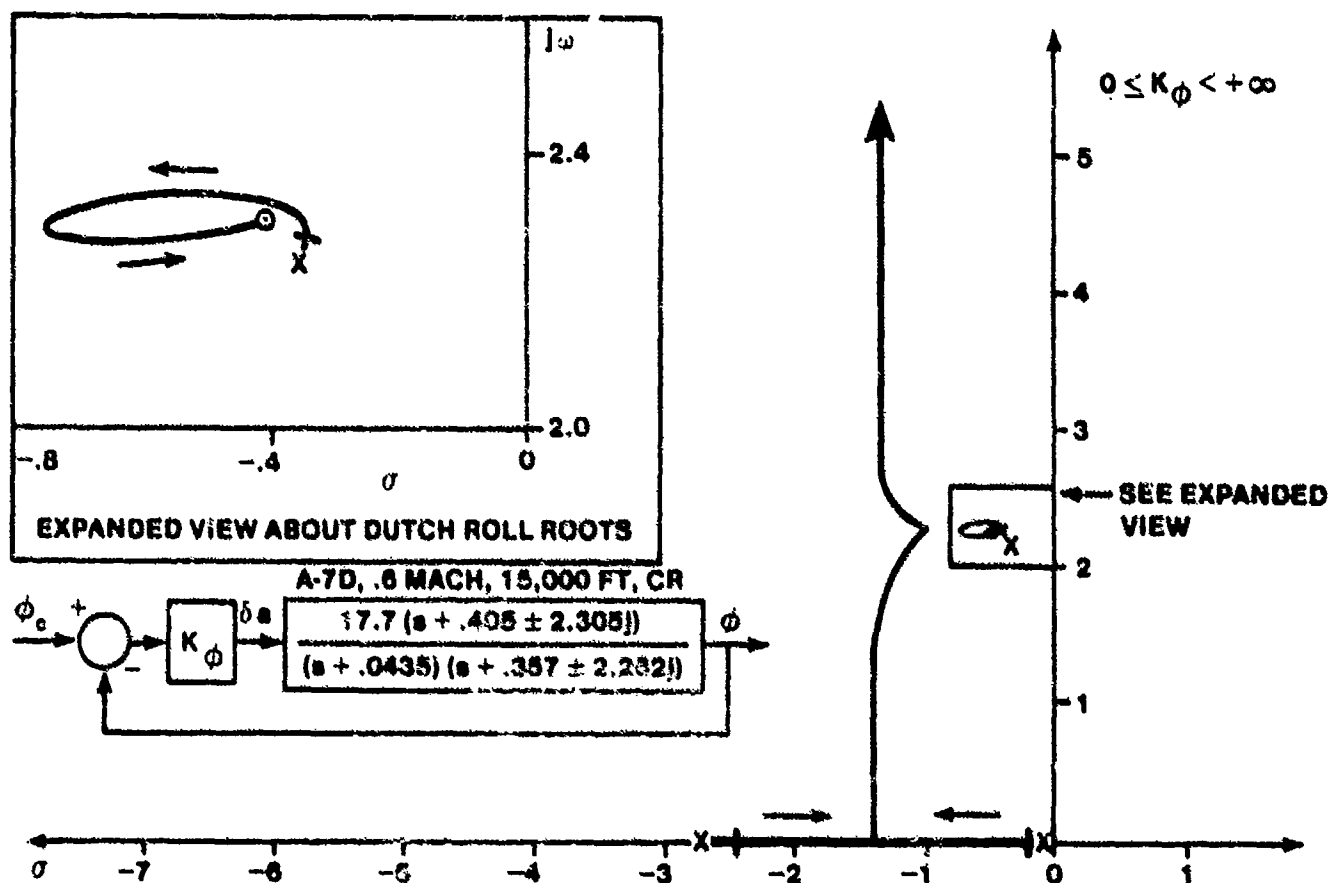
FIGURE 14.23. ROOT LOCUS PLOT OF ROLL ANGLE FEEDBACK TO AILERONS LOOP WITH SUPPRESSED DUTCH ROLL DYNAMICS

14.33

C·5A, .22 MACH, S.L., PA

$$\frac{.464\ (s + .165 \pm .411j)}{(s + .03)(s + 1.13)(s + .12 \pm .52j)}$$

ϕ_c + K_ϕ δ_a ϕ

$0 \leq K_\phi < +\infty$

$j\omega$

2

1

.5

σ

3

2

1

0
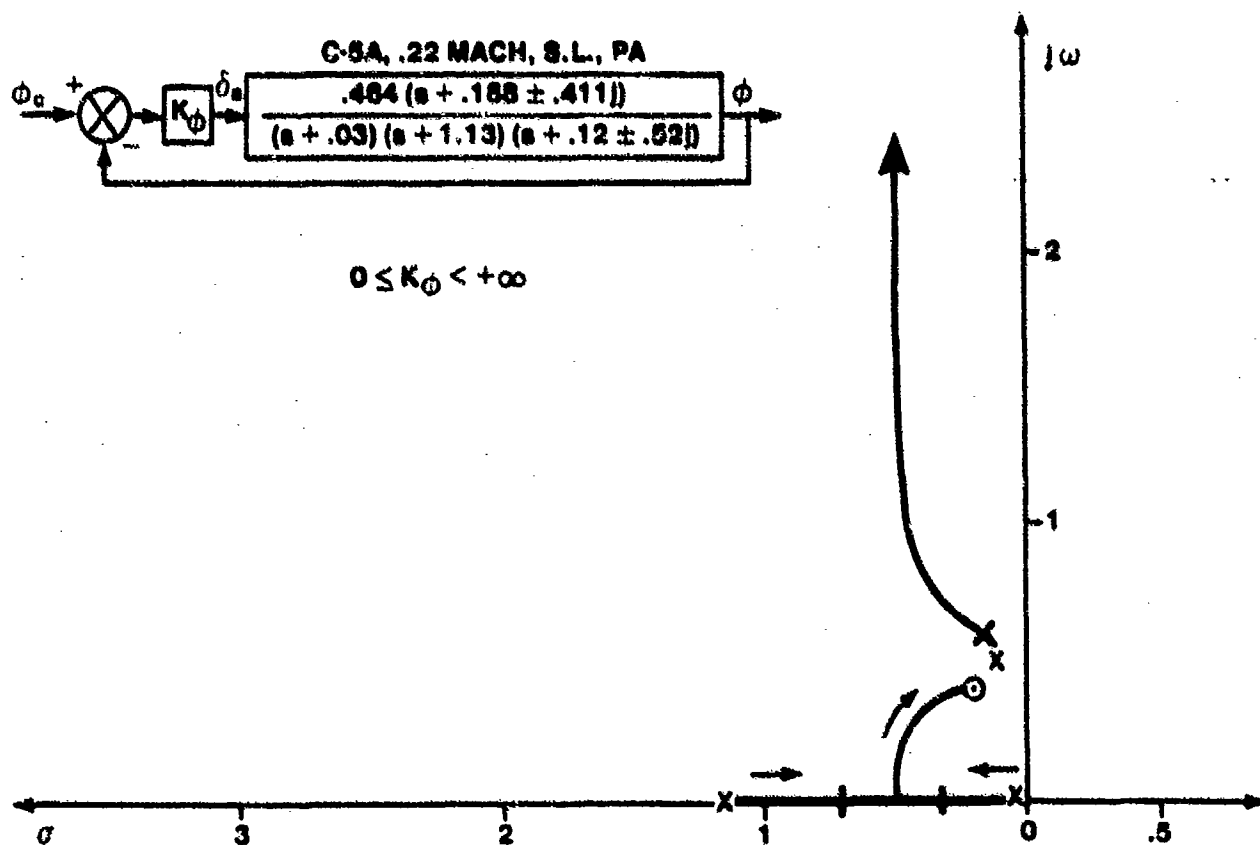
FIGURE 14.24. ROOT LOCUS PLOT OF ROLL ANGLE FEEDBACK TO THE AILERONS LOOP

14.2.3.2 <u>Roll Rate Feedback to the Ailerons</u>. As seen in the C-5 example of the last section, a roll control system based on roll angle feedback is often inadequate from the standpoint of tightness of control (good damping and reasonably fast response time) in response to disturbances and commands. This is due to the fact that, with pure roll attitude feedback, the open loop and closed loop total effective damping are the same. The total effective damping can be increased by feeding back a combination of roll angle and roll rate, such that the situation of Figure 14.23 is created.

Larger aircraft often employ roll dampers. The effect of the damper is to augment the roll damping derivative, L_p' which can reduce the

$$\phi/\beta \;=\; \left| \frac{L_\beta'}{N_\beta'} \right| \left[1 \Big/ \sqrt{1 + L_p'^2 \; N_\beta'} \right] \tag{14.14}$$

ratio of the Dutch roll mode if $\left| L_{p_{aug}}' \right| \Big/ \sqrt{N_\beta'} > 1$ where

$$L_{p_{aug}}' \;=\; L_p' - K_p L_{\delta_a}' \tag{14.15}$$

Modern fighters with full control augmentation systems use roll rate command systems for lateral control. Figure 14.25 shows the effect of a roll rate command system on the C-5A in the power approach configuration. The Dutch roll mode is effectively suppressed for relatively low values of gain. The roll mode time constant decreases slightly (maximum roll acceleration increases). The spiral mode is destabilized and, for high gain, may become unstable, although spiral dynamics which can be easily controlled by the pilot are retained.

C-5A, .22 MACH, S.L., PA
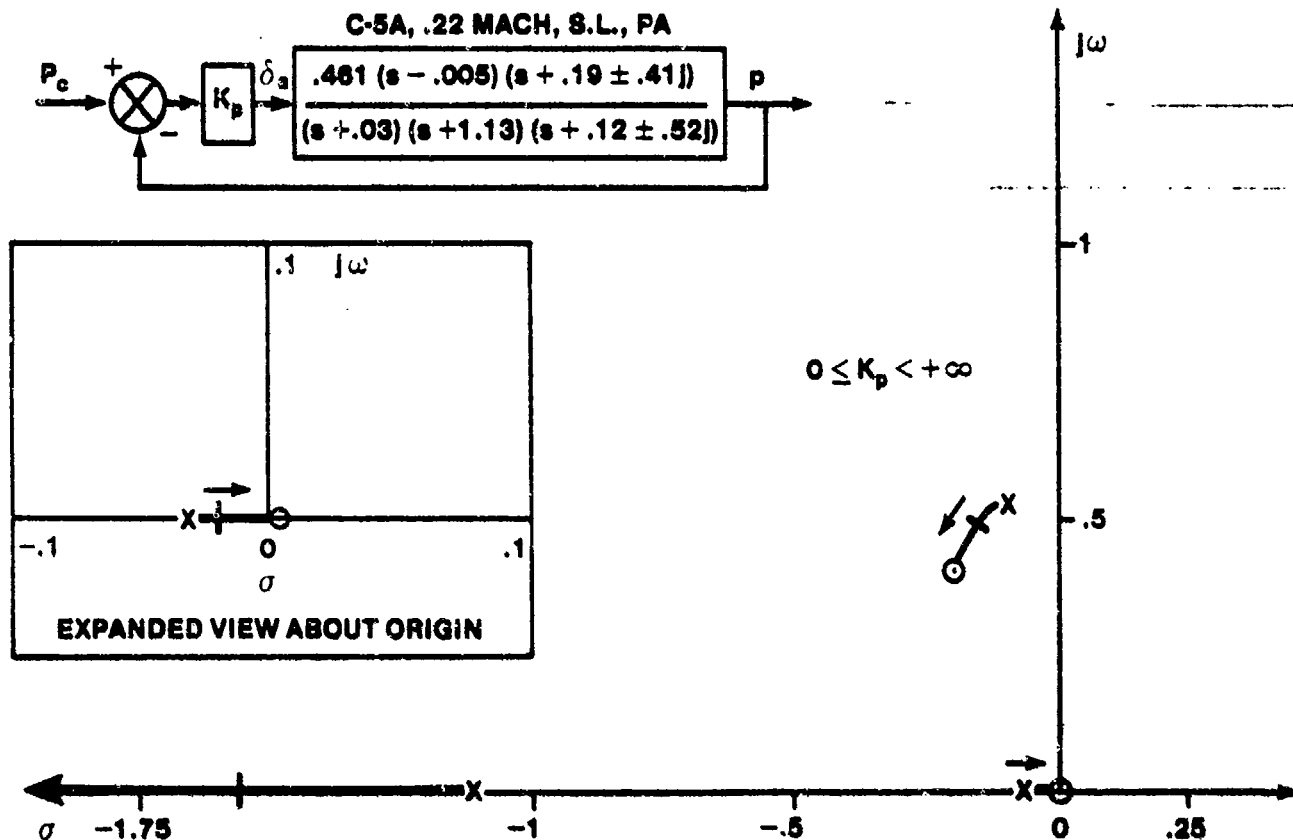
FIGURE 14.25. ROOT LOCUS PLOT OF ROLL RATE FEEDBACK TO THE AILERONS LOOP

14.2.3.3 Sideslip Angle or Yaw Rate Feedback to the Ailerons. These two feedbacks may be used under certain conditions if the aircraft possesses favorable characteristics for their employment.

The use of sideslip angle as a feedback to the ailerons alters the L_β' and N_β' stability derivatives and is seldom used (not used in any modern military aircraft). Sideslip angle feedback to the ailerons can provide some good features, such as spiral mode stabilization (increased effective

14.36

dihedral), but is usually accompanied by decreased Dutch roll damping or Dutch roll destabilization which outweigh the advantages, as shown in Figure 14.26.

C-5A, .22 MACH, S.L., PA

$$\beta_c \xrightarrow{+} \bigotimes \xrightarrow{} \boxed{K_\beta} \xrightarrow{\delta_a} \boxed{\frac{-.000443\,(s+.203)\,(s-2.75)\,(s+72.7)}{(s+.0283)\,(s+1.13)\,(s+.12\pm.52j)}} \xrightarrow{\beta}$$

$$0 \leq K_\beta \leq \infty$$

NOTE: GH = 0°

NOTE: AIRCRAFT POSSESSES PERVERSE YAW
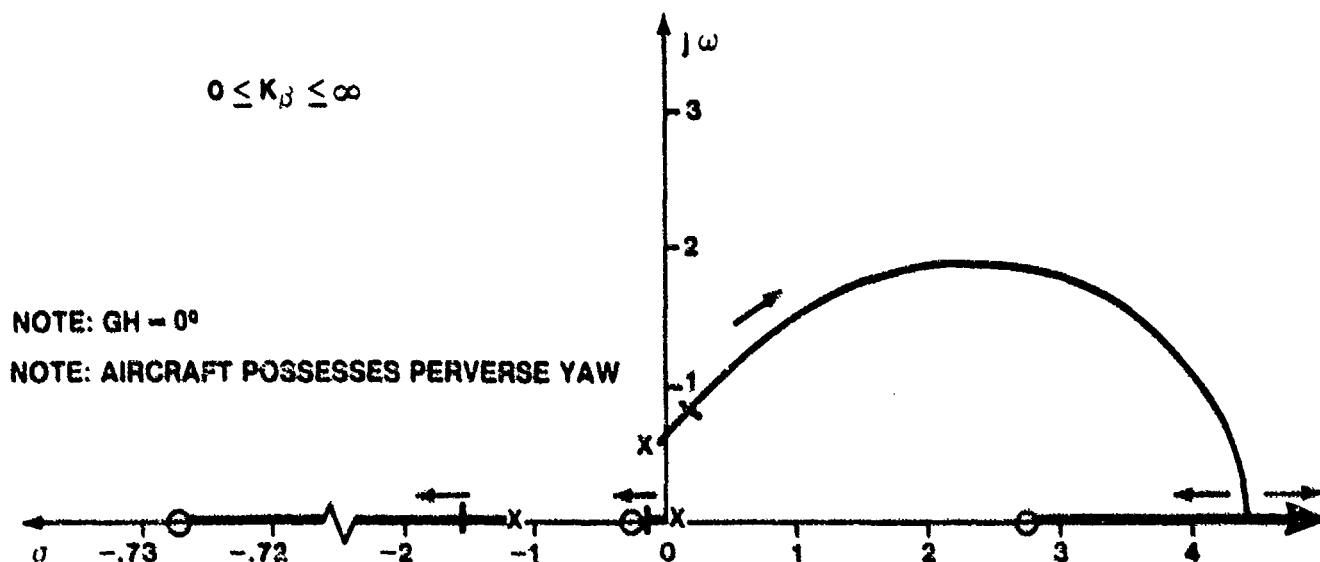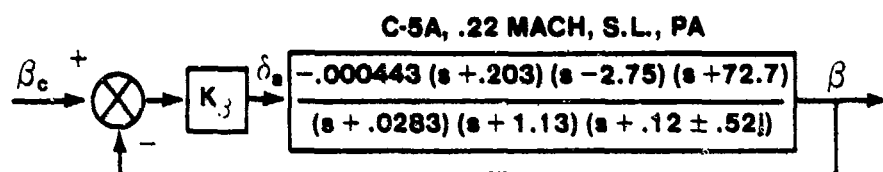
FIGURE 14.26.   ROOT LOCUS PLOT OF SIDESLIP ANGLE FEEDBACK TO THE AILERONS LOOP

The feedback of yaw rate to the ailerons can be an effective means of stabilizing the spiral mode by augmenting the L'_r derivative. If the basic aircraft possesses sufficient proverse yaw due to ailerons, the Dutch roll mode damping may also be improved, as shown in Figure 14.27. For the more common case of adverse yaw (or slight proverse yaw) due to the aileron, as shown in Figure 14.28, the yaw rate feedback gain cannot be increased too much without making the Dutch roll mode go unstable.
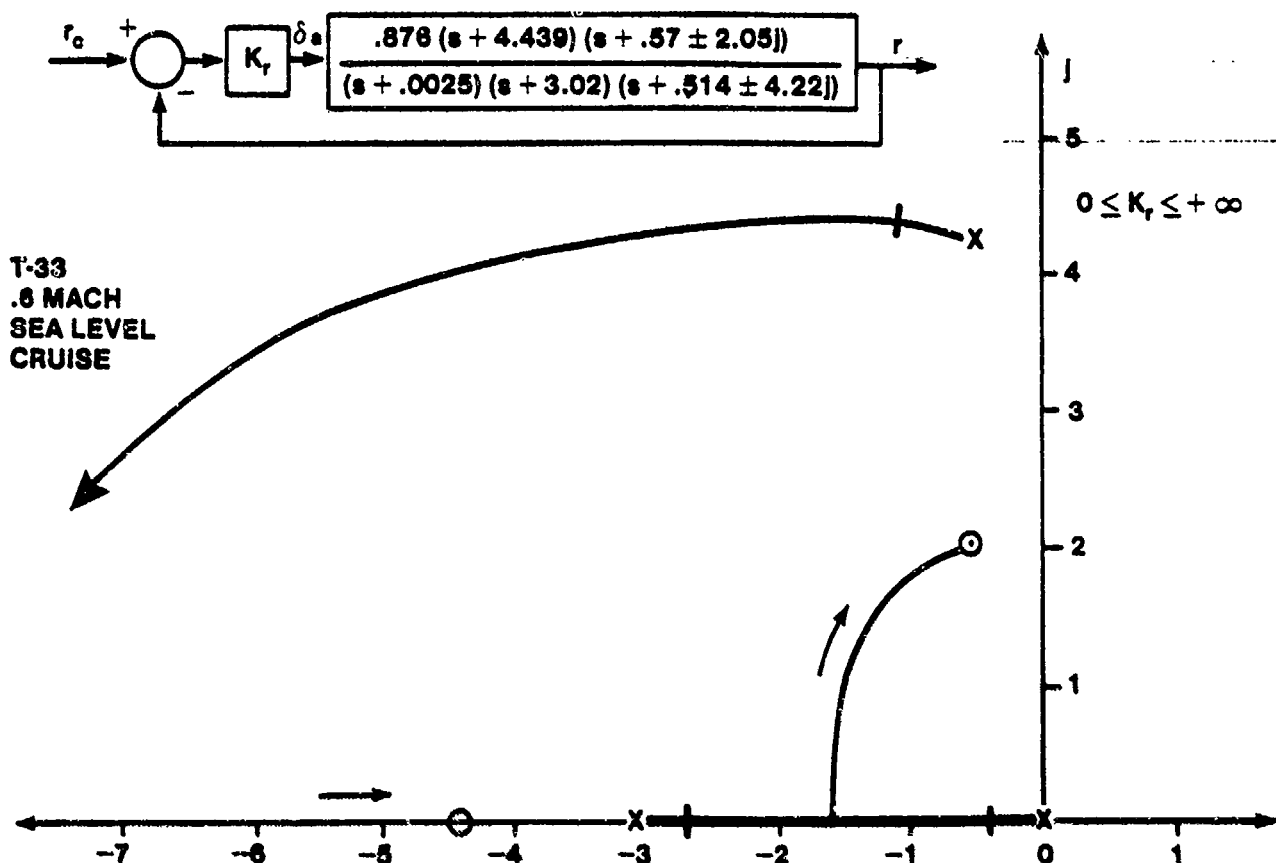
FIGURE 14.27. ROOT LOCUS PLOT OF YAW RATE FEEDBACK TO THE AILERONS LOOP
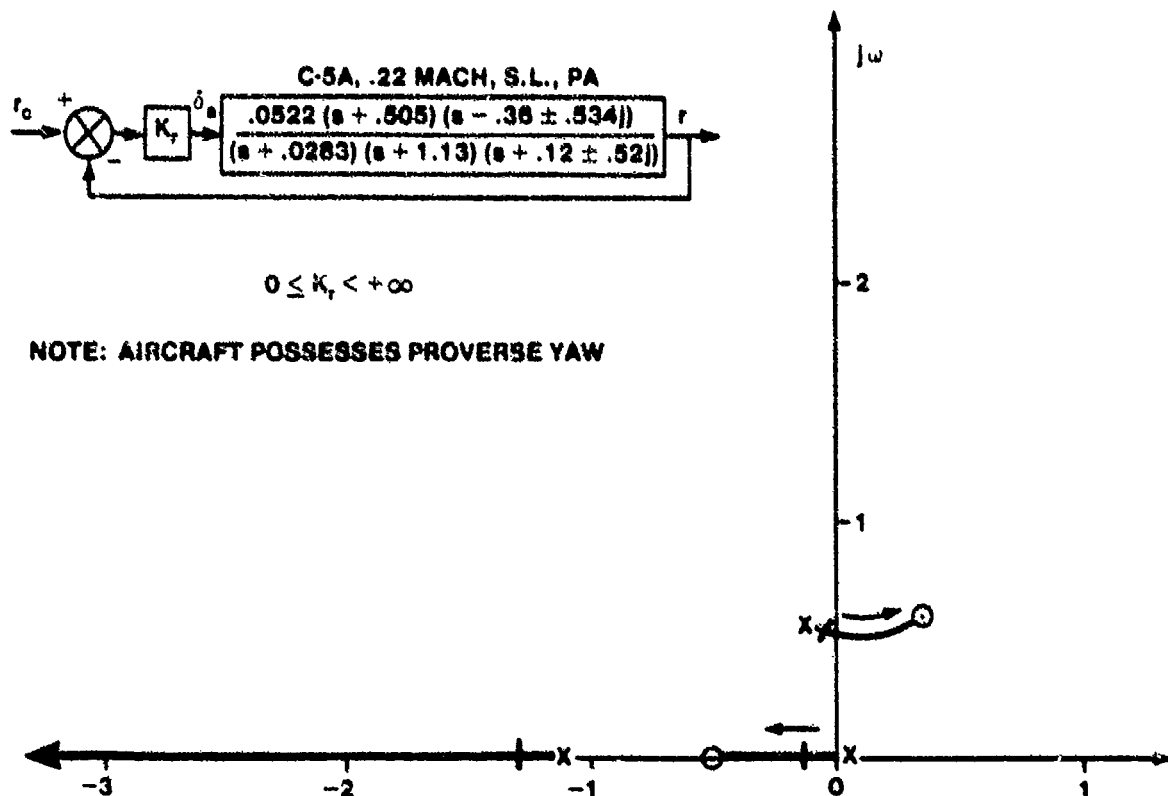
FIGURE 14.28. ROOT LOCUS PLOT OF YAW RATE FEEDBACK TO THE AILERONS LOOP

14.38

14.2.3.4 <u>Yaw Rate Feedback to the Rudder</u>. Yaw rate feedback to the rudder is commonly used to provide Dutch roll damping augmentation by increasing the magnitude of the N_r' derivative. The common mechanization is shown in Figure 14.30. The washout circuit acts as a highpass filter which does not allow the steady state (low frequency) yaw rate signals present in a steady turn to deflect the rudder from neutral. The transient signals (high frequency) present when the Dutch roll mode is excited are passed with unity gain and used to deflect the rudder to oppose the motion.

Figure 14.29 presents a yaw rate command system. The spiral mode is stabilized for low values of K_r and the Dutch roll damping increases rapidly as the gain increases. The roll mode time constant is not significantly affected for moderate values of gain but may decrease or increase slightly depending on the exact location of the real axis zero.
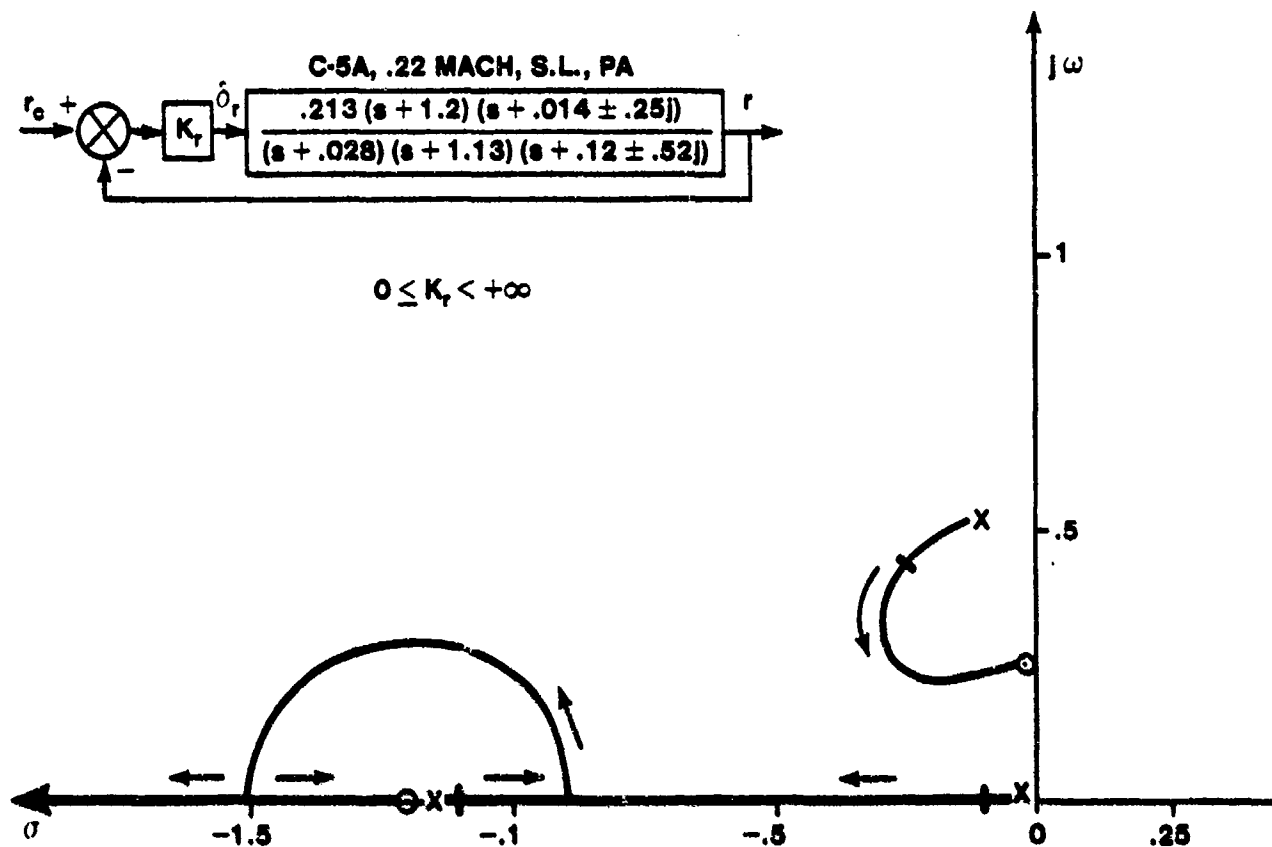
FIGURE 14.29. ROOT LOCUS PLOT OF YAW RATE FEEDBACK TO THE RUDDER LOOP
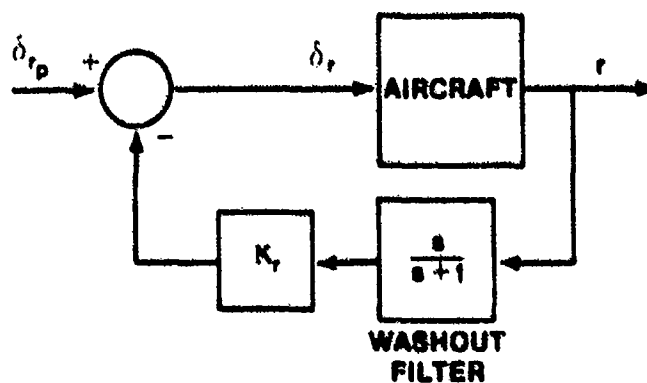
FIGURE 14.30. TYPICAL YAW DAMPER SYSTEM

14.2.3.5 <u>Sideslip Angle Feedback to the Rudder</u>. The feedback of sideslip angle to the rudder effectively augments the weathercock stability of the aircraft—the N'_β stability derivative. It is a useful way to provide aircraft coordination if properly implemented. Figure 14.31 shows the effect of sideslip angle feedback. The roll mode root location is not significantly altered. The spiral mode is destabilized but the time to double amplitude is long and is easily controlled by the pilot. The Dutch roll damping ratio is not changed until high values of gain are used, but the natural frequency increases rapidly for low gain. To increase the Dutch roll damping, yaw rate or sideslip angle rate feedback may be added as an additional feedback loop. The main disadvantage of the sideslip angle system is the practical one of instrumenting high quality sideslip sensors.
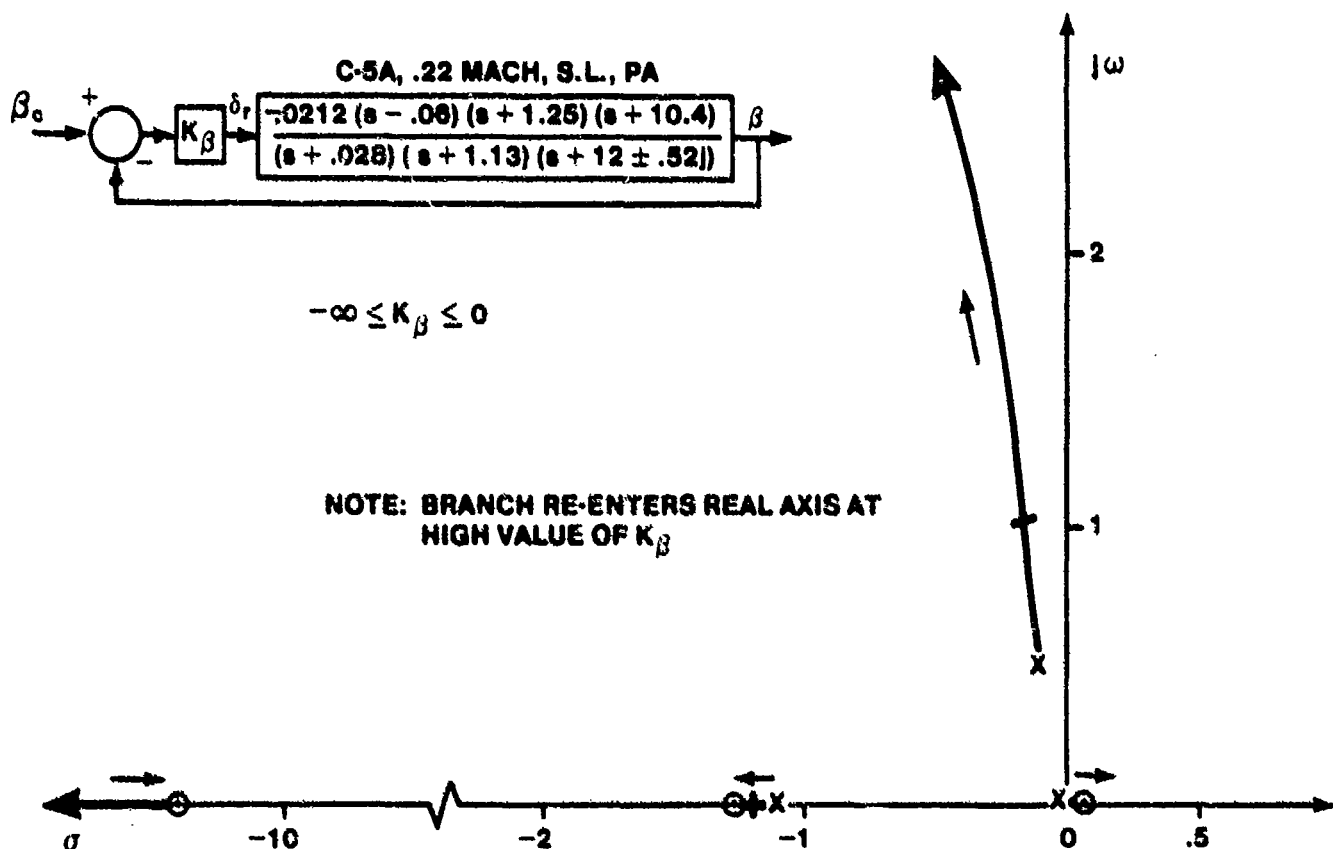
FIGURE 14.31. ROOT LOCUS PLOT OF SIDESLIP ANGLE FEEDBACK TO THE RUDDER LOOP

14.2.3.6 <u>Sideslip Angle Rate Feedback to the Rudder</u>. The use of computed sideslip angle rate feedback (commonly called a beta-dot system) to the rudder has been used extensively in fighter and attack aircraft, such as the A-10, F-16, and A-7D Digitac aircraft. The advantage of beta-dot feedback is that the aircraft can be made to roll about a depressed roll axis, usually slightly below the gun line, which can improve the aircraft handling qualities during aggressive maneuvers. Proper rudder coordination is applied by the augmentation system to keep the sideslip rate near zero.

The sideslip angle rate is computed from easily measured quantities as

$$\dot{\beta} = -r + \alpha p + \frac{g}{U_0} \sin \phi \cos \theta + \frac{a_{Y_{cg}}}{U_0} \qquad (U_0 = V_A) \qquad (14.16)$$

Often, if the gun line is designed to nearly coincide with the velocity vector of the aircraft, it is desirable to roll about an axis which is slightly depressed below the gun line to eliminate any pendulum effect in the fixed gunsight by providing initial pipper motion in the direction of the target as the roll is initiated. The estimate for sideslip angle rate is modified as

$$\dot{\beta} = -r + (\alpha + \alpha_B) p + \frac{g}{V_A} \sin \phi \cos \theta \qquad (14.17)$$

where α_B is a bias added to depress the roll axis below the relative velocity vector of the aircraft.

Often, the full equation is not used to estimate the sideslip angle rate. The system in the A-10 eliminates the pitch angle input into the equation, setting

$$\cos \theta = 1$$

When performing a loop or other vertical maneuver, the beta-dot system deflects the rudder fully whenever the aircraft nose passes through the verti-

cal, that is, whenever

$$\theta = \pm 90°$$

since the bank angle is undefined in this situation. The full authority rudder input causes a yaw transient. Implementations which do not use the full equation must be carefully studied to determine the impact of the simplification on the aircraft flying qualities.

Figure 14.32 presents a root locus plot of a sideslip angle rate feedback system. The Dutch roll mode damping is increased rapidly with increasing gain. The spiral and roll modes are hardly affected except for moderately large gain.
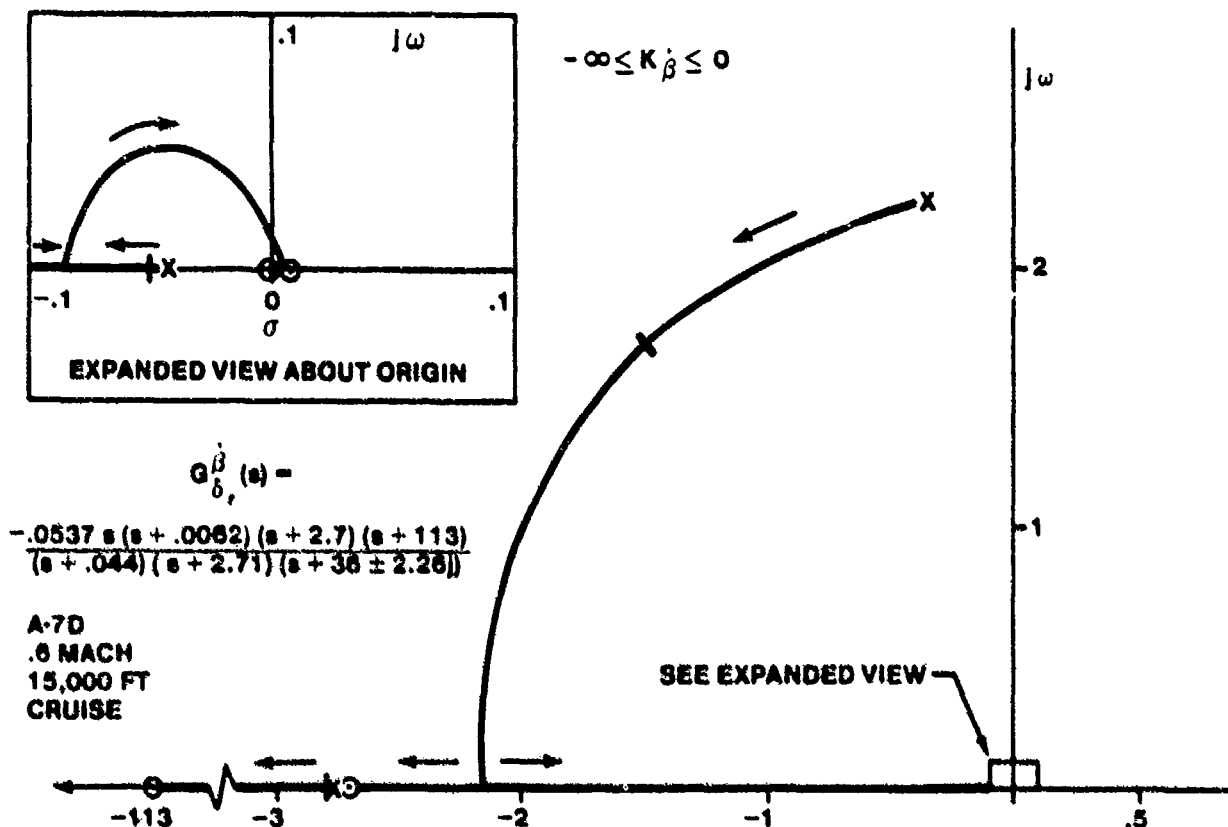
FIGURE 14.32. ROOT LOCUS PLOT OF SIDESLIP ANGLE RATE
FEEDBACK TO THE RUDDER LOOP

14.2.3.7 Lateral Acceleration Feedback to the Rudder. The difficulty in sensing sideslip angle can be overcome by using a properly located lateral accelerometer, where lateral acceleration can be expressed as (center of

14.43

gravity)

$$a_y = U_0 (\beta + r) - g \phi \cos \theta_0 \quad \text{(Stability Axis)} \qquad (14.18)$$

The accelerometer should be located close to

$$\ell_x = - Y_{\delta_r} N'_{\delta_r} \qquad (14.19)$$

so that the initial part of the lateral acceleration response to a step rudder input is proportional to the sideslip angle response due to a rudder deflection. This location corresponds to the instantaneous center of rotation about the Z body axis. The lateral acceleration feedback thus acts to provide aircraft coordination, and is used for this purpose in the A-7. Figure 14.33 shows the effect of lateral acceleration feedback with the accelerometer at the center of gravity. The effect of locating the lateral accelerometer away from the center of gravity will be discussed in Paragraph 14.3.
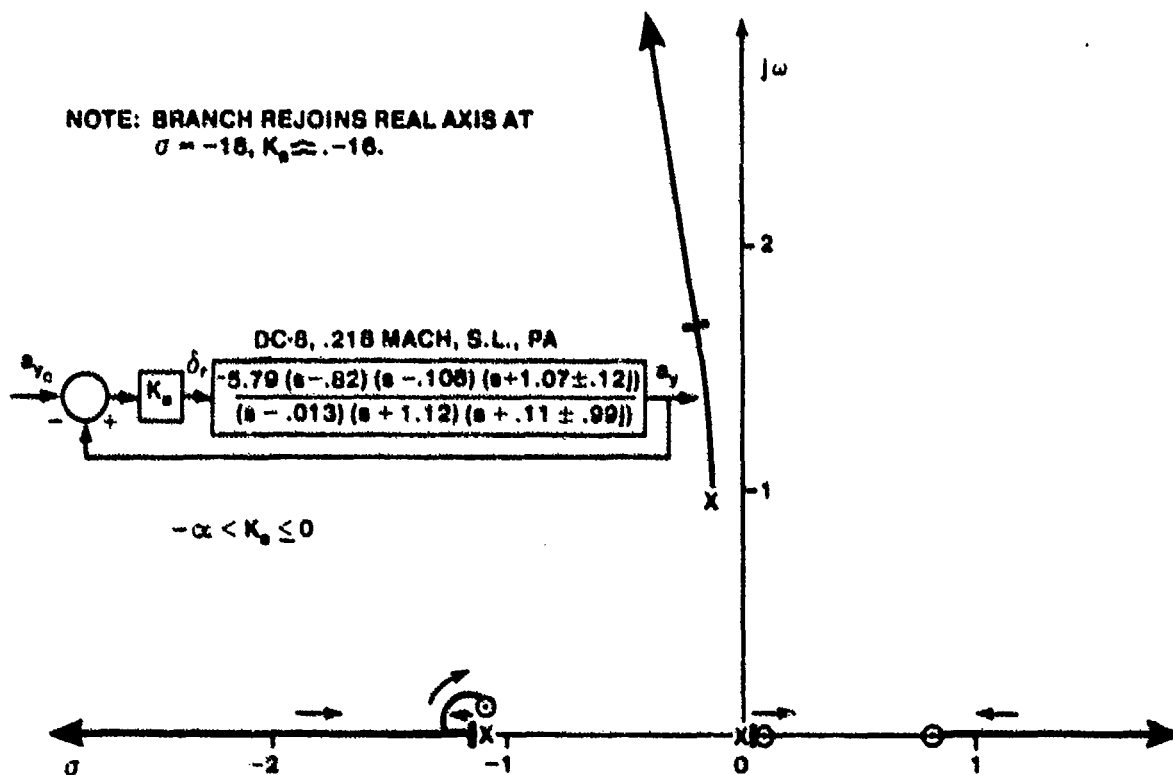
FIGURE 14.33. ROOT LOCUS PLOT OF LATERAL ACCELERATION
FEEDBACK TO THE RUDDER LOOP

14.44

14.2.4 Elementary Multiloop Compensation

Single parameter feedback strategies are common in less sophisticated flight control systems, where stability augmentation is the primary consideration. In single loop systems, if the desired flying qualities for the aircraft cannot be obtained as a result of the feedback strategy alone, then additional compensation (lead or lag filters) must be added to the flight control system. These additional compensator poles and zeros increase the order of the combined aircraft and flight control system, often causing an unanticipated degradation in flying qualities. Also, additional compensation is added to the flight control system to deal with difficulties such as structural resonance (flight control system excitation of the aircraft structure), sensor noise, or excessive steady state error.

The flying qualities of modern fighter aircraft are most frequently augmented through the feedback of two or more motion parameters to a single (or multiple) aerodynamic control surface. What is unique about the multiloop feedback approach is that the characteristics of the aircraft can be significantly altered to improve the flying qualities without introducing the additional poles and zeros of the compensators and filters. The best flight control systems will generally be the simplest--those that add a bare minimum of additional compensators and filters--relying instead on simple multiloop control strategies by taking advantage of the manner in which each feedback parameter influences the characteristic motions of the aircraft.

14.2.4.1 Pitch Rate and Pitch Angle Feedback to the Elevator. Pitch attitude feedback has the advantage of phugoid suppression and the disadvantage of reduction in short period damping. Pitch rate feedback has the advantages of increased short period damping and no effect on the phugoid mode. The advantages of both can be realized from the multiloop control system of Figure 14.34.

The composite root locus plot of Figure 14.35 clearly shows the advantages of the multiloop approach over both the single loop approaches for a typical autopilot application. The inner pitch rate loop increases the damping of the short period while not significantly altering the phugoid roots. The pitch attitude outer loop suppresses the phugoid roots. The combined effect yields improved short period damping and well suppressed phugoid motion.

Although this example is for an aircraft that exhibits classical aircraft properties, similar effects can be achieved in the presence of the unstable roots characteristic of the Mach tuck, an aft center of gravity or VTOL transition flight.
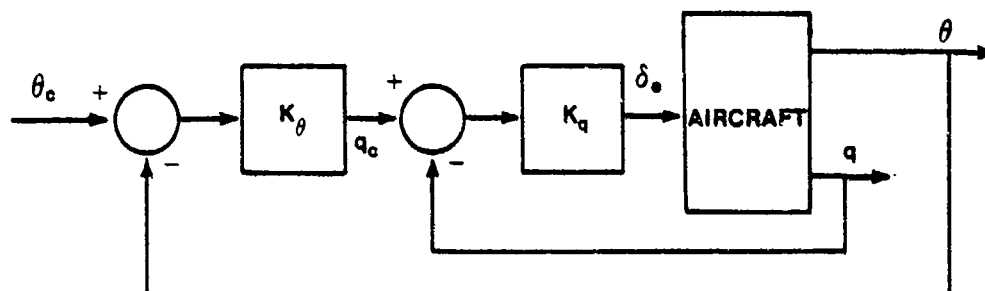
FIGURE 14.34. MULTILOOP PITCH ATTITUDE HOLD SYSTEM
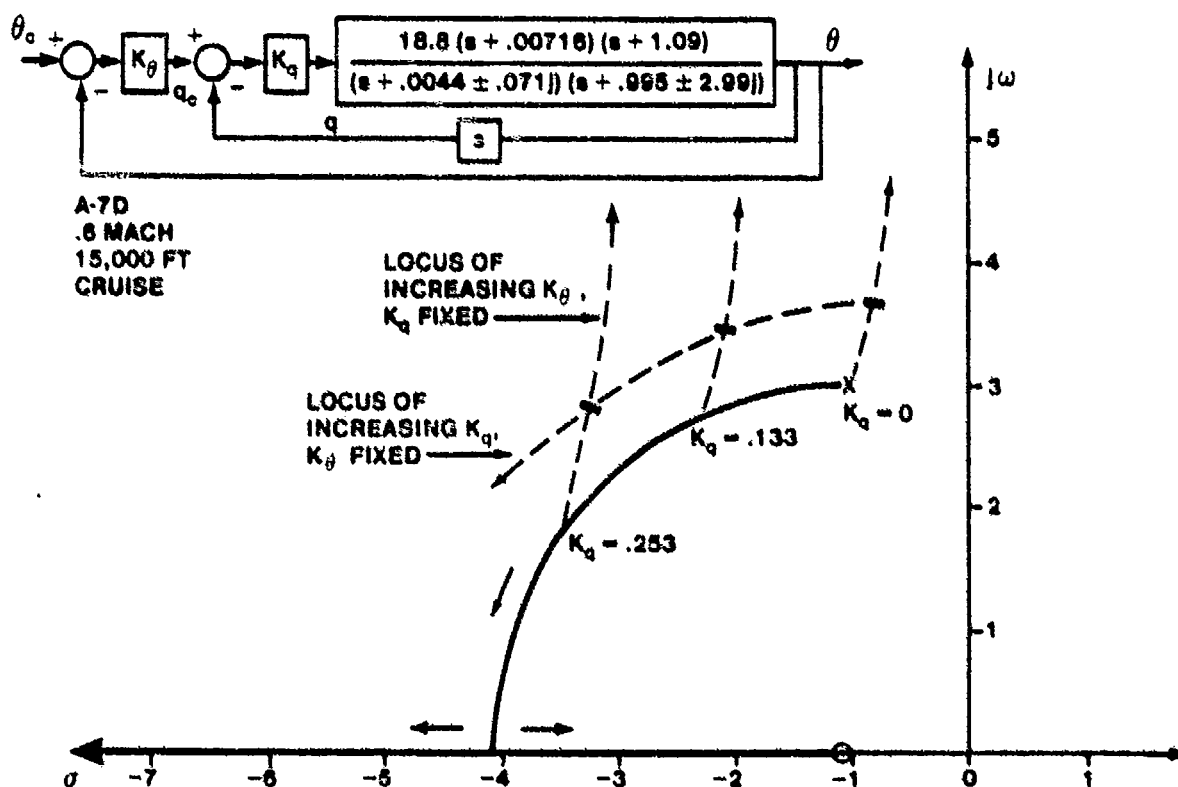
FIGURE 14.35. ROOT LOCUS PLOT OF SHORT PERIOD ROOT MIGRATION DUE TO PITCH RATE AND PITCH ATTITUDE FEEDBACK

14.2.4.2 Pitch Rate and Angle of Attack Feedback to the Elevator. Increased short period damping can also be achieved by feeding back pitch rate and angle of attack, as presented in Figure 14.36. This approach is more appropriate for piloted, versus autopilot-engaged, flight. Phugoid suppression does not occur in this situation since neither angle of attack nor pitch rate feedback are effective for this purpose. If normal acceleration is fed back as an outer loop parameter instead of angle of attack, the effect on the short period and phugoid roots is similar. An additional advantage of normal acceleration feedback is to help linearize the stick force gradient of the aircraft (used in the A-7D for this purpose).
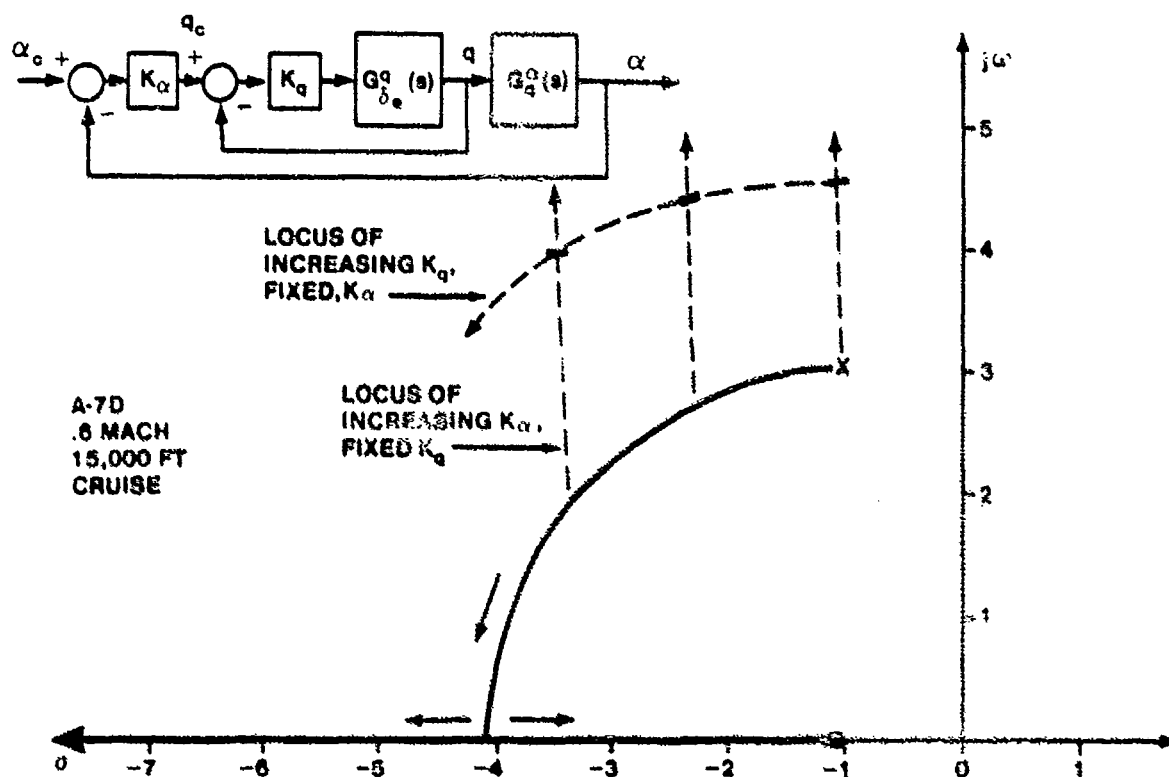
FIGURE 14.36. ROOT LOCUS PLOT OF SHORT PERIOD ROOT MIGRATION DUE TO PITCH RATE AND ANGLE OF ATTACK FEEDBACK

14.47

14.2.4.3 <u>Angle of Attack Rate and Angle of Attack Feedback to the Elevator.</u>
Angle of attack rate can be used for the inner loop instead of pitch rate to
achieve similar effects on the damping of the short period roots as those
achieved in the last section. Figure 14.38 presents the composite root locus
for an angle of attack rate and angle of attack system. The difficulty with
this system is in sensing the rate of change of angle of attack. It is almost
always inadvisable to attempt to differentiate the signal of a sensor since
noise and phase lag are introduced into the control system. One approach is
to compute the angle of attack rate from the equations of motion, using easily
measured parameters, as

$$\dot{\alpha} = \frac{1}{gU_0} (-n_z + \cos\theta \cos\phi) + \frac{g}{g} \qquad (14.20)$$

The nonlinear block diagram of Figure 14.37 can be used to compute the angle
of attack rate. Angle of attack rate is not currently used as a feedback
parameter except in some variable stability aircraft applications.
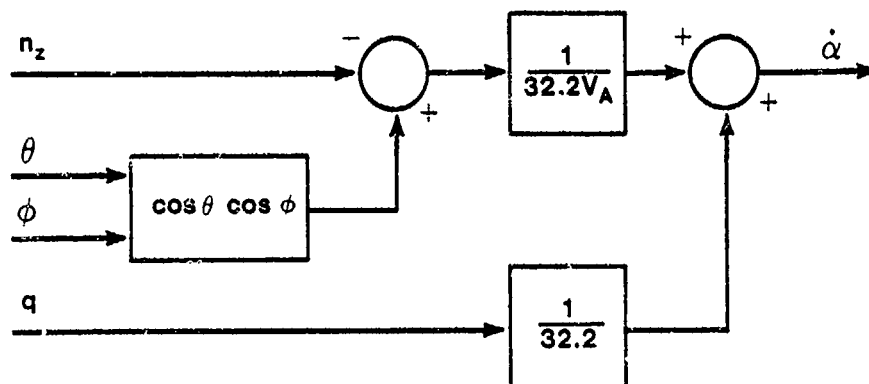
FIGURE 14.37. ANGLE OF ATTACK RATE COMPUTATION
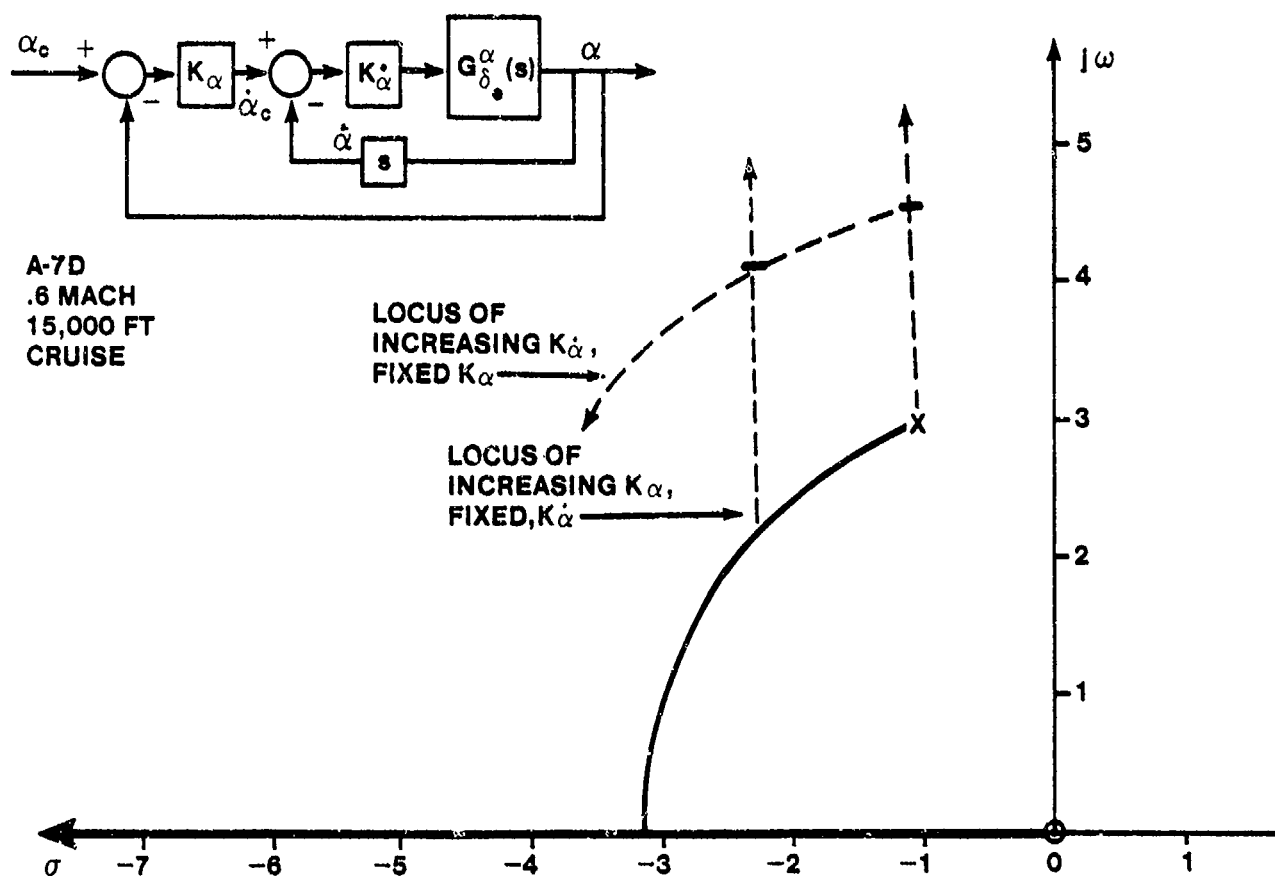
FIGURE 14.38. ROOT LOCUS PLOT OF SHORT PERIOD ROOT MIGRATION DUE TO ANGLE OF ATTACK AND AOA RATE FEEDBACK

14.2.4.4 <u>Altitude Rate and Altitude Feedback to the Elevator</u>. Paragraph 14.2.2.6 discussed the difficulties associated with the use of the elevator to control the aircraft's altitude. These difficulties can be avoided if the phugoid roots are suppressed by an inner altitude rate feedback loop. However, the short period roots are destabilized somewhat by altitude rate feedback. As can be seen from Figure 14.39, the inner altitude rate loop has the effect of moving the altitude low frequency roots from the right half well into the left half s-plane. The short period damping has decreased, however.

If altitude rate is computed as

$$\dot{h} = V_A (\theta - \alpha) \qquad (14.12)$$

then the perturbed altitude rate becomes

$$\dot{h} \cong u(\theta_0 - \alpha_0) + U_0(\theta - \alpha) \qquad (14.21)$$

If the airspeed perturbation is assumed small and the angle of attack is assumed nearly constant (as in the phugoid mode), such that

$$u \cong 0 \text{ and } \alpha \cong 0$$

then the perturbed altitude rate is proportional to the pitch attitude change. The aircraft altitude deviation can be fed back to the input of a pitch attitude hold system through a simple gain to achieve the same effect as the altitude rate plus altitude feedback scheme. A third pitch rate feedback loop could also be added to the pitch attitude system to improve the short period dynamics.
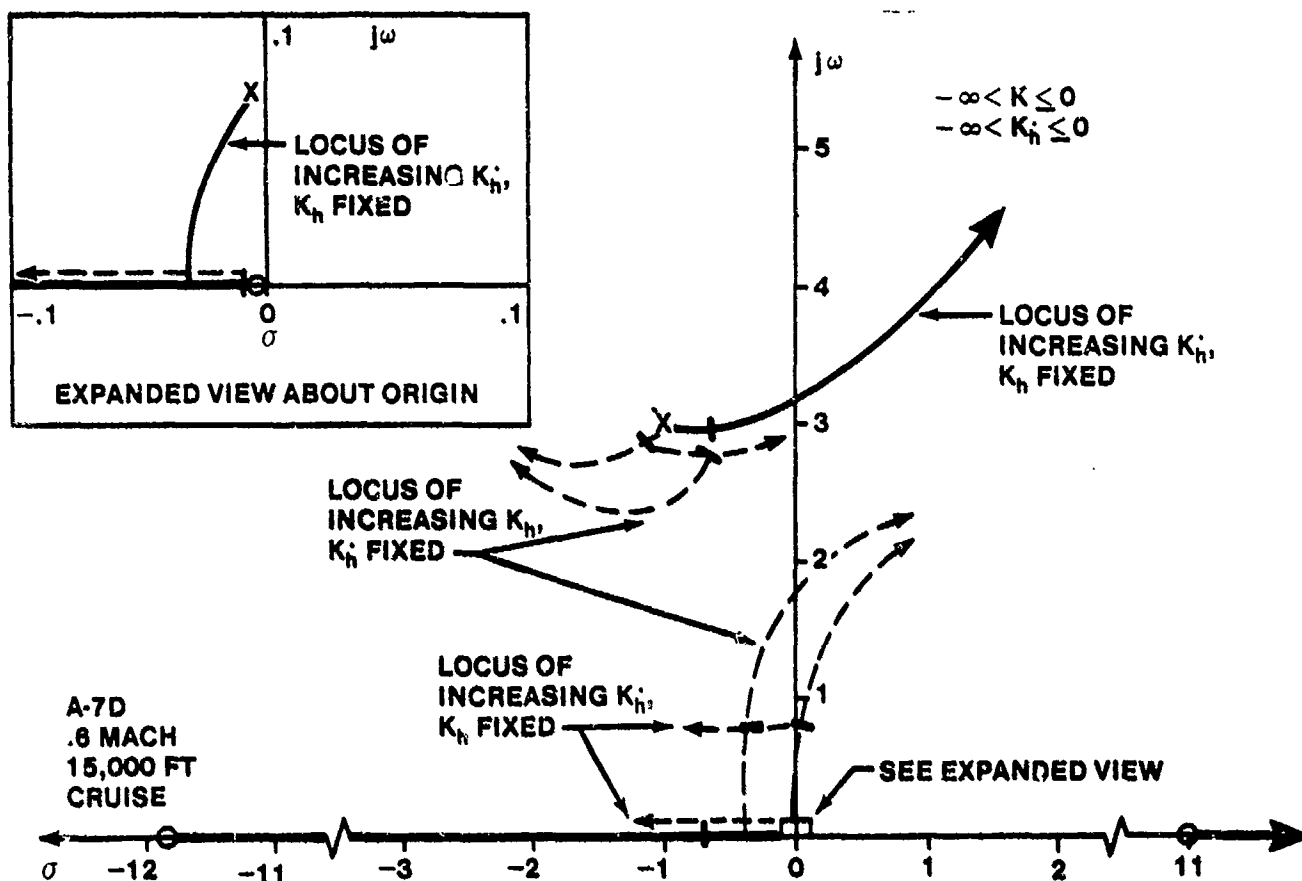
FIGURE 14.39. ROOT LOCUS PLOT OF ROOT MIGRATIONS DUE TO ALTITUDE AND ALTITUDE RATE MULTILOOP FEEDBACK

14.2.4.5 Roll Rate and Roll Attitude Feedback to the Ailerons. In the C-5 example of Paragraph 14.2.3.1, the Dutch roll roots were not well suppressed and the Dutch roll was not significantly altered by the augmentation system. Since the Dutch roll was lightly damped, objectionable bank angle oscillations could be expected. However, the Dutch roll roots of the A-7 example were reasonably well suppressed and would be expected to pose no problems. Roll rate feedback was shown to be effective in suppressing the Dutch roll motion which would otherwise be aggravated by aileron deflections. If roll rate is fed back as an inner loop to suppress the bank angle oscillation tendency of the C-5, and roll angle is fed back as an outer loop, the C-5 flying qualities could be improved (Figure 14.40).
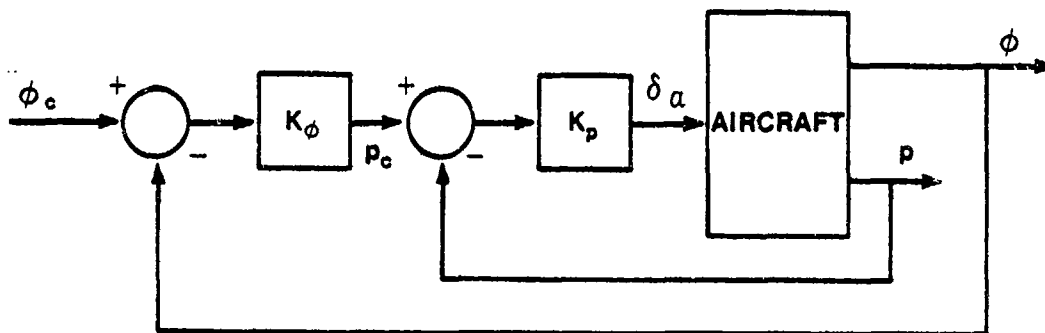
FIGURE 14.40.   ROLL ATTITUDE HOLD SYSTEM

14.2.4.6 Yaw Rate and Sideslip Angle Feedback to the Rudder. The purpose of
the washout filter in a typical yaw damper system was briefly discussed in
Paragraph 14.2.3.4. Yaw rate feedback, by itself, cannot eliminate a residual
sideslip angle during air-to-ground gunnery. Since this residual sideslip
angle greatly affects gunnery accuracy, coordination is required. The pilot
frequently has difficulty providing this coordination during minimum tracking
time attacks (curvilinear approach). Sideslip angle or lateral acceleration
feedbacks may be used to provide the desired coordination during strafing or
bombing. Figure 14.41 presents a composite root locus plot of a yaw rate and
sideslip angle multiloop feedback system. The yaw rate feedback, for low to
moderate gains, significantly increases the Dutch roll damping while not
altering the natural frequency. The Dutch roll roots can be moved
sufficiently far into the left half s-plane to provide heavy damping while the
sideslip angle feedback can improve the weathercock stability (turn
coordination) of the aircraft.
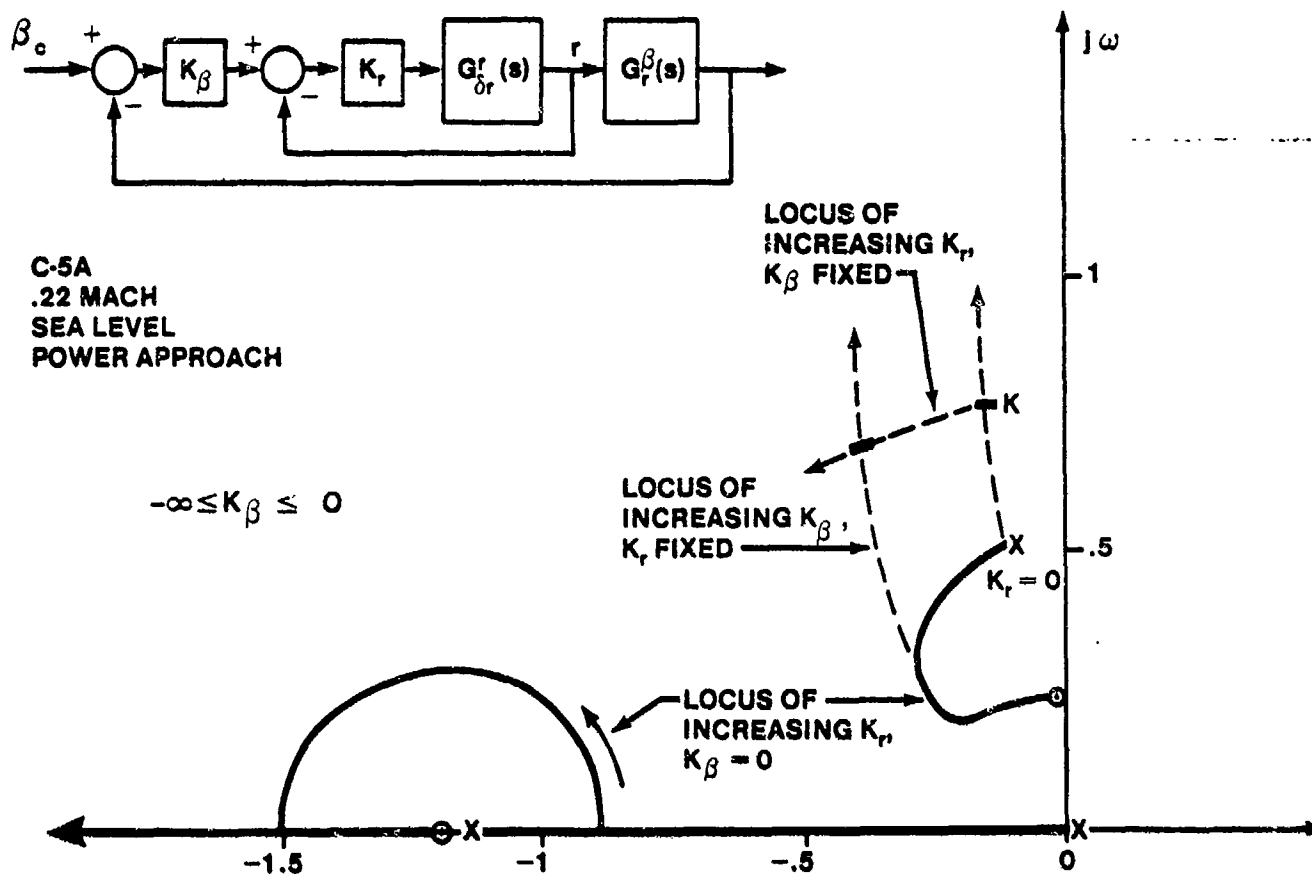
FIGURE 14.41.   ROOT LOCUS PLOT OF ROOT MIGRATIONS DUE TO YAW RATE AND SIDESLIP
ANGLE FEEDBACK

14.2.5 Summary

Table 14.3 summarizes single loop feedback control law effects on the
characteristic roots of the aircraft.   The effects of multiple loop systems
can be deduced from the effects of the individual loops.   Reference 14.1,
Chapters 7 and 8, contains an excellent in depth analysis of elementary
longitudinal and lateral-directional feedback control for aircraft.

TABLE 14.3

Summary of Aircraft Feedback Control Law Effects on the
Aircraft Characteristic Modes of Motion

1. Longitudinal Axis

Feedback Law	Effect on Short Period	Effect on Phugoid	Augmented Derivative	Figure
$\theta \rightarrow \delta_e$	Somewhat degraded characteristics-- damping slightly reduced, natural frequency slightly increased	Rapidly suppressed-- damping improves rapidly, two real axis roots appear		14.7(b)
	Stabilizes aircraft with aft C.G.	Stabilizes tuck mode		14.8 14.9
$q \rightarrow \delta_e$	Damping increases rapidly with gain, natural frequency slightly increased	Very little change--slightly reduced natural frequency	$M_{q_{AUG}} =$ $M_q + K_q M_{\delta_e}$	14.13
		Cannot stabilize tuck mode or aircraft with aft C.G. without compensation		14.14 14.15
$\alpha \rightarrow \delta_e$	Natural frequency increases rapidly with gain, damping ratio remains nearly constant except at very high gain	Very little effect-- natural frequency slightly reduced	$M_{\alpha_{AUG}} =$ $M_\alpha + K_\alpha M_{\delta_e}$	14.16 and 14.17
	Very effective in stabilizing aft C.G. aircraft, makes it look like conventional aircraft			

TABLE 14.3 (continued)

Summary of Aircraft Feedback Control Law Effects on the
Aircraft Characteristic Modes of Motion

Feedback Law	Effect on Short Period	Effect on Phugoid	Augmented Derivative	Figure
$n_z \rightarrow \delta_e$	Similar effects as AOA feedback-- natural frequency increases rapidly with gain, damping ratio not significantly affected	Little effect-- natural frequency somewhat reduced		14.18
$u \rightarrow \delta_e$	Not significantly affected--damping slightly reduced, natural frequency slightly increased	Greatly altered-- natural frequency rapidly increases with gain, damping improved somewhat	$M_{u_{AUG}} =$ $M_u - K_u M_{\delta_e}$	14.20
$h \rightarrow \delta_e$	Slight increase in damping ratio, natural frequency remains nearly constant	Driven unstable		14.22

2. Lateral-Directional Axes

Feedback Law	Effect on Dutch Roll	Effect on Roll Mode	Effect on Spiral Mode	Augmented Derivative	Figure
$\phi \rightarrow \delta_e$	If not excited by ailerons, no effect	Slightly increased time constant	Stabilized noticeably		14.23
	If excited by ailerons, damping increased slightly, natural frequency increased somewhat				14.24

TABLE 14.3 (continued)

Summary of Aircraft Feedback Control Law Effects on the
Aircraft Characteristic Modes of Motion

Feedback Law	Effect on Dutch Roll	Effect on Roll Mode	Effect on Spiral Mode	Augmented Derivative	Figure
$p \rightarrow \delta_a$	Suppresses excitation by aileron--damping increased somewhat, natural frequency decreased slightly	Time constant greatly reduced	Destabilized may go unstable	$L'_{p_{AUG}} =$ $L'_p - K_p L'_{\delta_a}$	14.25
$\beta \rightarrow \delta_a$	Destabilizes	Time constant decreases somewhat	Stabilized	$L'_{\beta_{AUG}} =$ $L'_\beta - K_\beta L'_{\delta_a}$	14.26
$r \rightarrow \delta_a$	Strong proverse Yaw--stabilizes	Time constant decreases somewhat	Stabilized		14.27
	Adverse or slight proverse Yaw--Destabilizes				14.28
$r \rightarrow \delta_r$	Damping increases greatly, natural frequency reduced somewhat	Time constant essentially unchanged	Stabilized somewhat	$N'_{r_{AUG}} =$ $N'_r + K_r N'_{\delta_r}$	14.31
$\beta \rightarrow \delta_r$	Natural frequency increases greatly, damping remains nearly constant	Time constant essentially unchanged	Destabilized	$N'_{\beta_{AUG}} =$ $N'_\beta - K_\beta N'_{\delta_r}$	14.31

TABLE 14.3 (continued)

Summary of Aircraft Feedback Control Law Effects on the
Aircraft Characteristic Modes of Motion

Feedback Law	Effect on Dutch Roll	Effect on Roll Mode	Effect on Spiral Mode	Augmented Derivative	Figure
$\beta \rightarrow \delta_r$	Natural frequency remains constant, damping greatly increased	Essentially unchanged	Very slightly stabilized		14.32
$n_y \rightarrow \delta_r$	Natural Frequency increases rapidly, damping remains essentially constant	Essentially Unchanged	Destabilized		14.33

14.3 FLIGHT CONTROL SYSTEM ELEMENTS

Complex flight control systems are comprised of various elements, from simple levers in mechanical systems to hydraulic actuators, washout filters, prefilters, sensors, electronic compensators and structural filters in full authority fly-by-wire systems.

14.3.1 Mechanical and Hydraulic Systems

14.3.1.1 Mechanical Systems. Conventional flight control systems use cables, rods, levers, bellcranks, and gears to transmit the pilot control stick or rudder pedal displacement to the aerodynamic control surface—or control actuator (in the case of hydraulically boosted or irreversible control systems). Additional elements, such as springs, dampers, and bobweights may be connected to the mechanical flight control system to improve the handling qualities of the aircraft by providing artificial feel. The F-15, which uses a parallel g-command electronic control augmentation system to improve

aircraft handling qualities, uses a bobweight in the mechanical path of its flight control system to provide acceleration feedback so that the mechanical system is a true load factor command system (zero steady state load factor error).

Figure 14.42 presents a simple mechanical control system for the A-10 ailerons. The system is made up of levers (control stick), bellcranks (devices which alter the direction of the applied force), rods and cables (which transmit the force over a distance), as well as electrical and hydraulic actuators (trim motor and walking beam control surface actuators respectively). The mechanical elements act as amplifiers and may be represented in a block diagram by a simple gain relating pilot control deflection to aerodynamic surface deflection. Figure 14.43 shows a simplified flight control system consisting of mechanical elements only. The stick deflection, y, is related to the rod movement, x as:

$$\frac{y}{x} = -\frac{a}{b} \qquad (14.22)$$

Bellcranks may have gains different than 1 if the two legs are of different lengths. For this example, both bellcranks have a gain of 1. Crossed cables have a net gain of -1. The surface deflection is related to the connecting rod deflection by

$$\sin \delta_e = -\frac{z}{\dfrac{r + \ell \tan \delta_e}{2}} \qquad (\ell \text{ usually zero}) \qquad (14.23)$$

which can be approximated as

$$\frac{z}{r} = -\delta_e \quad (\text{radians}) \qquad (14.24)$$

for small z. The block diagram of the system is shown in Figure 14.44.
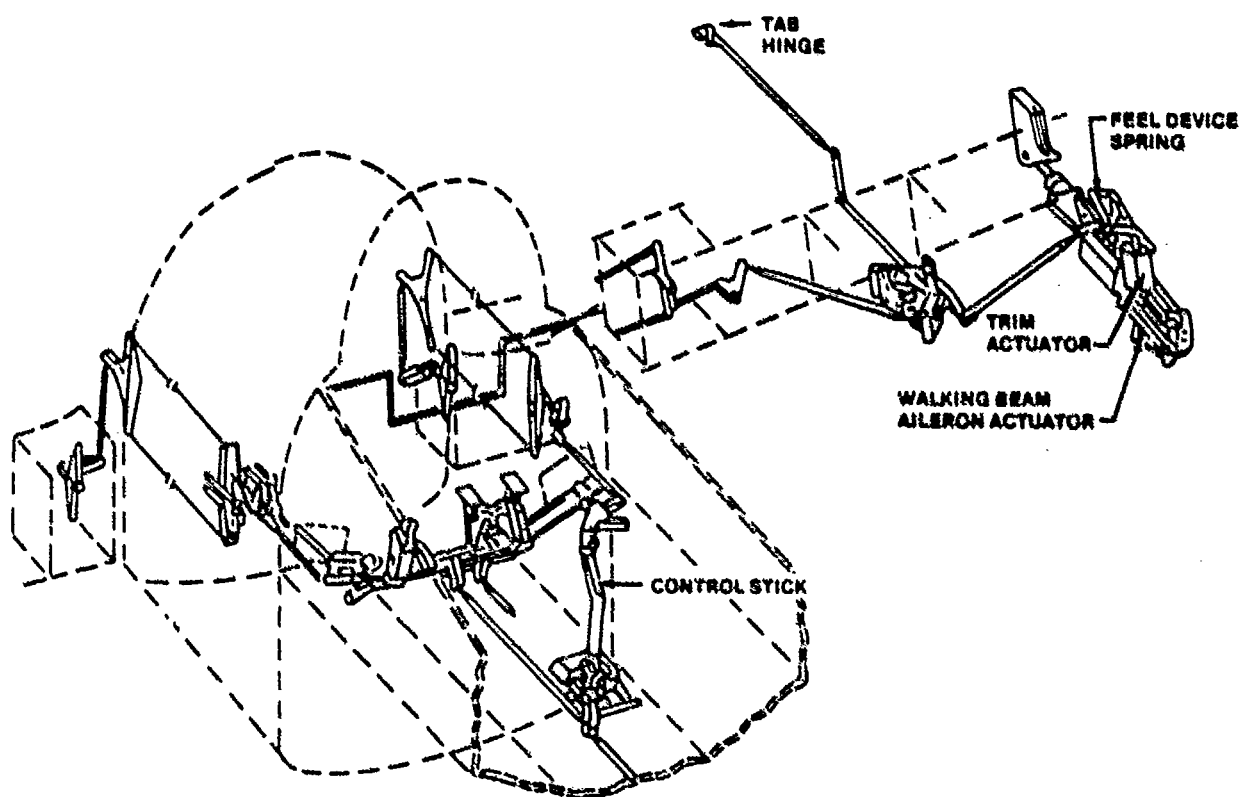
FIGURE 14.42.   SCHEMATIC DIAGRAM OF THE A-10 LATERAL CONTROL SYSTEM
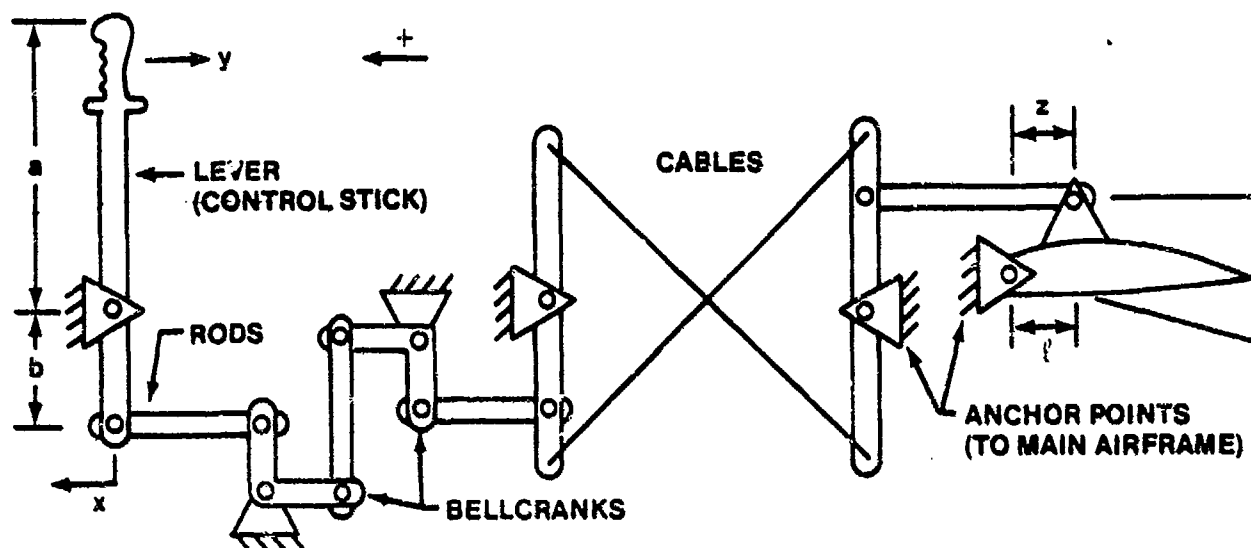
FIGURE 14.43. SIMPLE MECHANICAL FLIGHT CONTROL SYSTEM
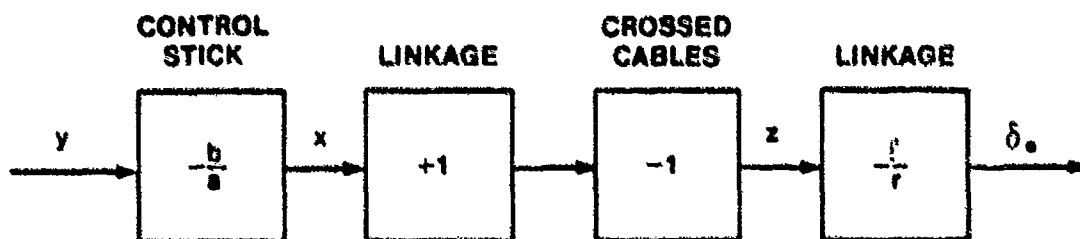
FIGURE 14.44. BLOCK DIAGRAM OF SIMPLE MECHANICAL FLIGHT CONTROL SYSTEM

In the F-15 pitch axis (Figure 14.45) the control stick deflection is sent directly to the hydraulic actuator through the ratio changer, a mechanical device that adjusts the stick to stabilator gearing as a function of dynamic pressure and Mach to keep the aircraft pitch response constant for a given stick deflection throughout the flight envelope. The air data system provides inputs to a device that adjusts the output rod position in the ratio changer slot, thus varying the gain of the ratio changer transfer function. The stick deflection is also sent to a mechanical accelerometer (bobweight) arrangement. This system senses an error between the commanded load factor (a function of stick position) and the actual load factor (as sensed by the bobweight). If the bobweight is displaced from the neutral position

the pitch trim compensator (a motor) activates to adjust the stabilator to correct to the commanded load factor. A block diagram of the system is shown in Figure 14.46. The spring and damper attached to the bobweight mechanism are omitted since they are a part of the mechanical accelerometer, the dynamics of which are negligible.
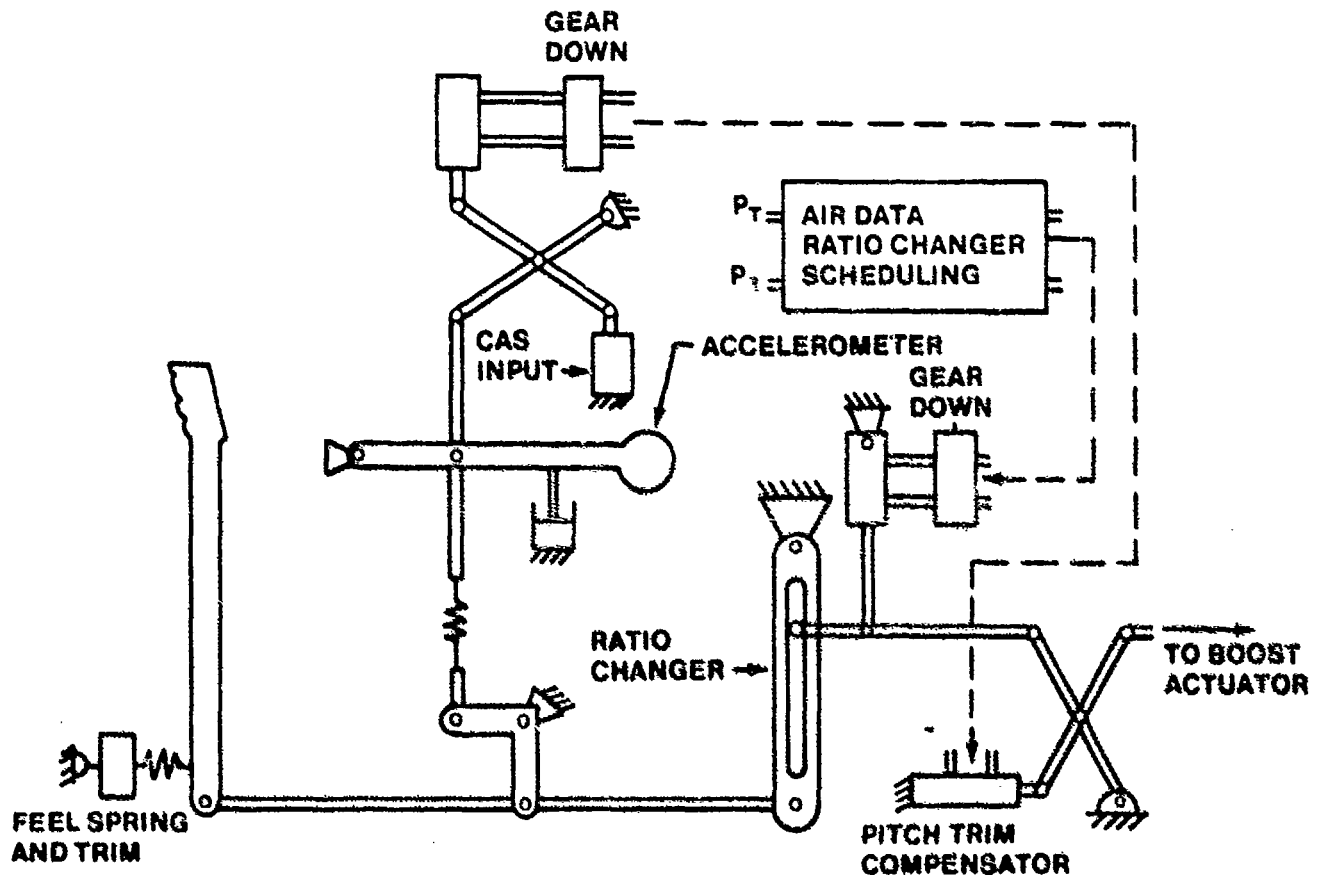
FIGURE 14.45. SCHEMATIC DIAGRAM OF THE F-15 LONGITUDINAL MECHANICAL CONTROL SYSTEM
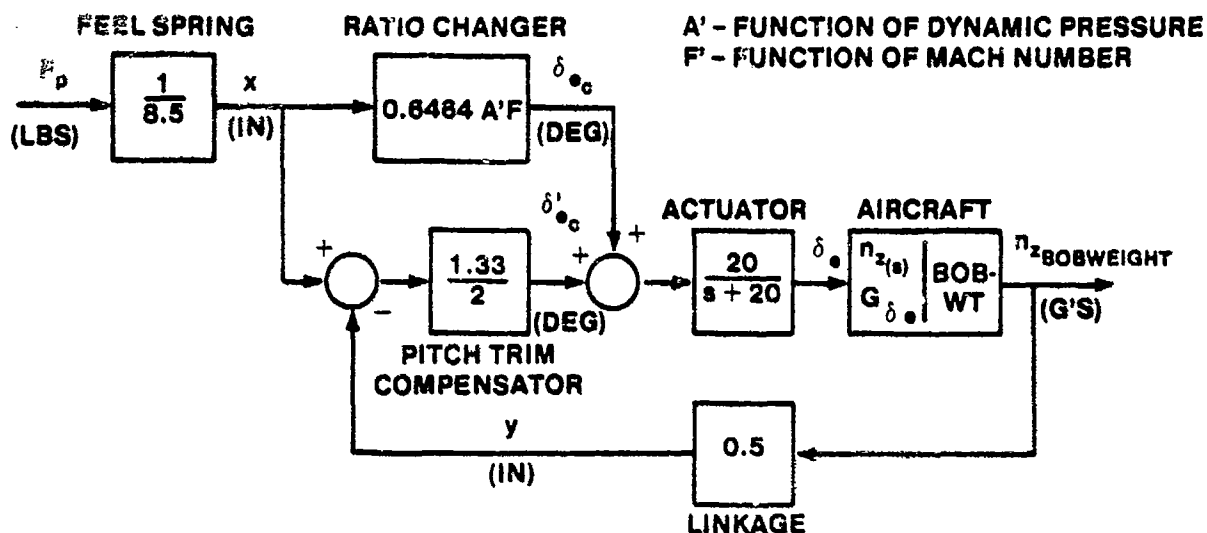
FIGURE 14.46. BLOCK DIAGRAM OF THE F-15 LONGITUDINAL MECHANICAL CONTROL SYSTEM

14.3.1.2 Hydraulic Systems. Figure 14.47 shows a schematic diagram of a typical hydraulic power actuator commonly used in high performance aircraft to deflect aerodynamic surfaces such as the primary flight controls, flaps, spoilers, and speedbrakes. A servo valve provides hydraulic fluid flow control to a power cylinder that amplifies the applied forces to move the control surface. The servo valve transforms a mechanical displacement to a fluid flow rate. The power cylinder transforms fluid pressure to a hinge moment to deflect the surface.

The control surface deflection is related to the power cylinder piston position as

$$y = \ell_1 \delta \qquad (14.25)$$

for small surface deflections, and the rate of hydraulic fluid flow into the power cylinder is related to the rate of piston movement as

$$Ay = q \qquad (14.26)$$

14.62
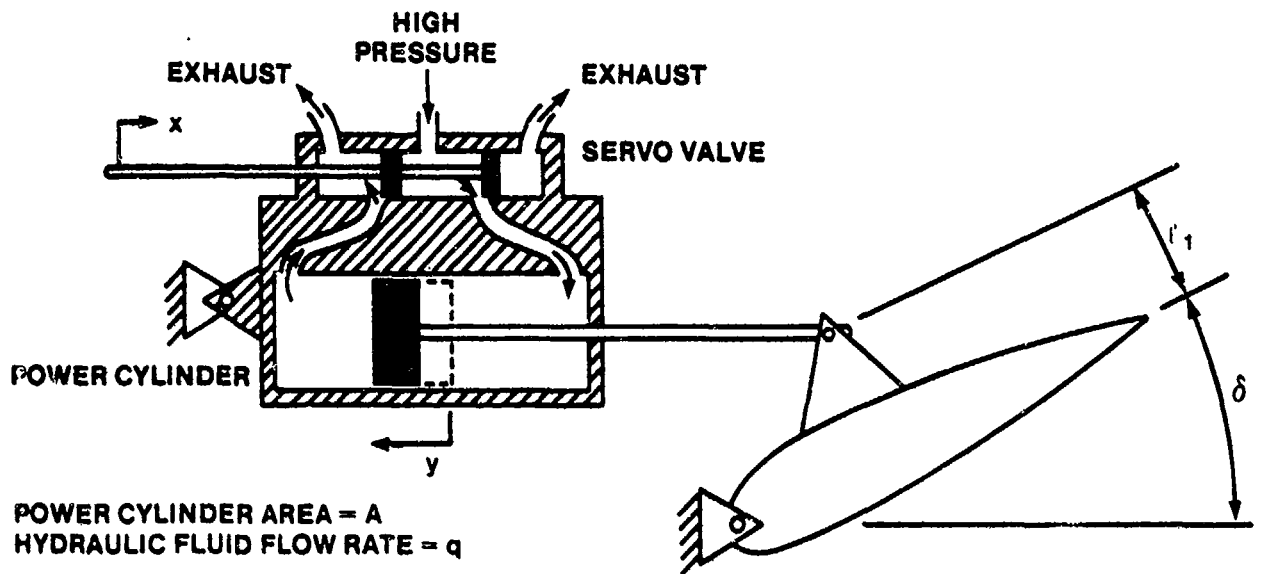
FIGURE 14.47.   SCHEMATIC DIAGRAM OF A HYDRAULIC ACTUATOR

The fluid flow rate through the series servo is assumed to be linear and may be expressed as a function of the displacement, x, as

$$q = Cx \qquad (14.27)$$

The transfer function between the aerodynamic surface deflection and the input mechanical rod displacement is derived as follows

$$\dot{y} = \ell_1 \dot{\delta} \qquad (14.28)$$

$$\frac{q}{A} = \ell_1 \dot{\delta} \qquad (14.29)$$

$$\frac{C}{A} x = \ell_1 \dot{\delta} \qquad (14.30)$$

$$\frac{\delta(s)}{x(s)} = \frac{C}{A\ell_1 s} = \frac{K}{s} \qquad (14.31)$$

The actuator is an integrator and a constant displacement of the valve results in a constant rate of change in the surface position.   This actuator response would be undesirable to a pilot since he would have to apply pulse inputs into the flight control system to obtain a change in elevator position.   Feedback

of the elevator position to the servo valve is required to change the integral action of the power cylinder so that the pilot input commands an aerodynamic surface position. This feedback can be accomplished mechanically or electrically.

Two implementations are possible--the actuator in parallel or in series with the pilot aerodynamic surface command. The parallel implementation is used in some mechanical flight control systems such as the T-33 and A-10 to boost the pilot command signals, thereby reducing the pilot control forces while providing a backup reversible control system capability. The series approach is used in irreversible flight control systems, such as systems in the T-38 and F-4. Aircraft with high authority control augmentation systems (A-7 and F-15) use a series actuator system which can be controlled mechanically and electrically--mechanically through the backup mechanical flight control system and electrically through the control augmentation system. Fly-by-wire aircraft, such as the F-16, control the hydraulic actuator electrically. The series servo position can be controlled electrically by either an electric motor or by a magnetic actuator.

Figure 14.46 shows a schematic of a manual boost servo configuration known as a walking beam actuator. The pilot command displacement, x, is applied to the walking beam. Initially, aerodynamic hinge moments effectively fix the mechanical feedback linkage from the aerodynamic surface to the walking beam so that the pilot input causes the servo valve to open. Hydraulic fluid causes the power cylinder to move, deflecting the aerodynamic surface. The mechanical linkage to the walking beam causes the walking beam to rotate about the fixed pilot input linkage, forcing the servo valve to close. Mathematically, the aerodynamic surface deflection is related to the piston movement as

$$\sin \epsilon = \frac{z}{\ell_3} \qquad (14.32)$$

which simplifies to

$$\epsilon = \frac{z}{\ell_3}$$

for small surface deflections. The servo valve position is related to the piston position and the pilot input linkage position as

$$y = \frac{\ell}{\ell_2} x - \frac{\ell_1}{\ell_2} z \qquad (14.33)$$

The rate of change of the piston position is related to the fluid flow rate (which is related to the servo valve position) as

$$A\dot{z} = q = Cy \qquad (14.34)$$

and the rate of change of the surface deflection is:

$$\dot{\varepsilon} = \frac{z}{\ell_3} \qquad (14.35)$$

Combining the above relations yields

$$\dot{\varepsilon} = \frac{C}{A\ell_3} y \qquad (14.36)$$
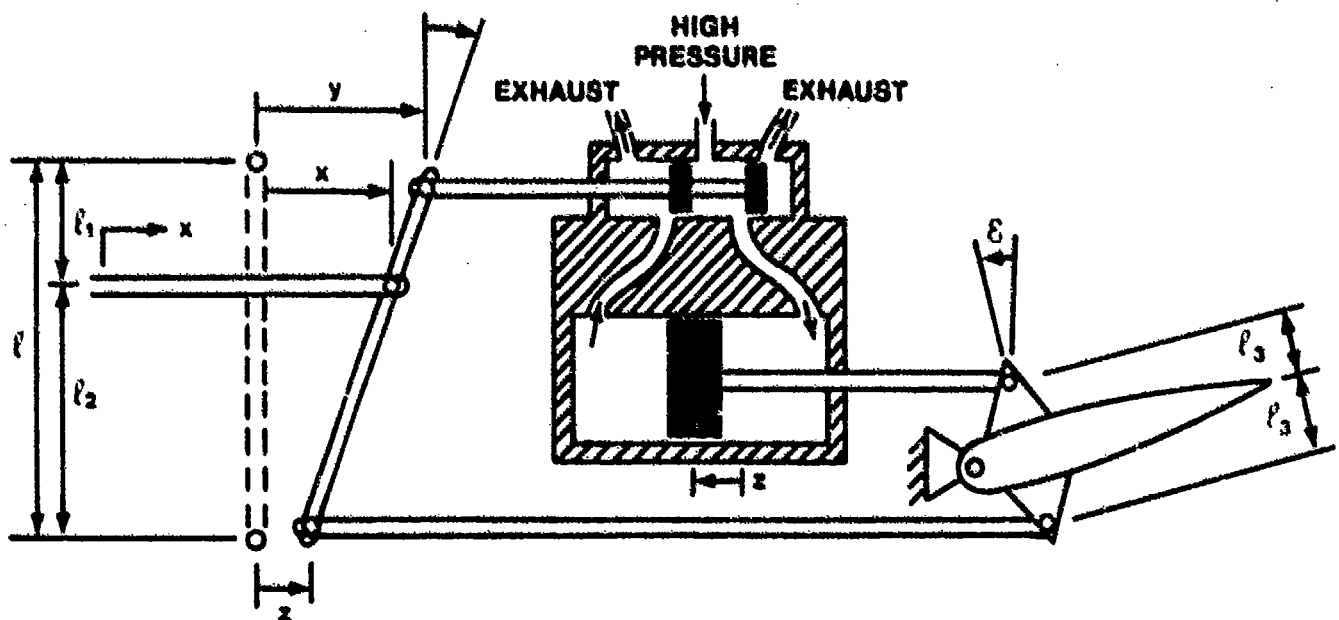
FIGURE 14.48. SCHEMATIC DIAGRAM OF A WALKING BEAM HYDRAULIC BOOST SYSTEM

$$\dot{\varepsilon} + \frac{C\ell_1}{A\ell_2}\,\varepsilon \;=\; \frac{C\ell}{A\ell_2\ell_3}\cdot x \qquad\qquad (14.37)$$

which, using the Laplace transform, provides the transfer function of the actuator

$$\frac{\varepsilon(s)}{x(s)} \;=\; \frac{\dfrac{C\ell}{A\ell_2\ell_3}}{s + \dfrac{C\ell_1}{A\ell_2}} \qquad\qquad (14.38)$$

Figure 14.49 shows a block diagram of the system. The mechanical feedback provides an actuator system which is a pure lag--the integrator action is controlled so that the aerodynamic surface is moved to a distinct position by a step input.
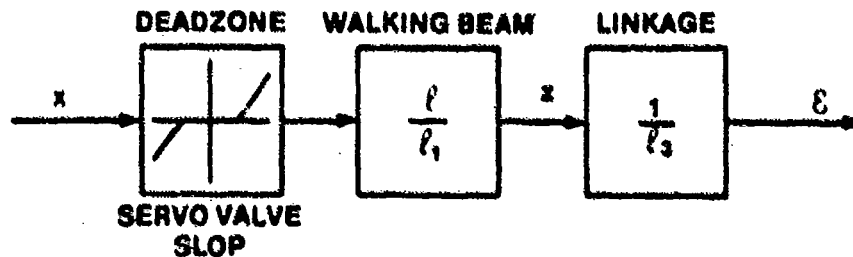
FIGURE 14.49. BLOCK DIAGRAM OF THE WALKING BEAM HYDRAULIC BOOST SYSTEM

In the event of a hydraulic system failure, the servo valve will move with little effort, causing mechanical slop in the system (deadzone effect—see Paragraph 14.3.6). Once moved to one of the stops, however, the pilot will exert force through the mechanical linkage to the aerodynamic surface. The flight control system is fully reversible and the pilot must overcome the surface hinge moments directly. Figure 14.50 shows the block diagram of the walking beam system in this situation.
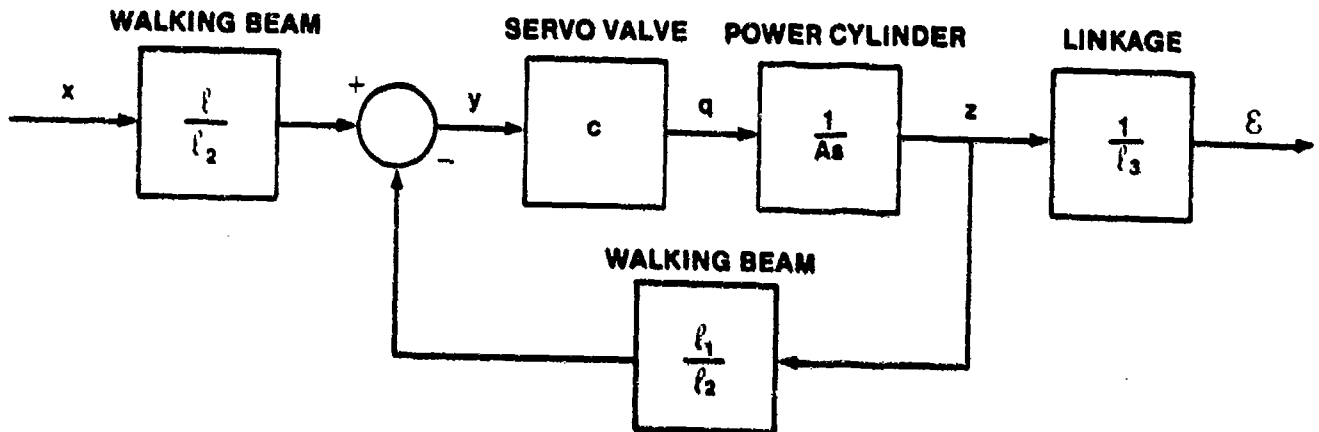
FIGURE 14.50. BLOCK DIAGRAM OF WALKING BEAM SYSTEM WITH HYDRAULIC
SYSTEM FAILURE

Figure 14.51 shows a servo actuator used in irreversible flight control systems. The pilot commanded displacement, x_1, causes the servo valve to allow hydraulic fluid flow. The piston, which is anchored to the aircraft at one end, causes the entire actuator housing to move displacing the aerodynamic surface. No direct linkage from the pilot to the surface is present. In the event of a hydraulic system failure, the pilot cannot move the aerodynamic surface through the actuator. The rate of fluid flow into the piston is related to the piston displacement and the pilot command is

$$q = C(x_1 - x_2) \qquad (14.39)$$

and the rate of piston displacement is

$$\dot{x}_2 = \frac{q}{A} \qquad (14.40)$$

yielding

$$\dot{x}_2 = \frac{C}{A}(x_1 - x_2) \qquad (14.41)$$
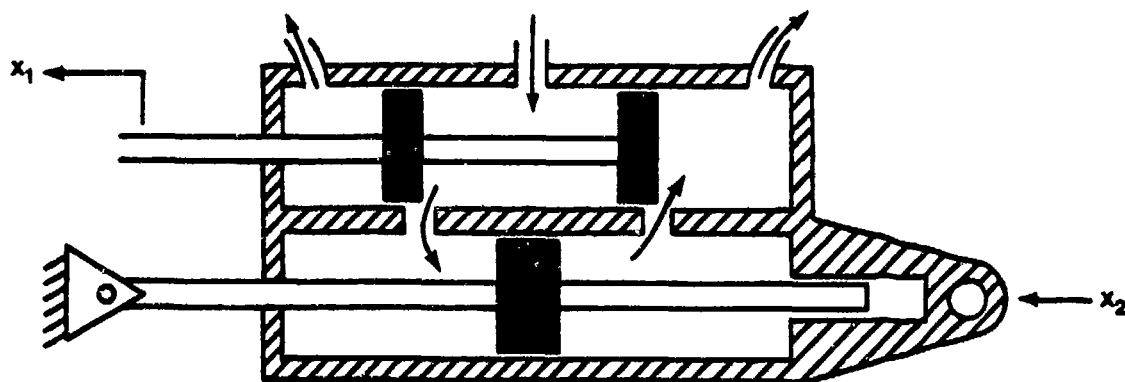
FIGURE 14.51. IRREVERSIBLE CONTROL SYSTEM ACTUATOR SCHEMATIC

The differential equation of the actuator is

$$\frac{A}{C} \dot{x}_2 + x_2 = x_1 \qquad (14.42)$$

resulting in the following transfer function

$$\frac{x_2(s)}{x_1(s)} = \frac{1}{\frac{A}{C} s + 1} = \frac{\frac{C}{A}}{s + \frac{C}{A}} \qquad (14.43)$$

Figure 14.52 presents a block diagram of the actuator system. A typical first order actuator model for a fighter aircraft is

$$\frac{\delta(s)}{\delta_c(s)} = \frac{20}{s + 20}$$
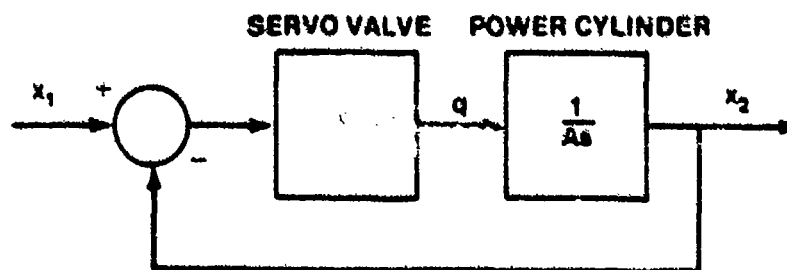
FIGURE 14.52. BLOCK DIAGRAM OF IRREVERSIBLE CONTROL SYSTEM HYDRAULIC ACTUATOR

If the leakage and compressibility effects within the actuator are not neglected, a third order actuator model is appropriate (see References 14.33 and 14.34), with the power cylinder modeled as a relatively low frequency (20 radians per second) first order lag and the servo valve modeled as a high frequency second order element. If a fly-by-wire system is modeled, an additional first order lag occurs as a result of the electrical actuation of the servo valve.

The F-16 actuator is modeled as

$$\frac{(20.2)(144.8)(71.4)^2}{(s + 20.2)(s + 144.8)(s + 52.55 \pm 48.34j)}$$

which may be simplified to

$$\frac{20.2}{s + 20.2}$$

The effect of the high frequency poles due to the servo valve and the electrical actuator is to add a slight bit of lag to the system so that if time response characteristics are compared, a closer first order approximation to the F-16 actuator is

$$\frac{13}{s + 13}$$

The change in dominant root locations during a simplified analysis of the F-16 flight control system is slight if the first approximation is used versus the second. The first approximation is found by inspection rather than through further analysis.

Figure 14.53 shows the effect of typical hydraulic actuator dynamics on the characteristics of a tactical aircraft (compare this root locus plot to Figure 14.7b). Notice that the added lag caused by the actuator forces the short period dynamics of the aircraft to become unstable at a relatively low system gain. The short period damping is reduced, for a given controller gain, to a greater extent than that revealed by the analysis of Paragraph 14.2. Figure 14.54 shows that a slower actuator has the effect of further destabilizing the aircraft. Slow actuators are typically used in transport or bomber aircraft. Figure 14.55 shows the time response for the system of Figure 14.53 at a selected controller gain. The additional lag introduced by the actuator is apparent.
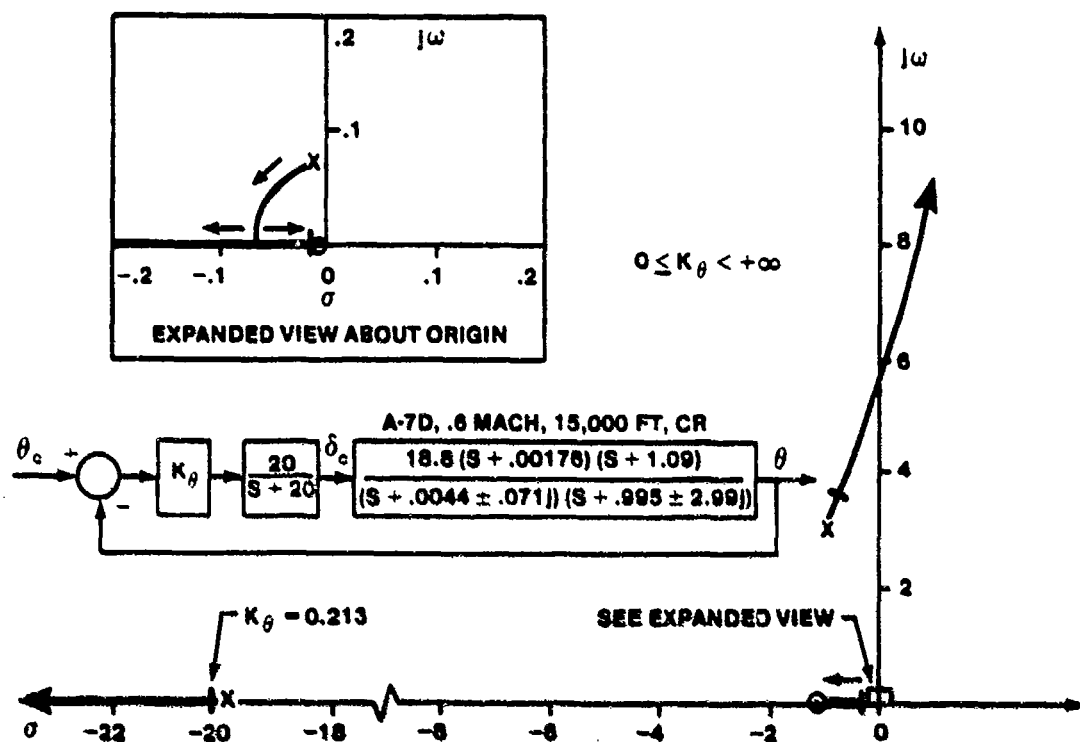
FIGURE 14.53. ROOT LOCUS PLOT OF PITCH ATTITUDE LOOP INCLUDING TYPICAL ACTUATOR CHARACTERISTICS
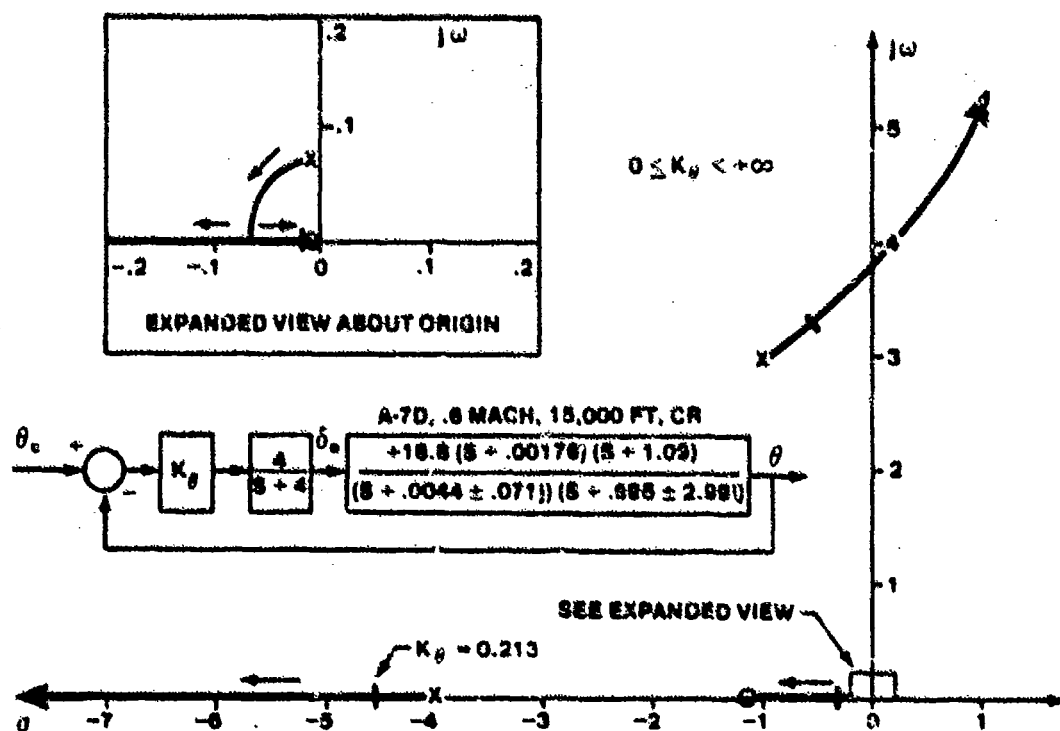
FIGURE 14.54. ROOT LOCUS PLOT OF PITCH ATTITUDE LOOP INCLUDING SLOW ACTUATOR CHARACTERISTICS
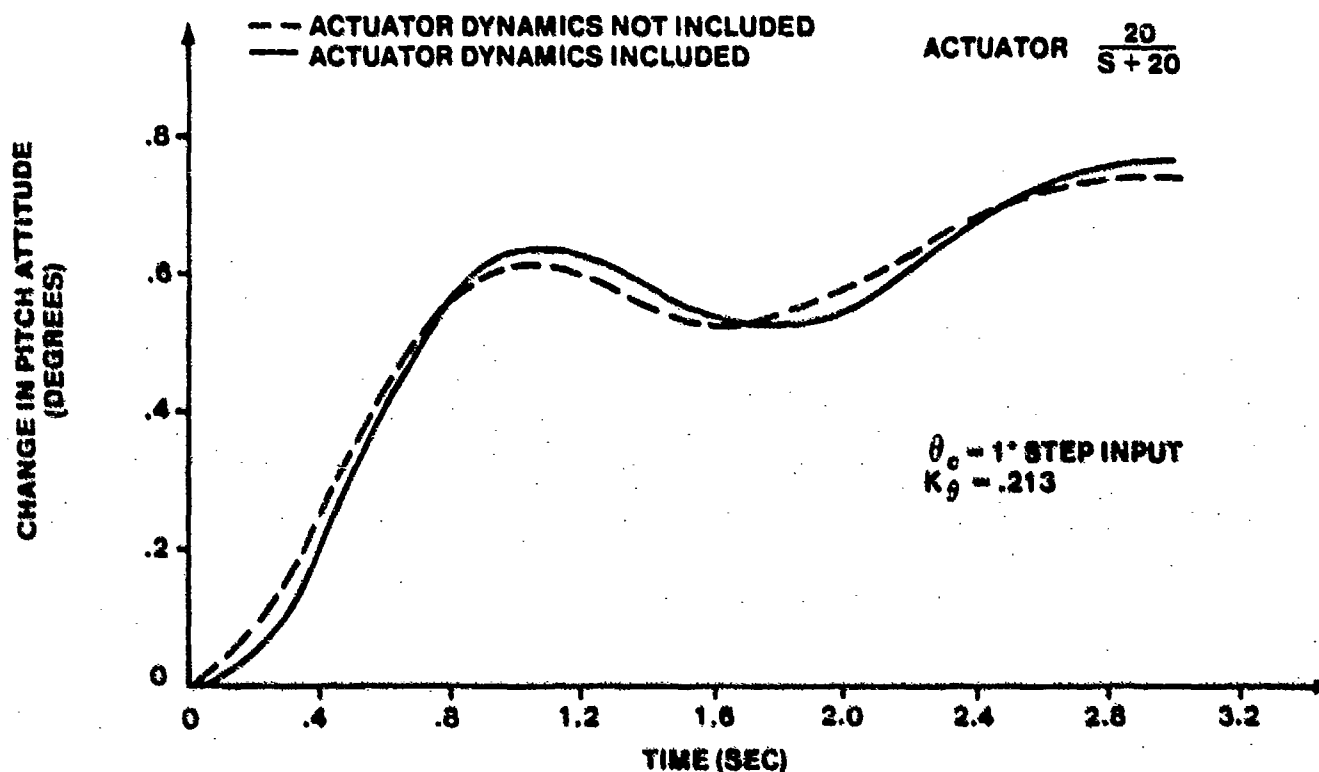
FIGURE 14.55. A-7D PITCH ATTITUDE RESPONSE COMPARISON SHOWING EFFECT OF
ACTUATOR DYNAMICS

In most applications, it is undesirable to reflect the control surface
movement which is caused by the augmentation system into the pilot controls
(the A-37 yaw damper causes the rudder pedals to move, which is often annoying
to the pilot). A dual servo actuator arrangement, as shown in Figure 14.56b,
could be used to prevent augmentation movement of the cockpit controls.

a. SURFACE MOVEMENT REFLECTED IN PILOT CONTROLLER

SAS INPUT

SAS INPUT

b. SURFACE MOVEMENT NOT REFLECTED IN PILOT CONTROLLER
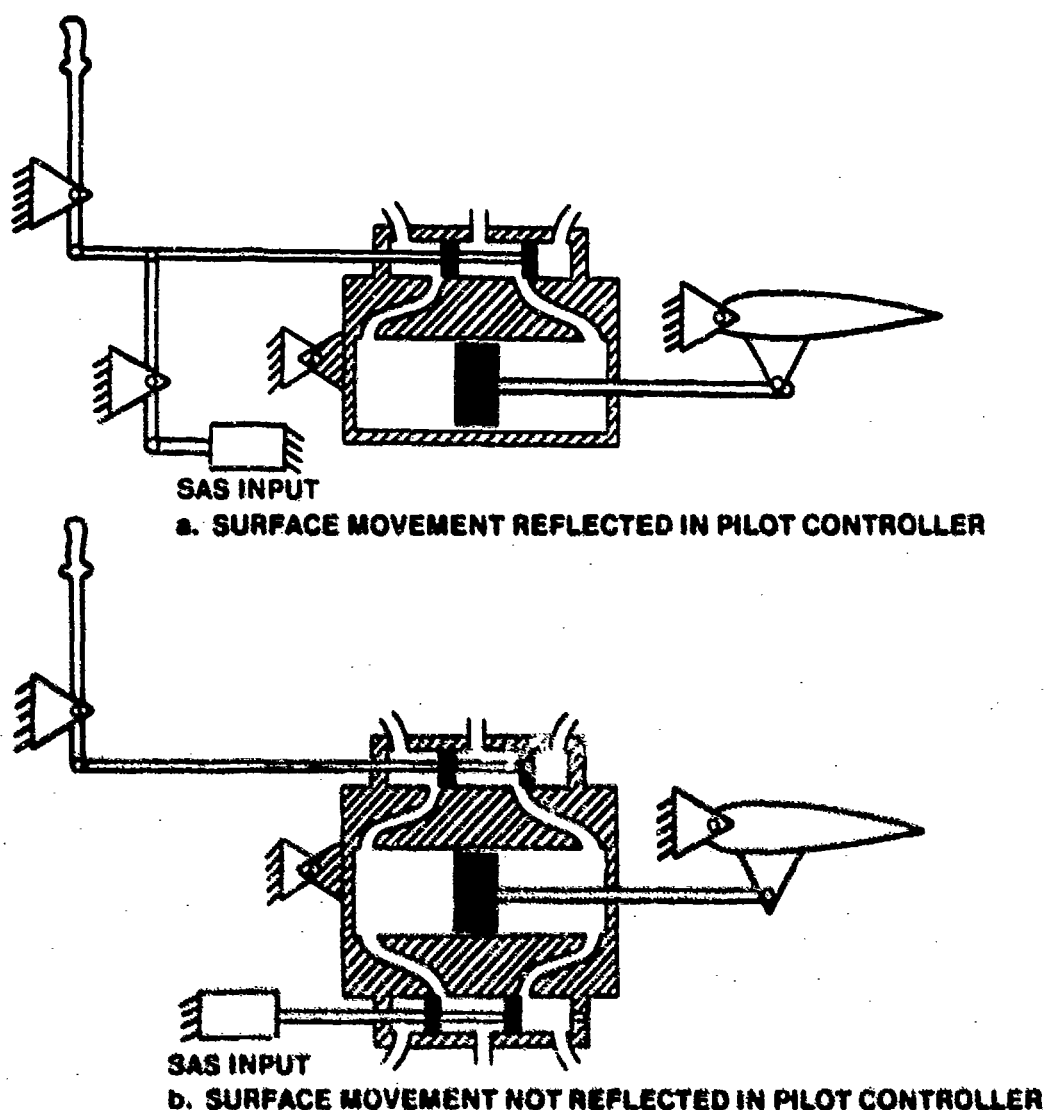
FIGURE 14.56. AUGMENTATION SYSTEM ACTUATOR INPUT IMPLEMENTATIONS

14.3.2 Artificial Feel Systems

High performance aircraft which use irreversible, hydraulically actuated
control surfaces and moveable pilot controllers require artificial feel
systems to simulate the control forces due to aerodynamic loads. Some
advanced aircraft which use fly-by-wire control systems (such as the F-16) use
isometric force controllers and lack artificial feel systems, although some
movement in the controller (proportional to the pilot force) has

proven to be helpful in reducing pilot-induced oscillation tendencies, especially in the roll axis.

14.3.2.1 Springs and Dampers. Springs are included in the flight control system to provide more pronounced speed stability cues to the pilot. The force exerted by the spring is proportional to the stick displacement.

Figure 14.57 shows the artificial feel system used in the F-4C. The bellows provides a spring gradient which is a function of Mach and altitude, effectively acting as a mechanical gain changer. On the ground, the springs exert no forces and the stick is moved to the forward stop by the force exerted by the bobweight. As the airspeed increases, the bellows dynamic pressure increases and the stick moves aft as the force of the spring increases.

The dampers provide stick forces which are proportional to the rate of stick deflection and prevent steady oscillations when the pilot releases the stick, improving controller centering characteristics. One damper is a function of the flight condition, being on a physical stop at most flight conditions so that

$$ b = \infty $$

and being off the stop at high altitudes and high Mach (above approximately 30,000 ft and 1.0 Mach), where

$$ b = 3.03 \text{ lb/in/sec} $$

A change in total stick damping is often necessary so that the dampers do not restrict the aircraft maneuverability at flight conditions where a high rate of elevator motion is desirable.

VISCOUS DAMPER
(∞ IF BOTTOMED OUT,
3.03 LB/IN/SEC OTHERWISE)

BELLOWS PRESSURE
(0.0569 $q_B p_3$ LB/IN)*

BELLOWS SPRING
(0.0157$q_B p_B$ LB/IN)*

LUMPED VISCOUS
DAMPING
(0.208 LB/IN/SEC)

BOBWEIGHT
(5.35 LB/G)

F-4C

F_s

LUMPED INERTIA
(0.0369 LB/IN/SEC²)

*THE PRODUCT $q_B p_B$ IS DETERMENED BY THE MA(
q, AND δ_e COMBINATION AT A
PARTICULAR FLIGHT CONDITION

AIRPLANE C.G.

EFFECTIVE BOBWEIGHT POSITION (39.3 FT)

FIGURE 14.57. SCHEMATIC DIAGRAM OF THE F-4C FEEL SYSTEM, INCLUDING THE
BOBWEIGHT

The transfer function of the feel system, consisting of the springs and dampers, can be determined by summing the moments about the stick pivot point, yielding (by reference to Figure 14.58)

$$J\ddot{\delta} = F_s \ell - b_1 \ell_1 \dot{x}_1 - k_1 \ell_2 x_2 - b_2 \ell_2 x_2 - b_2 \ell_3 (\dot{x}_3 - \dot{x}_4) \qquad (14.44)$$

where J is the stick moment of inertia about the pivot point. For small stick deflections

$$\delta = \frac{x_1}{\ell_1} = \frac{x_2}{\ell_2} = \frac{x_3}{\ell_3} = \frac{x}{\ell} \qquad (14.45)$$

and

$$\ell\ddot{\delta} = \ddot{x} \qquad (14.46)$$

The stick displacement, x, is related to the spring and damper displacements as

$$x = x_1 \frac{1}{\ell_1} = x_2 \frac{1}{\ell_2} = x_3 \frac{1}{\ell_3} \qquad (14.47)$$

The stick moment of inertia is approximated as

$$J = m\ell^2 \qquad (14.48)$$

if the mass of the stick is assumed to be concentrated at the feel grip and if the inertia of the feel grip about its own center of mass is assumed negligible (see Reference 14.36 for a discussion of moments of inertia). Substituting the above relationships into the original equation, and dividing
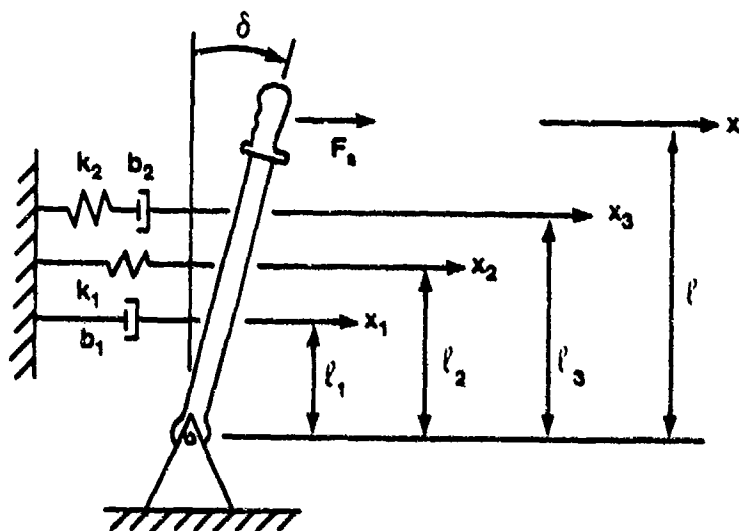
a. FEEL SYSTEM SCHEMATIC WITHOUT BOBWEIGHT
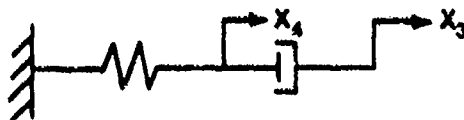
b. VISCOUS DAMPER AND BELLOWS PRESSURE SYSTEM

FIGURE 14.58. F-4C FEEL SYSTEM SCHEMATIC

by the length of the stick, yields

$$F_s - b_1 \frac{\ell_1}{\ell} \dot{x}_1 - k_1 \frac{\ell_2}{\ell} x_2 - b_2 \frac{\ell_3}{\ell} (\dot{x}_3 - \dot{x}_4) = \frac{m\ell^2}{\ell^2} \ddot{x}$$

or

$$F_s - B_1^* \dot{x} - k_1^* x - b_2^* (\dot{x} - \dot{y}) = m\ddot{x} \qquad (14.49)$$

A second equation arises by summing the forces about the point between the viscous damper and the bellows pressure, yielding

$$0 = - b_2^* (\dot{y} - \dot{x}) - k_2^* y \qquad (14.50)$$

where

$$b_1^* = \frac{\ell_1^2}{\ell^2} b_1 \ , \ b_2^* = \frac{\ell_3^2}{\ell^2} b_2 \ , \ k_1^* = \frac{\ell_2^2}{\ell^2} k_1 \ , \ k_2^* = \frac{\ell_3^2}{\ell^2} k_2 \ , \ y = \frac{\ell_3}{\ell} x_4$$

The two equations can be Laplace transformed and written in a matrix equation as

$$\begin{bmatrix} ms^2 + (b_1^* + b_2^*)s + k_1^* & - b_2^* s \\ \\ - b_2^* s & b_2^* s + k_2^* \end{bmatrix} \begin{bmatrix} x(s) \\ \\ y(s) \end{bmatrix} = \begin{bmatrix} 1 \\ \\ 0 \end{bmatrix} F_s$$

Cramer's rule can now be used to find the feel system transfer function. The characteristic equation is

$$[ms^2 + (b_1^* + b_2^*)s + k_1^*] (b_2^* s + k_2^*) - b_2^{*2} s^2$$

which is simplified to

$$[ms^2 + b_1^* s + k_1^*] (b_2^* s + k_2^*) + b_2^* k_2^* s \qquad (14.51)$$

The numerator for the transfer function which relates the stick grip longitudinal position to the applied pilot stick force is

$$b_2^* s + k_2^*$$

If both the numerator and the denominator of the transfer function are divided by the numerator and some algebra performed, the feel system transfer function becomes

$$\frac{x(s)}{F_s(s)} = \frac{1}{ms^2 + b_1^* s + k_1^* + \dfrac{k_2^*}{1 + \dfrac{k_2^*}{b_2^* s}}} \qquad (14.52)$$

Figure 14.59 shows the effect of pitch attitude feedback on the unaugmented F-4C aircraft (actuator dynamics included). The unstable tuck mode is quickly stabilized while the short period roots are not significantly affected for low to moderate values of gain.
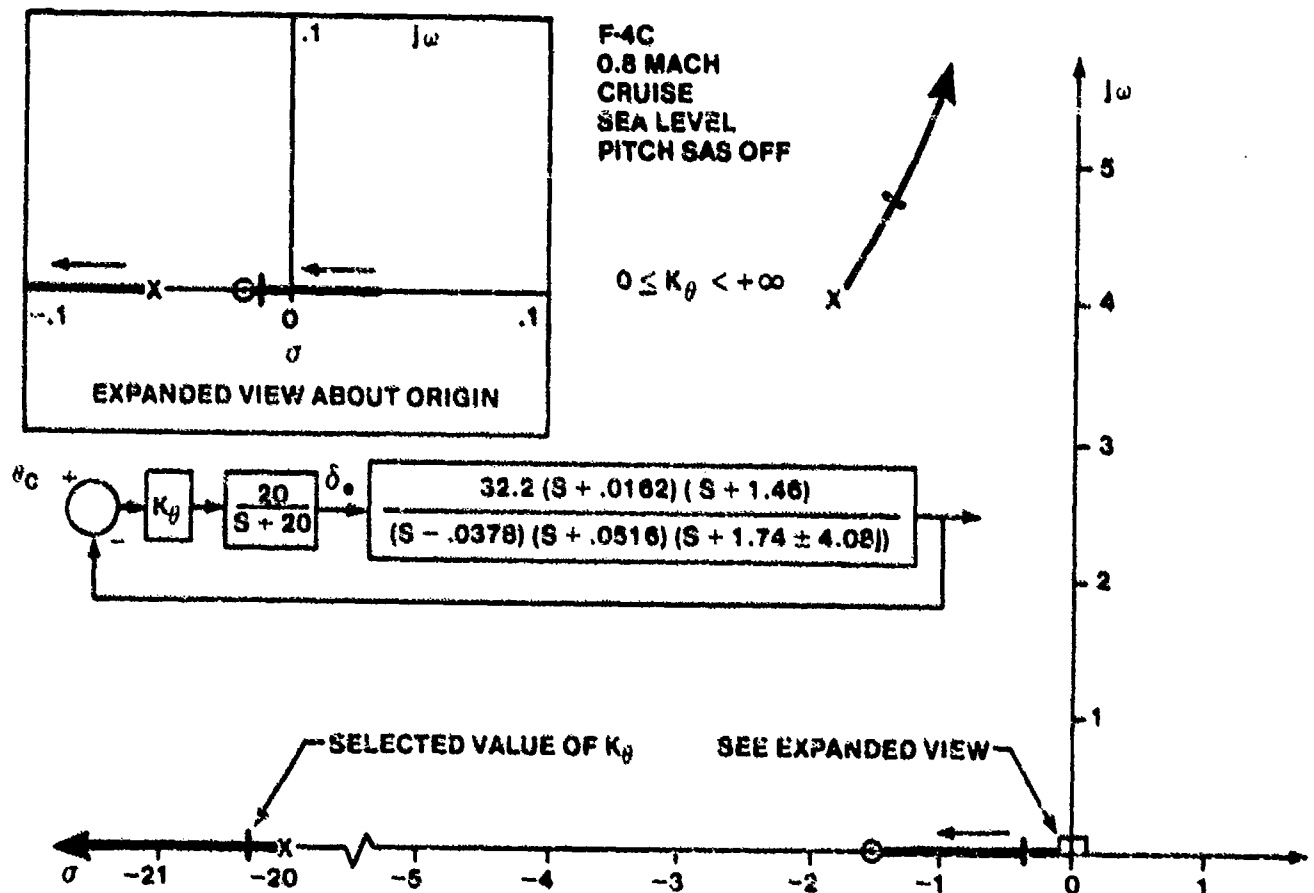
FIGURE 14.59.   PITCH ATTITUDE CONTROL LOOP FOR F-4C WITHOUT FEEL SYSTEM OR BOBWEIGHT

14.77

Figure 14.60 shows a block diagram of the F-4C feel system, including the bobweight effects. A simple pilot model is assumed—the pilot being a pure gain controller attempting to precisely control the aircraft's pitch attitude. More complex pilot models are possible, incorporating pilot delays and compensation, but this simple model is adequate to show the effects of the feel system. The pilot induced oscillation (PIO) susceptibility of the aircraft at this flight condition cannot be determined from the following simplified analysis, but an idea of the relative PIO susceptibility due to various feel system characteristics may be obtained by noting the relative pilot gain at which the pilot (pitch attitude control) loop becomes unstable. Initially, the effects of the bobweight are neglected, so that

$$W_B = 0$$
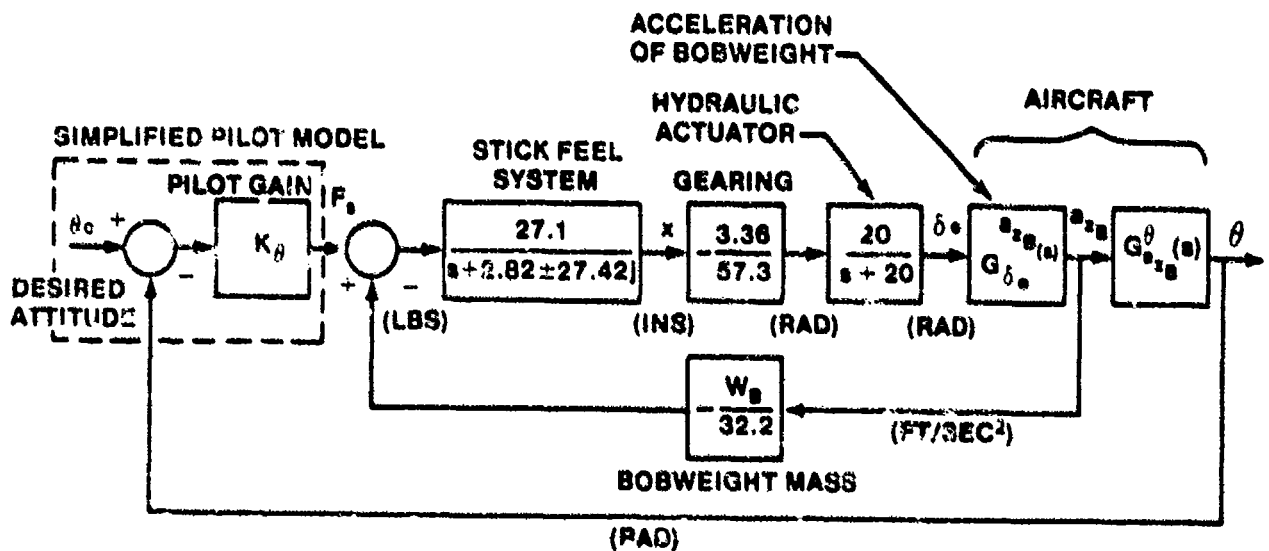
FIGURE 14.6C. BLOCK DIAGRAM OF THE F-4C FEEL SYSTEM WITH A SIMPLIFIED PILOT MODEL INCLUDED AS AN OUTER LOOP CONTROLLER

Figure 14.61 shows the effects of the production F-4C feel system. The feel system has light damping and a large natural frequency relative to the basic airframe characteristics. The pilot, by controlling the aircraft pitch attitude, is easily able to stabilize the tuck mode. The short period roots remain relatively well damped for low to moderate values of gain, but may be driven unstable at high pilot gain. The feel system roots are not appreciably affected, even by high pilot gains.
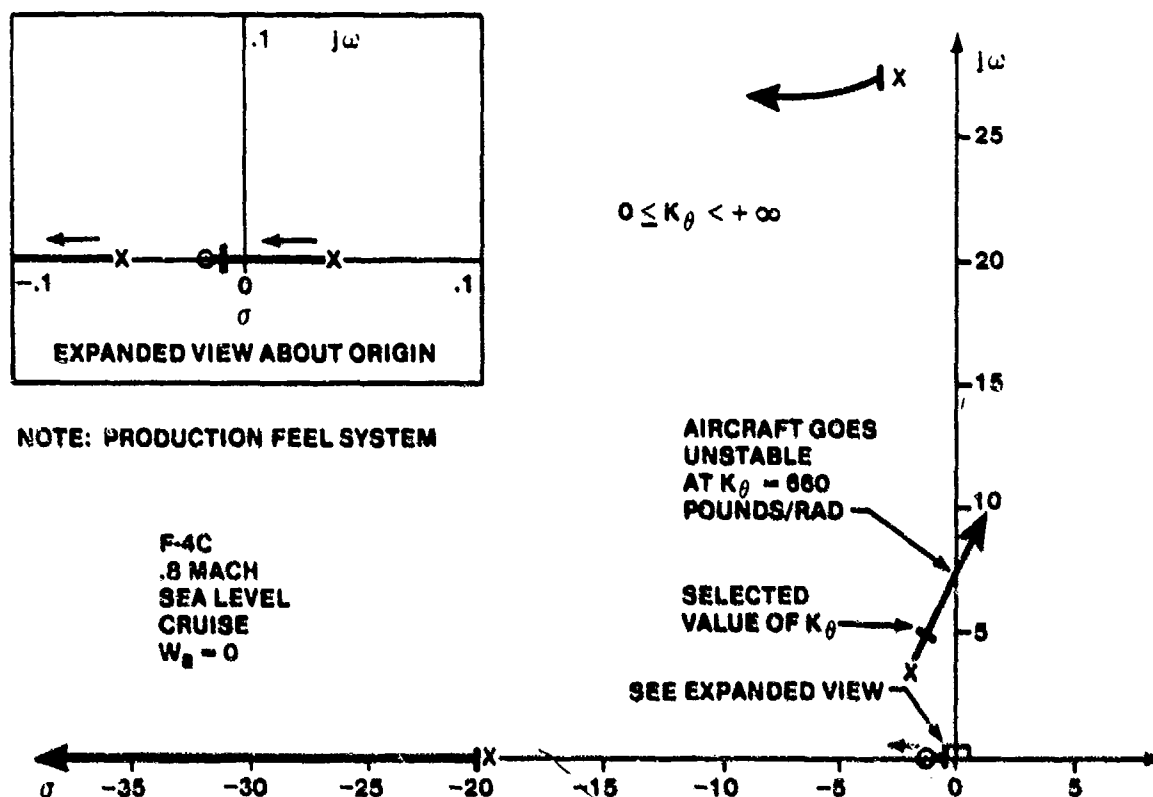
FIGURE 14.61. PITCH ATTITUDE CONTROL LOOP FOR F-4C WITH PRODUCTION FEEL SYSTEM NO BOBWEIGHT

Figure 14.62 shows the effect of reduced damping in the feel system. Although the feel system has no damping--resulting in a residual stick oscillation in the open loop response which causes the aircraft to oscillate in pitch at the feel system frequency--the pilot is able to provide the stick damping required to keep the pilot-aircraft combination stable. The basic airframe characteristics are not appreciably changed from the previous situation and the aircraft PIO susceptibility appears to be slightly reduced.

14.79

Even if slightly negative damping were present in the feel system, the pilot could stabilize the aircraft, although the open loop aircraft would be unstable due to the unstable feel system roots, even at flight conditions with a stable phugoid mode. If the pilot gain to stabilize the feel system were high (but attainable), the short period damping would be significantly reduced and poor flying characteristics and increased PIO susceptibility would result due to the high pilot workload and poor pitch attitude control. Under certain conditions, the feel system of the F-4C could become unstable at high Mach (with a bellows system failure) and the pilot would not be able to stabilize the feel system without driving the short period roots unstable. In this case, the pilot would lose control of the aircraft.
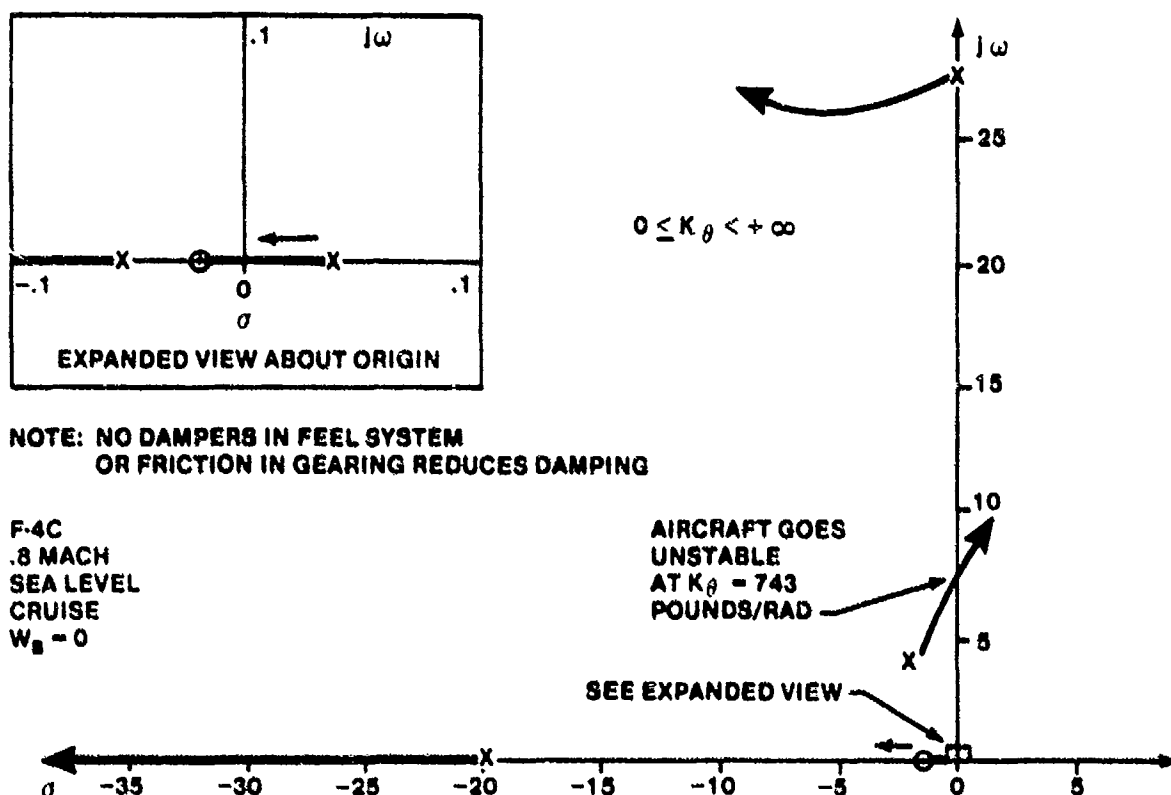
FIGURE 14.62. PITCH ATTITUDE LOOP FOR F-4C WITH NO FEEL SYSTEM DAMPING OR BOBWEIGHT

Figure 14.63 shows the effect of increased damping in the feel system. The added feel system forces due to the increased damping will reduce the rate at which the pilot can change the elevator position. The PIO susceptibility of the aircraft is slightly increased.

FIGURE 14.63. PITCH ATTITUDE LOOP FOR F-4C WITH INCREASED FEEL SYSTEM DAMPING FORCES, NO BOBWEIGHT

Figure 14.64 shows the effect of reduced spring forces in the feel system (reduced pilot control forces). The natural frequency of the feel system is much lower, bringing the roots in closer proximity to the basic airframe characteristics. The pilot is still able to control the pitch attitude of the aircraft, but the gain at which the short period roots are driven unstable is reduced, increasing the susceptibility of the aircraft to PIO's.

EXPANDED VIEW ABOUT ORIGIN

NOTE: REDUCED SPRING FORCES
OR INCREASED STICK MASS
REDUCES FEEL SYSTEM
NATURAL FREQUENCY

$0 \leq K_\theta < +\infty$

AIRCRAFT GOES
UNSTABLE AT
$K_\theta = 114$ POUNDS/RAD
FOR STICK MASS UNCHANGED

F-4C
.8 MACH
SEA LEVEL
CRUISE
$W_s = 0$

SEE EXPANDED
VIEW
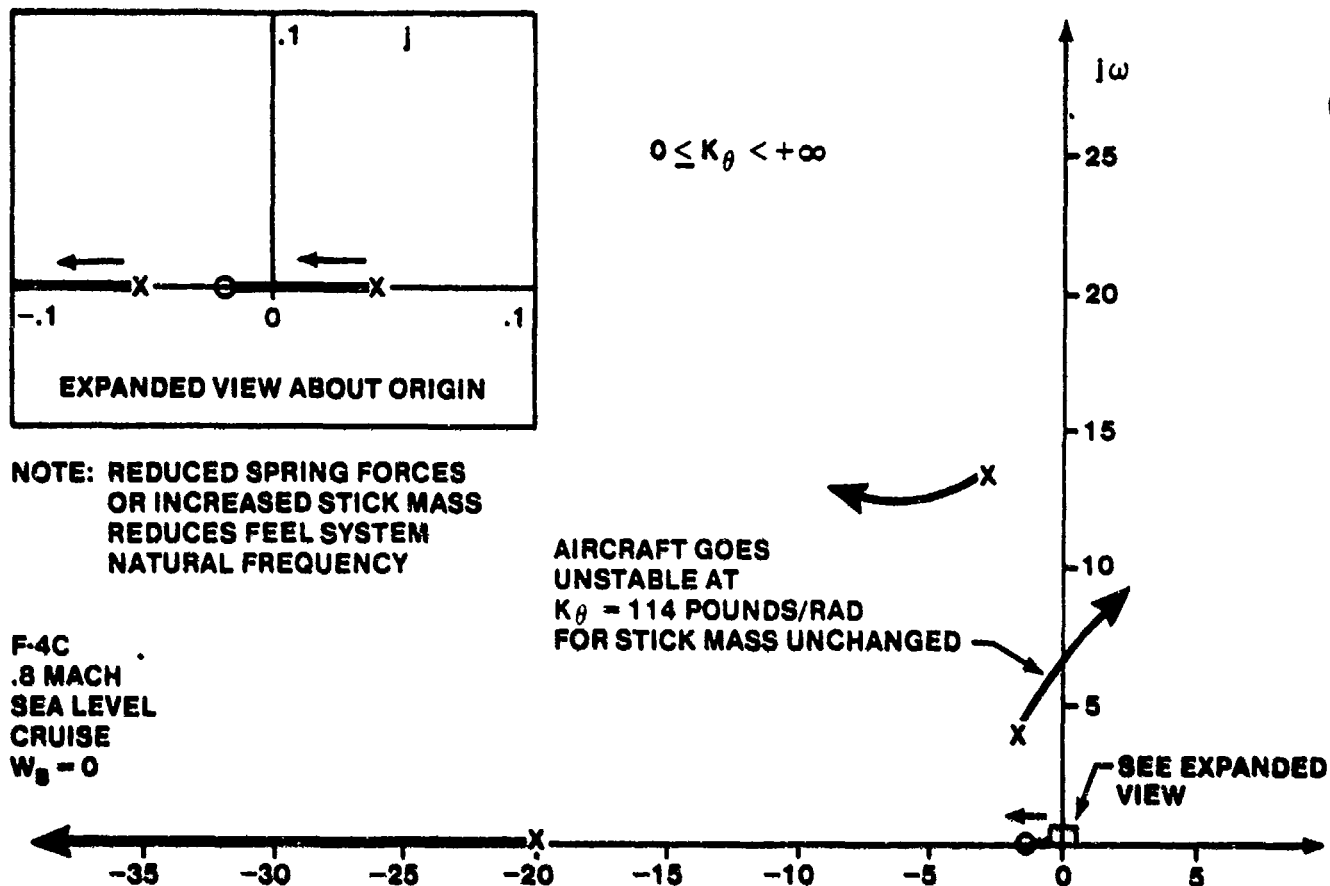
FIGURE 14.64.   PITCH ATTITUDE LOOP FOR F-4C WITH REDUCED FEEL SYSTEM SPRING
FORCES, NO BOBWEIGHT

Figure 14.65 shows what would happen in the absence of all feel system
forces (no damping or spring forces). If the pilot controls only pitch
attitude, he cannot stabilize the aircraft. The higher the pilot's gain, the
more unstable he drives the aircraft. However, if the pilot also uses stick
position as a feedback through his neuro-muscular system, resulting in the
modified pilot model of Figure 14.66, he may be able to control the aircraft
pitch attitude, although only by devoting his entire attention to flying the
aircraft. This aircraft is highly susceptible to PIO and must be very
carefully flown. If the pilot reverts to controlling the aircraft's pitch
attitude and does not concentrate on the position of the controller, the
aircraft will be driven unstable (this situation might occur during flare and
touchdown). Sticks with higher masses will require more pilot concentration
on the control position, resulting in a harder aircraft to fly. Feel systems
which possess friction, but which do not include a spring, will provide an
improvement if the pilot is able to fly using stick position cues.

EXPANDED VIEW ABOUT ORIGIN

$0 \leq K_\theta < +\infty$
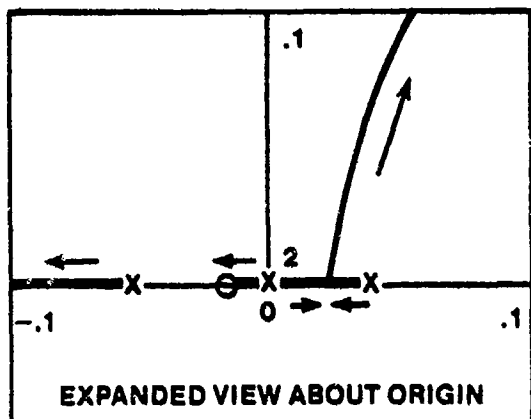
NOTE: ZERO FEEL SYSTEM FORCE OR DAMPING

F-4C
.8 MACH
SEA LEVEL
CRUISE
$W_e = 0$

AIRCRAFT UNSTABLE FOR ALL K_θ

SEE EXPANDED VIEW
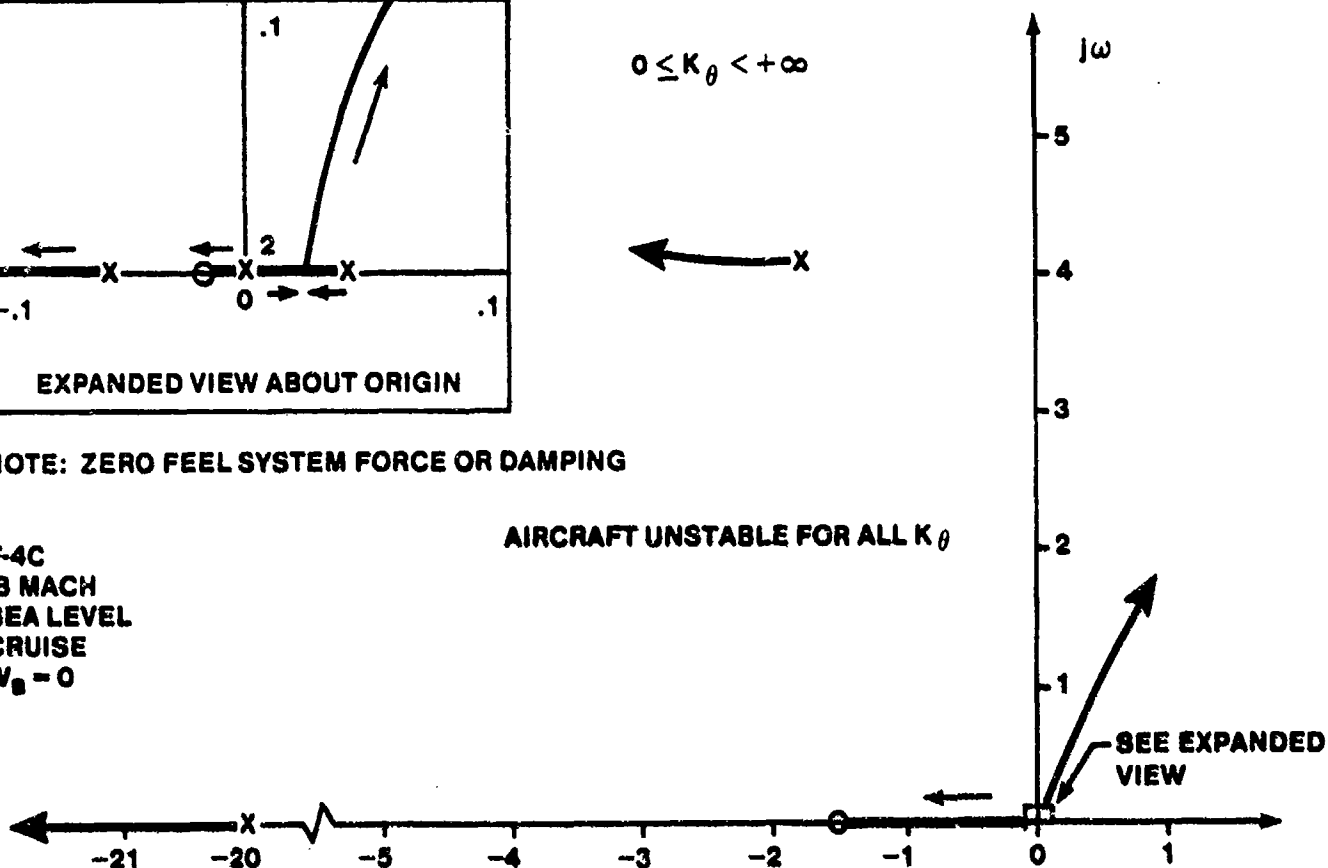
FIGURE 14.65.   PITCH ATTITUDE CONTROL LOOP WITH NO STICK DAMPING OR SPRING
FORCES, NO BOBWEIGHT

The observations obtained from this simplified analysis are:

1.   No conclusions about the overall PIO susceptibility of the aircraft
     are possible.

2.   Reduced feel system damping improves PIO resistance, but may cause
     poor stick centering characteristics and residual, high frequency
     oscillations. Increased feel system damping reduces PIO resistance.

3.   Reduced feel system spring forces greatly reduces PIO resistance.

4.   An absence of feel system spring and damper forces is extremely
     undesirable in aircraft with moveable controllers.
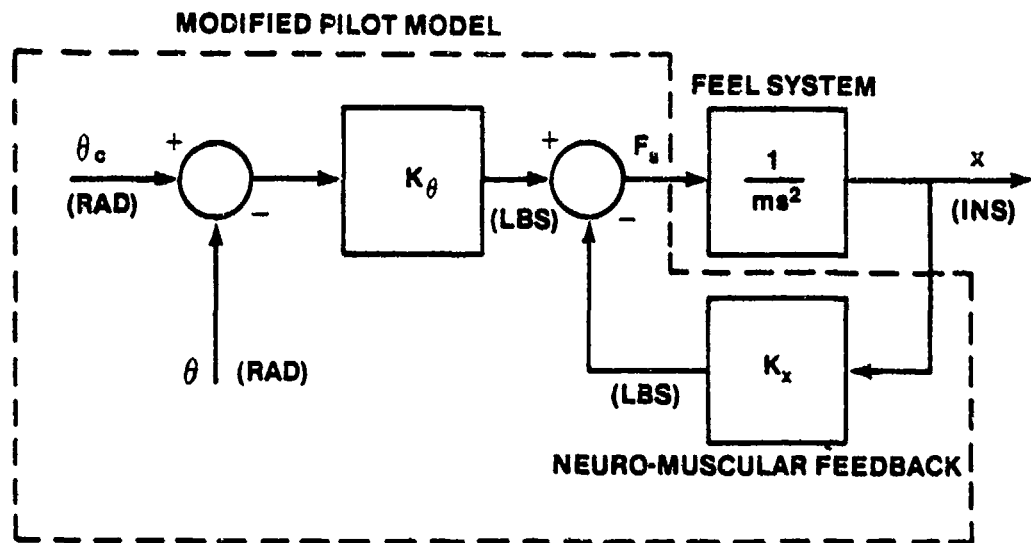
FIGURE 14.66. MODIFIED PILOT MODEL

14.3.2.2 Bobweight Effects. A bobweight is added to a flight control feel system to increase the stick free maneuvering stability of the aircraft (increased stick force per g). The speed stability of the aircraft is also increased somewhat.

A bobweight is effectively an acceleration feedback loop to the pilot applied stick forces (Figure 14.60). The location of the bobweight relative to the aircraft center of gravity, as well as the size of the bobweight mass, are the two variables to be analyzed in the following paragraphs. Both significantly affect the flying qualities of the aircraft.

The acceleration sensed at the bobweight station is given by

$$a_{z_B} = a_{z_{CG}} - \ell_x \dot{q} \qquad (14.7)$$

where ℓ_x is the distance from the center of gravity of the aircraft to the bobweight (positive forward). The effect of moving the bobweight forward is to change the location of the zeros in the acceleration transfer function

$$G_{\delta_e}^{a_{z_B}}(s)$$

Figure 14.67 shows the effect of moving the bobweight forward of the center of gravity for the F-4C aircraft. The zero in the right half s-plane, which has a strong destabilizing influence on the aircraft short period roots as the bobweight size increases, is rapidly moved into the left half s-plane

14-84

with only a slight movement of the bobweight forward. The further the bobweight is moved forward, the closer the zeros move to the proximity of the short period roots. The closer the zeros to the short period roots, the less the tendency will be for the short period roots to migrate towards the right half s-plane as the size of the bobweight is increased to achieve the desired stick force maneuver gradient.

NOTE: CENTER OF ROTATION
AT $\ell_x = 4.38$ FT

NOTE: ZEROS AT S = 0 AND
S = -.0148 DO NOT
MIGRATE WITH ℓ_x

$\ell_x = 6.13$ FT
$\ell_x = 7.0$ FT
$\ell_x = 7.9$ FT
$\ell_x = 8.76$ FT
$\ell_x = 11.38$ FT
$\ell_x = 14.0$ FT
$\ell_x = 29.77$ FT
$\ell_x = 43.78$ FT

F-4C
.8 MACH
SEA LEVEL
CRUISE

$\ell_x = 0$ FT $\ell_x = 0$ FT

-25   -20   -15   -10   -5   0   5   10   15
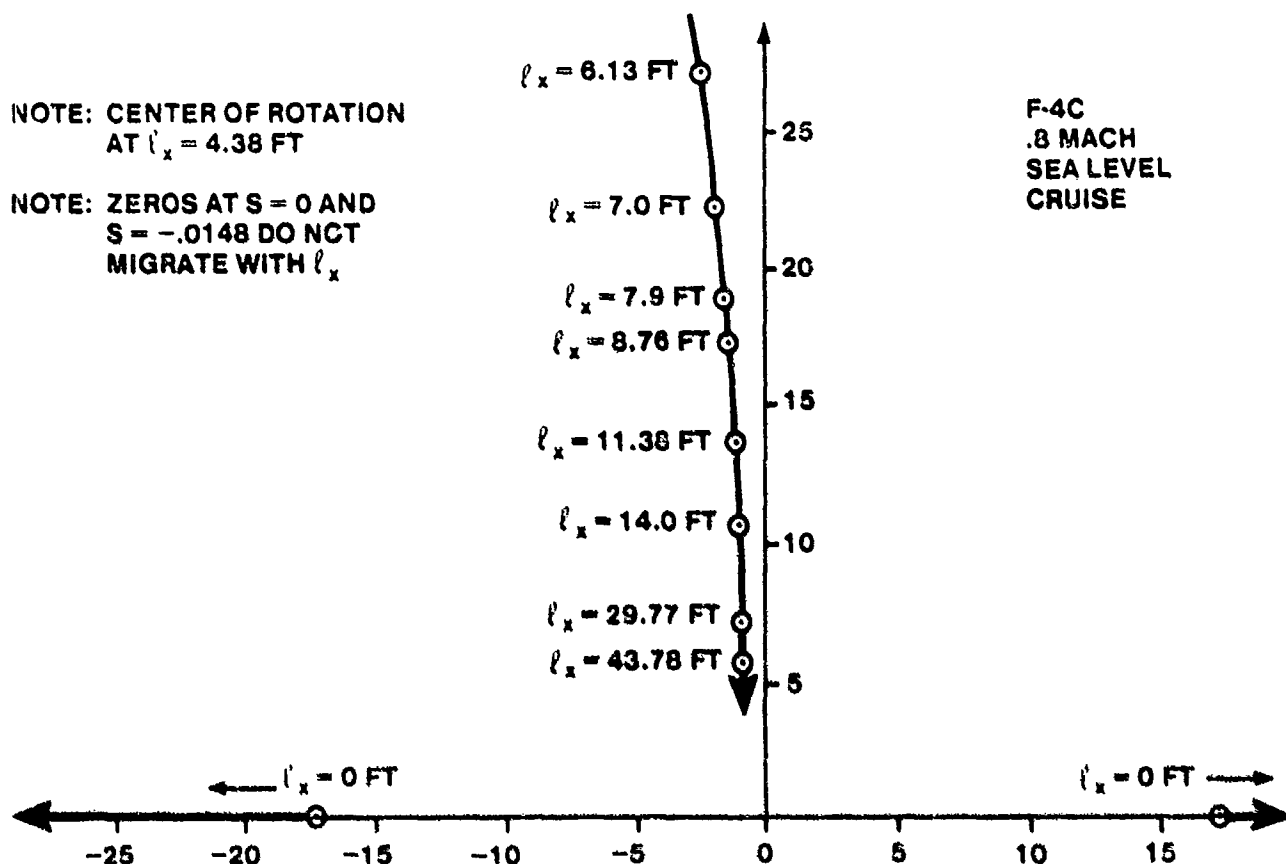
FIGURE 14.67.   MIGRATION OF ACCELERATION TRANSFER FUNCTION ZEROS AT ℓ_x INCREASES AHEAD OF C.G.

Figures 14.68 to 14.71 show the effect of the bobweight on the open loop aircraft characteristics with the feel system dynamics neglected. With the bobweight at the center of gravity, a very small bobweight (0.86 pounds) causes the short period roots to become unstable. As the bobweight is moved forward, the maximum size of the bobweight can increase before the short period is driven unstable. With the bobweight well forward of the center of gravity, an infinite bobweight size is possible (with the feel system dynamics

neglected) without driving the short period unstable. The bobweight, regardless of its location relative to the center of gravity, has the effect of reducing the short period damping - thereby increasing the PIO susceptibility of the aircraft. The feel system of the control stick will, however, impose further limitations on the size of the bobweight. Of course, the minimum and maximum size of the bobweight is also governed by the stick force gradient requirements of MIL-F-8785C.
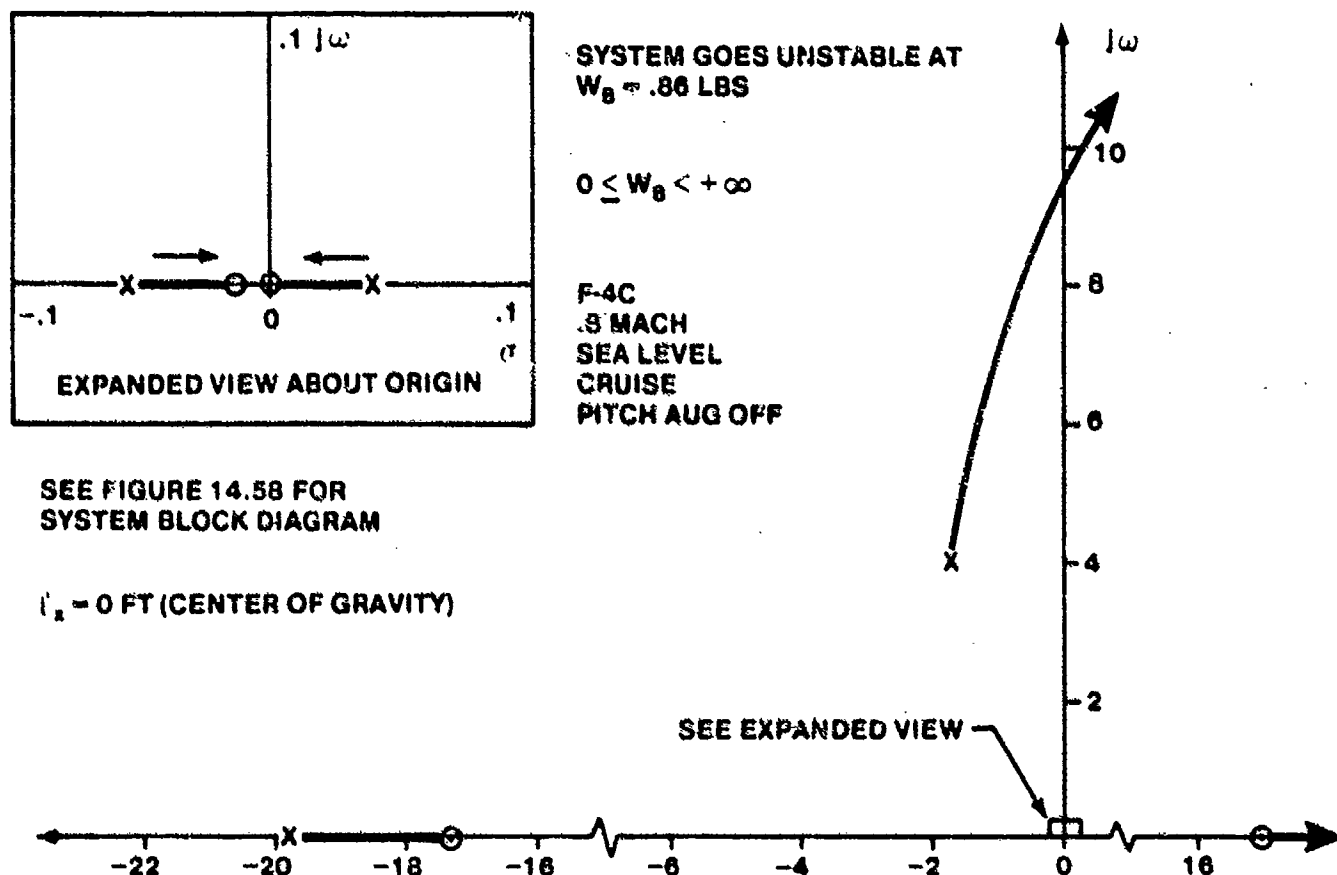
FIGURE 14.68. ROOT LOCUS PLOT OF BOBWEIGHT LOOP FOR THE F-4C WITHOUT FEEL SYSTEM
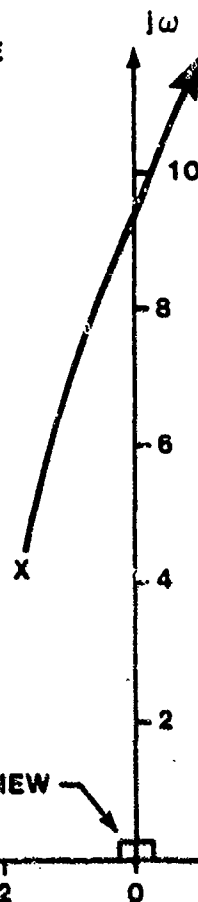
FIGURE 14.69.   ROOT LOCUS PLOT OF BOBWEIGHT LOOP FOR THE F-4C WITHOUT FEEL SYSTEM
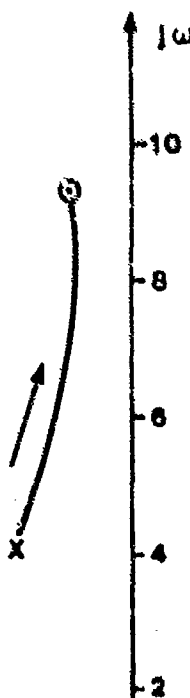
FIGURE 14.70.   ROOT LOCUS PLOT OF BOBWEIGHT LOOP FOR THE F-4C WITHOUT FEEL SYSTEM

FIGURE 14.71. ROOT LOCUS PLOT OF BOBWEIGHT LOOP FOR THE F-4C WITHOUT FEEL SYSTEM

Figures 14.72 to 14.75 show the effects of the bobweight with the feel system dynamics included. The maximum size of the bobweight without driving either the feel system or the snort period unstable occurs at the center of rotation. As the bobweight is moved forward of the center of rotation, increasing bobweight size drives the feel system unstable. The maximum allowable size of the bobweight is reduced to keep the feel system roots in the left hand s-plane.

Once the size of the bobweight is established by stability and stick force gradient considerations, the analysis of the last section concerning the pilot-in-the-loop handling qualities of the aircraft can be repeated. If the analysis is repeated (using multiloop analysis techniques to be discussed in Paragraph 14.4), the pilot gain at which the short period roots go unstable for
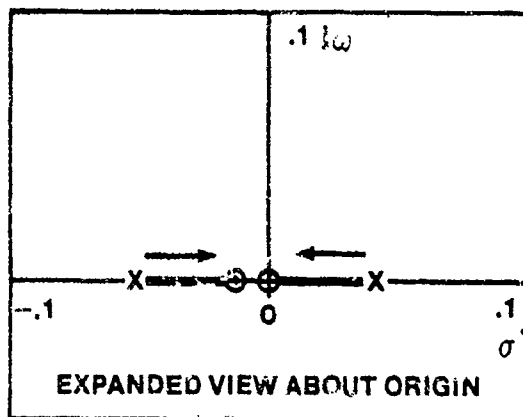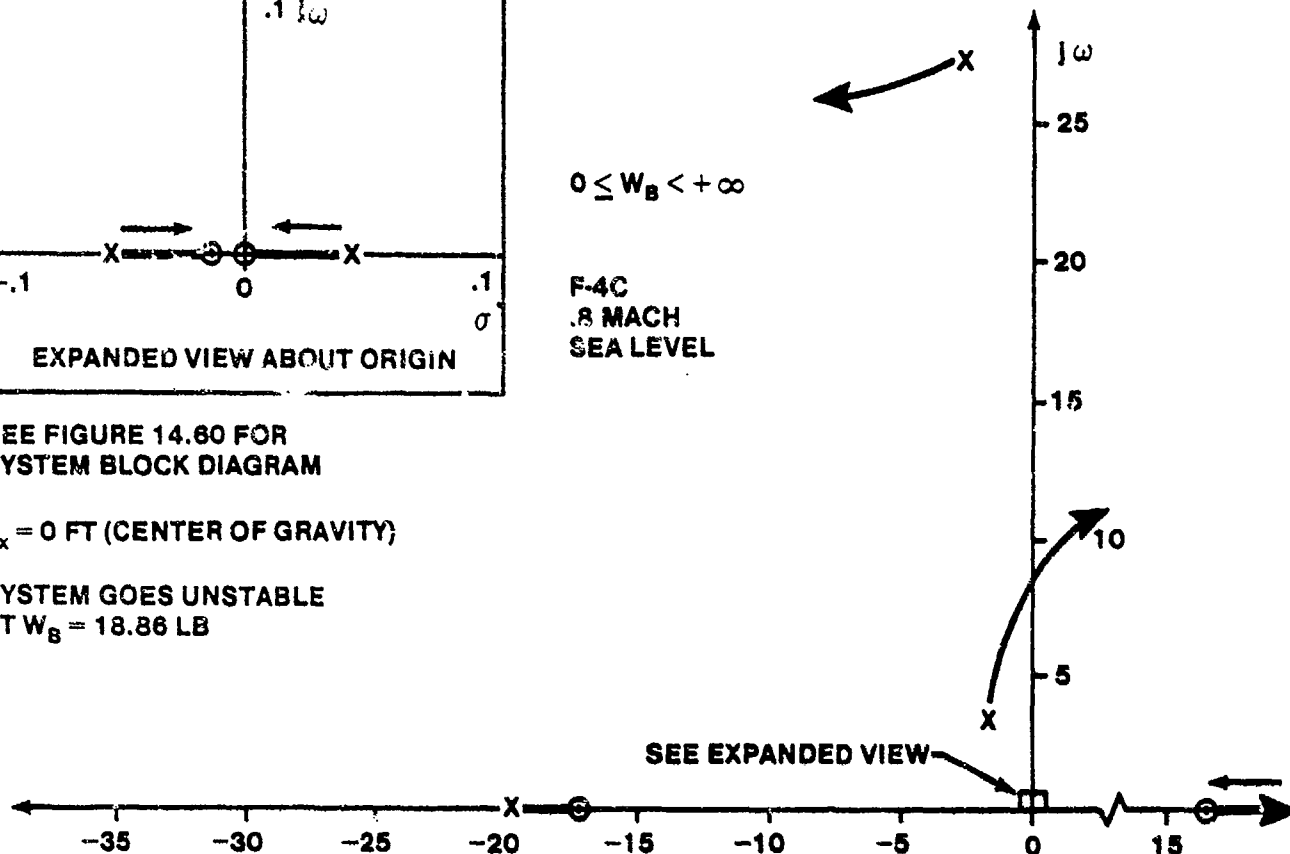
FIGURE 14.72.   ROOT LOCUS PLOT OF BOBWEIGHT LOOP FOR THE F-4C WITH FULL STICK FEEL SYSTEM.

FIGURE 14.73.   ROOT LOCUS PLOT OF BOBWEIGHT LOOP FOR THE F-4C WITH FULL STICK FEEL SYSTEM.

14.89

EXPANDED VIEW ABOUT ORIGIN
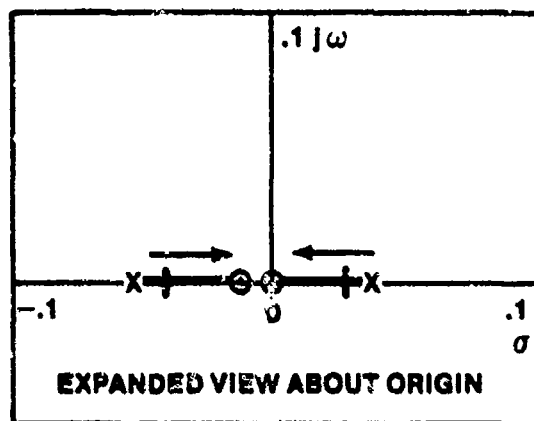
SYSTEM GOES UNSTABLE
AT W_B 17.6 LB

$0 \leq W_B < +\infty$

F-4C
.8 MACH
SEA LEVEL
CRUISE
PITCH AUG OFF

SEE FIGURE 14.60 FOR
SYSTEM BLOCK DIAGRAM
$\ell_x = 19.3$ FT

$N_{\delta_e}^{\ddot{\theta}} = -480.46 S (S + .0146) (S + .935 \pm 9.3j)$

$W_B = 5.35$ LB

SEE EXPANDED VIEW
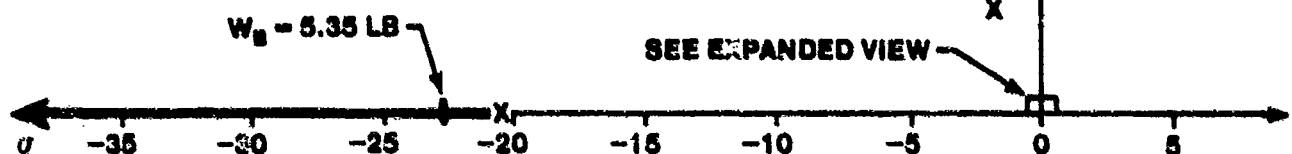
FIGURE 14.74. ROOT LOCUS PLOT OF BOBWEIGHT LOOP FOR THE F-4C WITH FULL STICK FEEL SYSTEM

$W_B = 5.35$ lbs and $\ell_x = 39.3$ feet

is

$K_\theta = 928$ lbs/rad

If the bobweight size is increased to

$W_B = 7.0$ lbs

then the short period roots go unstable at

$K_\theta = 997$ lbs/rad

Increasing the size of the bobweight reduces the PIO susceptibility

SYSTEM GOES UNSTABLE AT $W_B = 7.0$ LB

$0 \leq W_B < +\infty$

**F-4C
.8 MACH
SEA LEVEL
CRUISE
PITCH AUG OFF**

ROOT LOCATIONS WITH $W_B = 5.35$ LB (PRODUCTION W_B)

EXPANDED VIEW ABOUT ORIGIN

SEE FIGURE 14.60 FOR SYSTEM BLOCK DIAGRAM

$N_{\delta_e}^{\dot{x}} = -1127.68S\,(S + .0148)\,(S + .82 \pm 6.06j)$
$\ell_x = -39.3$ FT (PRODUCTION POSITION)

SEE EXPANDED VIEW
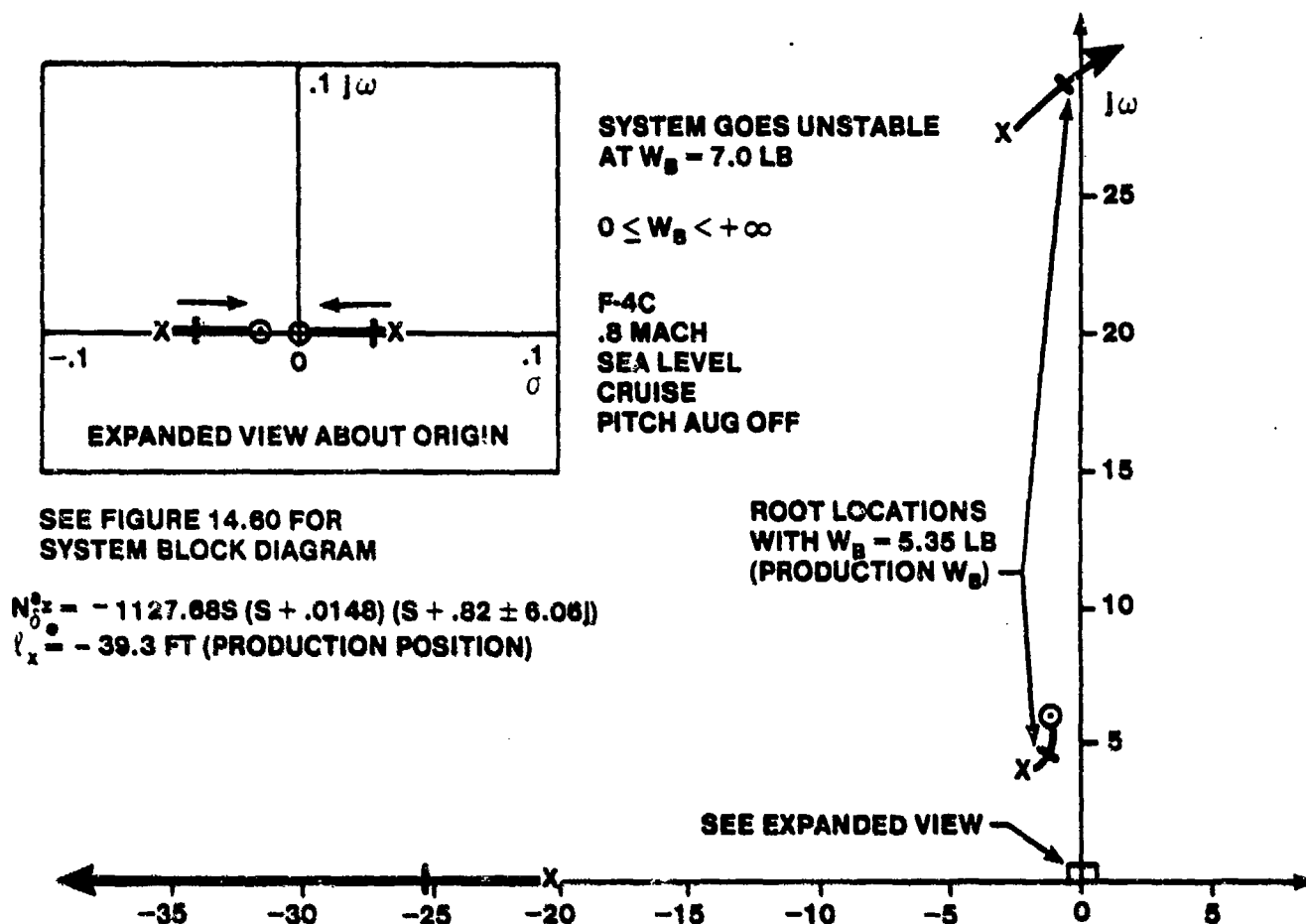
FIGURE 14.75. ROOT LOCUS PLOT OF BOBWEIGHT LOOP FOR THE F-4C WITH FULL STICK FEEL SYSTEM

but also reduces the stability of the feel system. If the bobweight is relocated so that

$$W_B = 5.35 \text{ lbs and } \ell_x = 19.3 \text{ feet}$$

then

$$K_\theta = 694 \text{ lbs/rad}$$

when the aircraft short period roots become unstable. This indicates that moving the bobweight closer to the center of gravity increases the PIO susceptibility of the aircraft.

14.91

The bobweight acts to:

1. Reduce the feel system damping.
2. Increase the feel system natural frequency.
3. Reduce the short period damping.
4. Increase the short period natural frequency.

Reducing bobweight size or moving the bobweight closer to the aircraft center of gravity increases the PIO susceptibility.

A bobweight may cause poor transient feel in high speed aircraft, if not properly designed, due to the lag between normal acceleration response and the pilot input. This may occur if the bobweight is too close to the center of gravity due to the elimination of the pitch acceleration term effects in the bobweight acceleration equation.

There is a possibility of coupling between the bobweight and the aircraft natural frequencies at high speeds, where the aircraft short period frequency is quite high (and may be of nearly the same magnitude as the feel system frequency for a system with light spring forces), which could result in uncomfortable or dangerous pitch oscillations in gusty conditions.

If the F-4C at Mach 1.1 is analyzed using the feel system dynamics present at 0.8 Mach, then the size of the bobweight must be significantly reduced to preclude the feel system from becoming unstable. The F-4C bellows spring prevents this from occurring normally since the spring forces increase proportionally with dynamic pressure. However, if a leak developed in the bellows, an unstable feel system could result which the pilot would not be able to stabilize without driving the short period roots unstable.

Figures 14.76 to 14.80 show the effect of the size of the bobweight (with and without the feel system dynamics) on the open loop F-4C short period response with the bobweight located at the production position. Figure 14.76 shows the basic aircraft short period response with the feel system and bobweight dynamics neglected. Figure 14.77 shows the same response with the feel system dynamics included. Note the slight deformations in the response at the first peak. These are due to the high frequency, lightly damped feel
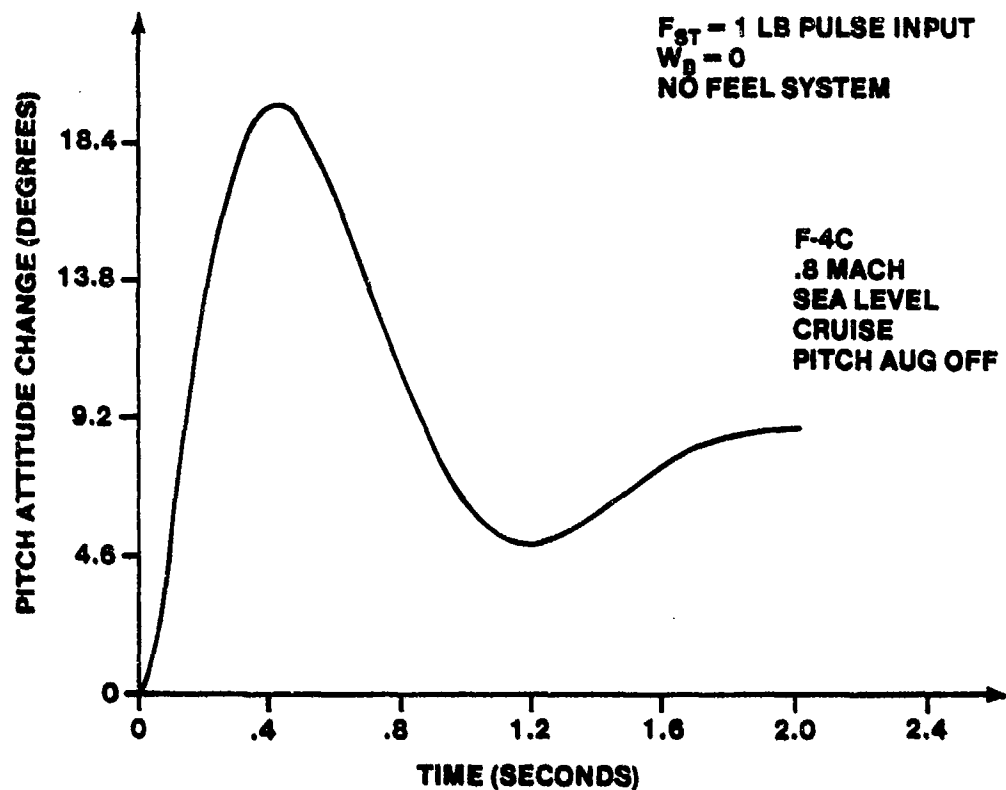
FIGURE 14.76. F-4C BASIC AIRCRAFT RESPONSE WITHOUT BOBWEIGHT OR FEEL SYSTEM
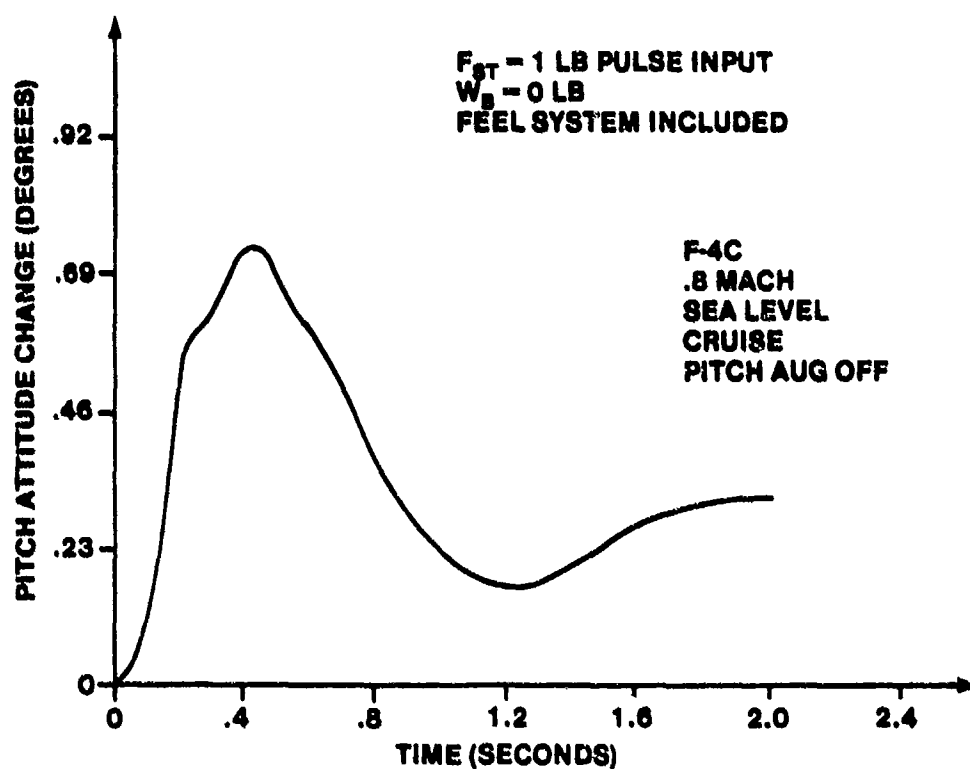
FIGURE 14.77. F-4C RESPONSE WITH FEEL SYSTEM, BOBWEIGHT OMITTED

14.93
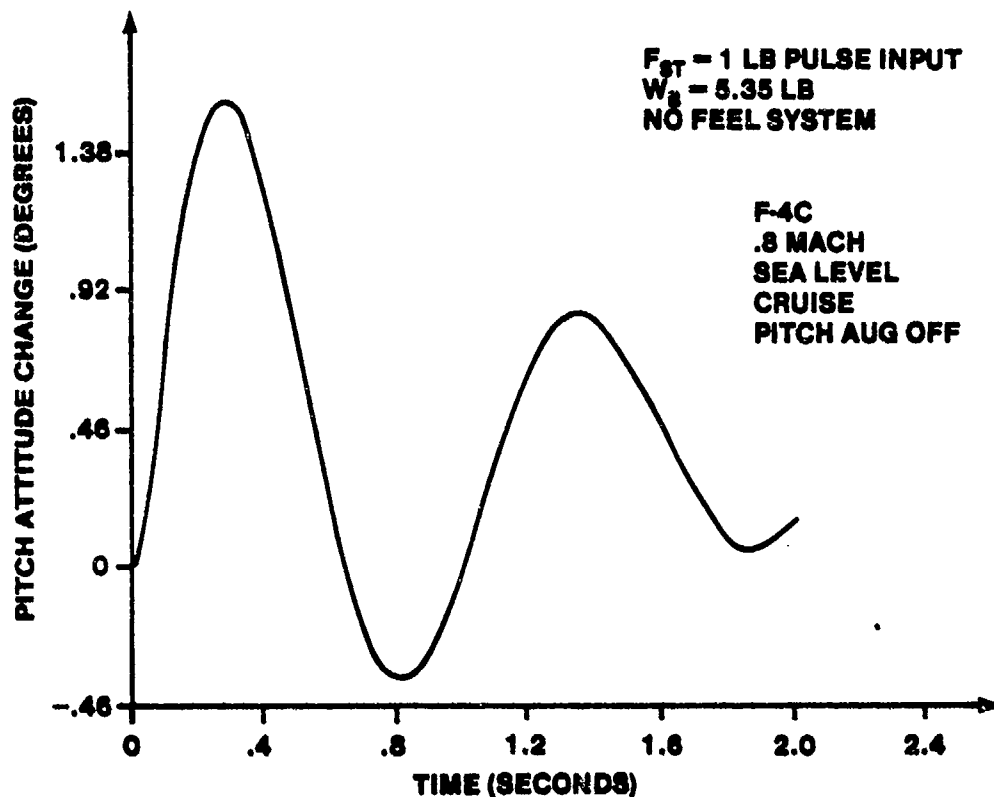
FIGURE 14.78. F-4C RESPONSE WITH BOBWEIGHT; FEEL SYSTEM OMITTED
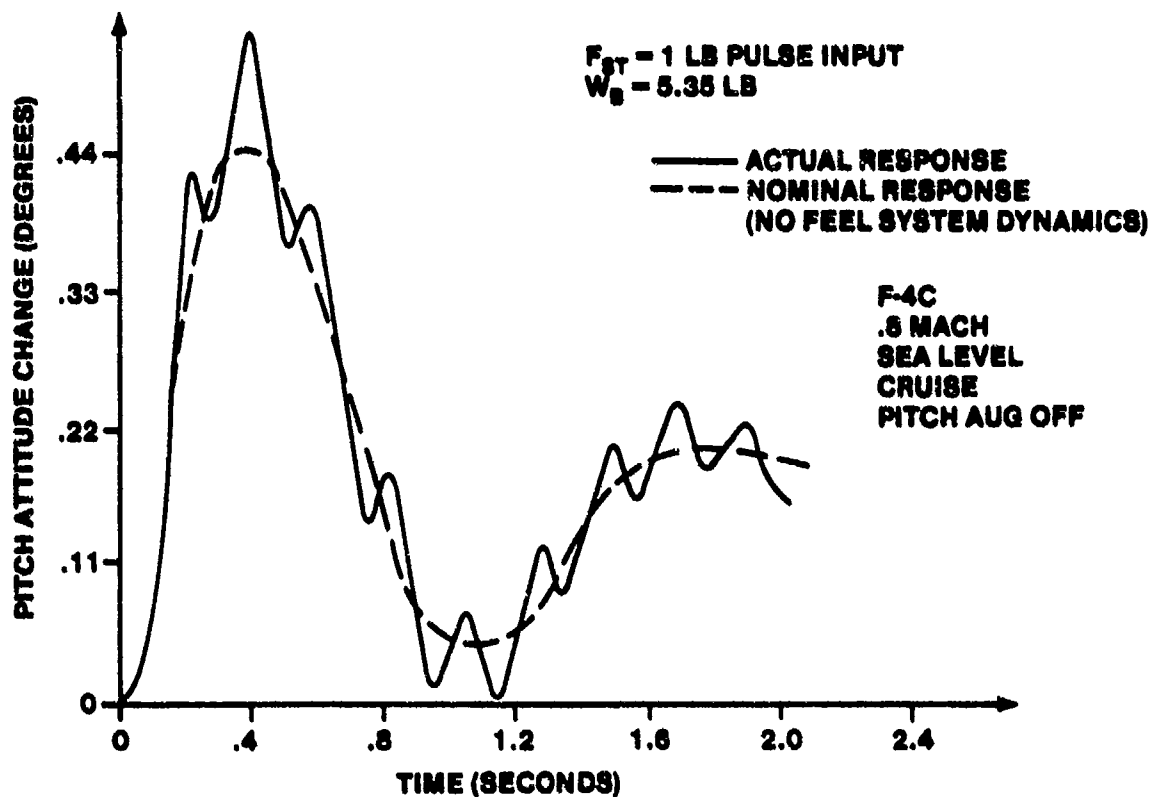
FIGURE 14.79. F-4C RESPONSE WITH PRODUCTION BOBWEIGHT
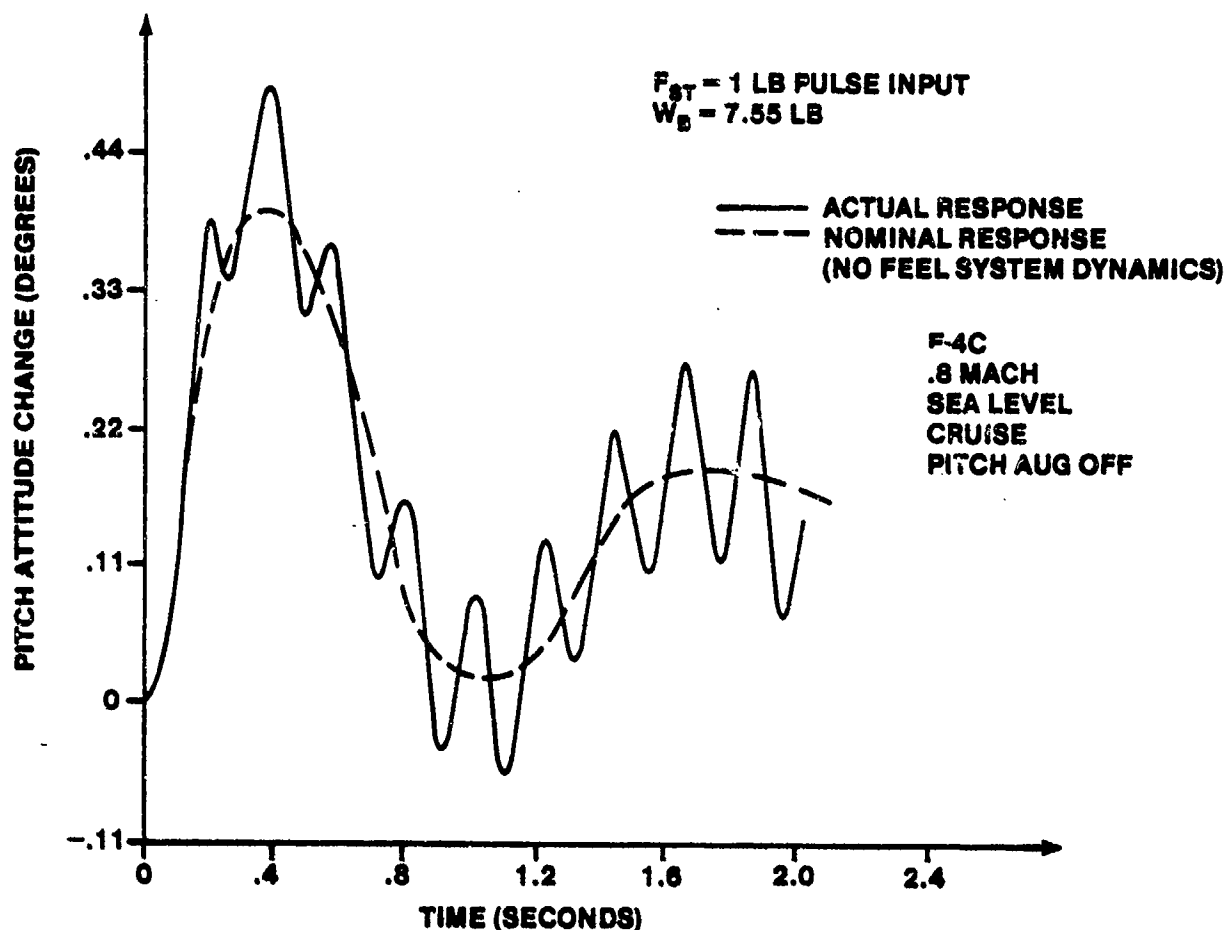
FIGURE 14.80.   F-4C RESPONSE WITH BOBWEIGHT TOO LARGE

system roots.   The damping of the short period is unchanged.   Figure 14.78
shows the effect of the bobweight, with the feel system omitted.   The short
period damping is reduced significantly.   Figure 14.79 shows the aircraft
response to a pulse stick input with the bobweight and feel system dynamics
included.   The short period damping is only slightly reduced from the basic
aircraft but the feel system dynamics are very evident.   Although the feel
system is stable, it appears to be very lightly damped.   Figure 14.80 shows
what happens to the feel system if the bobweight becomes too large.   The feel
system is driven unstable, appearing as a high frequency divergent motion
which is superimposed over the basic aircraft short period response.   Much
effort was required to achieve a bobweight configuration for the F-4C which
provided adequate maneuvering stick force characteristics while avoiding a
significant increase in the PIO susceptibility of the aircraft.   The pitch
damper which is included in the aircraft also helps to reduce the PIO
susceptibility of the aircraft.

14.3.3 Electronic Compensation Devices

14.3.3.1 Prefilter Effects. Prefilters are often added to the pilot command path of an electrical flight control system (Figure 14.81) to shape the response. A prefilter can be either a lead network, to provide a quickening of the initial aircraft response for a sluggish aircraft, or a lag network, to reduce the abruptness of the response of an overly sensitive aircraft. Figure 14.82 shows the effect of a lead network prefilter on the pitch rate response of an aircraft. Notice that the basic aircraft response is sluggish and heavily damped. With the lead prefilter on the pilot input, the response is much more abrupt. Figure 14.83 shows the effect of a lag prefilter on the pitch rate response of an aircraft with a pitch damper augmentation system. Notice that the larger the time constant of the prefilter, the more the aircraft response resembles the first order response of the prefilter.
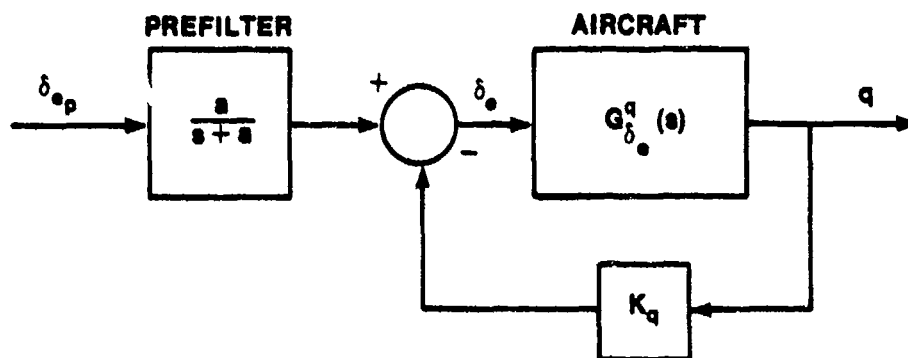
FIGURE 14.81. PREFILTER IMPLEMENTATION
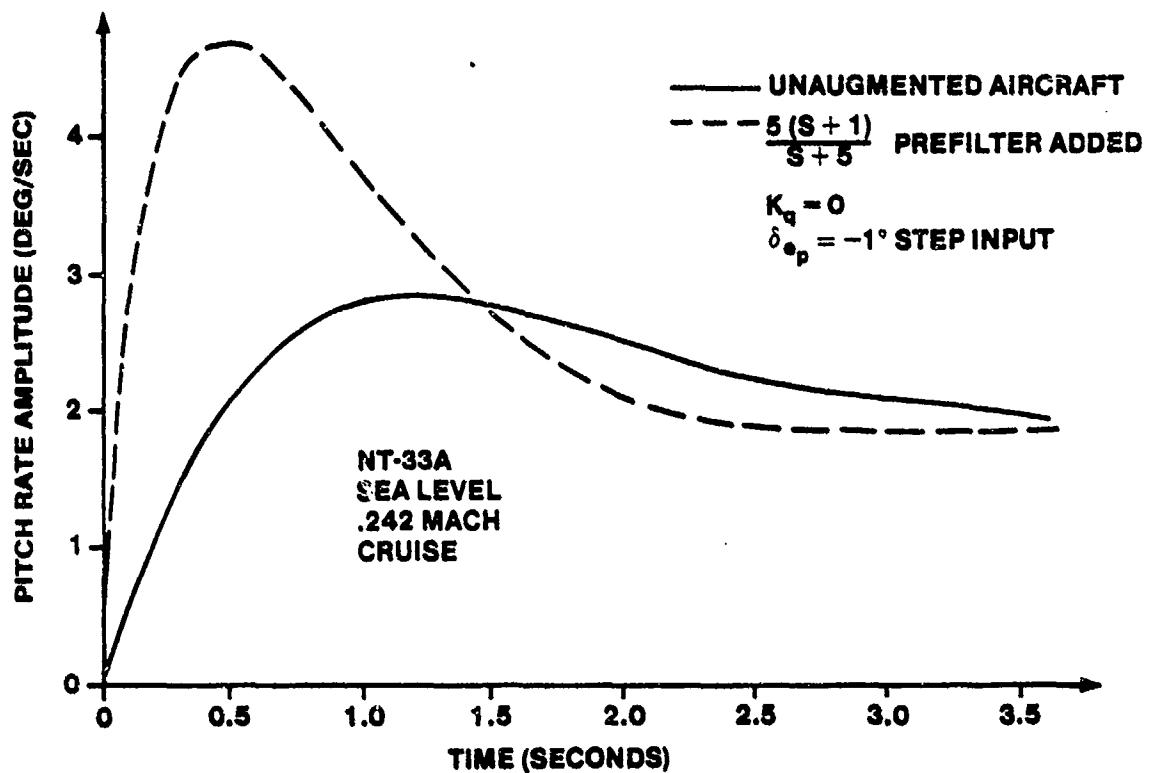
FIGURE 14.82. LEAD PREFILTER EFFECTS ON AIRCRAFT PITCH RATE RESPONSE
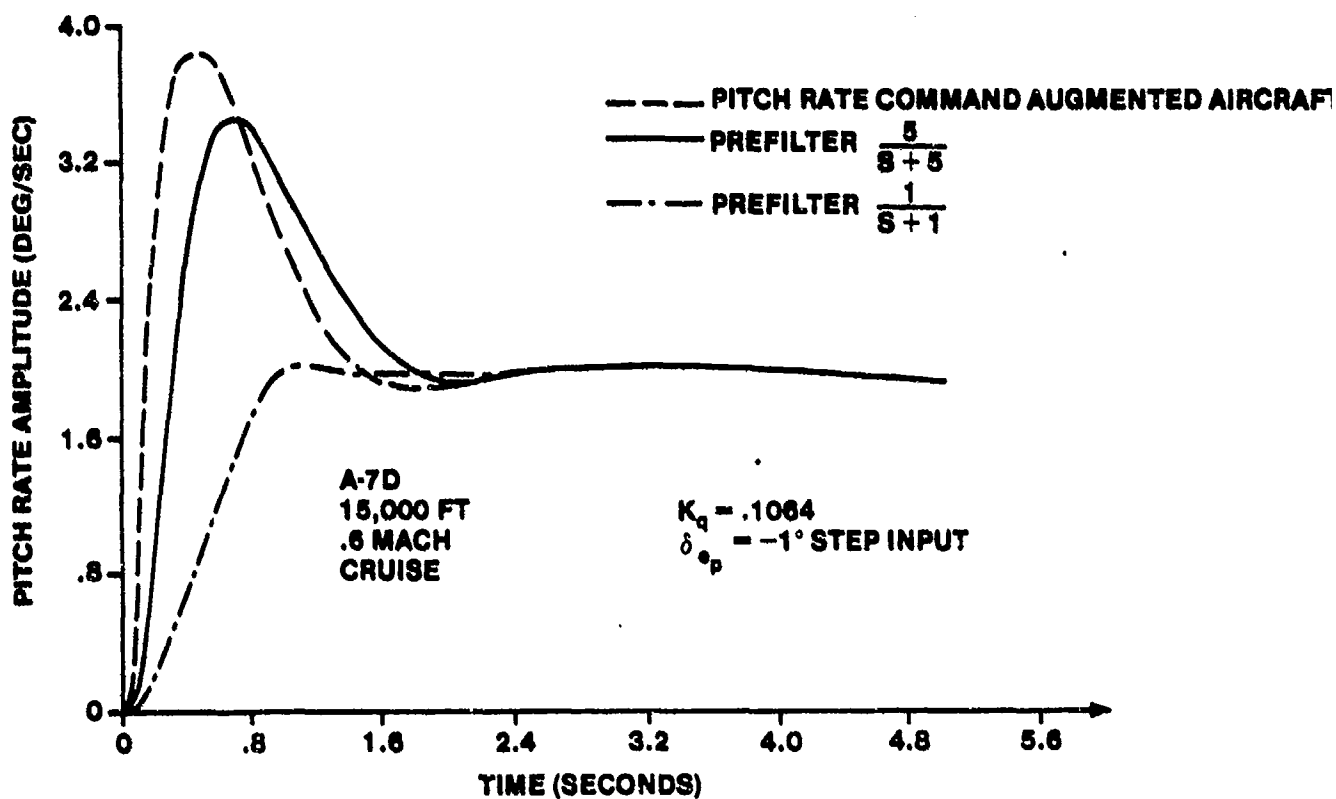
FIGURE 14.83. LAG PREFILTER EFFECTS ON AIRCRAFT PITCH RATE RESPONSE

14.3.3.2 Noise Filters. Low pass filters are frequently necessary in feedback paths to eliminate unwanted signal noise due to atmospheric turbulence, sensor dynamics, structural effects or electrical noise. Figure 14.84 presents the effect of the noise filter on the root locus of the angle of attack system discussed in paragraph 14.2 (compare to Figure 14.16). The noise filter does not appreciably alter the effect the control system has on the aircraft phugoid characteristics. The short period mode, however, is significantly altered. At a relatively low gain, the damping of short period is rapidly reduced and, at a low gain, becomes negative. Figure 14.85 shows the time response of the angle of attack of the aircraft and the shift in the feedback signal caused by the low pass filter. This phase shift causes the instability for higher gains since the error signal which drives the elevator does not represent the true angle of attack error. The second effect of the filter is to increase the order of the closed loop system, which effectively increases the initial lag in the aircraft response. A third effect is to attenuate high frequency angle of attack signals.
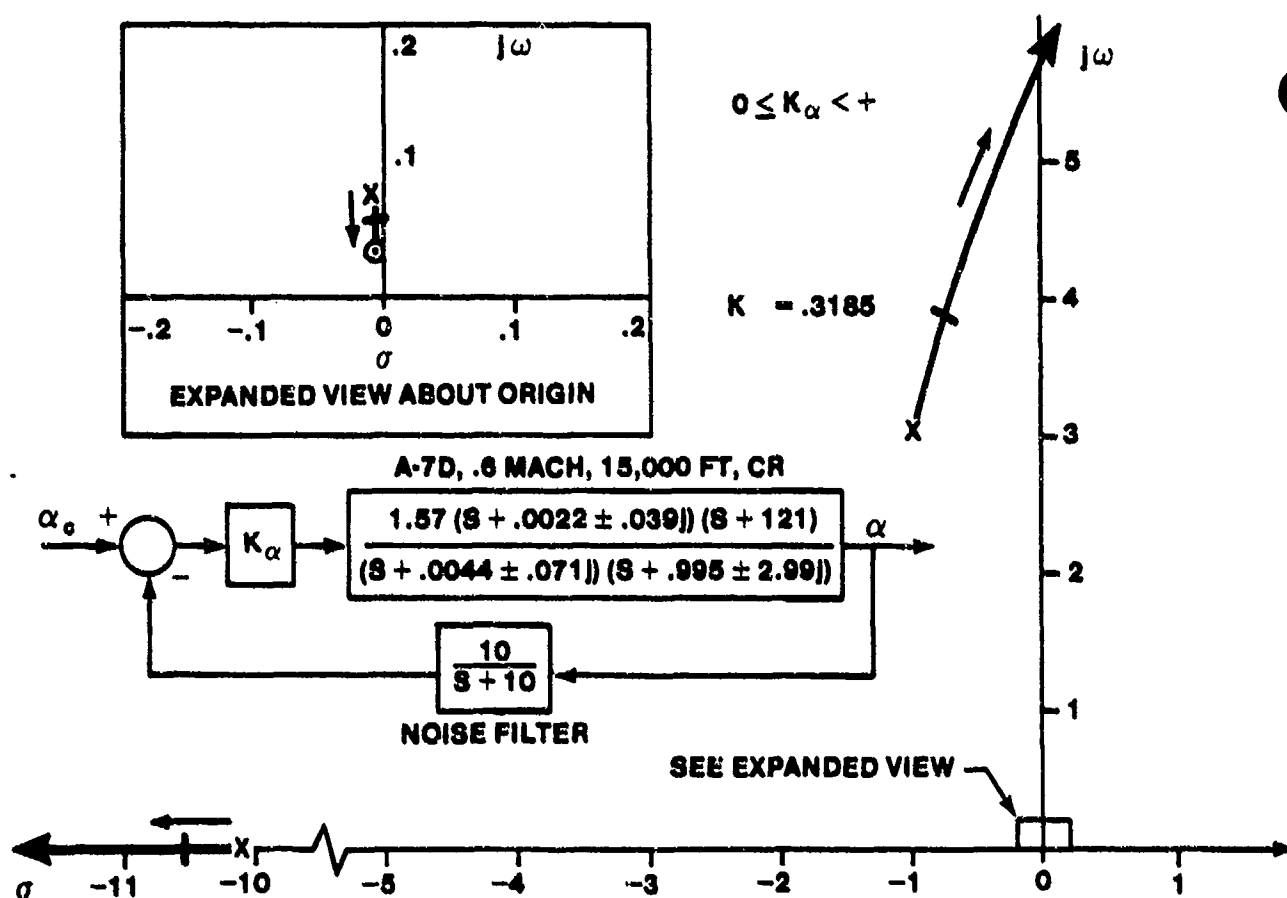
FIGURE 14.84. ROOT LOCUS PLOT OF ANGLE OF ATTACK LOOP WITH NOISE FILTER IN FEEDBACK PATH

14.98
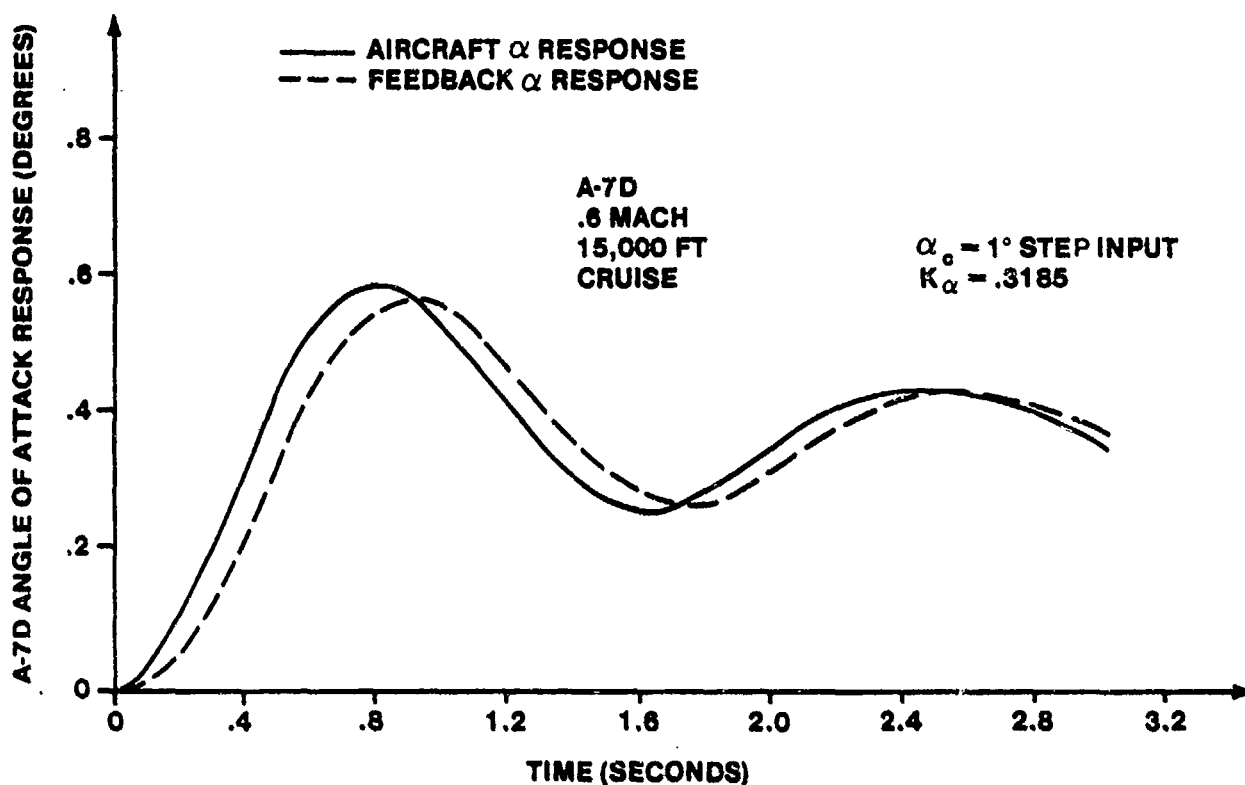
FIGURE 14.85.   A-7D ANGLE OF ATTACK RESPONSE FOR CONTROL SYSTEM WITH NOISE FILTER ON FEEDBACK

Noise filters are frequently used on sensors which detect atmospheric turbulence, such as angle of attack or sideslip sensors. Another approach is available to provide these signals for control system use to computationally derive the signals. This complementary filter approach is used to provide the flight control system with nearly noise free, turbulence resistant angular and angular rate signals with good high frequency quality for angle of attack or sideslip and has been successfully used in the variable stability Learjet and the A-7D Digitac aircraft. The computation scheme used in the A-7D Digitac to provide a high quality angle of attack signal to the directional axis (as part of a computed sideslip rate feedback control law) is shown in Figure 14.86.
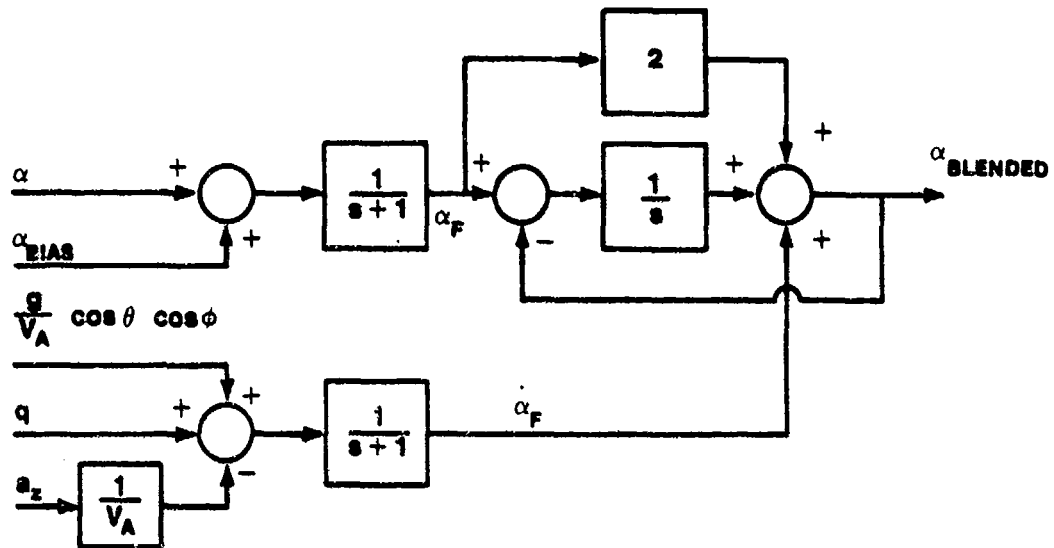
UNITS:
ANGULAR QUANTITIES - RADIANS OR RAD/SEC
ACCELERATIONS - FT/SEC²

NOTE: α_{BIAS} IS A CORRECTION OF REFERENCE
TO THE ROLL RATE GYRO PLANE

FIGURE 14.86.   ANGLE OF ATTACK COMPLIMENTARY FILTER USED IN THE A-7D DIGITAC
AIRCRAFT

The angle of attack derivation is based on the normal acceleration
equation

$$a_n = U_0 (q - \dot{\alpha}) + g \cos\theta \cos\phi \qquad \text{(positive up)} \qquad (14.53)$$

where a_n is the acceleration at the center of gravity.

The accelerometer location forward of the center of gravity is neglected
since it produces only a small error in the implementation.

The acceleration signal is subtracted from the pitch rate and gravity
signals to yield

$$\dot{\alpha} = - \frac{1}{V_A} a_n + q + \frac{g}{V_A} \cos\theta \cos\phi \qquad (U_0 = V_A) \qquad (14.54)$$

Neglecting the bias signal, and denoting the signal after the low pass filters as

$$\alpha_F \text{ and } \dot{\alpha}_F$$

then

$$\alpha_{BLENDED} = \dot{\alpha}_F + 2\alpha_F + \frac{1}{s}(\alpha_F - \alpha_{BLENDED})$$

or

$$(1 + \frac{1}{s}) \alpha_{BLENDED} = (s + 2 + \frac{1}{s}) \alpha_F$$

$$\frac{(s + 1)}{s} \alpha_{BLENDED} = \frac{(s + 1)^2}{s} \alpha_F$$

But

$$\alpha_{BLENDED} = (s + 1) \alpha_F = \dot{\alpha}_F + \alpha_F$$

$$\dot{\alpha}_F = \frac{1}{s + 1} \dot{\alpha}$$

$$\alpha_F = \frac{1}{s + 1} \alpha$$

so that

$$\alpha_{BLENDED} = \frac{1}{s + 1} \dot{\alpha} + \frac{1}{s + 1} \alpha \tag{14.55}$$

The angle of attack vane signal provides the low frequency (below 1 radian per second) portion of the signal and the angle of attack rate signal provides the high frequency part of the signal, since

$$\frac{1}{s + 1} \dot{\alpha} = \frac{s}{s + 1} \alpha$$

Looking at the Bode plot of Figure 14.87 it is apparent that high quality angle of attack magnitude information is passed through the filter.
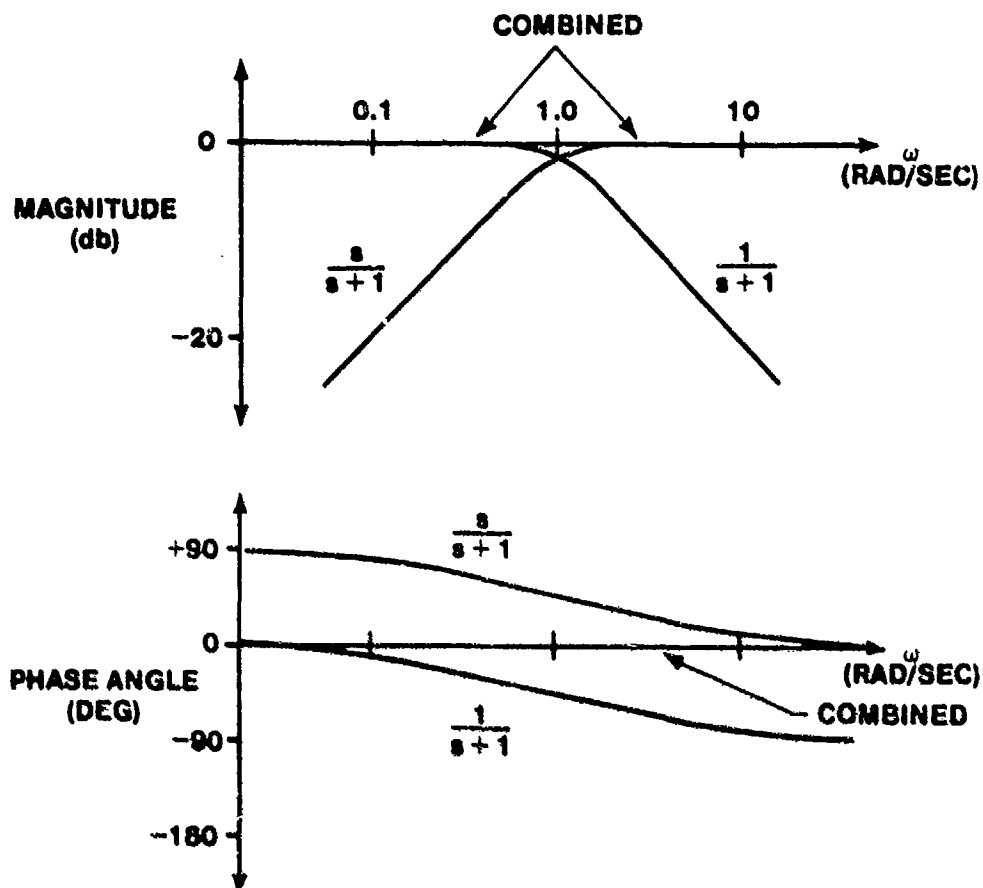
FIGURE 14.87. BODE PLOT FOR ANGLE OF ATTACK COMPLIMENTARY FILTER

If it is assumed that a signal which is attenuated more than 3 decibels does not contribute to the phase angle, then minimal phase shift is experienced by the output signal across the full spectrum of the angle of attack signal. Complimentary filters have excellent features which are just recently being realized.

14.3.3.3 **Steady-State Error Reduction.** Steady-state errors in feedback control systems are sometimes useful and sometimes undesirable. If speed stability is desired, a small steady-state error is necessary in the longitudinal axis of the control system. Since the aircraft will not precisely hold a commanded attitude or airspeed by itself, the pilot must provide a control input, either through the stick or trim system, to maintain the desired flight condition. The amount of additional control input or trim required is dependent on the aircraft characteristics and may be altered in several ways.

Perfect neutral speed stability is not attainable except with an altitude hold system but aircraft with nearly neutral speed stability can be realized with a 'g' command system. If nearly neutral speed stability is desired for piloted flight, an integrator is required in the forward path of a load factor command control system. Two implementations are possible--the addition of a pure integrator or the use of a proportional plus integral scheme. If speed stability is desirable, but a lower stick force gradient is required, then a lag filter may be added which reduces the steady-state error but does not completely eliminate it. Pure lag filters are not useful for error reduction. Similar uses for these methods of steady-state error reduction are applicable to the directional axis, especially in the elimination of sideslip (lateral acceleration).

The location of these devices to reduce steady-state error is limited to the forward path for the longitudinal axis. If a lag filter is used in the feedback path, the steady-state error will increase. If an integrator is used in the feedback path, the aircraft steady-state error will be unity.

In the lateral-directional axis, the use of an integrator in the feedback path of a lateral acceleration feedback system will maintain the sideslip angle at zero, a desirable feature in the elimination of unwanted lateral acceleration. The use of integrators in autopilots is common and is usually required to achieve the desired precision.

14.3.3.3.1 Effects of a Forward Path Integrator. If a pure integrator is placed in the forward path, a zero steady-state error for step inputs will result, since, for a pitch attitude system

$$e_{ss} = \lim_{s \to 0} \frac{1}{1 + \frac{K_\theta}{s} G_{\delta_e}^\theta (s)} = \frac{1}{1 + \infty} = 0 \qquad (14.56)$$

A similar result occurs for a load factor command system. If however, the integrator is used in a pitch rate command system, then a steady-state error occurs in the pitch rate but not in the pitch attitude. The use of integrators in the pitch rate command system for an unstable aircraft is discussed extensively in Paragraph 14.3.3.4.

Integrators will dramatically alter the root locus of the augmented aircraft from the characteristics discussed in the last chapter. Figure 14.88

shows the effect of an integrator added to the forward path of a simple pitch
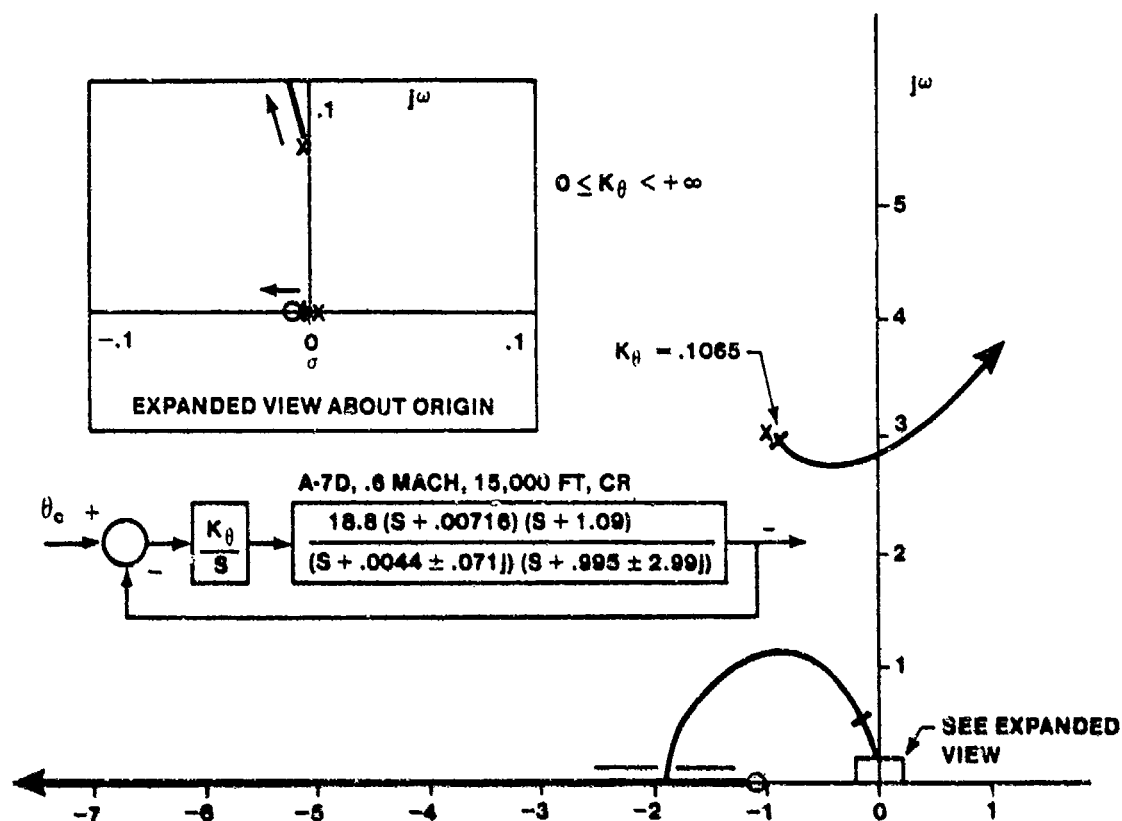
FIGURE 14.88. ROOT LOCUS PLOT OF PITCH ATTITUDE LOOP WITH FORWARD PATH
INTEGRATOR ADDED

attitude command system (compare this root locus to Figure 14.7b). The phugoid roots may move rapidly as the gain increases to a very high frequency (greater than 1.5 radians per second) while the short period roots very quickly become unstable. At low to moderate gain, two pairs of complex roots, those starting as the phugoid pair and those starting as the short period, can both occur in the angle of frequencies normally associated with the short period. The aircraft motion can no longer be described by a simple second order response and the requirements of MIL-F-8785C will be difficult to use. Figure 14.96 shows the time response of the aircraft pitch attitude with the pure integral controller. The excessive overshoot and poor convergence to the final aircraft pitch attitude is due to the lag introduced by the integrator. Notice the large initial time delay before the aircraft starts to respond to the pilot input. Better convergence can be achieved with higher integrator gains, but instability problems generally preclude the use of high gains.

If an integrator is added to a pitch rate command system, two effects will occur. The pitch rate command system root locus will be identical to the pitch attitude root locus, where the short period natural frequency increases and the damping ratio decreases while the phugoid characteristics are suppressed. This is not what would be expected from a pitch rate feedback system. Also, the integrator suppresses the large initial pitch rate overshoot which normally occurs in conventional aircraft. Excessive suppression of this characteristic is detrimental to acceptable handling qualities.

The use of a pure integrator in the forward path of a load factor command system provides apparent neutral speed stability, but is seldom used. The control strategy suffers because the pilot has no direct command path to the elevator. His inputs are applied to the integrator and the pilot must wait for the integration to occur before the aircraft responds. A large amount of lag is added to the system which can drive the short period roots unstable at a low system gain, as shown in Figure 14.89. The phugoid roots move rapidly to the real axis, creating an unsuppressed real root which can adversely affect the time response of the aircraft, as shown in Figure 14.98. Notice the significant effective time delay which initially occurs. Also, the integrator causes an unstable root near the origin which will eventually cause
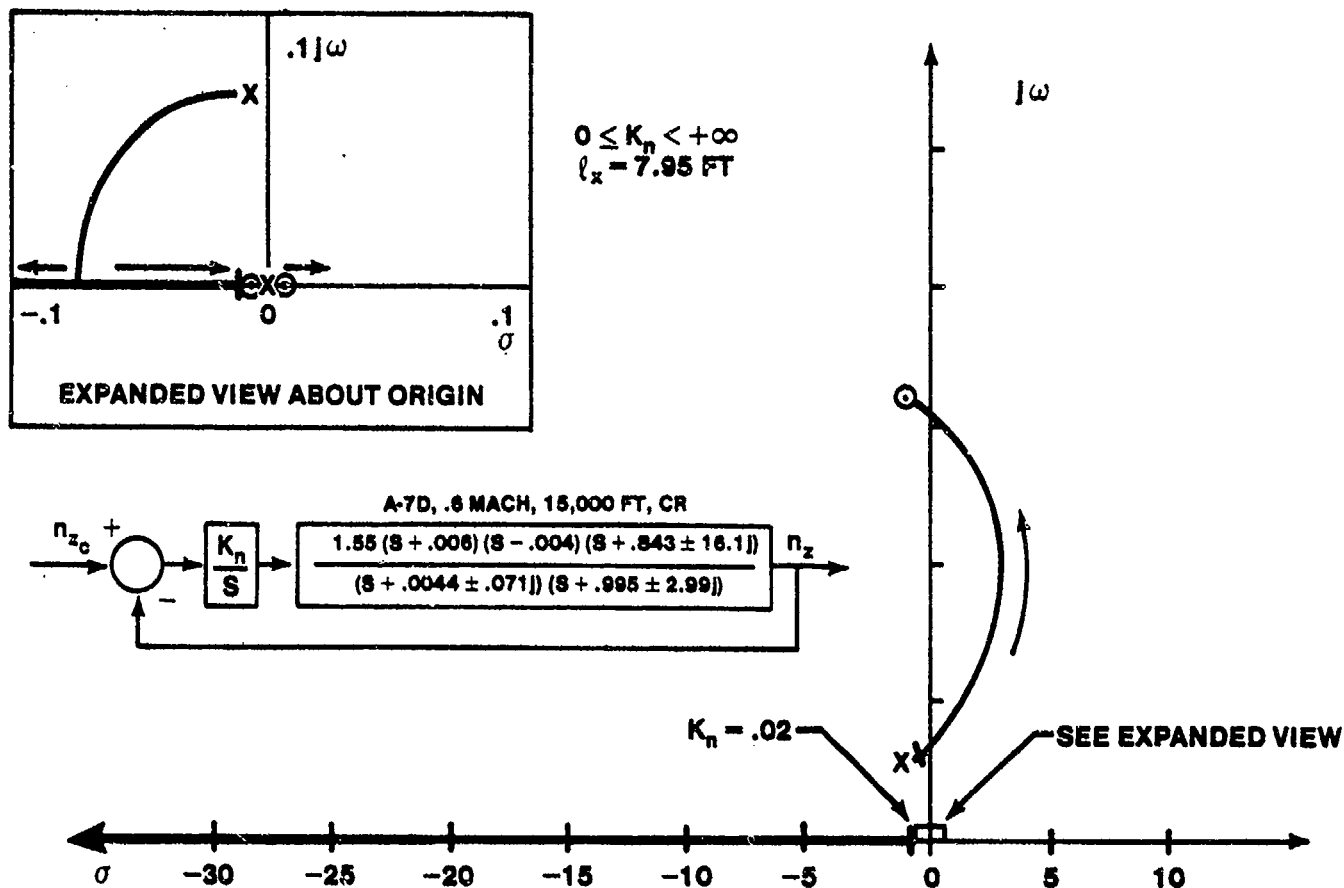
FIGURE 14.89. ROOT LOCUS PLOT OF 'G' COMMAND SYSTEM WITH INTEGRAL CONTROLLER

the aircraft to diverge (compare Figure 14.89 with Figure 14.19). However, if the time constant of the unstable root is long, neutral speed stability will be realized for all practical purposes.

14.3.3.3.2 Effects of a Lag Compensator. A lag compensator of the form

$$G(s) = \frac{s + Ka}{s + a} \quad (K > 1) \tag{14.57}$$

can be designed to approximate the action of the integrator at low frequencies. The gain, K, is usually not greater than 10, due to practical analog design considerations, so that the zero is not more than 10 times further from the origin than the pole.

The lag filter reduces the steady state error for a step input by a significant amount. For a system without the lag filter (Figure 14.7b)

14.106

$$e_{ss} = \lim_{s \to 0} \left[\frac{1}{1 + K_\theta G^\theta_{\delta_e}(s)} \right] = \frac{1}{1 + 2.92K_\theta} = 0.62 \quad (K_\theta = 0.213) \quad (14.58)$$

With the lag filter added

$$e_{ss} = \lim_{s \to 0} \left[\frac{1}{1 + \dfrac{K_\theta(s + 0.1)}{(s + 0.01)} G^\theta_{\delta_e}(s)} \right] = \frac{1}{1 + 29.2K_\theta} = 0.139 \quad (14.59)$$

A 78% reduction in the steady state error occurs. Larger percentage reductions can occur for higher gain, since high gain contribute to lower errors. However, in this system, high gain also cause low short period damping which would be unacceptable. A residual steady state error for step inputs exists since an integrator is not present. The lag filter is usually placed in the low frequency region so as not to affect the short period response of the aircraft while changing the phugoid response significantly. Referring to Figure 14.90, it is apparent that the phugoid natural frequency and damping are increased significantly while the short period response is not significantly altered from the system of Figure 14.7b. Figure 14.91 shows the time response of the aircraft pitch attitude illustrating the effects of the lag filter.
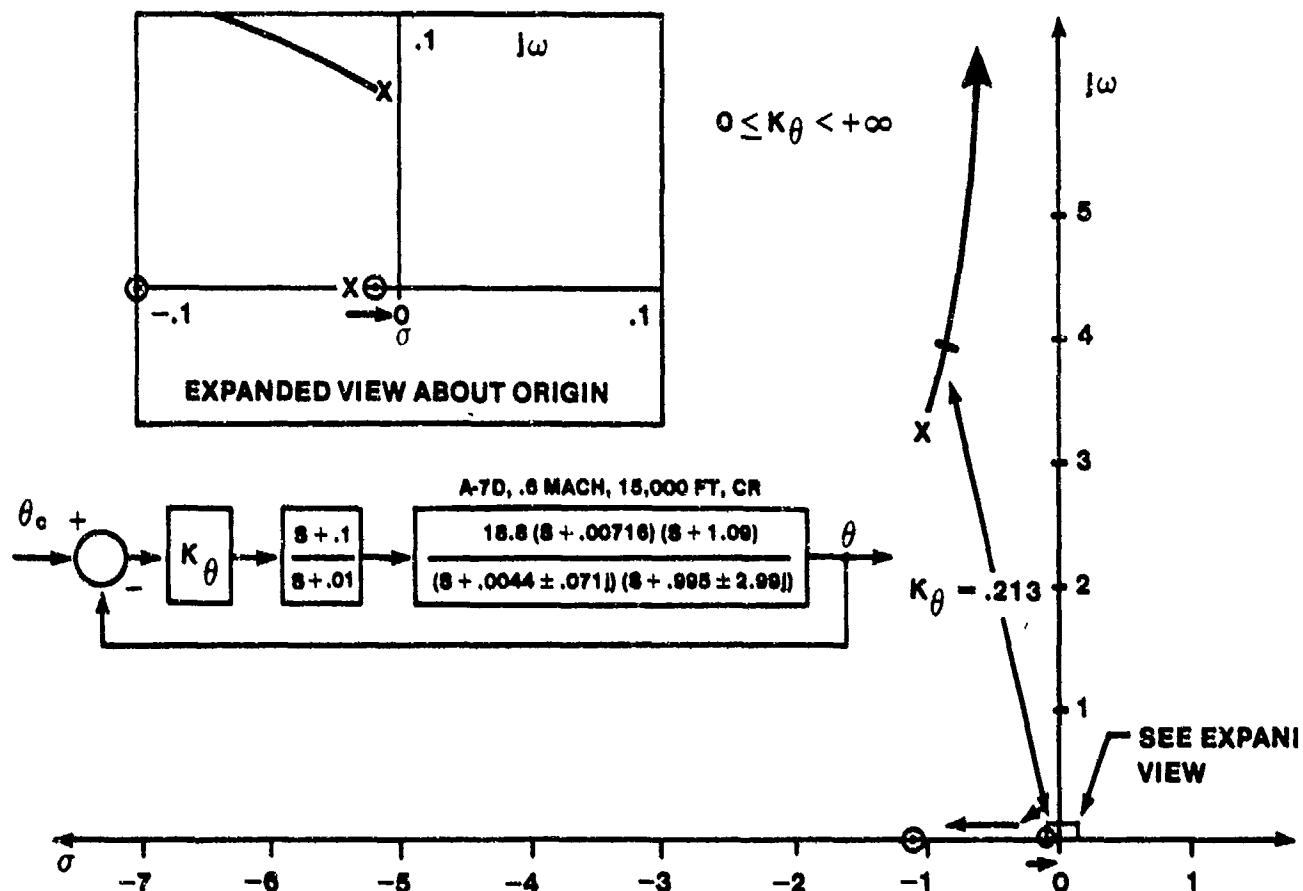
FIGURE 14.90. ROOT LOCUS PLOT OF PITCH ATTITUDE LOOP WITH LAG FILTER ADDED TO REDUCE e_{ss}

14.107
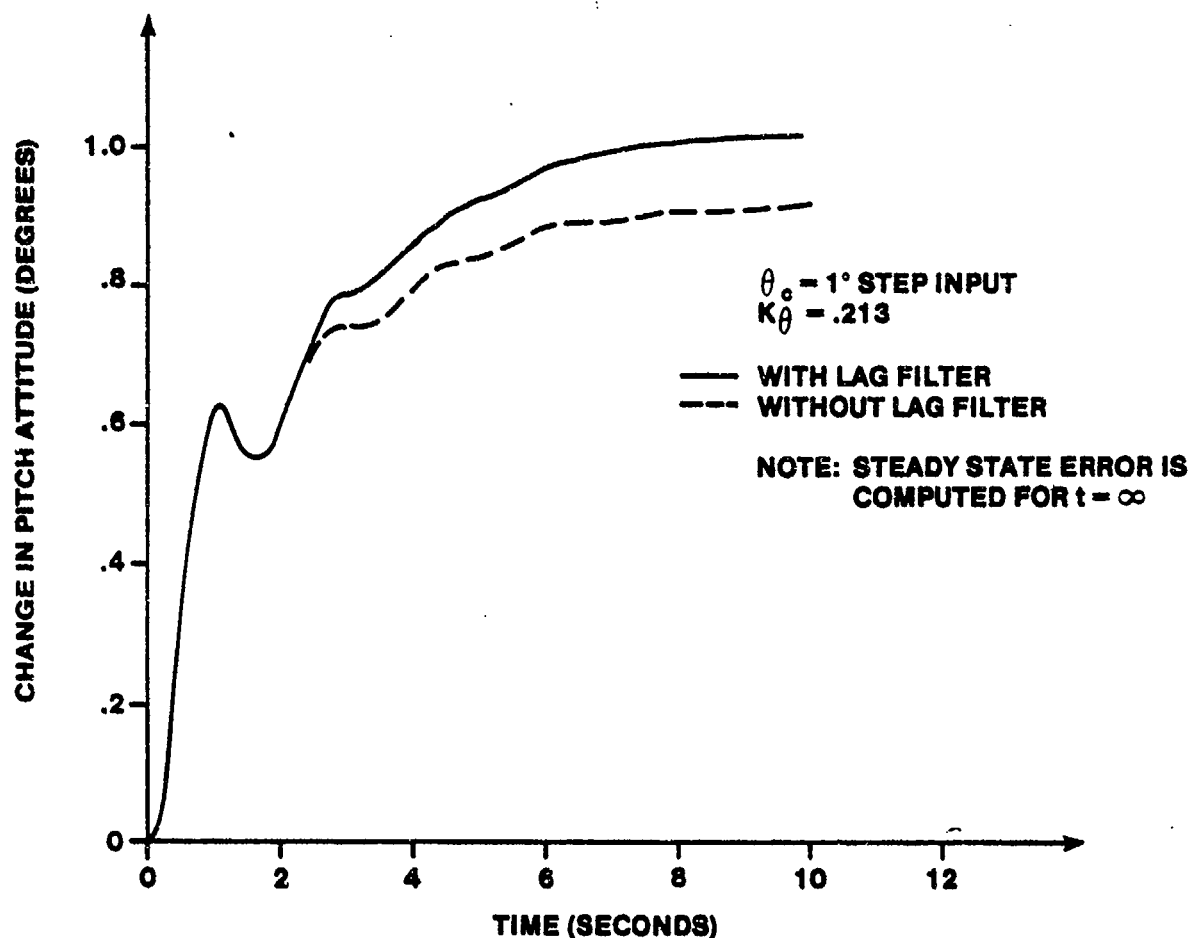
FIGURE 14.91. A-7D PITCH ATTITUDE RESPONSE WITH LAG FILTER

The A-7D digitac aircraft uses a lag filter in the pitch axis to reduce the speed stability of the aircraft relative to the normal A-7D, thereby reducing the pilot stick forces necessary to maintain a constant dive angle during dive bombing, where a speed increase from 300 kts at roll-in to 450 kts at bomb release is typical.

14.3.3.3.3 **Effects of Proportional Plus Integral Control.** A frequently used scheme to achieve neutral speed stability in a load factor command system while avoiding the main disadvantages (excessive lag and poor convergence characteristics) of the pure integral control implementation is the proportional plus integral network. A block diagram of this network is shown in Figure 14.92. The transfer function of this network is

$$G(s) \;=\; 1 + \frac{K}{s} \;=\; \frac{s + K}{s} \tag{14.60}$$

and the steady-state error of the pitch attitude command system for a step input is

$$e_{ss} = \lim_{s \to 0} \left[\frac{1}{1 + K_\theta \dfrac{(s + K)}{s} G^\theta_{\delta_e}(s)} \right] = \frac{1}{1 + \infty} = 0 \qquad (14.61)$$
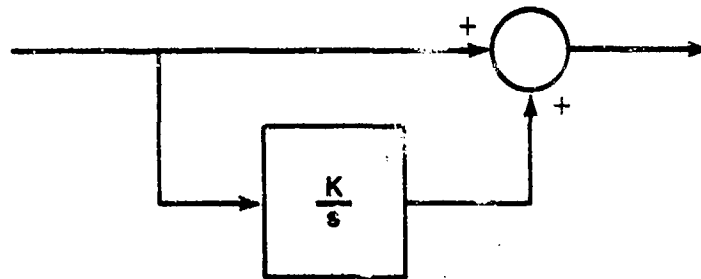
FIGURE 14.92.   PROPORTIONAL PLUS INTEGRAL CONTROLLER

The effect of proportional plus integral controllers on the augmented aircraft characteristics is nearly a direct function of the integrator gain, K. For high values of K the effect is similar to that of a pure integrator in the forward path (compare Figure 14.93 to Figure 14.88). The added zero due to the proportional plus integral controller causes the augmented aircraft roots to move further on the root locus plot for a specified gain than in the case of the pure integral controller, depending on the integrator gain, K. For low values of K, the effect more closely approximates that of the lag filter (compare Figure 14.94 to Figure 14.90) except that the step input steady state error is zero.

The main advantage this scheme has over the pure integrator approach is that the pilot is provided a direct path to the elevator and does not have to wait for an integration to occur prior to seeing the aircraft respond. The zero at s = -K helps to quicken the response over the pure integrator scheme at low values of K. Higher values of K contribute to an effective time delay due to the increased lag caused by the integrator. However, higher integrator gains are generally possible using a proportional plus integral scheme than when using a pure integral controller, shortening the convergence time of the

system to the commanded status.
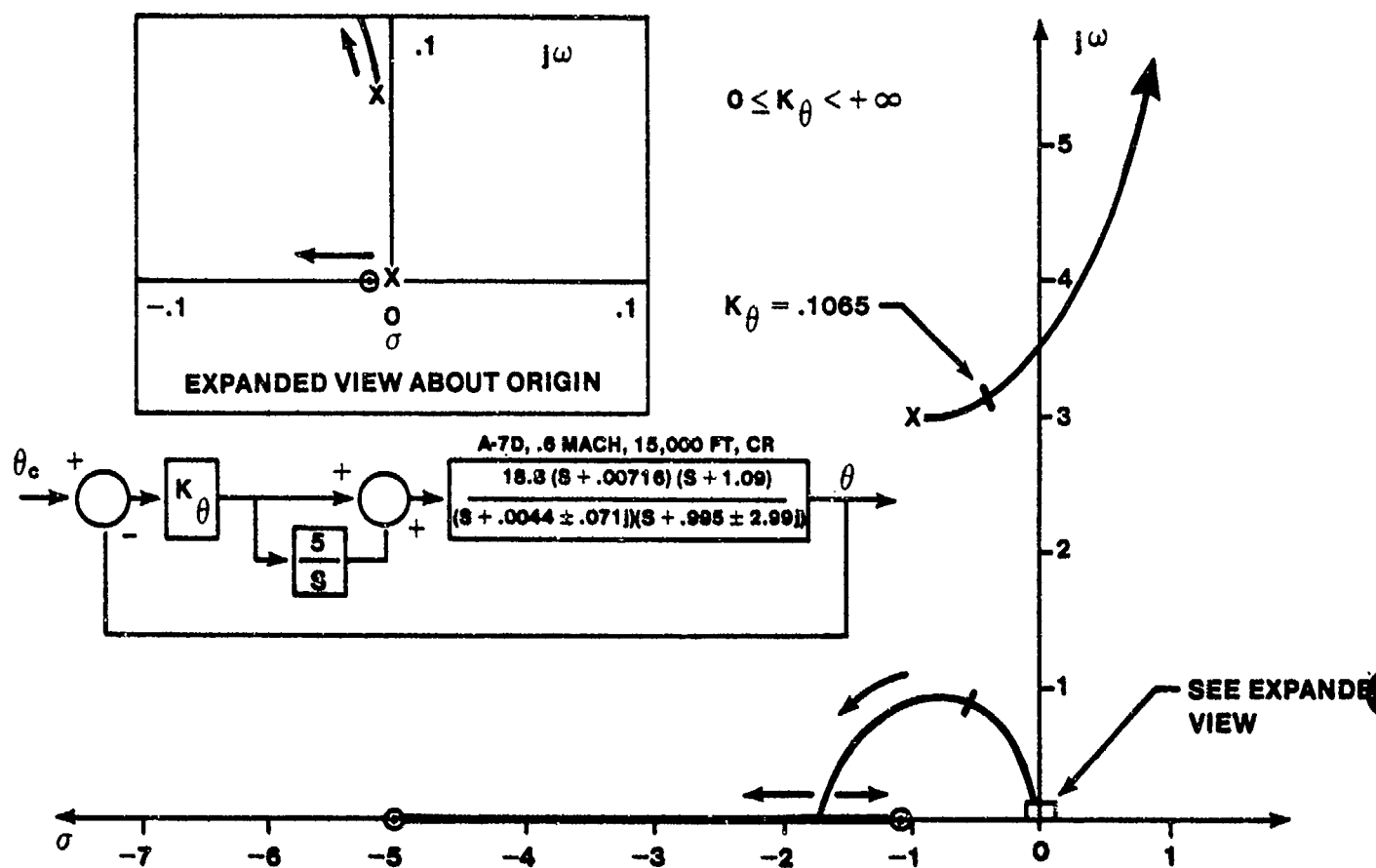
FIGURE 14.93.   ROOT LOCUS PLOT OF PITCH ATTITUDE LOOP WITH PROPORTIONAL PLUS
                INTEGRAL CONTROLLER, HIGH INTEGRATOR GAIN
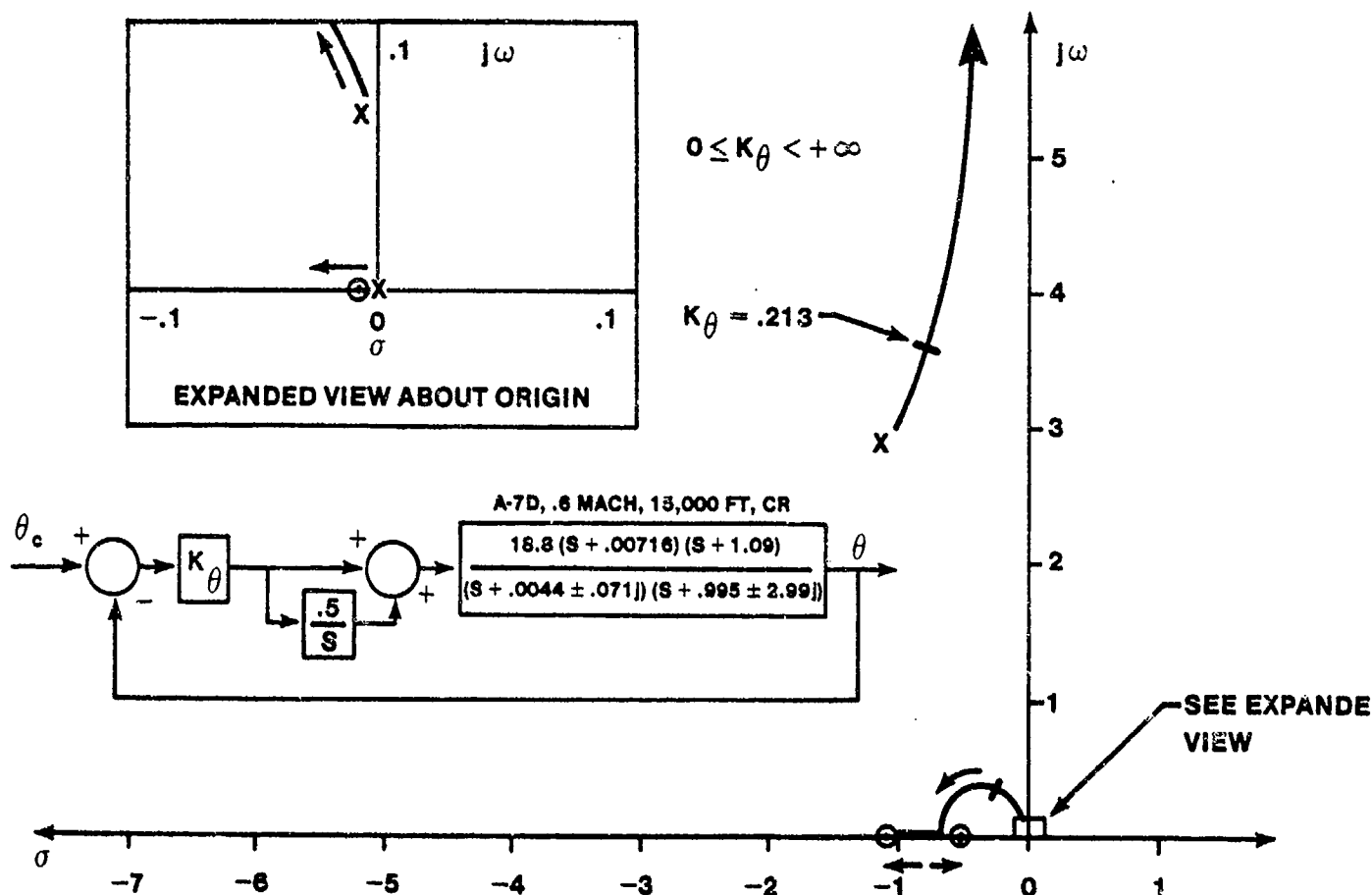
FIGURE 14.94. ROOT LOCUS PLOT OF PITCH ATTITUDE LOOP WITH PROPORTIONAL PLUS INTEGRAL CONTROLLER, LOW INTEGRATOR GAIN

If this system is added to the forward path of a pitch rate command system, the pitch rate overshoot characteristic of conventional aircraft is suppressed somewhat but not as severely as in the pure integrator case. For low values of K, the overshoot suppression is small. For high values of K, the overshoot suppression is substantial and approaches the poor flying qualities of the pure integrator scheme.

Figure 14.95 shows the root locus plot for a 'g' command system with a proportional plus integral controller. The zero added by the proportional path prevents the excessive lag present in the system with the pure integral controller so that the short period roots are not driven unstable at any system gain.

EXPANDED VIEW ABOUT ORIGIN

$.1 j\omega$

$-.1$ 0 $.1$
σ

$0 \leq K_n < +\infty$
$\ell_x = 7.95$ FT

A-7D, .6 MACH, 15,000 FT, CR

$$\frac{K_n (S + .5)}{S}$$

$$\frac{1.55 (S + .006)(S - .004)(S + .843 \pm 16.1j)}{(S + .0044 \pm .071j)(S + .995 \pm 2.99j)}$$

n_{z_c} $+$ $-$ n_z

$j\omega$

-25
-20
-15
-10
-5

$K_n = .02$

ROOT AT
$S = -.22$

SEE EXPAND VIEW

σ -35 -30 -25 -20 -15 -10 -5 0 5

FIGURE 14.95.   ROOT LOCUS PLOT OF 'G' COMMAND SYSTEM WITH PROPORTIONAL PLUS INTEGRAL CONTROLLER

Figure 14.96 shows the time response characteristics of a pitch attitude command system with a proportional plus integral controller in the forward path. Both responses are higher order and the requirements of MIL-F-8785 are difficult to apply. The higher integrator gain causes a faster rise time and more rapidly approaches the final value. Also note the difference in the initial response (below 0.2 seconds). The zero at s = -K does not aid the initial response of the system with the high integrator gain, resulting in an effective time delay of nearly 0.2 seconds (versus 0.1 seconds for the lower integrator gain). This effective time delay characteristic of highly augmented analog systems (no actual time delay occurs in analog systems, only in digital systems) has been correlated to a severe degradation in handling qualities when excessive.

FIGURE 14.96. A-7D PITCH ATTITUDE RESPONSE WITH PROPORTIONAL PLUS INTEGRAL CONTROL

Figure 14.97 shows the output signals associated with the proportional part of the network, the integrator, and the complete controller. Notice that the integrator rapidly assumes the majority of the error signal while the proportional path must act to reduce the total network output. The integrator actually causes the overshoot of the final pitch attitude value (commanded attitude) to occur.

Figure 14.98 compares the responses of two load factor command systems, one with a pure integral controller discussed in Paragraph 14.3.3.3.1, and one with a proportional plus integral controller. The effective time delay is reduced and the system convergence improved with the proportional plus integral controller.

14.113
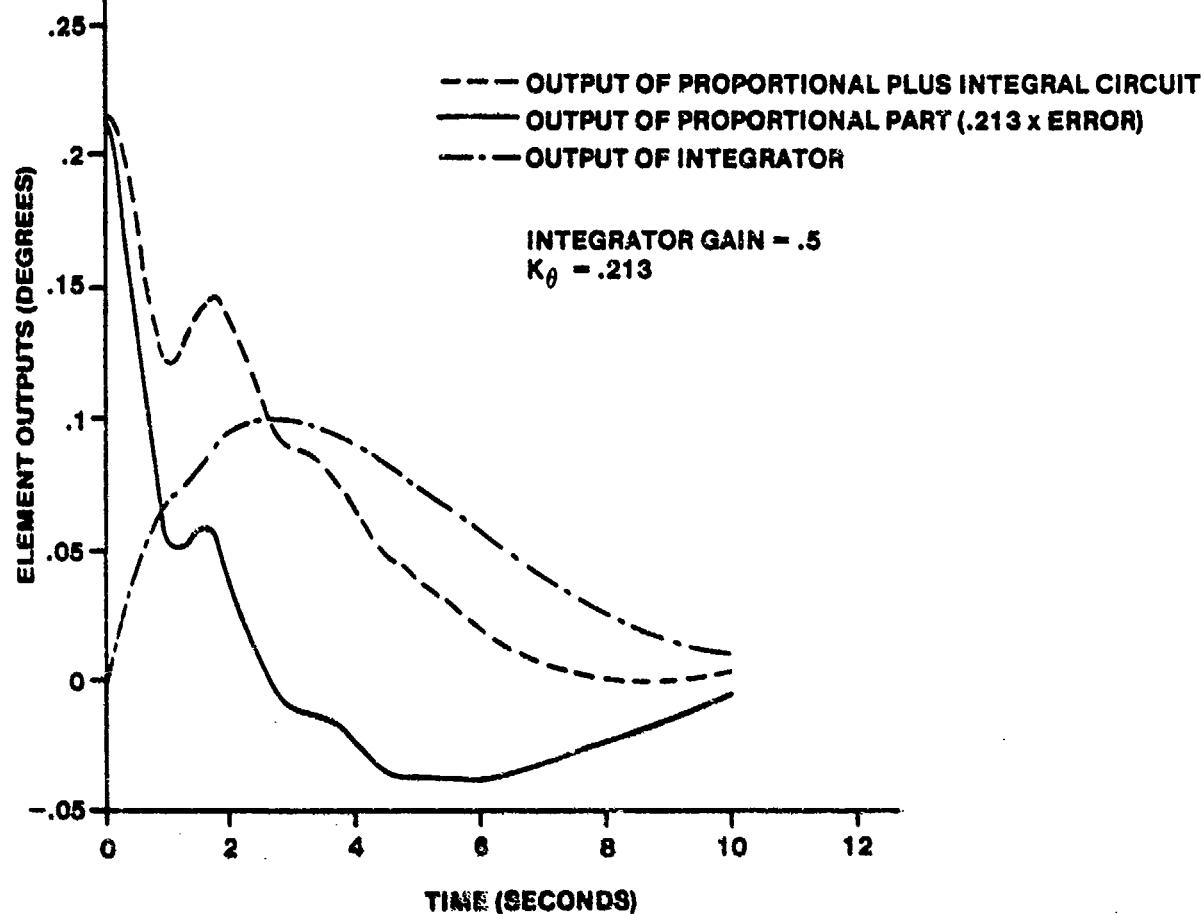
FIGURE 14.97. OUTPUTS OF PROPORTIONAL PLUS INTEGRAL CIRCUIT
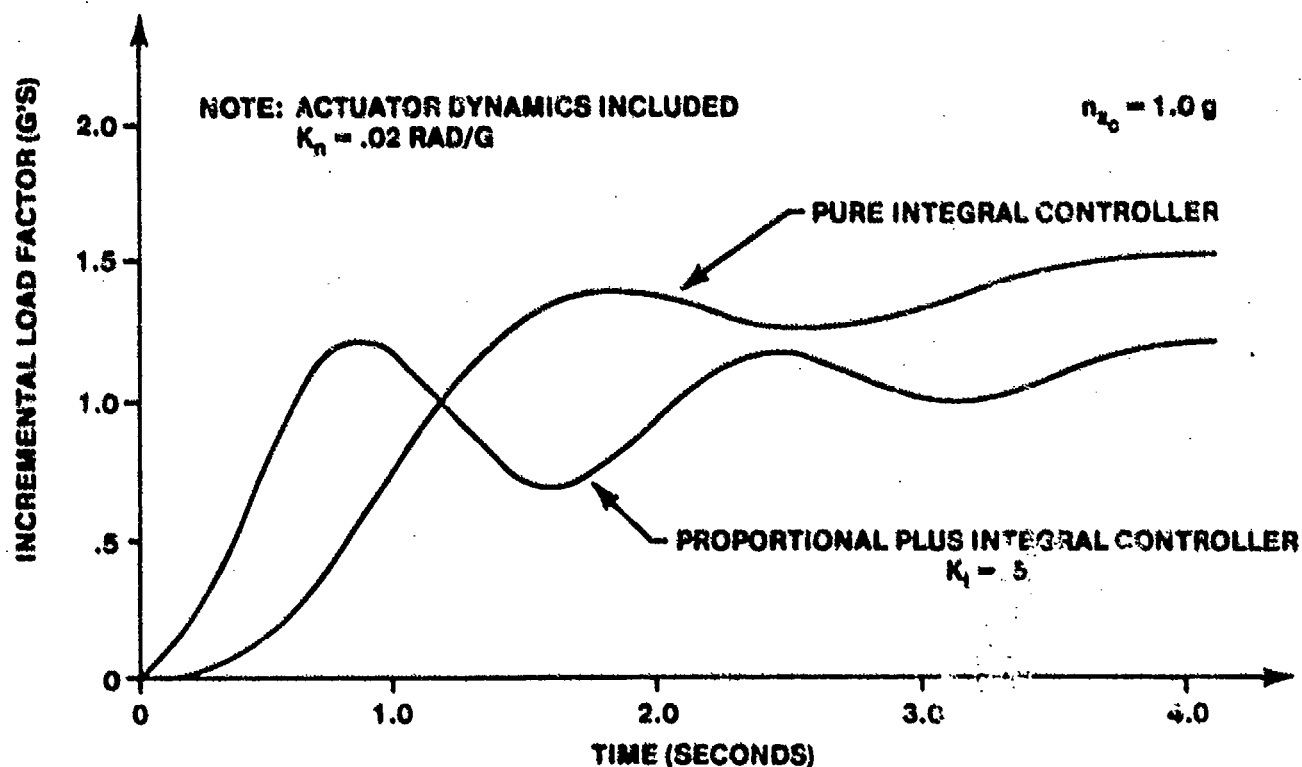
FIGURE 14.98. COMPARISON OF TIME RESPONSE CHARACTERISTICS FOR TWO 'G' COMMAND SYSTEMS

14.114

14.3.3.4 Use of Integral Control in Pitch Rate Command Systems. Pitch rate command systems are unsuccessful in stabilizing an unstable aircraft whose instability is due either to the tuck mode in the transonic regime or to a longitudinal static instability (Figure 14.14). This inability to stabilize the aircraft is due to the presence of the zero at the origin in the pitch rate transfer function. The use of an integrator in the forward loop to cancel the zero at the origin is a solution to this difficulty--but one with hidden difficulties for piloted flight (this solution may be quite successful for autopilot operation). With pure integral control, a decrease in the short period damping and an increase in the short period natural frequency occurs, the roots of the augmented aircraft migrating in a manner similar to a pitch attitude feedback system (Figure 14.9). A relatively high gain is required to stabilize the aircraft. Figure 14.99 shows the time response of the pitch rate command system with a pure integral controller. A large effective time delay is apparent and poor handling qualities could be expected due to the low response damping. Further compensation would be required to obtain acceptable characteristics.

$q_c = 1$ DEG/SEC
$K_q = 1.36$
PURE INTEGRAL CONTROL
$K_I = 1$

F-16
SEA LEVEL
135 KTAS
13° AOA
PA
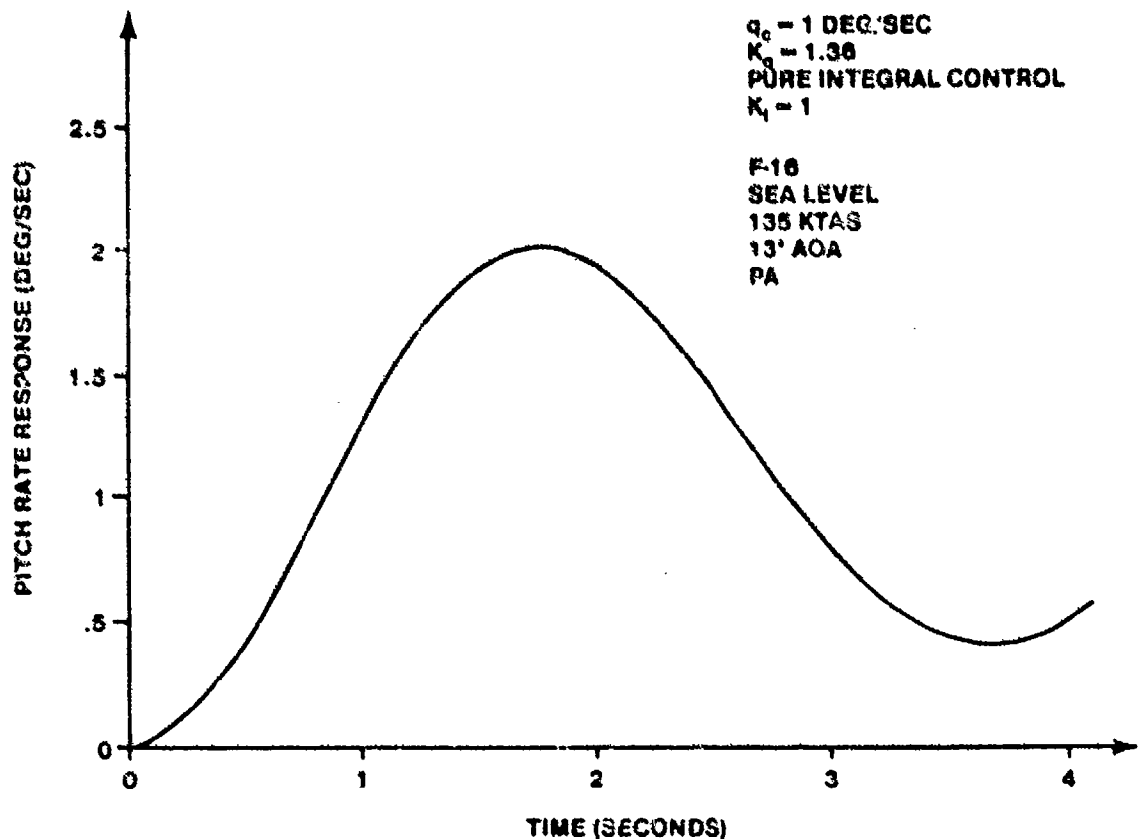
FIGURE 14.99. PITCH RATE RESPONSE FOR PITCH RATE SYSTEM WITH PURE INTEGRAL CONTROL, UNSTABLE AIRCRAFT

The use of a proportional plus integral controller may overcome the difficulties encountered when using the pure integral controller. Figures 14.100 and 14.101 illustrate the effects of two integral plus proportional controllers on the root locus of the pitch rate command system. The higher the integrator gain, the more closely the situation with the pure integral controller is approached. Figure 14.102 compares the time response of the two systems. The system with the lower integrator gain suppresses the pitch rate overshoot characteristic of the aircraft and may yield poor handling qualities as a result. The system with the higher integrator gain provides a response characteristic which is closer to what is obtained with conventional aircraft and generally preferred by pilots.
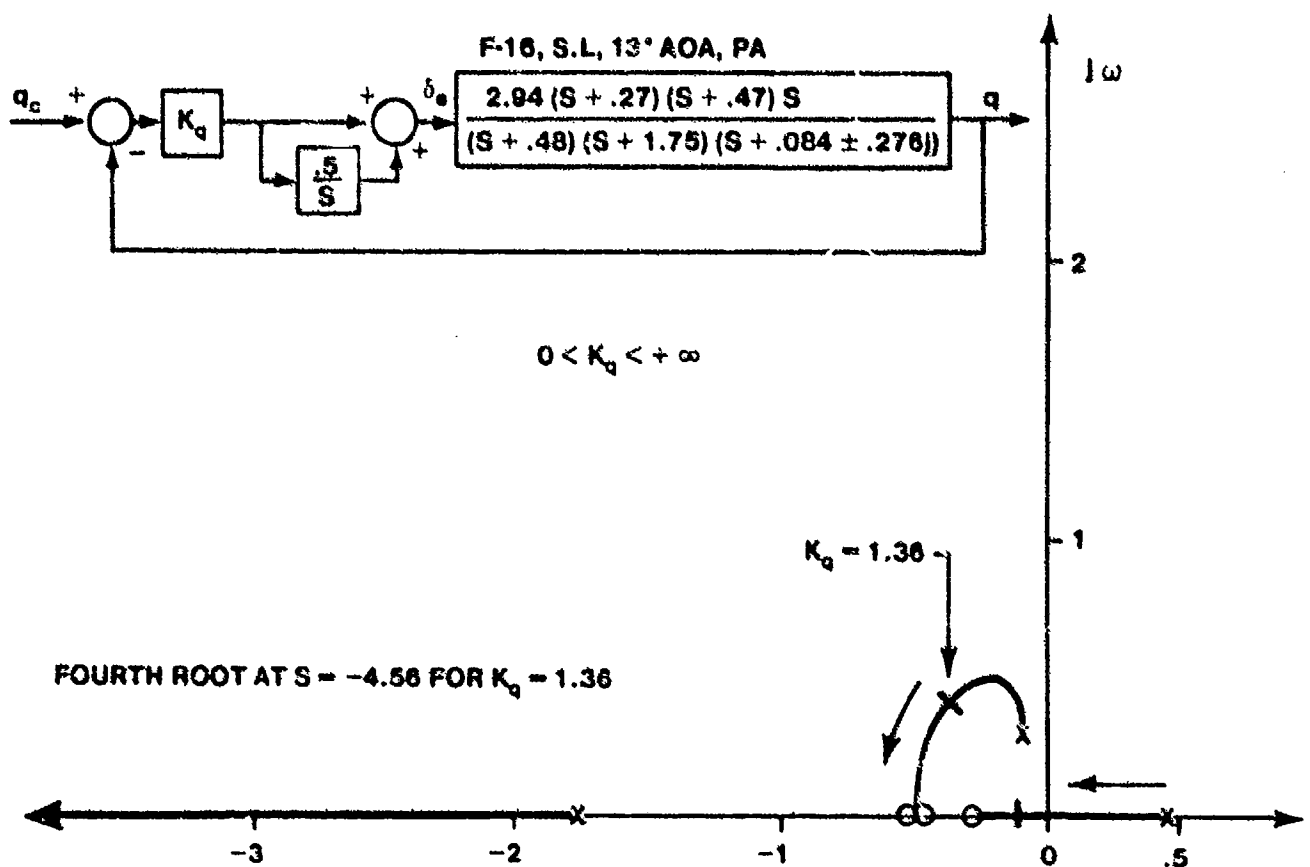
FIGURE 14.100.   EFFECT OF PROPORTIONAL PLUS INTEGRAL CONTROL ON A PITCH RATE SYSTEM FOR AN UNSTABLE AIRCRAFT

$0 \le K_q < +\infty$

$j\omega$

F-16, S.L., 13° AOA, PA

$$\frac{2.94\,(S+.27)\,(S+.47)\,S}{(S-.48)(S+1.75)(S+.084 \pm .276j)}$$
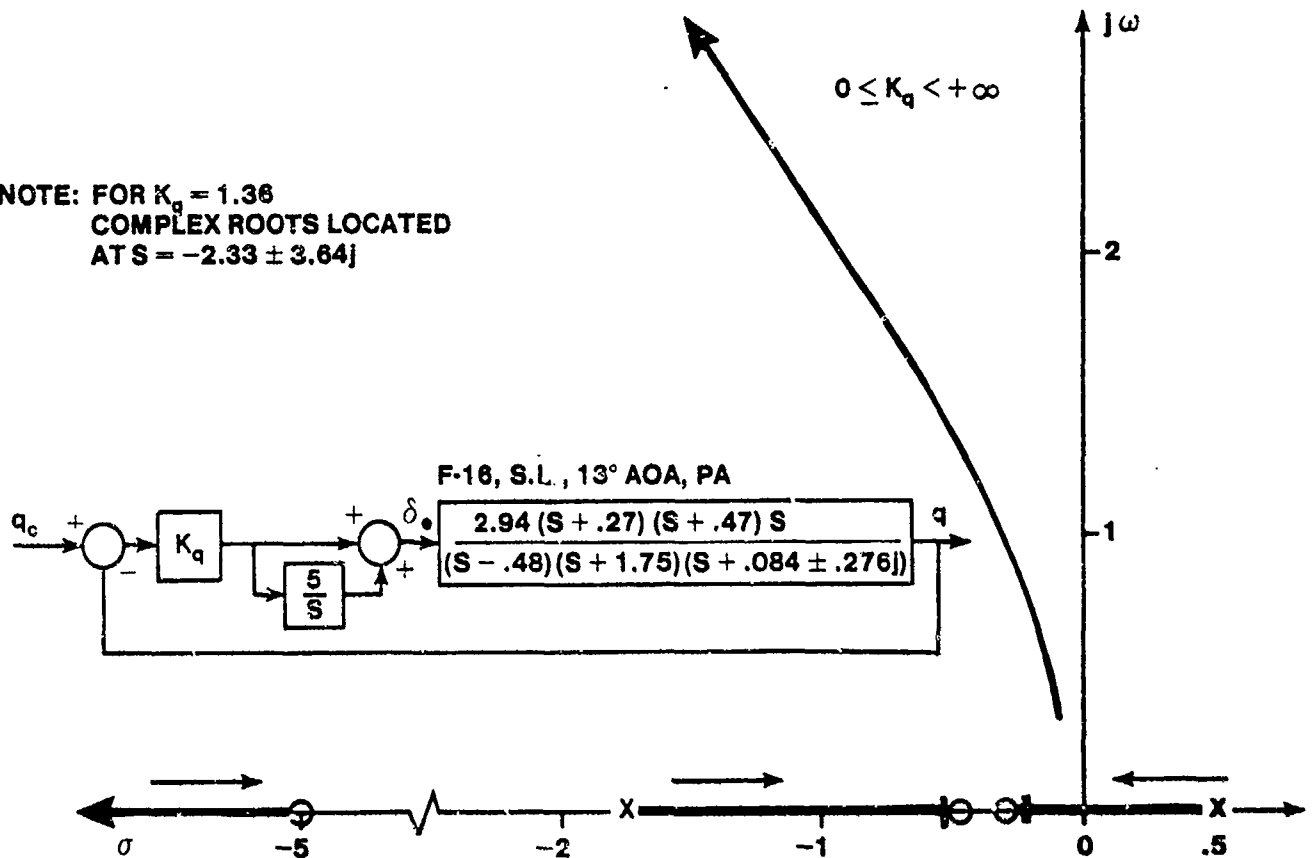
FIGURE 14.101.   EFFECT OF PROPORTIONAL PLUS INTEGRAL CONTROL ON A PITCH RATE
SYSTEM FOR AN UNSTABLE AIRCRAFT

$K_q = 1.36$
$q_c = 1$ DEG/SEC

PITCH RATE RESPONSE (DEG/SEC)

1.25

1.0

.75

.5

.25

0

F-16
SEA LEVEL
13' AOA
POWER APPROACH

INTEGRATOR GAINS
———— $K_I \approx .5$
– – – $K_I = 5$

NOTE: PROPORTIONAL PLUS INTEGRAL CONTROL

TIME (SECONDS)
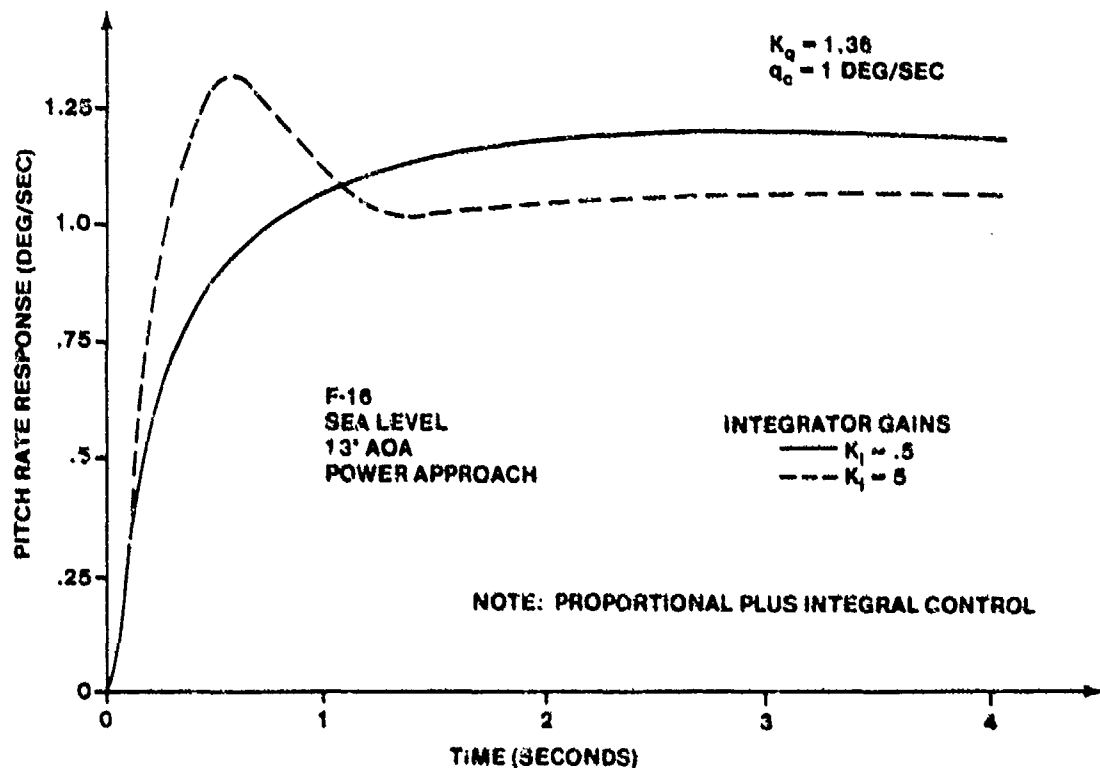
FIGURE 14.102.   COMPARISON OF PITCH RATE RESPONSE FOR PITCH RATE SYSTEMS WITH
INTEGRAL CONTROL, UNSTABLE AIRCRAFT

14.117

Engineers have postulated that the optimal location of the zero which arises from the proportional plus integral controller is such that it cancels the stable real root in the aircraft characteristic equation. Figures 14.103, 14.104, and 14.105 show the effect of varying the integrator gain about the stable real pole. Figure 14.106 compares the time responses of the three systems for a specified gain. It is apparent that the location of the zero relative to the pole does not significantly alter the aircraft response characteristics as long as the zero is relatively close to the pole. The higher the integrator gain, however, the lower the response rise time. The overshoot tendency of the pitch rate response is slight. Notice that if the system gain is reduced at a fixed integrator gain, the overshoot magnitude is increased somewhat but the response is also more sluggish (lower effective short period frequency).
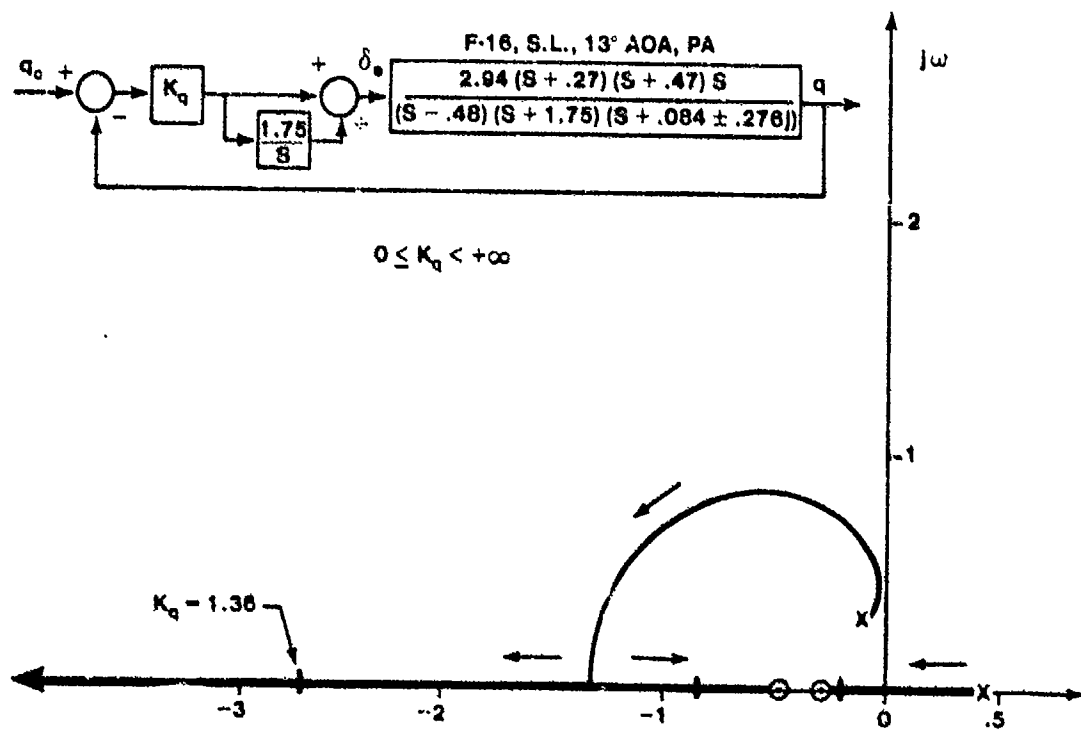
FIGURE 14.103. EFFECT OF PROPORTIONAL PLUS INTEGRAL CONTROL ON A PITCH RATE SYSTEM FOR AN UNSTABLE AIRCRAFT
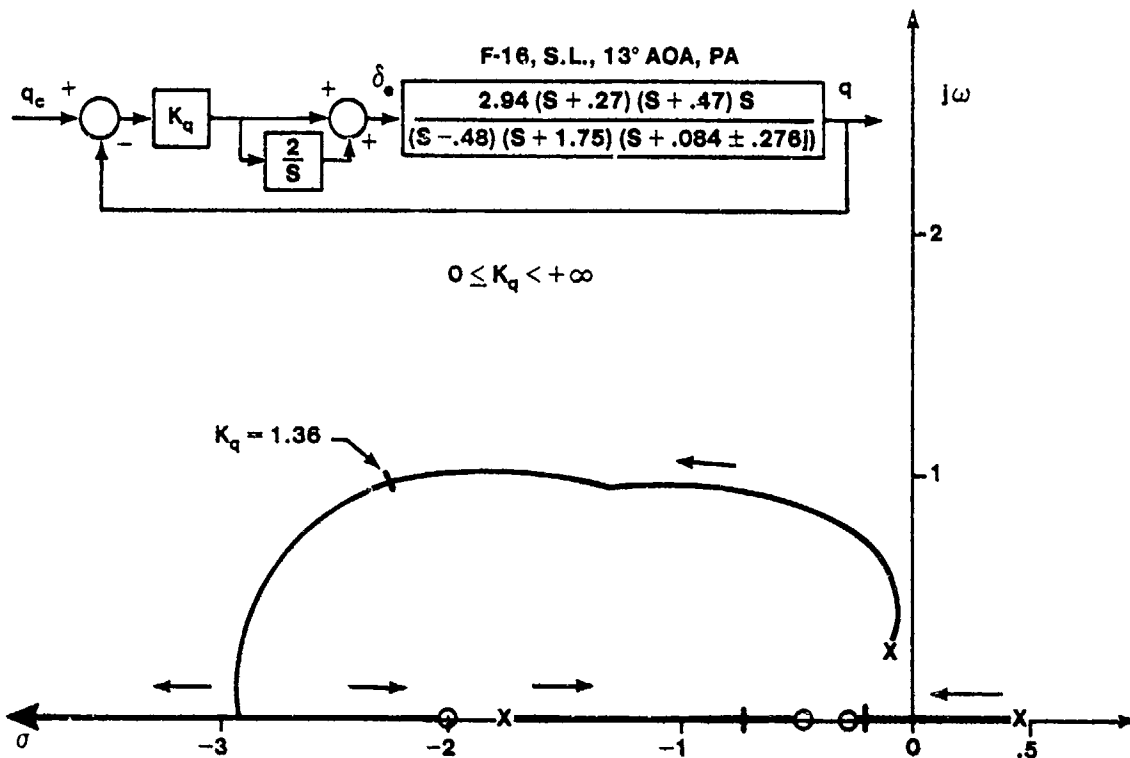
FIGURE 14.104. EFFECT OF PROPORTIONAL PLUS INTEGRAL CONTROL ON A PITCH RATE SYSTEM FOR AN UNSTABLE AIRCRAFT
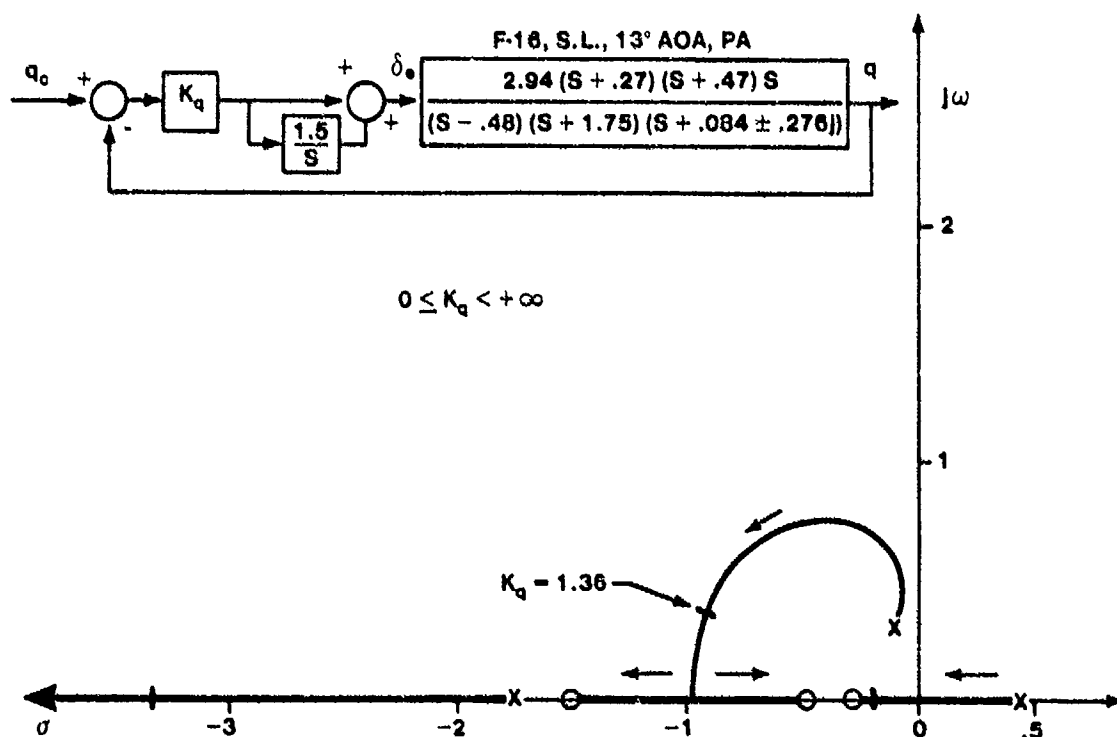
FIGURE 14.105. EFFECT OF PROPORTIONAL PLUS INTEGRAL CONTROL ON A PITCH RATE SYSTEM FOR AN UNSTABLE AIRCRAFT
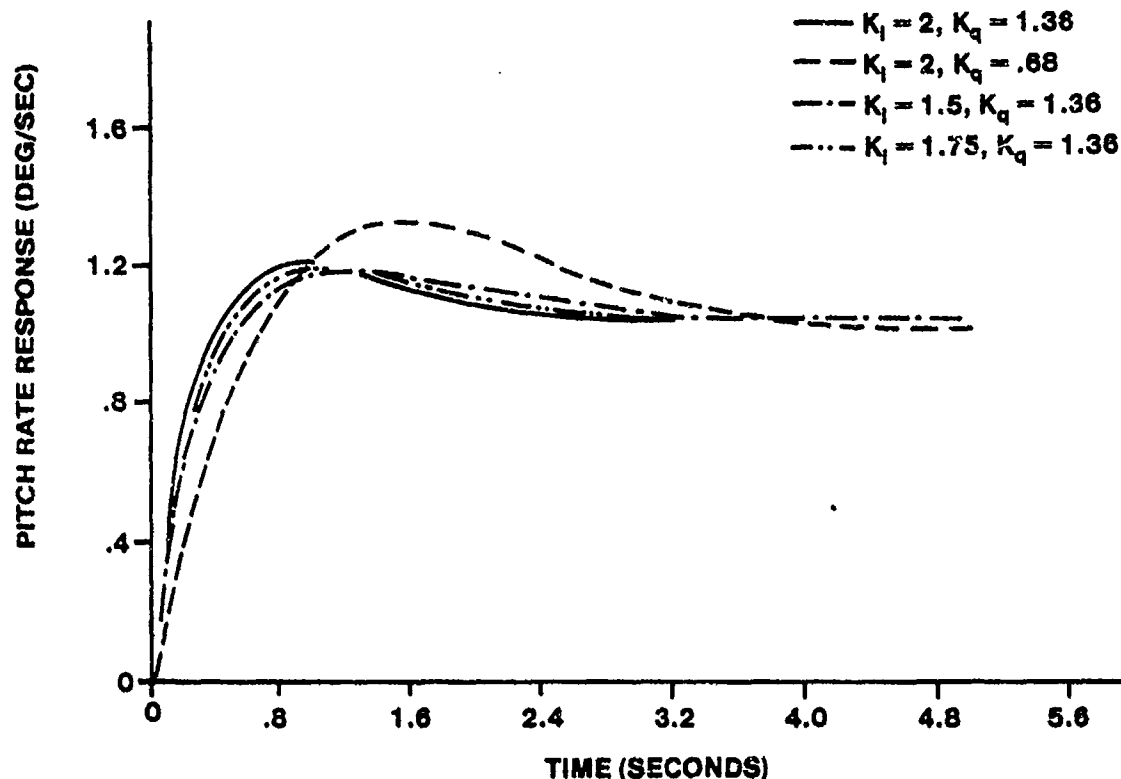
FIGURE 14.106. COMPARISON OF TIME RESPONSE CHARACTERISTICS FOR PITCH RATE
COMMAND SYSTEMS WITH PROPORTIONAL PLUS INTEGRAL CONTROLLERS

Using proportional plus integral control with relatively high integrator gain is preferred and cancellation of the stable real root may not be the optimal solution. The higher the integrator gain, the higher the frequency of the short period and the lower the short period damping for a fixed controller gain. The addition of lead compensation may be required to obtain the desired characteristics. Ground and in-flight simulations are required to assess the impact of the integrator gain on aircraft handling qualities.

14.3.3.5 Integrators as Memory Devices. Figure 14.107 shows a hypothetical pitch rate command system with an attitude hold feature. With the attitude hold feature disengaged, the pilot commands pitch rate. With the attitude hold feature engaged, the aircraft maintains the attitude at which the pilot releases the control stick. Proportional plus integral control is provided to precisely hold the commanded attitude. The purpose of the second integrator is to remember the attitude at which the pilot releases the control stick.

14.120

When the pilot applies enough force to engage the switch, the integrator output attempts to match the attitude of the aircraft. The speed at which the integrator output matches the aircraft attitude depends on the integrator gain, which is normally high. When the pilot releases the stick, the switch in the integrator path opens and the integrator maintains the last output (desired attitude) prior to the switch opening. Any deviations from this attitude result in a pitch rate command. The integrator is used as a memory device. This implementation is common in attitude hold system. The second switch, in the forward path of the attitude hold loop, insures that the attitude hold system does not provide inputs to the pitch rate command system during rapid maneuvers, where the integrator memory cannot cancel the actual aircraft attitude signal. The feedback path in the proportional plus integral controller cancels any residual signal retained by the integrator when the attitude hold mode is disengaged by driving the integrator to zero.
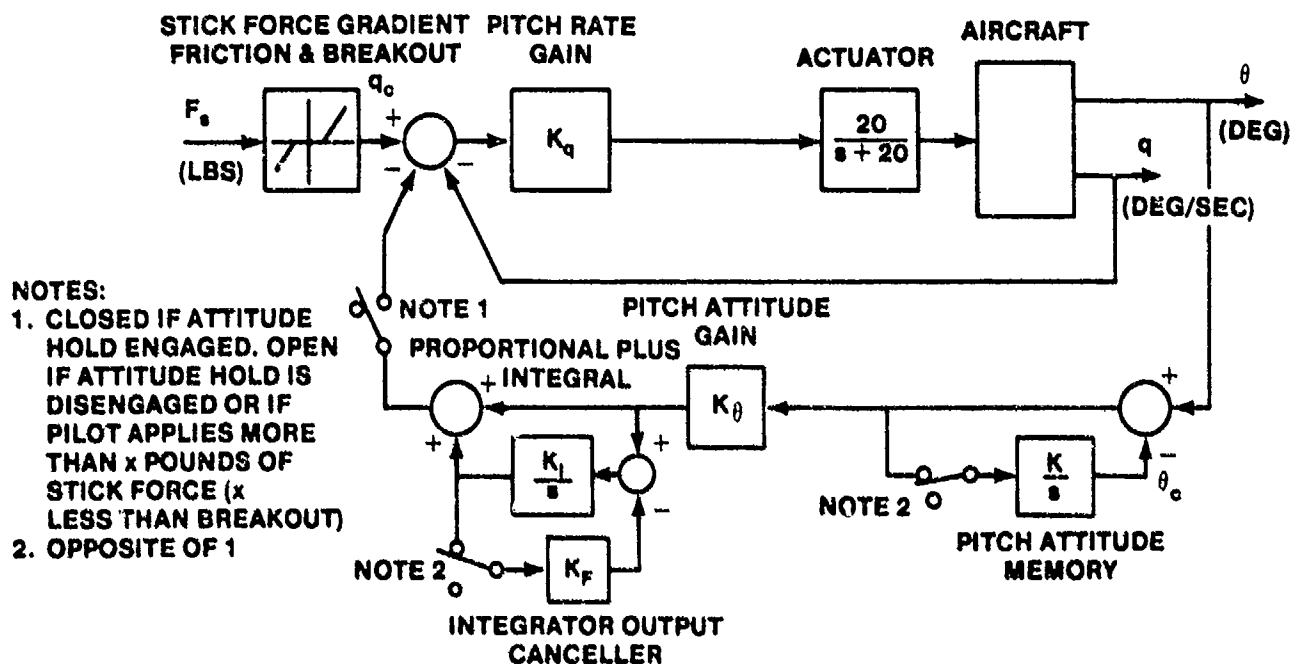
FIGURE 14.107. PITCH ATTITUDE HOLD SYSTEM CONFIGURATION

14.3.3.6 <u>Increasing the Phase Angle (Improved Stability)</u>. The phase angle of the control system is related to the time response damping ratio of the closed loop system by the following rough approximation (for second order systems).

$$= \frac{\text{Phase Margin (degrees)}}{100} \quad (\text{Phase Margin} < 70^\circ) \quad (14.62)$$

if the system damping ratio is low then the phase angle must be increased. The best way to improve the damping ratio is to provide a rate feedback loop as discussed in Paragraph 14.2.2.2. Another approach is to add lead compensation in either the forward or feedback path. The general form of the lead compensator is

$$\frac{\cdot \frac{1}{K} (s + Kb)}{s + b} \quad (K < 1)$$

where the zero occurs closer to the origin than the pole. The gain 1/K prevents an increase in the steady state error.

Figures 14.108 and 14.109 present the effects of a lead compensator (with two different values of K) on a pitch attitude command system. The lead compensator can significantly alter the closed loop response. The lead compensator is generally centered near the short period frequency so as to increase the phase angle in that region, thereby improving the system short period damping ratio. The more lead provided (small value of K), the more damping is improved. Practical limitations in components generally restrict K > 0.1 in analog systems. If the control loop gain is too high the damping ratio will decrease and the natural frequency will increase in the pitch attitude systems presented.
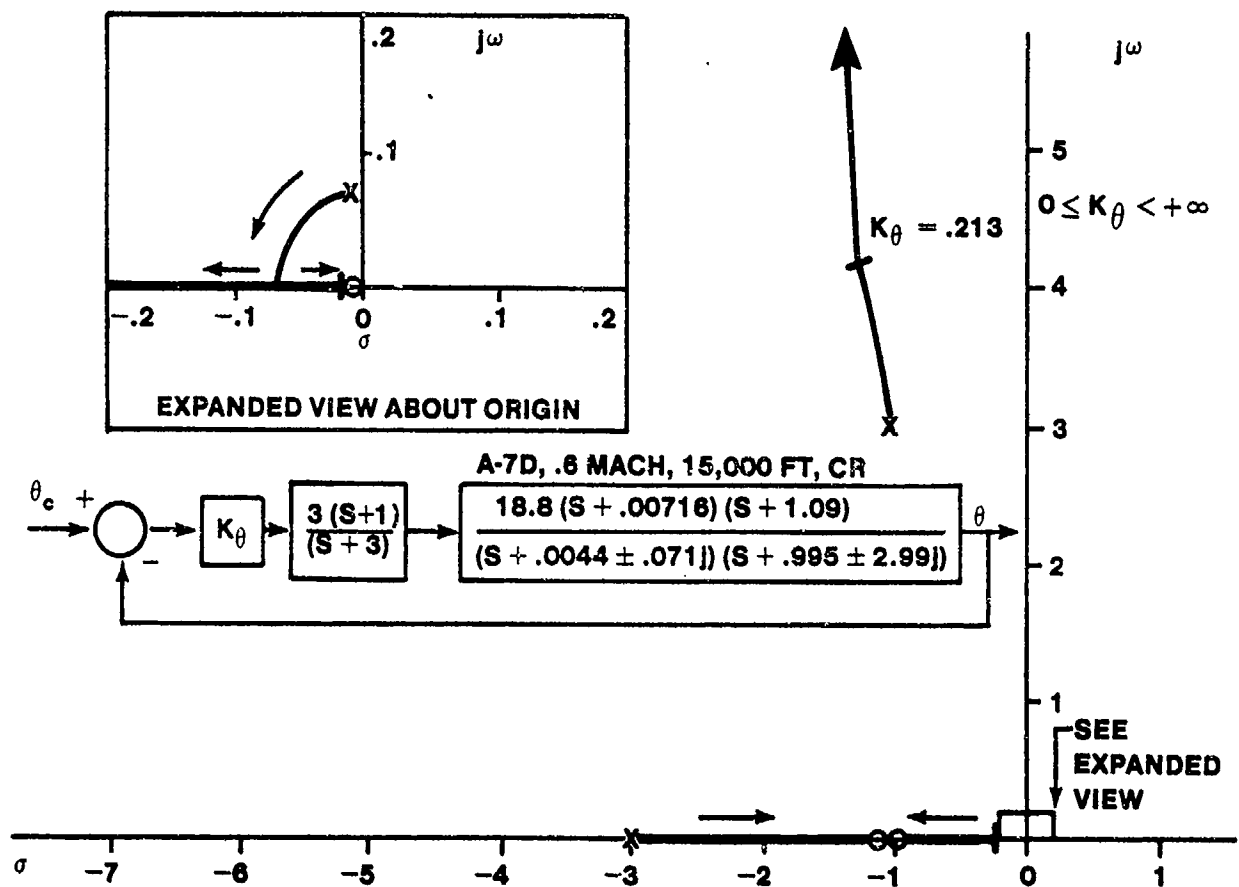
FIGURE 14.108.   ROOT LOCUS PLOT OF PITCH ATTITUDE LOOP WITH LEAD COMPENSATOR
ADDED
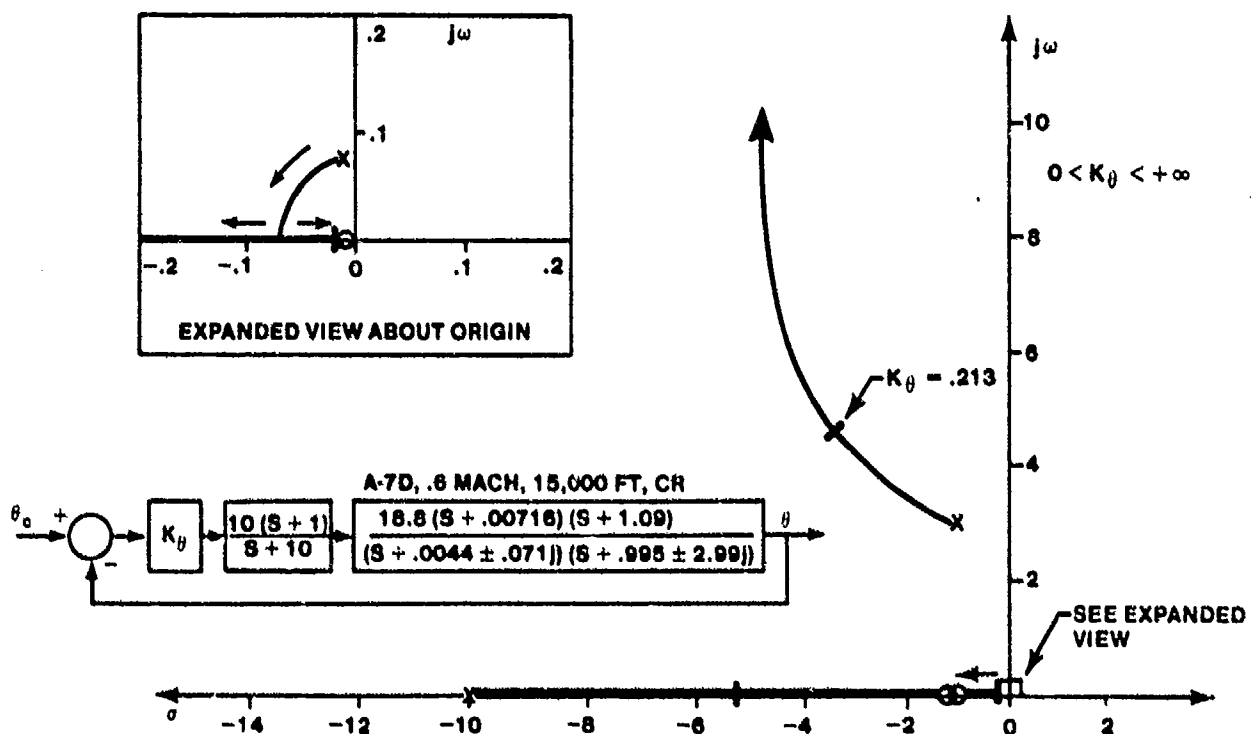
FIGURE 14.109.   ROOT LOCUS PLOT OF PITCH ATTITUDE LOOP WITH LEAD COMPENSATOR
ADDED

14.123

The location of the lead compensator in the forward versus the feedback path significantly impacts the time response (Figure 14.110). Both systems have the same closed loop roots. The only difference is the proximity of the zero--added to the system by the compensator--to the origin. Note that the response after several seconds is essentially exponential in character. The zero added by the feedback compensator is remote from the origin and the response is essentially exponential near the origin. The system is more sluggish than the original system. The forward path compensator zero is much closer to the origin and nearly cancels the exponential response due to the dominant low frequency real root, causing a more abrupt response. The damping of both compensated systems is higher than the damping of the uncompensated system with the same short period. The zero in the forward path compensator reduces the effective damping by causing the initial response overshoot.
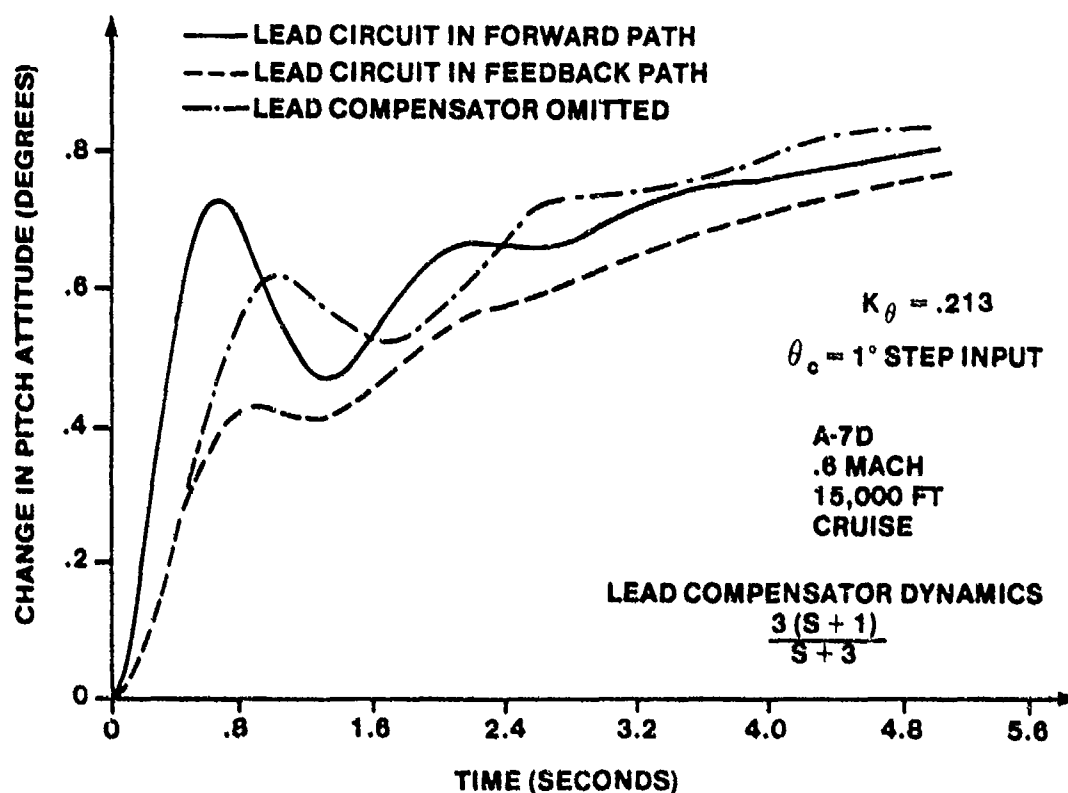
FIGURE 14.110.   A-7D PITCH ATTITUDE RESPONSE WITH LEAD COMPENSATOR ADDED

14.3.3.7 <u>Washout Filter</u>. A washout filter has the form

$$\frac{s}{s + b}$$

This is a high pass filter that passes signals above b radians per second while attenuating lower frequency signals. The steady state signal passing through this filter is zero. Signals will be passed only during the transient portion of the aircraft response and that the steady state signal will be attenuated.

This filter is very common in the feedback path of yaw damper systems. During a steady state level turn, a steady yaw rate is present. Since the aircraft is in a bank

$$r = \dot{\psi} \cos \phi \tag{14.63}$$

where $\dot{\psi}$ is the heading rate and ϕ is the bank angle. The yaw rate gyro feeds this signal back to the rudder to try to deflect the rudder to oppose the turn. Without a washout filter, a constant rudder deflection would occur which would try to roll the aircraft wings level. This wings level tendency in swept wing aircraft is caused by large sideslip due to rudder deflection and is undesirable during turns. The washout filter prevents the residual rudder deflection during the turn while still providing Dutch roll damping during rolling maneuvers.

The s in the numerator represents a differentiation. Therefore, the filter passes only the derivative of the incoming signal, which is zero for a constant amplitude signal. The attitude memory circuit in Figure 14.107 forms a washout filter when the attitude hold system is disengaged.

Figure 14.111 shows the washout filter in a pitch rate damper has little effect on the root locus of the pitch rate augmented aircraft. If the pole of the filter were located such that s < -1.09, the effect would be slight. If, however, the pole were located such that s << -1.09, the filter would nearly negate the effect of the feedback since it would pass only very

14.125

high frequency signals. Figure 14.112 shows the pitch rate response of the pitch damper augmented aircraft to a step pitch rate command. Figure 14.113 shows the output of the washout filter, which goes to zero after a short time.
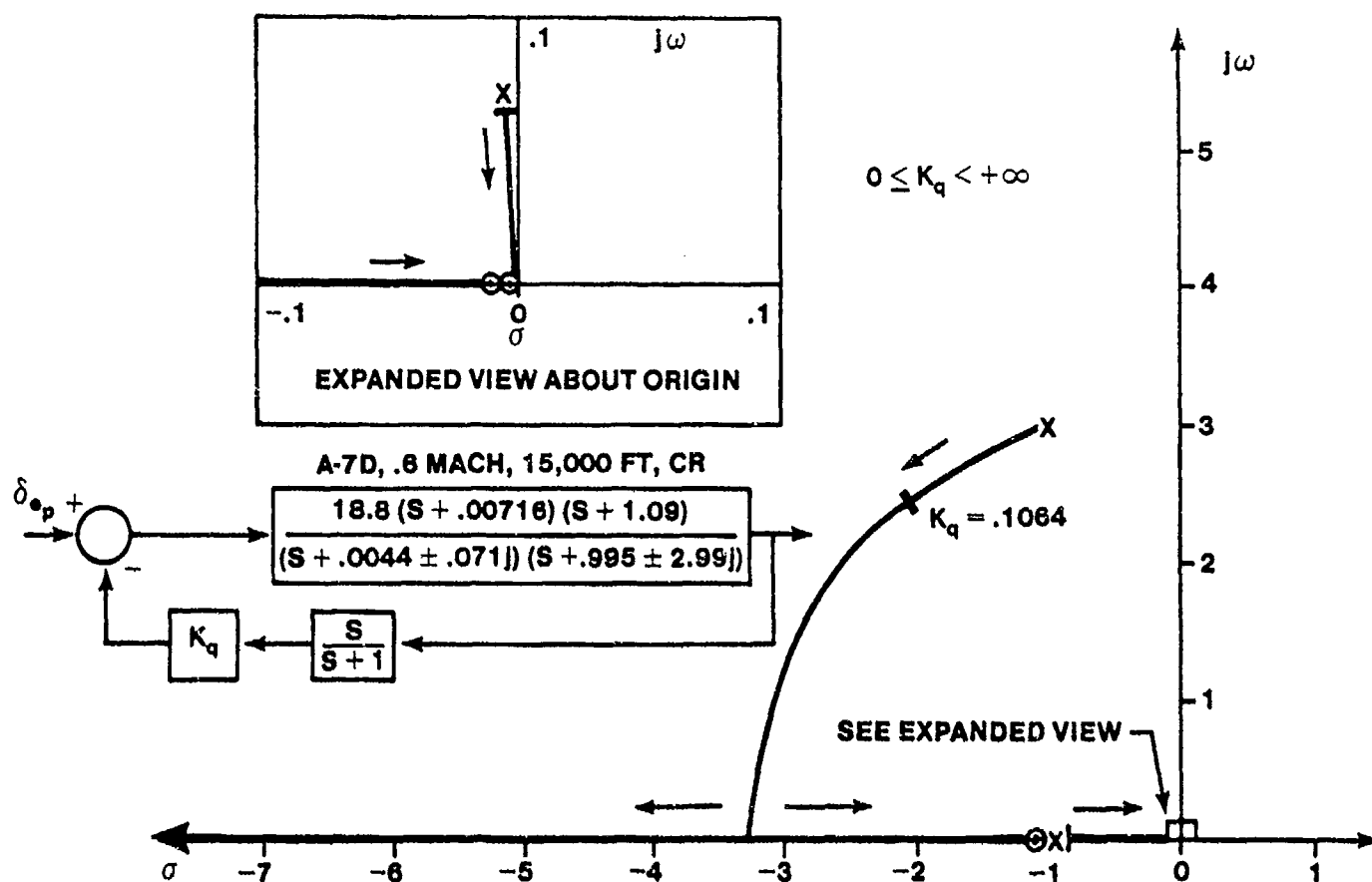
FIGURE 14.111. ROOT LOCUS PLOT OF PITCH DAMPER WITH WASHOUT PROVISION
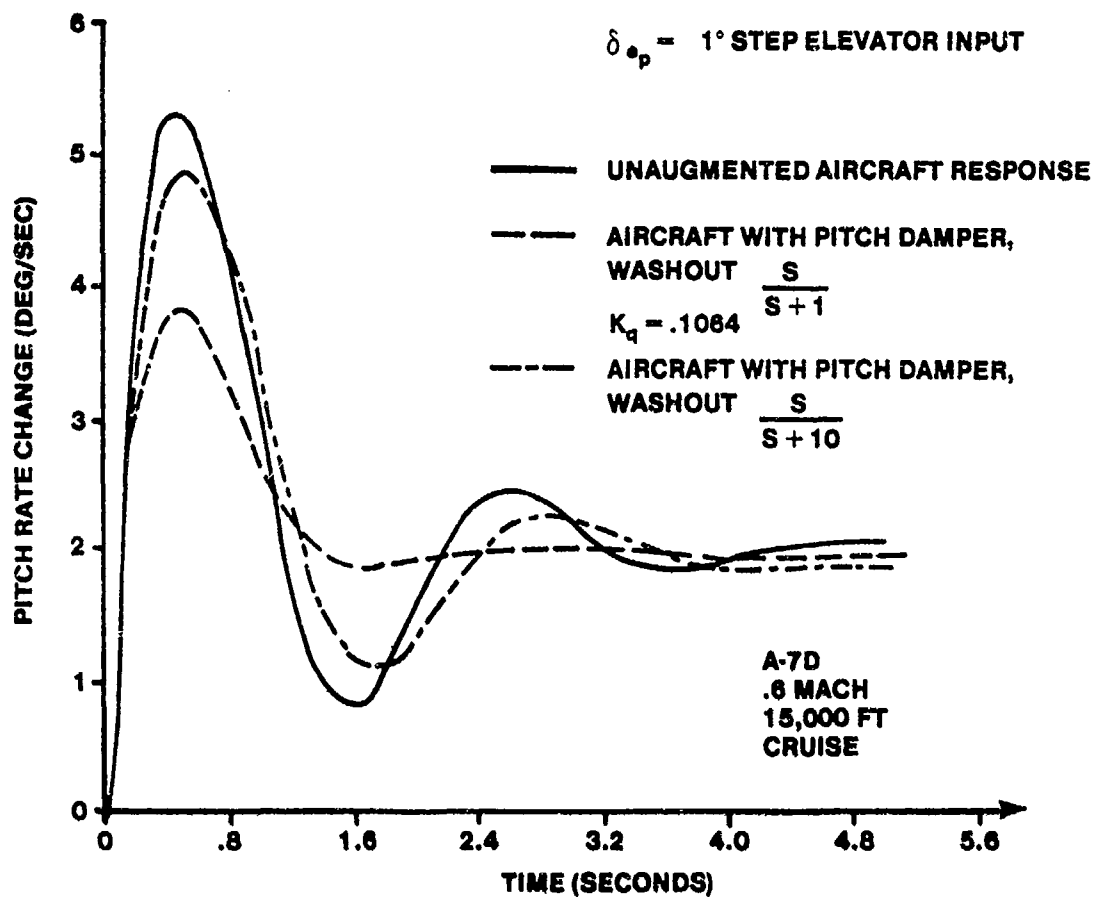
FIGURE 14.112.   COMPARISON OF PITCH RATE RESPONSE
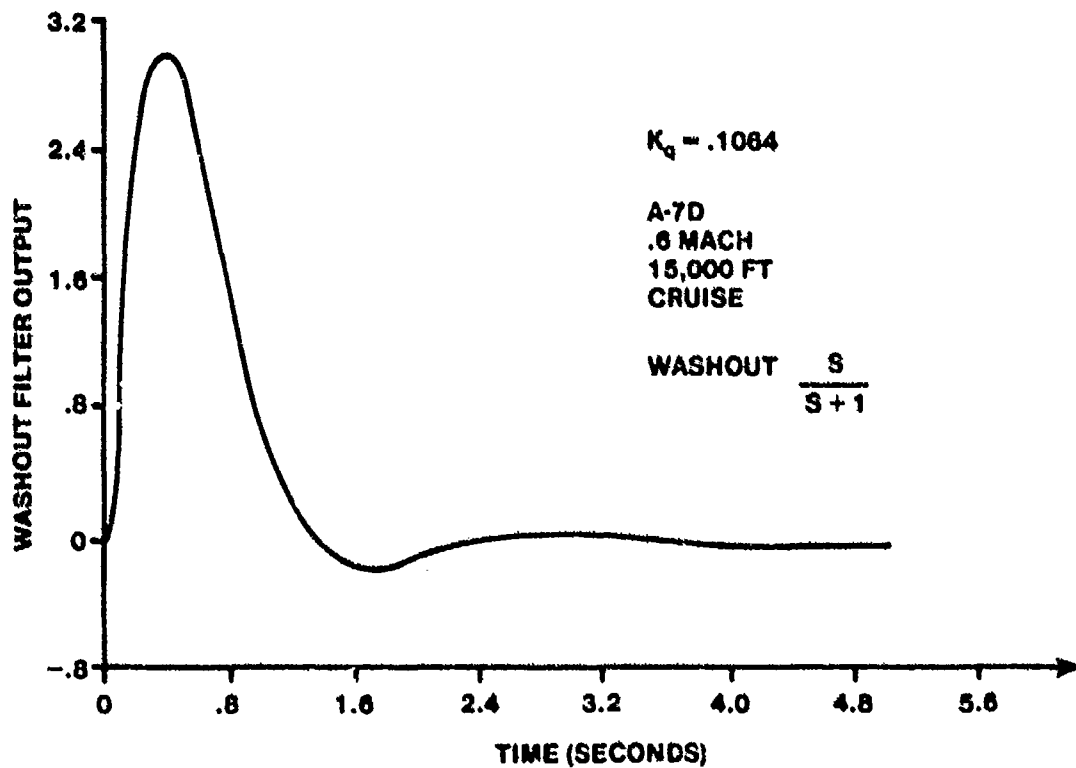
FIGURE 14.113.   PITCH DAMPER WASHOUT FILTER OUTPUT TIME RESPONSE

14.127

The use of a washout filter in a command or forward path is inadvisable. The command signal degrades to zero after a short time. For the pitch rate damper, for instance, if a washout filter were added to the command path and the pilot tried to maintain a constant aircraft pitch rate, he would be required to apply a constantly increasing stick force to maintain the rate. When the pilot reached a force or deflection limit in the feel system the aircraft pitch rate would go to zero and the pilot could no longer pitch the aircraft.

14.3.3.8 Gain Scheduling. It is frequently necessary to change the control system gains as a function of the flight condition for aircraft with large flight envelopes. The purpose of gain scheduling is to retain nearly constant handling qualities within a large region of the flight envelope. Gains are usually scheduled as a function of dynamic pressure or Mach, although other parameters may be used.

14.3.4 Sensor Placement in a Rigid Aircraft

A discussion of sensor dynamics is beyond the scope of this text. These dynamics are usually negligible for the analysis of aircraft control systems since the sensors are selected to be sufficiently fast (very high natural frequencies) so as to add a negligibly small amount of lag to the system. References 14.3, 14.33, and 14.37 discuss sensor dynamics.

The location of an angle of attack sensor must minimize local flow disturbances near the sensor so as to obtain steady measurements. Since flow near the aircraft is affected by upwash, the angle of attack measurement from the vane is not the true angle of attack, and must be corrected to indicate the true angle of attack. This correction may be determined experimentally during tower flyby pitot static tests for subsonic speeds or computed for supersonic speeds. The correction may be a function of altitude or Mach.

The placement of rate gyros is not critical in rigid aircraft. They are usually aligned to measure rotational motion about the aircraft body axes.

Accelerometers, however, must be located carefully. The acceleration at locations other than the aircraft center of gravity is computed as

$$\bar{a}_{ACCEL} = \bar{a}_{cg} + \dot{\bar{\omega}} \times \ell \tag{14.64}$$

where ω is the angular acceleration of the aircraft and ℓ is the location of the accelerometer relative to the center of gravity, expressed in the aircraft body axis system.

Computing the normal and lateral accelerations from

$$\bar{a}_{ACCEL} = a_{x_{cg}}\bar{i} + a_{y_{cg}}\bar{j} + a_{z_{cg}}\bar{k} + \begin{vmatrix} \bar{i} & \bar{j} & \bar{k} \\ \dot{p} & \dot{q} & \dot{r} \\ \ell_x & \ell_y & \ell_z \end{vmatrix}$$

yields

$$\bar{a}_{y_{ACCEL}} = \bar{a}_{y_{cg}} + \ell_x \dot{r}\bar{j} - \ell_z \dot{p}\bar{j} \tag{14.65}$$

and

$$\bar{a}_{z_{ACCEL}} = \bar{a}_{z_{cg}} + \ell_y \dot{p}\bar{k} - \ell_x \dot{q}\bar{k} \tag{14.66}$$

It is undesirable to locate the normal accelerometer away from the centerline of the aircraft to avoid sensing roll accelerations.

The desirability of locating the normal accelerometer ahead of the center of rotation of the aircraft was briefly discussed in Paragraph 14.2.2.4. The effect of accelerometer location on the acceleration transfer function zeros can be determined by plotting a root locus of

$$GH = \frac{-\ell_x s^2 N^{\theta}_{\delta_e}(s)}{N^{a_{z_{cg}}}_{\delta_e}(s)} \tag{14.67}$$

as a function of ℓ_x and, for feedback of lateral acceleration to the rudder, by plotting the root locus of either

$$GH = \frac{\ell_x s\, N^r_{\delta_r}(s)}{\dfrac{a_{y_{cg}}}{N_{\delta_r}}(s)} \tag{14.68}$$

or

$$GH = \frac{-\ell_z s\, N^p_{\delta_r}(s)}{\dfrac{a_{y_{cg}}}{N_{\delta_r}}(s)} \tag{14.69}$$

as ℓ_x and ℓ_z vary. The normal load factor transfer function is

$$G^{n_z}_{\delta_e}(s) = + \frac{1}{32.2} G^{a_z}_{\delta_e}(s) \tag{14.70}$$

The further the normal accelerometer is located ahead of the center of gravity, the closer two of the zeros in the

$$\left. G^{a_z}_{\delta_e}(s) \right|_{ACCEL}$$

transfer function move towards the short period roots. The further the accelerometer is located aft of the center of gravity, the more destabilizing

14.130

the effect of acceleration feedback on the short period roots and the lower the maximum gain of the system to maintain stability. Figure 14.114 shows the effect of normal accelerometer placement on the zeros of the acceleration transfer function. The gain of the acceleration transfer function changes as a function of the accelerometer location, and may be computed as

$$K_{\delta_e}^{a_{z_{ACCEL}}} = K_{\delta_e}^{a_{z_{cg}}} - \ell_x K_{\delta_e}$$

$$(14.71)$$
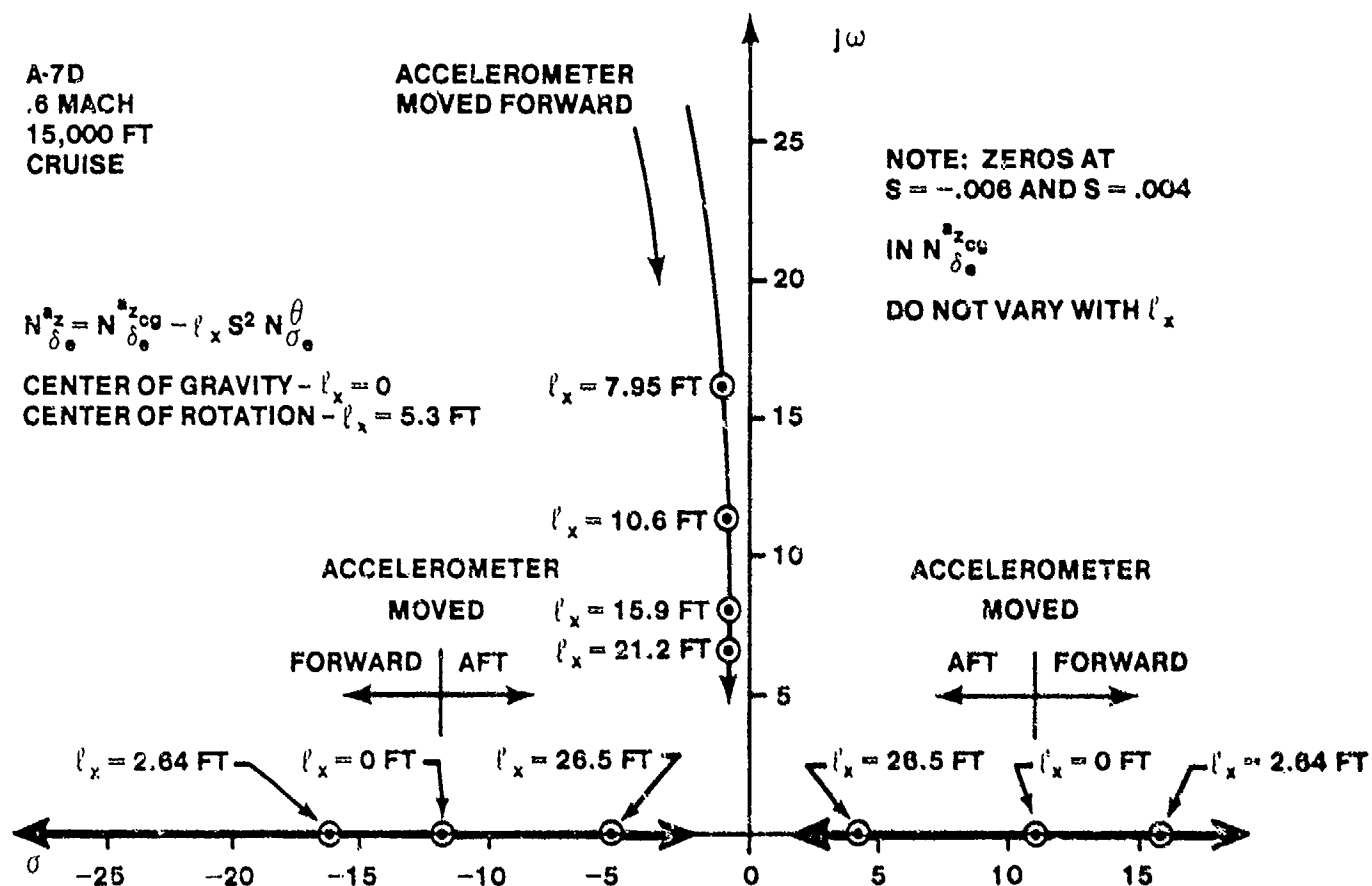
FIGURE 14.114. EFFECT OF NORMAL ACCELEROMETER LOCATION ON ZEROS OF ACCELERATION TRANSFER FUNCTION

where the two gains are associated with the numerator terms indicated. The center of rotation of the aircraft may be computed by setting the above expression equal to zero and solving for the distance from the center of gravity.

Figure 14.115 shows the effect of accelerometer location on the short period roots for three otherwise identical acceleration feedback systems. Actuator dynamics are included. As the accelerometer location moves aft of the center of gravity, the short period roots migrate to the right half s-plane at a much lower gain than if the sensor were at the center of gravity. At a relatively low gain, the system with the sensor at the center of gravity will also be driven unstable. With the accelerometer well in front of the center of gravity the system cannot cause the short period roots to become unstable for any gain.
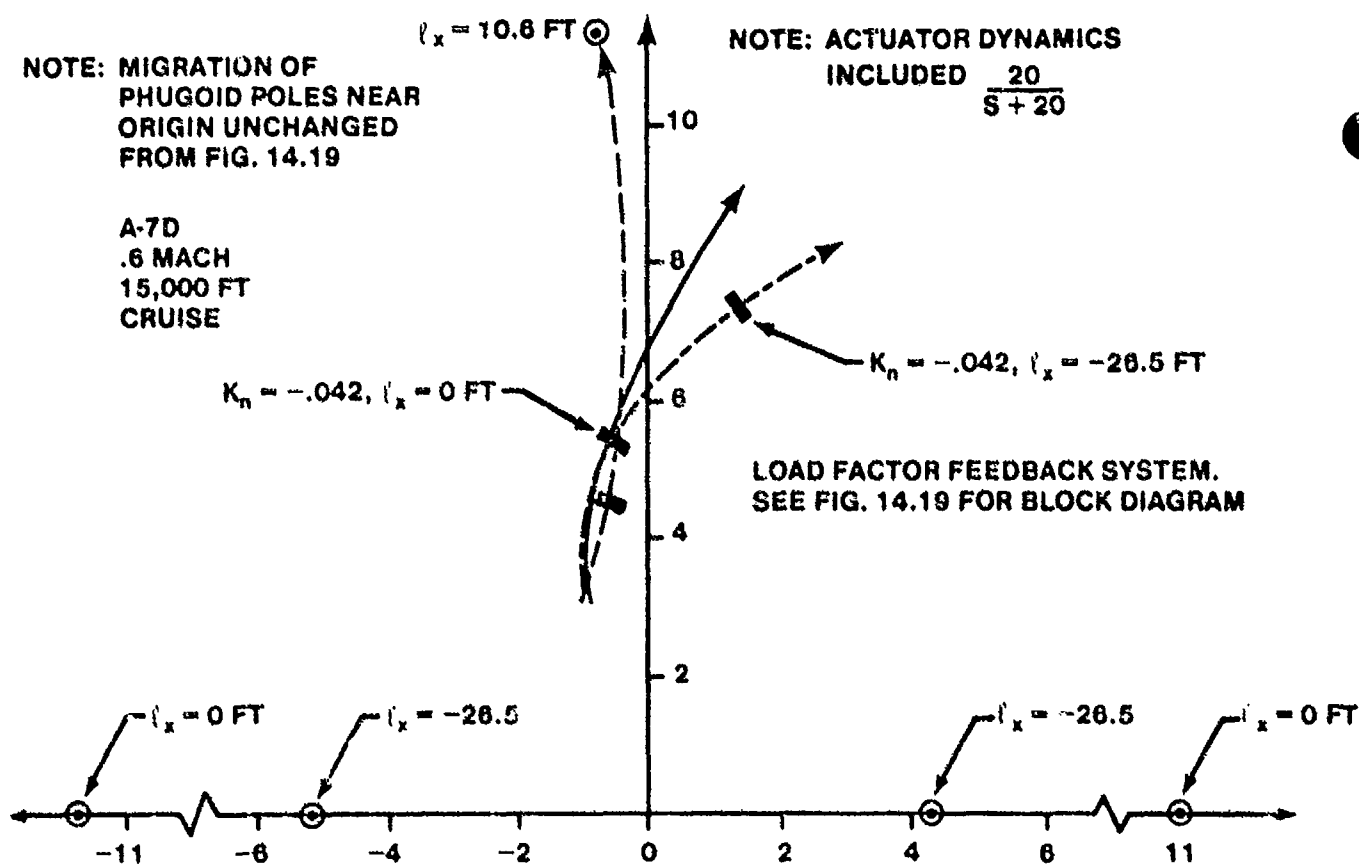
FIGURE 14.115. COMPARISON OF SHORT PERIOD ROOT MIGRATION DUE TO ACCELEROMETER LOCATION

The placement of lateral accelerometers is also important if the destabilizing influence of the acceleration transfer function zeros on the Dutch roll roots is to be minimized so that higher feedback gains can be realized. Figures 14.116 and 14.117 show the migration of the acceleration transfer function zeros with longitudinal and vertical displacement of the accelerometer, respectively. The lateral accelerometer should be located well forward of the center of rotation for the directional axis (ahead of the center of gravity). Locating the lateral accelerometer above the aircraft center of gravity will also minimize the number of zeros in the right half s-plane and minimize the destabilizing influence of these zeros on the Dutch roll roots. Locating the lateral accelerometer ahead of the directional center of rotation and above the center of gravity combines these two effects.
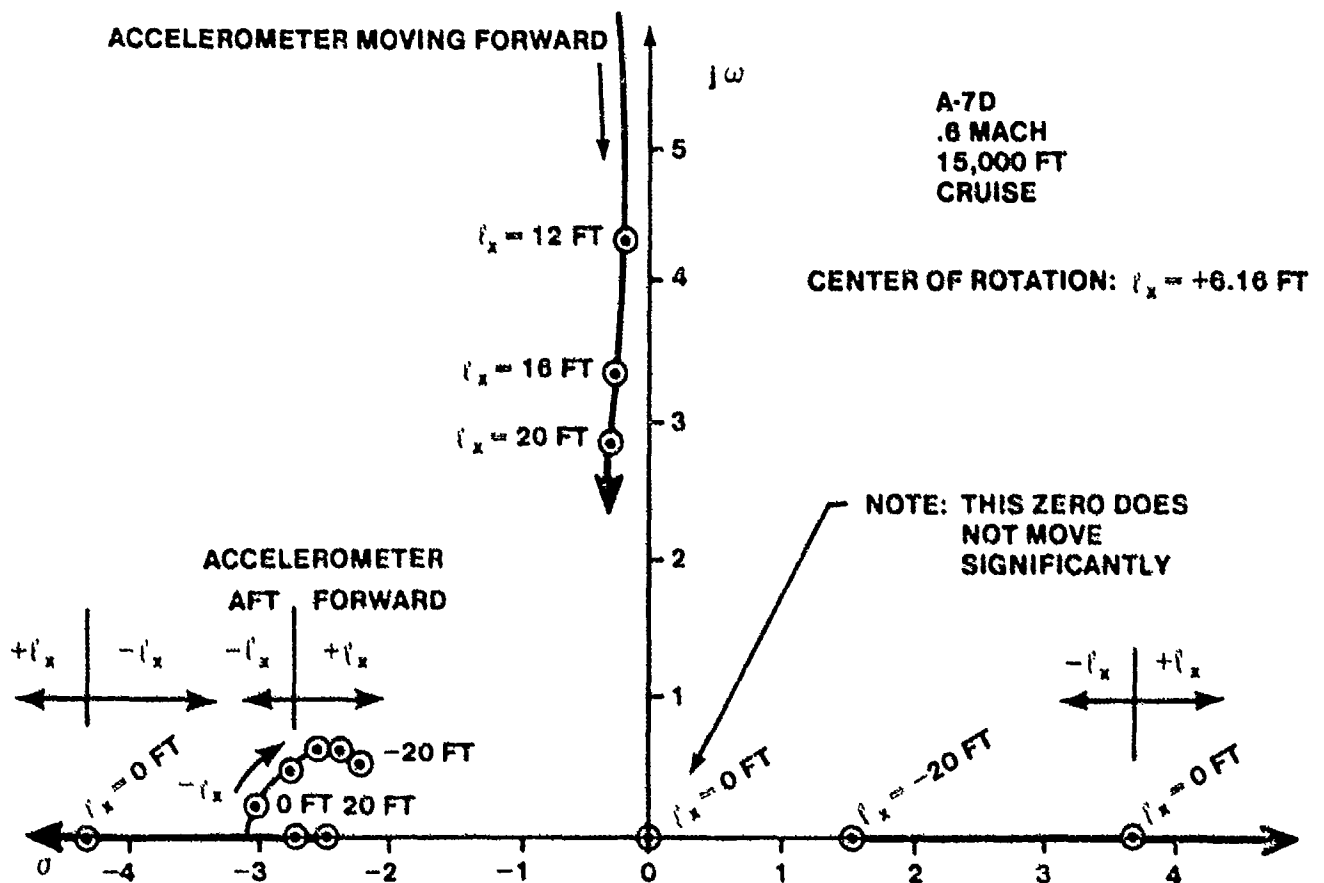
FIGURE 14.116. EFFECT OF LATERAL ACCELEROMETER LOCATION ON ZEROS OF LATERAL ACCELERATION TRANSFER FUNCTION

14.133

CENTER OF ROTATION: $x = 4.7$ FT
BELOW C.G.

A-7D
.6 MACH
15,000 FT
CRUISE

THIS ZERO MOVES QUICKLY TO $-\infty$
AND REENTERS AT $+\infty$ TO MOVE
TOWARDS ORIGIN FOR $+\ell_x$
$\ell_x = 2$ FT S $= -4.9$
$\ell_x = 4$ FT S $= -21.7$
$\ell_x = 6$ FT S $= +14.3$
$\ell_x = 8$ FT S $= +7.4$
$\ell_x = 10$ FT S $= -6.0$

NOTE: THIS ZERO DOES NOT
MIGRATE SIGNIFICANTLY

NOTE: THIS ZERO DOES NOT
MIGRATE SIGNIFICANTLY

DOWN   UP
$+\ell_z$ | $-\ell_z$

BELOW C.G.   ABOVE C.G.
$+\ell_z$ | $-\ell_x$

$j\omega$

σ -4   -3   -2   -1   0   1   2   3   4
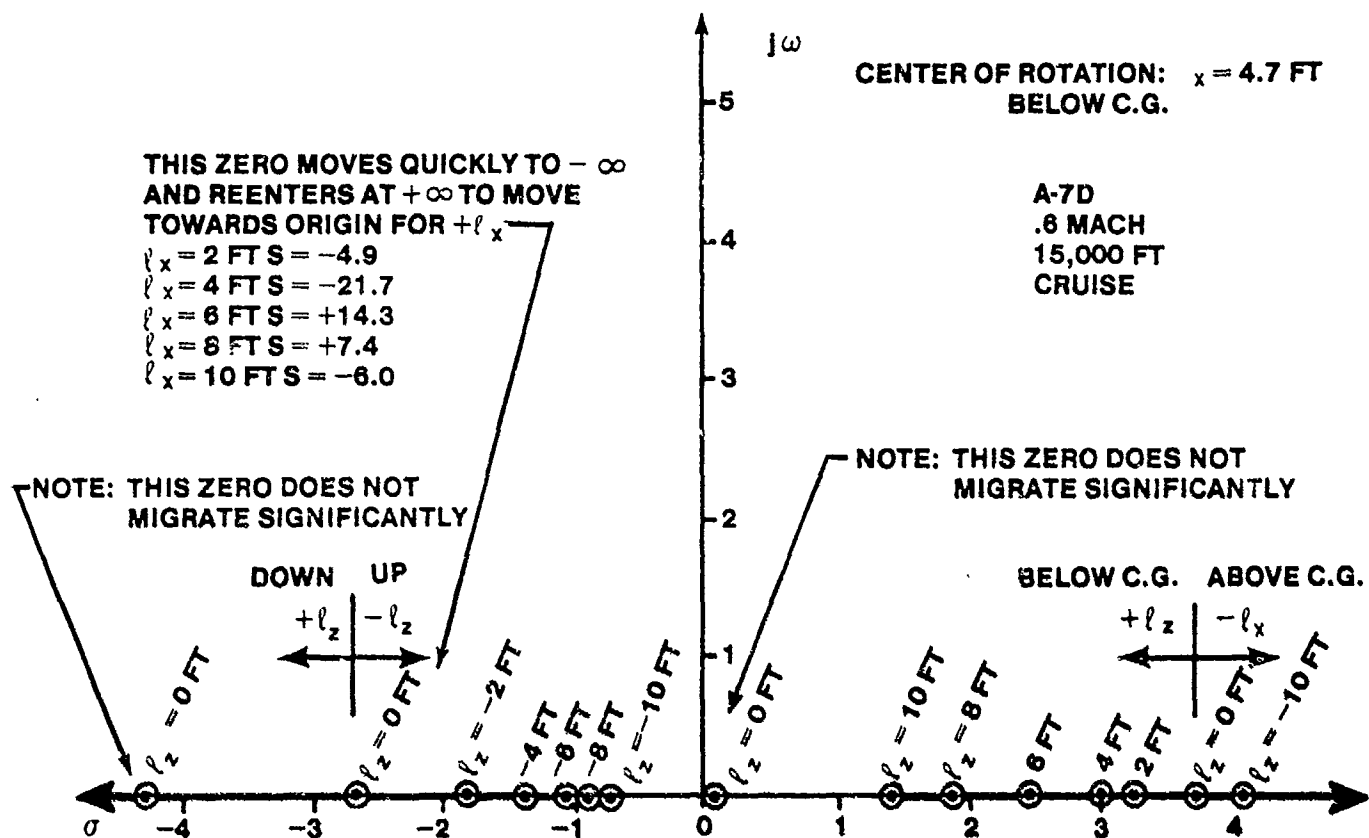
FIGURE 14.117.   EFFECT OF LATERAL ACCELEROMETER LOCATION ON ZEROS OF LATERAL
ACCELERATION TRANSFER FUNCTION

14.3.5 Fuselage Structural Bending

Fuselage bending is sensed by rate gyros and accelerometers at
frequencies below the cut-off frequency of the aircraft control system (the
maximum frequency at which the flight control system sensors can detect
motion). The effects of aeroelastic coupling due to the intermingling of the
aircraft structural motions with the rigid body motions can produce extraneous
control signals which can degrade handling qualities or controllability and
may even cause the flight control system to drive the structural motions
unstable.

References 14.2, 14.3, 14.40 and 14.41 discuss aeroelastic equations of
motion.

14.134

Longitudinal aeroelastic equations of motion are presented in Figure 14.118. The equations describe the aircraft pitch axis motion and the significant structural body bending for small perturbations of the aircraft from straight and level flight. The significant structural modes are the bending modes that are at a frequency that can be sensed and therefore interact with the flight control system. The first two equations represent the two degree of freedom short period dynamic characteristics and include aeroelastic coupling effects. The next three equations are the structural body bending equations of motion. The last two equations provide for the computation of aircraft pitch rate and normal acceleration that are sensed at the locations of the pitch rate gyro and normal accelerometer, respectively. A list of the dimensional stability derivatives used in the equations is presented in Table 14.4. Figure 14.119 presents an illustration of the variable definitions. Reference 14.39 presents a list of the coefficients for the equations of motion for the F-4E aircraft.

$$\dot{\alpha} - \dot{\theta} = Z_\alpha \alpha + Z_{\dot\theta}\dot\theta + Z_{\dot\eta_1}\dot\eta_1 + Z_{\eta_1}\eta_1 + Z_{\dot\eta_2}\dot\eta_2 + Z_{\eta_2}\eta_2 + Z_{\dot\eta_3}\dot\eta_3 + Z_{\eta_3}\eta_3 + Z_{\ddot\delta}\ddot\delta + Z_{\dot\delta}\dot\delta + Z_\delta\delta$$

$$\ddot\theta = M_\alpha \alpha + M_{\dot\alpha}\dot\alpha + M_{\dot\theta}\dot\theta + M_{\dot\eta_1}\dot\eta_1 + M_{\eta_1}\eta_1 + M_{\dot\eta_2}\dot\eta_2 + M_{\eta_2}\eta_2 + M_{\dot\eta_3}\dot\eta_3 + M_{\eta_3}\eta_3 + M_{\ddot\delta}\ddot\delta + M_{\dot\delta}\dot\delta + M_\delta\delta$$

$$\ddot\eta_1 = F_\alpha \alpha + F_{\dot\theta}\dot\theta + F_{\dot\eta_1}\dot\eta_1 + F_{\eta_1}\eta_1 + F_{\dot\eta_2}\dot\eta_2 + F_{\eta_2}\eta_2 + F_{\dot\eta_3}\dot\eta_3 + F_{\eta_3}\eta_3 + F_{\ddot\delta}\ddot\delta + F_{\dot\delta}\dot\delta + F_\delta\delta$$

$$\ddot\eta_2 = G_\alpha \alpha + G_{\dot\theta}\dot\theta + G_{\dot\eta_1}\dot\eta_1 + G_{\eta_1}\eta_1 + G_{\dot\eta_2}\dot\eta_2 + G_{\eta_2}\eta_2 + G_{\dot\eta_3}\dot\eta_3 + G_{\eta_3}\eta_3 + G_{\ddot\delta}\ddot\delta + G_{\dot\delta}\dot\delta + G_\delta\delta$$

$$\ddot\eta_3 = H_\alpha \alpha + H_{\dot\theta}\dot\theta + H_{\dot\eta_1}\dot\eta_1 + H_{\eta_1}\eta_1 + H_{\dot\eta_2}\dot\eta_2 + H_{\eta_2}\eta_2 + H_{\dot\eta_3}\dot\eta_3 + H_{\eta_3}\eta_3 + H_{\ddot\delta}\ddot\delta + H_{\dot\delta}\dot\delta + H_\delta\delta$$

$$\dot\theta_{M_j} = \dot\theta + [\frac{\partial\phi_1}{\partial x}]_j \dot\eta_1 + [\frac{\partial\phi_2}{\partial x}]_j \dot\eta_2 + [\frac{\partial\phi_3}{\partial x}]_j \dot\eta_3$$

$$n_{z_j} = -\frac{1}{32.2}[U_0(\dot\alpha - \dot\theta) - 1_x \ddot\theta + [\phi_1]_j \ddot\eta_1 + [\phi_2]_j \ddot\eta_2 + [\phi_3]_j \ddot\eta_3$$

FIGURE 14.118. LONGITUDINAL AEROELASTIC EQUATIONS OF MOTION

FRL – FUSELAGE REFERENCE LINE

$$\frac{2\phi_2}{2x}$$ IS THE LOCAL SLOPE OF THE FRL$_{ELASTIC}$

FRL$_{ELASTIC}$

η_2

FRL$_{RIGID}$
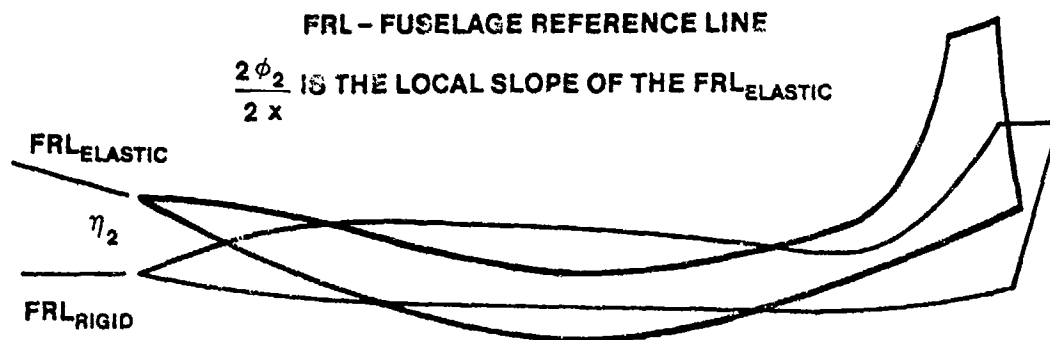
(a). FIRST FUSELAGE BENDING MODE

STABILATOR ROTATION MODE — EFFECTS DUE TO ROTATION OF STABILATOR ABOUT
THE STABILATOR HINGE LINE DUE TO ELASTICITY

FIRST STABILATOR BENDING MODE

(b). ELASTIC STABILATOR MODES

Z

X

1ST BENDING MODE

3RD BENDING MODE
2ND BENDING MODE
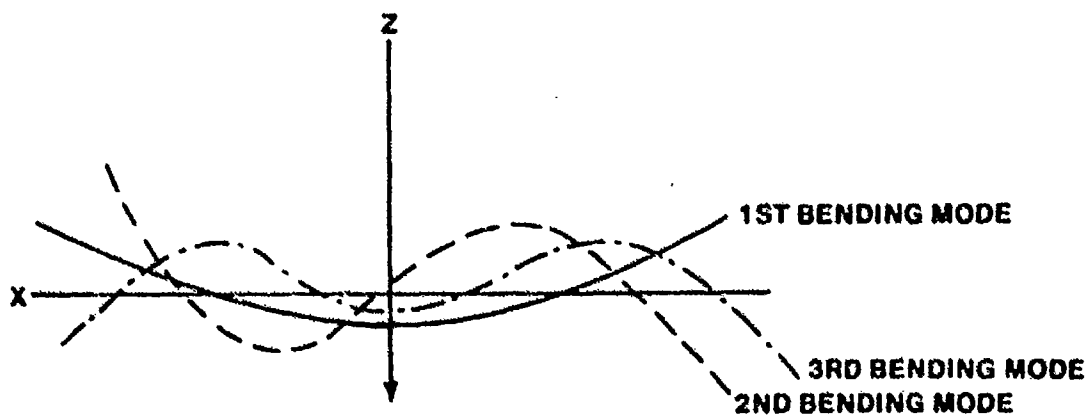
(c). BENDING MODE SHAPES

FIGURE 14.119. AEROELASTIC MODE AND VARIABLE DEFINITIONS

TABLE 14.4

AEROELASTIC EQUATIONS DIMENSIONAL STABILITY DERIVATIVE DEFINITIONS

F_α — Stabilator Bending Mode Acceleration due to Angle of Attack (1/sec squared)

$F_{\dot\theta}$ — Stabilator Bending Mode Acceleration due to Pitch Rate (1/sec)

F_δ, $F_{\dot\delta}$, $F_{\ddot\delta}$ — Stabilator Bending Mode Acceleration due to Stabilitator Deflection Acceleration (1/sec squared), Rate (1/sec), and Position (dimensionless), Respectively

F_{η_1}, $F_{\dot\eta_1}$ — Stabilitator Bending Mode Acceleration due to Stabilator Bending (1/sec squared) and Stabilator Bending Rate (1/sec), Respectively

F_{η_2}, $F_{\dot\eta_2}$, — Stabilator Bending Mode Acceleration due to First Fuselage Vertical Bending (1/sec squared) and Bending Rate (1/sec), Respectively

F_{η_3}, $F_{\dot\eta_3}$ — Stabilator Bending Mode Acceleration due to Stabilator Rotation Mode (1/sec squared) and Rotation Mode Rate (1/sec), Respectively

G_x — First Fuselage Vertical Bending Mode Acceleration due to Parameter x

H_x — Stabilator Rotation Mode Acceleration due to Parameter x

M_x — Pitching Angular Acceleration due to Parameter x

Z_x — Flight Path Angular Acceleration due to Parameter x

η_1, η_2, η_3 — Normalized Coordinates of Stabilator Bending Mode, First Fuselage Vertical Bending Mode and Stabilator Rotation Mode, Respectively. Displacement at Fuselage Station j is Positive Downward.

$(\phi_1)_j$, $(\phi_2)_j$, $(\phi_3)_j$ — Measured Normal Acceleration due to Stabilator Bending Mode, First Fuselage Vertical Bending Mode and Stabilator Rotation Mode at Fuselage Station j, Respectively

$\dfrac{\partial\phi_1}{\partial x}j$, $\dfrac{\partial\phi_2}{\partial x}j$, $\dfrac{\partial\phi_3}{\partial x}j$ — Slope of the Stabilator Bending Mode, First Fuselage Vertical Bending Mode and Stabilator Rotation Mode at Fuselage Station j, Respectively

Aircraft transfer functions can be found from the equations of motion. Figure 14.120 presents the equations in matrix format. Cramer's rule can be applied to develop the equations of motion including aeroelastic effects. This matrix equation may be partitioned to show the rigid and aeroelastic aircraft interplay as follows:

$$
\left[
\begin{array}{c|c}
\text{Rigid Body Equations} & \begin{array}{c}\text{Coupling Forces}\\ \text{and Moments due}\\ \text{to Bending}\end{array} \\
\hline
\begin{array}{c}\text{Coupling Forces}\\ \text{and Moments due}\\ \text{to Rigid Body}\\ \text{Motions}\end{array} & \text{Bending Mode Equations}
\end{array}
\right]
\left[
\begin{array}{c}
\alpha(s) \\
\theta(s) \\
\hline
\eta_1(s) \\
\eta_2(s) \\
\eta_3(s)
\end{array}
\right]
= \text{Control Effects} \quad \delta(s)
$$

$$
\left[
\begin{array}{cc|ccc}
s - Z_\alpha & -(Z_{\dot{\theta}}+1)s & -Z_{\dot{n}_1}s - Z_{n_1} & -Z_{\dot{n}_2}s - Z_{n_2} & -Z_{\dot{n}_3}s - Z_{n_3} \\
-M_\alpha - M_{\dot{\alpha}}s & s^2 - M_{\dot{\theta}}s & -M_{\dot{n}_1}s - M_{n_1} & -M_{\dot{n}_2}s - M_{n_2} & -M_{\dot{n}_3}s - M_{n_3} \\
\hline
-F_\alpha & -F_{\dot{\theta}}s & s^2 - F_{\dot{n}_1}s - F_{n_1} & -F_{\dot{n}_2}s - F_{n_2} & -F_{\dot{n}_3}s - F_{n_3} \\
-G_\alpha & -G_{\dot{\theta}}s & -G_{\dot{n}_1}s - G_{n_1} & s^2 - G_{\dot{n}_2}s - G_{n_2} & -G_{\dot{n}_3}s - G_{n_3} \\
-H & -H_{\dot{\theta}}s & -H_{\dot{n}_1}s - H_{n_1} & -H_{\dot{n}_2}s - H_{n_2} & s^2 - H_{\dot{n}_3}s - H_{n_3}
\end{array}
\right]
\left[
\begin{array}{c}
\alpha(s) \\
\theta(s) \\
\eta_1(s) \\
\eta_2(s) \\
\eta_3(s)
\end{array}
\right]
$$

$$
=
\left[
\begin{array}{c}
Z_{\ddot{\delta}}s^2 + Z_{\dot{\delta}}s + Z_{\delta} \\
M_{\ddot{\delta}}s^2 + M_{\dot{\delta}}s + M_{\delta} \\
F_{\ddot{\delta}}s^2 + F_{\dot{\delta}}s + F_{\delta} \\
G_{\ddot{\delta}}s^2 + G_{\dot{\delta}}s + G_{\delta} \\
H_{\ddot{\delta}}s^2 + H_{\dot{\delta}}s + H_{\delta}
\end{array}
\right]
\delta(s)
$$

FIGURE 14.120. LONGITUDINAL AEROELASTIC MATRIX EQUATION OF MOTION

If the natural frequency of the short period mode ω_{sp} is low relative to the natural frequency of the structural bending mode ω_{sb} such that $\omega_{sb}/\omega_{sp} > 5$ then the response of the rigid body aircraft and the structural bending effects are effectively decoupled. The principle of superposition can be used in this case to account for the aeroelastic effects. The block diagram, for the rate gyro measurement is Figure 14.121.
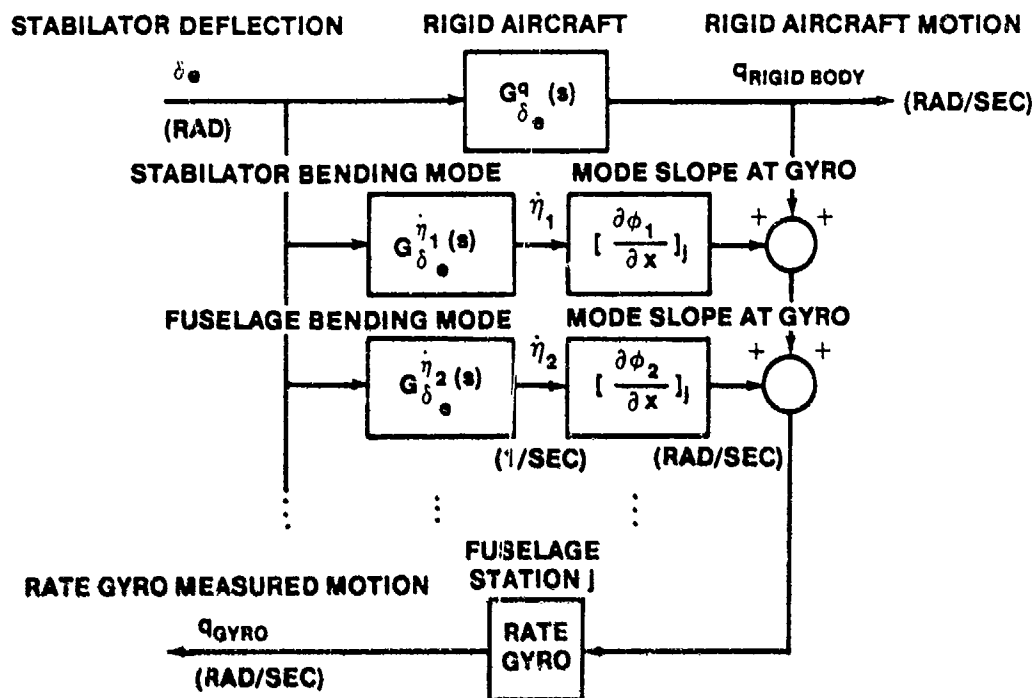
FIGURE 14.121. DECOUPLED AEROELASTIC AIRCRAFT MODEL

14.3.5.1 Accelerometer and Rate Gyro Sensor Placement. From the last two equations of the longitudinal aeroelastic equations of motion, the adverse effects of structural coupling can be reduced by the careful selection of the sensor locations. The ideal location for an accelerometer is where ϕ_1, ϕ_2 and ϕ_3 are zero (from a structural point of view) and a pitch rate gyro is ideally located where $\partial\phi_1/\partial x$, $\partial\phi_2/\partial x$, $\partial\phi_3/\partial x$ are zero. All six varibles are not all zero at the same point in reality. If the structural mode shapes are accurately represented by simple harmonic motion (sinusoidal in nature) then a reduction of structural mode coupling may be obtained by locating accelerometers on nodal points, or points of zero deformation η_1', η_2', $\eta_3' = 0$ where the bending mode shapes in Figure 14.119c cross the x axis and by locating rate gyros on anti-nodal points, or points of zero slope, where $\partial\phi_1/\partial x$, $\partial\phi_2/\partial x$, $\partial\phi_3/\partial x = 0$.

14.139

Design compromises are necessary due to interference of the bending and rotation modes and due to limitations on available space for sensor location. The normal accelerometer location is usually ahead of the aircraft center of rotation and close to the node of the first fuselage structural mode. The rate gyro is normally located close to the anti-node of the first fuselage bending mode. Rate gyros located forward of this point have a destabilizing effect on the structural mode, which may require compensation to prevent driving the structural mode unstable. Rate gyros located aft of the anti-node have a stabilizing effect on the structural mode. The location of the gyro in the rigid aircraft did not require any special consideration.

14.3.5.2 Structural Filter Compensation. The proper placement of sensors will not entirely eliminate adverse structural effects in the flight control system. Often structural filters are required to provide structural mode attentuation. A simple first order lag filter, similar to the noise filter previously discussed, and a notch filter are commonly used for this purpose. A notch filter has the form

$$ K \left[\frac{s^2 + 2\zeta_N \omega_N s + \omega_N^2}{s^2 + 2\zeta_D \omega_D s + \omega_D^2} \right] \qquad (K = \omega_D^2 / \omega_N^2) $$

Figure 14.126 shows a Bode plot of a typical notch filter. The notch depth and relative width are primarily a function of the ratio ζ_N ζ_D. As this ratio becomes smaller, the depth of the notch increases while its width in terms of frequency decreases. Conversely, an increase in the ratio produces the opposite effect—less depth and wider notch. The tuned frequency is governed by the frequencies ω_N and ω_D. If the notch filter is symmetric, then the tuned frequency is $\omega_N = \omega_D$. If the notch filter is asymmetric, then $\omega_N \neq \omega_D$ and the tuned frequency is determined by ω_N if $\zeta_N < \zeta_D$.

14.3.5.3 Notch Filter Effects. Figure 14.122 presents a block diagram for a C-star (C*) command system for a proposed fly-by-wire F-4E aircraft. C* is defined as

$$ C^* = - n_{z_{ACCEL}} + Kq \qquad (14.72) $$

This blended pitch rate and normal acceleration system was a common control law strategy in the late sixties and early seventies (A-7D uses a C* control law), but was found to be difficult to design for level 1 flying qualities.

The transfer function

$$\frac{C^*}{\delta_e} = \frac{1355.7(s + 2.63 \pm 5.05j)(s + 0.52 \pm 65.75j)}{(s + 4)(s + 2.08 \pm 7.02j)(s + 1.19 \pm 92.01j)} \qquad (g's/radian)$$

was found using the matrix transfer function of Figure 14.120 for the 1.2 Mach, 5000 feet flight condition (see Reference 14.39). The system designers minimized structural coupling through the pitch rate gyro by locating the gyro at a point where the first fuselage bending mode slope is essentially zero. However, the accelerometer detects some structural mode acceleration. Notice the poles and zeros at very high frequencies which result from the first fuselage bending mode.
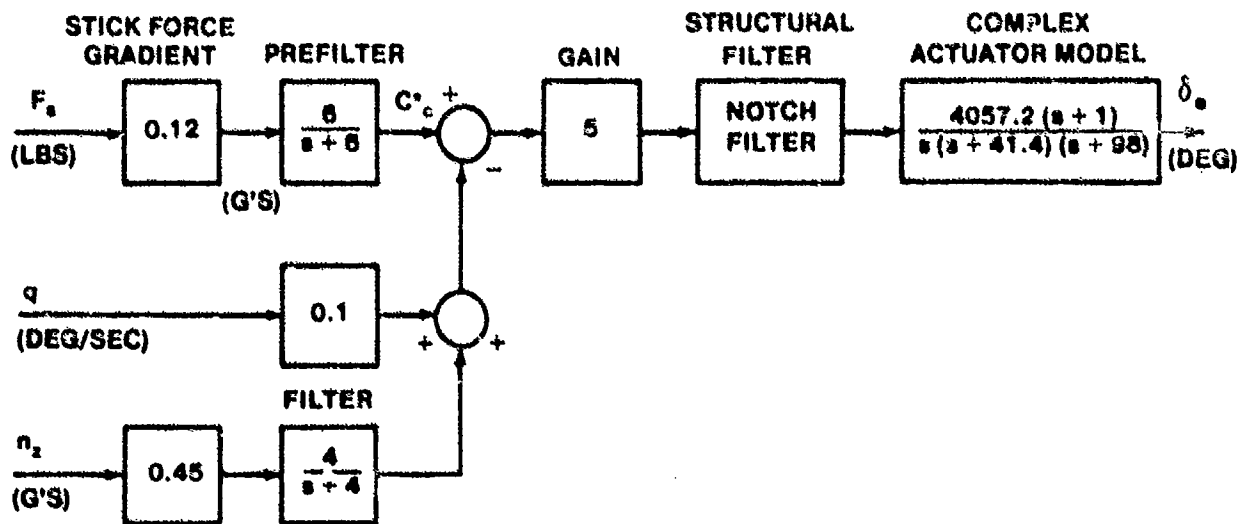
FIGURE 14.122.   PROPOSED FLY-BY-WIRE LONGITUDINAL FLIGHT CONTROL SYSTEM FOR THE F-4E AIRCRAFT

The control system block diagram may be redrawn for analysis, as shown in Figure 14.123. If the notch filter is neglected, the Bode diagram of Figure 14.124 and the root locus plot of Figure 14.125 result. Notice the instability near 92 radians per second which occurs due to the structural coupling between the first fuselage bending mode and the flight control system (zero gain or phase margin in the Bode diagram and a pair of high frequency oscillatory roots in the right half s-plane in the root locus plot). This instability is due to the accelerometer sensing structural bending mode accelerations and feeding the signals back to the stabilator through the flight control system to further excite the bending mode. The overall gain of the control system must be reduced by a minimum of 15 decibels (a factor of 5.6) to maintain stability, with an accompanying degradation of handling qualities due to a reduced bandwidth and poor short period damping, unless a filter can be added to the system to suppress the coupling.
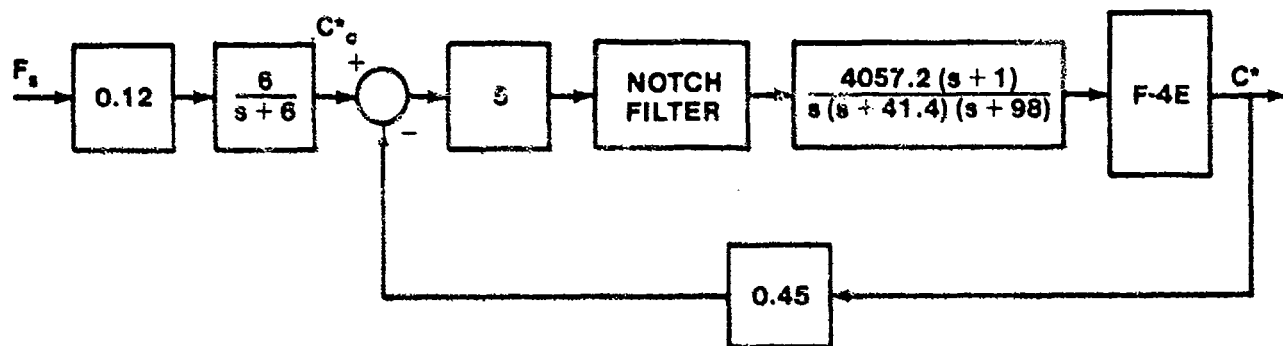
FIGURE 14.123. SIMPLIFIED LONGITUDINAL FLIGHT CONTROL SYSTEM PROPOSED FOR THE F-4E AIRCRAFT
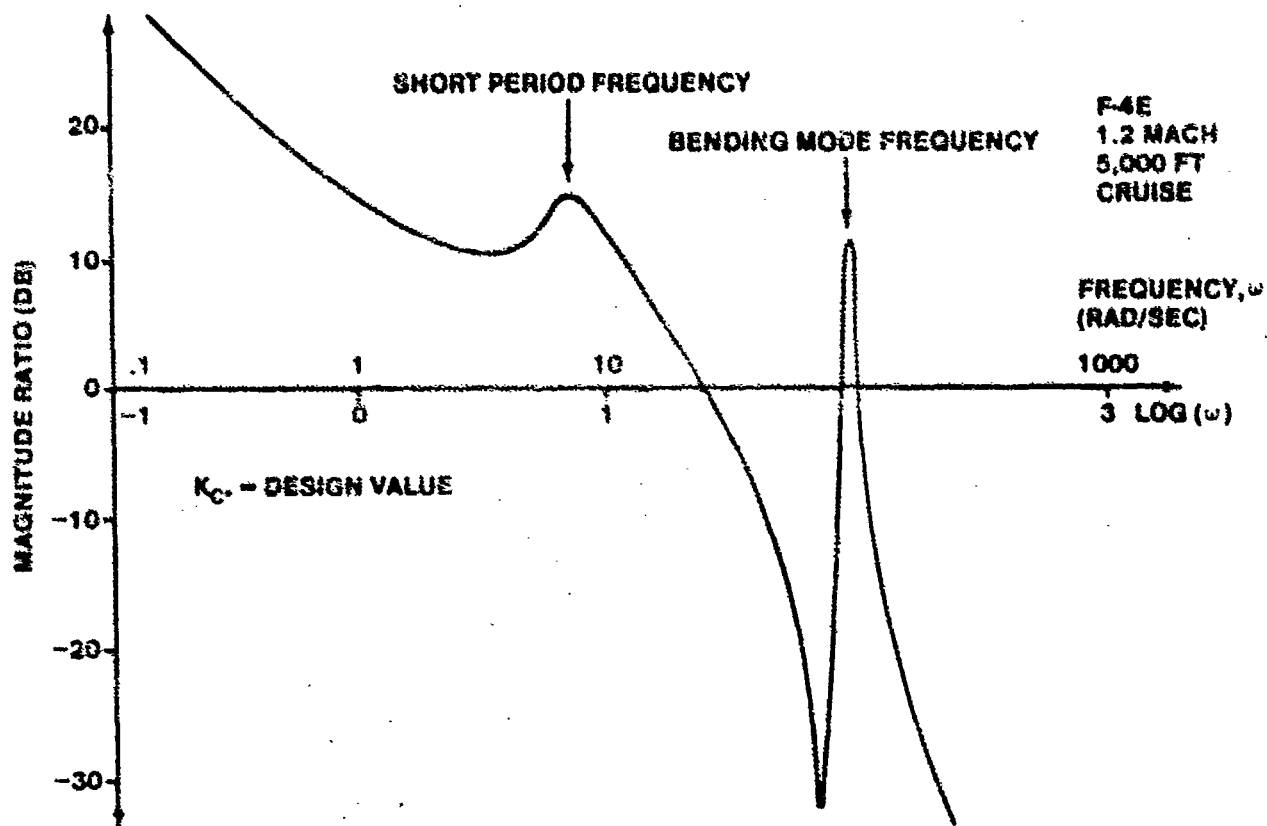
FIGURE 14.124A. BODE PLOT OF C* COMMAND SYSTEM FOR F-4E SHOWING EFFECTS OF FIRST FUSELAGE BENDING MODE

14.143
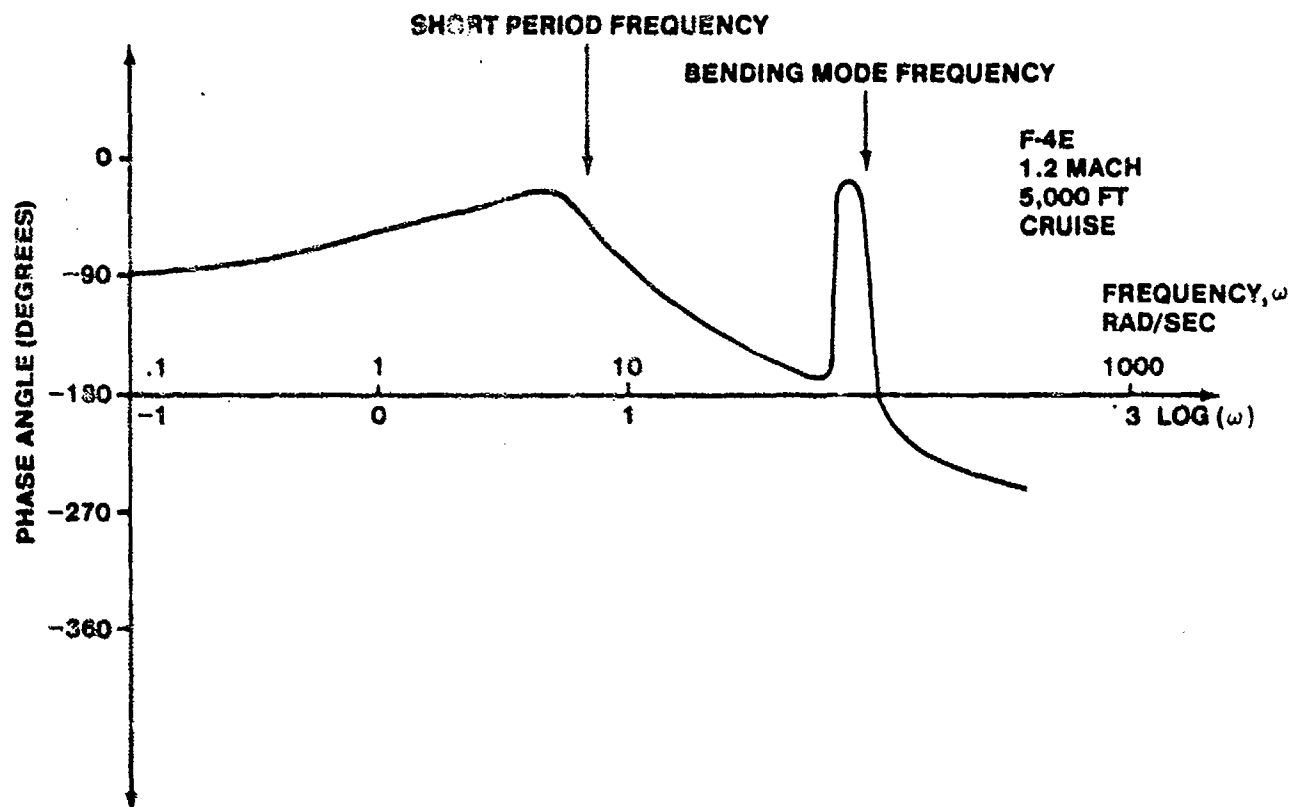
FIGURE 14.124B.   BODE PLOT OF C* COMMAND SYSTEM (CONTINUED)

The designers added a notch filter

$$G_{NF}(s) = \frac{0.96(s + 4.3 \pm 85.6j)}{s + 50.4 \pm 67.2j}$$

to the system.   Figure 14.126 plots a Bode diagram for this filter.   The
magnitude plot displays a large reduction in the ratio of the output signal to
the input signal near the structural bending mode frequency of 92 radians per
second, forming a notch.   The magnitude ratio at low frequencies (less than
about 16 radians per second) is essentially unaffected so that the short
period response is not distorted by the filter.   A very slight bit of phase
lag occurs in the short period frequency region (about 5°) which causes a
slight increase in the response time.

$0 \le K_{C^*} < + \infty$

F-4E
1.2 MACH
5,000 FT
CRUISE

POLE FOR
DESIGN K_{C^*}

POLE AND ZERO FOR
1ST FUSELAGE BENDING
MODE

POLE AT S = −119.3
FOR DESIGN K_{C^*}

COMPLEX ACTUATOR MODEL POLES

SEE FIG.
14.125b
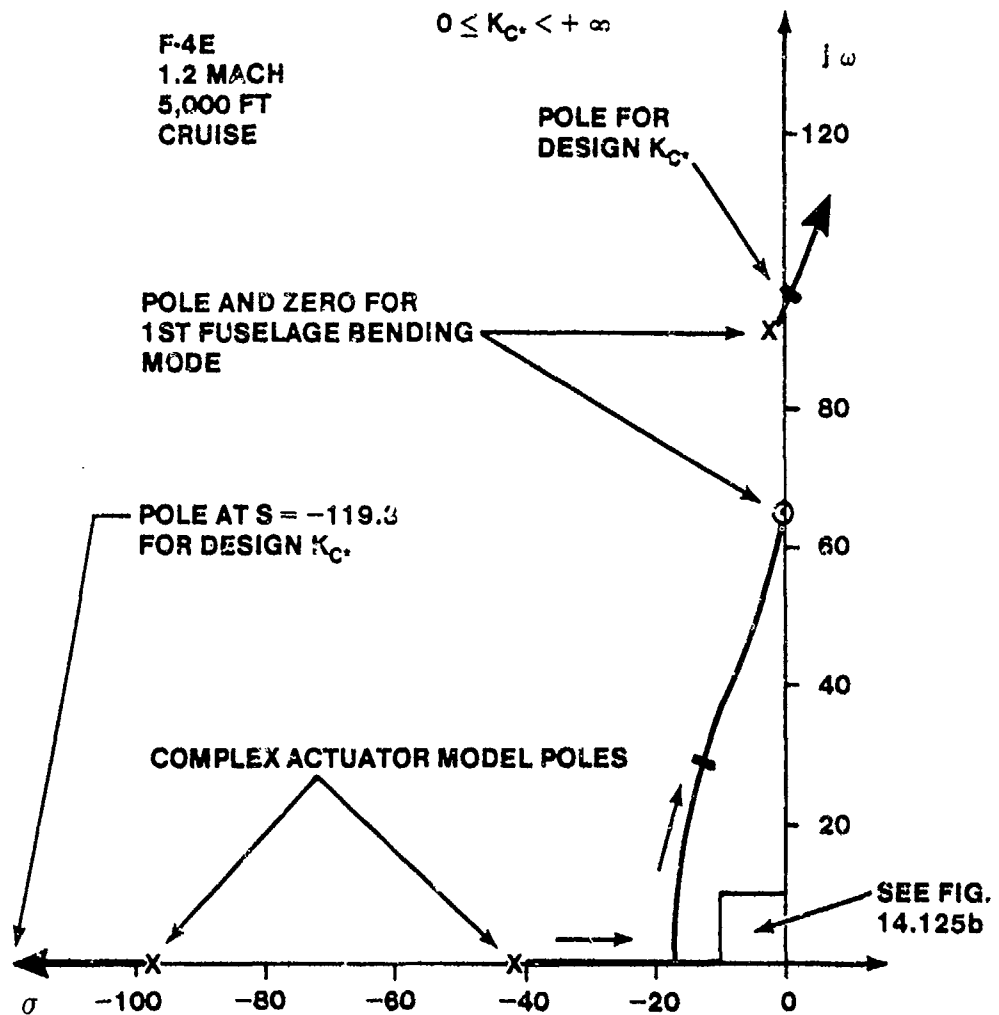
FIGURE 14.125A. ROOT LOCUS OF C* COMMAND SYSTEM FOR THE F-4E SHOWING
EFFECTS OF FIRST FUSELAGE BENDING MODE

$0 \leq K_{C^*} < +\infty$

F-4E
1.2 MACH
5,000 FT
CRUISE

POLE LOCATIONS
AT DESIGN K_{C^*}
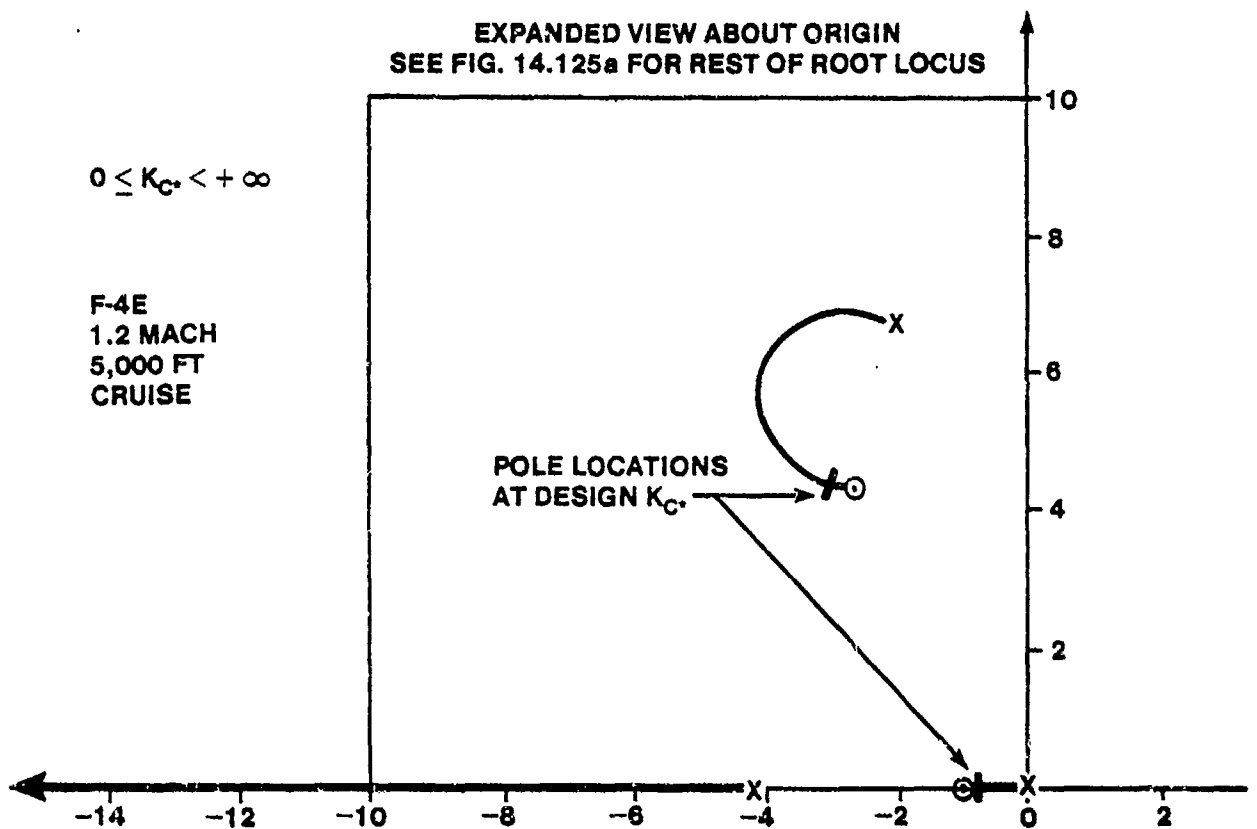
FIGURE 14.125B. EXPANDED ROOT LOCUS PLOT OF C* COMMAND SYSTEM FOR THE F-4E
INCLUDING BENDING MODE EFFECTS

TUNED
FREQUENCY

PHASE ANGLE PLOT

MAGNITUDE RATIO (DB)

PHASE ANGLE (DEGREES)

FREQUENCY
(RAD/SEC)

LOG (ω)

MAGNITUDE PLOT

SHORT PERIOD
FREQUENCY

BENDING MODE
FREQUENCY
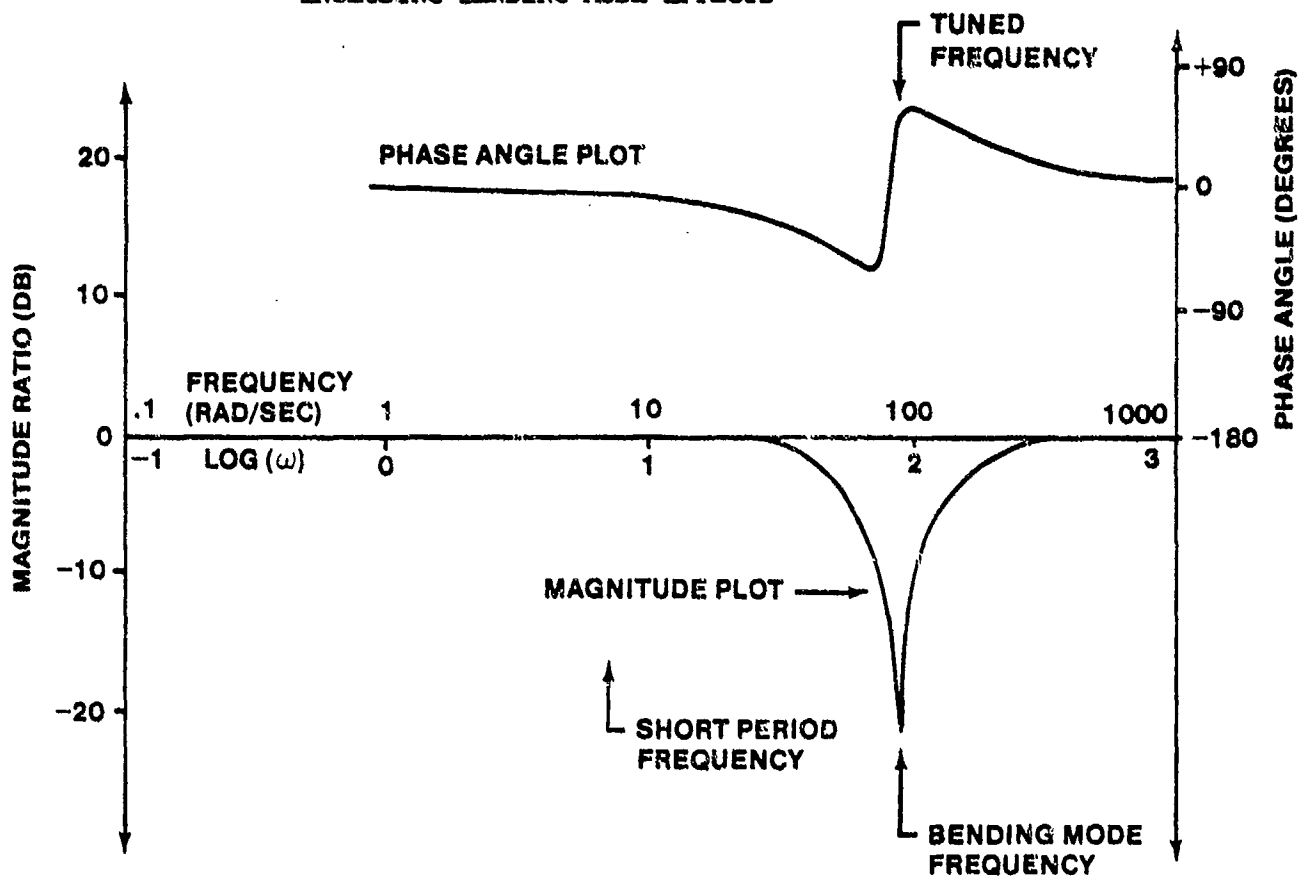
FIGURE 14.126. BODE PLOT OF NOTCH FILTER USED IN F-4E C* COMMAND FLIGHT
CONTROL SYSTEM

Figure 14.127 shows the effect of the notch filter on the proposed F-4E fly-by-wire flight control system. Notice the magnitude ratio is suppressed in the vicinity of the bending mode natural frequency. Figure 14.128 presents the root locus plot for the system incorporating the structural filter. Notice that all the augmented roots of the aircraft are stable.
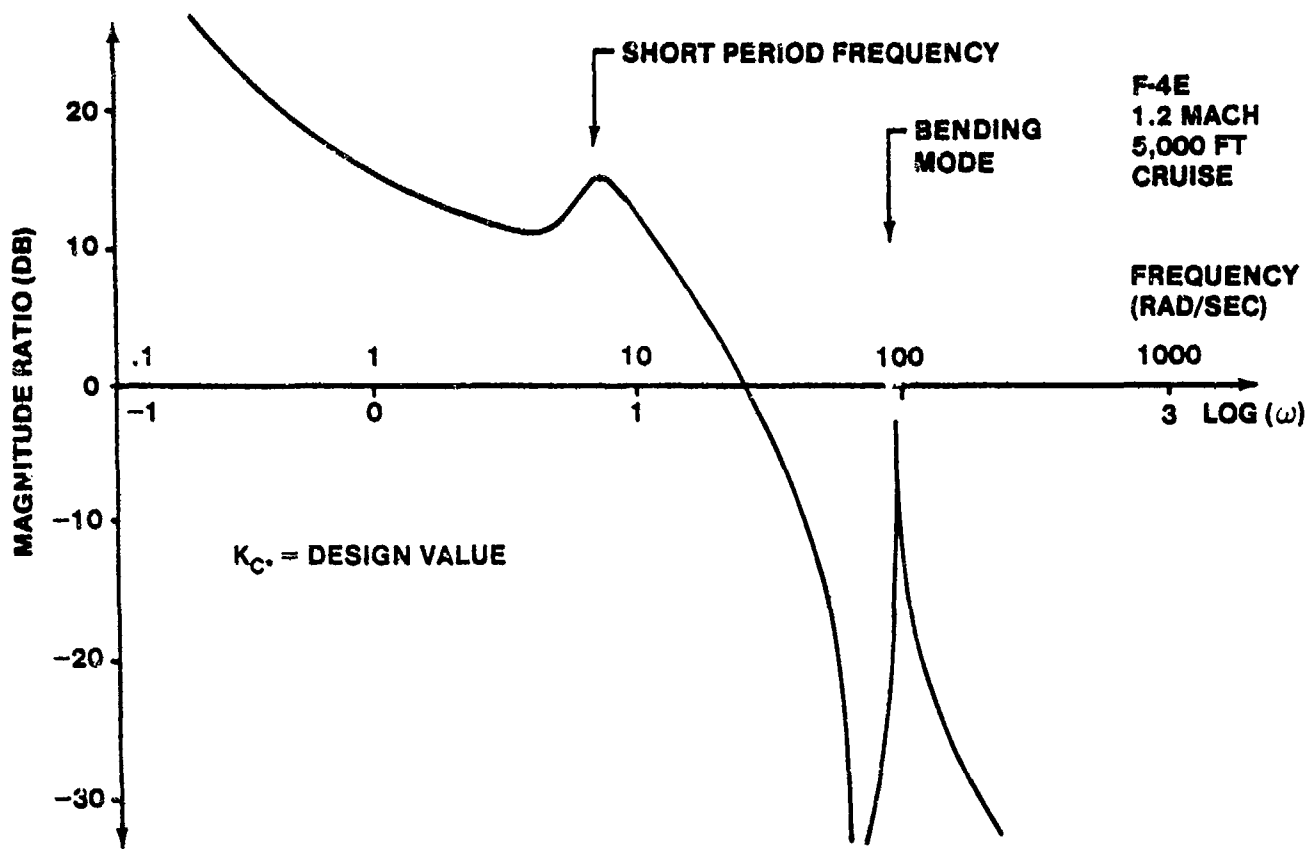
FIGURE 14.127A. BODE PLOT OF C* COMMAND SYSTEM FOR F-4E SHOWING SUPPRESSION
OF BENDING MODE BY STRUCTURAL FILTER
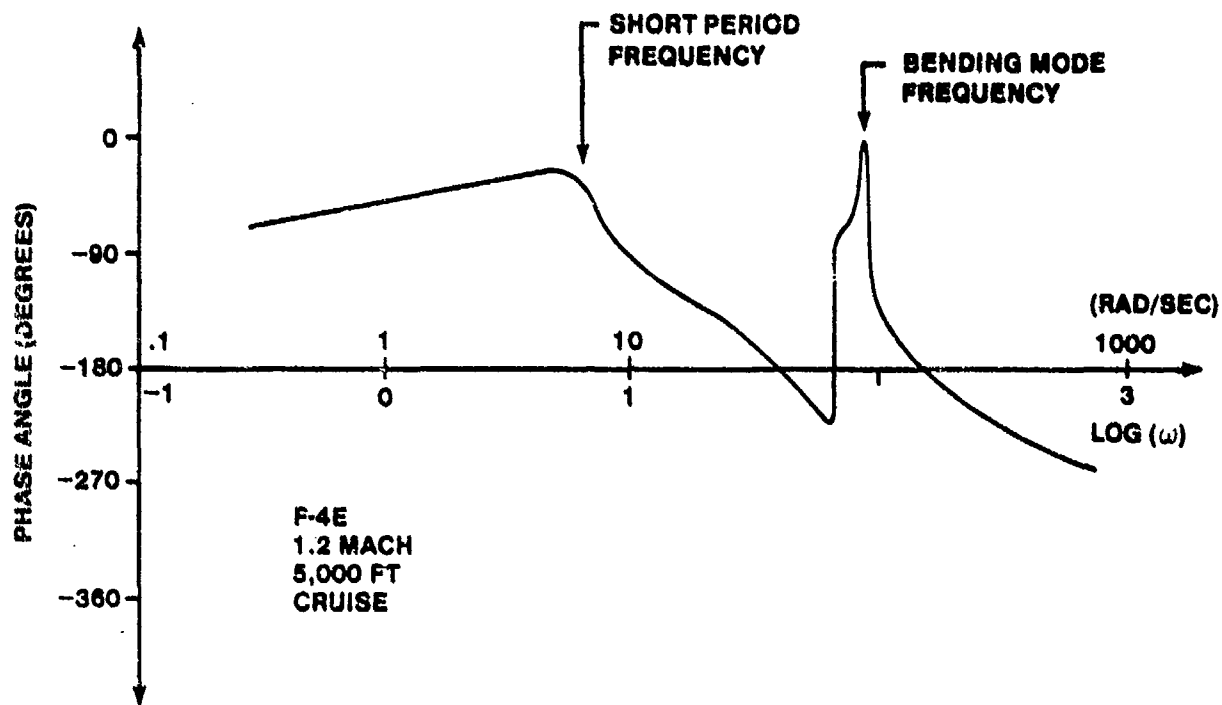
FIGURE 14.127B. BODE PLOT OF C* COMMAND SYSTEM (CONTINUED).
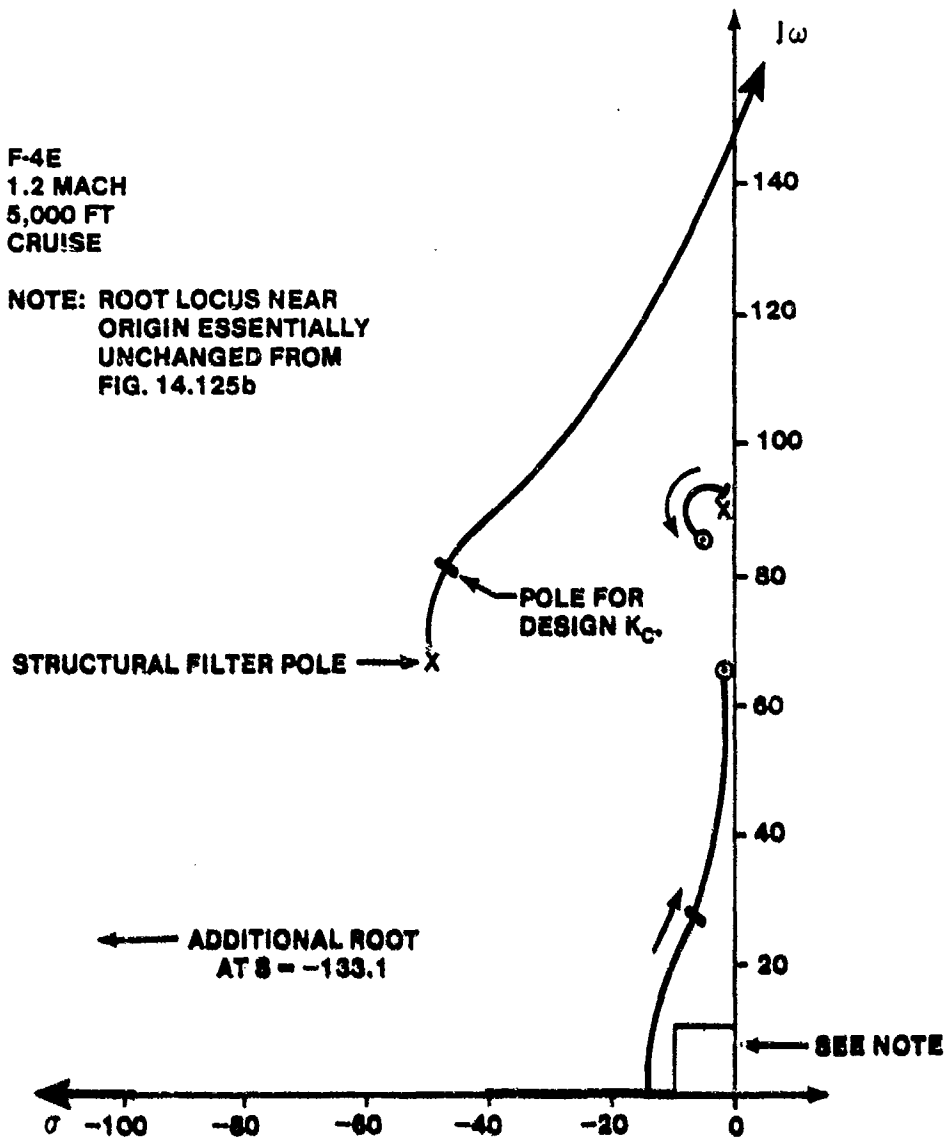
FIGURE 14.128. ROOT LOCUS PLOT OF F-4E WITH C* SYSTEM INCLUDING STRUCTURAL FILTER

14.3.6 Nonlinear Elements

Simplified linear analysis of complex systems often ignores important nonlinear effects which can greatly alter the response characteristics of closed loop control systems and may cause significant adverse or even catastrophic results. Nonlinearities in system elements, such as actuator rate limits, control surface deflection limits, mechanical hysteresis or friction, can cause system instabilities which are not evident from linear analysis. (Reference 14.31 discusses nonlinear analysis.)

Figure 14.129 presents four common nonlinearities encountered in flight control systems. The convention used for graphically representing nonlinear effects plots the input variable along the x axis and the output variable along the y axis. The input-output relationship must be understood when examining nonlinear elements.

The deadzone effect is typical of friction and breakout forces present in conventional pilot controller feel systems and occurs to some degree in most mechanical systems. The stick force is plotted as the input variable and the stick displacement is the output variable.

The limiter effect is typical of hydraulic actuators -- which can deflect an aerodynamic surface at a rate less than commanded depending on the surface aerodynamic hinge moment and which also have limited motion authority due to piston movement capacity. Mechanical stops are usually provided to limit aerodynamic surface range of motion.

Hysteresis is quite common and often undesirable in pitot static instruments. Hysteresis may be useful for other applications. The A-7D maneuvering flaps display hysteresis which was intentionally designed into the system to prevent premature flap extension or retraction. When increasing angle of attack past 14 units the flaps fully extend. As angle of attack is reduced past 11 units they retract.

The absolute value nonlinearity causes a signal to pass which is of the same magnitude as the input regardless of the sign of the input.

(a). DEADZONE

(b). LIMITER

(c). HYSTERESIS

(d). ABSOLUTE VALUE
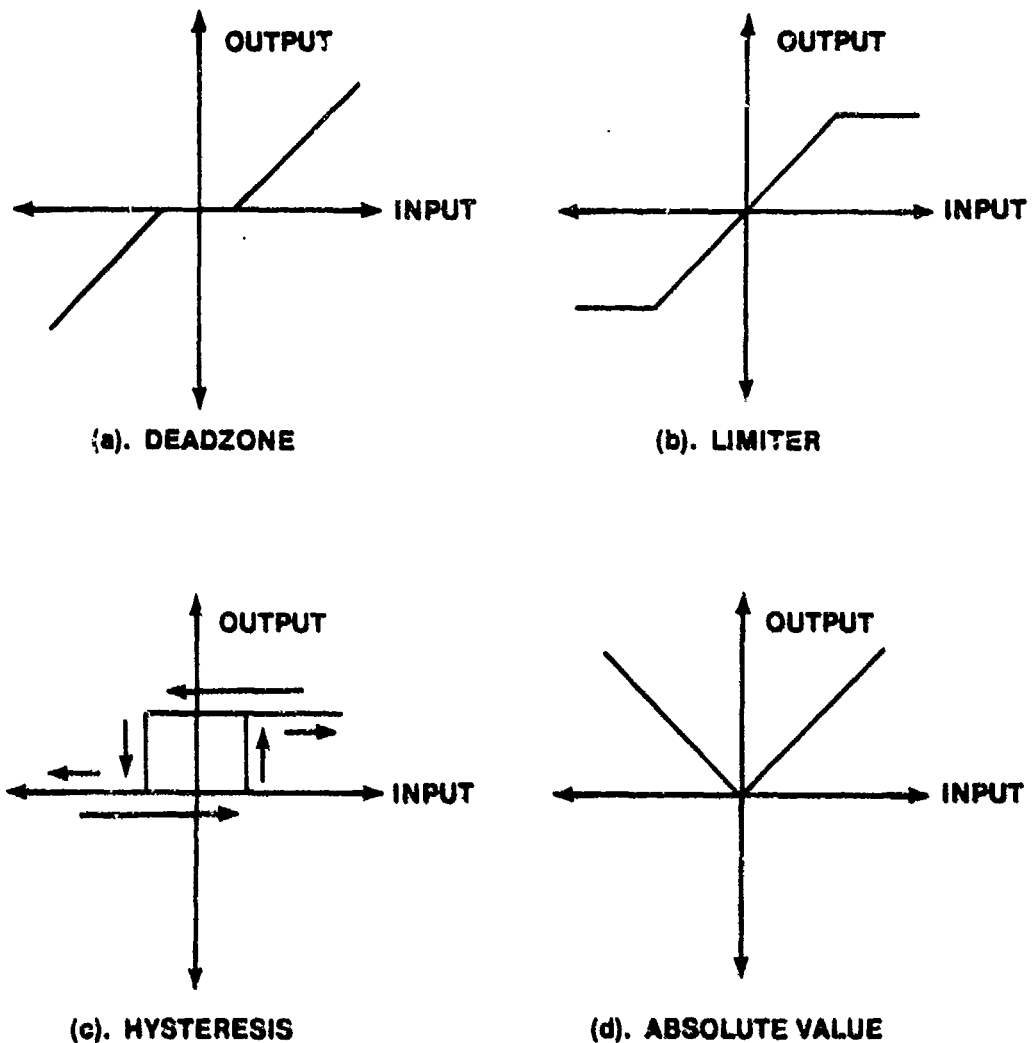
FIGURE 14.129. TYPICAL NONLINEARITIES

14.3.7 SAS and CAS Definitions

14.3.7.1 Stability Augmentation System (SAS). A stability augmentation system incorporates an electrical damper system in parallel with a conventional flight control system. The damper system obtains aircraft motion information from a sensor and applies an additional input to the control surface actuator to augment pilot input. If the pilot moves the aerodynamic surface directly (without the aid of an actuator), then an actuator must be provided for the damper system.

If the aircraft has irreversible flight control, the signal applied to the actuator by the damper will not normally be sensed by the pilot (no reflection of control surface movement in the controls).

In a boosted or reversible system the pilot may sense damper movement of the controls because of the direct link of the control to the aerodynamic surface. The pilot often senses an increase in control forces caused by the damper attempting to oppose transient aircraft motions, especially when using yaw damper systems during a wing-low crosswind landing (KC-135 or A-37).

14.3.7.2 Control Augmentation System (CAS). A CAS adds a record command path between the pilot controller and the control surface. The pilot actuates the mechanical and CAS electrical command path simultaneously. The electrical path typically uses a force sensor in the stick to provide an input to the electrical control system. With the CAS engaged, the aircraft response is heavily damped and the control system gains are scheduled to maintain constant aircraft response characteristics throughout the flight envelope. The sensors in the augmentation system provide feedback signals which are compared to the pilot input (usually a load factor, pitch rate or roll rate signal) to achieve the desired aircraft response.

The F-15 has a mechanical feedback path to alter the aircraft response characteristics somewhat with the CAS disengaged.

14.3.7.3 Effect of Parallel Mechanical and Electrical Systems. The analysis of control augmentation systems is complicated by the two command paths. An analysis of a CAS cannot ignore the effects of the mechanical system when examining the augmented aircraft response.

Figure 14.130 presents a block diagram of the F-15 longitudinal flight control system including the CAS interconnect servo. Since the steady state stick force gradients of the mechanical and electrical systems are different (4.25 pounds per 'g' for the mechanical system and 3.75 pounds per 'g' for the electrical system), the load factor feedback cannot satisfy both steady state conditions simultaneously. The inability of the load factor feedback to satisfy the two systems is alleviated via the CAS interconnect servo, which allows the pitch CAS gradient to be met by providing a bias signal to the mechanical path. This feature also causes a transfer of any steady state CAS series servo offset to the mechanical system so as to keep the series servo position near center, providing full CAS authority under most conditions and preventing large transients upon CAS disengagement. A full description of the F-15 control system is provided in Reference 14.42.

The aircraft transfer functions for the 0.9 Mach, sea level flight condition are

$$G_{\delta_e}^q(s) = \frac{37.48\,s\,(s + 0.069)\,(s + 3.337)}{(s + 0.035 \pm 0.147j)\,(s + 3.135 \pm 3.46j)} \quad (\text{deg/sec/deg})$$

$$G_{\delta_e}^{n_z}(s) = \frac{0.276\,s\,(s + 0.065)\,(s + 2.23 \pm 15.9j)}{(s + 0.035 \pm 0.147j)\,(s + 3.135 \pm 3.46j)} \quad (\text{g's/deg})$$

where the accelerometer is located 23 feet ahead of the center of gravity. Figure 14.131 compares the aircraft response with the CAS disengaged, with the CAS engaged and the effects of the mechanical system omitted, and of the augmented aircraft including the effects of both the CAS and the mechanical system. Notice that the mechanical system helps to make the augmented aircraft response more abrupt and to increase the initial load factor obtained for a given applied stick force. Without considering the effects of the mechanical system with the CAS engaged, one might wrongly conclude that the aircraft response is sluggish. Notice also that while the augmented aircraft steady state stick force gradient is 3.75 pounds per 'g', a closer approximation to the force gradient during practical maneuvering would be near 4.5 pounds per 'g', since the pilot would apply whatever additional force is necessary to attain the desired load factor as quickly as possible.
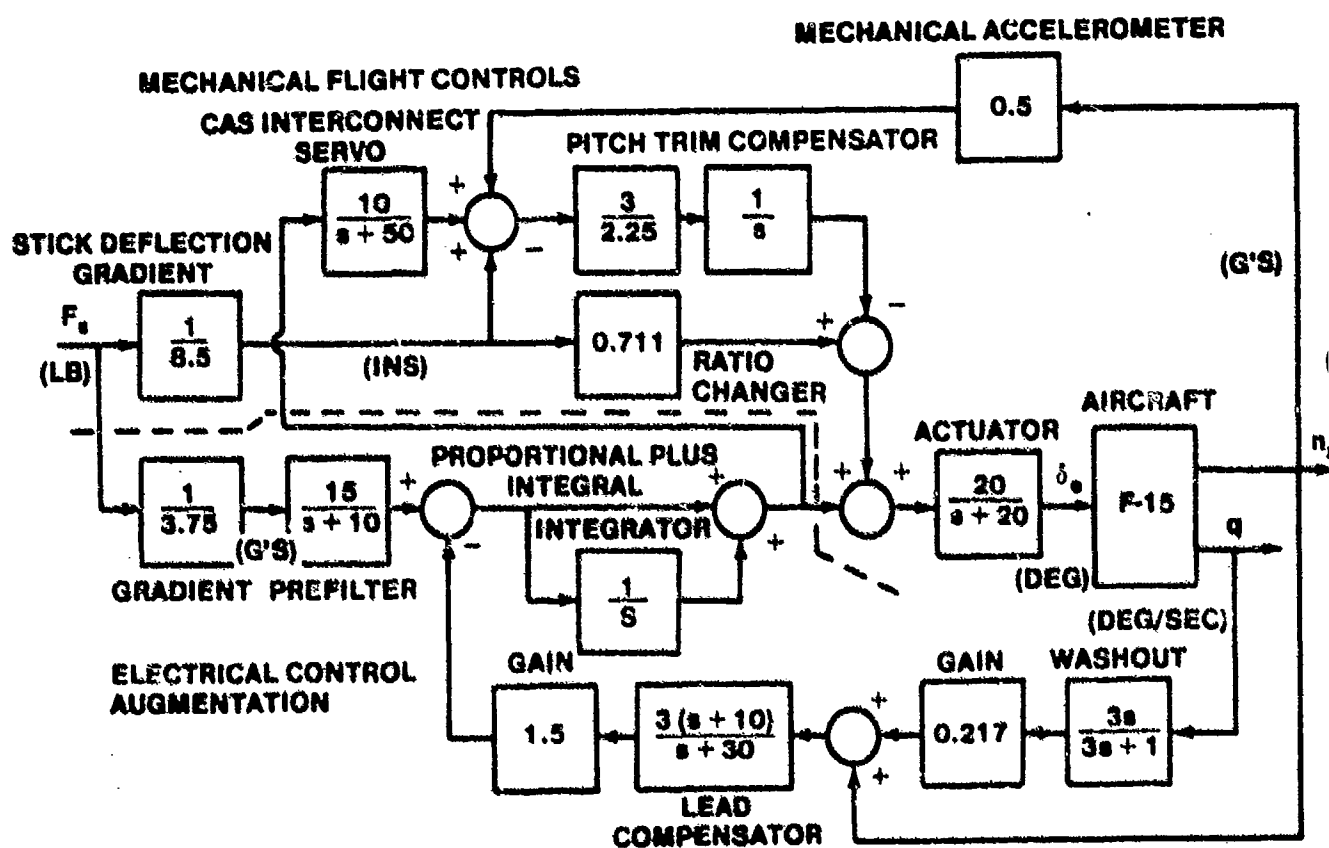
FIGURE 14.130. COMPLETE F-15 LONGITUDINAL FLIGHT CONTROL SYSTEM
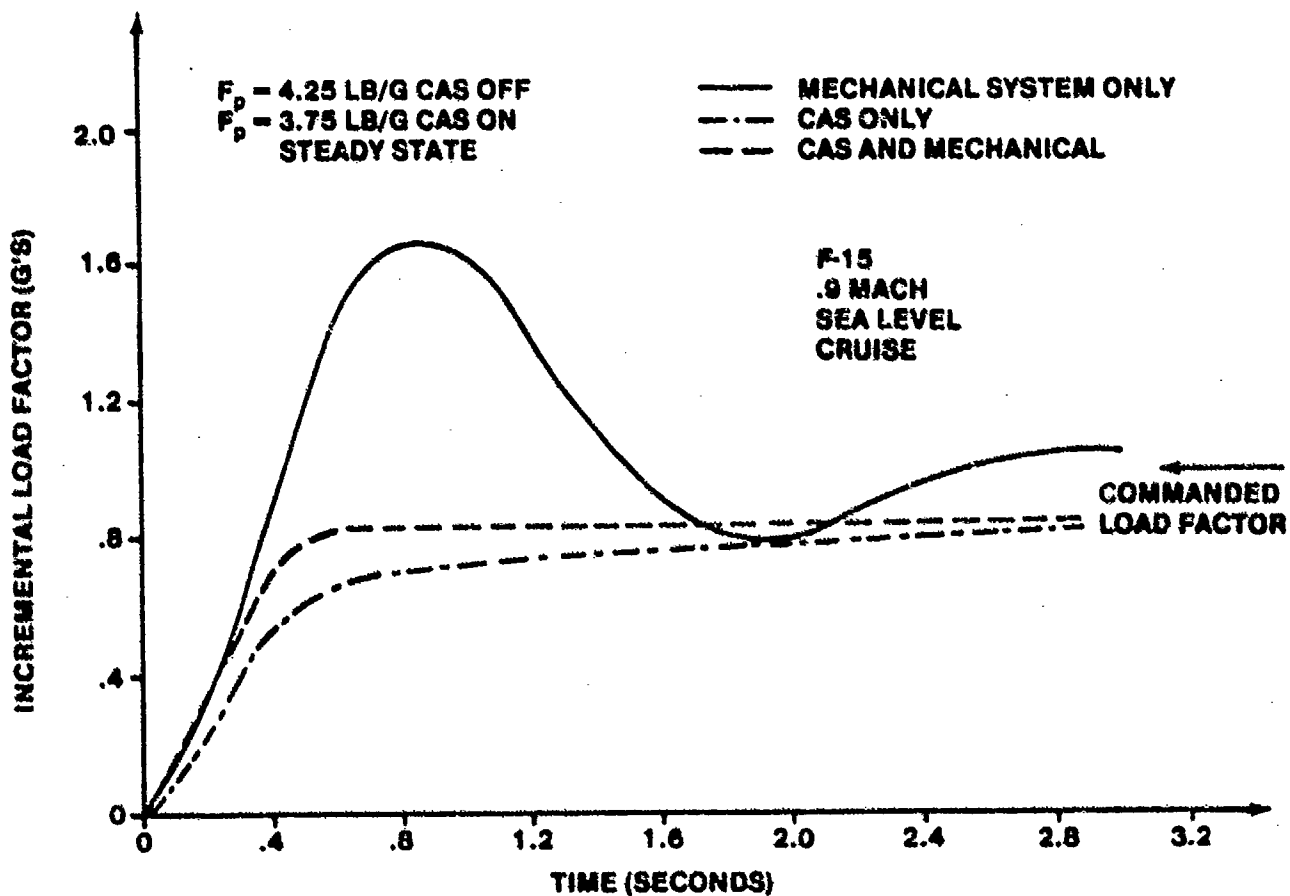
FIGURE 14.131. COMPARISON OF F-15 TIME RESPONSE CHARACTERISTICS

14.4 ANALYSIS OF MULTILOOP FEEDBACK CONTROL SYSTEMS

14.4.1 Uncoupled Multiloop Control Systems

Aircraft flight controls are frequently more complex than the simple single loop stability augmentation systems and usually incorporate several of the features discussed in Paragraph 14.3. Autopilots usually use an angular rate feedback as an inner loop to provide increased damping to the short period or Dutch roll mode and attitude feedback for comparison to the desired reference attitude as an outer loop. Figure 14.132 shows a block diagram of a multiloop attitude hold system.

14.4.1.1 Pitch Attitude Hold Control System. Figure 14.132 presents the pitch attitude control system to be analyzed in this section. The block diagram is reformulated to clearly show the multiloop nature of the system in Figure 14.133. The transfer function relating the pitch attitude to the pitch rate is

$$\frac{G^{\theta}_{\delta_e}(s)}{G^{q}_{\delta_e}(s)}$$

since

$$\frac{\theta}{q} = \left(\frac{\theta}{\delta_e}\right)\left(\frac{\delta_e}{q}\right) \tag{14.73}$$
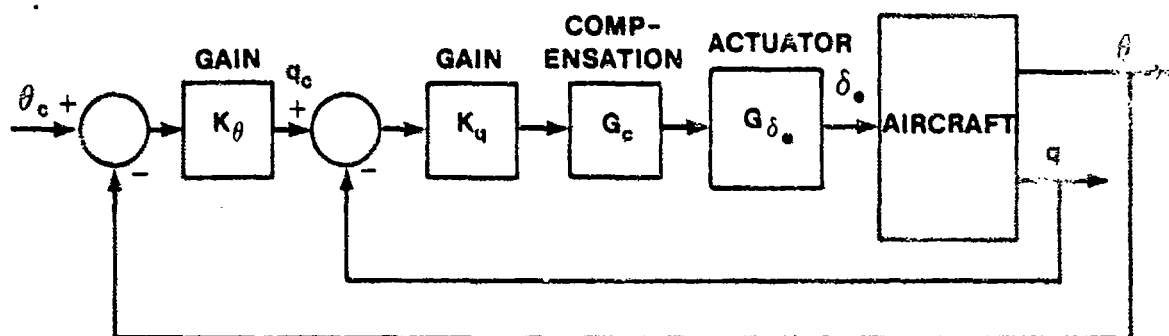
FIGURE 14.132.   PITCH ATTITUDE HOLD CONTROL SYSTEM
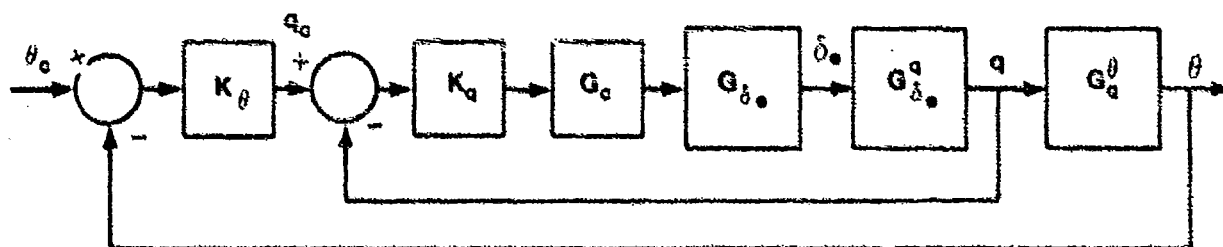
FIGURE 14.133.   REFORMULATED PITCH ATTITUDE CONTROL SYSTEM

which can be simplified to the ratio of the two transfer function numerators

$$\frac{N_{\delta_e}^{\theta}(s)}{N_{\delta_e}^{q}(s)}$$

The block diagram is now in a form which readily lends itself to multiloop analysis. The root locus of the inner pitch rate loop

$$GH_{q \text{ loop}} = K_q G_c G_{\delta_e} G_{\delta_e}^q \tag{14.74}$$

is plotted. The pitch rate augmented aircraft roots are determined from the root locus by selecting a value of K_q which meets the desired pitch rate in terms of response time and damping ratio. The pitch rate augmented aircraft transfer function (inner loop closed) is

$$G_{q_c}^q \Bigg|_{q \text{ AUG}} = \frac{K_q K_{\delta_e} N_c N_{\delta_e}^q}{\Delta_{q \text{ AUG}}} \tag{14.75}$$

where Δ_{AUG} are the characteristic roots of the pitch rate feedback loop augmented aircraft determined from the root locus analysis. The block diagram is simplified as shown in Figure 14.134.
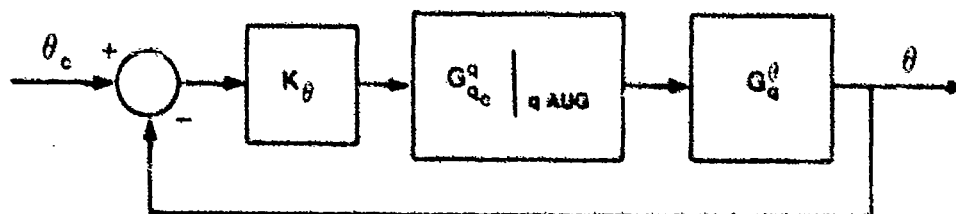
FIGURE 14.134.   SIMPLIFIED PITCH ATTITUDE CONTROL SYSTEM

The outer loop can now be analyzed by forming the open loop transfer function for the attitude hold system augmented aircraft

$$GH_{\theta \text{ loop}} = K_\theta G_q^\theta G_{q_c}^q \Bigg|_{q \text{ AUG}} \tag{14.76}$$

and plotting the root locus. The closed loop transfer function for the attitude hold system augmented aircraft becomes

$$G^{\theta}_{\theta_c}\bigg|_{\substack{q,\theta \\ AUG}} = \frac{K_{\theta}N^{\theta}_{q}N^{q}_{q_c}\big|_{q\ AUG}}{\Delta_{q,\theta}\big|_{AUG}} \qquad (14.77)$$

where $\Delta_{\substack{q,\theta \\ AUG}}$ are the augmented aircraft characteristic roots with both the pitch attitude and pitch rate feedback loops closed.

14.4.1.2 Simple Pitch Attitude Hold System. Figure 14.135 presents a block diagram for a proposed pitch attitude autopilot for the AV-8A Harrier VTOL aircraft. The aircraft transfer function (160 KTAS, sea level, zero engine nozzle angle) is

$$G^{\theta}_{\delta_e}(s) = \frac{6.59(s + 0.65)(s + 0.521)}{(s + 0.203)(s + 1.69)(s - 0.123 \pm 0.364j)} \quad (\text{deg/deg})$$

Figure 14.134 shows the block diagram reconfigured for analysis.

UNITS: θ_c DEGREES
θ DEGREES
q_c DEG/SEC
q DEG/SEC
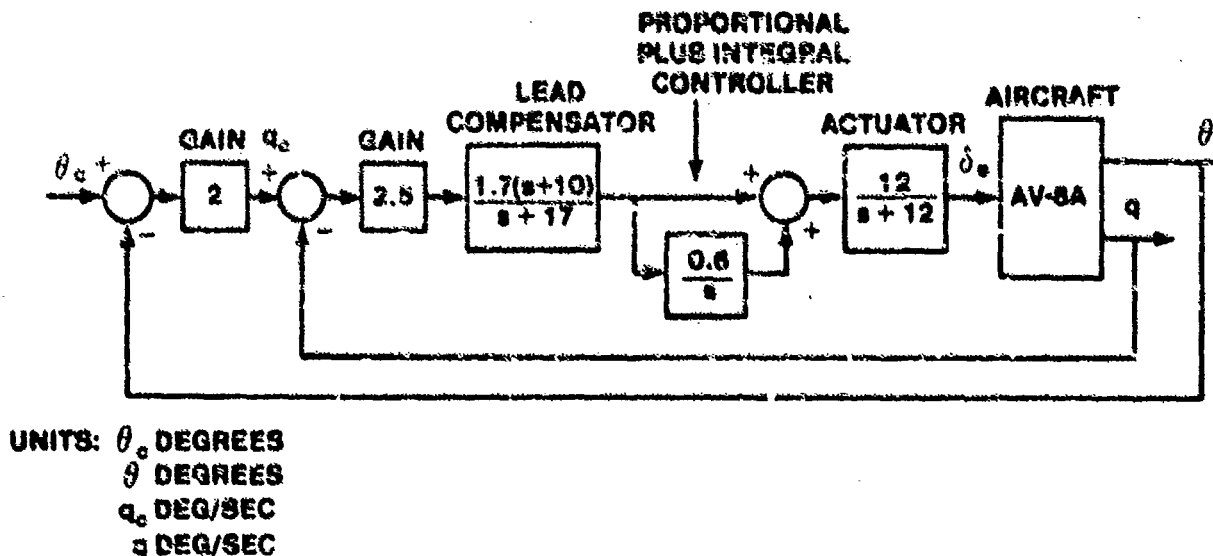
FIGURE 14.135. PROPOSED PITCH ATTITUDE HOLD SYSTEM FOR THE
AV-8A HARRIER FOR THE TRANSITION FLIGHT PHASE
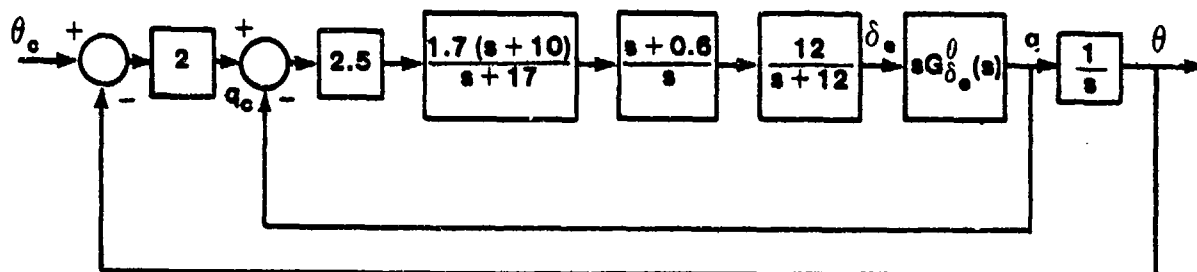
FIGURE 14.136. REFORMULATED PITCH ATTITUDE HOLD SYSTEM FOR THE
AV-8A HARRIER

The inner pitch rate feedback loop is analyzed first. The pitch rate
feedback loop will stabilize the unstable oscillatory root pair of the
unaugmented aircraft. The open loop transfer function for the inner loop is
formed as

$$GH_{q\ loop} = \frac{-6.59(2.5)\ (1.7)\ (12)\ s\ (s + 0.065)\ (s + 0.521)\ (s + 10)\ (s + 0.6)}{s(s + 0.203)\ (s + 1.69)\ (s - 0.123 \pm 0.364j)\ (s + 17)\ (s + 12)}$$

and the root locus is plotted for positive gains (since an odd number of
negative signs appears in the loop). Figure 14.137 presents the root locus
plot for the pitch rate feedback loop. The closed loop transfer function
characteristic roots corresponding to the design system gain of $K_q = 336.09$
are found from the root locus analysis. The closed loop transfer function
(for the inner loop) zeros are the zeros appearing in the forward path of the
loop. No other zeros are introduced since no feedback elements exist. The
gain of the closed loop transfer function is also found from the forward
elements. The closed loop transfer function for the inner loop is

$$G^q_{q_c}\ (s) = \frac{336.09(s + 0.065)\ (s + 0.521)\ (s + 0.6)\ (s + 10)}{(s + 0.074)\ (s + 0.53 \pm 0.165j)\ (s + 9.5)\ (s + 10.0 \pm 16.24j)}$$
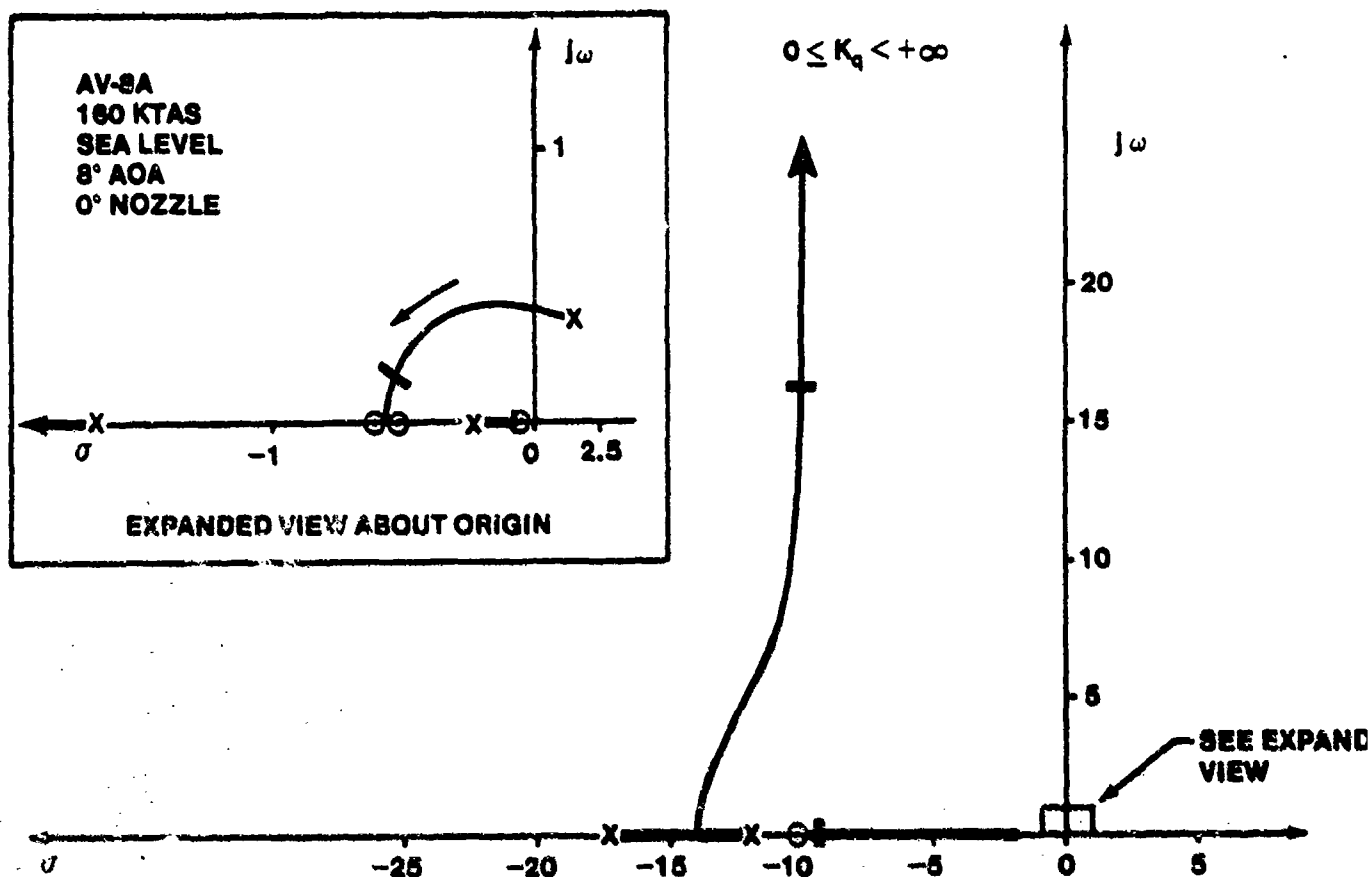
FIGURE 14.137.   ROOT LOCUS PLOT FOR PITCH RATE LOOP
OF PROPOSED AV-8A ATTITUDE AUTOPILOT

The inner loop is now replaced by a single block formed by the closed loop
transfer function of the inner loop (Figure 14.138).
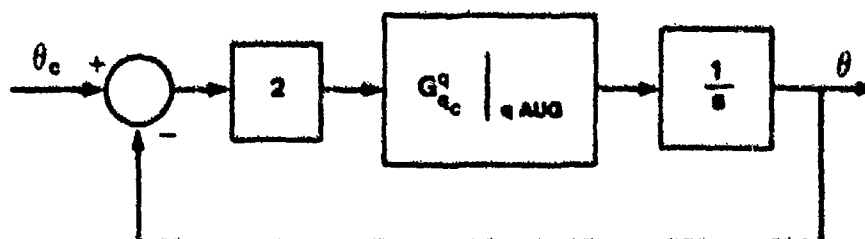
FIGURE 14.138.   SIMPLIFIED AV-8A PITCH ATTITUDE HOLD SYSTEM

14.161

The open loop transfer function for the outer loop is

$$GH_{\theta \ loop} = \frac{2}{s} G^{q}_{q_c} \ (s)$$

The root locus as K_{θ} varies as plotted in Figure 14.139 and the roots for the designed gain of $K_{\theta} = 672.18$ are plotted. The closed loop transfer function for the pitch attitude hold system is

$$G^{\theta}_{\theta_c} \ (s) = \frac{672.18 (s + 0.065) \ (s + 0.521) \ (s + 0.6) \ (s + 10)}{(s+0.065)(s+0.71) \ (s+0.47)(s+2.09)(s+9.32)(s+9.0\pm15.66j)}$$

and the final value for a unit step pitch attitude change is $\theta_{ss} = 1^{o}$ so that a zero steady-state error exists (as expected for a type 1 system). Notice that all the roots except for the root near $s = -2.1$ and the high frequency roots near $s = -9.0 \pm 15.66j$ are in fairly close proximity to zeros. This implies that they are suppressed and that the dominant root in the aircraft response is $s = -2.1$
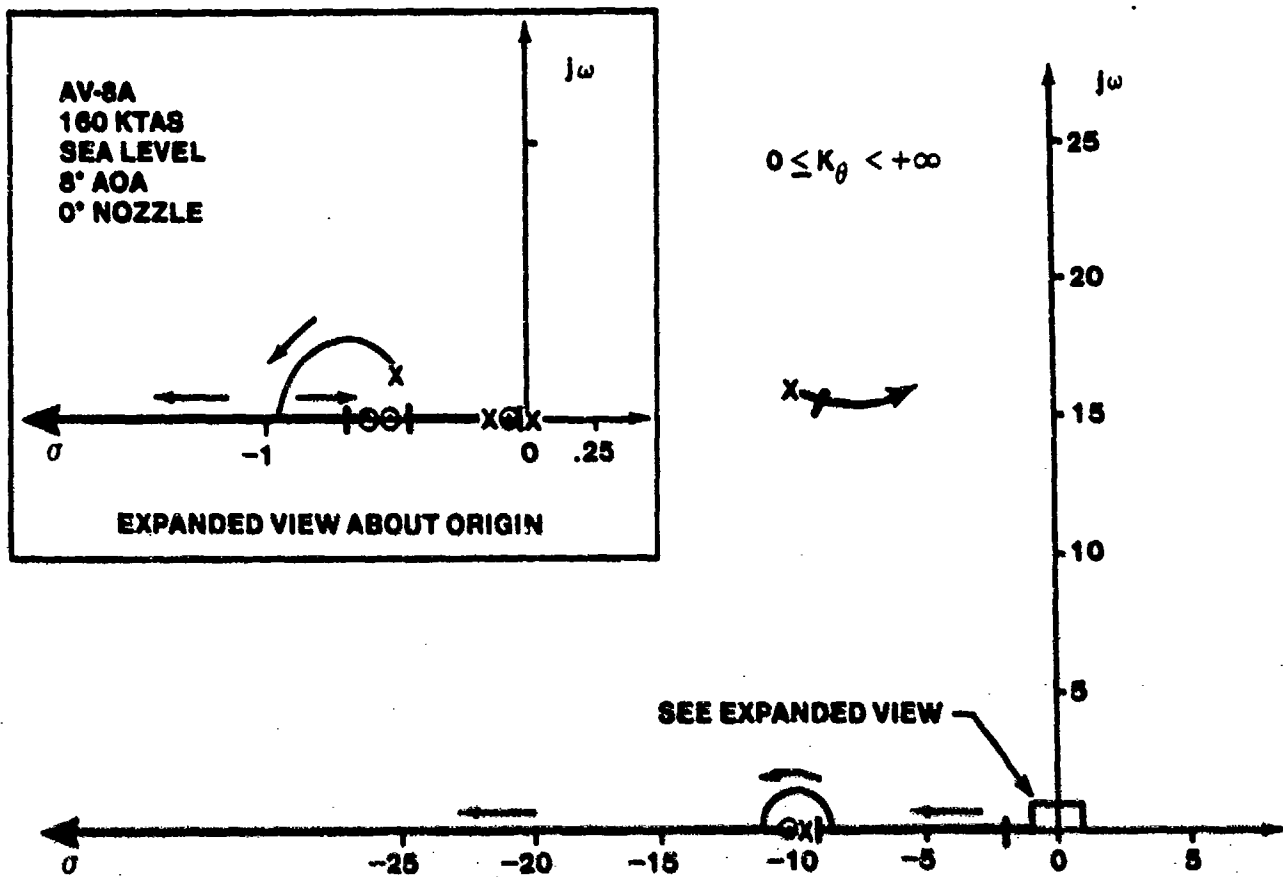
FIGURE 14.139. ROOT LOCUS PLOT FOR PITCH ATTITUDE LOOP
OF PROPOSED AV-8A ATTITUDE AUTOPILOT

The time response of the aircraft to a step input can therefore be closely approximated as $\theta(t) = 1 - e^{-2.1t}$ as shown in Figure 14.140, where the approximate and the actual responses are compared.

(a). ACTUAL AIRCRAFT RESPONSE

AV-8A
160 KTAS
SEA LEVEL
0° ENGINE NOZZLE

$\theta_c = 1°$ STEP INPUT
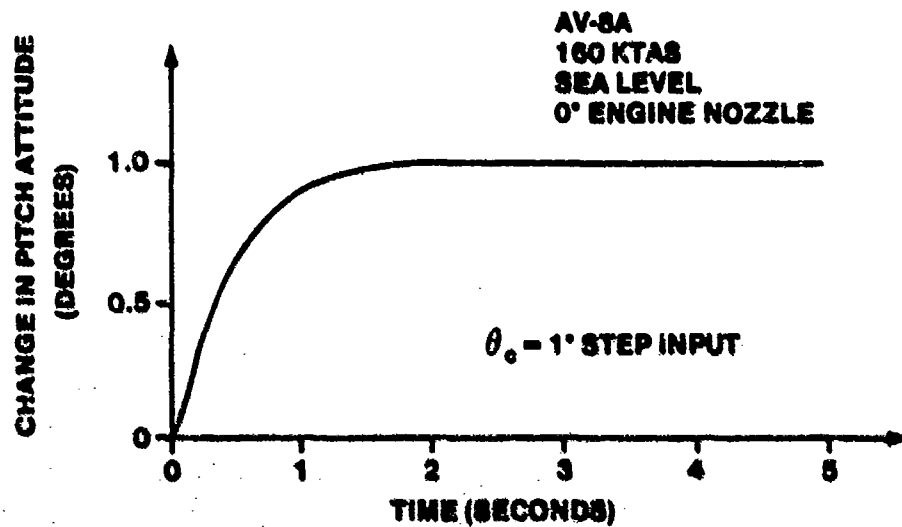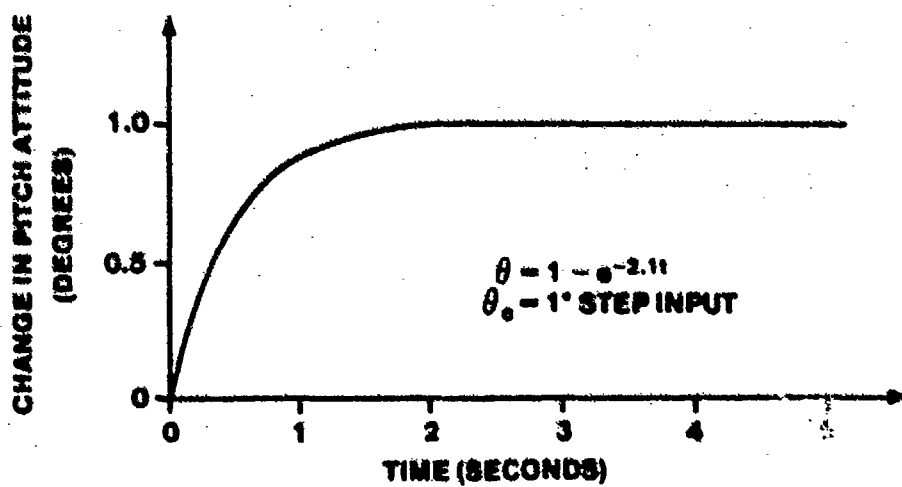
(b). APPROXIMATE AIRCRAFT RESPONSE

$\theta = 1 - e^{-2.1t}$
$\theta_c = 1°$ STEP INPUT

FIGURE 14.140.   COMPARISON OF ACTUAL AND APPROXIMATE
AV-8A PITCH ATTITUDE RESPONSES

14.4.1.3 Multiloop Longitudinal Flight Control System. Figure 14.141
presents a block diagram for the F-16 flight control system simplified for
linear analysis (leading edge flaps locked up). Gains F2 and F3 are scheduled
with the flight condition, gain F2 being a function of dynamic pressure
divided by static pressure and gain F3 being a function of dynamic pressure
alone. The gains shown are for the flight condition to be analyzed (0.6 Mach
at sea level). The aircraft transfer functions are:

$$\Delta(s) = (s - 0.087)(s + 2.373)(s + 0.098 \pm 0.104j)$$

$$N_{\delta_e}^{\alpha}(s) = 0.203(s + 0.0067 \pm 0.067j)(s + 106.47) \text{ deg/deg}$$

$$N_{\delta_e}^{q}(s) = 21.516\, s(s + 0.0189)(s + 1.5) \text{ deg/sec/deg}$$

$$N_{\delta_e}^{n_z}(s) = 0.0889\, s\,(s + 0.0158)(s + 1.165 \pm 11.437j) \text{ g's/deg}$$

where

$$G_{\delta_e}^{\alpha}(s) = \frac{N_{\delta_e}^{\alpha}(s)}{\Delta(s)}$$

and similarly for

$$G_{\delta_e}^{q}(s) \text{ and } G_{\delta_e}^{n_z}(s)$$

The load factor transfer function is for the accelerometer location.
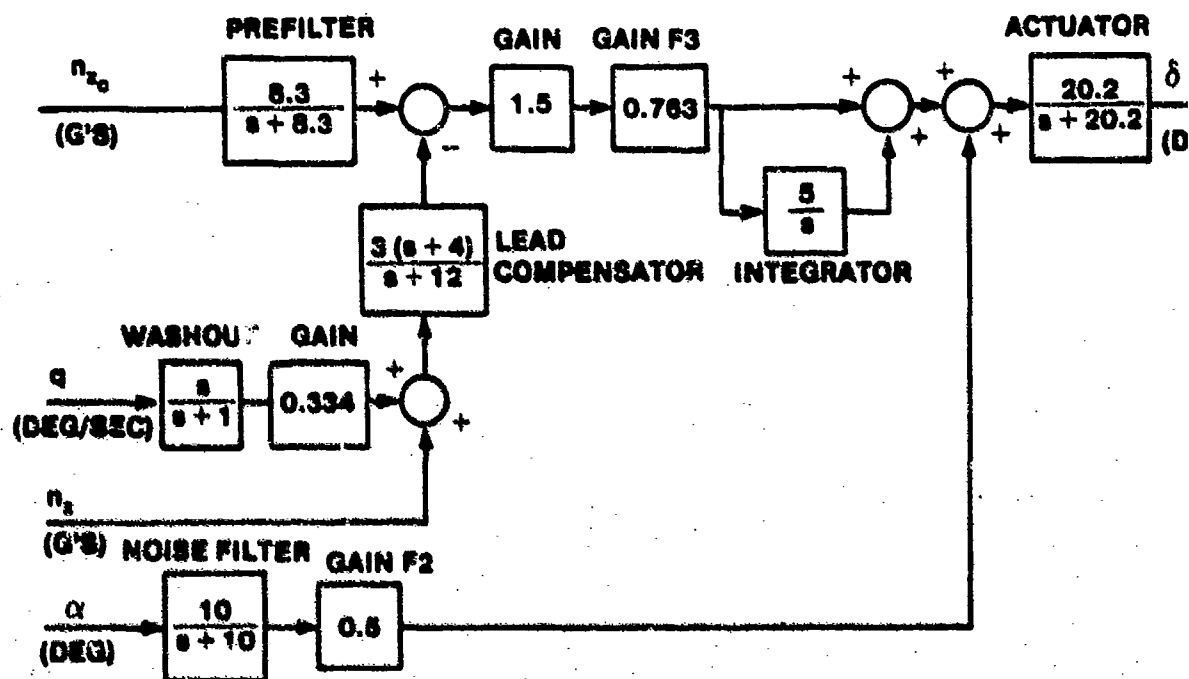
FIGURE 14.141. SIMPLIFIED F-16 LONGITUDINAL AXIS FLIGHT CONTROL SYSTEM, 0.6 MACH AT SEA LEVEL

Figure 14.142 presents the block diagram in a clearer format. The forward path gains have been combined and the integral plus proportional paths have been added together. Although this diagram shows the relationship of the feedback loops in a clearer format (since the angle of attack loop is clearly shown to be the innermost feedback loop) it is still not completely satisfactory for analysis purposes. The aircraft block needs to be simplified so that the elements of each loop analysis are clearly defined and the lead filter must be relocated so that the pitch rate and load factor feedback paths add directly to the forward path. Two options are possible for the lead filter: Adding it into the forward path, in which case a compensating filter must be added to the command path in accordance with block diagram reduction procedures (the inverse of the lead filter must be added), or adding the lead filter to each of the feedback paths which pass through it (pitch rate and load factor feedbacks) but separating the two feedback paths for clarity. The second option is chosen as being the most logical since the command path is left unchanged and all elements in each feedback path are accurately shown. Figure 14.143 shows the simplified block diagram for the analysis. The pitch rate and load factor loops could have been interchanged (pitch rate outer loop, load factor inner loop) with a corresponding change in the aircraft block diagrams, but the load factor loop is selected as the outermost loop since the pilot commands load factor.
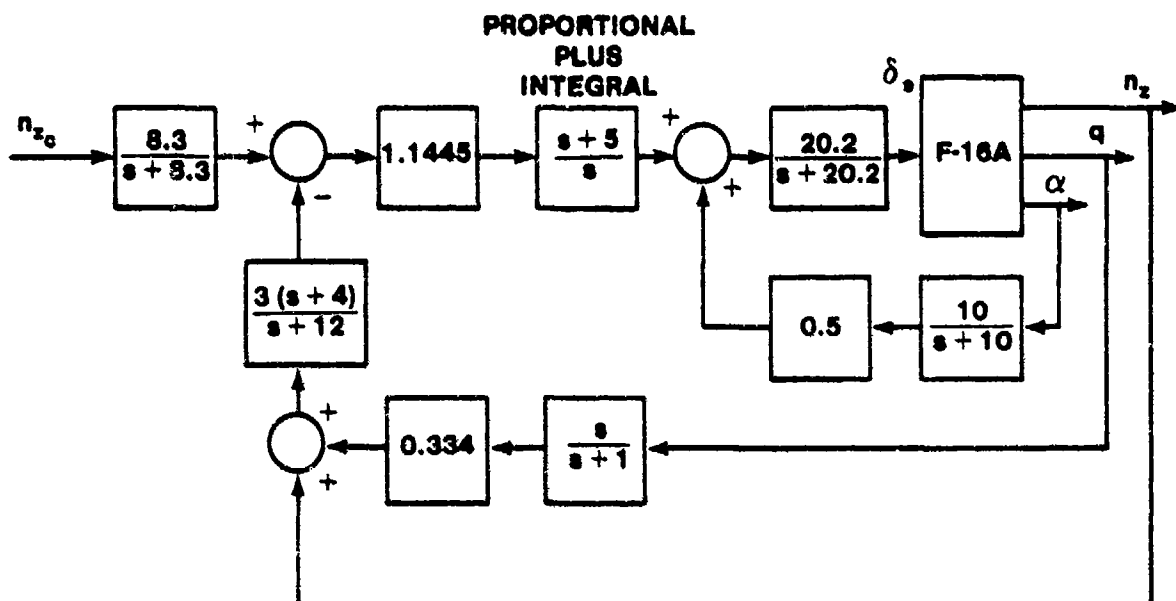
FIGURE 14.142.   SIMPLIFIED F-16 LONGITUDINAL AXIS FLIGHT CONTROL
SYSTEM SHOWING FEEDBACK LOOPS
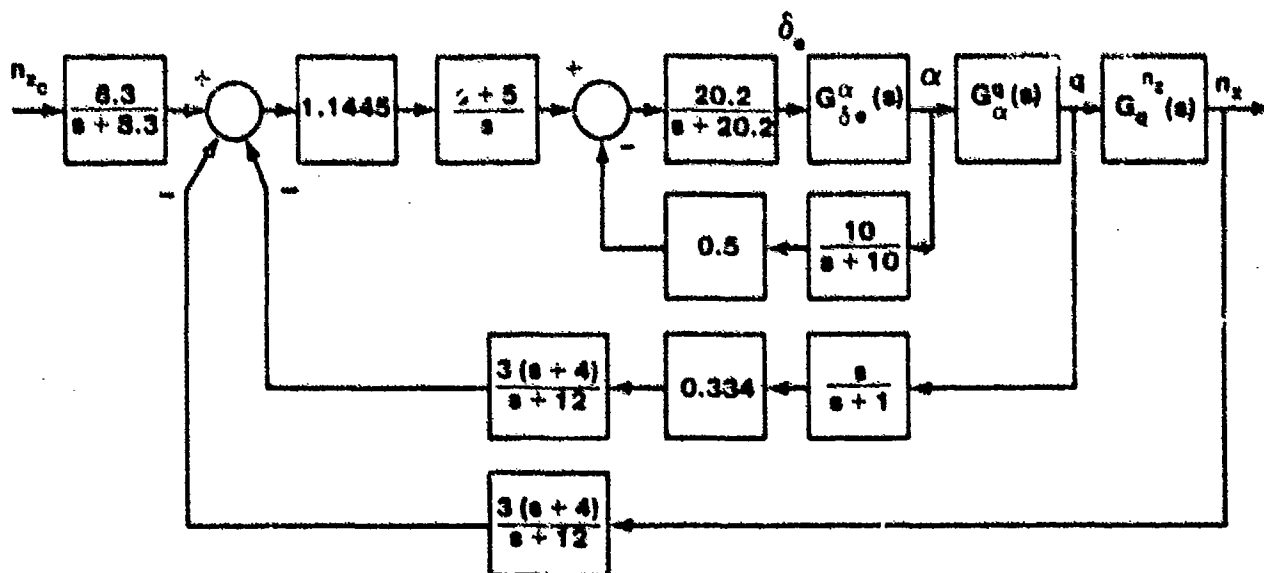
FIGURE 14.143.   SIMPLIFIED F-16 LONGITUDINAL FLIGHT CONTROL
SYSTEM IN FORMAT FOR ANALYSIS

The angle of attack feedback loop, being the innermost loop, is analyzed
first. Looking at the characteristic roots of the aircraft transfer function
and realizing that the F-16 is statically unstable due to an aft center of

gravity, the angle of attack feedback will stabilize the aircraft roots and should separate the nondistinct short period and phugoid characteristics into the more conventional configuration. Remembering that angle of attack feedback augments the M_α stability derivative which tends to stabilize a statically unstable aircraft and moves the short period to a higher natural frequency.

The open loop transfer of the innermost loop is

$$GH_{\alpha\ loop} = \underbrace{\frac{0.203\ (s + 0.0087 \pm 0.067j)\ (s + 106.47)}{(s - 0.087)\ (s + 2.373)\ (s + 0.098 \pm 0.104j)}}_{\text{Aircraft}} \underbrace{\frac{20.2}{s + 20.2}}_{\text{Actuator}} \underbrace{\frac{5}{s + 10}}_{\substack{\text{Feedback} \\ \text{Elements}}}$$

and the root locus is plotted in Figure 14.144. The closed loop transfer function characteristic equation (denominator poles) is found from the root locus analysis. The open loop gain is $K_{\alpha\ loop} = 20.5$. The points on the root locus corresponding to this gain are the closed loop characteristic roots. The closed loop gain is equal to the forward path gain, and the closed loop zeros are the forward path open loop zeros and the feedback path open loop poles. The closed loop transfer function becomes, for the design gains

$$\left. \frac{G^\alpha}{\alpha_c} \right|_{\substack{\alpha\ loop \\ closed}} = \frac{4.1\ (s + 0.0087 \pm 0.067j)\ (s + 106.47)\ (s + 10)}{(s + 0.0083 \pm 0.0643j)\ (s + 0.478 \pm 3.03j)\ (s + 12.1)\ (s + 19.6)}$$

where the $(s + 10)$ zero is from the feedback path. Notice the roots at $(s + 0.478 \pm 3.03j)$. These roots are the short period roots and, as a result of the angle of attack feedback, the aircraft has effectively acquired longitudinal static stability and looks like a conventional aircraft. The short period damping, however, is low, being $\zeta_{sp} = 0.156$ and must be augmented. The short period natural frequency is

$$\omega_{n_{sp}} = 3.07\ \text{rad/sec} \quad (n/\alpha = 29.6\ \text{g's/rad})$$

which is at the boundary between level 1 and level 2 in MIL-F-8785C. Pitch rate feedback is used to improve the short period damping but should not change the short period natural frequency significantly. The analysis thus far has indicated a potential handling qualities problem due to a low short period natural frequency.
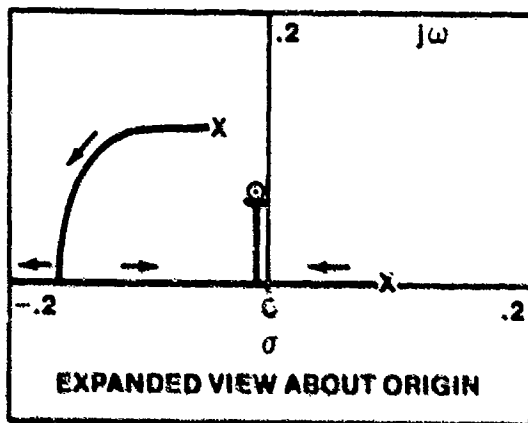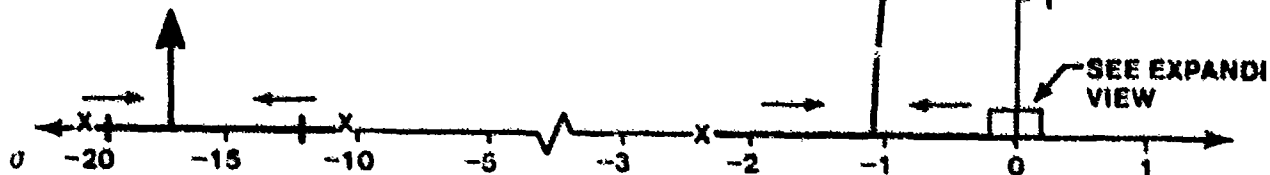
FIGURE 14.144. ROOT LOCUS PLOT OF ANGLE OF ATTACK FEEDBACK LOOP FOR THE F-16A AIRCRAFT

Simplifying Figure 14.143 further results in Figure 14.145.

AIRCRAFT TRANSFER FUNCTION
WITH AOA LOOP CLOSED
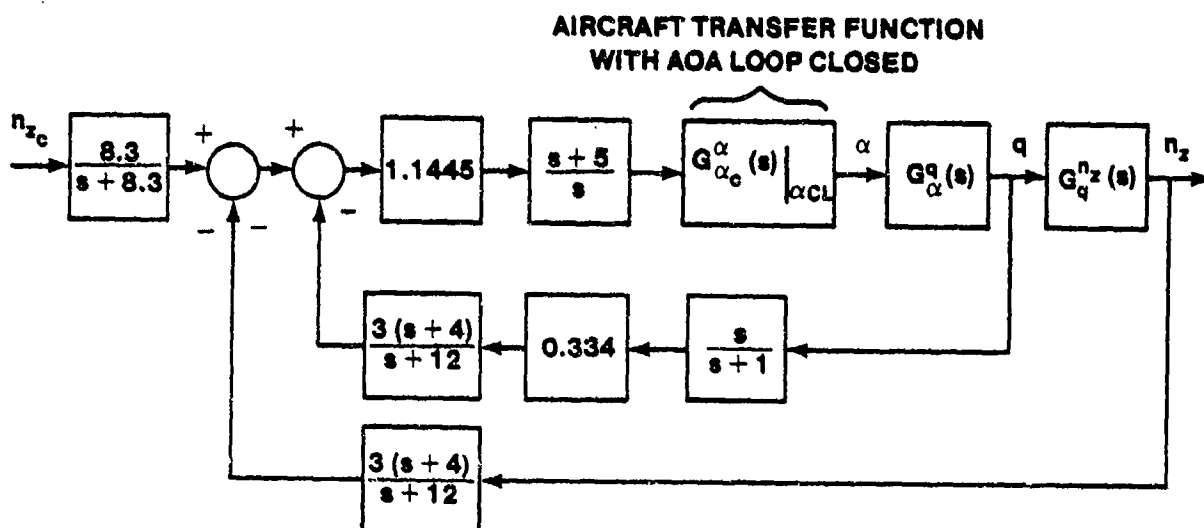
FIGURE 14.145.   SIMPLIFIED F-16 FLIGHT CONTROL SYSTEM WITH
ANGLE OF ATTACK CLOSED LOOP TRANSFER FUNCTION
REPLACING ANGLE OF ATTACK LOOP

Next, the transfer function

$$G_{\alpha_c}^{q}(s)\bigg|_{\substack{\alpha\ loop \\ closed}} = G_{\alpha_c}^{\alpha}\bigg|_{\substack{\alpha\ loop \\ closed}} G_{\alpha}^{q}(s) \qquad (14.78)$$

is formed, where

$$G_{\alpha}^{q}(s) = \frac{N_{\delta_e}^{q}(s)}{N_{\delta_e}^{\alpha}(s)} \qquad (14.79)$$

Notice that the zeros and gain of the pitch rate numerator replace the zeros and gain of the angle of attack closed loop transfer function, but that the zero which resulted from the noise filter on the angle of attack signal and the gain of the actuator remain. The open loop transfer function of the pitch rate loop becomes

$$GH_{q\ loop} = \underbrace{\frac{434.6232\ s(s + 0.0139)\ (s + 1.5)}{(s + 0.0083 \pm 0.0634j)\ (s - 0.478 \pm 3.03j)\ (s + 12.1)\ (s + 19.6)}}_{\text{Pitch Rate Transfer Function with a Loop Closed}}$$

14.171

$$\underbrace{\frac{1.1445\ (s + 5)}{s}}_{\substack{\text{Forward Path}\\\text{Elements}}} \qquad \underbrace{\frac{1.002\ s\ (s + 4)}{(s + 1)\ (s + 12)}}_{\substack{\text{Feedback}\\\text{Elements}}}$$

where $K_{OL} = 498.42$

Once again plotting the root locus (Figure 14.146) and selecting the roots matching the design open loop gain, the closed loop transfer function for the system with both the angle of attack and pitch rate feedback loops closed becomes

$$G\frac{q}{q_c}\ (s)\bigg|_{\alpha,q\ CL} = \frac{497.43\ (s + 0.0189)\ (s + 1.5)\ (s + 10)\ (s + 5)}{(s + 0.0093 \pm 0.023j)(s + 1.33)(s + 3.78 \pm 2.68j)(s + 10.2)}$$

$$\frac{(s + 1)\ (s + 12)}{(s + 13.3 \pm 20.2j)}$$
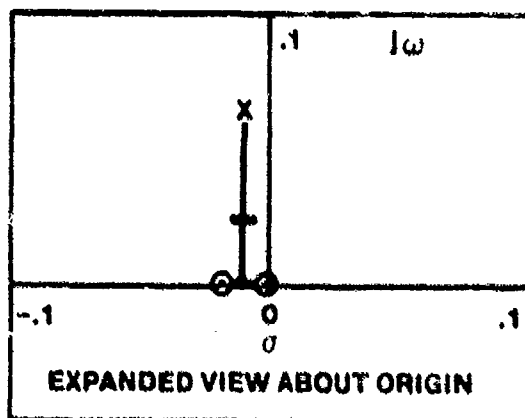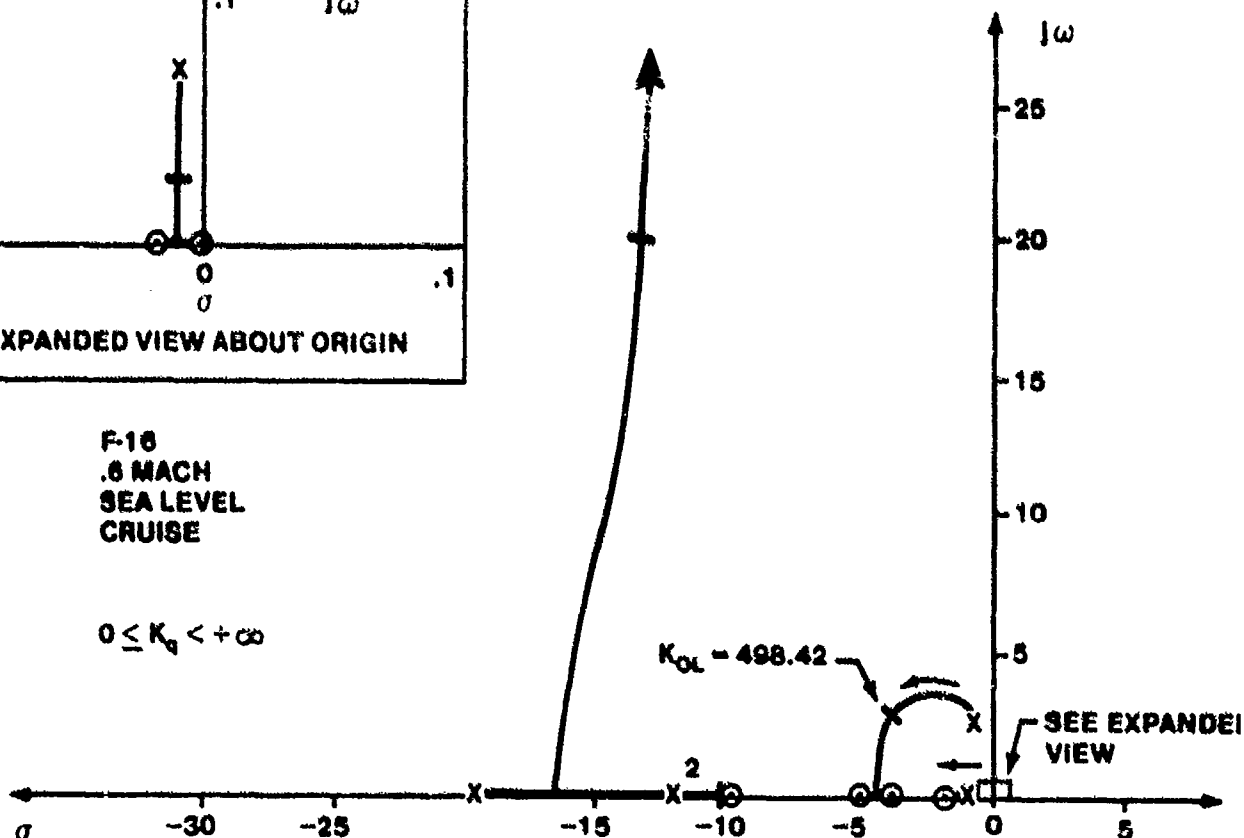
FIGURE 14.146. ROOT LOCUS PLOT FOR WASHED OUT PITCH RATE FEEDBACK LOOP FOR THE F-16A AIRCRAFT

The phugoid roots are altered slightly. Because of the zeros at (s + 4) and (s + 5) in the open loop equation, the frequency of the short period roots, (s + 3.78 ± 2.68j), has been increased significantly from $\omega_{n_{sp}}$ = 3.07 rad/sec to 4.63 rad/sec as well as the short period damping, from ζ_{sp} = 0.156 to 0.816. The pitch rate feedback loop has moved the short period natural frequency further into the level 1 area, but the frequency is still somewhat low and remains an area of concern for high gain tracking tasks. A new significant root has appeared at (S + 1.33). The effects of this root are of concern due to its low frequency. A zero is close by at (s + 1), but not really close enough to cancel completely the effects of the pole. This root should be kept in mind during the analysis of the outermost loop, the load factor feedback path.

Figure 14.147 shows the reduced block diagram for the analysis conducted thus far.
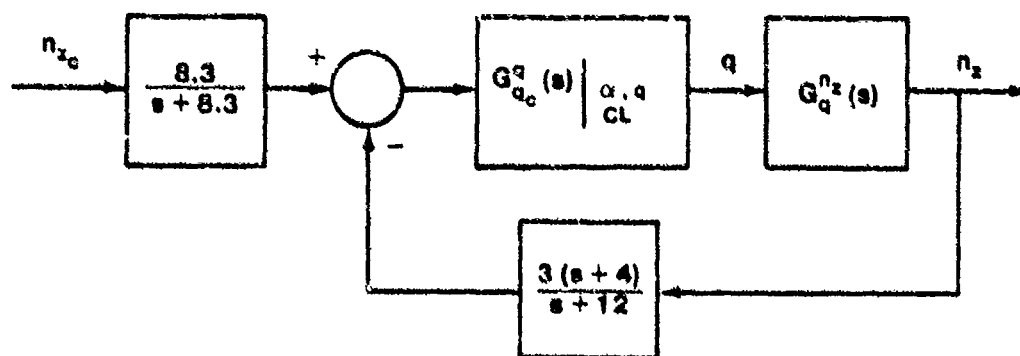
FIGURE 14.147.   SIMPLIFIED F-16 LONGITUDINAL FLIGHT CONTROL
SYSTEM WITH THE TWO INNER LOOPS CLOSED

The open loop transfer function for the outer loop becomes

$$GH_{n_z}\ loop = \frac{2.055\ (s + 0.0058)\ (s + 1.165 \pm 11.437j)\ (s + 10)\ (s + 5)\ (s + 1)}{\underbrace{(s + 0.0093 \pm 0.023j)\ (s + 1.33)\ (s + 3.78 \pm 2.68j)\ (s + 10.2)}_{\text{Forward Path Transfer Function}}}$$

$$\underbrace{\frac{s + 12}{(s + 13.3 \pm 20.2j)}}_{\substack{\text{Forward Path} \\ \text{Transfer Function}}} \underbrace{\frac{3(s + 4)}{(s + 12)}}_{\substack{\text{Feedback} \\ \text{Elements}}} \qquad K_{OL} = 6.165$$

From the root locus (Figure 14.148) it appears that the short period roots have moved to a slightly higher natural frequency and somewhat reduced damping. However, additional roots have appeared near the origin on the real axis which threaten to become dominant. The closed loop transfer function becomes

$$G_{\frac{n_z}{n_{z_c}}}(s)\Bigg|_{\alpha,q,n_z\ CL} = \frac{2.055\ (s + 0.0158)\ (s + 1.165 \pm 11.437j)\ (s + 10)}{(s + 0.0164)\ (s + 1.74)\ (s + 3.86 \pm 3.32j)\ (s + 0.637)}$$

$$\frac{(s + 5)\ (s + 1)\ (s + 12)}{(s + 10.3)\ (s + 15.7 \pm 17.6j)} \quad \underbrace{\frac{8.3}{(s + 8.3)}}_{\text{Prefilter}}$$
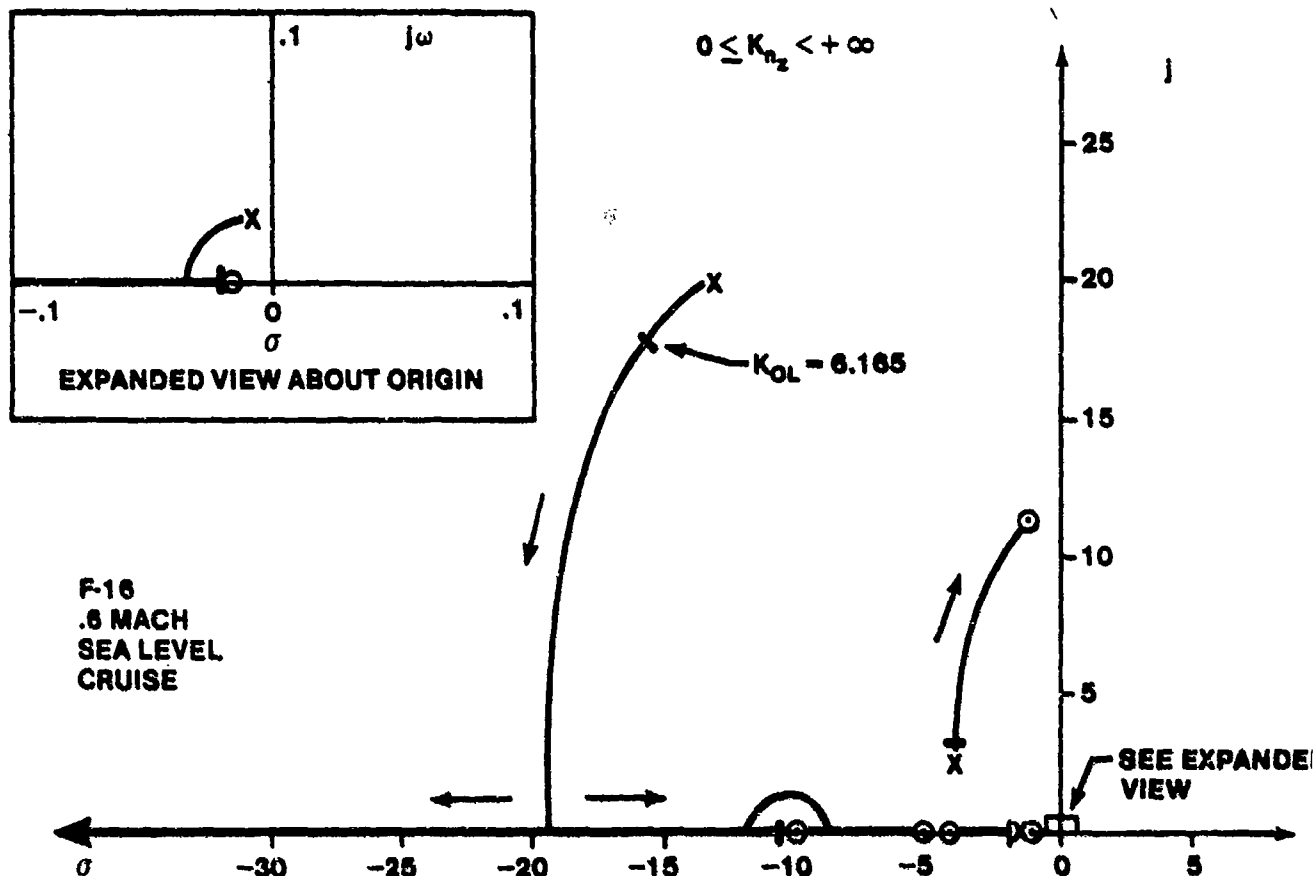
FIGURE 14.148. ROOT LOCUS PLOT OF LOAD FACTOR
FEEDBACK LOOP FOR THE F-16A AIRCRAFT

Two real roots have appeared in the denominator at (s + 1.74) and (s + .637). These roots are not well suppressed by any nearby zeros and represent the dominant short period roots in addition to the short period roots at (s + 3.84 +/- 3.32j). The high frequency roots have little impact on the aircraft response since their effects die out rapidly. The two real roots dominate the aircraft response. The initial response lag will be significant with this many unsuppressed roots dominating the response and may hinder tracking tasks. The natural frequency of the short period root (at s = -1.74) fails to meet the level 1 requirements of MIL-F-8785C. The steady state value to a step acceleration input is (final value theorem)

$$n_{z_{ss}} = \lim_{s \to 0} G_{n_{z_c}}^{n_z}(s)\Big|_{\alpha,q,n_z\,CL} = 0.96\ g's$$

The load factor time response of the aircraft with and without the prefilter in the command path are shown in Figures 14.149 and 14.150. With a prefilter, the response is relatively slow and exponential with the root at $(s + 1.74)$ dominating the short term response and the root at $(s + 0.637)$ dominating the longer term response. Significant time delay occurs initially, which is apparent from the plot. Without the prefilter, the initial response is slightly more abrupt. The pitch rate time response of the aircraft is shown in Figure 14.151 using the closed loop pitch rate transfer function

$$G_{n_{z_c}}^{q}(s)\bigg|_{\alpha,q,n_z CL} = \frac{497.43\ (s + 0.0189)\ (s + 1.5)\ (s + 10)\ (s + 5)\ (s + 1)}{(s + 0.0164)\ (s + 1.74)\ (s + 3.86 \pm 3.32j)\ (s + 0.637)}$$

$$\frac{(s + 12)}{(s + 10.3)\ (s + 15.7 \pm 17.6j)}$$

No initial overshoot of the final pitch rate value occurs. Inflight investigations using variable stability aircraft have shown that heavy suppression of the pitch rate overshoot tendency (present in conventional aircraft) results in objectionable handling qualities.
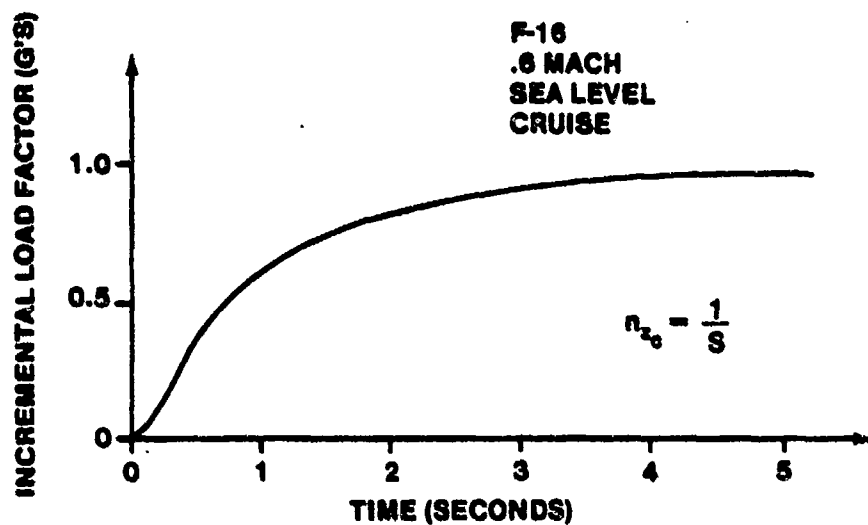
(a) ACTUAL AIRCRAFT LOAD FACTOR RESPONSE
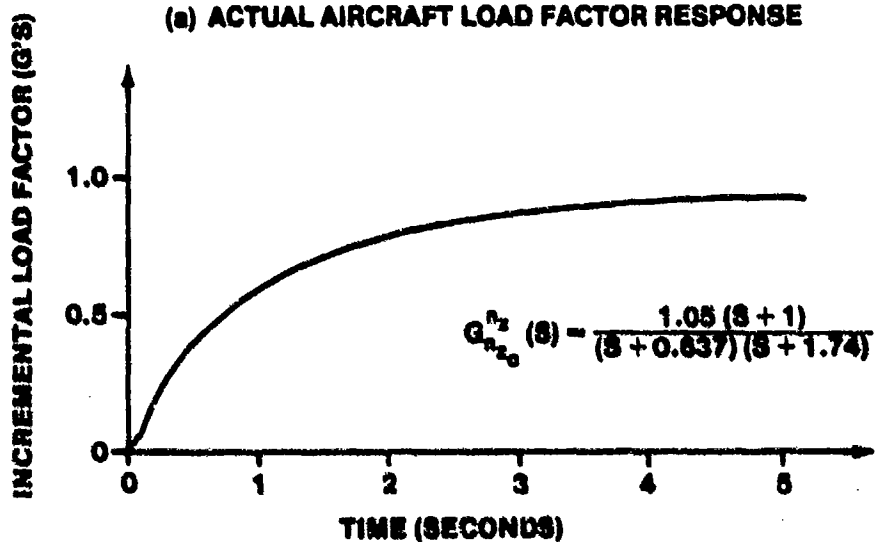
(b) APPROXIMATE AIRCRAFT LOAD FACTOR RESPONSE

FIGURE 14.149.   F-16A LOAD FACTOR RESPONSE, PREFILTER EFFECTS OMITTED
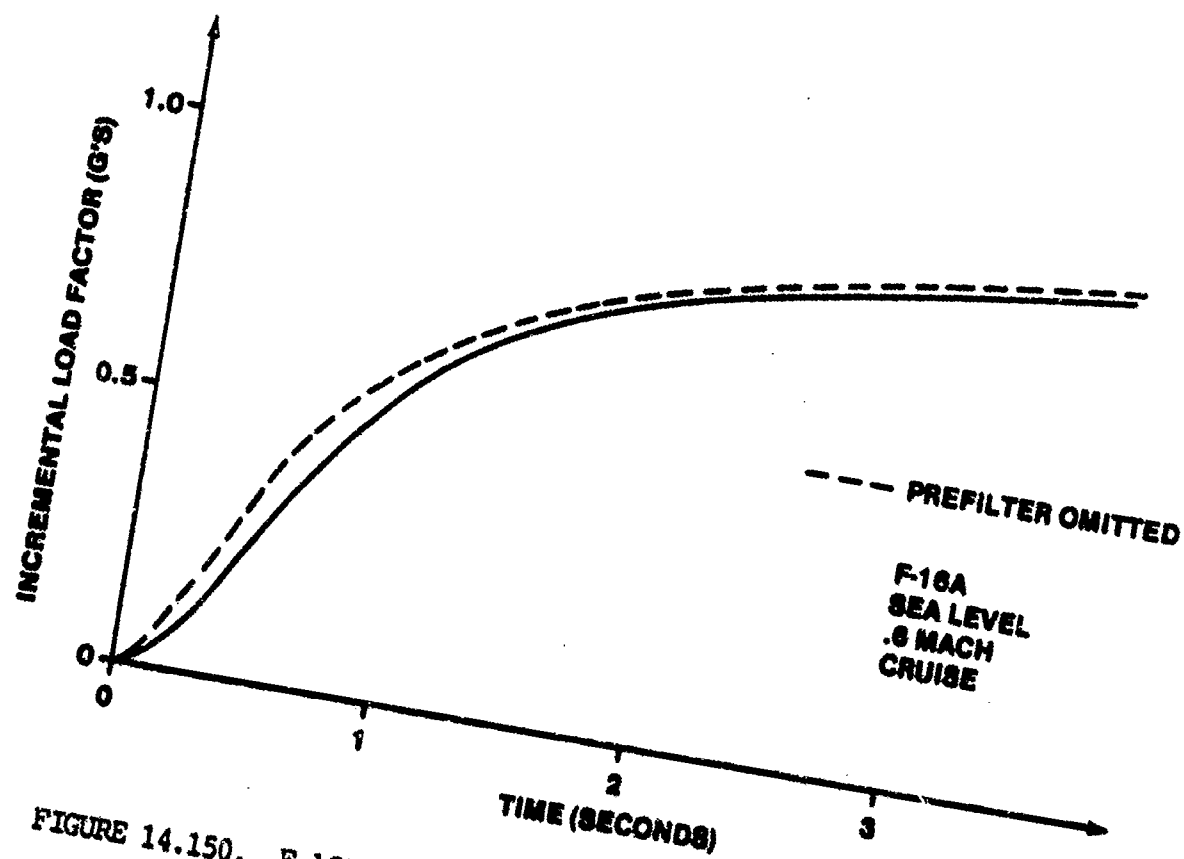
FIGURE 14.150. F-16A LOAD FACTOR RESPONSE, PREFILTER EFFECTS INCLUDED
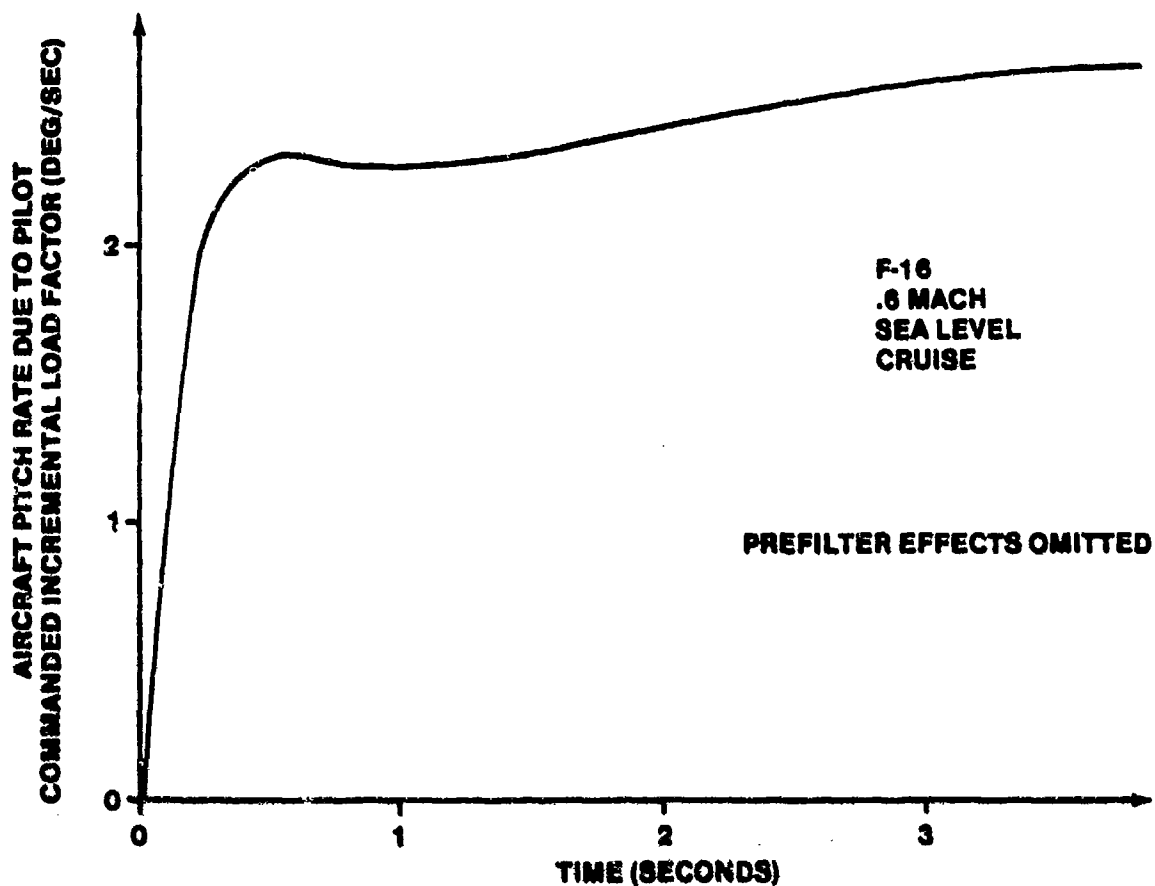
FIGURE 14.151. F-16A PITCH RATE RESPONSE DUE TO A PILOT
COMMANDED INCREMENTAL LOAD FACTOR

The handling qualities of the aircraft with the flaps locked up are
suspect at this flight condition since the load factor response is slow and
the pitch rate overshoot tendency is suppressed. Figure 14.152 shows the
block diagram of the system if the maneuvering flaps are allowed to move. The
analysis of this block diagram is more complex due to its multi-input
character, and will be discussed in Paragraph 14.4.2.8.
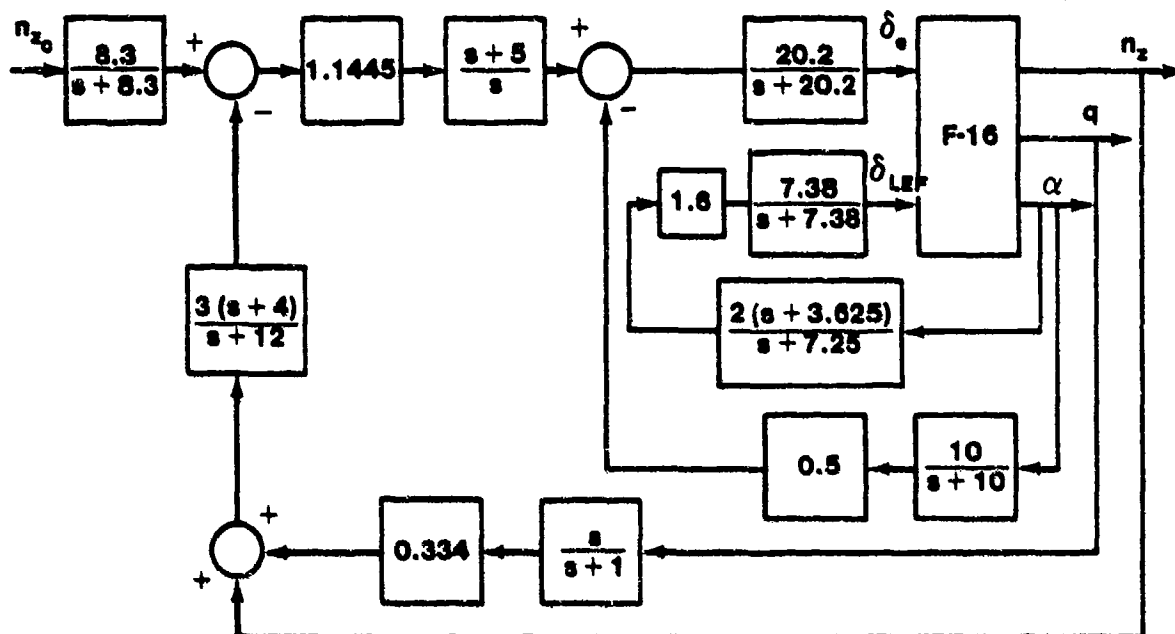
FIGURE 14.152.   LONGITUDINAL FLIGHT CONTROL SYSTEM WITH
LEADING EDGE FLAP SYSTEM ENGAGED

14.4.2   Coupled Multiloop Control Systems

The lateral-directional axes of the typical aircraft are coupled. This
is evident since both the aileron and rudder inputs control
lateral-directional dynamics such as sideslip, roll rate and yaw rate,
although to differing degrees of effectiveness.   In Paragraph 14.2, the
effects of various lateral-directional feedback augmentation schemes were
analyzed as to how they alter roll, Dutch roll, and spiral mode
characteristics.   No attention was given then to the coupling effects such
feedback augmentation systems have on the aircraft, nor was a presentation
made of the appropriate analytical tools needed to account for coupling
effects.   For instance, a commonly used lateral-directional stability
augmentation system is the yaw damper, where yaw rate is fed back to the
rudder.   The yaw damper not only affects the Dutch roll damping but alters the
roll mode time constant and spiral stability.   If the pilot applies a rudder
input, the aileron input can be considered to be zero and a simple analysis

results. However, if the pilot applies an aileron input, the analysis is not so straightforward. Using superposition for linear systems, the response due to separate aileron and rudder inputs may be added to yield the response due to simultaneous aileron and rudder inputs.

14.4.2.1 <u>Roll Rate Response with Yaw Damper Engaged</u>. Figure 14.153 presents the block diagram of a simple lateral-directional stability augmentation system with a yaw damper implemented using the rudder. It is desired to determine the effect of the yaw damper on the aircraft roll rate due to an aileron input. The augmented aircraft roots can be determined using the block diagram of Figure 14.154, in which aileron inputs are neglected and the $G_{\delta_{r_c}}^{r}$ (s) closed loop transfer function is found using single loop root locus analysis.
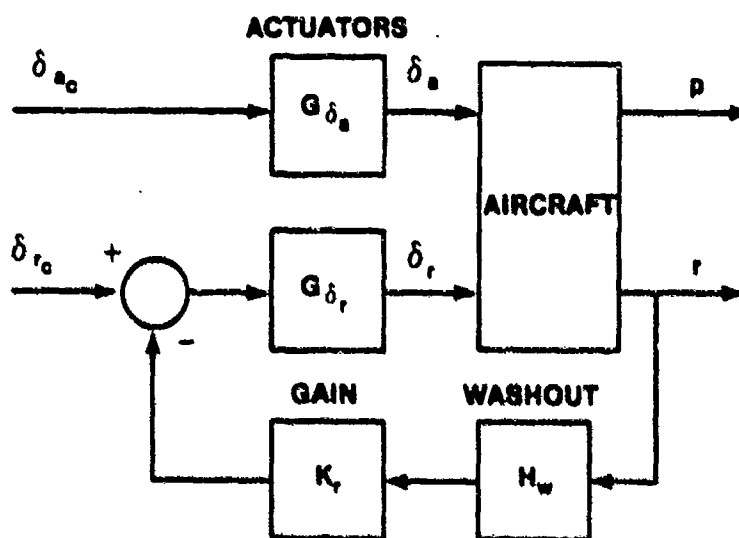
FIGURE 14.153. YAW DAMPER STABILITY AUGMENTATION SYSTEM

The open loop transfer function

$$GH = G_{\delta_r} G_{\delta_r}^{r} H_w K_r \tag{14.80}$$

root locus is plotted as a function of the gain and the augmented aircraft roots are determined to achieve the desired aircraft characteristic roots. These selected roots determine the value of K_r. The closed function becomes

$$G_{\delta_{r_c}}^r \Bigg|_{\substack{\text{YAW} \\ \text{AUG}}} = \frac{K_{\delta_r} N_{\delta_r}^r D_w}{\Delta\, D_{\delta_r}\, D_w + K_r\, N_{\delta_r}^r\, K_{\delta_r}\, N_w} \tag{14.81}$$

where Δ are the unaugmented aircraft characteristic roots, in this case $D_{\delta_r}^r$

D   denotes poles for other system elements (denominator terms for the transfer function denoted by the subscript)

N   denoted zeros for aircraft and other system element transfer function (numerator terms)

K   denotes system gains
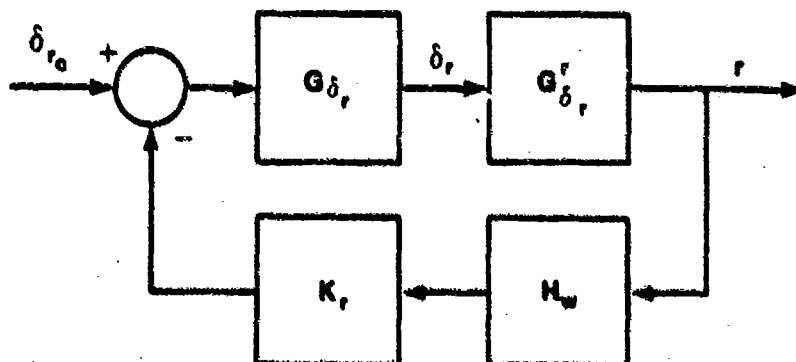
FIGURE 14.154.   DIRECTIONAL AXIS OF THE YAW DAMPER SAS ASSUMING ZERO AILERON INPUT

The zeros of the closed loop transfer function are determined from the zeros of the forward path elements and the poles of the feedback path elements. The gain of the closed loop equation is determined by the gains of the forward path elements only. The feedback gain and zeros affect the locations of the augmented system roots only.

The response to an aileron input is more complex. Not only is the deflected aileron causing a dynamic response in the aircraft, but the feedback of yaw rate to the rudder simultaneously causes rudder deflections which also affect the aircraft's dynamic response. By superposition, the roll response to simultaneous aileron and rudder inputs is:

$$p = G^p_{\delta_a} \delta_a + G^p_{\delta_r} \delta_r \qquad (14.82)$$

and the yaw rate response is:

$$r = G^r_{\delta_a} \delta_a + G^r_{\delta_r} \delta_r \qquad (14.83)$$

Since yaw rate feedback is used

$$\delta_r = G_{\delta_r} \left[S_{r_c} - K_r H_w r \right] \qquad (14.84)$$

whereas

$$\delta_a = G_{\delta_a} \delta_{a_c} \qquad (14.85)$$

Substituting the expressions for the surface deflections into the response equations, and assuming $\delta_{r_c} = 0$ (pilot's feet on the floor), the expressions become

$$p = G_{\delta_a} G^p_{\delta_a} \delta_{a_c} - K_r G_{\delta_r} H_w G^p_{\delta_r} r$$

$$r = G_{\delta_a} G^r_{\delta_a} \delta_{a_c} - K_r G_{\delta_r} H_w G^r_{\delta_r} r$$

Writing these two equations in matrix notation

$$\begin{bmatrix} 1 & K_r G_{\delta_r} H_w G^p_{\delta_r} & p \\ \\ 0 & 1 + K_r G_{\delta_r} H_w G^r_{\delta_r} & r \end{bmatrix} = \begin{bmatrix} G_{\delta_a} G^p_{\delta_a} \\ \\ G_{\delta_a} G^r_{\delta_a} \end{bmatrix} \delta_{a_c}$$

Using Cramer's rule, the characteristic equation is

$$1 + K_r G_{\delta_r} H_w G^r_{\delta_r}$$

The yaw rate due to an aileron input is found by substituting the aileron control matrix column into the yaw rate column, finding the determinant and dividing by the characteristic equation

$$
G_{\delta_{a_c}}^r \bigg|_{\substack{YAW \\ AUG}} \quad \frac{G_{\delta_a} G_{\delta_a}^r}{1 + K_r G_{\delta_r} H_w G_{\delta_r}^r} = \frac{\dfrac{K_{\delta_a} N_{\delta_a}^r}{D_{\delta_a} \Delta}}{1 + \dfrac{K_r K_{\delta_r} N_w N_{\delta_r}^r}{D_{\delta_r} D_w \Delta}}
$$

$$
= \frac{K_{\delta_a}}{D_{\delta_a}} \left[\frac{N_{\delta_a}^r D_{\delta_r} D_w}{\Delta D_{\delta_r} D_w + K_r K_{\delta_r} N_w N_{\delta_r}^r} \right] = G_{\delta_a} G_{\delta_a}^r \bigg|_{\substack{YAW \\ AUG}} \qquad (14.86)
$$

Note that despite the fact that an aileron input is applied, the characteristic roots of the

$$
G_{\delta_a}^r \bigg|_{\substack{YAW \\ AUG}}
$$

transfer function are exactly the same as those arrived at using the root locus analysis and assuming $\delta_{a_c} = 0$. This verifies that only feedback loops can alter the aircraft characteristic roots, not inputs. Only the zeros change to account for the different input and output relationships. The aileron actuator pole must be added to the denominator to account for additional lag in the total aircraft system.

$$G^p_{\delta_a} \Big|_{\substack{\text{YAW}\\\text{AUG}}} = \frac{G_{\delta_a}\left[G^p_{\delta_a} + K_r C_{\delta_r} H_w \left[G^p_{\delta_a} G^r_{\delta_r} - G^p_{\delta_r} G^r_{\delta_a}\right]\right]}{1 + K_r G_{\delta_r} H_w G^r_{\delta_r}} \qquad (14.87)$$

$G^p_{\delta_a} G^r_{\delta_r} - G^p_{\delta_r} G^r_{\delta_a}$ is the term to account for simultaneous aileron and rudder inputs which affect the roll rate. If the indicated algebra is performed on this term, the result is

$$G^p_{\delta_a} G^r_{\delta_r} - G^p_{\delta_r} G^r_{\delta_a} = \frac{\Delta\, N^{p\ r}_{\delta_a \delta_r}}{\Delta^2} = \frac{N^{p\ r}_{\delta_a \delta_r}}{\Delta} = G^{p\ r}_{\delta_a \delta_r} \qquad (14.88)$$

$N^{p\ r}_{\delta_a \delta_r}$ is determined in the same manner as presented in Appendix A. The roll rate due to an aileron input simplifies to

$$G^p_{\delta_a} \Big|_{\substack{\text{YAW}\\\text{AUG}}} = \frac{K_{\delta_a}}{D_\delta}\left[\frac{N^p_{\delta_a} D_{\delta_r} D_w + K_r K_{\delta_r} N_w N^{p\ r}_{\delta_a \delta_r}}{\Delta\, D_{\delta_r} D_w + K_r K_{\delta_r} N_w N^r_{\delta_r}}\right] = G_{\delta_a} G^p_{\delta_a} \Big|_{\substack{\text{YAW}\\\text{AUG}}} \qquad (14.89)$$

The characteristic equation is the same as previously determined using simple singe loop root locus analysis. The numerator, however, contains the coupling term $N^{p\ r}_{\delta_a \delta_r}$ to account for the roll rate due to simultaneous aileron input and rudder inputs augmentation system. Coupling numerator terms of the form $N^{x\ y}_{\delta_x \delta_x}$ or $N^{x\ x}_{\delta_x \delta_y}$

are both equal to zero, since, in the first case

$$G^{x\ y}_{\delta_x \delta_x} = G^x_{\delta_x} G^y_{\delta_x} - G^y_{\delta_x} G^x_{\delta_x} = 0 \qquad (14.90)$$

and in the second case

$$G^{x\ x}_{\delta_x \delta_y} = G^x_{\delta_x} G^x_{\delta_y} - G^x_{\delta_y} G^x_{\delta_x} = 0 \qquad (14.91)$$

14.4.2.2 <u>Simple Numerical Example</u>. Assume a coupled system with a block diagram shown in Figure 14.155 where

$$N\frac{y_1}{x_1} = 2 \ (s + 1.5) \qquad\qquad N\frac{y_1}{x_2} = -0.5 \ (s + 21)$$

$$N\frac{y_2}{x_1} = s + 5 \qquad\qquad Nx_2\frac{y_2}{} = 3 \ (s + 0.667)$$

$$\Delta(s) = s^2 + 4s + 9 = (s + 2 \pm 2.24j) \quad \text{where} \quad \zeta = 0.667 \text{ and } \omega_n = 3$$
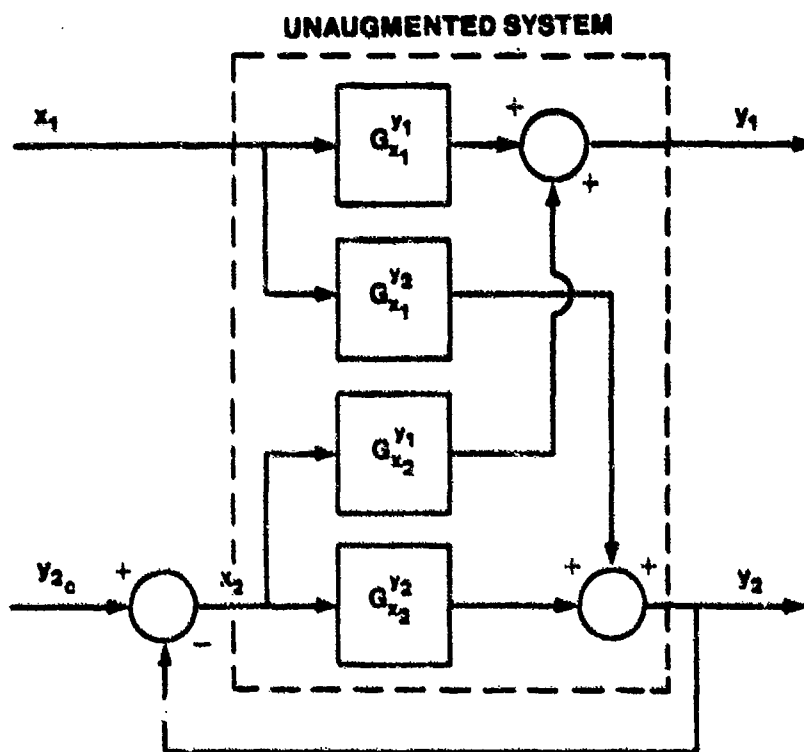
FIGURE 14.155.   FULLY COUPLED SYSTEM WITH SINGLE FEEDBACK PATH

To determine y_1 and x_1 for the augmented system only algebra is required, but the more complex systems encountered in flight control systems require a root locus program.

Assuming $x_1 = 0$ the block diagram reduces to that of Figure 14.156.
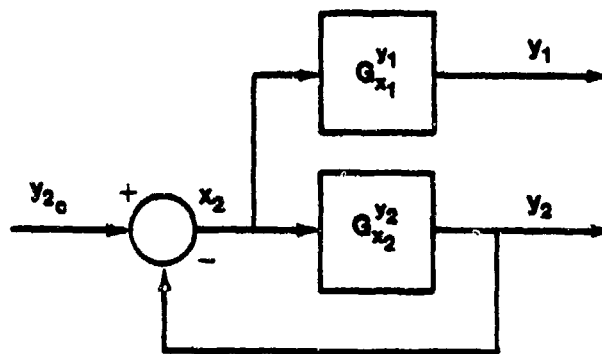
FIGURE 14.156. SIMPLIFIED SYSTEM ASSUMING INPUT ONE EQUALS ZERO

y_1 has no effect on the characteristics of the augmented system since it is not fed back to the control input. The y_2 feedback alters the system roots. Writing the equation for y_2 and simplifying yields

$$y_2 = G_{x_2}^{y_2} x_2$$

$$x_2 = y_{2_c} - y_2$$

$$y_2 = G_{x_2}^{y_2} \left[y_{2_c} - y_2 \right]$$

$$y_2 + G_{x_2}^{y_2} y_2 = G_{x_2}^{y_2} y_{2_c}$$

$$\frac{y_2}{y_{2_c}} = \frac{G_{x_2}^{y_2}}{1 + G_{x_2}^{y_2}}$$

This is the familiar closed loop transfer function. The closed loop roots are:

$$\frac{Y_2}{Y_{2_c}} = \frac{3(s + 0.667)}{s^2 + 7s + 11} = \frac{3(s + 0.667)}{(s + 2.38)(s + 4.62)}$$

The open loop transfer is

$$GH = \frac{3(s + 0.667)}{(s + 2 \pm 2.24j)}$$

If this is plotted as a root locus, allowing the gain to vary, and the roots corresponding to the gain K = 3 determined from the plot, the same roots are obtained (Figure 14.157). For complex systems, the root locus method is the best, yielding both the design closed loop roots as well as insight into the reasons for the design selected gain. The algebraic solution is more difficult usually and yields no insight into the design rationale.
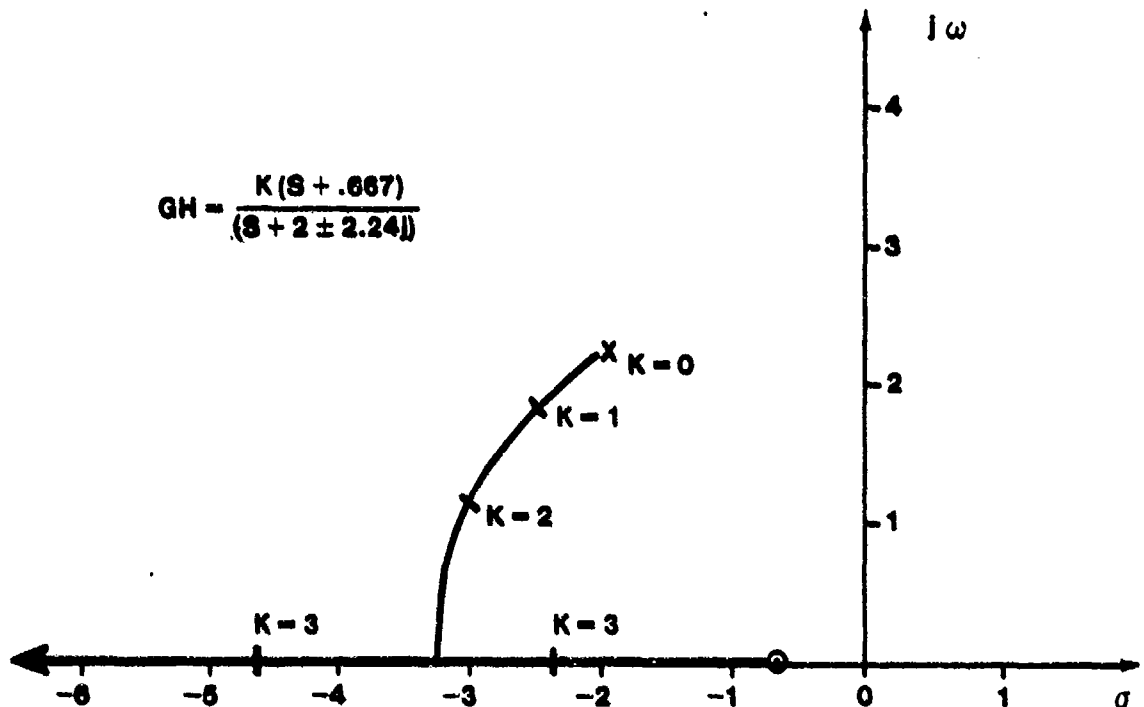
FIGURE 14.157. ROOT LOCUS PLOT OF THE OPEN LOOP TRANSFER FUNCTION FOR THE COUPLED SYSTEM EXAMPLE PROBLEM

14.188

The characteristics of the unaugmented system can only be altered through feedback augmentation. The roots of y_2 are therefore the roots of $\left. G_{x_1}^{y_1} \right|_{AUG}$

$G_{y_{2_c}}^{y_2}$

If $y_{2_c} = 0$ is assumed, the block diagram becomes that of Figure 14.158. Writing the algebraic equations

$$Y_1 = G_{x_1}^{y_1} x_1 + G_{x_2}^{y_1} x_2$$

$$Y_2 = G_{x_1}^{y_2} x_1 + G_{x_2}^{y_2} x_2$$

where $x_2 = -y_2$ so that

$$Y_1 = G_{x_1}^{y_1} x_1 - G_{x_2}^{y_1} y_2$$

$$Y_2 = G_{x_1}^{y_2} x_1 - G_{x_2}^{y_2} y_2$$
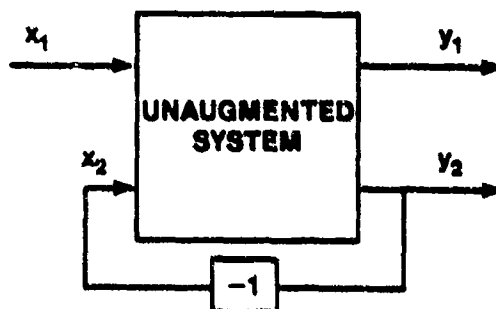
FIGURE 14.158. SIMPLIFIED SYSTEM ASSUMING INPUT TWO EQUALS ZERO

In matrix format

$$
\begin{bmatrix} 1 & G_{x_2}^{y_1} \\ 0 & 1 + G_{x_2}^{y_2} \end{bmatrix}
\begin{bmatrix} y_1 \\ y_2 \end{bmatrix}
=
\begin{bmatrix} G_{x_1}^{y_1} \\ G_{x_1}^{y_2} \end{bmatrix} x_1
$$

$$
G_{x_1}^{y_1}\Big|_{AUG} = \frac{G_{x_1}^{y_1} + G_{x_1 \; x_2}^{y_1 \; y_2}}{1 + G_{x_2}^{y_2}}
$$

where $G_{x_1 \; x_2}^{y_1 \; y_2} = G_{x_1}^{y_1} G_{x_2}^{y_2} - G_{x_1}^{y_2} G_{x_2}^{y_1}$ is the coupling numerator term.

Using the definition and solving algebraically yields

$$
G_{x_1 \; x_2}^{y_1 \; y_2} = \frac{(2s + 3)\,(3s + 2) + (0.5s + 10.5)\,(s + 5)}{(s^2 + 4s + 9)^2} = \frac{6.5\,(s^2 + 4s + 9)}{(s^2 + 4s + 9)^2}
$$

$$
= \frac{6.5}{s^2 + 4s + 9}
$$

If the system equations of motion are used (from which all the transfer functions may be derived), where the matrix equations are

$$
\begin{bmatrix} \dot{y}_1 \\ \dot{y}_2 \end{bmatrix}
=
\begin{bmatrix} -1 & -3 \\ 2 & -3 \end{bmatrix}
\begin{bmatrix} y_1 \\ y_2 \end{bmatrix}
+
\begin{bmatrix} 2 & -0.5 \\ 1 & 3 \end{bmatrix}
\begin{bmatrix} x_1 \\ x_2 \end{bmatrix}
$$

or, in Laplace form are

$$\begin{bmatrix} s+1 & 3 \\ -2 & s+3 \end{bmatrix} \begin{bmatrix} y_1 \\ y_2 \end{bmatrix} = \begin{bmatrix} 2 & -0.5 \\ 1 & 3 \end{bmatrix} \begin{bmatrix} x_1 \\ x_2 \end{bmatrix}$$

then, using Cramer's rule yields

$$G_{x_1 x_2}^{y_1 y_2} = \frac{\begin{vmatrix} 2 & -0.5 \\ 1 & 3 \end{vmatrix}}{\begin{vmatrix} s+1 & 3 \\ -2 & s+3 \end{vmatrix}} = \frac{6.5}{s^2 + 4s + 9}$$

which is the same result previously obtained. The Cramer's rule method is much preferred over the algebraic method to minimize numerical round-off errors and in generally much simpler in complex aircraft problems.

Now the transfer function

$$G_{x_1}^{y_1}\bigg|_{AUG} = \frac{\dfrac{2(s+1.5) + 6.5}{s^2 + 4s + 9}}{1 + \dfrac{3(s + 0.667)}{s^2 + 4s + 9}} = \frac{2(s + 4.75)}{(s = 2.38)\,(s + 4.62)}$$

Note that the characteristic roots are the same as those previously obtained, but that the zero is different than that of

$$G_{x_1}^{y_1} = \frac{2(s + 1.5)}{s^2 + 4s + 9}$$

This change in the zero is due to the coupling, since y_1 is affected by both inputs, x_1 and x_2 both of which are applied to the system simultaneously.

The zero can be found using the root locus program, which is advantageous for complex systems. Since

$$N \frac{Y_1}{X_1} \bigg|_{AUG} = 2(s + 1.5) + 6.5$$

$$= 2(s + 1.5) \left[1 + \frac{6.5}{2(s + 1.5)} \right]$$

$$= 2(s + 1.5) \left[1 + \frac{3.25}{s + 1.5} \right]$$

the open loop transfer function

$$GH = \frac{3.25}{s + 1.5}$$

can be entered into the root locus routine to find the closed loop zero location. The root locus program performs the required algebra by combining the two polynomials and factoring the result (which is all a root locus routine does anyway). Figure 14.159 shows the root locus of the above transfer function as the numerator gain varies. The resulting expression becomes

$$N \frac{Y_1}{X_1}_{AUG} = 2(s + 1.5) \left[\frac{s + 4.75}{s + 1.5} \right] = 2(s + 4.75)$$

as previously obtained.

$$GH = \frac{K}{s+1.5}$$

ZEROS OF $N_{x_1}^{y_1}$, $|_{AUG}$
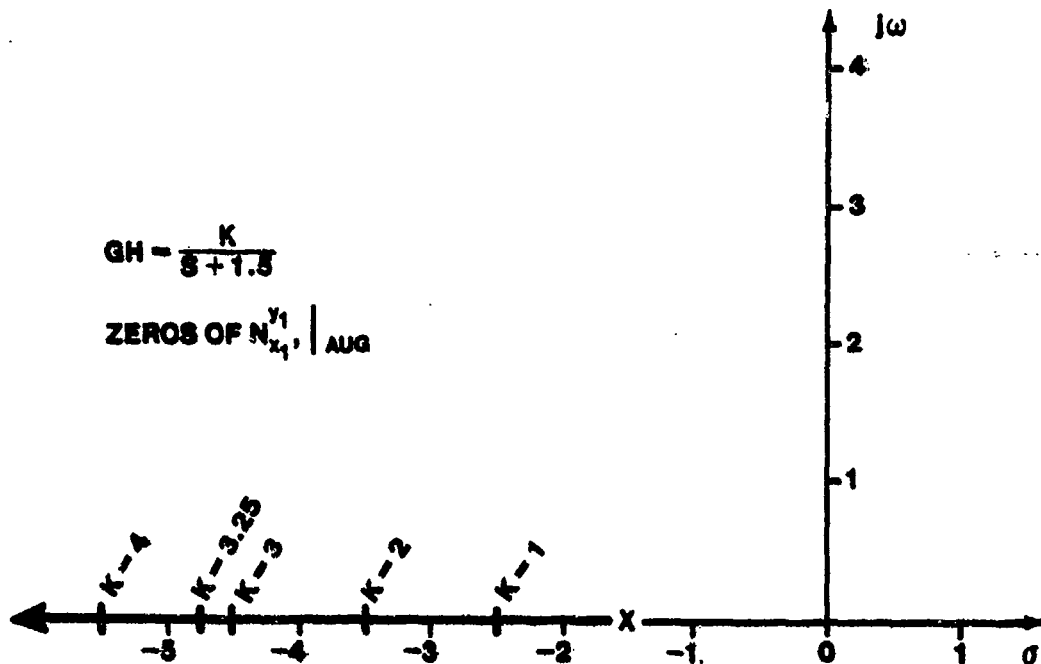
FIGURE 14.159. ROOT LOCUS USED TO COMBINE AND FACTOR
ZEROS OF A CLOSED LOOP COUPLED SYSTEM

A comparison of the time responses due to a unit step input

$$x_1 \; (s) \; = \; \frac{1}{s}$$

shows the effect of the coupling.

The time response for y_1 of the unaugmented system (Figure 14.160) shows
an initial overshoot characteristic of a second order system with a zero
closer to the origin than the poles. The system is heavily damped, as
evidenced by the slight overshoot at 1.6 seconds (the initial overshoot is not
caused by a lack of damping, but by the zero which is near the origin). The
time response for y_1 of the augmented system (Figure 14.161) is characterized
by an overdamped response (two real roots). Since the zero is farther from
the origin than the dominant pole, the initial overshoot does not occur. The
coupling of the system has resulted in a much changed response characteristic.
There is no straightforward technique for the designer to know whether an
improved or degraded response will occur due to the cross coupling. He must
design by trial and error to obtain acceptable zero locations.
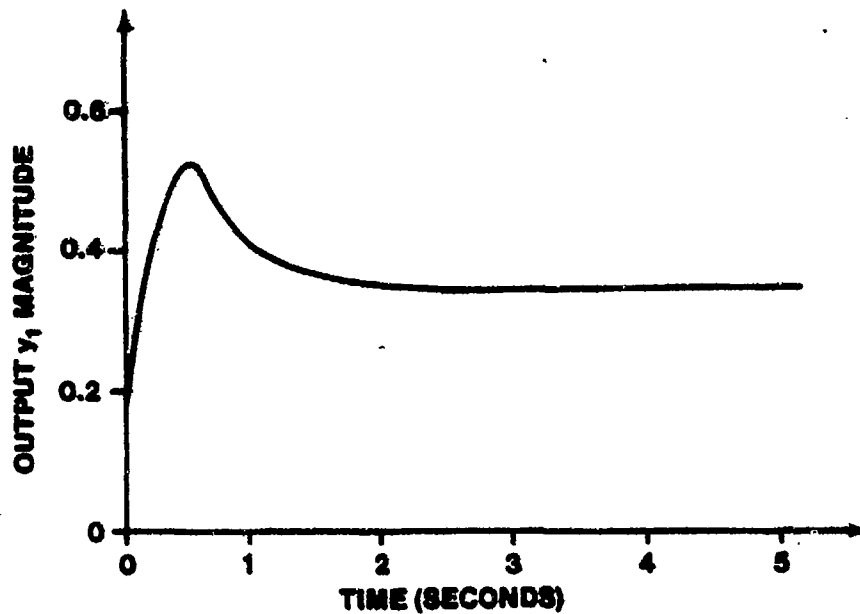
FIGURE 14.160. TIME RESPONSE OF UNAUGMENTED SYSTEM
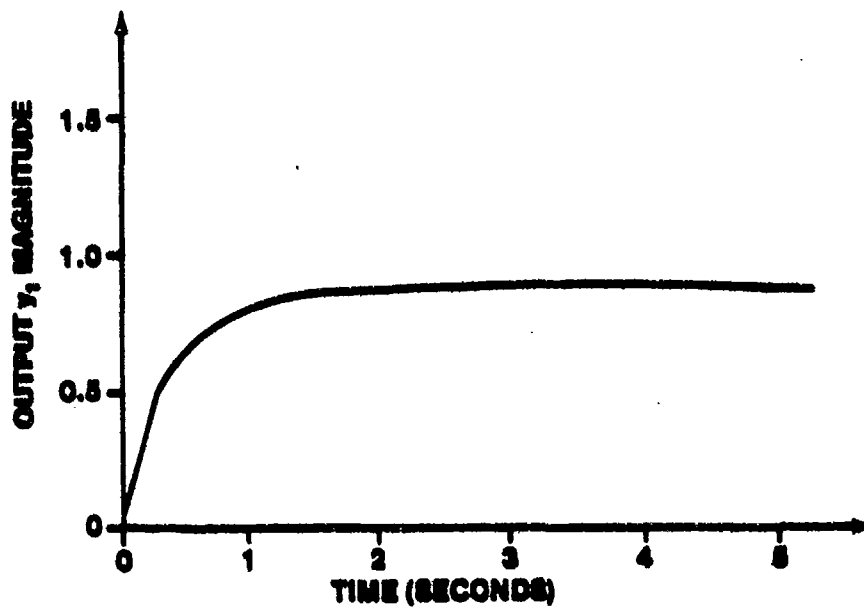
FIGURE 14.161. TIME RESPONSE OF AUGMENTED SYSTEM

14.4.2.3 Roll Rate and Yaw Rate Response with both Roll and Yaw Dampers Engaged. If a roll damper is now engaged in addition to the yaw damper of the last section, a simple root locus analysis of the block diagram of Figure 14.162 yields the roll-plus-yaw damper augmented roots of the aircraft. The open loop transfer function

14.194

$$GH_{p \text{ loop}} = K_p \, G_{\delta_a} \, G_{\delta_a}^p \bigg|_{\substack{\text{YAW} \\ \text{AUG}}} \tag{14.92}$$

is plotted, the augmented aircraft roots are selected for the desired transient response characteristics and K_p is determined by the root locations and their associated root locus gain. To prove this, the closed loop transfer function is computer and compared to the results of a more rigorous development similar to the last section. The closed loop transfer function is

$$G_{\delta_{a_c}}^p \bigg|_{\substack{\text{ROLL} \\ \text{YAW} \\ \text{AUG}}} = \cfrac{K_{\delta_a} \, G_{\delta_a}^p \bigg|_{\substack{\text{YAW} \\ \text{AUG}}}}{1 + K_p G_{\delta_a} \, G_{\delta_a}^p \bigg|_{\substack{\text{YAW} \\ \text{AUG}}}}$$
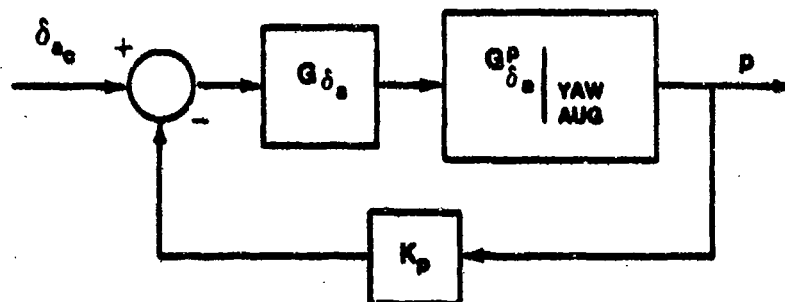
FIGURE 14.162. SIMPLIFIED FLIGHT CONTROL SYSTEM WITH ROLL DAMPER ENGAGED

which is simplified to

$$G_{\delta_{a_c}}^p \bigg|_{\substack{\text{ROLL} \\ \text{YAW} \\ \text{AUG}}} = \cfrac{K_{\delta_a} N_{\delta_a}^p \bigg|_{\substack{\text{YAW} \\ \text{AUG}}}}{D_{\delta_a} \Delta_{\text{YAW}} + K_p K_{\delta_a} N_{\delta_a}^p \bigg|_{\substack{\text{YAW} \\ \text{AUG}}}} \tag{14.93}$$

where $\Delta_{\substack{YAW \\ AUG}}$ is the characteristic equation of the yaw damper augmented aircraft.

$$\Delta_{\substack{ROLL \\ YAW \\ AUG}} = \Delta\, D_{\delta_a} D_{\delta_r} D_w + K_p K_{\delta_a} D_{\delta_r} D_w N_{\delta_a}^p + K_r K_{\delta_r} N_w D_{\delta_a} N_{\delta_r}^r + K_p K_{\delta_a} K_r K_{\delta_r} N_w N_{\delta_a}^p{}_{\delta_r}^r$$

Note that the numerator of

$$G_{\delta_{a_c}}^p \Bigg|_{\substack{ROLL \\ YAW \\ AUG}}$$

is identical to

$$G_{\delta_{a_c}}^p \Bigg|_{\substack{YAW \\ AUG}} .$$

It will be shown later that the numerator of

$$G_{\delta_{r_c}}^r \Bigg|_{\substack{YAW \\ AUG}}$$

must be modified to account for the aileron feedback loop.

To prove the expressions arrived at above, the analysis of the last section is modified to account for the aileron feedback loop. The total aircraft response to simultaneous aileron and rudder inputs are

$$p = G_{\delta_a}^p \delta_a + G_{\delta_r}^p \delta_r \tag{14.82}$$

$$r = G_{\delta_a}^r \delta_a + G_{\delta_r}^r \delta_r$$

Referring to Figure 14.163, the feedback of roll and yaw rate to the ailerons and rudder, respectively, modify the expressions for the aileron and rudder deflections to

$$\delta_a = \left(\delta_{a_c} - K_p \, p\right) G_{\delta_a} \qquad (14.94)$$

$$\delta_r = \left(\delta_{r_c} - K_r H_w \, r\right) G_{\delta_r} \qquad (14.95)$$
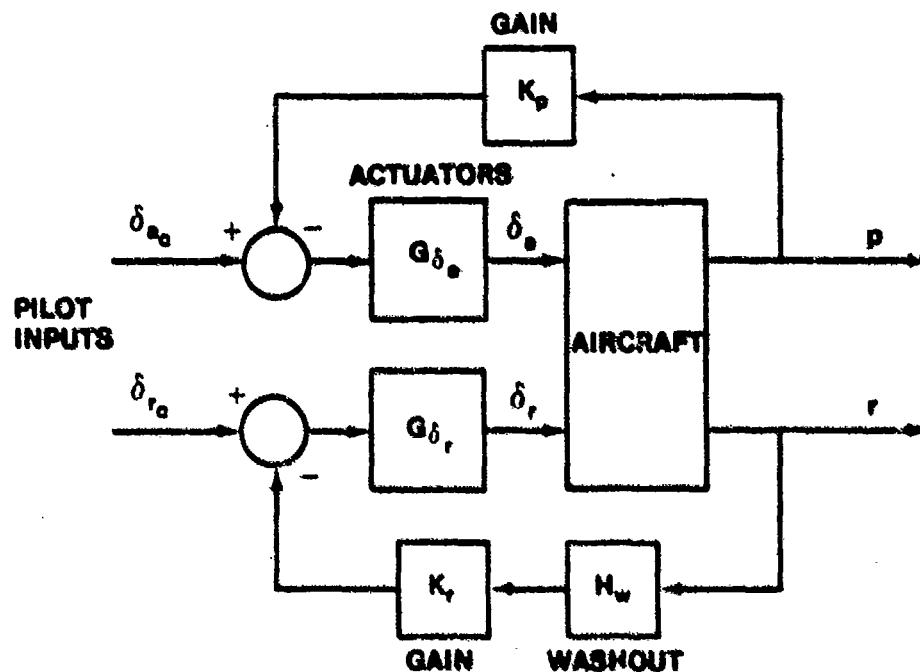
FIGURE 14.163. AIRCRAFT WITH BOTH ROLL AND YAW DAMPERS ENGAGED

The matrix equation can be written after the expressions for the aileron and rudder deflections are substituted into the aircraft response relationships

$$
\begin{bmatrix}
1 + K_p G_{\delta_a} G_{\delta_a}^p & K_r G_{\delta_r} H_w G_{\delta_r}^p \\
\\
K_p G_{\delta_a} G_{\delta_a}^r & 1 + K_r G_{\delta_r} H_w G_{\delta_r}^r
\end{bmatrix}
\begin{bmatrix}
p \\
\\
r
\end{bmatrix}
=
\begin{bmatrix}
G_{\delta_a} G_{\delta_a}^p & G_{\delta_r} G_{\delta_r}^p \\
\\
G_{\delta_a} G_{\delta_a}^r & G_{\delta_r} G_{\delta_r}^r
\end{bmatrix}
\begin{bmatrix}
\delta_{a_c} \\
\\
\delta_{r_c}
\end{bmatrix}
$$

Using Cramer's rule, the characteristic equation becomes

$$\Delta_{\substack{ROLL \\ YAW \\ AUG}} = \Delta\, D_{\delta_a} D_{\delta_r} D_w + K_p K_{\delta_a} D_{\delta_r} D_w N_\delta^p + K_r K_{\delta_r} N_w D_{\delta_a} N_\delta^r + K_p K_{\delta_a} K_r K_{\delta_r} N_w N_\delta^p{}_\delta^r$$

as previously determined. It can be readily proved that the numerator of

$$G_{\delta_{a_c}}^p \bigg|_{\substack{ROLL \\ YAW \\ AUG}}$$

is identical to

$$G_{\delta_{a_c}}^p \bigg|_{\substack{YAW \\ AUG}}$$

The numerator of the yaw rate due to aileron input transfer function,

$$G_{\delta_{a_c}}^r \bigg|_{\substack{ROLL \\ YAW \\ AUG}}$$

is the same as

$$G_{\delta_{a_c}}^r \bigg|_{\substack{YAW \\ AUG}}$$

so that only the characteristics roots change to account for the roll rate feedback. If the roll rate feedback loop incorporated a compensator with poles and zeros, this would not be true, however.

The

$$G^{r}_{\delta_{r_c}}\Bigg|\ \begin{matrix}\text{ROLL}\\\text{YAW}\\\text{AUG}\end{matrix}$$

transfer function would be modified, however, to account for the simultaneous deflection of the aileron due to the roll rate feedback loop, as

$$G^{r}_{\delta_{r_c}}\ \begin{matrix}\text{ROLL}\\\text{YAW}\\\text{AUG}\end{matrix} = \cfrac{+\ G_{\delta_r}G^{r}_{\delta_r}\ +\ K_p\ G_{\delta_a}\ G_{\delta_r}\ G^{p}_{\delta_r}\ r_\delta}{\cfrac{\Delta_{\text{ROLL}}}{\begin{matrix}\text{YAW}\\\text{AUG}\end{matrix}}\Big/\ \Delta\ D_{\delta_a}\ D_{\delta_r}\ D_w}$$

which is simplified to

$$G^{r}_{\delta_{r_c}}\ \begin{matrix}\text{ROLL}\\\text{YAW}\\\text{AUG}\end{matrix} = \cfrac{+\ K_{\delta_r}\ D_{\delta_a}\ D_w\ N^{r}_{\delta_r}\ +\ K_p\ K_{\delta_a}\ K_{\delta_r}\ D_w N^{p}_{\delta_a}\ r_{\delta_r}}{\Delta_{\begin{matrix}\text{ROLL}\\\text{YAW}\\\text{AUG}\end{matrix}}} \qquad (14.96)$$

The rules used for multiloop analysis can be applied to the lateral-directional axis to determine how the various feedback parameters change the aircraft characteristic roots, but that the numerator terms must be modified (cannot be determined as easily as for single input systems) to account for the simultaneous deflection of both the rudder and aileron. Here the rudder loop was closed first and a root locus analysis performed to determine the new aircraft characteristic roots. The numerator for the transfer function relating roll rate to an aileron command with the yaw damper engaged was computed, and then another root locus analysis was performed to determine the effect of the roll damper on the aircraft characteristic roots. 14.4.2.4 Aileron-Rudder Interconnect. Aileron-rudder interconnects are often used in flight control systems to counteract the adverse yaw induced by the deflecting ailerons. The aileron-rudder interconnect, if properly designed,

acts to minimize sideslip excursions during rolling maneuvers, but is occasionally designed to provide proverse yaw if roll rate can be increased. Figure 14.164 shows an aileron-rudder interconnect system for an aircraft with no augmentation systems engaged. The equation for the aircraft response is:

$$\beta = G_{\delta_a}^{\beta} \, \delta_a + G_{\delta_r}^{\beta} \, \delta_r \qquad (14.97)$$
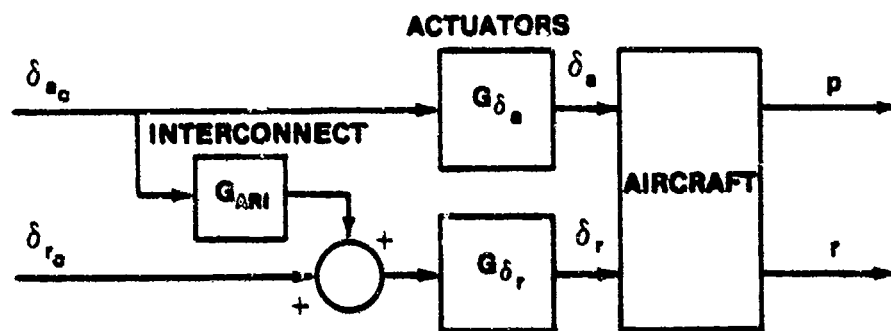
FIGURE 14.164. AIRCRAFT WITH AILERON-RUDDER INTERCONNECT FEATURE

Since no feedback is provided to either control surface, the characteristic roots of the unaugmented aircraft cannot be affected. If the interconnect provides perfect coordination then $\beta = 0$ and the ratio of rudder to aileron becomes

$$\frac{\delta_r}{\delta_a} = -\frac{G_{\delta_a}^{\beta}}{G_{\delta_r}^{\beta}} = -\frac{N_{\delta_a}^{\beta}}{N_{\delta_r}^{\beta}} = G_{ARI} \qquad (14.98)$$

The above expression yields the ideal aileron-rudder interconnect and is valid if the aileron and rudder actuators have the same dynamics. If the dynamics differ, then the aileron-rudder interconnect transfer function must account for the different actuator dynamics for perfect coordination, and becomes

$$G_{ARI} = -\frac{K_{\delta_a} D_{\delta_r} N_{\delta_a}^{\beta}}{K_{\delta_r} D_{\delta_a} N_{\delta_r}^{\beta}} \qquad (14.99)$$

If the above expression is substituted into the control surface equations $\delta_a = G_{\delta_a} \delta_{a_c}$ and $\delta_r = \left[G_{\delta_r} G_{ARI} \delta_{a_c} + \delta_{r_c} \right]$ where $\delta_{r_c} = 0$.

If the pilot is assumed to fly feet-on-the-floor (a realistic assumption in many high performance jet aircraft since high roll rates preclude good turn coordination). Then

$$\delta_r = -\frac{K_{\delta_a} N_{\delta_a}^{\beta}}{D_{\delta_a} N_{\delta_r}^{\beta}} \delta_{a_c}$$

and, substituting into the original expression

$$\beta = G_{\delta_a} G_{\delta_a}^{\beta} \delta_{a_c} - G_{\delta_a} G_{\delta_a}^{\beta} \delta_{a_c} = 0$$

The use of an exact expression for G_{ARI} is impractical in almost all cases since the dynamics of the aircraft change rapidly with airspeed, requiring the poles and zeros of G_{ARI} to be programmed with airspeed. Usually, a simple gain or first order lag is used, being selected to provide slightly proverse yaw during the roll. If the interconnect is approximated as a gain, then $G_{ARI} = K_{ARI}$ so that $\beta = G_{\delta_a} G_{\delta_a}^{\beta} \delta_{a_c} + G_{\delta_r} K_{ARI} G_{\delta_r}^{\beta} \delta_{a_c}$ and the aircraft transfer function for $G_{\delta_{a_c}}^{\beta}$ becomes

$$G_{\delta_{a_c}}^{\beta} = \frac{D_{\delta_r} K_{\delta_a} N_{\delta_a}^{\beta} + K_{ARI} K_{\delta_r} N_{\delta_r}^{\beta} D_{\delta_a}}{D_{\delta_a} D_{\delta_r} \Delta} \qquad (14.100)$$

The aileron-rudder interconnect affects the zeros of $G_{\delta_{a_c}}^{\beta}$.

Similarly, the roll rate due to an aileron input is affected by the interconnect, since the rudder is also deflected, the transfer function becomes

$$G_{\delta_{a_c}}^{p} = \frac{K_{\delta_a} D_{\delta_r} N_{\delta_a}^{p} + K_{ARI} K_{\delta_r} D_{\delta_a} N_{\delta_r}^{p}}{D_{\delta_a} D_{\delta_r} \Delta} \qquad (14.101)$$

The sideslip and roll response due to rudder inputs alone are unaffected by the interconnect. Notice that the Dutch roll, spiral and roll mode roots are unaffected by the aileron-rudder interconnect.

14.4.2.5 <u>Yaw Damper Engaged with an Aileron-Rudder Interconnect System</u>. If an aileron-rudder interconnect is used with a yaw damper, the aircraft characteristic equation is modified by the yaw damper and the expression for the zeros of the $G_{\delta_{a_c}}^{\beta}$ transfer function are modified by both the damper system and the interconnect. Similar results can be derived for roll rate or other transfer functions where the pilot commands an aileron input.
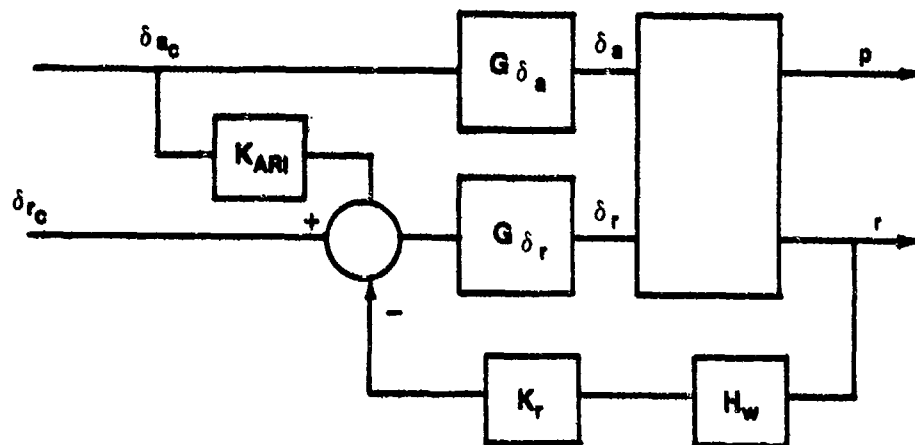
FIGURE 14.165. YAW DAMPER AND AILERON - RUDDER INTERCONNECT

The control expressions become

$$\delta_a = G_{\delta_a} \delta_{a_c}$$

$$\delta_r = G_{\delta_r} \left[K_{ARI} \delta_{a_c} - K_r H_w r + \delta_{r_c} \right]$$

14.202

where

$$\delta_{r_c} = 0$$

Substituting into the aircraft response relationships

$$\beta = G_{\delta_a} G_{\delta_a}^{\beta} \delta_{a_c} + G_{\delta_r} K_{ARI} G_{\delta_r}^{\beta} \delta_{a_c} - K_r G_{\delta_r} H_W G_{\delta_r}^{\beta} r$$

$$r = G_{\delta_a} G_{\delta_a}^{r} \delta_{a_c} + G_{\delta_r} K_{ARI} G_{\delta_r}^{r} \delta_{a_c} - K_r G_{\delta_r} H_W G_{\delta_r}^{r} r$$

The matrix equation becomes

$$\begin{bmatrix} 1 & K_r G_{\delta_r} H_W G_{\delta_r}^{\beta} \\ & \\ 0 & 1 + K_r G_{\delta_r} H_W G_{\delta_r}^{r} \end{bmatrix} \begin{bmatrix} \beta \\ \\ r \end{bmatrix} = \begin{bmatrix} G_{\delta_a} G_{\delta_a}^{\beta} + K_{ARI} G_{\delta_r} G_{\delta_r}^{\beta} \\ \cdot \\ G_{\delta_a} G_{\delta_a}^{r} + K_{ARI} G_{\delta_r} G_{\delta_r}^{r} \end{bmatrix} \delta_{a_c}$$

The characteristic equation of the augmented aircraft is unchanged by the aileron-rudder interconnect, being affected only by the yaw damper. The transfer function becomes

$$G_{\delta_{a_c}}^{\beta} \Big|_{\substack{YAW \\ AUG}} = \frac{G_{\delta_a} G_{\delta_a}^{\beta} + K_r G_{\delta_a} G_{\delta_r} H_W G_{\delta_a}^{\beta} G_{\delta_r}^{r} + K_{ARI} G_{\delta_r} G_{\delta_r}^{\beta}}{1 + K_r G_{\delta_r} H_W G_{\delta_r}^{r}}$$

which can be simplified to

$$G_{\delta_{a_c}}^{\beta} \Big|_{\substack{YAW \\ AUG}} = \frac{K_{\delta_a} \left[D_{\delta_r} D_W N_{\delta_a}^{\beta} + K_r K_{\delta_r} N_W N_{\delta_a}^{\beta} N_{\delta_r}^{r} + K_{ARI} \dfrac{K_{\delta_r}}{K_{\delta_a}} D_{\delta_a} D_W N_{\delta_r}^{\beta} \right]}{\left[D_{\delta_a} D_{\delta_r} D_W \Delta + K_r K_{\delta_r} N_W N_{\delta_r}^{r} \right]}$$

(14.102)

If a roll rate feedback loop is added to the aircraft, the augmented roots with both the yaw damper and roll stability augmentation systems engaged are affected by the aileron-rudder interconnect, since the zeros of $G_{\delta_a}^{p}\Big|_{\substack{YAW \\ AUG}}$ are changed by the aileron-rudder interconnect.

14.4.2.6 <u>Coupling Numerator Terms Involving Derived Response Parameters</u>. In many applications, lateral acceleration is fed back to the rudder to improve turn coordination. When analyzing the response of the aircraft to aileron inputs (roll rate response, for instance) coupling numerator terms like $G_{\delta_a \delta_r}^{p \ a_y}$ appear in the $G_{\delta_a}^{p}\Big|_{\substack{YAW \\ AUG}}$ transfer function. This coupling numerator term involves lateral acceleration, for which the transfer functions $G_{\delta_r}^{a_y}$ and $G_{\delta_a}^{a_y}$ must must be derived, as in Paragraph 14.2. The coupling numerator is most easily computed by noting that

$$G_{\delta_r}^{a_y} = U_0 s G_{\delta_r}^{\beta} + U_0 G_{\delta_r}^{r} + \ell_x s G_{\delta_r}^{r} - \ell_z s G_{\delta_r}^{p} - g G_{\delta_r}^{\phi} - U_0 \alpha_0 G_{\delta_r}^{p} \qquad (14.103)$$

and

$$G_{\delta_a}^{a_y} = U_0 s G_{\delta_a}^{\beta} + U_0 G_{\delta_a}^{r} + \ell_x s G_{\delta_a}^{r} + \ell_z s G_{\delta_a}^{p} - g G_{\delta_a}^{\phi} - U_0 \alpha_0 G_{\delta_a}^{p} \qquad (14.104)$$

where the lateral acceleration transfer function is computed in the body axis system. The term $\alpha_0 G_{\delta_a}^{p} = 0$ if the stability axis system is used, since $\alpha_0 = 0$. Assuming $\ell_z = 0$ and defining the coupling transfer function as

$$G_{\delta_a \delta_r}^{p \ a_y} = G_{\delta_a}^{p} G_{\delta_r}^{a_y} - G_{\delta_a}^{a_y} G_{\delta_r}^{p} \qquad (14.105)$$

the coupling numerator becomes, by substituting in the acceleration transfer function equations

$$N_{\delta_a \delta_r}^{p \ a_y} = U_0 s N_{\delta_a \delta_r}^{p \ \beta} + U_0 N_{\delta_a \delta_r}^{p \ r} + \ell_x s N_{\delta_a \delta_r}^{p \ r} \qquad (14.106)$$

14.204

where

$$-gN_{\delta_a}^p \frac{\phi}{\delta_r} = -\frac{g}{s} N_{\delta_a}^{\phi} \frac{\phi}{\delta_r} = 0 \quad (\phi = \frac{p}{s})$$

Similar derivations for coupling numerator terms must be made whenever the transfer function for a particular output parameter is a function of two or more transfer functions developed from the equations of motion for the aircraft.

14.4.2.7 Multiloop Lateral-Direction Flight Control System:

The A-7D control augmentation system uses all of the elements discussed in the last several subsections. With the yaw stabilizer engaged, yaw rate and lateral acceleration feedback are provided to the rudder in addition to an aileron-rudder interconnect. The control augmentation switch engages the pitch and roll control augmentation systems that, in the lateral axis, provides a roll rate command system with increased aileron control authority over the mechanical system. The response of the aircraft is analyzed under four conditions: no augmentation, yaw stabilization with no aileron-rudder interconnect, yaw stabilization with the aileron-rudder interconnect and roll rate command system engaged. Two output responses illustrate the effects of the various feedbacks and interconnects -- the roll rate response and the sideslip angle response. The effects of lateral stick commands, only, are examined. The effect of the mechanical control system acting in parallel with the yaw stabilizer and roll augmentation system will be neglected (the effect of the mechanical flight control system in parallel with an electrical control augmentation system is discussed in Paragraph 14.3).

Figures 14.166 and 14.167 present the A-7D lateral-directional control system in the format found commonly in the literature. The aileron-rudder interconnect gain is a function of the elevator deflection angle and the value presented is for 1 'g' trim flight condition at 0.6 Mach, 15,000 feet. The following body axis system transfer functions are required for the analysis:

$$\Delta(s) = (s + 0.0435)(s + 2.71)(s + 0.357 \pm 2.262j)$$

$$N_{\delta_a}^{\beta}(s) = -0.00655 (s + 2.71)(s - 1.63)(s + 23.2) \quad rad/rad$$

$$N_{\delta_r}^{\beta}(s) = -0.0537 \ (s - 0.00616) \ (s + 2.7) \ (s + 113) \qquad \text{rad/rad}$$

$$N_{\delta_a}^{r}(s) = 1.37 \ (s + 0.777) \ (s + 0.322 \pm 2.106j) \qquad \text{rad/sec/rad}$$

$$N_{\delta_r}^{r}(s) = 5.54 \ (s + 2.35) \ (s + 0.348 \pm 0.648j) \qquad \text{rad/sec/rad}$$

$$N_{\delta_a}^{a_y}(s) \bigg|_{CG} = -4.16 \ (s + 1.32) \ (s + 3.12) \ (s - 0.585 \pm 1.902j) \qquad \text{ft/sec}^2/\text{rad}$$

$$N_{\delta_r}^{a_y}(s) \bigg|_{CG} = -34.1 \ (s - 0.0227) \ (s + 2.69) \ (s + 4.3) \ (s - 3.69) \qquad \text{ft/sec}^2/\text{rad}$$

$$N_{\delta_a}^{p}(s) = 17.6 \ (s - 0.00347) \ (s + 0.405 \pm 2.305j) \qquad \text{rad/sec/rad}$$

$$N_{\delta_r}^{p}(s) = 7.27 \ (s - 0.00352) \ (s + 4.31) \ (s - 4.45) \qquad \text{rad/sec/rad}$$
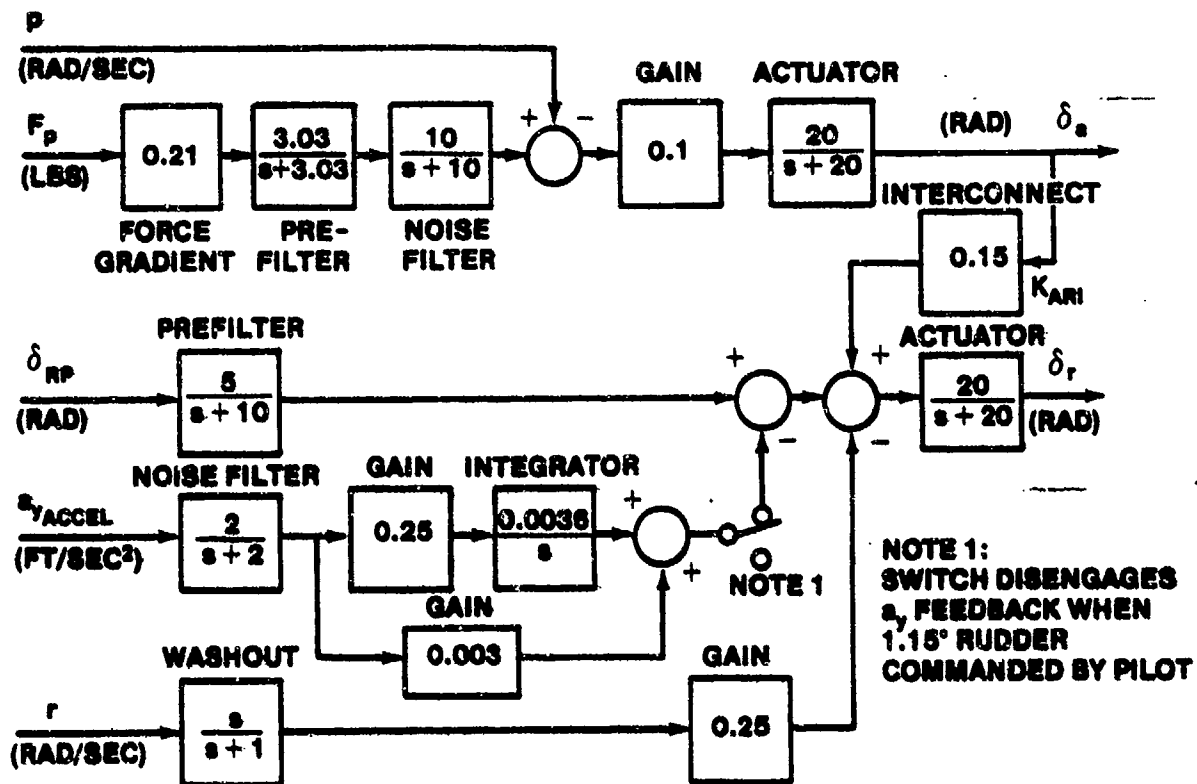
FIGURE 14.166.   A-7D LATERAL-DIRECTIONAL FLIGHT CONTROL SYSTEM
(YAW STAB AND CONT AUG ENGAGED)

14.207
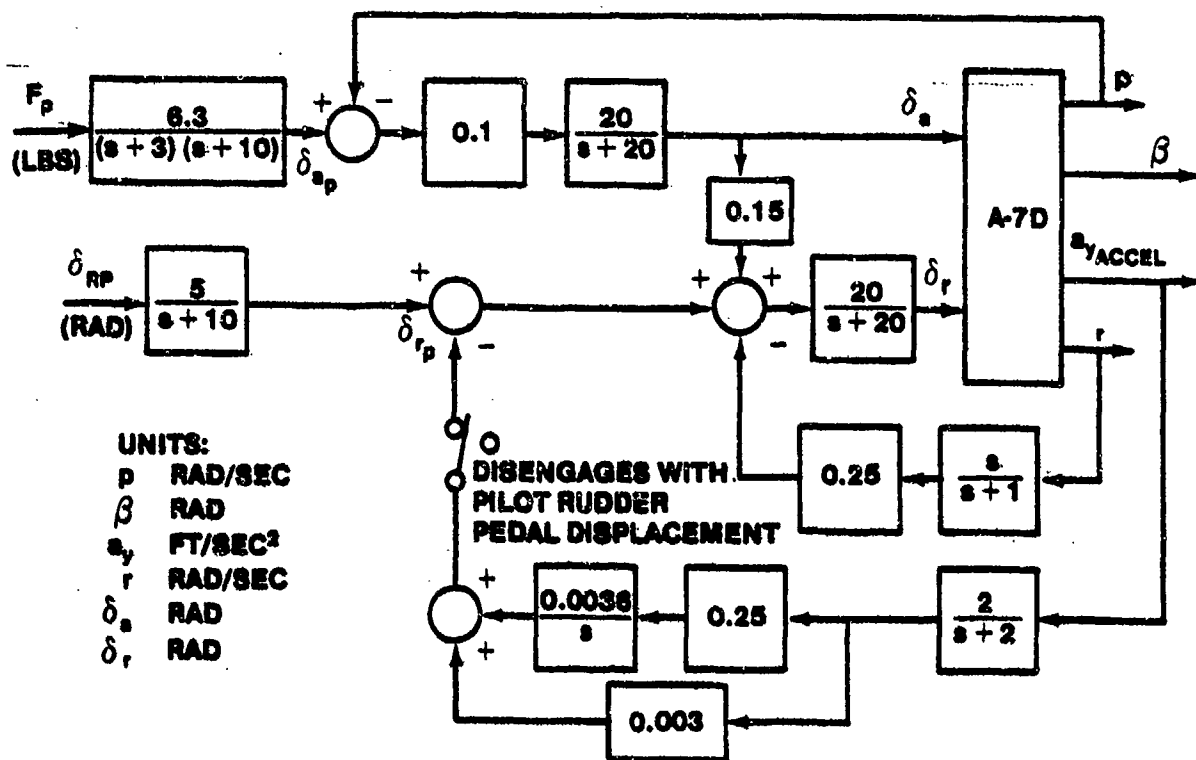
FIGURE 14.167. A-7D LATERAL-DIRECTIONAL AXIS BLOCK DIAGRAM

Figure 14.168 presents the roll rate and sideslip angle responses of the unaugmented aircraft to step aileron inputs.
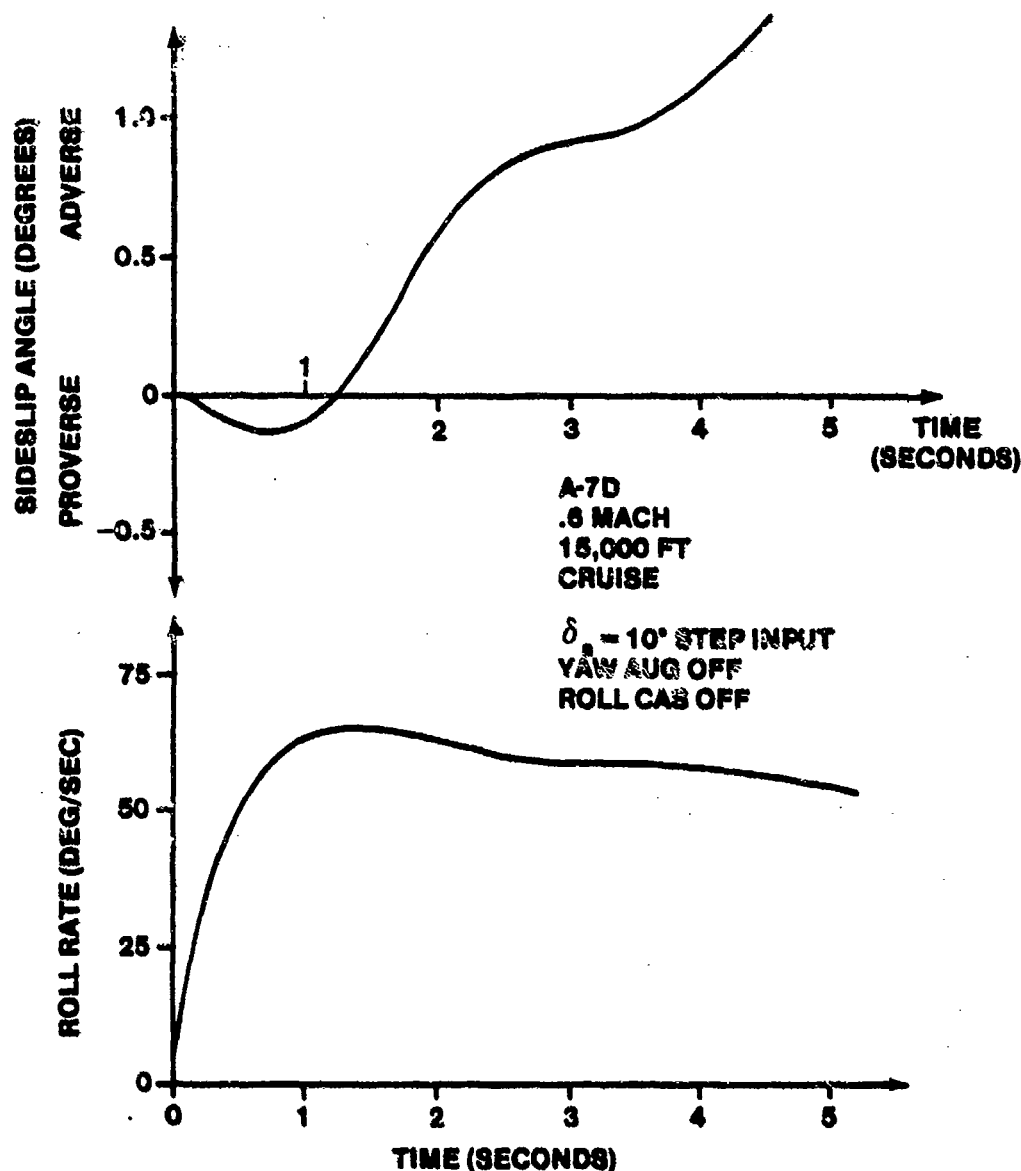
FIGURE 14.168. A-7D SIDESLIP ANGLE AND ROLL RATE RESPONSE
FOR THE UNAUGMENTED AIRCRAFT.

The aileron input is assumed to be zero and the control augmentation system is disengaged (no roll rate feedback to the ailerons). The analysis takes advantage of the superposition principle which states that the response of a linear system to multiple inputs is equal to the sum of the separate inputs applied individually. The yaw stabilizer is a multiloop system and can be handled, for rudder inputs, in a manner similar to the longitudinal

system analysis of paragraph 14.4.1.2. If the pilot applies a rudder pedal input, the lateral acceleration feedback path is opened.

Since the acceleration transfer functions provided are for the center of gravity, the transfer functions for the accelerometer position must be computed. The acceleration at the accelerometer is

$$a_{y_{accel}} = a_{y_{CG}} + \ell_x \dot{r} \quad \text{where } \dot{p} = 0 \tag{14.65}$$

so that the rudder transfer function becomes

$$G_{\delta_r}^{a_y}(s)\bigg|_{\ell_x} = \frac{N_{\delta_r}^{a_y}(s)\bigg|_{CG} + \ell_x s N_{\delta_r}^{r}(s)}{\Delta(s)}$$

where $\ell_x = 4.6$ ft

Looking at the numerator of the transfer function only

$$N_{\delta_r}^{a_y}(s)\bigg|_{CG} + \ell_x s N_{\delta_r}^{r}(s) = N_{\delta_r}^{a_y}(s)\bigg|_{CG} \left[1 + \frac{\ell_x s N_{\delta_r}^{r}(s)}{N_{\delta_r}^{a_y}(s)\bigg|_{CG}} \right]$$

The root locus program can be used to factor the numerator polynomial of the accelerometer transfer function by entering

$$GH = \frac{\ell_x s N_{\delta_r}^{r}(s)}{N_{\delta_r}^{a_y}(s)\bigg|_{CG}}$$

and determining the roots for the gain

$$\frac{\ell_x K_{\delta_r}^{r}}{K_{\delta_r}^{a_y}\bigg|_{CG}} = -0.747$$

The roots determined by this analysis are the zeros of the transfer function

$$G_{\delta_r}^{a_y}(s)\bigg|_{\ell_x}$$

The gain of this transfer function is found by considering that both parts of the numerator polynomial

$$N_{\delta_r}^{a_y}(s)\bigg|_{CG} + \ell_x\, s N_{\delta_r}^{r}(s)$$

are fourth order. The constants associated with the fourth power of the Laplace operator, s, are added to find the gain

$$K_{\delta_r}^{a_y}\bigg|_{\ell_x} = K_{\delta_r}^{a_y}\bigg|_{CG} + \ell_x K_{\delta_r}^{r} = 8.616$$

The acceleration transfer function is

$$G_{\delta_r}^{a_y}(s)\bigg|_{\ell_x} = \frac{8.616(s - 0.0222)\,(s + 2.6)\,(s + 9.12)\,(s - 7.69)}{\Delta(s)}$$

Figure 14.169 presents the yaw stabilizer block diagram with $\delta_{a_p} = 0$ and the roll control augmentation system disengaged. The block diagram is in a format which clearly shows the feedback loops. The proportional plus integral paths in the acceleration feedback path have been combined. The acceleration feedback path could have been represented as the inner loop, but since the yaw rate feedback is used to suppress the Dutch roll and the acceleration loop is used for turn (not roll) coordination, it is logical to analyze the loops in the order presented.
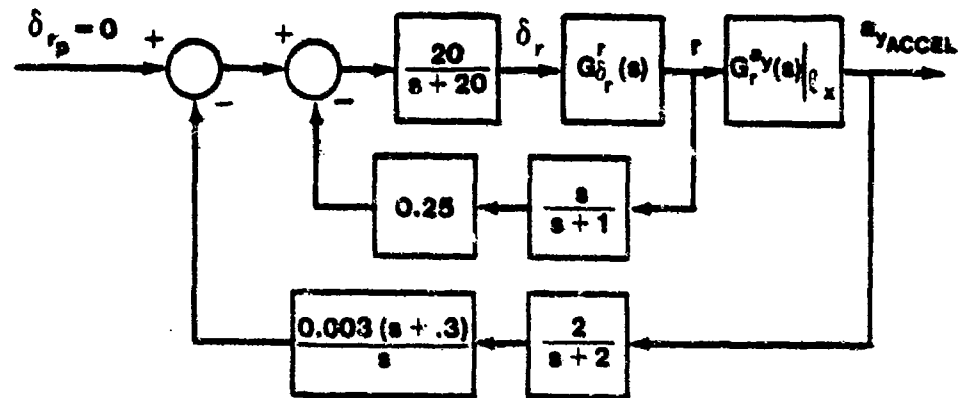
FIGURE 14.169.   SIMPLIFIED A-7D YAW STABILIZER CONTROL SYSTEM
WITH YAW STABILIZER ENGAGED

The open loop transfer function for the yaw rate loop

$$GH = \underbrace{\frac{+5.54(s + 2.35)\ (s + 0.348 \pm 0.648j)}{(s + 0.0435)\ (s + 2.71)\ (s + 0.357 \pm 2.62j)}}_{\text{Aircraft Transfer Function}} \underbrace{\frac{20}{s + 20}}_{\text{Actuator}} \underbrace{\frac{0.25\ s}{s + 1}}_{\substack{\text{Feedback}\\ \text{Elements}}}$$

is used to plot the root locus for the inner loop, Figure 14.170. The closed loop roots are found on the root locus, corresponding to the gain K_{OL} = 27.7. From the root locus, it is apparent that the yaw rate feedback increases the Dutch roll damping from ζ_{dr} = 0.156 to 0.407 while having only a small effect on the Dutch roll natural frequency, which changes from $\omega_{n_{dr}}$ = 2.29 rad/sec to 2.13 rad/sec as discussed in Paragraph 14.2. The roll mode time constant is decreased from

$$\tau_r = \frac{1}{2.71} \text{ to } \frac{1}{3.08}$$

and the spiral mode is somewhat destabilized. The closed loop transfer function for the inner yaw rate feedback loop becomes

$$G^{r}_{\delta_{r_p}}(s)\bigg|_{r\ CL} = \frac{+110.8(s + 0.348 \pm 0.648j)(s + 1)(s + 2.35)}{(s + 0.0387)(s + 0.869 \pm 1.95j)(s + 1.24)(s\ 3.08)(s + 18.4)}$$
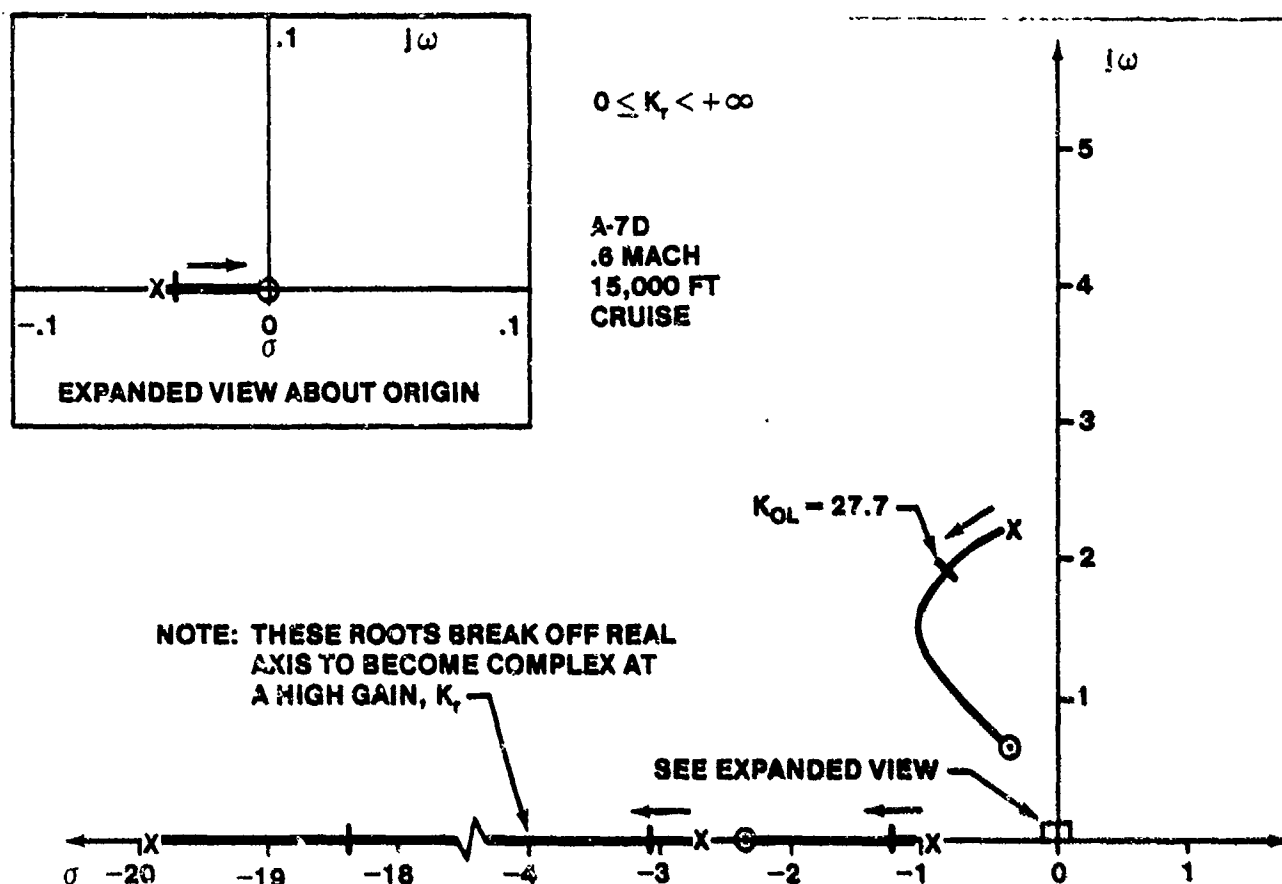
FIGURE 14.170.   ROOT LOCUS PLOT OF A-7D YAW RATE FEEDBACK LOOP

The (s + 1) zero is introduced by the washout filter in the feedback path (see Appendix F). Figure 14.171 shows the simplified block diagram of the acceleration feedback loop, where the closed loop transfer function of the yaw rate feedback loop is used to represent the effect of the inner loop already analyzed.
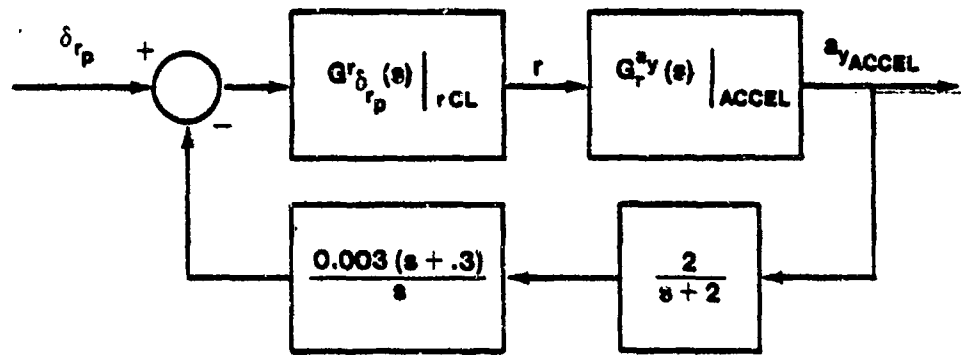
FIGURE 14.171.   SIMPLIFIED A-7D YAW STABILIZER BLOCK DIAGRAM

If a yaw rate response due to a rudder input (CAS disengaged) were desired, the analysis would end since the acceleration feedback is eliminated when the pilot applies the rudder. The yaw rate response would be described by

$$G_{\delta_{r_p}}^{r}(s) \Bigg|_{\substack{YAW \\ AUG}} = \frac{110.8(s +0.348 \pm 0.648j)\ (s+1)\ (s+2.35)}{(s+0.0387)(s+0.869 \pm 1.95j)(s+1.24)(s+3.08)(s+18.4)}$$

since a positive pilot rudder input is right rudder. If the transfer function due to the pilot rudder displacement were desired, then

$$G_{\delta_{RP}}^{r}(s) \Bigg|_{\substack{YAW \\ AUG}} = \frac{5}{s+10}\ G_{\delta_{r_p}}^{r}(s) \Bigg|_{\substack{YAW \\ AUG}}$$

It will be assumed that the pilot flies feet-on-the-floor so that the acceleration feedback loop is always engaged. This assumption will not alter the analysis process.

The transfer function for

$$G_{r}^{a_y}(s) \Bigg|_{\ell_x} = \frac{N_{\delta_r}^{a_y}(s) \Big|_{\ell_x}}{N_{\delta_r}^{r}(s)}$$

is required to perform the outer loop analysis, where the numerators for rudder inputs are used (rather than the numerators due to the aileron inputs). Substituting in the numerators and forming the open loop transfer function for the outer loop yields

$$GH = \underbrace{\frac{172.32(s - 0.0222)(s + 2.6)(s + 9.12)(s - 7.69)(s + 1)}{(s+0.0387)(s+0.869\pm1.95j)(s+1.24)(s+3.08)(s+18.4)}}_{\substack{\text{Aircraft Sensed Lateral Acceleration Transfer} \\ \text{Function with Yaw Rate Loop Closed}}} \cdot \underbrace{\frac{0.006(s + 0.3)}{s(s + 2)}}_{\substack{\text{Feedback} \\ \text{Elements}}}$$

The closed loop roots are obtained from the root locus plot (Figure 14.172), which reveals that the lateral acceleration feedback has the effect of increasing the Dutch roll natural frequency and reducing the Dutch roll damping (as discussed in Chapter 1).
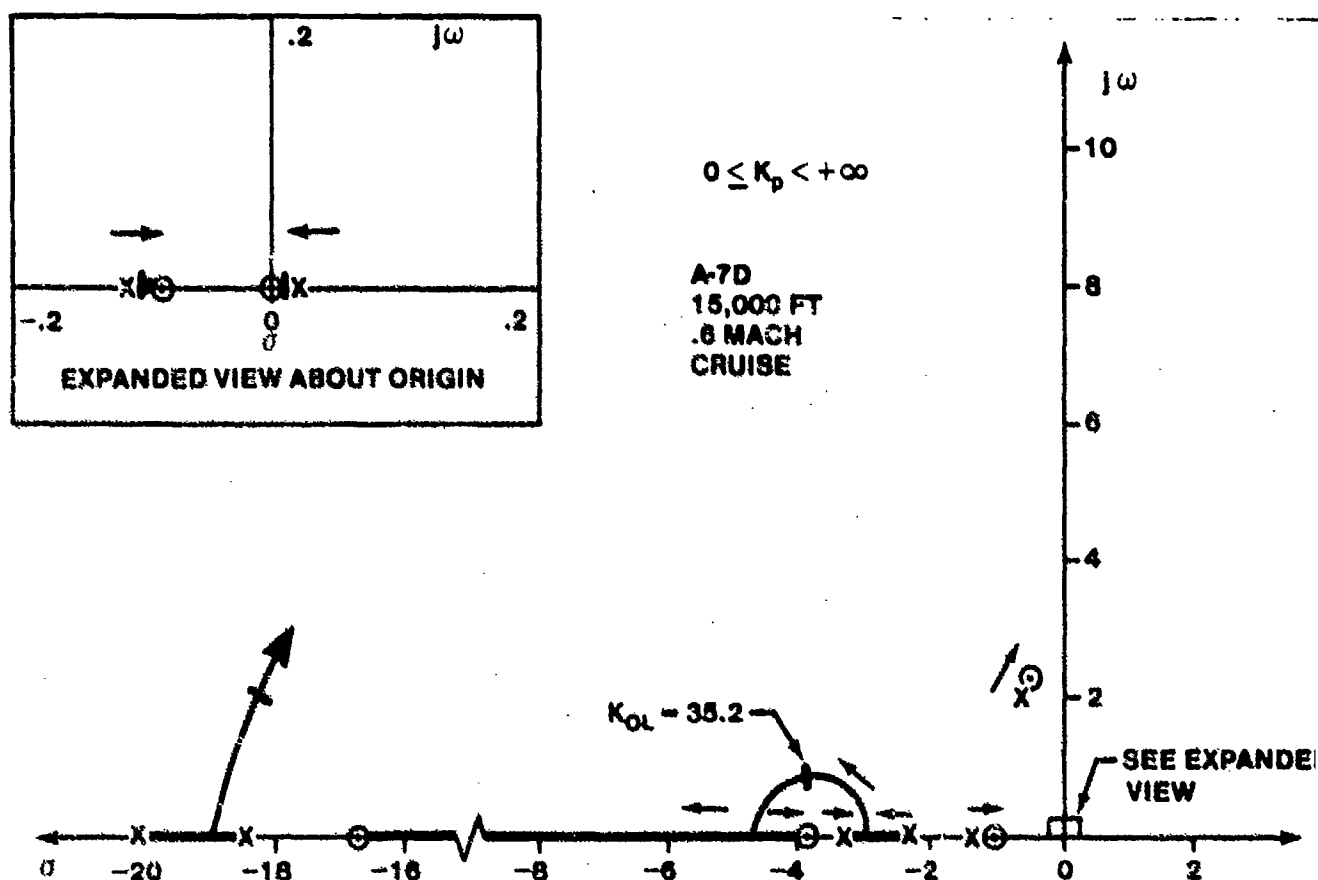
FIGURE 14.172. ROOT LOCUS OF A-7D LATERAL ACCELERATION FEEDBACK LOOP

The closed loop yaw rate transfer function for the yaw stabilizer augmented aircraft becomes

$$G_{\delta_{r_p}}^{r}(s)\bigg|_{\substack{YAW \\ AUG}} = \left[\frac{110.8(s+2.35)\ (s+0.348\pm0.648j)\ (s+1)\ (s+2)s}{(s-0.0141)\ (s+0.584\pm2.16j)\ (s+0.111)\ (s+1.14)}\right.$$

$$\left.\frac{1}{(s+2.31)\ (s+3.33)\ (s+18.5)}\right]$$

and for the lateral acceleration at the center of gravity becomes

$$G_{\delta_{r_p}}^{a_y}(s)\bigg|_{\substack{CG \\ YAW \\ AUG}} = \left[\frac{682.0(s-0.022)\ (s+2.69)\ (s+4.3)\ (s-3.69)\ (s+1)}{(s-0.0141)\ (s+0.584\pm2.16j)\ (s+0.111)\ (s+1.14)}\right.$$

$$\left.\frac{s(s+2)}{(s+2.31)\ (s+3.33)\ (s+18.5)}\right]$$

where

$$G_{\delta_{r_p}}^{r}(s)\bigg|_{\substack{YAW \\ AUG}} = G_{\delta_{r_p}}^{a_y}(s)\bigg|_{\substack{ACCEL \\ YAW \\ AUG}} \frac{N_{\delta_r}^{r}(s)}{N_{\delta_r}^{a_y}(s)}\bigg|_{\ell_x}$$

and

$$G_{\delta_{r_p}}^{a_y}(s)\bigg|_{\substack{CG \\ YAW \\ AUG}} = G_{\delta_{r_p}}^{a_y}(s)\bigg|_{\substack{ACCEL \\ YAW \\ AUG}} \frac{N_{\delta_r}^{a_y}(s)\big|_{CG}}{N_{\delta_r}^{a_y}(s)\big|_{\ell_x}}$$

The transfer function found from the root locus analysis of the acceleration loop is

$$G_{\delta_{r_p}}^{a_y} (s) \Bigg|_{\substack{ACCEL \\ YAW \\ AUG}} = \left[\frac{172.32 \ (s - 0.0222) \ (s + 2.6) \ (s + 9.12) \ (s - 7.69)}{(s - 0.141) \ (+ 0.584 \pm 2.16j) \ (s + 0.111) \ (s + 1.14)} \right.$$

$$\left. \frac{s(s + 1) \ (s + 2)}{(s + 2.31) \ (s + 3.33) \ (s + 18.5)} \right]$$

As a result of this feedback loop, the Dutch roll damping is reduced, from $\zeta_{dr} = 0.407$ to 0.261 but that it remains higher than the Dutch roll damping of the unaugmented aircraft. The Dutch roll natural frequency of the augmented aircraft remains about the same as for the unaugmented aircraft, $\omega_{n_{dr}} = 2.24$ rad/sec respectively. The spiral mode root has been driven unstable. The roots at $(s + 0.111)$ and $(s + 1.14)$ will play a significant role in the aircraft response, with the root at $(s + 0.111)$ causing the turn coordination or the response due to a sideslip angle upset to be sluggish.

The effect on the roll mode will now be analyzed. If a roll is accomplished with the rudder, then, with the yaw stabilizer engaged

$$G_{\delta_{r_p}}^{p} (s) \Bigg|_{\substack{YAW \\ AUG}} = G_{\delta_{r_p}}^{r} (s) \Bigg|_{\substack{YAW \\ AUG}} \frac{N_{\delta_r}^{p} (s)}{N_{\delta_r}^{r} (s)} \quad \begin{array}{l} \text{Acceleration} \\ \text{Path Open} \end{array}$$

and

$$G_{\delta_{r_p}}^{p} (s) \Bigg|_{\substack{YAW \\ AUG}} = \frac{145.4(s + 0.00352) \ (s + 4.31) \ (s - 4.45) \ (s + 1)}{(s + 0.0387)(s + 0.869 \pm 195.j)(s + 1.24)(s + 3.08)(s + 18.4)}$$

A similar technique could be used to find $G_{\delta_{r_p}}^{\beta} (s) \Bigg|_{\substack{YAW \\ AUG}}$

The aircraft response characteristics due to an aileron input with the yaw stabilizer engaged will be found. The relatively straight forward analysis conducted thus far cannot be applied to find

$$G_{\delta_{a_p}}^{p} (s) \Bigg|_{\substack{YAW \\ AUG}} \quad \text{or} \quad G_{\delta_{a_p}}^{\beta} (s) \Bigg|_{\substack{YAW \\ AUG}}$$

The roll control augmentation system is assumed off. From the block diagram (Figure 14.166 with the roll augmentation disengaged).

$$p = G^p_{\delta_a} \delta_a + G^p_{\delta_r} \delta_r$$

$$r = G^r_{\delta_a} \delta_a + G^r_{\delta_r} \delta_r$$

$$a_{y_{ACCEL}} = G^{a_y}_{\delta_a}\bigg|_{ACCEL} \delta_a + G^{a_y}_{\delta_r}\bigg|_{ACCEL} \delta_r$$

where

$$\delta_a = G_{\delta_a} \delta_{a_p}$$

$$\delta_r = \left[G_{\delta_r} G_{\delta_a} K_{ARI} \delta_{a_p} - K_r H_r r - H_s H_a a_{y_{ACCEL}} \right]$$

and where

$$\delta_{r_p} = 0$$

Substituting the expression for

$$\delta_a \text{ and } \delta_r$$

into the aircraft response equations yields

$$p = G^p_{\delta_a} G_{\delta_a} \delta_{a_p} + G^p_{\delta_r} G_{\delta_r} \left[G_{\delta_a} K_{ARI} \delta_{a_p} - K_r H_r r - H_s H_a a_{y_{ACCEL}} \right]$$

$$r = G^r_{\delta_a} G_{\delta_a} \delta_{a_p} + G^r_{\delta_r} G_{\delta_r} \left[G_{\delta_a} K_{ARI} \delta_{a_p} - K_r H_r r - H_s H_a a_{y_{ACCEL}} \right]$$

$$a_{y_{ACCEL}} = G^{a_y}_{\delta_a}\bigg|_{ACCEL} G_{\delta_a} \delta_{a_p} + G^{a_y}_{\delta_r}\bigg|_{ACCEL} G_{\delta_r} \left[G_{\delta_a} K_{ARI} \delta_{a_p} - K_r H_r r - H_s H_a a_{y_{ACCEL}} \right]$$

Formulating these equations into a matrix equation yields the equation of Figure 14.173.

$$\begin{bmatrix} 1 & +K_r H_r G_{\delta_r} G_{\delta_r}^p & +H_s H_a G_{\delta_r} G_{\delta_r}^p \\[4pt] 0 & 1+K_r H_r G_{\delta_r} G_{\delta_r}^r & +H_s H_a G_{\delta_r} G_{\delta_r}^r \\[4pt] 0 & +K_r H_r G_{\delta_r} G_{\delta_r}^{a_y}\Big|_{ACC} & 1+H_s H_a G_{\delta_r} G_{\delta_r}^{a_y}\Big|_{ACC} \end{bmatrix} \begin{bmatrix} p \\[4pt] r \\[4pt] a_{y_{ACCEL}} \end{bmatrix} =$$

$$\begin{bmatrix} G_{\delta_a}^p G_{\delta_a} + K_{ARI} G_{\delta_a} G_{\delta_r} G_{\delta_r}^p \\[6pt] G_{\delta_a}^r G_{\delta_a} + K_{ARI} G_{\delta_a} G_{\delta_r} G_{\delta_r}^r \\[6pt] G_{\delta_a}^{a_y}\Big|_{ACC} G_{\delta_a} + K_{ARI} G_{\delta_a} G_{\delta_r} G_{\delta_r}^{a_y}\Big|_{ACC} \end{bmatrix} \delta_{a_p}$$

FIGURE 14.173. MATRIX EQUATIONS FOR A-7D LATERAL-DIRECTIONAL
FLIGHT CONTROL SYSTEM ANALYSIS

The general strategy will be to find the numerator terms from the matrix equation. The denominator has already been obtained through the root locus analysis. The characteristic equation of the yaw stabilizer augmented aircraft is

$$1 + K_r H_r G_{\delta_r} G_{\delta_r}^r + H_s H_a G_{\delta_r} G_{\delta_r}^{a_y}\Big|_{ACCEL}$$

as obtained from the determinant of the output variable matrix. The numerator is obtained for the roll rate response, using Cramer's rule, as

$$G_{\delta_a} G_{\delta_a}^p + K_r H_r G_{\delta_r} G_{\delta_a} G_{\delta_a}^p G_{\delta_r}^r + H_s H_a G_{\delta_r} G_{\delta_a} G_{\delta_a}^p G_{\delta_r}^{a_y}\Big|_{ACCEL} + K_{ARI} G_{\delta_a} G_{\delta_r} G_{\delta_r}^p$$

where the coupling terms

$$G_{\delta_a}^p G_{\delta_r}^r \quad \text{and} \quad G_{\delta_a}^p G_{\delta_r}^{a_y}\Big|_{ACCEL}$$

14.219

appear (see Appendix A and Paragraph 14.4.2.6 for their definitions).

The aircraft equations of motion necessary to obtain the coupling numerator terms are

$$\begin{bmatrix} s + 0.187 & -0.07s - 0.051 & 1 \\ 29.2 & s^2 + 2.73s & -0.868 \\ -3.12 & 0.116 & s + 0.541 \end{bmatrix} \begin{bmatrix} \beta \\ \phi \\ r \end{bmatrix} = \begin{bmatrix} -0.00655 & 0.0537 \\ 17.6 & 7.27 \\ 1.37 & -5.54 \end{bmatrix} \begin{bmatrix} \delta_a \\ \delta_r \end{bmatrix}$$

Applying the definitions for the coupling terms yields

$$N^{\beta\ r}_{\delta_a \delta_r}(s) = -.037\,(s + 0.73)\,(s + 203.67) \quad rad^2/sec/rad^2$$

$$N^{p\ r}_{\delta_a \delta_r}(s) = -107.464\,s(s + 0.226) \quad rad^2/sec/rad^2$$

$$N^{p\ \beta}_{\delta_a \delta_r}(s) = 0.993\,s(s + 108.83) \quad rad^2/sec/rad^2$$

$$N^{\beta\ a_y}_{\delta_a \delta_r}(s)\bigg|_{l_x} = -0.17(s + 1.4 \pm 0.96j)\,(s + 82.48) \quad ft\text{-}rad/sec^2/rad^2$$

$$N^{p\ y}_{\delta_a \delta_r}(s)\bigg|_{l_x} = 136.24\,s(s - 9.68)\,(s + 11.7) \quad ft\text{-}rad/sec^2/rad^2$$

If each term in the numerator and denominator of

$$G^{p}_{\delta_{a_p}}(s) \bigg|_{\substack{YAW \\ AUG}}$$

is expressed as

$$G_{\delta_a} = \frac{K_{\delta_a}}{D_{\delta_a}} \quad H_r = \frac{N_r}{D_r} \quad and \quad G^{p\ r}_{\delta_a \delta_r} = \frac{N^{p\ r}_{\delta_a \delta_r}}{\Delta}$$

where Δ is the unaugmented characteristic equation of the aircraft.

14.220

Then

$$
G_{\delta_a}^{p}\bigg|_{\substack{YAW\\AUG\\ARI}} = \frac{K_{\delta_a}}{D_{\delta_a}} \frac{N_{\delta_a}^{p} D_r D_{\delta_r} D_s D_a - K_r N_r K_{\delta_r} N_{\delta_a}^{p}{}_{\delta_r}^{r} D_s D_a + K_{ARI} K_{\delta_r} D_a D_s D_r N_{\delta_r}^{p}\bigg|_{a_y}}{\Delta D_r D_{\delta_r} D_s D_a - K_r N_r K_{\delta_r} D_s D_a N_{\delta_a}^{r} - N_s N_r N_a K_{\delta_r} N_{\delta_r}^{a_y}\bigg|_{ACCEL}}\bigg|_{ACCEL}
$$

$$
\frac{- N_s N_a D_r K_{\delta_r} N_{\delta_a}^{p}{}_{\delta_r}^{a_y}\bigg|_{ACCEL}}{\Delta D_r D_{\delta_r} D_s D_a - K_r N_r K_{\delta_r} D_s D_a N_{\delta_a}^{r} - N_s N_r N_a K_{\delta_r} N_{\delta_r}^{a_y}\bigg|_{ACCEL}}
$$

where

$$
G_{\delta_a} = \frac{20}{s+20} \qquad G_{\delta_r} = \frac{20}{s+20} \qquad K_r = 0.25
$$

$$
H_r = \frac{s}{s+1} \qquad H_s = \frac{0.003\,(s+0.3)}{s} \qquad K_{ARI} = -0.15
$$

$$
H_a = \frac{2}{s+2}
$$

A similar result for $G_{\delta_a}^{\beta}\bigg|_{\substack{YAW\\AUG\\ARI}}$ is obtained by merely replacing the numerator terms for the roll rate transfer functions with the appropriate numerator terms for the sideslip angle transfer functions, including the coupling numerators. The technique for factoring and combining polynomials using the root locus program, as discussed previously when deriving

$$
G_{\delta_r}^{a_y}(s)
$$

is applied successively to the numerator. The denominator is already known from the root locus analysis of the yaw stabilizer.

The transfer function with $K_{ARI} = 0$ for aileron inputs are (roll augmentation system disengaged)

$$G^p_{\delta_a}(s)\bigg|_{\substack{YAW\\AUG}} = \frac{20}{s + 20}\left[\frac{17.6\,s(s + 0.1)\,(s + 3.864)\,(s + 0.37 \pm 2.07j)}{(s - 0.0141)\,(s + .584 \pm 2.16j)\,(s + 0.111)\,(s + 1.14)}\right.$$

$$\left.\frac{(s + 18.11)\,(s + 1)}{(s + 2.31)\,(s + 3.33)\,(s + 18.5)}\right]$$

$$G^\beta_{\delta_a}(s)\bigg|_{\substack{YAW\\AUG}} = \frac{20}{s + 20}\left[\frac{-0.00655\,(s + 0.0603)\,(s + 1.98)\,(s + 0.524 \pm 0.194j)}{(s - 0.0141)\,(s + 0.584 \pm 2.16j)\,(s + 0.111)\,(s + 1.14)}\right.$$

$$\left.\frac{(s - 7.255)\,(s + 25.47 \pm 13.06j)}{(s + 2.31)\,(s + 3.33)\,(s + 18.5)}\right]$$

and with the selected aileron-rudder interconnect gain of $K_{ARI} = +0.15$ are (roll augmentation system disengaged)

$$G^p_{\delta_a}(s)\bigg|_{\substack{YAW\\AUG\\ARI}} = \frac{20}{s + 20}\left[\frac{17.6\,s(s + 0.086)\,(s + 1)\,(s + 0.468 \pm 2.315j)}{(s + 0.0141)\,(s + 0.584 \pm 2.16j)\,(s + 0.111)\,(s + 1.14)}\right.$$

$$\left.\frac{(s + 3.824)\,(s + 16.73)}{(s + 2.31)\,(s + 3.33)\,(s + 18.5)}\right]$$

$$G^\beta_{\delta_a}(s)\bigg|_{\substack{YAW\\AUG\\ARI}} = \frac{20}{s + 20}\left[\frac{-0.00655\,(s + 0.484)\,(s + 1.97)\,(s + 1.0 \pm 0.583j)}{(s - 0.0141)\,(s + 0.584 \pm 2.16j)\,(s + 0.111)\,(s + 1.14)}\right.$$

$$\left.\frac{(s - 0.53)\,(s + 33.94 \pm 45.99j)}{(s + 2.31)\,(s + 3.33)\,(s + 18.5)}\right]$$

Figures 14.174 and 14.175 show the effect of the aileron-rudder interconnect on the roll and sideslip response characteristics of the aircraft due to an aileron deflection. Notice that the roll rate performance is improved with the aileron-rudder interconnect included in the system. The improved roll performance is due to the action of the aileron-rudder

interconnect, which provides proverse yaw when the pilot commands an aileron deflection. Without the aileron-rudder interconnect, the roll rate response slows due to the adverse yaw which develops.
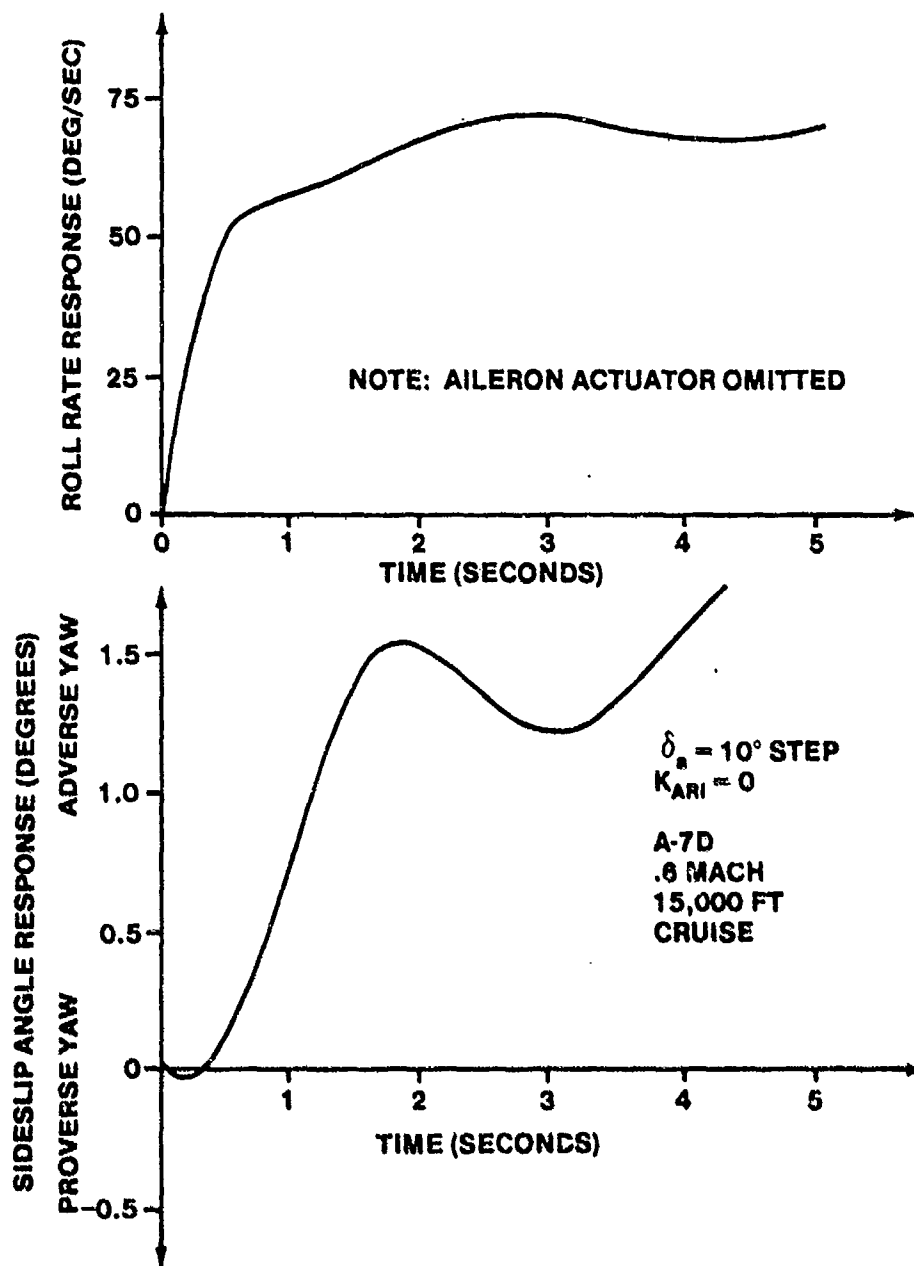
FIGURE 14.174. A-7D RESPONSE DUE TO AN AILERON INPUT, STAB ON, NO INTERCONNECT
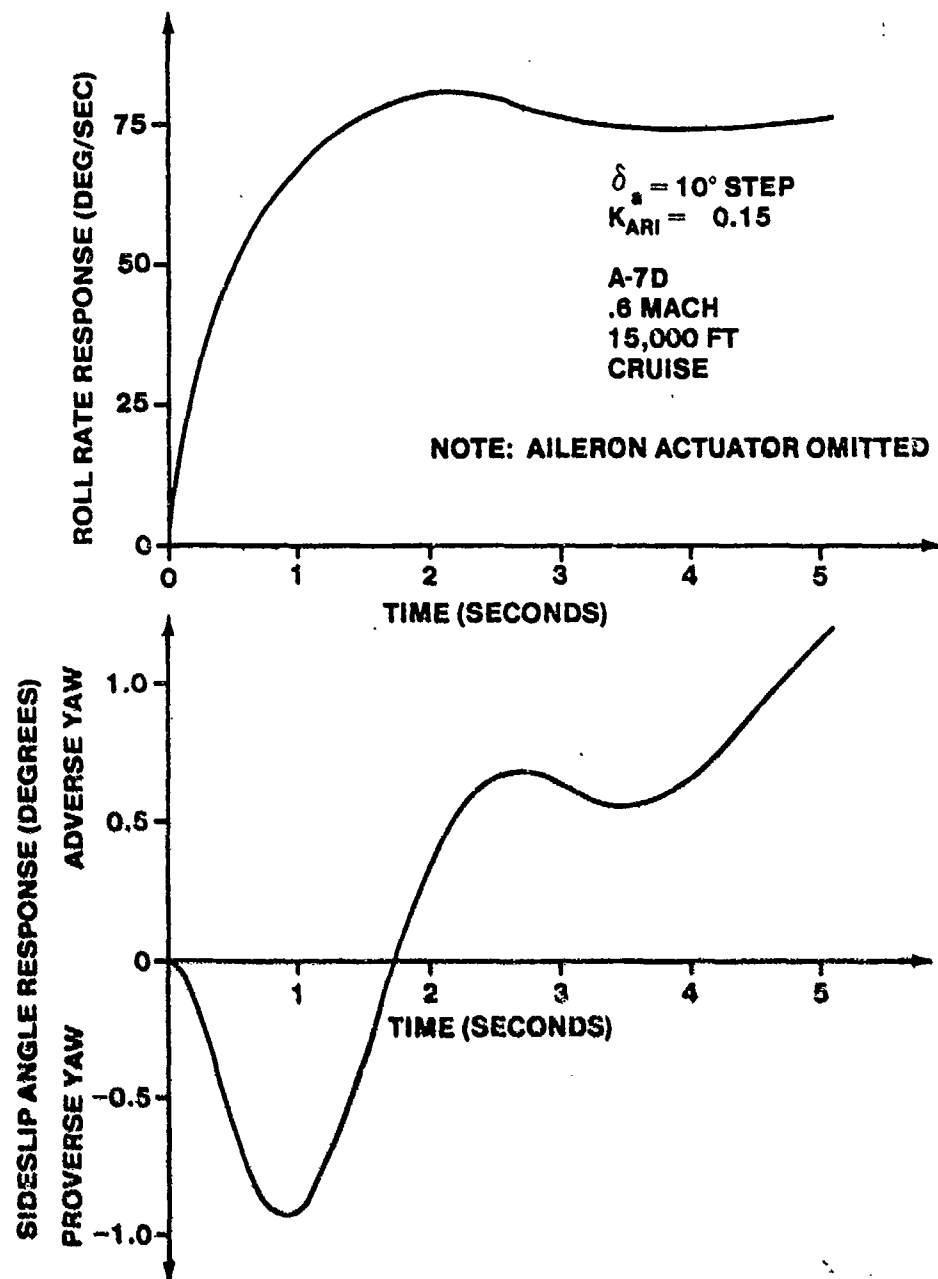
FIGURE 14.175.   A-7D RESPONSE DUE TO AN AILERON INPUT,
STAB ON, WITH INTERCONNECT

How the effect of the roll centered augmentation system can be determined. The block diagram of Figure 14.176 is used to find the root locus for

$$GH_{p\ loop} = \frac{35.2s\ (s + 0.086)\ (s + 1)\ (s + 0.468 \pm 2.315j)\ (s + 3.824)}{(s - 0.0141)\ (s + 0.584 \pm 2.16j)\ (s + 0.111)\ (s + 1.14)\ (s + 2.31)}$$

$$\times\ \frac{(s + 16.73)}{(s + 3.33)\ (s + 18.5)\ (s + 20)}$$

as the roll rate system gain varies (Figure 14.177), which yields the closed loop transfer function, including the effect of the prefilters on the pilot input, as

$$G^p_{\delta_p}(s)\bigg|_{AUG} = \left[\frac{224\ s(s + 0.086)\ (s + 1)\ (s + 0.468 \pm 2.315j)\ (s + 3.824)}{(s - 0.0087)\ (s + 0.1)\ (s + 0.503 \pm 2.19j)\ (s + 1.05)}\right.$$

$$\left.\frac{(s + 16.73)}{(s + 3.03)\ (s + 3.91 \pm 0.89j)\ (s + 18.28 \pm 2.07j)\ (s + 10)}\right]$$
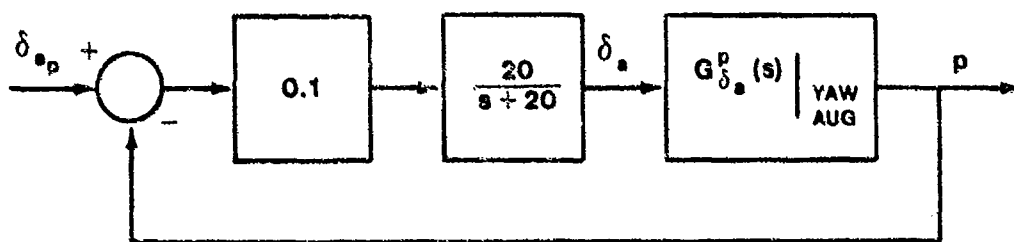
FIGURE 14.176.   A-7D ROLL CONTROL AUGMENTATION SYSTEM

The roll response of the aircraft is complex due to the large number of poles which influence the response. A look at the proximity of the various poles to the roll rate zeros provides a rough guess at the roll mode time constant for this flight condition of

$$\tau_r = \frac{1}{4} = 0.25 \text{ seconds}$$

A more accurate estimate of the roll mode time constant can be obtained from the roll rate time response. The effective roll mode time constant — that is, the roll mode time constant seen by the pilot -- must include the effect of the prefilters.
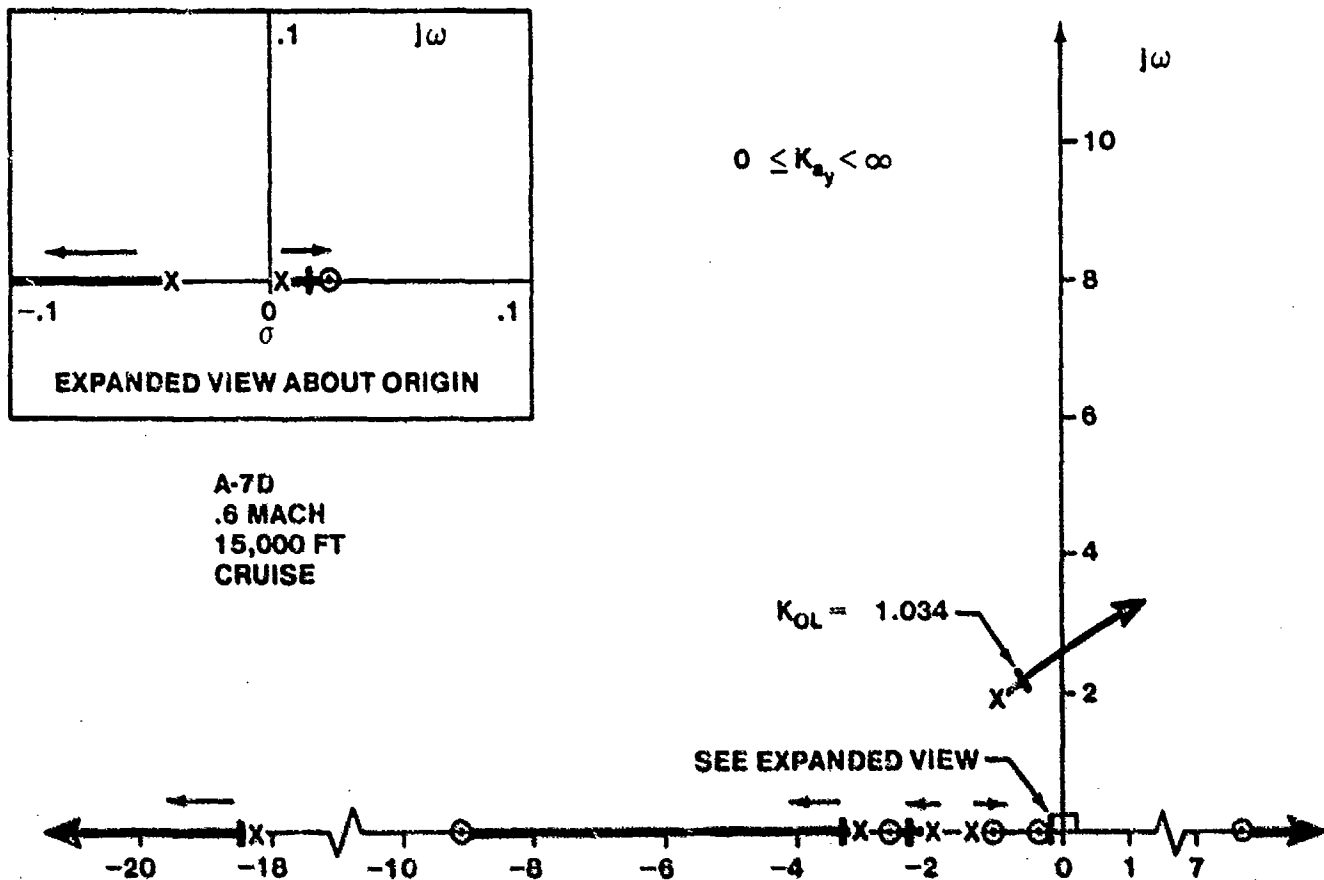
FIGURE 14.177. ROOT LOCUS PLOT OF A-7D ROLL RATE COMMAND SYSTEM

The roll rate and sideslip responses of the aircraft due to a step pilot lateral stick force are shown in Figure 14.178. The prefilters act to increase the response time of the aircraft roll rate. This should improve the pilots' opinion of the aircraft roll response by making it less abrupt. The prefilters introduce an effective time delay on the initial roll rate response. If excessive, the aircraft handling qualities will be degraded. The directional axis, including the effects of the aileron-rudder intercon·:·~·. is effective in coordinating the roll quite well.
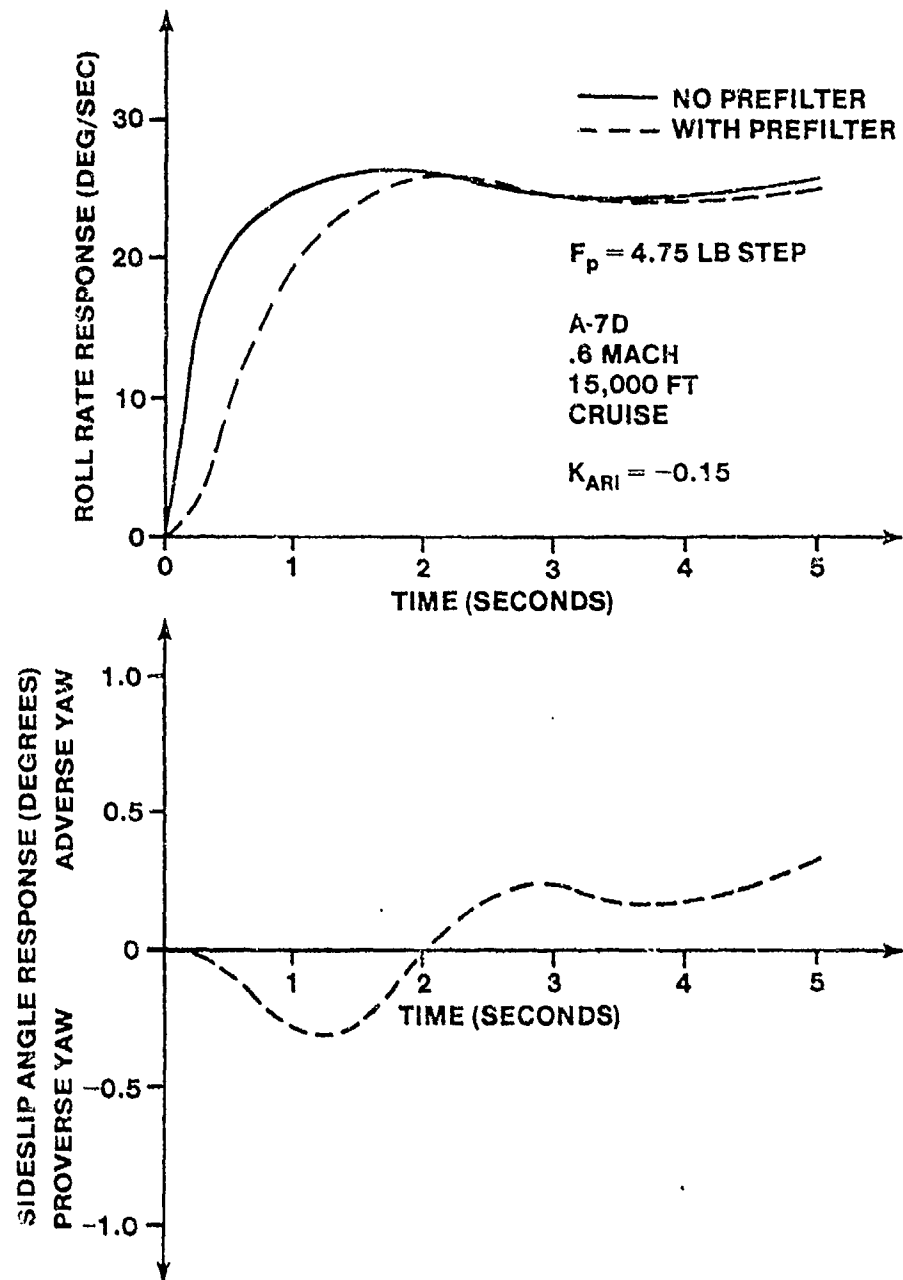
FIGURE 14.178. A-7D RESPONSE TO PILOT ROLL COMMAND,
YAW STAB AND ROLL CAS ON

14.4.2.8 Longitudinal Axis with Two Aerodynamic Control Surfaces. When the F-16 longitudinal flight control system (Paragraph 14.4.1.3) is modified to include the effects of the leading edge deflection, the block diagram of Figure 14.142 is changed to that of Figure 14.152. The angle of attack is fed back to the leading edge flap actuator through a lead compensator and a gain.

The aircraft lift coefficient may increase or decrease slightly as a result of the leading edge flap deflection, with total lift being reduced at very low angles of attack. At moderate to high angles of attack, the aircraft lift coefficient is increased. The stall angle of attack is higher with the leading edge flaps deflected. The airflow over the wing stays attached to the wing surface to a higher angle of attack with the leading edge flaps deployed, postponing separation buffet onset (stall warning). Leading edge flaps also aid directional stability at high angles of attack. While the pitching moment coefficient is reduced (slightly more negative) with the leading edge flaps deflected at low to moderate angles of attack, a noticeable positive pitching moment contribution occurs at high angles of attack, reducing the static and dynamic stability of the aircraft.

Modifying the aircraft equations of motion to account for the leading edge flaps (after obtaining leading edge flap stability derivative data from lift and moment coefficient curves for 0.6 Mach) yields

$$
\begin{bmatrix}
s + 0.0177 & 0.0269 & 0.048 \\
0.095 & s + 1.479 & -s \\
0 & 0.221\,s - 0.906 & s^2 + 0.752\,s
\end{bmatrix}
\begin{bmatrix}
u(s) \\
\alpha(s) \\
\theta(s)
\end{bmatrix}
=
$$

$$
\begin{bmatrix}
0.022 & 0 \\
-0.203 & -0.052 \\
-21.544 & -2.819
\end{bmatrix}
\cdot
\begin{bmatrix}
\delta_e(s) \\
\delta_{LEF}(s)
\end{bmatrix}
$$

The leading edge flaps provide a small positive contribution to aircraft lift, but also provide a net nose down pitching moment increment at the 1 'g' flight condition of interest.

In a similar manner to the coupled analysis conducted for the lateral-directional axis, the first step in analyzing the F-16 longitudinal axis is to assume that $\delta_e = 0$ and perform a root locus analysis of the aircraft leading edge flap loop (see Figure 14.152). The aircraft transfer function is

$$G^{\alpha}_{\delta_{LEF}}(s) = \frac{0.052\ (s + 0.009 \pm 0.067j)\ (s + 54.96)}{(s - 0.087)\ (s + 2.373)\ (s + 0.098 \pm 0.104j)}\ \text{deg/deg}$$

The open loop transfer function for the leading edge flap loop is

$$GH_{\delta_{LEF}} = \frac{1.228\ (s + 3.625)\ (s + 0.009 \pm 0.067j)\ (s + 54.96)}{(s - 0.087)(s + 2.373)(s + 0.098 \pm 0.104j)(s + 7.38)(s + 7.25)}$$

The root locus is plotted in Figure 14.178 as $K_{\alpha_{\delta_{LEF}}}$ varies. Notice that the leading edge flaps effectively stabilize the aircraft.

EXPANDED VIEW ABOUT ORIGIN

$0 \leq K\alpha_{\delta_{LEF}} < +\infty$
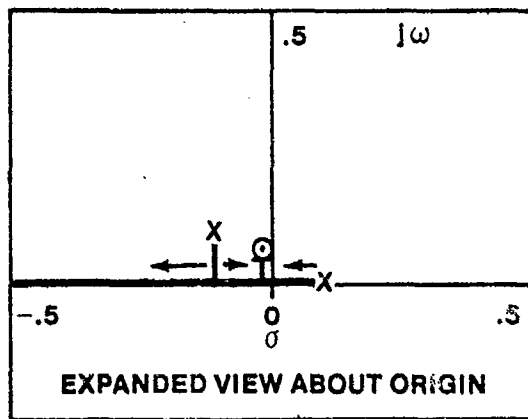
F-16
.6 MACH
SEA LEVEL
CRUISE

$K_{\alpha_{\delta_{LEF}}} = 1.6$

SEE EXP/
VIEW
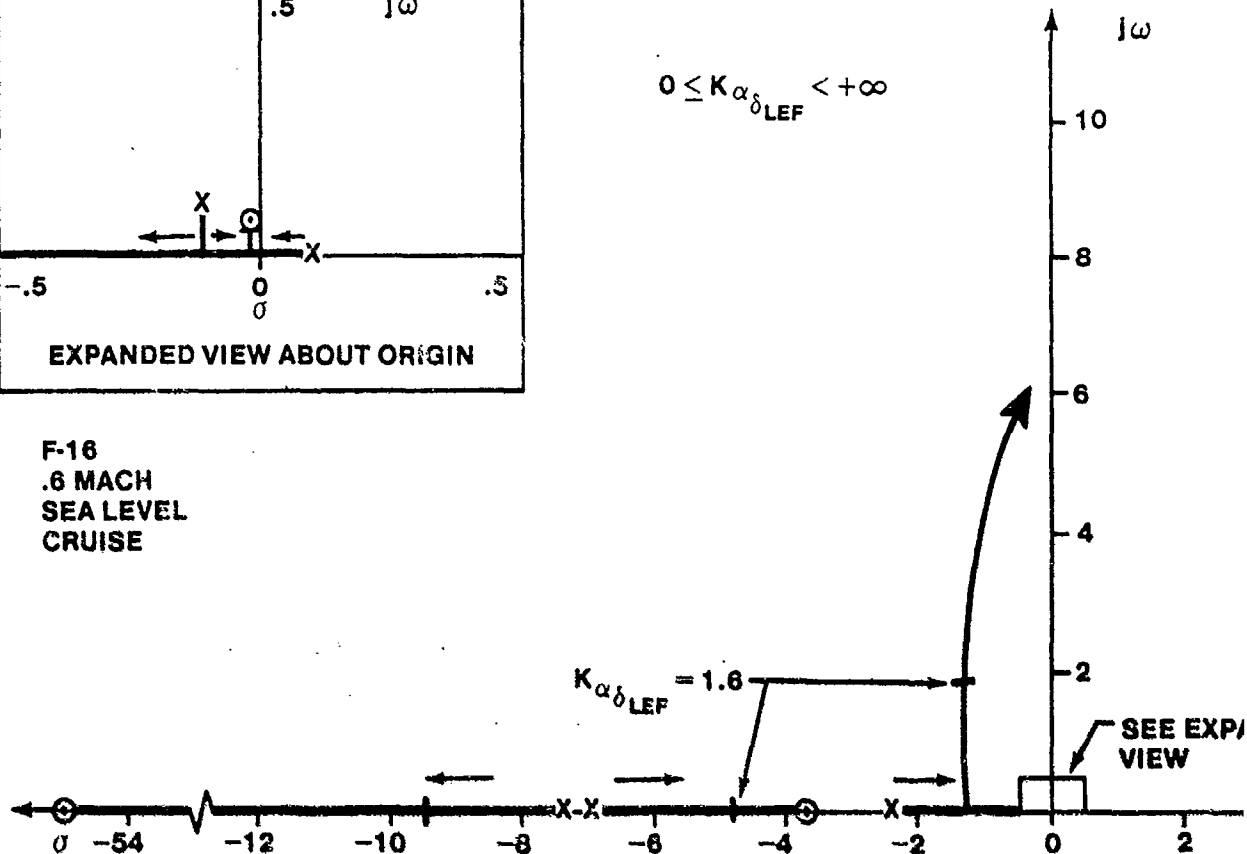
FIGURE 14.179. ROOT LOCUS PLOT OF F-16 LEADING EDGE FLAP CONTROL SYSTEM

The aircraft transfer functions

$$G^{\alpha}_{\delta_e}(s), \quad G^{q}_{\delta_e}(s) \quad \text{and} \quad G^{n_z}_{\delta_e}(s)$$

must be modified to account for the simultaneous leading edge flap deflections. For the angle of attack transfer function

$$\alpha = G^{\alpha}_{\delta_e}\delta_e + G^{\alpha}_{\delta_{LEF}}\delta_{LEF}.$$

where (from Figure 14.152)

$$\delta_{LEF} = K_{\alpha_{\delta_{LEF}}}H_{c_{\delta_{LEF}}}G_{\delta_{LEF}}\alpha$$

14.230

where

$$K_{\alpha_{\delta_{LEF}}} = 1.6$$

$$H_{c_{\delta_{LEF}}} = \frac{2(s + 3.625)}{s + 7.25}$$

$$G_{\delta_{LEF}} = \frac{7.38}{s + 7.38}$$

so that

$$\alpha = G^{\alpha}_{\delta_e} \delta_e + G^{\alpha}_{\delta_{LEF}} K_{\delta_{LEF}} H_{\delta_{LEF}} G_{\delta_{LEF}} \alpha$$

yielding

$$\frac{\alpha}{\delta_e} = \frac{G^{\alpha}_{\delta_e}}{1 - K_{\alpha_{\delta_{LEF}}} G_{\delta_{LEF}} H_{c_{\delta_{LEF}}} G^{\alpha}_{\delta_{LEF}}}$$

or, after simplifying

$$\frac{\alpha}{\delta_e} = \frac{N^{\alpha}_{\delta_e} D_{c_{\delta_{LEF}}} D_{\delta_{LEF}}}{\Delta D_{\delta_{LEF}} D_{c_{\delta_{LEF}}} - K_{\alpha_{\delta_{LEF}}} N^{\alpha}_{\delta_{LEF}} N_{c_{\delta_{LEF}}} K_{\delta_{LEF}}}$$

The aircraft angle of attack due to an elevator deflection transfer function includes two additional zeros (the poles of the leading edge flap actuator and lead compensator) as well as the closed loop poles obtained from the leading edge flap system analysis, yielding

$$G^{\alpha}_{\delta_e}(s)\Big|_{\delta_{LEF} \, CL} = \frac{0.203 \, (s + 0.0087 \pm 0.067j) \, (s + 7.25) \, (s + 7.38)}{(s + 0.0083 \pm 0.058j) \, (s + 1.39 \pm 1.92j) \, (s + 4.8) \, (s + 9.53)}$$

The pitch rate transfer function for the aircraft is found by writing the equations

$$q = G^q_{\delta_e} \delta_e + G^q_{\delta_{LEF}} \delta_{LEF}$$

14.231

$$\alpha = G_{\delta_e} \delta_e + G_{\delta_{LEF}} \delta_{LEF}$$

substituting in the expression for δ_{LEF} and writing the matrix equation

$$\begin{bmatrix} 1 - G^{\alpha}_{\delta_{LEF}} K_{\alpha_{\delta_{LEF}}} G_{\delta_{LEF}} H_{c_{\delta_{LEF}}} & 0 \\ - G^{q}_{\delta_{LEF}} K_{\delta_{LEF}} G_{\delta_{LEF}} H_{c\delta_{LEF}} & 1 \end{bmatrix} \begin{bmatrix} \alpha \\ q \end{bmatrix} = \begin{bmatrix} G^{\alpha}_{\delta_e} \\ G^{q}_{\delta_e} \end{bmatrix} \delta_e$$

yields

$$G^{q}_{\delta_e} \Big|_{\delta_{LEF} CL} = \frac{G^{q}_{\delta_e} - K_{\alpha_{\delta_{LEF}}} G_{\delta_{LEF}} H_{c_{\delta_{LEF}}} sG^{\beta \alpha}_{\delta_e \delta_{LEF}}}{\Delta_{\delta_{LEF} CL}}$$

where $\Delta_{\delta_{LEF}CL}$ are the roots of the leading edge flap system augmented aircraft, already obtained.

Simplifying yields

$$G^{q}_{\delta_e} \Big|_{\delta_{LEF} CL} = \frac{N^{q}_{\delta_d} D_{\delta_{LEF}} D_{c_{\delta_{LEF}}} - K_{\alpha_{\delta_{LEF}}} K_{\delta_{LEF}} N_{c_{\delta_{LEF}}} sN^{\theta \alpha}_{\delta_e \delta_{LEF}}}{\Delta_{\delta_{LEF} CL}}$$

Similarly

$$G^{n_z}_{\delta_e} \Big|_{\delta_{LEF} CL} = \frac{N^{n_z}_{\delta_e} D_{c_{\delta_{LEF}}} D_{\delta_{LEF}} - K_{\alpha_{\delta_{LEF}}} K_{\delta_{LEF}} N_{c_{\delta_{LEF}}} N^{n_z \alpha}_{\delta_e \delta_{LEF}}}{\Delta_{\delta_{LEF} CL}}$$

Since $n_z = \dfrac{1}{(57.3)(32.2)} [U_0 (\dot{\alpha} - q) - \ell_x \dot{q}]$ g's/deg and

$$N^{n_z \alpha}_{\delta_e \delta_{LEF}} = N^{n_z}_{\delta_e} N^{\alpha}_{\delta_{LEF}} - N^{\alpha}_{\delta_e} N^{n_z}_{\delta_{LEF}}$$

14.232

$$N_{\delta_e}^{n_z}\,\delta_{LEF}^{\alpha} = \frac{\ell_x}{(32.2)\,(57.3)}\ s\ s + \frac{U_0}{\ell_x}\ N_{\delta_e}^{\theta}\,\delta_{LEF}^{\alpha} = 0.0042\ s(s + 0.007)\ (s + 45.44)$$

from the aircraft equations of motion since the normal accelerometer is lo-located at $\ell_x = 14$ feet.

The aircraft pitch rate and normal acceleration transfer functions become

$$G_{\delta_e}^{q}\bigg|_{\delta_{LEF}\ CL} = \frac{21.516\ (s + 0.018)\ (s + 1.6)\ (s + 7.26 \pm 1.033j)}{(s + 0.0083 \pm 0.058j)\ (s + 1.39 \pm 1.92j)\ (s + 4.8)\ (s + 9.53)}$$

$$G_{\delta_e}^{n_z}\bigg|_{\delta_{LEF}\ CL} = \frac{0.0889\ s(s + 0.0155)\ (s + 6.36)\ (s + 8.46)\ (s + 1.07 \pm 11.594j)}{(s + 0.0083 \pm 0.058j)\ (s + 1.39 \pm 1.92j)\ (s + 4.8)\ (s + 9.53)}$$

The effects of the leading edge flap system are accounted for in the

$$G_{\delta_e}^{\alpha}\bigg|_{\delta_{LEF}\ CL} \qquad G_{\delta_e}^{q}\bigg|_{\delta_{LEF}\ CL} \qquad \text{and} \qquad G_{\delta_e}^{n_z}\bigg|_{\delta_{LEF}\ CL}$$

transfer functions. Now, all the modified aircraft transfer functions are available to repeat the analysis of Paragraph 14.4.1.3, the closed loop transfer function for the aircraft load factor response becomes

$$G_{n_{z_c}}^{n_z}\bigg|_{\substack{FULL \\ AUG}} = \frac{2.055\ (s + 0.0155)\ (s + 1)\ (s + 5)\ (s + 6.36)\ (s + 8.46)\ (s + 10)}{(s + 0.0164)\ (s + 0.58)\ (s + 1.7)\ (s + 10.24)\ (s + 5.87)\ (s + 7.97)}$$
$$\times \frac{(s + 1.07 \pm 11.594j)\ (s + 12)}{(s + 4.29 \pm 4.022j)\ (s + 15.77 \pm 17.55j)}$$

and the final load factor is

$$\lim_{s \to 0}\left[G_{n_{z_c}}^{n_z}\bigg|_{\substack{FULL \\ AUG}} \right] = 0.95\ \text{g's}$$

which is close to one, as expected (the error is due to round-off errors in the analysis introduced by the root locus factoring scheme). Notice that the dominant poles at (s + 0.58) and (s + 1.7) are nearly identical to the dominant poles at (s + 0.637) and (s + 1.74) obtained in Paragraph 14.4.1.3. This indicates that the aircraft response with the leading edge flaps is nearly the same as with the flaps locked up (for the low angle of attack flight condition analyzed). This would not be true at high angles of attack, where the leading edge flaps would provide improved lift characteristics and a pronounced destabilizing pitching moment.

14.4.3 Advanced Flight Control System Analysis Programs

The analytical techniques discussed in this chapter, are often laborious, especially if a large number of flight conditions are to be considered. Fortunately, a sophisticated flight control system analysis program is available to greatly simplify the process. The EASY program available at the Flight Test Center uses matrix techniques and a state space formulation of the aircraft equations of motion (See References 29, 30, and 31 for discussions of state space techniques) to allow the linearized aircraft model and the complete linearized control system to be programmed on the computer. Test inputs can be applied to the flight control system model. Several aircraft parameters and control surface motions can be recorded simultaneously. Bode and root locus plots of the various aircraft transfer functions, as specified by the user, are also easily obtained. Reference 28 provides further information.

14.5 ANALYSIS OF A COMPLEX FLIGHT CONTROL SYSTEM

Effective flight control testing depends on a thorough understanding of the flight control operation. The current trend in aircraft design is to rely ever more heavily on the flight control system to provide adequate flying qualities and apparent stability. Future designs use forward swept wings, canards, and decoupling of rotational and translational motions. Some aircraft do not use mechanical linkages between the pilot controls and the aerodynamic surfaces, relying on a totally electric flight control system. Analog and digital techniques are being used, with digital control becoming

more emphasized due to its inherent flexibility. Signal encoding and decoding methods are used to send control surface commands via redundant electrical or fiber optic cables. Fault tolerant techniques are being used to increase aircraft survivability.

Aircraft subsystems must be understood in terms of their effects on the flight control system. Electrical system deficiencies have caused out-of-control maneuvers in the A-10 and F-16 aircraft which have resulted in lost aircraft. Hydraulic system failures and sensor failures must also be investigated to determine their effects.

This section provides the test pilot and flight test engineer a background in flight control system simplification and analysis. The F-16 flight control system, as configured in 1979, is analyzed qualitatively. Several potential problem areas of interest for the flight test plan are discussed. This does not imply that problem areas exist within the F-16 flight control system, but, rather, is done to demonstrate the kinds of problems which should be considered during the analysis of a flight control system block diagram. Autopilot functions are not addressed. The sign convention in this analysis is that of the contactor's. You must be able to work with different sign conventions to fully understand flight control digrams from various sources.

192
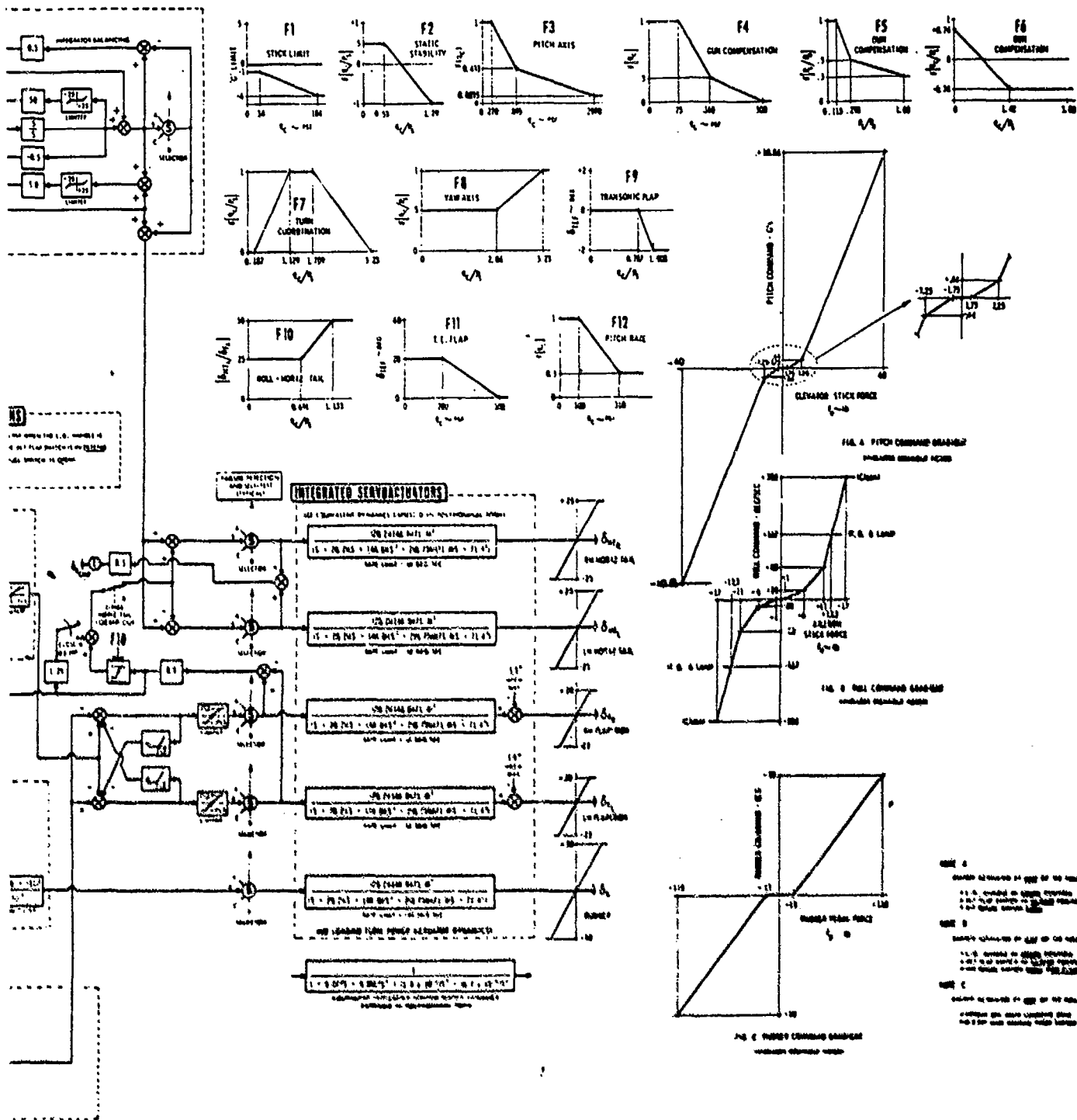
FIGURE 14.180. FLIGHT CONTROL SYSTEM BLOCK DIAGRAM

14.5.1 Longitudinal Axis Description

The longitudinal axis uses symmetrically deflected horizontal tail surfaces to provide pitch control.

14.5.1.1 Pilot Input and Load Factor Limiting System. Figure 14.181 shows the block diagram of the pilot load factor command path and the load factor limiter. The switches in the diagram are shown in their normal gear up flight positions.

The pilot stick forces are measured with strain gauges, stripped from the alternating current carrier frequency by the demodulator and converted to g command signals by the pitch command gradient. This gradient provides a +1.75 lb deadband to desensitize the stick to spurious small amplitude pilot inputs. A parabolic stick force gradient is used to desensitize the aircraft to low stick force inputs (high stick force gradient of 12.5 lbs/g) for small inputs, but provides for decreased stick force per g during maneuvering (3.12 lb/g). The pilot commands incremental load factors with 1g as the reference. The pilot command is added to the pitch trim command and sent to the load factor limiter.

The g limiter system uses two paths to determine the maximum and minimum g commands. Positive signals are limited to a maximum of 8 incremental g's for all flight conditions. Negative signals are limited based on the aircraft configuration. A pilot selectable switch provides an override capability to provide negative g command, subject only to the pitch command gradient limitations. With the gear up, negative g limiting is based on dynamic pressure and varies between -1 and -4 incremental g's (0 to -3 g's). With the gear down, the alternate flaps extended, or the air refueling door open, the negative g signal is limited to -4. It is important to note here, and will become apparent later in the discussion, that the g command input is really a g command or a blended g-alpha (angle of attack) command input, and the aircraft angle of attack and configuration determines which approach is in effect. The limiters operate on the command signal in effect.

The limited command signal normally has a unity gain providing normal pitch command gradient responses. When the weight is on the main gear, a higher gain is provided to effectively reduce the stick force required to operate the aircraft. When the angle of attack is very high and the pilot selects override, the higher gain and lack of negative command signal limiting

14.237

FIGURE 14.181.   BLOCK DIAGRAM OF F-16 PILOT COMMAND PATH FOR THE LONGITUDINAL AXIS

provides the pilot more elevator command authority for recovering from the deep stall mode of the aircraft. A prefilter (lag filter) is provided to smooth out the aircraft response. These are often provided in full authority systems to improve the handling qualities of an aircraft which is too responsive to pilot inputs. The fixed stick configuration of the F-16 also requires the prefilter to prevent abrupt pilot commands.

A linearized block diagram of this portion of the flight control system is shown in Figure 14.182. All limiters are neglected, the pitch command gradient is removed, the command signal is the pilot g command, the demodulator is omitted since it possesses a pole which is very remote from the origin, and all switches are assumed to be in their normal flight positions. The pitch trim signal is assumed to be zero.
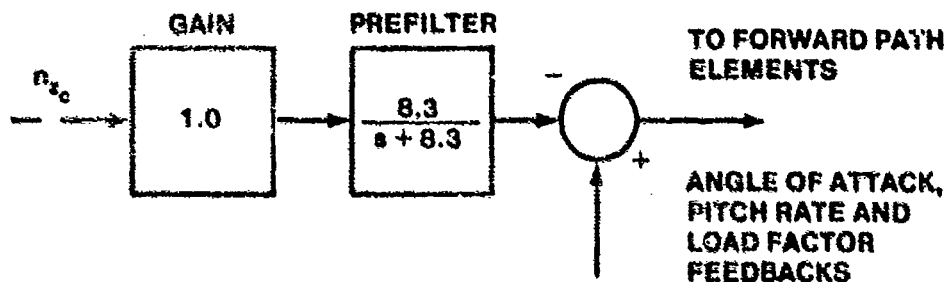
FIGURE 14.182. LINEARIZED PILOT COMMAND PATH

Some issues of concern are:

1. The prefilter, pitch command gradient, and deadband all have similar effects on the pilot's opinion of an aircraft which is too abrupt in its response. Deadbands, lag prefilters, and high stick force gradients tend to smooth out the response by slowing it somewhat (lag effect). The proper combination of these effects is important in the pilot's ability to perform tight tracking tasks. When the stick force gradient is reduced to 7.25 lbs, the abruptness of response increases and pilot opinion is of concern since additional lag is not provided to compensate for the increased pitch sensitivity. Also, operation near the knee in the gradient is likely to produce poor flying qualities. Too much lag in the command path can increase pilot-induced oscillation susceptibility.

2. The effect of the weight on wheels switch and the large decrease in pitch command signal magnitude just after liftoff is of concern. Pitch transients and pilot compensation must be investigated.

3. The effect of the override switch, if inadvertently left in the override position, should be investigated. For positive g maneuvering, it should have no effect. However, a negative g overstress could occur, although probably quite remote since -4 incremental g's is not likely to be commanded. Other implications arise concerning the static stability of the aircraft with the manual pitch switch in the override position, as will be discussed later.

4. The effect of changing the negative pitch command signal limiting when the gear are lowered, would probably be minimal since this would probably occur in relatively level, positive g flight.

14.5.1.2 Angle of Attack Feedback Paths. Angle of attack feedback is used for the following purposes:

1. To provide longitudinal static stability at subsonic speeds

2. To provide angle of attack limiting

3. To provide apparent longitudinal static stability (speed stability) to the pilot in the power approach configuration, during air refueling, and when flying at high angles of attack in the cruise configuration

4. To provide roll rate limiting in conjunction with dynamic pressure and elevator deflection inputs

5. To provide limiting on pilot rudder command authority in conjunction with roll rate inputs

6. To allow increased pitch command authority when the angle of attack exceeds 29° and the manual pitch switch is placed in the override position (see Section 4.1.1) as well as to activate other departure prevention features

7. To provide computed beta-dot feedback for the directional axis in conjunction with yaw rate, roll rate, and lateral acceleration feedbacks

8. To provide elevator saturation minimization in the pitch axis elevator deflection command

14.5.1.2.1 <u>Longitudinal Static Stability</u>. The angle of attack feedback path which provides longitudinal static stability is shown in Figure 14.183. True angle of attack (sensed angle of attack from several redundant sources compensated for upwash effects) is limited due to sensor limitations. Angle of attack feedback is eliminated from the flight control law when weight is on the main landing gear or at high angles of attack with the manual pitch switch in the override position. A low pass filter is employed to eliminate high frequency noise inputs. This filter adds up to 45° lag to the signal (signals at higher frequencies than 10 radians per second are attenuated, but do lag more than 45°). The signal goes through gain F2 which is a function of dynamic pressure divided by static pressure. At low Mach, the feedback stabilizes the aerodynamically unstable aircraft and creates distinct phugoid and short period roots so that the aircraft reacts like a conventional aircraft despite the aft center of gravity (see Paragraph 14.2). At high dynamic pressures, the center of lift moves aft of the center of gravity, providing a statically stable aircraft. At a ratio of dynamic to static pressure of 0.95, the sign of the angle of attack feedback changes. This occurs at about 1.16 Mach. In supersonic flight, the angle of attack feedback acts to reduce the short period natural frequency to prevent too much static stability.
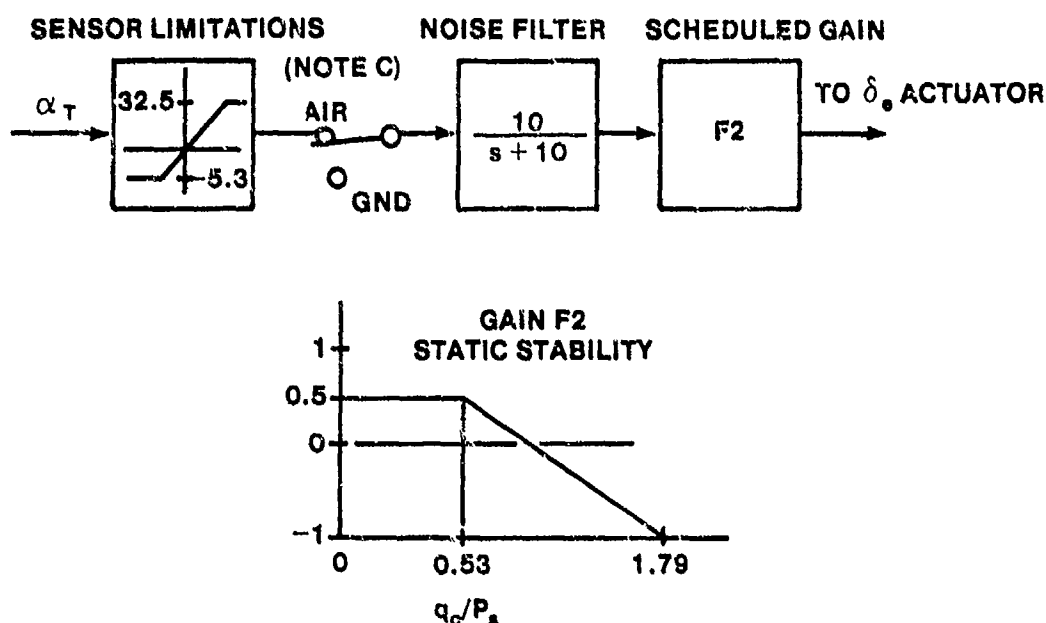
FIGURE 14.183. STATIC STABILITY CONTROL SYSTEM

The aircraft could be flown subsonically without this loop present, but would require close pilot attention. Also, the implementation of autopilot features requires a statically stable aircraft (no right half s-plane poles).

Areas of concern are:

1. Since lag is introduced into the angle of attack signal by the low-pass filter, what is the effect of rapid angle of attack changes on the low static stability (large inputs)?

2. Does gain F2 provide adequate stability margin throughout the flight envelope?

3. What is the effect of suddenly providing angle of attack feedback at liftoff or the effect of angle of attack control law changes during touch and go landings?

14.5.1.2.2 Angle of Attack Limiting. Two separate paths are provided for angle of attack limiting. Figure 14.184 shows the combined angle of attack limiting system.

True angle of attack is fed back only after the aircraft becomes airborne. This is important since angle of attack vanes are subject to wind effects with the aircraft at low speed on the ground. Undesirable elevator response to wind gusts on the ground is eliminated. Angle of attack feedback is also eliminated during very high angle of attack flight if the pilot selects override with the manual pitch switch. Above 32.5° or below -5.3° angle of attack, the angle of attack feedback is fixed at a constant value due to sensor limitations.

The noise filtered angle of attack signal is compared with two bias signals and, if greater than the value of the bias, is compared with the pitch command signal.

The first bias uses pitch rate and preset angle of attack values. The pitch rate signal from the rate gyro is demodulated (filtering out the AC carrier frequency). The pitch rate signal goes through a washout filter (high pass which allows high frequency transient signals to pass but attenuates low frequency and steady state signals. This is done in the context of the angle of attack limiting system so that overshoots of the limiter values are minimized during rapid pitch maneuvers, but steady state pitch rates do not lower the angle of attack attainable.

NOTE A:
SWITCH ACTIVATED BY ANY OF
THE FOLLOWING METHODS:
1. LANDING GEAR HANDLE IN DOWN
   POSITION
2. ALTERNATE FLAP SWITCH IN EXTEND
   POSITION
3. AIR REFUEL SWITCH OPEN

NOTE C:
SWITCH ACTIVATED BY ANY OF THE FOLLOWING
METHODS:
1. WEIGHT ON MAIN LANDING GEAR
2. ALPHA GREATER THAN 29 DEGREES
   AND MANUAL PITCH SWITCH IN OVERRIDE
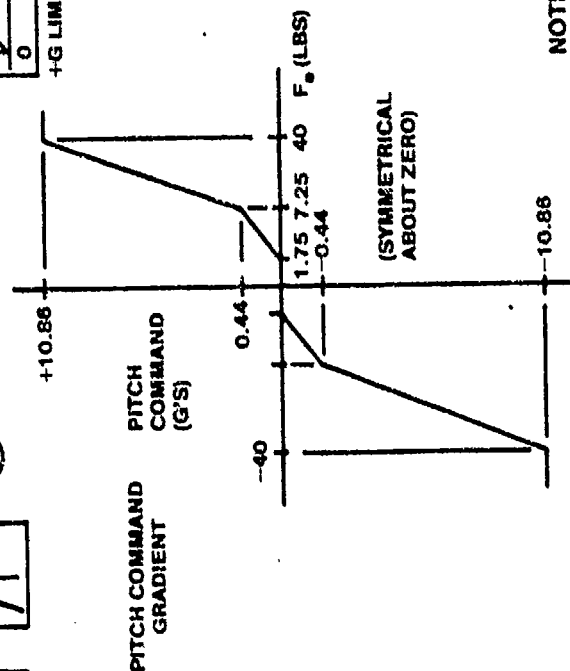
NOTE A & C
same as on Fig 14.180
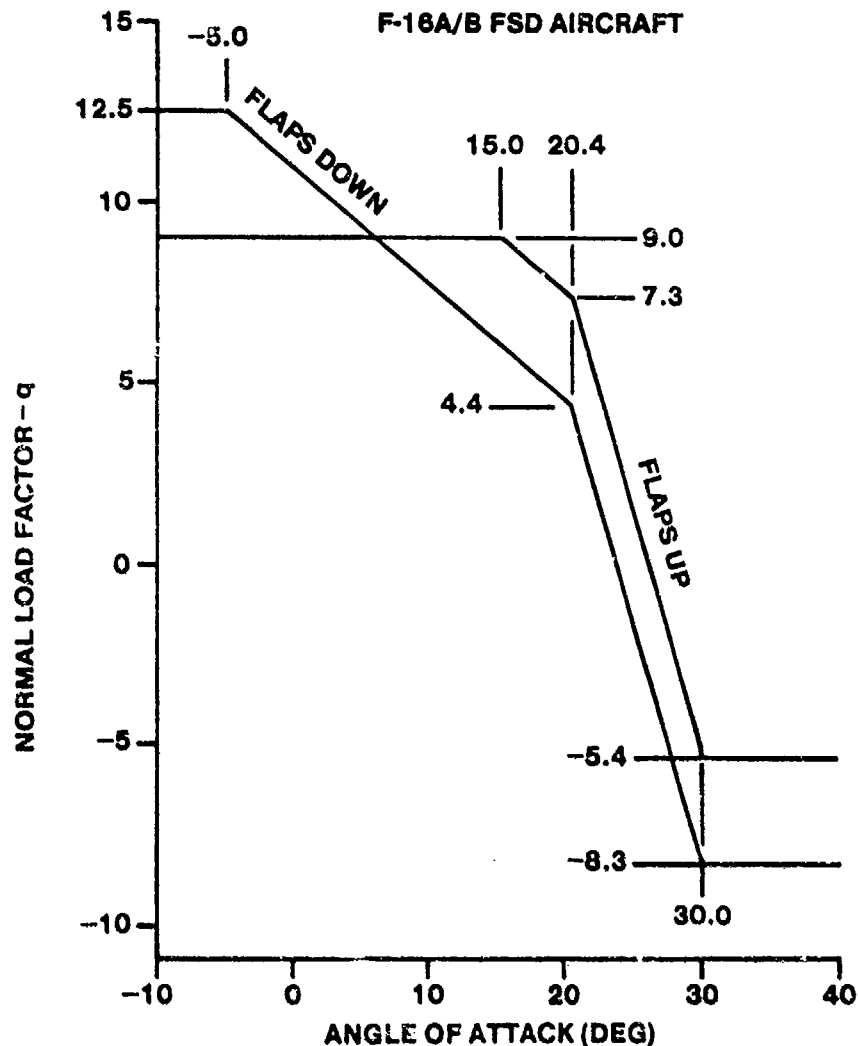
FIGURE 14. 184(B). ANGLE OF ATTACK LIMITER BOUNDARIES

During rapid pitch maneuvers, the effective angle of attack limit is lowered and as the pitch rate transients die out, the limit is again increased to its steady state value. Pitch rate passes through two gains, one a function of the dynamic pressure. It is then ready for comparison with the angle of attack signal. Two biases, one set at 6° angle of attack and one at 9° angle of attack, determine where angle of attack limiting begins. Neither bias signal is provided to the system with the gear down and the weight on the main gear. This avoids a biased tail deflection. The 6° bias only is used when airborne in the power approach configuration. Both biases are used during

up-and-away flight in the cruise configuration. The lag filters act to blend the bias into the system once the appropriate switch is closed. The 6° bias is blended into the system 0.3 sec after liftoff and the 9° bias is blended into the system over a 24 sec period. The signal equation can be determined from the filter transfer function by treating the bias as a step input. When the switch closes, the Laplace output of the filter is

$$B(s) = \frac{6}{s} \; \frac{10}{s + 10}$$

for the 6° bias, yielding a signal shape in the time domain of

$$b(t) = 6[1 - e^{-10t}]$$

The 9° bias time response is

$$b(t) = 9[1 - e^{-0.125t}]$$

The biases are blended out in a similar fashion when the switches are opened. This blending action prevents a sudden change in system configuration, minimizing transients.

The combined bias, pitch rate, and angle of attack signals pass through a gain of value 0.322. Positive signals are always passed on. Negative values are passed on only when the gear are down, the air refueling door is open, or when the alternate flaps are selected. The resulting signal is added to the load factor feedback signal so that, if a signal is present, the system reverts to a blended g-alpha system rather than a pure g command system.

The second bias signal uses a 20.4^O angle of attack bias and conditioned pitch and roll rate signals. The absolute value of the roll rate passes through a gain and a low pass filter. The filter has a relatively long time constant so that the angle of attack limit is not decreased initially by a high roll rate, but is lowered gradually as the roll continues to prevent roll coupling effects. The signal is passed through a threshold filter. Roll rates less than 20° degrees per second do not alter the maximum attainable

angle of attack. Roll rates greater than $56°$ per second reduce the maximum angle of attack limit by $5.4°$. Intermediate roll rates reduce the angle of attack limit by lesser amounts. The roll rate derived bias signal is summed with the 20.4 degree bias and pitch rate signal and then compared with the angle of attack signal. Positive values are then summed with the command signal. The pitch rate signal serves to minimize limiter overshoots during rapid pitch maneuvers and aids in minimizing roll coupling effects.

The angle of attack limiter operates when the pilot is on the positive g command limiter. When the commanded g is not obtainable without exceeding the angle of attack limit, the angle of attack and load factor feedback combination nulls out the signal sent to the elevator. If the angle of attack and load factor combination feedback exceeds the command signal, a nose down elevator command reduces the angle of attack toward the limit. If the aircraft is below the commanded limit, the pilot command signal exceeds the combination feedback signal and a nose up elevator command results.

The angle of attack limits can be found for various aircraft configurations from the block diagram. The pitch rate and roll rate feedbacks are assumed zero. The equations for the gear up configuration are (zero pitch rate and roll rate assumed)

$$n_{z_{TRIM}} + n_{z_c} = \alpha_T - 20.4 + 0.322(\alpha_T - 15) + n_z - 1 \qquad \alpha \geq 20.4°$$

$$n_{z_{TRIM}} + n_{z_c} = 0.322(\alpha_T - 15) + n_z - 1 \qquad 15° \leq \alpha < 20.4°$$

$$n_{z_{MAXIMUM}} = 9 \text{ g's} \qquad \alpha < 15°$$

where the left side of the first two equations may be set at the maximum aft stick input from the command path (8 incremental g's). For the power approach configuration

$$n_{z_{TRIM}} + n_z = \alpha_T - 20.4 + 0.322(\alpha_T - 6) + n_z - 1 \qquad \alpha \geq 20.4°$$

$$n_{z_{TRIM}} + n_z = 0.322(\alpha_T - 6) + n_z - 1 \qquad \alpha \leq 20.4°$$

The contractor's angle of attack limiter boundaries confirms the validity of the above equations. However, the contractor curve shows some situations which are not possible in the aircraft. For example, in the flaps-up configuration, the contractor equates 30° angle of attack with -5.4g, an impossible flight condition. Also, the curve implies a 9 g limit at negative angles of attack. The flaps up curve is valid for positive load factors and angles of attack only (above zero degrees angle of attack and zero commanded load factor) since positive angles of attack cannot physically produce negative load factors nor can positive load factors be obtained with negative angles of attack. It is possible to obtain higher angles of attack limiter boundary values by applying forward stick forces at low speeds. Although high angles of attack are achievable during zooms, it is unlikely that the pilot or angle of attack limiter can control the angle of attack during these basically ballistic maneuvers, although the angle of attack limiter system will command a nose down pitching motion as the airspeed is reduced. The minimum angle of attack at which a particular load factor can be obtained is dependent upon the flight condition and gross weight.

The flaps down curve is not meaningful as presented. A more pertinent curve relates the aircraft angle of attack to the pilot command signal at a particular load factor and trim setting, yielding an indication of the aircraft speed stability. Figure 14.185 plots pilot command signal versus angle of attack. The angle of attack is plotted backwards and can be related to airspeed in the power approach configuration, with slower airspeeds corresponding to lower angles of attack. Positive speed stability is provided. Notice that the flight manual suggested 13° angle of attack power approach situation occurs near the upper limit of the trim system authority (for zero pilot stick forces), so that it is not possible to trim the aircraft to too high a final approach angle of attack. Positive speed stability is also provided during air refueling and whenever alternate flaps are selected.
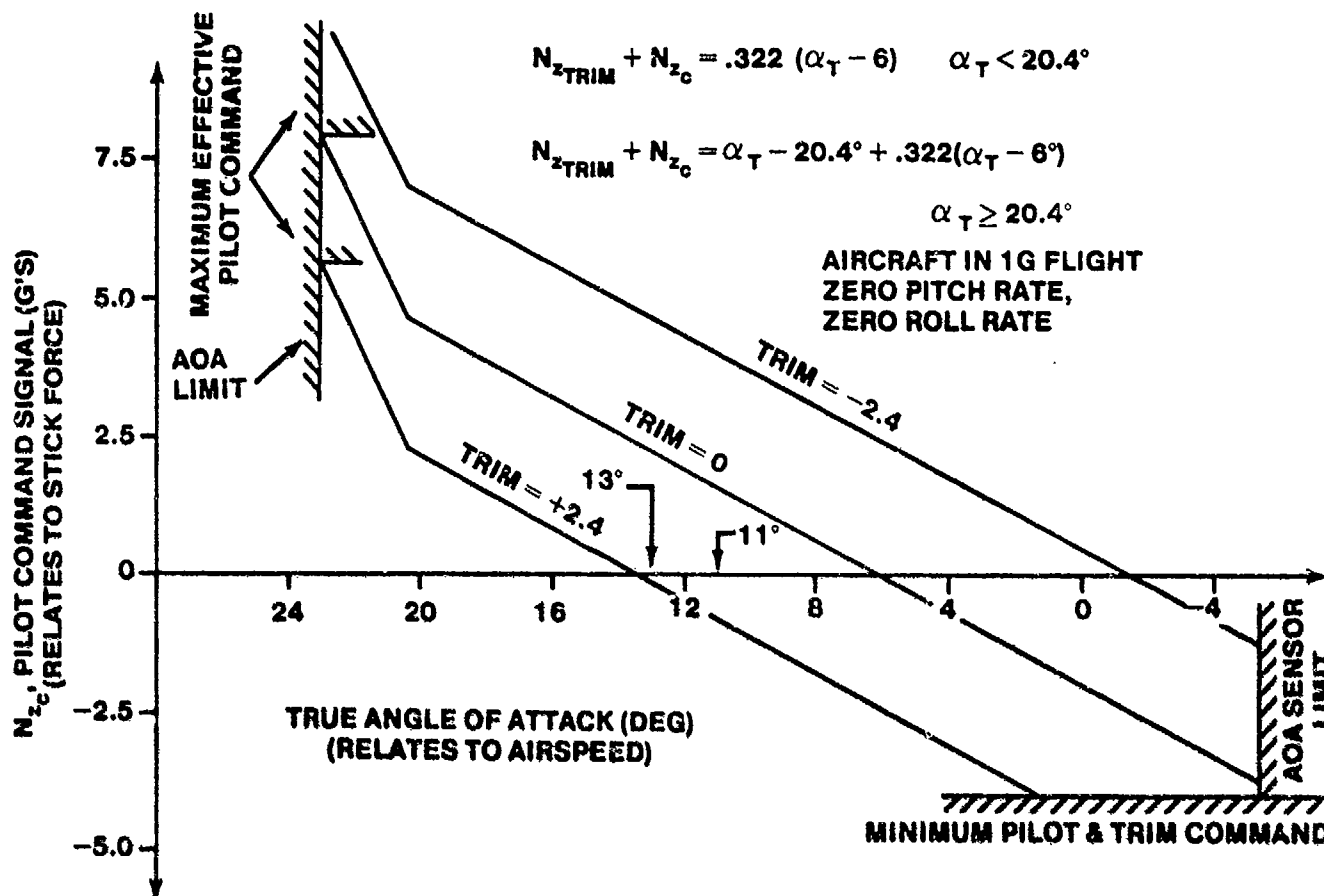
FIGURE 14.185. F-16A POWER APPROACH SPEED STABILITY CURVES

Above 15° angle of attack, positive speed stability is provided for the cruise configuration (slow speed flight), as shown in Figure 14.186. Notice that the pilot can trim the aircraft to alleviate the stick forces required for level flight up to an angle of attack which is well below the limiter value, but that he must hold aft stick forces to continue to decelerate in level flight. In 1 g flight, once the aircraft reaches the angle of attack limit with a maximum pilot plus trim command input, a nose down pitching motion will occur to try to maintain the aircraft angle of attack at the limiting value.

$$N_{z_{TRIM}} + N_{z_c} = \tau - 20.4° + .322(\tau - 15) \quad \tau \quad 20.4°$$

$$N_{z_{TRIM}} + N_{z_c} = .322(\tau - 15) \, 15° \quad \tau \quad 20.4°$$

AIRCRAFT IN lg FLIGHT,
ZERO PITCH RATE,
ZERO ROLL RATE

AOA LIMITER
SYSTEM NOT
IN EFFECT
BELOW 15°
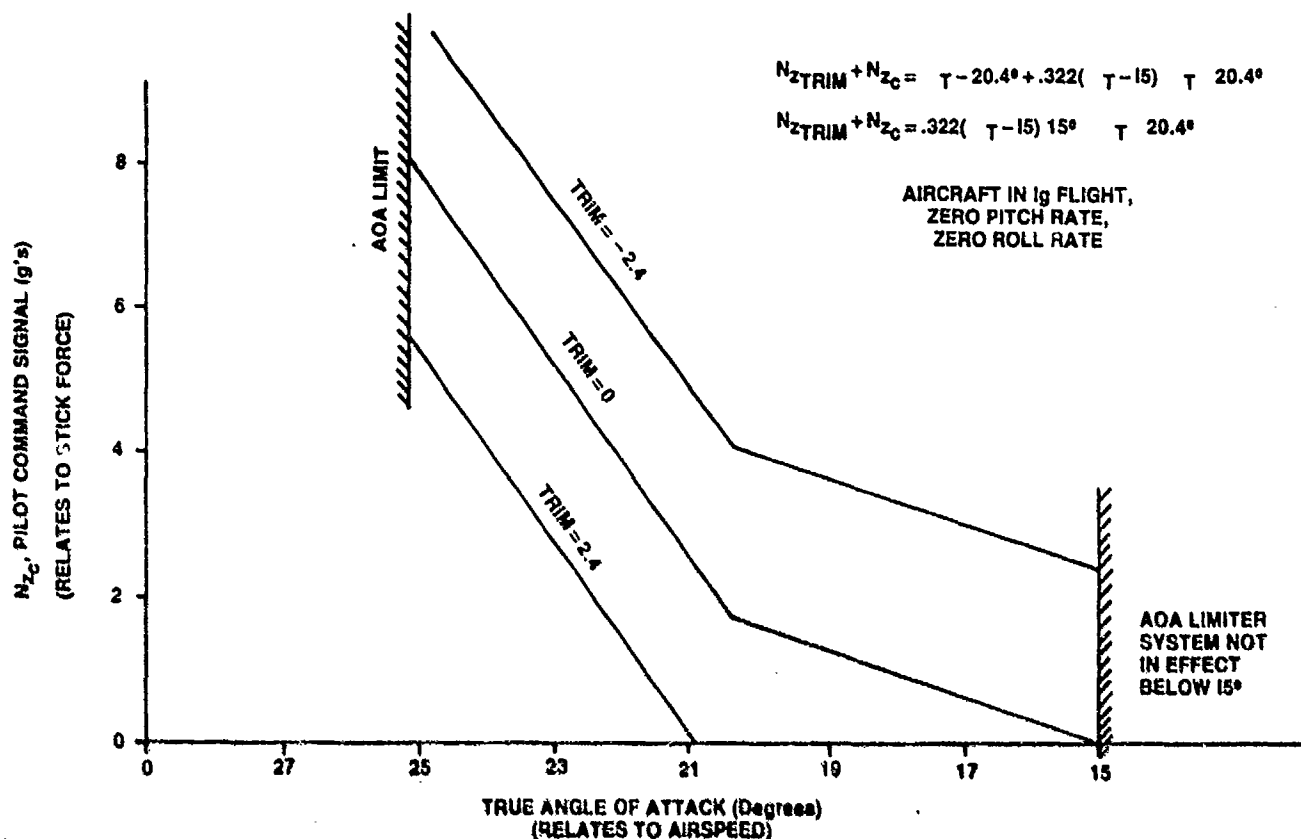
FIGURE 14.186.

The determination of the aircraft maneuvering stick force gradients could be accomplished in a manner similar to that used to determine the aircraft speed stability by plotting the pilot command input signal versus the angle of attack for a constant airspeed. The angle of attack would be plotted increasing to the right since increasing angle of attack corresponds to load factor. Pilot commanded load factor still corresponds to the pilot stick forces. The steady state maneuvering gradient when the aircraft angle of attack is below $15°$ is easily determined from the pilot pitch command gradient. This gradient is low relative to the effective gradient since a 1 g pilot command results in a load factor increase somewhat less than one in the near term, requiring the pilot to increase the command input to obtain the desired 1 g increase in the load factor until the integrator can relieve the additional stick forces. The concern here is the steady state maneuvering gradient, which occurs where the angle of attack limiter system is providing

angle of attack feedback during flight in the cruise configuration and in the power approach configuration. Analysis of the maneuvering gradients is not as simple as analyzing the speed stability because a simple aerodynamic model of the aircraft is required to determine the aircraft load factor. The effective maneuvering gradient would require a linear analysis of the system operation within the desired angle of attack range and a determination of the load factor change per unit of pilot command input. The gradient could be easily determined during ground simulations of the augmented aircraft.

Areas of concern for flight test include:

1. Transients at takeoff due to the 6° bias phase-in and angle of attack feedback closure

2. Transients during gear retraction and gear extension due to blending of the 9° bias and the 1.0 bias. Since the bias signals are blended over a 24 second period, no transients are expected

3. Angle of attack overshoot magnitudes during rapid g onset (rapid pilot command input) at low airspeeds in the cruise and power approach configuration

4. Angle of attack limiter operation during rolling maneuvers in the cruise and power approach configurations

5. g limiter operation during rapid g onset at high speeds

6. Speed stability gradients during power approach, at low speed during cruise and during air refueling

7. Stall and departure prevention due to angle of attack limiting system operation during cruise and power approach

8. Handling qualities with angle of attack feedback in the power approach configuration and at low speed in the cruise configuration

9. Deep stall recovery system operation

10. Angle of attack limiter operation during vertical zooms to very low airspeeds where the angle of attack system indicates a low angle of attack until the aircraft is no longer controllable

11. Adequacy of the trim system authority during approach to landing, especially when using the flight manual 13° angle of attack approach procedure

12. Maneuvering stick force gradients during power approach and during flight in the cruise configuration when operating at angles of attack above 15°.

14.5.1.3 Pitch Rate and Load Factor Feedback Paths. The pitch rate (non-alpha limiting function) and load factor feedback paths are shown in Figure 14.187.

NOTE C:
SWITCH ACTIVATED BY ANY OF THE FOLLOWING METHODS:
1. WEIGHT ON MAIN LANDING GEAR
2. AOA GREATER THAN 29 DEGREES AND MANUAL PITCH SWITCH IN OVERRIDE POSITION
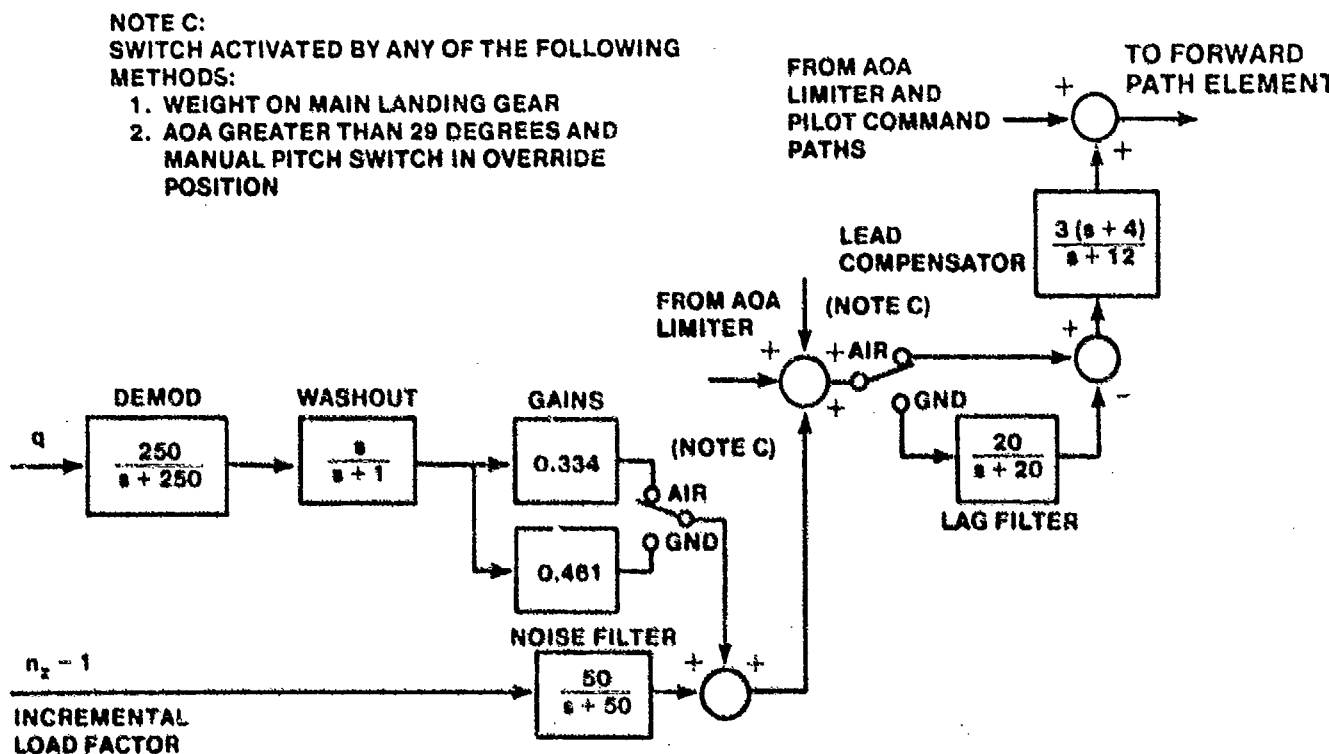
FIGURE 14.187. F-16 LOAD FACTOR AND STABILITY AUGMENTATION FEEDBACK PATHS

The purpose of the demodulator on the pitch rate feedback was discussed earlier. The washout filter is necessary since the normal flight mode is a pure g command system. In steady state maneuvers (1 g cruise or steady turns) the pitch rate feedback signal does not affect the system (washed out to zero) so that the actual g matches the commanded g (cruise only). However, load factor feedback, by itself, generally has an adverse effect on the short period dynamics of the aircraft (see Paragraphs 14.2 and 14.3). During tight tracking tasks such as formation flying and air-to-air tracking, pitch rate

feedback is used to improve handling qualities. High frequency pitch rate feedback is provided through the washout filter for this purpose during transient conditions present during high gain tracking tasks. Two gains are provided. Higher gain for takeoff is provided for improved pitch attitude control during rotation (more precision). The lag filter is provided to eliminate noise due to vibrations caused by the runway. The lag filter on the load factor feedback signal attenuates high frequency noise, such as due to structural bending modes. The lead filter in the feedback path helps improve the short period damping but also reduces the short period natural frequency slightly. Areas of interest concerning these feedback signals are:

1. Handling qualities during tracking

2. Transients at liftoff due to the gain change and the elimination of the lag filter

3. Structural resonance elimination

14.5.1.4 Forward Path Elements. The forward path elements are downstream of the point where the angle of attack limiter and pitch rate plus load factor feedback signals are summed with the pilot command signal. Figure 14.188 shows the block diagram.

The signal from the command path summed with the feedback and alpha limiter paths passes through two gains. The second gain is a parabolically shaped gain as a function of dynamic pressure which reduces the amount of elevator commanded as the elevator effectiveness increases with airspeed.

The complex block diagram encountered next is essentially a proportional plus integral feed forward element which reduces steady state load factor errors to zero. The integrator has a relatively high gain of 5.0 for fast response. The selector feature compares proportional plus integral controller elevator commands among the four redundant flight control computers and feeds back an error signal to keep the four integrators from drifting, a problem of physical integrators. When the aircraft is on the ground, the integrator has a -0.5 feedback gain and the result is equivalent to

$$G(s) = \frac{i(0)}{s + 2.5} \quad \text{or} \quad g(t) = i(0)\,[e^{-2.5t}]$$

where $i(0)$ is the integrator output at touchdown.
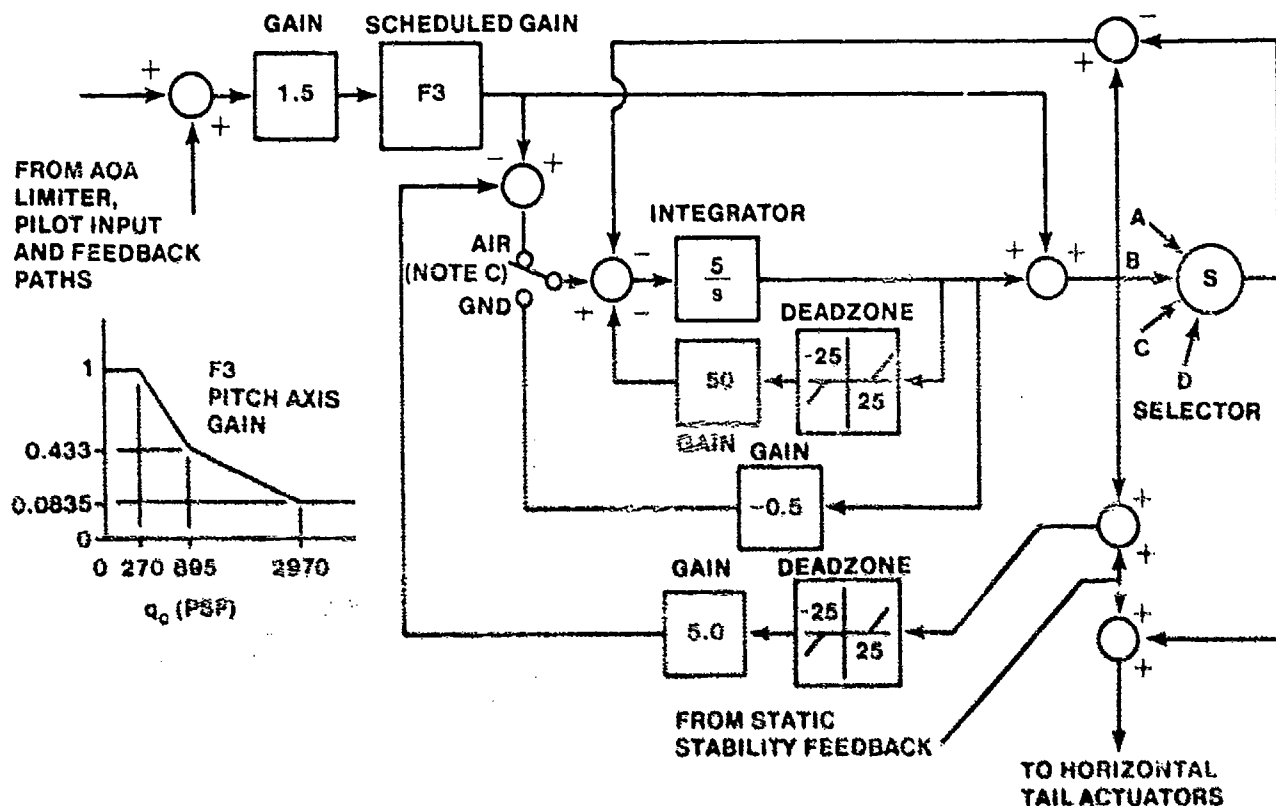
FIGURE 14.188. F-16 PROPORTIONAL PLUS INTEGRAL CONTROLLER CIRCUITRY

The integrator output is forced to zero after touchdown in a little over 1 second. If the integrator output exceeds 25° in either direction, feedback is provided to limit the integrator output. In this case, the closed loop transfer function is

$$G(s) = \frac{i(0) - 25}{s + 250} \quad \text{or} \quad g(t) = [i(0) - 25]\,[e^{-250t}]$$

where $i(0) \geq 25^{\circ}$.

The integrator output is very rapidly driven back towards 25° of elevator command.

The combined circuit output is also controlled at high angles of attack. It is highly desirable to keep the commanded horizontal tail angle within the 25° deflection limits. If the combined proportional plus integral signal and

angle of attack signal from the static stability loop exceeds 25° in either direction, then feedback is provided to drive the output of the circuit to a lower value. Without the feedback path, the angle commanded could reach a maximum of 55.85° at high angles of attack. It is difficult to analytically evaluate the action of the integrator due to its complex nonlinear nature. A nonlinear simulation of the combined circuitry, including both nonlinear feedback paths, yields horizontal tail angle commands as function of the pilot command (assuming the angle of attack is above the mechanical limits of the angle of attack vanes), as shown in Table 14.5. The combined circuit provides a soft limiter for the elevator command, but also prevents the pilot from recovering from the deep stall unless he selects override on the manual pitch switch. With override selected, the integrator output is driven to zero and the angle of attack feedbacks are eliminated so that the pilot has direct control of the elevator position. The integral plus proportional signal is added to the static stability feedback and becomes the elevator command signal.

Areas of concern are:

1. Effectiveness of integrator balancing

2. Effectiveness of gain F3 in maintaining nearly constant flying qualities throughout the speed envelope of the aircraft

3. Effectiveness of the integrator and the flying qualities associated with the relatively high integrator gain

4. Elevator saturation, especially at high angles of attack, and the effectiveness of saturation prevention features

5. Integrator action after touchdown

TABLE 14.5
STEADY STATE ELEVATOR COMMAND AT HIGH ANGLES OF ATTACK
VERSUS PILOT COMMANDED LOAD FACTOR

Pilot Command n_{z_c}	Steady State Elevator Command δ_{e_c}
8 g's	28.7°
0 g's	30.3°
-1 g's	30.5°

14.5.1.5 Elevator Actuator System for the Longitudinal Axis. The F-16
employs a rolling tail configuration. Both pitching and rolling moments are
created by the horizontal tail. Figure 14.189 shows the horizontal tail
configuration. Each half of the tail is controlled independently and each
half may be locked out of the system in case of battle damage. The elevator
command is provided to both horizontal tail actuators to produce symmetrical
elevator deflections. The rolling tail commands are provided to each half of
the horizontal tail by the lateral axis, the details of which will be
discussed in Paragraph 14.5.2. The commands provided to the aerodynamic
surface actuators are compared among the four channels of the flight control
system to ensure that the computer (only one computer actually flies the
aircraft, the others are used as comparators) in command is providing the
correct elevator command If the computer in command is providing erroneous
signals, it is voted out of the system and another computer takes over. The
average elevator deflection commanded is provided to the lateral axis command
gradient computation, to be discussed in Paragraph 14.5.2. The horizontal
tail actuators are limited to a deflection rate of 60° per second, which is
fairly fast. The tail deflection is limited to 25° in either direction due to
actuator mechanical deflection limitations.

One area of concern is the potential for crosstalk between the lateral
and longitudinal axes due to the rolling tail. Longitudinal tracking problems
could occur if the lateral inputs cause pitching motions. Another area of
concern is the control authority available and the handling qualities with one
of the elevators locked out.
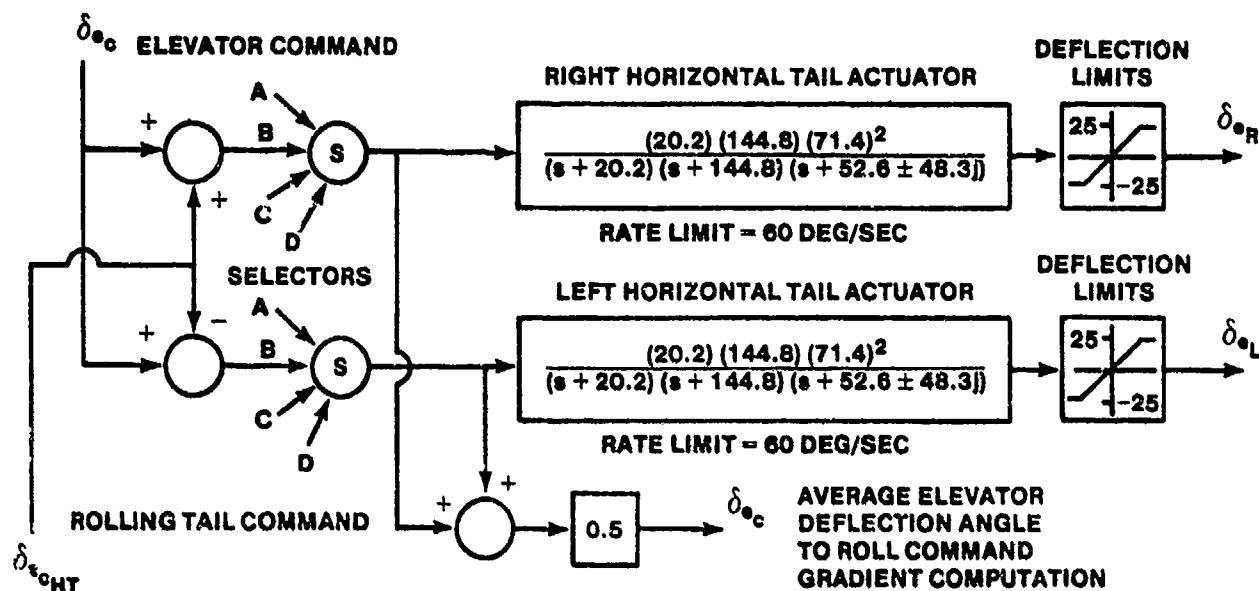
FIGURE 14.189. F-16 HORIZONTAL TAIL CONFIGURATION FOR PITCH CONTROL

14.5.1.6 Simplified Pitch Axis for Linear Analysis.

14.5.1.6.1 Cruise Configuration. Figure 14.189 shows a simplified pitch axis control system for the cruise configuration. It assumes that all signals are within limits specified (angle of attack and pilot g command limits) and that the deadzones in the integrator loop are not exceeded. The pilot input is the commanded load factor so that difficulties associated with the nonlinear pitch command gradient are avoided. Elements which have poles remote from the origin are neglected (some judgement is required here, but generally poles further from the origin than about 25 radians per second may be neglected). Gains F2 and F3 should be set at the trim flight condition value and assumed constant.
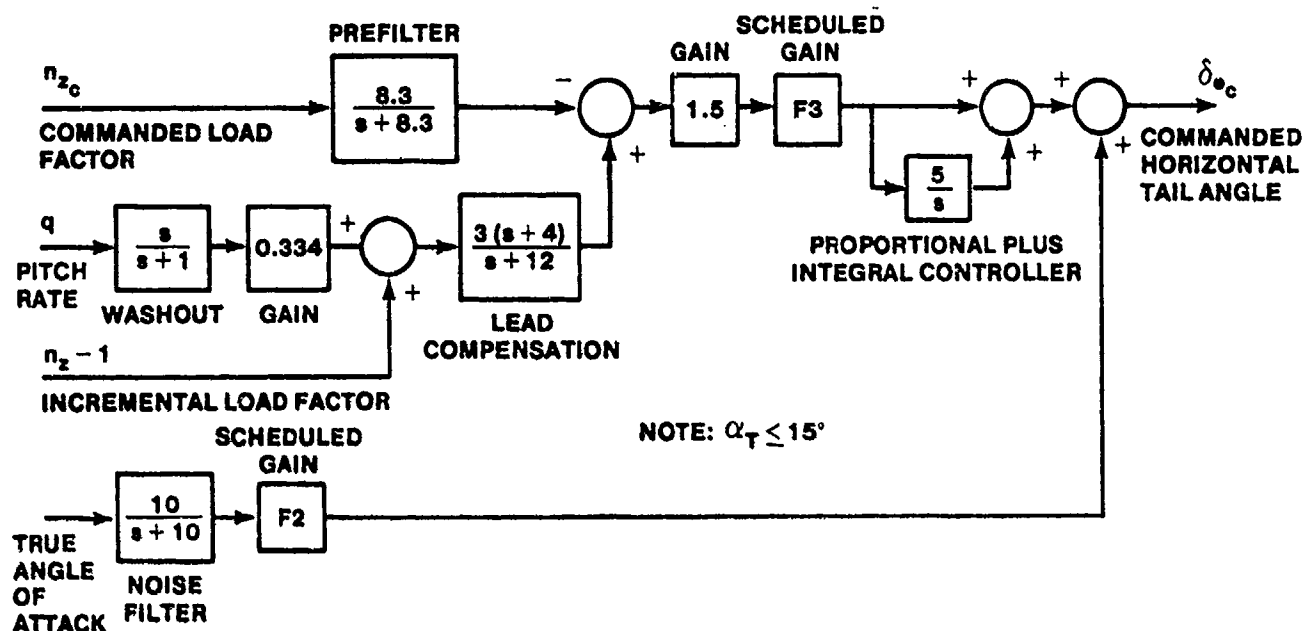
FIGURE 14.190. LINEARIZED LONGITUDINAL FLIGHT CONTROL SYSTEM FOR THE CRUISE
CONFIGURATION AT LOW ANGLES OF ATTACK

14.5.1.6.2 Power Approach Configuration. Figure 14.191 shows a
simplified block diagram of the pitch axis system for the power approach
configuration. Two angle of attack feedback loops are included, the second
loop coming from the alpha limiter loop which provides positive speed
stability. Gains F2, F3, and F12 should be set at the trim condition values
and assumed constant.

PREFILTER

n_{z_c}

$\dfrac{8.3}{s+8.3}$

WASHOUT

q

$\dfrac{s}{s+1}$

GAIN

0.334

SCHEDULED GAIN

0.7 → F12 → 0.322

GAIN   **GAIN**

$n_z - 1$

NOISE FILTER   **GAIN**

α_T

$\dfrac{10}{s+10}$ 0.322

LEAD COMPENSATOR

$\dfrac{3(s+4)}{s+12}$

NOTE: $\alpha_T \leq 20.4°$

SCHEDULED GAIN

F2

SCHEDULED GAIN   **SCHEDULED GAIN**

1.5   F3

$\dfrac{5}{s}$

PROPORTIONAL PLUS INTEGRAL CONTROLLER

δ_{e_c}
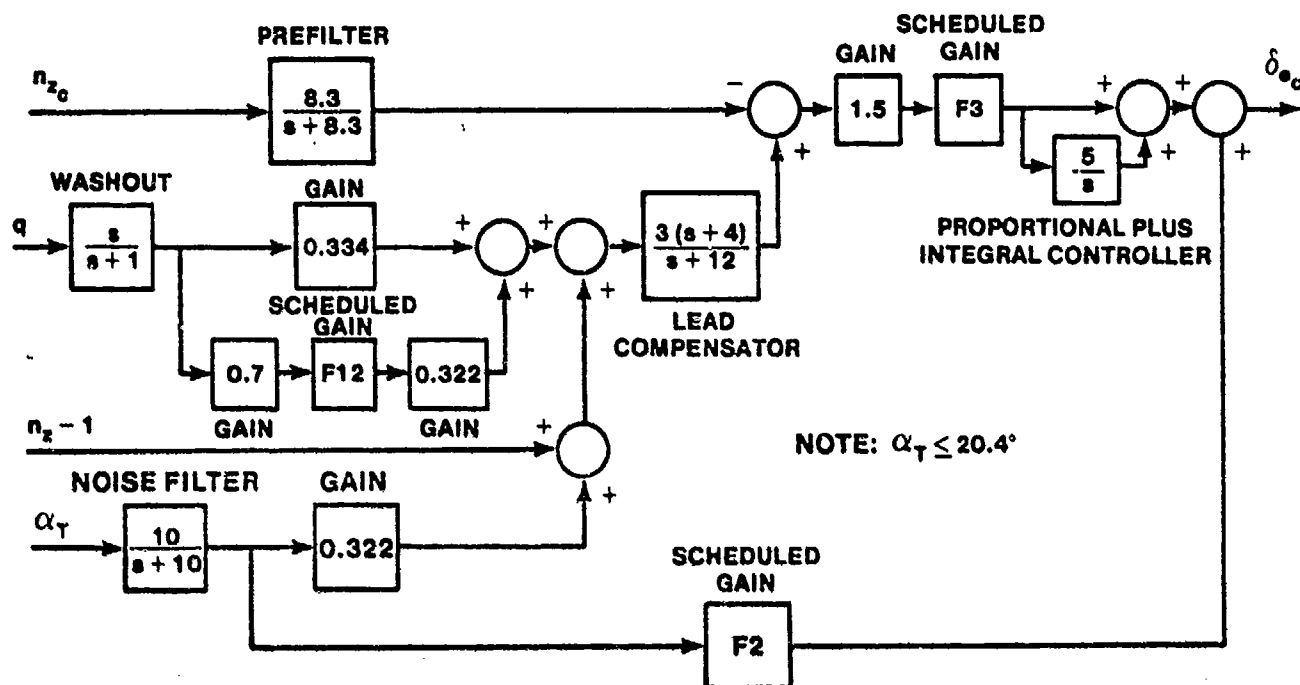
FIGURE 14.191.   LINEARIZED LONGITUDINAL FLIGHT CONTROL SYSTEM FOR THE POWER APPROACH CONFIGURATION, LOW ANGLES OF ATTACK

14.5.1.7   Longitudinal Axis Flight Control System Configuration with the Manual Power Switch in Override.   If the pilot enters a deep stall at near 60° of alpha, the circuitry around the proportional plus integral controller prevents the pilot from deflecting the elevator, as shown in Table 14.5.   To provide the "pitch out" maneuver and recover the aircraft from the deep stall condition, all of the angle of attack feedbacks to the longitudinal axis are eliminated from the flight control system.   The integrator in the forward path is also eliminated to preclude it from providing inputs to the elevator.   The negative load factor limiters are eliminated to provide the ability to command full elevator leading edge up.   The gain in the pilot command path is doubled to provide the ability to command 24° of elevator leading edge down.   An increased pitch rate feedback gain in conjunction with the load factor feedback provides aircraft augmentation.   The augmented aircraft is aerodynamically unstable in this situation, even when recovered from the out-of-control flight condition, but can be flown for a short period of time while airspeed is increased and angle of attack is reduced.   The flight control configuration in this situation is shown in Figure 14.192.   The flight

control system, with the exception of the negative load factor limiter is the same as that used for takeoff roll before liftoff.
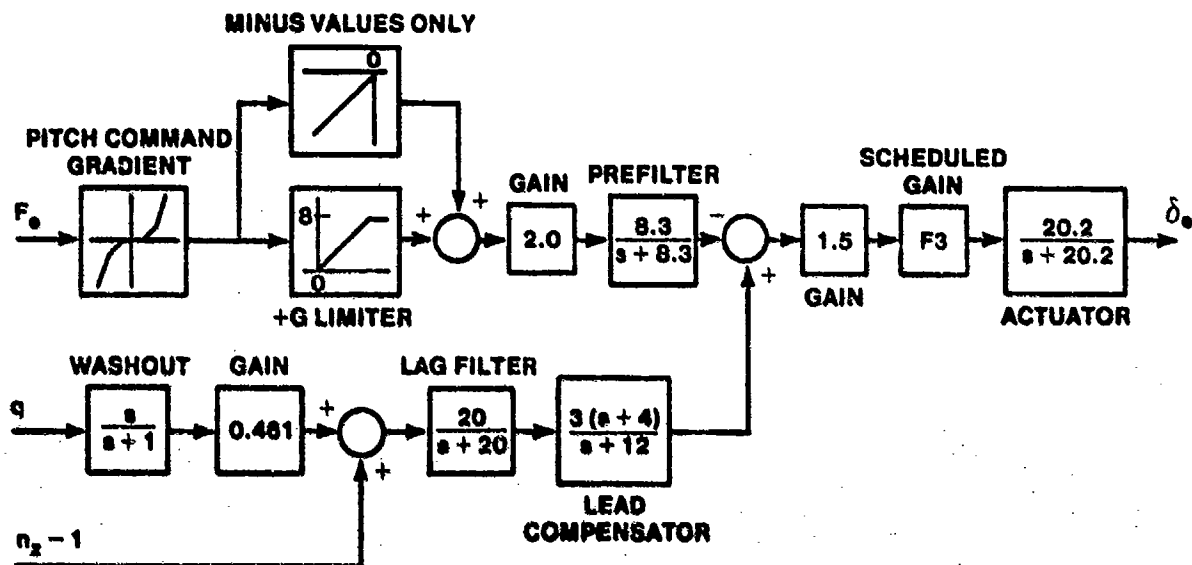
FIGURE 14.192. SIMPLIFIED LONGITUDINAL FLIGHT CONTROL CONFIGURATION WITH THE MANUAL PITCH SWITCH IN THE OVERRIDE POSITION

14.5.2 Lateral Axis Description

The lateral axis uses differential flaperons (combined ailerons and flaps) on the wings and differential horizontal tail control surfaces to provide roll control. It is important to understand the sign convention used for the ailerons and rolling horizontal tail during the analysis of the lateral axis. In Figure 14.180, a positive aileron deflection causes the trailing edge of the aileron to move down. The same convention is used for differential horizontal tail deflections.

14.5.2.1 Pilot Input and Roll Rate ·   ':   :·· System. Figure 14.193 presents the pilot command path for the roll axis. The stick force is converted to

a roll rate command by the roll command gradient. The maximum roll rate obtainable accounts for several factors in order to avoid aircraft departure and minimize roll coupling. At high speeds and low angles of attack with the gear up, the maximum roll rate is limited to 308° per second. The maximum roll rate is reduced at low dynamic pressures (low airspeeds or high altitudes), large elevator deflection angles and high angles of attack. The maximum commanded roll rate may be reduced to a minimum value of 80° per second when operating on the angle of attack limiter with full nose down elevator commanded and at very low airspeeds. With the gear handle down, the alternate flap switch in the extend position or the air refueling switch open, a maximum roll rate of 167° per second is provided. The roll command gradients are unchanged by the maximum roll rate limiter, only the maximum roll rate which can be commanded by the pilot changes. Still higher roll rates could be commanded using the trim system in addition to the stick input, but the slow roll trim system rate precludes this approach as a viable way to beat the system. The maximum roll rate actually achieved depends upon the aircraft aerodynamics as well as the roll rate limiter. It may be possible to saturate the ailerons before obtaining the commanded maximum roll rate under certain conditions. Roll performance tests are required to determine the actual roll rates obtainable throughout the flight envelope.
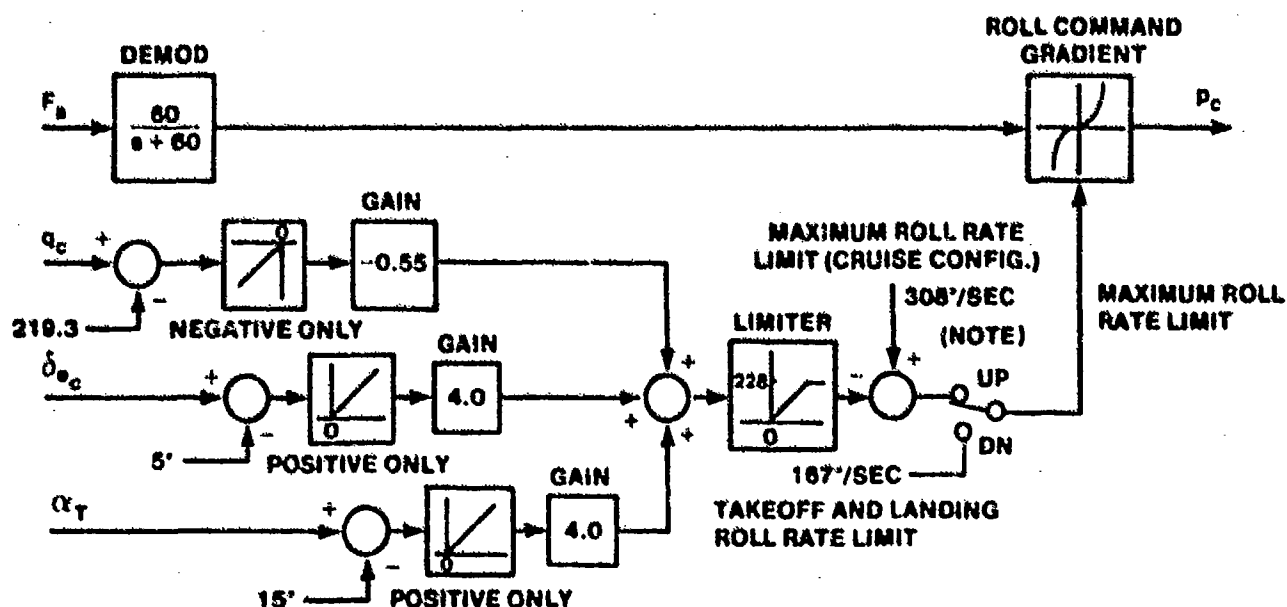
FIGURE 14.193. F-16 LATERAL AXIS PILOT COMMAND PATH

14.5.2.2. Nonlinear Prefilter and Roll Rate Feedback Elements. Figure 14.194 shows the nonlinear prefilter and feedback elements present in the roll rate command system. The s in the numerator of the washout filters performs a differentiation. The first nonlinearity in the upper feedback path of the prefilter passes a positive roll rate command signal. The washout filter differentiates the signal to determine that the pilot is indeed applying the signal. The second nonlinearity passes positive derivatives of the pilot command signal. If a steady pilot commanded roll rate signal, or a roll rate command signal with a negative derivative (the pilot relaxing the roll rate command), were detected by the washout filter, then the second nonlinearity would not allow the signal to be fed back. In this manner, the prefilter takes on two distinct characteristics, as shown in Figure 14.195. The second feedback path provides similar operation for negative roll rate command signals. When the pilot is applying the roll rate command input, the prefilter provides additional lag to smooth the aircraft response. This is often necessary with fixed stick controllers to avoid roll ratcheting caused by the pilot. When the pilot relaxes the roll rate command the prefilter introduces much less lag and the aircraft roll rate is halted more abruptly.
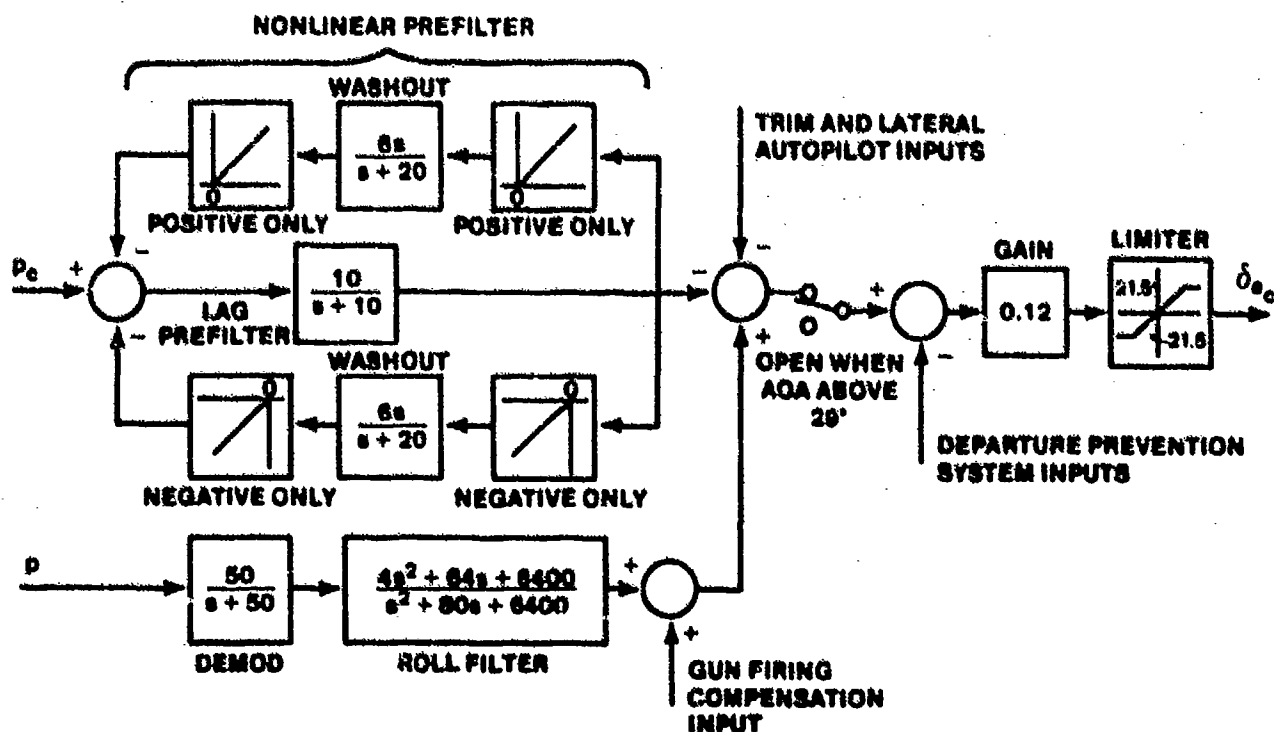
FIGURE 14.194. F-16 LATERAL AXIS NONLINEAR PREFILTER AND FEEDBACK AUGMENTATION SYSTEM

$$\frac{10}{s + 10}$$

$$\frac{6s}{s + 20}$$
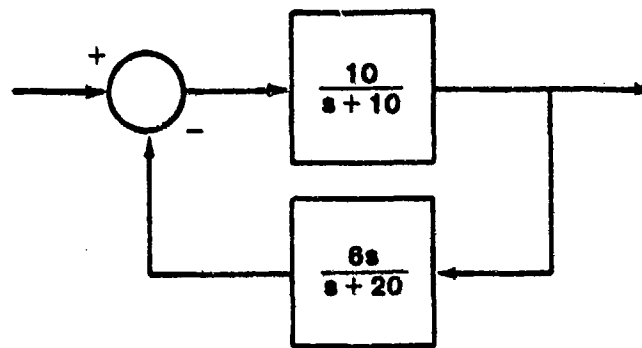
a. PILOT INPUT BEING APPLIED

$$\frac{10}{s + 10}$$
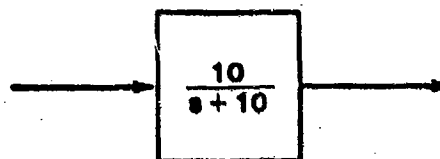
b. PILOT INPUT BEING REMOVED

FIGURE 14.195. LINEARIZED PREFILTER MODES

Three areas of concern:

1. Is the prefilter effect sufficient to prevent roll ratcheting which could cause poor handling qualities during high gain tracking tasks?

2. Is the pilot able to obtain the desired roll rate sufficiently fast to avoid overcontrolling the aircraft in roll?

3. Does the aircraft roll rate decrease sufficiently fast to avoid overshooting the desired roll attitude or is the pilot required to apply opposite roll rate commands to obtain precise roll attitude control?

The aircraft roll rate is sensed by the roll rate gyro and the signal is demodulated. A roll filter increases the phase angle of the lateral axis in the vicinity of 60 radians per second (lead filter), and reduces the effects of structural resonance in the lateral axis. The lateral axis is compensated during gun firing due to the location of the gun (in the left wing root area) to prevent a left rolling tendency. The pilot command, trim, and feedback

inputs are summed, multiplied by a gain, limited to 21.5° in either direction, and applied to the aileron actuators. Notice that the pilot command signal and the trim signal are applied as negative signals for a positive roll rate command. If the aircraft is above 29° angle of attack, the roll rate command, trim and feedback signals are cut out and aileron control reverts to the departure prevention system. This means that the pilot lateral control inputs are ignored when flying at high angles of attack. The major area of concern with regard to the departure prevention system is the impact of the system operation during very low speed vertical combat maneuvers. The aircraft is restricted from very low speed maneuvering flight, such as a near vertical scissors.

14.5.2.3 <u>Flaperon and Differential Horizontal Tail System</u>. The signals from the lateral axis are provided to the flaperon and differential horizontal tail surfaces through the system shown in Figure 14.196. Aileron command signals are applied to each flaperon actuator such that the flaperons move the same amount differentially. For a positive roll command signal, the right aileron is moved trailing edge up the same amount that the left aileron is moved trailing edge down. Two feedback paths are provided to allow the aircraft to roll with the flaps extended to 20°. With both flaps extended, the ailerons are both at the 21.5° command deflection limit. The roll command system cannot further deflect either aileron in the down direction. This signal is sent instead to the upward commanded aileron to double the upward deflection command signal. The aileron command signals pass through an additional limiter and are then compared with the flaperon command deflection signals of the other three flight control computers. The flaperon actuators possess the same characteristics as the horizontal tail actuators previously discussed. The flaperons possess a 1.5° electrical bias from the trailing edge flap system so that a zero flaperon deflection occurs in the absence of command inputs unless one of the flaperons are locked out. The flaperons may be controlled through angles from 20° trailing edge down to 23° trailing edge up. The aileron command deflections are summed (double the deflection due to the roll command with the flap command being eliminated) and multiplied by two gains, one of which is a function of the dynamic pressure divided by the static pressure. The resulting signal is applied to the horizontal tail

actuators to differentially deflect them. For a right roll command, the right horizontal tail is deflected trailing edge up and the left tail is deflected trailing edge down, exactly in the same manner as the flaperons. If either horizontal tail is locked out of the system due to battle damage, differential tail deflection commands are not provided to the horizontal tail. Signals to the aileron-rudder interconnect and for the departure prevention system are also provided by the aileron-elevator interconnect system. The departure prevention system uses the differential horizontal tail, if not locked out, in conjunction with the ailerons.

Areas of interest are: the roll performance of the aircraft, with and without the horizontal tail locked out, and the aircraft handling qualities during power approach, where significant lift losses during rolls due to the upward deflecting flaperon may cause flight path control problems.

14.5.2.4 Simplified Lateral Axis Control System for Linear Analysis. Figure 14.197 presents a simplified lateral axis control system. The pilot roll rate command is fed through the nonlinear prefilter as represented by either the prefilter present when the pilot applies the command input or the prefilter present when the pilot relaxes the control input. The results of the analysis where the pilot applies the roll command are directly provided by the time response program; the results where the pilot relaxes the roll command must be viewed as if the aircraft were in a steady rolling maneuver. Instead of starting at zero roll rate and approaching some final roll rate, the initial point is some steady roll rate and the final state is zero roll rate. The aircraft transfer function must represent the roll rate response for the combined flaperon and differential tail deflections, unless the tail is assumed to be locked out.
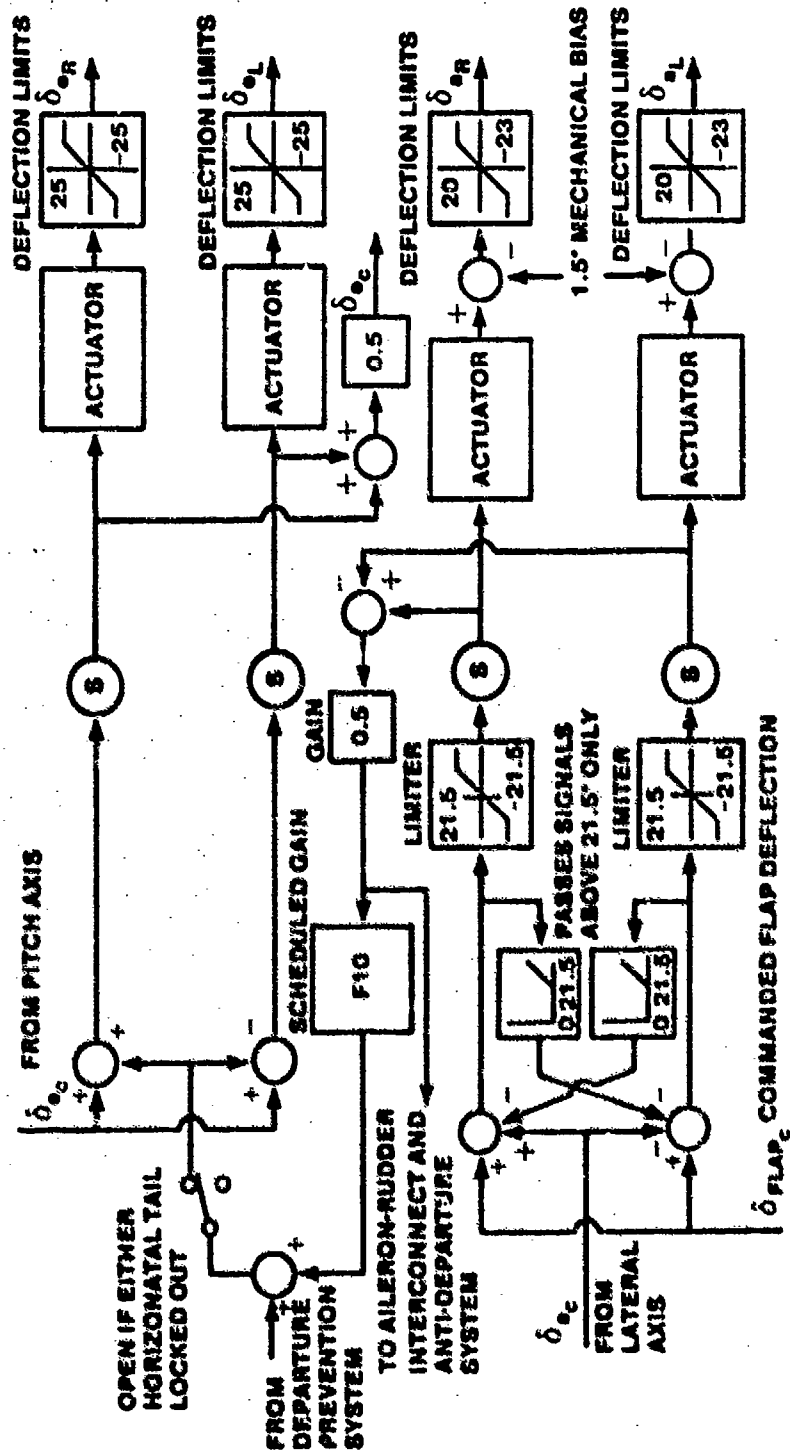
FIGURE 14.196. F-16 FLAPERON AND HORIZONTAL TAIL CONFIGURATION FOR ROLL CONTROL

NONLINEAR PREFILTER   **GAIN**   **ACTUATOR**
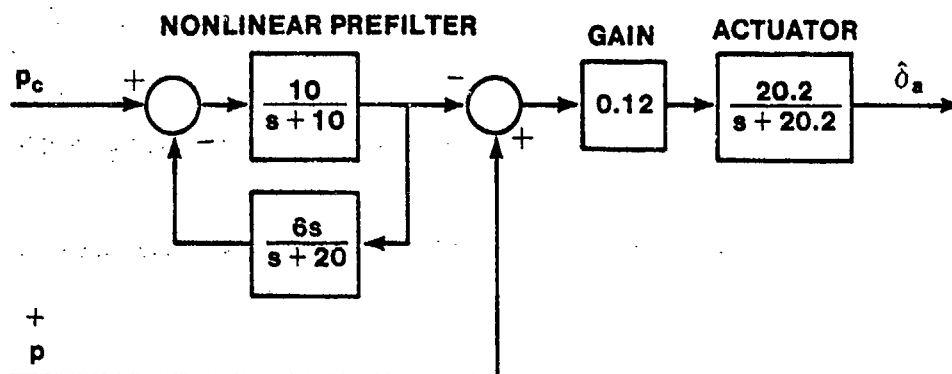
FIGURE 14.197. LINEARIZED LATERAL FLIGHT CONTROL SYSTEM

14.5.2.5 Lateral Axis Departure Prevention System. Figure 14.198 presents
the departure prevention system for the lateral axis. Above 29° angle of
attack, the pilot command, trim, and feedback signals are eliminated from the
system and provide no aileron commands. A yaw rate signal is provided to the
lateral axis such that one degree per second of yaw rate commands one degree
of aileron deflection. Yaw to the right (positive) causes the right aileron
to deflect up and the left aileron to deflect down. The differential
horizontal tail commands are increased by 1.25° differential tail per degree
of aileron. A positive yaw rate commands the left horizontal tail to deflect
trailing edge down and the right tail to deflect trailing edge up. Recall
from the proportional plus integral controller circuitry in the longitudinal
axis that above 32.5° angle of attack the horizontal tail is likely to be
saturated in the full trailing edge down direction regardless of the pilot
pitch command signal. The left horizontal tail will therefore not deflect
further. However, with sufficient yaw rate (about 2.5° per second with an 8 g
pilot command signal applied) the right horizontal tail will move off the
deflection limit so as to be less trailing edge down than the left tail. The
difference in drag provided by the differentially deflecting horizontal tails
and the adverse yaw due to the aileron both oppose the positive yaw rate.

If the aircraft does enter a spin, the departure prevention system
automatically applies anti-spin aileron (aileron with the spin for a swept
wing aircraft).

FIGURE 14.198.   LATERAL AXIS DEPARTURE PREVENTION SYSTEM

14.5.3 Directional Axis

The directional axis uses a conventional rudder to augment the directional stability of the aircraft and provide yaw control for the pilot.

14.5.3.1 Directional Axis Feedback Control Law.
The directional axis flight control system is presented in Figure 14.199. Unlike the longitudinal and lateral systems, the pilot does not command an aircraft motion in the

FIGURE 14.199. DIRECTIONAL AXIS FLIGHT CONTROL SYSTEM

directional axis. The pilot commands a rudder position directly. A yaw damper, using beta-dot feedback improves the aircraft pitch roll characteristics. The rudder pedals are essentially fixed (a slight bit of motion is provided) so that the pilot input is through force transducers mounted on the rudder pedals. The applied force signal is demodulated. Mechanical, friction, and breakout in the rudder pedals is combined with electrical breakout and the command gradient to form the rudder command shown in Figure 14.180. The rudder command is multiplied by a constant which varies between 0 and 1 as a function of the angle of attack, presented in Figure 14.200. Two parameters determine the angle of attack for the scheduled gain. The aircraft roll rate reduces the angle of attack at which the pilot rudder command is faded out. With less than 20° per second of roll rate present, the pilot can command full rudder up to 20° angle of attack and lesser amounts of rudder up to a maximum of 30° angle of attack. Above 30° angle of attack, the pilot can command no rudder deflection. As the roll rate

of the aircraft increases, the amount of rudder available at a particular angle of attack decreases, until, at 56° per second of roll rate, the pilot cannot command full rudder at positive angles of attack. The pilot rudder command fade out precludes using rudder to perform rolls at high angles of attack, decreasing the departure susceptibility of the aircraft.
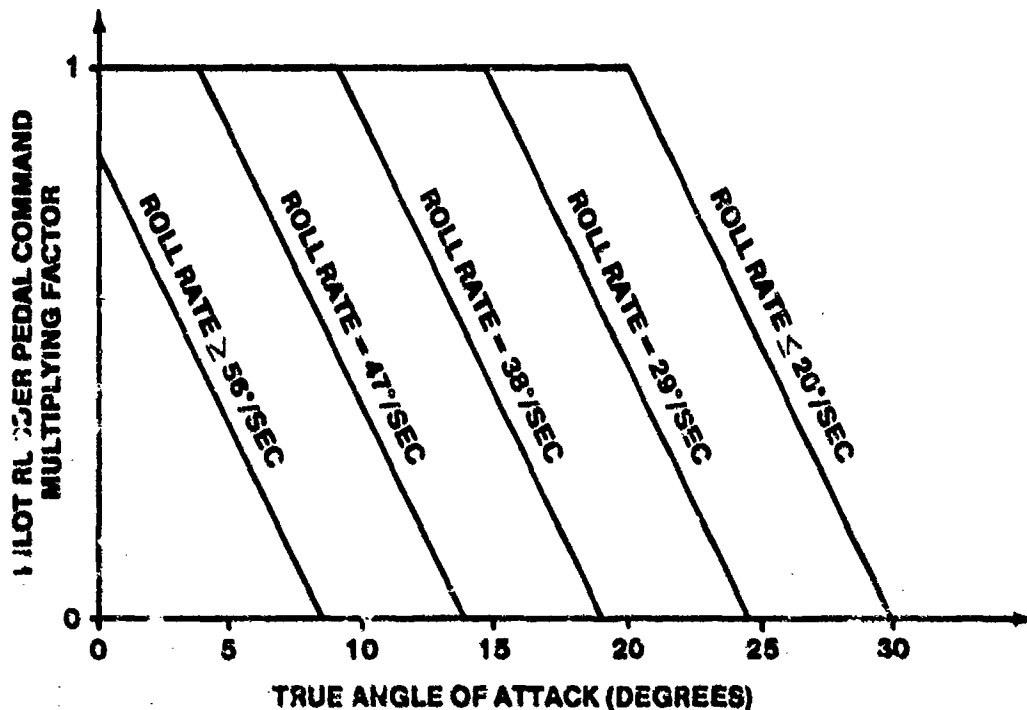
FIGURE 14.200. F-16A RUDDER PEDAL COMMAND FADEOUT GAIN

Four parameters are used to compute what is essentially a beta-dot feedback signal. The aircraft true angle of attack is multiplied by the aircraft roll rate (in rads/sec) and combined with the yaw rate. A lead compensator is provided, the purpose of which should be investigated during the linear analysis of the directional control system. A washout filter prevents rudder deflections during steady state turns due to the yaw rate feedback. The signal is combined with the lateral acceleration feedback to form the computed beta-dot feedback. The feedback signal is multiplied by

a scheduled gain which is a function of the dynamic pressure divided by the static pressure. A gun compensation input is provided during gun firing. Yaw trim, aileron-rudder interconnect, and departure prevention system inputs are provided. Despite the fact that the pilot rudder command can be washed out at high angles of attack and high roll rates, the pilot can still command 12° of rudder deflection via the rudder trim knob since the rudder trim input occurs after the pilot command fader. The resulting rudder command passes through a structural filter, is compared with the rudder commands of the other computers, and is sent to the rudder actuator.

The area of interest here is the departure susceptibility during typical tactical fighter maneuvers with combat configurations. The impact of the rudder fader during the performance of rudder reversals in air-to-air gun engagements should also be investigated.

14.5.3.2 Simplified Directional Axis for Linear Analysis - Figure 14.201. The roll rate and angle of attack are assumed sufficiently low to avoid pilot rudder command fade out. Gain F8 is set for the flight condition to be analyzed. The roll rate is multiplied by the aircraft trim angle of attack (expressed in radians) for the flight condition. Either the roll rate or the angle of attack must be converted to radians to keep the units consistent. Since the analysis of the lateral and directional axes will assume a constant angle of attack, it is convenient to change the control law slightly. The demodulators and the structural filter are omitted since they occur at relatively high frequencies.

δ_{r_p}

ACTUATOR

$\dfrac{20.2}{s + 20.2}$ → δ_r

+ +

r + −

TRIM AOA
(RAD)

α_{TRIM}

p

LEAD
COMPENSATOR

$\dfrac{3(s+5)}{s+15}$

WASHOUT

$\dfrac{1.5s}{s+1}$

+ +

SCHEDULED
GAIN

F8

GAIN

19.32

n_y
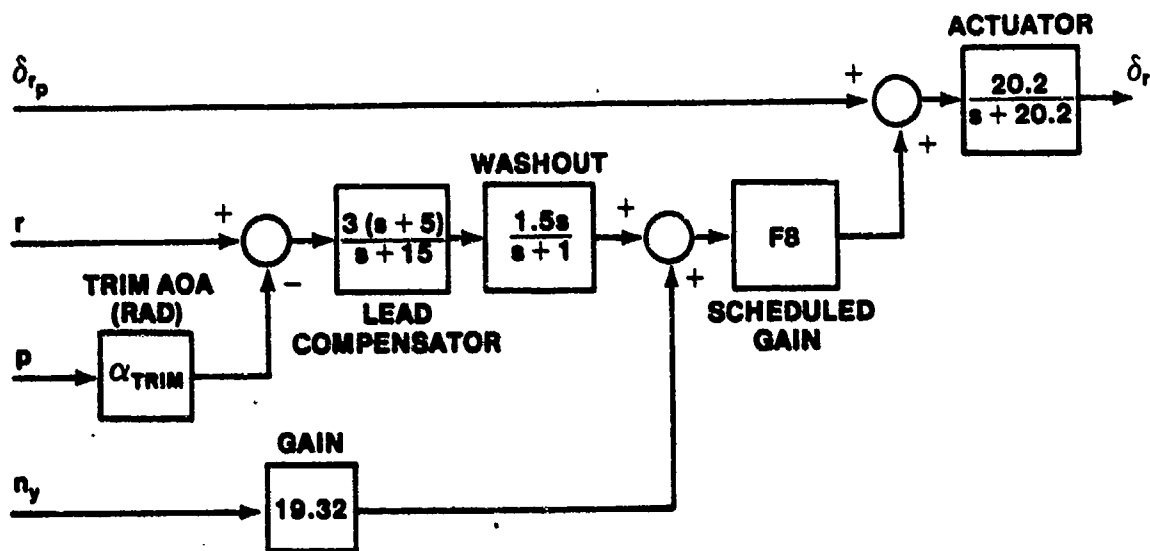
FIGURE 14.201. LINEARIZED DIRECTIONAL AXIS FLIGHT CONTROL SYSTEM

14.5.3.3 Aileron-Rudder Interconnect. An aileron-rudder interconnect improves the aircraft turn coordination below 29° angle of attack. Above 29° angle of attack or below 60 kts ground speed with the main landing gear on the ground, the ARI is omitted from the system. The ARI gain is a function of the aircraft angle of attack as well as the dynamic pressure divided by the static pressure. The aircraft possesses proverse yaw at low angles of attack and adverse yaw at higher angles of attack. For low angles of attack, a right roll will produce a left rudder deflection for coordination. At angles of attack above 10° as well as at very low or very high airspeeds, a right roll command will produce a right rudder deflection which, in turn, causes a nose right yawing motion to offset the adverse yaw.

The area of interest concerning the aileron-rudder interconnect involves a determination of its effectiveness in maintaining coordinated flight during turns.

14.5.3.4 Lateral Acceleration Canceller. During gunfiring, the directional axis cancels 0.2 g's of the lateral acceleration feedback signal. Since the gun is located in the left wing root, the lateral accelerometer detects a lateral acceleration caused by gun firing. The feedback of this acceleration

to the rudder could cause the aiming symbol to be pulled off of the target due to the rudder deflections. Referring to the directional axis of Figure 14.179 with the trigger in the non-firing position, the acceleration canceller output is zero. When the trigger is depressed, two switches are repositioned to provide an output signal after a 0.1 second delay to allow the gun to spin up and begin firing. The integrator acts as a memory device which holds whatever lateral acceleration is present when the trigger is depressed. The integrator signal is compared with the lateral acceleration sensed by the accelerometer and the difference is limited and compared with the lateral acceleration. The resulting lateral acceleration signal plus any additional lateral acceleration which exceeds the 0.2 g limits in the canceller circuit. Of concern are the aircraft directional handling qualities during gun firing and the adequacy of the canceller in preventing unwanted rudder inputs when the trigger is depressed.

14.5.3.5. **Departure Prevention System Operation for the Directional Axis.** The departure prevention system provides additional yaw rate feedback (0.75° of rudder deflection per degree per second of yaw rate) to the directional axis when the aircraft angle of attack is above 29°. The pilot rudder authority is decreased to zero so that no pilot rudder commands are possible. All feedback paths for the directional axis are available. If a right yaw rate develops, left rudder is commanded to oppose the yawing motion (anti-spin rudder).

Two areas of concern arise regarding the departure prevention system:

1. How effective is the departure prevention system in preventing yaw rates (which are necessary for entry into a spin) from developing? This question must be answered for all aircraft configurations and for a number of flight conditions which might precipitate in departure, including typical tactical air-to-air and air-to-surface maneuvers.

2. What is the impact of the departure prevention system on air-to-air tactics in this aircraft, especially during maneuvers in the vertical at low airspeeds?

14.5.4 **Additional Features**

14.5.4.1 **Gun Compensation.** Gun compensation is necessary to offset rolling

and yawing moments during gun firing as a result of the gun location in the left wing root. The gun compensation network block diagram is presented in Figure 14.180. When the trigger is pulled, a 0.1 second time delay is provided to allow the gun to spin up to firing speed and begin to fire. The bias signal of 1.0 passes through a lag filter which blends the signal to avoid an abrupt change in flight control laws. At low dynamic pressures, the signal passes through the lower path gain, which is a function of the dynamic pressure. At very low airspeeds or very high altitudes, the signal in the upper path is cancelled due to the bias signal and the multiplier. At high dynamic pressures, the lower path signal is driven to zero by the scheduled gain. The upper signal is multiplied by a gain which is a function of the static pressure divided by the standard day sea level atmospheric pressure. The upper and lower path signals are summed and passed through another scheduled gain, which is a function of the dynamic pressure divided by the static pressure. At approximately Mach 1.01, the signs of the roll rate and rudder commands are reversed. At lower Mach, a positive roll rate command and a negative rudder deflection command are generated to offset the rolling and yawing moments created by the gun recoil. Above Mach 1.01, the situation is reversed due to the drag of the downward deflecting aileron producing the desired yaw moments and the decreased rudder effectiveness in yawing the aircraft. The flaperons deflect symmetrically to a -2.0° position for transonic and supersonic drag reduction. During gunfiring, the aileron (left) is in a region of low drag while the down aileron (right) increases drag on the right wing to offset the gun recoil. The rudder deflects slightly but should have little effect in supersonic flight. The compensation provided to the yaw axis is limited to 6.6° of rudder deflection and, consequently, to 11° per second of roll rate.

14.5.4.2 Trailing Edge Flap System. Figure 14.180. The trailing edge flaps extend automatically whenever the gear handle is down, the alternate flap switch is in extend, or, for the two seat aircraft, when the air refueling door is open. The enlarged canopy of the two seat version provides minimal clearance for air refueling, necessitating a reduction of the aircraft angle of attack, and hence its deck angle, for air refueling. The commanded trailing edge flap position is a function of the dynamic pressure to avoid overspeed. The flaps are fully extended below 0.34 Mach and are fully blown

up above 0.58 Mach. Using the alternate flap switch, it is possible to improve the low speed maneuvering capability of the aircraft at low Mach using the additional lift provided by the flaps. The flaps may be flown in the alternate position at all times. However, the control laws of the pitch axis revert to the power approach configuration at all flight conditions. Because of the mechanical bias present in the flaperon system, a 20° flap command actually provides 21.5^O of flap deflection command due to an electrical bias which offsets the mechanical bias. A full trailing edge flap deflection of 20° is provided by the system. A 1.5^O bias is always provided via the trailing edge flap system to offset the mechanical bias present in the system so that no residual flaperon deflection is present. Transonically, the trailing edge flap is deflected upward to reduce drag. A maximum trailing edge up deflection of -2.0^O is provided in the flap circuitry to reduce the rate at which the flaps are deflected, the maximum flap deflection rate being 5° per second. Additionally, a lag filter is provided to further blend the flap deflection to reduce pitch transients during flap movement and allow the longitudinal axis integrator to keep the aircraft trimmed. The flap system is disabled if either flaperon is locked out due to battle damage to avoid asymmetric flap deflections. Of interest here are the pitch transients which occur during flap extension and retraction, the usefulness of the flaps for low speed maneuvering and the effect of the flaps on air-to-air gun tracking with the alternate flaps selected when the engagement transits regions where flap deflections and retractions occur.

14.5.4.3 <u>Standby System</u>. The air data system is nonredundant. In the event of a dynamic or static pressure system failure, standby gains are provided for all the scheduled gains in the system. A linear analysis of the system using these gains determines the aircraft handling qualities with the standby flight control configuration.

14.6 <u>FLIGHT CONTROL SYSTEM TESTING</u>

A through understanding of aircraft flight control systems is required to conduct safe, efficient, and thorough flight test programs on modern, highly augmented aircraft. The goal of both the designer and the tester is to

provide aircraft to operational units that can efficiently accomplish their design missions—aircraft which are easy to fly so that the crew can devote their attention to accomplishing mission objectives.

This section applies the background knowledge gained in previous sections to the verification testing of the performance of the flight control system.

14.6.1 Ground Tests

The flight control system and related subsystems should be thoroughly tested on the ground prior to the start of flight testing. This is critical in the case of flight control systems since the pilot's ability to fly the aircraft is directly dependent upon the proper operation of the flight control system. A comprehensive ground test phase will ensure that the system is installed correctly and functioning properly, and will reveal some flying qualities or flight control system design deficiencies which can impact flight safety.

14.6.1.1 Mandatory Ground Tests. Sufficient ground testing must be accomplished to ensure the aircraft is safe for flight. All system components must be tested to demonstrate their satisfactory performance and operation under the environmental extremes expected to be encountered during the flight test program. The complete flight control system must pass the following tests, either on an "Iron Bird" mockup coupled to a computer aerodynamic simulation of the aircraft where the flight control system is functionally, statically, and dynamically duplicated, or on the actual aircraft.

1. Power supply variation tests should be accomplished to demonstrate satisfactory system operation over the range of allowable power supply variations. The requirement states: "Sufficient electrical, hydraulic, and pneumatic power capacity shall be provided in all flight phases and with all corresponding engine speed settings such that the probability of losing the capability to maintain at least FCS Operational State III (Level 3 flying qualities) airplane performance shall not be greater than extremely remote when considering the combined probability of system and component failure and the cumulative exceedance probability of turbulence." Electrical, hydraulic, and other required power sources should be applied and calibrated at maximum rated positions. After warmup, the power sources should be varied and modulated throughout their specified ranges. No steady state or transient modulation changes in the power source, within permissible limits, should cause a variation or modulation in the flight control system's performance

which may result in undesirable or unsatisfactory operation. With rated power applied, all switches, controls, and components should be operated as in actual flight. The power source should not vary beyond permissible operational limits when the system is operated against load conditions varying from no load to full load. Power supply variations have caused several A-10 and F-16 in-flight loss of control incidents, some resulting in the loss of the aircraft. These tests should be performed on the operational mockup in accordance with the supporting documentation for MIL-F-9490.

2. Limited fatigue tests must be performed to ensure the structural integrity of the flight control system mechanical elements. A full fatigue life demonstration is not required prior to the first flight. Fatigue tests may be accomplished by cycling loads on components fixed in one or both hardover positions or in an intermediate position. Hydraulic system pressure impulse loads are applied to the system. An appropriate alternate test facility should be used, such as the aircraft fatigue test rig, rather than the actual aircraft.

3. Stability margin tests which cannot be economically or safely tested in-flight, should be accomplished. The frequency response tests, discussed in Paragraph 14.6.1.3 fulfill this requirement. These tests should be performed on the test aircraft when possible.

4. Tests should be performed to determine the effects of single and multiple flight control system component failures on the performance, safety, or mission accomplishment reliability of the aircraft as well as to develop emergency procedures to counteract the effects of failure. For essential and flight phase essential controls, the following tests of AFCS BIT (Automatic Flight Control System Built-In-Test) and failure reversion capability should be considered:

   a. Overtemperature tests of the AFCS computers, panels, and sensors should be performed to evaluate the BIT capability of detecting failures induced by progressive overheating.

   b. Wire hardness failures (shorts between wires and ground as well as open circuits) should be tested to evaluate the BIT capability to detect wiring damage or failures.

   The primary objective is to ensure that true redundancy exists in the flight control system by verifying that individual failures in each channel are detected, remedied, and are not the cause of multichannel failures. Much of this testing may have to be accomplished on the "iron bird" mockup of the flight control system rather than on the actual aircraft.

5. Flight control system wear life tests must be performed in accordance with MIL-F-9490 to identify areas where component wear is likely and where frequent inspection may be required.

6. Other tests should demonstrate the flight control system performance as well as compatibility among the flight control system elements and with interfacing systems, such as navigation, pitot static, or weapons delivery systems. A detailed discussion of possible test methods to be used to perform some of these tests is provided in Paragraph 14.6.1.3.

7. Temperature variation tests to duplicate the normal operation or failure of temperature regulating elements must be performed on any components whose performance is sensitive to temperature variations.

Analog and digital flight control computer program operation should be thoroughly tested using ground simulations, the "iron bird" mockup, and the aircraft, and should include simulated support system and flight control system failures. A real danger exists in the area of digital systems, where insidious programming bugs may occur, endangering flight safety.

14.6.1.1.2 <u>Aircraft Ground Tests</u>. Prior to the first flight:

1. Limit Cycle and structural resonance tests must bo performed. A procedure used at the Air Force Flight Test Center is discussed in Paragraph 14.6.1.2.

2. Functional, dynamic, and static tests must demonstrate that all flight control system equipment is properly installed. These tests should be conducted on the integrated flight control system and test instrumentation package, as installed in the test aircraft, to ensure proper flight control system operation as well as check that the test instrumentation does not impact the flight control system performance. Possible test methods are discussed in Paragraph 14.6.1.3.

3. Electromagnetic interference tests investigate the electrical interference between system components and with other aircraft systems and must be within the limits established by applicable military specifications as referenced in MIL-F-9490.

4. Flight control system integrity tests ensure the soundness of components and connections as well as the adequacy of component clearances and proper operation. The importance of this test is emphasized by an incident aboard an F-16 test aircraft due to an inadequate wire bundle clearance with the aircraft structure, which resulted in wire insulation wear and an electrical short. The aircraft was safely recovered, but the implications for a fly-by-wire aircraft are self evident.

5.	Taxi tests should be performed with increasing airspeed and all feedback loops closed to examine flight control system stability above zero airspeed. Flight control sensor outputs and control surface deflections should be analyzed for proper system operation.

6.	Unique features of the aircraft flight control system, such as the A-10 jammed control feature, should be tested thoroughly on the ground for proper implementation. It may not be possible to safely test these features or certain combinations of these features (A-10 jammed control followed by manual reversion) in flight, especially features provided for unique emergency situations. Ground or airborne simulations should be used to investigate the aircraft handling qualities in these situations.

14.6.1.2	Limit Cycle and Structural Resonance Tests. A limit cycle is a sustained closed loop oscillation of a control surface at a frequency usually less than 5 Hertz (31.5 radians per second). It is caused by nonlinear elements in the flight control system or nonlinear operation of control system elements. Some examples of nonlinear elements are: limiters, mechanical hysteresis or deadzones. A limit cycle occurs when the phase margin of the flight control system loop (consisting of the aircraft, motion sensors and control system elements) is zero degrees and the control system gain is high.

Two types of limit cycles occur -- stable and unstable. Stable limit cycles are low amplitude oscillations of the control surface as a result of nonlinearities about the null position, such as hysterisis or deadzones. Unstable limit cycles are a result of system saturation such as actuator rate limiting, and are large amplitude divergent oscillations of a control surface, which eventually cause the surface to oscillate between the mechanical limits at the maximum actuator rate. The low amplitude oscillation is undesirable in general, but is usually not catostrophic. The large amplitude oscillation is catostrophic in that loss of control could occur at low speed and structural failure will occur at high speed.

The limit cycle problem can be alleviated by lead compensation to increase the phase margin of the control system in the susceptible frequence range. Another approach to alleviate or reduce limit cycle problems is to reduce the system gain. The lead compensation is usually used so that a sufficiently high gain is maintained to provide the desired handling qualities, that would normally be degraded by a system gain reduction.

Aircraft structural resonance is characterized by a sustained high frequency oscillation of a control surface at a resonant structural frequency, usually above 10 Hertz (62.8 radians per second). It is usually caused by control system sensors (such as rate gyros) sensing small vehicle structural vibrations (caused by control surface .movement) and feeding these signals back to the control surface through the flight control system. At structural resonant frequencies, these signals are amplified and a phase lag of 180° may occur through the control system alone. If the phase lag from the sensor to the control surface is 180° and the total system gain is high enough, the surface motion will sustain itself and structural resonance will occur.

Since control system instabilities can adversely affect flight safety, ensure that these characteristics are well known for all new aircraft. Analytical math models can predict some of the interactions and instabilities that occur between the flight control system, the structure, the aerodynamics and the pilot, but are often limited by the validity of the input data. Ground testing flight hardware will better define these interactions prior to the first flight and following any significant flight control system modifications.

A reasonable approach to flight tests:

1. Conduct ground tests on the actual flight hardware installed in the test aircraft prior to the first flight to predict limit cycle and structural resonance characteristics.

2. Large gain margins for flight control system instabilities should be used for the first flight of a new aircraft to account for uncertainties in the analysis.

3. Carefully controlled inflight tests should be conducted early in the flight test program to establish the actual limit cycle and structural resonance characteristics of the aircraft. These tests may allow some relaxation of the large gain margins used for the initial flights.

14.6.1.2.1 Limit Cycle tests. Perform limit cycle tests on each axis separately unless coupling of the control system axes occurs, in which case multiple, or even all, axes should be tested simultaneously as well as separately.

14.6.1.2.1.1 Ground Tests. The equipment and instrumentation necessary to conduct ground limit cycle tests include: An analog computer in which the appropriate aircraft aerodynamic equations of motion are programmed, position transducers on the control surfaces, and strip recorders to document control surface position limit cycle amplitudes and frequencies. If a digital computer simulation of the aircraft aerodynamics is used in lieu of an analog simulation, the sampling rates must be well above the highest limit cycle frequency expected. Analog to digital and digital to analog converters must be used to convert continuous parameters (such as control surface position) to digital signals, and to convert digital outputs of the simulation (such as aircraft pitch rate) back to analog signals to simulate the sensor (rate gyro) outputs. Extreme care is required when using a digital aircraft simulation since the sampling and computation lag in the simulation may alter the limit cycle characteristics of the aircraft. An analog simulation is usually preferred for limit cycle tests.

A simulated aerodynamic loop is closed on the aircraft by sending the control surface position to the analog computer (in which the aerodynamic transfer functions of the aircraft are programmed for the simulated flight condition). The outputs of the analog computer are the dynamic motion parameters, such as pitch rate, angle of attack, or normal acceleration, and are scaled and fed back into the flight control system at the point where the sensor output occurs, thus completing the control system loops. The actual sensors should be disconnected since actual aircraft motions (due to the control surface motions) would be added to the system, altering the limit cycle characteristics. Insure the flight control system configuration (gain schedules, switch positions, etc.) is consistent with the simulated aerodynamic flight condition.

Small, (less than one degree control surface command) and larger (greater than one degree) amplitude step inputs are applied to the control system at the point where the pilot input is summed to the feedback paths. Alternate inputs are applied where the sensor inputs are provided to the flight control system. Small and large inputs should be applied to the system at progressively increasing values of total loop gain. The loop gain may be adjusted at any point in the loop--in the flight computer for digital system and in the analog computer simulation of the aircraft in the case of hardwired

14.280

analog flight control computers. Limit cycle amplitudes and frequencies are recorded at each gain setting by recording the control surface deflection on a strip chart recorder. The loop gains should be increased until a divergent oscillation is obtained.

14.6.1.2.1.2 Ground test Criterion. Based on experience obtained during test programs conducted at the Air Force Flight Test Center, a gain margin criterion has been established for limit cycle phenomenon. With a gain margin of 6 decibels used (double the normal system gain at any flight condition), no limit cycle is allowed which has an amplitude greater than 0.5° of control surface deflection, peak-to-peak, in any axis. The maximum speed envelope is restricted to ensure the gain margin is provided during initial flights, if necessary. This criterion is conservative to provide a safety margin due to the many uncertainties which exist is predicting limit cycle characteristics. For aircraft which schedule control system gains with airspeed, Mach, or dynamic pressure, the high speed condition may not be the most critical in terms of encountering a limit cycle. The high speed condition will, however, be critical from the structural integrity point of view if a limit cycle is encountered.

14.6.1.2.1.3 Flight Tests. Initial flights should use large gain margins for suspected limit cycle conditions by restricting the maximum speed using the ground test results. Before the flight envelope is expanded, carefully controlled inflight tests should determine the actual limit cycle characteristics of the aircraft and flight control system combination. Inflight tests are conducted by applying small, sharp step or pulse inputs into each axis of the flight control system at incrementally increasing stabilized airspeeds. Real time control surface data should be recorded at each flight condition. If no limit cycle tendency exists, the aircraft is cleared to the next test point. This procedure is continued until a tendency toward a large amplitude limit cycle is observed. At all times, the test pilot must be ready to disconnect the control system, reduce speed or reduce the control system gain, if possible, should a control system instability occur. The results obtained from inflight tests establish the maximum allowable control system gain or maximum allowable flight speed.

14.6.1.2.2 Structural Resonance Tests. Structural resonance occuring inflight can be destructive and result in the loss of the aircraft. The Air

Force Flight Test Center policy is to conduct ground tests on the actual flight control system and structure of a new aircraft (as opposed to mathematically modelling the aircraft control system and structure). This eliminates many uncertainties concerning control system response characteristics, structural model response and sensor location with regard to the structural wave shapes.

14.6.1.2.2.1 <u>Ground Tests.</u> Structural resonance for the worst case is assumed to be independent of aerodynamic flight conditions. No aerodynamic computations, such as those needed for limit cycle tests, are required. The tests apply relatively large, sharp inputs into each axis of the flight control system just prior to the surface servo actuators. The aircraft should be as close as possible to the actual flight configuration. All flight hardware and aircraft structure should be installed and secured. The landing gear struts should be deflated to a minimum allowable value to reduce gear frequencies as much as possible so that they will have minimal influence on the structural resonance frequencies. Tests should be performed on a range of fuel and external store configurations. The control surface frequency and amplitude for each axis are recorded to identify any structural resonance. The flight control system gains should be increased gradually to at least twice the maximum total system gain to be used inflight without encountering resonance.

Structural resonance can damage the aircraft. The flight control system must be disengaged as soon as resonance occurs. A good way to disengage the system is to disconnect the sensor by opening the sensor feedback path. For fly-by-wire aircraft, disconnect switches may be added to prevent feedback to the surface if resonance is encountered. The disconnect capability should be remote from the aircraft since large aircraft motions can be encountered during these tests. If a structural resonance problem is encountered, an aircraft flight control system redesign or gain reduction may be required.

14.6.1.2.2.2 <u>Ground Test Criterion.</u> Ground structural resonance tests have been performed with success during numerous aircraft test programs at the Air Force Flight Test Center. The current structural resonance criterion requires that all three axes of the flight control system (six degrees-of-freedom for control configured vehicles) be capable of operating on the ground at twice the maximum total axis gain to be used in flight without

sustaining structural mode vibrations. This conservative criterion was established due to the many uncertainties in predicting structural resonance. These uncertainties include inaccuracies in theoretical or experimental predictions of aeroelastic effects, atmospheric turbulence and variations in inertia and structural characteristics due to changes in fuel loads. It is therefore highly desirable to establish large gain margins for the first flight(s) where unexpected problems are likely to surface. As the system characteristics become known or actual inflight structural resonance characteristics are determined, this criterion may be relaxed somewhat.

14.6.1.2.2.3 Taxi Tests. Obtaining structural resonance data should definitely be an objective of any taxi test. The structural filter of the B-1 was modified as a result of structural resonance encountered during the initial high speed taxi tests conducted prior to its first flight.

14.6.1.2.2.4 Flight Tests. Structural resonance flight tests are performed using sharp pulse inputs through the flight control system or by using a structural mode exciter system. These tests may be conducted in conjunction with limit cycle tests or during aeroelastic testing. Structural resonance may be distinguished from limit cycle by the frequency of the control surface oscillation. Careful buildup test procedure should be used.

Further information concerning limit cycle and structural resonance test procedures is provided in Appendix E. An excellent discussion of limit cycle tests conducted on the A-7D DIGITAC is in Reference 14.8.

14.6.1.3 Ground Functional Tests. Flight control functional tests should be accomplished by measuring pilot applied forces and the resulting control deflections and then comparing these to the signals applied to the flight control system. For example, F-16 force gradients can be measured using a hand held force gauge and recording the output of the stick force sensors (strain gauges). The voltage output of the command gradient can be correlated to a physical command signal (g's commanded in the case of the F-16) and plotted versus pounds of stick force to yield the actual stick force gradient. A similar technique could be used on a mechanical system with hydraulically actuated control surfaces by plotting stick force versus stick deflection. For flight control systems that do not allow access to components within the system, the control input to control surface position output can be used to verify the force gradient.

Frequency response can be used to determine the open loop transfer functions of the flight control system or to obtain transfer function data on individual components within the system, such as actuators, filters or compensators. The procedure is shown in Figure 14.202. A sinusoidal test signal (from a calibrated oscillator) is applied to a given path of the flight control system (stick force input to control surface deflection or feedback sensor output to control surface deflection). The input and output sinusoidal signals are recorded. The amplitude ratio of the output to the input is computed, as well as the phase shift between the input and the output. A Bode plot of amplitude ratio versus frequency and phase shift versus frequency is constructed and compared directly with block diagram computed data. Transfer function testers are available to perform the frequency response tests and compute the transfer function Bode diagram automatically. However, if the flight control system has nonlinear elements which are frequency dependent (where exciting the system at a particular frequency changes the gain at all frequencies -- such as the Space Shuttle Pilot-Induced Oscillation suppressor) the results can be misleading. Another approach uses the Frequency Response Analysis (FPA) program available at the Air Force Flight Test Center and applies a standard input test signals to the flight control system. Output parameters are recorded at various points in the flight control system and the FPA program reduces the data and provides Bode plots of the transfer functions. The test signals are of small enough amplitude to avoid saturating system limiters and the effects of deadzones are considered or bypassed. The effects of nonlinearities in the flight control system can be obtained by varying the amplitude of the input test signals and recording the outputs. The flight control system configuration must be the same as the configuration at the flight condition of interest.

Gain schedules which depend on pitot static inputs are verified using pitot static test equipment. The static ports are connected to a vacuum pump and the ram air port is connected to a pressure source. A particular altitude is simulated by lowering the static pressure and an airspeed is simulated by increasing the pressure at the ram air port. This procedure is used during
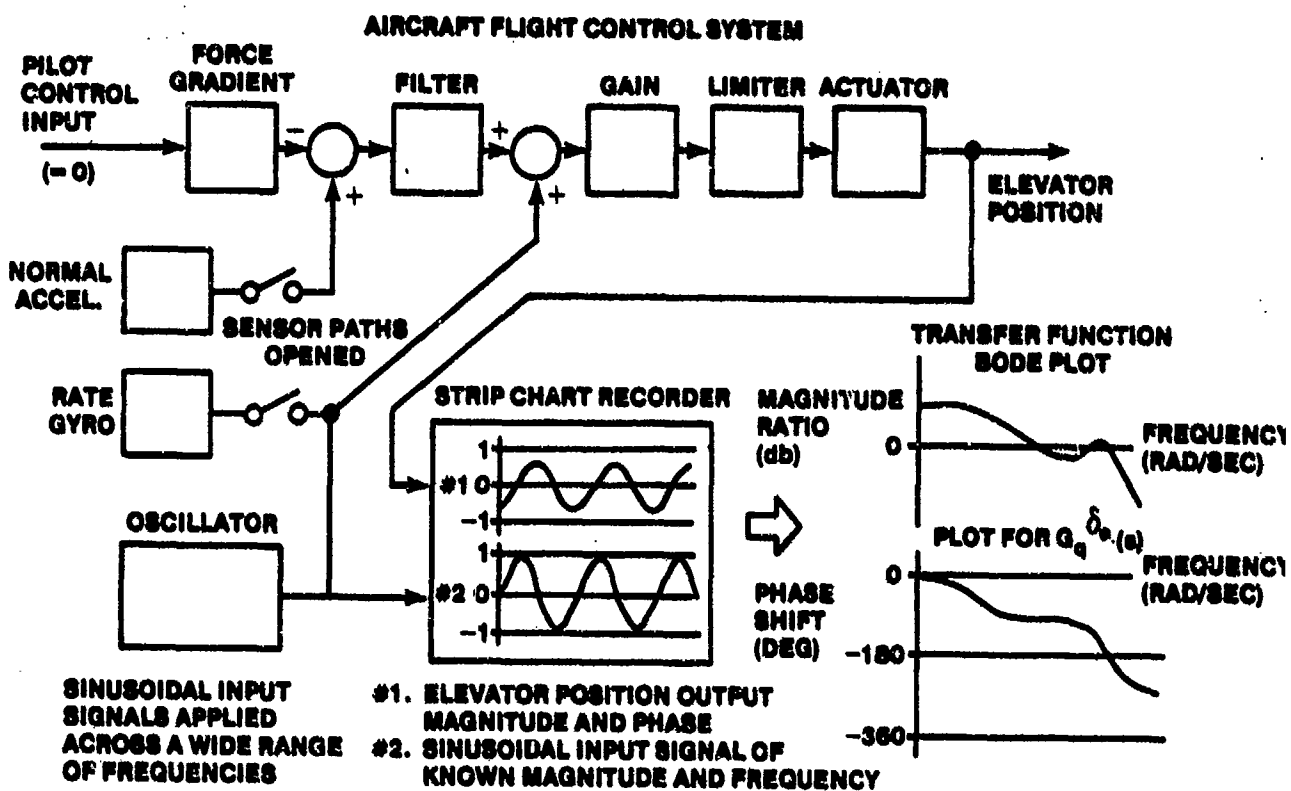
FIGURE 14.202. FREQUENCY RESPONSE TEST PROCEDURE

pitot static system leak checks. The airspeed and altitude combination are determined from the cockpit instruments. The control system gains (voltage outputs) are recorded for a number of flight conditions and compared to the design values. Wheels on the ground switches and other switches in the flight control system may have to be artificially placed in the flight position to obtain proper flight control system operation.

An end-to-end check is performed to determine flight control system operation under simulated dynamic conditions. The pitot static system simulates a particular flight condition to set scheduled gains at the appropriate values. A computer simulation simulates aircraft aerodynamic responses to control surface inputs. These responses are applied to the flight control system where the sensor outputs interface with the flight control system. The actual control surface positions are provided to the simulation, closing the complete flight control system loop. Pilot inputs are applied through the control path and parameters in the flight control system recorded. Comparing actual flight control responses to engineering simulations for similar inputs provides a good check on the system implementation across a wide range of aerodynamic conditions.

14.6.2 Flight Tests

Flight testing ensures that the aircraft flight control system meets the following general criteria:

1.   Contractual specifications

2.   Adequate flying qualities for mission accomplishment

3.   Proper system operation under a variety of flight conditions and situations

4.   Flight safety considerations

When testing the handling qualities of an aircraft, a thorough knowledge of the aircraft's design missions and required mission elements is essential. The test pilot often makes qualitative decisions regarding the mission suitability of the aircraft. He can only assess the suitability of the aircraft based on his flight experience, his training, and his understanding

of the intended mission. Sometimes an aircraft must be evaluated against a new mission, and the pilot must rely heavily upon his understanding of the tasks required to accomplish that mission rather than upon his personal flight experience. Table 14.6 provides a list of tasks that are elements of a multi-role fighter mission. A listing of this type is a first step in the design of a handling qualities test program. After the mission tasks are defined, the specific elements of each task should be determined to clearly define important considerations which contribute to task accomplishment (Table 14.7). Once the specific elements of a task are defined, flight test maneuvers may be specified to thoroughly evaluate the handling qualities of the aircraft.

14.6.2.1 Inflight Simulation. An inflight simulation effort, if pursued, should occur relatively early in the flight control system development—shortly after the major control system configuration decisions are finalized based on ground simulations, and as soon as adequate wind tunnel data are available to provide a realistic simulation of the aircraft. The idea is to perform inflight simulations early enough so that handling qualities deficiencies, especially in those flight phases which are not well simulated on the ground simulators, can be identified and corrected. Ground simulations are most deficient in areas where pilots make high frequency inputs to the aircraft, such as during landings, fingertip formation, air refueling, air-to-air and air-to-ground tracking, or other maneuvers where the pilot relies on visual or motion cues. Time delays due to digital sampling and computation which appear in the visual systems of ground simulators preclude the use of these simulations as a viable method for handling qualities determination and refinement during high gain piloting tasks.

TABLE 14.6.   TYPICAL FIGHTER MISSION PROFILE

MISSION EVENTS

Ground Checks
Taxi
Takeoff
- Rotation
- Gear and Flap Retraction
- Acceleration
Climb
Level Off
Cruise
- Steady Turns
Mission Tasks
- Subsonic, Transonic, Supersonic Flight
- Acrobatics
  - Lazy 8
  - Loop
- Air Refueling
- Air-to-Air Combat
  - Gunnery
  - Missiles
  - Break Turns
  - Jinkout Maneuvers
- Air-to-Ground Combat
  - Roll-ins
  - Strafe
  - Dive Bomb
  - Pop-ups
  - Rolling Pull-offs
- Low level
- Formation
  - Fingertip
  - Trail
  - Fighting Wing
  - Tactical
Descent
Approach
- IFR
- VFR
- Information
Landing
- Normal
- Minimum Run
- Crosswind
- Wet or Icy Runway
- Emergency
- Formation

TABLE 14.7. DETAILED TASK ANALYSIS

TASK: APPROACH AND LANDING

ELEMENTS:

Airspeed (Angle of Attack) Control
- Speed Stability
- Slow Speed Cue
- Flight Path Stability
- Engine Response
- Turbulence Effects

Flight Path Control
- Longitudinal Attitude Control, Predictability and Precision
- Aim Point Predictability and Precision
- Short Period Dynamics (High Gain Task)
- Control of Runway Alignment

Attitude Control
- Control Harmony
- Control Sensitivity
- Friction and Breakout
- Predictability and Precision
  - Touchdown
  - PIO Tendency
  - Float and Balloon Tendency
  - Turbulence Effects
  - Aerobraking

Touchdown Point Predictability, Precision and Repeatability

Gear Dynamics at Touchdown

Crosswind Effects

    IFR (Hood) Approaches
- Heading Control

Overhead Traffic Patterns
- Maneuvering Gradient

Heads-Up Display and Instrument Lag Effects
- Angle of Attack
- Attitude References
- Flight Path Reference
- Readibility

Approach Techniques
- Constant Angle of Attack to Touchdown
- Flare
- Wing Low
  - Lateral-Directional Stability
- Crab

Pilot Visibility

Current inflight simulators include:

1. The Total Inflight Simulator (TIFS), a six degree of freedom variable stability C-131 which is capable of purely digital, purely analog, or hybrid flight control simulations.

2. The variable stability NT-33, a three degree of freedom aircraft with analog or digital control system capabilities.

3. The variable stability X-22 Vertical Takeoff and Landing aircraft for V/STOL simulations.

4. Two variable stability Navions, one with a six degree of freedom capability.

5. A variable stability Learjet with three degrees of freedom and similar capabilities as the NT-33. This aircraft is not normally available for inflight simulations due to its use for student test pilot instruction at the Air Force and Naval Test Pilot Schools.

6. A variable stability F-16 is being planned for future use.

Airborne simulators have a limited ability to simulate aircraft performance, structural effects or cockpit environment of the test aircraft. It is essential to minimize the effect of those characteristics of the simulation aircraft which interfere with the desired evaluation.

14.6.2.2 **Flight Testing.** Flight tests should not be conducted in environmental conditions for which the system has not been thoroughly tested on the ground.

Preparation for the flight test requires a consolidation of experience from the following areas:

1. A through knowledge of the flight control system operation and design. Analysis of the flight control system block diagram will aid in understanding the system in detail and will help identify specific test objectives. The EASY program available at the Air Force Flight Test Center, as well as analysis methods discussed in this text, should be used.

2. Consideration of the results obtained during ground and airborne simulations. The limitations of each simulation method used must be kept in mind when evaluating the results of handling qualities tests.

3. Analysis of the results obtained during ground tests conducted on the flight test article.

4. Advantages and disadvantages of the various test methods available to determine the adequacy of the aircraft's handling qualities for the required mission phases.

14.6.2.2.1 <u>Control System Operation</u>. Particular attention should be given to the following flight control system areas:

1. Variable gain scheduling operation.

2. Single point failures and resulting flight control characteristics.

3. Effect of programmed control system reconfigurations, such as switch position gauges and feedback control law alterations (change from pitch rate feedback to blended pitch rate and load factor feedback, for instance).

4. Failure mode tests, concentrating on transients, proper operation of the degraded system and the adequacy of aircraft handling qualities.

5. Operation of automatic limiters, such as load factor or angle of attack limiters, during both slow and rapid maneuvers.

6. Operation of special features such as roll coupling prevention features during aileron and rudder rolls, under varying load factor conditions.

7. Effects of actual weapons employment on handling qualities, especially gun firing.

8. High angle of attack maneuvers including stall warning or prevention features incorporated into the flight control system. These should be tested during 1 g and accelerated maneuvers as well as during very slow flight conditions such as resulting from nose high zooming flight at speeds below the stall speed. Departure and spin characteristics with the flight control system engaged should be investigated as well as transients due to partial or complete flight control system disengagements as high angle of attack flight is approached (disengagement of the A-7 roll CAS at 22 units angle of attack, for example).

9. Pilot relief mode operation (auto-pilot features). These must meet the requirements of MIL-F-9490.

10. Engagements and disengagement transients during auto-pilot operation.

11. Operation of warning systems to advise the pilot of inadvertent auto-pilot disengagements. (An L-1011 crashed due to an unnoticed disengagement of the altitude hold mode with no accompanying cockpit warning.)

12. Effects of atmospheric turbulence, jet wash and runway crosswinds on the aircraft's handling qualities.

13. Verification of ground test data concerning limit cycle gain margins and structural resonance (Paragraph 14.6.1.2).

14. Effect of asymmetric store loads on all aspects of the control system operation and performance, especially regarding adequacy of control authority, automatic maneuver limiter operation and high angle of attack characteristics.

15. Effects of center of gravity location and gross weight on handling qualities.

16. Trim system rates and authority (including auto-trim features).

17. Electrical power transients or voltage reduction effects on control system operation and flying characteristics.

18. Hydraulic system failure effects.

19. Fault tolerance (ability to reconfigure or compensate for detected system failures) and redundancy management (voting schemes to detect faults).

20. Human factors associated with flight control system operation, pilot control actuation techniques, control harmony, friction, breakout, and control forces.

21. Operational environmental effects on control system components and overall system operation.

22. Environmental control system capabilities to provide adequate cooling for flight control system avionic components.

23. Operation of unconventional flight modes as well as associated human factors and handling qualities.

24. Structural implications of control system operation. This is critical in programs like the AFTI-16 where the control surface motions are changed relative to the F-16 to provide unconventional flight modes.

25. Effects of non-flight control system failures (such as engine failures in various configurations) on the handling qualities of the aircraft. These failures should be tested in conjunction with a fully operational flight control system (compatible with the failure) as well as with partial or complete flight control system failures.

26. Flight control system operation during maneuvers typical of the aircraft operational mission, including training maneuvers. The A-10 Beta-dot stability augmentation system (SAS) provides rudder inputs during maneuvers which pass through 90° of pitch (loops) and during turns when the SAS gain is suddenly changed according to a discrete, rather than a continuous, gain schedule with airspeed.

27. Effects of nonlinear force gradients on pilot-in-the-loop tasks, especially near gradient slope changes.

14.6.2.2.2 Flight Test Instrumentation. In addition to the data acquisition system configured for stability and control testing, the flight control computer should be instrumented to record:

1. Signals being supplied to the computer by sensors and pilot controllers.

2. Signals being sent by the computer to the actuators.

3. Internal signals within the flight control computer such as:

   a. Filter and integrator inputs and outputs.
   b. Switch positions.
   c. Inputs and outputs of nonlinear elements.
   d. Results of computations as well as signals being supplied to the computational algorithms.
   e. Operation of logic decisions.

A thorough instrumentation of digital flight control computer programs is extremely important during developmental testing. Thorough documentation of the operation of the flight control program will greatly aid data analysis, is essential to detecting and defining glitches in the program operation and is necessary to confirm the proper operation of the flight control system. Without this instrumentation, unexplained anomolies in the aircraft flying qualities will be difficult to explain and correct if they are a result of computer programming bugs.

14.6.2.2.3 Configuration Control. During developmental testing of digital flight control system.s it is critical to establish strict software configuration control policies. This is necessary to ensure that:

1. No software change is incorporated which results in the development of a flight safety hazard. Sufficient analysis must be performed to assess the impact of changes on the aircraft flying qualities.

2. The test configuration of the flight control system is known at all times. The configurations should be confirmed prior to flight using ground test procedures discussed in Paragraph 14.6.1.3.

3. Test results can be correlated to specific configurations.

4. Configuration changes are well documented.

Strict configuration control is required to ensure that proposed software changes are adequately reviewed prior to incorporation into the flight control system, and that the full impact of proposed changes are completely investigated (with adequate simulation, if available).

The procedures established to manage proposed software changes depend on the impact of those changes on the flight control system if the changes do not function properly, if unforeseen program operations occur, or if undesirable operations which already exist are further degraded. Software changes to the flight control program can fall into one of the following categories:

1. Nuisance failures which do not affect flight safety but may cause delays in some test accomplishment.

2. Mission failures which may degrade the flying qualities (reduce the level of flying qualities or cause reversion to backup flight control modes) and result in the loss of effective testing.

3. Flight safety failures which severely degrade flying qualities (cause large aircraft response transients or loss of control) and may result in loss of the aircraft as well as injury or death to the crew.

Flight control software changes are governed by Air Force Class II modification procedures and regulations (AFR 57-4 and AFSCR 80-33). These procedures are often unwieldly in software development efforts and alternate procedures must be established in the test plan. Strict software change review procedures should be used to ensure a complete technical and safety review of proposed changes as well as to formally document all changes (including a complete listing of the most recent software package with the changes incorporated). A possible way to manage this process is to create a

software review board to assess the technical and flight safety impact of all software changes. When proposed changes are considered, the changes must be carefully evaluated for the entire envelope for which the aircraft has been previously cleared. Often a change implemented to correct a deficiency at one flight condition can adversely impact the flying qualities in another flight regime. Additionally, attention must be devoted to the effects of changes on limit cycle and structural resonance characteristics.

14.6.2.3 <u>Test Techniques</u>. Table 14.8 contains a list of flight test techniques available to determine the performance of flight control system. Open loop (non-task related) techniques are useful for aircraft which are not highly augmented, and respond to a pilot input with essentially a classical second order short period or Dutch roll. Static tests are useful for maneuvering force gradient testing and determinating apparent static stability. A pilot control frequency sweep can generate time history data (similar to the tracking test technique data) which can be reduced to obtain Bode plots of the aircraft or flight control system transfer functions (Paragraph 14.5.1.3). Open loop tests provide data which can be compared to MIL-F-8785C requirements, and are thereby compared to characteristics experimentally determined to provide adequate handling qualities in various mission tasks. Even for classical aircraft, open loop tests cannot be relied on exclusively to determine the adequacy of the aircraft's handling qualities to accomplish mission related tasks.

Closed loop testing, where the pilot accomplishes a precision, well-defined, mission-related task, is essential. Tracking test techniques are currently the only methods available which can reveal handling qualities deficiencies in highly augmented aircraft (those in which the dynamic response characteristics of the aircraft are governed by the flight control system more so than by the aircraft aerodynamics.) A detailed discussion of closed loop (pilot-in-the-loop) test techniques is provided in subsequent sections.

TABLE 14.8. HANDLING QUALITIES FLIGHT TEST TECHNIQUES

OPEN LOOP TEST TECHNIQUES

Longitudinal Static Stability
    - Stabilized Method
    - Accel-decel Method
Maneuvering Stability
    - Stabilized 'g' Method (Pull-up Technique)
    - Slowly Varying 'g' Method
Lateral-Directional Stability
    - Stabilized Sideslip Method
    - Slowly Varying Sideslip Method
Roll Performance (1 g and Loaded)
Dynamics
    - Doublet Inputs
    - Step Inputs
Trim Change Tests
Sinusoidal Stick Pump (Frequency Sweep)

CLOSED LOOP TEST TECHNIQUES

HQDT
    - Air-to-Air
    - Air-to-Ground
Fingertip Formation
Air Refueling
Spot Landings
Precision Approaches
    - Meatball (Carrier Landing System)
    - ILS
Precision Attitude Changes
Horizon Tracking

14.6.2.3.1 Tracking Test Techniques. Open loop test techniques to identify the dynamic response characteristics of an aircraft do not adequately evaluate the dynamic modes of the aircraft. This is particularly true in two situations:

1. High gain pilot-in-the-loop mission related tasks, such as formation, air refueling, precision landings, air-to-air or air-to-ground target tracking.

2. Highly augmented aircraft where the aircraft response is more dependent on the characteristics of the flight control augmentation system than on the aerodynamic characteristics of the aircraft.

The handling qualities during tracking (HQDT) test technique was developed to excite dynamic modes that are not adequately excited by traditional open or closed loop test techniques. Tracking test techniques are a powerful tool for identifying handling qualities deficiencies, and were specifically developed to obtain engineering data to support pilot rating and comment data. An air-to-air tracking test is the most satisfactory precision tracking task, in terms of obtaining both qualitative pilot ratings and comments as well as quantitative time history data, although other tests are possible, such as air-to-ground tracking, precision formation flying or precision spot landings, as dictated by the aircraft's mission or flight phase. It is very important not to confuse tracking test techniques with the operational tracking and gun firing techniques associated with air-to-air combat. While it is expected that the results of tracking tests will provide information on the pilot's ability to precisely control the aircraft's attitude or flight path during combat maneuvers, the data gathered cannot be extrapolated to reflect specific operational mission effectiveness (such as kill ratios to be expected against typical adversaries).

The specific elements of closed loop handling qualities tests are:

1. Pilot flying the aircraft.

2. Mission oriented tasks.

3. Repeatable test maneuvers.

4. Rapid operational envelope scan.

5. Clearly defined performance standards and control strategies. Well-defined tracking tasks are normally used for test maneuvers.

6. Control strategies which are operationally significant but which possess adequate frequency content so as to excite the aircraft and flight control system dynamics over a wide frequency range. To ensure adequate frequency content in the aircraft response, the pilot must immediately, positively, and continuously correct any tracking errors which occur, no matter how small the errors are. This aggressive piloting technique increases the pilot's gain (assuring adequate frequency content) while amplifying the adverse impact of handling qualities deficiencies upon task accomplishment.

7. Adequate duration to separate transient and steady state residual motions and to provide adequate frequency resolution. In analyzing time history data, the frequency resolution and the lowest identifiable frequency are inversely proportional to the duration of the test maneuver.

8. Separation of the effect of noise variables, such as atmospheric turbulence or aerodynamic buffet.

The tracking test technique is philosophically based on the idea that a pilot performing a precision tracking task will be able to easily identify flying qualities deficiencies which make the task difficult to perform well. The pilot is in the loop, not merely providing a test input to obtain open loop data. The task is well defined and the pilot must perform aggressively to obtain the desired degree of precision.

Experience has shown that pilots who are unfamiliar with tracking test techniques or with the test aircraft and its flying qualities may require several familiarization maneuvers before good quality pilot comments and tracking data are obtained.

14.6.2.3.1.1 Precision Tracking Test Techniques. The precision tracking test ensures that the combined airframe and flight control system dynamics are initially and continually excited during the tracking task. An acquisition task is usually used to initially excite the augmented aircraft dynamics. For the remainder of the tracking task (20 to 30 seconds) the precision tracking technique serves to continually excite the combined pilot-aircraft dynamics.

The precision tracking technique used in flying qualities evaluations uses a fixed (noncomputing) gunsight. Computing gunsights are unacceptable since the gunsight dynamics may completely mask the actual aircraft handling qualities during aggressive tracking or the pilot will revert to operational tracking techniques which do not adequately excite the pilot-aircraft system dynamics. The gunsight pipper depression angle should be as nearly aligned with the roll axis as possible. It may be desirable to set the pipper depression angle to correspond to the actual roll axis for the test load factor (constant angle of attack tests).

For air-to-air tracking tests, a prominent feature should be selected on the target aircraft to be the precision aimpoint (like a tailpipe). During a tracking test, the tracking pilot must devote his entire mental concentration

14.298

and physical effort to keeping the pipper on the precision aimpoint. Even the smallest pipper excursion from the precision aimpoint must be immediately, positively and aggressively corrected. The pipper must not be allowed to float near the target, or to stabilize in order to facilitate returning the pipper to the aimpoint. The tracking pilot must use the selected precision aimpoint and resist the tendency to aim at the "center" of the target aircraft. The result of this technique is to make the tracking errors worse than if the pipper were allowed to float undisturbed near the target, especially if the aircraft exhibits poor flying qualities. Despite the reduced tracking accuracy, the precision tracking technique perpetuates the initial perturbation of the combined airframe, control system and pilot dynamics, and has proved to be the most effective test technique for uncovering and magnifying flying qualities deficiencies.

With certain exceptions, tracking tests must be accomplished without using the rudder (pilot's feet on the floor). This is due to the ability of some pilots to completely mask flying qualities deficiencies through rudder coordination. There are two exceptions to this general rule. First, if the pilot is relatively unfamiliar with the aircraft, he may be allowed to used the rudder during the early stages of tracking tests. Serious flying qualities deficiencies will still become apparent despite the rudder coordination while increasing the pilot's familiarity with the aircraft. Second, after flying qualities deficiencies have been discovered using the "feet on the floor" method, The tracking test should be conducted allowing the pilot to use the rudder. This aids in determining the effectiveness of using the rudder during tracking and in proposing modifications to correct the handling qualities deficiencies.

The aircraft must be trimmed prior to starting the tracking maneuver and must not be retrimmed during the tracking test.

14.6.2.3.1.2 **Air-to-Air Tracking Test Maneuvers.** Target aircraft tracking maneuvers can be tailored to the specific handling qualities data to be investigated, but must possess two important characteristics:

1. The maneuver must be repeatable. It must be simple enough so that airspeed and load factor combinations can be easily and accurately repeated from day to day and from target pilot to target pilot.

2.   The maneuver must require the tracking pilot to excite the aircraft and flight control system dynamics to be investigated.

Unless a specific problem is to be investigated, wind-up turns are recommended as the first tracking maneuvers performed. These maneuvers will allow the test team to quickly examine the aircraft's handling qualities throughout the useful range of angle of attack at various Mach and dynamic pressure test conditions.

14.6.2.3.1.2.1 Wind-up Turns. Once the desired Mach and altitude are attained, two techniques may be used to initiate the maneuver:

1.   The target establishes a 30° bank at the tracker's command with the tracker in trail. The tracker turns on the data systems (gun camera and onboard data acquisition system) and clears the target to maneuver. The target initiates the wind-up turn.

2.   The track aircraft is aligned slightly below and inside (the designated turn direction) with the target in 1 g wings-level flight. After turning on the data systems, the tracker clears the target to maneuver. The target initiates the wind-up turn.

In either case, after being cleared to maneuver, the target pilot increases the angle of attack in the wind-up turn at approximately one degree every two seconds while the evaluation pilot performs the acquisition maneuver. The tracker tries to precisely track the aimpoint throughout the remainder of the maneuver. One acquisition maneuver used requires the tracker to place the target on an outer ring of the gunsight reticle and then as rapidly as possible move the target to the pipper, where precision tracking is immediately begun.

The optimum tracking range is 1500 feet, plus or minus 500 feet. This range keeps the tracker close enough to the target to clearly distinguish the precision aimpoint to the pilot and on the gun camera record, and far enough back to keep the tracker from entering the target's jetwash. If possible, ranging radar or transponder data may be displayed in the tracker's gunsight. The target's wingspan may also be used to estimate and control the tracking range.

The maneuver is terminated on command of the tracker after the target aircraft calls that he has reached the maximum test angle of attack, when the tracker aircraft handling qualities deteriorate to the point that precision tracking is not possible at maximum pilot effort, anytime flight safety considerations dictate or when the desired test condition Mach and altitude tolerance bands are exceeded.

Tests conducted at supersonic speeds may require the sacrifice of altitude to maintain Mach, especially at high load factors. Mach can decrease rapidly in a poorly performed maneuver, and "transonic dig-in", a sudden increase in load factor as airspeed decreases through the Mach 1 region, may cause an aircraft overstress and should be avoided.

14.6.2.3.1.2.2 Constant Angle of Attack Tests. Camera, time history and pilot comment data from wind-up turns will allow the test team to identify angle of attack and Mach combinations which warrant further testing.

The procedure used to accomplish constant angle of attack tests is similar to the wind-up turn. Upon command of the tracker, the target establishes a 30° banked turn at the test Mach and altitude. The tracker sets up approximately 1500 feet in trail. When the data systems have been turned on, the tracker clears the target to maneuver. The target smoothly increases angle of attack (load factor) at the desired Mach. The tracker moves the target to the desired location in the gunsight for the acquisition maneuver. The target calls when he is established at the desired Mach and angle of attack. The tracker begins precision tracking for 20 to 30 seconds.

If the effect of large perturbations on the pilot's ability to precisely track the target are desired, rapid constant load factor barrel-rolling reversals of the turn direction may be incorporated into the constant angle of attack tracking turns. These reversals are performed at near combat reversal rates. A rolling reversal may be sandwiched between two constant angle of attack tracking maneuvers.

14.6.2.3.1.2.3 Transonic Tests. If the target and tracker aircraft each have sufficient engine thrust to maintain transonic speeds and angles of attack, tracking tests in the transonic region may be performed in a manner similar to subsonic tests. If insufficient thrust is available, transonic

handling qualities can be examined using the constant angle of attack technique by starting the maneuver supersonic and permitting the Mach number to slowly decay through the transonic region while continuing to track.

14.6.2.3.1.3 Test Point Selection. During the early phases of flight control testing, tracking tests should begin near the middle of the flight envelope. As experience with the aircraft and control system accumulates, tracking test points where handling qualities deficiencies are expected or near the boundaries of the envelope are investigated. Knowledge of the aircraft's design mission role and mission flight arena will aid in test point selection. Also, a thorough knowledge of the flight control system operation, such as flight conditions where gains change, nonlinearities are encountered or the control system configuration changes will help define additional test points.
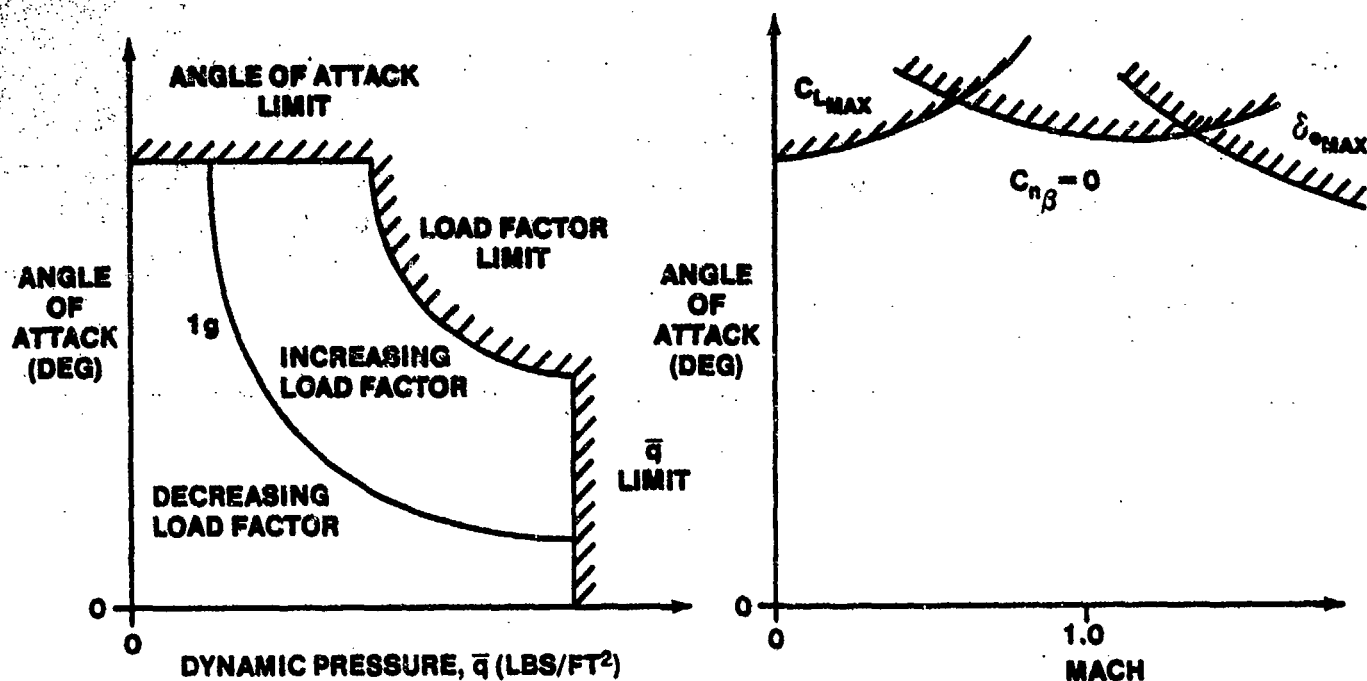
FIGURE 14.203. FLIGHT ENVELOP LIMITS OF AN AIRCRAFT AS FUNCTIONS OF ANGLE OF ATTACK VERSUS DYNAMIC PRESSURE OR MACH

Initial flight control system optimization should be conducted at a limited number of mission relevant test points -- a representative air combat point (0.85 Mach at 15,000 ft) or a typical supersonic point (1.2 Mach at 30,000 ft), for example. Once acceptable handling qualities are achieved at these typical flight conditions a survey of the remainder of the flight envelope should be accomplished. Selecting a limited number of mission relevant points at which to conduct the bulk of the handling qualities developmental testing will establish a standard of acceptable handling qualities while reducing test time, cost, and uncertainty.

14.6.2.3.1.4 Air-to-Ground Tracking Maneuvers. The technique used for air-to-air tracking tests can be successfully used in air-to-ground tests when a target aircraft is not available. The disadvantages of air-to-ground tests are that only points near 1 g flight (load factor equals the cosine of the dive angle) can be investigated and the target range cannot be held constant. Strafing gunsight settings and shallow dive angles are preferred to steep dive angles or large gunsight depressions. Strafing passes allow more tracking time and better airspeed control. Tests should be conducted as close to a constant airspeed as possible in a shallow dive. A range of test airspeeds should be selected. The ground target selected should be prominent and well

defined. The test aircraft should set up on the test condition with the target offset in the gunsight. The pilot attempts to rapidly acquire the target to excite the flight control dynamics. Precision tracking of the target should then be accomplished for 10 to 20 seconds. The tracking pilot must be cognizant of the hazards of target fixation during these tests. If desirable, the target may be changed after tracking the initial target. An initial acquisition maneuver is performed to move the pipper to the new target followed by precision tracking of the new target. This allows further investigation of the handling qualities in either the longitudinal or lateral axis by additional excitation of a particular axis of the aircraft.

14.6.2.3.1.5 Mission Briefing Items.

1. Review of Maneuvers and Test Conditions
   a. Target maneuvers to be flown
   b. Test conditions
   c. Conditions at which maneuvers will be terminated

2. Review of Test Techniques
   a. Target pilot responsibilities
   b. Maneuver initiation technique
   c. Initial excitation technique
   d. Trim consideration (trim prior to maneuver initiation)
   e. Rudder technique (feet on the floor)
   f. Precision tracking test technique review (aimpoint, aggressive tracking)
   g. Desired test range
   h. Duration of the maneuver parts (20 seconds minimum)
   i. Maneuver termination procedures

3. Pilot Evaluations
   a. Pilot comment and rating procedures (use of the rating scales)
   b. Particular aspects of flying qualities or task performance to which the tracking pilot should direct attention

4. Other Considerations
   a. Gunsight depression angle
   b. Time correlation procedures for data
   c. Camera or gunsight filters
   d. Gun camera and data acquisition system speeds
   e. Marking of film magazines for identification
   f. Check film magazine after each maneuver to assure proper operation

5. Safety
   a. Procedures for avoiding jetwash
   b. Special considerations (high angle of attack, departure, transonic dig-in)

14.6.2.3.1.6 Mission Debriefing Items.

1. General Pilot Comments and Impressions

2. Discussion of Each Maneuver
   a. Were the test conditions met?
   b. Was the tracking aircraft trimmed for straight and level flight prior to the maneuver?
   c. Did the tracking pilot retrim during the maneuver?
   d. Was correct tracking range maintained?
   e. Were the rudder pedals used?
   f. Was the precision aimpoint used?
   g. Was the aimpoint persistently tracked? Was the pipper allowed to float?
   h. Was jetwash encountered?
   i. Pilot comments and impressions of task performance and aircraft flying qualities
   j. Cooper-Harper rating of flying qualities for the maneuver, based on step by step progress through the rating scale
   k. What flying qualities improvements are desirable?

14.6.2.3.1.7 **Data.** Three sources of data are necessary to define flying qualities deficiencies using tracking test techniques: Pilot comments and Cooper-Harper ratings, gun camera film records of the pipper position relative to the target, and time history records of aircraft parameters such as pilot control forces and deflections, control surface positions, aircraft motion, and flight control system parameters.

The single most important source of data for discovering handling qualities deficiencies is the pilot comments and Cooper-Harper ratings. The best technique for gathering pilot comments is to record them as the test maneuver is performed, or as soon as possible after the maneuver is completed. Cooper-Harper numerical ratings must be carefully awarded using the rating scale. Two other rating scales are also useful in defining handling qualities deficiencies: The pilot induced oscillation (PIO) rating scale and the turbulence rating scale. Taken together with the pilot comments, the three rating scales can provide meaningful comparative data during a flight control optimization.

The gun camera film is a physical measure of what the pilot observes during the tracking test. Taken by itself, pipper motion analysis (Figure 14.204) is not a reliable quantitative measure of the aircraft's flying qualities. It supplements pilot comments and ratings. Reference 14.14 gives

a detailed description of gun camera film analysis. If a video recorder system is used in place of a gun camera, the video may be effectively used during the debrief of each test maneuver and may result in additional pilot comment data.

The time history record of aircraft and flight control system parameters is obtained from the stability and control data acquisition system. These data are important in defining the cause of handling qualities deficiencies — which is essential if design modifications are required.

An accurate method of time correlating all three of the data sources is extremely important. This can be effectively accomplished using a data correlation switch (ideally the gun trigger). Activation of the switch should turn on a light in the gun camera field of view and provide a signal trace in the data acquisition system. A pilot comment into the tape recorder will correlate a voice recorder other than the voice track of the data acquisition system.

14.6.2.3.2 Closed Loop Handling Qualities Tests. During the initial testing of a new fighter aircraft, air-to-air or air-to-ground tracking tests should be performed since the characteristics of the aircraft and flight control systems are unknown. Major up-and-away handling qualities deficiencies will surface as a result of these tests. Initial tracking tasks for large aircraft, or for fighter aircraft in the power approach configuration, may be limited to precision tracking of mountain peaks or the horizon while in level flight. For aircraft which are not normally equipped with a gunsight, a series of reference lines should be provided on the windscreen to provide a reference for precision tracking. Heads Up! Tests in the proximity of other aircraft or the ground are hazardous since poor handling qualities could cause a PIO, mid-air collision or loss of control.
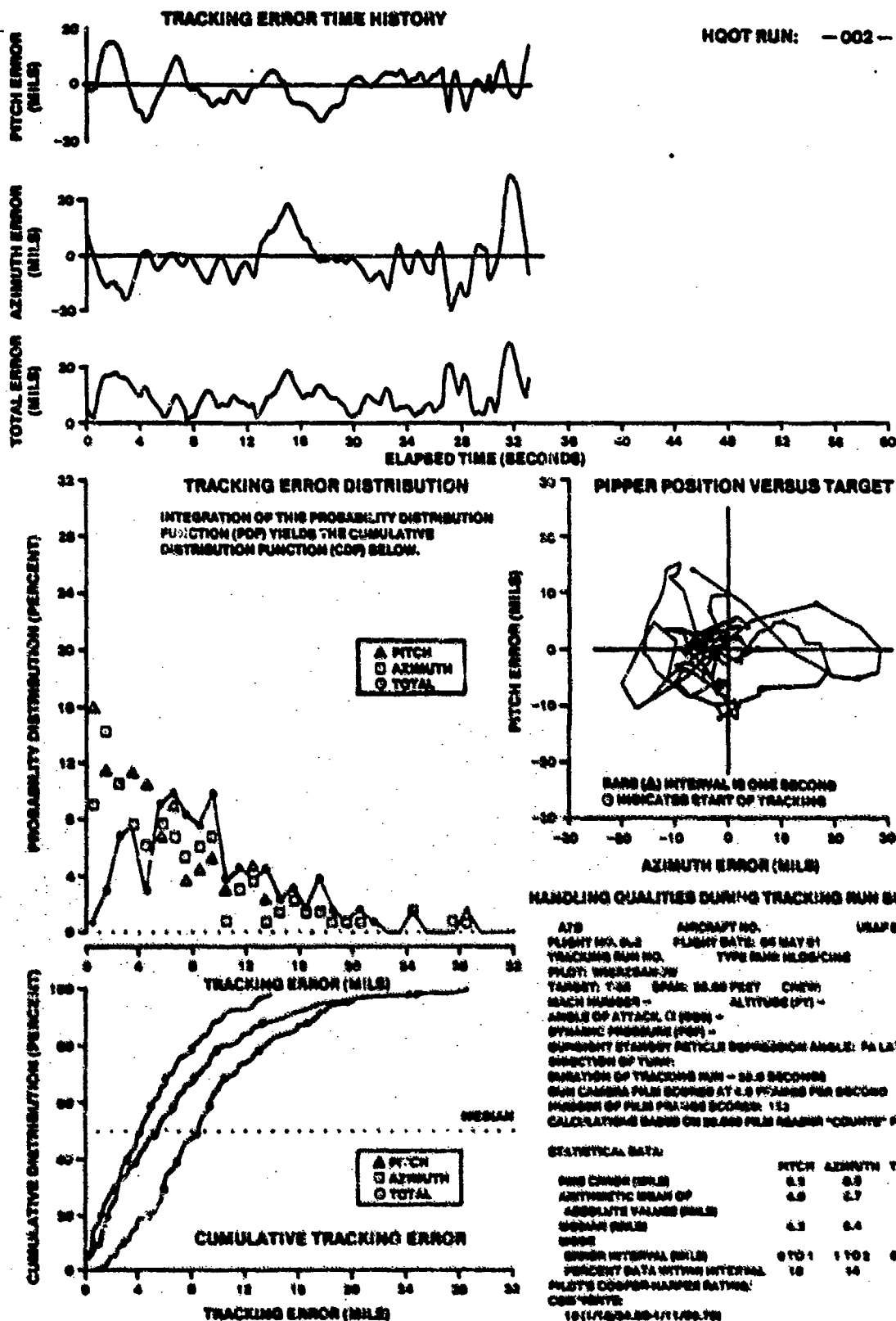
FIGURE 14.204.   CALCOMP PLOT TRACKING ANALYSIS OF AN
AIR-TO-AIR TRACKING TASK

14.6.2.3.2.1 Formation. Fingertip is the preferred formation for handling qualities investigation for formation tasks. The fingertip position should be well defined and adequate visual references should be provided to define the position accurately. The test aircraft should be flown to remain in the desired position precisely. Level flight, steady turns and Lazy 8 type maneuvers over a range of airspeeds and load factors should be performed. Pilot comments, Cooper-Harper ratings and time history data should be collected throughout the maneuver. The precision formation task is a high pilot gain task. Fingertip formation in the power approach configuration is an excellent way to uncover handling qualities deficiencies associated with approach and landing.

14.6.2.3.2.2 Air Refueling. Proximity tests should be performed initially without trying for an actual hook-up. This will reveal the effects of the refueling aircraft's wake on the handling qualities of the receiver. Precise positioning should be achieved by visual cues and boom operator direction. Once the general handling qualities near the tanker are understood, the aircraft should be flown to an actual hook-up to investigate the effects of the boom proximity to the aircraft as well as the handling qualities during precision formation (trail formation) flying. For tankers, the effects of various large receiver aircraft in the air refueling position (such as the B-52 or C-5) should be investigated to determine the change in handling qualities associated with these aircraft during refueling operations.

14.6.2.3.2.3 Approach and Landing. Precision approaches can be flown using a Navy optical landing system or instrument landing system (ILS) approach. These tasks provide general handling qualities information for landing tests and reveal handling qualities deficiencies associated with instrument approaches. The optical landing system suffers due to the lack of trend information as well as a changing vertical position sensitivity with decreasing range from touchdown. The ILS approach suffers in that the dynamics of the approach system indicators in the cockpit are included in the pilot loop. Another test technique available to evaluate handling qualities during the approach phase is the air-to-air tracking test technique at constant angle of attack in the power approach configuration.

Precision landing tests should be performed using spot landings. These tests reveal handling qualities deficiencies associated with precise pitch

attitude and airspeed control, ground effect, and touchdown. Spot landings
are difficult to perform in aircraft that require, an extensive flare prior to
touchdown.   Several practice approaches must be performed to determine the
aircraft performance characteristics during the flare and landing phase before
meaningful pilot rating data can be obtained.   It is essential to establish
desired and acceptable touchdown zones and to award ratings according to the
performance actually achieved during the spot landings.

14.6.3 Pilot Ratings

Pilot ratings are meaningful only for closed loop task performance.
Pilot ratings are not assigned during classical open loop stability and
control tests, nor are they assigned to aircraft performance characteristics.
Specific closed loop tasks must be devised to determine how stability and
control characteristics obtained during open loop testing affect pilot task
accomplishment.   These are the Cooper-Harper rating, the pilot induced
oscillation (PIO) susceptibility rating and the turbulence effect rating. All
three ratings should be given when appropriate.

14.6.3.1 <u>Cooper-Harper Rating Scale</u>. The Cooper-Harper rating is a numerical
assessment of the aircraft's handling qualities as they affect the pilot's
ability to perform a specific task (Figure 14.205).

HANDLING QUALITIES RATING SCALE
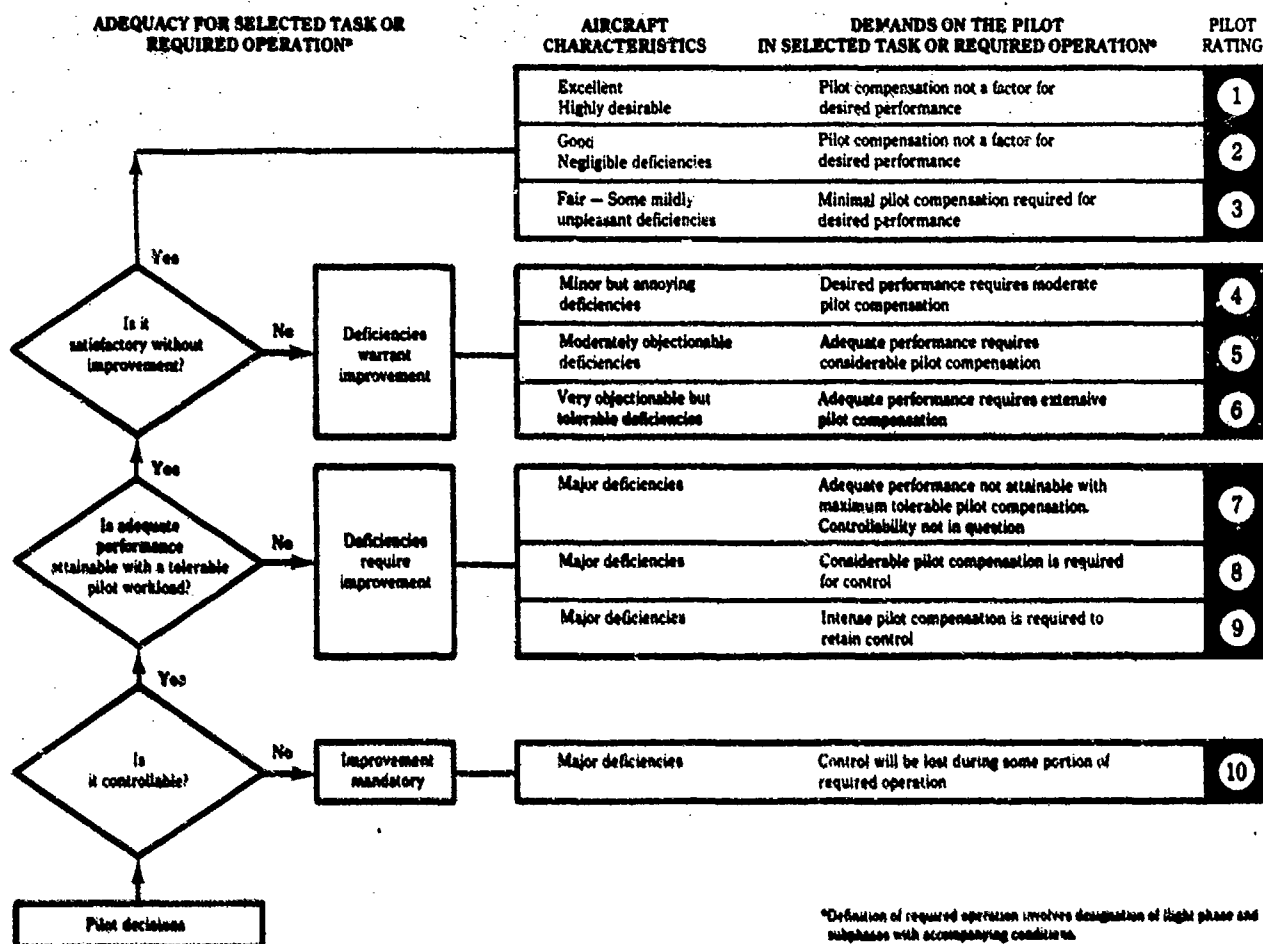
FIGURE 14.205.   HANDLING QUALITIES RATING SCALE

The consistency of the ratings between pilots requires a clear understanding of the definition of the key decision making terms. The following discussion of these terms is paraphrased from Reference 14.15.

The determination of aircraft controllability must be made within the framework of the defined mission or intended use. An example of considerations which must be addressed when deciding if the aircraft is controllable might occur during an evaluation of fighter handling qualities during air-to-air tracking. The pilot encounters a situation in which aircraft control could be maintained only by devoting his complete and undivided attention to flying the aircraft. In this situation, the aircraft is controllable in the strict sense, but the pilot maintains control only by restricting the tasks he can perform and by giving the flying of the aircraft his undivided attention. For the pilot to answer that the aircraft is controllable in this task, he must be able to retain control in all mission required tasks. Therefore, in the example discussed, the appropriate decision is that the aircraft is not controllable (control will be lost during some portion of the required operations) since all tasks could not be performed and those that could be performed required all the pilot's attention and effort, forcing him to neglect elements of his overall duties. Major aircraft deficiencies exist which require mandatory improvement.

Aircraft adequacy must be determined within the context of the task to be accomplished and the level of effort (pilot workload) that must be expended. A yes answer at this decision point in the rating scale means that the flight phase or task can be adequately accomplished, that the evaluation pilot would agree to use the aircraft for the designated role and that the deficiencies which exist can be tolerated. Although the task can be accomplished with adequate precision, its accomplishment may require considerable effort and concentration on the part of the pilot. However, the workload required to achieve adequate precision in the task is tolerable and not unreasonable in the context of the aircraft's intended use. A no answer does not necessarily mean that the task cannot be achieved or that the pilot workload necessary to accomplish the task are of such a magnitude that the pilot rejects the aircraft for this aspect of the mission. Deficiencies and objectionable characteristics exist which require improvement.

The determination of whether the aircraft's handling qualities are satisfactory must be made in the context of the level of precision with which the required task can be performed and the workload required to attain the level of precision. The pilot's judgment of desired versus adequate performance must be considered. Satisfactory handling qualities does not imply that the aircraft is perfect, but rather that desired task performance is achievable without aircraft improvement. Unsatisfactory handling qualities imply that although the task can be adequately accomplished, the desired level of precision cannot be achieved (Cooper-Harper ratings of 5 and 6). A rating of 4 implies that although desired performance is achievable, it is attained at a higher than desired pilot workload.

The rating scale includes further subdivisions of quality within each of the primary categories. These subdivisions provide descriptions to define quality differences separating each numerical rating. The pilot should not award ratings of 3.5, 6.5 or 9.5 since this indicates a reluctance to make fundamental decisions with respect to a primary category, nor should he break his ratings down any finer than half ratings. The proper use of the rating scale requires the pilot to refer to the rating scale itself and sequentially answer each question.

14.6.3.2 <u>Pilot Induced Oscillation (PIO) Rating Scale.</u> The PIO rating scale (Figure 14.205) is useful in conjunction with the Cooper-Harper rating scale to provide further insight into the aircraft handling qualities.

DESCRIPTION	NUMERICAL RATING
No tendency for pilot to induce undesirable motion.	1
Undesirable motions tend to occur when pilot initiates abrupt maneuvers or attempts tight control. These motions can be prevented or eliminated by pilot technique.	2
Undesirable motions easily induced when pilot initiates abrupt maneuvers or attempts tight control. These motions can be prevented or eliminated, but only at sacrifice to task performance or through considerable pilot attention and effort.	3
Oscillations tend to develop when pilot initiates abrupt maneuvers or attempts tight control. Pilot must reduce gain or abandon task to recover.	4
Divergent oscillations tend to develop when pilot initiates abrupt maneuvers or attempts tight control. Pilot must open loop by releasing or freezing the stick.	5
Disturbance or normal pilot control may cause divergent oscillation. Pilot must open control loop by releasing or freezing the stick.	6

FIGURE 14.206. PIO RATING SCALE

14.313

A pilot induced oscillation is an unwanted, inadvertent and atypical closed loop coupling between the pilot and the aircraft response. Factors which contribute to PIO include:

1. Excessive stick force to control surface lag

2. Rate saturated controls

3. High stick force friction

4. High bobweight friction

5. High bobweight contribution to stick force per g

6. Low short period damping

7. Low stick force per g or elevator deflection per g

8. Excessive control sensitivity

The PIO will increase pilot workload to accomplish a given task, force the pilot to divert his attention from task accomplishment to aircraft control, or cause the pilot to lose control of the aircraft. If aircraft control is lost, the only successful recovery technique is for the pilot to either freeze or release the flight controls.

The PIO rating scale should be used in conjunction with the Cooper-Harper scale to rate the aircraft handling qualities during high gain pilot-in-the-loop tasks such as air-to-air tracking, precision formation flying or spot landings. The pilot should physically refer to the rating scale descriptions after completing a given task and award a PIO numerical rating along with a Cooper-Harper rating. These two ratings provide a more complete picture of the aircraft's handling qualities than either rating standing alone.

14.6.3.3 Turbulence Rating Scale. The turbulence rating scale (Figure 14.207) is designed to show the effect of turbulence on the handling qualities of an aircraft during precision, high gain tasks. If turbulence is

encountered during handling qualities testing, this scale should be used in conjunction with the Cooper-Harper and PIO rating scales.

INCREASE OF PILOT EFFORT WITH TURBULENCE	DETERIORATION OF TASK PERFORMANCE WITH TURBULENCE	RATING
No Significant Increase	No Significant Deterioration	A
More Effort Required	No Significant Deterioration	B
	Minor	C
	Moderate	D
Best Efforts Required	Moderate	E
	Major (But Evaluation Tasks Can Still Be Accomplished)	F
	Large (Some Tasks Cannot Be Performed)	G
Unable To Perform Tasks		H

FIGURE 14.207. TURBULENCE RATING SCALE

14.6.3.4 Confidence Factor. A confidence factor scale (Figure 14.208) may be used to indicate the level of confidence the pilot has that the task performed during a particular test was representative of the defined task. This factor is not to be used as an indication of the rater's inability to make a decision regarding the test aircraft's handling qualities. It is useful in judging the significance of the data, since data collected during non-representative tasks may not be useful. Both the tracker and the target pilots may assign confidence factors to the test maneuver to indicate if the task was flown as defined.

DESCRIPTION	CLASSIFICATION
The pilot rating was assigned with a high degree of confidence.	A
The pilot rating was assigned with only a moderate degree of confidence because of uncertainties introduced by moderate differences in environmental conditions, or in aircraft configuration or state, or in the task, from what was desired.	B
The pilot rating was assigned with minimum confidence because of important differences between the desired and the actual environmental conditions, aircraft configuration or state, or task, requiring considerable pilot extrapolation.	C

FIGURE 14.208.   CONFIDENCE FACTOR SCALE

14.6.3.5 Control System Optimization. It is frequently necessary to obtain a concensus of opinion among a group of test pilots when optimizing a flight control configuration. Establishing criteria which the test pilots agree are important to the accomplishment of the required task is imperative.

Suggested criteria:

1. Desired performance limits for the task (these must be specified — for example, track the target within 5 mils of the aimpoint 80% of the time).

2. Adequate performance limits for the task (for example, track the target within 10 mils 50% of the time). Performance outside these limits is, by definition, not adequate and should be accompanied by Cooper-Harper ratings between 7 and 9.

3. Aircraft flight path predictability

4. Control harmony

5. Control forces

6. Control sensitivity

7. Workload required to accomplish the task

Additional criteria may be required as problems are identified.

If pilot comments and ratings show a clear preference for a particular configuration then the data is capable of clearly supporting a conclusion. Discussion of the individual impressions of the various configurations is undesirable in general since the results could become biased. However, a clear preference is usually not apparent from the data and a discussion of the results and impressions is necessary to differentiate between the configurations tested.

The first step in arriving at a consensus is to rank the relative importance of the criteria. The test pilots must then discuss the various configurations, their ranking relative to the criteria, and the overall ranking of the configuration options. No one individual or group can dominate the discussion.

14.6.4 Evaluation Criteria

The purpose of the evaluation criteria for flight control systems is twofold:

1. To provide criteria which are easily used by the flight control designer and which provide the designer with a high confidence that a design meeting the criteria will have satisfactory handling qualities. The criteria must, therefore, relate to pilot opinions and ratings obtained during actual flight testing of aircraft flight control systems with similar characteristics.

2. To provide the tester with criteria which can be easily compared to flight test data to determine contractual compliance.

Flight control systems must meet the following requirements:

1. The general flying qualities requirements of MIL-F-8785C for fixed wing aircraft or V/STOL aircraft in conventional flight. Other specifications apply to helicopter flying qualities or to the flying qualities of V/STOL aircraft during low speed flight.

2. Special performance requirements of the procurement detail specification.

3. Requirements of MIL-F-9490 concerning auto-pilot functions and flight load factor alleviation systems.

4.   The requirements of the flight control system specification.

14.6.4.1. MIL-F-8785C, "Flying Qualities of Piloted Aircraft". This specification applies to the flying qualities of fixed wing aircraft in conventional modes of flight (requirements for V/STOL aircraft in transition are covered in MIL-F-83300 and for helicopters in MIL-F-8501A). The requirements are written in terms of the cockpit controls which produce conventional pitching, rolling or yawing motions. No specific requirements are currently provided for unconventional flight modes -- such as direct lift, sideforce or fuselage pointing -- although these modes are not precluded. The handling qualities are specified for four classes of aircraft (the classes being divided by mission group). Also, three phases or types of tasks are defined which further delineate handling qualities requirements. Three levels of handling qualities are defined -- corresponding to three of the four primary categories of the Cooper-Harper rating scale (not including Cooper-Harper ratings of 10) as follows:

1.   Level 1. Flying qualities which are adequate for the mission flight phase (Cooper-Harper ratings of 1 to 3).

2.   Level 2. Flying qualities which are adequate to accomplish the mission flight phase but some increase in pilot workload or some degradation in mission effectiveness, or both, exists (Cooper-Harper ratings of 4 to 6).

3.   Level 3. Flying qualities such that the airplane can be controlled safely, but pilot workload is excessive or mission effectiveness is inadequate, or both (Cooper-Harper ratings of 7 to 9).

The requirements of the specification apply to the full range of operational center of gravity and gross weight conditions, including external store configurations (symmetric and asymmetric) as well as all aircraft configurations used in operational tasks. Requirements for both normal operation and failure states are provided and aircraft operation, service and permissible flight envelopes are defined. Level 1 flying qualities are allowed within the service flight envelope and during failure state operation (based on the probability of the failure occurring).

These requirements are based to a large extent on flight experiments conducted in variable stability aircraft using well-defined, precision, high

gain tasks. Cooper-Harper ratings of the defined tasks were correlated to the aircraft characteristics to determine the characteristics which result in level 1, 2 or 3 flying qualities. Open loop tests determine the test aircraft's characteristics, which are compared to the data derived from the flight experiments to determine the adequacy of the closed loop handling qualities. In theory this method should work -- and it was reasonably successful for conventional unaugmented or slightly augmented aircraft. The use of these requirements to assure adequate flying qualities for modern, highly augmented aircraft has been unsuccessful for two reason:

1. The flight control system effectively masks or alters the basic aerodynamic characteristics of the aircraft.

2. Flight control system engineers have not used the requirements of the specification as design guidelines.

14.6.4.2 MIL-F-9490 "Flight Control Systems - Design, Installation and Test of Piloted Aircraft, General Specification For". This specification applies to the general performance of flight control systems in Air Force piloted aircraft. Five flight control operational states are defined as follows:

1. Operational State I (normal operation). The normal state of flight control system (FCS) performance, safety and reliability. The level 1 flying qualities requirements of MIL-F-8785C are met within the operational envelope.

2. Operation State II (restricted operation). The state of less than normal equipment operation or performance which involves degradation or failure of only a non-critical portion of the overall flight control system. A moderate increase in crew workload and degradation in mission effectiveness may result but the intended mission may be accomplished. The level 2 flying qualities requirements of MIL-F-8785C are met within the operational envelope.

3. Operational State III (minimum safe operation). The state of degraded flight control system performance, safety or reliability which permits safe termination of precision tracking or maneuvering tasks, and safe cruise, descent and landing at the destination of original intent or alternate but where the pilot workload is excessive or mission effectiveness inadequate. Phases of the intended mission involving precision tracking or maneuvering cannot be completed satisfactorily. The level 3 flying qualities requirements of MIL-F-8785C are met.

14.319

4. Operational State IV (controllable to an immediate emergency landing). The state of degraded FCS operation at which continued safe flight is not possible. However, sufficient control remains to allow engine restart attempts, a controlled descent and emergency landing.

5. Operational State V (controllable to an evacuable flight condition). The state of degraded FCS operation at which the flight control system capability is limited to maneuvers required to reach a flight condition at which crew evacuation may be safely accomplished.

Additionally, flight control system functions are classified according to their criticality as follows:

1. Essential. Loss of function results in an unsafe condition or inability to maintain FCS Operation State III.

2. Flight phase essential. Loss of the function results in an unsafe condition or inability to maintain FCS Operational State III only during specific flight phases.

3. Noncritical. Loss of the function does not affect flight safety or result in control capability below that required for FCS Operation State III.

Flight control system requirements are provided in the following areas:

1. Manual flight control system requirements (piloted flight) — must meet the general flying requirements of MIL-F-8785C (or other appropriate specifications) and the special performance requirements of the procurement detail specification.

2. Automatic flight control system performance requirements
   a. Attitude hold (pitch and roll)
   b. Heading hold
   c. Heading select
   d. Lateral acceleration and sideslip limits (AFCS engaged)
   e. Altitude hold
   f. Mach hold
   g. Airspeed hold
   h. Automatic navigation
   i. Automatic instrument low approach system
   k. Flight load fatigue alleviation
   l. Ride smoothing
   m. Flutter suppression
   n. Gust and maneuver load alleviation
   o. Automatic terrain following
   p. Control stick steering

3. General flight control system design
   a. Redundancy
   b. Failure immunity and safety
   c. System operation and interface
      1. Warm up
      2. Disengagements
      3. Mode compatibility
      4. Failure transients
   d. Trim controls
   e. Stability
   f. Operation in turbulence
   g. System arrangement
   h. Residual oscillations
   i. System test and monitoring provisions (BIT)

4. Manual flight control system design
   a. Augmentation system compatibility
   b. Control centering, breakout forces and freeplay
   c. Reversion to backup modes
   d. Controller kinematics
   e. Mechanical systems
   f. Electrical systems

5. Automatic flight control system design
   a. Interface provisions
   b. Emergency provisions

6. Mission accomplishment reliability

7. Flight safety

8. Survivability (all engines out)

9. Invulnerability
   a. Natural environments
      1. Sand and dust
      2. Fungus
      3. Extreme temperatures
      4. Humidity, corrosion and icing
      5. Altitude
      6. Combined temperature and altitude
   b. Lightning strikes and static atmospheric electricity
   c. Induced environments (projected for mission)
      1. Temperature
      2. Acceleration
      3. Vibration
      4. Noise and shock
      5. Pressure
      6. Electromagnetic interference
      7. Nuclear radiation

14.321

      d.   Onboard failures of other systems and equipment (critical engine or engine pair)
      e.   Maintenance error
      f.   Pilot and flight crew inaction and error

10. Maintenance provisions

11. Structural integrity

12. Subsystem and component design requirements
      a.   Pilot controls and displays
      b.   Sensors
      c.   Signal transmission
      d.   Signal computation
      e.   Control power (hydraulic, electrical and pneumatic systems)
      f.   Actuation systems
      g.   Component design, fabrication and installation

Methods for demonstrating compliance with the requirements of the specification fall into the following categories:

1. Analysis

2. Inspection

3. Test
      a.   Laboratory (including piloted simulations)
      b.   Airplane ground
      c.   Airplane flight

To the maximum extent possible, compliance with quantitative requirements shall be demonstrated by actual tests. The specific ground tests required prior to flight are discussed in Paragraph 14.5.1.

Refer to MIL-F-9490 for detailed descriptions of the requirements of the specification. A background document is provided for more information as well as the history and rationale behind each specification.

14.6.4.3 <u>New Requirements</u>. The requirements of MIL-F-8785C are not well suited to the evaluation of modern, highly augmented aircraft which do not respond to pilot inputs with classical second order short period or Dutch roll characteristics. To overcome the inadequacies of the specification when dealing with these aircraft, several new criteria have been proposed during

the past several years. Two of the criteria are the equivalent lower order system approach and the bandwidth criteria. Several other criteria are available, such as C*, Neal-Smith and time response characteristic envelopes, and are useful as design criteria.

14.6.4.3.1 Equivalent Lower Order Systems. The equivalent lower order systems approach attempts to fit the Bode gain and phase angle plots of a high order augmented aircraft transfer function (aircraft pitch rate response due to a pilot stick force input, for example) with an equivalent lower order transfer function (a transfer function which nearly matches the Bode gain and phase angle curves over a wide range of frequencies, typically 0.1 to 20 radians per second). The approach concentrates on those characteristics which greatly influence aircraft handling qualities -- the short period, Dutch roll, and roll mode parameters. Once the equivalent lower order system is obtained, the requirements of MIL-F-8785C are applied to the aircraft parameters, such as short period damping ratio and natural frequency, as identified from the equivalent lower order transfer functions.

Classical aircraft dynamics theory provides a second order transfer function relating the aircraft pitch rate response to the elevator deflection, which is of the form

$$\frac{\dot{\theta}(s)}{\delta_e(s)} = \frac{K_\theta \, (s + 1/T_{\theta_2})}{s^2 + 2\zeta_{sp}\omega_{n_{sp}} s + \omega_{n_{sp}}^2} \qquad (14.107)$$

where $1/T_{\theta_2}$ is a parameter which relates to the aircraft's load factor change to an angle of attack change (n/α) as

$$\frac{n}{\alpha} = \frac{V(1/T_{\theta_2})}{g} \qquad (14.108)$$

where

K_θ is the aircraft elevator effectiveness, M_{δ_e}

ζ_{sp} is the short period damping ratio

$\omega_{n_{sp}}$ is the short period natural frequency

n is the load factor change

α is the angle of attack change, in radians

V is the true airspeed, in feet per second .

g is the acceleration of gravity, in feet per second squared

The above equation is limited in its ability to match phase angle shifts of an actual aircraft transfer function which are due to the compensators, actuators, integrators, filters and other elements present in the flight control system. The equivalent system procedure augments the equation with the addition of a time delay factor to introduce phase lag without affecting the gain characteristics. The resulting system transfer function is

$$\frac{\dot{\theta}(s)}{\delta_e(s)} = \frac{K_\theta \, (s + 1/T_{\theta_2}) \, e^{-\tau s}}{s^2 + 2\zeta_{sp}\omega_{n_{sp}} s + \omega_{n_{sp}}^2} \qquad (14.109)$$

where τ is the equivalent time delay, in seconds.

Flight test data obtained by the System Identification from Tracking test procedure (see Paragraph 14.5.4.2.3) is provided to a computer program (LCNG FIT) currently available at the Air Force Flight Test Center (and to be provided with the revised MIL-F-8785C) to obtain the equivalent lower order system transfer function. Requirements are being established for the time delay parameter (MIL-F-87850 places a limit on the apparent time delay as seen by the pilot).

The advantages of the equivalent lower order systems approach include the retention of the current MIL-F-8785C requirements with minor additions to account for the equivalent time delay due to the flight control system dynamics. The data on aircraft handling qualities obtained through years of inflight experimentation are retained. The effective time delay has significant effects on the flying qualities of aircraft. This approach is not

yet completely accepted by the aerospace industry. Much disagreement exists concerning the best way to achieve the curved fit to the actual aircraft transfer function. References 14.10 and 14.18 through 14.20 discuss the theory, curve fitting scheme and proposed requirements.

14.6.4.3.2 Bandwidth Criteria. The bandwidth requirement is a task oriented criterion motivated by the hypothesis that each aircraft task can be accomplished well if the aircraft has good response characteristics over a sufficiently wide range of pilot control input frequencies. This is essentially what MIL-F-8785C attempts to achieve through open loop test requirements. It is especially applicable to highly augmented aircraft.

The beauty of this approach over the equivalent lower order systems method is that the data obtained from flight test using the System Identification from Tracking test procedure can be used directly without further computer analysis.

Two criteria are specified -- an equivalent time delay to account for the higher order dynamics of the aircraft and the bandwidth of the aircraft transfer function. The bandwidth is calculated two ways. The frequency and gain where the phase angle is -180°, ω_{180} is determined. The frequency at the gain which is 6 db above the ω_{180} gain is defined as the bandwidth $\omega_{BW_{GAIN}}$ due to the gain margin. The frequency at a phase margin of 45° $\omega_{BW_{PHASE}}$ is found and is defined as the bandwidth due to the phase margin. The lesser of $\omega_{BW_{GAIN}}$ and $\omega_{BW_{PHASE}}$ is the bandwidth of the aircraft (Figure 14.209).

To determine the level of compliance with the proposed MIL-F-8785C criteria, the equivalent time delay is also needed. This is computed using the formula

$$\tau_p = -\frac{(\phi_{2\omega_{180}} + 180)}{2(57.3)\ (\omega_{180})} \tag{14.110}$$

where $\phi_{2\omega_{180}}$ is the phase angle at twice the frequency where -180° of phase angle occurs.
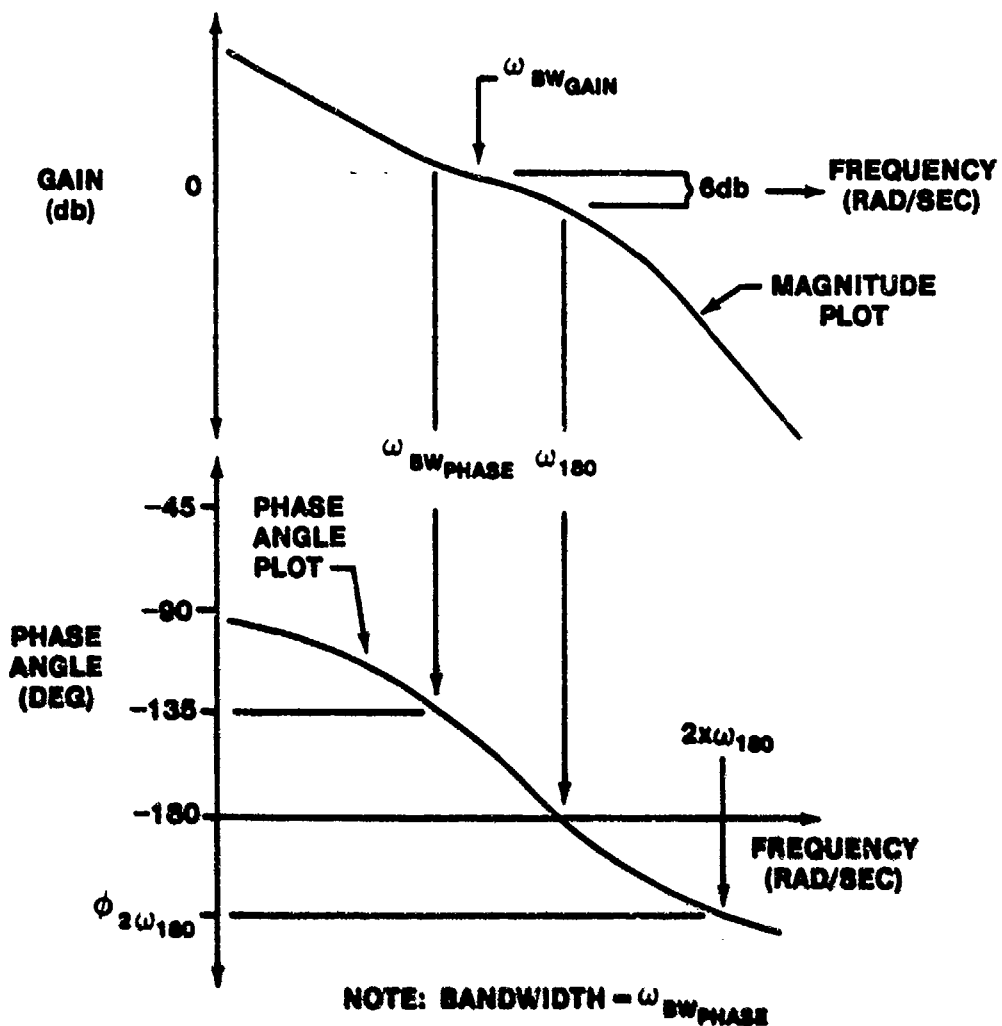
FIGURE 14.209.   DEFINITION OF BANDWIDTH

Figure 14.210 shows an example of the proposed bandwidth criteria. The advantage of the bandwidth criteria is its simplicity of application, both for the flight control engineer and the flight test organization. The basic assumptions of the criteria are widely accepted in industry, but some controversy exists as to its exact application, especially the lack of any specification on the control sensitivity of the aircraft (gain margin criteria). References 14.10, 14.21 and 14.22 contain further information.
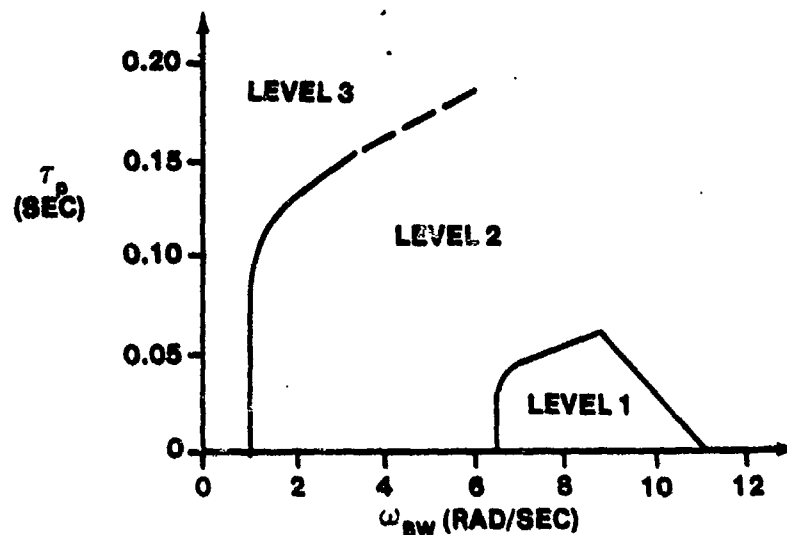
a. REQUIREMENTS FOR CATEGORY A FLIGHT PHASES

NOTE: REQUIREMENTS FOR $G_{F_s}^{\theta}$ (s)
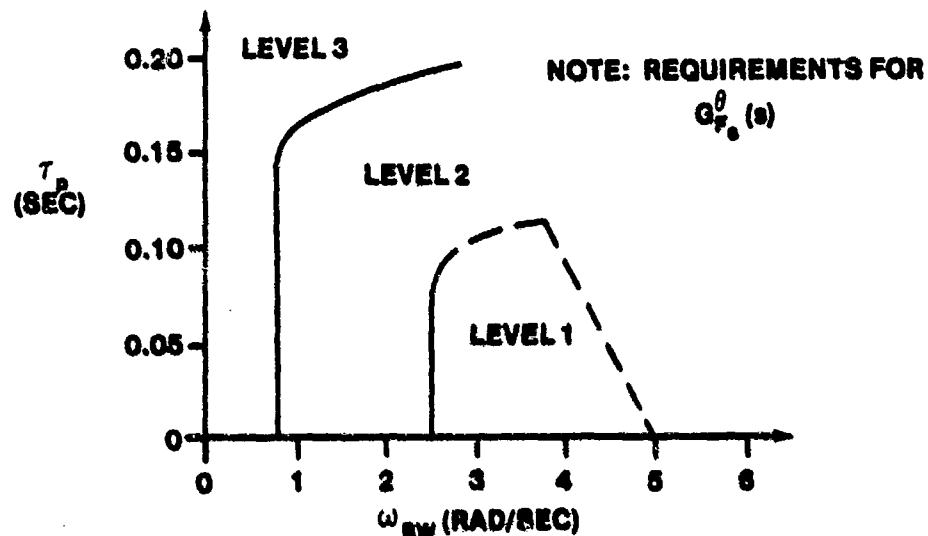
b. REQUIREMENTS FOR CATEGORY C FLIGHT PHASES

FIGURE 14.210.   PROPOSED BANDWIDTH REQUIREMENTS FOR
CLASS IV AIRCRAFT (PITCH ATTITUDE
CHANGE DUE TO PILOT STICK FORCE)

14.6.4.4 Flight Test Data Analysis.

14.6.4.4.1 System Identification From Tracking. System Identification from Tracking (SIFT) is a flight test data analysis technique for evaluating the pilot-in-the-loop handling qualities of highly augmented aircraft. Normal stability and control flight test parameters are recorded by the onboard data acquisition system during pilot-in-the-loop, mission oriented, precision tracking maneuvers (open loop sinusoidal stick pumps - frequency sweeps - may also be used, but tracking tasks are much preferred). The data are analyzed

14.327

in the frequency domain (using the Fast Fourier Transform -- see Reference 14.24 to obtain frequency response transfer functions). The transfer function data of the combined aircraft and flight control system, can be used to verify aircraft compliance with the proposed flying qualities requirements using either the equivalent lower order system approach or the bandwidth criteria.

The preferred maneuver for obtaining this data is a constant angle of attack, Mach, and altitude, high gain air-to-air tracking task. Good frequency content in the pilot inputs and controlled test conditions are important to acquiring useful data. Use of the rudder is required if directional axis data are desired.

The quantitative test data, in the form of time histories of aircraft motion, control surface positions or flight control system parameters acquired during the test maneuver are analyzed using the Frequency Response Analysis program available at the Air Force Flight Test Center (Reference 14.27). This program uses a Fast Fourier Analysis scheme to provide user specified Bode plots. These Bode plots may be specified as the airframe aerodynamics (pitch rate due to elevator input transfer function, for example), the flight control system (elevator deflection due to pitch rate feedback signal transfer function), the overall aircraft (pitch rate due to pilot command input) or some other component or subsystem in the flight control system (elevator actuator displacement due to electrical signal input). An advantage of the Bode plots identified through SIFT, versus aerodynamic data obtained through parameter identification tests, is that the actual system is identified directly rather than using a "best estimate".

The quantitative data obtained during tracking tests have been extremely valuable in isolating the cause of handling qualities deficiencies. An example occurred in the F-15 flight test program. A two to three mil pitch bobble was observed during precision tracking maneuvers. Classical stability and control tests did not uncover the problem. Once observed, several attempts to isolate the cause of the pitch bobble and correct the problem failed. The SIFT technique isolated the pitch bobble frequency at twice the Dutch roll frequency by analyzing the augmented aircraft pitch rate due to elevator input transfer function Bode diagram obtained during precision

tracking. The problem was found to be a cross-coupling of the lateral-directional dynamics into the pitch axis due to the rolling tail. Once isolated, the problem was corrected through flight control system redesign.

14.6.4.4.2 <u>Dynamic Parameter Analysis</u>. The dynamic parameter analysis relies on identification of aircraft stability derivatives from flight test data by using specialized test inputs and maneuvers. Stability derivative data is obtained by reducing flight test data using a maximum likelihood data reduction scheme (References 14.22 and 14.23).

Flight test determined stability derivatives are used to update analytical models (transfer functions) of the aircraft for improved flight control system design and analysis and to improve ground and airborne simulations of the aircraft and the flight control system. The updated aircraft transfer function data can be used to conduct an analysis of the augmented aircraft and a comparison of the results can be made to the requirements of MIL-F-8785C. The SIFT method is greatly preferred over the Dynamic Parameter Analysis technique for flight control system contractual compliance verification and handling qualities evaluation.

14.1. A-7D Pitch CAS Analysis

The block diagram of the pitch CAS for the A-7D is shown in Figure 14P.1. The aircraft transfer functions for several flight conditions are presented in Figure 14P.2. The aircraft normal accelerometer sensor is located 8.78 feet ahead of the center of gravity.
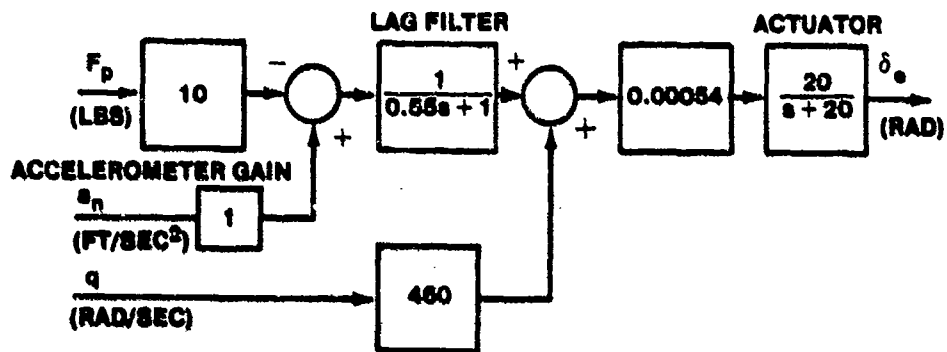
FIGURE 14P.1. A-7D PITCH CONTROL AUGMENTATION SYSTEM

For the flight conditions assigned:

1. Determine the units of each gain in the block diagram. The units at each summing junction must be compatible. It is not uncommon to find errors in the block diagram. These errors are usually unit conversion errors and result in gain errors by factors of 32.2 feet per second squared (gravitational acceleration) or 57.3° per radian (angular relationship). Hint: The units of the accelerometer gain is deg/g. It may be helpful to try to convert the block diagram to one which uses accelerations in g's and angular parameters in degrees. A determination of the number of degrees of elevator commanded per unit error of acceleration or pitch rate may reveal unit conversion errors.

2. From Figure 14P.2, determine the aircraft transfer functions for the flight condition to be examined. The pitch rate and acceleration at the center of gravity are the two transfer functions of interest in this analysis. Comment on the open loop pitch attitude (what the

14.330

pilot observes) response of the aircraft. Plot the pitch attitude response of the unaugmented aircraft to a one degree elevator input. Include the actuator dynamics in the analysis. Label the units of the response curve obtained from the computer.

3. Determine the acceleration transfer function at the accelerometer. Use the root locus program technique discussed in class for combining the transfer function zeros. Two hints: a) only the gain and zero locations of the acceleration transfer function change to account for the accelerometer location, and b) the output of the accelerometer is in the same reference frame as that used by the pilot (positive acceleration up). It may be interesting to plot a root locus of the zero locations as a function of the accelerometer location to realize why the accelerometer is located ahead of the center of gravity. Determine the center of rotation of the aircraft longitudinal axis. The proper sign of the accelerometer output may be obtained by multiplying the acceleration transfer function by a factor of -1 to change the reference from positive down (aircraft body axis system) to positive up (pilot load factor reference frame).

4. Determine how the pitch rate feedback loop affects the characteristics of the aircraft. Allow the feedback gain to vary and plot a root locus for this loop. Comment on the root locus. Determine the closed loop pitch rate transfer function for the inner pitch rate loop at the design gain. Find the pitch rate augmented short period and phugoid natural frequencies and damping ratio to aid in your discussion and analysis of this loop. How does the effect of this loop on the A-7D compare to the discussion of the effects of pitch rate feedback presented in paragraph 14.2?

5. Find the aircraft acceleration transfer function for the accelerometer location for the pitch rate augmented aircraft. Determine how the acceleration feedback loop affects the augmented roots found in part 4. Plot a root locus for the acceleration loop and comment. Determine the closed loop transfer function for the fully augmented aircraft which relates the pilot stick force to the aircraft load factor. Determine the augmented aircraft short period and phugoid characteristics and compare to the unaugmented aircraft characteristics. Does the aircraft meet the level 1 requirements of MIL-F-8785C (short period and phugoid modes), where

$$\frac{n}{\alpha} = \frac{V(1/T_{\theta_2})}{g}$$

What is the effect of the lag filter and why do you suppose it is included in the system?

6. Plot the time response characteristics for the augmented aircraft, including the aircraft load factor, pitch rate and pitch attitude responses, for a 3.22 pound pilot stick force input. Compare the augmented aircraft pitch attitude response characteristics to the unaugmented response. The response magnitude of the two responses may differ since the characteristics of the mechanical flight

control system were not included in the analysis (the amount of elevator deflection per pound of pilot force is not give). The damping and natural frequency characteristics, as well as the response rise time, settling time and overshoot characteristics, are accurate.

TABLE 14P.1. MACH AND TRUE AIRSPEED CONVERSIONS

Altitude (feet)	Mach	True Airspeed (feet/second)
0	0.25	279
0	0.6	670
0	0.9	1005
15000	0.3	317
15000	0.6	635
15000	0.9	952
15000	1.1	1164
35000	0.6	584
35000	0.9	876

14.2. T-38 Lateral-Direction Axis Analysis

An engineer has suggested retrofitting the T-38 with an aileron-rudder interconnect in addition to the yaw SAS. Your task is to analyze the proposal presented in Figure 14P.3, and provide a recommendation to the SPO on whether to implement the proposed configuration into a flight test vehicle for further evaluation. For simplification, your analysis will be performed at only one assigned flight condition. Your task will be to compare the performance improvements afforded by the proposed system over the existing system and determine if these improvements are sufficient to warrant further system evaluation. The requirements of MIL-F-8785C should be considered during your analysis and discussion.

The aircraft transfer function data is provided in Figure 14P.5 and 14P.6. The yaw rate feedback gain is scheduled as a function of the dynamic pressure (Figure 14P.8) and, for the design proposed in this study, the ARI is included for all flight conditions and the gain set at the value presented in the block diagram.

ACTUATORS
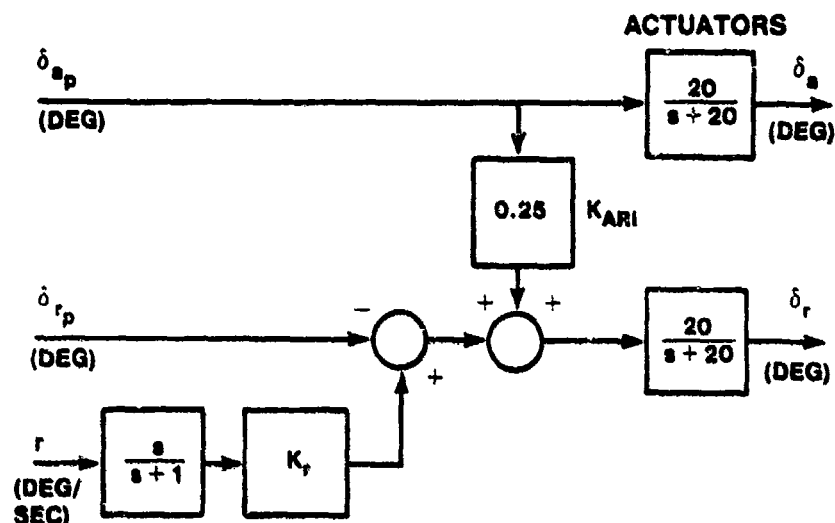
FIGURE 14P.3. T-38 LATERAL-DIRECTION AXIS INCLUDING AN
AILERON-RUDDER INTERCONNECT FEATURE

1. With the pilot flying feet-on-the-floor plot the unaugmented
    aircraft sideslip angle response for a one degree aileron pulse
    input command (for the unaugmented aircraft, the ARI gain is zero).
    The impulse input may more closely approximate a pilot aileron input
    than a step command since the step command results in continuous
    rolls and may exceed the validity of the linear analysis. Comment
    on the aircraft response characteristics. Determine the Dutch roll
    frequency and damping, the roll mode time constant and the spiral
    mode time constant. Compare these results to the requirements of
    MIL-F-8785C. Does the aircraft possess proverse or adverse yaw
    characteristics?

2. Plot a root locus of the aircraft yaw SAS loop as the yaw rate
    feedback gain varies. How are the characteristic modes of motion of
    the aircraft affected? Determine the closed loop transfer function
    which relates the aircraft yaw rate to the pilot rudder command.
    Find the Dutch roll damping and frequency, the roll mode time
    constant and the spiral mode time constant for the augmented
    aircraft and compare these to the unaugmented aircraft
    characteristics and MIL-F-8785C.

3. Using the generalized analysis techniques presented in Chapter 3,
    determine a general transfer function for the closed loop transfer
    aileron command input. Since the denominator of this transfer
    function is the characteristic equation of the augmented aircraft

14.333

and is the same as that found in part 2, only the numerator need be found from the matrix equations. Include the ARI effects in the general expression and reduce the expression to its simplest form.

4. If the ARI gain is zero, determine the numerator of the transfer function relating the sideslip angle response due to an aileron command input using the root locus program technique discussed in class to combine the two parts of the transfer function numerator. It is difficult to find the required coupling numerator terms needed for the analysis using the transfer functions provided by Figures 14P.5 and 14P.6 and the coupling term definitions presented in Paragraph 14.4. The equations of motion provided in Appendix A and the dimensional stability derivatives of Figure 14P.4 should be used for this purpose. Determine the sideslip angle response of the augmented aircraft due to a pilot aileron pulse input. Compare this response with the response obtained in part 1. Remember to label your plots obtained from the computer. Does the aircraft possess proverse or adverse yaw characteristics? How much adverse or proverse yaw is generated per degree of aileron input (use the maximum initial sideslip excursion to determine this value)? How does this compare to the unaugmented aircraft sideslip excursion?

5. For the ARI gain set to the design value, repeat the analysis of Part 4. The effects of the ARI may be easily included in the analysis by modifying the transfer function relating the sideslip response due to a pilot aileron command input contained in Part 4 using the root locus program technique. Does the aircraft possess proverse of adverse yaw? How much yaw is generated per degree of aileron input? How does this compare to the unaugmented aircraft response and to the augmented aircraft response without the ARI? What is your assessment of the value of the ARI at the flight condition evaluated? Should the ARI be incorporated into the T-38 fleet?

Normally the effect of the yaw damper and the ARI on the aircraft roll response would also need to be examined (however, these effects may be omitted for the purposes of this analysis). These effects may be determined using the same analysis procedure outlined above by finding the transfer function of the augmented aircraft which relates the aircraft roll rate to the pilot aileron command (step 3) and then accomplishing steps 4 and 5. An aileron step command would be used to determine how the steady state roll rate of the aircraft is affected by the yaw damper and the ARI.

FIGURE 14P.2. ELEVATOR LONGITUDINAL TRANSFER FUNCTION FACTORS FOR THE A-7

Note: Data for body-fixed centerline axes, clean flexible airplane

		FLIGHT CONDITION								
		1	2	3	4	5	6	7	8	9
	h	0	0	0	15,000	15,000	15,000	15,000	35,000	35,000
	M	0.25	0.6	0.9	0.3	0.6	0.9	1.1	0.6	0.9
Δ	ζ_{sp}	0.367	0.383	0.395	0.277	0.316	0.316	0.185	0.225	0.230
	ω_{sp}	1.76	4.21	6.76	1.63	3.15	5.48	8.81	2.08	3.63
	$\zeta_p(1/T_{p_1})$	0.0594	0.100	0.790	0.118	0.0620	(0.0688)	0.589	0.0449	(0.0616)
	$\zeta_p(1/T_{p_2})$	0.156	0.0698	0.0472	0.140	0.0710	(−0.0513)	0.0372	0.751	(−0.0501)
$N^{\theta}_{\delta_e}$	A_{θ}	−5.43	−30.6	−58.4	−45.1	−18.8	−41.6	−44.3	−8.18	−20.2
	$1/T_{\theta_1}$	−0.214	0.0122	0.0728	−0.00823	0.00716	0.0.443	0.0422	−0.00316	0.0202
	$1/T_{\theta_2}$	0.731	1.79	3.19	0.506	1.09	1.97	2.02	0.516	0.933
$N^{u}_{\delta_e}$	A_u	5.75	8.34	11.6	5.63	6.96	9.13	11.2	5.70	6.61
	$1/T_u$	51.1	123	186	8.5	120	190	234	109	177
	$\zeta_u(1/T_{u_2})$	(0.411)	0.665	(1.22)	(0.369)	0.627	0.854	(0.899)	0.925	0.753
	$\omega_u(1/T_u)$	(1.05)	1.30	(2.28)	(0.387)	0.890	1.24	(1.23)	0.466	0.719

14.335

A_w	-99.4	-43.2	-220	-209	-99.6	-23.8	-318	-165	-29.0
$1/T_{w_1}$	178	110	234	191	121	58.9	187	126	51.7
$\zeta_w(1/T_{w_2})$	0.419	-0.0553	(-0.0131)	(-0.00939)	0.0567	-0.0444	(-0.00603)	0.239	-0.110
$\omega_w(1/T_{w_3})$	0.0219	0.0494	(0.0530)	(0.0518)	0.0386	0.0990	(0.0773)	0.0210	0.105
A_h	99.7	43.6	221	209	99.8	24.5	318	165	29.6
$1/T_{h_1}$	0.0173	-0.0154	0.0412	0.0431	0.00225	-0.0549	0.0719	0.00956	-0.0624
$1/T_{h_2}$	13.2	7.64	22.2	20.0	11.8	5.41	25.3	15.6	6.21
$1/T_{h_3}$	-12.5	-7.22	-21.2	-18.7	-11.0	-4.92	-23.3	-14.3	-5.57
A_{a_z}	-99.4	-43.2	-220	-209	-99.6	-23.8	-318	-165	-29.0
$1/T_{a_{z_1}}$	-0.00250	-0.00170	-0.00139	-0.00147	-0.00405	-0.00417	-0.00117	-0.00248	-0.00998
$1/T_{a_{z_2}}$	0.0197	-0.0136	0.0425	0.0445	0.00627	-0.0497	0.0729	0.0120	-0.0506
$1/T_{a_{z_3}}$	13.2	7.69	22.2	20.0	11.8	5.55	25.3	15.6	6.33
$1/T_{a_{z_4}}$	-12.5	-7.28	-21.3	-18.7	-11.0	-5.08	-23.3	-14.3	-5.73

Row groupings: $N_{\delta_e}^w$ (A_w, $1/T_{w_1}$, $\zeta_w(1/T_{w_2})$, $\omega_w(1/T_{w_3})$); $N_{\delta_e}^h$ (A_h, $1/T_{h_1}$, $1/T_{h_2}$, $1/T_{h_3}$); $N_{\delta_e}^{a_z}$ CG (A_{a_z}, $1/T_{a_{z_1}}$, $1/T_{a_{z_2}}$, $1/T_{a_{z_3}}$, $1/T_{a_{z_4}}$)

FIGURE 14P.4. LATERAL NONDIMENSIONAL STABILITY DERIVATIVES FOR THE T-38

Note: Data are for body fixed centerline axes, cruise configuration

	FLIGHT CONDITION							
	1	2	3	4	5	6	7	
h (ft)	0	0	0	25,000	25,000	50,000	50,000	40,(
M (-)	0.6	0.8	1.0	0.4	1.0	0.8	1.0	4.:
V_{T_o} (ft/sec)	670	893	1117	406	1017	774	968	12.
C_{y_β}	-0.175	-1.27	-1.35	-1.26	-1.35	-1.26	-1.41	-1..
$C_{y_{\delta_a}}$	0	0	0	0	0	0	0	0
$C_{y_{\delta_r}}$	0.155	0.172	0.103	0.160	0.132	0.183	0.126	0.09
C_{ℓ_β}	-0.057	-0.0063	-0.085	-0.097	-0.086	-0.086	-0.080	-0.05
C_{ℓ_p}	-0.320	-0.330	-0.275	-0.270	-0.365	-0.335	-0.390	-0.29
C_{ℓ_r}	0.080	0.095	0.110	0.155	0.115	0.140	0.135	0.13
$C_{\ell_{\delta_a}}$	0.037	0.030	0.0069	0.040	0.026	0.053	0.032	0.01
$C_{\ell_{\delta_r}}$	0.016	0.018	0.012	0.017	0.015	0.021	0.016	0.01(
C_{n_β}	0.262	0.315	0.332	0.240	0.335	0.286	0.340	0.31

C_{n_p}	0.076	0.078	0.084	0.085	0.078	0.052	0.070	0.0
C_{n_r}	-0.470	-0.435	-0.490	-0.340	-0.490	-0.380	-0.500	-0.5
$C_{n_{\delta_a}}$	0.013	0.0143	0.0126	0.0069	0.0126	0.0149	0.0137	0.01
$C_{n_{\delta_r}}$	-0.092	-0.092	-0.063	-0.103	-0.086	-0.106	-0.086	-0.06

LATERAL DIMENSIONAL DERIVATIVES FOR THE T-38

Note: Data are for body-fixed centerline axes, cruise configuration.

	FLIGHT CONDITION							
	1	2	3	4	5	6	7	
h (ft)	0	0	0	25,000	25,000	50,000	50,000	40,
M (-)	0.6	0.8	1.0	0.4	1.0	0.8	1.0	1.
Y_v	-0.311	-0.737	-0.98	-0.151	-0.4	-0.0982	-0.137	-0.
Y_{δ_a}	0	0	0	0	0	0	0	
Y_{δ_r}	0.0675	0.1	0.075	0.191	0.0391	0.0143	0.0122	0.
L_β	-29.69	-58.29	-123.03	-8.491	-46.24	-9.293	-13.46	-2
L_p	-3.14	-4.316	-4.5	-0.727	-2.435	-0.588	-0.8544	-1
L_r	0.785	1.242	1.8	0.417	0.767	0.246	0.296	0
L_{δ_a}	19.27	27.75	9.987	3.503	13.89	5.727	5.383	7
L_{δ_r}	8.334	16.65	17.37	1.489	8.065	2.269	2.691	4
N_δ	17.65	37.71	62.18	2.72	23.31	4.0	7.402	1
N_p	0.0965	0.132	0.178	0.296	0.0673	0.0118	0.0198	0.
N_r	-0.597	-0.736	-1.037	-0.1185	-0.423	-0.086	-0.142	-
N_{δ_a}	0.876	1.712	2.36	0.0782	0.877	0.2084	0.298	0
N_{δ_r}	-6.2	-11.01	-11.8	-1.167	-5.984	-1.482	-1.872	-3

Note: Data for body-fixed centerline axes, cruise configuration

$S = 170 \text{ ft}^2$, $b = 25.25$ ft, $c = 7.73$ ft

$W = 10,000$ lbs, $m - 311.0$ slugs, c.g. at 23% MAC

$I_x = 4,400$ slug-ft^2, $I_y = 30,000$ slug-ft^2, $I_z = 34,000$ slug-ft^2, $I_{xz} = 0$

				FLIGHT CONDITION				
	1	2	3	4	5	6	7	
h (ft)	0	0	0	25,000	25,000	50,000	50,000	40
M (-)	0.6	0.8	1.0	0.4	1.0	0.8	1.0	1
a (ft/sec)	1117	1117	1117	1016	1016	968.5	968.5	9
ρ (slug/ft^3)	0.002378	0.002378	0.002378	0.001065	0.001065	0.000367	0.000367	0.0
V_{T_0} (ft/sec)	670	893	1117	406	1016	774	968.5	1
$q = \rho V_T^2/2$ (lb/ft^2)	535	950	1482	88	550	109	170	
α_0 (deg)	1.1	0.8	0.6	8.7	1.5	5.0	3.1	
7_0 (deg)	0	0	0	0	0	0	0	
U_0 (ft/sec)	669.8	892.8	1116.8	401.2	1015.7	771.3	965	1
W_0 (ft/sec)	12.7	12.5	11.7	61.3	26.6	67.4	52.3	

FIGURE 14P.5. AILERON LATERAL TRANSFER FUNCTION FACTORS FOR THE T-38

Note: Data for body-fixed centerline axes, cruise configuration

		FLIGHT CONDITION							
		1	2	3	4	5	6	7	
h		0	0	0	25,000	25,000	50,000	50,000	40,
M		0.6	0.8	1.0	0.4	1.0	0.8	1.0	1.
Δ	$1/T_s$	0.0025	−0.0014	0.00141	−0.013	0.00016	−0.00594	−0.0031	−0.0
	$1/T_\beta$	3.0197	4.145	4.185	0.605	2.275	0.548	0.803	1.2
	ζd	0.121	0.133	0.146	0.102	0.1	0.527	0.585	0.0
	ω_d	4.251	6.2	7.97	1.98	4.94	2.187	2.847	4.1
$N_{\delta_a}^p$	A_p	19.273	27.75	10.0	3.50	13.98	5.727	5.383	7.9
	$1/T_{p_1}$	−0.00091	−0.0005	−0.0003	−0.012	−0.00082	−0.00362	−0.0018	−0.00
	ζ_p	0.108	0.12	0.127	0.0852	0.085	0.0473	0.052	0.00
	ω_p	4.382	6.473	9.628	1.703	5.137	2.081	2.856	4.3
$N_{\delta_a}^\phi$	A_p	19.29	27.78	10.01	3.515	14.0	5.745	5.4	7.9
	$1/T_{p_1} (\zeta_p)$	(0.108)	(0.12)	(0.127)	(0.0829)	(0.0853)	(0.047)	(0.0522)	(0.0
	$1/T_{p\delta} (\omega_p)$	(4.381)	(6.471)	(9.617)	(1.719)	(5.135)	(2.086)	(2.856)	(4.3
$N_{\delta_a}^r$	A_r	0.876	1.712	2.36	0.782	0.877	0.2084	0.298	0.8
	$1/T_r$	4.439	5.405	4.80	0.535	1.52	0.484	0.638	1.4
	ζ_r	0.267	0.423	0.47	0.192	0.405	0.0827	0.129	0.1
	ω_r	2.127	2.113	1.523	4.345	2.95	3.19	2.765	1.8
$N_{\delta_a}^\beta$	A_β	−0.511	−1.323	−2.255	0.446	−0.511	0.289	−0.0074	−0.
	$1/T_{\beta_1} (\zeta_\beta)$	−0.167	−0.0832	−0.0353	(0.706)	−0.0843	(0.58)	−0.21	−0.0
	$1/T_{\beta_2} (\omega_\beta)$	6.926	7.439	5.334	(0.287)	4.90	(0.283)	18.624	1.7
	$1/T_{\beta_3}$	−−	−−	−−	−−	−−	−−	−−	−

FIGURE 14P.6. RUDDER LATERAL TRANSFER FUNCTION FACTORS FOR THE T-38

Note: Data are for body-fixed centerline axes, cruise configuration.

		FLIGHT CONDITION							
		1	2	3	4	5	6	7	
h		0	0	0	25,000	25,000	50,000	50,000	40,
M		0.6	0.8	1.0	0.4	1.0	0.8	1.0	1.
Δ	$1/T_s$	0.0025	-0.0014	0.00141	-0.013	0.00016	-0.00594	-0.0031	-0.0
	$1/T_R$	3.0197	4.145	4.185	0.605	2.275	0.348	0.803	1.
	ζ_d	0.121	0.133	0.146	0.102	0.1	0.527	0.585	0.0
	ω_d	4.251	6.2	7.97	1.98	4.94	2.187	2.847	4.
$N^p_{\delta_r}$	A_p	8.33	16.65	17.37	1.49	8.065	2.27	2.691	4.
	$1/T_{p_1}$	-0.00092	-0.0005	-0.0003	-0.0119	-0.00082	-0.00361	-0.0018	-0.00
	$1/T_{p_2}(\zeta_p)$	-2.07	-0.797	-4.522	-2.06	-3.311	-1.454	-1.395	(0.0
	$1/T_{p_3}(\omega_p)$	2.154	1.10	4.79	1.905	3.341	1.423	1.408	(0.6
$N^\phi_{\delta_r}$	A_ϕ	8.215	16.5	17.245	1.31	7.91	2.14	2.59	4.2
	$1/T_{\phi_1}(\zeta_\phi)$	-2.11	-0.827	-4.557	-2.293	-3.372	-1.526	-1.443	(-0.0
	$a/T_{\phi_2}(\omega_p)$	2.15	1.09	4.79	1.994	3.350	1.451	1.42	(0.6
$N^r_{\delta_r}$	A_r	-6.2	-11.01	-11.8	-1.167	-5.984	-1.482	-1.872	-3.2
	$1/T_{r_1}$	3.0	4.114	4.196	0.561	2.252	0.519	0.78	-0.0
	$\zeta_r(1/T_{r_2})$	0.206	(0.0302)	0.674	0.14	0.373	0.11	0.196	(0.1
	$\omega_r(1/T_{r_3})$	0.309	(0.367)	0.465	0.833	0.456	0.502	0.346	(1.

$N^\beta_{\beta_r}$	A_β	0.067	0.0998	0.0748	0.0191	0.0391	0.0143	0.0122	0.188
	$1/T_\beta$	−0.00065	−0.0016	−0.00212	−0.0372	−0.0034	−0.0107	−0.0052	−0.0041
	$1/T_{\beta_2}$	2.994	4.075	4.205	0.655	2.302	0.558	0.810	1.23
	$1/T_{\beta_3}$	94.93	113.63	161.56	72.21	159.0	117.48	164.64	178.02
$N^{a_y}_{\delta_r}$ CG	A_{n_y}	45.24	89.16	83.53	7.852	39.77	11.08	11.88	22.72
	$1/T_{a_{y_1}}$	−0.0057	−0.0018	−0.00447	−0.0496	−0.00561	−0.014	−0.0063	−0.003
	$1/T_{a_{y_2}}$	3.89	3.795	4.223	0.683	2.322	0.565	0.813	1.2?
	$1/T_{a_{y_3}}$	−3.027	−6.248	−9.098	−2.525	−5.987	−2.536	−3.709	−4.7?
	$1/T_{a_{y_4}}$	2.882	7.327	10.416	2.736	6.529	2.66	3.90	5.0?

14.343
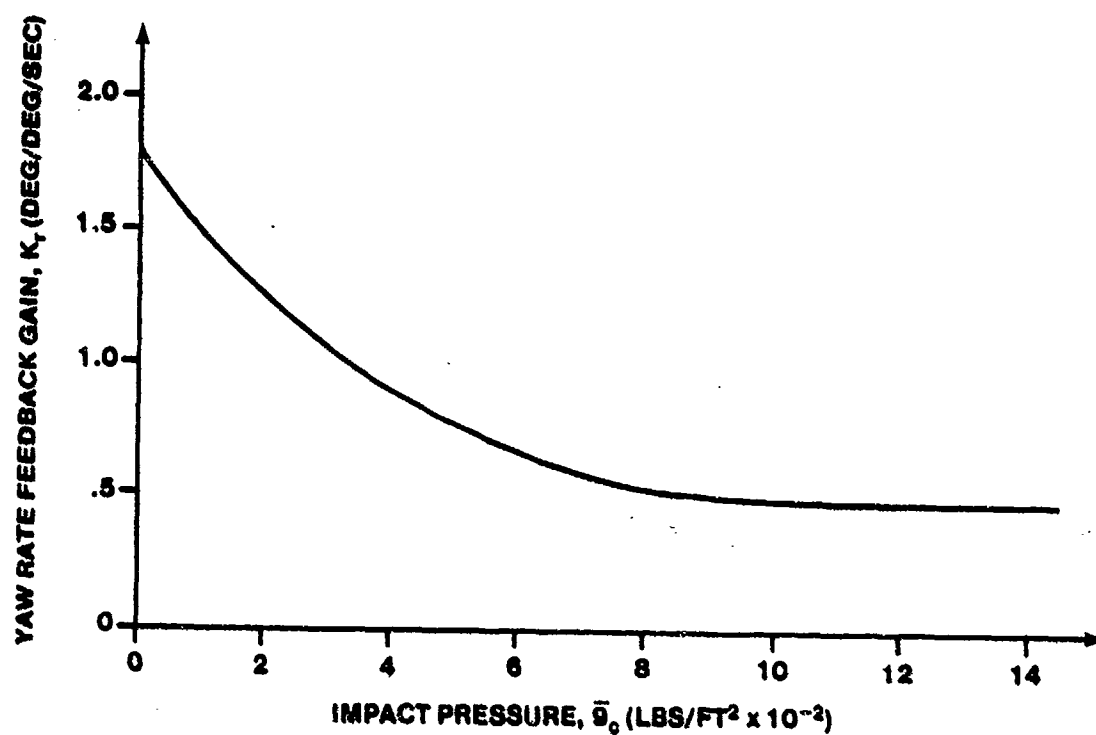
FIGURE 14P.8. T-38 YAW RATE FEEDBACK GAIN SCHEDULED
AS A FUNCTION OF DYNAMIC PRESSURE

14.344

Bibliography

14.1.   McRuer, Duane, Irving Ashkenas and Dustan Graham. *Aircraft Dynamics and Automatic Control.* Princeton University Press, Princeton, New Jersey. 1973.

14.2.   Blakelock, John H. *Automatic Control of Aircraft and Missiles.* John Wiley and Sons, Inc., New York, New York. 1965.

14.3.   Roskam, Jan. *Airplane Flight Dynamics and Automatic Flight Controls.*

14.4.   Pape, James K. and Michael P. Garland. *F-16A/B Flying Qualities Full Scale Development Test and Evaluation.* Final Report, AFFTC-TR-79-10. Air Force Flight Test Center, Edwards AFB, CA. September, 1979.

14.5.   Anonymous. *F-16 Air Combat Fighter: Technical Description.* Volume 8. "Flight Control System." General Dynamics Report F-16-060-8. General Dynamics, Fort Worth, Tx. 12 August 1975.

14.6.   Hoh, Roger H., T. T. Myers, I. L. Ashkenas, R. F. Ringland and S. J. Craig. *Development of Handling Quality Criteria for Aircraft with Independent Control of Six Degrees of Freedom.*

14.7.   Hooker, David S., Rober L. Kisslinger, George R. Smith and M. Sheppard Smyth. *Survivable Flight Control System.* Interim Report No. 1: "Studies, Analyses and Approach". Technical Report, AFFDL-TR-71-20. Air Force Flight Dynamics Laboratory, Wright-Patterson AFB, OH. May 1971.

14.8.   Damman, Lawrence, et. al. *Flight Test Development and Evaluation of a Multimode Digital Flight Control System Implemented in an A-7D (DIGITAC).* AFFTC-TR-76-15. Air Force Flight Test Center, Edwards AFB, CA. June 1976.

14.9.   Kirsten, Paul W. *Flight Control System Structural Resonance and Limit Cycle Results.* Air Force Flight Test Center, Edwards AFB, CA. Undated.

14.10.   Hoh, Roger H., et. al. *Proposed MIL Handbook -- Handling Qualities of Piloted Airplanes.* Systems Technology, Inc., Hawthorne, CA. December, 1981. Preliminary.

14.11.   Anonymous. *Background Information and User Guide for MIL-XXXX, Flight Control Systems.* Northrop Corporation, Hawthorne, CA. Undated. Draft Version.

14.12.   Anonymous. *Background Information and User Guide for MIL-F-9490D.* AFFDL-TR-74-116. The Boeing Company, Wichita Division, Wichita, Kansas. January, 1975.

14.13. Clark, Robert, et. al. A-7D Digital Multimode Flight Control System Flight Test and Weapon Delivery Evaluation. AFFDL-TR-76-121. Honeywell, Inc., St. Louis Park, MN. December, 1976.

14.14. Twisdale, Thomas R. and Capt. David L. Franklin. Tracking Test Techniques for Handling Qualities Evaluation. AFFTC-TD-75-1. Air Force Flight Test Center, Edwards AFB, CA. May, 1975.

14.15. Martin, Roy and George Muellner. Systems Theory and Flight Test Techniques. Chapter 12, "Closed-Loop Handling Qualities." USAF Test Pilot School, Edwards AFB, CA. February, 1979.

14.16. Twisdale, Thomas R. and Tice A. Ashurst, Jr. System Identification from Tracking (SIFT), A New Technique for Handling Qualities Test and Evaluation. AFFTC-TR-77-27 . Air Force Flight Test Center, Edwards AFB, CA. November, 1977. Initial Report.

14.17. Twisdale, Thomas R. SIFT Pilot-in-the-Loop Handling Qualities Test and Analysis Techniques. Air Force Flight Test Center, Edwards AFB, CA. Undated.

14.18. Bischoff, David E. "Equivalent Systems Definition of Longitudinal Flying Qualities." Proceedings of the 1981 Science and Engineering Symposium. Volume III. Wright-Patterson AFB, OH. 27-29 October 1981.

14.19. Hodgkinson, J., R. L. Berger and R. L. Bear. "Analysis of High Order Aircraft/Flight Control System Dynamics Using an Equivalent System Approach." Seventh Annual Pittsburgh Conference on Modeling and Simulation. 26-27 April, 1976.

14.20. Hodgkinson, J., W. J. LaManna and J. L. Heyde. "Handling Qualities of Aircraft with Stability and Control Augmentation Systems — A Fundamental Approach." Aeronautical Journal. February, 1976.

14.21. Hoh, Roger H. Thomas T. Myers and Irving L. Ashkenas. "Development of a Tentative Flying Qualities Criterion for Aircraft with Independent Control of Six Degrees of Freedom — Analysis and Flight Test." Systems Technology, Inc., Hawthorne, CA. Undated.

14.22. Nagy, Christopher J. A New Method for Test and Analysis of Dynamic Stability and Control. AFFTC-TD-75-4. Air Force Flight Test Center, Edwards AFB, CA. May, 1976.

14.23. Jones, Raymond L. Dynamic Parameter Analysis. USAF Test Pilot School, Edwards AFB, CA. August, 1978. Revised September, 1980.

14.24. Hamming, R. W. Numerical Methods for Scientists and Engineers. Second Edition. McGraw-Hill, Inc., New York, NY, 1973.

14.25. Teper, Gary L. Aircraft Stability and Control Data. STI Technical
        Report 176-1. Systems Technology, Inc., Hawthorne, CA. April,
        1969. Prepared for Ames Research Center, NASA.

14.26. Heffley, Rober K. and Wayne F. Jewell. Aircraft Handling
        Qualities Data. STI Technical Report 1004-1. Systems Technology,
        In.c, Hawthorne, CA. May, 1972. Prepared for Flight Research
        Center, NASA.

14.27. Kitto, William and Tom Twisdale. The New FRA (Frequency Response
        Analysis) Program Users Guide. Edition 1.2. Computer Printout.
        Air Force Flight Test Center, Edwards AFB, CA. July 1981.

14.28. Anonymous. EASY5 Simulation at the AFFTC. Software Management
        Branch, Computer Sciences Division, Air Force Flight Test Center,
        Edwards AFB, CA. 6 March, 1981.

14.29. Schultz, Donald G. and James L. Melsa. State Functions and Linear
        Control Systems. McGraw-Hill Book Company, New York. 1967.

14.30. D'Azzo, John J. and Constantine H. Houpis. Linear Control System
        Analysis and Design: Conventional and Modern. McGraw-Hill, Inc.,
        New York. 1975.

14.31. Katshuhiko, Ogata. State Space Analysis of Control Systems.
        Prentice-Hall, Inc., Englewood Cliffs, N.J. 1967.

14.32. Anonymous. The Artificial Feel System. Bureau of Aeronautics
        Report AE-61-4-V. Northrop Aircraft, Inc. May, 1953.

14.33. Cannon, Rober H., Jr. Dynamics of Physical Systems. McGraw-Hill
        Book company, New York. 1967.

14.34. Lago, Gladwyn V. and Lloyd M. Benningfield. Circuit and System
        Theory. John Wiley and Sons, New York. 1979.

14.35. Anonymous. The Hydraulic System. Bureau of Aeronautics Report
        AE-61-4-IV. Northrop Aircraft, Inc. March, 1953.

14.36. Beer, Ferdinand P. and E. Russell Johnston, Jr. Vector Mechanics
        for Engineers: Statics and Dynamics. McGraw-Hill Book Company, New
        York. 1962.

14.37. Hjorten, Major Alvin P. The Foundations of Inertial Navigation and
        Automatic Guidance. Department of Astronautics, USAF Academy, CO.
        1986.

14.38. Anonymous. Flying Qualities of Piloted Airplanes. Military
        Specification MIL-F-8785C. 5 November 1980.

14.39. Kisslinger, Robert L. and George J. Vetsch. *Survivable Flight Control System, Interim Report No. 1: Studies, Analysis and Approach. Supplement for Control Law Development Studies.* AFFDL-TR-71-20, Supplement - 2. McDonnel Aircraft Company, McDonnell Douglas Corporation, St. Louis, MO. May, 1971.

14.40. Abramson, Norman. *An Introduction to the Dynamics of Airplanes.* Dover Publications, Inc., New York. 1971.

14.41. Bisplinghoff, Raymond L. and Hold Ashley. *Principles of Aeroelasticity.* Dover Publications, Inc., New York. 1962.

14.42. Guenther, L. H. and D. A. Smith. *F-15 Flight Control Analysis: Part I, Flight Control Design Analysis.* McConnell Aircraft Company, St. Louis, MO. 3 August 1970. Classification cancelled 4 January 1979.

14.43. Brandeau, G. *Task Oriented Flying Qualities for Air-to-Ground Gun Attack.* Fairchild Republic Company, Farmingdale, NY. June, 1978. Prepared for AFDL Symposium on Flying Qualities, September, 1978.

14.44. Jeske, R. A. and R. P. Anderson. *Final Engineering Report: Automatic Flight Control System for the A-D/E Aircraft.* Vought Aeronautics Division, LTV Aerospace Corporation, Dallas, TX. Undated.

14.45. Wilde, W. C. *F-16 Flight Control Design Analysis Report.* General Dynamics, Fort Worth Division, Ft. Worth, TX. 13 July 1976.

14.46. Gelb, Arthur and Wallace E. Vaner Velde. *Multiple-Input Describing Functions and Nonlinear System Design.* McGraw-Hill Book Company, New York. 1968.

APPENDIX A

AIRCRAFT TRANSFER FUNCTIONS

A.1 EQUATIONS OF MOTION REVIEW

The aircraft stability derivatives are normally presented in two formats. Aerodynamic wind tunnel data usually presents a plot of the nondimensional stability derivative value versus airspeed or Mach for normal (1g) flight conditions (stability derivatives may be plotted as a function of angle of attack or sideslip for spin or departure analysis). The nondimensional stability derivative equations of motion making the usual assumptions are:

Longitudinal axis (body axes)

$$\left(\frac{mU_0}{Sq_0}\dot{\hat{u}} - C_{x_u}\hat{u}\right) + \left(-\frac{c}{2U_0}C_{x_{\dot{\alpha}}}\dot{\alpha} - C_{x_\alpha}\alpha\right) + \left(-\frac{c}{2U_0}C_{x_q}\dot{\theta} + \frac{mg}{Sq_0}(\cos\theta_0)\theta\right)$$

$$= C_{x_{\delta_e}}\delta_e$$

$$-\left(C_{z_u}\hat{u}\right) + \left[\left(\frac{mU_0}{Sq_0} - \frac{c}{2U_0}C_{z_{\dot{\alpha}}}\right)\dot{\alpha} - C_{z_\alpha}\alpha\right] + \left[-\left(\frac{mU_0}{Sq_0} - \frac{c}{2U_0}C_{z_q}\right)\dot{\theta} + \right.$$

$$\left. \frac{mg}{Sq_0}(\sin\theta_0)\theta\right] = C_{z_{\delta_e}}\delta_e$$

$$-\left(C_{m_u}\hat{u}\right) + \left(-\frac{c}{2U_0}C_{m_{\dot{\alpha}}}\dot{\alpha} - C_{m_\alpha}\alpha\right) + \left(\frac{I_y}{Sq_0c}\ddot{\theta} - \frac{c}{2U_0}C_{m_q}\dot{\theta}\right) = C_{m_{\delta_e}}\delta_e$$

where $\hat{u} = u/U_0$ (nondimensional velocity perturbation)

q_0 is the trim dynamic pressure

$q = \dot{\phi}\cos\phi + \dot{\psi}\sin\psi\cos\theta$

$q = \dot{\theta}$ (pitch rate if bank angle is zero)

$C_{x_{\dot{\alpha}}} = C_{x_q} = C_{x_{\delta_e}} = 0$

and

$\dot{\alpha} = w/U_0$

Lateral-directional axes

$$- \frac{b}{2U_0} C_{y_p} \dot{\phi} - \frac{mg}{Sq_0} (\cos \theta_0)\phi + \left(\frac{mU_0}{Sq_0} - \frac{b}{2U_0} C_{y_r} \right) r + \frac{mU_0}{Sq_0} \dot{\beta} - C_{y_\beta} \beta$$

$$= C_{y_{\delta_a}} \delta_a + C_{y_{\delta_r}} \delta_r$$

$$\frac{I_x}{Sq_0 b} \ddot{\phi} - \frac{b}{2U_0} C_{l_p} \dot{\phi} - \frac{I_{xz}}{Sq_0 b} \dot{r} - \frac{b}{2U_0} C_{l_r} r - C_{l_\beta} \beta = C_{l_{\delta_a}} \delta_a + C_{l_{\delta_r}} \delta_r$$

$$\frac{I_{xz}}{Sq_0 b} \ddot{\phi} - \frac{b}{2U_0} C_{n_p} \dot{\phi} - \frac{I_z}{Sq_0 b} \dot{r} - \frac{b}{2U_0} C_{n_r} r - C_{n_\beta} \beta = C_{n_{\delta_a}} \delta_a + C_{n_{\delta_r}} \delta_r$$

where

$$p = \dot{\phi} - \dot{\psi} \sin \theta$$

$$= \dot{\phi} \text{ (roll rate if pitch attitude is zero or small)}$$

$$C_{y_p} = C_{y_r} = C_{y_{\delta_a}} = 0$$

and

$$\beta = v/U_0$$

Sometimes nondimensional stability derivative data are tabulated as a function of angle of attack and Mach to cover the entire aircraft flight envelope. Equations of motion for other than 1 g flight can be obtained from this format given the angle of attack corresponding to a particular load factor.

Dimensional stability derivative data are usually the format found in textbooks or NASA published aircraft stability and control data reports. The dimensional stability derivative equations are

Longitudinal axis (body axes)

$$\dot{u} - X_u^* u - X_w w + W_0 \dot{\theta} + g (\cos \theta_0)\theta = X_{\delta_e} \delta_e$$

$$-Z_u^* u + (1 - Z_{\dot{w}})\dot{w} - Z_w w - U_0\dot{\theta} + g\,(\sin\theta_0)\theta = Z_{\delta_e}\delta_e$$

$$-M_u^* u - M_{\dot{w}}\dot{w} - M_w w + \ddot{\theta} - M_q\dot{\theta} = M_{\delta_e}\delta_e$$

where

$$w_0 = V_A \sin\alpha_0$$

V_A is the trim velocity of the aircraft (true airspeed)

$$X_u^* = \frac{X_u}{U_0} \quad Z_u^* = \frac{Z_u}{U_0} \text{ and } M_u^* = \frac{M_u}{U_0}$$

Stability derivatives in terms of angle of attack can be written by recalling that

$$\alpha = w/U_0$$

Therefore

$$M_\alpha = M\left(\frac{w}{U_0}\right) = U_0 M_w$$

Similarly

$$U_0 X_w = X_\alpha \text{ and } U_0 Z_w = Z_\alpha$$

Lateral-directional axes (body axes)

$$\dot{\beta} - Y_v\beta - \frac{w_0}{V_A}\dot{\phi} - \frac{g}{V_A}(\cos\theta_0)\phi + \frac{U_0}{V_A}r = Y_{\delta_a}^*\delta_a + Y_{\delta_r}^*\delta_r$$

$$-L_\beta'\beta + \ddot{\phi} - L_p'\dot{\phi} - L_r'r = L_{\delta_a}'\delta_a + L_{\delta_r}'\delta_r$$

$$-N_\beta'\beta - N_p'\dot{\phi} + \dot{r} - N_r'r = N_{\delta_a}'\delta_a + N_{\delta_r}'\delta_r$$

The NASA publications (references 25 and 26) also tabulate the aircraft transfer functions directly, as will be discussed later.

A.2 <u>TRANSFER FUNCTIONS</u>

If the Laplace transform of the above equations is taken, assuming zero initial conditions, and the equations are written in matrix notation, the following equations result (in terms of dimensional stability derivatives for the aircraft body axes system):

Longitudinal axis

$$
\begin{bmatrix}
s - X_u^* & -X_w & W_0 s + g \cos \theta_0 \\
-Z_u^* & (1 - Z_{\dot{w}})s - Z_w & -U_0 s + g \sin \theta_0 \\
-M_u^* & -M_{\dot{w}}s - M_w & s^2 - M_q s
\end{bmatrix}
\begin{bmatrix}
u \\
w \\
\theta
\end{bmatrix}
\begin{bmatrix}
X_{\delta_e} \\
Z_{\delta_e} \\
M_{\delta_e}
\end{bmatrix}
\delta_e
$$

Lateral-directional axes

$$
\begin{bmatrix}
s - Y_v & -\alpha_0 s - \dfrac{g \cos \theta_0}{U_0} & 1 \\
-L'_\beta & s^2 - L'_p s & -L'_r \\
-N'_\beta & -N'_p s & s - N'_r
\end{bmatrix}
\begin{bmatrix}
\beta \\
\phi \\
r
\end{bmatrix}
=
\begin{bmatrix}
Y^*_{\delta_a} & Y^*_{\delta_r} \\
L'_{\delta_a} & L'_{\delta_r} \\
N'_{\delta_a} & N'_{\delta_r}
\end{bmatrix}
\begin{bmatrix}
\delta_a \\
\delta_r
\end{bmatrix}
$$

If the stability axes system is used, then

$$\theta_0 = W_0 = \alpha_0 = 0$$

Furthermore, the above equations assume

$$U_0 = V_A$$

In reality, $U_0 \approx V_A \cos \alpha \cos \beta$, but assuming α and β to be small, then the above relation is valid. A reasonable assumption for small angles of attack. Transfer functions in terms of angle of attack can be found as

$$\frac{\alpha(s)}{\delta_e(s)} = \frac{1}{U_0} \frac{w(s)}{\delta_e(s)}$$

so that the above matrix equations are all that are needed for transfer function derivation.

The transfer function for

$$\frac{w(s)}{\delta_e(s)}$$

can be found, using Cramer's rule, as

$$\frac{w(s)}{\delta_e(s)} = \frac{\begin{vmatrix} s - X_u^* & X_{\delta_e} & W_0 s + g \\ -Z_u^* & Z_{\delta_e} & -U_0 s + g\theta_0 \\ -M_u^* & M_{\delta_e} & s^2 - M_q s \end{vmatrix}}{\begin{vmatrix} s - X_u^* & -X_w & W_0 s + g \\ -Z_u^* & (1 - Z_w)s - Z_w & -U_0 s + g\theta_0 \\ -M_u^* & -M_w s - M_w & s^2 - M_q s \end{vmatrix}}$$

where the determinant in the denominator yields the characteristic equation of the unaugmented aircraft. Similar derivations can be used to find any single input, single output transfer function for the longitudinal or lateral-directional axes.

Often, in the analysis of coupled axes, such as the lateral-directional axes, a coupling term arises in the closed loop transfer function. For instance, when a transfer function relating roll rate to aileron input is desired for an aircraft with a yaw damper engaged, the coupling transfer function which arises accounts for the simultaneous deflection of the aileron (by the pilot) and the rudder (by the yaw damper).

The coupling transfer function is found as

$$
G^{\beta \; r}_{\delta_a \delta_r}(s) = \frac{\begin{vmatrix} Y^*_{\delta_a} & -\alpha_0 s - \dfrac{g}{U_0} & Y^*_{\delta_r} \\[2ex] L'_{\delta_a} & s^2 - L'_p s & L'_{\delta_r} \\[2ex] N'_{\delta_a} & -N'_p s & N'_{\delta_r} \end{vmatrix}}{\begin{vmatrix} s - Y_v & -\alpha_0 s + \dfrac{g}{U_0} & 1 \\[2ex] -L'_\beta & s^2 - L'_p s & -L'_r \\[2ex] -N'_\beta & -N'_p s & s - N'_r \end{vmatrix}}
$$

where both control columns are substituted into the appropriate output parameter columns to find the numerator. The denominator yields the characteristic equation of the aircraft.

Sometimes if three controls are available, such as using vertical canards in addition to the ailerons and rudder controls, another coupling term arises of the form

$$
G^{\beta \; \phi \; r}_{\delta_a \delta_{vc} \delta_r}(s)
$$

which is found by substituting all three control columns from the control matrix into the appropriate motion parameter columns.

It is often convenient to express the transfer functions in the body axis system, especially for control system analysis, since the sensors on the aircraft are usually fixed to the aircraft.

A.3 DIMENSIONAL STABILITY DERIVATIVE DEFINITIONS

The definitions of dimensional stability derivatives, in terms of non-dimensional stability derivatives, are presented in Table A.1.

A.4 BODY AXES TRANSFORMATIONS

The stability axes system stability derivatives are related to the body axes system stability derivatives as shown in Table A.2.

A.5 DATA PRESENTATION

Examples of three formats used to present aircraft transfer function data are shown in Figure A.1 and Tables A.3 and A.4 for the lateral-directional axes of the A-7A.

The data presented in Figure A.1 can be used in the nondimensional stability derivative equations. The data presented in Table A.3 can be used in the dimensional stability derivative equations. Both approaches yield the same transfer functions. The data in Table A.4 is presented in transfer function format already (body axes system in this case).

$$\Delta$$

is the lateral-directional characteristic equation (denominator term). The numerator terms are presented as

$$N^{output}_{input} (s)$$

A.7

For example

$$N^p_{\delta_a}(s)$$

is the numerator for roll rate due to aileron deflection.

$$1/T$$

denotes real axis poles or zeros.

$$\zeta \text{ and } \omega$$

denotes damping ratio and natural frequency of poles or zeros. These must be converted to the form

where

$$s = \sigma \pm \omega_d j$$

$$\sigma = \zeta \omega_n \text{ and } \omega_d = \omega_n \sqrt{1 - \zeta^2}$$

A is the root locus gain of the transfer function.

For example, the transfer function

$$G^p_{\delta_a}(s) = \frac{N^p_{\delta_a}(s)}{\Delta(s)}$$

at 0.6 Mach, sea level is found, where

$$\Delta(s) = (s + 0.0411)(s + 4.46)(s^2 + 2(0.202)(2.91)s + (2.91)^2)$$

or

$$\Delta(s) = \underbrace{(s + 0.0411)}_{\substack{\text{Spiral} \\ \text{mode} \\ \text{root}}} \underbrace{(s + 4.46)}_{\substack{\text{Roll} \\ \text{mode} \\ \text{root}}} \underbrace{(s + 0.59 \pm 2.85j)}_{\substack{\text{Dutch Roll} \\ \text{roots}}}$$

and

$$N^p_{\delta_a}(s) = 28.4(s - 0.00234)(s^2 + 2(0.217)(3.05)s + (3.05)^2)$$

or

$$N^p_{\delta_a}(s) = 28.4(s - 0.00234)(s + 0.66 \pm 2.98j)$$

The units are

$$p \quad \text{radians per second}$$

$$\delta_a \quad \text{radians}$$

or

$$p \quad \text{degrees per second}$$

$$\delta_a \quad \text{degrees}$$

since both the input and output parameters have similar units. If the input and output parameters have different units, as is the case in the transfer function

$$N_{\delta_a}^{a_y} (s)$$

then the units are

$$a_y \quad \text{feet per second squared}$$

$$\delta_y \quad \text{radians}$$

If in doubt about units, always assume radians for angular parameters.

A.6 TRANSFER FUNCTION DERIVATION FROM FLIGHT TEST DATA

The use of flight test derived aircraft stability derivative data, using dynamic parameter identification flight test techniques (see Section 5.4.3.2 and Reference 23) frequently requires an estimate of certain stability derivatives (those which influence the aircraft phugoid characteristics) from the aircraft lift and drag curves. This is necessary since the flight test techniques are successful in identifying those stability derivatives which influence the short period characteristics of the aircraft, but are not successful in identifying those stability derivatives which are due to airspeed or drag variations. Generally, the identification of the lateral-directional stability derivatives is more complete. Figures A.2 and A.3 provide useful information when deriving an aircraft model using flight test derived data. Refer to Reference 2 (Pages 19 and 112) for more details.

DIMENSIONAL STABILITY DERIVATIVE DEFINITIONS

The same symbols are used for body - and stability-axes dimensional derivatives. Note: Prior to using these definitions for the derivatives that follow, check the units to ensure the same normalizing factor has been used.

A. Longitudinal Body Axes

$$X_u^* = X_u + T_u \cos \xi_0 \qquad \text{1/sec}$$

$$X_u = \frac{\rho S U_0}{m} \left(-\frac{M}{2} C_{X_M} - C_X + \frac{W_0}{2U_0} C_{X_\alpha} \right) \qquad \text{1/sec}$$

$$X_w = \frac{\rho S U_0}{2M} \left[-C_{X_\alpha} - 2 \frac{W_0}{U_0} \left(C_X + \frac{M}{2} C_{X_M} \right) \right] \qquad \text{1/sec}$$

$$X_{\delta_e} = -\frac{\rho S V_{T_0}^2}{2m} C_{X_{\delta_e}} \qquad \frac{\text{ft}}{\text{sec}^2 \text{rad}}$$

$$Z_u^* = Z_u - T_u \sin \xi_0 \qquad \text{1/sec}$$

$$Z_u = \frac{\rho S U_0}{m} \left(-\frac{M}{2} C_{N_M} - C_n + \frac{W_0}{2U_0} C_{N_\alpha} \right) \qquad \text{1/sec}$$

$$Z_w = \frac{\rho S U_0}{2m} \left[-C_{n_\alpha} - 2 \frac{W_0}{U_0} \left(C_n + \frac{M}{2} C_{N_M} \right) \right] \qquad \text{1/sec}$$

$$Z_w = -\frac{\rho S c}{4m} \frac{U_0}{V_{T_0}} C_{N_\alpha}$$

$$Z_{\delta_e} = - \frac{\rho S V_{T_0}^2}{2m} C_{n_{\delta_e}} \qquad \frac{\text{ft}}{\text{sec}^2 \text{rad}}$$

$$M_u^* = M_u + \frac{\ell_{th}}{I_y} T_u \qquad \frac{1}{\text{sec-ft}}$$

$$M_u = \frac{\rho S c U_0}{I_y} \left[\frac{M}{2} C_{m_M} + C_m - \frac{W_0}{2U_0} C_{m_\alpha} \right] \qquad \frac{1}{\text{sec-ft}}$$

$$M_w = \frac{\rho S c U_0}{2I_y} C_{m_\alpha} + \frac{2W_0}{U_0} \left[\left(C_m + \frac{M}{2} C_{m_M} \right) \right] \qquad \frac{1}{\text{sec-ft}}$$

$$M_{\dot{w}} = \frac{\rho S c^2}{4I_y} \frac{U_0}{V_{T_0}} C_{m_{\dot\alpha}} \qquad \frac{1}{\text{sec-ft}}$$

$$M_\alpha = U_0 M_w \qquad 1/\text{sec}^2$$

$$M_{\dot\alpha} = U_0 M_{\dot{w}} \qquad 1/\text{sec}$$

$$M_q = \frac{\rho S c^2 V_{T_0}}{4I_y} C_{m_q} \qquad 1/\text{sec}$$

$$M_{\delta_e} = \frac{\rho S c V_{T_0}^2}{2I_y} C_{m_{\delta_e}} \qquad 1/\text{sec}^2$$

$$T_u = \frac{1}{am} \, \partial T / \partial M \qquad 1/\text{sec}$$

B. Lateral Body Axis

$$Y_v = \left(\rho S V_{T_0}/2m\right) C_{y_\beta} \qquad\qquad \text{1/sec}$$

$$Y_\beta = V_{T_0} Y_v \qquad\qquad \text{ft/sec}^2$$

$$Y_{\delta_a} = \left(\rho S V_{T_0}^2/2m\right) C_{y_{\delta_a}} \qquad\qquad \text{ft/sec}^2$$

$$Y_{\delta_r} = \left(\rho S V_{T_0}^2/2m\right) C_{y_{\delta_r}} \qquad\qquad \text{ft/sec}^2$$

$$Y_{\delta_r} = \left(\rho S V_{T_0}/2m\right) C_{y_{\delta_r}} \qquad\qquad \text{1/sec}$$

$$L_\beta = \left(\rho S V_{T_0} b/2I_x\right) C_{l_\beta} \qquad\qquad \text{1/sec}^2$$

$$L_p = \left(\rho S V_{T_0} b^2/4I_x\right) C_{l_p} \qquad\qquad \text{1/sec}$$

$$L_r = \left(\rho S V_{T_0} b^2/4I_x\right) C_{l_r} \qquad\qquad \text{1/sec}$$

$$L_{\delta_a} = \left(\rho S V_{T_0}^2 b/2I_x\right) C_{l_{\delta_a}} \qquad\qquad \text{1/sec}^2$$

$$L_{\delta_r} = \left(\rho S V_{T_0}^2 b/2I_x\right) C_{l_{\delta_r}} \qquad\qquad \text{1/sec}^2$$

$$Y_{\delta_a} = \left(\rho S V_{T_0}/2m\right) C_{y_{\delta_a}} \qquad\qquad \text{1/sec}$$

$$N_\beta = \left(\rho S V_{T_0}^2 b / 2 I_z\right) C_{n_\beta} \qquad 1/\text{sec}^2$$

$$N_p = \left(\rho S V_{T_0} b^2 / 4 I_z\right) C_{n_p} \qquad 1/\text{sec}$$

$$N_r = \left(\rho S V_{T_0} b^2 / 4 I_z\right) C_{n_r} \qquad 1/\text{sec}$$

$$N_{\delta_a} = \left(\rho S V_{T_0}^2 b / 2 I_z\right) C_{n_{\delta_a}} \qquad 1/\text{sec}^2$$

$$N_{\delta_r} = \left(\rho S V_{T_0}^2 b / 2 I_z\right) C_{n_{\delta_r}} \qquad 1/\text{sec}^2$$

$$L_\beta' = \left(L_\beta + I_{xz} N_\beta / I_x\right) G \qquad 1/\text{sec}^2$$

$$L_p' = \left(L_p + I_{xz} N_p / I_x\right) G \qquad 1/\text{sec}$$

$$L_r' = \left(L_r + I_{xz} N_r / I_x\right) G \qquad 1/\text{sec}$$

$$L_{\delta_r}' = \left(L_{\delta_r} + I_{xz} N_{\delta_r} / I_x\right) G \qquad 1/\text{sec}^2$$

$$L_{\delta_a}' = \left(L_{\delta_a} + I_{xz} N_{\delta_a} / I_x\right) G \qquad 1/\text{sec}^2$$

$$N_\beta' = \left(N_\beta + I_{xz} L_\beta / I_z\right) G \qquad 1/\text{sec}^2$$

$$N_p' = \left(N_p + I_{xz} L_p / I_z\right) G \qquad 1/\text{sec}$$

DIMENSIONAL STABILITY DERIVATIVE DEFINITIONS

$$N_r' = \left(N_r + I_{xz}L_r/I_z\right)G \qquad\qquad 1/\text{sec}$$

$$N_{\delta_r'} = \left(N_{\delta_r} + I_{xz}L_{\delta_r}/I_z\right)G \qquad\qquad 1/\text{sec}^2$$

$$N_{\delta_a'} = \left(N_{\delta_a} + I_{xz}L_{\delta_a}/I_z\right)G \qquad\qquad 1/\text{sec}^2$$

$$G = \frac{1}{1 - \dfrac{I_{xz}^2}{I_x I_z}}$$

TABLE A.2
TRANSFORMATION OF STABILITY AXES DERIVATIVES TO BODY AXES

A. Nondimensional Stability Axes to Body Axes

$$U_o = V_{T_o} \cos \alpha_o$$

$$W_o = V_{T_o} \sin \alpha_o$$
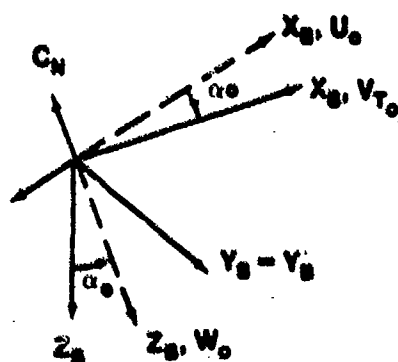
Longitudinal

Body Axes

$$C_N = C_L \cos \alpha_0 + C_D \sin \alpha_0$$

$$C_X = C_D \cos \alpha_0 - C_L \sin \alpha_0$$

$$C_{N_{\dot\alpha}} = C_{L_{\dot\alpha}} \cos \alpha_0 - C_L \sin \alpha_0 + C_{D_\alpha} \sin \alpha_0 + C_D \cos \alpha_0$$

$$C_{N_\alpha} = C_{L_\alpha} \cos \alpha_0$$

$$C_{N_q} = C_{L_q} \cos \alpha_0$$

$$C_{N_M} = C_{L_M} \cos \alpha_0 + C_{D_M} \sin \alpha_0$$

$$C_{N_\delta} = C_{L_\delta} \cos \alpha_0 + C_{D_\delta} \sin \alpha_0$$

$$C_{X_\alpha} = C_{D_\alpha} \cos \alpha_0 - C_D \sin \alpha_0 - C_{L_\alpha} \sin \alpha_0 - C_L \cos \alpha_0$$

$$C_{X_{\dot\alpha}} = -C_{L_{\dot\alpha}} \sin \alpha_0$$

$$C_{X_q} = -C_{L_q} \sin \alpha_0$$

$$C_{X_M} = C_{D_M} \cos \alpha_C - C_{L_M} \sin \alpha_0$$

$$C_{X_\delta} = C_{D_\delta} \cos \alpha_0 - C_{L_\delta} \sin \alpha_0$$

$$C_m, \ C_{m_\alpha}, \ C_{m_{\dot\alpha}}, \ C_{m_q}, \ C_{m_M}, \ C_{m_\delta} \quad = \quad \text{UNCHANGED}$$

TRANSFORMATION OF STABILITY AXES DERIVATIVES TO BODY AXES

Lateral

Body Axes

$$\left(C_{l_\beta\ B}\right) = C_{l_\beta}\ \cos\alpha_0 - C_{n_\beta}\ \sin\alpha_0$$

$$\left(C_{l_p\ B}\right) = C_{l_p}\ \cos^2\alpha_0 - \left(C_{l_r} + C_{n_p}\right)\ \sin\alpha_0\ \cos\alpha_0 + C_{n_r}\ \sin^2\alpha_0$$

$$\left(C_{l_r\ B}\right) = C_{l_r}\ \cos^2\alpha_0 - \left(C_{n_r} - C_{l_p}\right)\ \sin\alpha_0\ \cos\alpha_0 + C_{n_p}\ \sin^2\alpha_0$$

$$\left(C_{l_\delta\ B}\right) = C_{l_\delta}\ \cos\alpha_0 - C_{n_\delta}\ \sin\alpha_0$$

$$\left(C_{n_\beta\ B}\right) = C_{n_\beta}\ \cos\alpha_0 + C_{l_\beta}\ \sin\alpha_0$$

$$\left(C_{n_p\ B}\right) = C_{n_p}\ \cos^2\alpha_0 - \left(C_{n_r} - C_{l_p}\right)\ \sin\alpha_0\ \cos\alpha_0 - C_{l_r}\ \sin^2\alpha_0$$

$$\left(C_{n_r\ B}\right) = C_{n_r}\ \cos^2\alpha_0 + \left(C_{l_r} + C_{n_p}\right)\ \sin\alpha_0\ \cos\alpha_0 + C_{l_p}\ \sin^2\alpha_0$$

$$\left(C_{n_\delta\ B}\right) = C_{n_\delta}\ \cos\alpha_0 + C_{l_\delta}\ \sin\alpha_0$$

$$C_{y_\beta},\ C_{y_{\delta_R}},\ C_{y_{\delta_a}} \quad - \quad \text{UNCHANGED}$$

Longitudinal

$$(X_u)_b = X_u\ \cos^2\alpha_0 - (X_w + Z_u)\ \sin\alpha_0\ \cos\alpha_0 + Z_w\ \sin^2\alpha$$

$$(X_{\dot{u}})_b = Z_{\dot{w}}\ \sin^2\alpha_0$$

$$(X_w)_b = X_w \cos^2 \alpha_0 + (X_u - Z_w) \sin \alpha_0 \cos \alpha_0 - Z_u \sin^2 \alpha_0$$

$$(X_{\dot{w}})_b = X_{\dot{w}} \cos^2 \alpha_0 - Z_{\dot{w}} \sin \alpha_0 \cos \alpha_0$$

$$(X_{q;\delta})_b = X_{q;\delta} \cos \alpha_0 - Z_{q;\delta} \sin \alpha_0$$

$$(Z_u)_b = Z_u \cos^2 \alpha_0 - (Z_w - X_u) \sin \alpha_0 \cos \alpha_0 - X_w \sin^2 \alpha_0$$

$$(Z_{\dot{u}})_b = -Z_{\dot{w}} \sin \alpha_0 \cos \alpha_0$$

$$(Z_w)_b = Z_w \cos^2 \alpha_0 + (Z_u + X_w) \sin \alpha_0 \cos \alpha_0 + X_u \sin^2 \alpha_0$$

$$(Z_{\dot{w}})_b = Z_{\dot{w}} \cos^2 \alpha_0 + X_{\dot{w}} \sin \alpha_0 \cos \alpha_0$$

$$(Z_{q;\delta})_b = Z_{q;\delta} \cos \alpha_0 + X_{q;\delta} \sin \alpha_0$$

$$(M_u)_b = M_w \cos \alpha_0 - M_u \sin \alpha_0$$

$$(M_{\dot{u}})_b = -M_{\dot{w}} \sin \alpha_0$$

$$(M_w)_b = M_w \cos \alpha_0 + M_u \sin \alpha_0$$

$$(M_{\dot{w}})_b = M_{\dot{w}} \cos \alpha_0$$

$$(M_{q;\delta})_b = M_{q;\delta}$$

$$(I_y)_b = I_y$$

Lateral-Directional

$$(Y_{v;\delta})_b = Y_{v;\delta}$$

TRANSFORMATION OF STABILITY AXES DERIVATIVES TO BODY AXES

$$(Y_v)_b = Y_v$$

$$(Y_p)_b = Y_p \cos \alpha_0 - Y_r \sin \alpha_0$$

$$(Y_r)_b = Y_r \cos \alpha_0 + Y_p \sin \alpha_0$$

$$(L'_{v;\delta})_b = L_{v;\delta} \cos \alpha_0 - N_{v;\delta} \sin \alpha_0$$

$$(L'_v)_b = L'_v \cos \alpha_0 - N'_v \sin \alpha_0$$

$$(L'_p)_b = L'_p \cos^2 \alpha_0 - (L'_r + N'_p) \sin \alpha_0 \cos \alpha_0 + N'_r \sin^2 \alpha_0$$

$$(L'_r)_b = L'_r \cos^2 \alpha_0 - (N'_r - L'_p) \sin \alpha_0 \cos \alpha_0 - N'_p \sin^2 \alpha_0$$

$$(N'_{v;\delta})_b = N'_{v;\delta} \cos \alpha_0 + L'_{v;\delta} \sin \alpha_0$$

$$(N'_v)_b = N'_v \cos \alpha_0 + L'_v \sin \alpha_0$$

$$(N'_p)_b = N'_p \cos^2 \alpha_0 - (N'_r - L'_p) \sin \alpha_0 \cos \alpha_0 - L'_r \sin^2 \alpha_0$$

$$(N'_r)_b = N'_r \cos^2 \alpha_0 + (L'_r + N'_p) \sin \alpha_0 \cos \alpha_0 + L'_p \sin^2 \alpha_0$$

$$(I_x)_b = I_x \cos^2 \alpha_0 + 2I_{xz} \sin \alpha_0 \cos \alpha_0 + I_z \sin^2 \alpha_0$$

$$(I_z)_b = I_z \cos^2 \alpha_0 - 2I_{xz} \sin \alpha_0 \cos \alpha_0 + I_x \sin^2 \alpha_0$$

$$(I_{xz})_b = (I_z - I_x) \sin \alpha_0 \cos \alpha_0 + I_{xz}(\cos^2 \alpha_0 - \sin^2 \alpha_0)$$
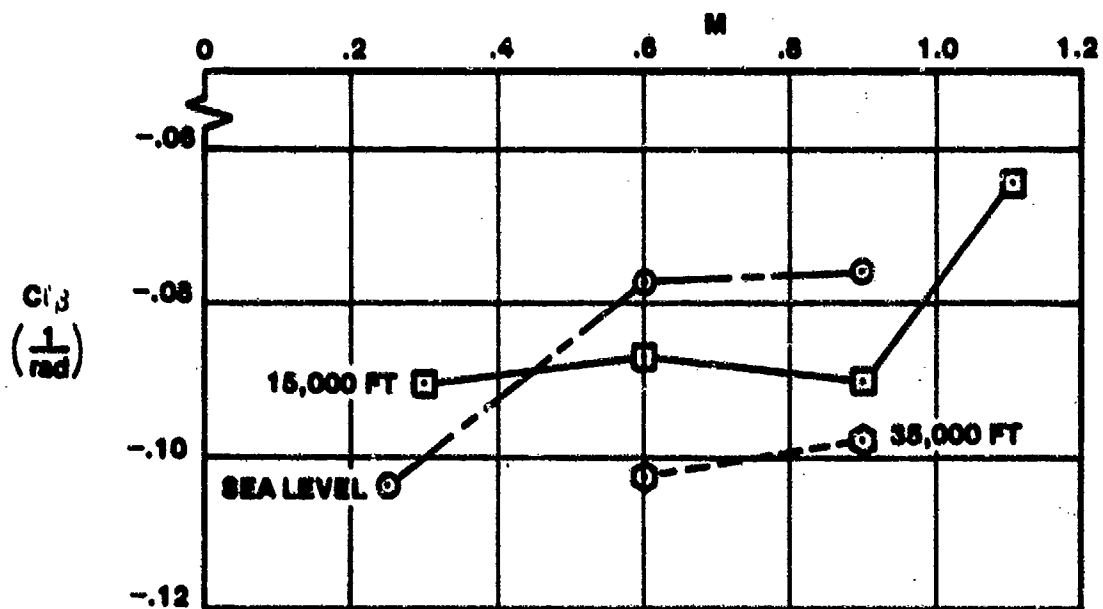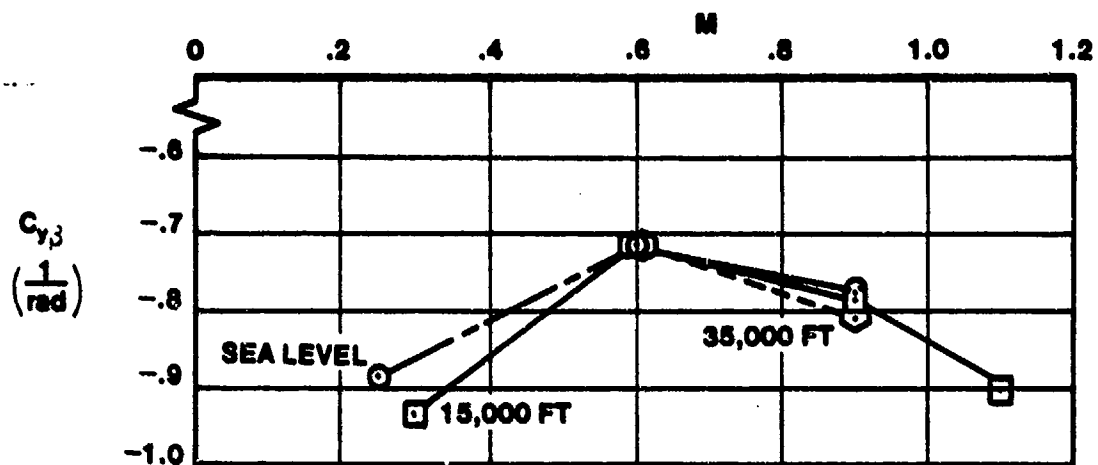
FIGURE A.1. STABILITY DERIVATIVE DATA
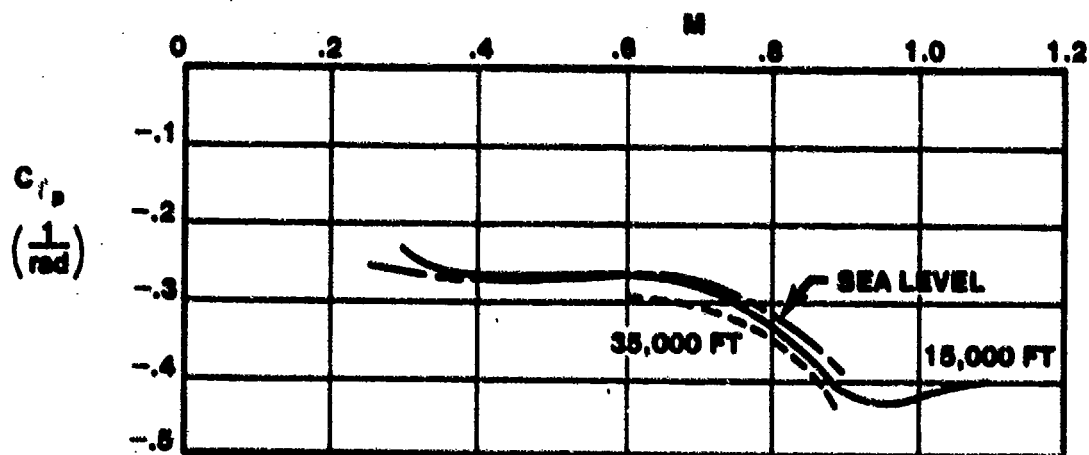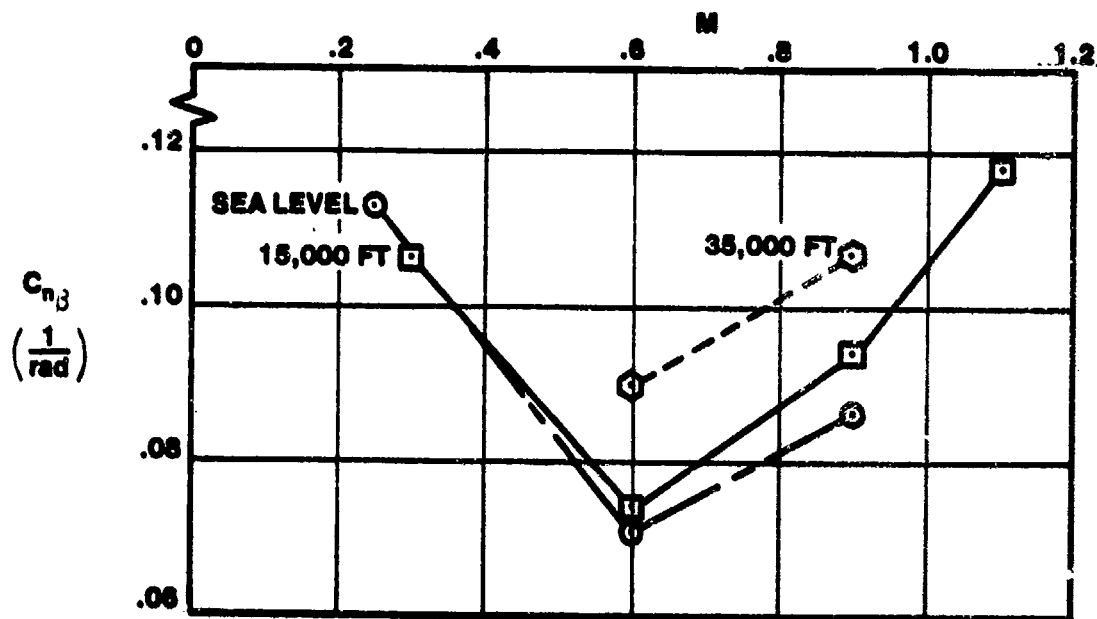
FIGURE A.1. STABILITY DERIVATIVE DATA (continued)
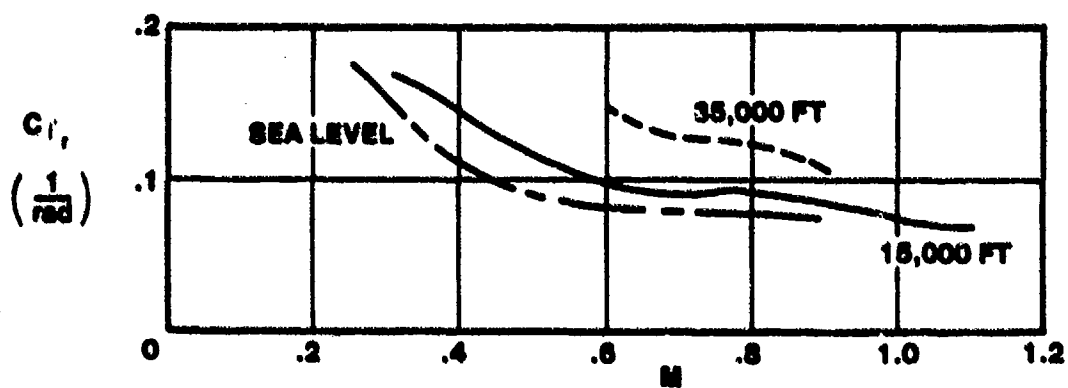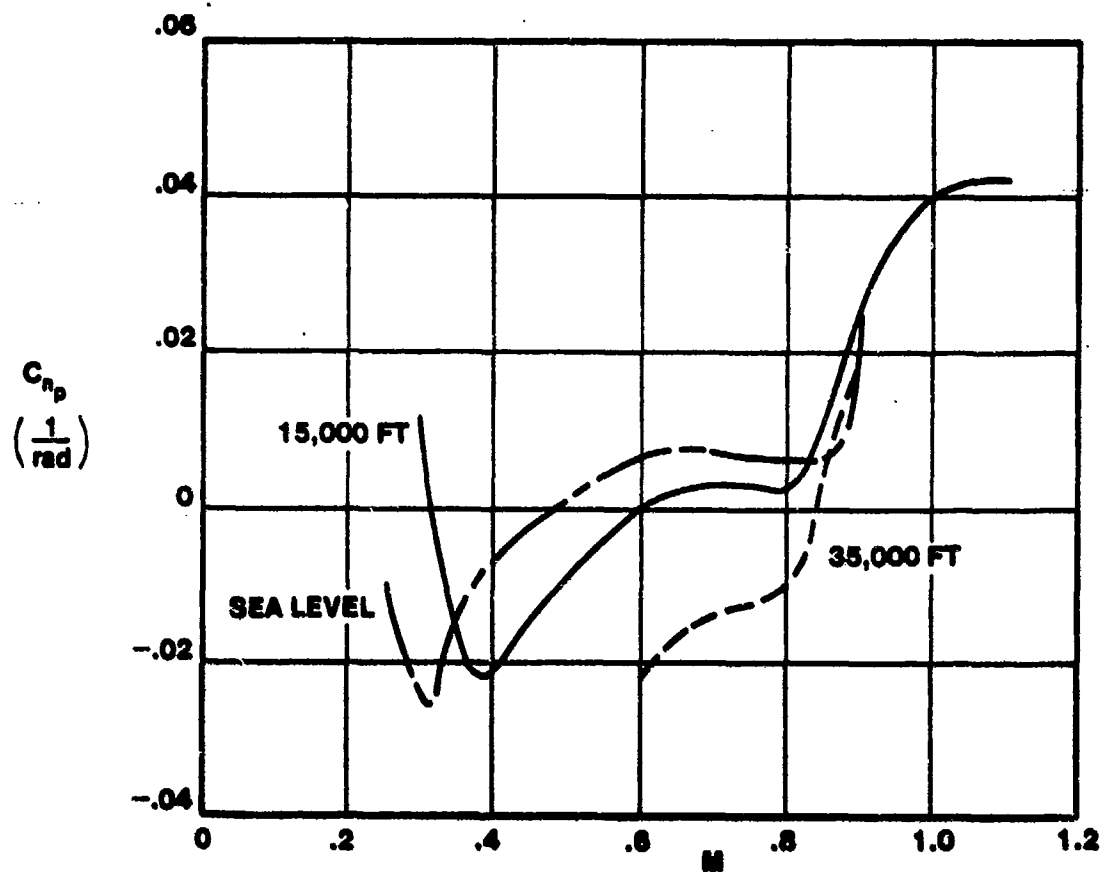
FIGURE A.1. STABILITY DERIVATIVE DATA (continued)
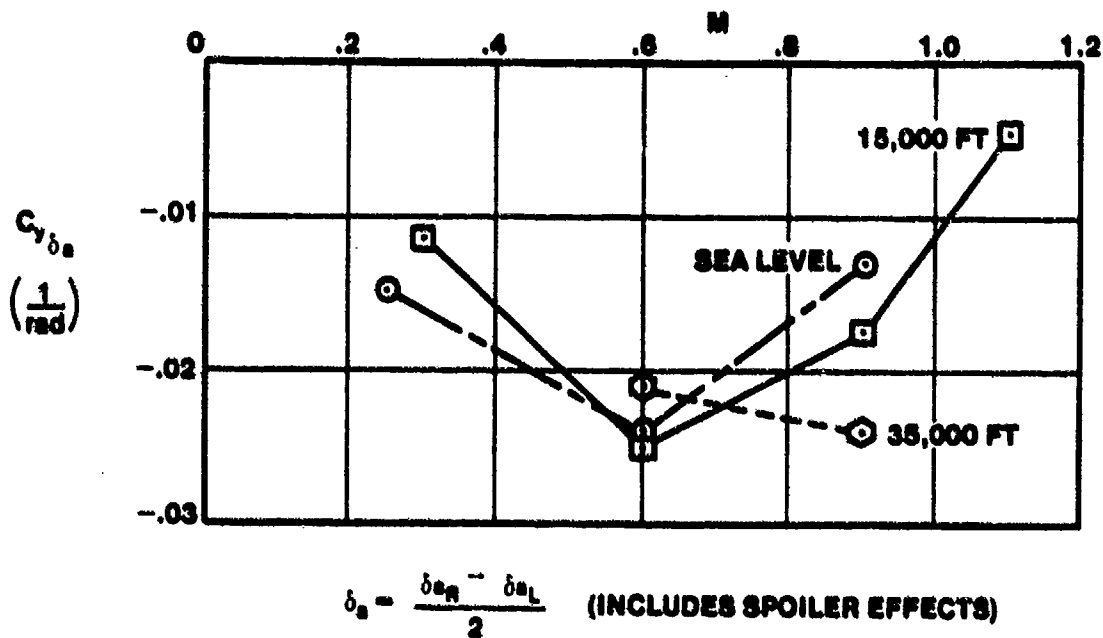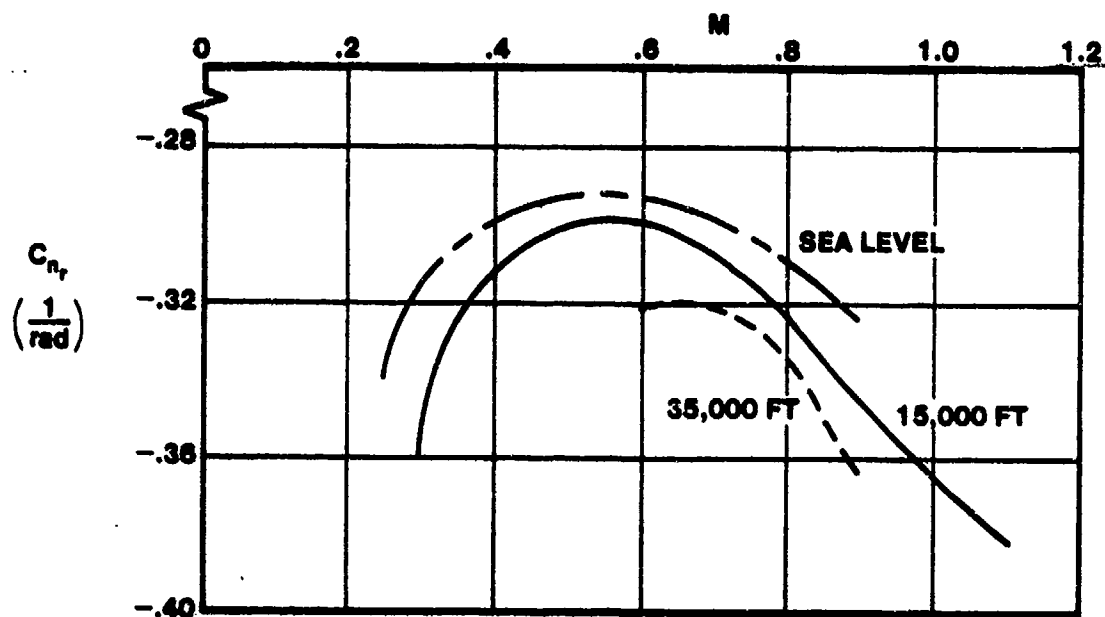
FIGURE A.1. STABILITY DERIVATIVE DATA (continued)
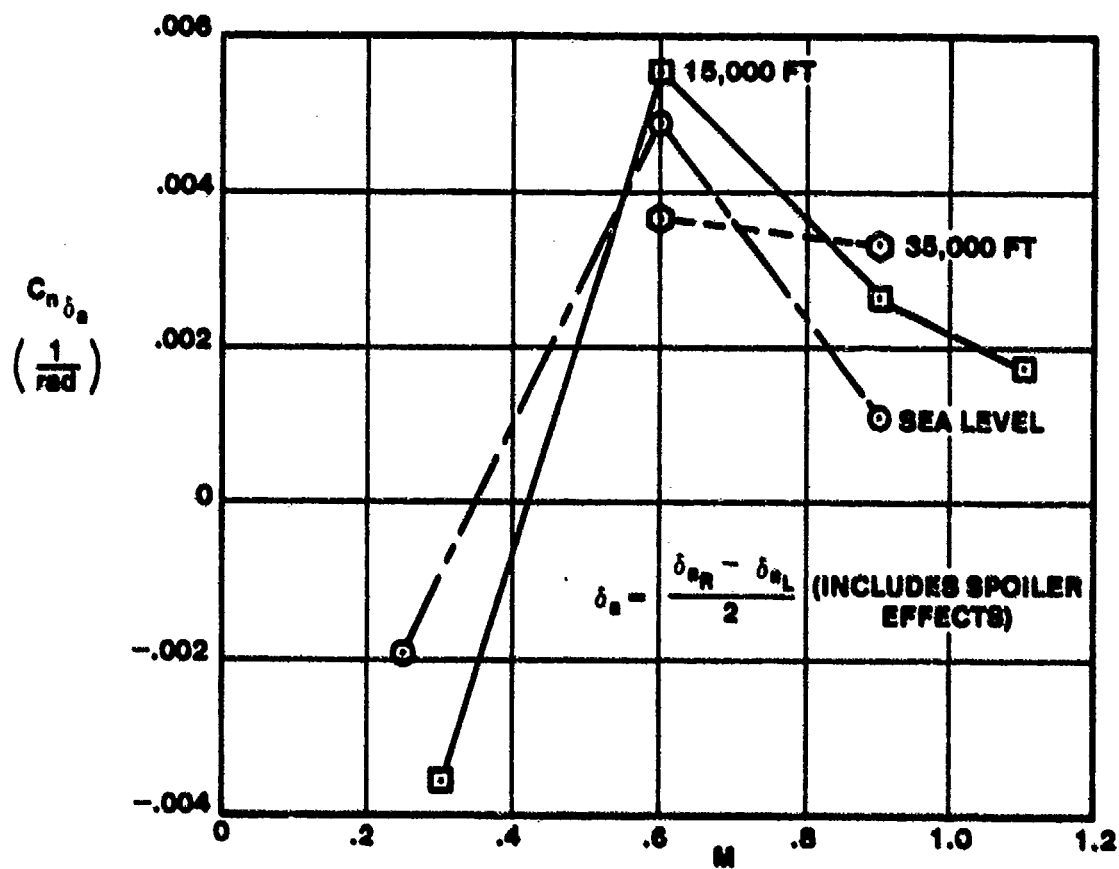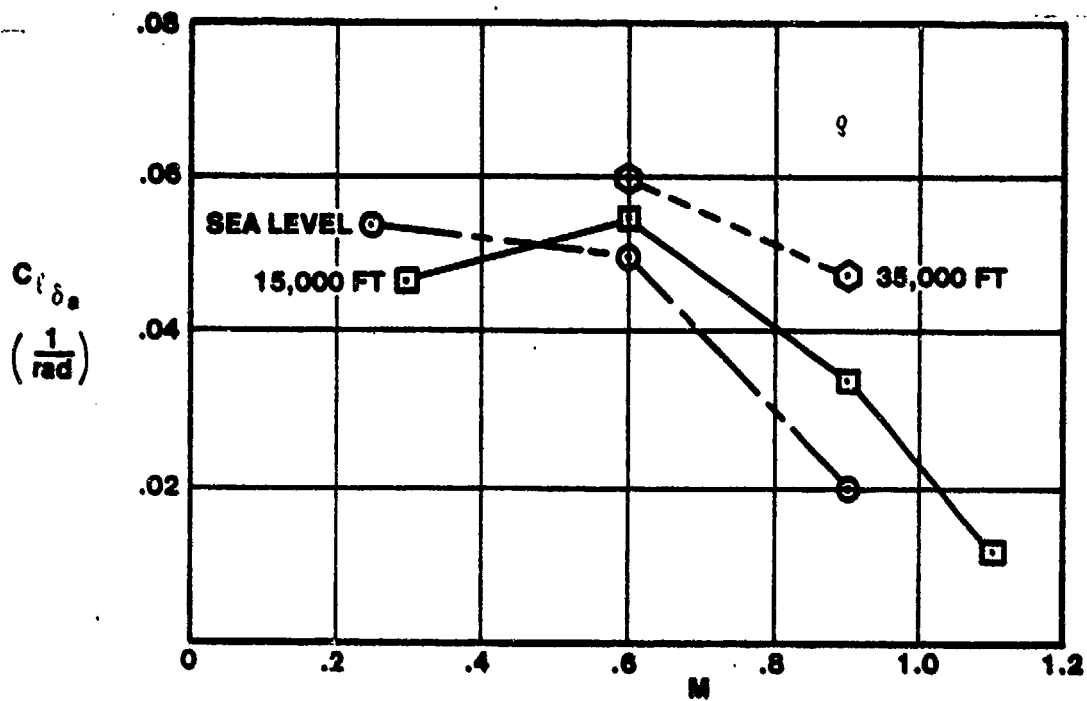
FIGURE A.1.   STABILITY DERIVATIVE DATA (continued)
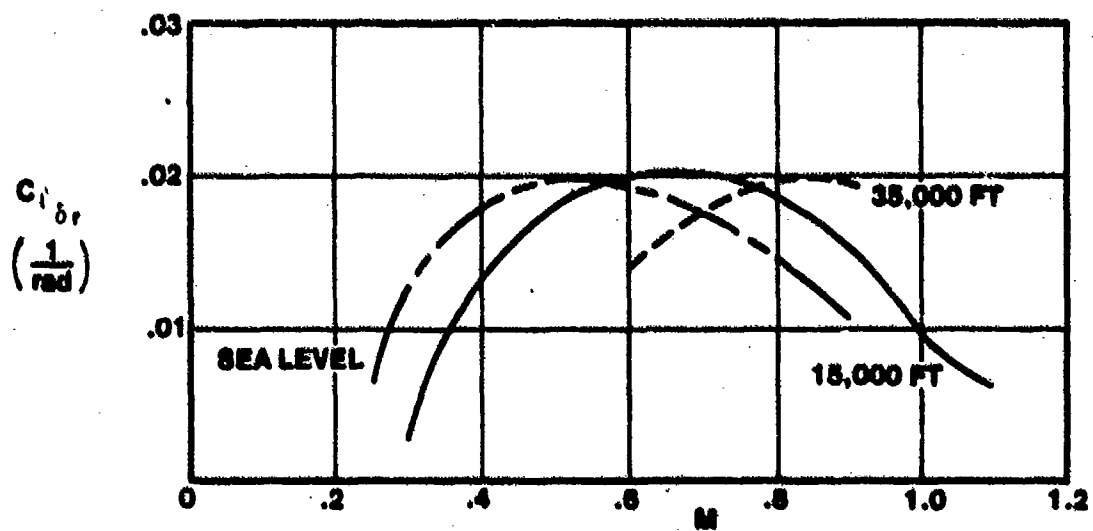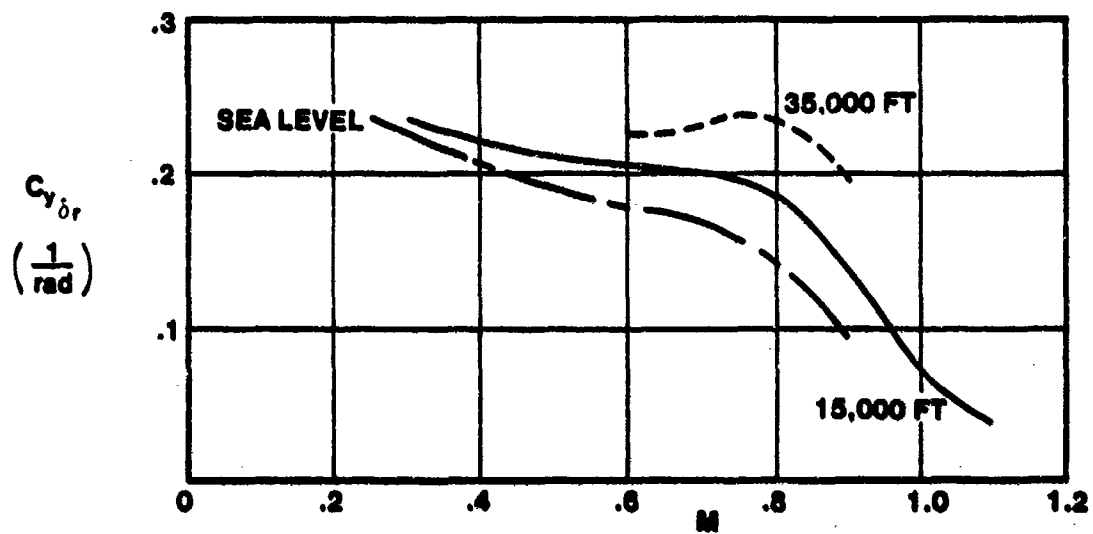
FIGURE A.1. STABILITY DERIVATIVE DATA (continued)
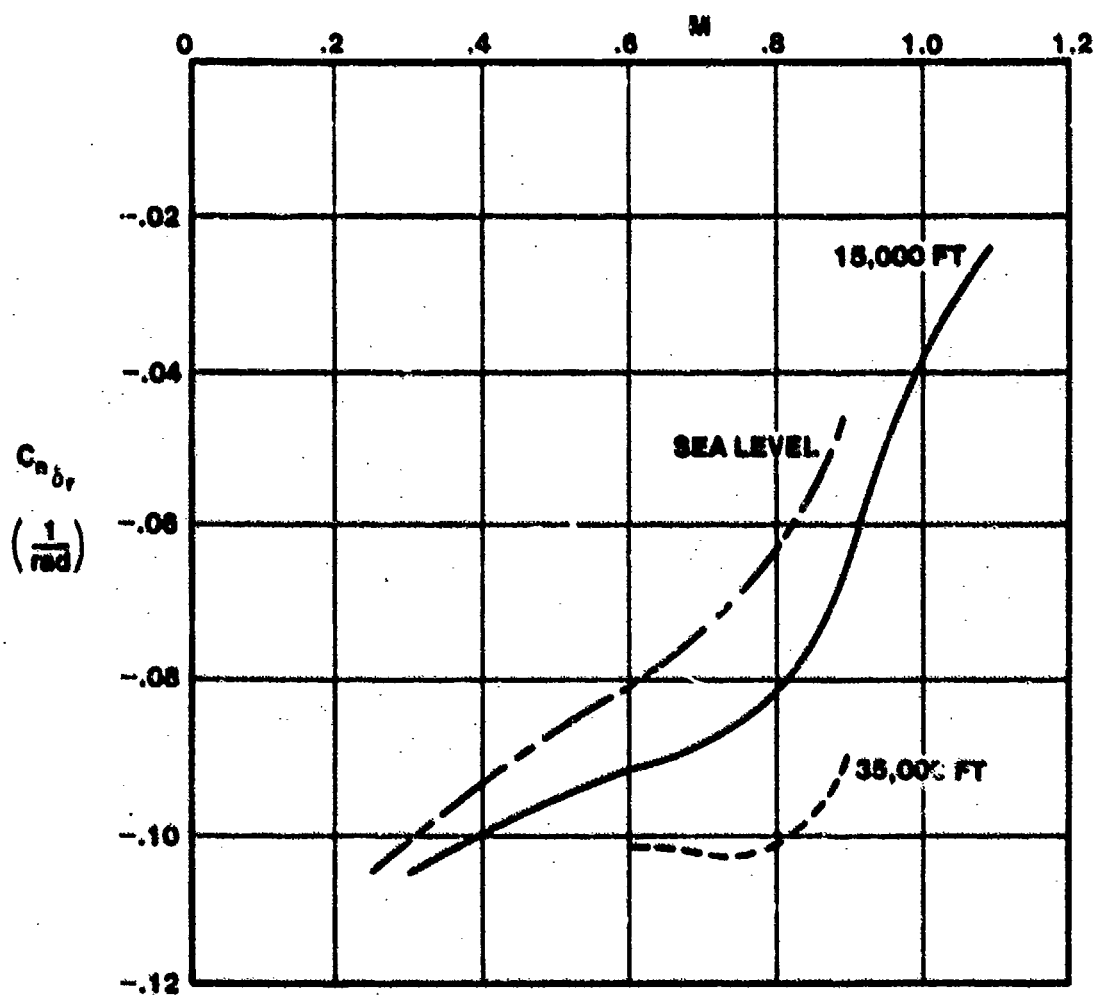
FIGURE A.1. STABILITY DERIVATIVE DATA (continued)

TABLE A.3

LATERAL DIMENSIONAL DERIVATIVES FOR THE A-7A

Note: Data are for body-fixed centerline axes, clean flexible airplane

	FLIGHT CONDITION								
	1	2	3	4	5	6	7	8	9
h	0	0	0	15,000	15,000	15,000	15,000	35,000	35,000
M	0.25	0.6	0.9	0.3	0.6	0.9	1.1	0.6	0.9
Y_v	−0.162	−0.314	−0.514	−0.122	−0.187	−0.310	−0.435	−0.0847	−0.143
$Y^*_{\delta_a}$	−0.00274	−0.0105	−0.00857	−0.00150	−0.00655	−0.00691	−0.00318	−0.00287	−0.00427
$Y^*_{\delta_r}$	0.0430	0.0760	0.0626	0.0307	0.0537	0.0560	0.0192	0.0667	0.0347
L'_β	−11.9	−44.8	−98.0	−8.79	−29.2	−68.0	−71.2	−14.9	−30.6
L'_p	−2.00	−4.46	−9.75	−1.38	−2.73	−6.19	−7.31	−1.40	−3.00
L'_r	1.18	1.15	1.38	0.857	0.888	0.843	0.859	0.599	0.563
L'_{δ_a}	5.34	38.4	28.2	3.75	17.8	34.1	12.8	7.95	14.2
L'_{δ_r}	2.22	11.4	13.2	1.82	7.27	11.2	7.27	3.09	6.55
N'_β	1.29	5.74	17.2	0.948	3.12	10.2	21.9	1.38	4.72
N'_p	−0.0670	−0.188	−0.319	−0.0310	−0.116	−0.207	−0.169	−0.0790	−0.112
N'_r	−0.339	−0.906	−1.54	−0.271	−0.541	−0.975	−1.33	−0.347	−0.456
N'_{δ_a}	0.402	2.08	1.56	0.200	1.37	1.64	1.04	0.652	1.01
N'_{δ_r}	−1.93	−8.61	−11.1	−1.56	−5.54	−8.50	−4.83	−2.54	−5.11

TABLE A.4

AILERON LATERAL TRANSFER FUNCTION FACTORS FOR THE A-7

Note: Data are for body-fixed centerline axes, clean flexible airplane

		FLIGHT CONDITION								
		1	2	3	4	5	6	7	8	9
	h	0	0	0	15,000	15,000	15,000	15,000	35,000	35,000
	M	0.25	0.6	0.9	0.3	0.6	0.9	1.1	0.6	0.9
Δ	$1/T_s$	0.0462	0.0411	0.0180	0.0449	0.0435	0.0214	0.0102	0.0319	0.0191
	$1/T_R$	1.62	4.46	9.75	0.968	2.71	6.17	7.15	1.28	2.92
	ζ_d	0.237	0.202	0.218	0.231	0.156	0.175	0.189	0.114	0.128
	ω_d	1.81	2.91	4.68	1.55	2.29	3.66	5.03	1.81	2.58
$N^p_{\delta_a}$	A_p	5.34	28.4	25.2	3.75	17.6	24.1	12.5	7.96	14.2
	$1/T_{p_1}$	−0.0219	−0.000?	−0.00113	−0.0232	−0.00347	−0.00144	−0.00137	−0.00718	−0.00241
	ζ_p	0.217	0.217	0.222	0.191	0.173	0.176	0.173	0.122	0.124
	ω_p	1.49	3.05	4.91	1.27	2.34	3.87	5.33	1.62	2.64
$N^\phi_{\delta_a}$	A_ϕ	5.42	28.5	25.2	3.81	17.7	24.1	12.5	8.04	14.3
	ζ_ϕ	0.210	0.217	0.222	0.183	0.173	0.177	0.175	0.119	0.124
	ω_ϕ	1.51	3.05	4.91	1.29	2.34	3.87	5.32	1.62	2.64
$N^r_{\delta_a}$	A_r	0.402	2.08	1.56	0.260	1.37	1.64	1.04	0.653	1.01
	$1/T_{r_1}$	0.596	1.12	1.13	0.445	0.777	0.944	0.581	0.420	0.593
	ζ_r	0.0852	0.287	0.597	0.146	0.151	0.446	0.638	0.0198	0.193
	ω_r	2.35	2.29	3.26	2.18	2.13	2.78	3.99	2.03	2.45
$N^\beta_{\delta_a}$	A_β	−0.00274	−0.0105	−0.00857	−0.00150	−0.00655	−0.00661	−0.00216	−0.00267	−0.00427
	$1/T_{\beta_1}$ (ζ_β)	(0.885)	3.26	7.76	(0.726)	2.21	5.77	10.7	0.793	(0.872)
	$1/T_{\beta_2}$ (ω_β)	(0.667)	−0.627	−0.254	(0.471)	−1.63	−0.245	−0.113	−0.422	(10.6)
	$1/T_{\beta_3}$	−233	63.1	78.2	−391	23.2	86.8	188	−147	−0.545
$N^{a_y}_{\delta_a}$ CG	A_{a_y}	−0.766	−7.06	−6.61	−0.477	−4.16	−6.58	−2.51	−1.56	−0.6374
	$1/T_{a_{y_1}}$ ($\zeta_{a_{y_1}}$)	(0.943)	2.29	−1.16	(0.758)	1.32	−0.596	−0.146	0.290	(0.801)
	$1/T_{a_{y_2}}$ ($\omega_{a_{y_2}}$)	(0.648)	5.92	−1.84	(0.461)	3.12	−2.66	−7.93	0.961	(2.34)
	ζ_{a_y} ($1/T_{a_{y_3}}$)	0.0896	−0.810	(3.65)	0.0573	−0.294	(3.79)	0.897	0.0499	−0.113
	ω_{a_y} ($1/T_{a_{y_4}}$)	6.37	1.76	(10.7)	7.10	1.99	(−6.63)	9.31	3.92	1.30

TABLE A.4 (continued)

AILERON LATERAL TRANSFER FUNCTION FACTORS FOR THE A-7

Note: Data are for body-fixed centerline axes, clean flexible airplane

		FLIGHT CONDITION								
		1	2	3	4	5	6	7	8	9
	h	0	0	0	15,000	15,000	15,000	15,000	35,000	35,000
	M	0.25	0.6	0.9	0.3	0.6	0.9	1.1	0.6	0.9
Δ	$1/T_s$	0.0462	0.0411	0.0180	0.0449	0.0435	0.0214	0.0102	0.0319	0.0191
	$1/T_R$	1.62	4.46	9.75	0.968	2.71	6.17	7.15	1.28	2.92
	ζ_d	0.237	0.202	0.218	0.231	0.156	0.175	0.189	0.114	0.128
	ω_d	1.61	2.91	4.68	1.65	2.29	3.66	5.03	1.61	2.58
$N_{\delta_r}^{p}$	A_p	2.22	11.4	13.2	18.2	7.27	11.2	7.27	3.09	6.55
	$1/T_{p_1}$	−0.0234	−0.00242	−0.00117	−0.0237	−0.00352	−0.00147	−0.00141	−0.00723	−0.00243
	$1/T_{p_2}$	3.68	5.35	8.31	2.33	4.31	6.63	5.56	3.16	4.39
	$1/T_{p_3}$	−3.38	−5.31	−7.88	−2.79	−4.45	−6.33	−4.55	−3.44	−4.38
$N_{\delta_r}^{\phi}$	A_ϕ	1.84	10.9	12.8	1.45	6.89	10.8	7.03	2.75	6.21
	$1/T_{\phi_1}$	2.78	5.37	8.29	2.48	4.35	6.64	5.53	3.27	4.43
	$1/T_{\phi_2}$	−4.11	−5.53	−8.16	−3.48	−4.68	−6.57	−4.76	−3.79	−4.61
$N_{\delta_r}^{r}$	A_r	−1.93	−8.61	−11.1	−1.56	−5.54	−8.80	−4.83	−2.54	−5.11
	$1/T_{r_1}$	1.13	4.33	9.87	0.553	2.35	6.12	7.31	0.578	2.84
	ζ_r	0.538	0.475	0.674	0.414	0.473	0.535	0.790	0.440	0.526
	ω_r	1.02	0.642	0.502	1.17	0.735	0.541	0.381	1.12	0.585
$N_{\delta_r}^{\beta}$	A_β	0.0430	0.0769	0.0626	0.0307	0.0537	0.0550	0.0192	0.0267	0.0347
	$1/T_{\beta_1}$	−0.0524	−0.00190	0.000366	−0.0503	−0.00616	0.000578	0.00271	−0.0178	−0.00216
	$1/T_{\beta_2}$	1.73	4.45	9.76	1.14	2.70	6.17	7.11	1.32	2.94
	$1/T_{\beta_3}$	54.7	120	186	63.6	113	170	272	110	180
$N_{\delta_r}^{a_y}$ CG	A_{a_y}	12.0	51.5	62.9	9.74	34.1	52.3	22.4	15.6	30.4
	$1/T_{a_{y_1}}$	−0.123	−0.0145	−0.00502	−0.108	−0.0227	−0.00654	0.000648	−0.0436	−0.0107
	$1/T_{a_{y_2}}$	1.87	4.43	9.57	1.27	2.69	6.16	7.04	1.36	2.97
	$1/T_{a_{y_3}}$	−2.00	−4.97	−7.84	−1.96	−3.69	−5.78	−8.91	−2.28	−5.81
	$1/T_{a_{y_4}}$	2.60	5.92	9.57	2.45	4.30	6.80	10.5	2.61	4.30

STABILITY DERIVATIVE	EQUATION	TYPICAL VALUE
C_{x_u}	$-2C_D - U_o [\, \partial C_D / \, \partial u\,]$	-0.05
C_{x_α}	$C_L - [\, \partial C_D / \, \partial \alpha\,]$	$+0.1$
C_{z_u}	$-2C_L - U_o [\, \partial C_L / \, \partial u\,]$	$-.05$
C_{z_α}	$-C_D - [\, \partial C_L / \, \partial \alpha\,]$	-4
$C_{z_{\dot\alpha}}$		-1
C_{z_q}		-2
C_{m_u}	Neglect for Jets	
C_{m_α}		-0.3
$C_{m_{\dot\alpha}}$		-3
C_{m_q}		-8

NOTE: EFFECTS OF $C_{m_{\dot\alpha}}$ AND C_{m_q} ARE USUALLY COMBINED WHEN USING FLIGHT TEST DATA.

FIGURE A.2. DEFINITIONS AND TYPICAL VALUES FOR LONGITUDINAL NONDIMENSINAL STABILITY DERIVATIVES

STABILITY DERIVATIVE	TYPICAL VALUE
C_{y_β}	-0.6
C_{l_β}	-0.06
C_{l_p}	-0.4
C_{l_r}	$+0.06$
C_{n_β}	$+0.11$
C_{n_p}	-0.015
C_{n_r}	-0.12
C_{y_p}	Neglect
C_{y_r}	Neglect

FIGURE 3. TYPICAL VALUES FOR LATERAL-DIRECTIONAL NONDIMENSIONAL STABILITY DERIVATIVES

APPENDIX B

FLYING QUALITIES

CLOSED LOOP TRANSFER FUNCTION FORMULATION

Determining closed loop poles and zeros of a control system transfer function can often be confusing (Figure B.1). The following general rules apply.

B.1 NO POLES OR ZEROS IN OPEN LOOP TRANSFER FUNCTION CANCEL

If no poles or zeros in the open loop transfer function cancel, then the zeros of the closed loop transfer function are determined as

    a. The zeros of the forward path transfer function, $G(s)$

    b. The poles of the feedback path transfer function, $H(s)$

If

$$G(s) = \frac{K_F \prod\limits_{i=1}^{m}\left(s - z_{i_F}\right)}{\prod\limits_{j=1}^{n}\left(s - p_{j_F}\right)} \quad \text{and} \quad H(s) = \frac{K_B \prod\limits_{k=1}^{\rho}\left(s - z_{k_B}\right)}{\prod\limits_{\ell=1}^{q}\left(s - p_{\ell_B}\right)}$$

then the zeros for the closed loop transfer function are

$$\prod\limits_{i=1}^{m}\left(s - z_{i_F}\right) \quad \prod\limits_{\ell=1}^{q}\left(s - p_{\ell_B}\right)$$

The closed loop transfer function gain is always the product of the gains of the forward path elements.

**COMBINED FORWARD PATH
TRANSFER FUNCTION**

**COMBINED FEEDBACK PATH
TRANSFER FUNCTION**
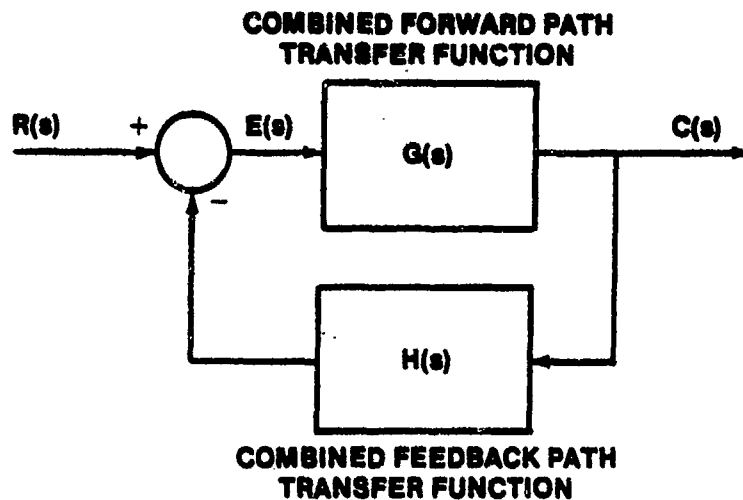
FIGURE B.1.   SIMPLIFIED FEEDBACK CONTROL SYSTEM

The closed loop roots are obtained from the root locus analysis of

$$G(s)H(s)$$

and correspond to the roots at the open loop transfer function gain

$$K_F K_B$$

B.2   POLE IN FORWARD PATH CANCELED BY ZERO IN FEEDBACK PATH

If a pole and a zero in the open loop transfer function cancel, where the pole is part of the forward path transfer function and the zero is in the feedback path transfer function, such that

$$G'(s) = \frac{N_G(s)}{(s + a)D_G(s)} \quad \text{and} \quad H'(s) = \frac{(s + a)N_H(s)}{D_H(s)}$$

so that

$$G(s)_{CL} = \frac{\dfrac{N_G(s)}{(s + a)D_G(s)}}{\left[1 + \dfrac{N_G(s)\ (s + a)N_H(s)}{(s + a)D_G(s)D_H(s)}\right]}$$

then

$$G(s)_{CL} = \frac{N_G(s)\, D_H(s)}{(s + a)D_G(s)D_H(s) + N_G(s)N_H(s)}$$

It is apparent that the zeros are determined as in Paragraph B.1. However, the canceled pole in the open loop transfer function appears in the denominator of the closed loop transfer function as a distinct root of the closed loop characteristic equation. The other poles are found, as before, from the root locus analysis of

$$G'(s)H'(s) = \frac{N_G(s)N_H(s)}{D_G(s)D_H(s)}$$

B.3 ZERO IN FORWARD PATH CANCELED BY POLE IN THE FEEDBACK PATH

If a zero and a pole in the open loop transfer function cancel, where the zero is part of the forward path transfer function and the pole is in the feedback path, then

$$G'(s) = \frac{(s + a)N_G(s)}{D_G(s)} \quad \text{and} \quad H'(s) = \frac{N_H(s)}{(s + a)D_H(s)}$$

so that

$$G(s)_{CL} = \frac{\dfrac{(s + a)\, N_G(s)}{D_G(s)}}{\left[1 + \dfrac{(s + a)N_G(s)N_H(s)}{D_G(s)\,(s + a)D_H(s)} \right]}$$

and

$$G(s)_{CL} = \frac{(s + a)N_G(s)N_H(s)}{D_G(s)D_H(s) + N_G(s)N_H(s)}$$

It is apparent that the zeros of the closed loop equation include the canceled zero to the first power. The numerator contains all the zeros of the original forward path transfer function, but excludes the canceled pole in the feedback path.

B.4 POLE AND ZERO CANCEL WHICH ARE BOTH IN THE FORWARD PATH OR BOTH IN THE FEEDBACK PATH

If a pole and a zero which are both in the forward path cancel, or if a pole and a zero which are both in the feedback path cancel, then neither the pole nor the zero appear in the closed loop transfer function. For example, if

$$G'(s) = \frac{(s + a)N_G(s)}{(s + a)D_G(s)} \quad \text{and} \quad H'(s) = \frac{(s + b)N_H(s)}{(s + b)D_H(s)}$$

then

$$G(s)\Big|_{CL} = \frac{N_G(s)D_H(s)}{D_G(s)D_H(s) + N_G(s)N_H(s)}$$

B.5 MULTIPLE POLE AND ZERO CANCELLATIONS

If a slight variation of the previous situation occurs, such that

$$G'(s) = \frac{(s + a)N_G(s)}{(s + b)D_G(s)} \quad \text{and} \quad H'(s) = \frac{(s + b)N_H(s)}{(s + a)D_H(s)}$$

then

$$G(s)\Big|_{CL} = \frac{(s + a)N_G(s)D_H(s)}{(s + b)D_G(s)D_H(s) + N_G(s)N_H(s)}$$

which is a combination of Rules B.2 and B.3. It is advisable to perform a simple analysis, similar to the analysis of this appendix, when in doubt about the composition of the closed loop transfer function zeros. The poles of the closed loop transfer function are always obtained from the root locus analysis, except as noted above where a canceled pole appears in the closed loop transfer function also.

APPENDIX C

QUALITATIVE FLIGHT TESTING

C.1 PURPOSE

Qualitative flight testing determines the maximum amount of information in the minimum amount of flying time in order to evaluate an aircraft with respect to its entire mission or some specific area of interest.

Qualitative flight testing has essentially the same purpose as quantitative flight testing, i.e., to determine how well the aircraft flies and how well it will perform its designed mission. To accurately evaluate an aircraft from quantitative data requires analysis of large amounts of precisely measured data. The best a pilot can hope to do on a qualitative evaluation is to measure a limited amount of quantitative data. Thus, the test pilot's opinion on the acceptability of the aircraft is the important result and measured quantitative data (when available) is used primarily to support this opinion. Quantitative values of stick forces measured with a hand gage, for example, should be included in the report to support the pilot's opinion of acceptability. Estimates of stick forces can be made if no reliable measurements are available or qualifying terms such as "heavy", "medium", or "light" can be used to describe the forces. The point is that the difference in evaluating an aircraft qualitatively and quantitatively is a matter of degree. "Use what you've got." Pilot opinion supported by measured data is primary in qualitative testing, while the reverse is true in quantitative testing. The general rule is to first decide how well the aircraft does its job and then use the quantitative data you can get to support your opinion.

C.2 PILOT OPINION

Naturally, all pilots will not have exactly the same opinion regarding the acceptability of a particular aircraft characteristic. No two people think exactly alike. However, the opinions of pilots with similar experience and background will usually not differ greatly, particularly with respect to the capability of an aircraft to perform a specific mission. In other respects, such as cockpit arrangements, the opinions may vary more markedly.

For this reason, it is important for the qualitative test pilot to be as objective as possible in his evaluation. Guides which specify military requirements, such as MIL-STD-203F and MIL-F-8785C, should be used wherever possible to establish acceptability. However, mere compliance with a set of requirements does not necessarily yield a satisfactory aircraft. The primary question is "will it do the job?", not "does it meet the specifications?"

C.3 MISSION PREPARATION

A very limited amount of flight time is normally available for a qualitative evaluation. To acquire the information necessary to write an accurate and comprehensive report on an aircraft in this limited time requires a great deal of preflight study and planning.

The preflight preparation for a qualitative test is extremely important. It is almost impossible to put in too much time in planning for the flights. The amount of information acquired in the air will be directly proportional to the amount of preparation put in on the ground. A pilot who doesn't know what he is looking for is not likely to find it, and to know exactly what to look for in the evaluation requires considerable knowledge of the aircraft and its mission.

The precise mission of the aircraft is important in determining what specific investigations should be made in the evaluation. All fighters, for instance, do not have the same mission, and the characteristics of particular importance may not be the same. The roll characteristics of an air superiority fighter would be more important than for a long range strategic fighter, and the specific test plan should take this fact into account. Expected outstanding characteristics or weaknesses should also receive particular emphasis. Of course, the evaluation must be conducted within the cleared flight envelope of the aircraft, and the amount of flight time available may limit the number of altitudes, airspeeds, and tests that can be investigated. However, concentration on the extremes of altitudes, airspeeds, etc., and the

areas dictated by the primary mission will provide the best approach to the test planning.

An outline of the test to be conducted and the various altitudes, airspeeds, and configurations to be used will aid in organizing the flights and planning the flight data cards. The points included in the outline should be compatible with the time available for the. evaluation but it is always wise to overplan the flight and include more than seems possible to accomplish in the allotted time. Leave yourself the option of skipping the less important parts of your plan if time or fuel runs short. The sequence of tests should be such that as little time as possible is wasted. With proper planning a continuous flow from one investigation to the next is possible.

C.4 FLIGHT DATA CARDS

Before planning the flight data cards, as much as possible should be learned about the aircraft. Study the pilot's handbook if one is available, discuss the aircraft with the engineers, or with other pilots who have flown it, and get adequate cockpit time. The more the pilot knows about the aircraft and the more comfortable he is in it, the more thorough the evaluation will be. A pilot who doesn't know the aircraft procedures, both normal and emergency, or who has to spend most of his time in the air looking for controls or switches will not be able to do much evaluating.

The flight data cards should be self explanatory and should include all the points to be investigated during the flight. They should be designed so that a minimum of writing is required in the air because time will not be available to write down more than a word or two about each point. Remember, however, to provide places in the flight plan to write down these necessary comments. Numerous forms for the data cards are possible but completeness and legibility are essential.

Figures C.1 through C.4 present some possible formats and ideas for flight evaluation cards.

QUAL EVALUATION _____ AIRCRAFT

DATE _____   LOCATION _____

CONFIGURATION _____

_____

CALL SIGN _____   OPS # _____   TAIL # _____
G.W. _____   CG _____ %   FUEL LOAD _____ GAL/LBS

IMPORTANT MISSION LIMITATIONS

BATTERY POWER TIME _____

ICS TIME _____
IGNITION TIME _____
TEMP _____ ' TIME _____
TEMP _____ ' TIME _____
TEMP _____ ' TIME _____
FLAP SETTING ° OR % _____

IDLE LIMITS

RPM	_____ ±	_____
EGT	_____ ±	_____
FF	_____ ±	_____
OIL P.	_____ ±	_____
HYD	_____ ±	_____
PNEU	_____ ±	_____
TORQUE	_____ ±	_____
NOZ/TOP/TIT	_____ ±	_____

MAX CANOPY SPEED _____
MAX NGS SPEED _____

MAX TAXI SPEED _____
LINE UP CHECK

RPM	_____ ±	_____
EGT	_____ ±	_____
FF	_____ ±	_____
OIL P.	_____ ±	_____
OIL QTY	_____ ±	_____
TORQUE	_____ ±	_____

NOZZLE _____
TOP/TIT _____
GEAR LIMIT SPEED _____
FLAP SCHED _____ 1 _____
                   2 _____
FLAP LIMIT SPEED _____
EJECTION ENVELOPE/BANK
AS/ALT _____ BK _____
AS/ALT _____ BK _____
AS/ALT _____ BK _____

MAXIMUM AIRSPEED _____
MAXIMUM MACH # _____
MAX G (S) _____ WT _____
MAX G (S) _____ WT _____
MAX G (S) _____ WT _____
MAX G (A) _____ WT _____
MAX G (A) _____ WT _____

ENGINE LIMITS

	MIL	MAX
RPM	_____ %	_____ %
EGT	_____ '	_____ '
FF	_____	_____
OIL P	_____	_____
TORQUE	_____	_____
TOP/TIT	_____	_____
RPM OVERSPEED	_____	

AOA _____ AOA _____
LOAD/VOLT MTRS _____ ± _____
CG LIMITS % _____ TO _____
STORE LIMITS
       AIRSPEED _____
       G LIMIT _____ S _____ A
       JETTISON _____
ZERO G. LIMITS _____

_____

NEGATIVE G. LIMIT _____

_____

PROHIBITED MANEUVERS
1 _____
2 _____
3 _____
4 _____
NG LIFT OFF _____
MAIN GEAR T/O _____

FIGURE C.1.   TYPICAL AIRCRAFT QUALITATIVE EVALUATION FLIGHT CARD

A. Support Equipment
   1. Power Unit
      Type
      Capacity
   2. Other

B. Cargo Compartment
   1. Entrance
   2. Egress
   3. Systems Accessibility
   4. Other

C. Flight Deck
   1. Crew Stations
      a. Pilot
         Seat Adjustment
         Clearance
         Vision
         Rudder
         Pedal Adjustment
         Restrictions
         Other

      b. Copilot

      c. Flight Mechanic

      d. Navigator

   2. Instrument Panel
      a. Flight Instruments
         Grouping
         Readability
         Adequacy

      b. Engine Instruments
         Grouping
         Readability
         Adequacy

      c. Warning Lights
         Placards
         Switches
         Controls

   3. Pedestal
      a. Engine Controls
         System Controls
         Switches
         Guards
         Placards
         Lights
         Feel Identification
         Accessibility
         Confusion Factor
         Arrangement

      b. Remarks

   4. Overhead Panel
      a. Engine Controls
         System Controls
         Switches
         Guards
         Lights
         Placards
         Accessibility
         Feel Identification
         Confusion Factor
         Arrangement

      b. Remarks

   5. Side Panels
      a. Switches
         CBs
         Lights

      b. Remarks

   6. Flight Controls
      a. Rudder
         Break-out Force
         Travel
         Adjustment
         Clearance
         Stop
         Friction

      b. Elevator
         Break-out Force
         Travel
         Stop
         Friction
         Clearance

      c. Control Wheel
         Aileron Break-out Force
         Travel
         Stop
         Friction
         Clearance
         Grip
         Switches

   7. General Comments

FIGURE C.2.   TYPICAL LARGE AIRCRAFT QUALITATIVE EVALUATION FLIGHT CARDS

5. Vibration
   a. Noise
   b. Air vent deflectors
   c. Ventilation/heating
6. Control Required To Maintain Proper Taxi Speed
7. Remarks:

D. Pre-Take-Off (line up at even 1,000 feet and check W/V)
   1. Flight Control Check With Boost Operating
      a. b/o force
      b. rate
      c. deflection
      d. slop
      e. friction
   2. Flaps Set _____ Trim Set _____
   3. Engine Power Check
      a. Acceleration
         Idle _____ to _____ (MRP) _____ Sec.
         Asymmetric _____
         Overshoot _____
      b. Stabilized conditions: OAT _____

Eng	% RPM	Torque	TIT	Throttle Pos
1				
2				
3				
4				

   4. Brakes Hold At MIL PWR
   5. Fuel reading _____ lbs. W/V _____ kts.

E. Take-Off. (Use flight data on knee board)
   1. Start Time Form BRAKE RELEASE TO START CLIMB _____
   2. Brake Release Action
   3. Directional Control. Rudder Effective _____ kts.
   4. Elevator Effective (nose wheel off) _____ kts.
   5. Aileron Control _____ kts.
   6. T.O. Distance _____ ft. Lift-Off Speed _____ kts. Time _____ sec.
   7. Control Force _____ Pitch _____ Trim _____
   8. Trim-Out – Raise Gear
      Time _____ sec.
      Yaw _____
      Trim _____
   9. Trim-Out – Raise Flaps
      Time _____ sec.
      Trim _____
   10. Acceleration to MINIMUM CONTROL SPEED
   11. Acceleration to Climb Speed (1,000 ft)
   12. Visibility and Pitch Angle _____
   13. Remarks:

FIGURE C.2. TYPICAL LARGE AIRCRAFT QUALITATIVE EVALUATION FLIGHT CARDS
            (CONTINUED)

F. Climb (M N _____ ', 80° to W/V).
    1. Visibility _____
       Pitch Angle _____
    2. Record: FUEL at START CLIMB _____

TIME	HI	VI	R/C	TI	% RPM	TORQUE	TPT	Wf
_____	4M							
_____	6M							
_____	8M							
_____	10M							
_____	12M							
_____	14M							
_____	16M							
_____	18M							
_____	20M							
_____	22M							
_____	24M							
_____	26M							
_____	28M							
_____	30M							
_____	32M							

      FUEL at LEVEL-OFF _____

    3. Check Cabin Pressurization:
       10M _____
       15M _____
       20M _____
       25M _____
       30M _____ Note any fluctuations or surges.

    4. Cabin Heat Adequacy
      a. Heat glass

    5. Remarks

G. Cruise
    1. Vmax
      a. HI _____
      b. VI _____
      c. OAT _____
      d. Flt. Controls _____
      e. RPM _____
      f. Torque _____
      g. TIT _____
      h. Wf _____
      i. FUEL _____

FIGURE C.2.   TYPICAL LARGE AIRCRAFT QUALITATIVE EVALUATION FLIGHT CARDS
        (CONTINUED)

2. Dynamics (HI _____ VI _____) Note Control Position
   a. Phugoid
      1. Trim _____ VI_{in} _____ V_{max} _____ V_{min} _____
      2. Sec/cyc _____° _____ Damping _____
   b. Porpoise Mode. input _____ cycls _____ ampl. _____
   c. Spiral stability
      1. RT @ 10° _____°/_____ sec.
      2. LFT " " _____°/_____ sec.
      3. Remarks:

   d. Dutch Roll
      1. RT sideslip s/c _____ Roll _____ Yaw _____
         Damping _____ (1) _____ (2) _____ (3) _____
      2. LFT sideslip s/c _____ Roll _____ Yaw _____
         Damping _____ (1) _____ (2) _____ (3) _____
      3. (1) Norm (2) Damper Off (3) Rudder Power Off.
   e. Short Period
      1. Fixed (1.0g) Damping _____
      2. Fixed (−1.0g) Damping _____
      3. Free (1.0g) Damping _____
      4. Free (−1.0g) Damping _____
      5. Remarks:

3. Maximum Range Data
   a. HI _____ VI _____ OAT _____ FUEL _____
   b. RPM _____ Torque _____ TPT _____ Wf _____
   c. Remarks:

4. Systems Check: HI _____ VI _____
   a. Engine shut-down, No. _____
      1. Time to feather _____ Control force _____
      2. Procedure, etc:
   b. Engine restart
      1. Time to Normal power _____ Surge _____ Trim _____
      2. Procedure, etc:
   c. Anti-icing/de-icing system
      1. Full operation effect on engines _____
      2. Nasi glass
         Other
      3. Remarks:

   d. GTU/ATM operation _____
   e. Pressurization/heating _____
   f. Other:

5. Emergency Descent, HI _____ VI _____ (Initial)
   a. Time from cruise to start descent _____
   b. Procedure: G and F _____ Clean _____ Pressurization _____
   c. Time _____ from CR to HI _____ at VI _____
   d. Visibility _____ Pitch _____ Control _____
   e. Remarks:

FIGURE C.2. TYPICAL LARGE AIRCRAFT QUALITATIVE EVALUATION FLIGHT CARDS
            (CONTINUED)

6. Static Longitudinal Stability and Performance HI _____
   a. Acceleration check Trim at Max Range VI _____
      1. Decel to VI _____ Control Force *(Trim setting)
      2. Speed/Pwr VI _____ RPM _____ Tq _____ TIT _____ OAT _____
         Speed/Pwr VI _____ RPM _____ Tq _____ TIT _____
      3. Acceleration, (RESET TRIM), Time/10 kts (MRP) Initial VI _____
         10 _____
         20 _____
         30 _____
         40 _____
         50 _____
         60 _____
         70 _____
         80 _____
         V/S _____ ft/min. Control forces/gradient
      4. Remarks: FUEL _____

   b. Trim Changes: HI _____ VI _____
      1. Control boost off _____ on _____
      2. Runaway Trim: Elev _____ Ail _____ Rud _____
         5 sec delay (build-up)
   c. Turning Performance and Aileron Rolls. Cruise. (Build-up). FULL DEFLECT
      1. 60° ∅, Time 360° _____ V$_{max}$ _____ HI _____
      2. 45° Lft – 45° Rt (FIX) Time for 90° _____
      3. 45° Rt – 45° Lft (FIX) Time for 90° _____
      4. 60° ∅, Time 360° _____ VI _____ HI _____
      5. 45° Lft – 45° Rt (FIX) Time for 90° _____
      6. 45° Rt – 45° Lft (FIX) Time for 90° _____
      7. 60° ∅, Time 360° _____ VI _____ HI _____
      8. 45° Lft – 45° Rt _____ (FIX) Time for 90° _____
      9. 45° Rt – 45° Lft (FIX) Time for 90° _____
         POWER APPROACH
      10. 45° Lft – 45° Rt (FIX) Time for 90° _____
      11. 45° Rt – 45° Lft (FIX) Time for 90° _____
   d. Spiral Stability PA HI _____ VI _____ Pwr _____
      1. Rt ∅ 10° _____ °/_____ sec. (½ - 2).
      2. Lft 10° _____ °/_____ sec. (½ - 2).
   e. Phugoid (HI C$_L$) _____
   f. Sideslips, TRIM (L) HI _____ VI _____
      1. Rt _____°, Fr _____ Fs _____ Fs _____ dr _____ da _____ de _____
      2. Lft _____°, Fr _____ Fs _____ Fs _____ dr _____ da _____ de _____
         TRIM (CR) HI _____ VI _____
      3. Rt _____°, Fr _____ Fs _____ Fs _____ dr _____ da _____ de _____
      4. Lft _____°, Fr _____ Fs _____ Fs _____ dr _____ da _____ de _____
      5. D.E. with rudder (Pick up wing) _____
      6. Remarks: FUEL _____

7. Stalls, Gross Weight _____ HI Trim _____ _____
   a. CR 1.0g TRIM VI _____ Vw _____ Vs _____ HI _____
   b. CR 2.0g TRIM VI _____ Vw _____ Vs _____ HI _____
   c. Remarks:

   d. PA 1.0g TRIM VI _____ Vw _____ Vs _____ HI _____
   b. PA 1.5g TRIM VI _____ Vw _____ Vs _____ HI _____

FIGURE C.2.   TYPICAL LARGE AIRCRAFT QUALITATIVE EVALUATION FLIGHT CARDS
              (CONTINUED)

8. Asymmetric Power - III _____
   a. Climb configuration (MRP, Climb VI, Trimmed-out)
     NTC _____ Feather _____ No. 1 Eng. Rudder Free, 2 sec.
     Decel to 1.4 Vsl _____ kts. $\emptyset$ and sideslip
     (Cond. permitting check 2 out on one side)
   b. T.O. Configuration at V_{max} Gear and T.O. Flaps (165 kts.)
     Fail 1 and 2 and decelerate holding $\emptyset$ = ZERO.
     VI_{min} _____ . Check $\emptyset$ = 5° and SIDESLIP = ZERO.
   c. AT Min control speed fail 3 and 4, Fr _____ , Fa _____
     Fs _____ TRIM OUT HANDS OFF AT 1, 2 Vsl _____
   d. Remarks:

9. Boost OFF Operation HI _____ VI _____ Pwr _____
   a. Asymmetric Control 1 and 2 idle, 3 and 4 MRP
   b. Response _____ Fr _____ Fa _____ Fs _____
   c. Remarks:

10. Descent
   a. CR Configuration VI _____ V/S _____
     1. Visibility _____ Attitude _____
     2. Engine operation at idle _____
     3. Pressurization, systems, etc. _____
     4. Remarks:

   b. L Configuration VI _____ V/S _____
     1. Visibility _____ Attitude _____
     2. Engine operation at idle _____
     3. Remarks:

11. Trim Changes Trim at Placard Speed, PLF
   a. Flaps to 50% VI _____ HI _____ PLF/Trim
   b. Gear DOWN VI _____ HI _____ PLF/Trim
   c. Flaps to 100% VI _____ HI _____ PLF/Trim
   d. Power to IDLE VI _____ HI _____ Trim
   e. Idle to HRP VI _____ Att _____ Trim
   f. Gear UP VI _____ V/S _____ Trim
   g. Flaps UP VI _____ V/S _____ Trim

12. Asymmetric Power Go-around
   a. _____ Out, Pa VI _____ HI _____ Pwr _____
   b. Fr _____ Fa _____ Fe _____ Response and Control
   c. Remarks:

13. General Comments Prior to Completion of Flying.

FIGURE C.2.   TYPICAL LARGE AIRCRAFT QUALITATIVE EVALUATION FLIGHT CARDS
             (CONTINUED)

H. Approach and Landing
    1. Pre-landing check: Operating Weight _____
       Alt Setting _____ Fuel Weight _____
       W/V _____ Landing GR WT _____
       Runway _____ Best Flare Speed _____
       (Pilot Pwr and Steer) Touchdown speed _____
       (Copilot Ailerons) VS$_L$ _____

    2. Traffic pattern:
       a. Visibility _____ Control
       b. Power response _____
       c. Remarks:

    3. Landing:
       a. Flare _____ Response _____ Control _____
       b. Float _____ Characteristics in ground effect _____
       c. Touchdown _____ Nose-wheel off _____ Grd idle _____
          Reverse _____ Brakes _____ Steering _____
       d. Directional control with ailerons _____
       e. Stopping distance _____

    4. Remarks:

I. Post-flight and Shut-down
    1. Normal procedures. Ease and time to accomplish _____
    2. Coordination _____
    3. Fuel _____
    4. Flight Time _____
    5. Squawks _____

J. Re-evaluate Cockpit and A/C in General

FIGURE C.2.   TYPICAL LARGE AIRCRAFT QUALITATIVE EVALUATION FLIGHT CARDS
              (CONTINUED)

EXTERNAL INSPECTION

TOD START _____
TOD FINISH _____

Remarks:

....

COCKPIT EVALUATION

1. Ease of Entry

      Ladder _____

      Steps _____

2. Location of Instruments and Controls
3. Adjustment of Seat and Controls
4. Comfort
5. Ease of Identification of:
   Switches
   Controls
   Emergency Devices
   Warning Lights
6. Egress – ground and Airborne

BEFORE STARTING CHECKS

TOD _____

   Remarks

     Complexity:

FIGURE C.3.   TYPICAL FIGHTER AIRCRAFT QUALITATIVE EVALUATION FLIGHT CARDS
          (2 hour flight)

STARTING ENGINES   Fuel_____TOD_____

   Complexity:

   Ground Support:

      Equipment_____

      Personnel_____

BEFORE TAXI CHECKS   TOD_____

   Estimated Break-out Force

      Longitudinal +_____# −_____#

      Lateral+_____# −_____#

      Directional+_____# −_____#

   Trim rate (Longitudinal) Aft_____ Sec

                 Fore_____ Sec

   Flap Extension_____ sec   Retraction_____ sec

TAXIING   Fuel_____TOD_____

                                RPM req to move_____

   Visibility

   Steering   N.W.S.

                                Brakes

   Visibility

   Power required_____RPM, fuel/flow_____ pph

   Runway temp_____°F. P.A._____ ft.

FIGURE C.3.   TYPICAL FIGHTER AIRCRAFT QUALITATIVE EVALUATION FLIGHT CARDS
(2 hour flight) (CONTINUED)

TAKEOFF   Fuel _____#TOD _____

    Do brakes hold in MIL PWR   Yes   No

    Symmetry of brake release

    Directional control

    Rudder effective speed _____ knots

    Ease of rotation

    Lift-off speed _____ knots

    Estimated T/O distance _____ feet

    Gear up time _____ sec   Flaps up time _____ sec

    Trim changes   Landing gear + – _____#

                     Flaps + – _____#

Are placards hard to exceed?   Yes   No

    Visibility during T/O and Initial Climb

    Adequacy of T/O trim setting:

    Speed stability during acceleration:

CLIMB   Fuel _____#TOD _____

    Control during climb

        Longitudinal

        Directional

        Lateral

Climb Schedule		
5000 ft.	.89IMN	550
10000 ft.	.89IMN	510
15000 ft.	.90IMN	470
20000 ft.	.905IMN	430
25000 ft.	.910IMN	390
30000 ft.	.915IMN	360
35000 ft.	.92IMN	320
39000 ft.	.92IMN	

FIGURE C.3.   TYPICAL FIGHTER AIRCRAFT QUALITATIVE EVALUATION FLIGHT CARDS
(2 hour flight) (CONTINUED)

LEVEL OFF Fuel _____ #TOD _____

   EASE

   Attitude Change _____ °

****

CRUISE   **90% RPM**   **.86IMN (recommended cruise)**

  Start   **Fuel** _____ #   **TOD** _____

                                                                                 Linear?

Sideslip:	C_{ℓ_β}	Hvy	Med	Lt	Yes	No
	C_{n_β}	Hvy	Med	Lt	Yes	No

Dutch Roll   Period _____ sec

                  Damping   Hvy   Med   Lt

  Cycles to Damp _____

CRUISE cont.   **39,000 ft.**   **.86IMN**

  PIO Tendency   Yes   No

  Short Period   Cycles to Damp _____

                 Period _____ sec

    Do controls have dynamic tendency?

                            Yes   No

Aileron Rolls: t90

                            R   L   Adv. Yaw

½ deflection   _____ sec _____ sec

Full deflect.   _____ sec _____ sec

*********************************** DAMPERS OFF ***********************************

                                                                                 Linear?

Sideslip:	C_{ℓ_β}	Hvy	Med	Lt	Yes	No
	C_{n_β}	Hvy	Med	Lt	Yes	No

Dutch Roll: Period _____ sec

                 Damping   Hvy   Med   Lt

                 Cycles to Damp _____

PIO Tendency   Yes   No

Short Period: Cycles to Damp _____

                 Period _____ sec

FIGURE C.3. TYPICAL FIGHTER AIRCRAFT QUALITATIVE EVALUATION FLIGHT CARDS
(2 hour flight) (CONTINUED)

```
************************************ DAMPERS ON ************************************
        Finish:              Fuel_____#              TOD_____
      Speed brake trim change        Hvy    Med    Lt
              Extend            Push    Pull
              Retract           Push    Pull
MANEUVERING FLIGHT                         .9 IMN                39-35,000 ft.
   Fuel_____#
   Initial buffet_____ g
   Heavy buffet_____ g  $n_{max}$_____ g
   Stick force      Hvy    Med    Lt
   Linear           Yes    No
*****************************************************************************************

ACCELERATION TO 1.2 IMN at 35,000 ft. (trim .9 IMN)
   Start:              Fuel_____#              TOD_____
   NB   Light L_____ sec  R_____ sec
   NB   Trim Change_____# Push    Pull
   Stick force gradient_____
   Transonic trim change_____
   Finish fuel_____#              TOD_____
*****************************************************************************************

CRUISE 1.15 IMN                                         35,000 ft.
   Start              Fuel_____#              TOD_____
                                                        Linear?
   Sideslip:     $C_{\ell_\beta}$    Hvy    Med    Lt         Yes    No
                 $C_{n_\beta}$       Hvy    Med    Lt         Yes    No
   Dutch Roll:   Period_____ sec
                 Damping    Hvy    Med    Lt
                 Cycles to Damp_____
   PIO Tendency     Yes    No
```

FIGURE C.3.   TYPICAL FIGHTER AIRCRAFT QUALITATIVE EVALUATION FLIGHT CARDS
        (2 hour flight) (CONTINUED)

CRUISE cont 1.15 IMN 35,000 ft.

Short Period: Cycles to Damp _____

                    Period _____ sec

*************************************** **DAMPERS OFF** **

Linear?

Sideslip:	C_{ℓ_β}	Hvy	Med	Lt	Yes	No
	C_{n_β}	Hvy	Med	Lt	Yes	No

Dutch Roll: Period _____ sec

             Damping   Hvy Med Lt

             Cycles to Damp _____

PIO Tendency   Yes No

Short Period: Cycles to Damp _____

             Period _____ sec

*************************************** **DAMPERS ON** **

Aileron Rolls: t 90   Adverse Yaw

                                R L

    ½ deflection   _____ sec _____ sec

    Full deflect.   _____ sec _____ sec

    Finish: Fuel _____   TOD _____

****

SPEED BRAKE TRIM CHANGE 1.15-1.1 IMN

Hvy   Med   Lt

Extend   Push   Pull

Retract   Push   Pull

MANEUVERING FLIGHT   1.1 IMN   35-35,000 ft.

Fuel _____ #

Initial buffet _____ g   Heavy buffet _____ g

n_{max} _____ g

Stick force   Hvy   Med   Lt

Linear?   Yes   No

FIGURE C.3.   TYPICAL FIGHTER AIRCRAFT QUALITATIVE EVALUATION FLIGHT CARDS (2 hour flight) (CONTINUED)

DECELERATION TO 210 knots 30,000 ft. (Long Stat)

   Stick Force gradient _____

* * *

CRUISE   **210 knots**   **30,000 ft.**

   Start: Fuel _____#   TOD _____

                                                                            Linear?

   Sideslips: C_{ℓ_β} Hvy   Med   Lt   Yes   No

                C_{n_β} Hvy   Med   Lt   Yes   No

   Dutch Rolls: Period _____ sec

                Damping   Hvy   Med   Lt

                Cycles to Damp _____

   PIO Tendency   Yes   No

   Short Periods: Cycles to Damp _____

                Period _____ sec

* * * **DAMPERS OFF** * * *

                                                                            Linear?

   Sideslips: C_{ℓ_β} Hvy   Med   Lt   Yes   No

                C_{n_β} Hvy   Med   Lt   Yes   No

CRUISE   **210 knots at 30,000 ft.**

   Dutch Roll: Period _____ sec

                Damping   Hvy   Med   Lt

                Cycles to Damp _____

   PIO Tendency   Yes   No

   Short Periods: Cycles to Damp _____

                Period _____ sec

   Finish: Fuel _____#   TOD _____

FIGURE C.3.   TYPICAL FIGHTER AIRCRAFT QUALITATIVE EVALUATION FLIGHT CARDS (2 hour flight) (CONTINUED)

·· DAMPERS ON ··

AILERON ROLLS   **t90**   **Adverse Yaw**

    ½ deflection   R_____ sec   L_____ sec

    Full deflect.   R_____ sec   L_____ sec

···

MANEUVERING FLIGHT at 210 knots

    Fuel _____#

    Initial Buffet _____ g   Heavy Buffet _____ g

    "max" _____ g

    Stick force gradient: Hvy   Med   Lt

···

STALLS   Cruise Configuration 25,000 ft.

    Fuel _____#

Cr   **Vw** _____ knots   **Ve** _____ knots

GLIDE   **Vw** _____ knots   **Ve** _____ knots

Remarks

POWER APPROACH CONFIGURATION

    Gear extension _____ sec

    Flap extension _____ sec

    Asymmetric power at 155 knots

    MIL RWR Rudder Force   Hvy   Med   Lt

    MAX TWR Rudder Force   Hvy   Med   Lt

    Trimability   MIL _____ MAX

STALLS: Fuel _____

Vw _____ knots   **Ve** _____ knots

Remarks:

FIGURE C.3.   TYPICAL FIGHTER AIRCRAFT QUALITATIVE EVALUATION FLIGHT CARDS
(2 hour flight) (CONTINUED)

Trim at 160 knots

Sideslip:	C_{ℓ_β}	Hvy	Med	Lt		Yes	No
	C_{n_β}	Hvy	Med	Lt		Yes	No

Dutch Roll: Period _____ sec

                  Damping   Hvy Med Lt

                  Cycles to Damp _____

PIO Tendency   Yes No

Short Period: Cycles to Damp _____

                  Period _____ sec

** **DAMPERS OFF** **

Dutch Roll: Period _____ sec

                  Damping   Damping   Hvy Med Lt

                  Cycles to Damp _____

PIO Tendency   Yes No

Short Period: Cycles to Damp _____

                  Period _____ sec

** **DAMPERS ON** **

AILERON ROLLS   t90   **Adverse Yaw**

   ½ deflection   R _____ sec L _____ sec

   Full deflect   R _____ sec L _____ sec

****

ACROBATICS

   Loop

   Immelman

   Barrel Roll

FIGURE C.3.   TYPICAL FIGHTER AIRCRAFT QUALITATIVE EVALUATION FLIGHT CARDS (2 hour flight) (CONTINUED)

INSTRUMENTS

Holding at 20,000 ft.	250 knots	90-92%
Penetration S/B	270 knots	90%
Initial Clean	220 knots	94%

Low Cone   gear, 86%, flaps, 155 knots

LANDING

Normal traffic pattern   60% flaps

Single engine go-around closed pattern

Full stop   Full flaps

   Touchdown speed_____ knots' marker_____

••

TAXIING   Fuel_____#TOD_____

   Engine acceleration idle to mil_____ sec

   Turning radius_____ feet

   Re-evaluate cockpits

ENGINE SHUTDOWN

   Check servicing for turn-around

            Time_____

            Oil_____ qts

            Hydraulic fluid_____ qts

            LOX_____ liters

FIGURE C.3.   TYPICAL FIGHTER AIRCRAFT QUALITATIVE EVALUATION FLIGHT CARDS
            (2 hour flight) (CONTINUED)

TOD _____ beside A/C

START   **Procedure**

F Flow _____ RPM _____ F Flow _____

Before Taxi Check

TOD _____

TAXI

     Power to Roll _____ Brakes   S   NS

     Nosewheel steering   Turn Rad. _____

     NWS Off   Brake turn _____

     Canopy Operation

     Visibility

TOD _____

LINE UP

     Brakes Mil Pwr _____

     Pump one brake

     Engine Acc Time _____

RPM _____ EGT _____ FF _____

Throttle friction   S   NS

FUEL   L _____   R _____

TOD _____

FIGURE C.4.   TYPICAL AIRCRAFT QUALITATIVE EVALUATION FOR A PILOT TRAINING MISSION (1 hour flight)

TAKEOFF

    Brake release

    A/B light

    NWS rel at Rudder Eff   A/S _____

    CONTROL FORCES   L M H _____ lbs

    NW LIFT OFF _____

    T.O. ROLL _____ ft A/S _____

GEAR UP _____ sec.   FLAPS UP _____ sec

    Trim Changes _____

    Noises

    Press. Sys

    Acceleration   Rotation

CLIMB

    Schedule   .9 to 35M

    Control

    Trim

    Visibility

    Dampers

    35M   Time _____   Fuel L _____ R _____

                    Throttle Mil   Level Off

TOD _____

FIGURE C.4. TYPICAL AIRCRAFT QUALITATIVE EVALUATION FOR A PILOT TRAINING MISSION (1 hour flight) (CONTINUED)

SUPERSONIC

    A/B Light   time_____

    TRIM CHANGES

    STABILITY

	DAMPERS	PULSE	CYCLE	TIME
	ON	Elev		
		Rud		
	OFF	Elev		
		Rud		

    45° Roll

ONE ENGINE IDLE

Wind Up Turn to g Max.

    A/S_____   **"g"**_____

    Stick force gradient

    Buffet

    FUEL   L_____   R_____

    TOD_____

FIGURE C.4.   TYPICAL AIRCRAFT QUALITATIVE EVALUATION FOR A PILOT TRAINING MISSION (1 hour flight) (CONTINUED)

TURNING PERFORMANCE   **300 Kts**_____ **sec**

    Zoom to Slow A/C

PWR STALL   **WARN**_____   **STALL**_____

230 Kts. Flight   **Roll**

    STABILITY

	DAMPERS	PULSE	CYCLE	TIME
	ON	Elev		
		Rud		
	OFF	Elev		
		Rud		
	Sideslip	6° Approx.		

CUT ONE ENGINE

    EMERGENCY GEAR EXTENSION_____ **sec**

    AIRSTART

    170 knots   **Flaps Down**

      Aileron Power

    Cycle gear   **Flaps up**   **TRIM**

    FUEL   L_____   R_____

TOD_____

FIGURE C.4.   TYPICAL AIRCRAFT QUALITATIVE EVALUATION FOR A PILOT TRAINING MISSION (1 hour flight) (CONTINUED)

DIVE   **450 Kts**   **12M**

    CLOVERLEAF
    BARREL ROLL
    IMMELMAN
       Level at 20M Inbound to   **VOR**
       200 Kts   **F FLOW** _____
       250 Kts   **F FLOW** _____
       300 Kts   **F FLOW** _____

HIGH CONE
    240 Kts.   **Gear Flaps**   **Dive Brakes**
    1 g stall
    200 Kts.

                          STABILITY   **Check**
STALL RIGHT TURN   **190 Kts**
Clean up A/C   **275 Kts.**   **turn to ILS**

    350 Kts.   **Speed Brakes**   **Decelerate**
ISL Gear, Flaps, D/C   **170 Kts**

TOD _____

FIGURE C.4.   TYPICAL AIRCRAFT QUALITATIVE EVALUATION FOR A PILOT TRAINING
                MISSION (1 hour flight) (CONTINUED)

SINGLE ENGINE GO-AROUND

SINGLE ENGINE TOUCH AND GO

RE-ENTER
      PITCH OUT   **NO FLAP LANDING**

      TRIM CHANGES

TAXI

      AFTER LANDING CHECK

      SHUTDOWN

FIGURE C.4.   TYPICAL AIRCRAFT QUALITATIVE EVALUATION FOR A PILOT TRAINING MISSION (1 hour flight) (CONTINUED)

C.5 GENERAL TECHNIQUES

The cockpit evaluation can normally be made while getting cockpit time prior to the first flight. MIL-STD-203F specifies the standard cockpit arrangement for the various types of aircraft in considerable detail and should be used as a guide in making the cockpit evaluation. However, a summary of some of the points to note may prove helpful. These include ease of entry, comfort, adjustment of seat and controls, location of basic flight instruments, size and legibility of instruments, accessibility of switches and controls, ease of identification of switches and controls, location and identification of emergency switches and controls, methods of escape (both on the ground and airborne), and general impression of cockpit layout.

Several points should be observed and recorded during the start and while preparing the aircraft for flight. These should be weighed against the aircraft's mission requirements. An all-weather interceptor, for example, should be capable of fast, uncomplicated starts to meet its alert and scramble requirements. Starts for other types may not be so critical; however, no starting procedure should be unnecessarily complex or confusing. Evaluation of the start should include: complexity of start, time to prepare for start, time to start, external power and ground support equipment required, ground personnel required, and time from start to taxi. The system checks and normal procedure requirements from start to taxi should also be evaluated.

An evaluation of the ground handling characteristics can be made while taxiing. How much power is required to start moving and to taxi at the desired speed? Is braking action required to prevent taxiing too fast? Is the visibility adequate? Is the directional control satisfactory? Is the braking action satisfactory? What is the turning radius of the aircraft? Does the aircraft require any auxiliary equipment such as removable wheels, escape ladders, etc? Is there any problem with clearing obstacles with any part of the aircraft?

The takeoff distance may be difficult to determine without assistance from outside personnel, but an estimate should be made using whatever aid is available such as runway distance markers. Use the recommended takeoff procedure; don't try to make a maximum performance takeoff. The normal ground roll will be of more interest than the minimum possible. Some of the other

points to note in the takeoff include: ability of brakes to hold in military power, directional control during ground roll, rudder effective speed, nose lift-off speed, visibility after nose up and during initial acceleration and climb, force required to raise nose, any over-controlling tendencies, airborne speed, adequacy of recommended takeoff trim settings, time to retract gear and flaps, trim changes with retraction of gear and flaps, any tendency to exceed gear or flap speed limitations, effectiveness of trimming action during acceleration, and any distracting noises or vibrations.

The in-flight techniques differ very little from the techniques used in flying quantitative tests. However, it generally is not necessary to be as precise in holding airspeeds and altitudes. To do so would only waste time because differences caused by variations of a few hundred feet in altitude or a few knots in airspeed will not be qualitatively discernible. This is not an endorsement for being lax in flying the aircraft. Just don't waste time with precision that will not contribute to the evaluation of the aircraft. If speeds are critical, such as in the climb or in the pattern, then maintain them as closely as possible. Otherwise, use good judgment in determining how close to an aim condition it is necessary to be and fly accordingly.

If the climb rate of the aircraft is relatively slow, it may be possible to get some stability information in the climb, i.e., stick pulses, sideslips, etc. Most present day fighter aircraft climb so rapidly that this may not be practical. If so, just record climb performance data (time, fuel, and in-dicated speed) at intervals of approximately 5,000 feet. Start the time at brake release. Intercept the climb schedule at a comfortable altitude and attempt to fly the recommended schedule precisely. Continue the climb only as far as necessary to meet the objective of the flight. Unless climb perform-ance is of primary importance, this will probably be to the altitude selected for the first series of investigations. General aircraft characteristics should be observed during the climb. How difficult is it to maintain the recommended climb schedule? Are the control responses smooth, too fast, too slow? Is visibility adequate? Is there any buffet, vibration or excessive noise? Are the ventilation and pressurization systems satisfactory? Are the normal procedures complicated or excessively distracting? If dampers or other artificial stability devices are provided, check the applicable charac-teristics with them ON and OFF.

The altitude selected for the first series of stability investigations may be at the tropopause since this is where the aircraft will probably have its best performance. However, if the designed operating altitude is considerably higher it may be advisable to select an altitude at or near the aircraft's operating altitude. The stability maneuvers performed will be essentially the same at all the altitudes and airspeeds selected. These should be sufficiently spaced to assure discernible qualitative differences in the aircraft's characteristics.

The stability characteristics investigated should include longitudinal and directional static stability, longitudinal and directional dynamic stability, aileron rolls, and maneuvering flight at several different airspeeds and altitudes. An investigation of the transonic trim changes also should be made. All the dynamic characteristics should be checked with the stability augmentation devices, if any, both ON and OFF. With proper planning these investigations can be made in a minimum amount of time. The longitudinal static stability can be checked while accelerating to V_{max}, for instance. Once at V_{max}, the aircraft can be trimmed for approximately hands-off flight and the static directional stability checked by entering a steady sideslip out to maximum rudder deflection (if the aircraft is cleared to that limit). The periods of the dynamic modes can be timed using a stop watch or counting the seconds. Estimate the number of the cycles to damp completely or to one-half amplitude, as the case may be, for all the modes.

Approach the aileron rolls cautiously. Make several partial deflection rolls before making any full deflection rolls. The time to reach 90° of roll and the time to roll 360° can be estimated using a stopwatch or again by counting the seconds. It is advisable to make rapid reversals of ailerons and other rolling maneuvers if these can be expected in operational use of the aircraft. The rolling characteristics should also be checked in accelerated flight as well as 1g flight.

After completion of investigations at V_{max}, a windup turn to limit load factor can be made to check the maneuvering stability of the aircraft. Then zoom back to the original altitude and repeat these investigations at the second airspeed. The other altitudes and airspeeds can be checked in the same

manner. Any differences resulting from altitude or speed changes should be noted.

If the aircraft is cleared for stalls, they should be investigated cautiously in all configurations and types of entry. Determine the approximate stall warning margin, what defines the warning and the stall, and the aircraft characteristics in the stall and the recovery. If possible, determine the best method of breaking the stall and altitude loss in recovery from several points in the stall.

If possible, check the tactical mission capability of the aircraft. Simulated dive bombing runs or LABS maneuvers could be made for a tactical fighter for example. All the information obtainable will be helpful in writing an accurate and comprehensive report.

Fly the traffic pattern as recommended and, if fuel permits, make a go-around on the first pass. Note the power response, power required in the pattern, airspeed control and sink rate, trim changes with gear and flap extension, trimming action, buffet with gear extension, and general aircraft feel in the pattern. On the go-around, recheck the trim changes with gear and flap retraction and with drag device reaction. Don't forget to look at engine out characteristics if time and fuel permit. On the first landing in the aircraft it is probably not advisable to attempt to get the minimum landing roll. Make a normal touchdown and use normal braking action (use the drag chute if provided). Note the touchdown speed, the effects of any crosswind, directional control, nose lowering speed, etc. As with the takeoff, the normal landing roll is of more importance than the minimum possible.

Review the flight while taxiing back to the parking area. Re-evaluate the cockpit, and attempt to determine whether the aircraft will perform its design mission and is safe and comfortable to fly. Your opinion with everything fresh in mind is probably the most accurate. Put everything you remember about the flight and your impressions of the aircraft down on paper immediately after leaving the aircraft. Do this immediately and before talking to anyone about the airplane or the flight. Waiting or discussing points with other people may alter first hand impressions or cause important aspects of the flight to be forgotten.

C.6 INITIAL FLIGHT REPORT

The test pilot's ability to qualitatively evaluate an aircraft in limited flying time is only part of the evaluation. His ability to communicate his finding is an extremely important step that must not be neglected. An "Initial Flight Report" should be written as soon as possible after the flight. At the Flight Test Center this is accomplished on the AFFTC Form 365, (Figure 5). The report should express everything learned about the aircraft. A narrative form is normally used for qualitative reports. Comparisons with other aircraft can be used to assist in describing the aircraft. Take care to ensure that only aircraft familiar to most readers are used for comparison. Otherwise the comparison will mean nothing to them.

Keep in mind the purpose of the qualitative evaluation while writing the report. Mere figures are normally not enough to describe the stability of the aircraft, particularly on a qualitative evaluation since the data obtained are very limited. Analyze the aircraft's characteristics in light of its ability to perform its design mission, give opinions of the aircraft's ability to do the job and support these opinions with the facts obtained on the evaluation flights. Comment on anything personally disliked but be objective in condemning any shortcomings. Recommendations for specific changes in the aircraft are to be included in the report. The exact manner in which the aircraft should be fixed should not be specified or recommended. The test pilot's job is to evaluate the existing hardware and state what should be changed. It is then the manufacturer's responsibility to determine how to make the necessary changes.

DAILY/INITIAL FLIGHT TEST REPORT	1. AIRCRAFT TYPE	2. SERIAL NUMBER

3.	CONDITIONS RELATIVE TO TEST	
A. PROJECT/MISSION NO	B. FLIGHT NO/DATA POINTS	C. DATE
D. FRONT COCKPIT (Left Seat)	E. FUEL LOAD	F. JON
G. REAR COCKPIT (Right Seat)	H. START UP OR WT/CG	I. WEATHER
J. TO TIME/SORTIE TIME	K. CONFIGURATION/LOADING	L. SURFACE CONDITIONS
M. CHASE ACFT/SERIAL NO	N. CHASE CREW	O. CHASE TO TIME/SORTIE TIME

4. PURPOSE OF FLIGHT/TEST POINTS

5. RESULTS OF TESTS (Continue on reverse if needed)

(SHOWN 75 PERCENT ACTUAL SIZE)

6. RECOMMENDATIONS

COMPLETED BY	SIGNATURE	DATE

AFFTC FORM 365   PREVIOUS EDITION IS OBSOLETE
MAR 84

FIGURE C.5. AFFTC FORM 365